Indian Point Probabilistic Safety Study

Power Authority of the State of New York
Consolidated Edison Company of New York, Inc.

— NOTICE —

THE ATTACHED FILES ARE OFFICIAL RECORDS OF THE DIVISION OF DOCUMENT CONTROL. THEY HAVE BEEN CHARGED TO YOU FOR A LIMITED TIME PERIOD AND MUST BE RETURNED TO THE RECORDS FACILITY BRANCH 016. PLEASE DO NOT SEND DOCUMENTS CHARGED OUT THROUGH THE MAIL. REMOVAL OF ANY PAGE(S) FROM DOCUMENT FOR REPRODUCTION MUST BE REFERRED TO FILE PERSONNEL.

Docket # 50-247
Control # 8203110003
Date 03-05-82 of Document
REGULATORY DOCKET FILE

DEADLINE RETURN DATE

REGULATORY DOCKET FILE COPY

RECORDS FACILITY BRANCH

Volume 8

Indian Point Probabilistic Safety Study

Copyright 1982 by
Power Authority of the State of New York
Consolidated Edison Company of New York, Inc.

Volume 8

Copy No. 15

REGULATORY DOCKET FILE COPY

SECTION 4
CONTAINMENT TRANSIENT ANALYSIS

TABLE OF CONTENTS

Section			Page
4.0	OVERVIEW		4.0-1
	4.0.1	Introduction	4.0-1
	4.0.2	Transient Analysis Approach	4.0-2
	4.0.3	Conclusions	4.0-4
4.1	ANALYTICAL TOOLS		4.1-1
	4.1.1	The MARCH Code	4.1-1
	4.1.2	COCOCLASS9 Code	4.1-3
	4.1.3	Analysis Model for the Dispersive Event	4.1-6
	4.1.4	Phenomenological Model Modifications	4.1-9
4.2	ANALYTICAL INPUT		4.2-1
	4.2.1	Containment Capability	4.2-1
	4.2.2	Class I Sequence	4.2-1
	4.2.3	Class II Sequence	4.2-4
	4.2.4	Class III Sequence	4.2-4
	4.2.5	Class IV Sequence	4.2-7
	4.2.6	Class V Sequence	4.2-7
	4.2.7	Class VI Sequence	4.2-9
4.3	RESULTS		4.3-1
	4.3.1	Class I Sequence	4.3-1
	4.3.2	Class II Sequence	4.3-2
	4.3.3	Class III Sequence	4.3-4
	4.3.4	Class IV Sequence	4.3-6
	4.3.5	Class V Sequence	4.3-7
	4.3.6	Class VI Sequence	4.3-10
	REFERENCES		4-1
4.4	APPENDICES		
	4.4.1	Containment Capability of Indian Point Power Plant Unit Nos. 2 and 3 for Internal Pressure Load	
	4.4.2	Structural Heat Transfer Modeling	
	4.4.3	Flame Temperature Calculation	
	4.4.4	MARCH In-Vessel Pressure Spike	
	4.4.5	Steam Generator Tube Integrity Evaluation For A Postulated Class-9 Event Loading	
	4.4.6	Particle Size For MARCH Code Reactor Cavity Steam Spike Analysis	
	4.4.7	Gas Radiation Model Used In COCO	
	4.4.8	Input Parameters For Containment Analysis	
	4.4.9	Compilation of Results	

LIST OF TABLES

Tables		Page
4.2.1-1	Description of Various Classes of Accidents	4.2-10
4.3.1-1	Class I Cases	4.3-12
4.3.2-1	Class II Cases	4.3-13
4.3.3-1	Class III Cases	4.3-14
4.3.4-1	Class IV Cases	4.3-18
4.3.5-1	Class V Cases	4.3-20
4.3.6-1	Class VI Cases	4.3-24

LIST OF FIGURES

Figure		Page
4.0.2-1	Calculation Approach	4.0-5
4.0.2-2	General Shape of the Rates of Steam and Water Releases into the Containment Atmosphere vs. Time	4.0-6
4.0.2-3	General Shape of the Rates of Hydrogen Release into the Containment Atmosphere vs. Time	4.0-7
4.0.2-4	General Shape of the Rates of Heat Release from Fission Products into the Containment Atmosphere vs. Time	4.0-8
4.1.1-1	MARCH Code Treatment of a Postulated Reactor Accident	4.1-14
4.1.2-1	Hydrogen Burn Characteristics in Dry Air	4.1-15
4.1.2-2	Percent Hydrogen Burn Versus Hydrogen Concentration	4.1-16
4.1.2-3	Hydrogen Burn Pressure Rise Versus Hydrogen Concentration	4.1-17
4.3.1-1	Pressure (In Containment) vs. Time, Class I, Best Estimate Case	4.3-25
4.3.1-2	Flame Temperature (In Containment) vs. Time, Class I, Best Estimate Case	4.3-26
4.3.1-3	Pressure (In Containment) vs. Time, Class I, Case 1	4.3-27
4.3.1-4	Flame Temperature (In Containment) vs. Time, Class I, Case 1	4.3-28
4.3.1-5	Pressure (In Containment) vs. Time, Class I, Case 3	4.3-29
4.3.1-6	Pressure (In Containment) vs. Time, Class I, Case 4	4.3-30
4.3.2-1	Pressure (In Containment) vs. Time, Class II, Best Estimate Case	4.3-31
4.3.2-2	Flame Temperature (In Containment) vs. Time, Class II, Best Estimate Case	4.3-32
4.3.2-3	Pressure (In Containment) vs. Time, Class II, Case 4	4.3-33
4.3.3-1	Pressure (In Containment) vs. Time, Class III, Best Estimate Case	4.3-34
4.3.3-2	Flame Temperature (In Containment) vs. Time, Class III, Best Estimate Case	4.3-35
4.3.3-3	Flame Temperature (In Containment) vs. Time, Class III, Case 3	4.3-36
4.3.3-4	Pressure (In Containment) vs. Time, Class III, Case 9	4.3-37
4.3.3-5	Pressure (In Containment) vs. Time, Class III, Case 11	4.3-38
4.3.3-6	Pressure (In Containment) vs. Time, Class III, Case 12	4.3-39
4.3.3-7	Pressure (In Containment) vs. Time, Class III, Case 13	4.3-40
4.3.3-8	Pressure (In Containment) vs. Time, Class III, Case 15	4.3-41
4.3.3-9	Pressure (In Containment) vs. Time, Class III, Case 16	4.3-42
4.3.4-1	Pressure (In Containment) vs. Time, Class IV, Best Estimate Case	4.3-43

LIST OF FIGURES (Continued)

Figure		Page
4.3.4-2	Flame Temperature (In Containment) vs. Time, Class IV, Best Estimate Case	4.3-44
4.3.4-3	Pressure (In Containment) vs. Time, Class IV, Case 1	4.3-45
4.3.4-4	Pressure (In Containment) vs. Time, Class IV, Case 2	4.3-46
4.3.4-5	Pressure (In Containment) vs. Time, Class IV, Case 3	4.3-47
4.3.4-6	Pressure (In Containment) vs. Time, Class IV, Case 4	4.3-48
4.3.4-7	Pressure (In Containment) vs. Time, Class IV, Case 6	4.3-49
4.3.4-8	Pressure (In Containment) vs. Time, Class IV, Case 7	4.3-50
4.3.5-1	Pressure (In Containment) vs. Time, Class V, Best Estimate Case	4.3-51
4.3.5-2	Flame Temperature (In Containment) vs. Time, Class V, Best Estimate Case	4.3-52
4.3.5-3	Pressure (In Containment) vs. Time, Class V, Case 1	4.3-53
4.3.5-4	Flame Temperature (In Containment) vs. Time, Class V, Case 1	4.3-54
4.3.5-5	Pressure (In Containment) vs. Time, Class V, Case 2	4.3-55
4.3.5-6	Flame Temperature (In Containment) vs. Time, Class V, Case 2	4.3-56
4.3.5-7	Pressure (In Containment) vs. Time, Class V, Case 7	4.3-57
4.3.5-8	Flame Temperature (In Containment) vs. Time, Class V, Case 7	4.3-58
4.3.5-9	Pressure (In Containment) vs. Time, Class V, Case 9	4.3-59
4.3.5-10	Pressure (In Containment) vs. Time, Class V, Case 12	4.3-60
4.3.5-11	Flame Temperature (In Containment) vs. Time, Class V, Case 12	4.3-61

SECTION 4

CONTAINMENT TRANSIENT ANALYSIS

4.0 OVERVIEW

4.0.1 Introduction

This section describes the methods and the results of analyses for containment pressure transients for a variety of core meltdown event sequences as set forth in the evaluation of the containment event tree in Section 2.

Section 4.1 describes the Meltdown Accident Response Characteristics (MARCH)* and COCOCLASS9** computer models, which have been used to analyze the progression of core melt and the resulting physical conditions. The code used to model the dispersive event identified by the phenomenological evaluation in Section 3 is also presented in this section.

Section 4.2 summarizes results of the assessments of the ultimate strength of the containment to withstand internal pressure loadings. These serve as the criteria against which peak pressures from the containment transients are compared to determine the likelihood of containment overpressure failure. Section 4.2 also defines the sequence classes analyzed. These encompass thousands of postulated accidents that can lead to a damaged core. The principal parameters used in the analysis and some alternative cases investigated for each of the sequence classes are also discussed.

Finally, Section 4.3 discusses the results obtained for the expected accident progression within each class sequence and other less likely accident progressions. A sufficient variety of accident progressions, including phenomenological alternatives, were analyzed to establish containment pressure status for the many nodal points of the containment event trees presented in Section 2. These containment transient results were used as the basis for establishing the probability of containment failure as used at the various branches of the containment event tree (Section 2).

---

* A description of MARCH is provided in Section 4.1.1

** A description of COCOCLASS9 is provided in Section 4.1.2

4.0.2 Transient Analysis Approach

During a postulated damaged core event a variety of constituents are calculated to be released into the containment atmosphere. These could include the following:

(1) Steam/Water
(2) Hydrogen
(3) Carbon Dioxide
(4) Carbon Monoxide
(5) Heat
(6) Core Debris

The magnitude and timing of these releases are dependent on the accident considered. The computational approach used in this study is illustrated in Figure 4.0.2-1. The MARCH computer code was used to analyze the sequence classes by defining the appropriate input based on applicable core melting phenomenology. The appropriate bounds are dependent on the type of accident being investigated, the path within the accident being scrutinized, and the variations in physical phenomena being analyzed. Mass and energy releases from transients calculated by MARCH were used as input to the COCOCLASS9 computer code. COCOCLASS9 was used with the appropriate additional input to determine the containment response. Additional experimental, analytical or parametric results were used to support the results obtained.

Figures 4.0.2-2 through 4.0.2-4 illustrate shapes of various release rates into the containment. The transient can be divided into five basic phases depending on the scenario chosen:

1. Initial blowdown
2. Core overheat
3. Core slump
4. Reactor vessel failure
5. Long-term releases

The release rates will vary for these phases.

The first phase is the initial blowdown. During this phase of the accident, only steam and water are released. Figure 4.0.2-2 illustrates three cases for steam release. For a large break Loss-of-Coolant Accident (LOCA), the steam and water release rates are large in magnitude, but short in duration. The entire inventory of the primary system can be released in 12 to 30 seconds. For a small break LOCA, the release rates are considerably less, but last a good deal longer, approximately one hour. If there is no break, such as in a transient event, there are no releases until the secondary side boils dry. After the secondary side dries out, steam is released as the pressurizer safety valves open and close. For a transient event, the initial blowdown lasts a few hours.

The second phase of the accident is the core overheating period. During this time, the core is still intact and the zirconium-water ($Zr-H_2O$) reaction begins. As Figure 4.0.2-2 illustrates, steam releases are fairly constant. The hydrogen releases during core overheating are dependent on the scenario. For a large break, hydrogen is released as it is formed. Therefore, as Figure 4.0.2-3 shows, hydrogen release rates into the containment are high compared to the small break and transient cases for which much of the hydrogen may be retained in the primary system, since it may be forming faster than it can be vented. During this stage of the accident, some fission products may also be released into the containment. These fission products can provide heat directly to the containment atmosphere.

The third phase of the accident is the core slump. For the large break case, both steam and hydrogen are released at approximately the same time that they are formed (see Figures 4.0.2-2 and 4.0.2-3). Consistent with the preceeding discussion, hydrogen and steam releases for the small break and transient cases are flow-limited, and tend to accumulate in the reactor coolant system. Fission product releases have similar trends.

The next phase is the failure of the reactor vessel. At this time, two major incidents occur. The first event is the interaction of the core debris with water that is present in the lower reactor cavity, or water that could subsequently be dumped onto the debris. This water-debris effect could result in rapid pressurization for the cases that have limited venting from the reactor coolant system (i.e., small break and transient cases). These releases are illustrated in Figure 4.0.2-2 and in the top two curves in Figure 4.0.2-3. The second incident is the release of the steam, hydrogen, and fission products which have accumulated in the reactor coolant system. The magnitude of the steam spike can vary depending upon the model used for the interaction between the water and the debris. At this point in the transient, all of the fission products have been released, and the heat transfer rate of these fission products in the containment atmosphere is constant (see Figure 4.0.2-4).

The final phase of the accident is the "long-term release" period. Two extremes, defined as coolable and noncoolable debris beds, are illustrated in Figures 4.0.2-2 and 4.0.2-3. The coolable debris bed generates steam as long as water is present for interaction with the core debris, while the noncoolable debris bed leads to debris/concrete interaction and carbon monoxide, carbon dioxide, hydrogen, and steam generation.

4.0.3 Conclusions

The analysis indicates that for the vast majority of accident progressions, the containment capability of 141 psia provides a substantial margin against overpressure failure. For the best estimate analyses performed, containment failure is not predicted for any sequence classes during

1. Initial blowdown
2. Core overheat
3. Core slump
4. Reactor vessel failure

In fact, only those few accidents that involve a loss of all active containment safeguards (i.e., fan coolers and sprays) result in a significant probability of an overpressure failure. Failure is not generally predicted even for cases analyzed with overly conservative assumptions that bound the containment pressure and temperature transient.

The best estimate maximum calculated blowdown pressure for the large break with active containment safeguards is 61 psia. The maximum calculated pressure for the best estimate small break is 51 psia at vessel failure. Both these values are well below the containment failure pressure. For the transient accident for which no active safeguards are available, the best estimate calculation predicts containment failure will not occur for at least 12 hours after the initiation of the incident. This calculation assumes no primary or secondary system cooling, or active containment safeguards for the entire period.

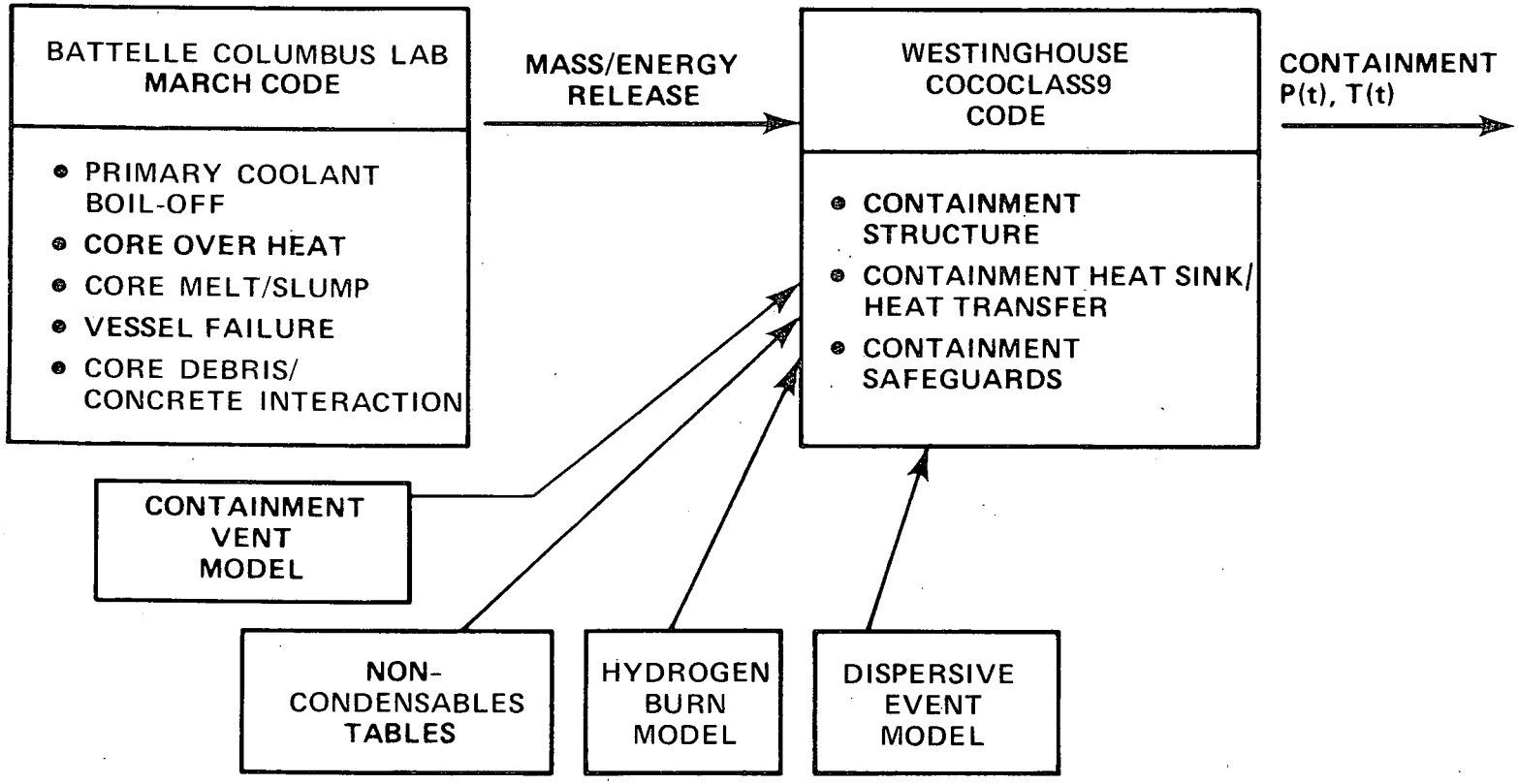
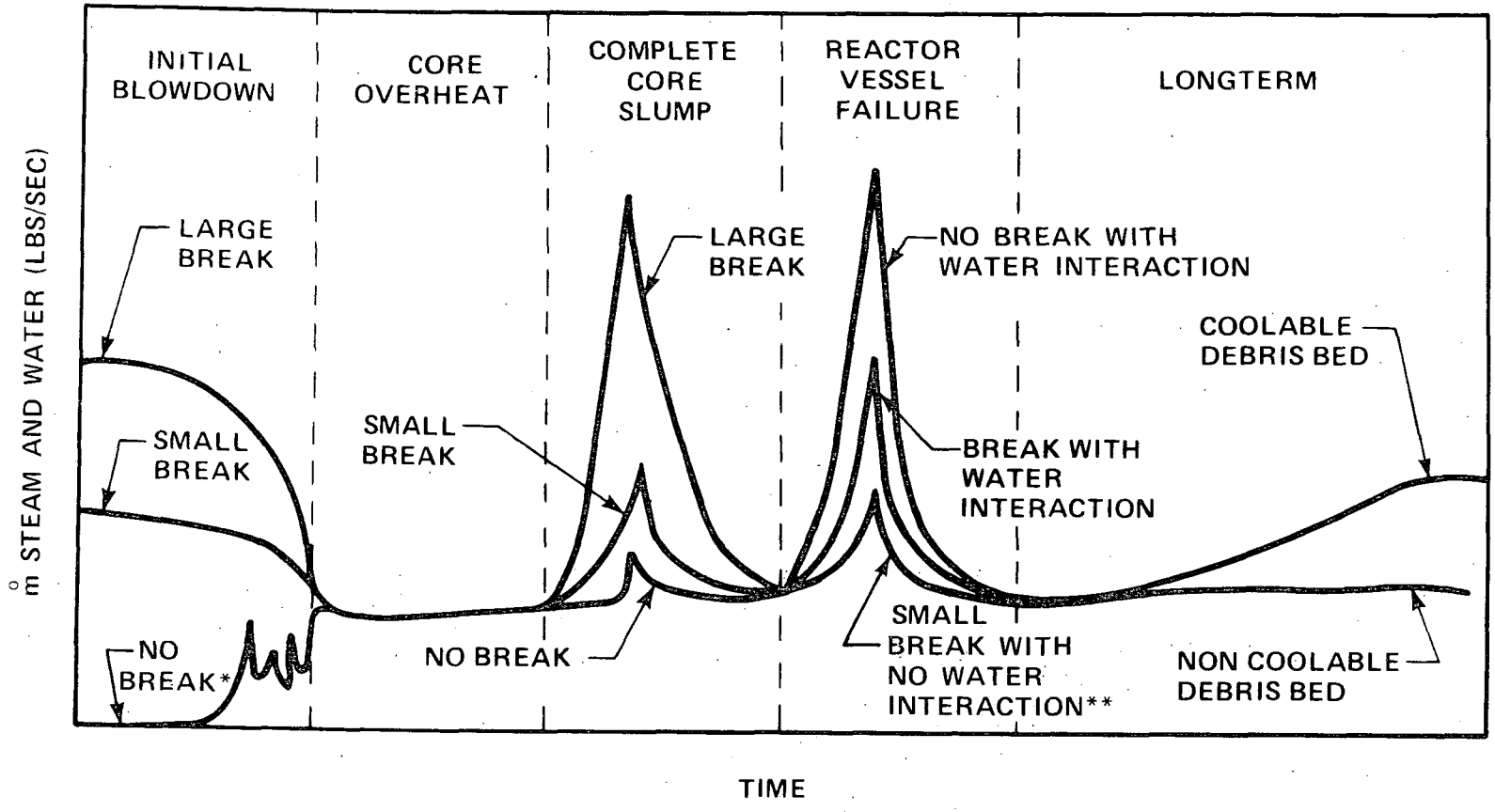


Figure 4.0.2-1. Calculation Approach



*NO BREAK REFERS TO A TRANSIENT EVENT
**FOR A LARGE BREAK WITH NO WATER INTERACTION, THERE IS NO SPIKE

Figure 4.0.2-2. General Shape of the Rates of Steam and Water Releases into the Containment Atmosphere vs. Time

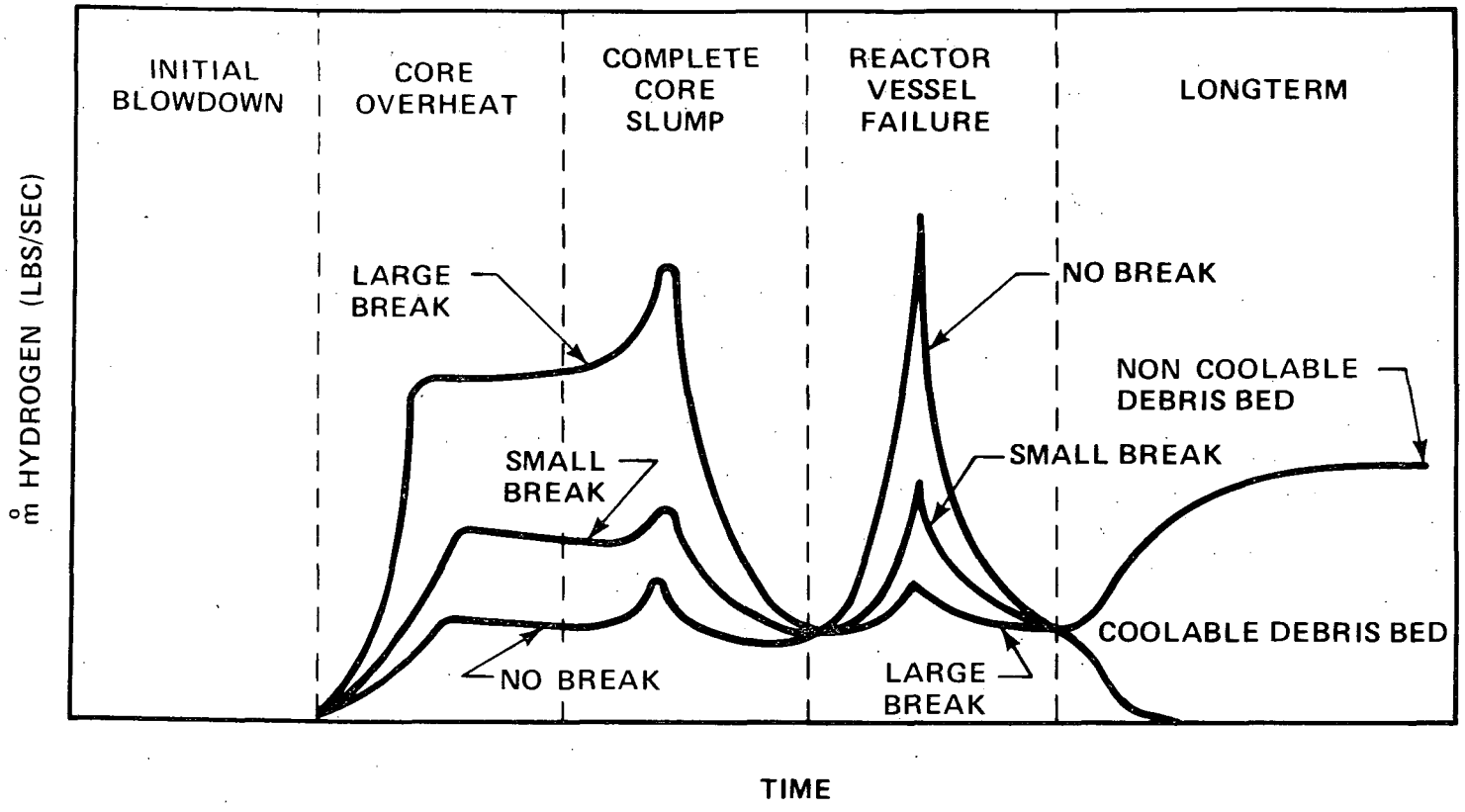


Figure 4.0.2-3. General Shape of the Rates of Hydrogen Release into the Containment Atmosphere vs. Time

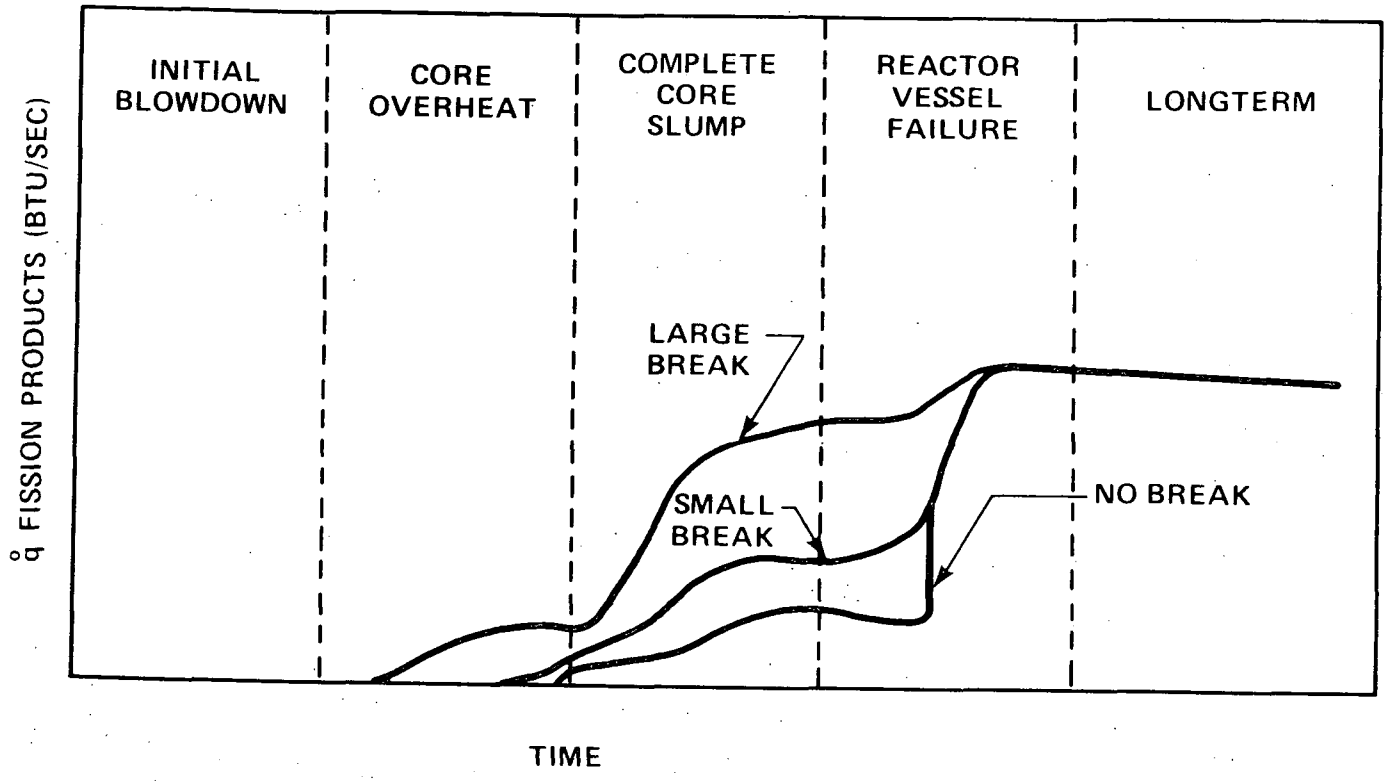


Figure 4.0.2-4. General Shape of the Rates of Heat Release from Fission Products into the Containment Atmosphere vs. Time

4.1 ANALYTICAL TOOLS

This section gives a short description of the computer codes used to perform the transient analysis of the sequence classes. A current version of MARCH was used to perform the transient analysis. This code was used to model the core and primary system behavior and to obtain the steam and water mass and energy releases for (1) the entire transient for the nondispersed cases and (2) until vessel failure for the dispersed cases. These mass and energy releases formed the input for the other computer code used to evaluate the containment response for the nondispersive cases.

The other computer code, COCOCLASS9, is a modified version of the Westinghouse COCO computer code. COCOCLASS9 was used instead of the MARCH containment module (MACE), because a more refined treatment of heat sinks and hydrogen burn phenomena was needed.

To analyze the event where debris is dispersed from the reactor cavity to the containment floor at vessel failure, additional modeling capability was developed since neither MARCH nor COCOCLASS9 model such an event. Therefore, a description of the model is included in Section 4.1.3.

4.1.1 The MARCH Code

The MARCH computer code (Ref. 4.1.1-1) was developed for the NRC by Battelle Columbus Laboratories.

The MARCH code simulates the response of the Light Water Reactor (LWR) primary system and containment to transients and LOCAs. These transients and LOCAs may result in core meltdown if failures of engineered safety features are postulated. The code performs calculations starting from the blowdown phase through core heat-up, coolant boil-off, core meltdown, melting and failure of the reactor vessel bottom head, core debris-water interaction in the reactor cavity, and thermal interaction between the concrete basemat and the debris. In each phase of the accidents, mass and energy additions to the containment with operable or inoperable engineered safety features are calculated to determine the pressure and temperature histories in the containment. Possible Pressurized Water Reactor (PWR) engineered safety features modeled in the code include Emergency Core Cooling System (ECCS), containment sprays, fans coolers, ice condensers, and ECCS and containment spray recirculation heat exchangers. The code also contains physical models that calculate the release of the volatile fission products from the melted fuel and their transport to the containment or to the atmosphere.

The five phases of core meltdown accident sequences are analyzed by five subroutines: INITIAL, BOIL, HEAD, HOTDROP and INTER. The INITIAL subroutine is only used in the large break accident sequence. In other accident sequences, the blowdown is calculated by subroutine PRIMP which is called from BOIL. These subroutines are run in sequence and can be independently coupled to a code that calculates the containment response to each stage of a core meltdown accident sequence. Figure 4.1.1-1 is a flow chart of the subroutines.

The main program MARCH calls various subroutines to perform appropriate calculations during an accident sequence and regulates program flow. PRIMP and its associated subroutines evaluate the primary system thermal-hydraulics for small LOCAs and transient accidents. They also compute the amounts of water and steam leaked into the containment through a small break and/or safety-relief valve. BOIL and its associated subroutines perform calculations of heat generation and heat transfer in the core, boil-off of water from the reactor vessel, melting and slumping of the core materials into the reactor vessel bottom head, Zr-H_2O reaction in the core and in the bottom head, and the primary system thermal-hydraulics. HEAD and its associated subroutines perform heat transfer calculations for thermal interaction between the vessel bottom head and the melted core debris and determine the bottom head failure time. HOTDROP and its associated subroutines simulate the interaction of core debris with water in the reactor cavity following the melt-through of the bottom head, including debris fragmentation, heat transfer, and metal-water reactions. INTER and its associated subroutines simulate the penetration of the core melt into the containment concrete basemat. INTER was originally developed at Sandia National Laboratories as a separate computer program (Ref. 4.1.1-2), and has been incorporated into the MARCH code as a subroutine.

The MARCH code was intended for reactor risk studies and focused on accident sequences involving gross core melting. Because of the increasing importance of damaged core phenomenology, MARCH has been applied to core conditions close to complete core melting, and to the evaluation of core meltdown accident-mitigating features. The MARCH code models a wide variety of physical processes including metal-water reactions, core debris-water interaction, and core debris-concrete interaction. In view of some of the uncertainties and complexities associated with the meltdown accident phenomenology, the modeling of the meltdown phenomena was simplified in order to develop a fast-running, integral meltdown code.

The MARPLT plotting subroutine in the code was modified for this study to be compatible with the Westinghouse system plotting package. Output from MARCH is used as input, after preprocessing by MARCO, to the COCOCLASS9 code (Section 4.1.2). With the recent inclusion of the hydrogen burn and core debris dispersive models, MARCH is used for containment transient analysis in this study.

In a study of this type, MARCH has a number of limitations. It will not predict the exact course a particular type of core meltdown will take. This is, in part, because (1) the models used in MARCH are simplified to increase computational speed, (2) MARCH does not model certain physical phenomena, and (3) the exact characteristics of an LWR core melt are not known. Instead, MARCH is used in conjunction with a variety of other analyses that either support or replace MARCH calculations that are important to the work being performed.

4.1.2 COCOCLASS9 Code

The COCO computer code that is used to calculate containment conditions for a number of accidents is a sophisticated mathematical model of a generalized reactor containment. The accuracy and flexibility of the program permits evaluation of containment designs for a broad spectrum of containment pressure transient calculations including analyses of containment integrity for main steamline and reactor primary coolant system ruptures, and emergency core cooling system minimum containment backpressure.

COCO is based on the time-dependent conservation equations of mass and energy, data from steam tables, equations of state for the noncondensables, and other auxiliary relationships. The containment's steam/gas/water atmospheric mixture and the sump water are modeled by a single volume having average properties, and transient conditions are determined for both. An energy equation is applied to the containment structures to obtain transient temperature gradients and heat storage and conduction through the structure. Heat removal by internal and external sprays, containment vents, fan coolers, and sump recirculation can be considered. Mass and energy additions are generally treated as boundary conditions. For a description of the COCO version that was used to perform standard plant safety analyses see References 4.1.2-2 to 4.1.2-7.

To perform containment response calculations to damaged core accidents, the following modifications were made to the basic COCO code:

1. Separate mass conservation equations were written for nitrogen, hydrogen, oxygen, a carbon monoxide/carbon dioxide mixture, steam, and water.

2. The system energy equations were rewritten to include all of the new constituents.

3. Equations of state for all the constituents were added. (Ideal gas laws are used for the noncondensables and the ASME steam tables are used for steam and water.)

4. The structural heat transfer model was modified to include the effects of condensation, convection, and radiation. Appendix 4.4.2 gives the techniques used to model these phenomena.

One point worth noting is the manner in which steam condensation is treated.

The COCOCLASS9 computer code sets the condensation heat transfer rate equal to an equivalent steam condensation rate from the containment atmosphere, or

$$m_{condensation} = q_{condensation}/h_{fg}$$

where

$m_{condensation}$ = the rate of steam condensation (lb/sec)

$q_{condensation}$ = the heat rate due to condensation (BTU/sec)

h_{fg} = the latent heat of vaporization (BTU/lb)

The convection and radiation heat rates are simply treated as heat rates in the energy equation.

5. A model was developed to determine the potential for nonbenign combustion in the containment atmosphere. (A nonbenign combustion is one that results in a significant pressure rise.)

   Figures 4.1.2-1 through 4.1.2-3 illustrate hydrogen burn characteristics in dry air, and can be used to illustrate the difference between benign and nonbenign burns. As Figure 4.1.2-1 shows, at approximately a 4 percent mole fraction, a burn can propagate upward. At approximately a 6 percent mole fraction, it can propagate sideways, and at approximately 8.5 percent mole fraction, it can proceed in all three directions. At 8.5 percent, a significant fraction of the hydrogen will burn and a significant pressure rise may occur. This is illustrated in Figures 4.1.2-2 and 4.1.2-3 which plot data from Ref. 4.1.2-8.

   The physical reason for this flammability limit is the exponential dependence of the reaction rate in the combustion wave on temperature. Therefore, the temperature of the flame is the criterion for the flammable limit. When the Flame Temperature Criterion is established, the calculated flame temperature for a mixture can be compared to it to determine the flammability of the mixture.

   The Flame Temperature Criterion for hydrogen/air or hydrogen/carbon monoxide/air mixtures has been determined to be 710°C (Ref. 4.1.2-9). Appendix 4.4.3 presents the method for calculating the flame temperature.

6. The capability of calculating various types of hydrogen burns was added to the COCO computer code. These include a continuous hydrogen burn, a continuous burn after a specified time, a burn from a given concentration down to another given concentration, a complete burn at a given time, and a complete burn if the flame temperature exceeds the Flame Temperature Criterion.

The following method is used to calculate mass and energy additions into the containment atmosphere during a burn.

Let Δt_B = the time over which the hydrogen is burned*

Then if a complete burn is assumed:

$$H_{BURN} = M_{HYD}/\Delta t_B$$

$$CO_{BURN} = M_{CO}/\Delta t_B$$

$$OX_{BURN} = 8.0\ H_{BURN} + 0.57\ CO_{BURN}$$

$$Q_{BURN} = \Delta H_{RX,\ H_2}\ H_{BURN} + \Delta H_{RX,CO}\ CO_{BURN}$$

$$STM_{FORM} = 9.0\ H_{BURN}$$

$$CO2_{FORM} = 1.57\ CO_{BURN}$$

where

M_{HYD} = Mass of hydrogen in containment, (lb)

M_{CO} = Mass of carbon monoxide in containment, (lb)

H_{BURN} = Hydrogen burn rate, (lb/sec)

CO_{BURN} = Carbon monoxide burn rate, (lb/sec)

OX_{BURN} = Oxygen burn rate, (lb/sec)

$\Delta H_{RX,\ H_2}$ = Heat released per pound of hydrogen burned, (BTU/lb_{H_2})

$\Delta H_{RX,\ CO}$ = Heat released per pound of carbon monoxide burned, (BTU/lb_{CO})

STM_{FORM} = Steam formed from hydrogen combustion, (lb/sec)

$CO2_{FORM}$ = Carbon dioxide formed from carbon monoxide combustion (lb/sec)

In an early version of COCOCLASS9, the heat of reaction for the hydrogen burn ($\Delta H_{RX,\ H_2}$) was taken to be 62,050 BTU/lb-H_2 BURNED. This heat of reaction includes the energy associated with the steam formation. Since the enthalpy change in the steam formed by the combustion process was also being tracked, a double accounting was occurring: an overprediction of the heat associated with the hydrogen burn, and an overprediction of the calculated containment

* This was generally taken to be 20 sec for a containment burn. It should also be noted that this method is not applicable for a continuous burn.

pressure. The heat of reaction for the hydrogen burn, which does not include the energy associated with the steam, is 52,060 BTU/lb-H_2 BURNED. Therefore, the pressure rise because of the burn would have to be reduced to 84 percent for such a calculation:

$$\frac{52,060}{62,050} (100) = 84 \text{ percent}$$

The version of the code that contains the overprediction was used to perform some calculations whose results are presented in this section. For these cases, the pressure rise due to a hydrogen burn was reduced to 85 percent before inclusion in the event trees. This corrected for the overprediction.

7. An interface code, MARCO, was developed to take mass and energy release rates from the MARCH calculation for use as boundary conditions to the containment analysis. This code took the results of the mass and energy release calculations and put them into a format that could be used directly by COCOCLASS9. Care was taken to keep the integrals of mass and energy consistent with MARCH and COCOCLASS9.

8. The COCOCLASS9 code was given the capability to estimate the adiabatic pressure resulting from a complete burn of a hydrogen/carbon monoxide/air/steam mixture. This technique uses the first law of thermodynamics and is simply a constant volume heat up calculation.

9. The COCOCLASS9 code was also given the capability to include all of the constituents (including the airborne fission products) in a containment vent flow calculation.

This new version of COCO has the capabilities needed to analyze the accidents addressed in this report.

4.1.3 Analysis Model for the Dispersive Event

For the sequence classes in which the reactor coolant system remains at a significant pressure until the reactor vessel fails, the large volume of pressurized steam and hydrogen present in the reactor coolant system at vessel failure is expected to forcibly eject the core melt debris from the vessel into the lower reactor cavity and subsequently into the containment. This is called the Time Phased Dispersive Model and is discussed in Section 3.1.7. The modeling techniques are described in this section.

Time Phased Dispersive Model

The principal characteristics of the Time Phase Dispersive Model are described in 3.1.7 and sections of 3.2. The modeling is identical to the gravity-type discharge modeling, as described by the MARCH computer

code, until just before core slump. Until this time, boundary conditions for the containment (steam, water, hydrogen, and heat release rates) are taken directly from MARCH. The initial blowdown and core overheat portions of the accident are unchanged. At the time of core slump, use of the MARCH code is discontinued. Conditions resulting from the primary system discharge and dispersion of the core debris are provided by calculations outside of MARCH. As discussed in Section 3, the phenomena modeled are

1. Loss of reactor vessel integrity due to failure of the instrumentation tubes;

2. Molten fuel discharge and scatter over the lower reactor cavity floor;

3. Initiation of vessel gas discharge and coincident dispersal of fuel from the lower reactor cavity;

4. Vaporization of containment water and continuation of gas/vapor discharge;

5. The emptying of the reactor vessel and the end of gas/vapor discharge;

6. Long-term mass and energy release into the containment.

Based on the material presented in Section 3.1, calculations indicate that the molten fuel is discharged from the vessel into the lower reactor cavity within a few seconds following vessel failure and hydrogen gas and steam begin to discharge from the failed vessel. This high velocity jet rapidly disperses the molten fuel from the lower reactor cavity. Now, two events are happening concurrently: (1) the vessel is discharging a steam/hydrogen mixture and (2) the molten core debris is boiling water on the containment floor.

The steam and hydrogen blowdown from the reactor vessel can be described by following the methods outlined in Section 3 and is calculated as follows:

Assuming ideal gas behavior for both the hydrogen and the steam, and an isothermal blowdown, the total mass flow rate out of the vessel is approximated by an isothermal process defined by

$$\dot{m} = 0.6(P_{new})A_b\ (1/RT)^{1/2}$$

where A_b is the area of the breach in the vessel,
T is the absolute gas temperature,
R is the gas constant,
and P_{new} is the decaying pressure of the vessel defined by

$$P_{new} = P_o \exp\left[\frac{-0.6\ A_b\ (RT)^{1/2} t}{V}\right]$$

where V is the vessel volume,
P_o is the original vessel pressure,
and t is the elapsed time since blowdown started.

The mass flow rate of each gas is the total rate times the mass fraction of that specific gas. The "less-than-ideal" gas behavior of the gas/vapor mixture is accounted for by adjusting the mass flows to preserve a mass balance.

The boiling of the water from the containment floor is modeled using a saturated critical heat flux (CHF) equation. A constant steam boil-off rate from the molten core debris/water interaction conditions is assumed for the duration of core cooling. Boil-off time is determined by dividing the heat contained within the dispersed fuel by the heat loss rate as determined by the CHF correlation. The CHF correlation used is

$$q/A = 0.14\ (\rho_g)^{1/2}\ (g\ \sigma\ (\rho_f - \rho_g))^{1/4} h_{fg}$$

where q/A is the CHF,
ρ_g is the density of saturated vapor,
ρ_f is the density of saturated liquid,
σ is the liquid/vapor surface tension,
h_{fg} is the latent heat of vaporization,
and g is the gravitational acceleration.

The above equation, when multiplied by the containment floor area, provides the heat loss rate of the dispersed fuel. The amount of steam produced during boil-off is defined as

$$m_{steam} = q_{core} / h_{fg}^*$$

where q_{core} is the heat contained within the dispersed fuel,
and h_{fg}^* is the latent heat of vaporization between the liquid at containment pressure before vessel failure and the vapor at the expected average containment pressure during steaming.

In addition, once the vessel pressure falls below the accumulator pressure (~600 psia), the water in the accumulators discharges by the equation:

$$\dot{m} = \left[\frac{2\ \rho_f \left(A_a\right)^2}{(fL/D)} \ (P_a - P_v) \right]^{1/2}$$

where ρ_f is the water density,
A_a is the flow area from the accumulators,
(fL/D) is the friction loss term,
P_a is the accumulator pressure,
and P_v is the vessel pressure.

The total steam and hydrogen addition rates into the containment atmosphere is the sum of the flow rates due to blowdown and boil-off. Accumulator discharge is routed to the floor as water and is not entrained. The total heat energy addition to the containment is the sum of each flow rate multiplied by the enthalpy at its physical state.

4.1.4 Phenomenological Model Modifications

There are several areas in the core meltdown progression in which the phenomena expected are different from those modeled in the MARCH code. These areas are the degree of coherency and the rates at which core melt debris is released to the lower plenum of the reactor vessel, the mode of reactor vessel failure, in-vessel and ex-vessel steam spikes, the potential for dispersing core debris when the reactor vessel fails, the hydrogen burn treatment, and the coolability of the debris bed in the reactor cavity. These phenomena are discussed in detail in Section 3. Tney are reviewed in the following paragraphs which identify the alternatives analyzed, discuss the probable phenomena, and outline the approaches used in the containment analysis.

The above differences, where possible, have been accommodated by working within the constraints of MARCH inputs and options, by providing other models to replace portions of MARCH, or by performing separate studies as needed.

Coherency of Core Meltdown

Based on NSAC-TMI-2 Code analyses described in Section 3.1.2, at vessel failure less than 50 percent of the core would be involved in short-term molten material flow into the bottom of the reactor vessel or into the reactor cavity. This is because of the radial temperature gradients in the core that result from power distribution and substantial radiation heat sinks afforded by structures around the core. MARCH does not model these. Instead, all of the core immediately and instantaneously drops into the lower plenum once the core plate is assumed to overheat whereas some portion of the presumed blockage is expected to melt first, providing a drain path through which only the molten portion of the core debris would drain at a finite but rapid rate. Here the MARCH treatment was used "as-is" except that in the dispersive vessel failure evaluation, the amount of core debris assumed to be ejected from the reactor cavity was limited to 50 percent in the expected case and 75 to 80 percent in the bounding case. Also, as will be discussed later, the in-vessel pressure spike calculated in MARCH when the core plate collapses was not modified for determining containment steam additions, but is not considered realistic in evaluation of Reactor Coolant System (RCS) boundary integrity. A more appropriate methodology is presented in Appendix 4.4.4.

Mode of Reactor Vessel Failure

An examination of the lower reactor vessel structure indicates that the partial penetration welds at the vessel's inner surface are logical candidates for failure in the event of overheating. This is substantiated by the analyses presented in Appendix 3.4.6 and Section 3.1. The first shows that under a substantial heat flux applied to the lower reactor vessel head, the inside penetration welds would overheat, lose strength and fail before vessel wall failure. In addition, an even more severe thermal loading occurs when a flow path develops in the blockage at the core plate. Because of the pouring of the molten core onto the penetrations, the heating of the welds is quickened due to the forced convection and conduction heat transfer between the molten core and the penetrations. The vessel failure would occur shortly thereafter, and the failure mode would thus be failure of the penetration(s) and subsequent expulsion of molten material through the hole that is formed. This flow of molten debris causes ablation of the adjacent vessel wall, widens the hole, and results in expulsion of the core debris over a period of five to 30 seconds (Section 3.1.7.2). MARCH does not model these phenomena mechanistically, but estimates the time it takes for the vessel boundary to fail and then assumes the debris and vessel head to be instantly deposited in the reactor cavity. Since the time for vessel failure as calculated by MARCH is also short (i.e., less than 1 to 10 minutes after core slump depending on RCS pressure), the results were not modified. However, in the analysis of the dispersive event, consideration of the expected hole size and the debris and gaseous discharge flow rates were used to determine the velocities and the time interval for the dispersal (Section 3.1.7.2).

In-Vessel and Ex-Vessel Steam Spikes

The MARCH code calculates large steam spikes when the core plate fails. They can also occur when the reactor vessel fails discharging molten core debris into the water in the bottom of the reactor vessel or in the reactor cavity. The large in-vessel steam spike calculated by MARCH results from evaporating the water in the vessel over an unrealistically short time period and from the assumed increase in the steam gas constant* when the last drop of water evaporates. Evaluations in Section 3.1.6 and Appendix 4.4.4 show that with physical limits on the rate of steam generation, the installed safety valve capacity limits overpressure to the valve actuation pressure. In addition, Appendix 4.4.5 shows that steam generator tubes can withstand much higher differential pressures (4500 psi) even if severe degradation is assumed. Hence, the core meltdown progression will not jeopardize primary-to-secondary system barrier integrity.

For the ex-vessel steam spike, the MARCH model assumes radiation and convective heat transfer from a hot particle to a surrounding medium of saturated water, but ignores hydrodynamic limitations associated with the cavity dimensions. Therefore, if a small particle diameter is

*The code assumes that steam is a perfect gas and uses an ideal gas law as the equation of state. The gas constant is updated during the transient, basing it on the temperature of the reactor coolant from the previous time step. Refer to Appendix 4.4.4 for a more detailed description.

input, the debris is quenched at a higher rate than is physically possible. Based on a heat removal rate corresponding to CHF as applied to the reactor cavity cross-sectional area, the steam rates should be adequately handled by containment safeguards and heat sinks without resulting in any pressure spike. A second physical limitation is that the rate of steam generation must be less than that which would carry off the particles by the resulting drag forces. Analysis in Appendix 4.4.6 shows that with this consideration and the MARCH heat transfer model, particles less than approximately 2 inches in diameter would be carried off by the steam flow. Therefore, for the analyses in which the debris was retained in the cavity, a 2-inch diameter particle was used as input to MARCH to produce steam generation that is still phenomenologically conservative. This results in a moderate steam spike. Sensitivity analyses have also been performed using a 3 mm diameter particle. This results in a substantial steam spike when the debris is quenched over a time interval of a few seconds. However, these results would not be realistic for a case in which the debris is confined to the reactor cavity cross-sectional area.

Dispersive Core Ejection

For sequences in which the primary system pressure is still substantial when the instrument penetrations fail, the evaluation (Section 3.1.7.2) of the dynamics associated with the steam discharge that follows core debris expulsion from the vessel has indicated that the core debris would be dispersed from the cavity. For these cases, the MARCH description of the core melt progression was bypassed at the beginning of core slump, and the dispersive model described in Section 4.1.3 was used to create input for the containment analysis model. The model developed for this study is based on time phasing of events as discussed in Section 3.2. It was assumed that either 50 or 75 percent of the molten core debris would be ejected from the vessel and discharged onto the containment floor where its heat would be lost to the water by quenching with subsequent steam generation. For these analyses, the debris was assumed to be ejected as a large mass over approximately 15 seconds.

In support of the time phase dispersive calculations, scoping analyses were performed to determine the sensitivity of containment response to parameters in the dispersive event. A limiting upper bound on containment pressure was calculated because of the parameters used and the assumuptions made. Following is a list of the assumptions:

1. The debris dispersed was entrained in the vessel blowdown of the primary system. This resulted in direct heating of the containment atmosphere and a heat transfer mechanism that, per unit of heat addition, causes a more rapid pressurization of the containment atmosphere than energy addition by the production of steam.

2. The debris has a very large heat transfer area by assuming it is divided into thousands of small particles.

3. All of the zirconium and stainless steel was at elevated temperatures so that significant oxidation occurred resulting in an additional mass of hydrogen in the containment.

4. A very rapid steaming rate was produced by assuming all of the debris dispersed was immediately quenched when it contacted the containment floor water.

5. To ensure an extremely conservative calculation of the containment pressure rise, the undispersed debris remaining in the reactor was immediately dropped and quenched in the cavity within the first few seconds after vessel failure.

Studies within the scoping analyses were performed, where, regardless of the flame temperature calculated, all of the hydrogen in containment was assumed to burn. This method compounds the pressure rise in containment by superimposing a hydrogen burn spike, a steam spike, and a heat addition spike.

These calculations, termed "entrained dispersive" in Table 4.3.1-1 through Table 4.3.6-1, resulted in very conservative upper bound pressures for the dispersive event and were used solely as an aid in determining the confidence in the containment failure probability. As can be seen in Tables 4.3.6-1 through 4.3.6-6, and as will be discussed in the following sections, the containment limit is rarely exceeded even with the compounding effects listed previously.

Hydrogen Burn Treatment

A continuous hydrogen burn is possible in some break cases in which a hydrogen/steam jet would entrain the appropriate amount of air if either an ignition source was present at the break, or if the gas was sufficiently hot. However, this favorable case was generally not considered because there is substantial uncertainty that the required conditions exist.

Instead of assuming continuous localized burning at low (4 percent) hydrogen concentrations, a general approach was followed. Hydrogen was allowed to accumulate until it reached a level at which a propagating burn would be expected if an ignition source such as a spark were present. A Flame Temperature Criterion described in Appendix 4.4.3 was used to determine the conditions and time interval over which such a burn is possible in the transient. The most probable time for burn, if an appropriate ignition source were present, would be the time at which the criterion was first satisfied. Because of the inability to guarantee a continuous spark ignition, the time when such a burn would yield the highest pressure was determined, and the burn was assumed to occur at that point. This treatment clearly covers the worst possible situation and is likely to be conservative for those cases in which a continuous ignition source is present.

The one exception to this approach is that in scoping the containment response to the dispersive event, the multitude of very hot particles entering the containment were sometimes considered as possible localized burn sources. For such cases, a global burn was forced although the

criterion for a propagating burn was not satisfied. This conservative assumption was used even in those cases in which the hydrogen concentration was below the 4 percent lower flammability limit normally considered necessary for hydrogen/air mixture combinations at room temperature.

Debris Coolability in the Reactor Cavity

The MARCH code treats core debris in the reactor cavity as a molten slab with simultaneous heat transfer to the concrete below and, if present, to the overlying water. The analysis and data presented in Appendix 3.4.5 indicate that with water in the reactor cavity, a coolable debris bed should be formed so that no significant concrete/debris interaction results. This is based on the evidence that a permeable particle bed would form and the dimensions and power density of the bed would not lead to bed dryout unless unreasonable and extremely small (submillimeter) diameter particles were formed. Therefore, in the base analysis for nondispersive gravity drop type core melts, the INTER concrete penetration mode of MARCH was bypassed when water was present in the cavity and heat removal mechanisms were available. The improbable situation of having no coolable debris bed even when water is present was analyzed. For these cases, the INTER routine of MARCH was used. In these cases, substantial concrete debris interaction is predicted, (i.e., penetration of several feet occurs before the debris freezes and a large quantity of H_2, CO, and CO_2 is added to the containment).

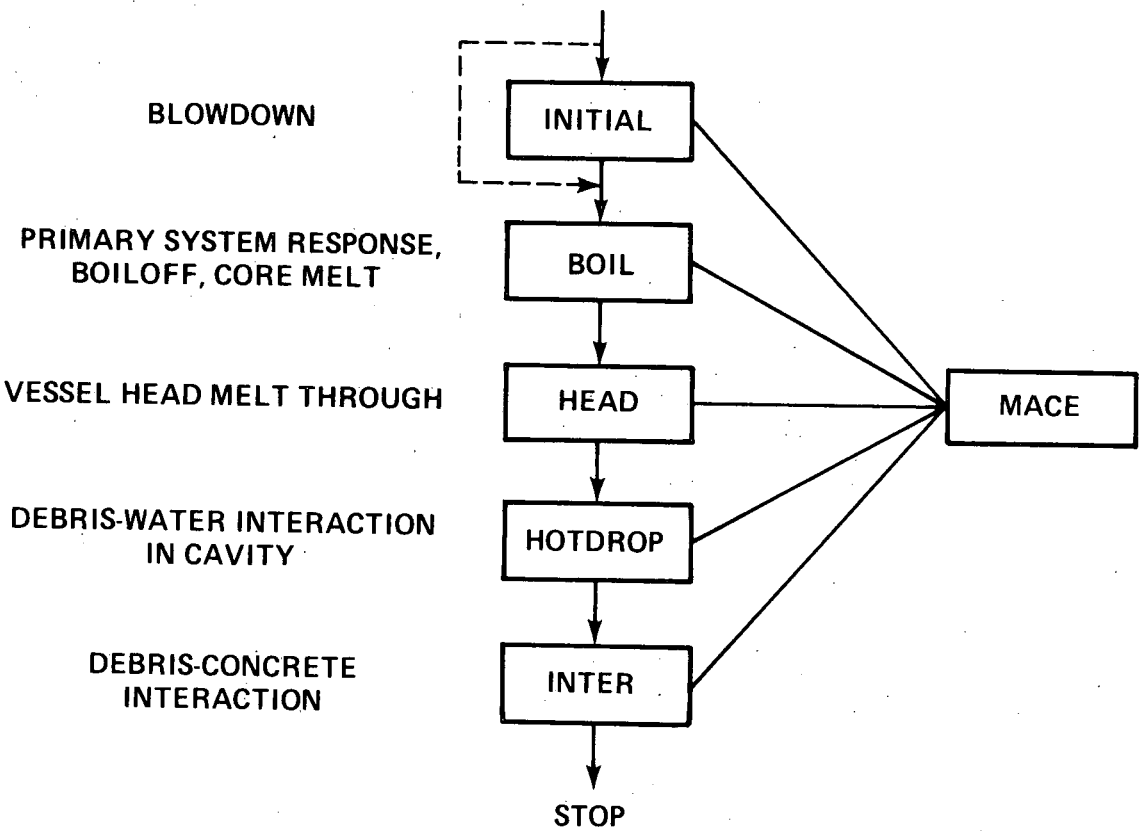


Figure 4.1.1-1. MARCH Code Treatment of a Postulated Reactor Accident

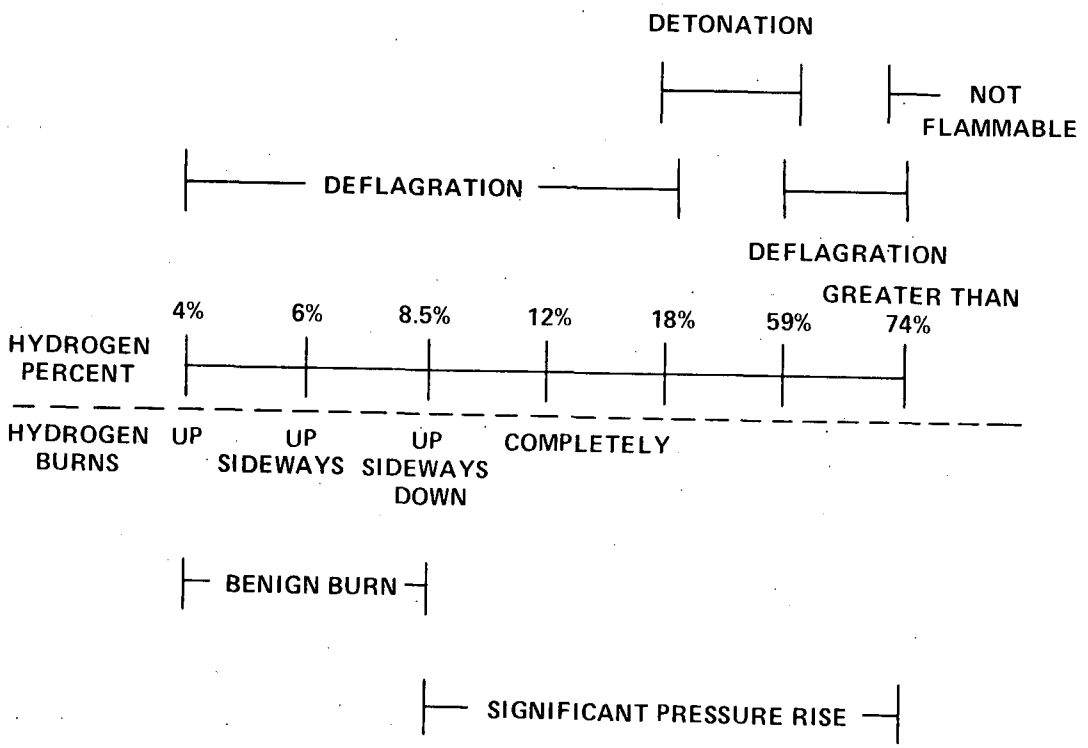


Figure 4.1.2-1. Hydrogen Burn Characteristics in Dry Air

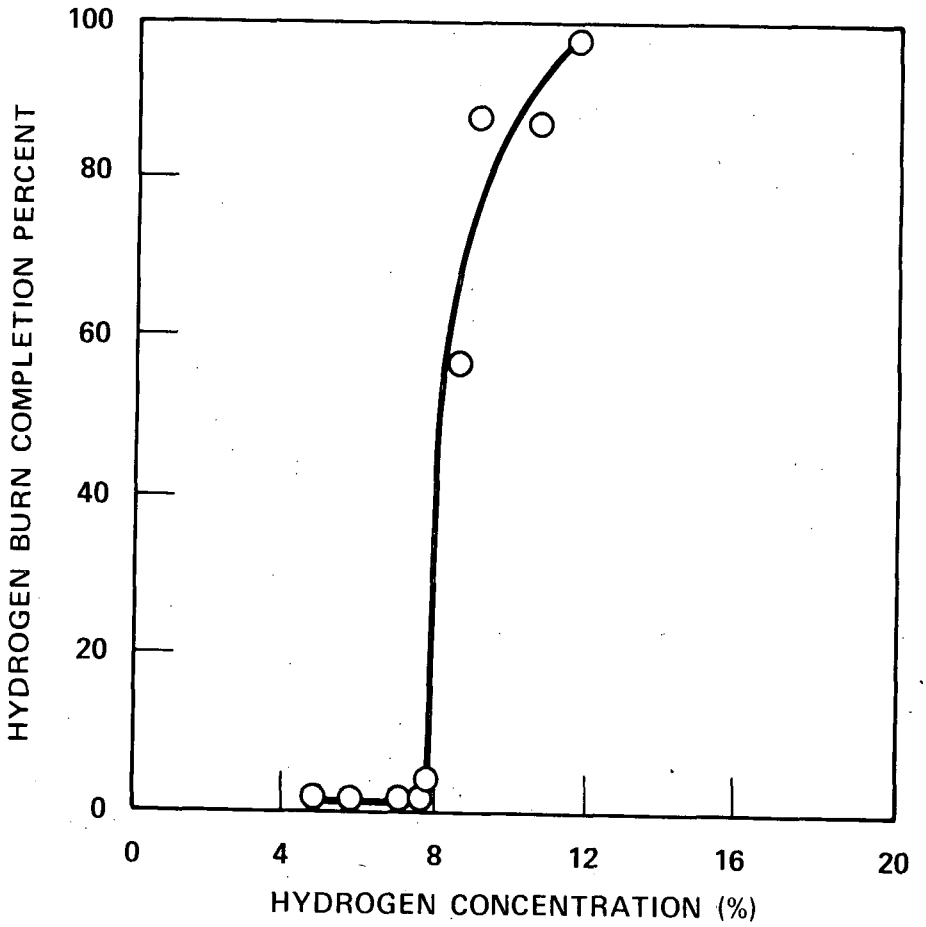


Figure 4.1.2-2. Percent Hydrogen Burn versus Hydrogen Concentration

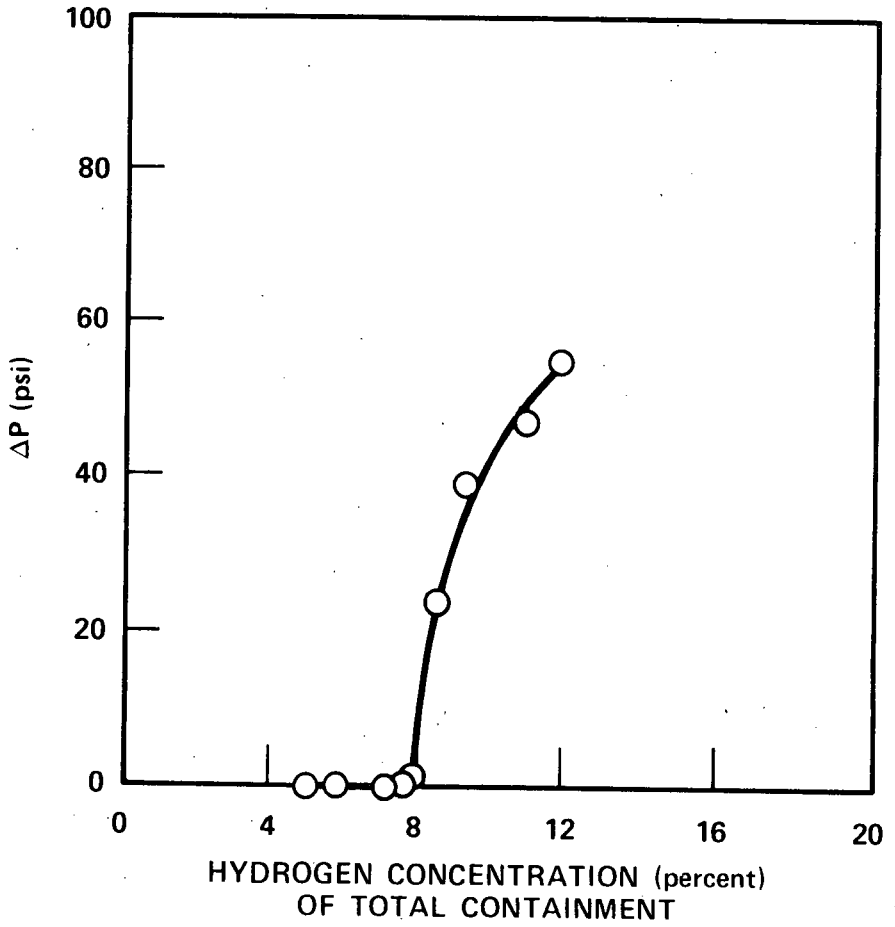


Figure 4.1.2-3. Hydrogen Burn Pressure Rise versus Hydrogen Concentration

4.2 ANALYTICAL INPUT

Section 4.1 described the models and analytical tools used in evaluating the transient behavior of the containment during postulated core damaging accidents. This section describes the containment capability and the sequence classes which were considered in these evaluations. Six typical sequence classes were analyzed (Section 2.3). These are described in the following sections, and are selected to encompass the many accident progressions possible (see Table 4.2.1-1). The results of the analysis were used to assign the probabilities for the many paths of the containment event tree.

4.2.1 Containment Capability

An essential element of risk evaluation for degraded core events is a realistic lower bound ultimate containment building capability for withstanding internal pressure load. This capability has been determined to be 141 psia for the Indian Point containment building based on a failure criterion defined as the state of having reached general yield in the reinforced walls. At pressures higher than 141 psia, the strains start to significantly increase and radial deflections of the containment wall may become unacceptably large. Thus, the nominal estimate for lower bound containment ultimate capacity has been taken as 141 psia consistent with attainment of general yield in the reinforced wall.

A complete description of the analysis models, material properties, failure modes and criteria, and analysis results is contained in the United Engineers and Constructors report included as Appendix 4.4.1.

4.2.2 Class I Sequence

The Class I sequence is typical of a postulated large break LOCA without safety injection, but with properly functioning minimum containment safeguards. The initial conditions for this event are a reactor system at 100 percent power with an average vessel temperature of 580°F. Following a large break, the reactor shuts down. A rapid blowdown occurs during the first few seconds of the transient and adds enough mass and energy to the containment atmosphere to actuate both the containment sprays and the fan coolers. The fan coolers remove heat, and in addition, one of two spray pumps is assumed to operate. This heat removal capability of the active containment safeguards and the passive wall heat sinks are the basis for heat removal from the containment atmosphere as calculated by COCOCLASS9. In this sequence, active containment safeguards continue to function during the remainder of the transient.

Following the initial blowdown, the reactor vessel is filled up to the vessel nozzles with water. Since ECCS has been assumed to fail and the accumulators have previously emptied, the core uncovers as the water in the reactor vessel boils off. After a significant portion of the core has uncovered, substantial core degradation will take place. In a short time, a portion of the core will begin to migrate downward as a molten

mass. When a significant fraction of the core has melted, it will migrate into the lower plenum causing failure of the reactor vessel instrumentation tubes and loss of reactor vessel integrity. Since active containment safeguards are operational, the containment pressure will have decayed significantly following the initial blowdown peak and will be at a relatively low pressure at this time. As the molten core is poured into the lower reactor cavity, significant steam will be generated and a subsequent spike in containment pressure will occur. Once the debris settles in the reactor cavity, it will be coolable because of a continued supply of water resulting from the operation of containment heat removal systems.

To correctly model an event, many phenomena must be characterized correctly. For a Class I event, the following major phenomena and their probable characterization must be considered in order to calculate the containment response. A description of the most probable characterization of the phenomena follows:

1. The coherency or noncoherency of the melt.

   This refers to the amount of molten core available to interact during vessel failure. As discussed in Section 3.1.2, analyses with the NSAC-TMI-2 computer code indicate that less than 50 percent of the core would be molten at the time major material migration into the lower plenum would be expected. Vessel failure would result shortly after the initiation of the core melt migration. Thus an assumption of 50 percent of the molten core debris being released from the vessel would be realistic. However, a coherent core melt and a drop of 100 percent of the core for all Class I events is conservatively assumed.

2. The amount of $Zr-H_2O$ reaction and the resultant hydrogen formation.

   For Class I events, 20 percent of the unreacted zirconium just before core slump (the time the core falls into the lower plenum of the reactor vessel) was considered to react. The resulting hydrogen was assumed available for release to the containment along with the hydrogen already predicted to be in the primary system. The basis for this 20 percent assumption is the $Zr-H_2O$ reaction data described in Section 3.1.3.3*. When this 20 percent assumption is made for the Class I sequence, the amount of hydrogen formed in the transient will be termed "Experimentally Based".

---

* The reaction of 20 percent of the unreacted zirconium is based on low pressure test data simulating the drop of molten zirconium into water. This percentage is a conservative assessment considering the competitive process of quenching and chemical reaction in conjunction with the lack of a mechanism for producing fine particles (Section 3.1.3.2). This conservatism was retained to encompass variations in the actual accident progressions.

3. The mode of molten core release from the failed reactor vessel.

Two modes of release have been identified, the Dispersive and the Gravity Drop. Since the Dispersive mode can only occur when the reactor system is at a significant pressure, and this is not the case for a Class I Sequence, only the Gravity Drop case was modeled.

4. The interaction between water and molten debris in the lower reactor cavity following vessel failure.

Analyses discussed in Section 3.1.1.3 indicate that the rate of steam generation would be limited by the CHF and/or the hydrodynamic limitations. This limiting rate was the criterion used to evaluate the best estimate Class I event.*

5. The long-term coolability of the debris bed is another important parameter in the calculation.

The discussion in Appendix 3.4.5 indicates that the ex-vessel debris bed would be coolable provided that sufficient water is supplied. The amount of water in the reactor cavity represents the spillage from the containment floor over the curb surrounding the reactor cavity. Data defining these containment parameters are used as input into the MARCH computer code. Calculations indicate that there is sufficient water to cool the core debris at vessel failure. A continued supply of water is ensured from the operation of containment heat removal systems. Thus, a coolable debris bed represents the probable phenomena for a Class I transient.

6. The assumed behavior of the hydrogen in the containment (i.e., whether it would ignite).

The Flame Temperature Criterion discussed in Section 4.1.2 provides a methodology to evaluate the flammability of the containment atmosphere. Since it is not known beforehand whether the containment atmosphere is flammable, a calculation is performed initially that assumes no combustion and determines the flammability and the adiabatic burn pressure versus time. If the containment atmosphere is calculated to be flammable for a significant period of time, then combustion is assumed to occur. The time of ignition is assumed to correspond to either a containment pressure spike, or the time of the maximum adiabatic burn pressure. For the best estimate Class I accident progression, the containment atmosphere is never flammable.

To define the probability of a Class I accident progression for all the paths of the containment event tree, parametric studies were made that considered the following:

1. 100 percent Zr-H_2O reaction.

* This was modeled by adjusting the particle size used by MARCH to get a CHF-limited boil-off rate during this period of time.

2. Steam generation resulting from interaction between the molten core debris and the water in the lower reactor cavity not limited by hydrodynamic limitations and/or the CHF.*

3. A noncoolable debris bed and the subsequent core debris/concrete interaction.

4. Hydrogen burns resulting from parametric study assumptions 1 and 3.

These results are reported in Section 4.3.1. Using these results, the appropriate probabilities could be assigned to all the paths on the containment event tree. Table 4.3.1-1 lists the best estimate, and the parameters varied for bounding cases in a Class I sequence analysis.

4.2.3 Class II Sequence

The Class II sequence is a large break LOCA, similar to Class I, except that the vessel safety injection and containment safeguards (fans and sprays) function until the switchover to recirculation is attempted. A failure is then assumed to occur at the recirculation switchover rendering the vessel injection and containment sprays inoperative. This event coincides with the emptying of the Refueling Water Storage Tank (RWST). However, the fan coolers are assumed not to fail. In the large break sequence, the combination of low pressure safety injection and containment spray flow would empty the RWST in approximately one hour. Core heatup would subsequently cause progression to a state of core degradation similar to the Class I sequence previously described, but the timing would be shifted.

The phenomena that occur (i.e., coherency, Zr-H_2O reaction, mode of core debris release from the failed reactor vessel, steaming from the lower reactor cavity, debris bed coolability, and hydrogen flammability), and the expected manner of occurrence for these phenomena are the same for Class II and Class I sequences. Therefore, the assumptions will not be reiterated. See Table 4.3.2-1 for a list of the best estimate and the parameters varied for bounding cases.

4.2.4 Class III Sequence

The Class III sequence is typical of a postulated small break LOCA in which safety injection fails at the initiation of the event, but minimum active containment safeguards function properly for the entire event. The initial conditions for this event are a reactor system at 100 percent power and an average vessel temperature of 580°F. Following the break, the reactor shuts down. The initial blowdown activates the containment fan coolers, but the containment spray is not activated

* This was accomplished by adjusting particle sizes in MARCH.

until vessel failure. Since minimum safeguards are assumed, three out of five fan coolers and one spray train (2500 gpm at 100°F) operate. The heat removal capability of the active containment safeguards and the passive containment heat sinks are the basis for the heat removal from the containment atmosphere. The core melt sequence progresses through blowdown, core overheat (with subsequent zirconium-water reaction and hydrogen formation), core slump, reactor vessel failure, and long-term releases. As the accident progresses through these events, a number of phenomena may occur. For a Class III event, the following major phenomena and their most probable characterization must be considered to calculate the containment response:

1. The coherency or noncoherency of the melt.

   This refers to the amount of molten core available to interact in the containment at vessel failure. As discussed in Section 3.1.2, analyses with the NSAC-TMI-2 computer code show less than 50 percent of the core would be molten at vessel failure. The most probable Class III accident progression was modeled using MARCH input options.

2. The amount of Zr-H_2O reaction and the resultant hydrogen formation.

   The most probable Class III event is the Zr-H_2O reaction up until core slump. The remaining Zr-H_2O reaction is estimated to be negligible. The amount of hydrogen formed during hydrogen generation up until core slump is taken directly from MARCH and termed "MARCH Calculated Prior to Slump, No Additional H_2 Produced" in the Tables of results.

3. The mode of molten core release from the failed reactor vessel.

   Two modes of release have been identified, the Dispersive and the Gravity Drop. Because the primary system will likely be at high pressure, the Dispersive mode of vessel failure and associated core debris release are the most probable phenomena for the Class III event. For this type of release, the molten core debris is discharged from the lower reactor cavity and spread over the containment floor.

4. The interaction between water and molten debris on the containment floor and the resultant steam generation following vessel failure.

   As discussed in Section 4.2.1, the steam boil-off will be limited by the CHF. This limiting rate is used in the analysis of the best estimate Class III event.

5. The long-term coolability of the debris bed.

   The discussion in Appendix 3.4.5 indicates that the ex-vessel debris bed would be coolable provided that sufficient water is supplied. For a Class III event, core debris exists both on the containment floor and in the lower reactor cavity. The amount of water in the

reactor cavity represents the spillage from the containment floor over the curb surrounding the reactor cavity plus possible accumulator discharge. Data defining these containment parameters are used as input into the MARCH code. Calculations indicate that there is sufficient water on the containment floor and in the lower reactor cavity to cool the core debris at vessel failure. A continued supply of water is ensured from the operation of containment heat removal systems. Thus, a coolable debris bed represents the probable phenomena for a Class III transient.

6. The assumed behavior of the hydrogen in the containment (i.e., whether it would ignite).

   The Flame Temperature Criterion discussed in Section 4.1.2 provides a methodology to evaluate the flammability of the containment atmosphere. Since it is not known a priori whether the containment atmosphere is flammable, a calculation is performed initially that assumes no combustion and determines the flammability and the adiabatic burn pressure versus time. If the containment atmosphere is flammable for a significant period of time, then combustion is assumed to occur. The time of ignition corresponds either to a containment pressure spike, or to the time of the maximum adiabatic burn pressure. For the best estimate Class III accident progression, the containment atmosphere is never flammable.

To define the probability of the Class III accident progressions for all the paths of the containment event tree, parameter studies were made that considered the following:

1. Zr-H_2O reaction corresponding to more than that predicted by MARCH at core slump.

2. Gravity drops with various amounts of Zr-H_2O reaction.

3. Gravity drops with larger reactor cavity steaming not limited by hydrodynamic considerations and/or the critical heat flux.

4. Scoping dispersive events considering entrainment and fast quench.

5. Hydrogen burns for items 2 and 4.

6. Continuous hydrogen burns for a Time Phased Dispersive event.

Best estimate and selected bounding case results are presented in Section 4.3.3 and in Table 4.3.3-1. Using these results, the appropriate probabilities could be assigned to the paths on the containment event tree.

4.2.5 Class IV Sequence

The Class IV sequence is a small break LOCA similar to Class III which assumes initial operation of the High Pressure Safety Injection (HPSI) system providing in-vessel core cooling. HPSI system failure is assumed to occur at the time of recirculation switchover. Under the assumptions of this sequence, the containment sprays do not actuate because the containment pressure never exceeds the containment spray pressure setpoint until vessel failure, by which time the spray system is assumed to have failed. However, the containment fan coolers actuate early in the transient when their pressure setpoint is reached. They continue to operate for the remainder of the transient.

Except for slight differences, the accident progressions and options used with Class III also apply to the Class IV sequence. Therefore, the major phenomena and the most probable characterization of these phenomena will not be reiterated. For a listing of the best estimate and the parameters varied for bounding cases, see Table 4.3.4-1 and Section 4.2.4.

4.2.6 Class V Sequence

Accidents that belong to Class V have the characteristics of a transient-initiated event with failure of primary and secondary cooling, and failure of containment safeguards.* The initial conditions for the event are a reactor at 100 percent power with an average vessel temperature of 580°F. Following the transient, the reactor shuts down. The accident can be initiated by incidents such as spurious reactor trip, loss of load on the turbine, or loss of offsite power with coincident loss of auxiliary turbine feed and diesels. Once the reactor trip has occurred, the primary system continues natural circulation, relieving heat through the steam generators until dry-out occurs. The primary system will then pressurize to the safety relief valve setpoint and begin to discharge steam to the containment, eventually uncovering the core approximately three or four hours into the accident. After the core is uncovered, substantial core damage will take place, and within a few minutes it will begin to migrate as a molten mass toward the lower plenum. As soon as a significant fraction of the core has melted, it will slump into the lower plenum causing almost immediate failure of the in-core instrumentation tubes. Because no containment safeguards are available, the containment will have slowly pressurized before core slump and will be at a pressure approximately 40 psia.

---

* Another analytical class has been defined (Class VI) to analyze a transient initiated event with failure of primary and secondary cooling but with minimum containment safeguards operational. This class is described in the next section.

At reactor vessel failure, the primary system will probably be close to the safety valve setpoint. If water is present in the cavity, the molten core will probably exit as a jet into the reactor cavity within 5 to 20 seconds causing a limited steam explosion. Next, the blowdown of approximately 60,000 pounds of steam and hydrogen in the primary system through the now ablated instrumentation tube penetration will push the molten debris out of the instrument tunnel and disperse it over the containment floor. Because the debris will be well scattered, it should be cooled by the water from the primary system and the accumulators. Since containment safeguards are not available, the containment is predicted to continue to pressurize.

In analyzing the Class V event, as in other classes, a number of variations in phenomena are considered. These phenomena and their most probable characterizations are

1. The coherency or noncoherency of the melt.

   In the Class V events, this refers to the amount of core that slumps coherently into the reactor vessel lower plenum and to the amount of core ejected at one time to the reactor cavity and then dispersed. As stated in previous sections, the NSAC-TMI-2 computer code shows that less than 50 percent of the core would be molten at vessel failure. As a result, the expected case for this sequence of events is one in which a noncoherent mass of molten core slumps into the lower plenum. Because analysis of the instrument tubes shows that they will fail almost immediately upon core slump, it is also expected that a noncoherent mass of core debris will be pushed from the reactor cavity. Nevertheless, to define the consequences for all nodes on the containment event tree, both a coherent, approximately 75 percent mass of debris, and a noncoherent, 50 percent mass of debris, were considered for the dispersive cases.

2. The amount of zirconium reaction and the resultant hydrogen formation.

   For the best estimate Class V case, the Zr-H_2O reaction until core slump, was taken directly from MARCH calculations. The remaining Zr-H_2O reaction was assumed to be negligible.

3. The mode of molten core release from the failed reactor vessel.

   As stated in Section 4.2.4, there are two possible modes of vessel failure and debris motion. The most probable is Time Phased Dispersive, and the other is Gravity Drop. The Time Phased Dispersive is more probable for the reasons stated in Section 4.2.4 and in the description of the dispersive model, Section 4.1.3.

4. Rate of steaming from the containment floor.

   As stated in Section 4.2.1, the steam boil-off rate will be limited in the best estimate case by the CHF.

5. Coolability of the debris long-term on the containment floor.

The discussion in Appendix 3.4.5 indicates that the ex-vessel debris bed will be coolable if sufficient water is provided. For the Class V event, water is limited to that in the primary system and in the accumulators. Calculations show that even with this limited amount of water there should be enough to continue to cool the debris for approximately eight to twelve hours into the accident. Because no safeguards are available, it is possible although unlikely, that debris-concrete interaction may begin at this time. However, because of the extent of the dispersion and the shallow depth of the debris, the probability is that the dispersed debris will interact with the concrete to a major extent. Therefore, the debris will be termed coolable even though portions of it may become uncovered.

6. The assumed behavior of the hydrogen in the containment (i.e. whether it would ignite).

This has been discussed in detail in Section 4.2.4 for the Class III sequence and the considerations are the same. The procedure used to determine the burn time is the same. For all of the Class V cases, so much steam is present in the containment that a significant hydrogen burn is not predicted.

For the phenomena listed above, parameters were varied to bracket the possible forms that an accident in the Class V sequence might take. In this way, the appropriate probabilities could be assigned to the paths of the containment event tree. Table 4.3.5-1 lists the best estimate and selected bounding case parameters as used in performing Class V sequence analysis. Because the parameters used in the analysis of the Class V sequence are identical to those of the Class III sequence, they will not be reiterated here. Therefore, refer to Section 4.3.3 to determine the parameters varied.

4.2.7 Class VI Sequence

Class VI accidents are similar to those in Class V except that containment safeguards are assumed to be operational. The expected accident progression is the same with two exceptions. First, the containment will not continue to overpressurize long-term because the heat removal capacity of the safeguards is present. Therefore, containment failure by overpressure long-term is not predicted. Second, because sprays are operational, water can be introduced to containment and the debris bed will very probably be coolable.

Because of the similarity between Class VI and Class V accidents, all of the parameters listed in Section 4.2.6 for Class V are varied in the same manner. For a description and results of the best estimate and parameters varied for bounding cases in the Class VI analysis, see Section 4.2.6 and Table 4.3.6-1.

TABLE 4.2.1-1

DESCRIPTION OF VARIOUS CLASSES OF ACCIDENTS

Containment Class	Initiating Event	BLOWDOWN	ECCS		CONTAINMENT SAFEGUARDS	
			INJECTION	RECIRC	SPRAYS	FANS
I	LARGE LOCA	FAST (≤ 30 sec)	OFF	-	(1)	(2)
II	LARGE LOCA	FAST (≤ 30 sec)	ON	NO	(1)(3)	(2)
III	SMALL LOCA	SLOW	OFF	-	(4)	(2)
IV	SMALL LOCA	SLOW	ON	NO	(5)	(2)
V	LOSS OF ALL AC POWER	NONE	OFF	-	(5)	(5)
VI	LOSS OF ALL AC POWER*	NONE	OFF	-	(6)	(7)

(1) INITIATED AT BLOWDOWN (1 of 2 OPERABLE)
(2) INITIATED AT BLOWDOWN (3 of 5 OPERABLE)
(3) TERMINATED AT ECCS RECIRC SWITCHOVER
(4) INITIATED AFTER VESSEL FAILURE (1 of 2 OPERABLE)
(5) NOT INITIATED
(6) INITIATED JUST PRIOR TO VESSEL FAILURE (1 of 2 OPERABLE)
(7) INITIATED AT START OF TRANSIENT (3 of 5 OPERABLE)

* EXCEPT CONTAINMENT SAFEGUARDS

4.3 RESULTS

In the following paragraphs, the phenomenological path that is believed most likely to occur within each of the six sequence classes analyzed will be identified and the results described. The results of the best estimate case for each sequence class and some less likely cases will be discussed. This approach was used to bound the phenomena that might occur within the containment and to aid in assigning probabilities to the unlikely paths of the containment event tree.

4.3.1 Class I Sequence

The Class I sequence is typical of a large break LOCA with loss of emergency coolant injection. Within the matrix of Class I cases, given in Table 4.3.1-1, the case with a limited Zr-H_2O reaction of approximately 36 percent, nondispersive core ejection, limited steam generation rate, coolable debris bed, and no hydrogen burn, is believed to best represent this class. This case is designated as the best estimate in Table 4.3.1-1.

Figure 4.3.1-1 shows the pressure profile for this case and Figure 4.3.1-2 is a plot of the flame temperature throughout the transient. The peak pressure of 61 psia during blowdown does not severely challenge the 141 psia containment limit. Following the blowdown spike, two other peaks appear on the pressure plot. The first one, at the lower grid plate failure, is because of the steam generation from the lower plenum water and core debris interaction. The second pressure spike, at vessel failure, is because of steam generation from core debris-water interaction in the lower reactor cavity. Both peaks result in pressures less than 40 psia. These relatively low peak pressures occur based on the phenomenology associated with a Class I sequence. The nondispersive vessel failure and the experimentally based Zr-H_2O reaction contribute in determining that these pressure peaks are well below the containment limit. At no time in the transient is the hydrogen concentration sufficient to support a propagating flame. As shown on the plot of Figure 4.3.1-2, the peak flame temperature is reached just as the vessel fails. This peak of approximately 800°F is well below the 1310°F Flame Temperature Criterion. Therefore, a hydrogen burn for the best estimate Class I sequence is not realistic.

Case 1 (Table 4.3.1-1), with an assumed 100 percent Zr-H_2O reaction and a rapid steam generation rate in the reactor cavity, shows a peak pressure rise at vessel failure. Figure 4.3.1-3 illustrates the total pressure versus time and shows that a maximum pressure of 79 psia occurs at vessel failure. In this case in which a 100 percent zirconium reaction at core slump is considered, hydrogen is flammable just before vessel failure (Figure 4.3.1-4).

Although a hydrogen burn is unrealistic for the Class I best estimate case, the peak pressure from a hydrogen burn is estimated. In Case 2 (Table 4.3.1-1), a burn initiated at vessel failure in the best estimate case will cause a larger pressure peak than a burn at any other time. The peaks representing the blowdown, 61 psia, and the lower grid plate failure, less than 40 psia, would remain essentially unchanged because

of the small amount of hydrogen available. However, the pressure peak at vessel failure will be the sum of the pressure associated with steam generation because of core debris-water interaction in the lower cavity and the simultaneous burn of the hydrogen released.

Case 3 (Table 4.3.1-1), assumes a 100 percent Zr-H_2O reaction with ignition sources present to force hydrogen burn at vessel failure. To obtain the upper bound pressure, the pressure spike from the hydrogen burn is combined with the pressure from steam generation that results from debris-water interaction in the lower cavity. The resulting pressure of 139 psia is shown in Figure 4.3.1-5. This case is extremely conservative for two reasons. First, the pressure peak due to the hydrogen burn will be reduced because of the assumed 100 percent Zr-H_2O reaction and only approximately half of the 2200 lbs of hydrogen burned would ever be available. Second, the steam spike will be reduced because of hydrodynamic limitations. Either one of these reasons will significantly lower the containment pressure.

In Case 4 (Table 4.3.1-1), the final case analyzed in evaluating the Class I sequence, the debris on the containment floor is assumed to be noncoolable. Significant debris-concrete interaction is modeled after vessel failure releasing large concentrations of hydrogen and carbon monoxide in the containment. The analysis assumes the containment atmosphere to be flammable after debris-concrete interaction approximately nine hours into the accident. This results in an extremely conservative pressure spike for the Class I sequence. Figure 4.3.1-6 shows the pressure profile, with the peak pressure of 144 psia at the late burn. Although this pressure is slightly above the containment limit, there are two reasons why this will never exist. First, it is not probable that significant debris-concrete interaction will ever occur for a Class I sequence because the debris bed is coolable. Second, it is expected that the hydrogen will burn earlier in time, thereby preventing massive accumulations of hydrogen and carbon monoxide.

4.3.2 Class II Sequence

The Class II sequence is characterized as a large break LOCA with failure of ECCS to start recirculation. The most likely accident progression consists of melt beginning at approximately two hours into the accident followed by a nondispersive type of vessel failure at approximately three and a half hours. The debris will gradually pour into the reactor cavity where there will be enough water available to maintain a coolable debris bed. For this case, the Zr-H_2O reaction is expected to be less than 50 percent. This case is designated as the best estimate case in Table 4.3.2-1.

Figure 4.3.2-1 shows the calculated pressure profile for this case. The peak pressure occurs at the end of blowdown and is 61 psia. Two other peaks occur. One is at core slump into the lower plenum and the other is at vessel failure. Both peaks are approximately 30 psia. As shown in Figure 4.3.2-2, the atmosphere never develops a flammable mixture. This is because the containment maximum hydrogen concentration is less than 6.5 percent. Therefore, the expected accident progression for the large LOCA with failure at recirculation is very similar to the best

estimate Class I accident progression. It differs primarily in the timing of major events such as core slump and vessel failure.

In Case 1 (Table 4.3.2-1), a variation on the expected progression, a much more rapid steaming rate is theorized at vessel failure. The peak pressure then occurs at vessel failure and is 73 psia. For this case, more steam is added to the containment atmosphere making the containment less flammable.

In Case 2 (Table 4.3.2-1), another variation on the best estimate case, hydrogen burn at vessel failure is assumed even though the containment atmosphere is not flammable. For this case, the pressure rise because of the hydrogen burn is approximately 25 psi and a peak pressure of approximately 55 psia is obtained. The blowdown pressure is expected to be higher than this.

In Case 3 (Table 4.3.2-1), to bracket the effects of hydrogen burn, 100 percent of the zirconium is assumed to react. This produces approximately 2200 lbs of hydrogen just before vessel failure. The containment atmosphere is flammable from core slump to vessel failure, when the steam produced in the reactor cavity makes it inert for about one hour. The containment safeguards then bring the steam concentration back down, and the containment once again becomes flammable. The worst pressure is achieved if a burn occurs just before vessel failure, causing the hydrogen burn spike to be added to the steam spike that began at vessel failure. The peak pressure because of the very rapid steaming rate is about 73 psia. A hydrogen burn adds another 57 psi to this pressure, for a total pressure of 130 psia. This pressure is still below the containment limit of 141 psia. Assuming that the more likely smaller steam spike occurs, the estimated pressure* will be even lower, approximately 105 psia. If the burn does not coincide exactly with vessel failure, then a pressure even lower than 105 psia will result. Therefore, even for a 100 percent Zr-H_2O reaction, any pressure rise from a hydrogen burn at vessel failure is expected to be well within the containment limit.

In Case 4 (Table 4.3.2-1), the effect of hydrogen and carbon monoxide generation on the containment because of debris-concrete interaction was analyzed although the debris bed is coolable. The worst time for a late burn is at approximately 11 hours, when the hydrogen mass has accumulated to 3300 lbs. The burn causes a pressure change of approximately 100 psi. However, because the safeguards have reduced the containment pressure to about 34 psia, the pressure in containment reaches only 134 psia as illustrated in Figure 4.3.2-3. Therefore, the containment is predicted to survive even if massive amounts of hydrogen and carbon monoxide are allowed to accumulate after debris-concrete interaction has begun.

* This pressure can be estimated by comparing bounding cases 2 and 3 in Table 4.3.2-1 and the best estimate case.

For the most probable progression of an accident within this class, the worst containment pressure is during blowdown. Therefore, the pressures are within the design pressure of the Indian Point containment. Table 4.3.2-1 gives a description of the Class II accidents analyzed. Active containment safeguards provide the necessary heat removal mechanism to keep the containment pressure down and the debris bed coolable.

4.3.3 Class III Sequence

Class III accidents are small break LOCAs with failure of emergency coolant injection. The expected amount of hydrogen before core slump for this accident type is approximately 26 percent. At core slump, the vessel will fail quickly because of the melt-through of one or more in-core instrumentation tubes, followed by a high pressure blowdown and the dispersal of the molten core debris over a wide area of the containment floor. Very little additional hydrogen, beyond that already produced at core slump, is expected to be produced, and the containment is not expected to be flammable at any time during the transient. Thus, the best estimate accident progression assumes noncoherent slump, 50 percent dispersion, MARCH-based hydrogen generation, no hydrogen burn, CHF-limited steaming, and a coolable debris bed. Figure 4.3.3-1 shows the pressure profile for this case, and Figure 4.3.3-2 is a plot of the Flame Temperature Criterion throughout the transient. For this case, the peak containment pressure occurs at vessel failure and for the noncoherent mass (50 percent of core involved) is approximately 51 psia.

In addition to the best estimate case for this sequence, 16 other calculations were performed. They were used to assign probabilities and ranges of probabilities for all the nodes on the containment event tree. The phenomena and peak pressures associated with the best estimate case and each of the selected cases are detailed in Table 4.3.3-1. A discussion of these selected cases follows.

In Case 1 (Table 4.3.3-1), when 75 percent of the core mass is involved in the dispersive event, the containment becomes less flammable because of additional steaming. This steaming is from the additional boil-off caused by the additional 25 percent of the core dispersed on the containment floor and results in a pressure spike of approximately 59 psia.

In Cases 2 and 3 (Table 4.3.3-1), the amount of hydrogen produced because of the reaction of the zirconium or stainless steel during vessel failure and the subsequent dispersion of debris were considered. To account for this possible extra hydrogen generation, a 69 percent $Zr\text{-}H_2O$ reaction (one half of that which has not already reacted prior to core slump plus that reacted at core slump) is assumed for both the likely noncoherent case and the less likely coherent case. As in the best estimate case, neither is flammable and the highest flame temperature calculated is 954°F (Figure 4.3.3-3), well below the Flame Temperature Criterion of 1310°F. Therefore, a propagating hydrogen burn is not likely for these cases that represent an upper bound on hydrogen generation according to experimental evidence.

In Cases 4 and 5 (Table 4.3.3-1), the possibility of combustion because of a continuous burn of hydrogen as it exits the reactor cavity at

vessel failure is considered. For the worst of these cases, the peak pressure of 84 psia is caused by the steam spike at vessel failure (65 psia) for a coherent dispersion and a hydrogen burn increase in pressure of 19 psi.

In Case 6 (Table 4.3.3-1), a propagating hydrogen burn is assumed to fully scope the effects of hydrogen burn for the dispersive event. Even in the extremely improbable event of 50 percent extra Zr-H_2O reaction and a coherent dispersive event, the peak pressure is below 111 psia, within the containment limit.

In Cases 7 and 8 (Table 4.3.3-1), scoping cases for the dispersive type of failure that yield an upper bound on containment pressure are analyzed. They represent an upper bound because the dispersed debris is assumed to be ejected at high velocity into the containment atmosphere, thereby directly heating it. It is also because the undispersed core and debris in the reactor vessel is assumed to fall immediately into the reactor cavity water and quench over 30 seconds. These cases were analyzed with varying amounts of core dispersed and varying amounts of zirconium reacted. None of these are flammable until well after vessel failure. The worst of these pressure spikes without a burn is 37 psi below the containment limit.

Cases 9 and 10 (Table 4.3.3-1) are scoping calculations which were performed assuming a hydrogen burn at vessel failure. For the calculations that use an experimentally based Zr-H_2O reaction and force a hydrogen burn at vessel failure, the peak calculated pressures are 131 psia and 135 psia at vessel failure for the 50 percent and 80 percent assumptions of debris dispersion. Figure 4.3.3-4 presents the pressure transient for Case 9.

The highest pressure calculated for any Class III sequence is for an Entrained Dispersive Event in which a 100 percent Zr-H_2O reaction is assumed, and a hydrogen burn is modeled during the core dispersion. The probability of the actual accident progression adhering to this conservative set of modeling assumptions is small. This progression adds the pressure spikes from direct heating during the dispersion, rapid quench of dispersed and undispersed core debris, and a hydrogen burn. The pressure transient is illustrated in Figure 4.3.3-5, and the details are given in Table 4.3.3-1, Case 11.

In Case 12 (Table 4.3.3-1), the core debris pouring in a nondispersive manner (Gravity Drop) into the reactor cavity was also analyzed since the primary system pressure at vessel failure can vary greatly for this class of accident. These cases are similar to those analyzed for the Class I and II accidents. If such a nondispersive case occurs, it will likely involve limited hydrogen generation (less than 100 percent Zr-H_2O reaction) and a hydrodynamically limited steam generation rate. It will not be flammable until a few hours after vessel failure and the peak pressure, as shown in Figure 4.3.3-6, will be 40 psia.

For a nondispersive case with hydrogen production corresponding to 100 percent Zr-H_2O reaction (Case 13), the containment barely becomes

flammable just at vessel failure. The peak pressure is 77 psia (Figure 4.3.3-7) given a very rapid steaming rate. When a hydrogen burn is added (Case 15), the total pressure becomes 135 psia (Figure 4.3.3-8). The 135 psia pressure is below the containment limit, and the pressure caused by an actual nondispersive accident will be less because both the rapid steaming rate and the 100 percent Zr-H_2O reaction would never occur.

In Case 16 (Table 4.3.3-1), the long-term effect of the various accidents after vessel failure is expected to be minimal because of active containment safeguards and abundant water on the containment floor. The base pressure should remain around 25 psia and almost no additional combustible gas should be added to the atmosphere because of debris-concrete interaction. If debris and concrete do interact, the containment may eventually become flammable. However, the resulting pressure from a burn should be within the containment limit. At approximately 11 hours, a burn for a nondispersive case with a massive amount of hydrogen and carbon monoxide present because of debris-concrete interaction results in a containment pressure of 137 psia, as shown in Figure 4.3.3-9.

The results for the Class III sequence demonstrate that containment failure either by overpressure or by basemat penetration is unlikely. The most expected accident progression has a peak pressure of 51 psia at vessel failure with a possible higher pressure occurring later in the transient because of a small hydrogen burn. As a result, the containment limit will probably not be reached.

4.3.4 Class IV Sequence

The Class IV sequence encompasses those accidents that are similar to small break LOCAs with failure of emergency coolant injection at the start of recirculation. As in the Class III sequences, the best estimate case is a noncoherent, dispersive vessel failure with limited Zr-H_2O reaction and no debris-concrete inateraction. Figure 4.3.4-1 shows the pressure profile for this case and Figure 4.3.4-2 is a plot of the flame temperature throughout the transient. The maximum pressure for this case is 56 psia, and the containment atmosphere is not flammable up to and through vessel failure.

As in the Class III sequence for the expected dispersive event, numerous other calculations were performed to bound the possible Class IV phenomena and to assign probabilities and ranges of probabilities for all the nodes on the containment event tree. The phenomena and peak pressures associated with the best estimate case and each of the selected bounding cases are detailed in Table 4.3.4-1. As illustrated in this table, the containment is never severely challenged even for the coherent dispersive case in which a continuous burn at vessel failure is considered.

For Cases 1 and 2 (Table 4.3.4-1), in which the entrainment of the core debris by the primary system blowdown causes bounding containment pressure spikes, the maximum pressure is 75 psia from the steam spike alone and 96 psia for the steam spike combined with a hydrogen burn. This is illustrated in Figure 4.3.4-3 for Case 1 and Figure 4.3.4-4 for Case 2. None of these entrained dispersive cases severely threatens the containment limit.

For Cases 3 and 4 (Table 4.3.4-1), in which the debris is pouring in a nondispersive manner into the reactor cavity (Gravity Drop) and accumulating, the peak pressure occurs at vessel failure if the containment remains inert. For the hydrodynamically limited steaming rate, the pressure spike magnitude is only 33 psia (Figure 4.3.4-5), and for the rapid steaming rate it is 63 psia (Figure 4.3.4-6).

In Case 6 (Table 4.3.4-1), when a 100 percent Zr-H_2O reaction is assumed prior to vessel failure, the containment becomes flammable just before vessel failure and the combination of a rapid steaming rate and a hydrogen burn yields a pressure of 118 psia (Figure 4.3.4-7). If the burn does not occur at vessel failure, then the containment will become inert for a few minutes following vessel failure. Flammability will return when the fan coolers lower the steam concentration and pressure. A burn at this time will yield a pressure lower than the 118 psia because the containment pressure to which the burn spike is being added is lower than the pressure at vessel failure.

In Case 7 (Table 4.3.4-1), a nondispersive core drop with debris-concrete interaction and a late burn of a massive amount of accumulated hydrogen and carbon monoxide was considered. The burn is conservatively assumed to occur at 23 hours into the accident. However, the containment was actually flammable with lower concentrations of hydrogen and carbon monoxide for the previous nine hours. As seen in Figure 4.3.4-8, the containment pressure reaches 127 psia, well within the 141 psia containment limit.

Similar to the Class III sequences, the Class IV accidents are not predicted to fail containment. The highest pressure for the best estimate case is not expected to be beyond design limit pressure, and enough water is available within the containment to prevent basemat penetration. Even the most conservative models do not cause pressures to be calculated that exceed the containment limit.

4.3.5 Class V Sequence

Accidents within this class are typically initiated by a transient event with loss of both primary and secondary cooling and loss of safeguards. Because there are no operational containment safeguards, all accidents in this class will ultimately lead to containment failure by long-term overpressure, provided earlier types of failure have not been predicted.

As shown in Table 4.3.5-1, the best estimate case is characterized by an experimentally and analytically based Zr-H_2O reaction, a noncoherent dispersive ejection of less than 50 percent of the core onto the containment floor, a floor steam generation rate limited by CHF, a coolable debris bed and no hydrogen burn. Figure 4.3.5-1 shows the pressure profile for this case until just after vessel failure. The peak pressure of 75 psia occurs during the core debris dispersion immediately following reactor vessel failure and does not approach the 141 psia containment limit. As indicated, a conservative calculation predicts that long-term overpressure would occur 10 hours or more into the

accident. As Figure 4.3.5-2 shows, the peak flame temperature is reached just as the vessel fails and the core is dispersed. This peak of approximately 500°F is well below the 1310°F critical Flame Temperature Criterion. Therefore, dispersive cases that include a hydrogen burn do not realistically represent the Class V sequence.

If a hydrogen burn during dispersion is modeled for the best estimate case, a burn initiated at the conclusion of the core debris discharge will yield a maximum pressure peak. This pressure peak will be the sum of the dispersive steam pressure spike and the hydrogen burn pressure spike. The resulting pressure is estimated to be approximately 16 psi above the no-burn pressure which indicates that a total pressure of approximately 91 psia is expected. This does not exceed the 141 psia containment limit.

In Case 1 (Table 4.3.5-1), a coherent dispersive ejection of approximately 75 percent of the core debris, a best estimate Zr-H_2O reaction, a CHF limited steam generation rate, a coolable debris bed and no hydrogen burn is analyzed. The distinction between this and the best estimate case is the increase in the quantity of discharged core. As shown in Figure 4.3.5-3, the peak pressure during vessel failure and core discharge is 83 psia. Up to this point in the transient, the pressure profile is identical to that of the best estimate case. Figure 4.3.5-4 shows that the hydrogen is not flammable at any point in the transient.

In Case 2 (Table 4.3.5-1), the amount of zirconium reacted is increased by reacting 50 percent of the previously unreacted zirconium. This causes a moderately higher pressure after vessel failure and core discharge. Figure 4.3.5-5 illustrates the containment pressure and indicates that the peak pressure of 85 psia occurs at vessel failure and core discharge. This represents a 10 psi increase over the best estimate case. This case is unrealistic in that it is assumed phenomenologically that the quantity of zirconium reacted at core slump correctly represents the amount of reaction during the transient. In fact, further significant Zr-H_2O reaction during and after vessel failure is deemed improbable. Similar to the best estimate case, Figure 4.3.5-6 shows that even with additional hydrogen, the containment is unable to support a propagating flame during the transient because the maximum flame temperature calculated is approximately 780°F.

In Case 3 (Table 4.3.5-1), as in the best estimate case, the sensitivity to the amount of Zr-H_2O reaction was studied. This case assumed a dispersive ejection of 75 percent of the core debris, an increased Zr-H_2O reaction, a coolable debris bed, and a CHF limited containment steaming rate. The calculated flame temperature for the transient indicates that the containment is not flammable, and a peak pressure of 93 psia occurs at vessel failure.

Cases 4 and 5 (Table 4.3.5-1) are results of calculations performed to study the possibility that hot core debris could serve as an ignition

source* for the hydrogen as it exited from the failed reactor vessel. These cases are identical to Cases 2 and 3 except that hydrogen was burned continuously as it exited the reactor vessel. The peak pressures for these two calculations were estimated to be less than 106 psia and 114 psia, respectively.

In Case 6 (Table 4.3.5-1), the Time Phased Dispersive model assumed a hydrogen burn at vessel failure. It has a coherent discharge of approximately 75 percent of the core debris, an increased Zr-H_2O reaction and a CHF limited containment steaming rate. To maximize the pressure at reactor vessel failure, a complete hydrogen burn was initiated following the blowdown of the reactor vessel. However, the occurrence of this hydrogen burn is unlikely because the flame temperature indicates that the mixture is nonflammable. The peak pressure of 117 psia during the burn does not exceed the containment limit.

As described in Section 4.1.4, scoping calculations were performed with the Entrained Dispersive model. For these cases, the core debris is carried into and scattered in the containment volume atmosphere where a Zr-H_2O reaction can take place with the steam. The result is a higher pressure spike at core discharge and the potential for sufficient hydrogen production to cause flammability.

In Case 7 (Table 4.3.5-1), a noncoherent core melt with an experimentally based Zr-H_2O reaction, a rapid steam generation rate, a coolable debris bed, and no hydrogen burn was analyzed. Figure 4.3.5-7 illustrates the containment pressure profile for this transient, indicating a peak pressure of 122 psia at vessel failure. The high pressure observed is because of the entrainment of the core debris by the steam and hydrogen discharged from the vessel and the subsequent direct heating of the atmosphere. At no time in the transient is the hydrogen concentration sufficient to support a propagating flame. The peak flame temperature, as shown on the plot in Figure 4.3.5-8, is reached just as the vessel fails and the core is dispersed. This peak of approximately 1050°F is below the 1310°F critical Flame Temperature Criterion. The peak containment pressure is 122 psia and does not exceed the containment limit of 141 psia.

If a burn is assumed in the previous case, a conservative pressure is calculated if the burn is concurrent with the entrained dispersion of the core at vessel failure (Case 9). If all other characteristics remain the same, the hydrogen burn at the conclusion of the dispersion causes a pressure profile as shown in Figure 4.3.5-9. The peak pressure of 160 psia represents a burn in addition to the vessel failure pressure spike. This value exceeds the containment limit by 19 psi. This case and the previous one are highly improbable because of the extremely conservative phenomenology assumed.

* The ignition of the hydrogen blowdown is not likely since it will probably be inerted by the steam mixed with it.

Scoping cases similar to those described in Table 4.3.5-1, Cases 7 and 9, but assuming an 80 percent dispersion, were also studied. The results of these calculations, Cases 8 and 10, are given in Table 4.3.5-1.

Analysis of the nondispersive cases in this class, Cases 11 to 15 (Table 4.3.5-1), reveals that the containment limit is not exceeded by vessel failure. The highest steam pressure spike is characterized by Case 12 in which 100 percent of the zirconium is assumed reacted with a rapid steam generation rate. Figure 4.3.5-10 shows that the pressure peak at vessel failure is 110 psia which is below the 141 psia containment limit. As shown in Figure 4.3.5-11, at no time is the hydrogen concentration sufficient to support a propagating flame. Even if the containment cavity drys out, allowing debris-concrete interaction that produces 6000 lbs of hydrogen, the peak flame temperature of 1240°F is below the 1310°F critical Flame Temperature Criterion.

4.3.6 Class VI Sequence

Accidents that belong to Class VI are similar to those initiated by a transient that result in a loss of all capability to remove heat from the primary system and the loss of the primary system safeguards. However, containment safeguards are operational. The most likely progression involves approximately 30 percent Zr-H_2O reaction, a dispersive vessel failure, a noncoherent mass of debris, long-term debris bed coolability and no hydrogen burn. This case should be similar to the best estimate Class V case with sprays initiated at the 37.7 psia setpoint. The fan coolers will actuate early in the transient and continue operating. Therefore, the standard Class V cases will provide an upper bound on containment pressure.

For the best estimate Class VI case, as described in Table 4.3.6-1, the containment pressure peaks at 75 psia when the vessel fails and the core debris is dispersed. The pressure will be reduced by approximately 15 psi with safeguards operational before vessel failure. Analysis indicates that the containment is well below flammability limits with a peak flame temperature of no more than 900°F just before vessel failure. After vessel failure, the containment pressure will drop to 25 to 30 psia and no long-term static overpressure will occur as in the Class V transients. With the debris bed coolable, the amount of hydrogen generated is insignificant and therefore, the increase in pressure because of the hydrogen burn will not cause the containment limit to be exceeded.

In Case 3 (Table 4.3.6-1), a nondispersive case, the containment will again have safeguards operational and pressure spikes less than those given for the corresponding cases in Class V. For rapid steam generation at vessel failure and a nondispersive event, the peak pressure is 96 psia. This is 14 psi lower than the comparable Class V case and does not threaten containment. The containment atmosphere is not flammable before or during vessel failure even though a 100 percent Zr-H_2O

reaction is modeled. Because the containment safeguards are operational, the steam concentration will be continuously decreased, and the containment will become flammable. However, a burn will not cause containment failure because of the reduced base pressure and the unlikelihood of debris-concrete interaction.

Table 4.3.6-1 gives details for some of the selected cases studied in analyzing this sequence.

The conclusion reached for the Class VI sequence is that the containment is unlikely to fail because of the operation of safeguards. With sprays initiated, enough water will be present to cool the core debris. Therefore, debris-concrete interaction is not likely. The operation of fan coolers early in the transient keeps the base pressure low. Therefore, the pressure because of the steam spike and hydrogen burn would still result in a pressure well below the containment limit of 141 psia.

CLASS I CASES

Phenomena Investigated \ Case	Best Estimate	Selected Bounding Cases 1	2	3	4
Debris Disposition at Vessel Failure	Nondispersed	Nondispersed	Nondispersed	Nondispersed	Nondispersed
Coherency of Core	Noncoherent slump, Assumed coherent drop	Noncoherent slump, Assumed coherent drop	Noncoherent slump, Assumed coherent drop	Noncoherent slump, Assumed coherent drop	Noncoherent slump, Assumed coherent drop
Amount of Hydrogen Formed	Experimentally Based	100% Zr Reacted	Experimentally Based	100% Zr Reacted	100% Zr Reacted
Debris Bed Coolability	Coolable, no debris-concrete interaction	Coolable, no debris-concrete interaction	Coolable, no debris-concrete interaction	Coolable, no debris-concrete interaction	Noncoolable
Hydrogen Burn Time	No burn, flame temperature criteria not met	No burn	Forced burn at vessel failure	Burn at vessel failure	Burn at worst time after vessel failure
Containment Steaming Rate	Hydrodynamically limited	Rapid quench	Hydrodynamically limited	Rapid quench	Rapid quench
Resulting Peak Pressures	61 psia at blowdown, 30 psia at vessel failure	∿ 79 psia at vessel failure	61 psia at blowdown, ∿ 54 psia at vessel failure	139 psia at vessel failure	144 psia at burn

TABLE 4.3.1-1

CLASS II CASES

Phenomena Investigated \ Case	Best Estimate	Selected Bounding Cases 1	2	3	4
Debris Disposition at Vessel Failure	Nondispersed	Nondispersed	Nondispersed	Nondispersed	Nondispersed
Coherency of Core	Noncoherent slump, Assumed coherent drop	Noncoherent slump, Assumed coherent drop	Noncoherent slump, Assumed coherent drop	Noncoherent slump, Assumed coherent drop	Noncoherent slump, Assumed coherent drop
Amount of Hydrogen Formed	Experimentally based	100% Zr Reacted	Experimentally Based	100% Zr Reacted	100% Zr Reacted
Debris Bed Coolability	Coolable, no debris-concrete interaction	Coolable, no debris-concrete interaction	Coolable, no debris-concrete interaction	Coolable, no debris-concrete interaction	Noncoolable
Hydrogen Burn Time	No burn, flame temperature criteria not met	No burn, flame temperature criteria not met	Forced burn at vessel failure	Burn at vessel failure	Burn at worst time after vessel failure
Containment Steaming Rate	Hydrodynamically limited	Rapid quench	Hydrodynamically limited	Rapid quench	Rapid quench
Resulting Peak Pressures	61 psia at blowdown, 30 psia at vessel failure	∿ 73 psia at vessel failure	61 psia at blowdown, ∿ 55 psia at vessel failure	130 psia at vessel failure	134 psia at burn

TABLE 4.3.2-1

CLASS III CASES

Phenomena Investigated \ Case	Best Estimate	Selected Bounding Cases 1	2	3	4
Debris Disposition at Vessel Failure	Dispersed, time phased	Dispersed, time phased	Dispersed, time phased	Dispersed, time phased	Dispersed, time phased
Coherency of Core	Noncoherent slump, 50% dispersed	Coherent slump, 75% dispersed	Noncoherent slump, 50% dispersed	Coherent slump, 75% dispersed	Noncoherent slump, 50% dispersed
Amount of Hydrogen Formed	MARCH calculated prior to slump, no additional hydrogen produced	MARCH calculated prior to slump, no additional hydrogen produced	MARCH calculated prior to slump, 50% remainder Zr reacted	MARCH calculated prior to slump, 50% remainder Zr reacted	MARCH calculated prior to slump, 50% remainder Zr reacted
Debris Bed Coolability	Coolable, no debris-concrete interaction	Coolable, no debris-concrete interaction	Coolable, no debris-concrete interaction	Coolable, no debris-concrete interaction	Coolable, no debris-concrete interaction
Hydrogen Burn Time	No burn, flame temperature criteria not met	No burn, flame temperature criteria not met	No burn, flame temperature criteria not met	No burn, flame temperature criteria not met	Continuous burn of hydrogen exiting tunnel
Containment Steaming Rate	CHF limited	CHF limited	CHF limited	CHF limited	CHF limited
Resulting Peak Pressures	51 psia at vessel failure	59 psia at vessel failure	58 psia at vessel failure	65 psia at vessel failure	~ 77 psia at burn

TABLE 4.3.3-1

CLASS III CASES (Continued)

Phenomena Investigated \ Case	Selected Bounding Cases 5	6	7	8
Debris Disposition at Vessel Failure	Dispersed, time phased	Dispersed, time phased	Dispersed, entrained debris	Dispersed, entrained debris
Coherency of Core	Coherent slump, 75% dispersed	Coherent slump, 75% dispersed	Noncoherent slump, 50% dispersed	Coherent slump, 80% dispersed
Amount of Hydrogen Formed	MARCH calculated prior to slump, 50% remainder Zr reacted	MARCH calculated prior to slump, 50% remainder Zr reacted	Experimentally based	Experimentally based
Debris Bed Coolability	Coolable, no debris-concrete interaction	Coolable, no debris-concrete interaction	Coolable, no debris-concrete interaction	Coolable, no debris-concrete interaction
Hydrogen Burn Time	Continuous burn of hydrogen exiting tunnel	Forced burn at vessel failure	No burn, flame temperature criteria not met	No burn, flame temperature criteria not met
Containment Steaming Rate	CHF limited	CHF limited	Rapid quench 100% core	Rapid quench 100% core
Resulting Peak Pressures	∿ 84 psia at burn	∿ 111 psia at vessel failure	95 psia at vessel failure	104 psia at vessel failure

TABLE 4.3.3-1

CLASS III CASES (Continued)

Phenomena Investigated \ Case	Selected Bounding Cases 9	10	11	12	13
Debris Disposition	Dispersed, entrained debris	Dispersed, entrained debris	Dispersed, entrained debris	Nondispersed	Nondispersed
Coherency of Core	Noncoherent slump, 50% dispersed	Coherent slump, 80% dispersed	Coherent slump, 80% dispersed	Noncoherent slump, Assumed coherent drop	Noncoherent slump, Assumed coherent drop
Amount of Hydrogen Formed	Experimentally based	Experimentally based	100% Zr Reacted	Experimentally based	100% Zr Reacted
Debris Bed Coolability	Coolable, no debris-concrete interaction	Coolable, no debris-concrete interaction	Coolable, no debris-concrete interaction	Coolable, no debris-concrete interaction	Coolable, no debris-concrete interaction
Hydrogen Burn Time	Forced burn at vessel failure	Forced burn at vessel failure	Burn at vessel failure	No burn, flame temperature criteria not met	No burn, flame temperature criteria not met
Containment Steaming Rate	Rapid quench 100% core	Rapid quench 100% core	Rapid quench 100% core	Hydrodynamically limited	Rapid quench
Resulting Peak Pressures	131 psia at vessel failure	135 psia at vessel failure	147 psia at vessel failure	40 psia at vessel failure	77 psia at vessel failure

TABLE 4.3.3-1

CLASS III CASES (Continued)

Phenomena Investigated \ Case	Selected Bounding Cases 14	15	16
Debris Disposition at Vessel Failure	Nondispersed	Nondispersed	Nondispersed
Coherency of Core	Noncoherent slump, Assumed coherent drop	Noncoherent slump, Assumed coherent drop	Noncoherent slump, Assumed coherent drop
Amount of Hydrogen Formed	Experimentally based	100% Zr Reacted	100% Zr Reacted
Debris Bed Coolability	Coolable, no debris-conrete interaction	Coolable, no debris-concrete interaction	Noncoolable
Hydrogen Burn Time	Forced burn at vessel failure	Forced burn at vessel failure	Burn at worst time after vessel failure
Containment Steaming Rate	Rapid quench	Rapid quench	Rapid quench
Resulting Peak Pressures	~ 104 psia at vessel failure	135 psia at vessel failure	137 psia at burn

TABLE 4.3.3-1

CLASS IV CASES

Phenomena Investigated \ Case	Best Estimate	Selected Bounding Cases 1	2	3	4
Debris Disposition	Dispersed, time phased	Dispersed, entrained debris	Dispersed, entrained debris	Nondispersed	Nondispersed
Coherency of Core	Noncoherent slump, 50% dispersed	Coherent slump, 80% dispersed	Coherent slump, 80% dispersed	Noncoherent slump, Assumed coherent drop	Noncoherent slump, Assumed coherent drop
Amount of Hydrogen Formed	MARCH calculated prior to slump, no additional hydrogen produced	Experimentally based	Experimentally based	Experimentally based	100% Zr Reacted
Debris Bed Coolability	Coolable, no debris-concrete interaction	Coolable, no debris-concrete interaction	Coolable, no debris-concrete interaction	Coolable, no debris-concrete interaction	Coolable, no debris-concrete interaction
Hydrogen Burn Time	No burn, flame temperature criteria not met	No burn, flame temperature criteria not met	Forced burn at vessel failure	No burn, flame temperature criteria not met	No burn
Containment Steaming Rate	CHF limited	Rapid quench 100% core	Rapid quench 100% core	Hydrodynamically limited	Rapid quench
Resulting Peak Pressures	56 psia at vessel failure	75 psia at vessel failure	96 psia at vessel failure	33 psia at vessel failure	63 psia at vessel failure

TABLE 4.3.4-1

CLASS IV CASES (Continued)

Phenomena Investigated \ Case	Selected Bounding Cases		
	5	6	7
Debris Disposition	Nondispersed	Nondispersed	Nondispersed
Coherency of Core	Noncoherent slump, Assumed coherent drop	Noncoherent slump, Assumed coherent drop	Noncoherent slump, Assumed coherent drop
Amount of Hydrogen Formed	Experimentally based	100% Zr Reacted	100% Zr Reacted
Debris Bed Coolability	Coolable, no debris-concrete interaction	Coolable, no debris-concrete interaction	Noncoolable
Hydrogen Burn Time	Forced burn at vessel failure	Burn at vessel failure	Burn at worst time after vessel failure
Containment Steaming Rate	Rapid quench	Rapid quench	Rapid quench
Resulting Peak Pressures	~ 98 psia at vessel failure	118 psia at vessel failure	127 psia at burn

TABLE 4.3.4-1

CLASS V CASES

Phenomena Investigated \ Case	Best Estimate	Selected Bounding Cases 1	2	3	4
Debris Disposition	Dispersed, time phased	Dispersed, time phased	Dispersed, time phased	Dispersed, time phased	Dispersed, time phased
Coherency of Core	Noncoherent slump, 50% dispersed	Coherent slump, 75% dispersed	Noncoherent slump, 50% dispersed	Coherent slump, 75% dispersed	Noncoherent slump, 50% dispersed
Amount of Hydrogen Formed	MARCH calculated prior to slump, no additional hydrogen produced	MARCH calculated prior to slump, no additional hydrogen produced	MARCH calculated prior to slump, 50% remainder Zr Reacted	MARCH calculated prior to slump, 50% remainder Zr Reacted	MARCH calculated prior to slump 50% remainder Zr Reacted
Debris Bed Coolability	Coolable, no debris-concrete interaction	Coolable, no debris-concrete interaction	Coolable, no debris-concrete interaction	Coolable, no debris-concrete interaction	Coolable, no debris-concrete interaction
Hydrogen Burn Time	No burn, flame temperature criteria not met	No burn, flame temperature criteria not met	No burn, flame temperature criteria not met	No burn, flame temperature criteria not met	Continuous burn of hydrogen exiting tunnel
Containment Steaming Rate	CHF limited	CHF limited	CHF limited	CHF limited	CHF limited
Resulting Peak Pressures	75 psia at vessel failure, long-term overpressure	83 psia at vessel failure, long-term overpressure	85 psia at vessel vessel failure, long-term overpressure	93 psia at vessel failure, long-term overpressure	$\leq$ 106 psia at vessel failure, long-term overpressure

TABLE 4.3.5-1

CLASS V CASES (continued)

Phenomena Investigated \ Case	Selected Bounding Cases 5	6	7	8
Debris Disposition at Vessel Failure	Dispersed, time phased	Dispersed, time phased	Dispersed, entrained debris	Dispersed, entrained debris
Coherency of Core	Coherent slump, 75% dispersed	Coherent slump, 75% dispersed	Noncoherent slump, 50% dispersed	Coherent slump, 80% dispersed
Amount of Hydrogen Formed	MARCH calculated prior to slump, 50% remainder Zr reacted	MARCH calculated prior to slump, 50% remained Zr reacted	Experimentally based	Experimentally based
Debris Bed Coolability	Coolable, no debris-concrete interaction	Coolable, no debris-concrete interaction	Coolable, no debris-concrete interaction	Coolable, no debris-concrete interaction
Hydrogen Burn Time	Continuous burn at hydrogen exiting tunnel	Forced burn at vessel failure	No burn, flame temperture criteria not met	No burn, flame temperature criteria not met
Containment Steaming Rate	CHF limited	CHF limited	Rapid quench 100% core	Rapid quench 100% core
Resulting Peak Pressures	$\leq$ 114 psia at vessel failure, long-term overpressure	117 psia at vessel failure, long-term overpressure	122 psia at vessel failure, long-term overpressure	132 psia at vessel failure, long-term overpressure

TABLE 4.3.5-1

CLASS V CASES (continued)

Phenomena Investigated \ Case	Selected Bounding Cases 9	10	11	12
Debris Dispostion at Vessel Failure	Dispersed, entrained debris	Dispersed, entrained debris	Nondispersed	Nondispersed
Coherency of Core	Noncoherent slump, 50% dispersed	Coherent slump, 80% dispersed	Noncoherent slump, Assumed coherent drop	Noncoherent slump, Assumed coherent drop
Amount of Hydrogen Formed	Experimentally based	Experimentally based	Experimentally based	100% Zr Reacted
Debris Bed Coolability	Coolable, no debris-concrete interaction	Coolable, no debris-concrete interaction	Coolable, no debris-concrete interaction	Coolable, no debris-concrete interaction
Hydrogen Burn Time	Forced burn at vessel failure	Forced burn at vessel failure	No burn, flame temperature criteria not met	No burn, flame temperature criteria not met
Containment Steaming Rate	Rapid quench 100% core	Rapid quench 100% core	Hydrodynamically limited	Rapid quench
Resulting Peak Pressures	160 psia at vessel failure, long-term overpressure	169 psia at vessel failure, long-term overpressure	82 psia at vessel failure, long-term overpressure	110 psia at vessel failure, long-term overpressure

TABLE 4.3.5-1

CLASS V CASES (continued)

Phenomena Investigated \ Case	Selected Bounding Cases		
	13	14	15
Debris Disposition at Vessel Failure	Nondispersed	Nondispersed	Nondispersed
Coherency of Core	Noncoherent slump, Assumed coherent drop	Noncoherent slump, Assumed coherent drop	Noncoherent slump, Assumed coherent drop
Amount of Hydrogen Formed	Experimentally based	100% Zr Reacted	100% Zr Reacted
Debris Bed Coolability	Coolable, no debris-concrete interaction	Coolable, no debris-concrete interaction	Noncoolable
Hydrogen Burn Time	Forced burn at vessel failure	Forced burn at vessel failure	Forced burn after vessel failure
Containment Steaming Rate	Rapid quench	Rapid quench	Rapid quench
Resulting Peak Pressures	$\sim$ 157 psia at vessel failure, long-term overpressure	$\leq$ 180 psia at vessel failure	After $\sim$ 40,000 sec. containment limit exceeded

TABLE 4.3.5-1

CLASS VI CASES

Phenomena Investigated \ Case	Best Estimate	Selected Bounding Cases 1	2	3	4
Debris Disposition at Vessel Failure	Dispersed, time phased	Dispersed, time phased	Dispersed, entrained debris	Nondispersed	Nondispersed
Coherency of Core	Noncoherent slump, 50% dispersed	Coherent slump, 75% dispersed	Noncoherent slump, 50% dispersed	Noncoherent slump, Assumed coherent drop	Noncoherent slump, Assumed coherent drop
Amount of Hydrogen Formed	MARCH calculated prior to slump, no additional hydrogen produced	MARCH calculated prior to slump, 50% remainder Zr reacted	Experimentally based	100% Zr Reacted	100% Zr Reacted
Debris Bed Coolability	Coolable, no debris-concrete interaction	Coolable, no debris-concrete interaction	Coolable, no debris-concrete interaction	Coolable, no debris-concrete interaction	Noncoolable
Hydrogen Burn Time	No burn, flame temperature criteria not met	No burn	Forced burn at vessel failure	No burn, flame temperature criteria not met	Burn at worst time after vessel failure
Containment Steaming Rate	CHF limited	CHF limited	Rapid quench 100% core	Rapid quench	Rapid quench
Resulting Peak Pressures	∿ 60 psia at vessel failure	∿ 78 psia at vessel failure	111 psia at vessel failure	96 psia at vessel failure	138 psia at burn

TABLE 4.3.6-1

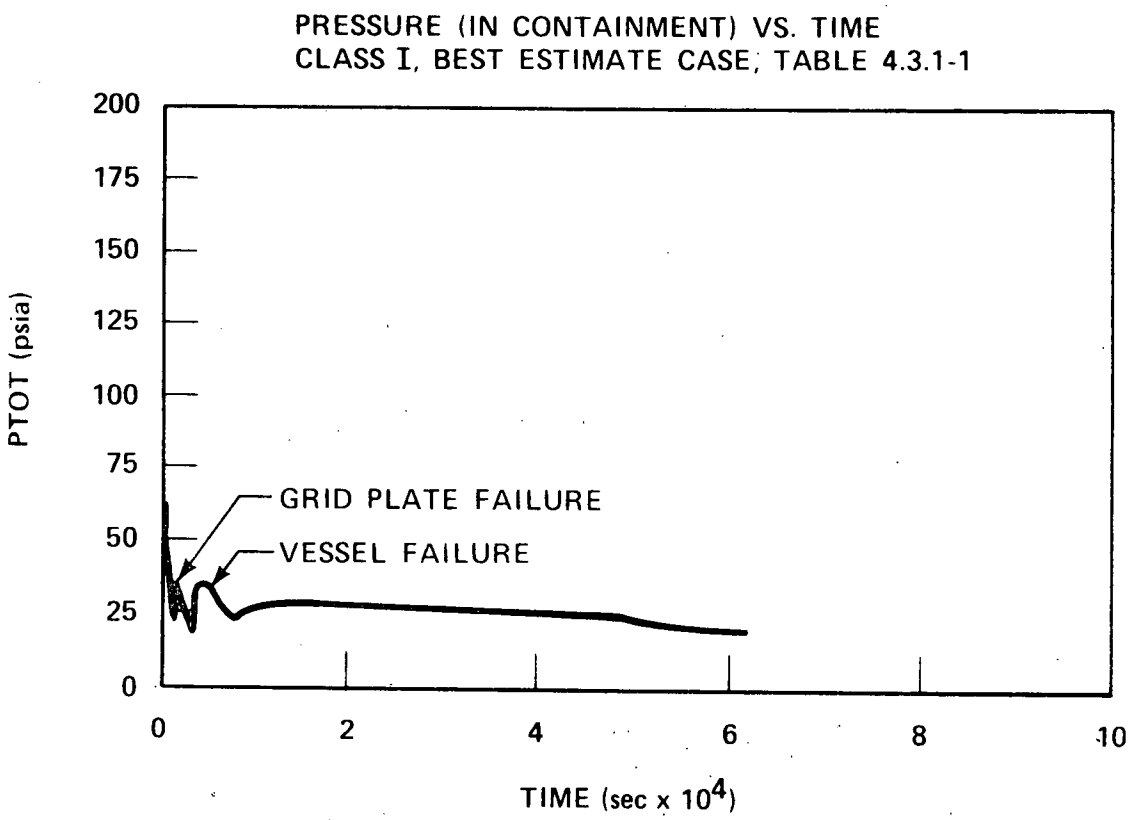

PRESSURE (IN CONTAINMENT) VS. TIME
CLASS I, BEST ESTIMATE CASE; TABLE 4.3.1-1
PTOT (psia)
200
175
150
125
100
75
50
25
0
GRID PLATE FAILURE
VESSEL FAILURE
0
2
4
6
8
10
TIME (sec x 10^4)

Figure 4.3.1-1

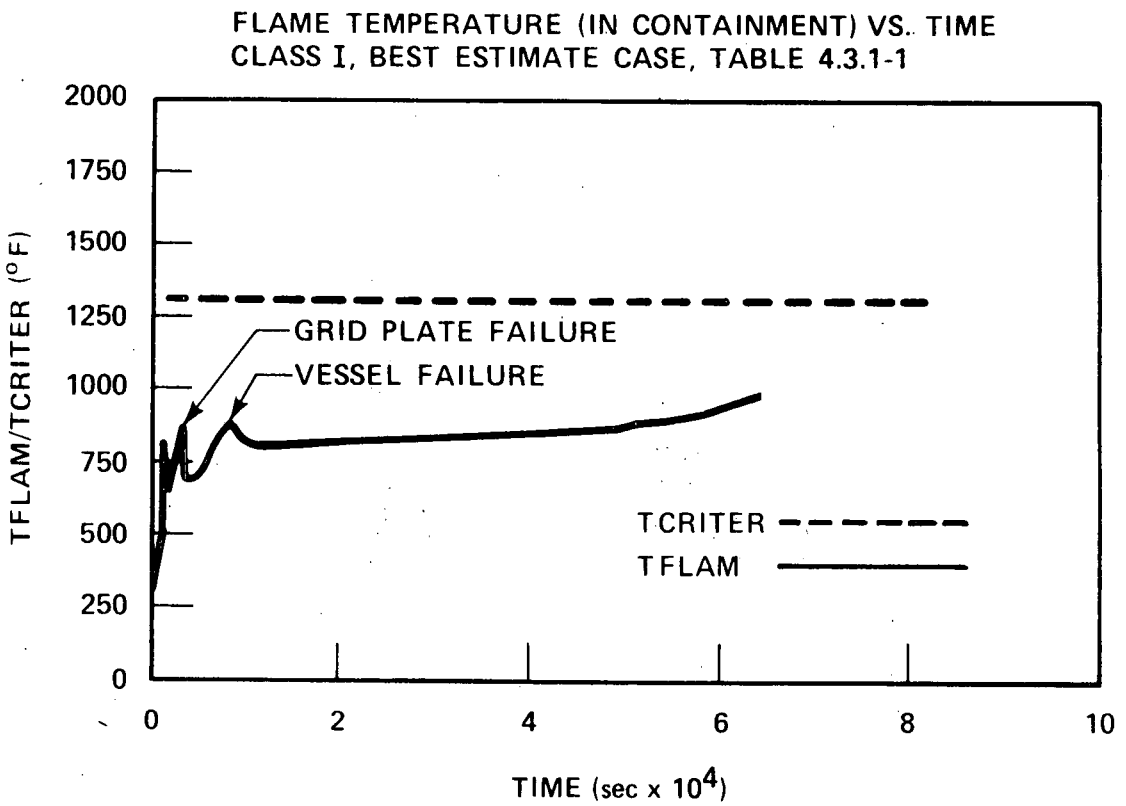

FLAME TEMPERATURE (IN CONTAINMENT) VS. TIME
CLASS I, BEST ESTIMATE CASE, TABLE 4.3.1-1
TFLAM/TCRITER (°F)
2000
1750
1500
1250
1000
750
500
250
0
GRID PLATE FAILURE
VESSEL FAILURE
TCRITER
TFLAM
0
2
4
6
8
10
TIME (sec x 10^4)

Figure 4.3.1-2

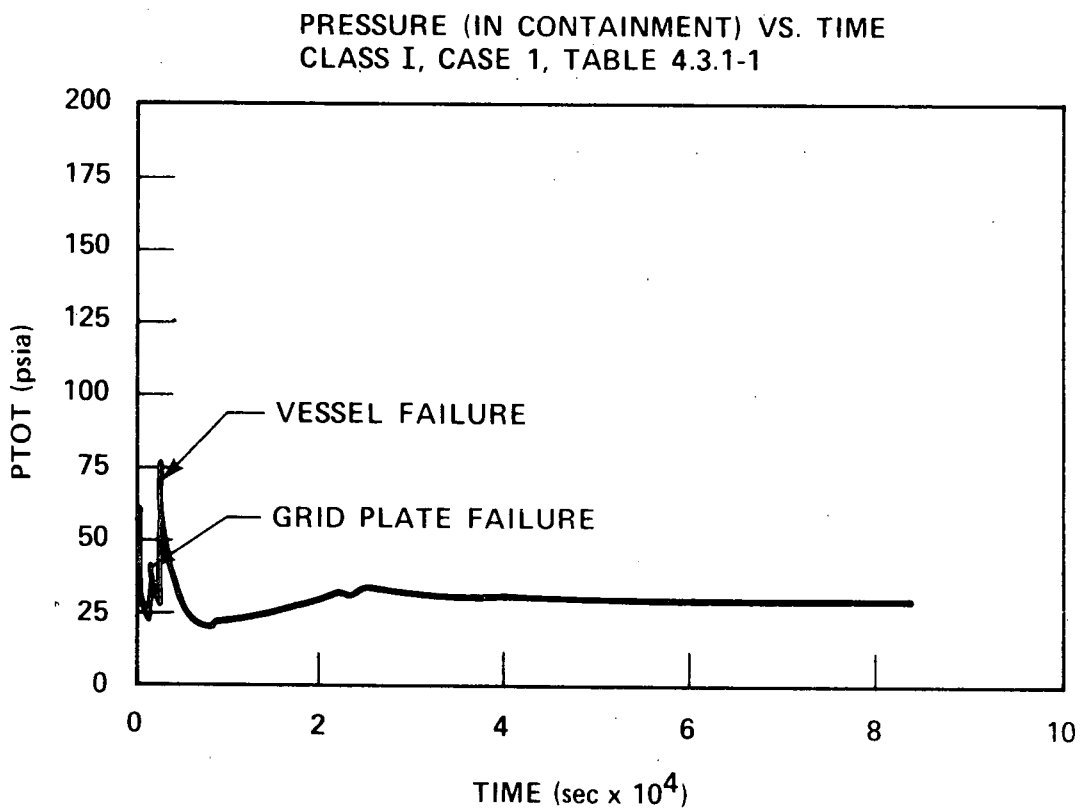

PRESSURE (IN CONTAINMENT) VS. TIME
CLASS I, CASE 1, TABLE 4.3.1-1
PTOT (psia)
200
175
150
125
100
75
50
25
0
VESSEL FAILURE
GRID PLATE FAILURE
0
2
4
6
8
10
TIME (sec x 10^4)

Figure 4.3.1-3

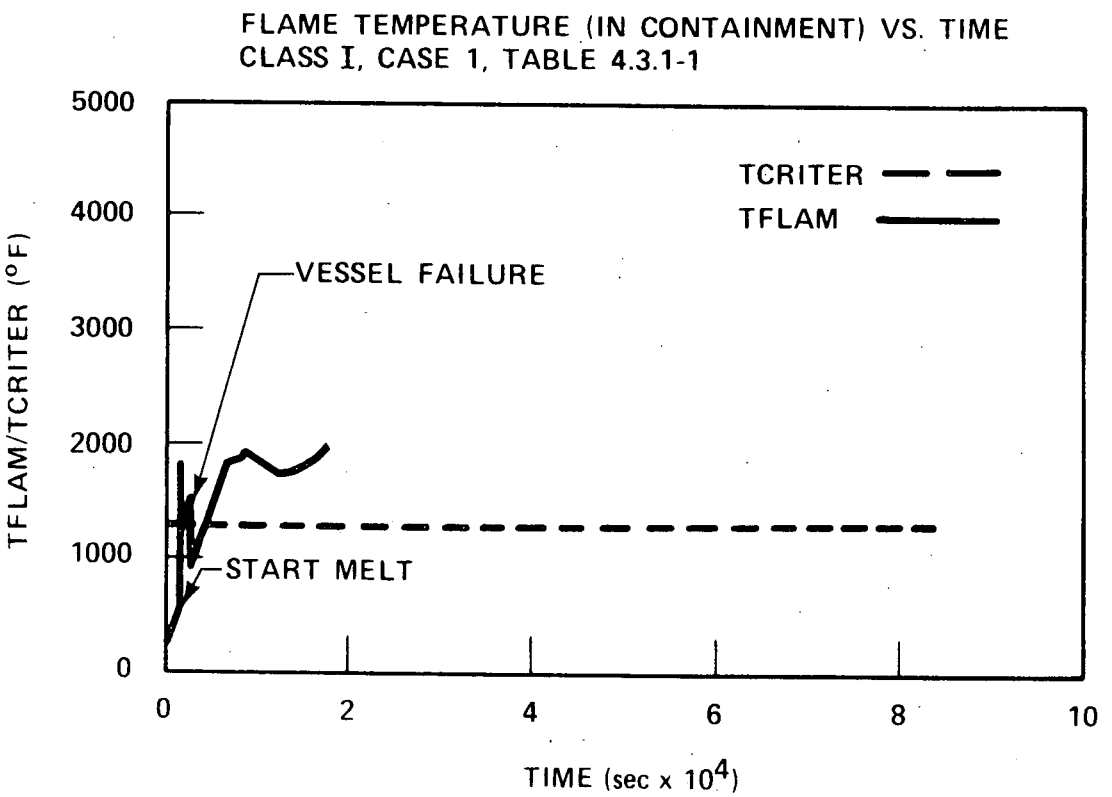

FLAME TEMPERATURE (IN CONTAINMENT) VS. TIME
CLASS I, CASE 1, TABLE 4.3.1-1
TFLAM/TCRITER (°F)
5000
4000
3000
2000
1000
0
TCRITER
TFLAM
VESSEL FAILURE
START MELT
0
2
4
6
8
10
TIME (sec x 10^4)

Figure 4.3.1-4

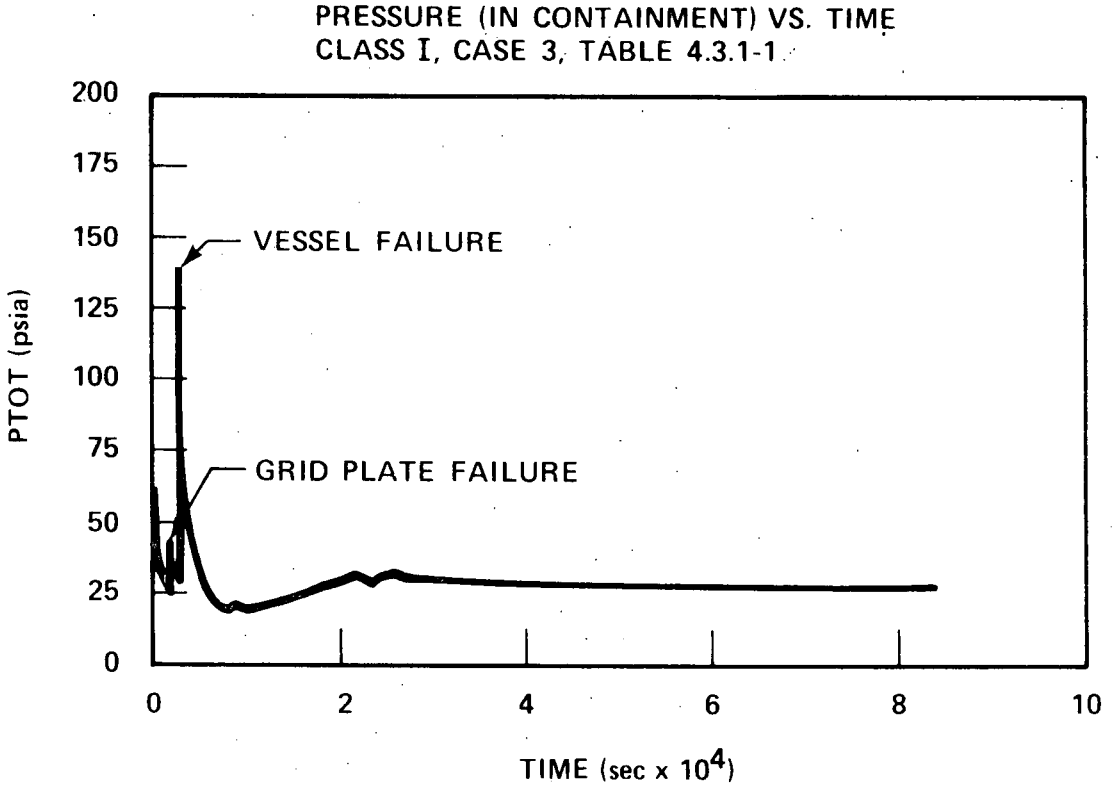

PRESSURE (IN CONTAINMENT) VS. TIME
CLASS I, CASE 3, TABLE 4.3.1-1
PTOT (psia)
200
175
150
125
100
75
50
25
0
VESSEL FAILURE
GRID PLATE FAILURE
0
2
4
6
8
10
TIME (sec x 10^4)

Figure 4.3.1-5

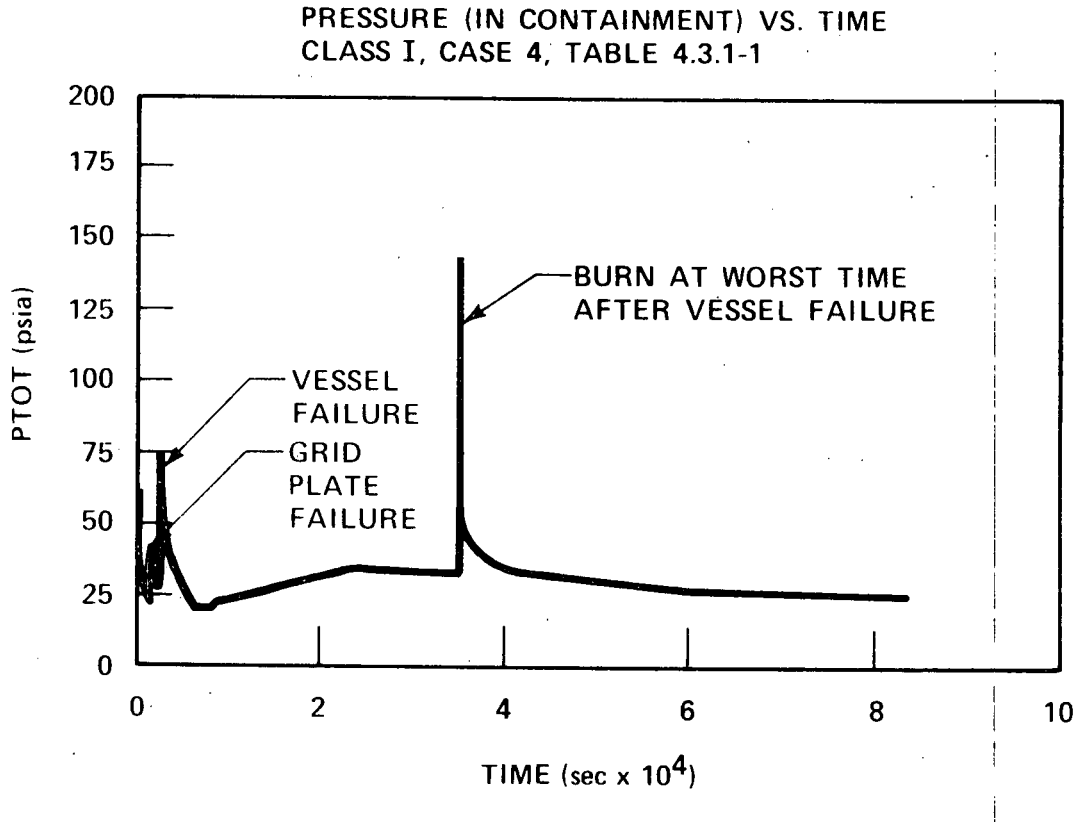

PRESSURE (IN CONTAINMENT) VS. TIME
CLASS I, CASE 4, TABLE 4.3.1-1
PTOT (psia)
200
175
150
125
100
75
50
25
0
BURN AT WORST TIME
AFTER VESSEL FAILURE
VESSEL
FAILURE
GRID
PLATE
FAILURE
0
2
4
6
8
10
TIME (sec x 10^4)

Figure 4.3.1-6

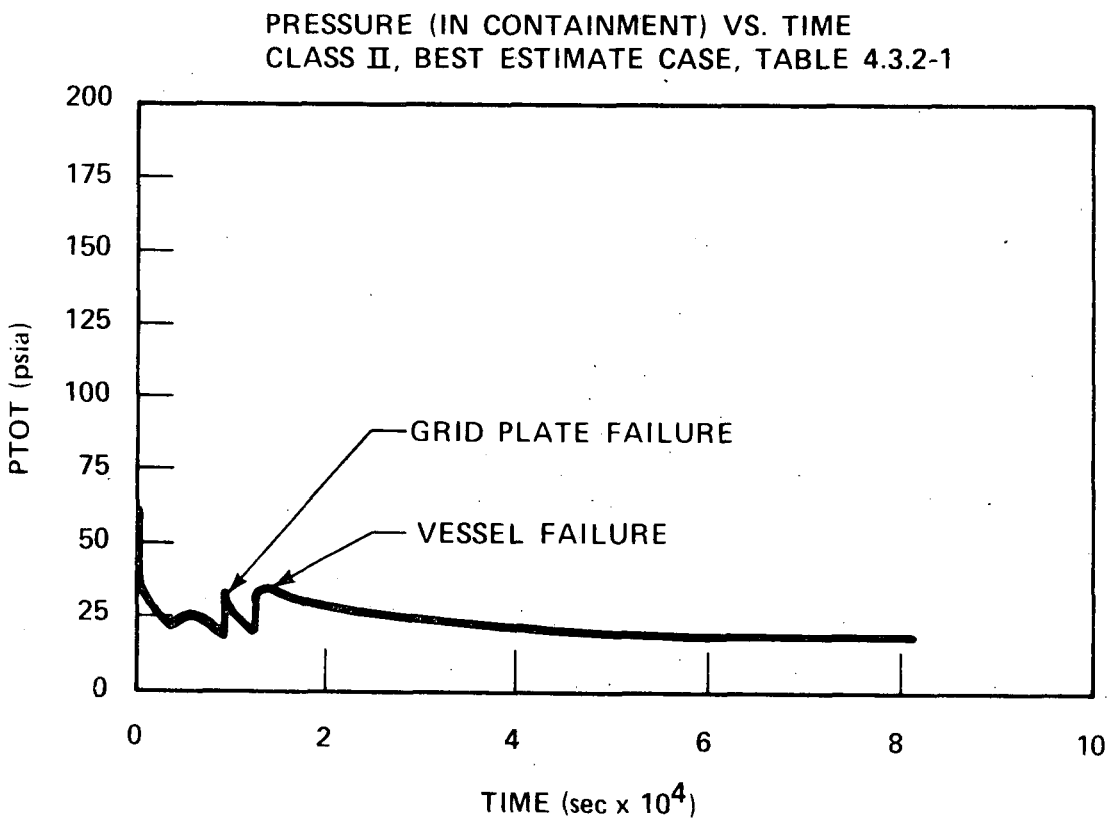

PRESSURE (IN CONTAINMENT) VS. TIME
CLASS II, BEST ESTIMATE CASE, TABLE 4.3.2-1
PTOT (psia)
200
175
150
125
100
75
50
25
0
GRID PLATE FAILURE
VESSEL FAILURE
0
2
4
6
8
10
TIME (sec x 10^4)

Figure 4.3.2-1

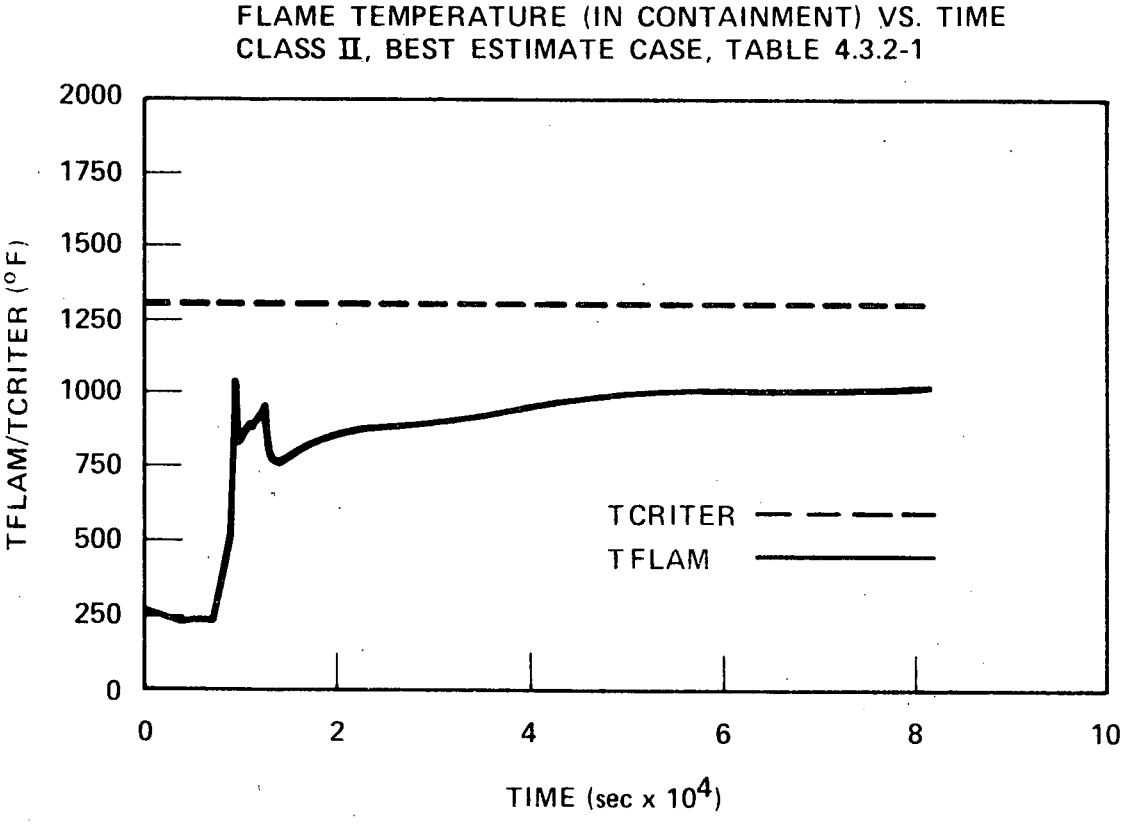

FLAME TEMPERATURE (IN CONTAINMENT) VS. TIME
CLASS II, BEST ESTIMATE CASE, TABLE 4.3.2-1
TFLAM/TCRITER (°F)
2000
1750
1500
1250
1000
750
500
250
0
0
2
4
6
8
10
TIME (sec x 10^4)
TCRITER
TFLAM

Figure 4.3.2-2

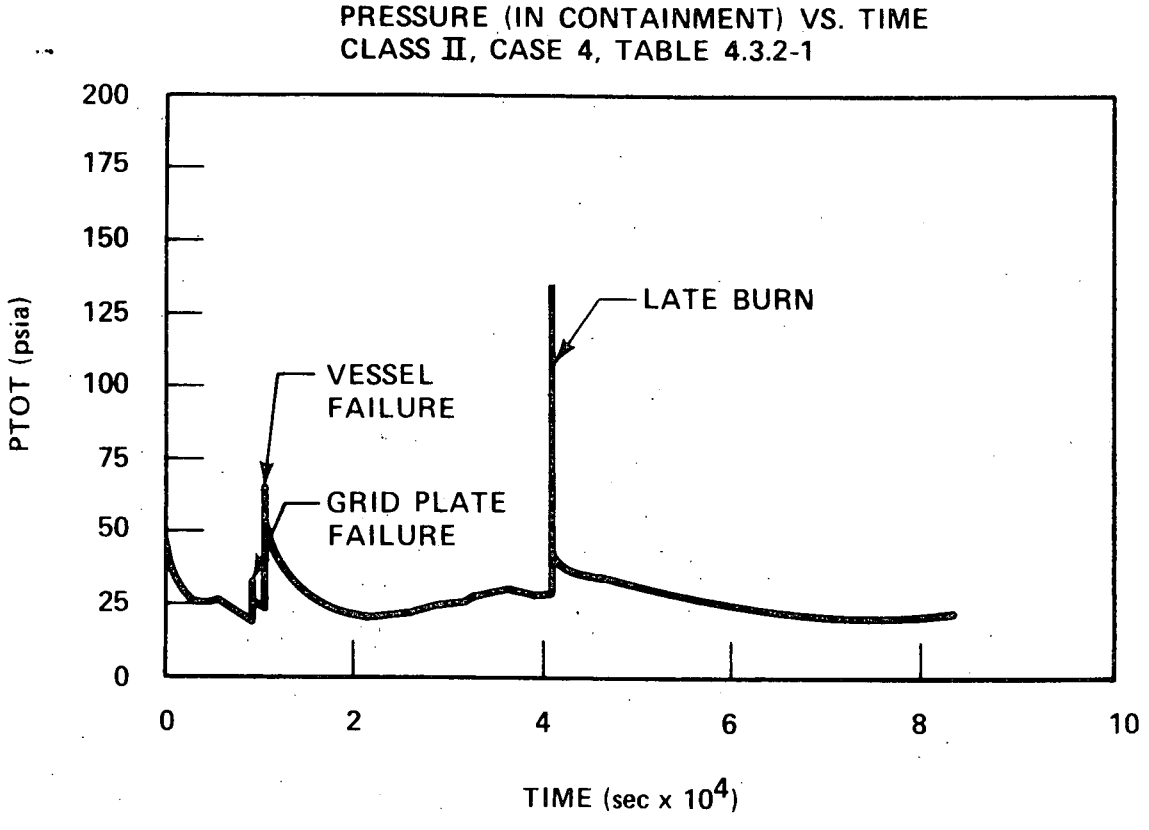

PRESSURE (IN CONTAINMENT) VS. TIME
CLASS II, CASE 4, TABLE 4.3.2-1
PTOT (psia)
200
175
150
125
100
75
50
25
0
VESSEL FAILURE
GRID PLATE FAILURE
LATE BURN
0
2
4
6
8
10
TIME (sec x 10^4)

Figure 4.3.2-3

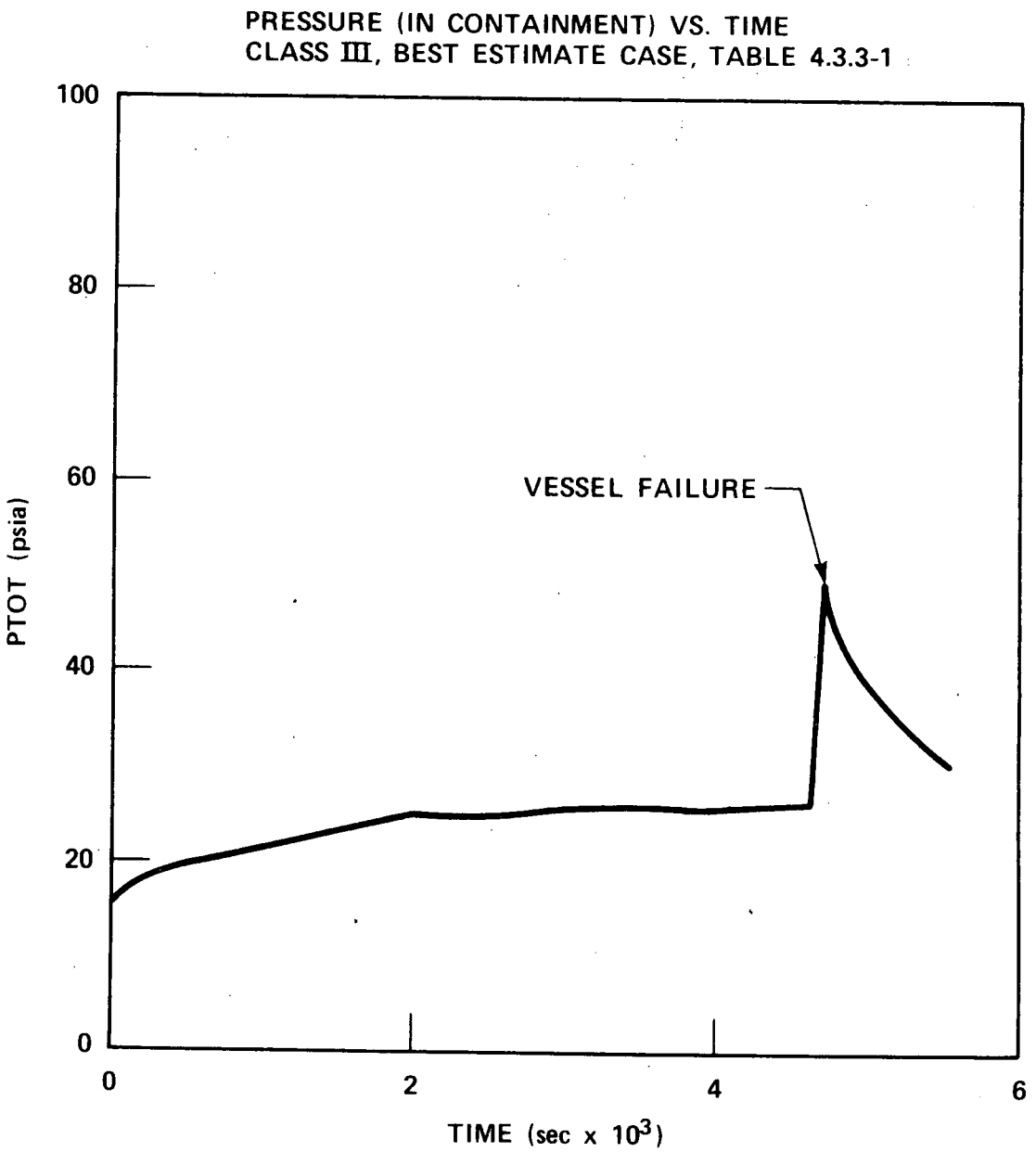
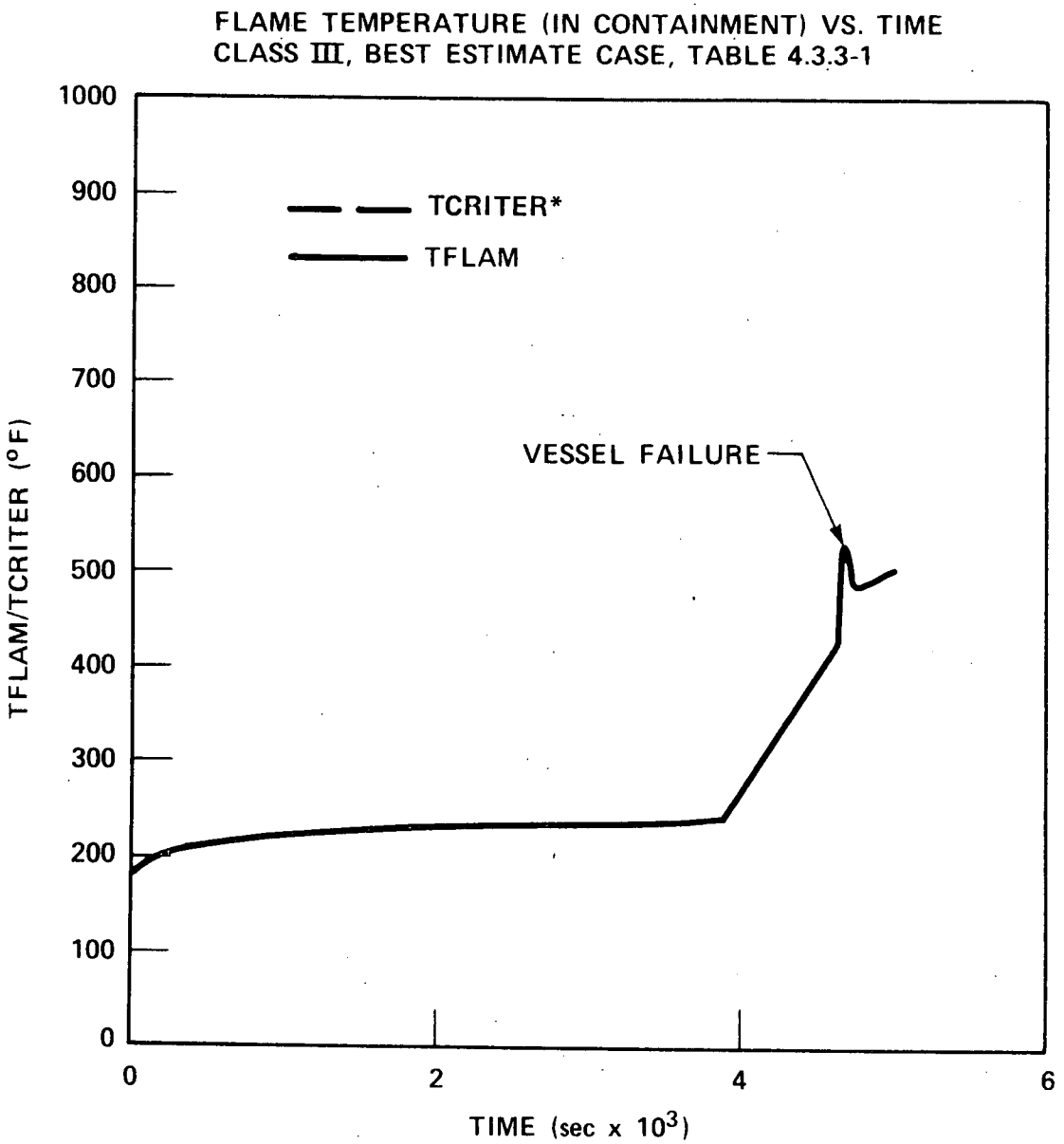

PRESSURE (IN CONTAINMENT) VS. TIME
CLASS III, BEST ESTIMATE CASE, TABLE 4.3.3-1
100
80
60
40
20
0
PTOT (psia)
VESSEL FAILURE
0
2
4
6
TIME (sec x 10³)

Figure 4.3.3-1



*TCRITER = 1310°F AND IS OFF THE SCALE OF THIS GRAPH

Figure 4.3.3-2

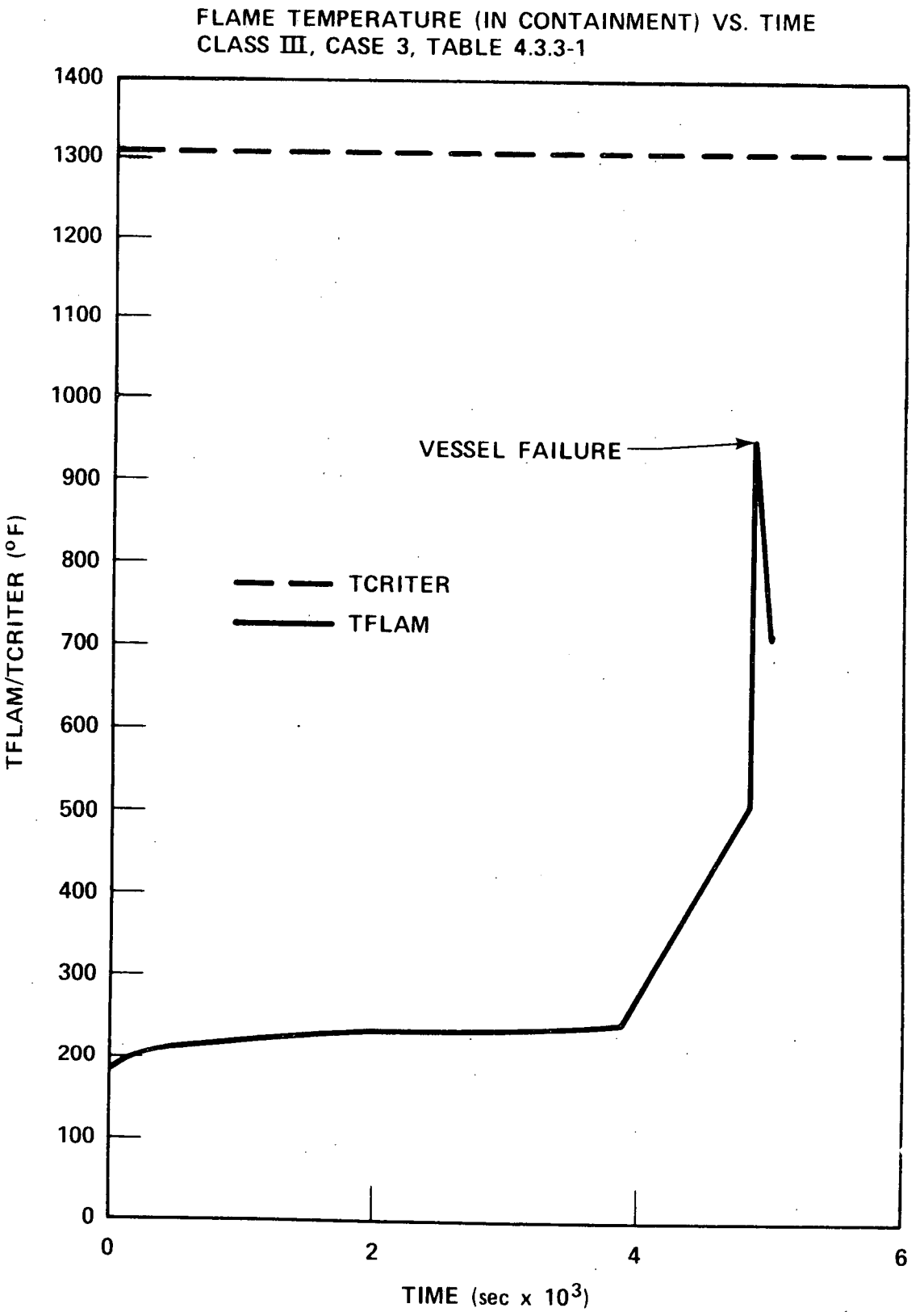

FLAME TEMPERATURE (IN CONTAINMENT) VS. TIME
CLASS III, CASE 3, TABLE 4.3.3-1
1400
1300
1200
1100
1000
900
800
700
600
500
400
300
200
100
0
TFLAM/TCRITER (°F)
VESSEL FAILURE
TCRITER
TFLAM
0
2
4
6
TIME (sec x 10³)

Figure 4.3.3-3

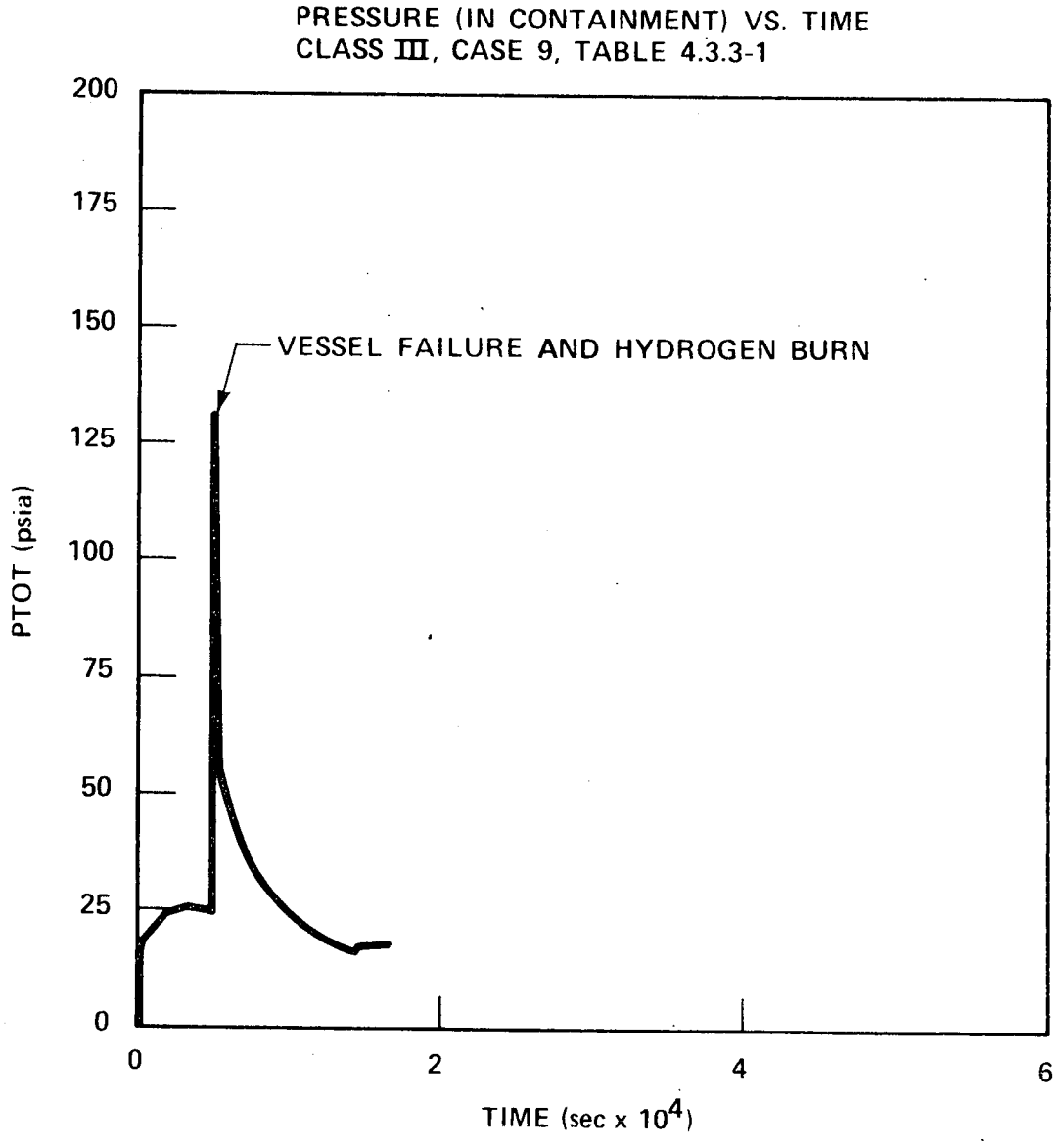

PRESSURE (IN CONTAINMENT) VS. TIME
CLASS III, CASE 9, TABLE 4.3.3-1
200
175
150
125
100
75
50
25
0
PTOT (psia)
VESSEL FAILURE AND HYDROGEN BURN
0
2
4
6
TIME (sec x 10^4)

Figure 4.3.3-4

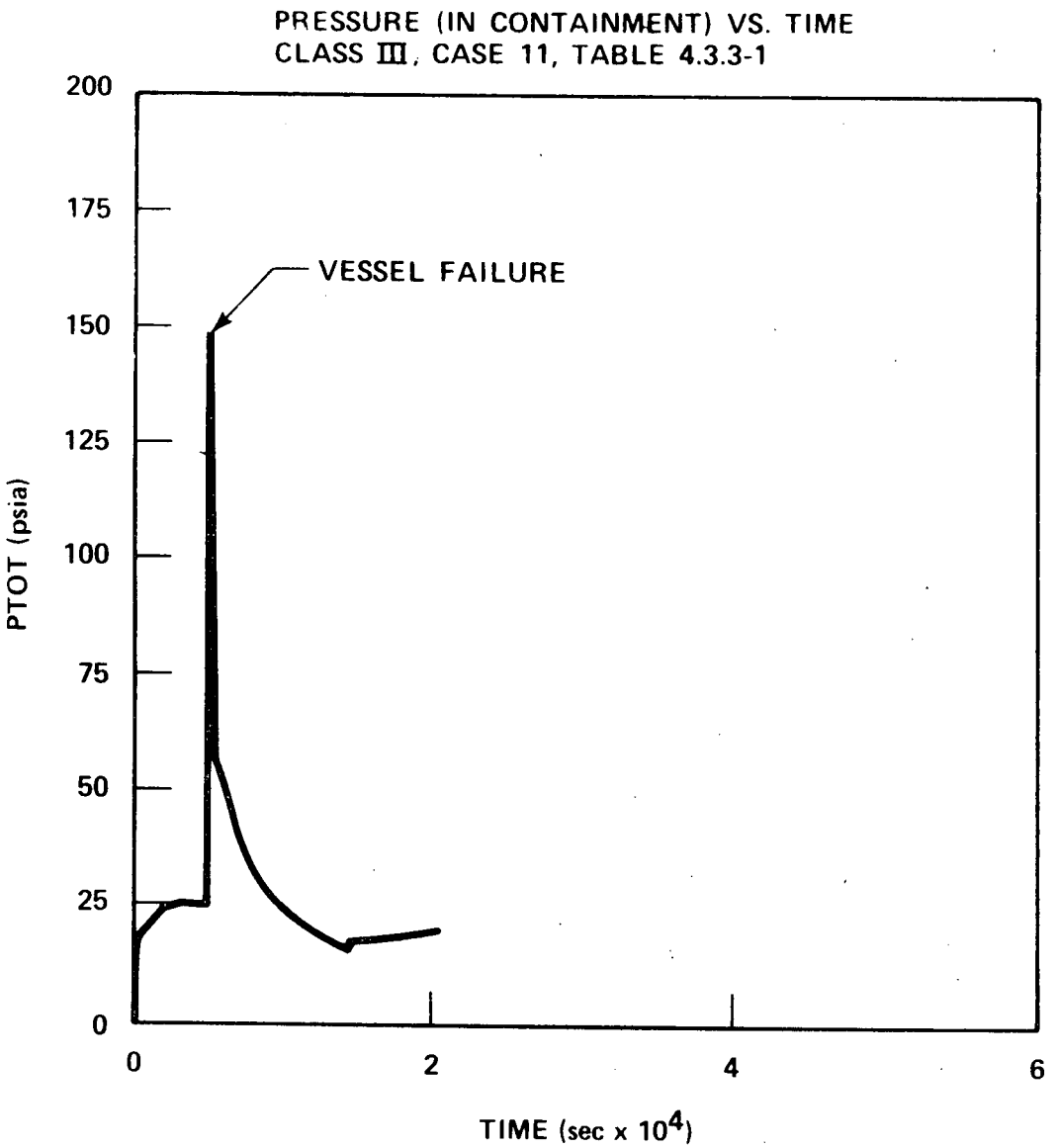

PRESSURE (IN CONTAINMENT) VS. TIME
CLASS III, CASE 11, TABLE 4.3.3-1
200
175
150
125
100
75
50
25
0
PTOT (psia)
VESSEL FAILURE
0
2
4
6
TIME (sec x 10^4)

Figure 4.3.3-5

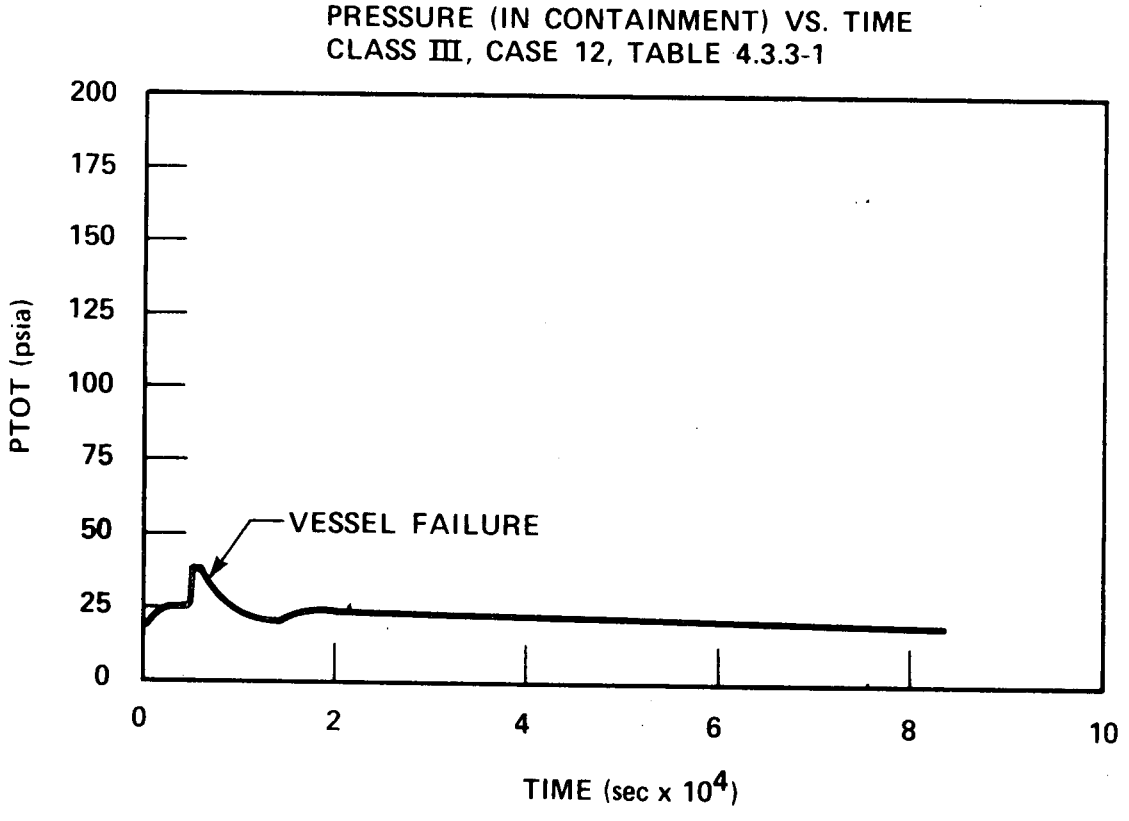

PRESSURE (IN CONTAINMENT) VS. TIME
CLASS III, CASE 12, TABLE 4.3.3-1
PTOT (psia)
200
175
150
125
100
75
50
25
0
VESSEL FAILURE
0
2
4
6
8
10
TIME (sec x 10^4)

Figure 4.3.3-6

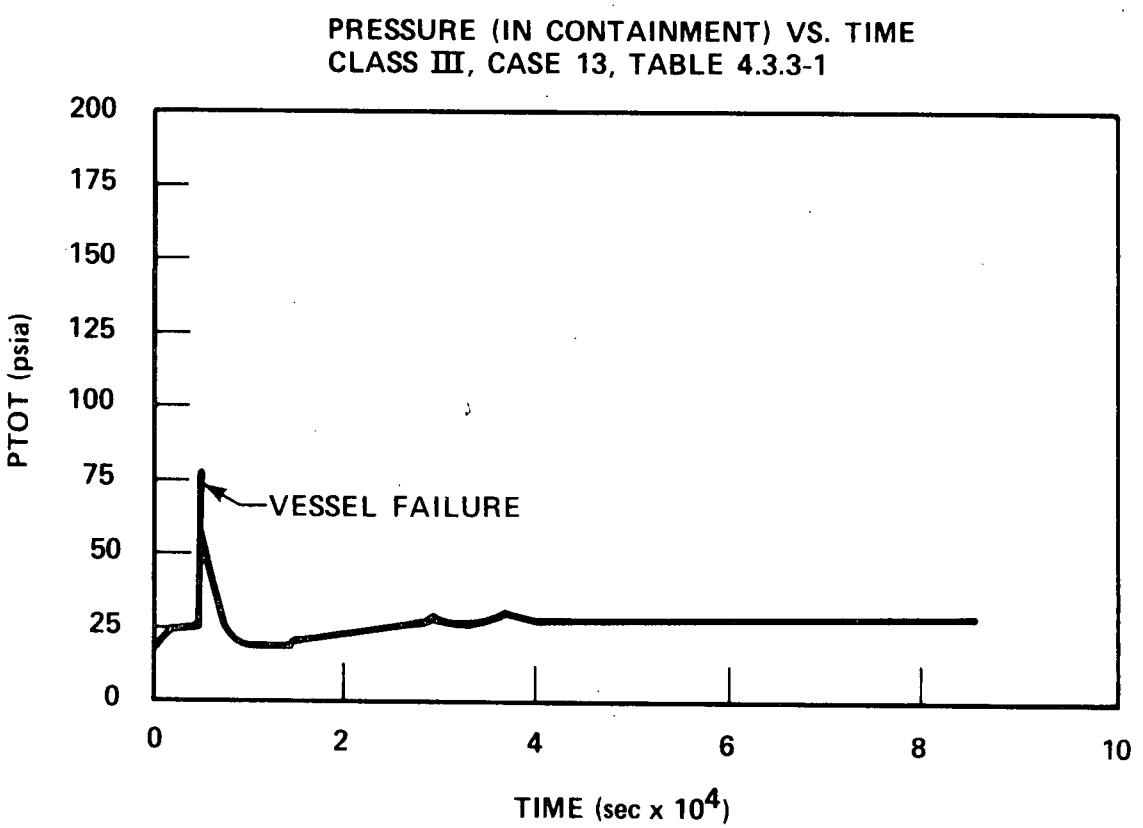

PRESSURE (IN CONTAINMENT) VS. TIME
CLASS III, CASE 13, TABLE 4.3.3-1
PTOT (psia)
200
175
150
125
100
75
50
25
0
VESSEL FAILURE
0
2
4
6
8
10
TIME (sec x 10^4)

Figure 4.3.3-7

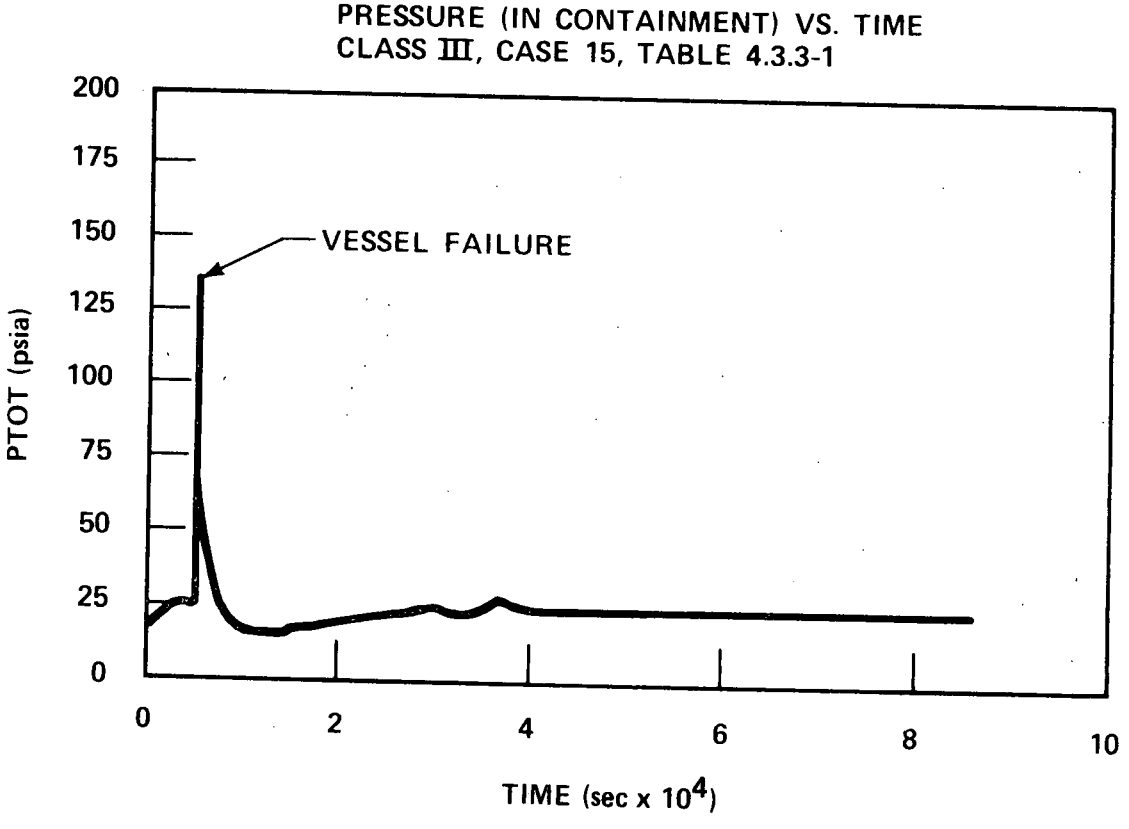

PRESSURE (IN CONTAINMENT) VS. TIME
CLASS III, CASE 15, TABLE 4.3.3-1
200
175
150
125
100
75
50
25
0
PTOT (psia)
VESSEL FAILURE
0
2
4
6
8
10
TIME (sec x 10^4)

Figure 4.3.3-8

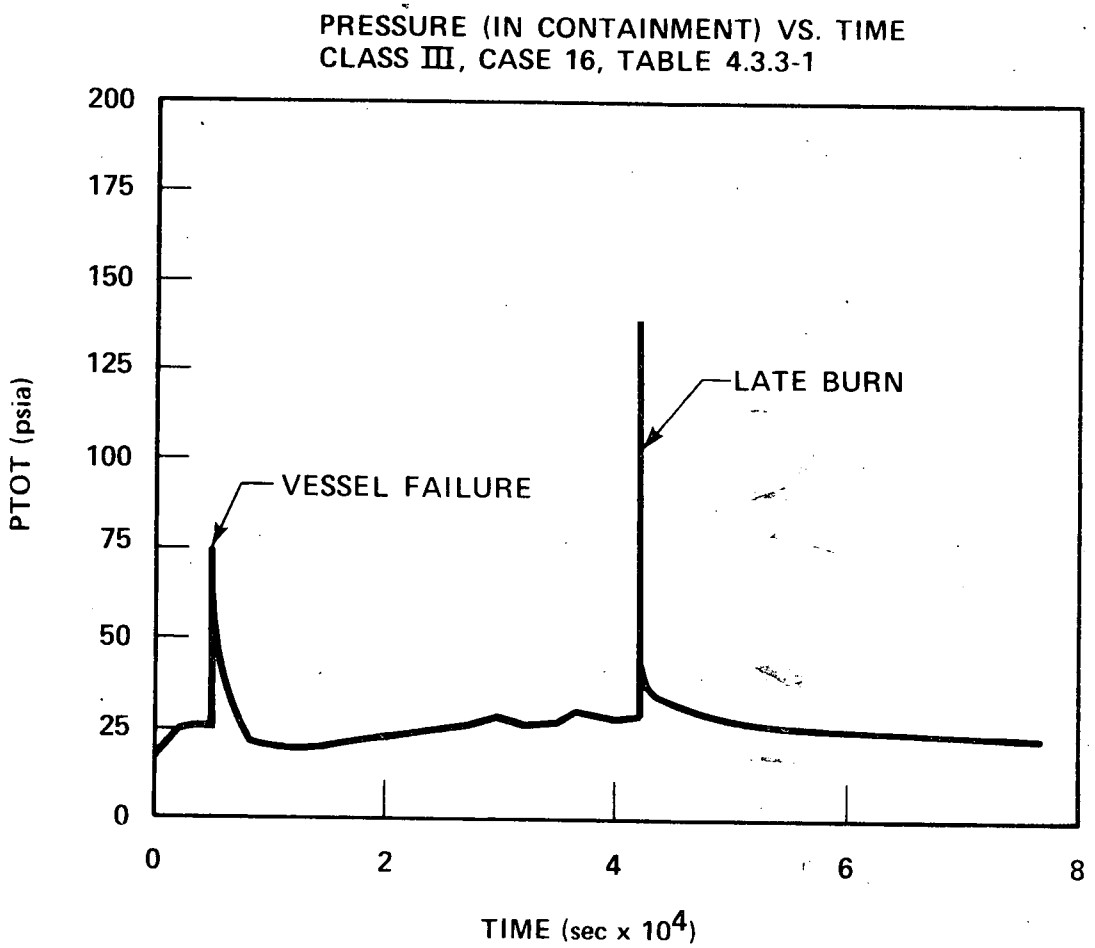

PRESSURE (IN CONTAINMENT) VS. TIME
CLASS III, CASE 16, TABLE 4.3.3-1
PTOT (psia)
200
175
150
125
100
75
50
25
0
VESSEL FAILURE
LATE BURN
0
2
4
6
8
TIME (sec x 10^4)

Figure 4.3.3-9

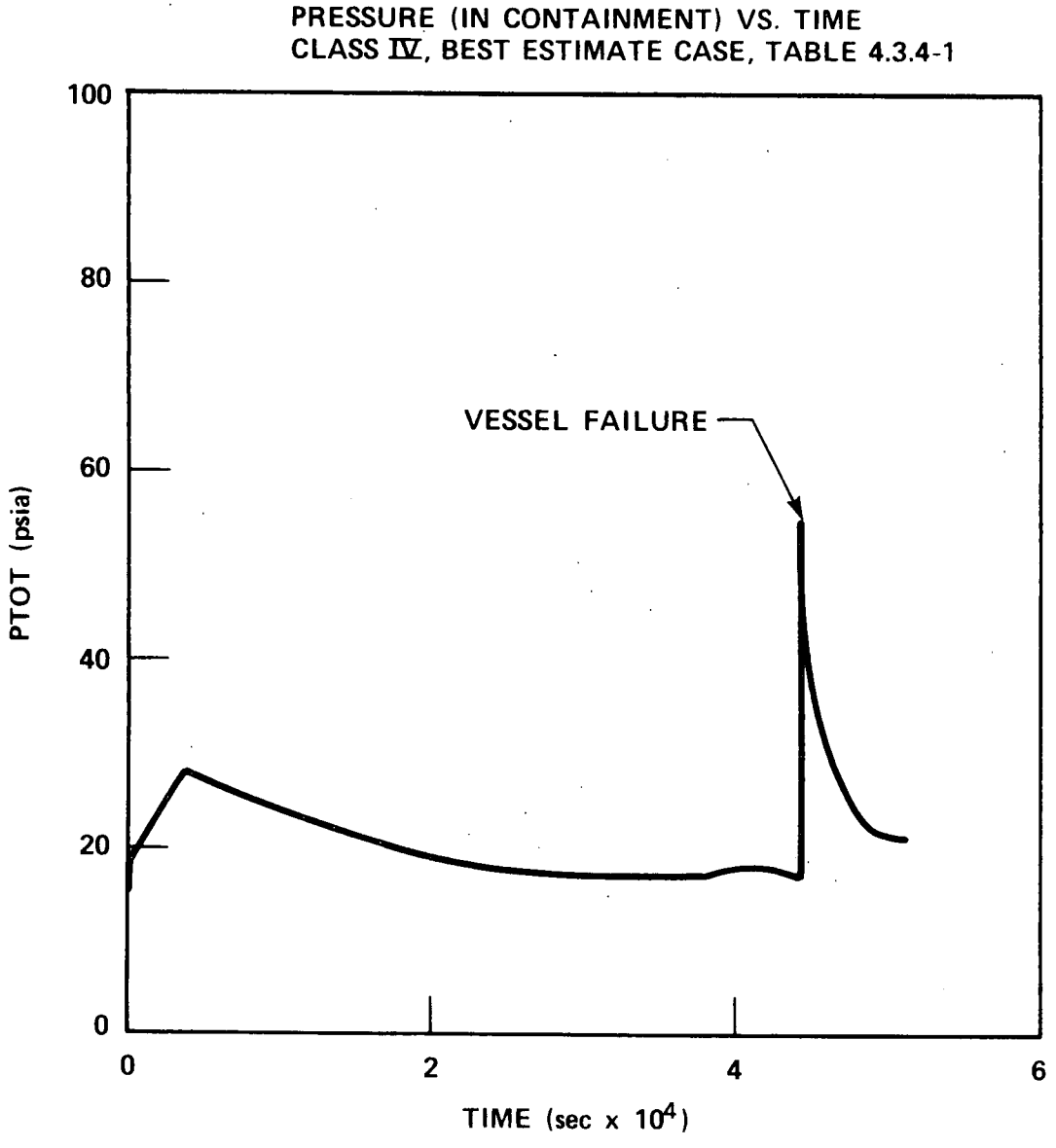

PRESSURE (IN CONTAINMENT) VS. TIME
CLASS IV, BEST ESTIMATE CASE, TABLE 4.3.4-1
100
80
60
40
20
0
PTOT (psia)
VESSEL FAILURE
0
2
4
6
TIME (sec x 10^4)

Figure 4.3.4-1

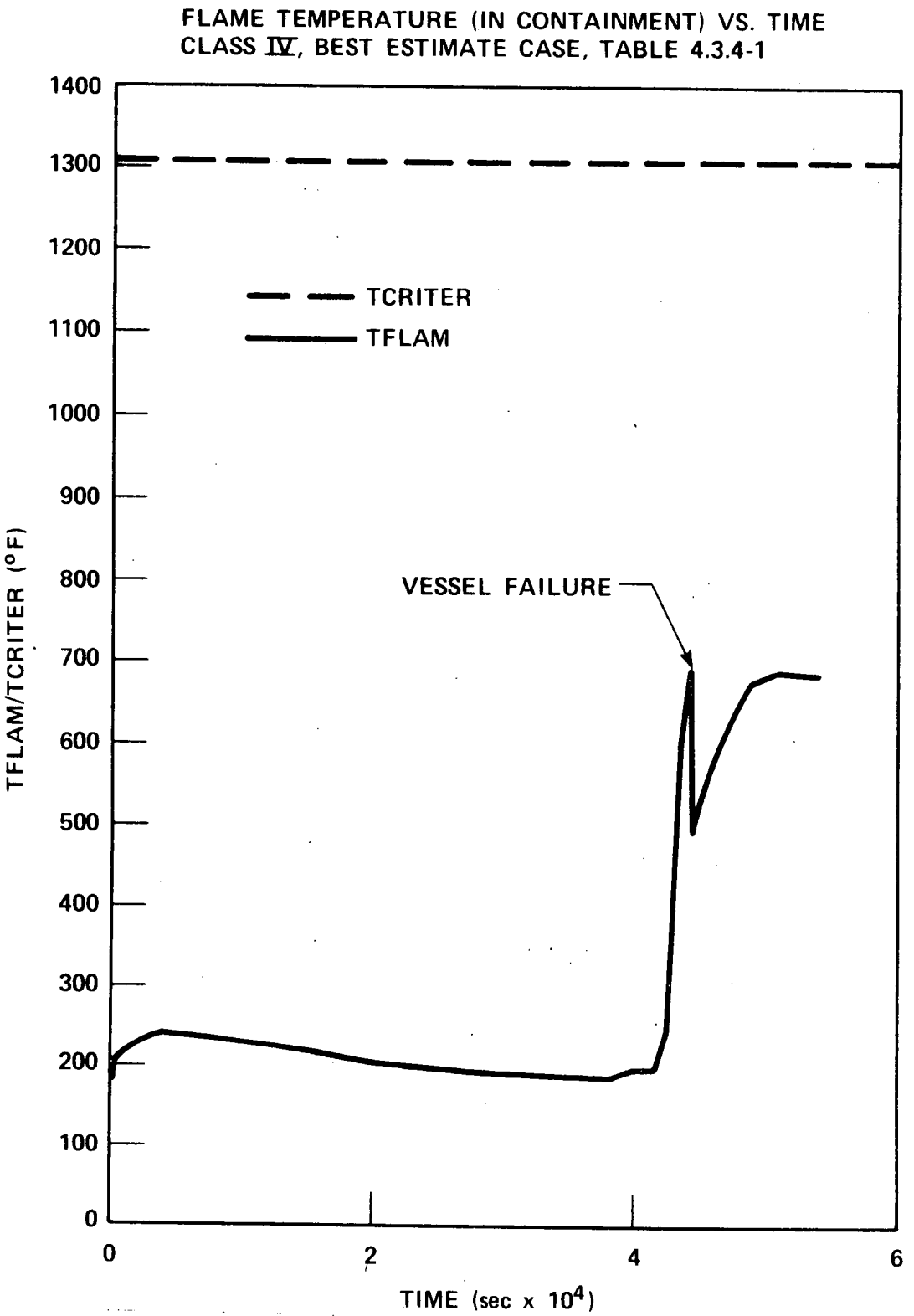

FLAME TEMPERATURE (IN CONTAINMENT) VS. TIME
CLASS IV, BEST ESTIMATE CASE, TABLE 4.3.4-1
TCRITER
TFLAM
VESSEL FAILURE
TFLAM/TCRITER (°F)
TIME (sec x 10^4)
1400
1300
1200
1100
1000
900
800
700
600
500
400
300
200
100
0
0
2
4
6

Figure 4.3.4-2

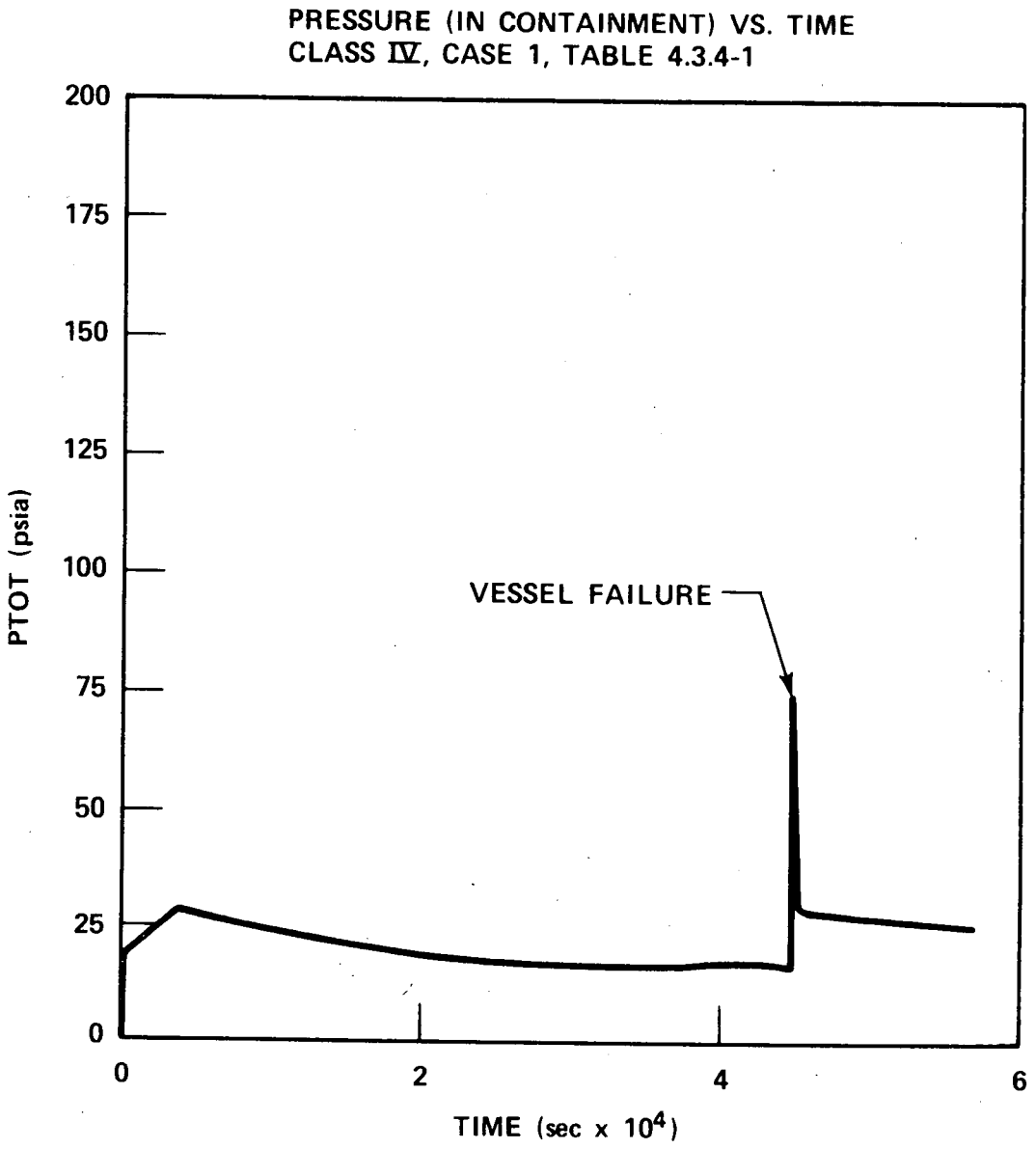

PRESSURE (IN CONTAINMENT) VS. TIME
CLASS IV, CASE 1, TABLE 4.3.4-1
PTOT (psia)
200
175
150
125
100
75
50
25
0
VESSEL FAILURE
0
2
4
6
TIME (sec x 10^4)

Figure 4.3.4-3

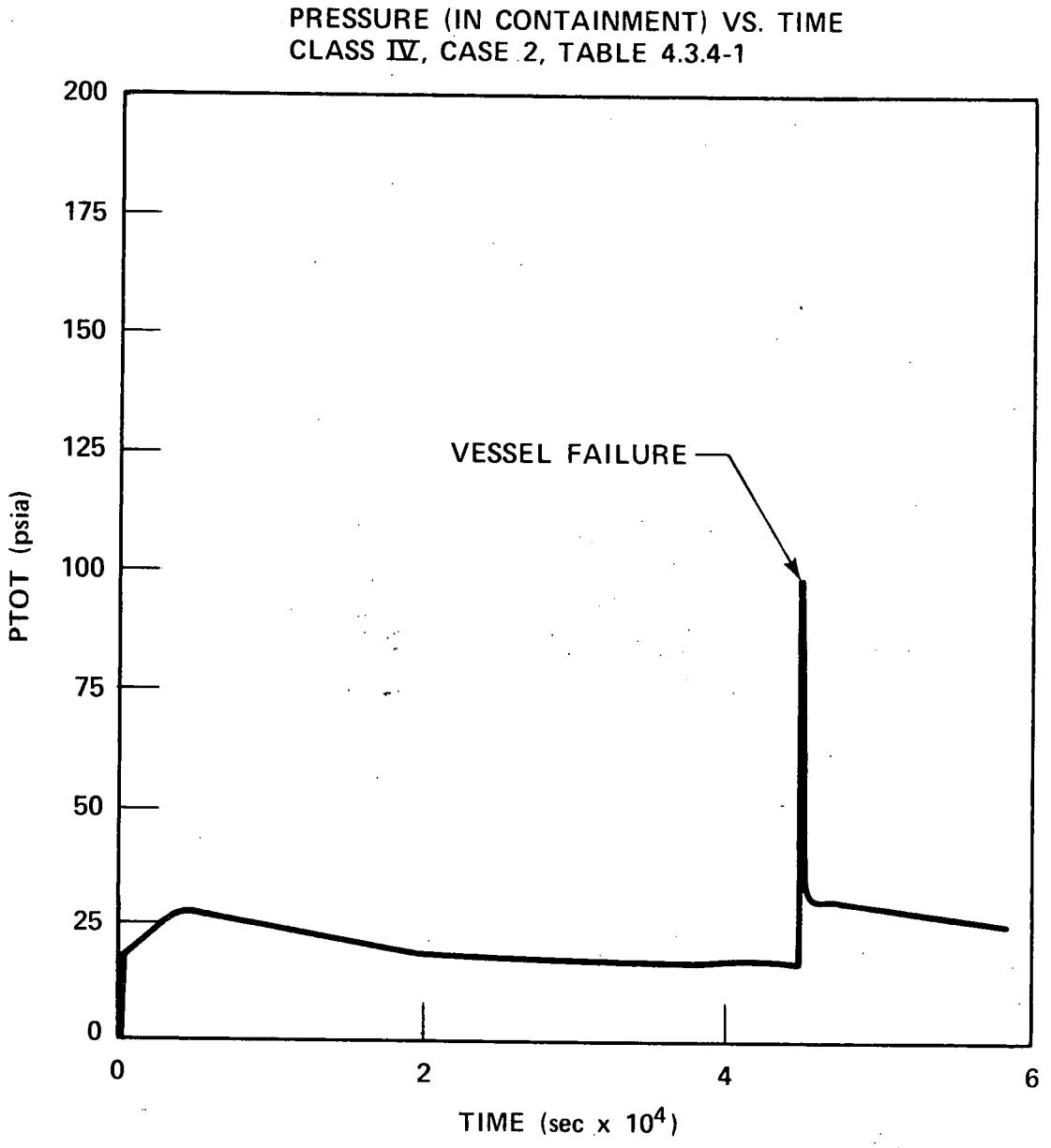

PRESSURE (IN CONTAINMENT) VS. TIME
CLASS IV, CASE 2, TABLE 4.3.4-1
200
175
150
125
100
75
50
25
0
PTOT (psia)
VESSEL FAILURE
0
2
4
6
TIME (sec x 10^4)

Figure 4.3.4-4

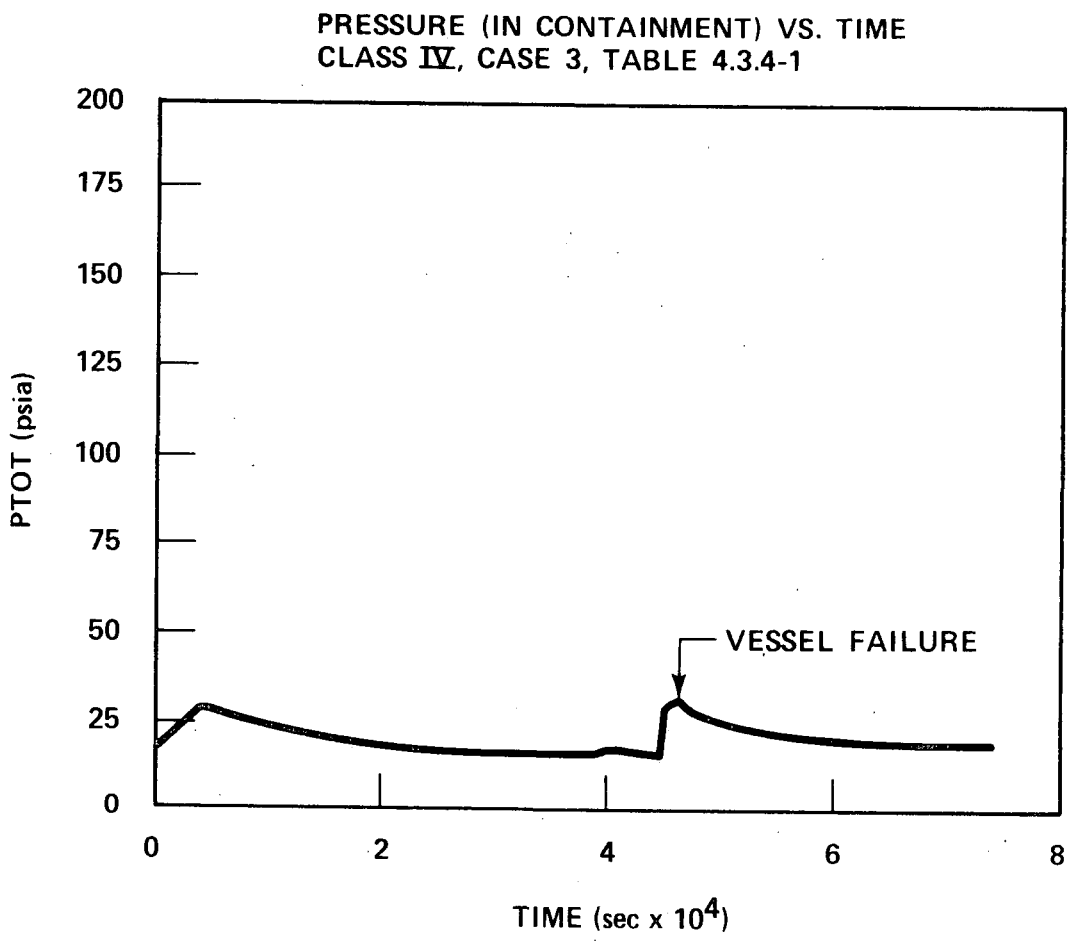

PRESSURE (IN CONTAINMENT) VS. TIME
CLASS IV, CASE 3, TABLE 4.3.4-1
PTOT (psia)
200
175
150
125
100
75
50
25
0
VESSEL FAILURE
0
2
4
6
8
TIME (sec x 10^4)

Figure 4.3.4-5

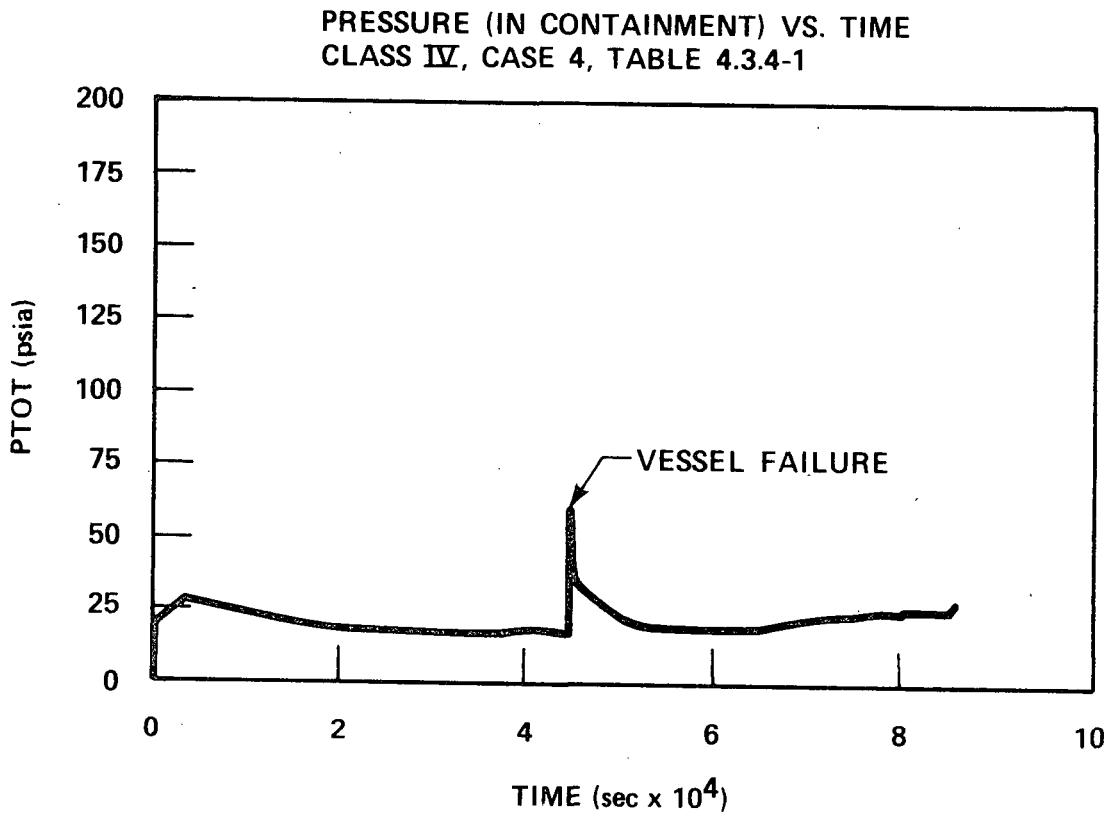

PRESSURE (IN CONTAINMENT) VS. TIME
CLASS IV, CASE 4, TABLE 4.3.4-1
PTOT (psia)
200
175
150
125
100
75
50
25
0
VESSEL FAILURE
0
2
4
6
8
10
TIME (sec x 10^4)

Figure 4.3.4-6

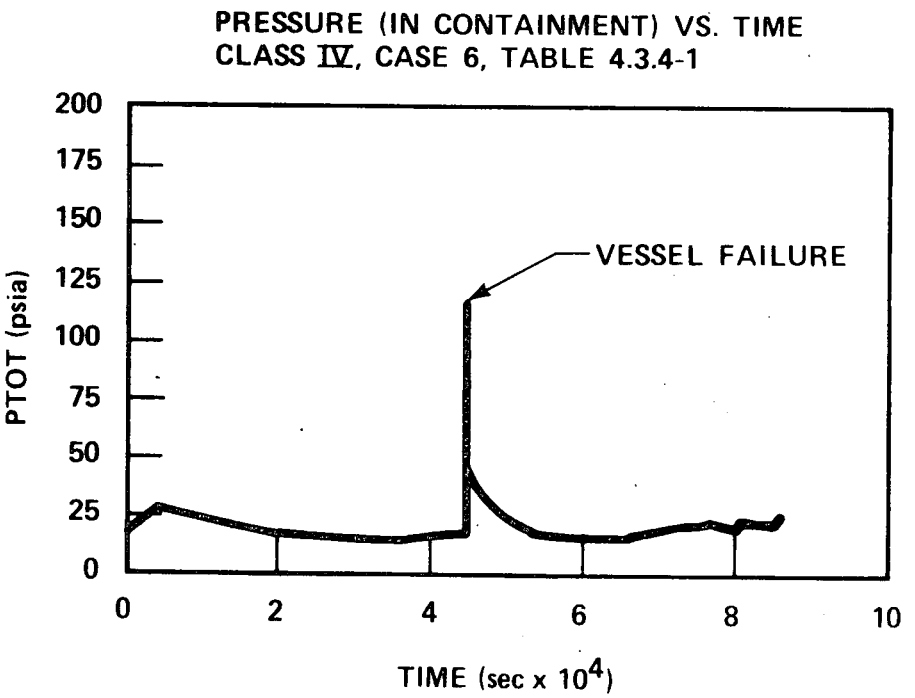

PRESSURE (IN CONTAINMENT) VS. TIME
CLASS IV, CASE 6, TABLE 4.3.4-1
PTOT (psia)
200
175
150
125
100
75
50
25
0
VESSEL FAILURE
0
2
4
6
8
10
TIME (sec x 10^4)

Figure 4.3.4-7

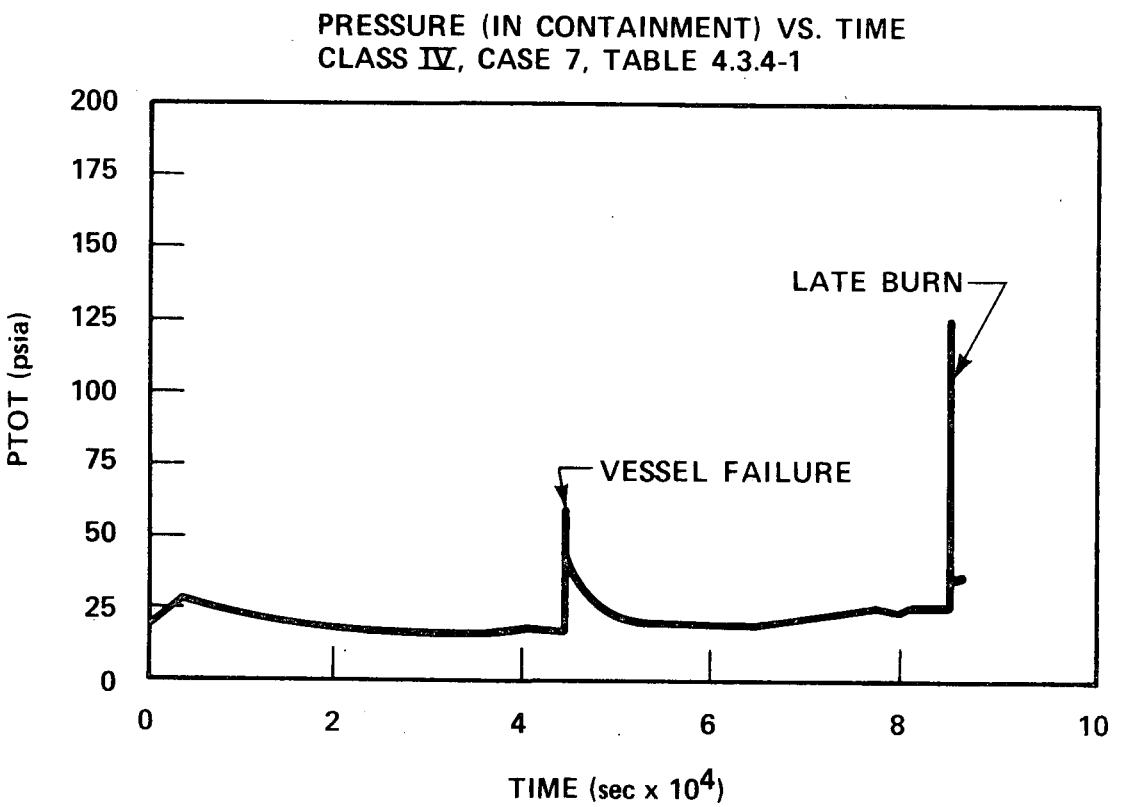

PRESSURE (IN CONTAINMENT) VS. TIME
CLASS IV, CASE 7, TABLE 4.3.4-1
PTOT (psia)
200
175
150
125
100
75
50
25
0
LATE BURN
VESSEL FAILURE
0
2
4
6
8
10
TIME (sec x 10^4)

Figure 4.3.4-8

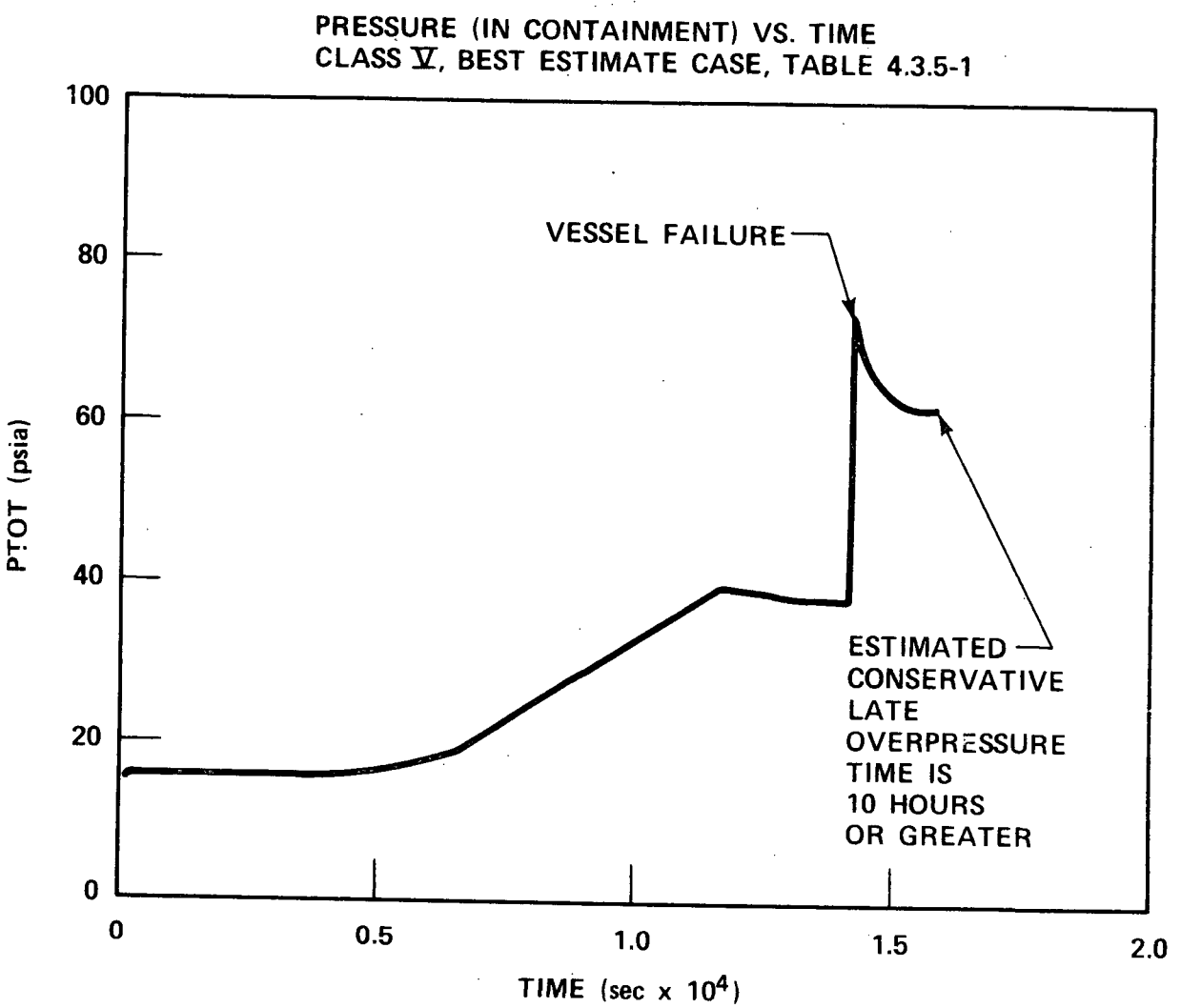
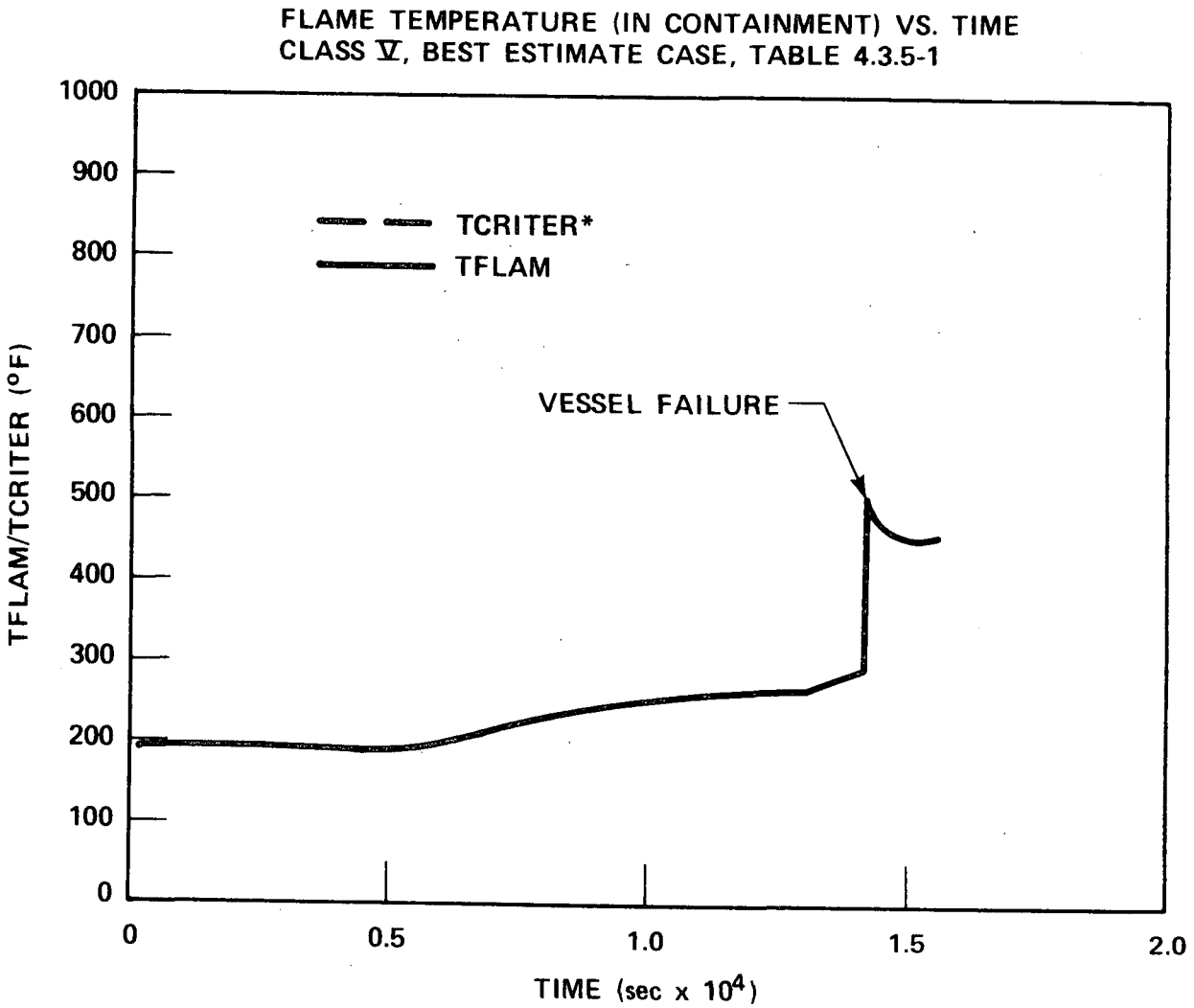

PRESSURE (IN CONTAINMENT) VS. TIME
CLASS V, BEST ESTIMATE CASE, TABLE 4.3.5-1
100
80
60
40
20
0
PTOT (psia)
VESSEL FAILURE
ESTIMATED
CONSERVATIVE
LATE
OVERPRESSURE
TIME IS
10 HOURS
OR GREATER
0
0.5
1.0
1.5
2.0
TIME (sec x 10^4)

Figure 4.3.5-1



*TCRITER = 1310°F AND IS OFF THE SCALE OF THIS GRAPH

Figure 4.3.5-2

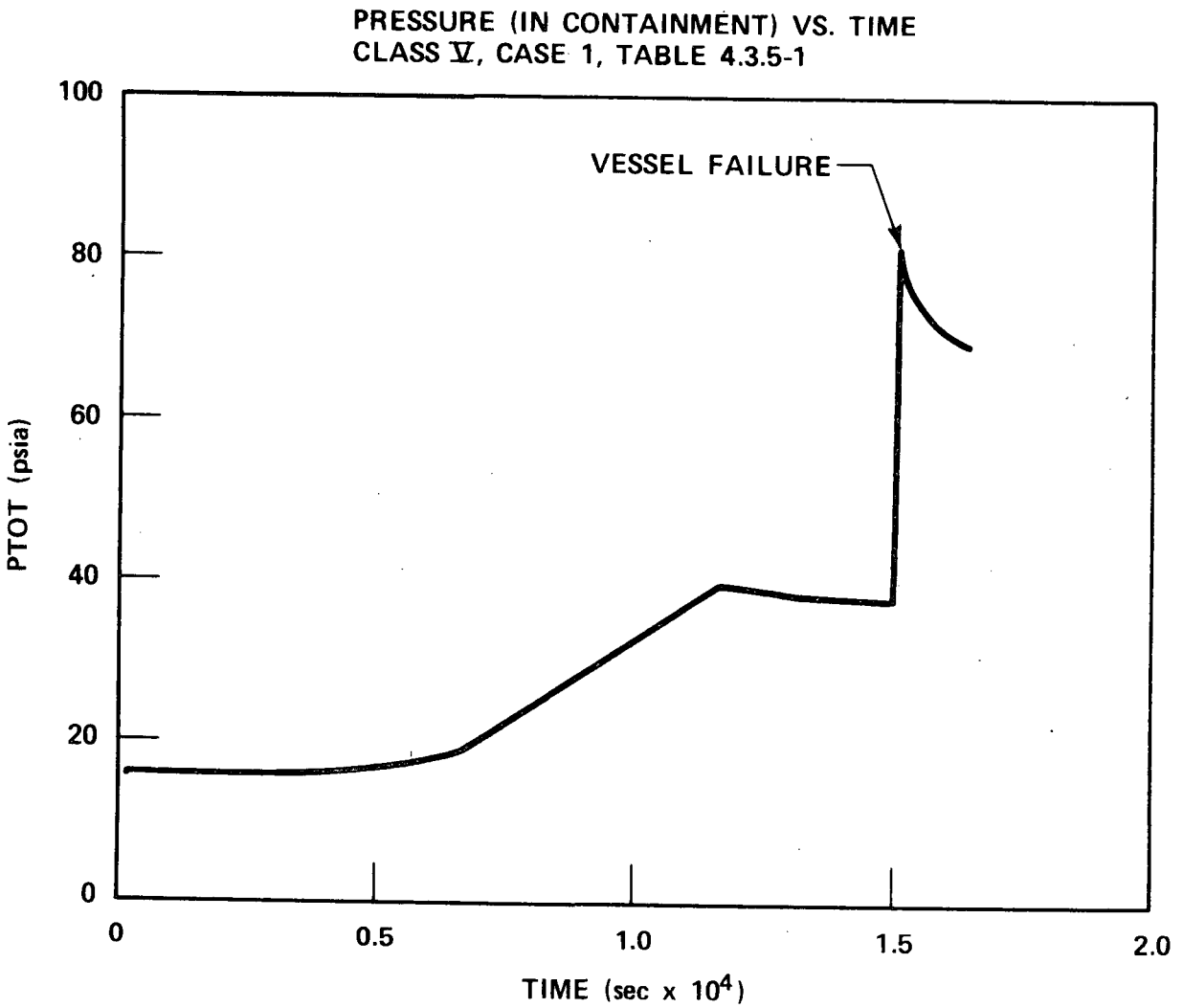

PRESSURE (IN CONTAINMENT) VS. TIME
CLASS V, CASE 1, TABLE 4.3.5-1
VESSEL FAILURE
PTOT (psia)
100
80
60
40
20
0
0
0.5
1.0
1.5
2.0
TIME (sec x 10^4)

Figure 4.3.5-3

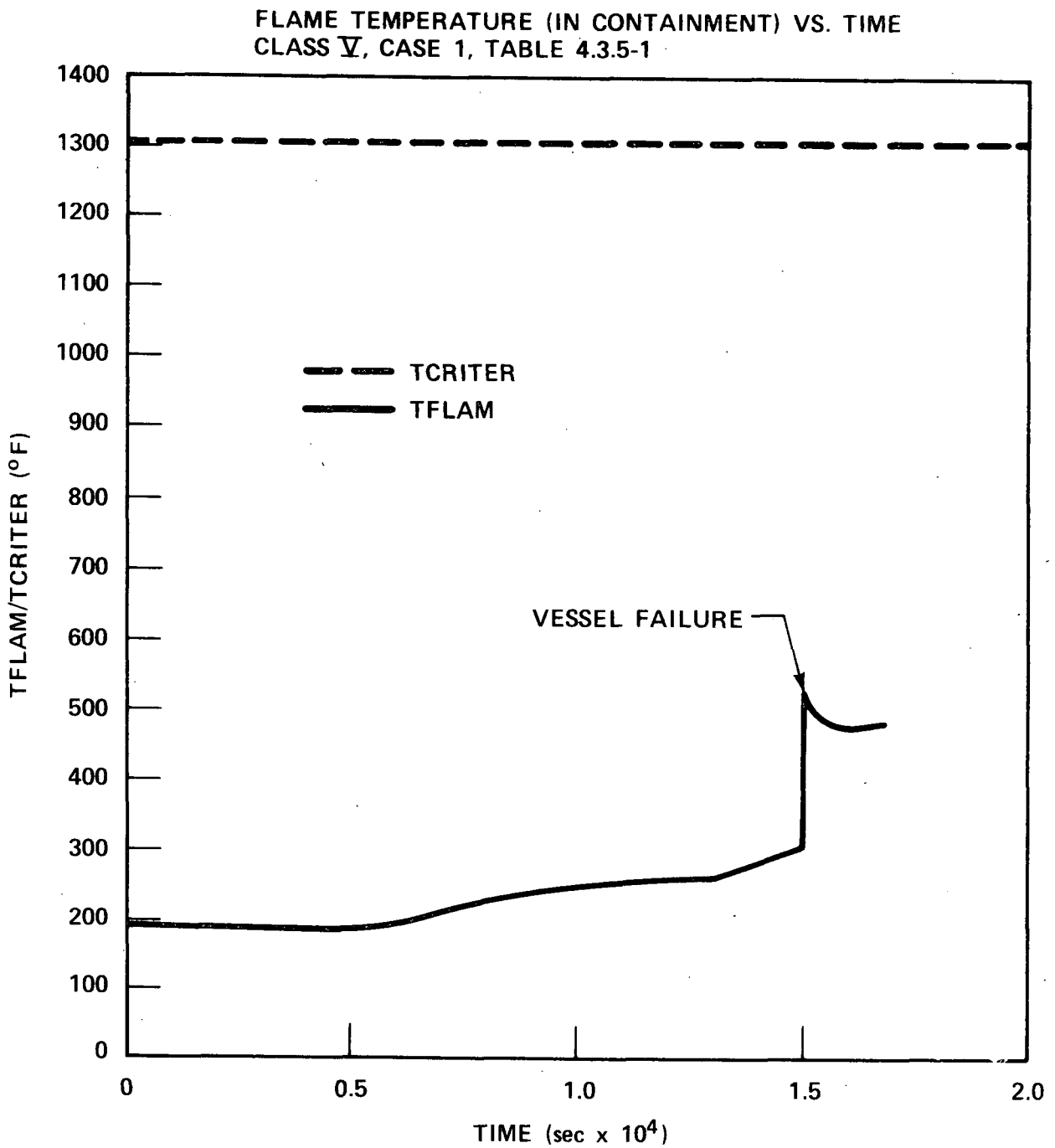

FLAME TEMPERATURE (IN CONTAINMENT) VS. TIME
CLASS V, CASE 1, TABLE 4.3.5-1
TFLAM/TCRITER (°F)
1400
1300
1200
1100
1000
900
800
700
600
500
400
300
200
100
0
TCRITER
TFLAM
VESSEL FAILURE
0
0.5
1.0
1.5
2.0
TIME (sec x 10^4)

Figure 4.3.5-4

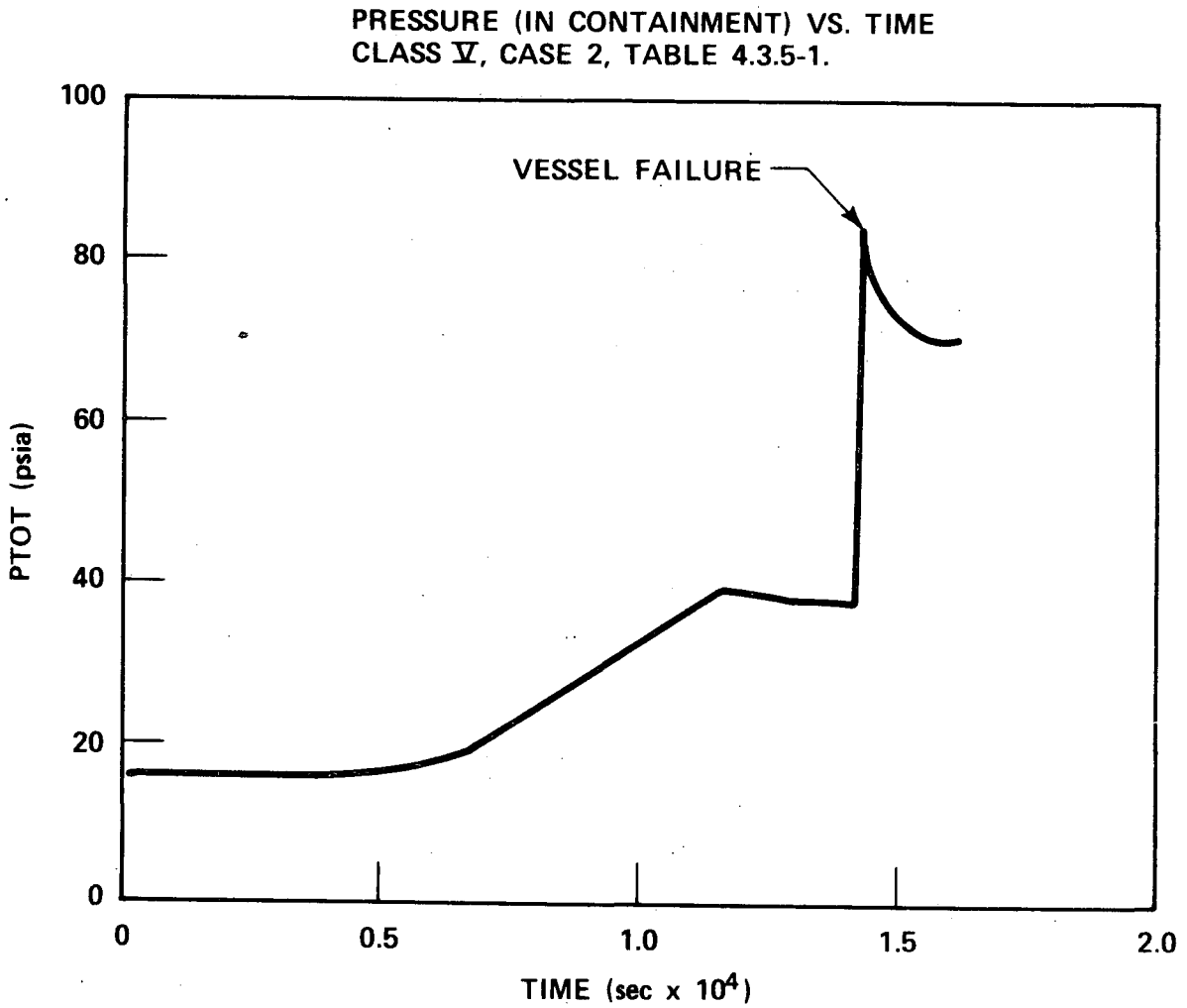
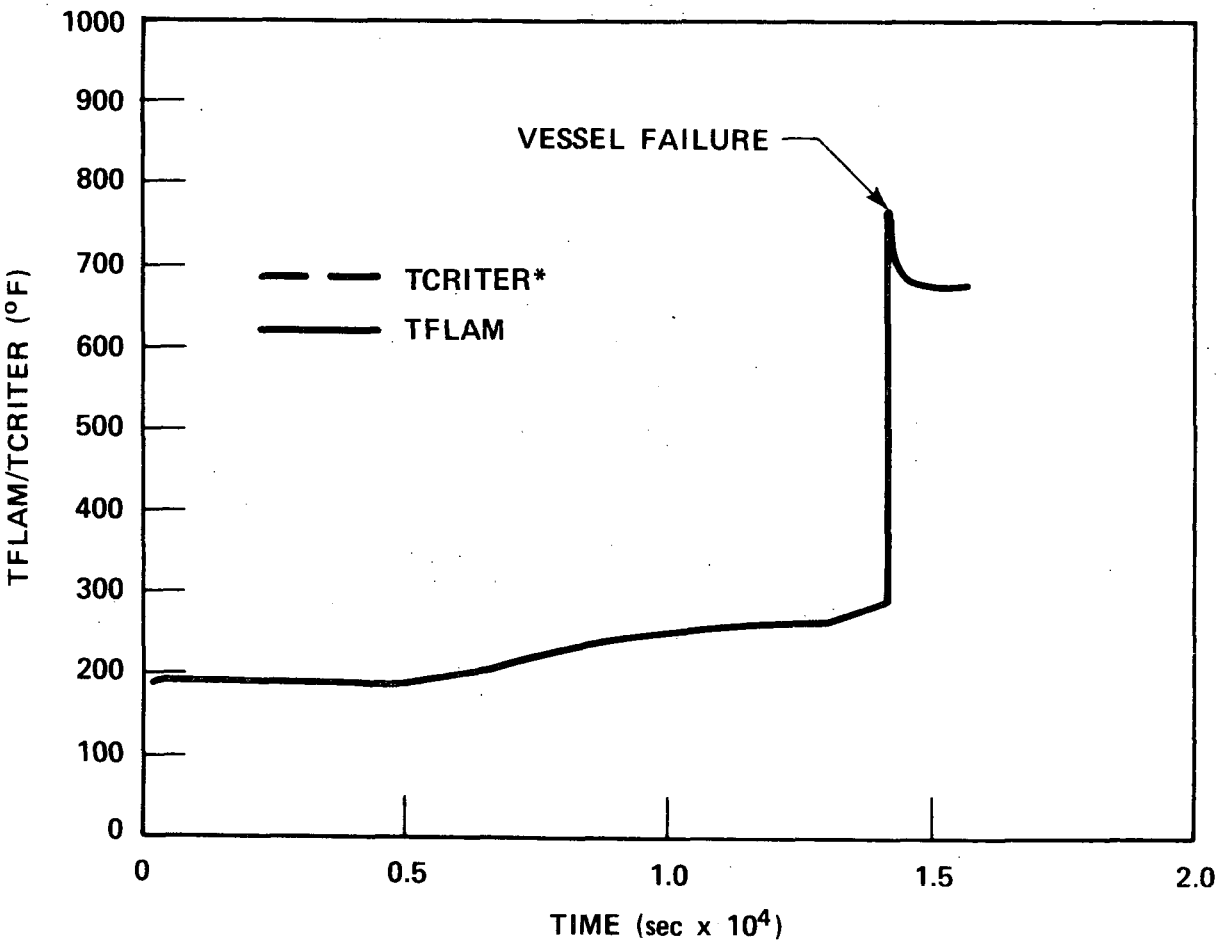

PRESSURE (IN CONTAINMENT) VS. TIME
CLASS V, CASE 2, TABLE 4.3.5-1.
VESSEL FAILURE
PTOT (psia)
100
80
60
40
20
0
0
0.5
1.0
1.5
2.0
TIME (sec x 10^4)

Figure 4.3.5-5

FLAME TEMPERATURE (IN CONTAINMENT) VS. TIME
CLASS V, CASE 2, TABLE 4.3.5-1



*TCRITER = 1310°F AND IS OFF THE SCALE OF THIS GRAPH

Figure 4.3.5-6

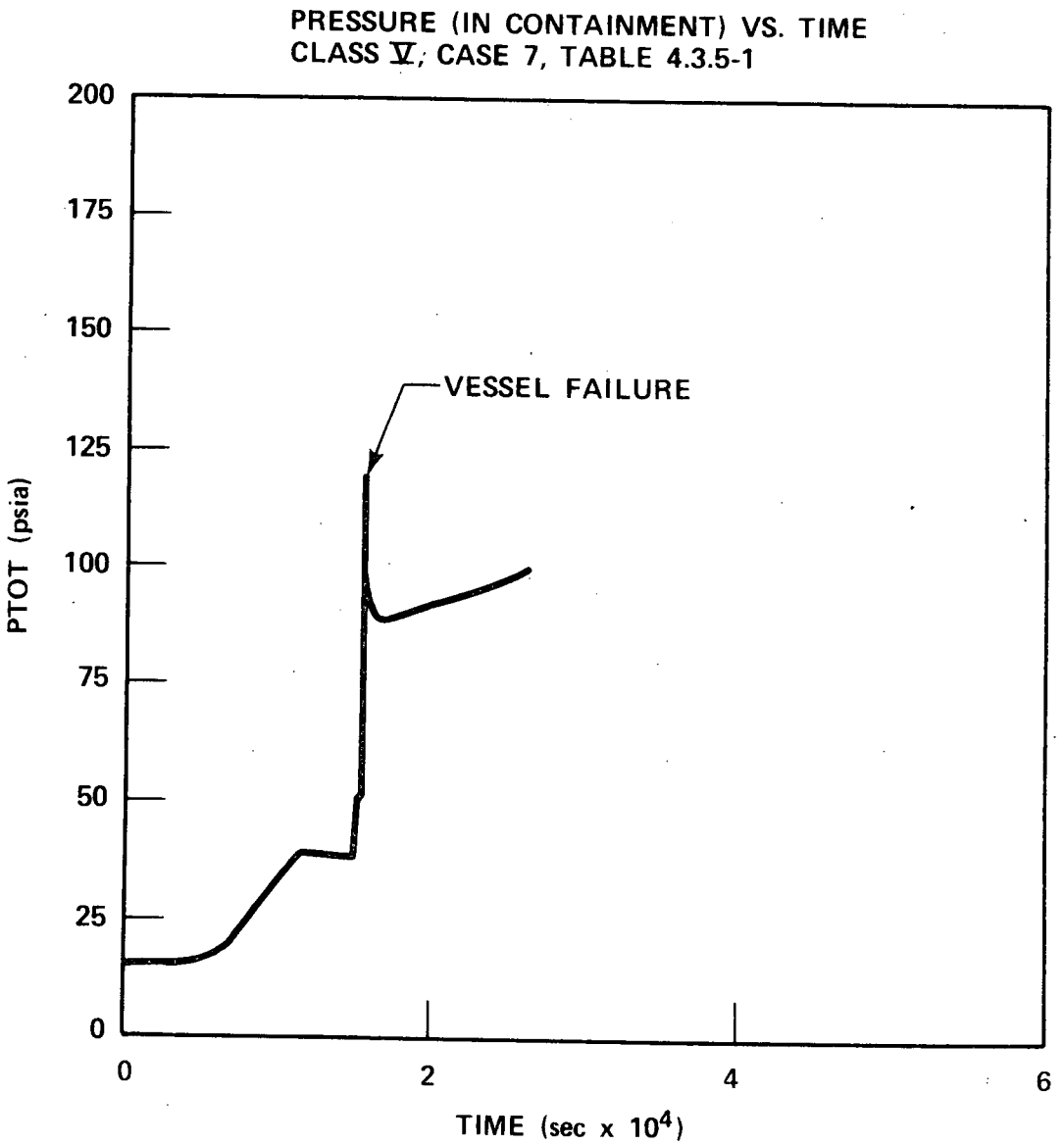

PRESSURE (IN CONTAINMENT) VS. TIME
CLASS V, CASE 7, TABLE 4.3.5-1
200
175
150
125
100
75
50
25
0
PTOT (psia)
VESSEL FAILURE
0
2
4
6
TIME (sec x 10^4)

Figure 4.3.5-7

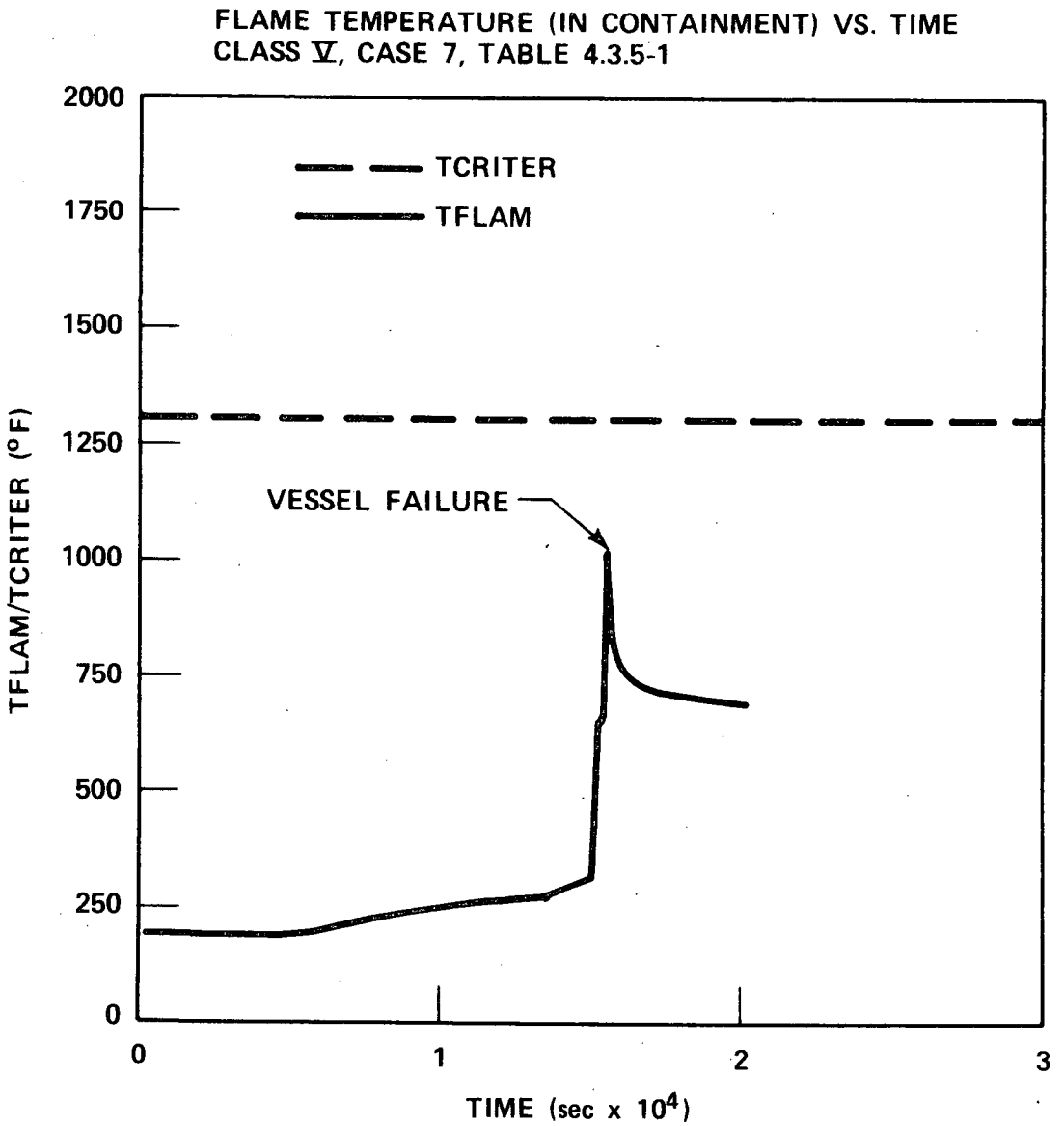

FLAME TEMPERATURE (IN CONTAINMENT) VS. TIME
CLASS V, CASE 7, TABLE 4.3.5-1
TCRITER
TFLAM
VESSEL FAILURE
TFLAM/TCRITER (°F)
2000
1750
1500
1250
1000
750
500
250
0
0
1
2
3
TIME (sec x 10^4)

Figure 4.3.5-8

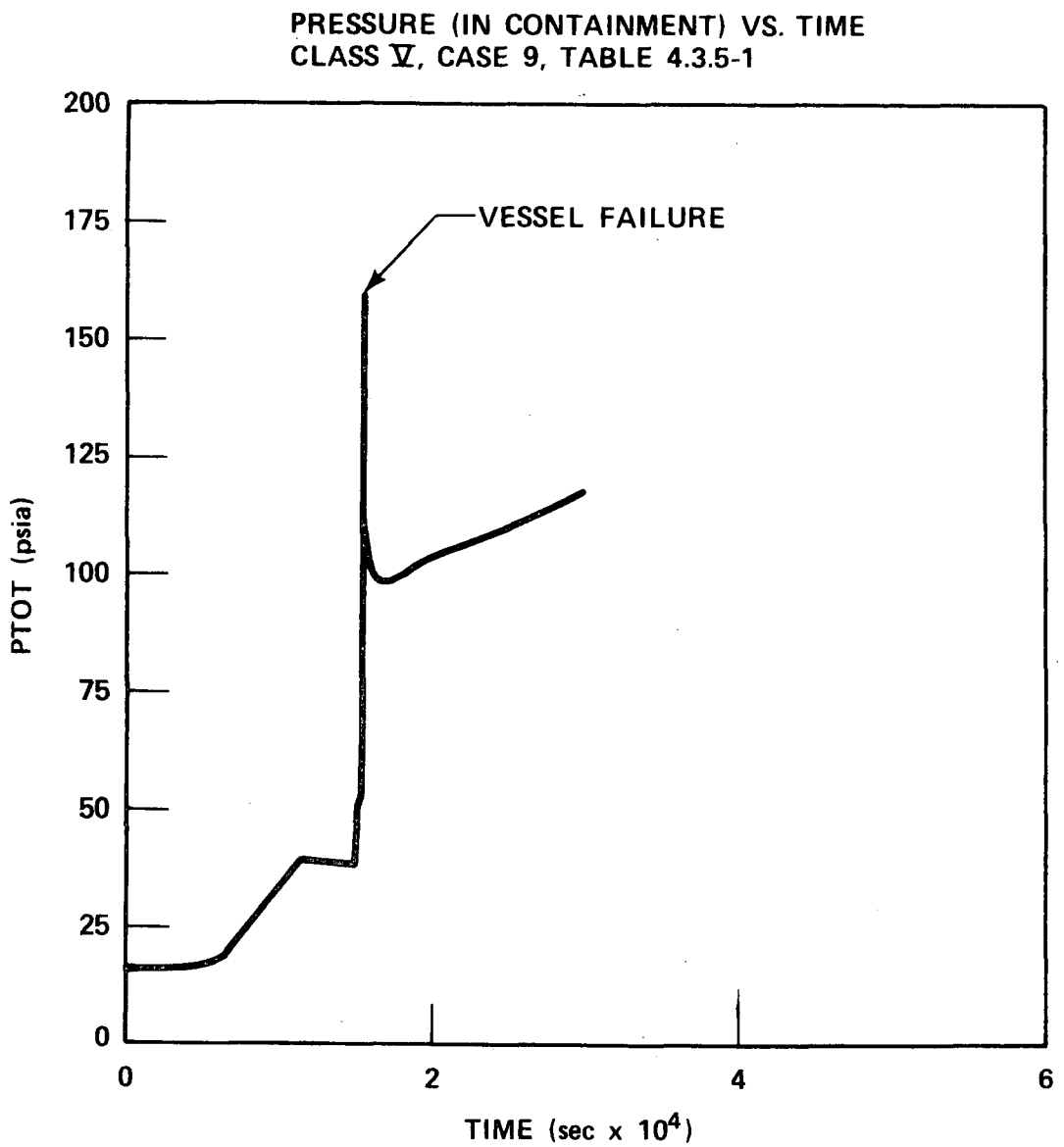

PRESSURE (IN CONTAINMENT) VS. TIME
CLASS V, CASE 9, TABLE 4.3.5-1
200
175
150
125
100
75
50
25
0
PTOT (psia)
VESSEL FAILURE
0
2
4
6
TIME (sec x 10^4)

Figure 4.3.5-9

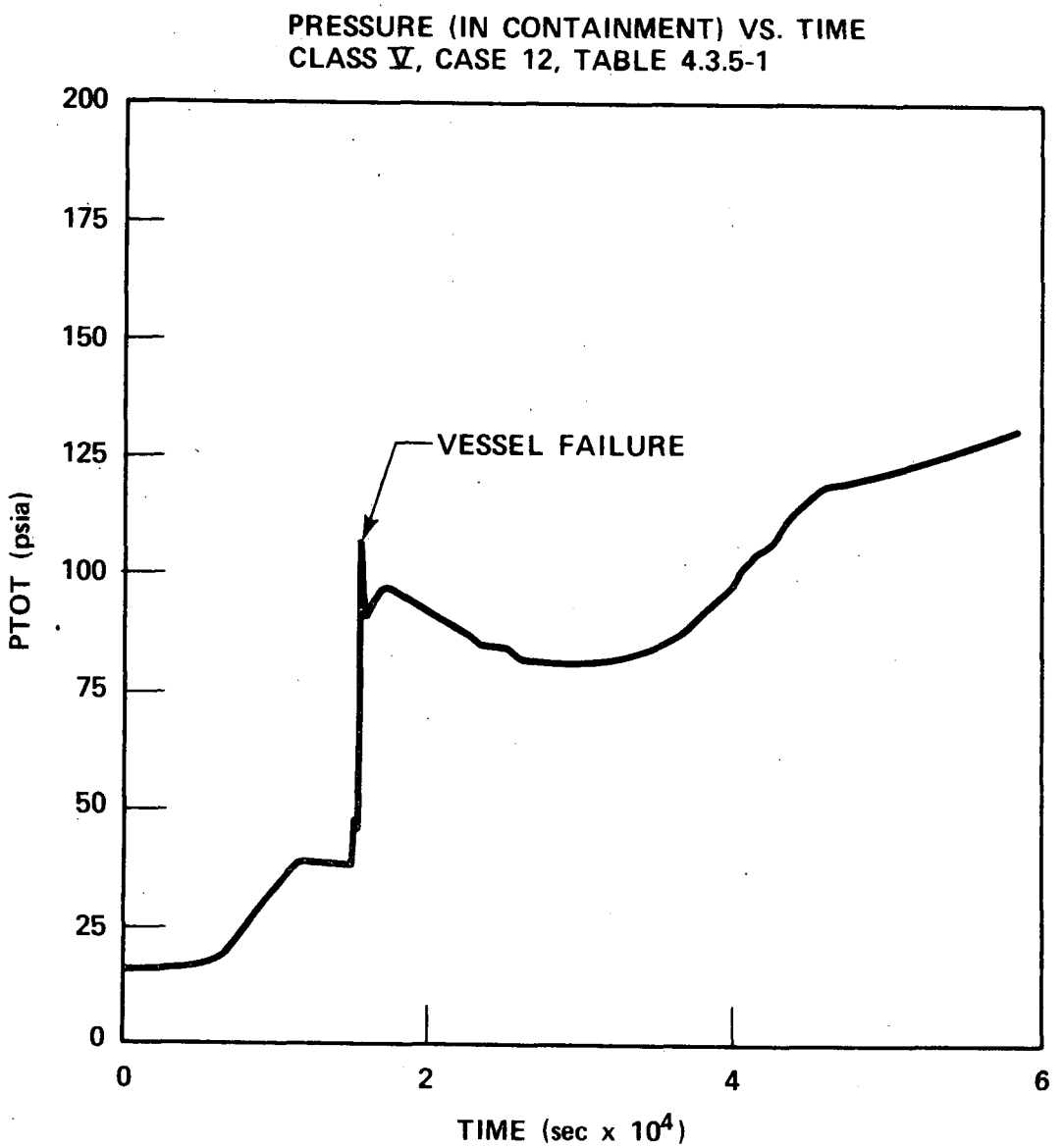


Figure 4.3.5-10

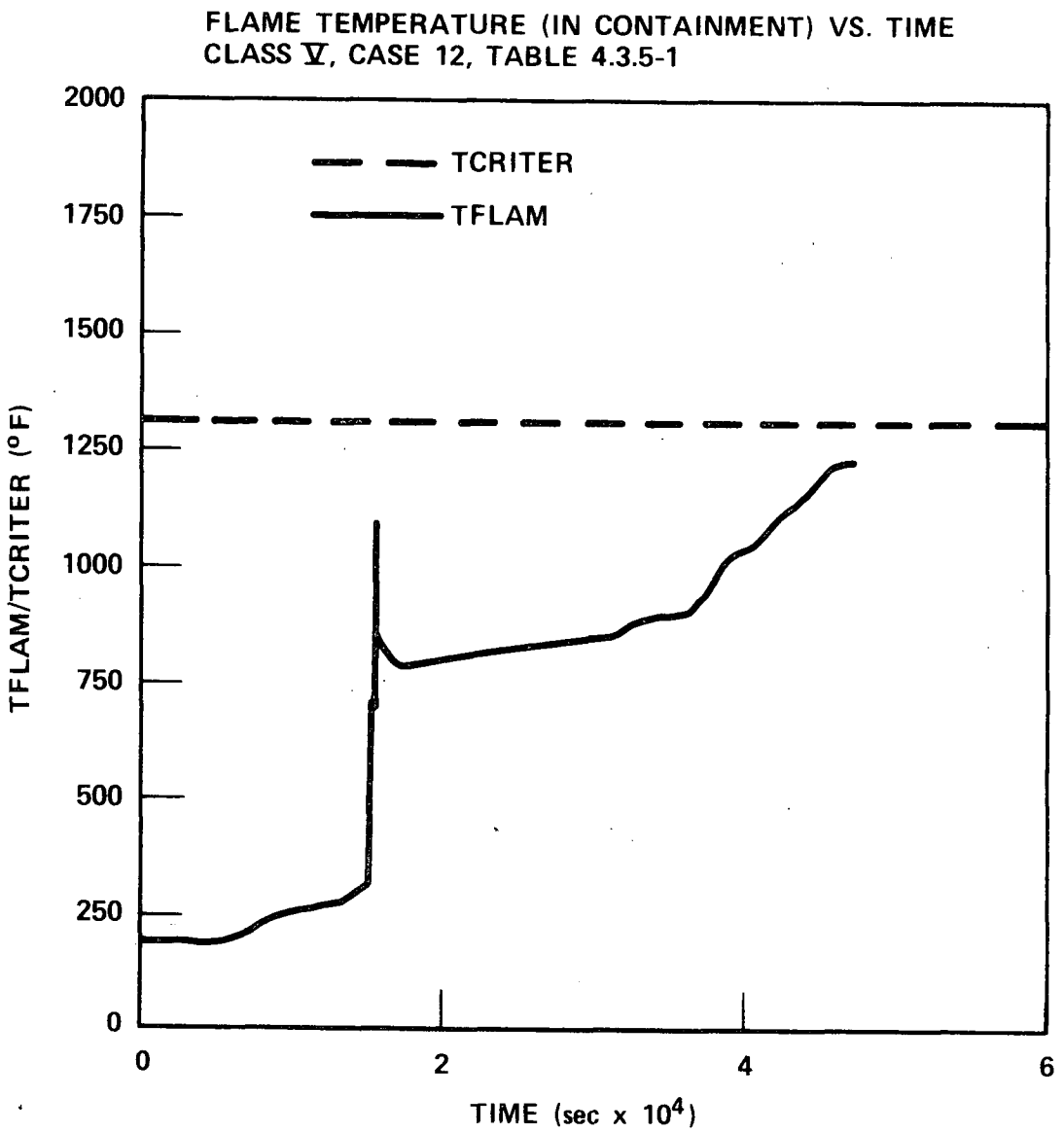


Figure 4.3.5-11

SECTION 4

REFERENCES

4.1.1-1 Wooton, R. O. and Avci, H. I., "MARCH Code Description and User's Manual," NUREG/CR-1711 (BMI-2064), Battelle Columbus Laboratories, October 1980.

4.1.1-2 Murfin, W. B., "A Preliminary Model for Core/Concrete Interactions," SAND 77-0370, Sandia Laboratories, August 1977.

4.1.2-1 Bordelon, F. M. and Murphy, E. T., WCAP-8327 Containment Pressure Analysis Code (COCO) July 1974.

4.1.2-2 Letter to Mr. D. B. Vassallo, Chief, Light Water Reactors Project, Branch 6, USNRC from Mr. C. Eicheldinger, Manager, Nuclear Safety, Westinghouse Electric Corporation, Dated March 17, 1976 (NS-CE-992).

4.1.2-3 Letter to Mr. D. B. Vassallo, Chief, Light Water Reactors Project, Branch 6, USNRC from Mr. C. Eicheldinger, Manager, Nuclear Safety, Westinghouse Electric Corporation, Dated July 10, 1975 (NS-CE-692).

4.1.2-4 Letter to Mr. D. B. Vassallo, Chief, Light Water Reactors Project, Branch 6, USNRC from Mr. C. Eicheldinger, Manager, Nuclear Safety, Westinghouse Electric Corporation, Dated April 7, 1976 (NS-CE-1021).

4.1.2-5 Letter to Mr. J. F. Stolz, Chief, Light Water Reactors Project, Branch 6, USNRC from Mr. C. Eicheldinger, Manager, Nuclear Safety, Westinghouse Electric Corporation, Dated August 27, 1976 (NS-CE-1183).

4.1.2-6 Hsieh, T. et. al., WCAP-8936, "Environment Qualification Instrument Transmitter Temperature Transient Analysis, February 1977.

4.1.2-7 Letter to John F. Stolz, Chief, Light Water Reactors Project, Branch 6, USNRC from C. Eicheldinger, Manager, Nuclear Safety, Westinghouse Electric Corporation, Dated June 14, 1977 (NS-CE-1453).

4.1.2-8 Furno, A. L., Cook, E. B., Kutcha, J. M. and D. S. Burgess, "Some Observations on Near-Limit Flames", 13th Combustion Symposium (International) 1970, pp. 593-99.

4.1.2-9 Lewis, B. and Karlovitz, B., Hydrogen Explosion Hazard of Pressurized Water Nuclear Reactor Containment, Combustion and Explosives Research Inc., Pittsburgh, Pa., January 16, 1980.

APPENDIX 4.4.1

Containment Capability Of

Indian Point Power Plant

Unit Nos. 2 and 3

For Internal Pressure Load

A Study Prepared For
The Power Authority Of The State Of New York
And
Consolidated Edison
By
United Engineers & Constructors, Inc.

TABLE OF CONTENTS

		PAGE
1.	Introduction	1
2.	Study Methodology	2
3.	Containment Description	3
	3.1 Physical Description	3
	3.2 Mechanical Properties	4
	3.3 Design Criteria	5
	3.4 Design Loads	6
4.	Analyses and Results	9
	4.1 Shell and Base Mat	9
	4.2 Liner System	11
	4.3 Penetrations	11
	4.4 Piping Penetration Assemblies	12
5.	Conclusions	14

1. Introduction

An evaluation of the capability of the Indian Point Units 2 and 3 Containment Vessels was performed for conditions representative of a core melt accident (Class 9 event). The evaluation was performed on a realistic basis and included actual material properties and the strength of the liner. For purposes of this investigation, capability was defined as the maximum combination of temperature and pressure to produce a general yield state, a condition which represents the limit of small displacement elastic response. By defining capability in this manner, a confident lower bound of functional capability could be defined without accounting for the additional available strength due to strain hardening in the reinforcing steel. The actual capability is higher.

The following regions of the Containment were evaluated:

A. Membrane region of the dome and cylinder.

B. Discontinuity region at the springline.

C. Discontinuity region at the base of the cylinder.

D. Base mat.

E. Large penetrations - equipment hatch and personnel airlock.

F. Several small penetrations.

G. Liner.

The methods used to evaluate the above regions were principally classical analysis methods performed by hand. Accurate results were possible because extensive prior experience with computer-based finite element numerical analyses and analyses by classical methods have shown that hand calculations produce excellent agreement with the computer analyses when coupled with a thorough understanding of the behavior of reinforced concrete containment shells under pressure and thermal loads.

2. Study Methodology

For this study, capability was defined, as the maximum combination of temperatures and pressure required to produce a general yield state in the shell's reinforcement steel, a condition which represents the limit of small displacement elastic response. All possible modes of failure which might occur prior to this limit condition, and thereby affect containment capability, were carefully reviewed. By defining capacity in this manner, a confident lower bound on functional capability could be defined without accounting for the additional available strength due to strain hardening in the reinforcing steel.

The development of a description of the containments' behavior during pressure and temperature loads was based on the experience gained in prior designs and analyses (both computer-based and classical methods) and review of the Indian Point Units 2 and 3 performances during their structural integrity tests. The difficulties and subjectiveness associated with the determination of the "weakest" failure mode among the numerous possible failure modes (both bursting and leaking) were recognized, especially as regards the need for extensive knowledge of 'real' properties of materials, effects of construction and manufacturing details and the nonlinear behavior of the structure at the pressure levels expected to produce failure. For this reason, the above approach to defining containment capability as the limiting state on small-displacement, elastic behavior was selected.

The use of hand calculations to evaluate selected regions of the containment was the approach chosen since comparisons made in prior analyses have demonstrated their accuracy. The membrane and discontinuity regions of the shell are good examples. The forces in the membrane regions, for pressure and temperature loads are statically determinate, while forces and moments at the base and springline due to pressure and temperature are readily determined from classical shell theory. The role of concrete cracking on shell stiffness, stress resultants and strength is well understood and incorporated into the hand calculations as required.

Special purpose computer codes were used in the evaluation of other regions in the containment including the liner and liner/anchor system under thermal loads. Hand calculations for penetration regions in the containment drew upon knowledge of their behavior from prior analyses.

3.0 Containment Description

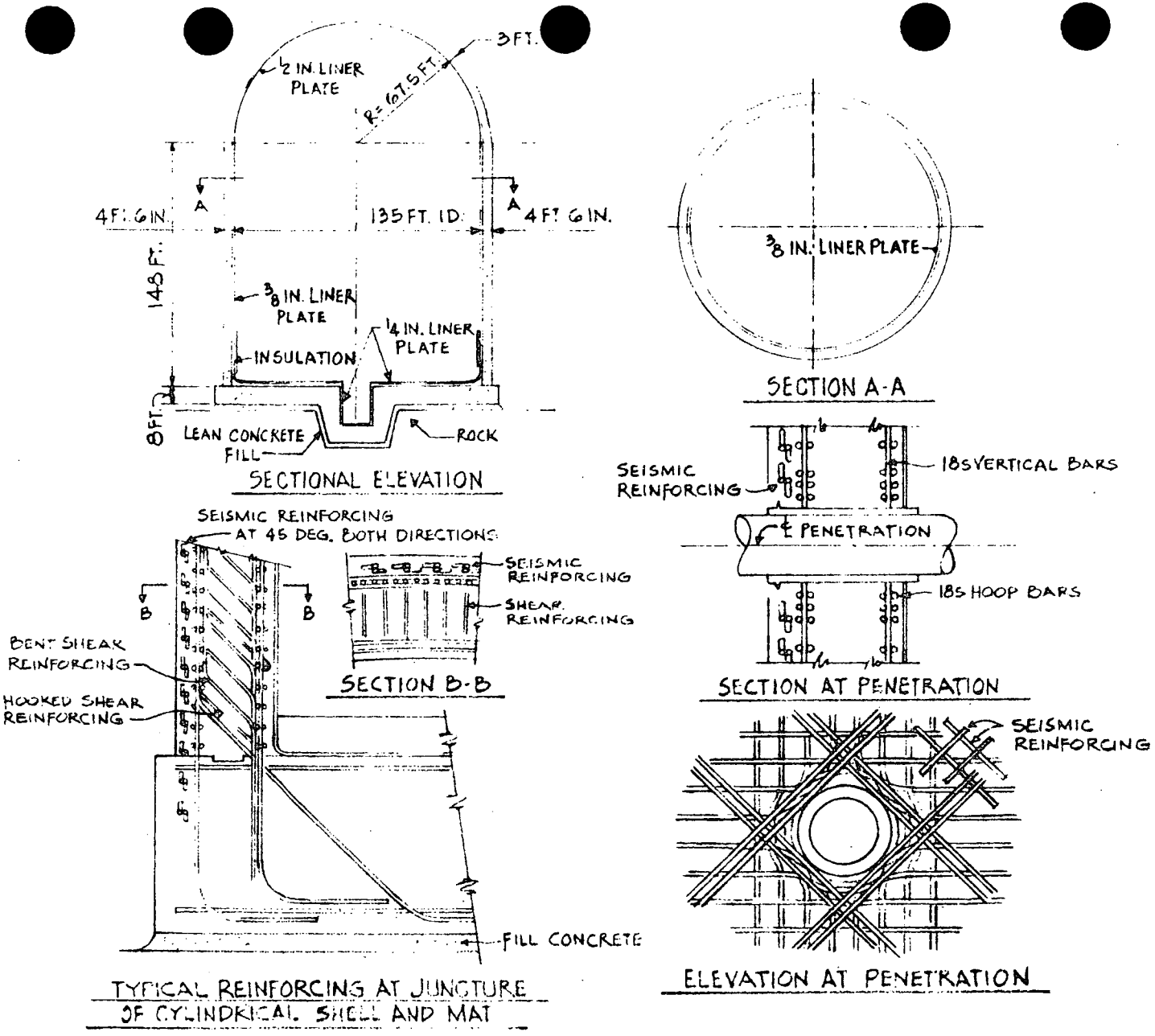
3.1 Physical Description

The containment structure is a reinforced concrete vertical right cylinder with a flat base and hemispherical dome. A welded steel liner with a minimum thickness of 1/4 inch is attached to the inside face of the concrete to ensure a high degree of leak-tightness. The design objective of the containment structure is to contain all radioactive material which might be released from the core following a loss-of-coolant accident. The structure serves as both a biological shield and a pressure container.

The structure, as shown on Figure 1, consists of side walls measuring 148 feet from the liner on the base to the springline of the dome, and has an inside diameter of 135 feet. The side walls of the cylinder and the dome are 4 feet 6 inches and 3 feet 6 inches thick, respectively. The inside radius of the dome is equal to the inside radius of the cylinder so that the discontinuity at the springline due to the change in thickness is on the outer surface. The flat concrete base mat is 9 feet thick with the bottom liner plate located on top of this mat. The bottom liner plate is covered with 3 feet of concrete, the top to which forms the floor of the containment. Such reinforcement is illustrated in Figures 2 through 5.

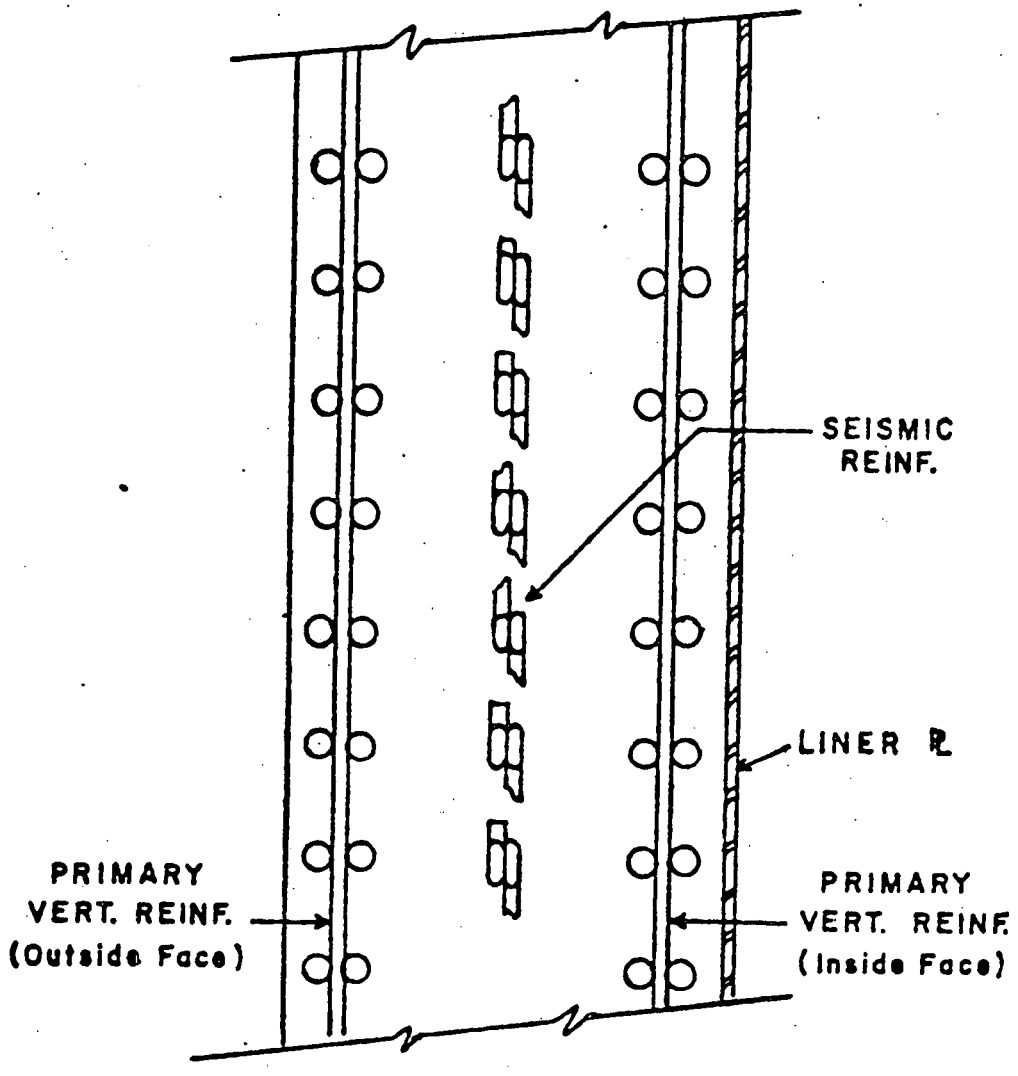
There are two large openings in the Indian Point Containment Structures. In Unit No. 3 the Personnel Lock is located in the South East quadrant with a center line evaluation of 83 feet 6 inches and an opening size of 8 feet 6 inches diameter. The Equipment Hatch is located in the North East quadrant of the Containment with a center line elevation of 101 feet 6 inches and opening size of 16 feet 0 inches diameter. Both of these openings along with their thickened reinforced concrete bosses are located at elevation 43 feet 0 inches distance above the fixed base mat. The thickened boss is heavily reinforced in addition to the dense reinforcement which already exists in the 4 feet 6 inches thick Containment cylinder wall. Figure 6 illustrates a typical section.

The basic structural elements considered in the design of the containment structure are the base slab, side walls and dome acting as one structure under all possible loading conditions. The liner is anchored to the concrete shell by stud anchors so that it forms an integral part of the entire composite structure under all membrane loadings as seen in Figure 7. The reinforcing in the structure has an elastic response to all primary loads with limited maximum strains to ensure the integrity of the steel liner. The lower 20 feet of the cylindrical liner is insulated to avoid excess deformation of the liner due to restricted radial growth when subjected to a rise in temperature.



CONTAINMENT STRUCTURE

FIGURE 1



SECTION OF CYLINDRICAL SHELL
I.P. UNITS 2 AND 3

FIGURE 2

CYLINDER REINFORCEMENT
INDIAN POINT UNIT-2

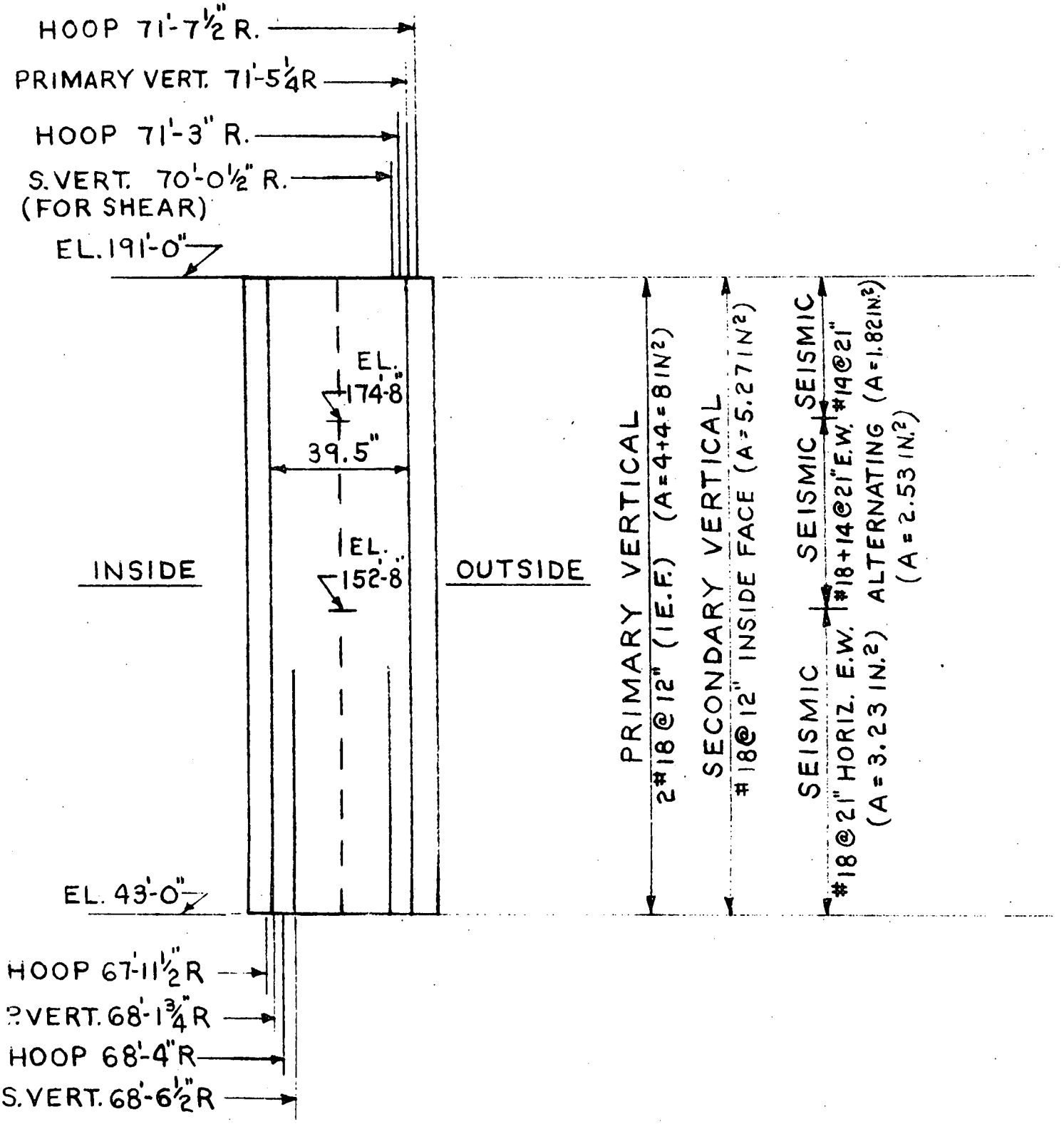


FIGURE 3

CYLINDER REINFORCEMENT
INDIAN POINT UNIT-3

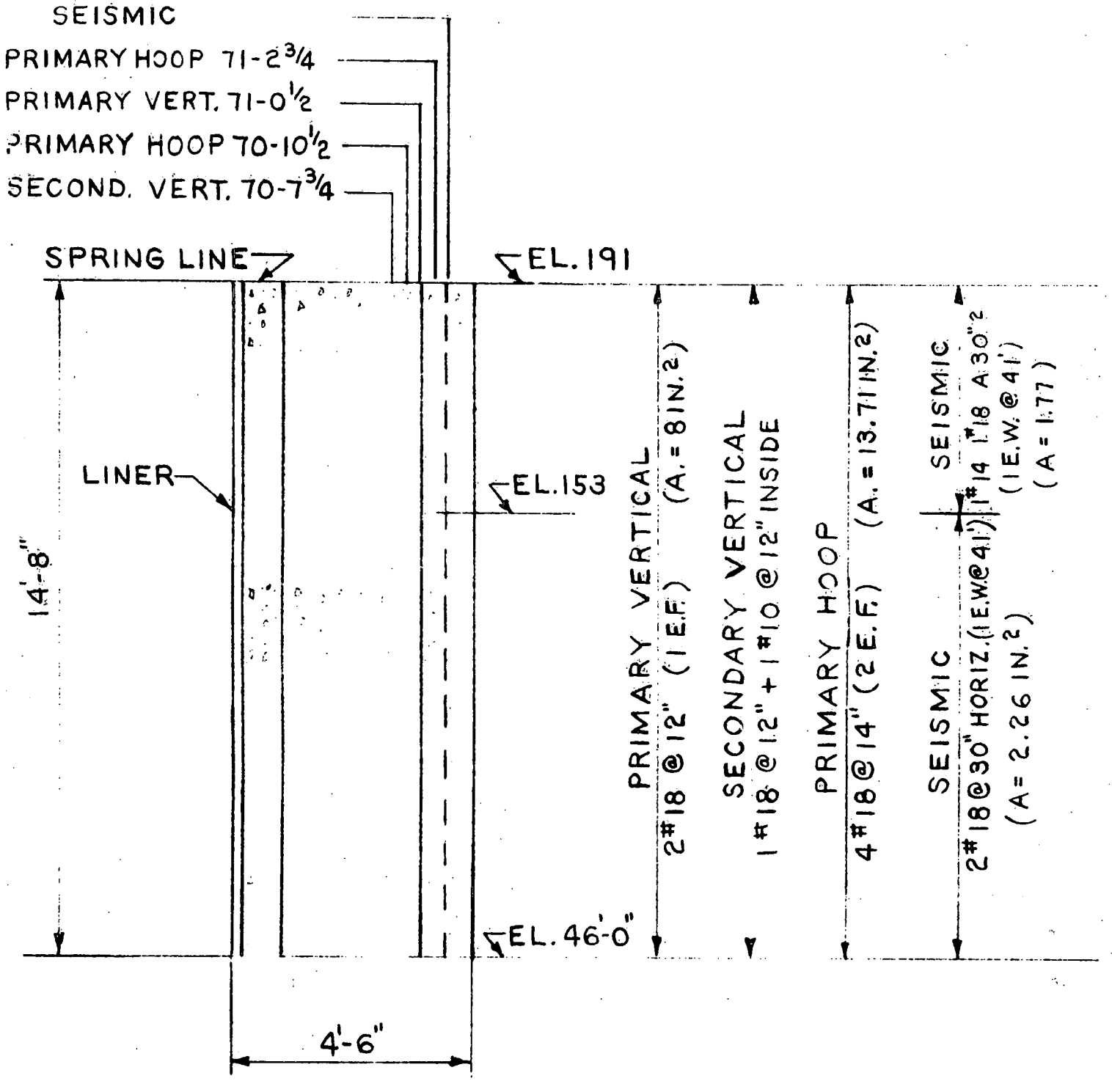
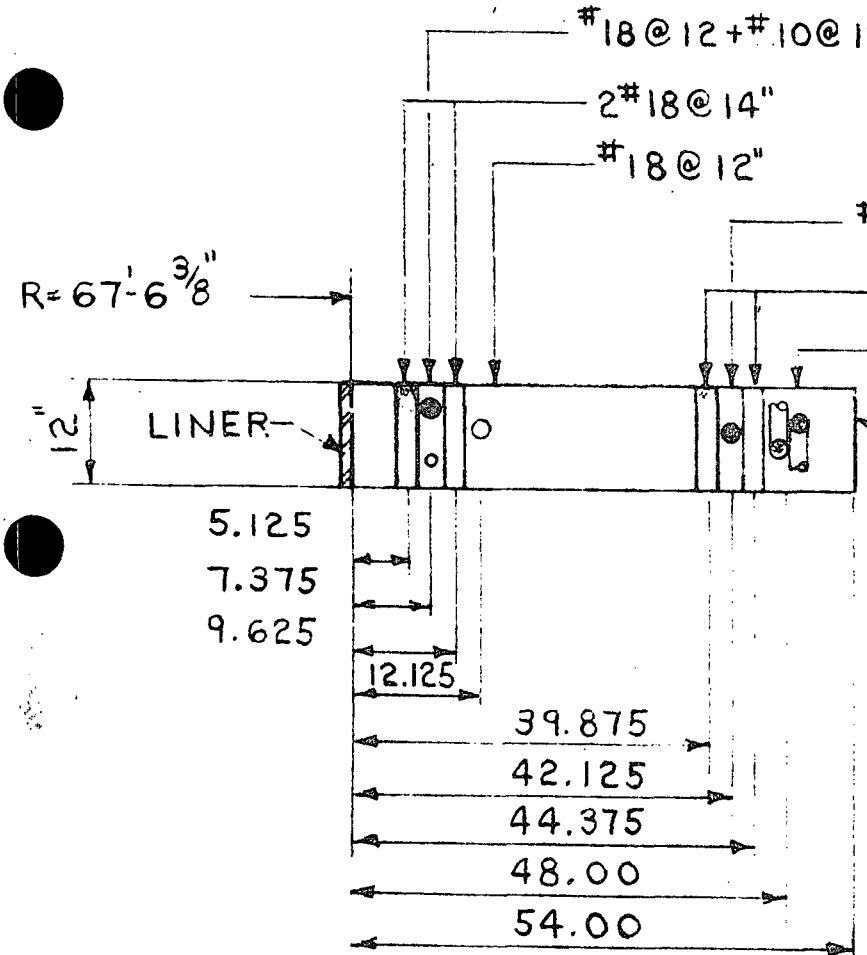


FIGURE 4

REINFORCEMENT DETAILS
INDIAN POINT UNITS 2 & 3
(SEISMIC ON OUTSIDE)

SECTION 1-1 @ MAT

NOTE: LINER IS NEGLECTED



VERTICAL:

INSIDE REBAR

$A_i = 4 + 1.27 + 4 = 9.27$ IN.^{2}

$$C.G. = \frac{5.27(7.375) + 4(12.125)}{9.27} = 9.42 \text{ IN.}$$

OUTSIDE REBAR

EQUIVALENT VERTICAL AREA OF SEISMIC REBAR.

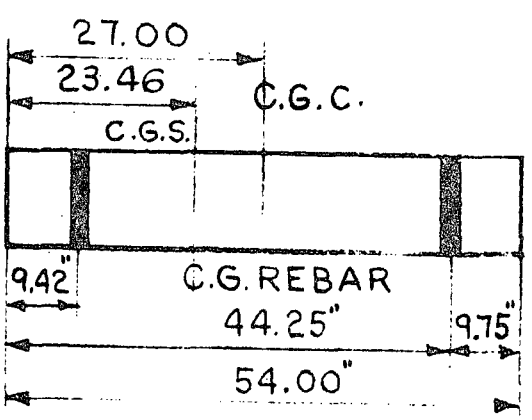
$A_v = 2(4 \sin 45)(12/30) = 2.26$ IN.^{2}/FT.

$A_o = 4 + 2.26 = 6.26$ IN.^{2}

$$C.G. = \frac{4(42.125) + 226(48)}{6.26} = 44.25"$$

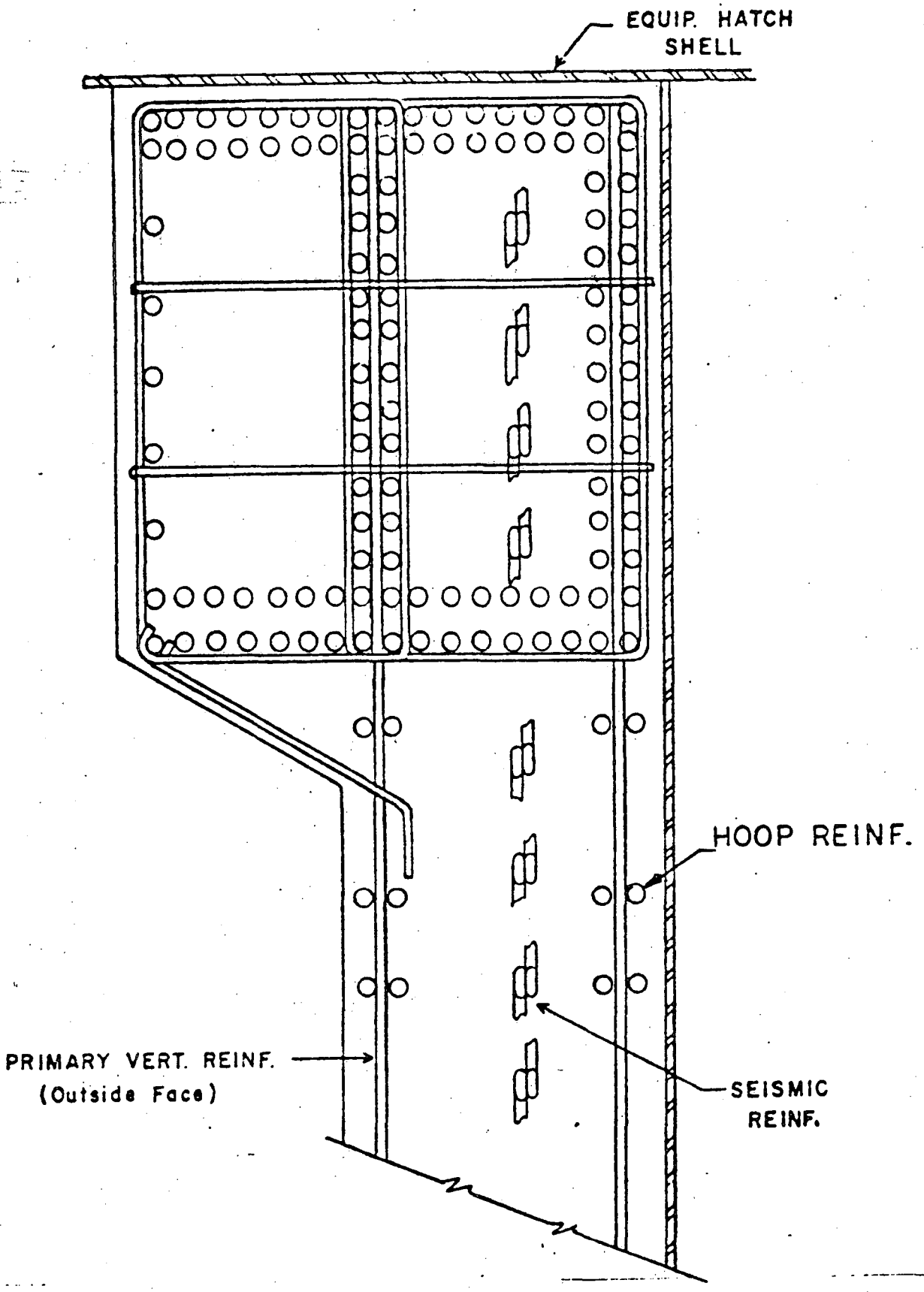
$d = 54 - 9.42 = 44.58$ IN.

EQUIV. SECTION MERIDIONAL



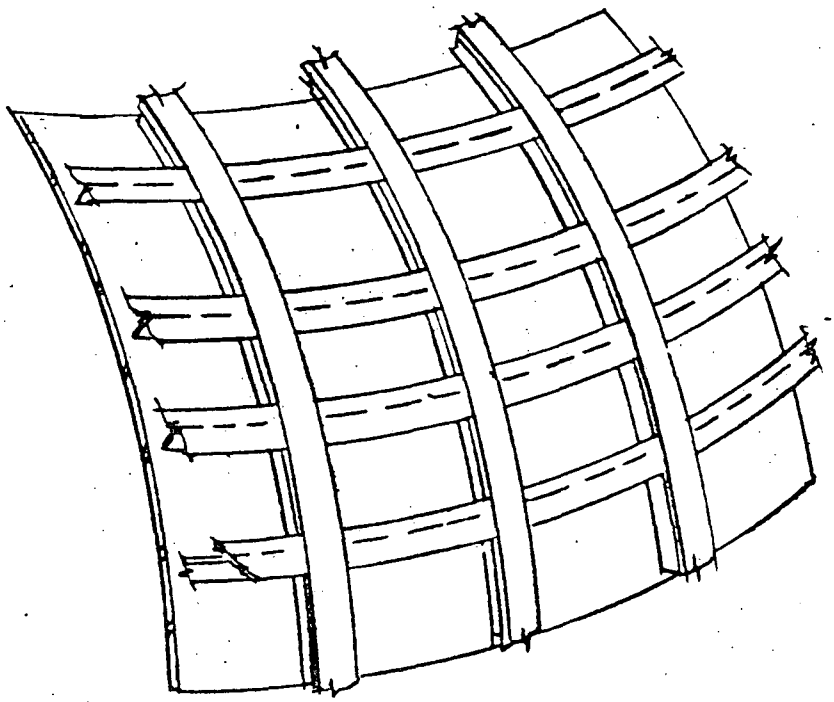
$A_T = 9.27 + 6.26 = 15.53$ IN.^{2}

FIGURE 5

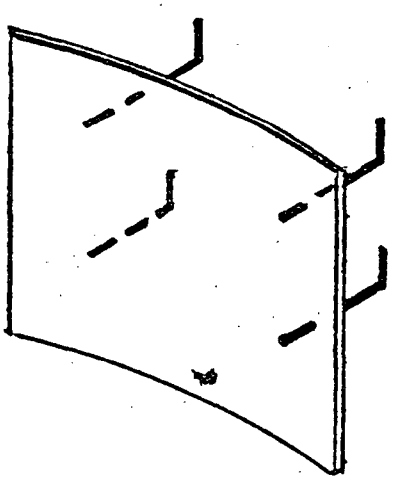


SECTION THROUGH DISCONTINUITY
REGION AROUND EQUIPMENT HATCH

FIGURE 6



ATTACHMENT TO DOME



ATTACHMENT TO CYLINDER

ATTACHMENT OF LINER TO CONCRETE

FIGURE 7

3.2 Mechanical Properties

Basically, four materials are used for the construction of the containment vessel. These are:

A) Concrete

B) Reinforcing Steel

C) Plate Steel Liner

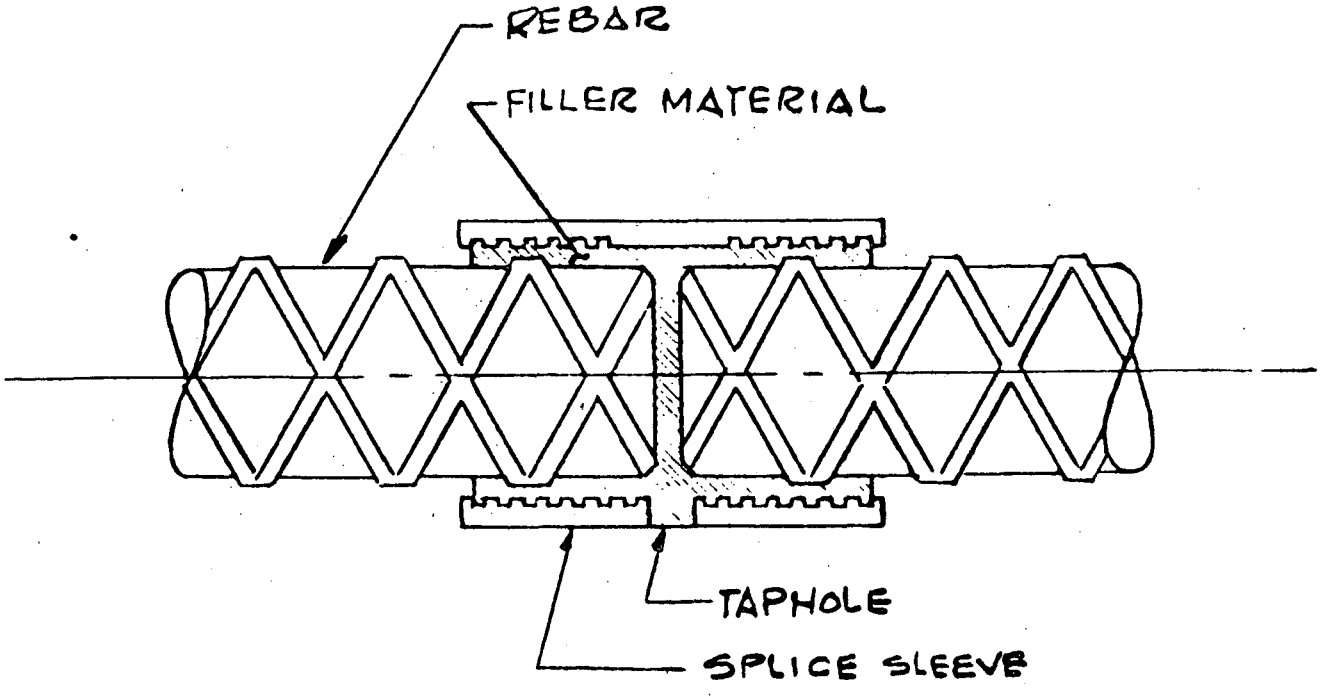
D) Insulation

Basic specifications for these materials are:

A) Concrete is a dense, durable mixture of sound coarse aggregate, fine aggregate, cement and water with a design minimum ultimate strength f'_c = 3,000 psi. Aggregates conform to American Society for Testing Materials Specification (ASTM) C-33 "Standard Specification for Concrete Aggregates".

B) Reinforcing steel for the dome, cylindrical walls and base is high-strength deformed billet steel bars conforming to ASTM Designation A432-65 "Specification for Deformed Billet Steel Bars for Concrete Reinforcement with 60,000 psi Minimum Yield Strength" (Revised ASTM A615-68, Grade 60). This steel has a minimum yield strength of 60,000 psi, a minimum tensile strength of 90,000 psi, and a minimum elongation of 7 percent in an 8-inch specimen. Reinforcing bars No. 11 and smaller in diameter are lapped spliced in the base for flexural loadings and spliced by the Cadweld process in the walls and dome for tension loading. Bars No. 14S and 18S are spliced by the Cadweld process only, illustrated in Figure 8. A certification of physical properties and chemical content of each heat of the reinforcing steel delivered to the job site was issued from the steel supplier. The splices used to join reinforcing bars were sample tested to ensure that they will develop at least 125 percent of the minimum yield point stress of the bar. The test program required cutting out approximately 2 percent of the completed splices and testing to determine their breaking strength thus confirming the strength of both the bars and the splice.

C) The plate steel liner is carbon steel conforming to ASTM Designation A442-65 "Standard Specification for Carbon Steel Plates with Improved Transition Properties", Grade 60. This steel has a minimum yield strength of 32,000 psi and minimum tensile strength of 60,000 psi with an elongation of 22 percent in an 8-inch gauge length at failure.



TYPICAL CADWELD SPLICE

FIGURE 8

The liner is 1/4 inch thick at the bottom, 1/2 inch thick in the first three courses and 3/8 inch thick for remaining portion of cylindrical walls except 3/4 inch thick at penetrations and 1/2 inch thick in the dome. The liner material has been tested to ensure an Net Ductility Transition (NDT) temperature 30°F lower than the minimum operating temperature of the liner material.

Impact testing was done in accordance with Section N331 of Section III of the ASME Boiler and Pressure Vessel Code. A 100 percent visual inspection of the liner anchors was made before pouring concrete.

D) The material for insulating the liner plate is urethane foam covered with gypsum board and a stainless steel jacket and backed with asbestos paper on the unexposed side. This insulation has been selected to withstand the calculated accident temperature and pressure conditions.

E) Quality of both materials and construction of the containment vessel has been ensured by a continuous program of quality control and inspection.

3.3 Design Criteria

The design was based upon limiting load factors which are used as the ratio by which loads are multiplied for design purposes to ensure that the loading deformation behavior of the structure is one of elastic, tolerable strain behavior. The load factor approach was used in this design as a means of making a rational evaluation of the isolated factors which must be considered in esuring an adequate safety margin for the structure. This approach permitted the designer to place the greatest conservatism on those loads most subject to variation and which most directly control the overall safety of the structure. In the case of the containment structure, therefore, this approach placed minimum emphasis on the fixed gravity loads and maximum emphasis on accident and earthquake or wind loads. The loads used to determine the required limiting capacity of any structural element on the containment structure are presented in Section 3.4.

The load factors used in this design were based upon the load factor concept used in Part IV-B, "Structure Analysis and Proportioning of Members Ultimate Strength Design" of ACI 318-63. Because of the refinement of the analysis and the restrictions on construction procedures, the load factors in the design primarily provide for a safety margin on the load assumptions. Specific combined load equations used in design are presented. All structural components have been designed to have a capacity required by the most severe loading combination.

The design included the consideration of both primary and secondary stresses. The load capacity in structural members was based on the ultimate strength values presented in Part IVB of American Concrete Institute ACI-318 as reduced by the capacity reduction factor"Ø" which provides for the possibility that small adverse variations in material strengths, workmanship, dimensions, and control, while individually within required tolerances and the limits of good practice, ocasionally may combine to result in under capacity. For tension members, the factor "Ø" is 0.95. The factor "Ø" is 0.90 for flexure and 0.85 for diagonal tension, bond and anchorage.

For the liner steel the factor "Ø" is 0.95 for tension. For compression and shear, the primary membrane liner stress is maintained below 0.95 yield and elastic stability was ensured as a function of liner anchorage requirements. The liner was designed to ensure that no strains greater than the strain at the guaranteed yield point will occur at the factored loads except in regions of local stress concentrations or stresses due to secondary load effects in which case the liner strain is limited to .5 percent. Sufficient anchorage is provided to ensure elastic stability of the liner. The basic design concept using stud anchorage of the liner plate to the concrete structure ensures stud failure due to shear, tension or bending stress without the stud connnection causing failure or tearing of the liner plate. The studs in the 1/2 inch plate are on 24 inch horizontal and 28 inch vertical grid and in the 3/8 inch plate on a 24 inch horizontal and 14 inch vertical grid. The design considered the possibility of daily stress reversals due to ambient temperature changes for the life of the plant, and fatigue limit of the studs exceeds the design requirements.

3.4 Design Loads

The design was based upon limiting load factors which were used as the ratio by which loads were multiplied for design purposes to ensure that the loading formation behavior of the structure was one of elastic, tolerable strain behavior. The load factor approach was used in this design as a means of making a rational evaluation of the isolated factors which must be considered in ensuring an adequate safety margin for the structure. The loads used to determine the required limiting capacity of any structural element on the containment structure are:

A) $C = 1.0D \pm 0.05D + 1.5P + 1.0\ (T + TL)$

B) $C = 1.0D \pm 0.05D + 1.25P + 1.0\ (T' + TL') + 1.25E$

C) $C = 1.0D \pm 0.05D + 1.0P + 1.0\ (T'' + TL'') + 1.0E'$

D) $C = 1.0D \pm 0.05D + 1.0W'$

Symbols used in these formulae are defined as follows:

C = Required load capacity section.

D = Dead load of structure and equipment loads.

P = Accident pressure load as shown on pressure-temperature transient curves.

T = Load due to maximum temperature gradient through the concrete shell and mat based upon temperatures associated with 1.5 times accident pressure.

TL = Load exerted by the liner based upon temperatures associated with 1.5 times accident pressure.

T' = Load due to maximum temperature gradient through the concrete shell based upon temperatures associated with 1.25 times accident pressure.

TL' = Load exerted by the liner based upon temperatures associated with 1.25 times accident pressure.

E = Load resulting from operational basis earthquake.

T" = Load due to maximum temperature gradient through the concrete shell based upon temperature associated with the accident pressure.

TL" = Load exerted by the liner based upon temperatures associated with the accident pressure.

E' = Load resulting from design basis earthquake.

W' = Tornado wind load and the pressure drop effect.

Load conditions A) indicate that the containment has the capacity to withstand loadings at least 50 percent greater than those calculated for the postulated loss-of-coolant accident (LOCA) alone.

All structural components have been designed to have a capacity required by the most severe loading combination. The loads resulting from the use of these equations will hereafter be termed "factored loads".

3.4.1 Accident Pressure Loads

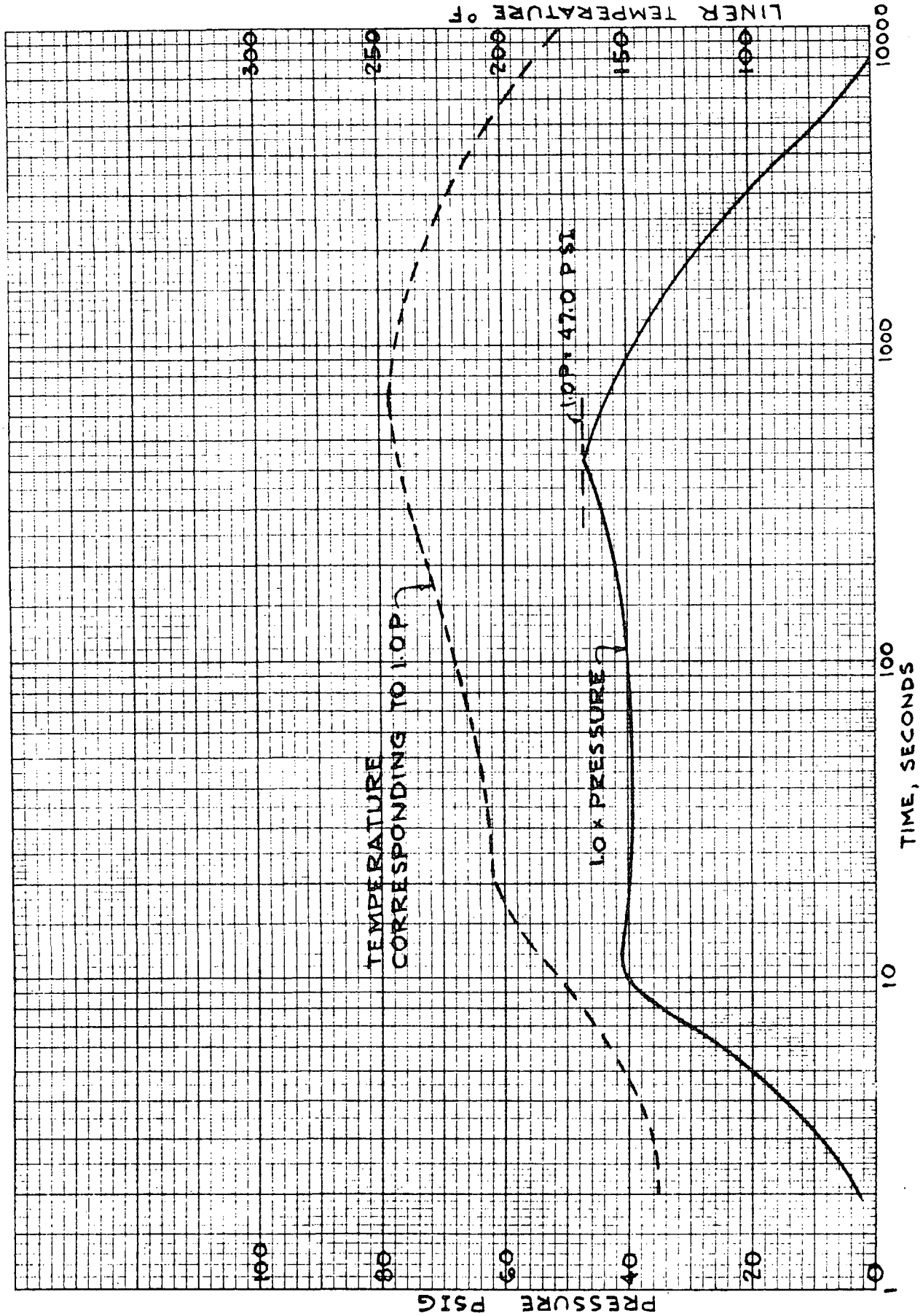
The design basis accident pressure load is shown in Figure 9 as a function of time. This design value is at least 5 percent in excess of maximum calculated containment pressure as shown in the FSAR.

3.4.2 Accident Temperature Loads

The design basis accident containment temperature assumed in the design of the containment is also shown in Figure 9 as a function of time. This containment temperature induces loads in the concrete shell as the concrete acts to restrain liner thermal expansion. This thermal load effect on the liner is combined with pressure load effects to develop design basis accident load requirements as a function of time. Accident temperature induced thermal gradients through the wall are not a factor in concrete shell design since the accident temperature effect penetrates approximately 10 percent of the containment wall thickness during the significant overpressure phase of the accident The cracking of the concrete shell due to containment pressurization acts to relieve secondary stresses induced by thermal gradient effect.

3.4.3 Loads At Penetrations

The effect of growth of the liner due to accident conditions has been considered in the design of penetrations and sleeves together with the effects of lateral loads due to thermal expansion of pipes, seismic motion, pipe break loads and pressure loads. In addition, stress concentration effects on large penetrations have been considered.



DESIGN PRESSURE-TEMPERATURE TRANSIENT

FIGURE 9

4. Analyses And Results

4.1 Shell And Base-Mat

The shell is comprised of the cylinder and the dome. The radius to thickness ratio of both is sufficiently large such that thin shell theory is applicable. Accordingly, the shell's behavior under pressure, and other axisymmetric loadings, can be separated into primary (membrane) and secondary (bending) actions and analyzed as such.

Membrane region - The statically determinate force system is independent of material properties and was calculated as follows:

DOME

$$\text{HOOP FORCE} = \frac{PR}{2} \qquad \text{MERIDIONAL FORCE} = \frac{PR}{2}$$

CYLINDER

$$\text{HOOP FORCE} = PR \text{ (GOVERNING CONDITION)}$$

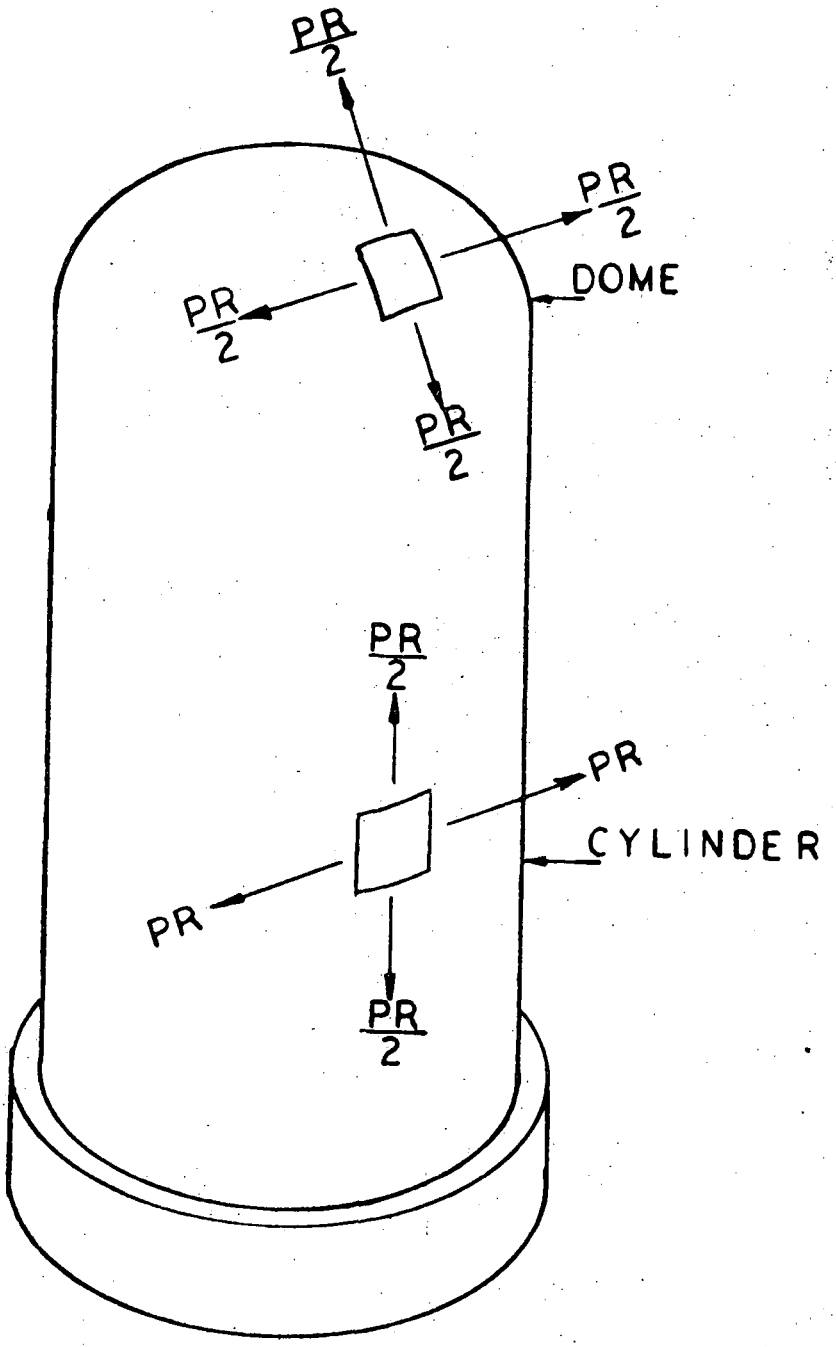
$$\text{MERIDIONAL FORCE} = \frac{PR}{2} - D$$

These force resultants are the shell forces in regions removed from discontinuities. Figure 10 illustrates this primary force system on the shell.

The shell's membrane capacity was calculated including the contributions of liner and seismic rebar, Figure 2. A general yield state in tension was assumed. Hoop capacity in the cylinder controls from observing the $N_\theta = PR$ term and reviewing steel areas. Because seismic rebar quantities decrease with shell height, the shell capacity was found to be a minimum in the region below the springline. The mean value of yield stress from the results of rebar tests for the Indian Point containments was incorporated in the strength evaluation, Figure 11 and Table 1. Cadwell test data were reviewed to ensure that the full rebar yield stress could be developed.

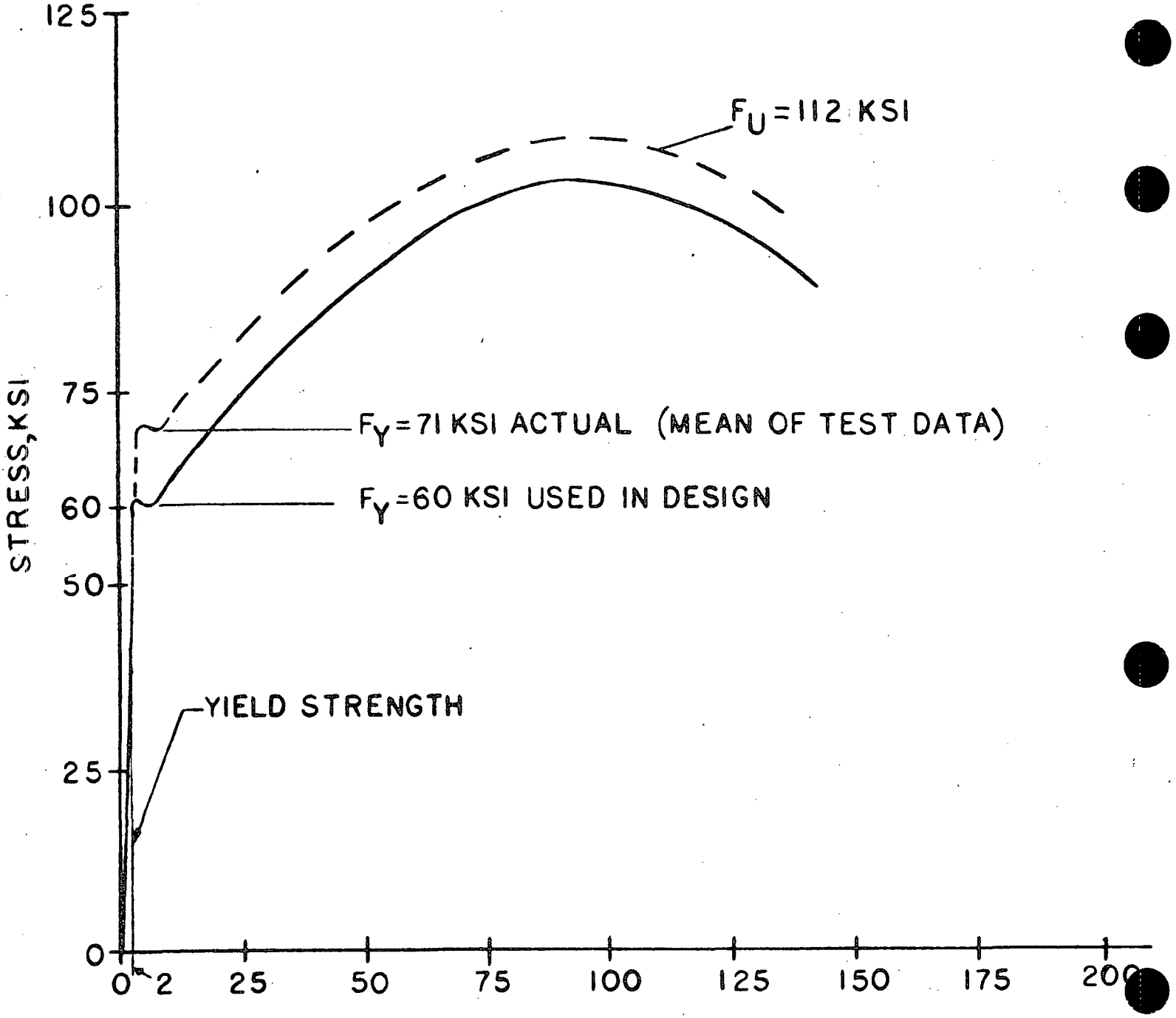
The specific composite nature of this reinforced concrete structure and the ductile behavior of the reinforcement allow this structure to develop a capacity characteristic of the average rebar strength. Table 2 summarizes the shell capacity as governed by hoop membrane capacity.

Only the minimum yield strength of the liner was included in these calculations. The actual yield is higher. Temperature plays no role in the capacity of the section at a state of general yield unless high enough to produce reductions in the material properties. A temperature spike on the liner will only increase the shell's radial displacement as illustrated in Figures 12 and 13.



MEMBRANE FORCES IN CONTAINMENT DUE TO PRESSURE

FIGURE 10



STRESS-STRAIN CURVE OF ASTM A-615-60 STEEL

FIGURE 11

TABLE 1

Main Reinforcing Steel - Test Results

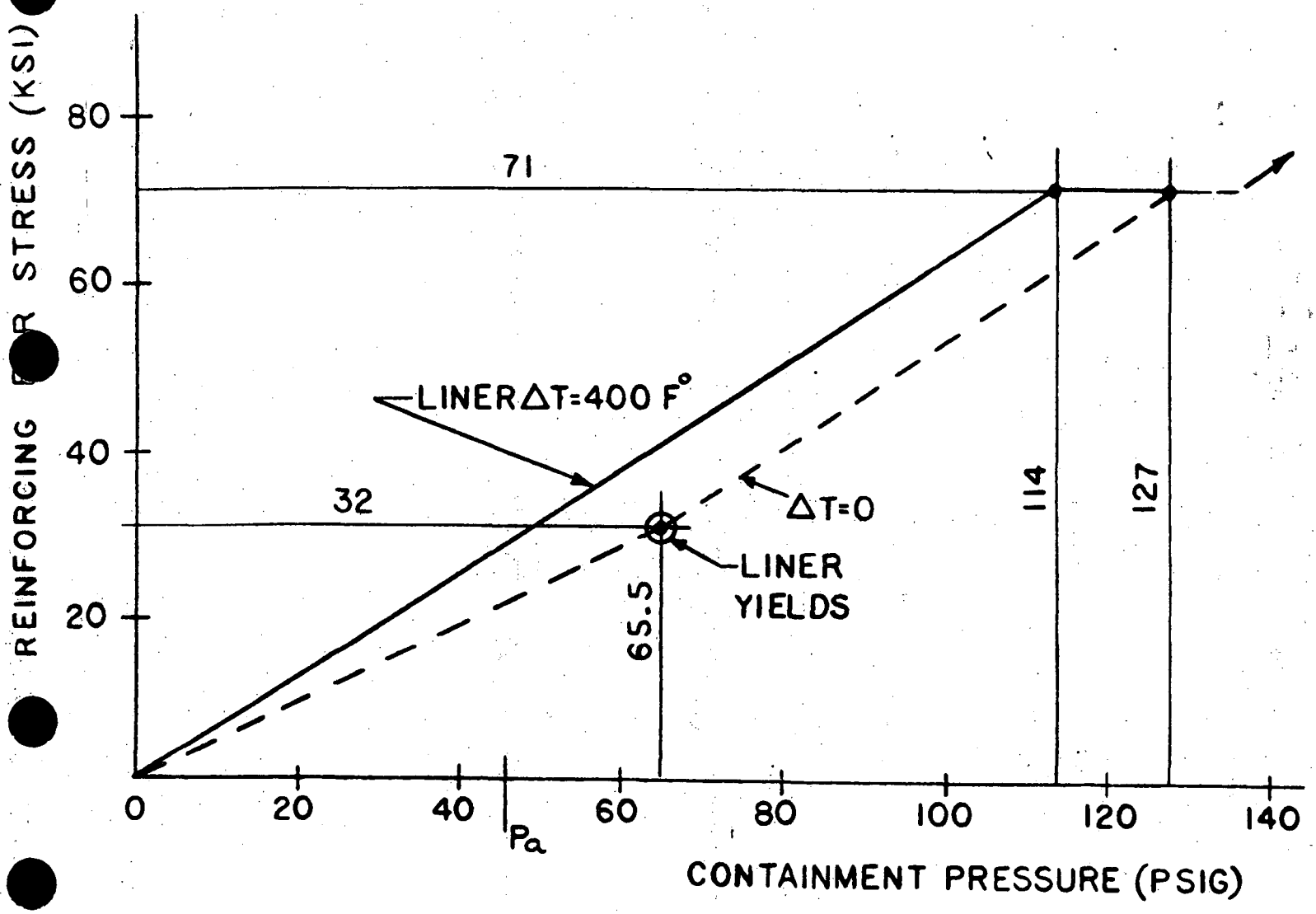
No. 18S Bars

Sample Size	N = 62
Mean Yield Stress	F_y = 71.82 KSI
Standard Deviation	S = 5.18 KSI

TABLE 2

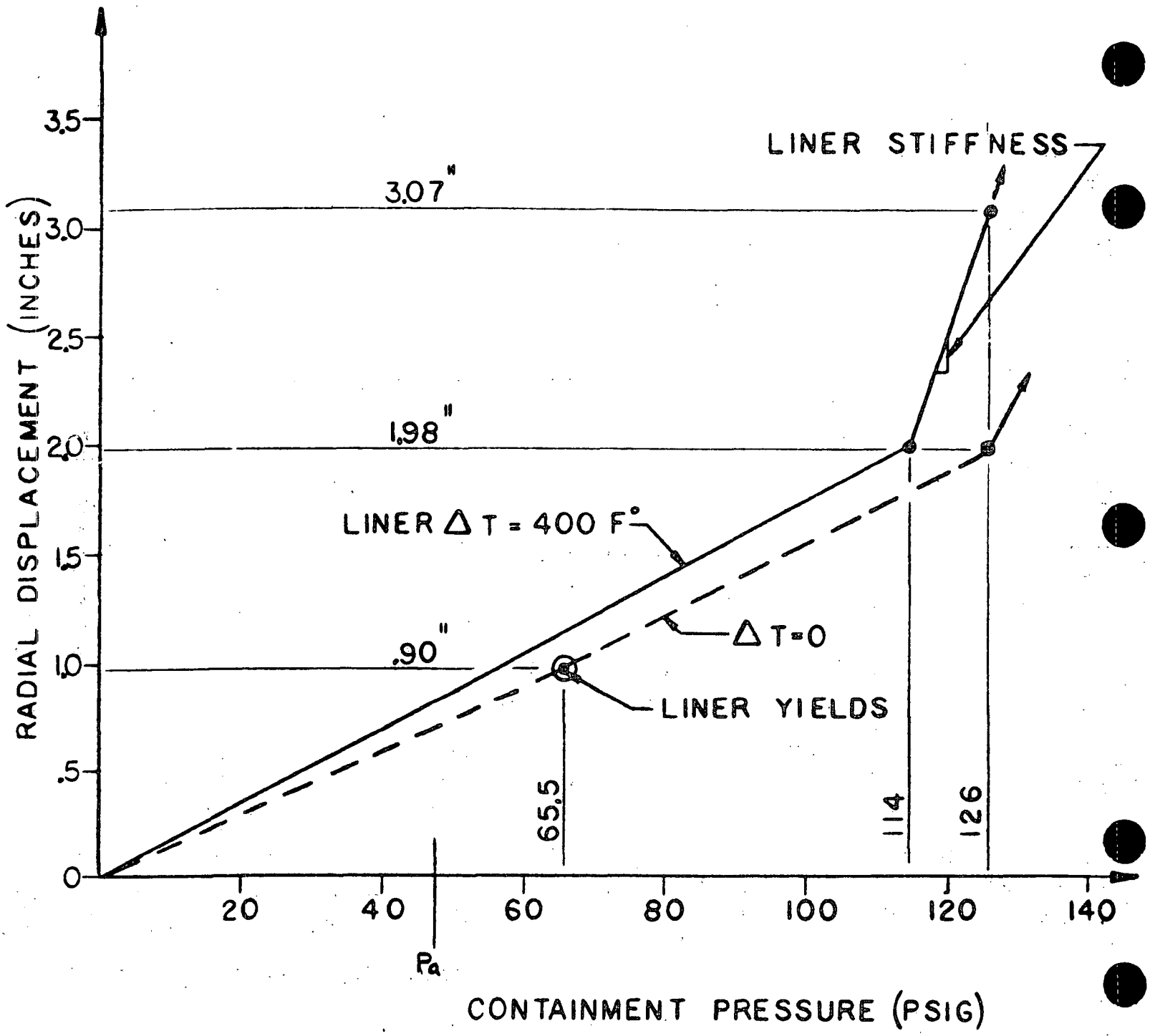
Maximum Pressures - Hoop Membrane Controlled

Unit	Region	Rebar	Liner	Total
No. 2	Base to 132'-8	121.1 PSI	14.8 PSI	135.9 PSI
	132'-8 to 174'-8	116.1 PSI	14.8 PSI	130.9 PSI
	174'-8 to 191'-0	111.1 PSI	14.8 PSI	125.9 PSI
No. 3	Base to 153'-0	114.2 PSI	14.8 PSI	129.0 PSI
	153'-0 to 191'-0	110.7 PSI	14.8 PSI	125.5 PSI



PLOT OF HOOP REBAR STRESS VERSUS CONTAINMENT PRESSURE—REGION OF CYLINDER WHERE SEISMIC REBAR IS REDUCED

FIGURE 12



PLOT OF RADIAL DISPLACEMENT VERSUS CONTAINMENT PRESSURE — REGION OF CYLINDER WHERE SEISMIC REBAR IS REDUCED

FIGURE 13

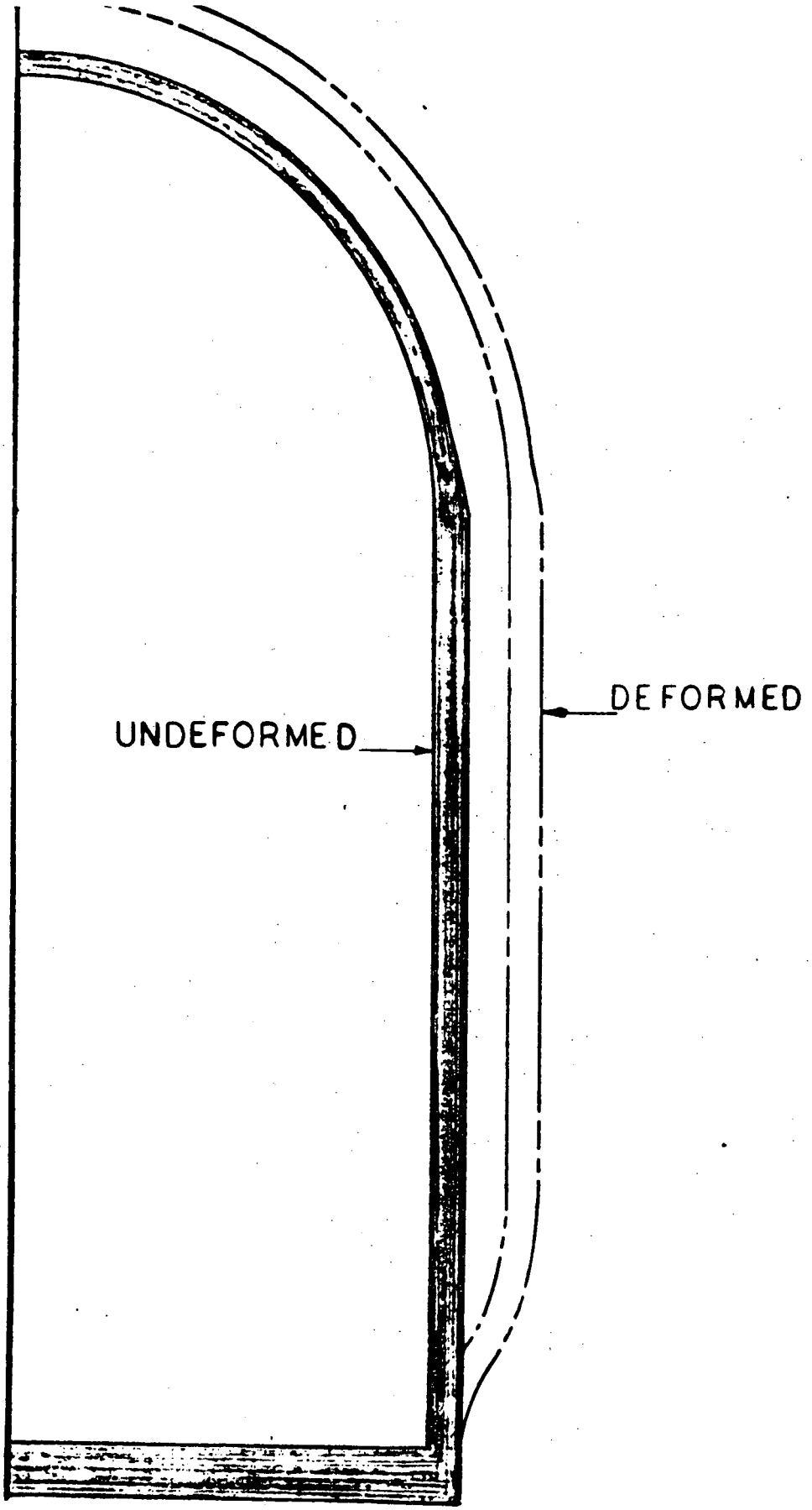
Discontinuity Regions - Forces and moments are induced in these regions because of the mismatch in radial displacements of base-mat, cylinder and dome under pressure loads, Figures 14, 15 and 16. At the springline, meridional moments and shears are secondary and are not large due to a designed compatible hoop stiffness at the dome-cylinder junction. The region was not critical. Meridional shears and moments at the base of the cylinder are also secondary but are large. Their magnitudes were computed with the classical beam on elastic foundation equations. Figure 17 illustrates the shells' force and moment distributions for design load combination "A". The shells' shear and moment capacities at the base were evaluated with allowance for the presence of meridional tension. The shear reinforcement, Figure 18, was designed to fully resist the radial shear forces. Additional meridional reinforcement near the inside surface of the wall increases the total quantity of meridional reinforcement to that far greater than required to resist meridional forces alone. In addition, the hoop reinforcement of the membrane region is contained in full quantity to the base. The hoop reinforcement at the base is not relied upon to transmit load but provides a redundancy for the base capacity. This region of the containment was found to have sufficient capacity so as not to be critical.

Table 3 summarizes the shell's moment and shear capacity at the base and the corresponding internal pressure capability of the containment.

The moment and shear capacities at the base of the containment are sufficient to withstand containment pressures in excess of 126 psi. In addition, yielding of meridional rebar 'softens' the end fixity and results in base moments and shears which increase with pressure in a nonlinear, lessened rate. This provides additional capacity not accounted for here. Dowel action of the main rebar also is not accounted for providing additional conservatisms in shear. Failure of the containment base in shear is precluded before general yield in the membrane regions of the shell. Insulation on the liner surface results in negligible thermal effects on base shear and moment.

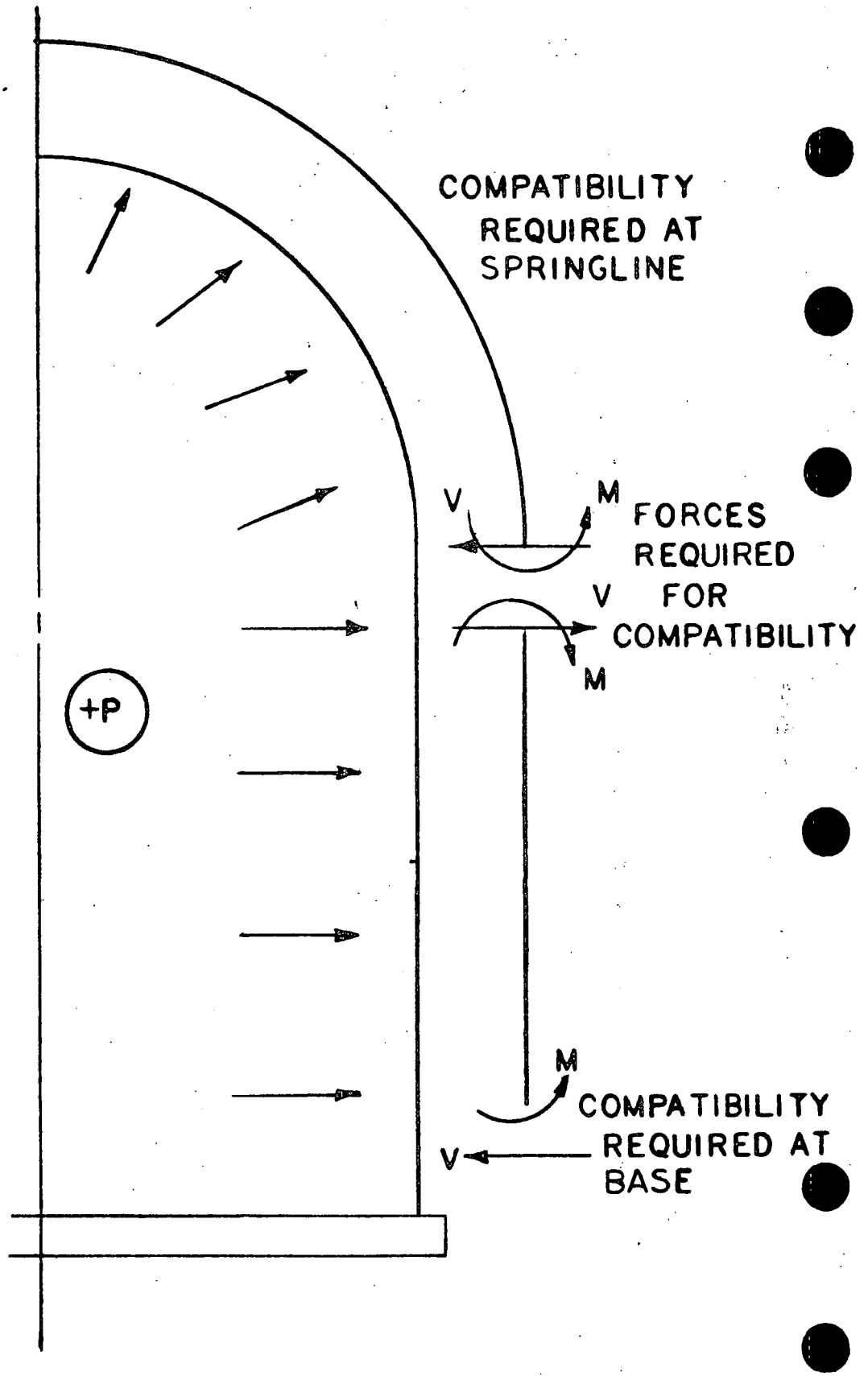
Base-Mat - The shear and tension forces and bending moments induced in the base mat during the pressure and temperature loads were evaluated on the basis of compatibility and equilibrium with the cylindrical shell, Figure 19. The reinforcement details were reviewed and the capability of the mat evaluated including the presence of tension on shear and moment capacities, Figure 20. This region of the containment was found not to be critical.

The meridional force in the wall due to pressure load is reduced by dead weight loading and applied to the base mat as shear. Axial tension and moment in the mat are similarly calculated. The foundation reaction was approximated by a uniform distribution but with the edge uplifting. The shear capacity was shown to permit containment pressures in excess of 126 psi. Yielding of rebar due to moment is predicted. However, this nonlinear effect will result in moments less than predicted by linear analysis.



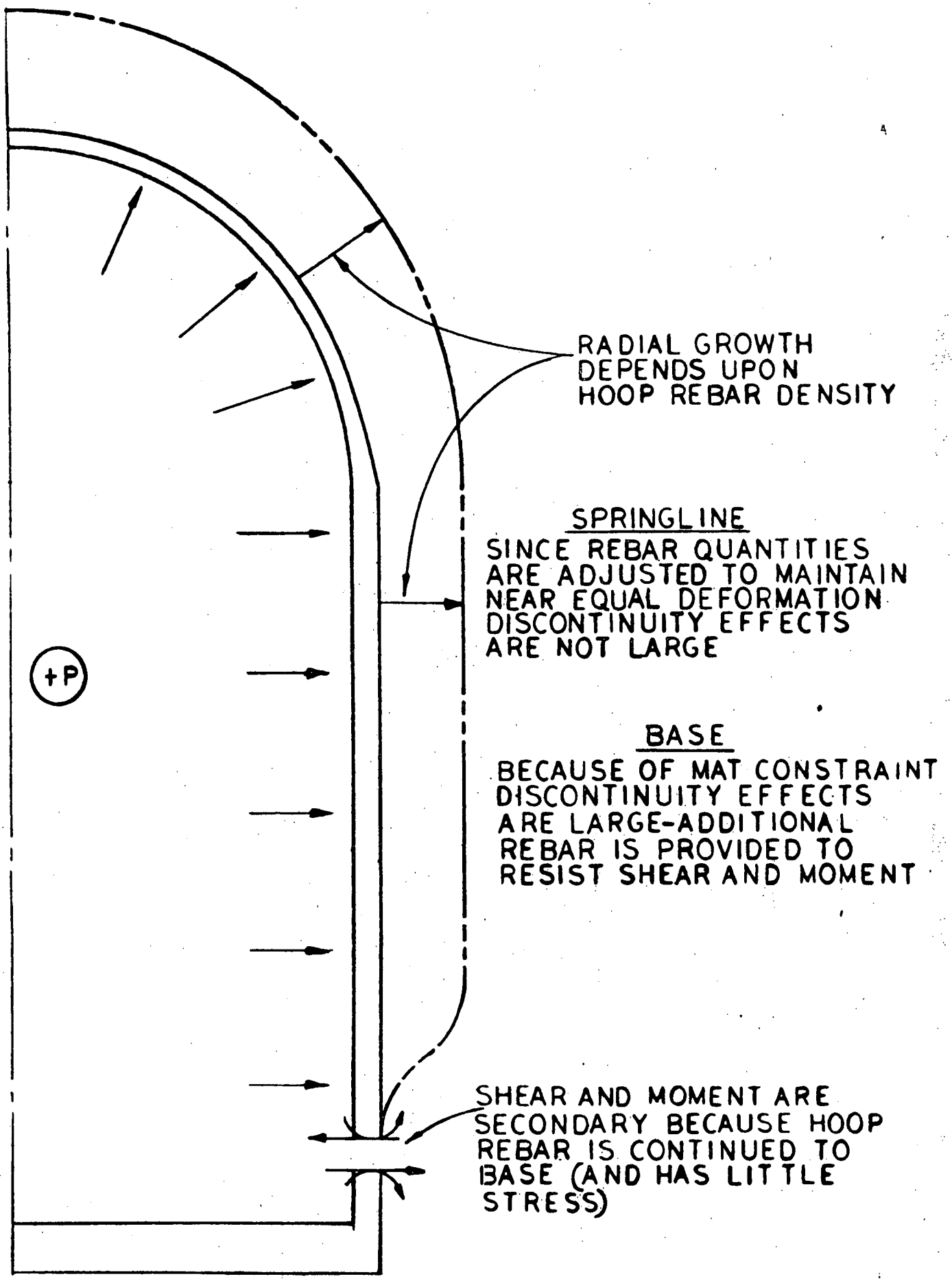
SKETCH OF DEFORMED SHAPE UNDER TEMPERATURE AND PRESSURE LOADING

FIGURE 14



DEFORMED SHAPE OF CONTAINMENT BEFORE IMPOSITION OF COMPATIBILITY

FIGURE 15



DEFORMED SHAPE OF CONTAINMENT AFTER IMPOSITION OF COMPATIBILITY (EXAGGERATED)

FIGURE 16

$$C = 1.0D \pm 0.05D + 1.5P + 1.0(T+TL)$$

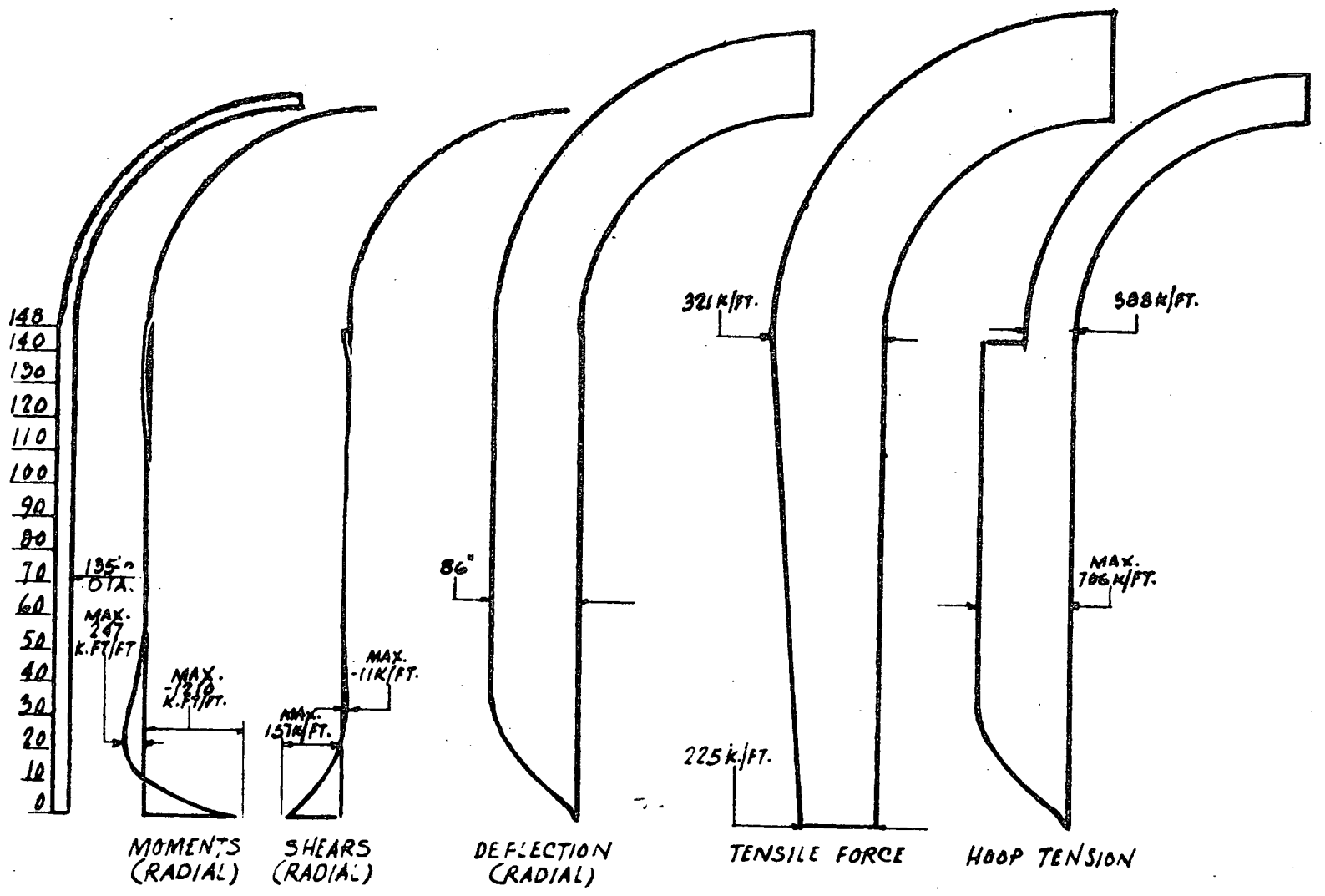
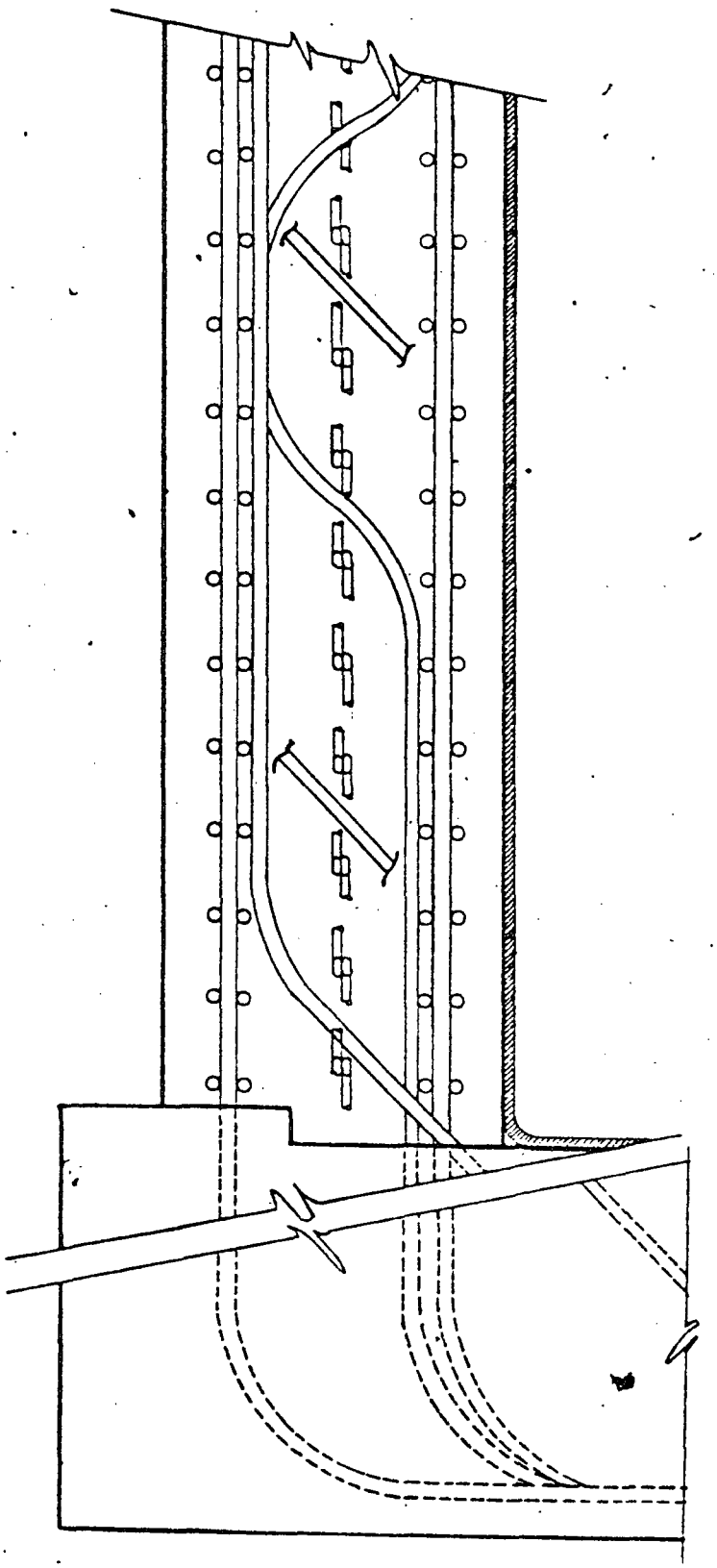


FIGURE 17

REVISED 8/20/81



DISCONTINUITY REGION AT
BASE OF CONTAINMENT SHELL

FIGURE 18

TABLE 3

Moment And Shear Capacity At Base Of Containment Wall

Section Moment Capacity

Mu = 23628 K·in/ft for Fy = 71.82 KSI

Section Moment As = 9.27 in^2 (tension steel)

Mo = 158.4 K·in/ft/psi for Fixed Base
= 0 for Hinged Base

Maximum Containment Pressure = 149 psi for fixed base

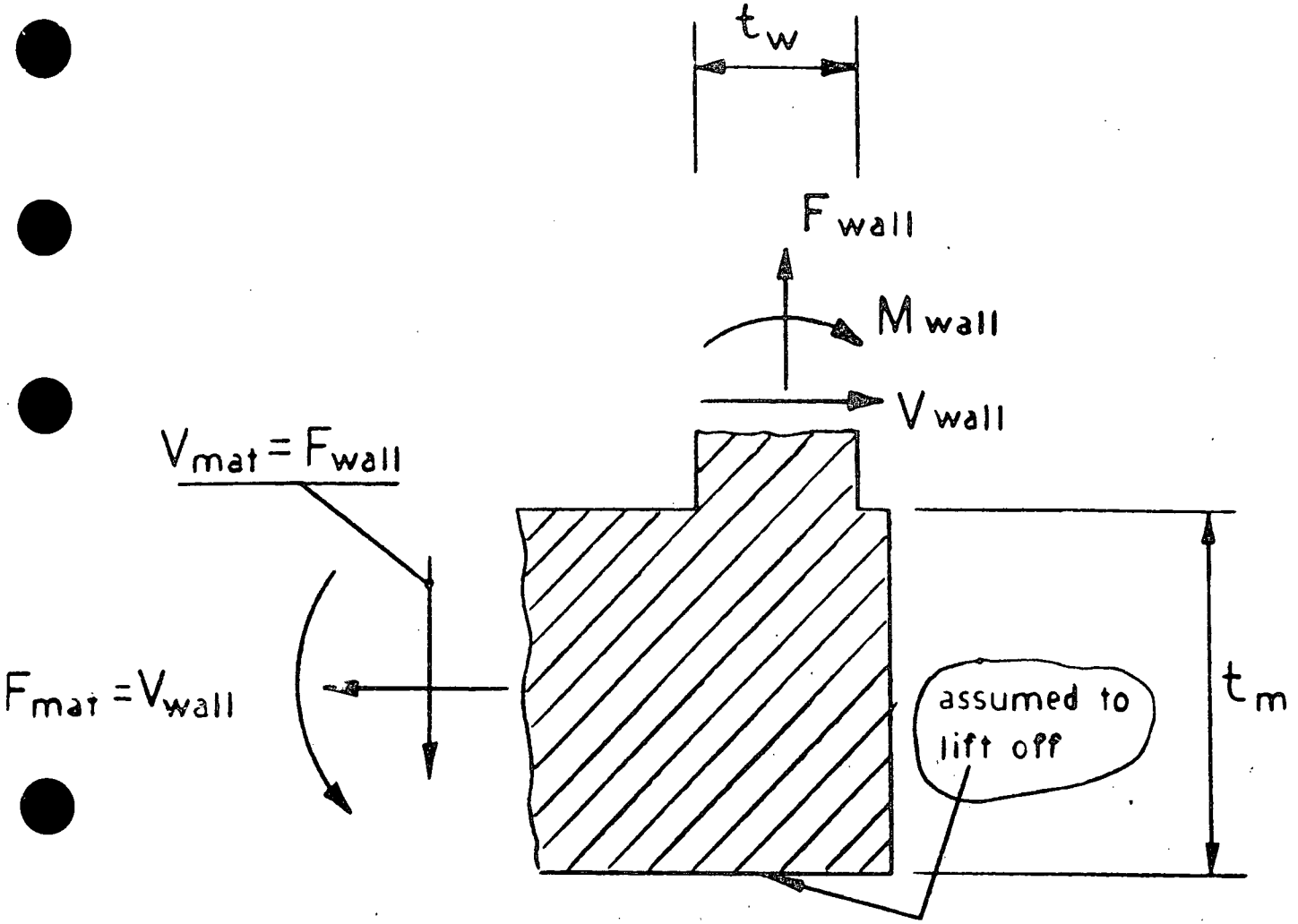
Section Shear Capacity

Vu = 256 K/ft for fy = 71.82 KSI; V_c = 0

Section Shear

Vo = 1.95 K/ft/psi for Fixed Base
= 0.975 K/ft/psi for Hinged Base

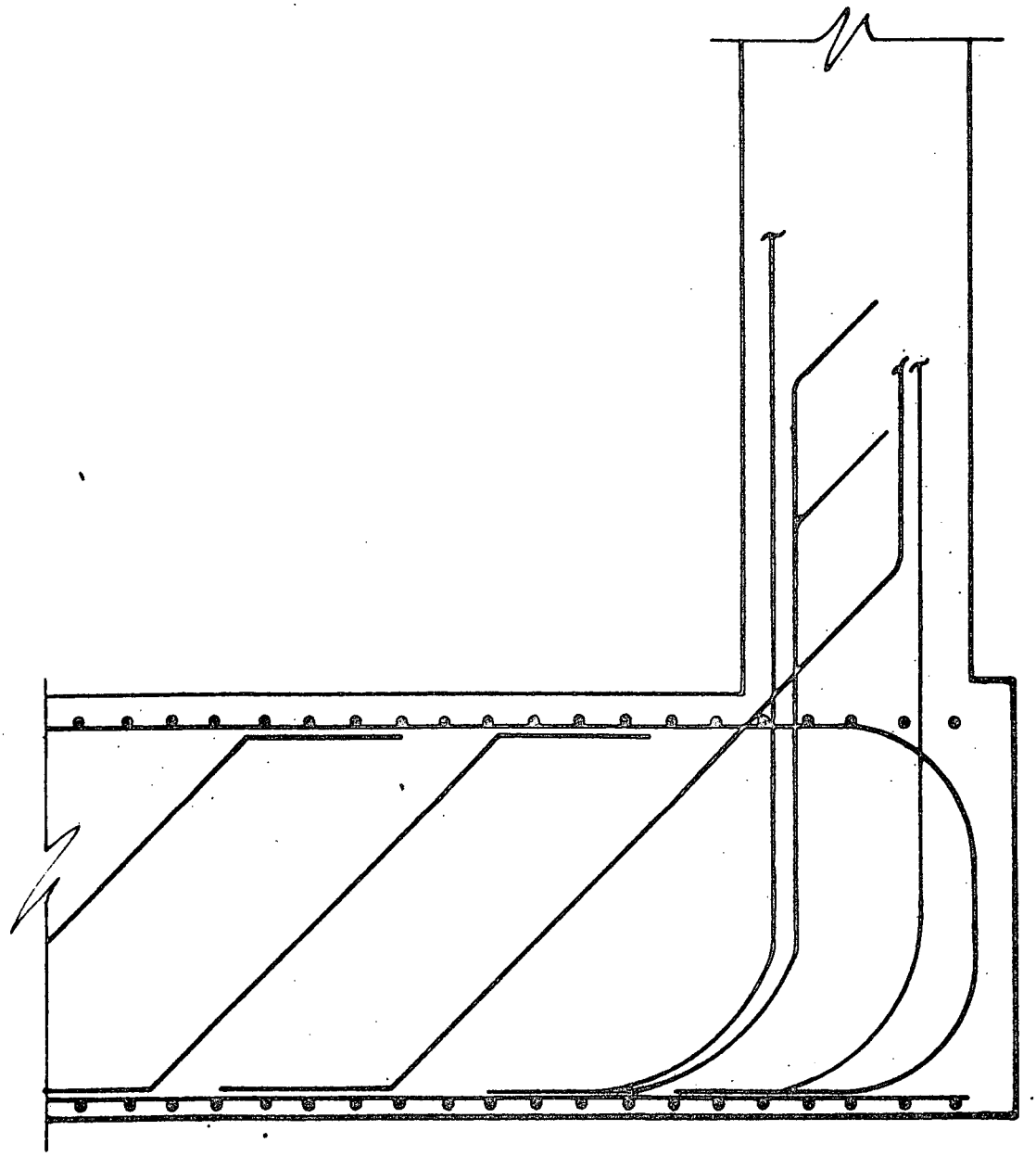
Maximum Containment Pressure = 131 psi for Fixed Base



$$M_{mat} = M_{wall} + V_{wall} \frac{t_m}{2} - F_{wall} \frac{t_w}{2}$$

DISCONTINUITY REGION SHOWING MAT FORCES

FIGURE 19



SECTION THROUGH MAT BELOW

CONTAINMENT WALL

FIGURE 20

Conclusion - The limiting zone of the containment was found to be in the membrane region of the cylinder below the springline where the quantity of seismic reinforcing steel is reduced. Membrane hoop forces produce the limiting condition at a pressure of 126 psig (141 psia). The region is one of high ductility. When pressure is sufficient to produce the general yield state in the shell reinforcement, the effect of temperature is to alter the shells state of strain only, Figures 12 and 13. The final strain state is load history dependent.

4.2 Liner and Liner Anchorage

A feedwater line break at Unit No. 2 and subsequent study[1] were reviewed for consequences of accident temperature on the liner and liner anchorage system. During this incident, the liner experienced local temperatures near 300°F. The liner plate in the immediate area was deformed and nine studs appeared to be damaged. The liner integrity was not violated by the incident. The liner deformation and damaged studs are sited in the regions known to be most highly stressed by thermal loads. As a result of this incident and study, thermal insulation on the liner was extended to 81 feet 9 inches in selected areas.

Pressures to 126 psi do not induce excessive strains in the liner plate. Pressure induced shell deformation relieves liner plate thermal effects. It was concluded that temperatures to at least 300°F when combined with a pressure of 126 psi will not result in loss of liner integrity.

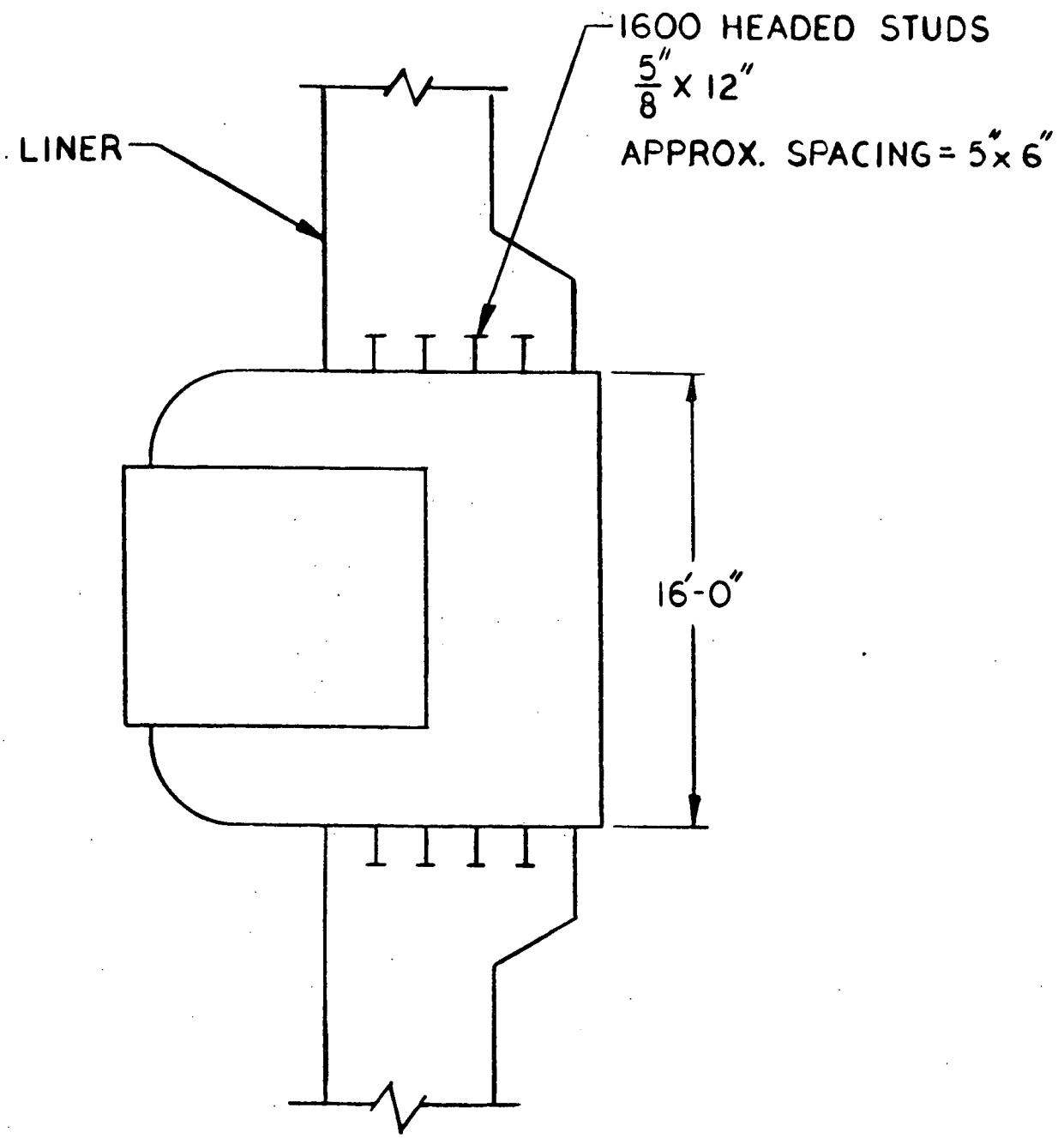
4.3 Penetrations

Large Penetrations - The equipment hatch, Figure 21, and personnel airlock were evaluated for their capacity under pressure loading equal to that which induces the general yield state in the membrane regions of the shell, previously defined as the limiting capability of the shell for this study. Primary membrane plus bending were considered in the evaluation of these steel components. The anchorages to the concrete shell were also checked.

The reinforced concrete shell capacity in the regions next to these large penetrations was reviewed, giving consideration to the sharp increase in forces and moments local to the hole. The shell designs incorporate a boss region, Figure 6, with substantial increases in reinforcement to resist these local effects. The induced moments, shear and increase in membrane forces rapidly decreases with distance away from the hole. It was concluded that any yielding which might occur would be local and that the bulk of the boss regions would remain elastic. The structural integrity tests support this conclusion as no excessive crack widths were found. The qualitative conclusion was that the capability of the reinforcement next to the large penetrations was sufficient so that these regions were not critical.

---

[1] Feedwater Line Incident Report, Indian Point Unit No. 2, Consolidated Edison Company, January 14, 1974



SKETCH OF EQUIPMENT HATCH

FIGURE 21

Small Penetrations - Representative piping penetrations were evaluated for pressure loading and applied piping reactions. The anchorage to the concrete shell was also reviewed. The design capacity of these details was found to be sufficient so as not to be critical. The local capability of the reinforced concrete shell was assessed. The small penetrations introduce force concentrations but negligible moments. These forces are resisted by an increase in reinforcement density. The local rebar stress increase is substantially less than the force concentration. If yielding did occur, it would only be in reinforcement immediately next to the hole and the magnitude of the strain would be limited since the remainder of the section is elastic. The structural integrity tests have shown no excessive crack widths near penetrations. These regions were judged not to be critical.

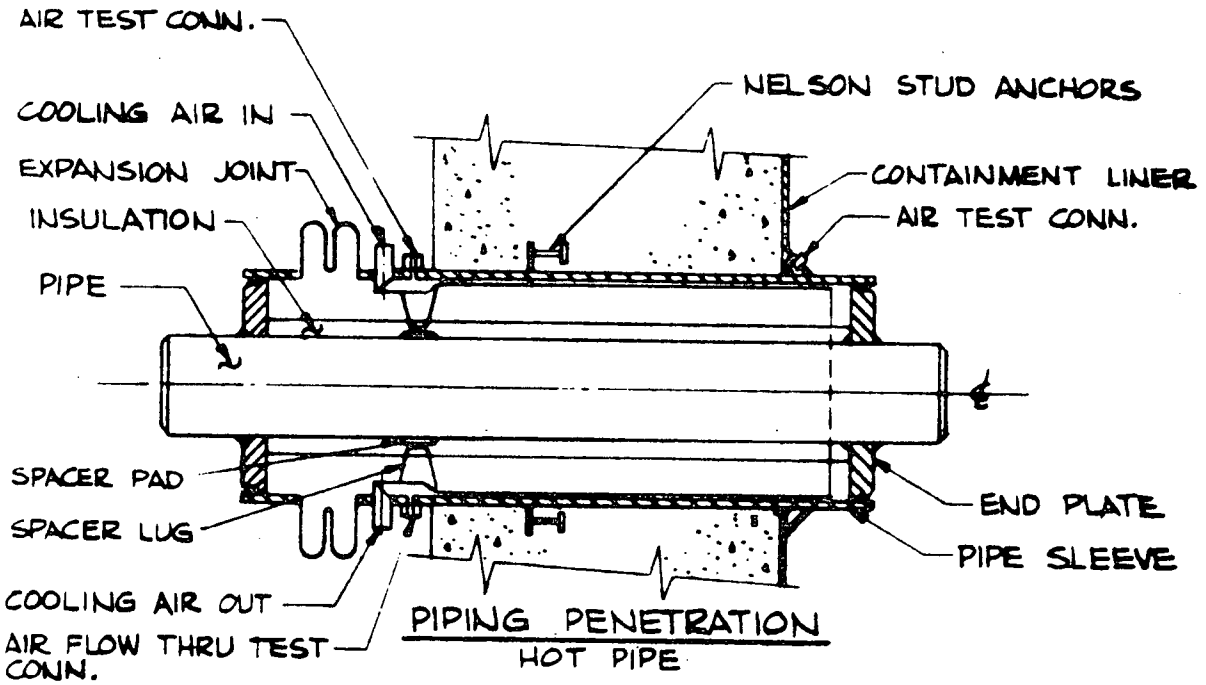
4.4 Piping Penetration Assemblies

For purposes of studying the piping penetrations, as represented in Figure 22, the containment structure was subjected to a range of temperatures at a given internal pressure of 160 psig. The load capability of the sleeve, the end plate, and the end plate to process pipe weld size were evaluated separately. The lowest limit was chosen to represent the limiting threshold. The loads on the penetrations included the effect of combined deadweight, seismic and thermal moment loads, plus, containment pressure of 160 psi. The maximum weld stress was limited to the value obtained by applying a faulted factor of 1.5 to the allowable weld stress from Table NF 3292.1-1 of ASME III, Subsection NF.

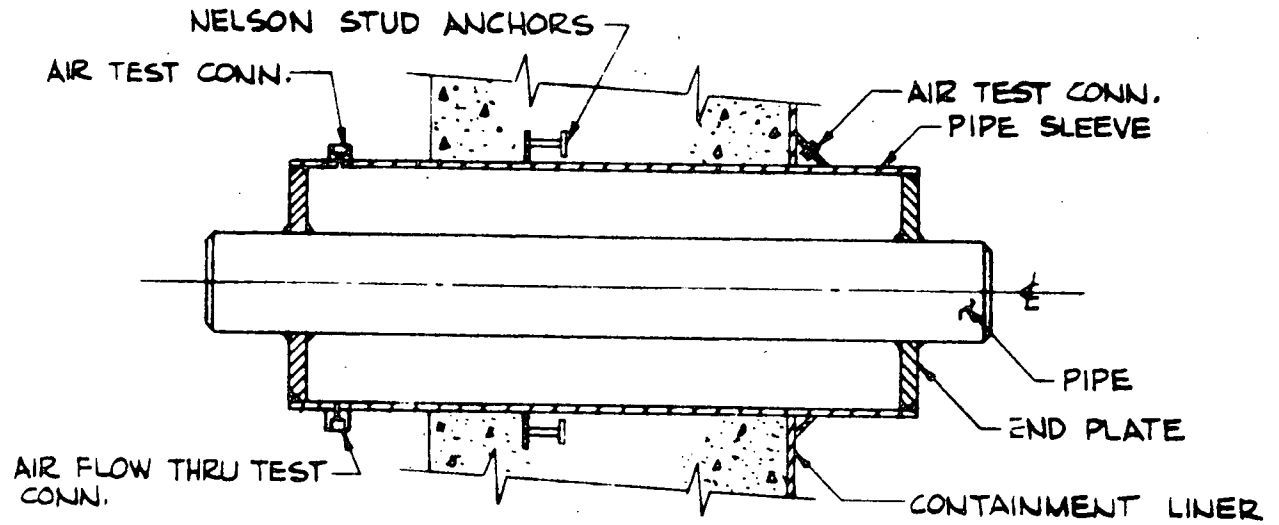
Based on these assumptions, temperature on piping penetration welds was found to be the limiting factor. Under these conditions an internal containment temperature of 317°F would raise one point of a weld up to the maximum NF allowable stress. As the temperature would increase, the maximum allowable stress would spread throughout the whole weld.

These results do not include the effect of the growth of the containment wall under pressure loading or any growth of the containment wall due to absorbing heat from within the containment. Both of these effects would tend to decrease stresses in the sleeve and would increase the thermal capability of the pipe penetrations. Per Westinghouse test data records, the containment electrical penetrations can successfully withstand pressures well above those encountered in the containment during and after a postulated LOCA. Also, these same penetrations can withstand a containment temperature of 400°F and still preserve integrity of the containment boundary. Temperature is therefore also the limiting condition for the containment electrical penetrations.

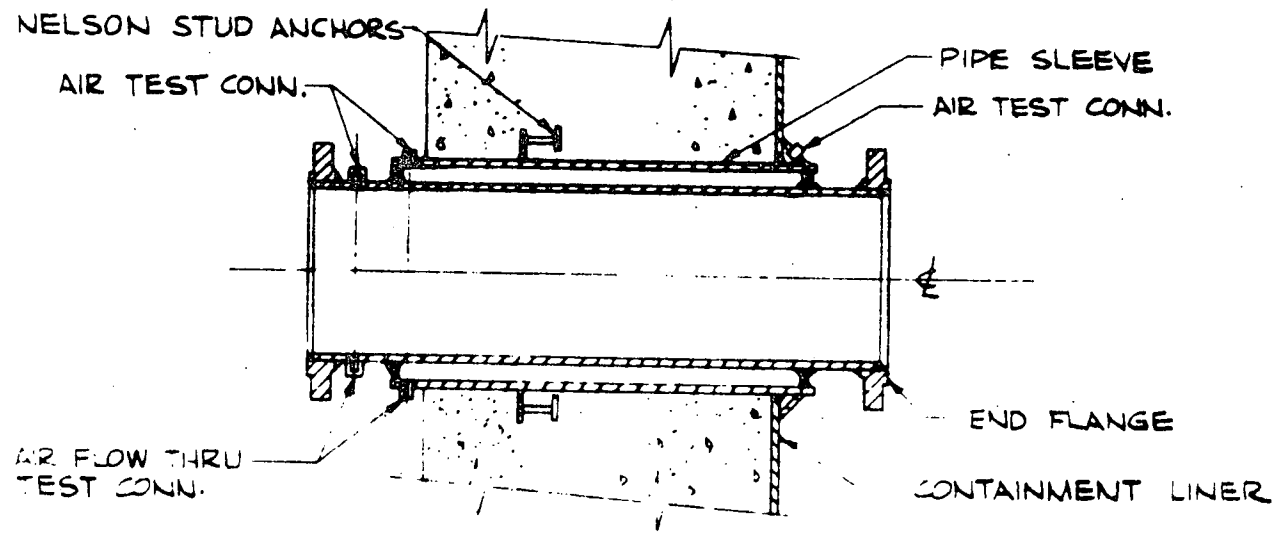
As part of penetration, the 10 inch Containment Pressure Relief butterfly valves and the 36 inch Containment Atmosphere Purge butterfly valves have also been evaluated. The following data were obtained:



PIPING PENETRATION
HOT PIPE



PIPING PENETRATION
COLD PIPE



PIPE PENETRATION
PURGE PIPING

FIGURE 22

The 10-inch valves are lined with EPT seat material which can withstand up to 300°F and 150 psig. The 36 inch valves are lined with EPDM seat material which can withstand 270°F at 50 psig. This indicates that at these P-T limits, "plastic" seats do show signs of softening. The results could be a possible air leakage past the seat of the first of each of the two redundant valves (the valves in contact with the inside containment). The second isolation valve being further away from the containment will be exposed to a lower temperature due to distance-created gradient.

In actuality, there is also a 52 psi air "buffer" injected between each of the redundant 10 inch, and each of the 36 inch valves. This "backup" pressure will allow the 10 and 36 inch valve seats to withstand a containment P-T build-up to about 300°F at 202 psig and 270°F at 102 psig, respectively.

Similarly, structural failure of the valve discs will be delayed by the 52 psi "buffer", resulting in the 10 inch valve disc being able to withstand a containment P-T of up to about 260 psig at 275°F, and the 36 inch valve disc being capable to withstand a containment P-T increase of up to about 130 psig at 275°F.

5. Conclusions

Results of this evaluation show that the Indian Point Units 2 and 3 Containment Vessels can withstand a pressure of 126 psig (141 psia), 2.7 times the design accident pressure, without impairing the functional capability of the containment. Other than inducing thermal strains in the containment, temperature to at least 300°F was found to have little or no effect on capability.

The following regions of the containment were evaluated:

A) Membrane region of the dome and cylinder.

B) Discontinuity region at the springline.

C) Discontinuity region at the base of the cylinder.

D) Base-mat

E) Large penetrations - equipment hatch and personnel airlock.

F) Several small penetrations.

G) Liner.

The limiting region was found to be in the cylinder below the springline in a zone where the seismic reinforcing steel is reduced. The membrane hoop forces produce this limiting condition.

The actual yield strength of the reinforcing steel was established by computing the mean of the test data from full scale tests of containment reinforcing steel. The actual yield strength was found to be 18 percent higher than the minimum yield strength used in design. The actual strength of the liner and concrete was also found to be significantly higher than assumed in design. However, these effects were conservatively neglected in this evaluation.

The discontinuity regions and the base mat were evaluated for shear and bending in the presence of tension and were not governing. The overall response of the equipment hatch and personnel airlock was evaluated. Primary membrane and bending stresses were computed and found to be within acceptable limits. In addition, the anchorage of the equipment hatch and personnel airlock to the concrete was evaluated to ensure that pressure loads could be transmitted to the concrete.

Several representative piping penetration assemblies were evaluated for pressure and applied piping reactions. The penetrations and their attachments to the concrete were found not to be critical.

In summary, the limiting zone of the containment was found to be below the springline in the region where the seismic reinforcing steel is reduced. Membrane hoop forces produce the limiting condition which occurs in a region of high ductility away from discontinuities. The discontinuity regions were found to have at least the conservatism as the membrane region which is con-

sistent with the philosophy of the ACI 318-63 Building Code used in the original design. This code mandates additional conservatism in regions of low ductility. Shear, anchorage and compression do not govern design.

The maximum pressure that the containments can withstand based upon the conservative definition of capability established for the purpose of this evaluation is 126 psig (141 psia) or 2.7 times the design accident pressure.

The 2.7 factor directly corresponds to conservatisms applied in the original design. These are identified below:

1.	Application of load factors	(1.5)
2.	Application of capacity reduction factors	(1.11)
3.	Strength of liner not accounted for	(1.15)
4.	Minimum strength of material considered	(1.18)
5.	Seismic rebar resisting LOCA loads	(1.12)
6.	Designer Conservatism	(1.06)

The product of these factors is 2.7 and represents the level of conservatism present in the original design. Thus, the 2.7 times the design accident pressure of 47 psig or 126 psig represents a confident lower bound of functional capability and represents limit of elastic response. The actual capability is higher.

APPENDIX 4.4.2

STRUCTURAL HEAT TRANSFER MODELING

APPENDIX 4.4.2

STRUCTURAL HEAT TRANSFER MODELING

The heat flux to a structural heat sink is the sum of radiation, convection, and condensation, or

$$q''_{STRUCTURAL,\ TOTAL} = q''_{RADIATION} + q''_{CONVECTION} + q''_{CONDENSATION}$$

where

$q''_{STRUCTURAL,\ TOTAL}$ = Total structural heat flux (Btu/hr-ft^2)

$q''_{RADIATION}$ = Radiation heat flux (Btu/hr-ft^2)

$q''_{CONVECTION}$ = Convection heat flux (Btu/hr-ft^2)

$q''_{CONDENSATION}$ = Condensation heat flux (Btu/hr-ft^2)

The heat flux due to radiation can be represented by

$$q''_{RADIATION} = H_{RADIATION} (T_{ATMOSPHERE} - T_{SURFACE})$$

where

$H_{RADIATION}$ = Heat transfer coefficient due to radiation*, (Btu/hr-ft^2-^{o}F)

$T_{ATMOSPHERE}$ = Containment atmosphere temperature, (^{o}F)

$T_{SURFACE}$ = Structural surface temperature, (^{o}F)

The heat flux due to convection can be represented in a similar manner.

---

*See Appendix 4.4.7.

$$q''_{CONVECTION} = H_{CONVECTION} (T_{ATMOSPHERE} - T_{SURFACE})$$

where the heat transfer coefficient due to convection ($H_{CONVECTION}$) is defined using the correlation given in reference (1).

The heat flux due to condensation is calculated in the following manner.

$$q''_{CONDENSATION} = H_{CONDENSATION} (T_{SATURATION} - T_{SURFACE})$$

where the new variables are

$H_{CONDENSATION}$ = Condensation heat transfer coefficent**. ($Btu/hr\text{-}ft^2\text{-}^oF$)

$T_{SATURATION}$ = Containment saturation temperature (^oF)

The surface temperature is determined from the simultaneous solution of the heat transfer equations (as just described in this appendix) and the conduction equations through the structure.

**The stagnant Tagami correlation is utilized to define $H_{CONDENSATION}$. (Ref. 2)

REFERENCES

1. F. Kreith, Principles of Heat Transfer, fifth printing, January 1962, copyright 1958 by the International Textbook Company, Scranton Pa., Chapter 7, pg. 310.

2. Tagami, Takasi, Interim Report on Safety Assessments and Facilities Establishment Project in Japan for Period Ending June, 1965 (No. 1).

APPENDIX 4.4.3

FLAME TEMPERATURE CALCULATION

APPENDIX 4.4.3
FLAME TEMPERATURE CALCULATION

As noted in Section 4.2.2, a model has been developed to determine when there is sufficient hydrogen in the containment atmosphere to support combustion. To establish the validity of this model, tests are being performed to define the flammability threshold (i.e., establish the Flame Temperature Criterion) by Fenwal Incorporated at their test site in Ashland, Massachusetts. In addition to verifying the Flame Temperature Criterion these tests should provide an empirical basis for the laminar burn velocity; help define the time period over which combustion can occur; and illustrate the effect of containment sprays on retarding hydrogen burn.

Two different test chambers will be used. The majority of the tests will be performed in a 3 foot vessel with a 100 joule source. To investigate scaling, sprays, and multiple ignition, a 5 foot vessel will be used to run selected tests.

The test matrix has been set up to cover a range of postulated accident conditions. They are as follows:

Initial Pressure	15-60 psia
Initial Temperature	20-350^{o}C
Water Mole Fraction	0-80%
Hydrogen Mole Fraction	6-14%

The model currently used to establish the Flame Temperature Criterion is given below.

Let Y_i = Mole fraction of i in containment atmosphere.

Then, for one mole of containment atmosphere*:

$$Y_{HYD} + Y_{OX} + Y_{STM} + Y_{CO_2} + Y_{NT} + Y_{CO} =$$

$$(Y_{HYD} - A) + (A + Y_{STM}) + (B + Y_{CO_2}) + (Y_{OX} - A/2 - B/2)$$

$$+ (Y_{CO} - B) + Y_{NT}$$

where:

A = Moles of H_2 reacted
B = Moles of CO reacted

---

* Subscripts are defined as follows: HYD = hydrogen, STM = steam, NT = nitrogen, OX = oxygen, CO_2 = carbon dioxide, CO = carbon monoxide

Note that reaction stoichiometry without inerts is as follows:

$$(A)\ H_2 + (A)/2\ O_2 = (A)\ H_2O$$
$$(B)\ CO + (B)/2\ O_2 = (B)\ CO_2$$

The heat of the reaction is

$$(A)\ \Delta H_{FORMATION,\ H\ O_2} + (B)\ (\Delta H_{FORMATION,\ CO_2} - \Delta H_{FORMATION,\ CO}) = Q_{REACTION}$$

$$Q_{REACTION} = \Sigma\ (Y_{PRODUCTS}\ H_{PRODUCTS} - Y_{REACTANTS}\ H_{REACTANTS})$$

where

H = molal enthalpy, which is a function of temperature.

Since

$T_{REACTANTS}$, $Y_{REACTANTS}$, $H_{REACTANTS}$ and $Y_{PRODUCTS}$ are known,

$T_{PRODUCTS}$ and $H_{PRODUCTS}$ can be calculated.

$T_{PRODUCTS}$ is known as the flame temperature (T_{FLAME}).

If $T_{FLAME} > T_{CRITERION}$; bulk combustion can be sustained.

APPENDIX 4.4.4

MARCH IN-VESSEL PRESSURE SPIKE

APPENDIX 4.4.4

MARCH IN-VESSEL PRESSURE SPIKE

Following the 60 day study, one area identified for further investigation was the in-vessel pressure spike. It was this spike of approximately 2500 psi,* caused by vaporization of water in the reactor vessel's lower plenum, that other investigators indicated could cause loss of containment integrity as a result of steam generator tube failure. Because initially this was not identified as a mode for containment failure, relatively little work was spent in developing techniques to calculate the magnitude of this pressure spike in the development of the MARCH computer code. Therefore this study was divided into two parts:

1. Review MARCH calculations to determine the validity of the techniques MARCH uses to calculate the in-vessel pressure spike.

2. Perform a separate set of calculations to estimate the magnitude of the in-vessel pressure spike.

Because the pressure spike was caused by the core debris/water interaction in the lower plenum of the reactor vessel and the associated vaporization of the water, a number of MARCH calculations were performed that varied the assumed mass of water in the lower plenum. These results are summarized by the first four cases in Table 4.4.4-1. As these results demonstrate, the sensitivity of the MARCH calculated in-vessel pressure spike to the assumed water mass in the reactor vessel lower plenum was not as great as expected. In fact, with only 100 lbs of water vaporized, a pressure rise of 954 psi occurred. This indicated that further study was needed to understand the MARCH calculational and modeling techniques.

Discussions with the developer of the MARCH computer code (Battelle Columbus Laboratories), indicated that these results could be the result of a calculational technique used by MARCH. To calculate the steam pressure, the code assumes that steam is a perfect gas and uses an ideal gas law as the equation of state**. The gas constant is updated during

---

* Detailed analysis of the steam generator tubes (See Appendix 4.4.5) has demonstrated that steam generator tubes would not fail under these conditions.

** Hand calculations indicate that the gas constant based on saturated conditions at 32°F is a factor of two greater than the gas constant for saturated conditions at 2500 psia.

the transient, always basing it on the temperature of the water in the reactor coolant from the previous time step. When the reactor coolant system's water mass goes to zero, the code uses saturated steam at 32°F to define the gas constant. Battelle Columbus Laboratories provided an input variable that could be used to set a minimum value for the RCS water mass, thus providing a means to identify more realistic conditions for the definition of the gas constant. Cases 5 and 6 in Table 1 were then run with a minimum RCS water mass of 50 lbs specified.

Cases 1 and 5 are identical except that case 5 provides a minimum RCS water mass of 50 lbs so that the gas constant can be better defined, and it also provides an indication of the step change effect caused by the manner in which the gas constant is defined. In case 1, a pressure rise of 2667 psi was calculated versus a pressure rise of 489 psi in case 5. It appears that this difference occurs only because of the manner in which the gas constant is defined. This shows that within the constraints of the MARCH calculational model, the majority of the in-vessel pressure rise reported by other investigators was probably caused by a questionable calculational technique. A more realistic MARCH calculated upper bound of the in-vessel steam spike for the scenario studied is 489 psi. Case 6 showed that, as expected, the in-vessel pressure spike approaches zero as the reactor vessel lower plenum water mass approaches zero.

Further reviews of the MARCH calculations also indicated another inappropriate analysis technique in this area. It appears that all of the water in the lower plenum of the reactor vessel is vaporized over a single timestep. While the timesteps over which the vaporization occurs can vary for different calculations, the magnitude of the timestep is not based on any physical criteria or constraint. Therefore, a better basis for the rate of vaporization is needed before the magnitude of the in-vessel pressure spike can be determined.

This review of the MARCH calculational technique indicates that the basis for the concern about steam generator tube failure from an in-vessel steam spike is not valid. Therefore, a separate set of calculations was performed to estimate the in-vessel pressure spike. The following discussion describes these calculations.

When damaged core material for a set of postulated accident conditions comes into contact with water, the vaporization rate should be limited by the hydrodynamic characteristics of the water. This means that if the core quenching takes place in a very short time, the resulting vapor will displace the water away from the heat source. Therefore, the maximum rate at which energy extraction can occur from such a system would be determined by the critical heat flux, that establishes the maximum rate at which vapor can be removed from the system in the presence of water moving downward toward the heated surface. An expression for the critical heat flux is given by

$$q/A = 0.14\, h_{fg}\, (\rho_g)^{1/2} \left(g\sigma\, (\rho_f - \rho_g)\right)^{1/4} \qquad (1)$$

which involves the densities of the two phases (ρ_g, ρ_f), the latent heat of vaporization (h_{fg}), the acceleration of gravity (g), and the liquid-vapor surface tension (σ). This expression maximizes at a pressure of about 7.0 MPa and a heat flux of approximately 4 Mw per square meter. Given this heat flux, the available area through which such removal can be effected could be that cross-sectional area of the core barrel itself (πr^2), which corresponds to approximately 10 square meters. Or, the damaged core could be in a hemispherical configuration in which the available surface area would be $2\pi r^2$ (20 square meters). If the system pressure is assumed to be 15.5 MPa (2250 psia) and the corresponding critical heat flux is 2.5 Mw per square meter, the above surface areas correspond to heat removal rates of 25 to 50 Mw, respectively. Assuming that the total core (100,000 kg) is heated to a temperature of 3000°C, and must be quenched to a temperature of approximately 300°C, the stored energy to be removed is 162,000 MJ. Assuming that the decay power left within the melt at this point in time is approximately 15 Mw, the above mechanism would result in a net cooling of 10 and 35 Mw, respectively. Given a total energy that must be removed and the energy removal rate, the times involved for the total quench of the damaged core state are 4.5 hours in the first case and 1.3 hours in the second case.

To study the response of the reactor coolant system to various boil-off rates, two COCOCLASS9 models of the reactor coolant system were developed. The only difference between the two models is that one modeled the reactor coolant system structures as heat sinks and the other did not. The heat sinks were initialized at the same temperature as the reactor coolant system. All calculations modeled pressurizer safety release valves and assumed a boil-off of 48,000 lbs of water from the lower plenum of the reactor vessel at a constant rate. The time over which the vaporization occurred was varied between cases. Table 4.4.4-2 presents the results.

For a two minute vaporization time, a 610 psi pressure rise resulted and for a 5 minute boil-off time no significant pressure rise results. A comparison of these results with an estimated minimum boil-off time between 1.3 and 4.5 hours, demonstrates that no in-vessel pressure spike would be expected.

TABLE 4.4.4-1

IN-VESSEL PRESSURE SPIKE MARCH CALCULATIONS - TE

Case	Reactor Vessel Lower Plenum Water Mass	Minimum RCS** Water Mass	RCS Pressure* Increase
1	48000 lbs	0	2667 psi
2	24000 lbs	0	1935 psi
3	12000 lbs	0	1625 psi
4	100 lbs	0	954 psi
5	48000 lbs	50 lbs	489 psi
6	100 lbs	50 lbs	0 psi

* RCS pressure before pressure rise is approximately 2550 psia

** MARCH variable WDED in deck NLBOIL

TABLE 4.4.4-2

IN-VESSEL PRESSURE SPIKE COCOCLASS9 CALCULATIONS

Case	Boil-off Time (min)	Structures Modeled	Calculated RCS Pressure Increase (psi)
1	2	yes	610
2	5	yes	negligible
3	5	no	negligible

APPENDIX 4.4.5

STEAM GENERATOR TUBE INTEGRITY EVALUATION FOR A POSTULATED CLASS-9 EVENT LOADING

STEAM GENERATOR TUBE INTEGRITY EVALUATION FOR A POSTULATED CLASS-9 EVENT LOADING

1.0 INTRODUCTION

The draft Sandia report, "Assessment of Core Penetration of Primary Containment and Particulate Debris Coolability in TMLB, S_2D, and ABG Accidents", indicates that during a Class-9 event, the steam generator tubing can be subjected to about 4500 psi primary-to-secondary differential pressure loading with the tube wall temperature reaching approximately 1000°F. Since the steam generator tubing is a critical barrier against the release of radioactivity, it is important to verify that the structural integrity of the tubing is maintained during these events.

2.0 CONSIDERATION OF TUBE DEGRADATION

During operation, the tubes may experience some damage, and the effect of such damage must be considered in evaluating the tube integrity. Based on operating experiences at Zion and Indian Point, the tube damage may be separated into two distinct categories: (1) denting, and (2) thinning and/or cracking. In light of the postulated Class-9 loadings, a discussion of the effect of these two types of defects on the tube integrity follows.

Numerous studies on the effects of various modes of tube damage on the burst strength of steam generator tubing have been reported. The results are based on test data reported in Reference [1]. All of the tests were conducted in a simulated steam generator environment at 600°F for 0.875 in x .050 in size, I-600 mill-annealed tubing. Three different material heats were tested to evaluate the effect of heat-to-heat variations in the mechanical properties of a typical tube bundle. Mechanical properties were obtained by averaging the results of five test samples for each heat. The average values ranged from 39.8 to 47.6 ksi for yield stress, and 93.0 to 98.7 ksi for the ultimate strength. The effect on tube burst strength because of property variations in these ranges is negligible and well within the expected test scatter.

Because these tests were conducted at 600°F and the maximum predicted tube wall temperature during a Class-9 event is about 1000°F, the effect of this higher temperature on the reported test results should also be considered. Theories on ductile failure indicate that the flow stress is approximately proportional to the sum of the material yield and ultimate strength [2]. Therefore, the burst pressures at 1000°F can be predicted by adjusting the reported data using the flow stress ratio given below. The strength properties used in this calculation are typical of mill-annealed I-600 material [3].

Temperature, °F	σy, ksi	σu, ksi	$\sigma y + \sigma u$	Flow Stress Ratio
600°F	43	94	137	
1000°F	41	82	123	R1000/600 = 0.9

The expected burst strengths at 1000°F would be 10 percent lower than the values reported in this study. The reported data at 600°F can be lowered by 10 percent to adjust for the higher temperature. Otherwise, the evaluation can be based using 600°F data and increasing the Class-9 event pressure loading from 4500 psi to about 5000 psi.

2.1 THINNING/CRACKING TYPE DEFECTS

In the case of thinning, the defects were produced by uniformly machining the tube's outside diameter (OD). In addition to the undefected new specimens, combinations of three different penetration depths and four defect lengths were tested. Results of these tests are shown in Figures 1A and 1B. For a tube with a 1.5 inch long defect, 50 percent of the nominal wall thickness is required to withstand the Class-9 event loading. For shorter and/or nonuniform defects, the allowable damage would be somewhat greater than 50 percent.

To study the effect of tight cracks, the defects were simulated mechanically by EDM slots. Slot lengths of 0.25 inch, 0.5 inch, and 1.5 inch and slot depths in the range of 25-30 percent, 55-60 percent, and 85-90 percent of nominal wall were tested. The results of these tests are shown in Figures 2A and 2B. Again, the results demonstrate that a tube with a 1.5 inch long and 50 percent through-wall crack would be able to withstand the postulated Class-9 event loading without rupturing.

At Indian Point 3, pitting exists on the secondary side of the steam generator tubes. It has been determined that this pitting will affect the tubes in a similar manner to thinning. In fact, per percentage of the wall thickness degraded, pitting will affect the ability of the tube to withstand pressure less than would the same degree of thinning. Therefore, it is concluded that the pitted tubes at Indian Point 3 will be able to withstand the postulated Class 9 event loading.

2.2 TUBE DENTING

Because of the inherent mechanism of denting, the corrosion of carbon steel tube support plates, the dented region of tubes is confined within the support plate thickness. Denting was simulated by hot-swagging a carbon steel ring onto the tube. The ring was 0.75 inches thick, simulating the thickness of the support plate. The nominal denting depth was 0.04 to 0.05 inch.

To investigate the effects of tube thinning near a dent, tests were also performed on specimens with denting and uniform thinning as well as denting with elliptical wastage defects.

Results of burst pressure tests with various denting and thinning configurations are summarized in Figure 3 and Table 1. These results clearly indicate that denting does not lower the burst strength of a tube with either the nominal or wasted wall. A similar conclusion has been derived regarding the strength of a dented tube with superimposed cracks [4]. Thus, the observations made previously regarding the required wall thickness to withstand the Class-9 event loads are unaffected by the presence of denting.

TABLE 1

Comparison of Burst Pressures of Elliptically Wasted .875 OD x .050 Wall Tubing with and without denting [1].

Radius of Cutter (in)	Wrap Angle (degrees)	Depth (Wall)	Burst Pressures (psi) Without Denting		With Denting	
24	0	25-30	8155,	8150	7905,	8150
24	45	25-30	7615,	7940	9200,	8060
24	135	25-30	5200,	7780	7800,	7770
12	0	55-60	5550,	5635	5520,	5605
12	45	55-60	5680,	5840	5650,	5675
12	135	55-60	5610,	5455	5320,	5230

3.0 SUMMARY

The results of burst pressure tests on tubes with a combination of wastage, cracking and denting damage demonstrate that a tube with 50 percent damage can safely withstand the postulated Class-9 event loads.

References:

1. Vagins, M., et. al., "Steam Generator Tube Integrity Program - Phase I Report", NUREG/CR-0718, PNL-2937, September 1979.

2. Eiber, R. J., et. al., "Investigation of the Initiation and Extent of Ductile Pipe Rupture (Final Report)", BMI-1908, June 1971.

3. Huntingdon Alloys Handbook.

4. Harrod, D. L., and Kaminski, D. A., "Burst Strength of Dented and Cracked 1600 Steam Generator Tubes", Westinghouse R+D Memo 79-102-DEFIN-MI, January 1977.

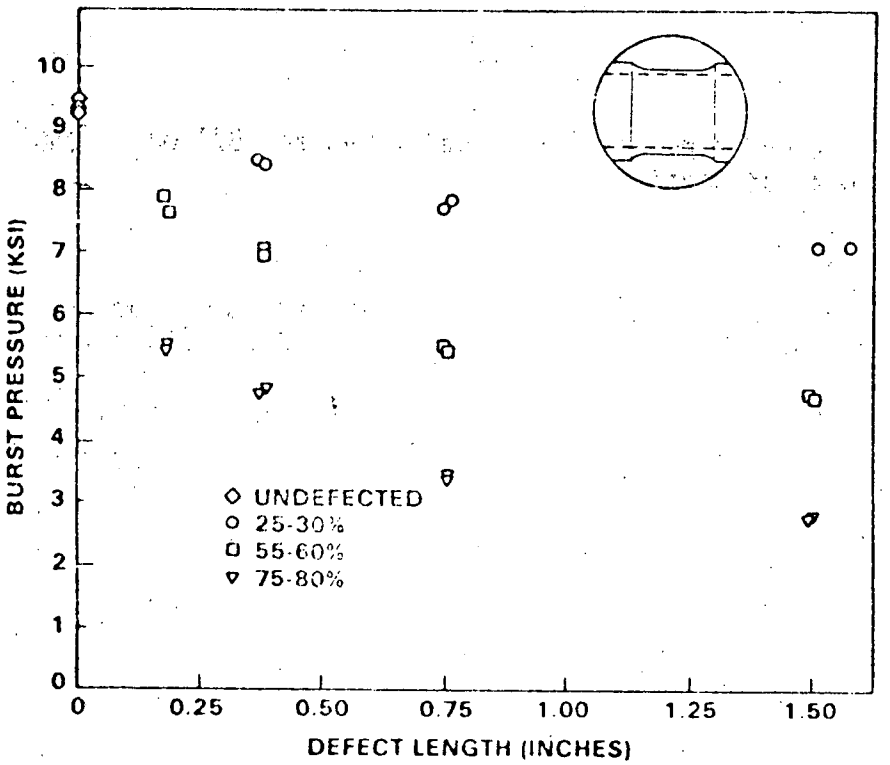


FIGURE 1A. Burst Data for 0.875 x 0.050 Uniform Thinning Specimens - Defect Length Variation [1]

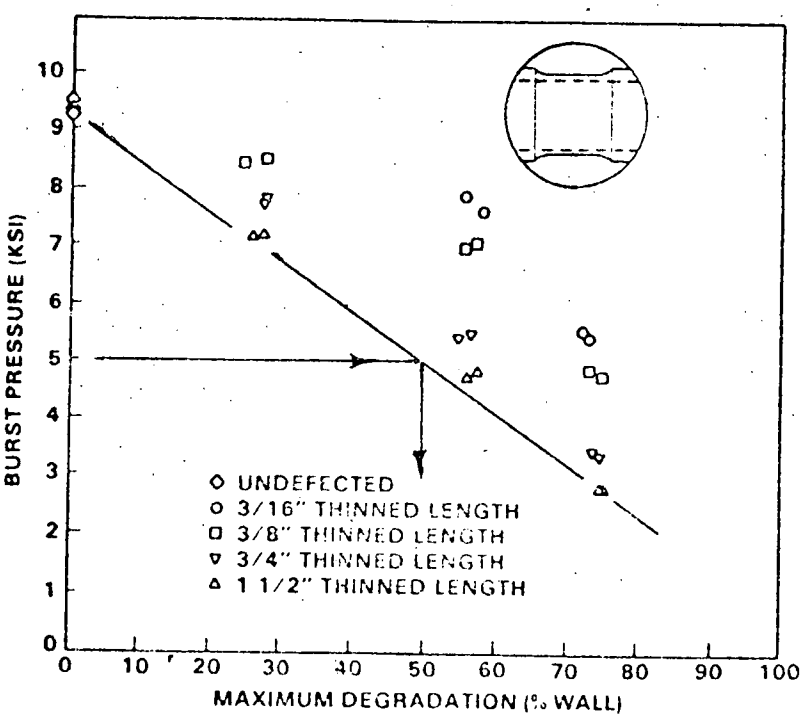


FIGURE 1B. Burst Data for 0.875 x 0.050 Uniform Thinning Specimens - Defect Depth Variation [1]

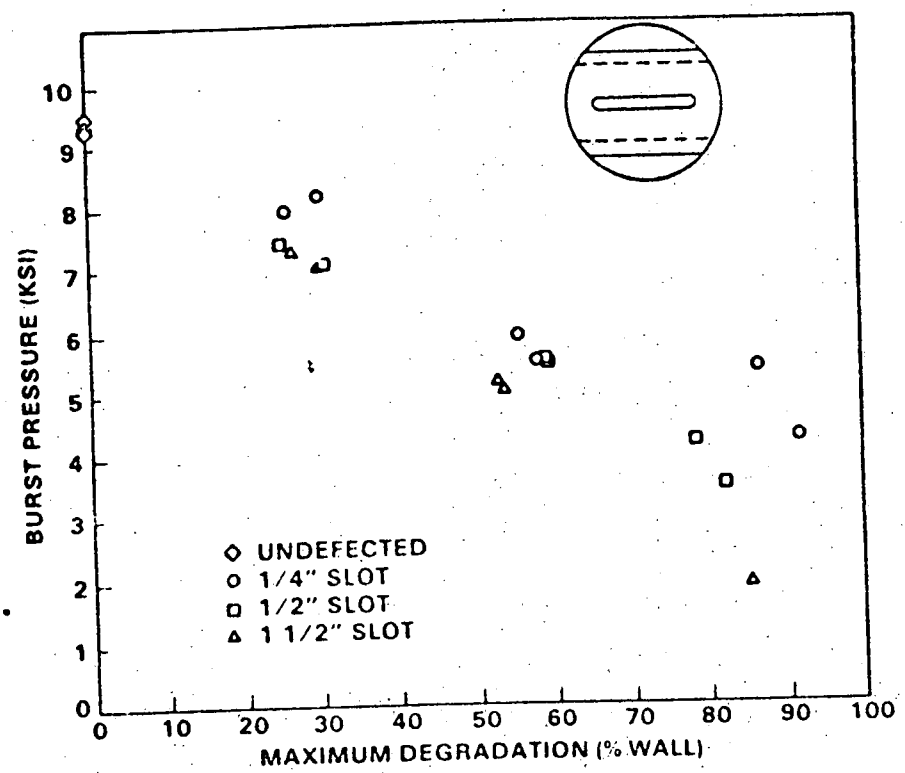


FIGURE 2A. Burst Data for 0.875 x 0.050 EDM Slot Specimens - Defect Depth Variation [1]

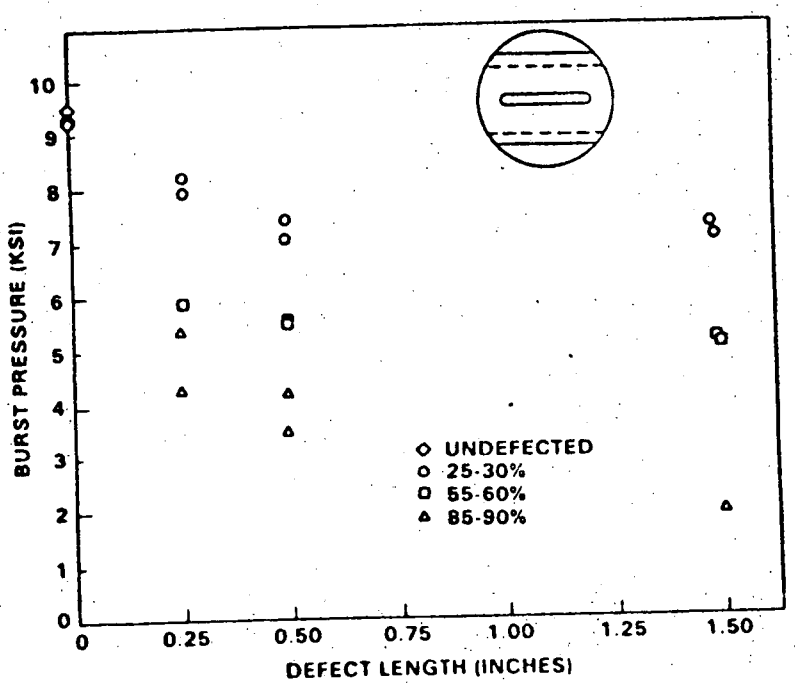


FIGURE 2B. Burst Data for 0.875 x 0.050 EDM Slot Specimens - Defect Length Variation [1]

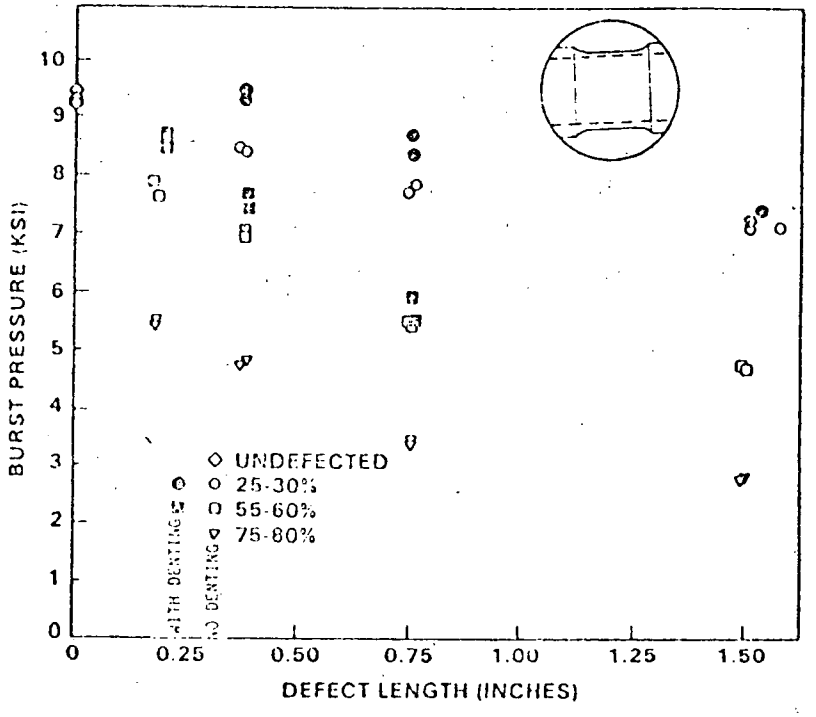


FIGURE 3. Burst Pressure Data of 0.875 x 0.050 Uniform Thinning Specimens With and Without Denting [1]

APPENDIX 4.4.6

PARTICLE SIZE FOR MARCH CODE REACTOR CAVITY STEAM SPIKE ANALYSIS

APPENDIX 4.4.6

PARTICLE SIZE FOR MARCH CODE REACTOR CAVITY STEAM SPIKE ANALYSIS

The MARCH code has a fixed model for the heat transfer for the quench and cooldown of debris entering the reactor cavity. This is based on radiation and convection to the water surrounding the debris particles. The user does have control over the particle diameter, an input. Some cases have typically used ~3 mm which results in very high heat transfer and steam generation rates, and hence a large steam spike immediately after vessel failure.

The cavity has a limited cross-sectional area. The mass of core debris, its initial temperature, and the heat transfer model in conjunction with the particle surface area (dependent on particle diameter) define the steam generation rate. The resultant steam flow through the bed may carry away the particles if the steam velocity yields drag forces in excess of the gravity force. Hence, there is a lower bound on the particle diameter below which the particle size is not consistent (physically realistic) with the heat transfer model employed.

The steam velocity which will lift a particle of radius R as a result of drag force is

$$1) \quad V = \frac{8}{3}\left(\frac{\rho}{\rho_g}\right)\frac{g}{C_D}\left(R\right)^{1/2}$$

ρ = particle density = 500 lbs/ft^3

ρ_g = gas (steam) density = 0.0727 lb/ft^3 at 30 psia

C_D = drag coefficient = 0.5

R = particle radius (ft)

$V = 1086 \cdot R^{1/2}$

The steam velocity developed by heat transfer from particles is

$$2) \quad V = \frac{hA\Delta T}{h_{fg} A_c \rho_g} \times \frac{1}{\alpha} \times \frac{1}{3600}$$

h = heat trans coefficient (Btu/hr-ft^2-°F)
ΔT = temperature difference between particles and water
h_{fg} = heat of vaporization of water 945 Btu/lb
A_c = cavity cross sectional area 420 ft^2
ρ_g = gas density = 0.0727 lb/ft^3
α = particle bed void fraction ~0.4
3600 = conversion from hours to sec

The primary mode of heat transfer is by radiation at high temperature. MARCH uses an emissivity of 0.4 which gives h = 96.8 Btu/hr-ft^2-°F if a ΔT of 4250°F is used. For spherical particles the ratio of area to volume is

$$\frac{A}{V} = \frac{3}{R}$$

The total volume for 350,000 lbs of melt at an average density of 500 lb/ft^3 is 700 ft^3. The total particle heat transfer area is thus

$$A = V \times A/V = 700 \times 3/R$$

$$T = 4500 - 250 = 4250°F$$

Based on these, $V = 20.8/R$

Equating results of 1) and 2) gives

$$V = 1086 \cdot R^{1/2} = 20.8/R$$

$$\text{or} \quad R^{3/2} = \frac{20.8}{1086} = 0.0192$$

$R = 0.72$ ft
$= 0.867$ in.

Based on the above considerations, the debris bed particles would have to be nearly 0.9 inches in radius to not be carried off by the initial steam generation in cooling from 4500°F using the MARCH heat transfer model. Therefore, a 2 inch diameter is used in MARCH analysis in the cavity.

It is noted that a criterion such as maximum critical heat flux based on the cavity cross-sectional area would give a much slower rate of energy removal (and hence steam generation) than the above.

APPENDIX 4.4.7

GAS RADIATION MODEL USED IN COCO

APPENDIX 4.4.7

GAS RADIATION MODEL USED IN COCO

The gas radiation module simulates the heat transfer via radiation from a gas medium to its surrounding walls. Only heteropolar gases (e.g., CO_2, CO, H_2O, NH_3, etc.) absorb and reradiate thermal radiation. At high partial pressures and large mean beam lengths, these gases approach blackbody radiators having an emissivity near unity.

The amount of heat transferred from a gas is given by

$$q = \frac{W_g - W_w}{\frac{1 - \varepsilon_w}{A_w \varepsilon_w} + \frac{1}{A_w \varepsilon_g}} \qquad (1)$$

where

q is the amount of heat (Btu/hr),

W_g is the emissive power of the gas (Btu/hr-ft^2),

W_w is the emissive power of the wall (Btu/hr-ft^2),

A_w is the wall area (ft^2),

ε_w is the emissivity of the wall,

and

ε_g is the emissivity of the gas.

The emissive power is defined by

$$W = \sigma \varepsilon T^4$$

where

σ is the Stefan-Boltzman constant,

ε is the emissivity of the radiating medium,

and

T is the absolute temperature of the radiating medium.

The calculated quantity of heat transferred is used in determining the effective radiative heat transfer coefficient:

$$h_r = q/(A_w (T_g - T_w)) \qquad (2)$$

where

h_r is the coefficient (Btu/hr-ft^2-F),

q is the heat transferred (Btu/hr),

A_w is the wall area (ft^2),

T_g is the gas temperature (°F),

and

T_w is the wall temperature (°F).

The value of the radiative coefficient is combined with the convective heat transfer coefficient describing the total heat transferred from the gas medium to its surrounding walls.

The gas emissivity is the variable which is difficult to calculate. It is a function of the gas composition, its thermodynamic state and its size and shape. A graphical solution is used to determine the emissivity of a specific gas. These graphs have been transformed into sets of data points for use in the computer module. Linearly interpolating, the computer calculates the emissivity based on the gas temperature, pressure, size and shape of the occupied volume. A correction factor in graphical format which accompanies the emissivity graphs, approaches unity at high pressures and large volumes, and it is not included.

The total gas emissivity is the sum of the values for each gas component less a small correction due to the presence of more than one gas. The total emissivity is used with the emissive power of the gas medium and the surrounding wall to calculate the amount of heat transferred between the gas and the walls. Finally, the radiative heat transfer coefficient is formed by dividing the total heat transferred to the wall by the wall surface area and the temperature difference between the gas medium and the wall.

REFERENCES

1. Principles of Heat Transfer, 3rd Edition, Frank Kreith, Intext Educational Publishers, New York, 1973.

2. Heat Transmission, 3rd Edition, William H. McAdams, New York, 1954.

APPENDIX 4.4.8

INPUT PARAMETERS FOR CONTAINMENT ANALYSIS

APPENDIX 4.4.8

INPUT PARAMETERS FOR CONTAINMENT ANALYSES

Tables 1 through 5 provide the initial conditions and plant parameters used for the containment analyses. A majority of the calculations were performed using the parameters for a representative plant. A few analyses, however, were performed with specific parameters for Indian Point plants 2 and 3 to show that the results would be essentially the same as those obtained with the representative plant parameters.

TABLE 1

OVERALL INITIAL CONDITIONS

	INDIAN POINT 2	INDIAN POINT 3	REPRESENATIVE PLANT
Net Free Volume (ft^3)	2.6×10^6	2.6×10^6	2.6×10^6
Initial Pressure (psia)	15.0	15.0	15.0
Initial Temperature (^oF)	100	100	100
Number of Fan Cooler (min/max)	3/5	3/5	3/5
Fan Cooler Initiation Pressure (psig)	2.0	3.0	3.5
Fan Cooler Initiation Time Delay (sec)	58.0	58.0	58.0
Number of Spray Pump (min/max)	1/2	1/2	1/2
Spray Flow per Spray Pump (gpm)	2500	2500	2500
Spray Initiation Pressure (psig)	30.0	23.0	23.0
Spray Initiation Time Delay (sec)	43.0	43.0	43.0
Spray Water Temperature (^oF)	100	100	100
Refueling Water Storage Tank Tank Capacity (gal.)	350,000	350,000	350,000
Reactor Cavity Volume (ft^3)	9857	9857	9857

TABLE 2

SPECIFIC INITIAL CONDITIONS FOR A REPRESENTATIVE PLANT

Core:	
Zircaloy Mass (lbs)	47,671
UO_2 Mass (lbs)	221,564
Miscellaneous Metal (lbs)	9,843
Vessel:	
Mass of Bottom Head (lbs)	67,865
Mass of Grid Plates and Structures Below Core (lbs)	73,706
Primary System Initial Conditions:	
Volume (ft^3)	12,990
Initial Vessel Water Temp. (^oF)	580
Core Power (MWt)	3,025

TABLE 3

SPECIFIC INITIAL CONDITIONS FOR THE INDIAN POINT PLANTS

	INDIAN POINT 2	INDIAN POINT 3
Core:		
Zircaloy Mass (lbs)	48,057	47,400
UO_2 Mass (lbs)	222,143	220,300
Miscellaneous Metal (lbs)	10,229	9,800
Vessel:		
Mass of Bottom Head (lbs)	67,865	67,865
Mass of Grid Plates and Structures Below Core (lbs)	73,706	73,706
Primary System Initial Conditions:		
Volume (ft^3)	12,224	12,242
Initial Vessel Water Temp. (^oF)	549	542.6
Core Power (MWt)	2,758	3,025

TABLE 4-a

CONTAINMENT STRUCTURAL HEAT SINKS FOR INDIAN POINT 2

WALL #	AREA (ft^2)	THICKNESS (ft)	LAYER COMPOSITION
1	49838.	0.00033/0.00021/0.0312/4.5	$Paint_1$/$Paint_2$/Steel/Concrete
2	32072.	0.00033/0.00021/0.0417/3.5	$Paint_1$/$Paint_2$/Steel/Concrete
3	15000.	1.0	Concrete
4	10000.	0.03125/1.0	Steel/Concrete
5	61000.	1.0	Concrete
6	68792.	0.00033/0.00021/0.0417	$Paint_1$/$Paint_2$/Steel
7	79904.	0.00033/0.00021/0.03125	$Paint_1$/$Paint_2$/Steel
8	27948.	0.00033/0.00021/0.0208	$Paint_1$/$Paint_2$/Steel
9	69800.	0.00033/0.00021/0.01563	$Paint_1$/$Paint_2$/Steel
10	3000.	0.01042	Steel
11	22000.	0.01152	Steel
12	10000.	0.00033/0.00021/0.00521	$Paint_1$/$Paint_2$/Steel
13	565.	0.00033/0.00021/0.0625/3.0	$Paint_1$/$Paint_2$/Steel/Concrete
14	7634.	0.00016/0.1058/0.04167/3.0	Stainless/Insulation/Steel/Concrete
15	1800.	0.03125	Steel

TABLE 4-b

CONTAINMENT STRUCTURAL HEAT SINKS FOR INDIAN POINT 3

WALL #	AREA (ft^2)	THICKNESS (ft)	LAYER COMPOSITION
1	49848.	0.00034/0.03125/3.0	Paint/Steel/Concrete
2	32072.	0.00054/0.04167/3.0	Paint/Steel/Concrete
3	15000.	1.0	Concrete
4	10000.	0.03125/1.0	Steel/Concrete
5	61000.	1.0	Concrete
6	68792.	0.00033/0.00021/0.0417	$Paint_1/Paint_2/Steel$
7	79904.	0.00033/0.00021/0.03125	$Paint_1/Paint_2/Steel$
8	27948.	0.00033/0.00021/0.0208	$Paint_1/Paint_2/Steel$
9	69800.	0.00033/0.00021/0.01563	$Paint_1/Paint_2/Steel$
10	3000.	0.01042	Steel
11	22000.	0.01152	Steel
12	10000.	0.00033/0.00021/0.00521	$Paint_1/Paint_2/Steel$
13	565.	0.00033/0.00021/0.0625/3.0	$Paint_1/Paint_2/Steel/Concrete$
14	7634.	0.1058/0.04167/3.0	Insulation/Steel/Concrete
15	1800.	0.03125	Steel

TABLE 5

REPRESENTATIVE PLANT CONTAINMENT STRUCTURAL HEAT SINKS

WALL #	AREA (ft^2)	THICKNESS (ft)	LAYER COMPOSITION
1	49838.	0.00033/0.00021/0.0312/3.0	$Paint_1$/$Paint_2$/Steel/Concrete
2	32072.	0.00033/0.00021/0.0417/3.0	$Paint_1$/$Paint_2$/Steel/Concrete
3	15000.	1.0	Concrete
4	10000.	0.03125/1.0	Steel/Concrete
5	61000.	1.0	Concrete
6	68792.	0.00033/0.00021/0.0417	$Paint_1$/$Paint_2$/Steel
7	79904.	0.00033/0.00021/0.03125	$Paint_1$/$Paint_2$/Steel
8	27948.	0.00033/0.00021/0.0208	$Paint_1$/$Paint_2$/Steel
9	69800.	0.00033/0.00021/0.01563	$Paint_1$/$Paint_2$/Steel
10	3000.	0.01042	Steel
11	22000.	0.01152	Steel
12	10000.	0.00033/0.00021/0.00521	$Paint_1$/$Paint_2$/Steel
13	565.	0.00033/0.00021/0.0625/3.0	$Paint_1$/$Paint_2$/Steel/Concrete
14	7634.	0.00016/0.1058/0.04167/3.0	Stainless/Insulation/Steel/Concrete
15	1800.	0.03125	Steel

APPENDIX 4.4.9

COMPILATION OF RESULTS

APPENDIX 4.4.9
COMPILATION OF RESULTS

To provide a short, quick reference for the peak pressures of the runs made, and to help compare pressures between scenarios, Table 1 of this appendix lists all of the runs analyzed with their corresponding peak pressures. Next, Table 2 includes the more extensive set of summary sheets and important containment plots.

This appendix includes representative results of MARCH/COCOCLASS9 runs made for the accident classes analyzed in this study. Each of the cases identified in Tables 4.3.1-1 through 4.3.6-1 of Section 4.3 is partially supported by the results presented here. For each run represented, a summary sheet in Table 2 of this appendix details important information pertaining to that run. Following the summary sheet is a set of plots for the run. These summary sheets and plots are presented to give a sample listing of the computer obtained transient analysis data used in this study. The results depicted by this information represent one of the sources used to establish the sensitivity of containment to parameter changes and as such, were used in the assignment of containment event tree probabilities. The plots are presented as obtained from the MARCH/COCOCLASS9 analyses. No attempt has been made to specify the error range per plot or the significance of the plot. See Section 4.3 for a discussion, organized by class, of the significant results obtained from the information in this appendix. Note that there is not a one-to-one correspondence between the cases of Tables 4.3.1-1 to 4.3.6-1 and the runs presented here.

One correction must be made when analyzing the figures in Table 2 for the Class I, II, III and V events, if the run was made before December 12, 1980, as is indicated by the date on the summary sheet. Before this date, the burn model in COCOCLASS9 used a heat of reaction that resulted in pressure rises about 17 percent too high. Therefore, for cases before the 12th, the burn peaks must be reduced appropriately. Likewise, for such cases, the peak burn pressures given on the summary sheets must be reduced. The Class IV results are correct because they were made using a corrected version of COCOCLASS9 after December 12th. For convenience, all of the pressures listed in Table 1 are already corrected, and Table 1 may be used in conjunction with the sets of data in Table 2 to interpret the correct burn peaks at the different times in a transient.

TABLE 1

SUMMARY OF RESULTS

CLASS	CASE	CASE TYPE*		P@VF (psia)	Pmax (psia)
I	1A	RSG, MxZr, CA	No Burn	79	79- (1)
I	1B	RSG, MxZr, CA	Burn @ VF	139	139- (2)
I	1C	RSG, MxZr, CA	Burn @ T_{max}	75	144- (3)
I	2A	LSG, LZr	No Burn	30	61- (4)
II	1A	RSG, MxZr, CA	No Burn	73	73- (2)
II	1B	RSG, MxZr, CA	Burn @ VF	122	122- (2)
II	1C	RSG, MxZr, CA	Burn @ T_{max}	63	134- (3)
II	2A	LSG, LZr	No Burn	30	61- (2)
III	1A	RSG, MxZr, CA	No Burn	77	77- (1)
III	1B	RSG, MxZr, CA	Burn @ VF	135	135- (2)
III	1C	RSG, MxZr, CA	Burn @ T_{max}	75	130- (3)
III	2A	LSG, LZr	No Burn	40	40- (1)
III	5A	LSG, LZr	E Dispersive 80%, No Burn	104	104- (1)
III	5B	LSG, LZr	E Dispersive 80%, Burn @ VF	135	135- (2)
III	6A	LSG, LZr	E Dispersive 50%, No Burn	95	95- (1)
III	6B	LSG, LZr	E Dispersive 50%, Burn @ VF	131	131- (2)
III	7A	RSG, MxZr	E Dispersive 80%, No Burn	104	104- (1)
III	7B	RSG, MxZr	E Dispersive 80%, Burn @ VF	147	147- (2)
III	4A	LSG, LZr (26%)	T Dispersive 50%	51	51- (1)
III	3A	LSG, LZr (33%)	T Dispersive 75%	59	59- (1)
III	3A'	LSG, LZr (66%)	T Dispersive 75%	65	65- (1)
III	4A'	LSG, LZr (61%)	T Dispersive 50%	58	58- (1)
IV	1A	RSG, MxZr, CA	No Burn	63	63- (1)

TABLE 1

SUMMARY OF RESULTS

CLASS	CASE	CASE TYPE*		P@VF (psia)	Pmax** (psia)
IV	1B	RSG, MxZr, CA	Burn @ VF	118	118- (2)
IV	1C	RSG, MxZr, CA	Burn @ T_{max}	60	127- (3)
IV	2A	LSG, LZr	No Burn	33	33- (1)
IV	2B	LSG, LZr	Burn @ VF	70	70- (2)
IV	5A	LSG, LZr	E Dispersive 80% No Burn	75	75- (1)
IV	5B	LSG, LZr	E Dispersive 80% Burn @ ES	96	96- (5)
IV	7B	RSG, MxZr	E Dispersive 80% Burn @ ES	105	105- (5)
IV	4A'	LSG, LZr (26%)	T Dispersive 50%	56	56- (1)
IV	3A'	LSG, LZr (64%)	T Dispersive 75%	61	61- (1)
V	1A	RSG, MxZr, CA	No Burn	110	147- (6)
V	2A	LSG, LZr	No Burn	82	136- (6)
V	5A	LSG, LZr	E Dispersive 80% No Burn	132	132- (1)
V	5B	LSG, LZr	E Dispersive 80% Burn @ ES	169	169- (5)
V	6A	LSG, LZr	E Dispersive 50% No Burn	122	122- (1)
V	6B	LSG, LZr	E Dispersive 50% Burn @ ES	160	160- (5)
V	7A	RSG, MxZr	E Dispersive 100% No Burn	124	124- (1)
V	7B	RSG, MxZr	E Dispersive 100% Burn @ ES	173	173- (5)
V	3A	LSG, LZr (28%)	T Dispersive 75%	83	83- (1)
V	4A	LSG, LZr (21%)	T Dispersive 50%	75	75- (1)
V	3A'	LSG, LZr (64%)	T Dispersive 75%	93	93- (1)
V	4A'	LSG, LZr (63%)	T Dispersive 50%	85	85- (1)

TABLE 1

SUMMARY OF RESULTS

CLASS	CASE	CASE TYPE*		P@VF (psia)	Pmax (psia)
VI	1A	RSG,MxZr, CA	No Burn	96	96- (1)
VI	1A'	RSG, MxZr, CA	Burn @ T_{max}	96	138- (3)
VI	1A"	RSG, MxZr, CA	No Burn	89	89- (1)

* Abbreviations:

E Dispersive X%: Entrained Dispersive X% dispersed
T Dispersive X%: Timed Dispersive X% dispersed
RSG: Rapid Steam Generation Rate
LSG: Limited Steam Generation Rate
MxZr: 100% Zr/H_2O Reaction
LZr: Limited Zr/H_2O Reaction
CA: Concrete Attack
VF: Vessel Failure
T_{max}: Maximum Flame Temperature after vessel failure
ES: End of Dispersion
P_{max}: Maximum Pressure During the Transient

** For the P_{max} column: time or event when P_{max} occurred:

(1) Vessel Failure
(2) Burn @ VF
(3) Burn @ T_{max}
(4) Blowdown
(5) Burn @ ES
(6) Late Overpressurization

TABLE 2

SUMMARY SHEETS AND FIGURES

CASE: CLASS: I, CASE 1A, AD, B, NO BURN

DISPERSIVE: NO PERCENT CORE: _____ FRACTION IN CAVITY: _____

RUN #: AALABNL DATE: 11/13/80

BLOWDOWN PEAK: 59 PSIA TIME: ~12 SEC.

HYDROGEN BURN?: NO CRITERIA: _____

TIME @ BURN: _____ SEC, PRESSURE: _____ PSIA, TEMPERATURE: _____ °F

PEAKS:

PRESSURE: 79 PSIA, TIME: 2659 SEC, WHY?: VESSEL FAILURE

TEMPERATURE: 487.3 °F, TIME: ≈1691 SEC, WHY?: GRID PLATE FAILURE

DISPERSIVE: NO

PRESSURE: _____ PSIA, TIME: _____ SEC,

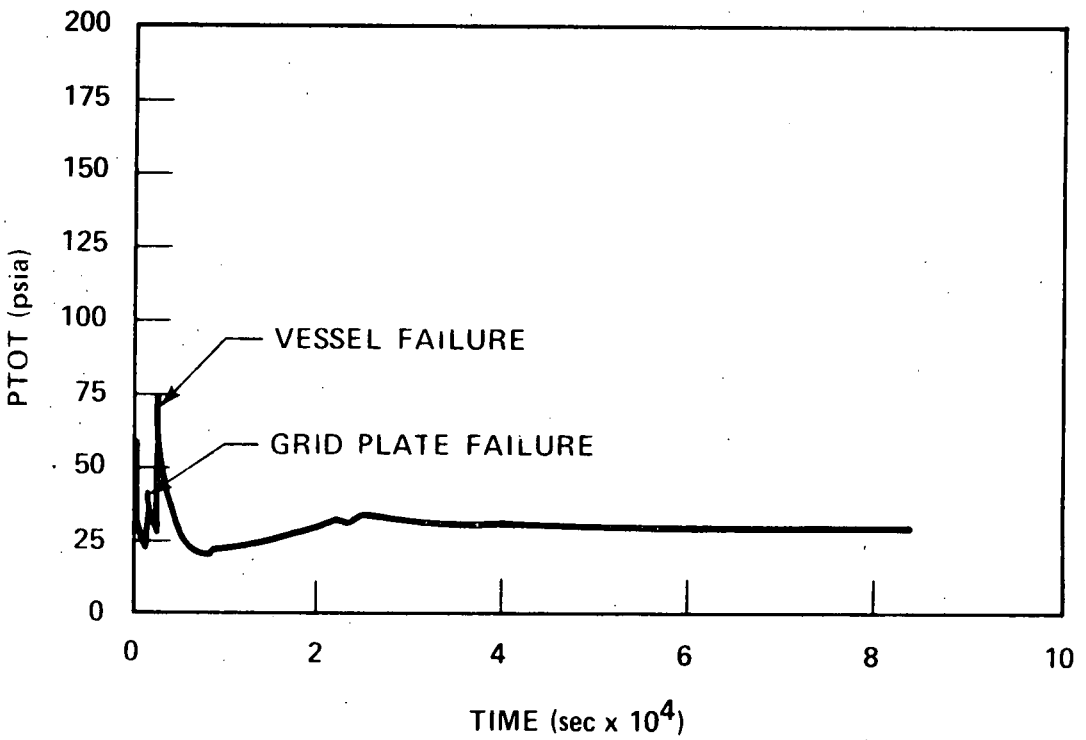
TEMPERATURE: _____ °F, TIME: _____ SEC,

END OF BOIL: 1812 SEC. END OF HEAD: 2652 SEC.

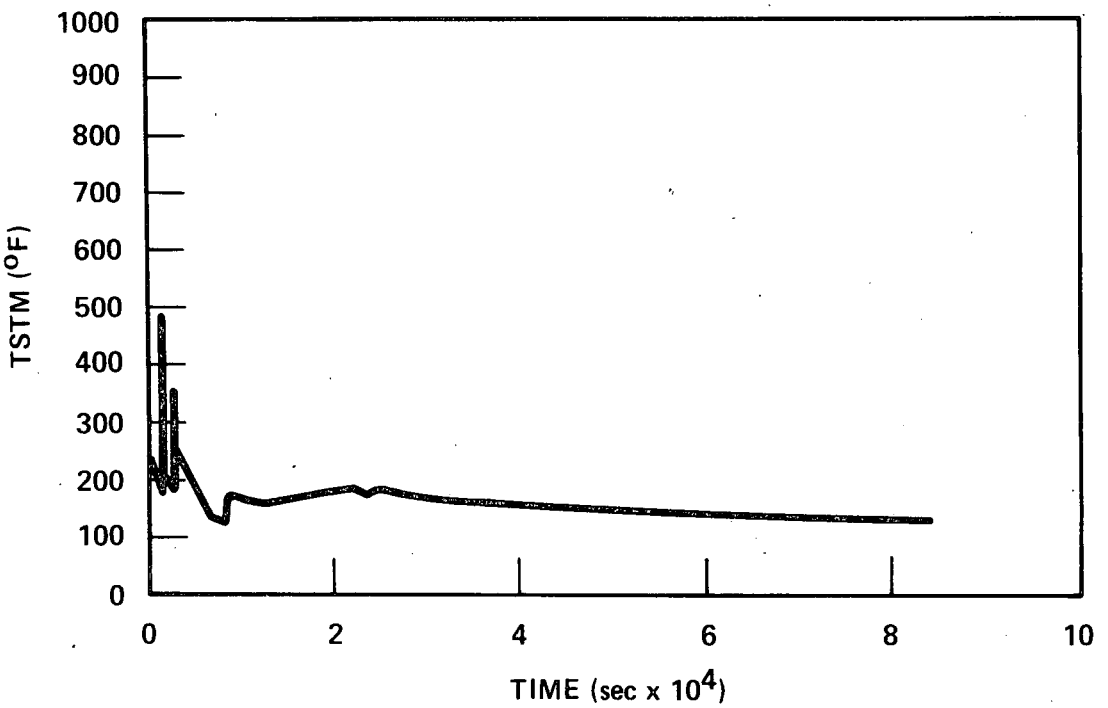
VESSEL FAILURE: 2652 SEC. END OF HOTDROP: 7579 SEC.

END OF INTER: 86480 SEC.

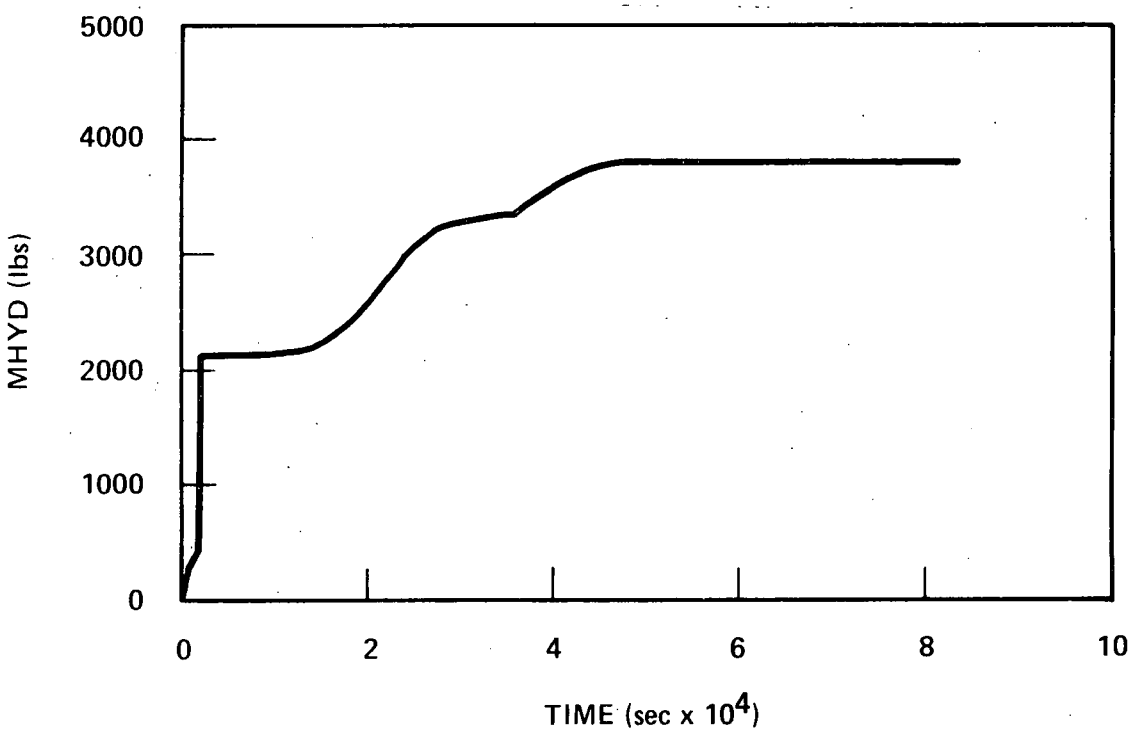
Class I, Case 1A



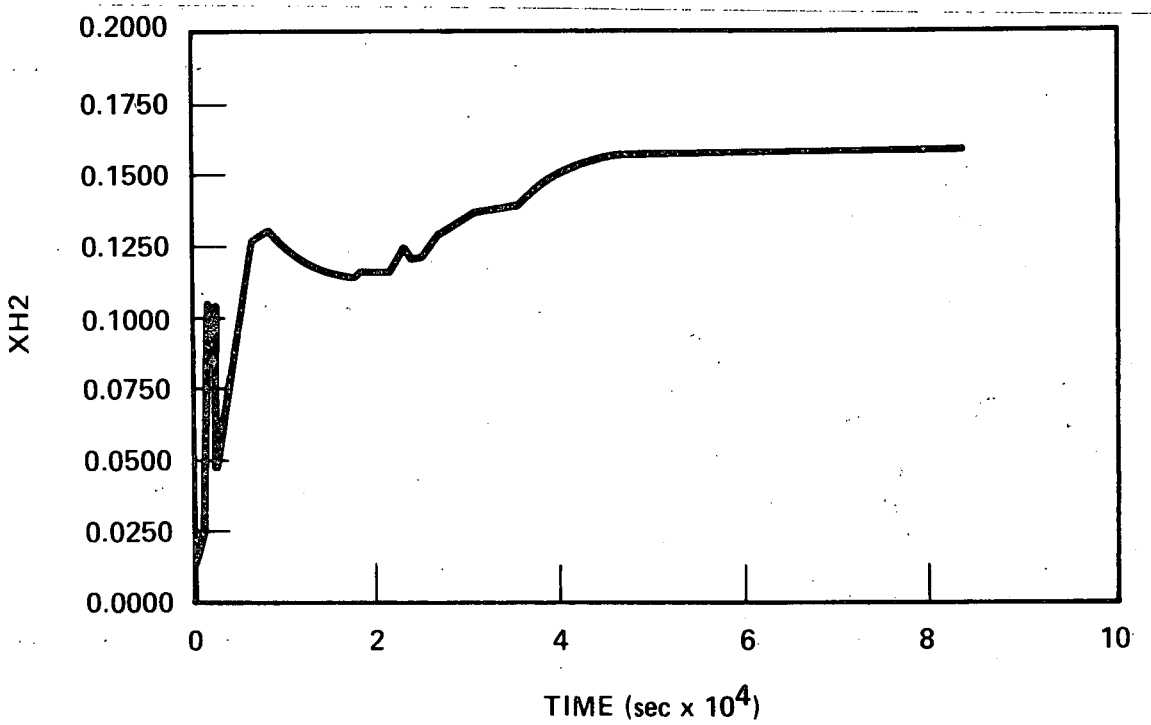
Pressure (in Containment) vs. Time
AD, B, No Burn
Class I, Case 1A



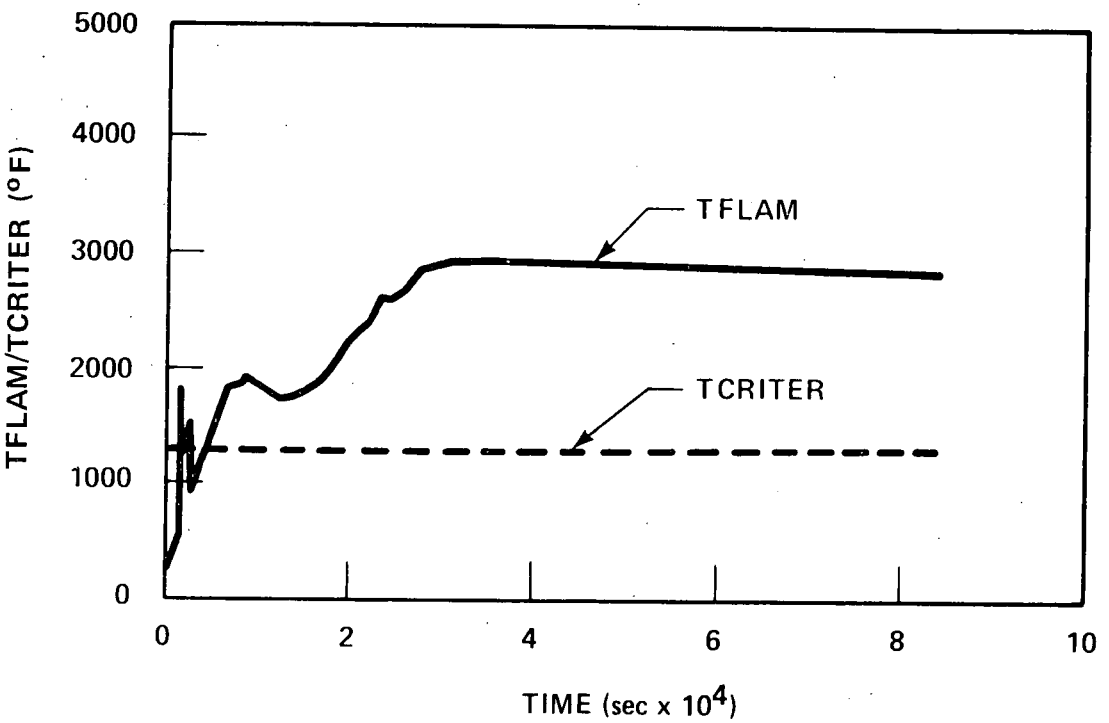
Temperature (in Containment) vs. Time
AD, B, No Burn
Class I, Case 1A



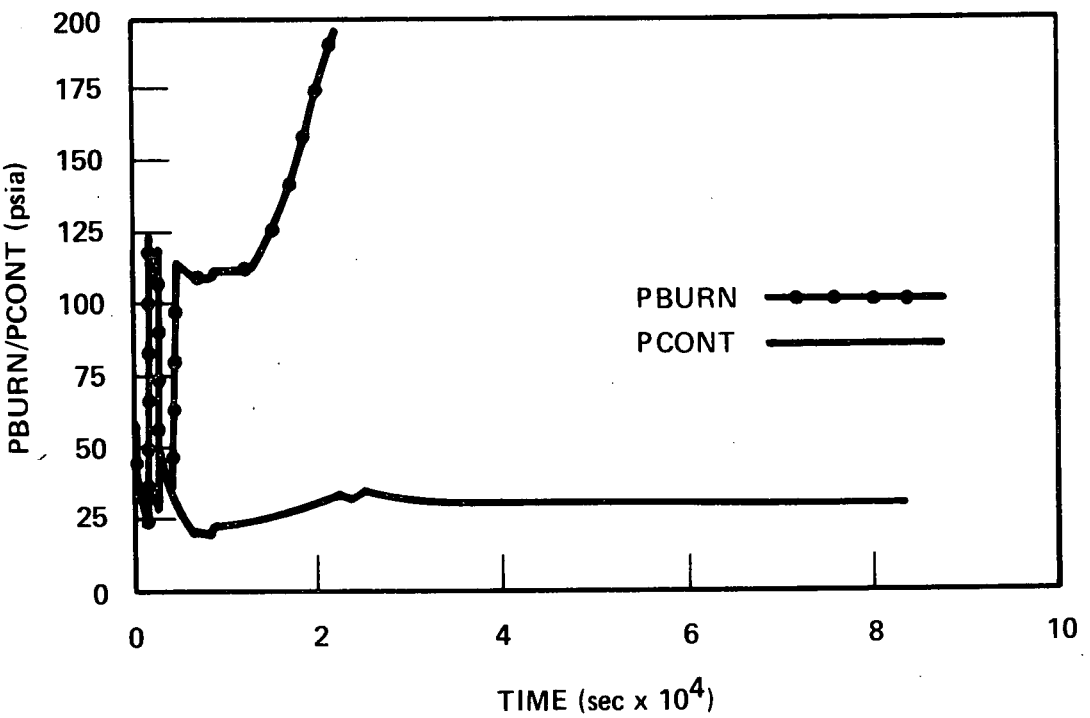
Mass Hydrogen (in Containment) vs. Time
AD, B, No Burn
Class I, Case 1A



Mole Fraction H_2 (in Containment) vs. Time
AD, B, No Burn
Class I, Case 1A



Flame Temperature (in Containment) vs. Time
AD, B, No Burn
Class I, Case 1A



Adiabatic Burn Pressure/Pressure in Containment vs. Time
AD, B, No Burn
Class I, Case 1A

CASE: CLASS I, CASE 1B, AD, B, BURN @ VESSEL FAILURE

DISPERSIVE: NO PERCENT CORE: ____ FRACTION IN CAVITY: ____

RUN #: AALABNY DATE: 11/13/80

BLOWDOWN PEAK: 59 PSIA TIME: ~12 SEC.

HYDROGEN BURN?: YES CRITERIA: VESSEL FAILURE

TIME @ BURN: 2653 SEC, PRESSURE: 149 PSIA, TEMPERATURE: 1129 °F

PEAKS:

PRESSURE: 149 PSIA, TIME: 2673 SEC, WHY?: VESSEL FAILURE/H_2 BURN

TEMPERATURE: 1129 °F, TIME: 2673 SEC, WHY?: VESSEL FAILURE/H_2 BURN

DISPERSIVE: NO

PRESSURE: ____ PSIA, TIME: ____ SEC,

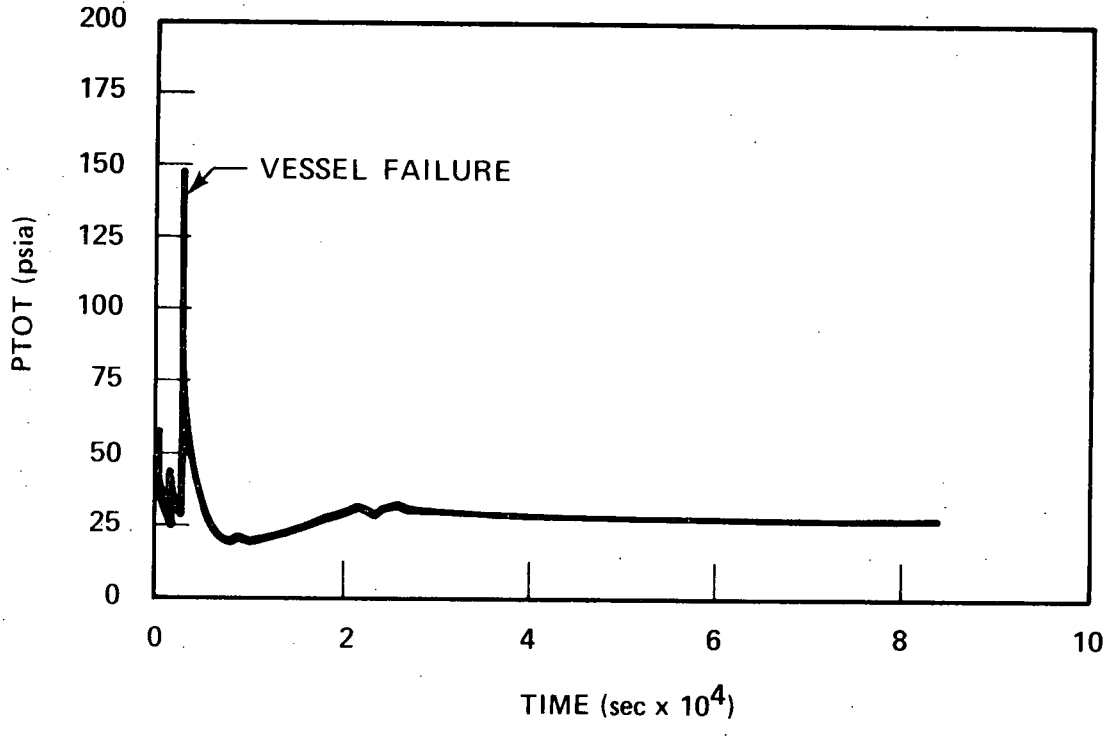
TEMPERATURE: ____ °F, TIME: ____ SEC,

END OF BOIL: 1812 SEC. END OF HEAD: 2652 SEC.

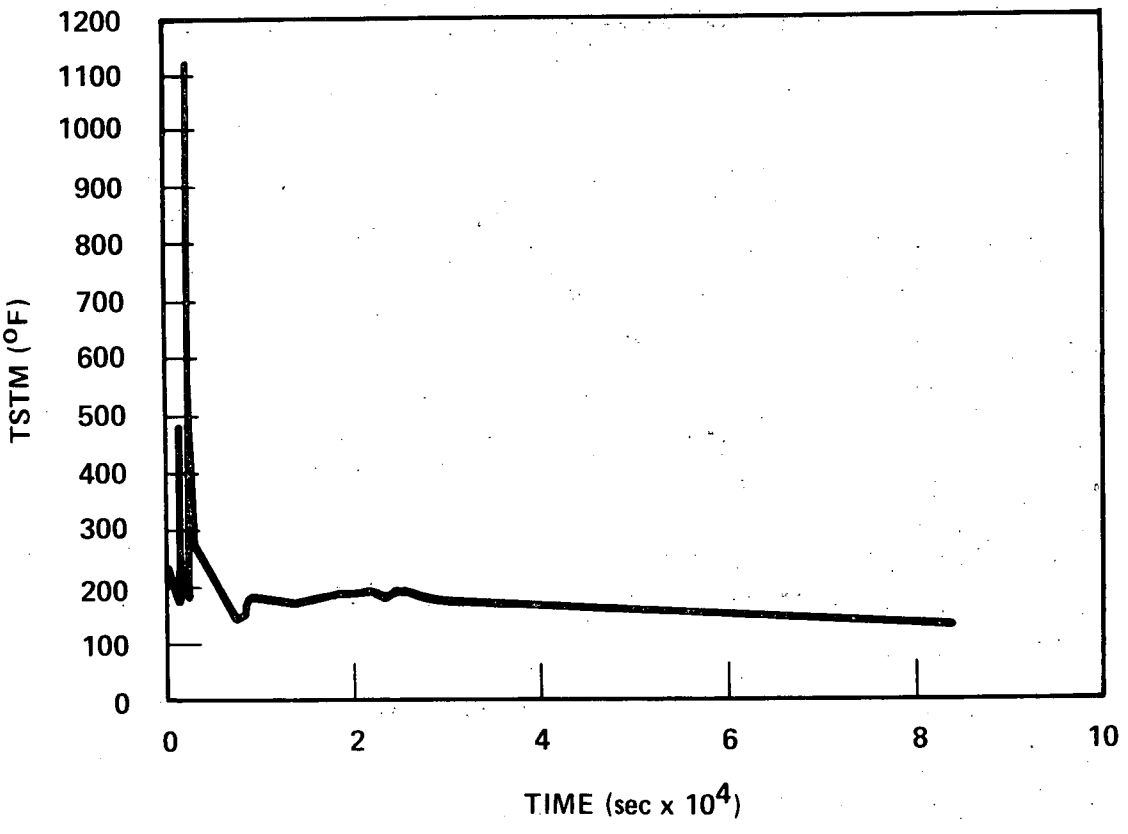
VESSEL FAILURE: 2652 SEC. END OF HOTDROP: 7579 SEC.

END OF INTER: 86480 SEC.

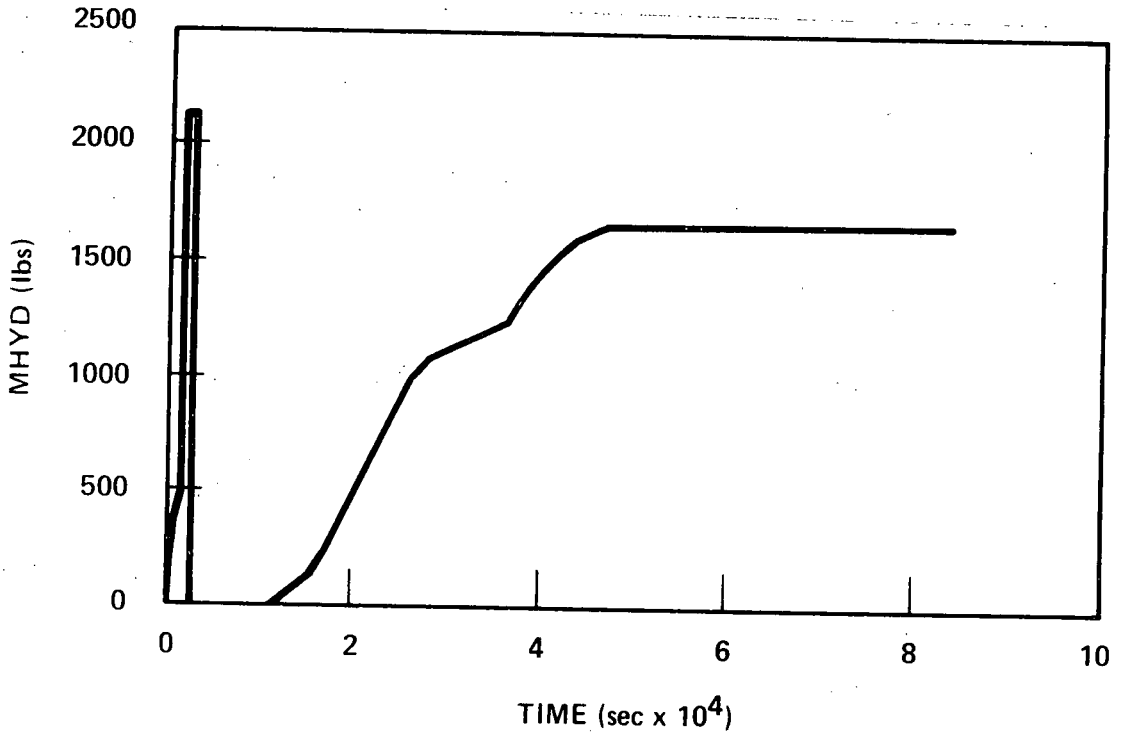
Class I, Case 1B



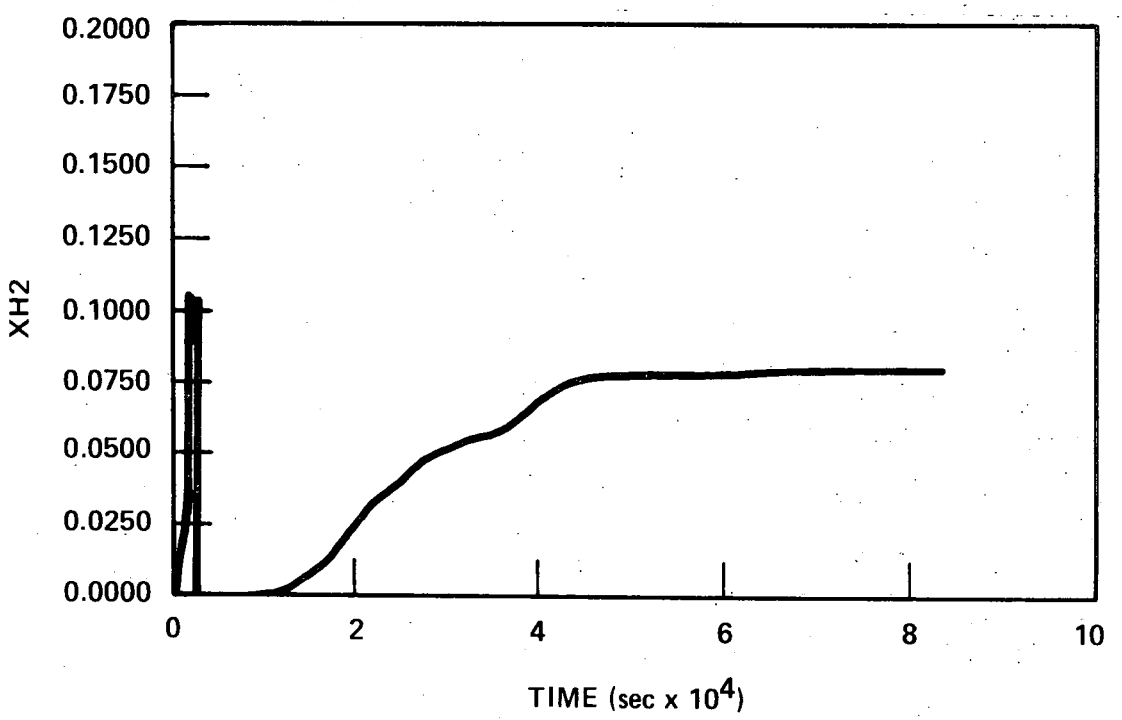
Pressure (in Containment) vs. Time
AD, B, Burn @ Vessel Failure
Class I, Case 1B



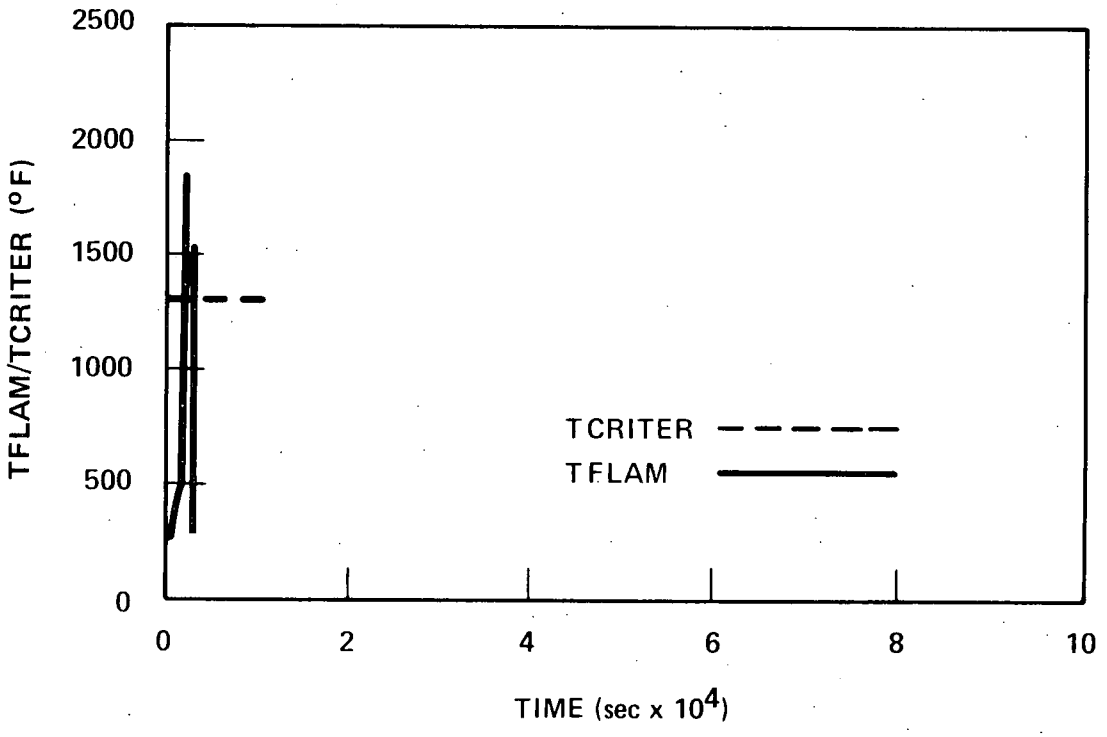
Temperature (in Containment) vs. Time
AD, B, Burn @ Vessel Failure
Class I, Case 1B



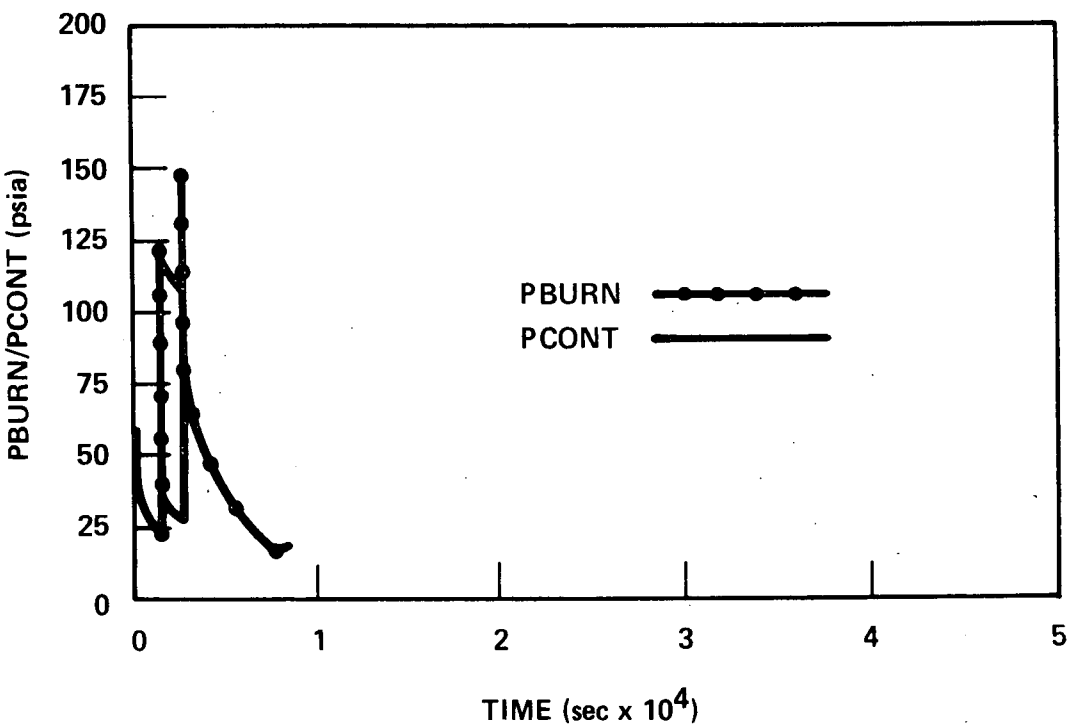
Mass Hydrogen (in Containment) vs. Time
AD, B, Burn @ Vessel Failure
Class I, Case 1B



Mole Fraction H_2 (in Containment) vs. Time
AD, B, Burn @ Vessel Failure
Class I, Case 1B



Flame Temperature (in Containment) vs. Time
AD, B, Burn @ Vessel Failure
Class I, Case 1B



Adiabatic Burn Pressure/Pressure in Containment vs. Time
AD, B, Burn @ Vessel Failure
Class I, Case 1B

CASE: CLASS I, CASE 1C, AD, B, BURN @ T_{MAX}

DISPERSIVE: NO PERCENT CORE: _____ FRACTION IN CAVITY: _____

RUN #: AALABOB DATE: 11/14/80

BLOWDOWN PEAK: 59 PSIA TIME: ~12 SEC.

HYDROGEN BURN?: YES CRITERIA: @ T_{MAX}

TIME @ BURN: 35091 SEC, PRESSURE: 155 PSIA, TEMPERATURE: 2968 °F

PEAKS:

PRESSURE: 155 PSIA, TIME: 35225 SEC, WHY?: H_2 BURN

TEMPERATURE: 2968 °F, TIME: 35225 SEC, WHY?: H_2 BURN

DISPERSIVE: NO

PRESSURE: _____ PSIA, TIME: _____ SEC,

TEMPERATURE: _____ °F, TIME: _____ SEC,

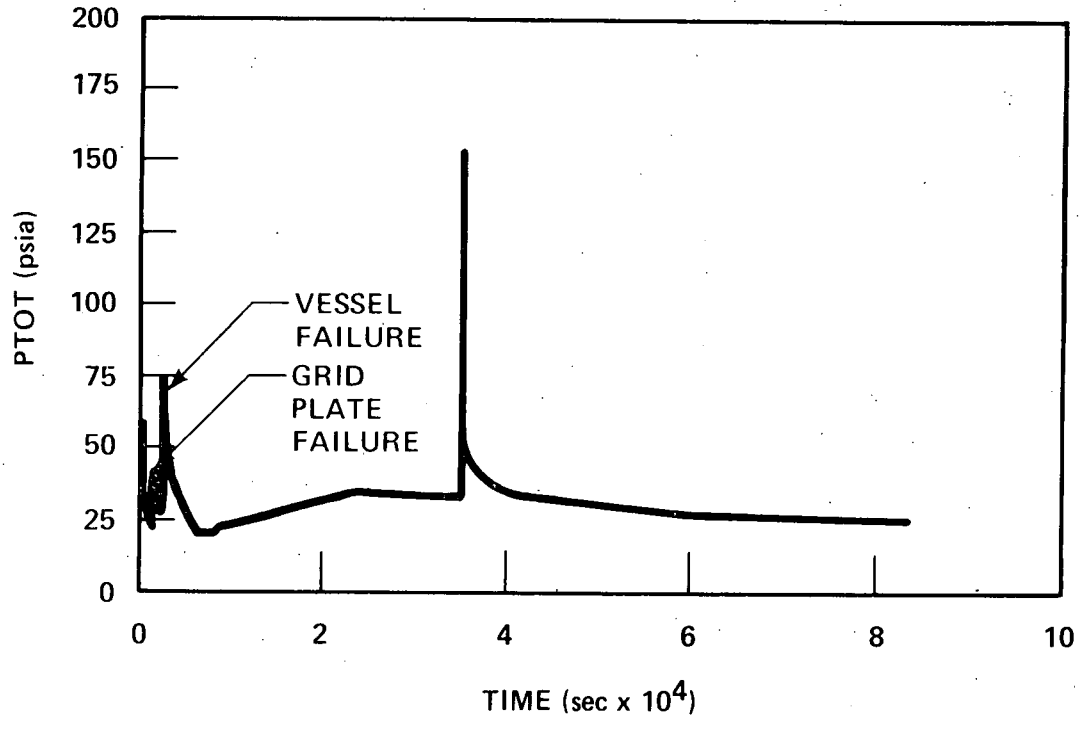
END OF BOIL: 1812 SEC. END OF HEAD: 2652 SEC.

VESSEL FAILURE: 2652 SEC. END OF HOTDROP: 7579 SEC.

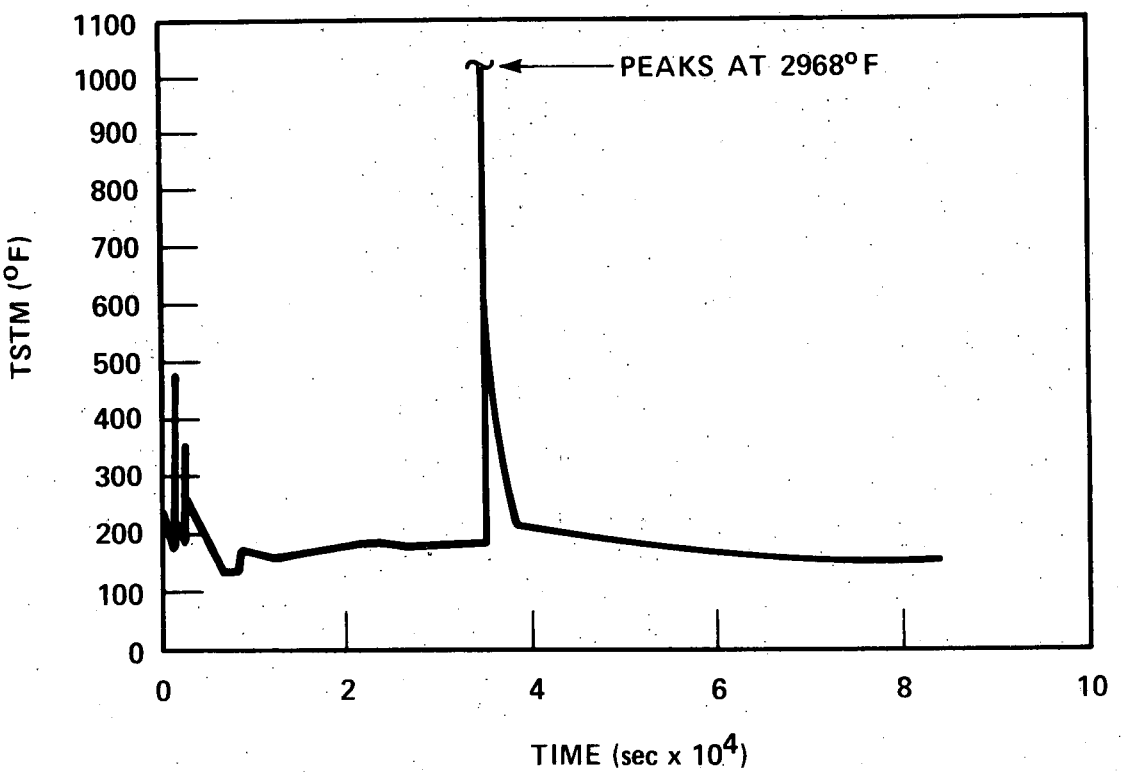
END OF INTER: 86480 SEC.

Class I, Case 1C

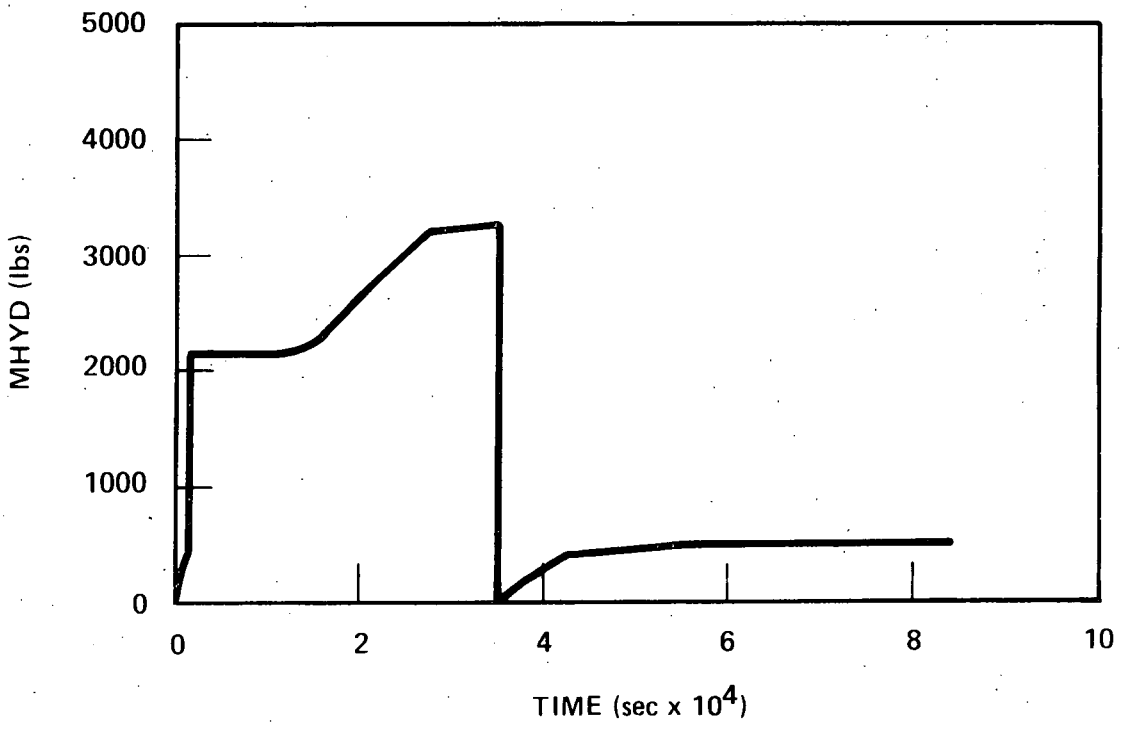
Sheet 1 of 7



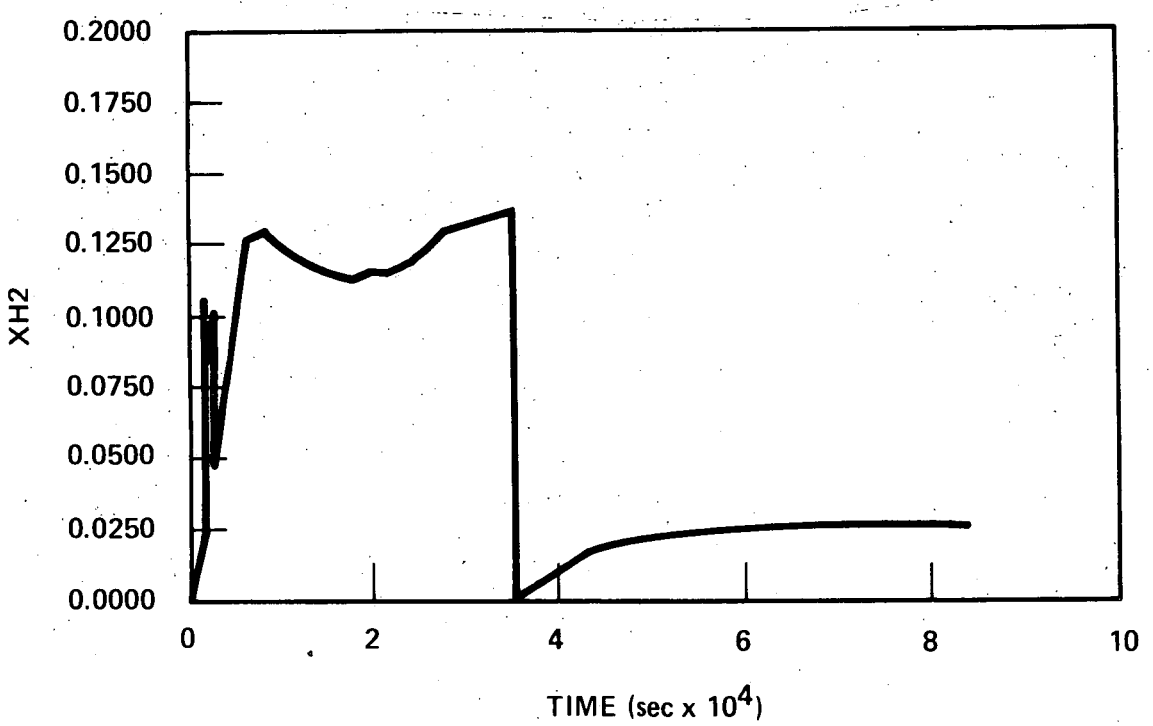
Pressure (in Containment) vs. Time
AD, B, Burn @ T_{MAX}
Class I, Case 1C



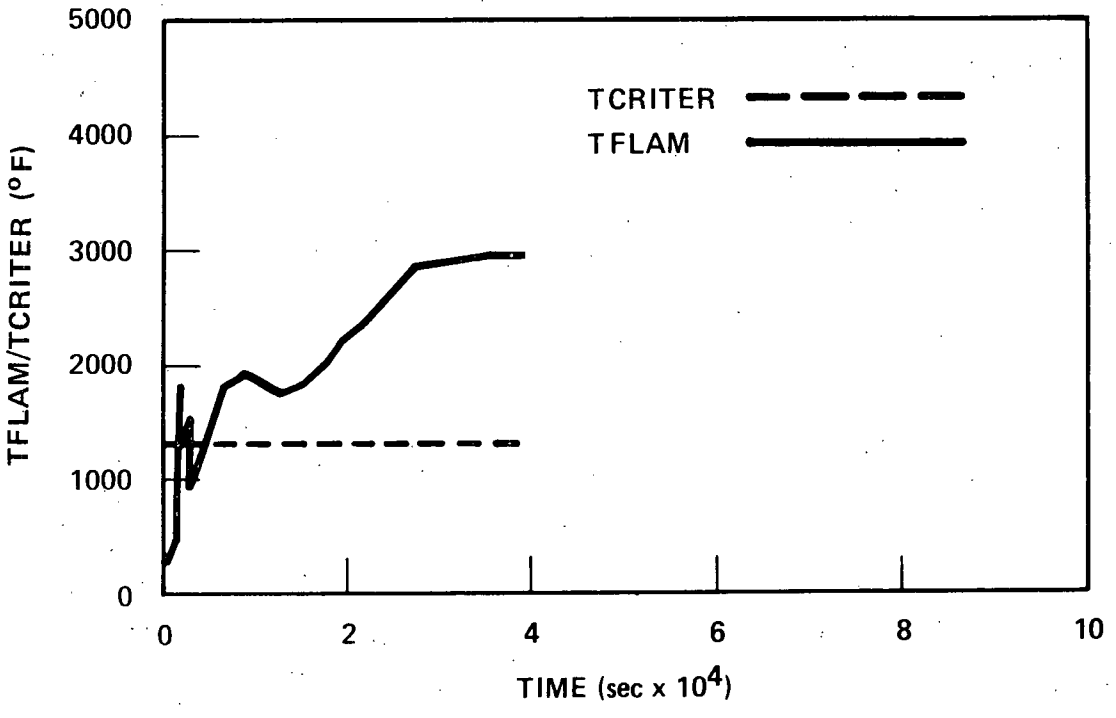
Temperature (in Containment) vs. Time
AD, B, Burn @ T_{MAX}
Class I, Case 1C



Mass Hydrogen (in Containment) vs. Time
AD, B, Burn @ T_{MAX}
Class I, Case 1C

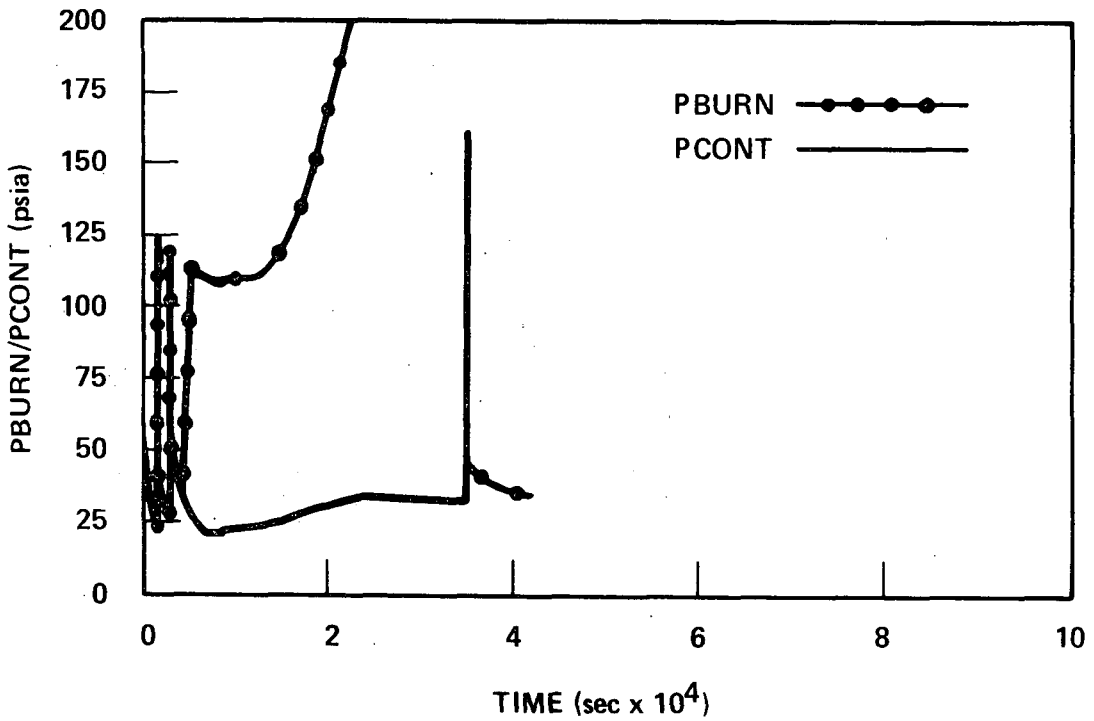


Mole Fraction H_2 (in Containment) vs. Time
AD, B, Burn @ T_{MAX}
Class I, Case 1C



Flame Temperature Criteria (in Containment) vs. Time
AD, B, Burn @ T_{MAX}
Class I, Case 1C

Sheet 6 of 7



Adiabatic Burn Pressure/Pressure in Containment vs. Time
AD, B, Burn @ T_{MAX}
Class I, Case 1C

CASE: CLASS I, CASE 2A, AD, W, NO BURN

DISPERSIVE: NO PERCENT CORE: ____ FRACTION IN CAVITY: ____

RUN #: AALAAYK DATE: 11/14/80

BLOWDOWN PEAK: 61 PSIA TIME: 12.0 SEC.

HYDROGEN BURN?: NO CRITERIA: ____

TIME @ BURN: ____ SEC, PRESSURE: ____ PSIA, TEMPERATURE: ____ °F

PEAKS:

PRESSURE: 61 PSIA, TIME: 12 SEC, WHY?: BLOWDOWN

TEMPERATURE: 325 °F, TIME: 12 SEC, WHY?: BLOWDOWN

DISPERSIVE: NO

PRESSURE: ____ PSIA, TIME: ____ SEC, WHY?: ____

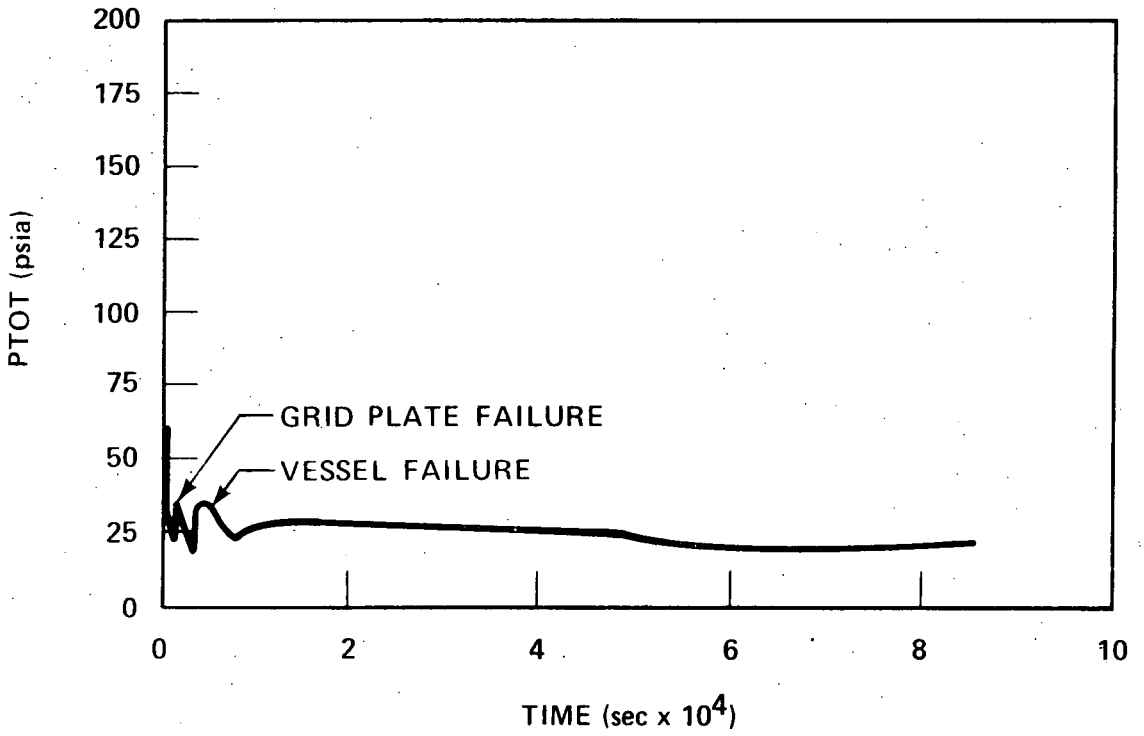
TEMPERATURE: ____ °F, TIME: ____ SEC, WHY?: ____

END OF BOIL: 1752 SEC. END OF HEAD: 3672 SEC.

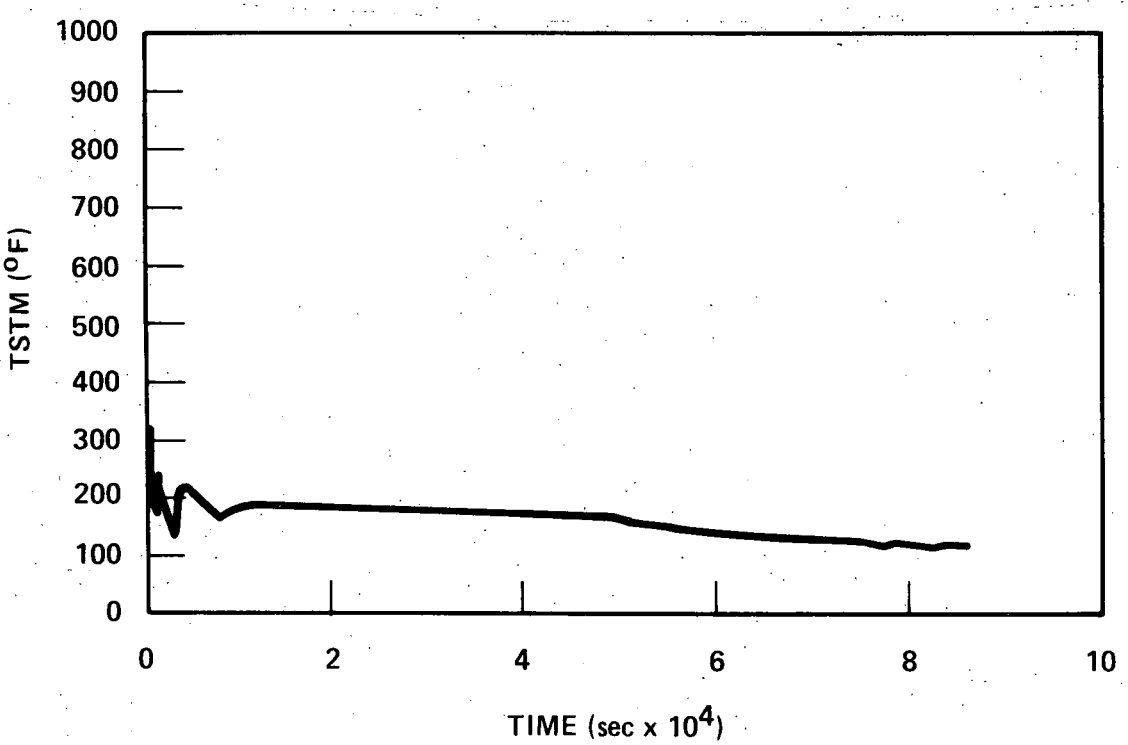
VESSEL FAILURE: 3672 SEC. END OF HOTDROP: 64369 SEC.

END OF INTER: 86288 SEC.

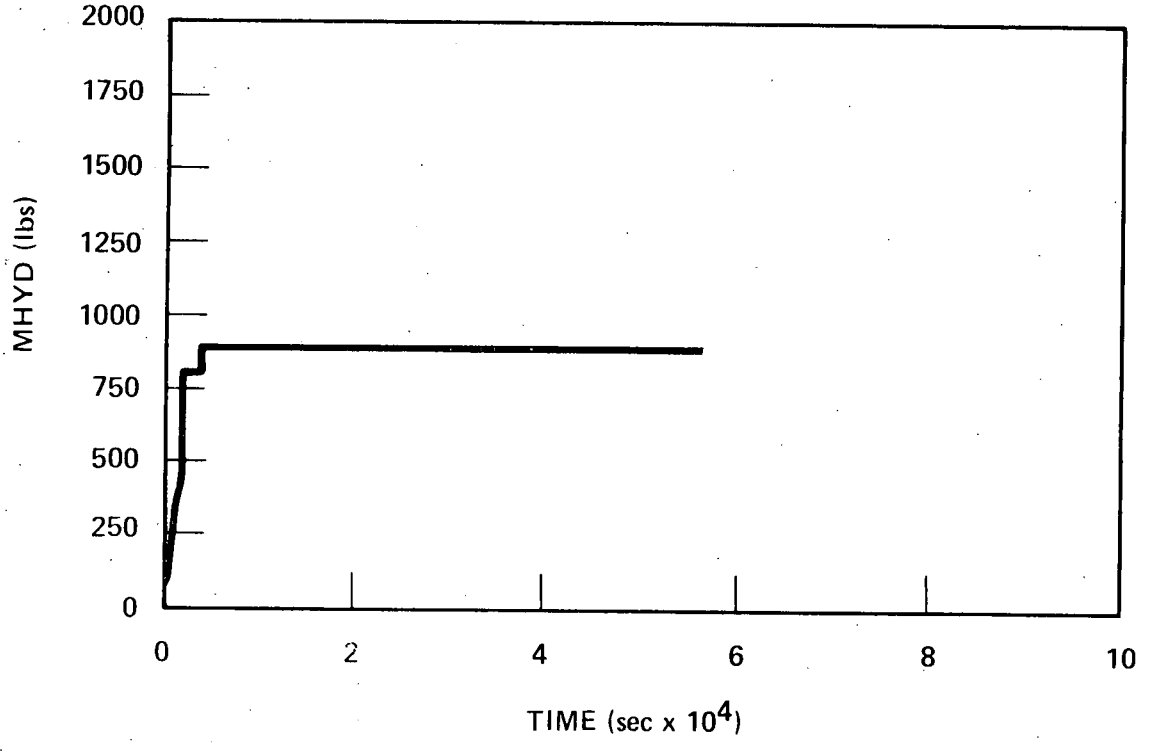
Class I, Case 2A



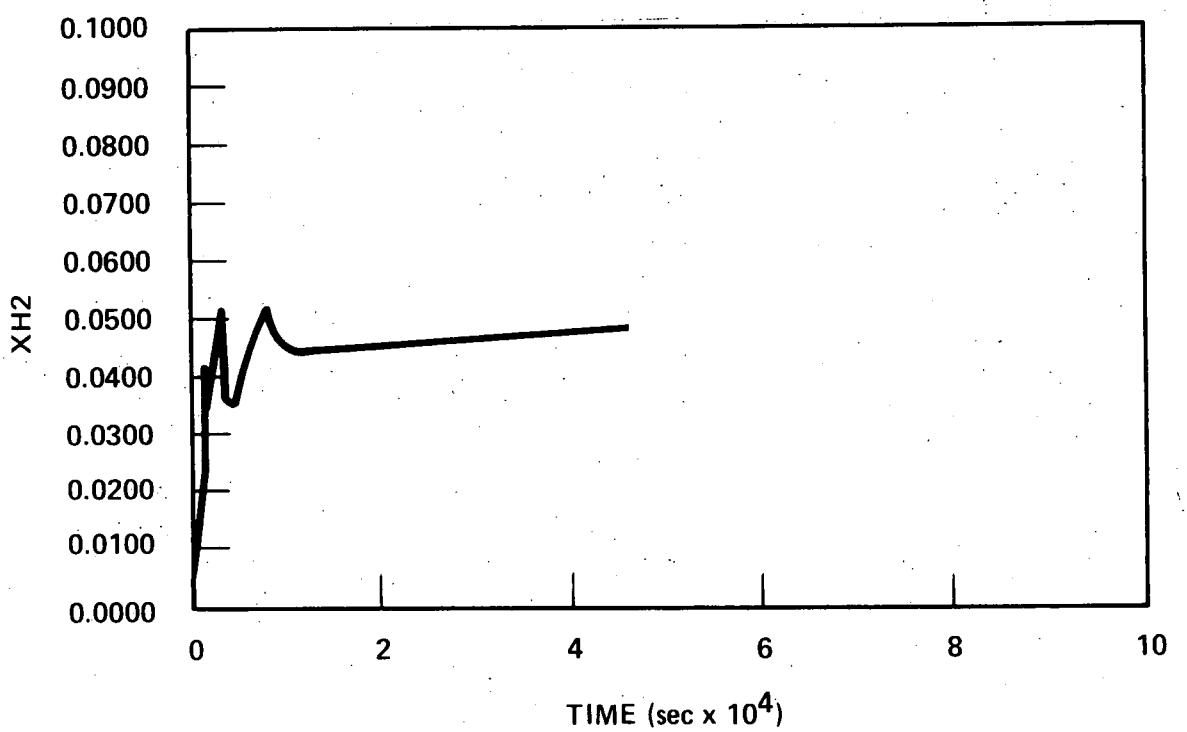
Pressure (in Containment) vs. Time
AD, W, No Burn
Class I, Case 2A



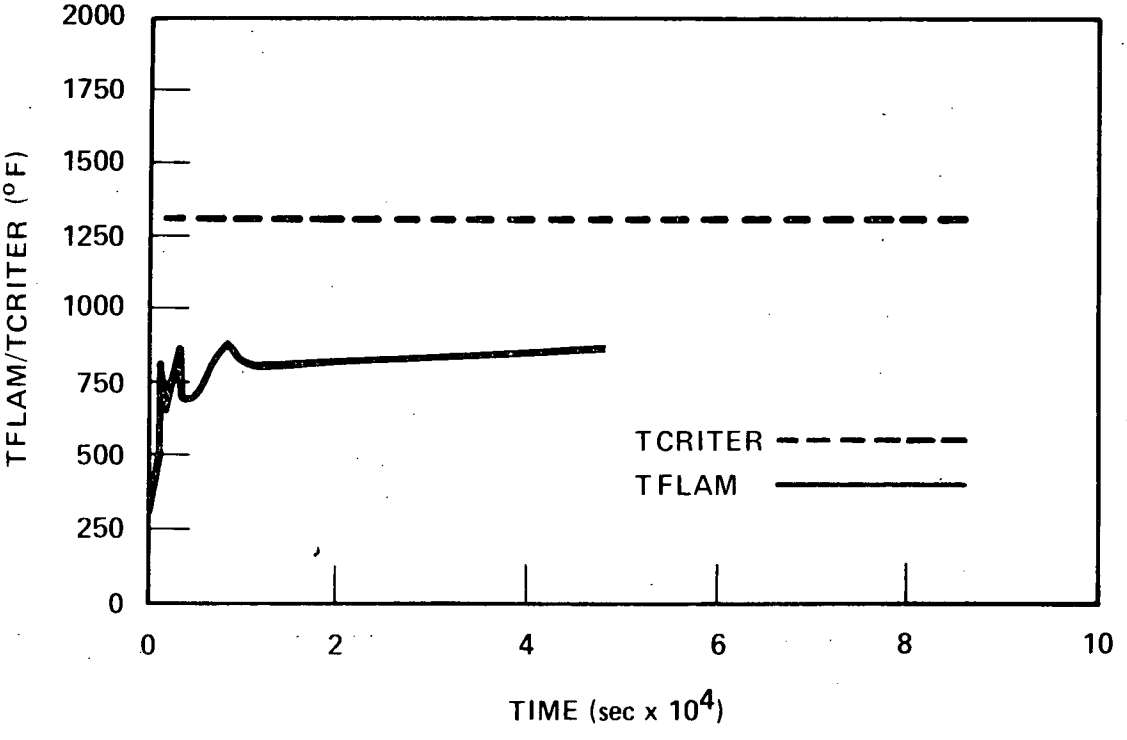
Temperature (in Containment) vs. Time
AD, W, No Burn
Class I, Case 2A



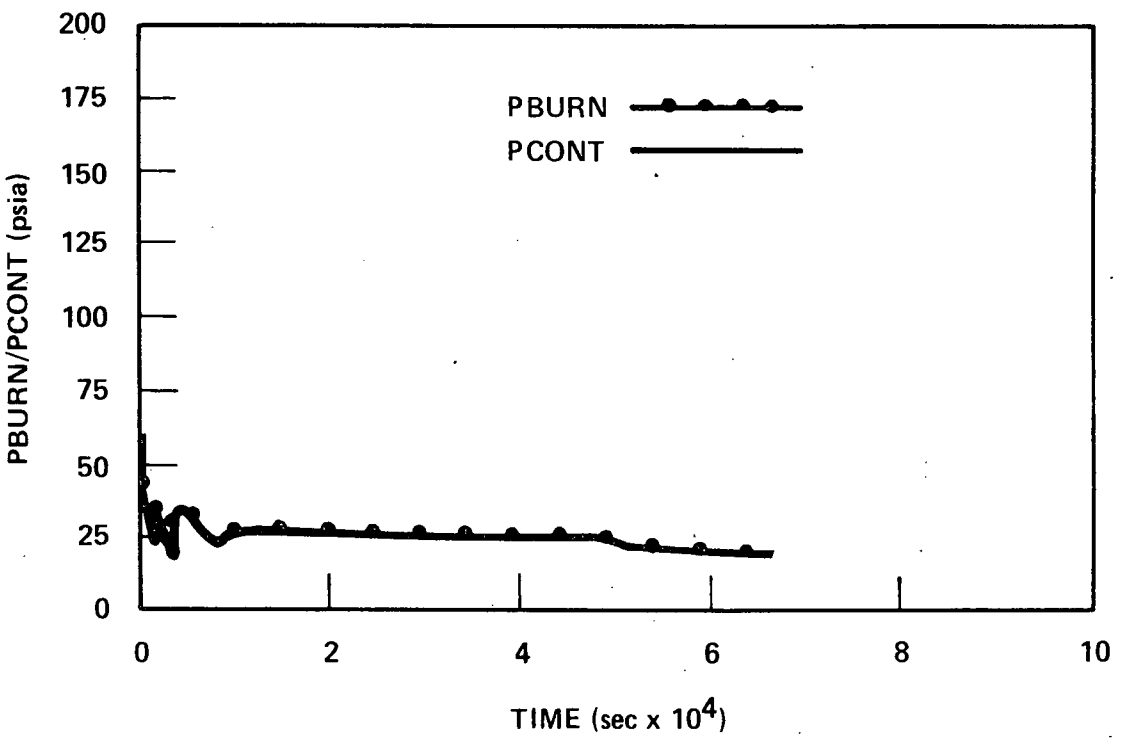
Mass Hydrogen (in Containment) vs. Time
AD, W, No Burn
Class I, Case 2A



Mole Fraction H_2 (in Containment) vs. Time
AD, W, No Burn
Class I, Case 2A



Flame Temperature (in Containment) vs. Time
AD, W, No Burn
Class I, Case 2A



Adiabatic Burn Pressure/Pressure in Containment vs. Time
AD, W, No Burn
Class I, Case 2A

Sheet 7 of 7

CASE: CLASS II, CASE 1A, AHF, B, NO BURN

DISPERSIVE: NO PERCENT CORE: ____ FRACTION IN CAVITY: ____

RUN #: AALABNR DATE: 11/13/80

BLOWDOWN PEAK: 59 PSIA TIME: ~12 SEC.

HYDROGEN BURN?: NO CRITERIA: ____

TIME @ BURN: ____ SEC, PRESSURE: ____ PSIA, TEMPERATURE: ____ °F

PEAKS:

PRESSURE: 72 PSIA, TIME: 10760 SEC, WHY?: VESSEL FAILURE

TEMPERATURE: 407 °F, TIME: ≈9372 SEC, WHY?: GRID PLATE FAILURE

DISPERSIVE: NO

PRESSURE: ____ PSIA, TIME: ____ SEC,

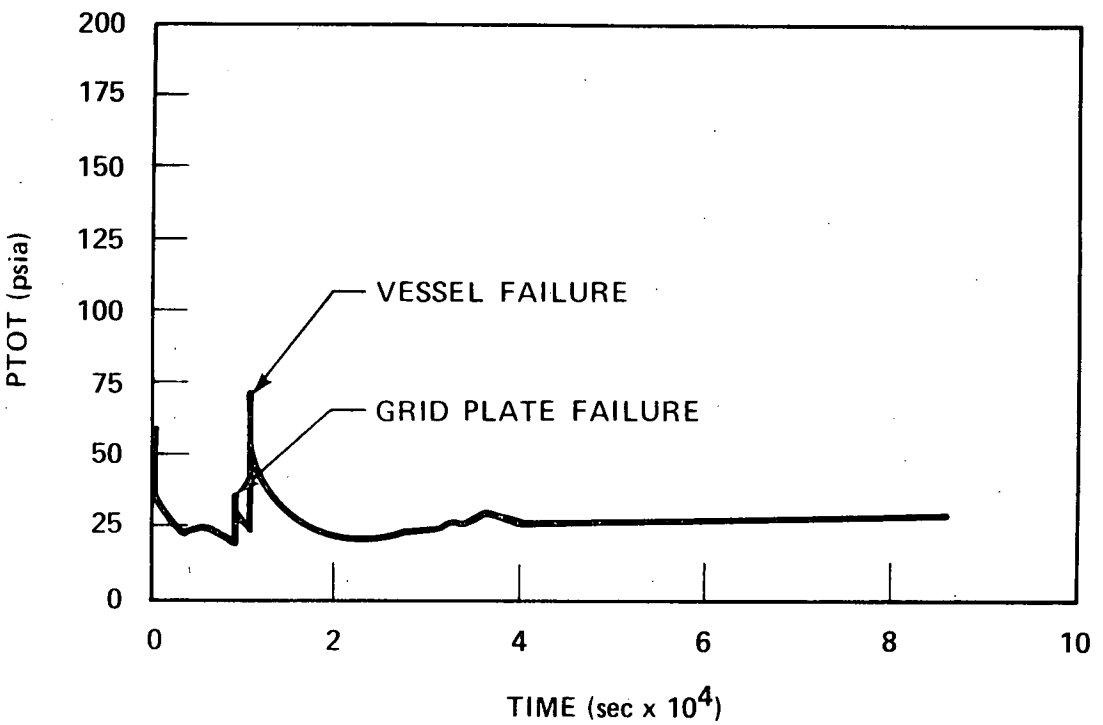
TEMPERATURE: ____ °F, TIME: ____ SEC,

END OF BOIL: 9432.6 SEC. END OF HEAD: 10753 SEC.

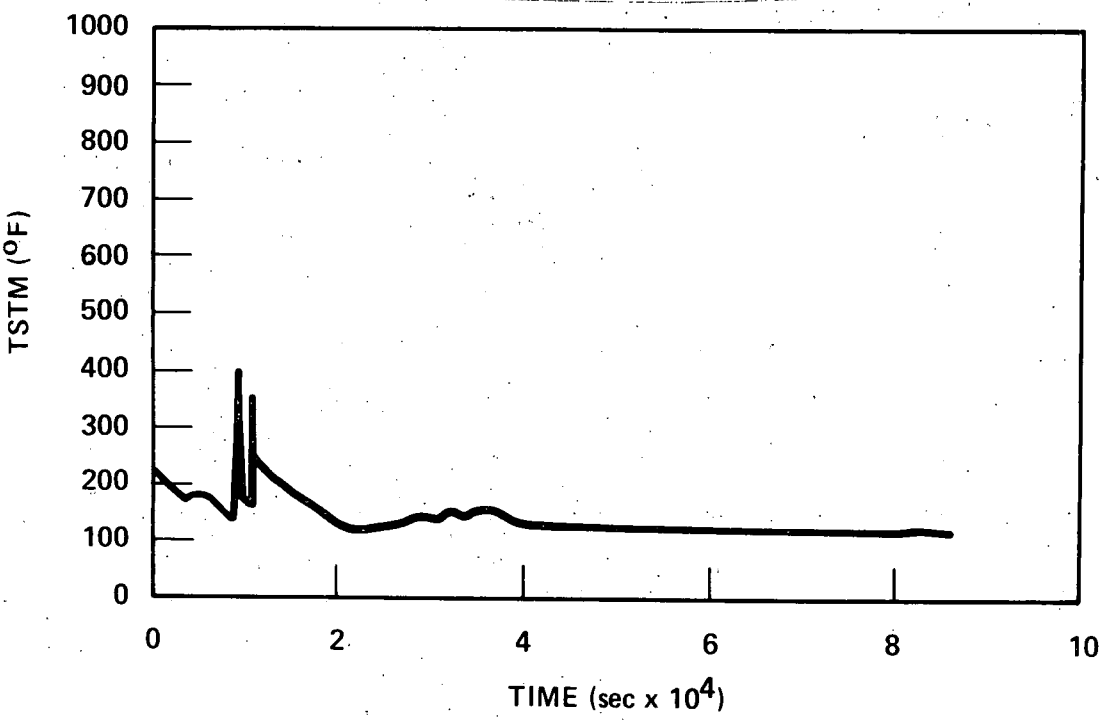
VESSEL FAILURE: 10753 SEC. END OF HOTDROP: 17360. SEC.

END OF INTER: 86883 SEC.

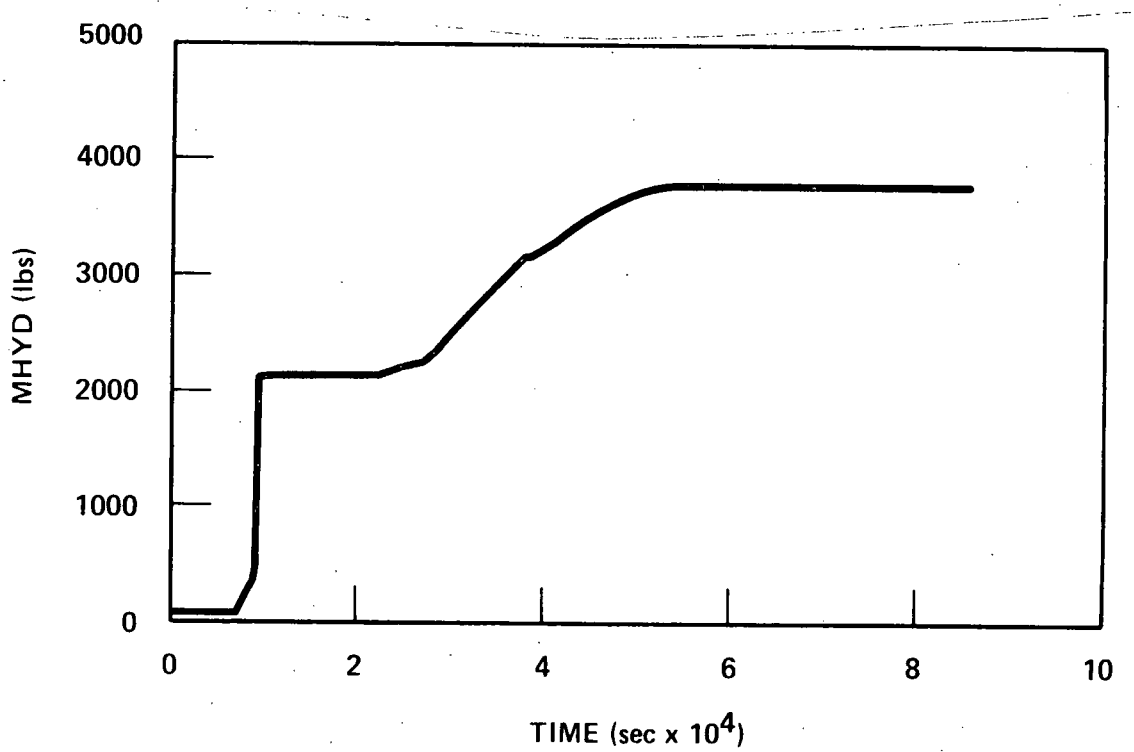
Class II, Case 1A



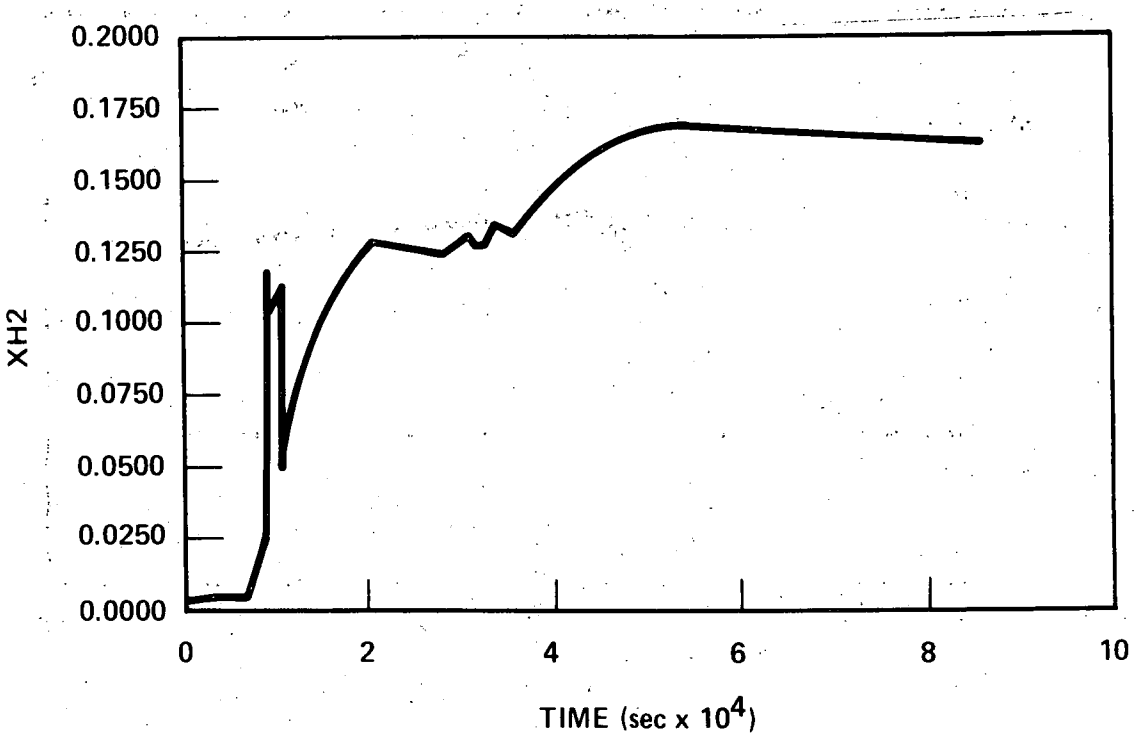
Pressure (in Containment) vs. Time
AHF, B, No Burn
Class II, Case 1A



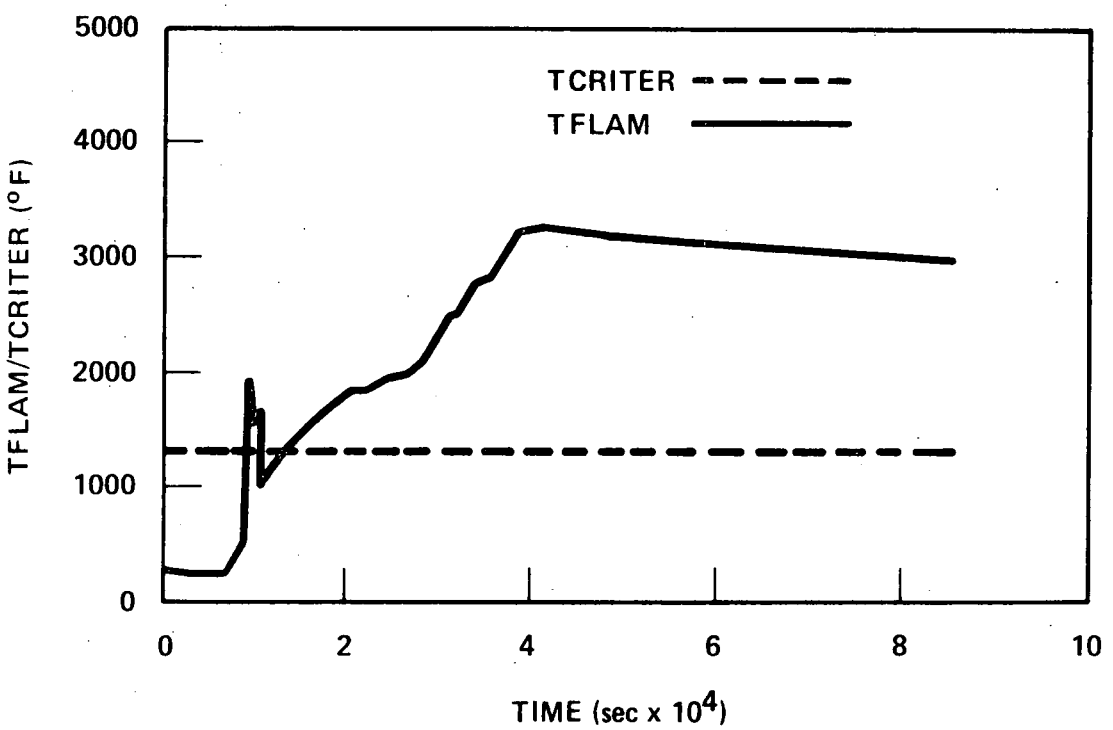
Temperature (in Containment) vs. Time
AHF, B, No Burn
Class II, Case 1A



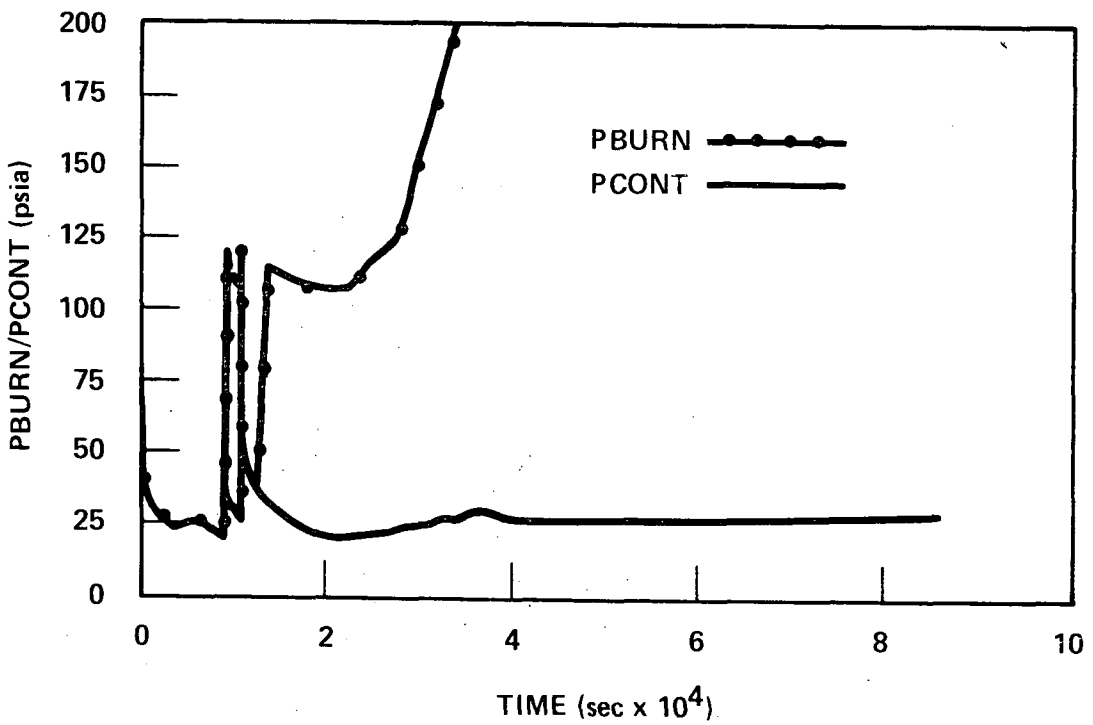
Mass Hydrogen (in Containment) vs. Time
AHF, B, No Burn
Class II, Case 1A



Mole Fraction H_2 (in Containment) vs. Time
AHF, B, No Burn
Class II, Case 1A



Flame Temperature (in Containment) vs. Time
AHF, B, No Burn
Class II, Case 1A



Adiabatic Burn Pressure/Pressure in Containment vs. Time
AHF, B, No Burn
Class II, Case 1A

CASE: CLASS II, CASE 1B, AHF, B, BURN @ VESSEL FAILURE

DISPERSIVE: NO PERCENT CORE: _____ FRACTION IN CAVITY: _____

RUN #: AALABAH DATE: 11/15/80

BLOWDOWN PEAK: 59 PSIA TIME: ~12 SEC.

HYDROGEN BURN?: YES CRITERIA: VESSEL FAILURE

TIME @ BURN: 10755 SEC, PRESSURE: 136 PSIA, TEMPERATURE: 1211 °F

PEAKS:

PRESSURE: 136 PSIA, TIME: 10775 SEC, WHY?: VESSEL FAILURE/H_2 BURN

TEMPERATURE: 1211 °F, TIME: 10775 SEC, WHY?: VESSEL FAILURE/H_2 BURN

DISPERSIVE: NO

PRESSURE: _____ PSIA, TIME: _____ SEC, WHY?: _____

TEMPERATURE: _____ °F, TIME: _____ SEC, WHY?: _____

END OF BOIL: 9432.6 SEC. END OF HEAD: 10753 SEC.

VESSEL FAILURE: 10753 SEC. END OF HOTDROP: 17360 SEC.

END OF INTER: 86883 SEC.

Class II, Case 1B

NO PLOTS MADE FOR RUN

AALABAH 11/15/80

CASE: CLASS II, CASE 1C, AHF, B, BURN @ T_{MAX}

DISPERSIVE: NO PERCENT CORE: _____ FRACTION IN CAVITY: _____

RUN #: AALAAZZ DATE: 11/15/80

BLOWDOWN PEAK: 59 PSIA TIME: ~12 SEC.

HYDROGEN BURN?: YES CRITERIA: @ T_{MAX}

TIME @ BURN: 40915 SEC, PRESSURE: 144 PSIA, TEMPERATURE: 3145 °F

PEAKS:

PRESSURE: 144 PSIA, TIME: 40950 SEC, WHY?: H_2 BURN

TEMPERATURE: 3145 °F, TIME: 40950 SEC, WHY?: H_2 BURN

DISPERSIVE: NO

PRESSURE: _____ PSIA, TIME: _____ SEC,

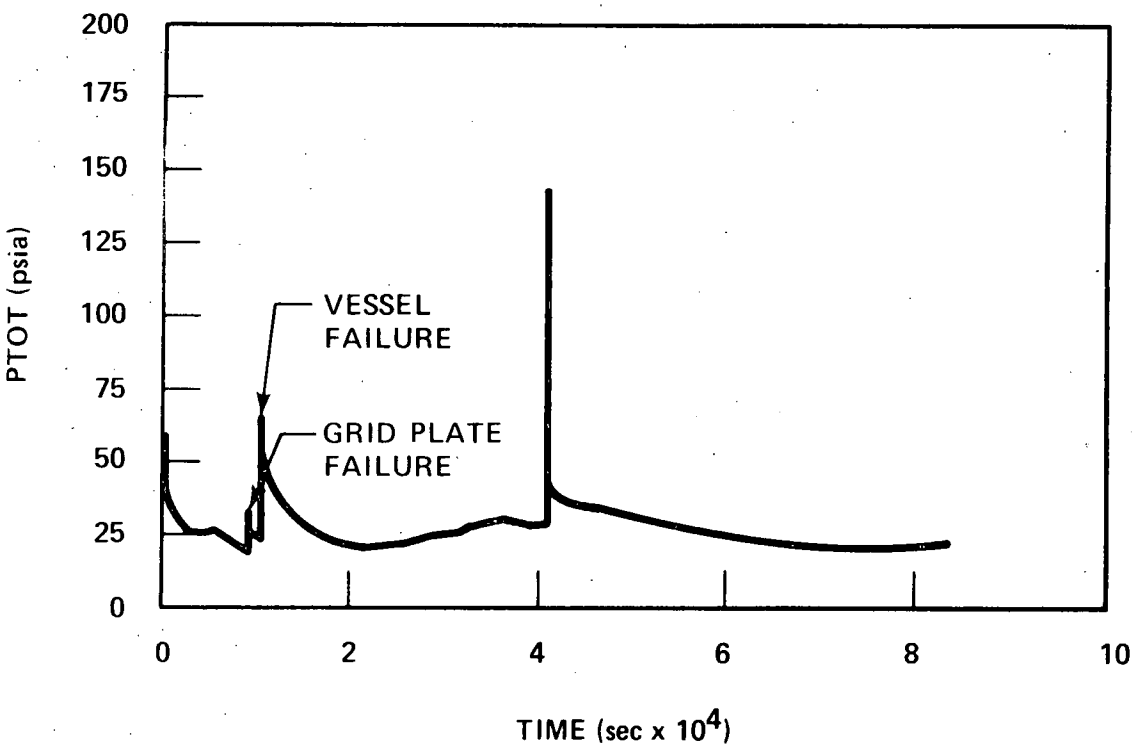
TEMPERATURE: _____ °F, TIME: _____ SEC,

END OF BOIL: 9432.6 SEC. END OF HEAD: 10753 SEC.

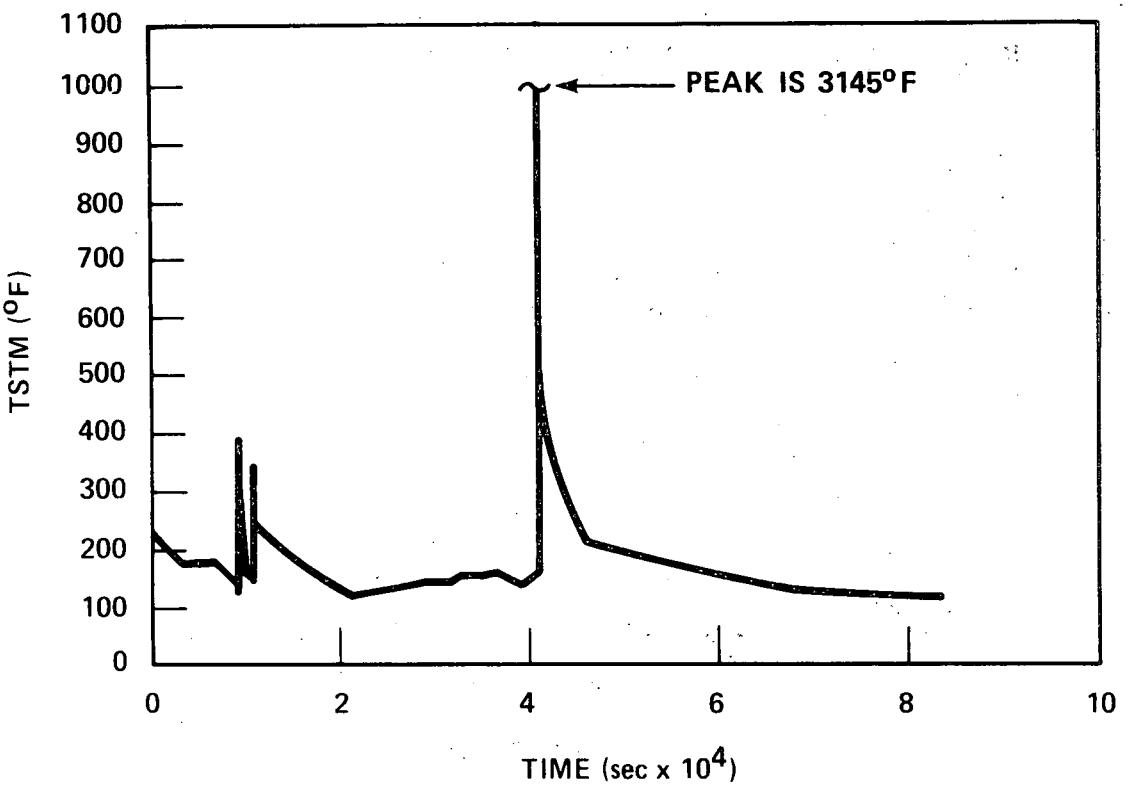
VESSEL FAILURE: 10753 SEC. END OF HOTDROP: 17360 SEC.

END OF INTER: 86883 SEC.

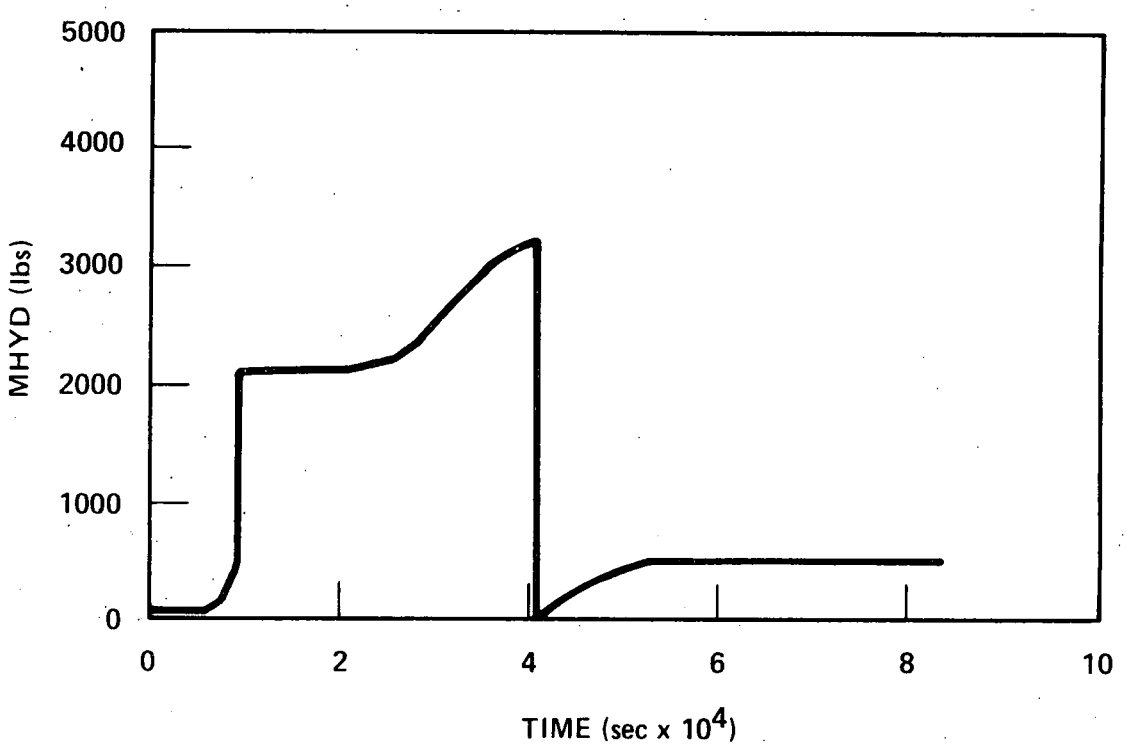
Class II, Case 1C



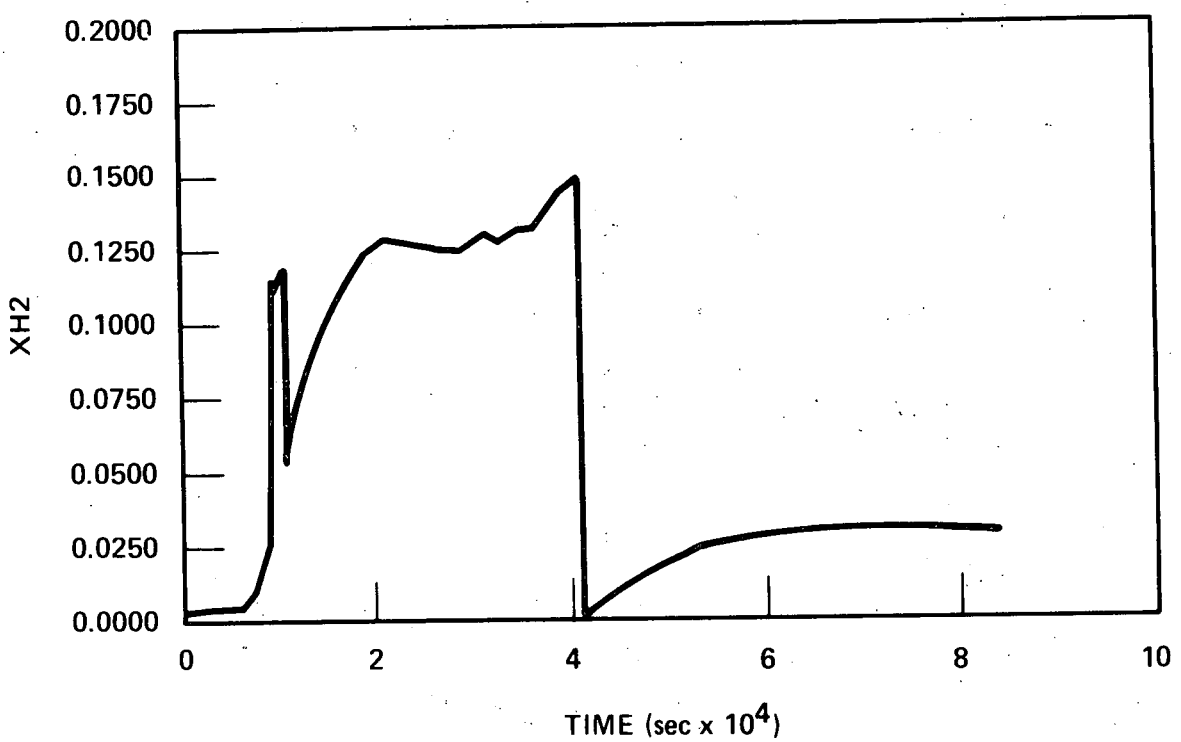
Pressure (in Containment) vs. Time
AHF, B, Burn @ T_{MAX}
Class II, Case 1C



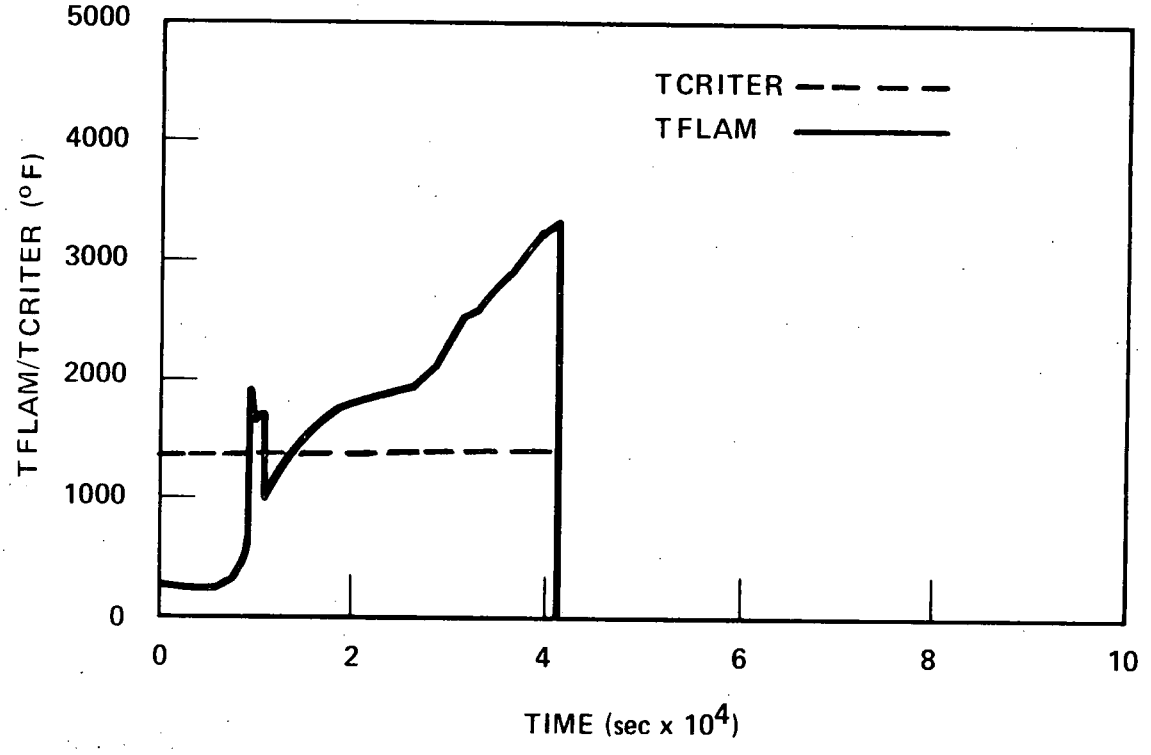
Temperature (in Containment) vs. Time
AHF, B, Burn @ T_{MAX}
Class II, Case 1C



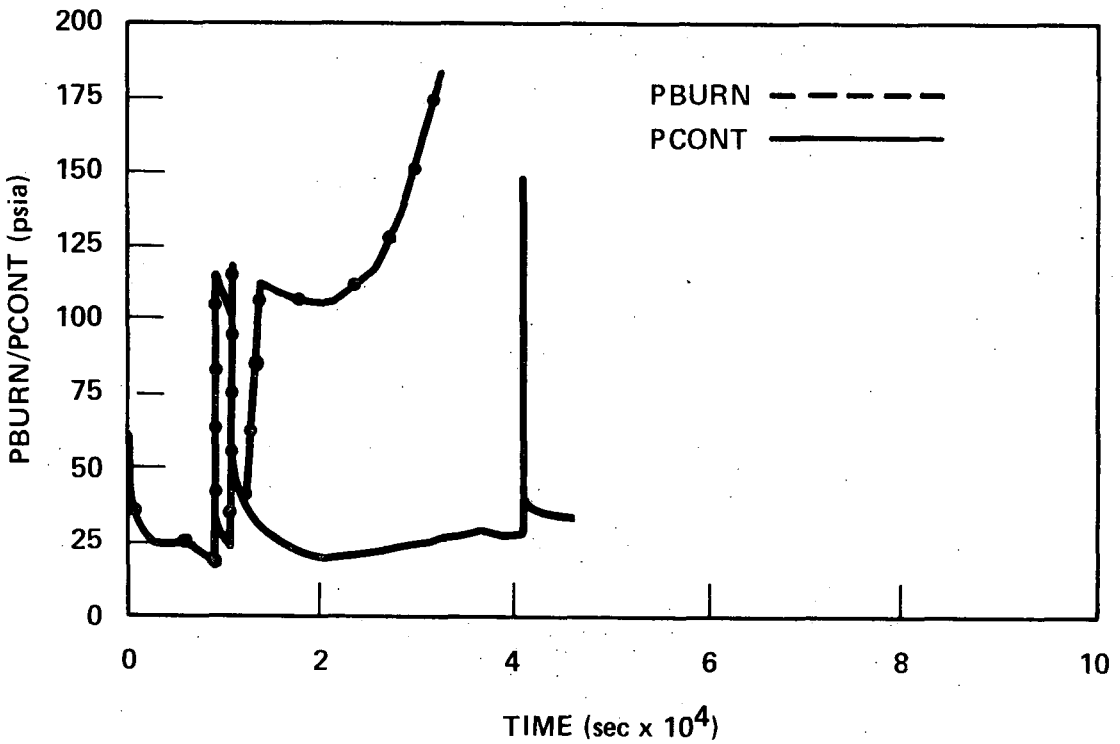
Mass Hydrogen (in Containment) vs. Time
AHF, B, Burn @ T_{MAX}
Class II, Case 1C



Mole Fraction H_2 (in Containment) vs. Time
AHF, B, Burn @ T_{MAX}
Class II, Case 1C



Flame Temperature (in Containment) vs. Time
AHF, B, Burn @ T_{MAX}
Class II, Case 1C



Adiabatic Burn Pressure/Pressure in Containment vs. Time
AHF, B, Burn @ T_{MAX}
Class II, Case 1C

CASE: CLASS II, CASE 2A, AHF, W, NO BURN

DISPERSIVE: NO PERCENT CORE: ____ FRACTION IN CAVITY: ____

RUN #: AALAAYV DATE: 11/14/80

BLOWDOWN PEAK: 61 PSIA TIME: 12 SEC.

HYDROGEN BURN?: NO CRITERIA: ____

TIME @ BURN: ____ SEC, PRESSURE: ____ PSIA, TEMPERATURE: ____ °F

PEAKS:

PRESSURE: 61 PSIA, TIME: 12 SEC, WHY?: BLOWDOWN

TEMPERATURE: 325 °F, TIME: 12 SEC, WHY?: BLOWDOWN

DISPERSIVE: NO

PRESSURE: ____ PSIA, TIME: ____ SEC,

TEMPERATURE: ____ °F, TIME: ____ SEC,

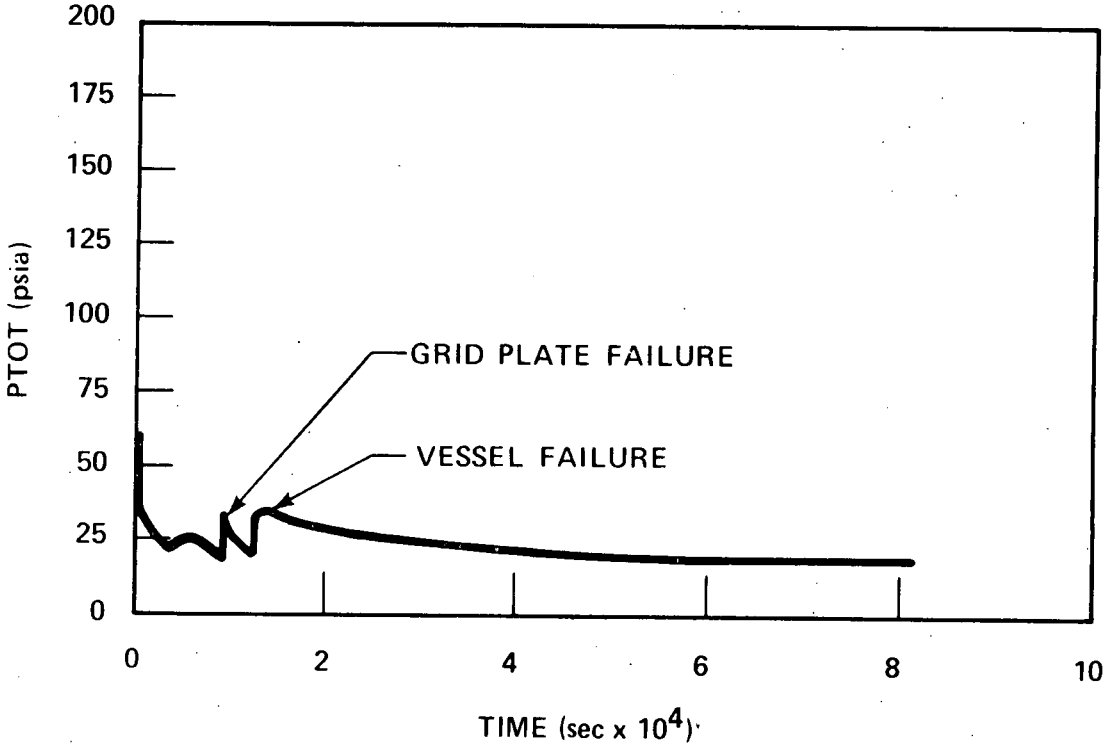
END OF BOIL: 9432 SEC. END OF HEAD: 12432 SEC.

VESSEL FAILURE: 12432 SEC. END OF HOTDROP: ____ SEC.

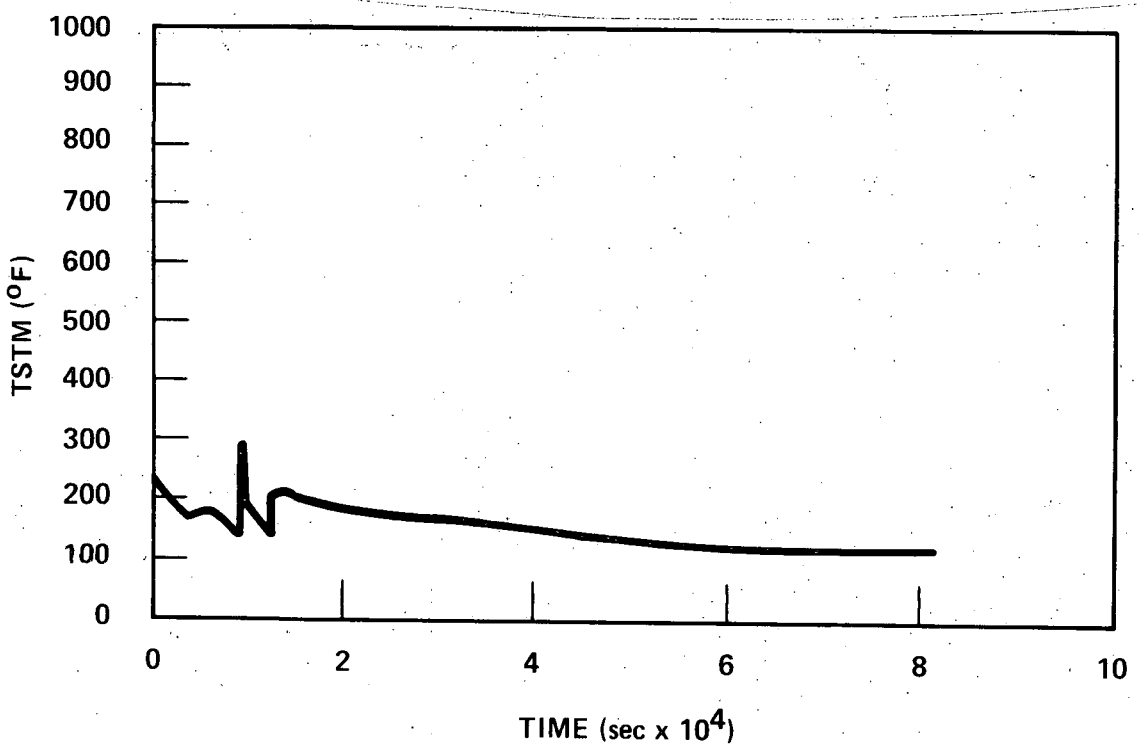
END OF INTER: 86776 SEC.

Class II, Case 2A

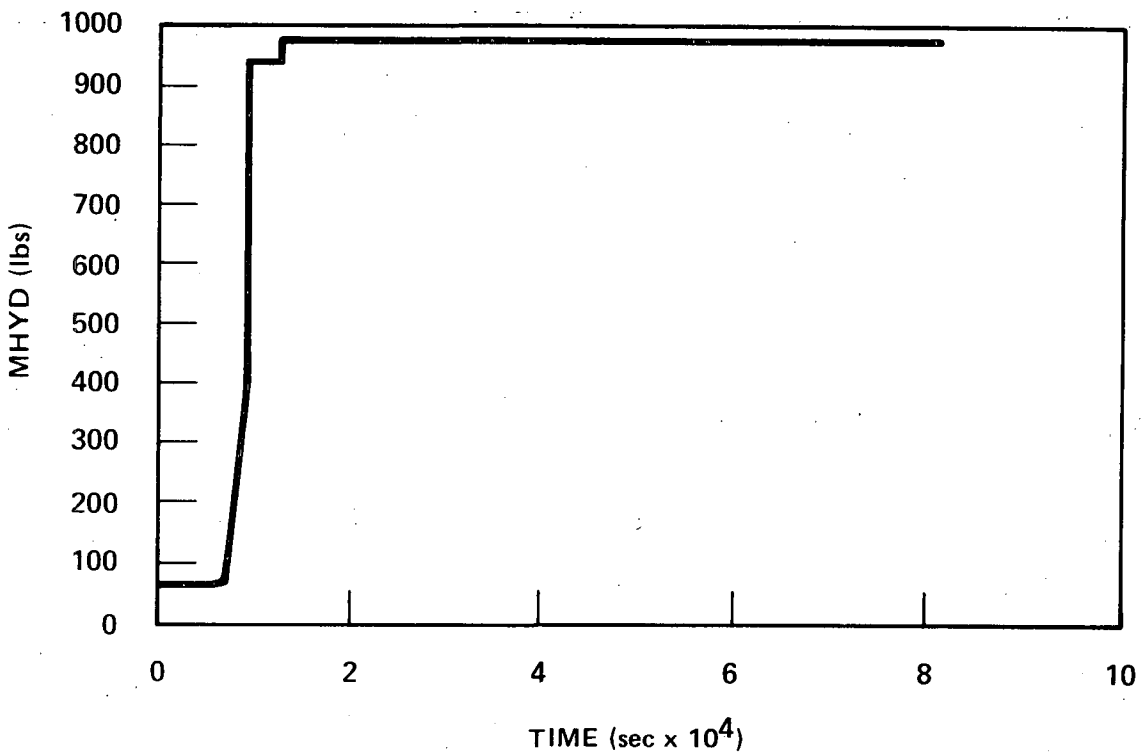
Sheet 1 of 7



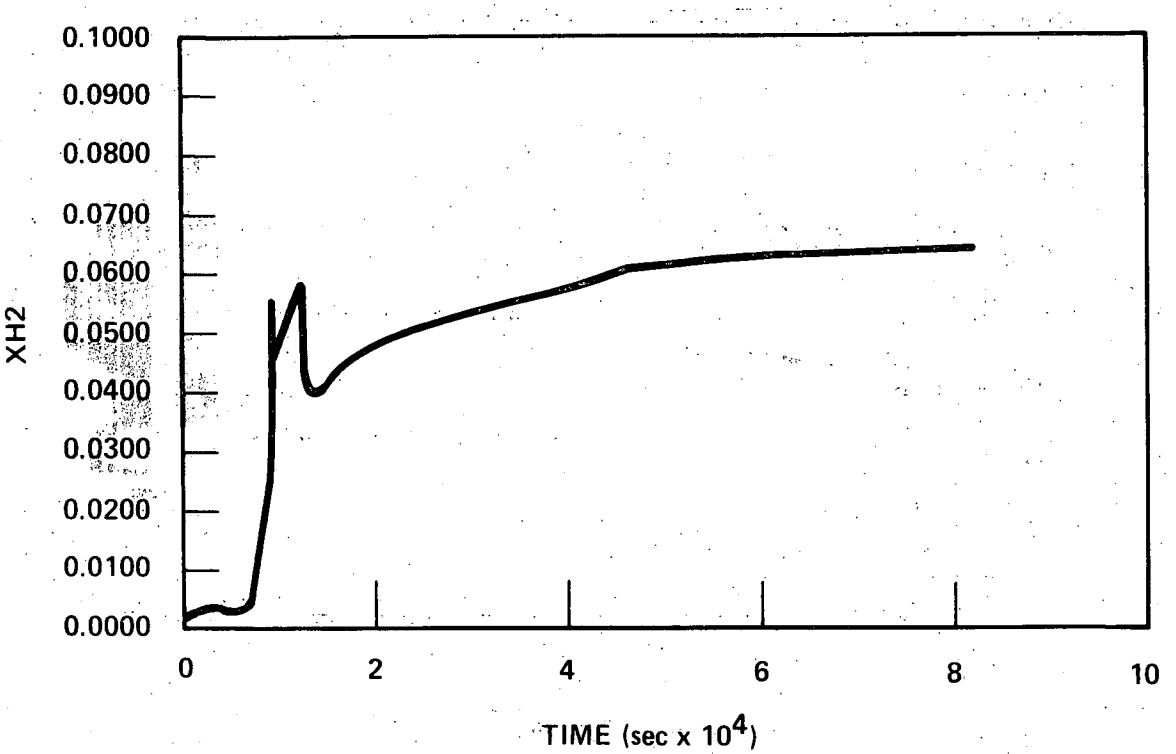
Pressure (in Containment) vs. Time
AHF, W, No Burn
Class II, Case 2A



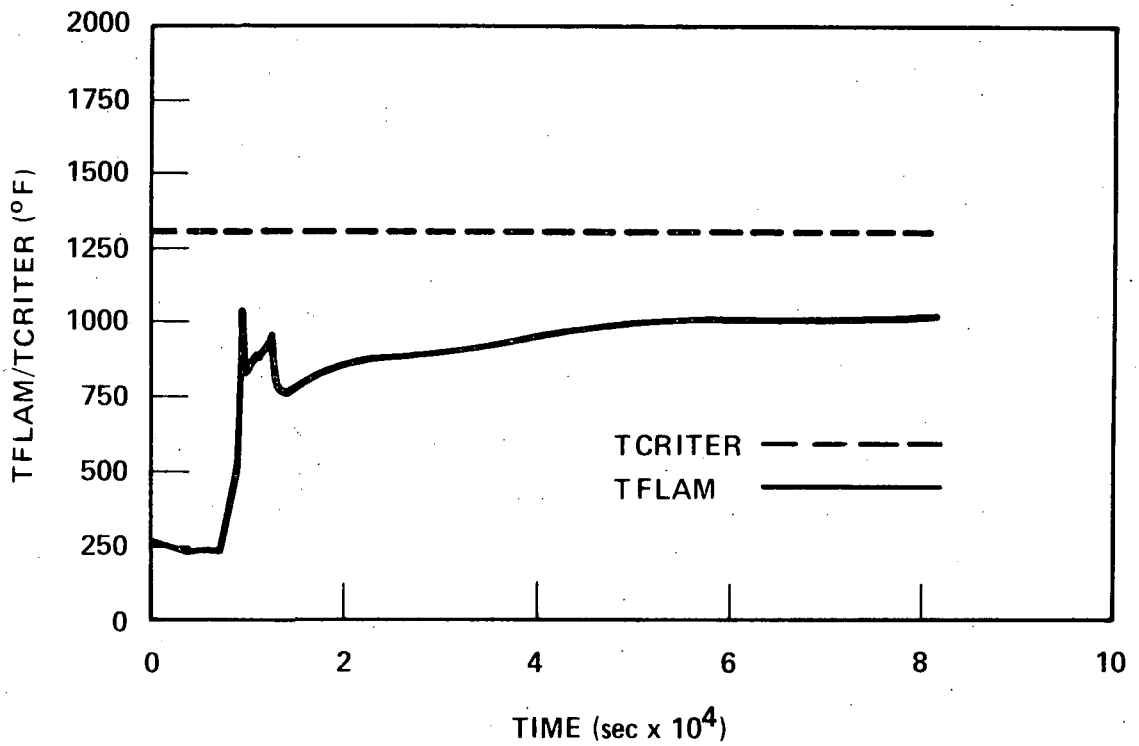
Temperature (in Containment) vs. Time
AHF, W, No Burn
Class II, Case 2A



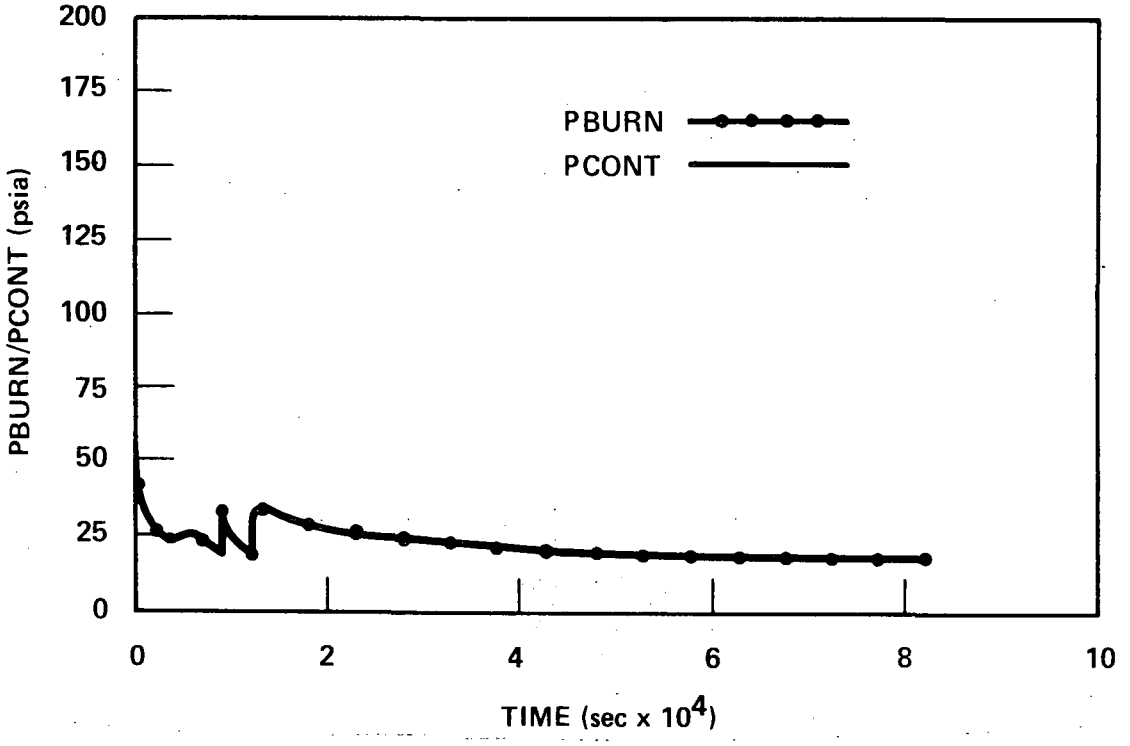
Mass Hydrogen (in Containment) vs. Time
AHF, W, No Burn
Class II, Case 2A



Mole Fraction H_2 (in Containment) vs. Time
AHF, W, No Burn
Class II, Case 2A



Flame Temperature (in Containment) vs. Time
AHF, W, No Burn
Class II, Case 2A



Adiabatic Burn Pressure/Pressure in Containment vs. Time
AHF, W, No Burn
Class II, Case 2A

CASE: CLASS III, CASE 1A, S2D, B, NO BURN, NON-DISPERSIVE

DISPERSIVE: NO PERCENT CORE: _____ FRACTION IN CAVITY: _____

RUN #: AALAADS DATE: 11/15/80

BLOWDOWN PEAK: _____ PSIA TIME: _____ SEC.

HYDROGEN BURN?: NO CRITERIA: _____

TIME @ BURN: _____ SEC, PRESSURE: _____ PSIA, TEMPERATURE: _____ °F

PEAKS:

PRESSURE: 77 PSIA, TIME: 4874 SEC, WHY?: VESSEL FAILURE

TEMPERATURE: 401 °F, TIME: 4874 SEC, WHY?: VESSEL FAILURE

DISPERSIVE: NO

PRESSURE: _____ PSIA, TIME: _____ SEC,

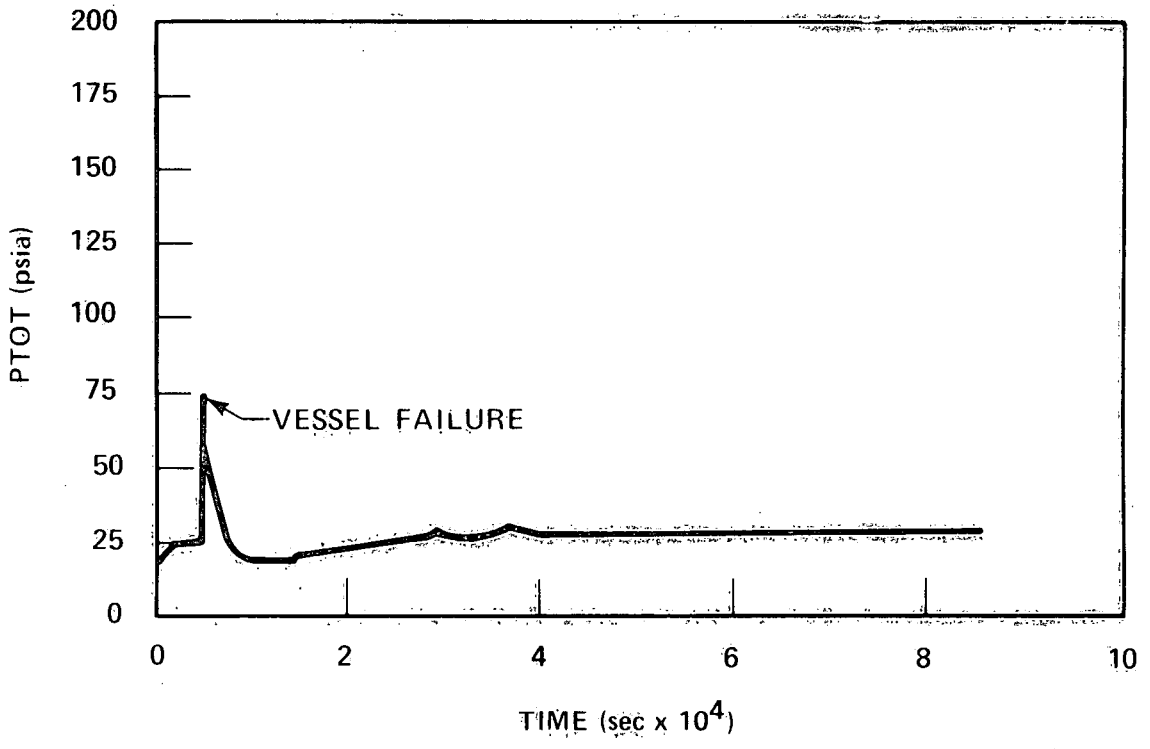
TEMPERATURE: _____ °F, TIME: _____ SEC,

END OF BOIL: 4864.5 SEC. END OF HEAD: 4867.1 SEC.

VESSEL FAILURE: 4867.1 SEC. END OF HOTDROP: 10394. SEC.

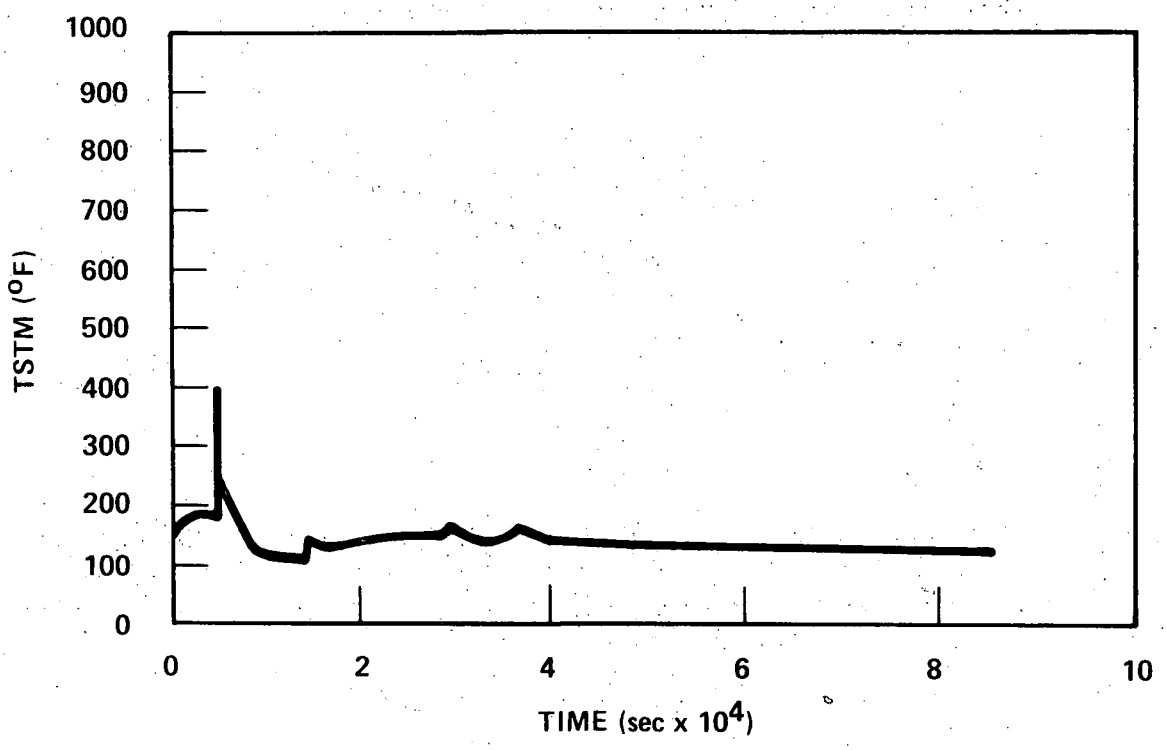
END OF INTER: 86947 SEC.

Class III, Case 1A



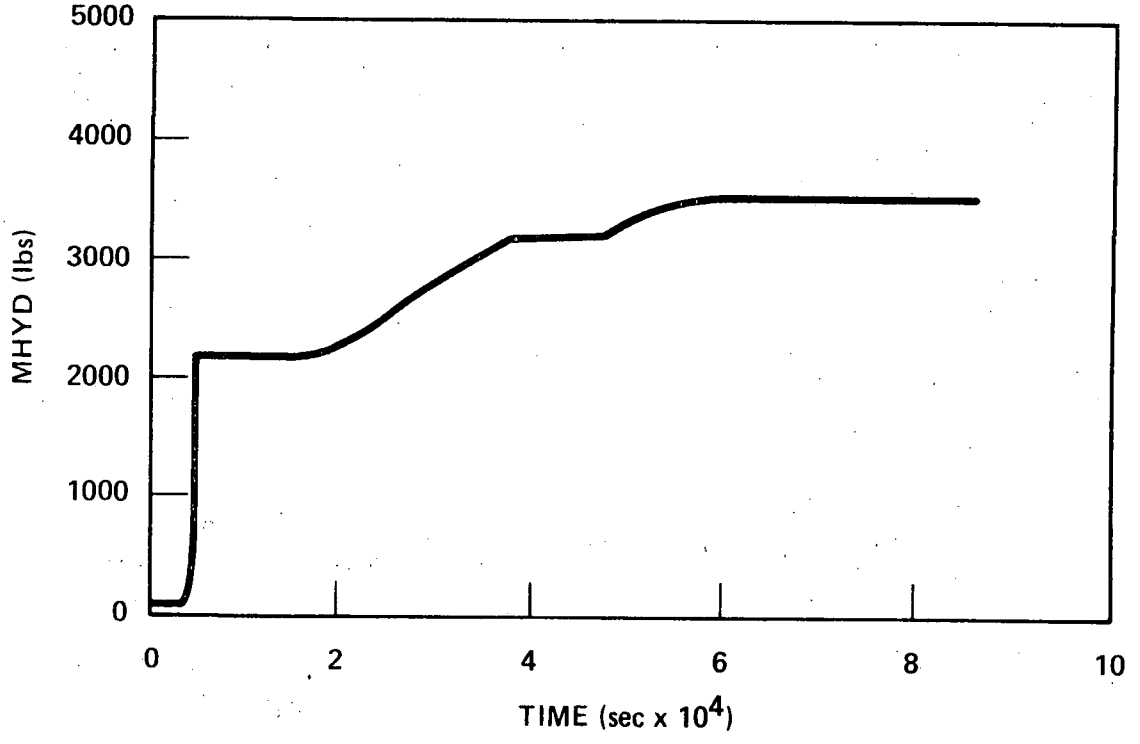
Pressure (in Containment) vs. Time
S2D, B, No Burn
Class III, Case 1A

Sheet 2 of 7

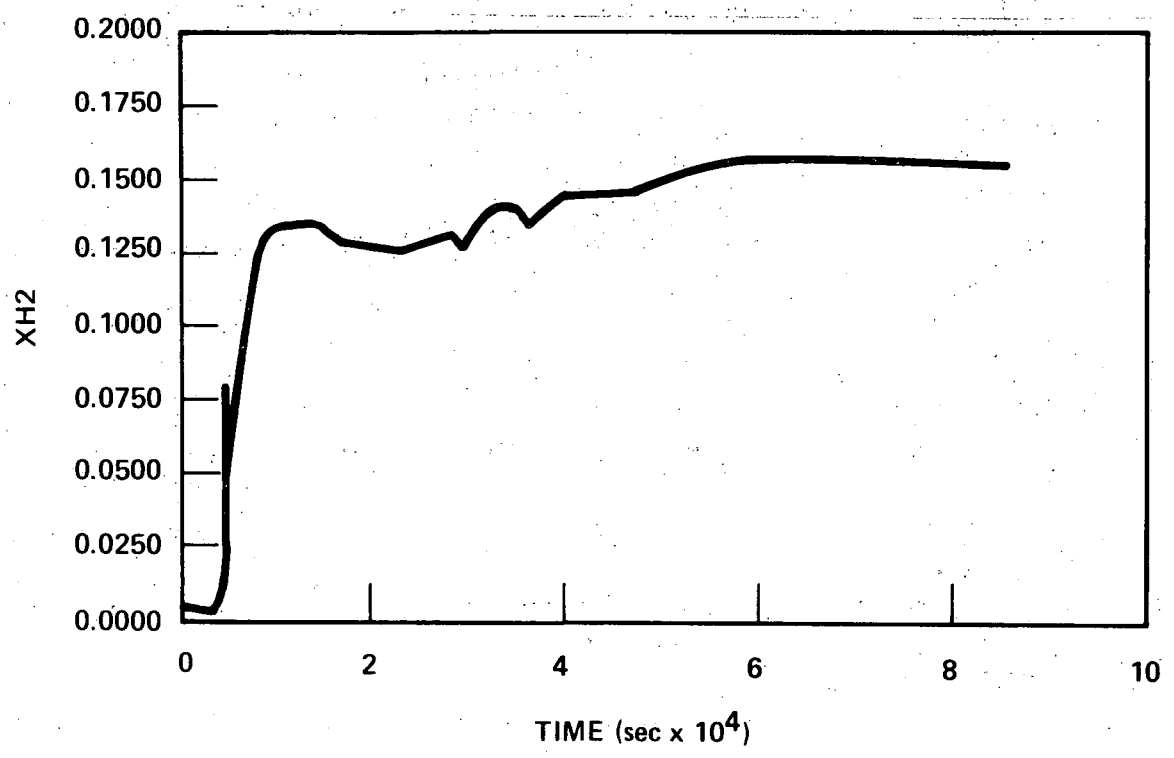


Temperature (in Containment) vs. Time
S2D, B, No Burn
Class III, Case 1A

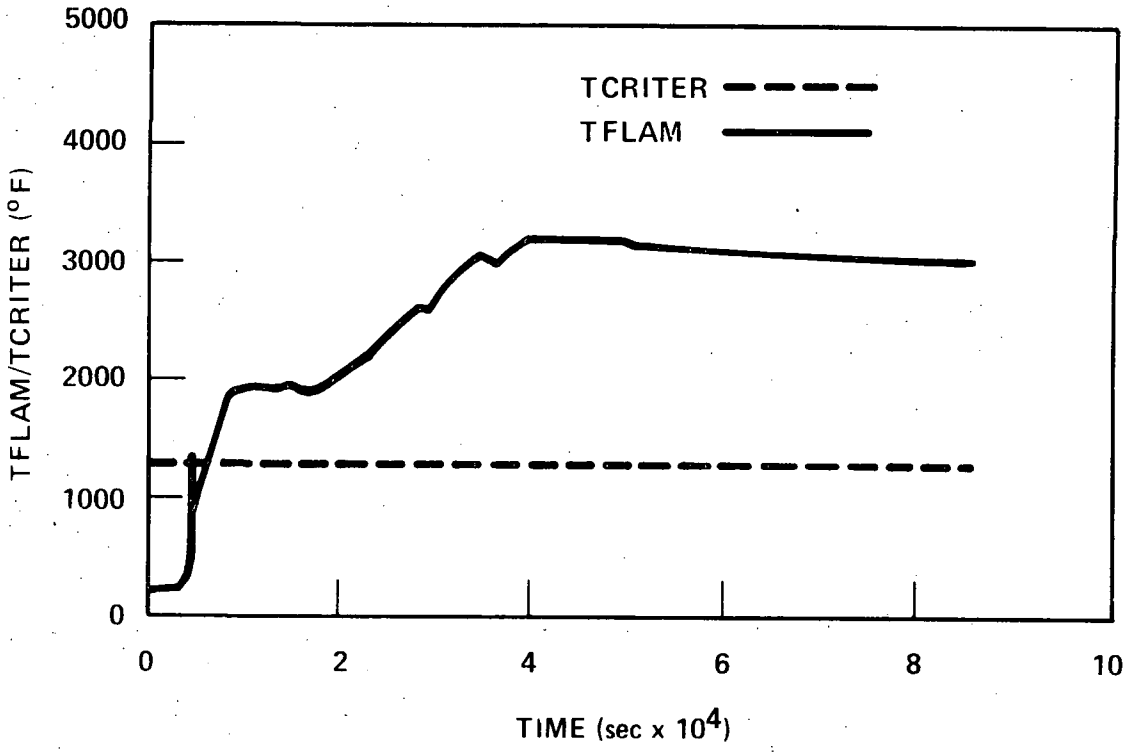
Sheet 3 of 7



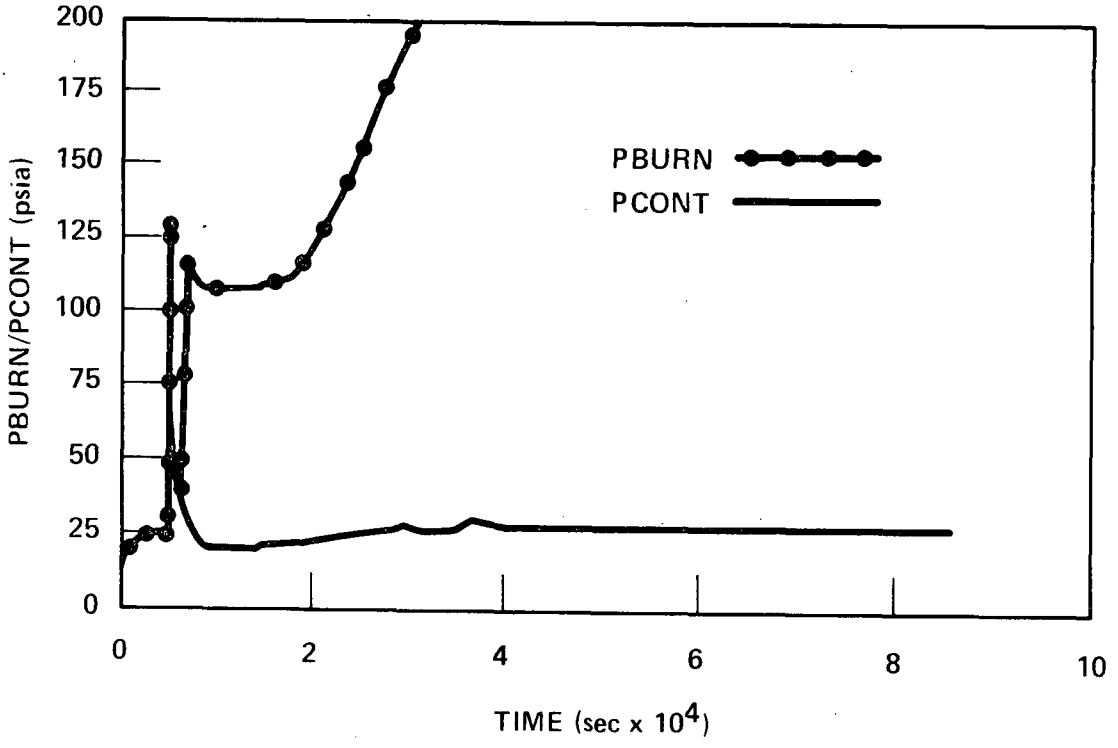
Mass Hydrogen (in Containment) vs. Time
S2D, B, No Burn
Class III, Case 1A



Mole Fraction H_2 (in Containment) vs. Time
S2D, B, No Burn
Class III, Case 1A



Flame Temperature (in Containment) vs. Time
S2D, B, No Burn
Class III, Case 1A



Adiabatic Burn Pressure/Pressure in Containment vs. Time
S2D, B, No Burn
Class III, Case 1A

CASE: CLASS III, CASE 1B, S2D, B, BURN @ VESSEL FAILURE, NON-DISPERSIVE

DISPERSIVE: NO PERCENT CORE: _____ FRACTION IN CAVITY: _____

RUN #: AALAAFV DATE: 11/15/80

BLOWDOWN PEAK: _____ PSIA TIME: _____ SEC.

HYDROGEN BURN?: YES CRITERIA: VESSEL FAILURE

TIME @ BURN: 4867 SEC, PRESSURE: 45 PSIA, TEMPERATURE: 361 °F

PEAKS:

PRESSURE: 145 PSIA, TIME: 4887 SEC, WHY?: VESSEL FAILURE, H_2 BURN

TEMPERATURE: 1198 °F, TIME: 4887 SEC, WHY?: VESSEL FAILURE, H_2 BURN

DISPERSIVE: NO

PRESSURE: _____ PSIA, TIME: _____ SEC,

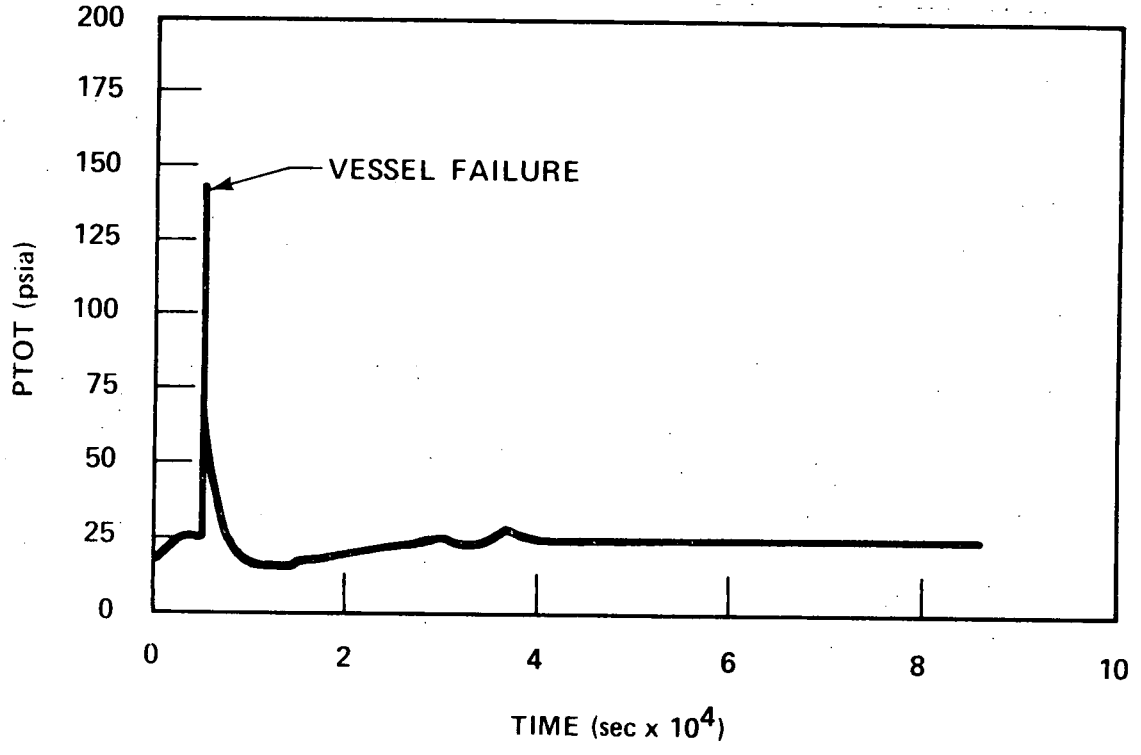
TEMPERATURE: _____ °F, TIME: _____ SEC,

END OF BOIL: 4864.5 SEC. END OF HEAD: 4867.1 SEC.

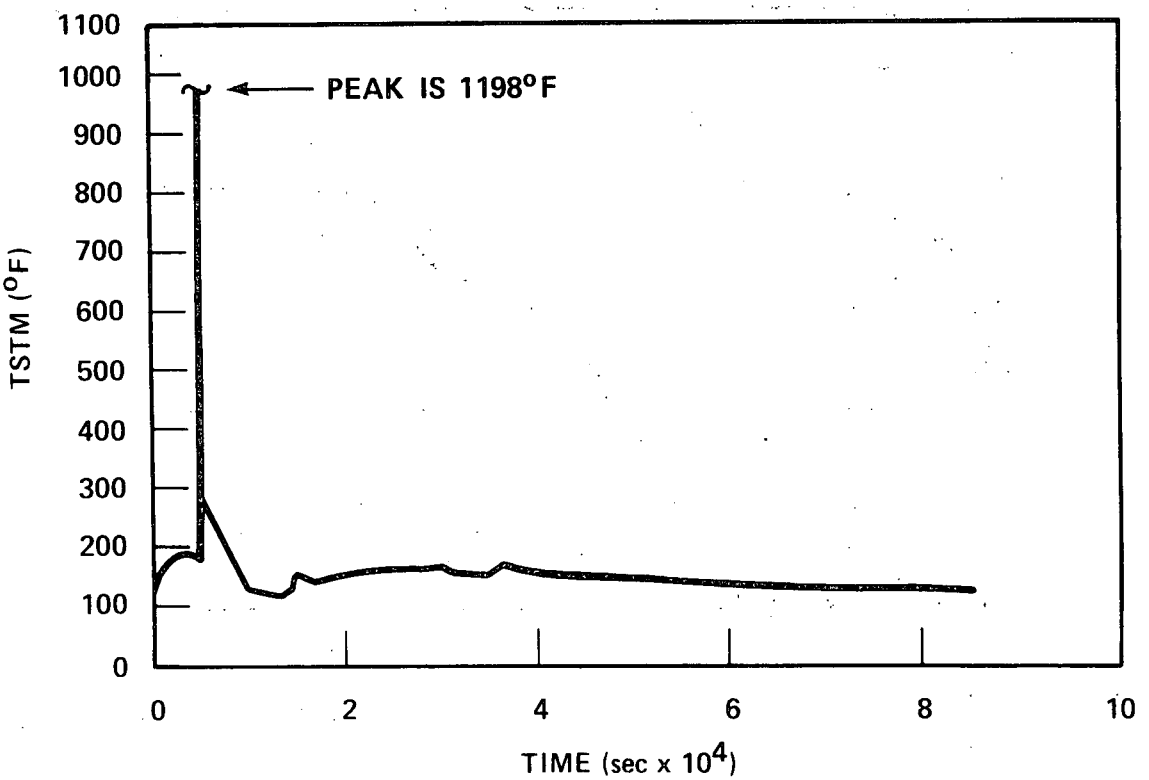
VESSEL FAILURE: 4867.1 SEC. END OF HOTDROP: 10394 SEC.

END OF INTER: 86947 SEC.

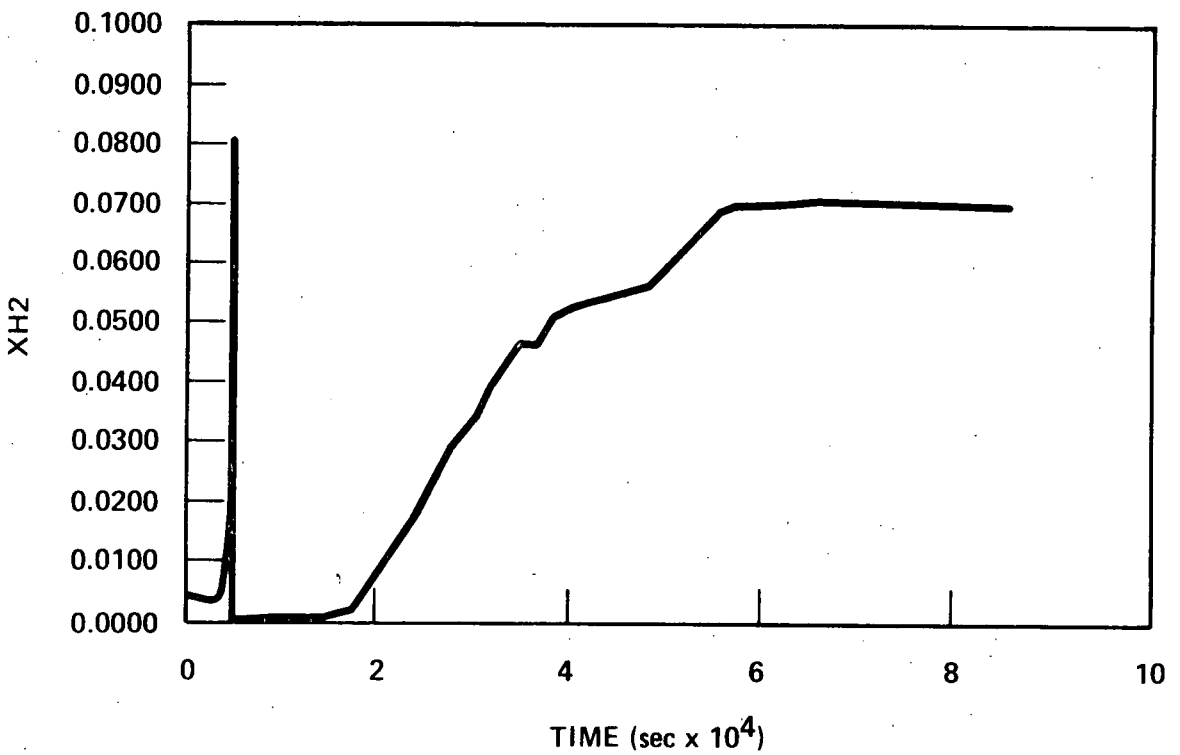
Class III, Case 1B



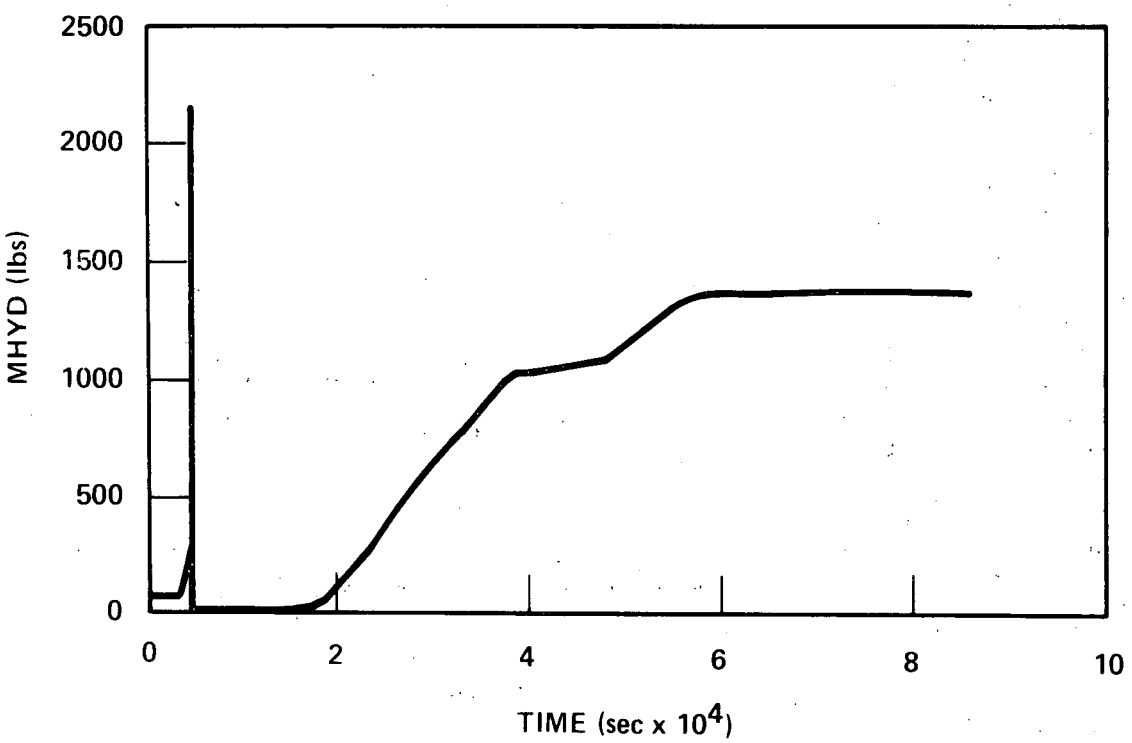
Pressure (in Containment) vs. Time
S2D, B, Burn @ Vessel Failure
Class III, Case 1B



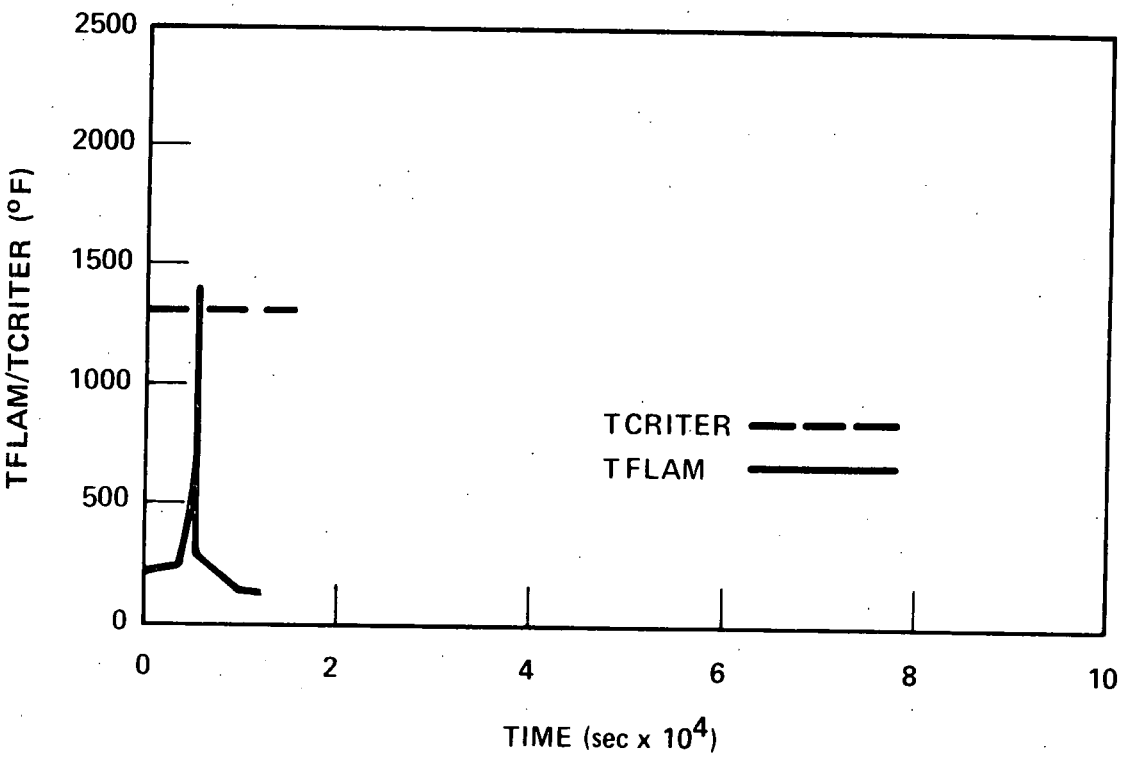
Temperature (in Containment) vs. Time
S2D, B, Burn @ Vessel Failure
Class III, Case 1B



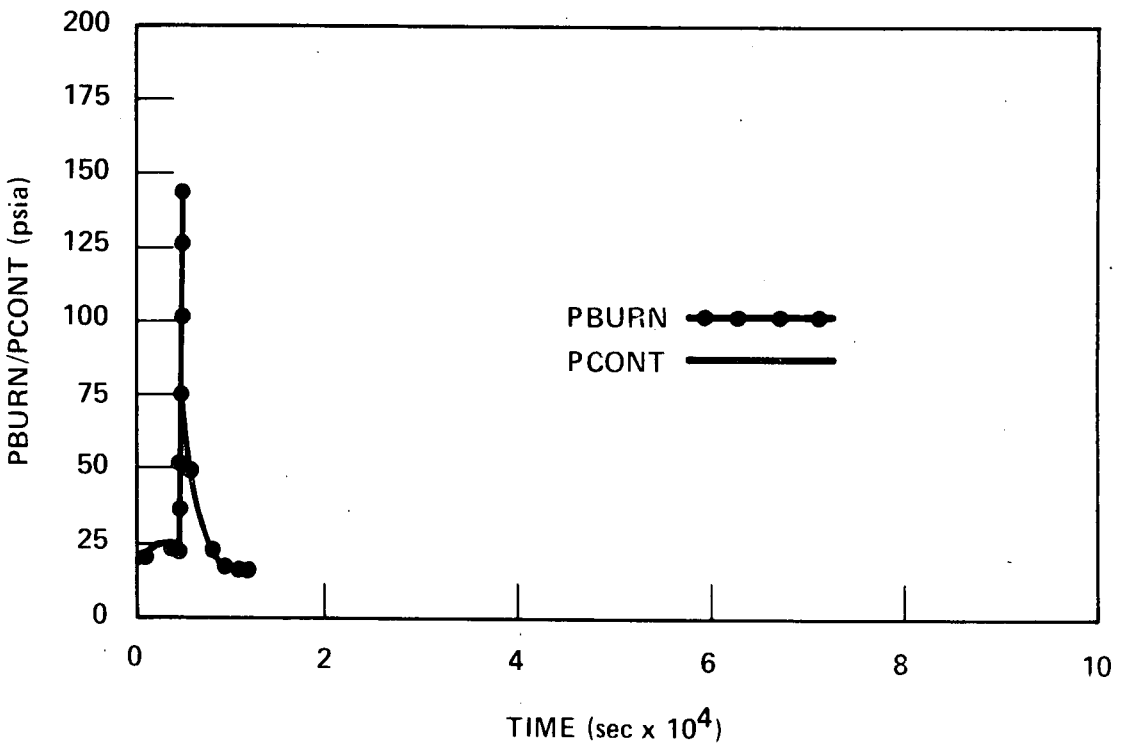
Mole Fraction H_2 (in Containment) vs. Time
S2D, B, Burn @ Vessel Failure
Class III, Case 1B



Mass Hydrogen (in Containment) vs. Time
S2D, B, Burn @ Vessel Failure
Class III, Case 1B



Flame Temperature (in Containment) vs. Time
S2D, B, Burn @ Vessel Failure
Class III, Case 1B



Adiabatic Burn Pressure/Pressure in Containment vs. Time
S2D, B, Burn @ Vessel Failure
Class III, Case 1B

CASE: CLASS III, CASE 1C, S2D, B, BURN @ T_{MAX}, NON-DISPERSIVE

DISPERSIVE: NO PERCENT CORE: _____ FRACTION IN CAVITY: _____

RUN #: AALAAFW DATE: 11/15/80

BLOWDOWN PEAK: _____ PSIA TIME: _____ SEC.

HYDROGEN BURN?: YES CRITERIA: T_{MAX}

TIME @ BURN: 42097 SEC, PRESSURE: 28 PSIA, TEMPERATURE: 140 °F

PEAKS:

PRESSURE: 147 PSIA, TIME: 42117.3 SEC, WHY?: H_2 BURN

TEMPERATURE: 3104.0 °F, TIME: 42117 SEC, WHY?: H_2 BURN

DISPERSIVE: NO

PRESSURE: _____ PSIA, TIME: _____ SEC,

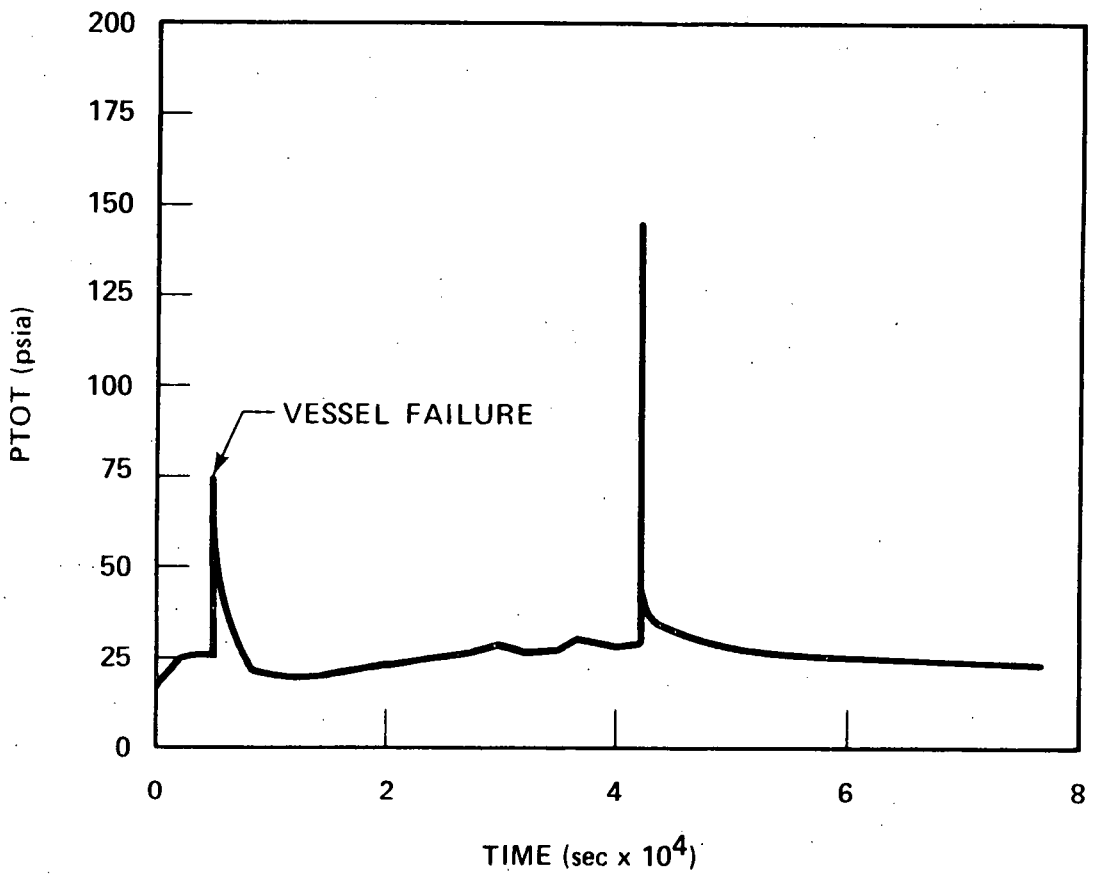
TEMPERATURE: _____ °F, TIME: _____ SEC,

END OF BOIL: 4864.5 SEC. END OF HEAD: 4867.1 SEC.

VESSEL FAILURE: 4867.1 SEC. END OF HOTDROP: 10394 SEC.

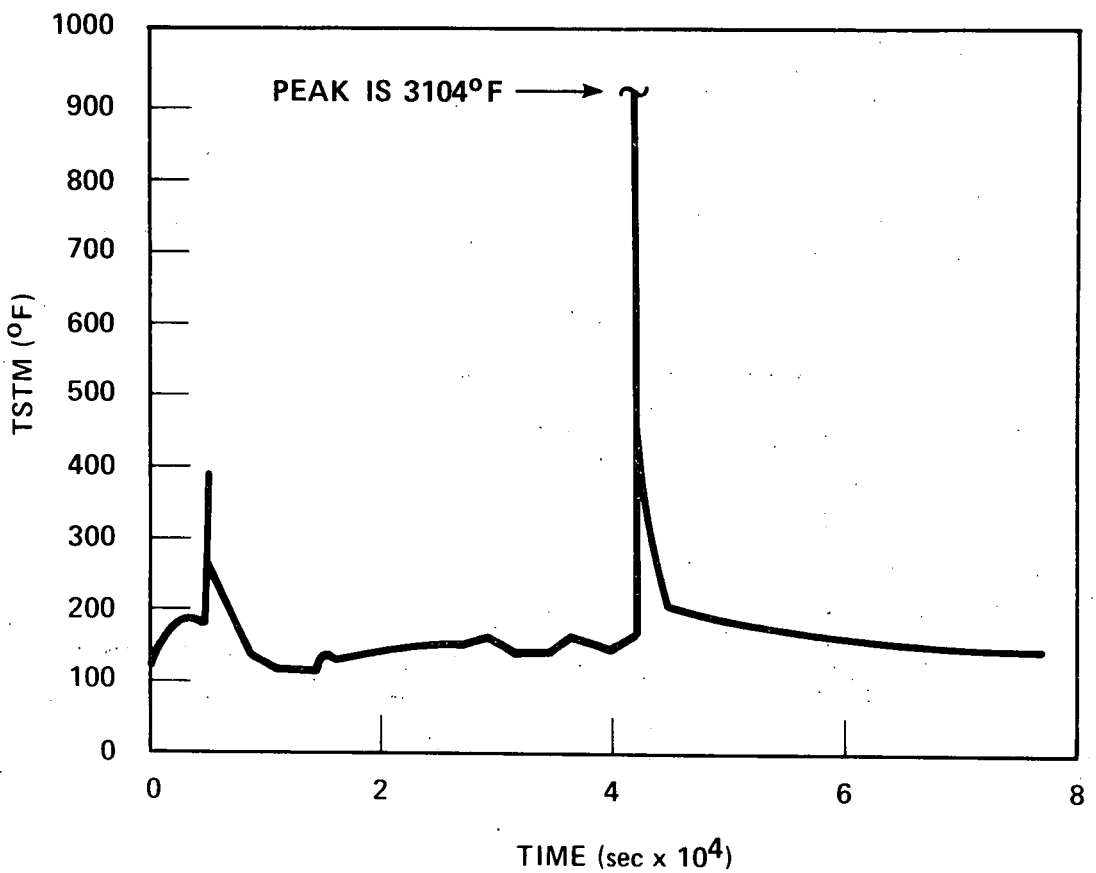
END OF INTER: 86947 SEC.

Class III, Case 1C

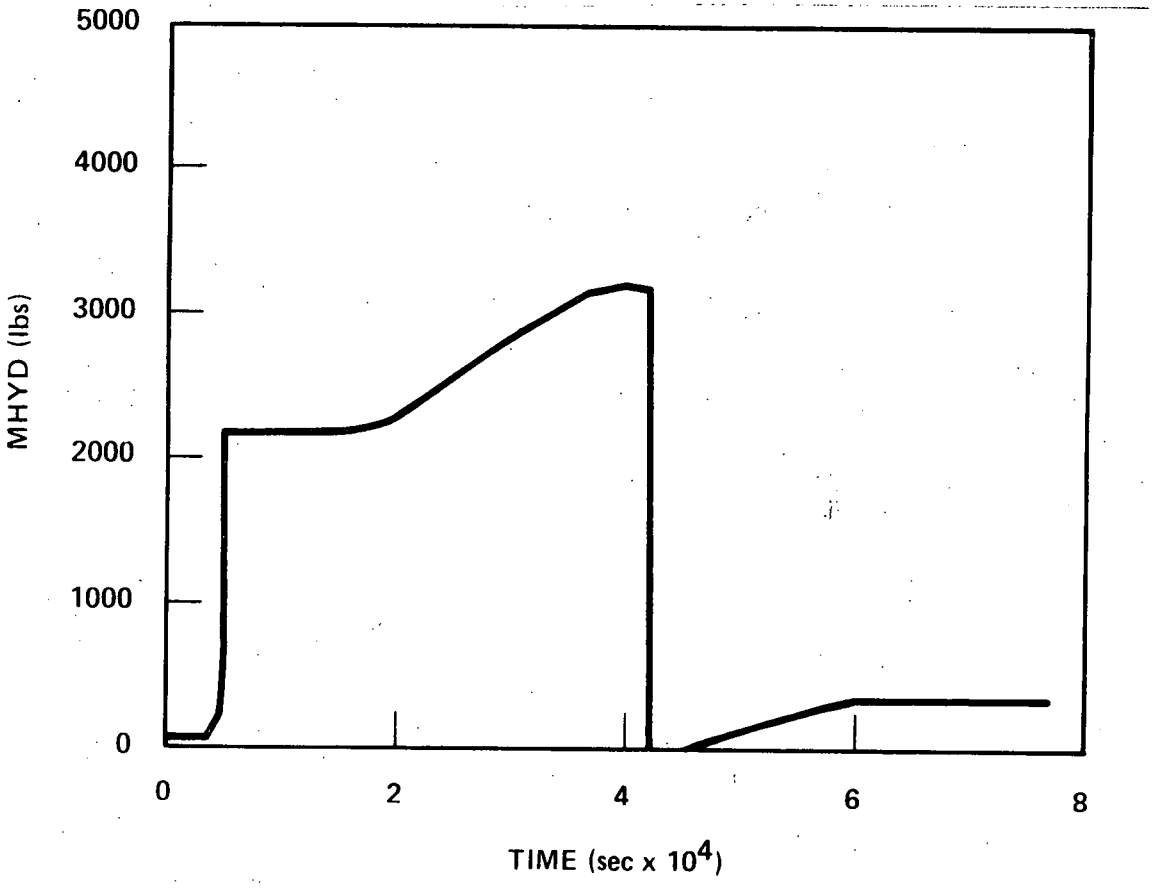


Pressure (in Containment) vs. Time
S2D, B, Burn @ T_{MAX}
Class III, Case 1C

Sheet 2 of 7

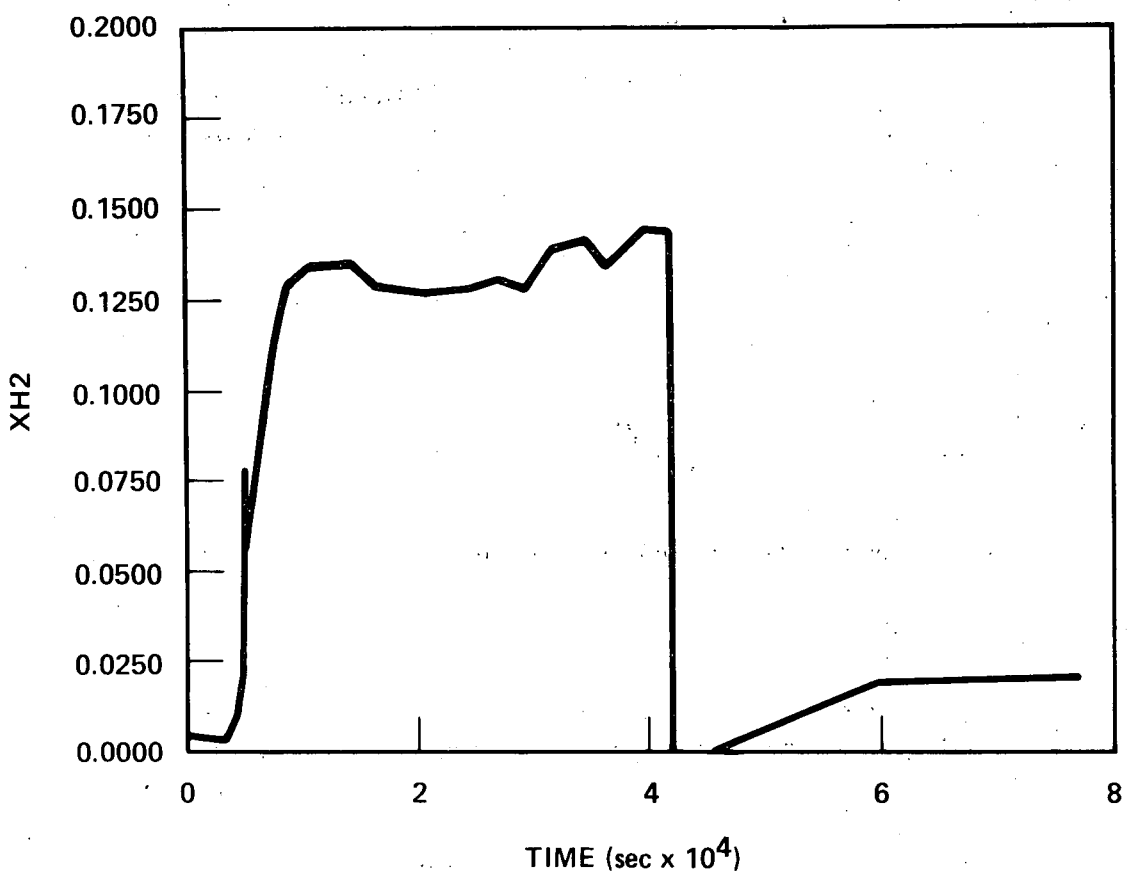


Temperature (in Containment) vs. Time
S2D, B, Burn @ T_{MAX}
Class III, Case 1C

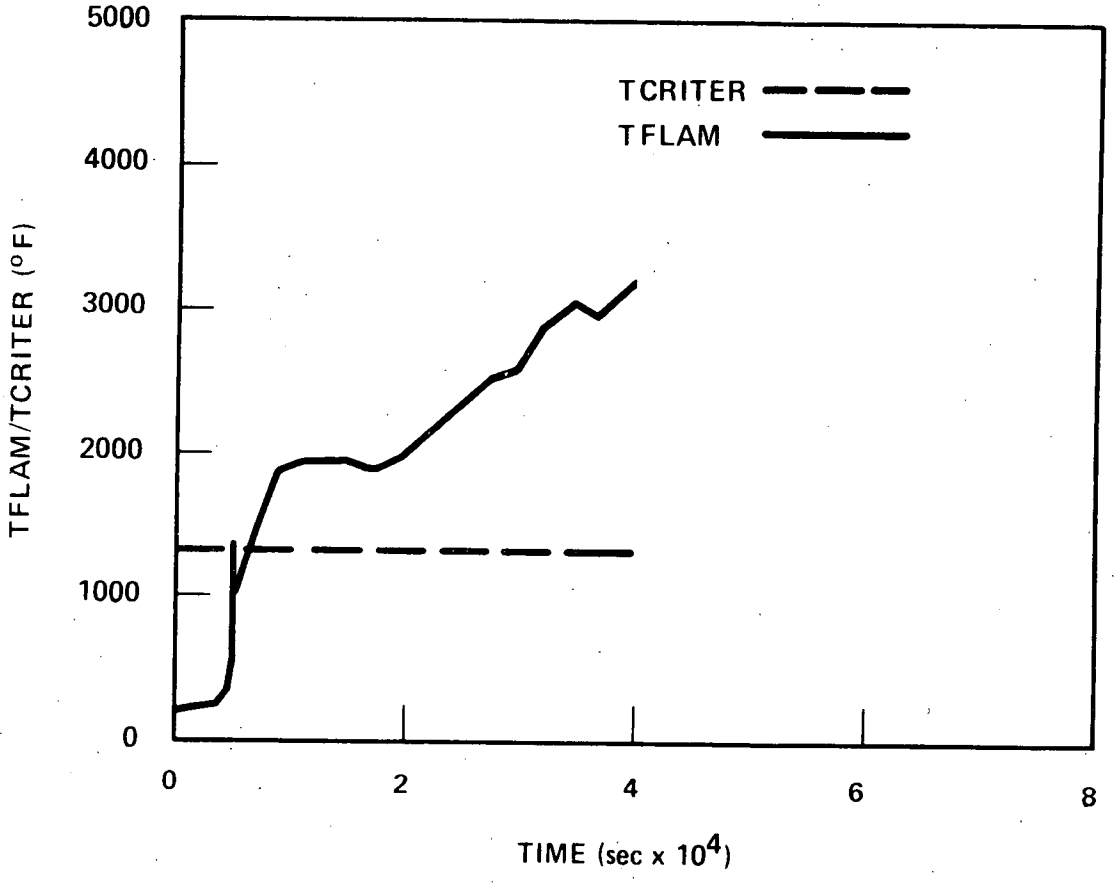


Mass Hydrogen (in Containment) vs. Time
S2D, B, Burn @ T_{MAX}
Class III, Case 1C

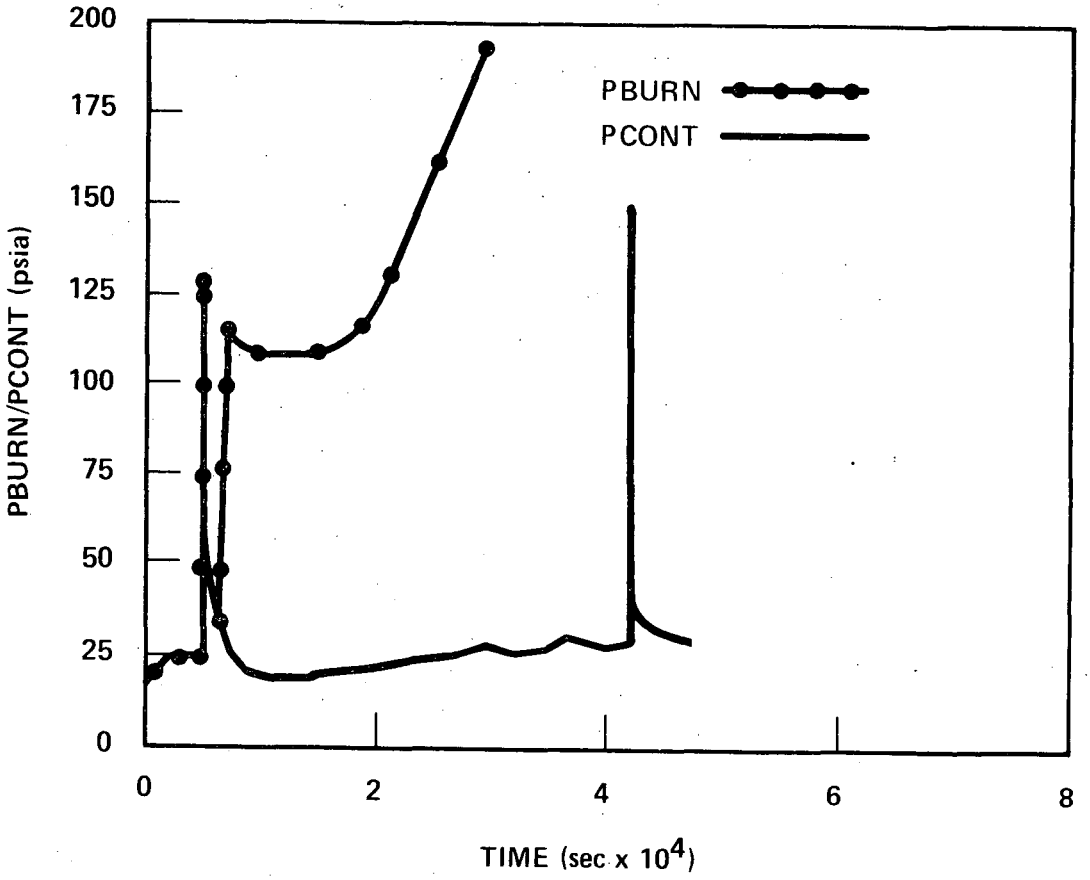
Sheet 4 of 7



Mole Fraction H_2 (in Containment) vs. Time
S2D, B, Burn @ T_{MAX}
Class III, Case 1C



Flame Temperature (in Containment) vs. Time
S2D, B, Burn @ T_{MAX}
Class III, Case 1C



Adiabatic Burn Pressure/Pressure in Containment vs. Time
S2D, B, Burn @ T_{MAX}
Class III, Case 1C

CASE: CLASS III, CASE 2A, S2D, W, NO BURN, NON-DISPERSIVE

DISPERSIVE: NO PERCENT CORE: _____ FRACTION IN CAVITY: _____

RUN #: AALAACB DATE: 11/15/80

BLOWDOWN PEAK: _____ PSIA TIME: _____ SEC.

HYDROGEN BURN?: NO CRITERIA: _____

TIME @ BURN: _____ SEC, PRESSURE: _____ PSIA, TEMPERATURE: _____ °F

PEAKS:

PRESSURE: 41 PSIA, TIME: 4868.3 SEC, WHY?: VESSEL FAILURE

TEMPERATURE: 291 °F, TIME: 4868 SEC, WHY?: VESSEL FAILURE

DISPERSIVE: NO

PRESSURE: _____ PSIA, TIME: _____ SEC,

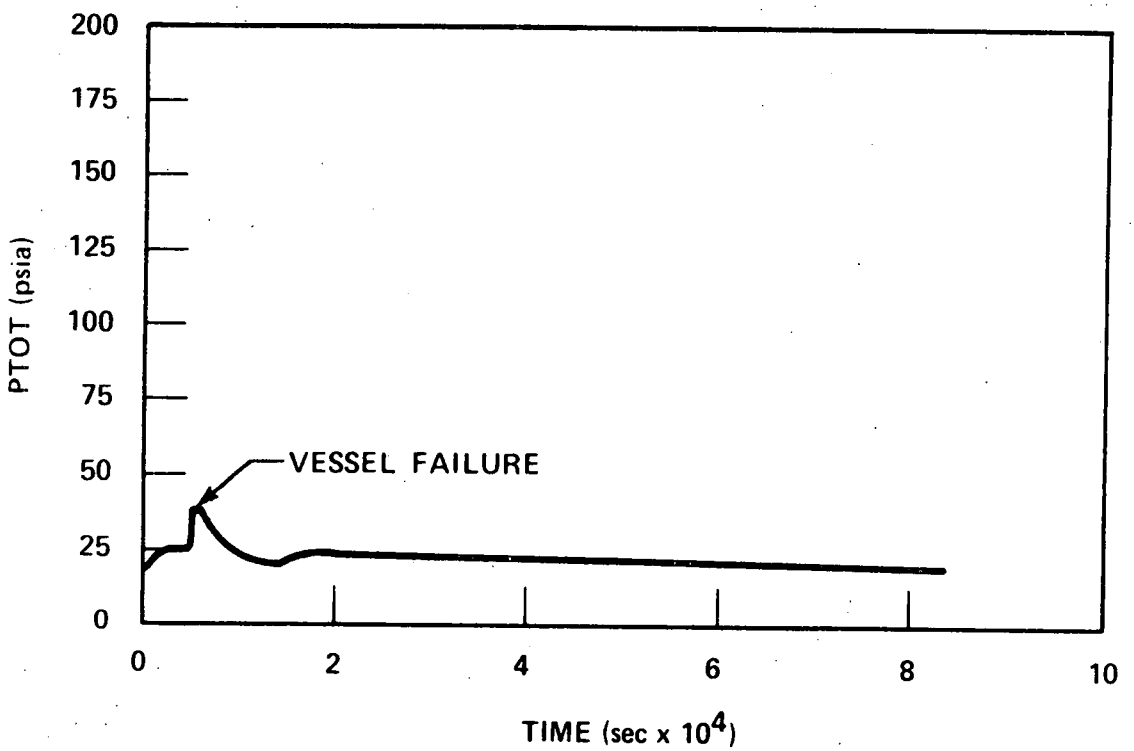
TEMPERATURE: _____ °F, TIME: _____ SEC,

END OF BOIL: 4865.4 SEC. END OF HEAD: 4868.3 SEC.

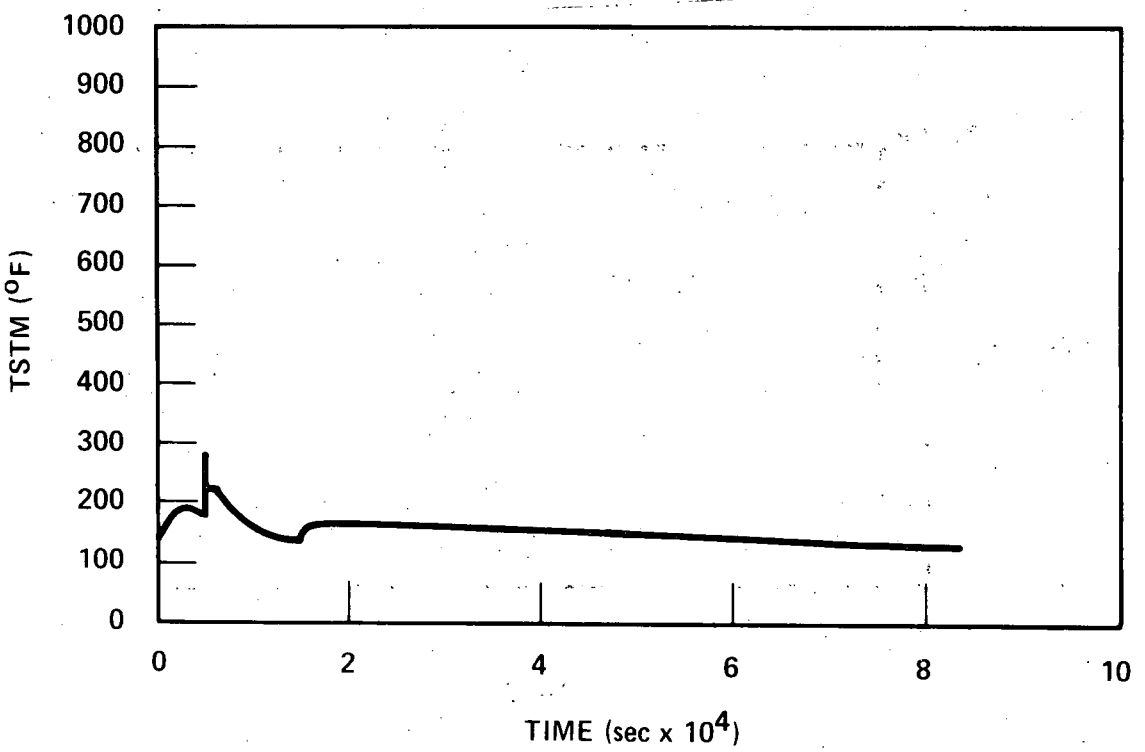
VESSEL FAILURE: 4868.3 SEC. END OF HOTDROP: _____ SEC.

END OF INTER: 86319 SEC.

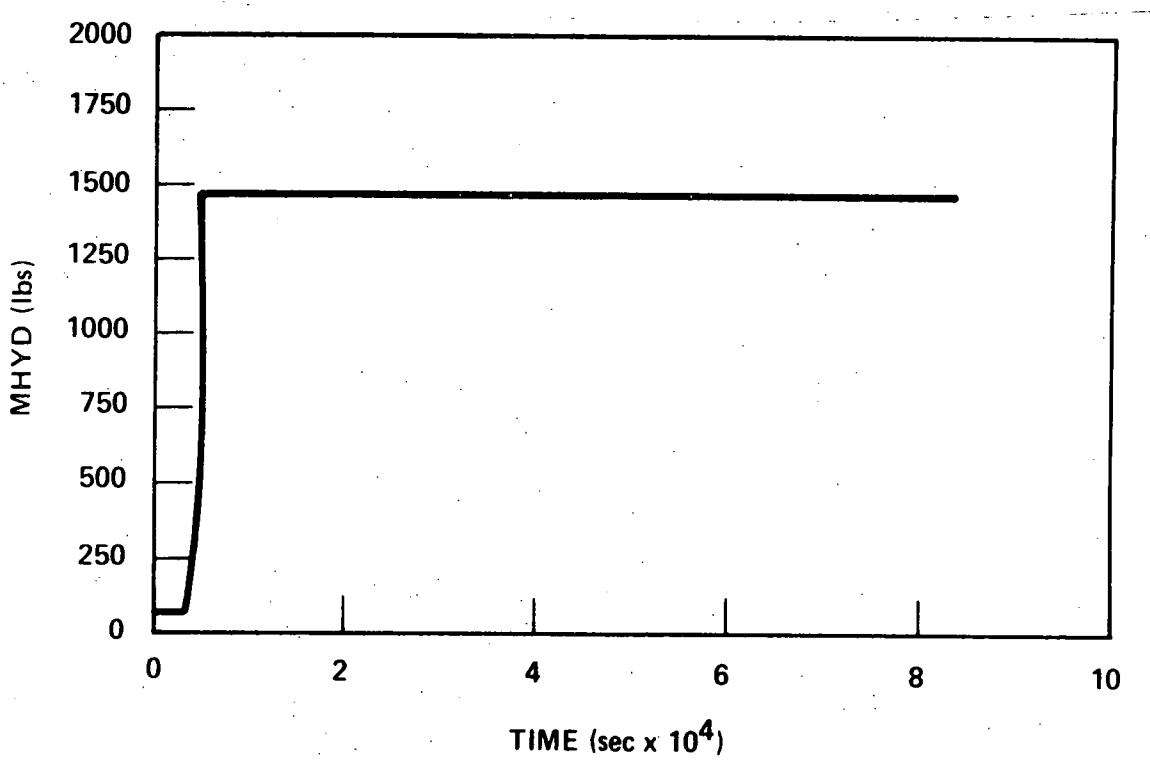
Class III, Case 2A



Pressure (in Containment) vs. Time
S2D, W, No Burn
Class III, Case 2A

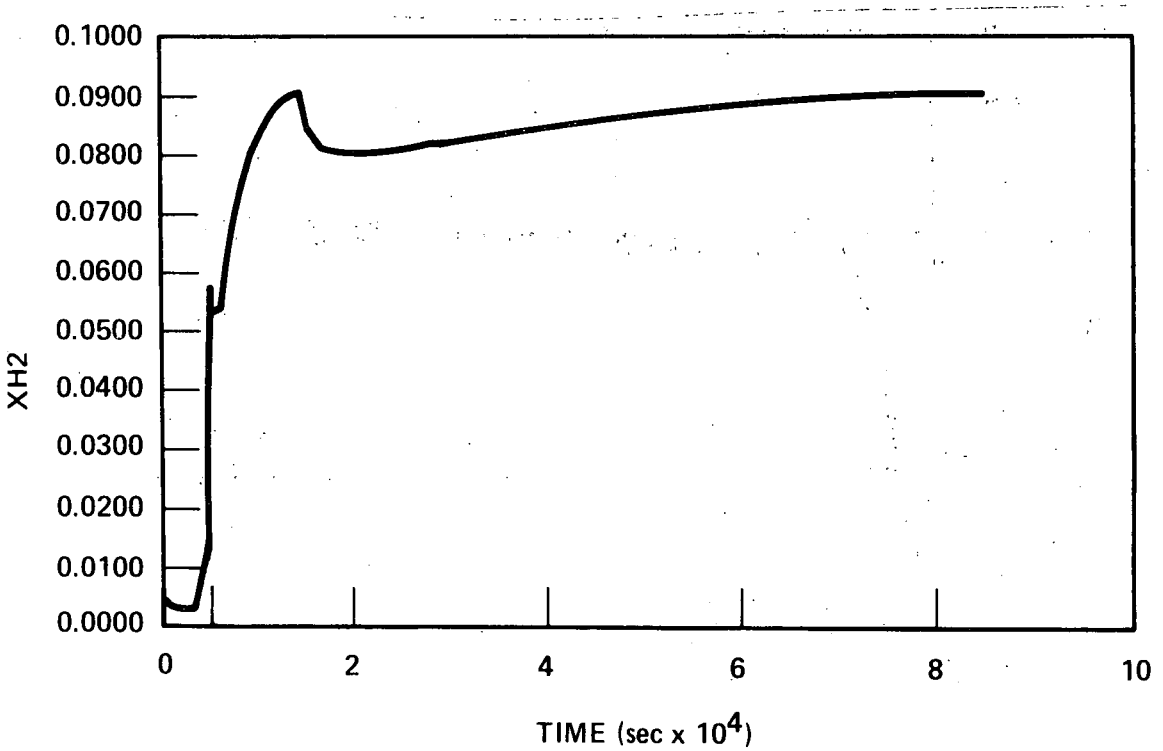


Temperature (in Containment) vs. Time
S2D, W, No Burn
Class III, Case 2A

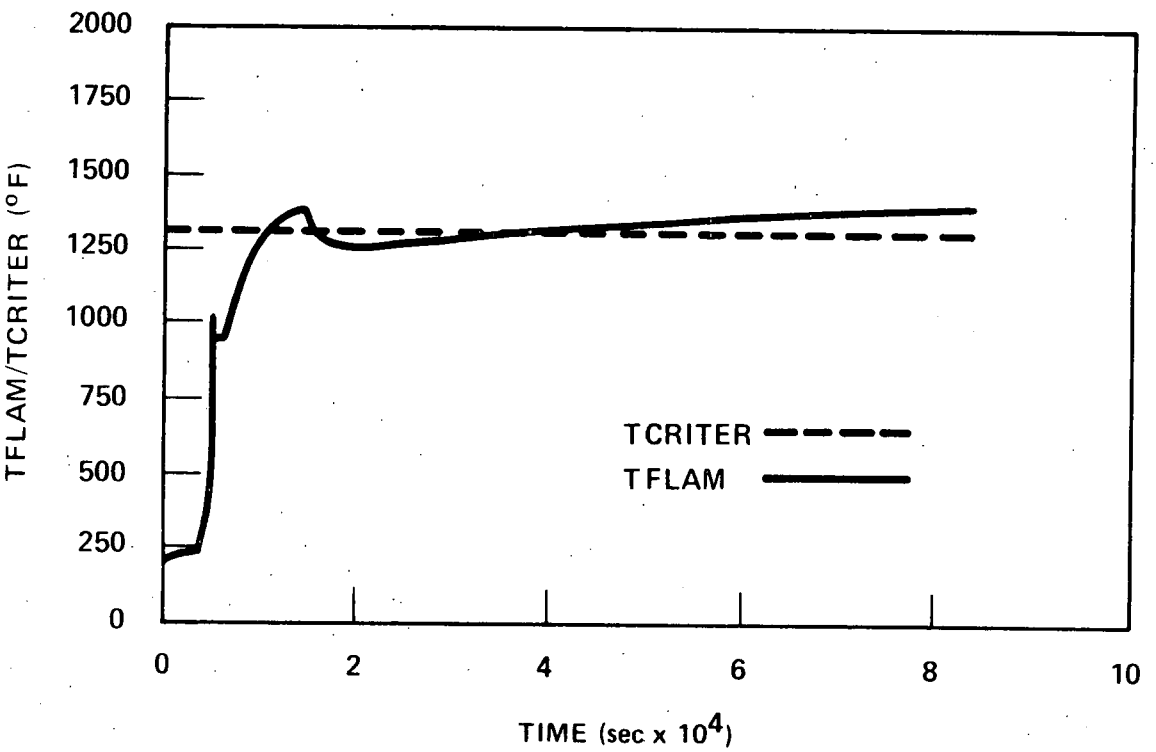


Mass Hydrogen (in Containment) vs. Time
S2D, W, No Burn
Class III, Case 2A

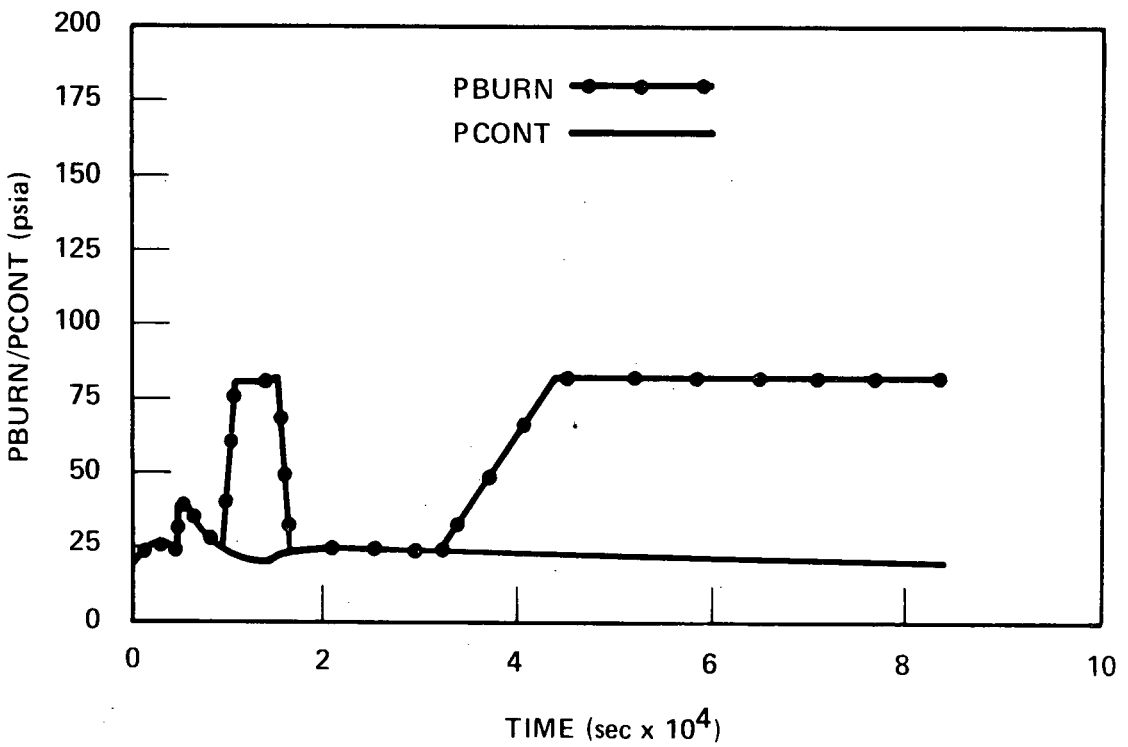
Sheet 4 of 7



Mole Fraction H_2 (in Containment) vs. Time
S2D, W, No Burn
Class III, Case 2A



Flame Temperature (in Containment) vs. Time
S2D, W, No Burn
Class III, Case 2A



Adiabatic Burn Pressure/Pressure in Containment vs. Time
S2D, W, No Burn
Class III, Case 2A

CASE: CLASS III, CASE 3a, S2D, TIME PHASED, 75% DISPERSIVE, NO BURN, 33% Zr REACTED

DISPERSIVE: YES PERCENT CORE DISPERSED: 75 FRACTION IN CAVITY: 0

RUN #: AB3YAXG DATE: 3/8/81 PERCENT Zr REACTED: 33

BLOWDOWN PEAK: N/A PSIA TIME: _____ SEC.

HYDROGEN BURN?: NO CRITERIA: _____

TIME @ BURN: _____ SEC, PRESSURE: _____ PSIA, TEMPERATURE: _____ °F

PEAKS:

PRESSURE: 59 PSIA, TIME: 4963.6 SEC, WHY?: VESSEL FAILURE

TEMPERATURE: 285 °F, TIME: 4919.9 SEC, WHY?: VESSEL FAILURE

DISPERSIVE: YES

PRESSURE: 59 PSIA, TIME: 4963.6 SEC,

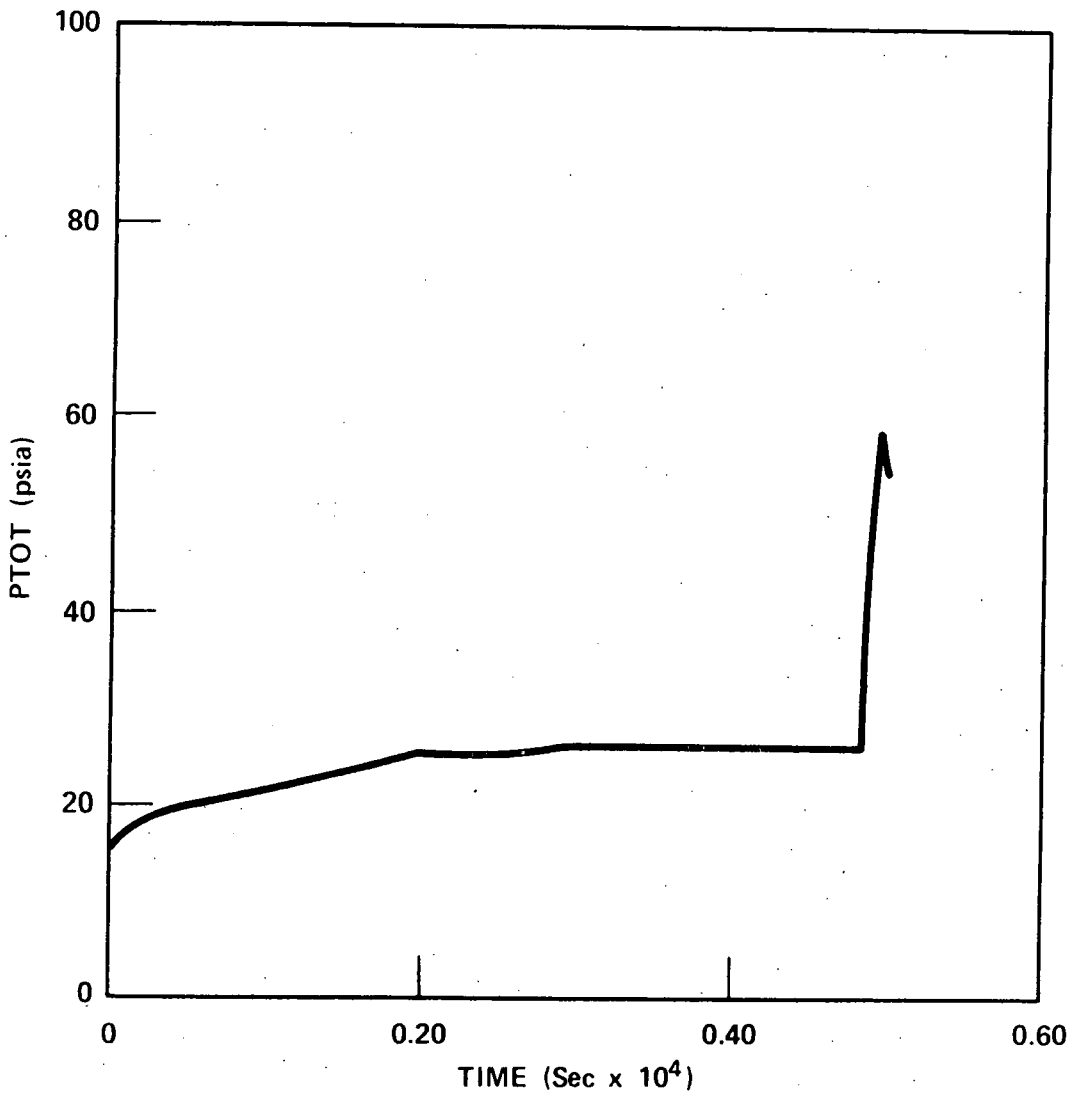
TEMPERATURE: 289 °F, TIME: 4963.6 SEC,

END OF BOIL: 4833 SEC. END OF HEAD: _____ SEC.

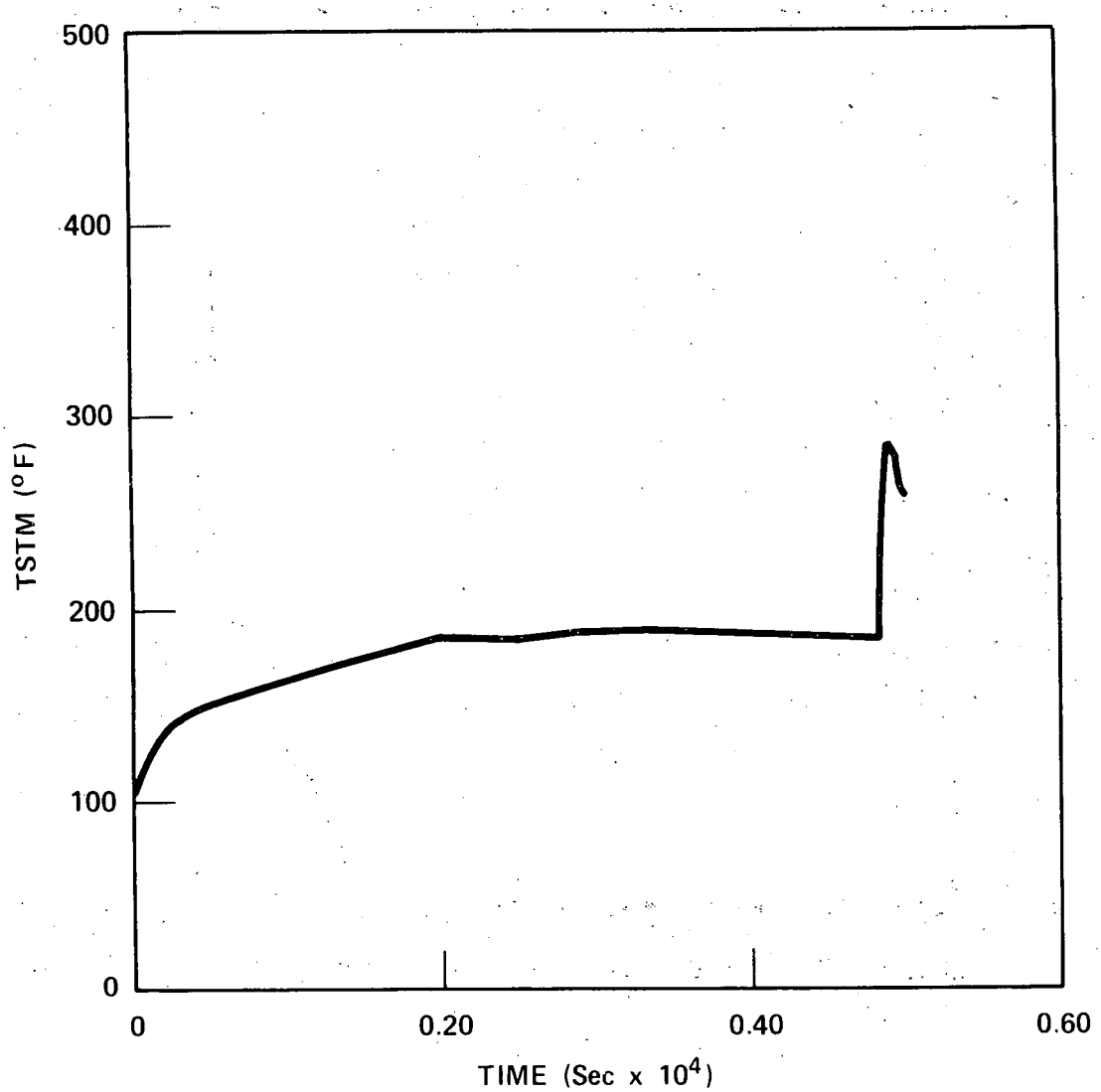
VESSEL FAILURE: 4833 SEC. END OF HOTDROP: _____ SEC.

END OF INTER: _____ SEC.

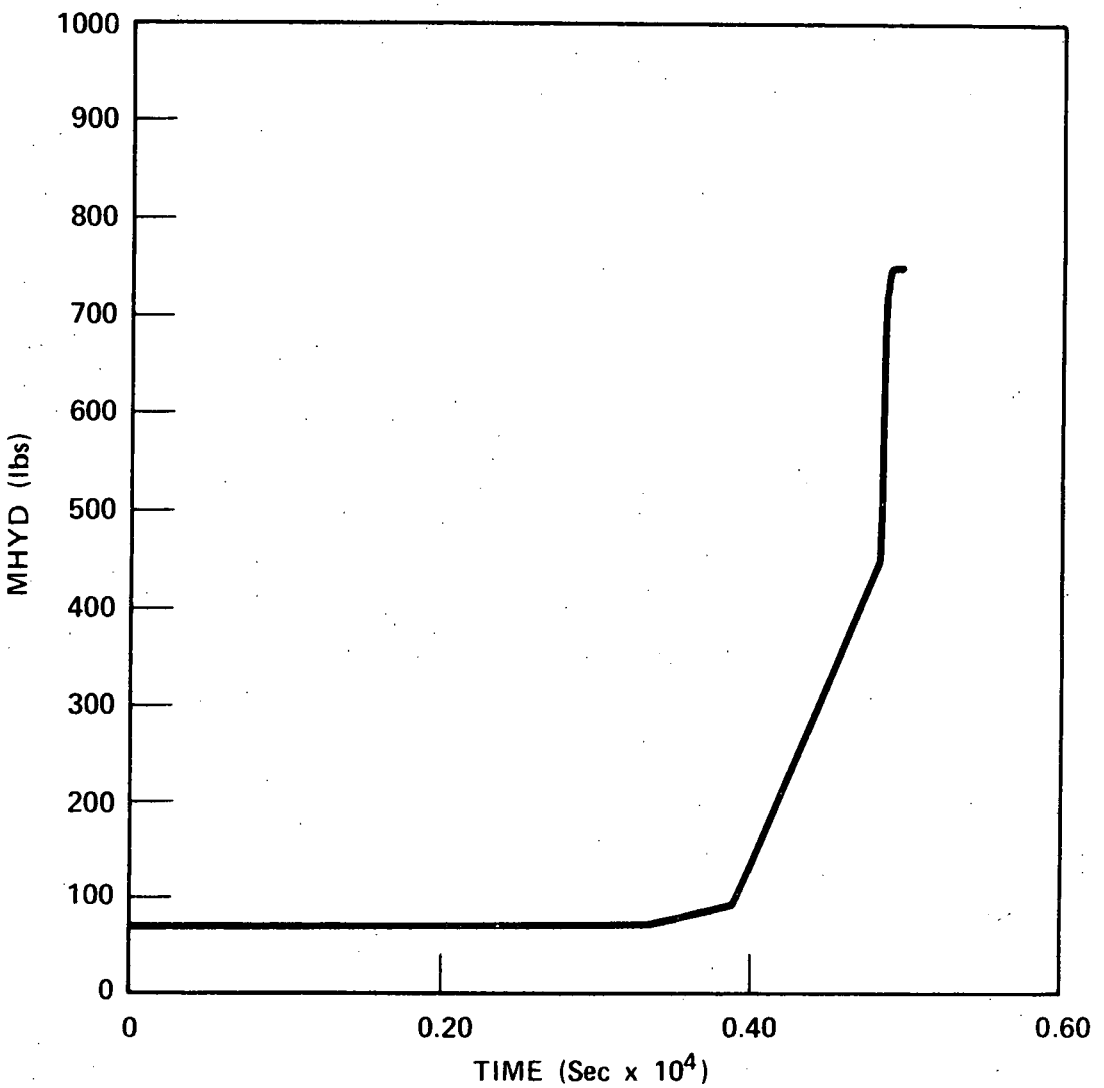
Class III, Case 3a



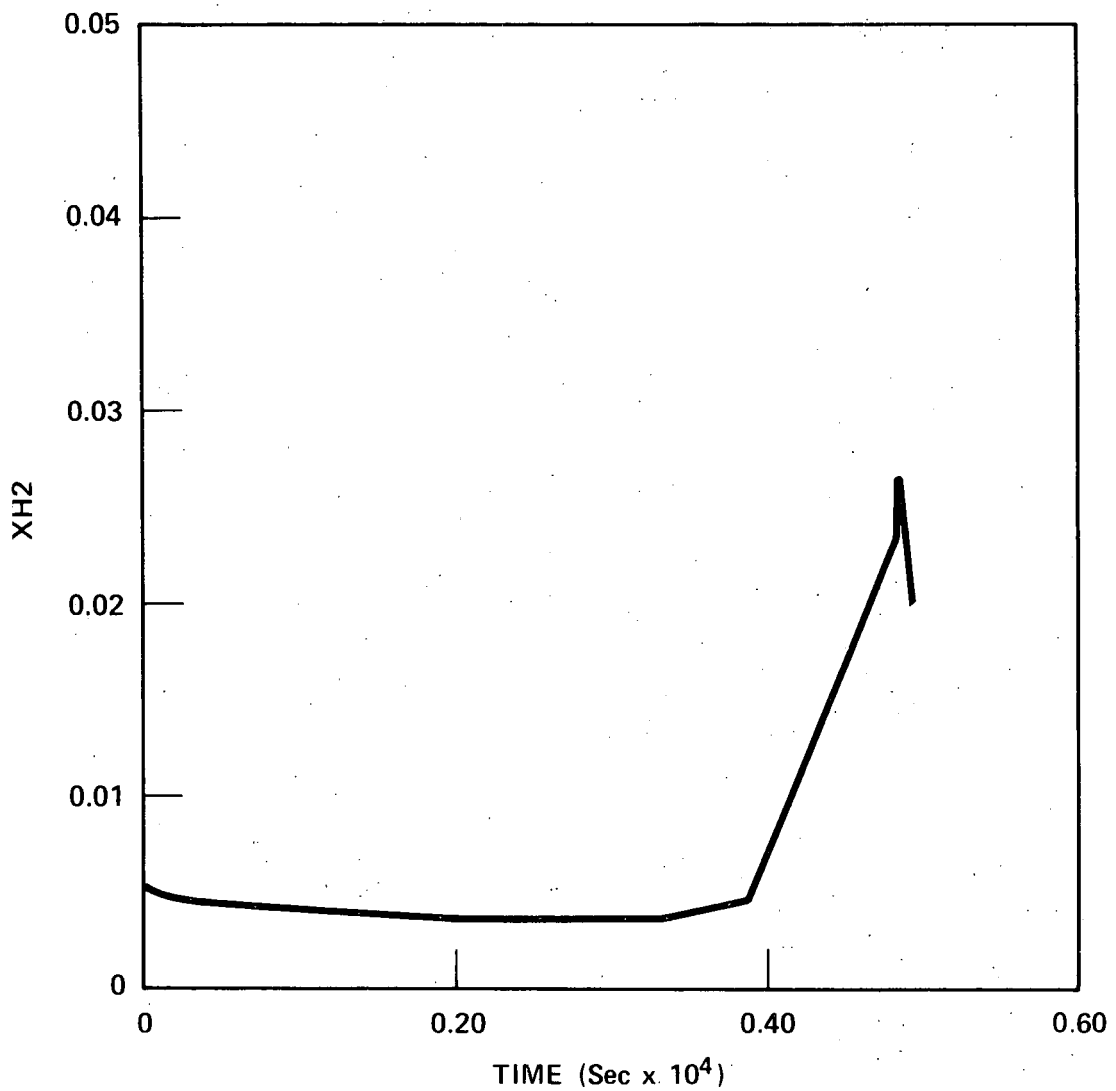
Pressure (in Containment) vs. Time
S2D, Time Phased, 75% Dispersive, No Burn, 33% Zr Reacted
Class III, Case 3a



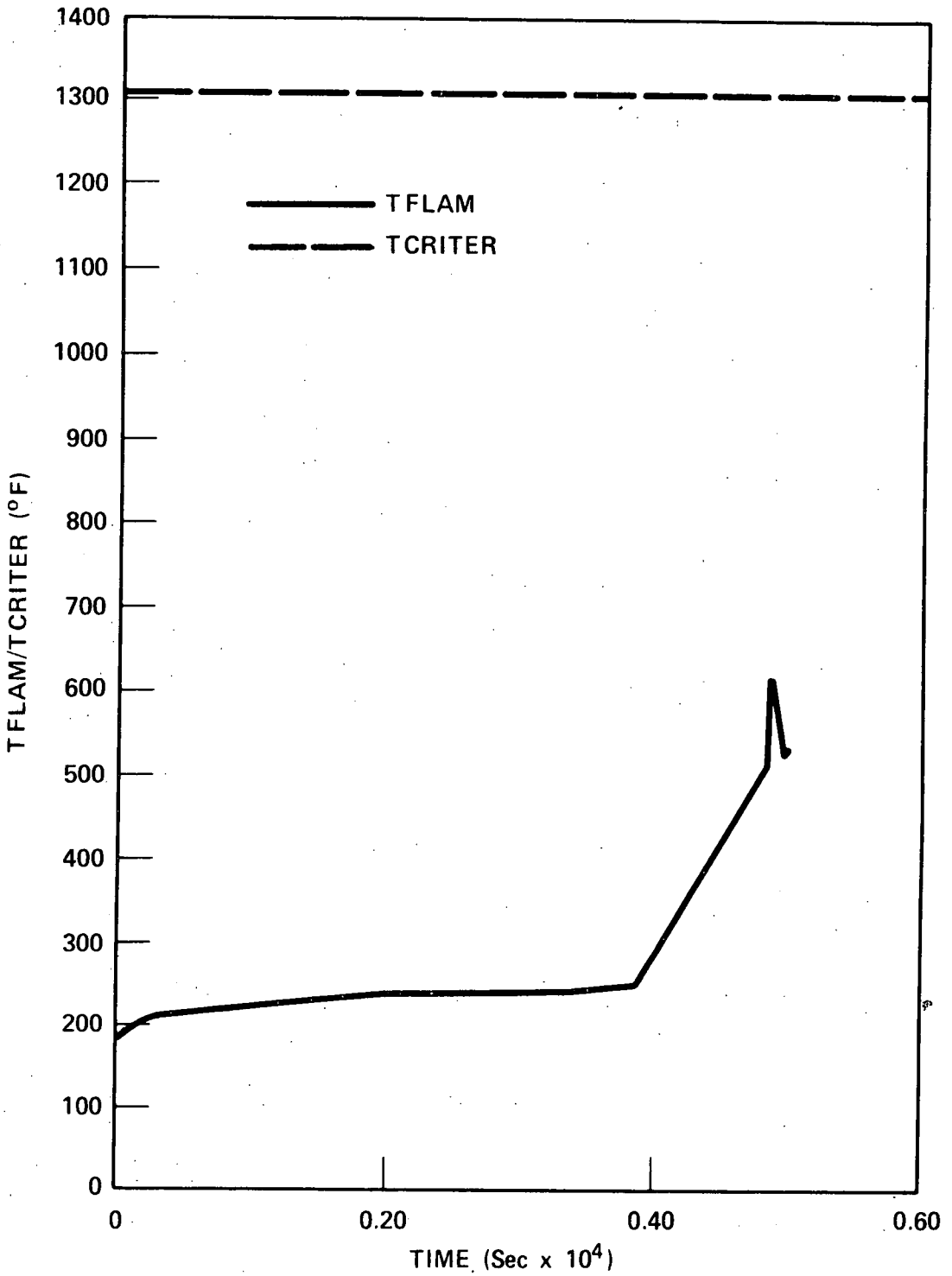
Temperature (in Containment) vs. Time
S2D, Time Phased, 75% Dispersive, No Burn, 33% Zr Reacted
Class III, Case 3a



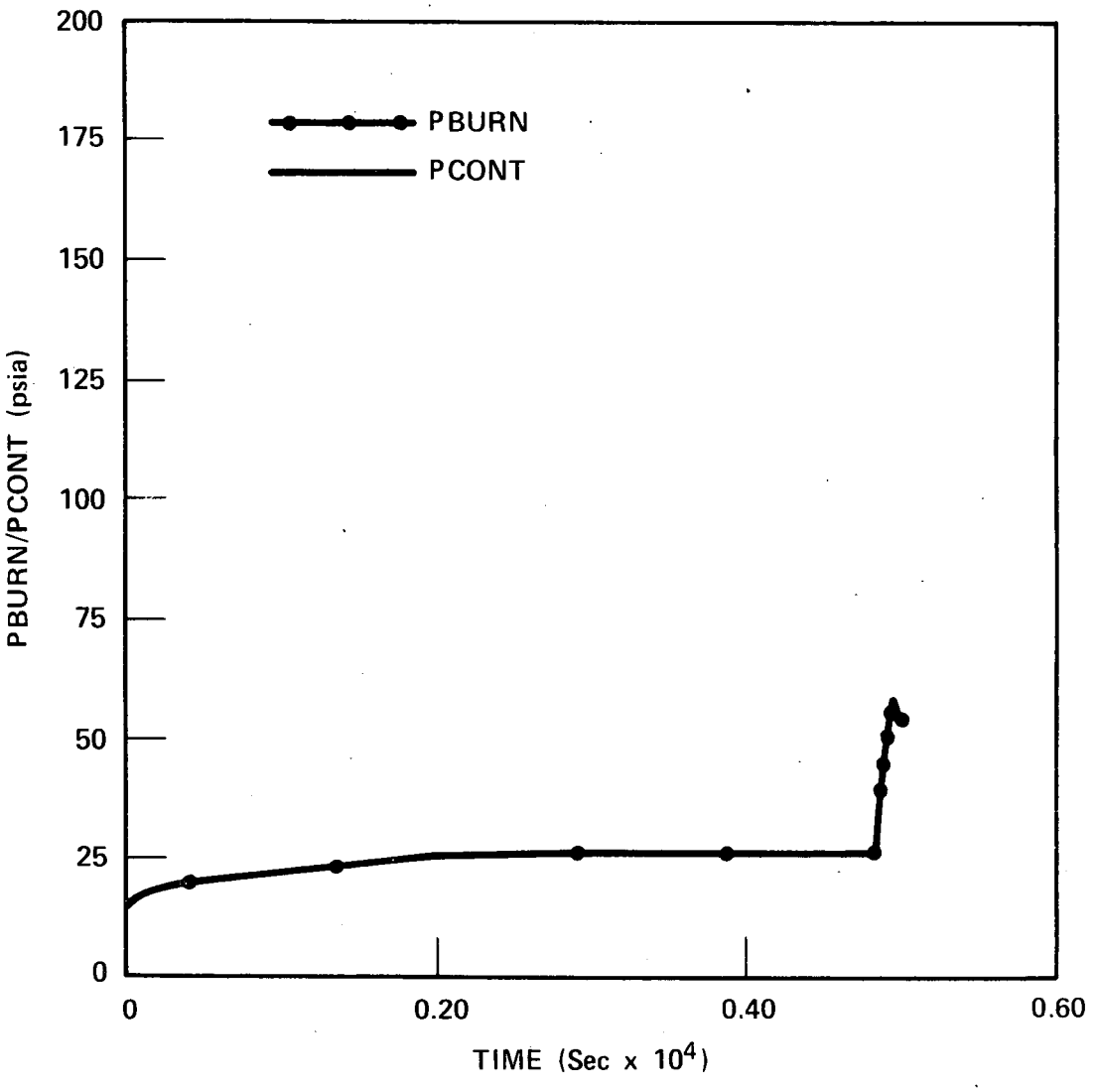
Mass Hydrogen (in Containment) vs. Time
S2D, Time Phased, 75% Dispersive, No Burn, 33% Zr Reacted
Class III, Case 3a



Mole Fraction H_2 (in Containment) vs. Time
S2D, Time Phased, 75% Dispersive, No Burn, 33% Zr Reacted
Class III, Case 3a



Flame Temperature (in Containment) vs. Time
S2D, Time Phased, 75% Dispersive, No Burn, 33% Zr Reacted
Class III, Case 3a



Adiabatic Burn Pressure/Pressure in Containment vs. Time
S2D, Time Phased, 75% Dispersive, No Burn, 33% Zr Reacted
Class III, Case 3a

CASE: CLASS III, CASE 3a', S2D, TIME PHASE, 75% DISPERSED, NO BURN,66% Zr REACTED

DISPERSIVE: YES PERCENT CORE DISPERSED: 75 FRACTION IN CAVITY: 0

RUN #: AB3YAXL DATE: 3/8/81 PERCENT Zr REACTED: 66

BLOWDOWN PEAK: N/A PSIA TIME: _____ SEC.

HYDROGEN BURN?: NO CRITERIA: _____

TIME @ BURN: _____ SEC, PRESSURE: _____ PSIA, TEMPERATURE: _____ °F

PEAKS:

PRESSURE: 65 PSIA, TIME: 4998.5 SEC, WHY?: VESSEL FAILURE

TEMPERATURE: 288 °F, TIME: 4917.6 SEC, WHY?: VESSEL FAILURE

DISPERSIVE: YES

PRESSURE: 65 PSIA, TIME: 4998.5 SEC, WHY?: _____

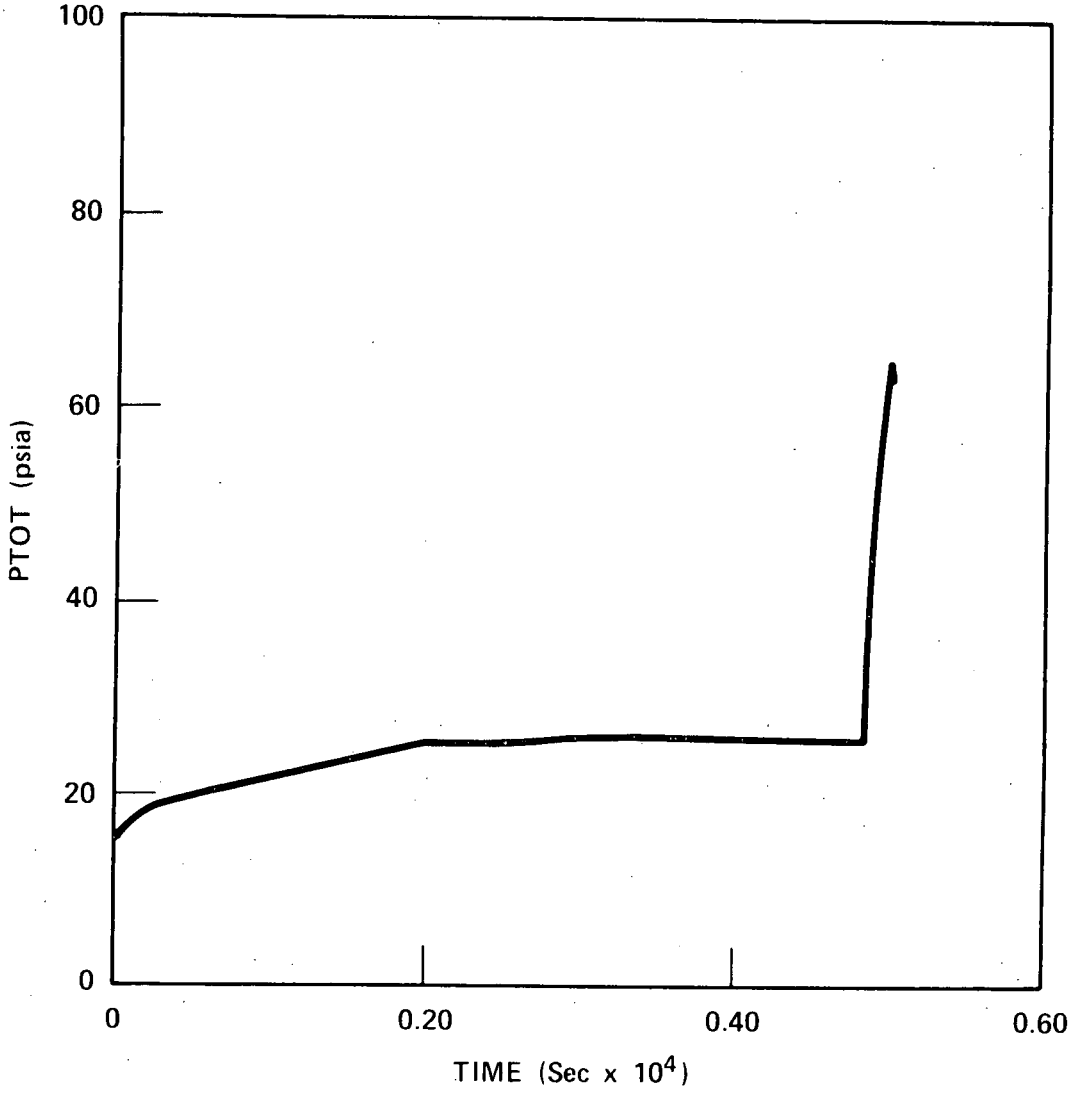
TEMPERATURE: 275 °F, TIME: 4998.5 SEC, WHY?: _____

END OF BOIL: 4833 SEC. END OF HEAD: _____ SEC.

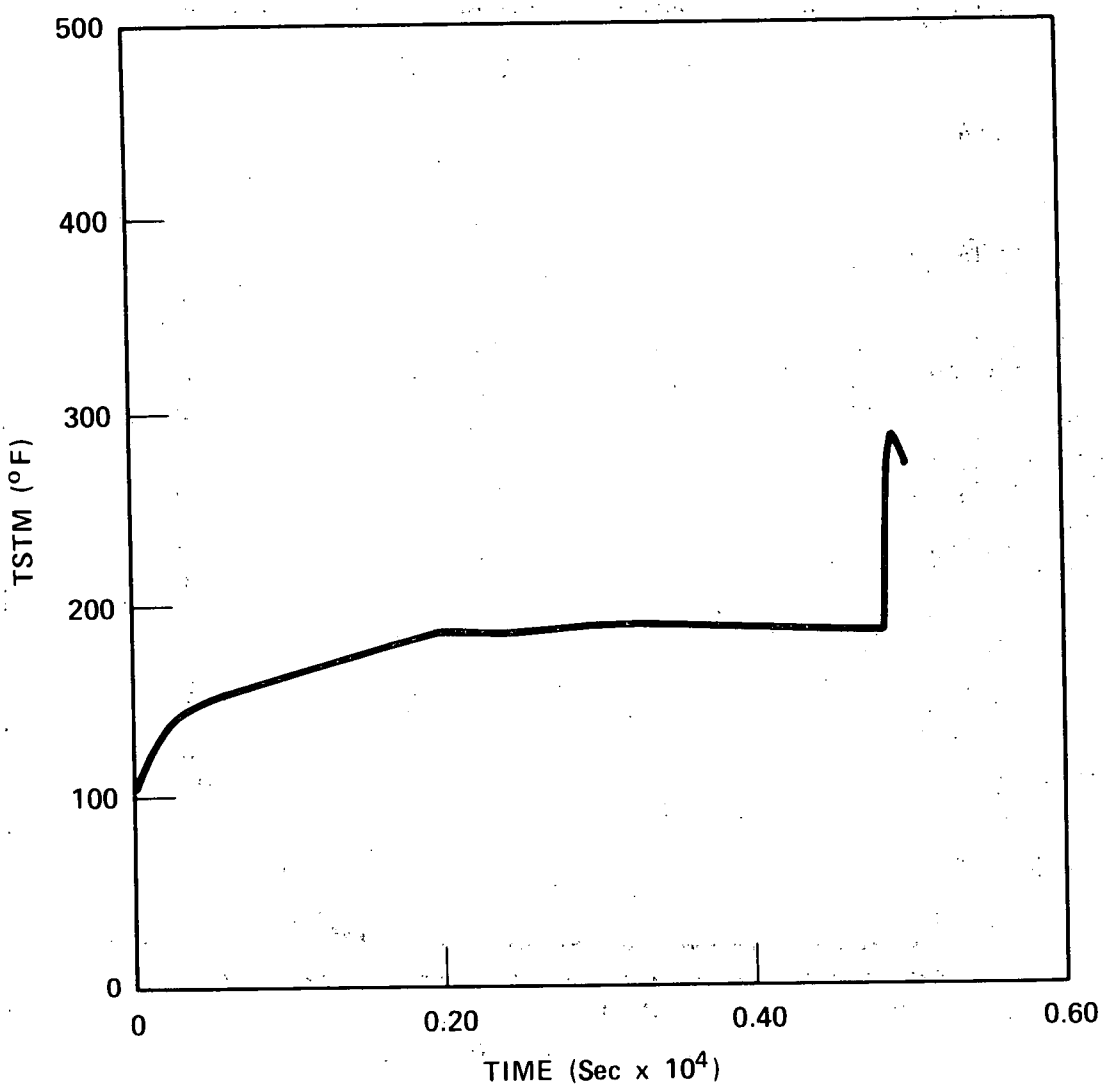
VESSEL FAILURE: 4833 SEC. END OF HOTDROP: _____ SEC.

END OF INTER: _____ SEC.

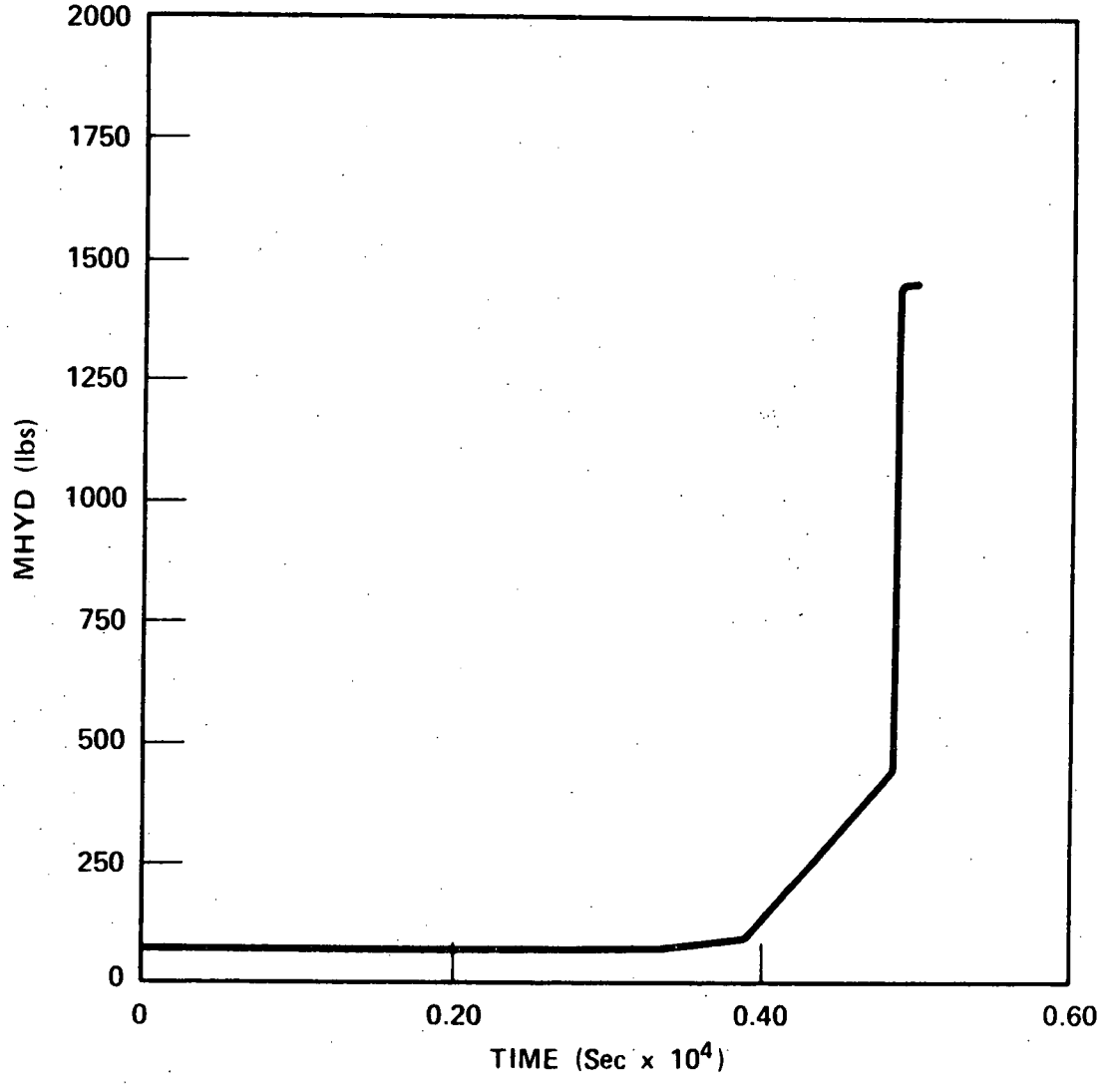
Class III, Case 3a'



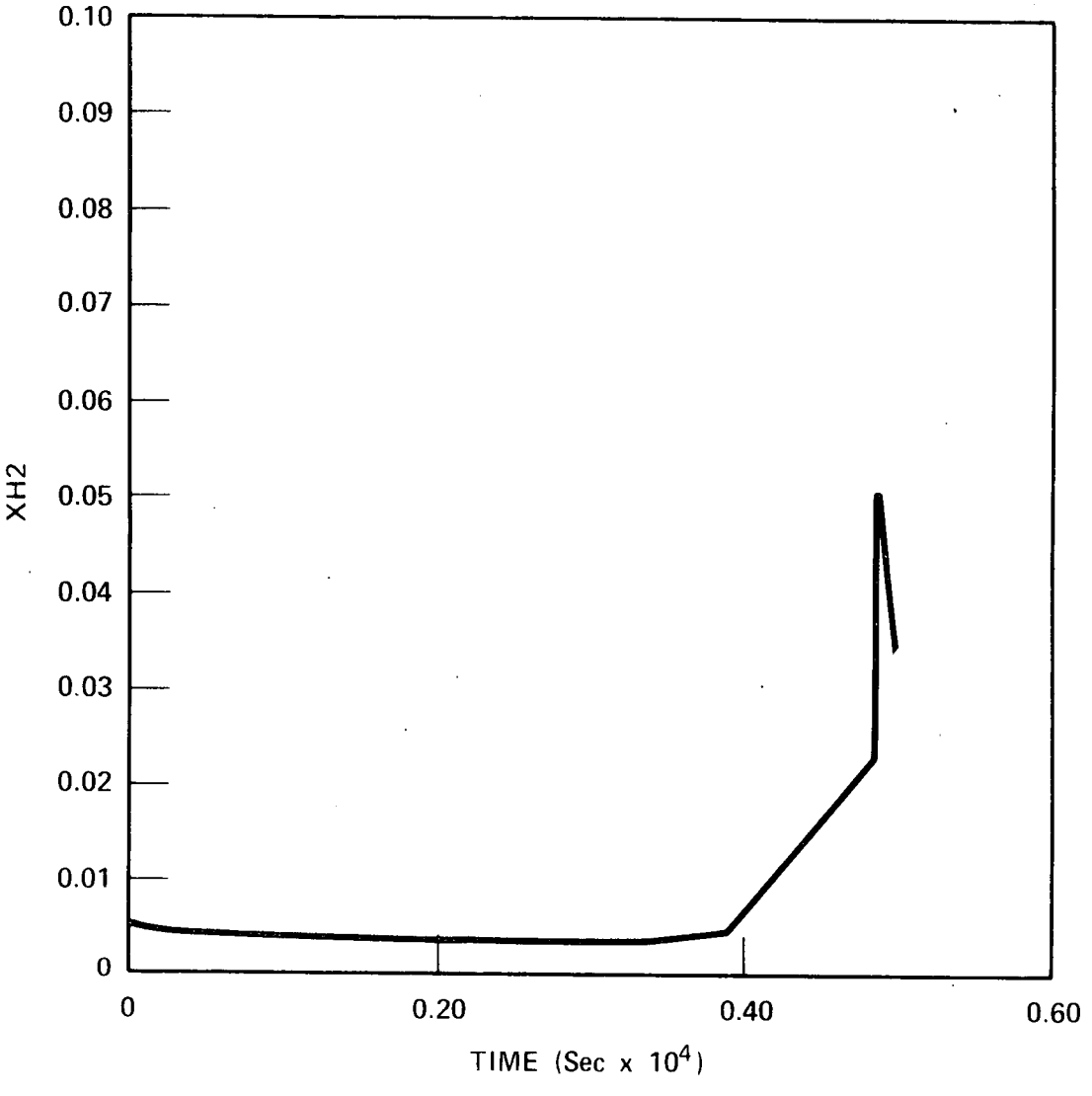
Pressure (in Containment) vs. Time
S2D, Time Phased, 75% Dispersive, No Burn, 66% Zr Reacted
Class III, Case 3a'



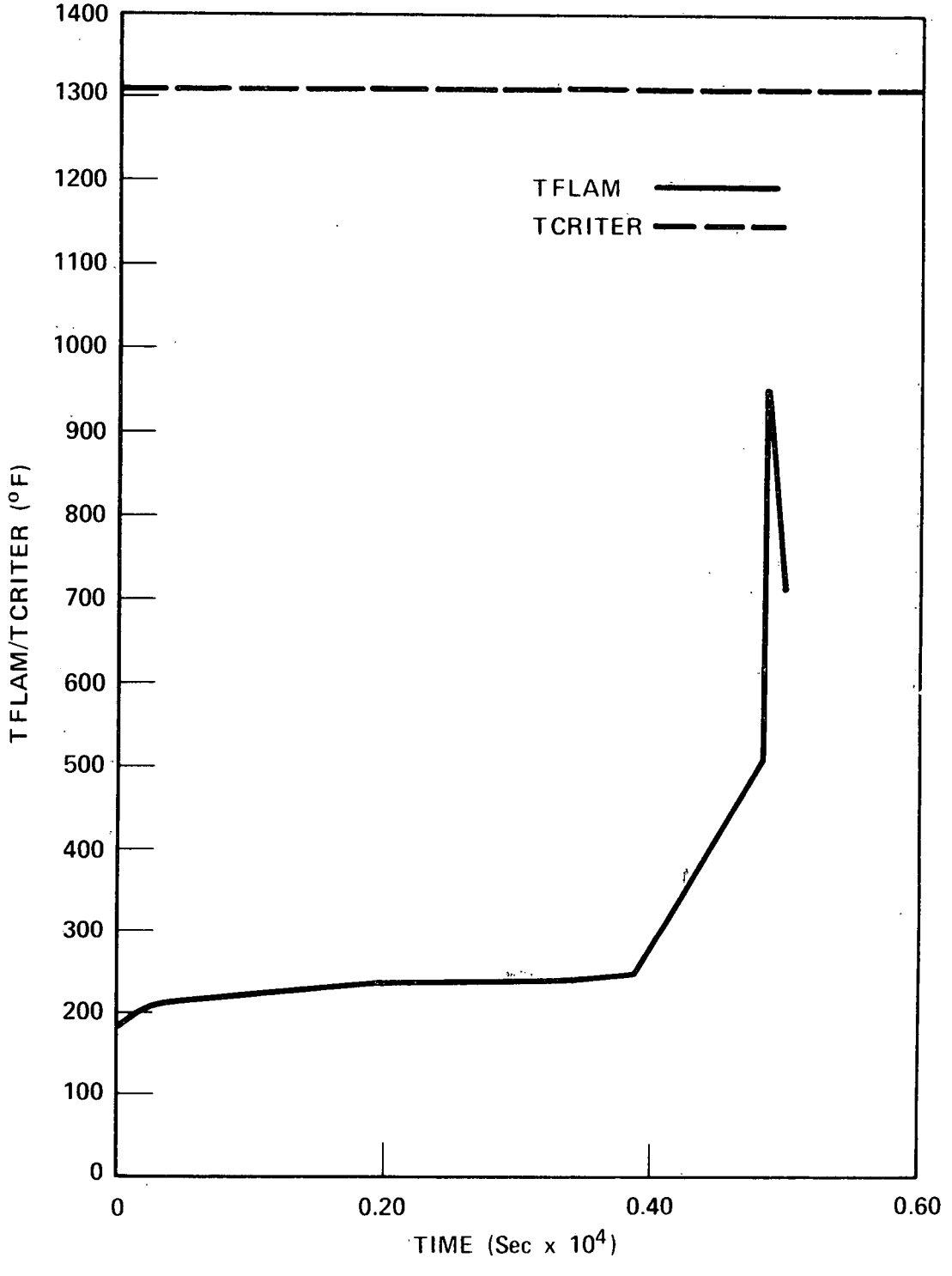
Temperature (in Containment) vs. Time
S2D, Time Phased, 75% Dispersive, No Burn, 66% Zr Reacted
Class III, Case 3a'



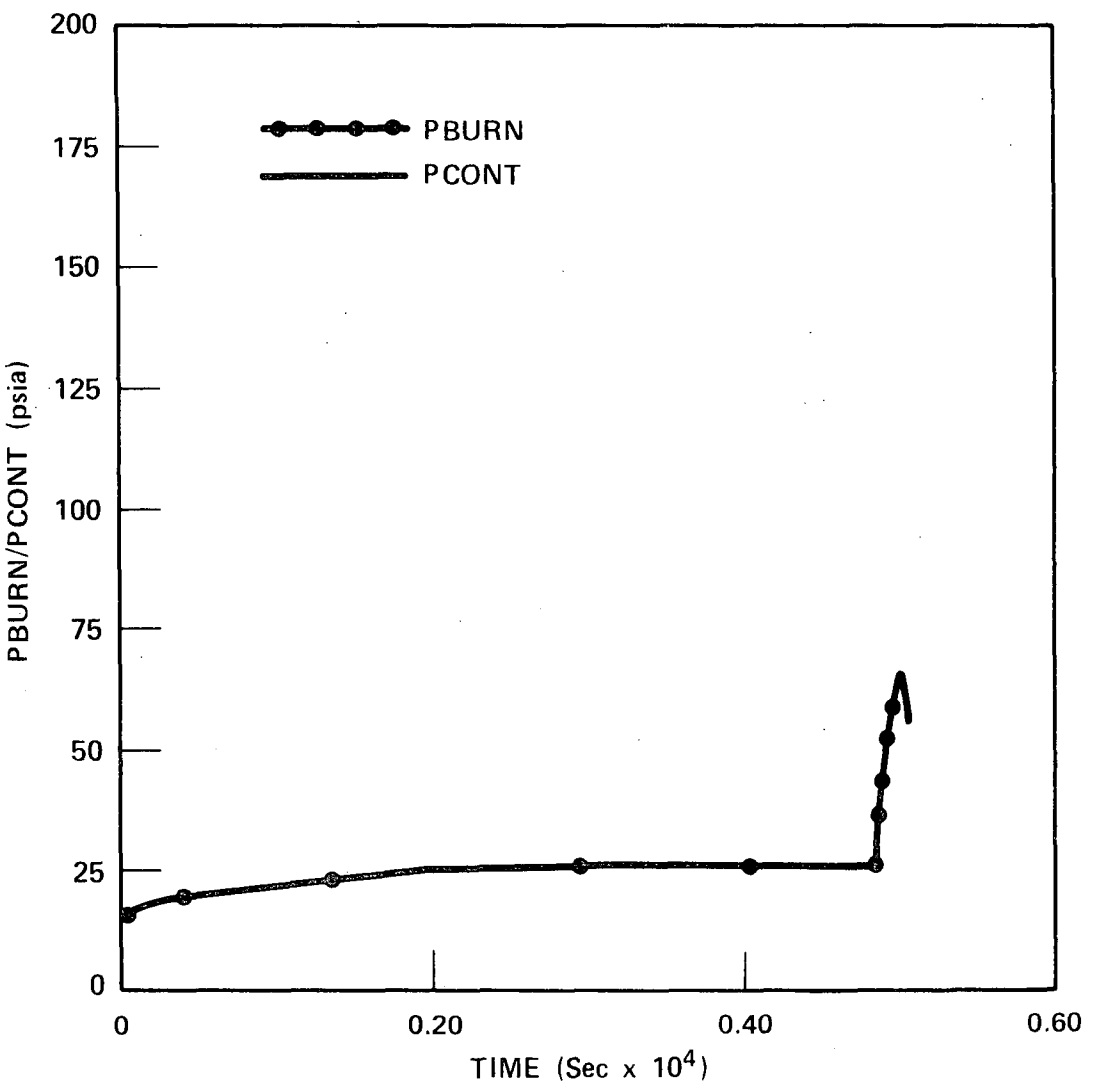
Mass Hydrogen (in Containment) vs. Time
S2D, Time Phased, 75% Dispersive, No Burn, 66% Zr Reacted
Class III, Case 3a'



Mole Fraction H_2 (in Containment) vs. Time
S2D, Time Phased, 75% Dispersive, No Burn, 66% Zr Reacted
Class III, Case 3a'



Flame Temperature (in Containment) vs. Time
S2D, Time Phased, 75% Dispersive, No Burn, 66% Zr Reacted
Class III, Case 3a'



Adiabatic Burn Pressure/Pressure in Containment vs. Time
S2D, Time Phased, 75% Dispersive, No Burn, 66% Zr Reacted
Class III, Case 3a'

CASE: CLASS III, CASE 4a, S2D, TIME PHASED, 50% DISPERSED, NO BURN, 26% Zr REACTED

DISPERSIVE: YES PERCENT CORE DISPERSED: 50 FRACTION IN CAVITY: 0

RUN #: AB3YCUG DATE: 3/6/81 PERCENT ZR REACTED: 26

BLOWDOWN PEAK: N/A PSIA TIME: _____ SEC.

HYDROGEN BURN?: N/A CRITERIA: _____

TIME @ BURN: _____ SEC, PRESSURE: _____ PSIA, TEMPERATURE: _____ °F

PEAKS:

PRESSURE: 51 PSIA, TIME: 4701 SEC, WHY?: VESSEL FAILURE

TEMPERATURE: 286 °F, TIME: 4699 SEC, WHY?: VESSEL FAILURE

DISPERSIVE: YES

PRESSURE: 51 PSIA, TIME: 4701 SEC, WHY?: _____

TEMPERATURE: 286 °F, TIME: 4701 SEC, WHY?: _____

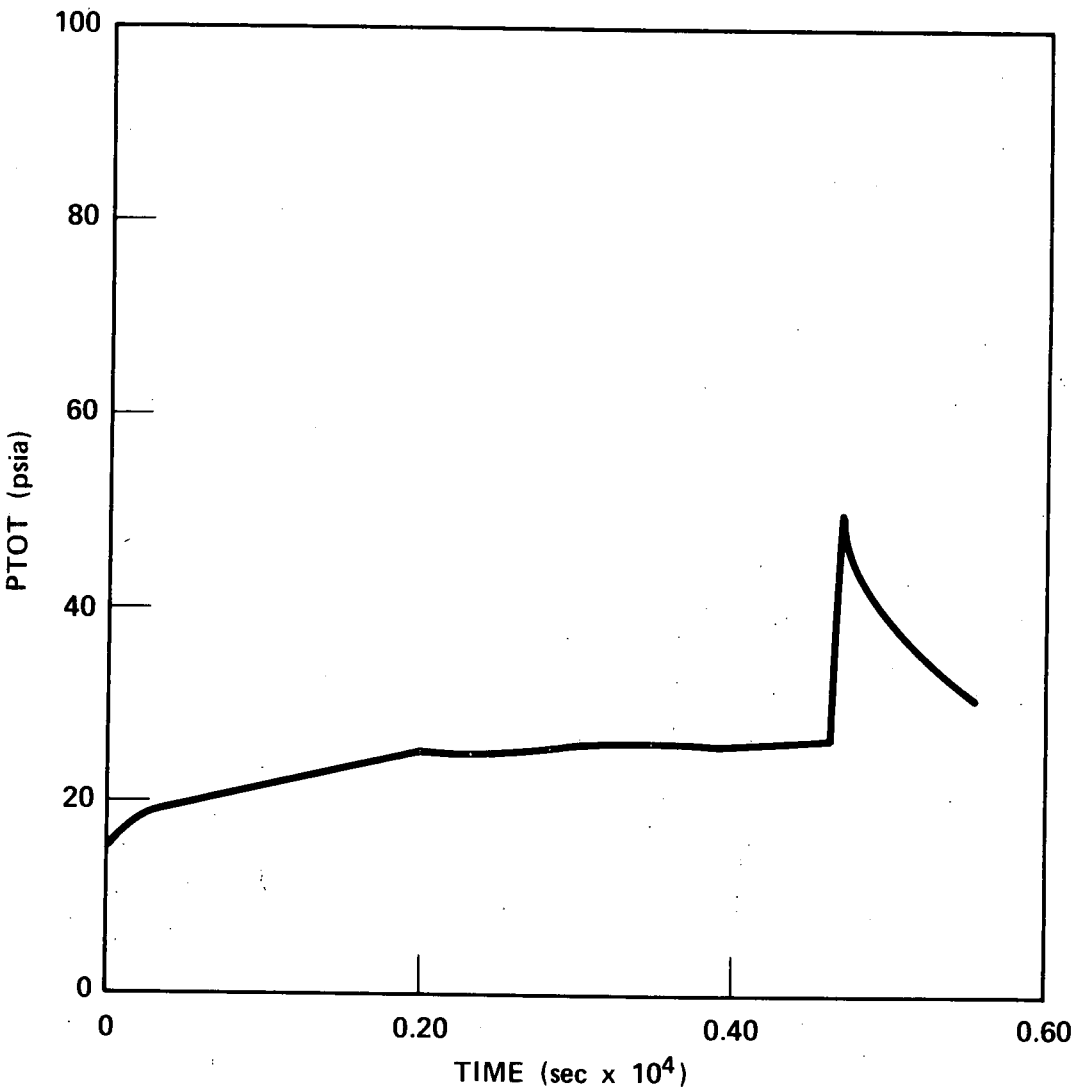
END OF BOIL: 4608.6 SEC. END OF HEAD: _____ SEC.

VESSEL FAILURE: 4608.6 SEC. END OF HOTDROP: _____ SEC.

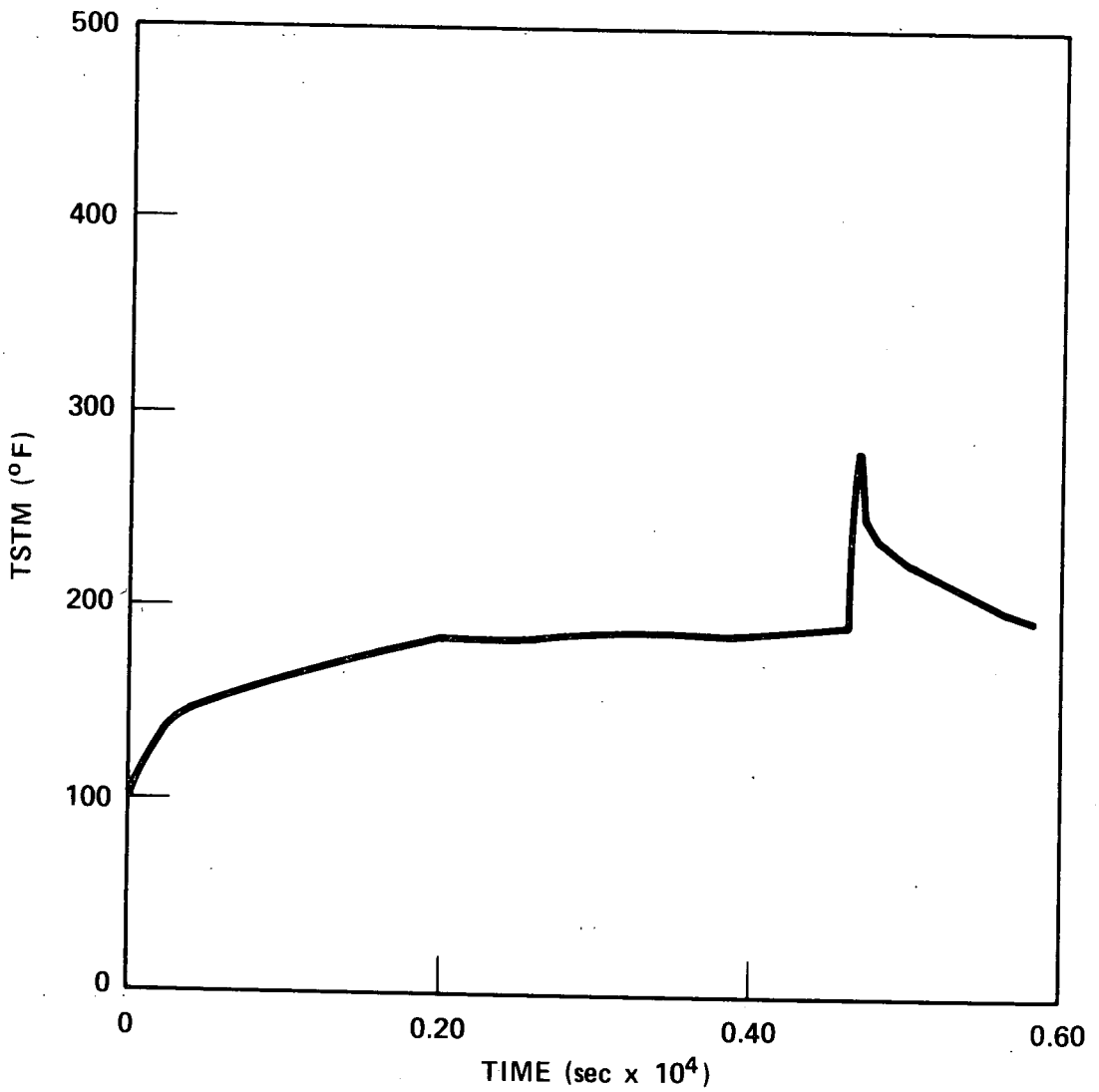
END OF INTER: _____ SEC.

Class III, Case 4a

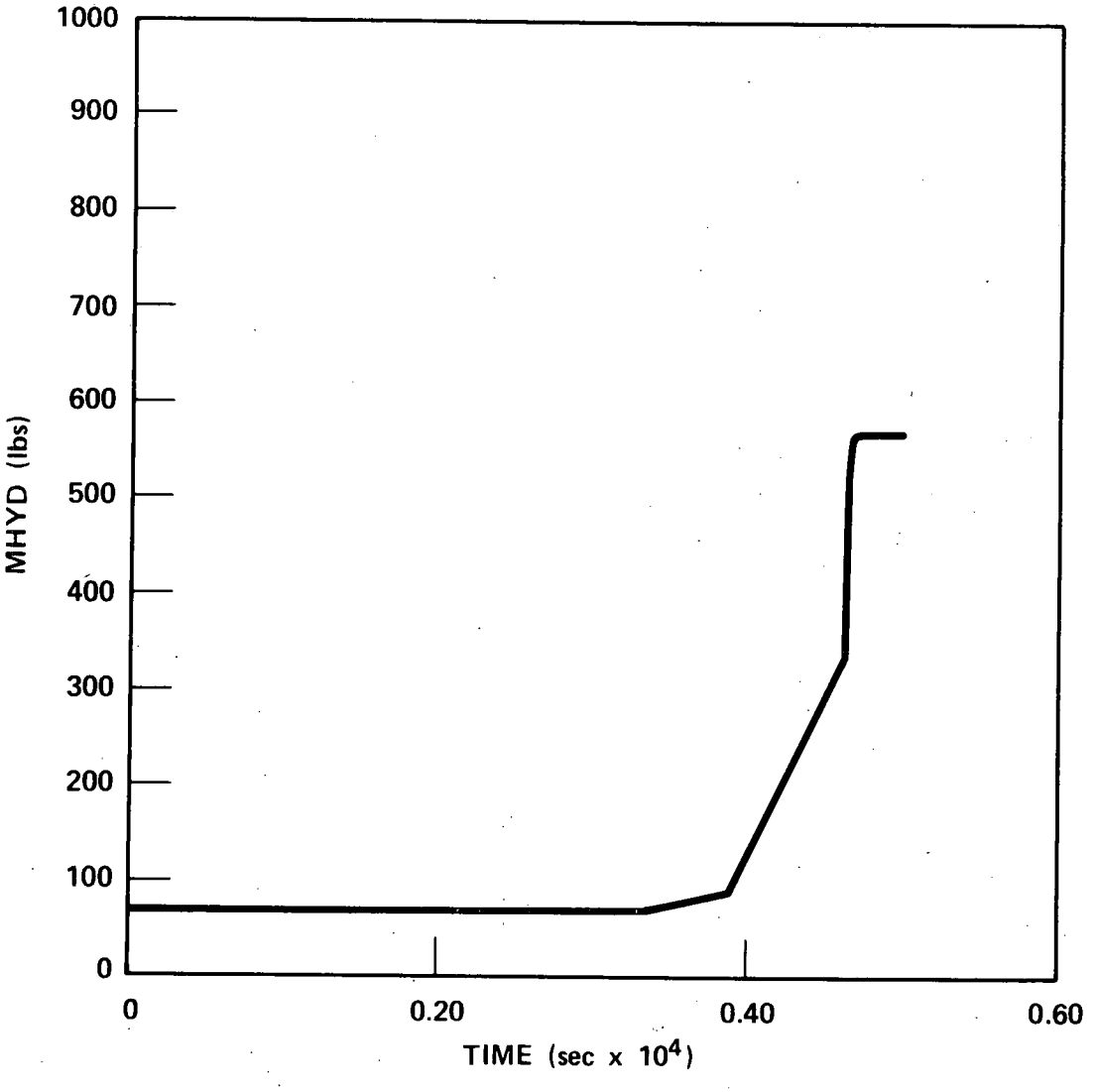
Sheet 1 of 7



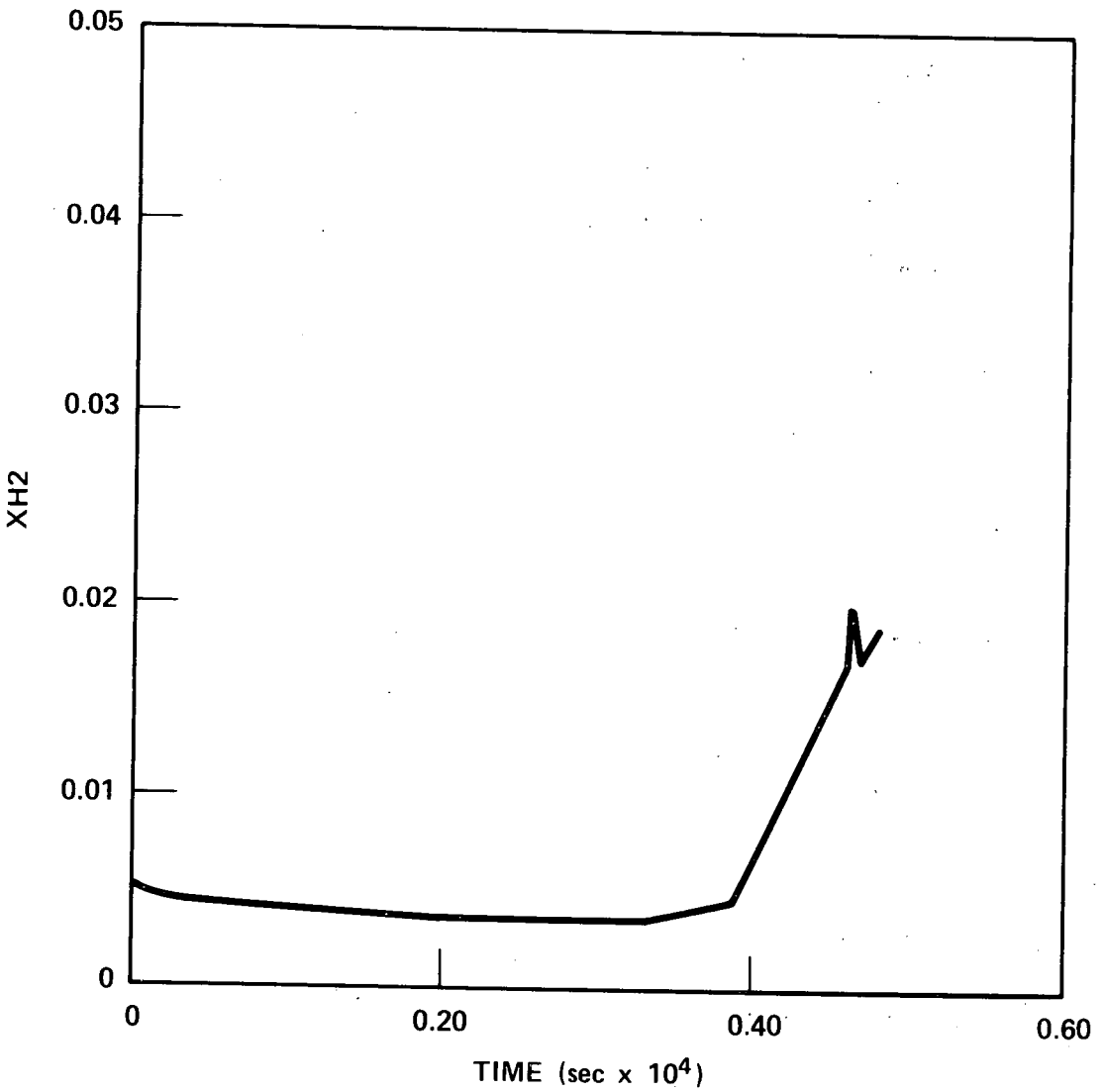
Pressure (in Containment) vs. Time
S2D, Time Phased, 50% Dispersive, No Burn, 26% Zr Reacted
Class III, Case 4a



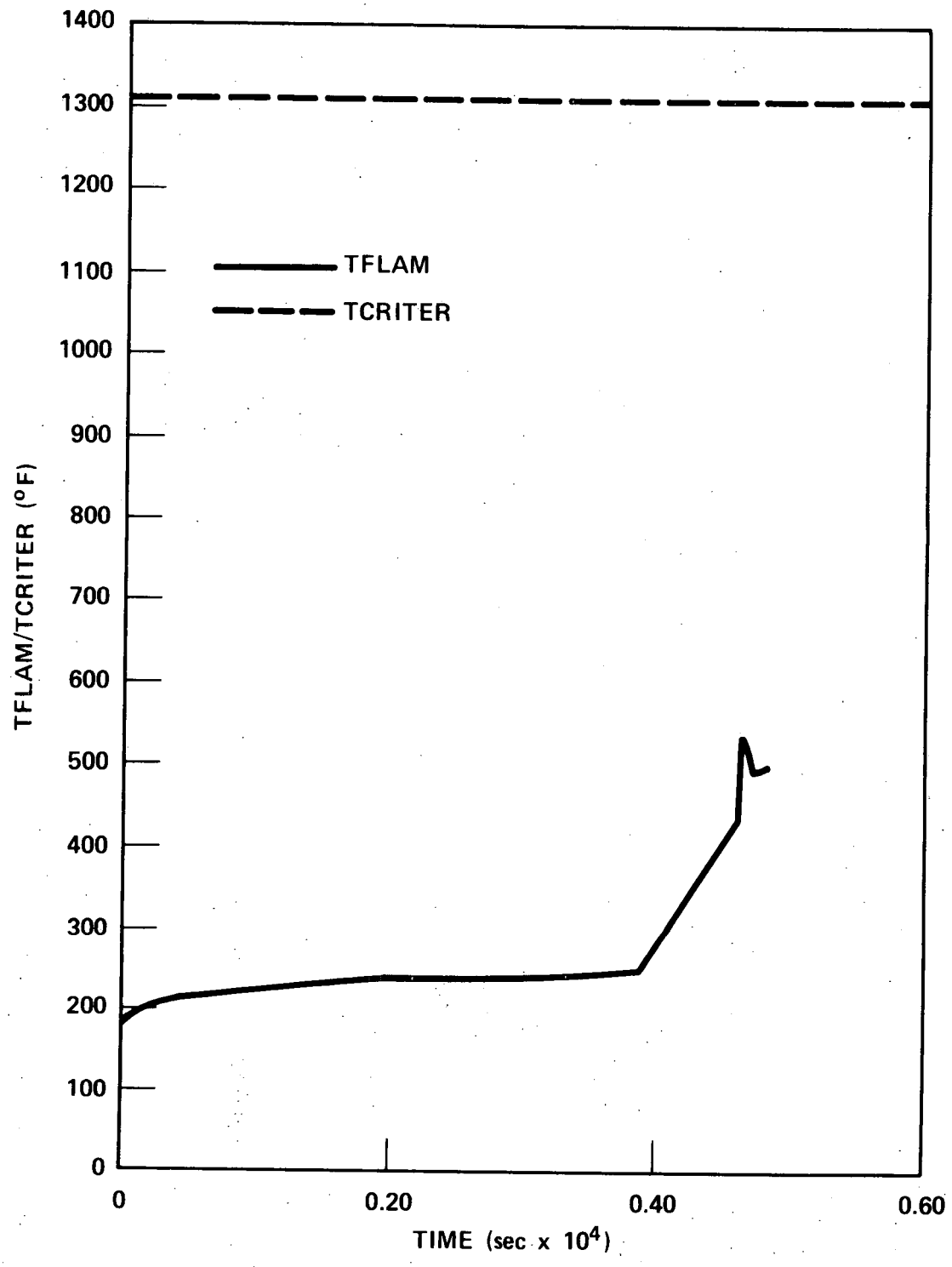
Temperature (in Containment) vs. Time
S2D, Time Phased, 50% Dispersive, No Burn, 26% Zr Reacted
Class III, Case 4a



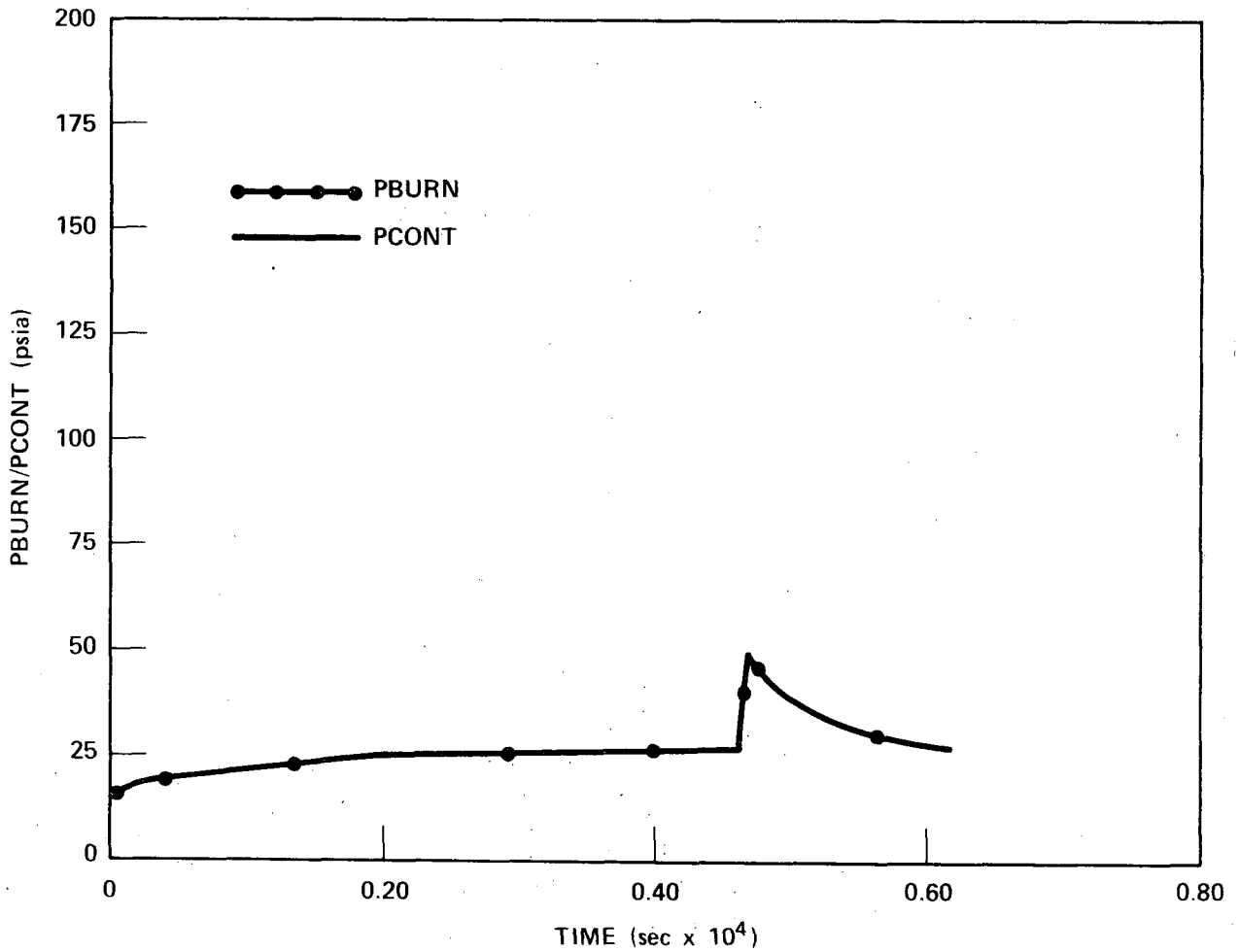
Mass Hydrogen (in Containment) vs. Time
S2D, Time Phased, 50% Dispersive, No Burn, 26% Zr Reacted
Class III, Case 4a



Mole Fraction H_2 (in Containment) vs. Time
S2D, Time Phased, 50% Dispersive, No Burn 26% Zr Reacted
Class III, Case 4a



Flame Temperature (in Containment) vs. Time
S2D, Time Phased, 50% Dispersive, No Burn, 26% Zr Reacted
Class III, Case 4a



Adiabatic Burn Pressure/Pressure in Containment vs. Time
S2D, Time Phased, 50% Dispersive, No Burn, 26% Zr Reacted
Class III, Case 4a

CASE: CLASS III, CASE 4a', S2D, TIME PHASED, 50% DISPERSED, NO BURN, 61% Zr REACTED

DISPERSIVE: YES PERCENT CORE DISPERSED: 50 FRACTION IN CAVITY: 0

RUN #: AB3YCRH DATE: 3/10/81 PERCENT ZR REACTED: 61

BLOWDOWN PEAK: N/A PSIA TIME: _____ SEC.

HYDROGEN BURN?: NO CRITERIA: _____

TIME @ BURN: _____ SEC, PRESSURE: _____ PSIA, TEMPERATURE: _____ °F

PEAKS:

PRESSURE: 58 PSIA, TIME: 4737.5 SEC, WHY?: VESSEL FAILURE

TEMPERATURE: 289 °F, TIME: 4697.5 SEC, WHY?: VESSEL FAILURE

DISPERSIVE: YES

PRESSURE: 58 PSIA, TIME: 4737.5 SEC, WHY?: _____

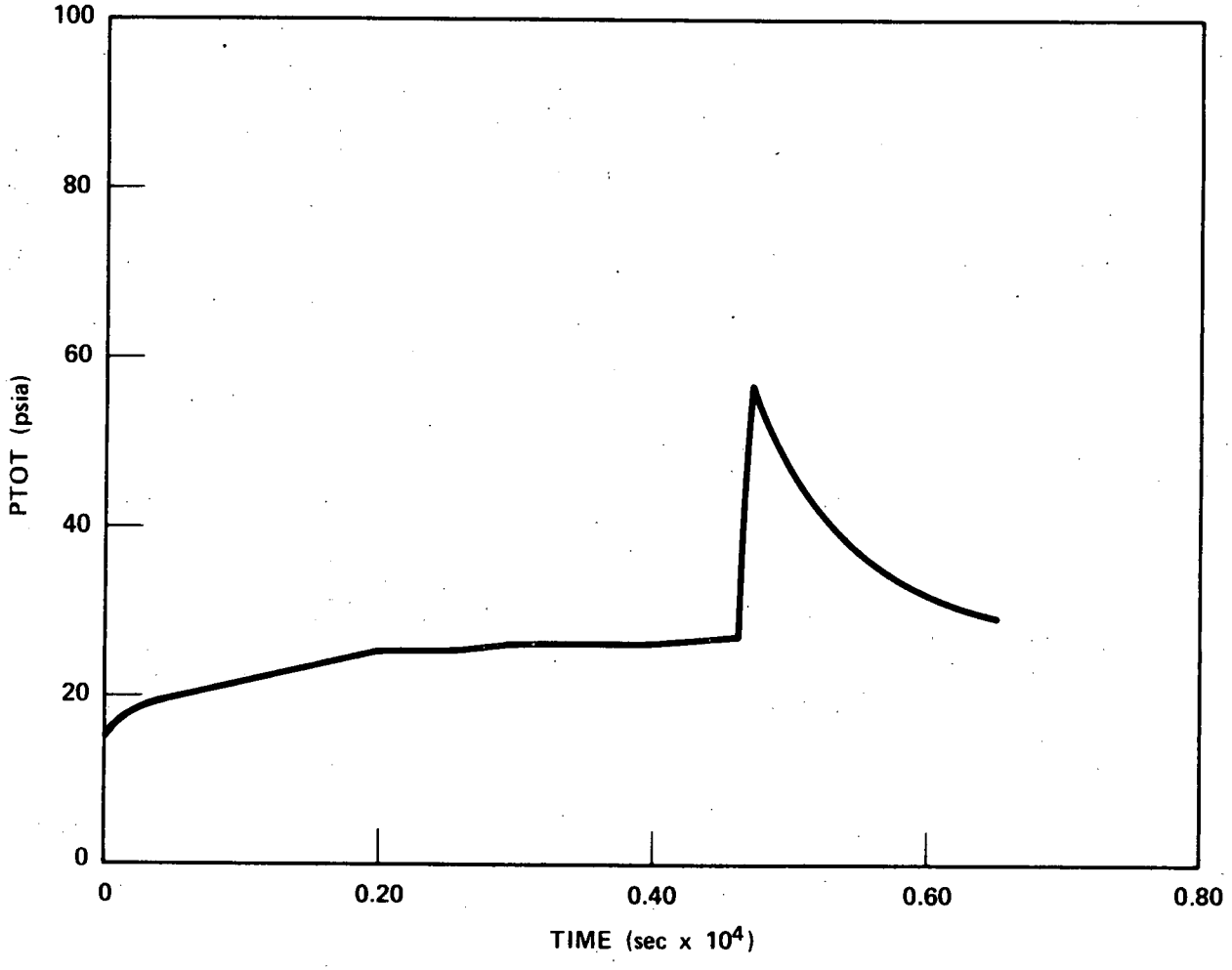
TEMPERATURE: 281 °F, TIME: 4737.5 SEC, WHY?: _____

END OF BOIL: 4608.6 SEC. END OF HEAD: _____ SEC.

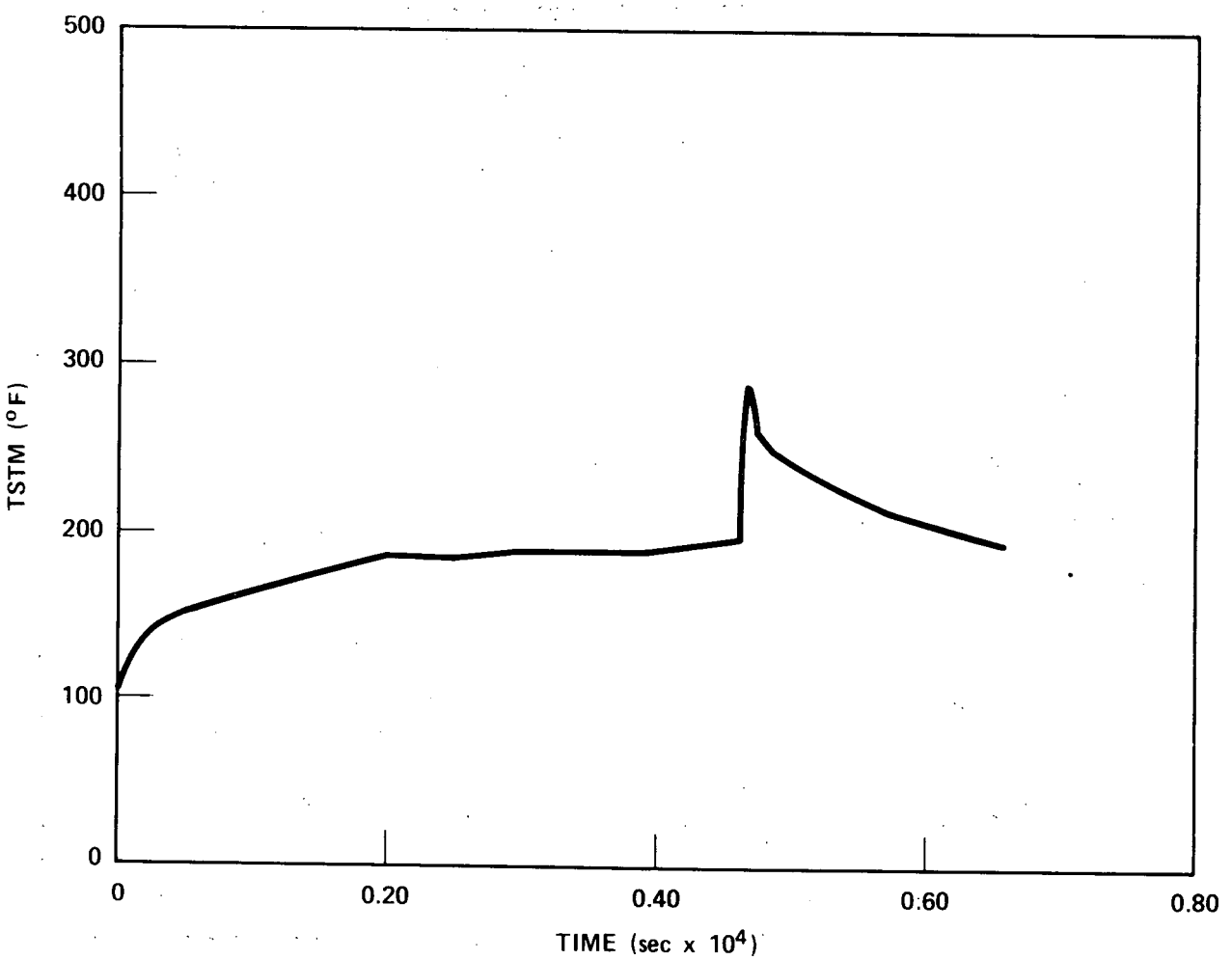
VESSEL FAILURE: 4608.6 SEC. END OF HOTDROP: _____ SEC.

END OF INTER: _____ SEC.

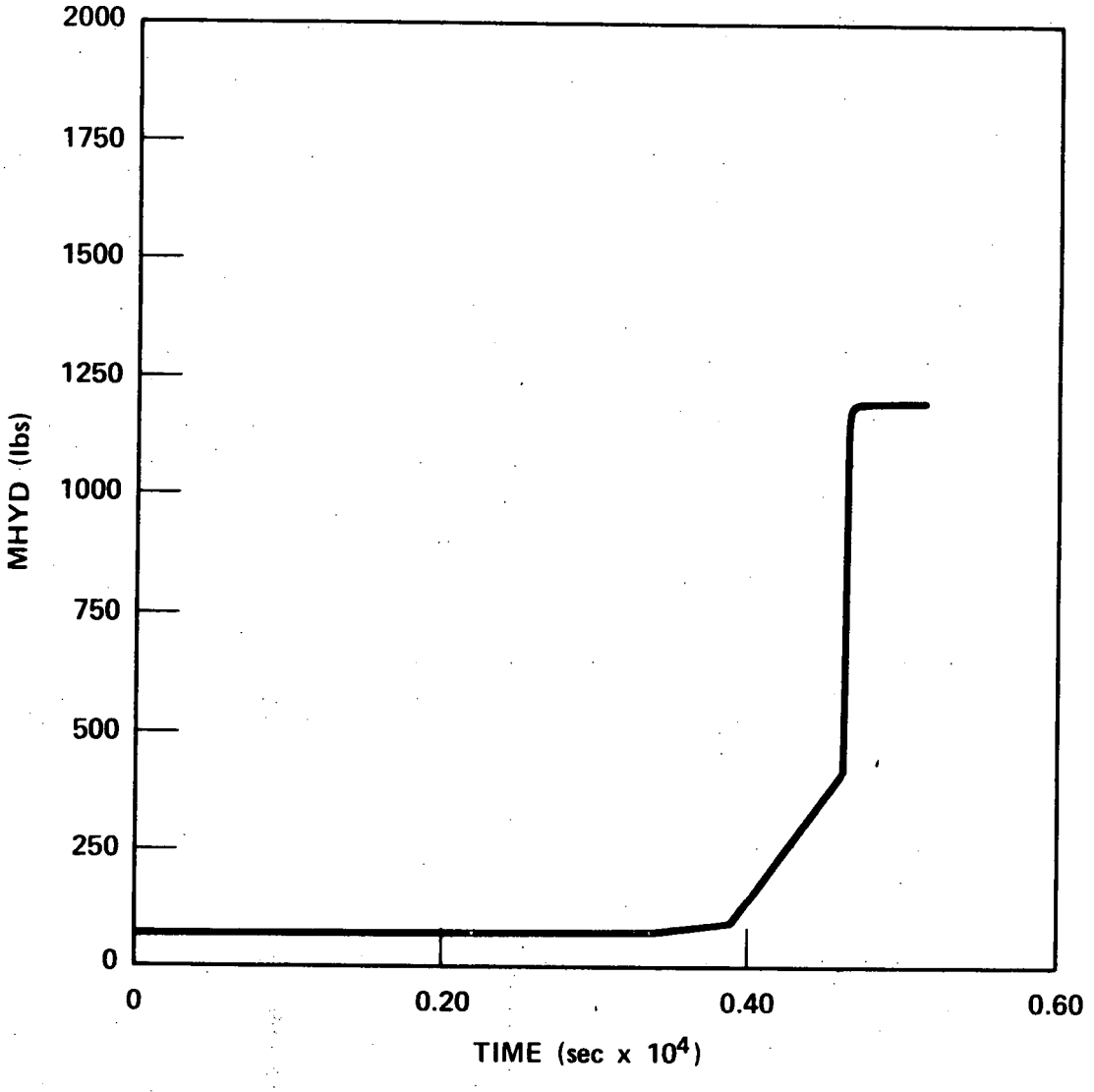
Class III, Case 4a'



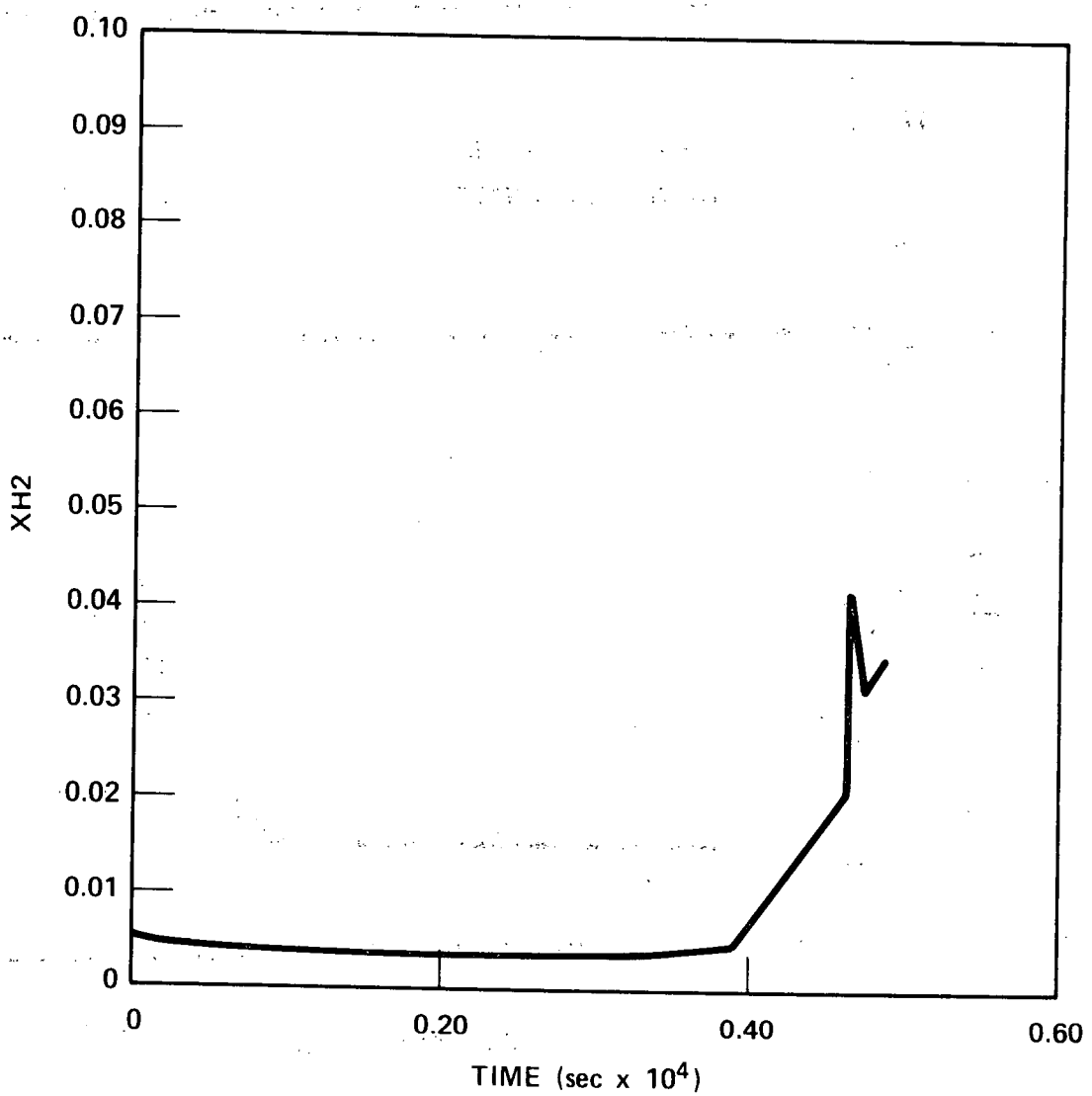
Pressure (in Containment) vs. Time
S2D, Time Phased, 50% Dispersive, No Burn, 61% Zr Reacted
Class III, Case 4a'



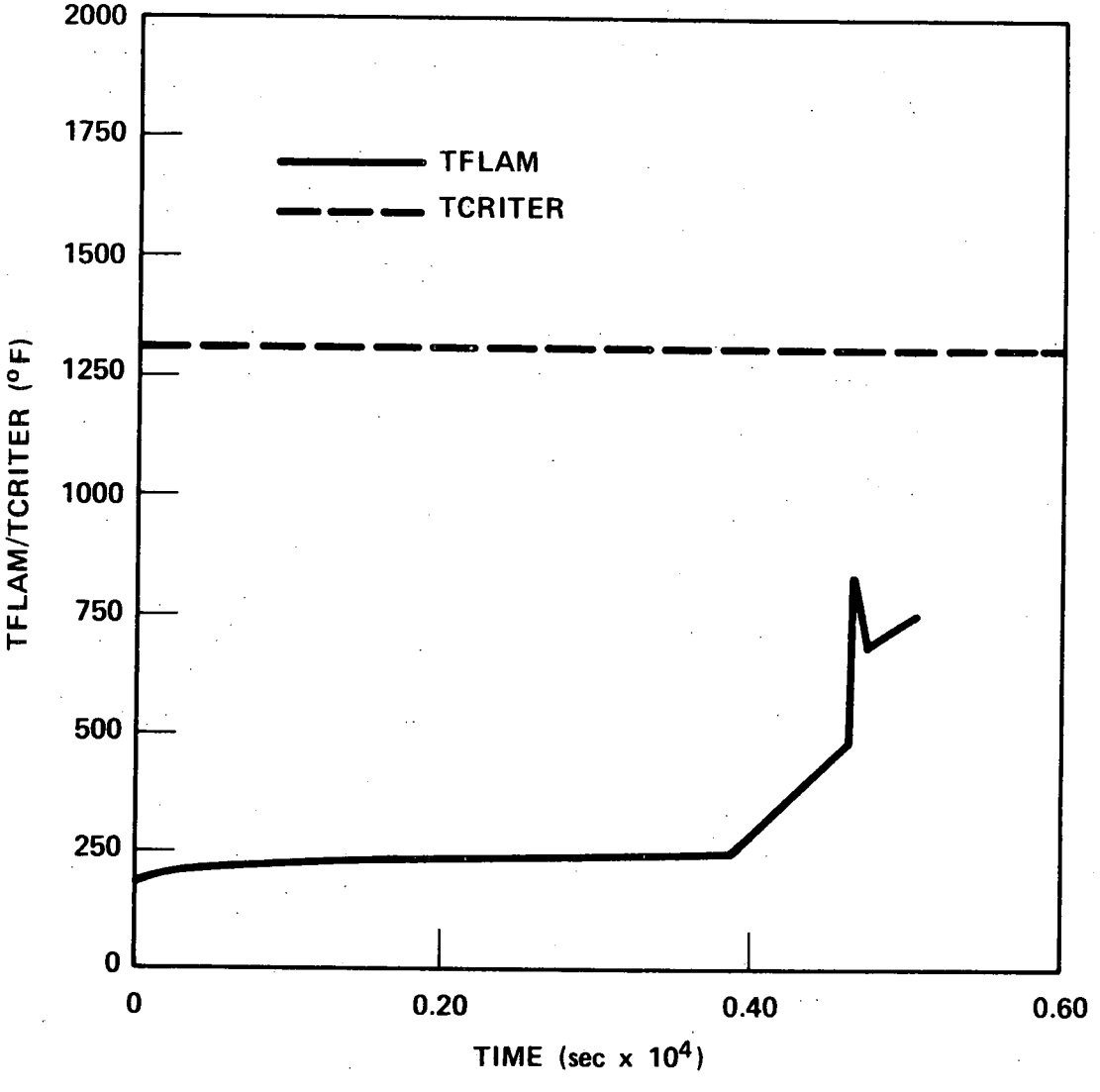
Temperature (in Containment) vs. Time
S2D, Time Phased, 50% Dispersive, No Burn, 61% Zr Reacted
Class III, Case 4a'



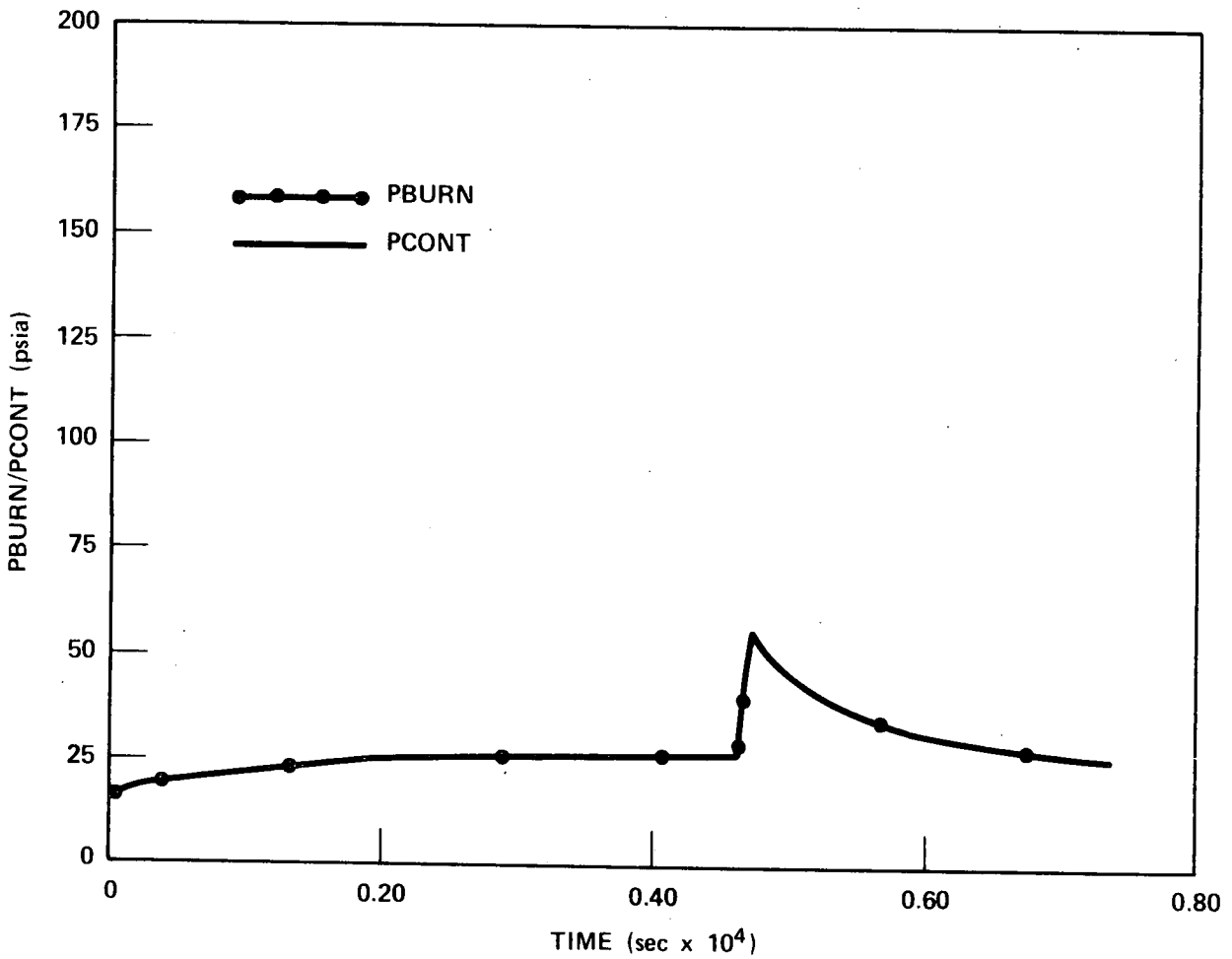
Mass Hydrogen (in Containment) vs. Time
S2D, Time Phased, 50% Dispersive, No Burn, 61% Zr Reacted
Class III, Case 4a'



Mole Fraction H_2 (in Containment) vs. Time
S2D, Time Phased, 50% Dispersive, No Burn; 61% Zr Reacted
Class III, Case 4a'



Flame Temperature (in Containment) vs. Time
S2D, Time Phased, 50% Dispersive, No Burn, 61% Zr Reacted
Class III, Case 4a'



Adiabatic Burn Pressure/Pressure in Containment vs. Time
S2D, Time Phased, 50% Dispersive, No Burn, 61% Zr Reacted
Class III, Case 4a'

CASE: CLASS III, CASE 5A, S2D, W, 80% DISPERSIVE, NO BURN

DISPERSIVE: YES PERCENT CORE: 80 FRACTION IN CAVITY: 0.20

RUN #: AALAAGP DATE: 11/15/80

BLOWDOWN PEAK: _____ PSIA TIME: _____ SEC.

HYDROGEN BURN?: NO CRITERIA: _____

TIME @ BURN: _____ SEC, PRESSURE: _____ PSIA, TEMPERATURE: _____ °F

PEAKS:

PRESSURE: 104 PSIA, TIME: 4898.5 SEC, WHY?: END OF DISPERSION

TEMPERATURE: 932 °F, TIME: 4898 SEC, WHY?: END OF DISPERSION

DISPERSION: YES

PRESSURE: 104 PSIA, TIME: 4868.3 SEC,

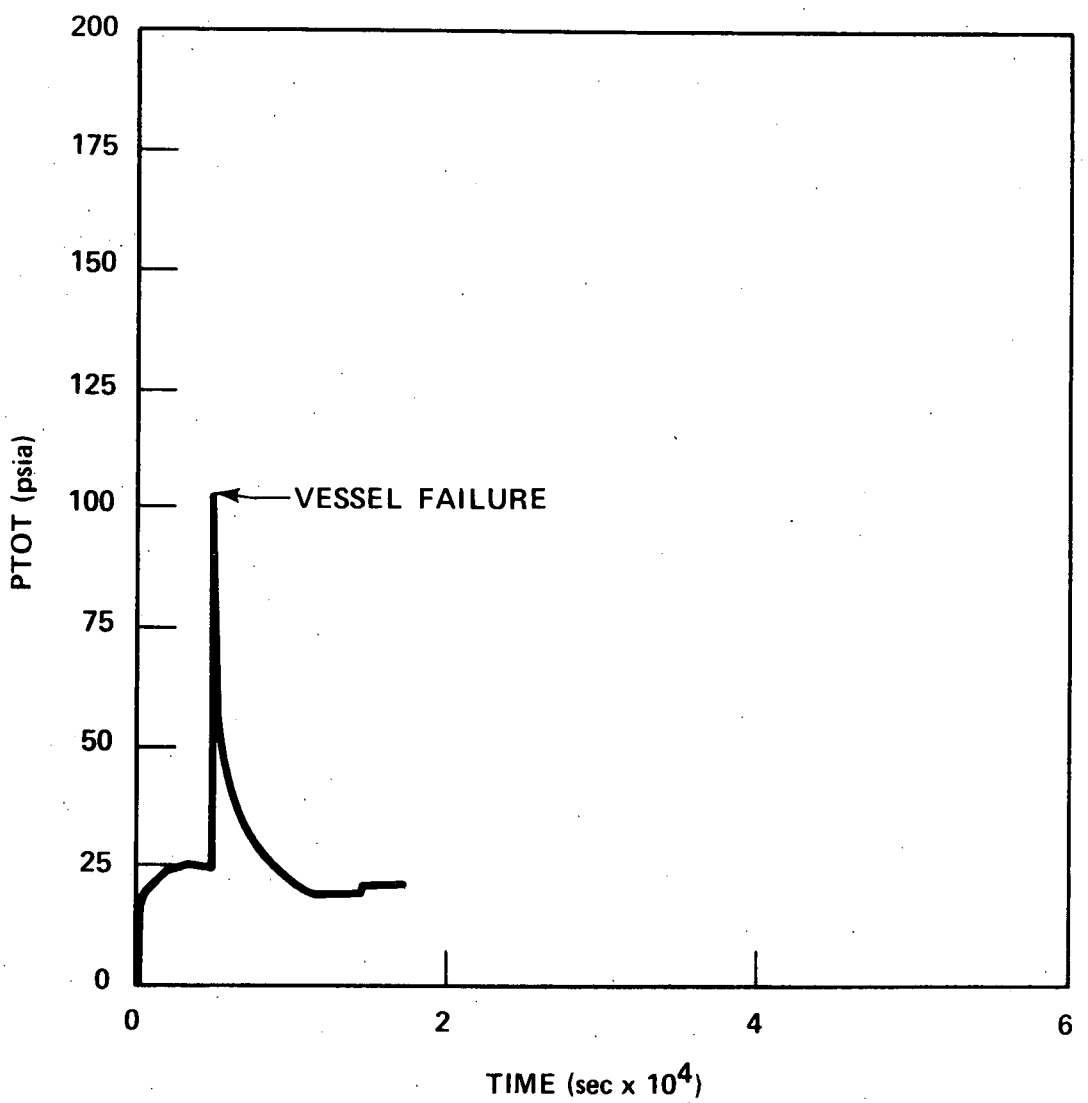
TEMPERATURE: 932 °F, TIME: 4868.3 SEC,

END OF BOIL: 4865.4 SEC. END OF HEAD: 4868.3 SEC.

VESSEL FAILURE: 4868.3 SEC. END OF HOTDROP: _____ SEC.

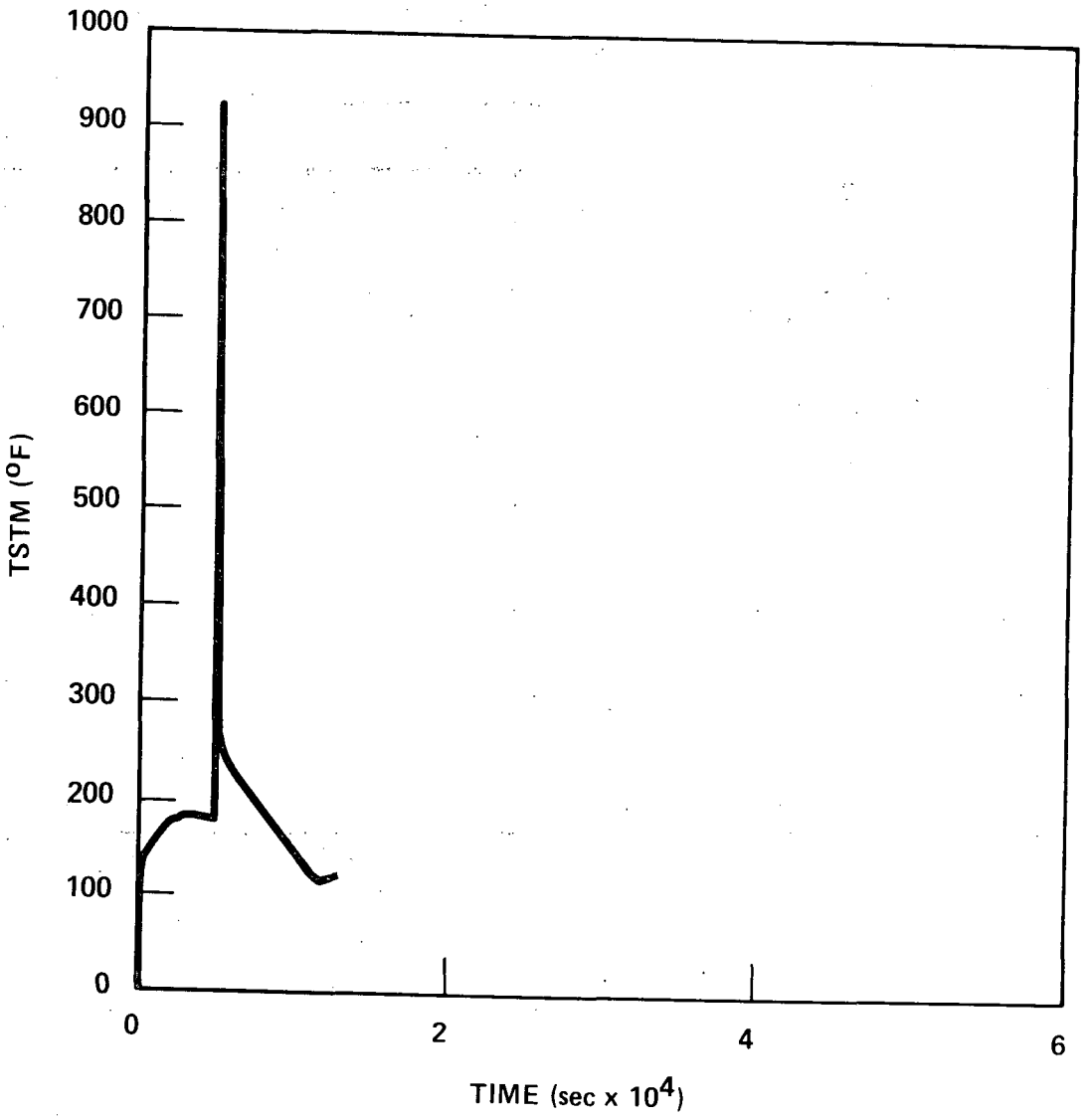
END OF INTER: 86319 SEC.

Class III, Case 5A

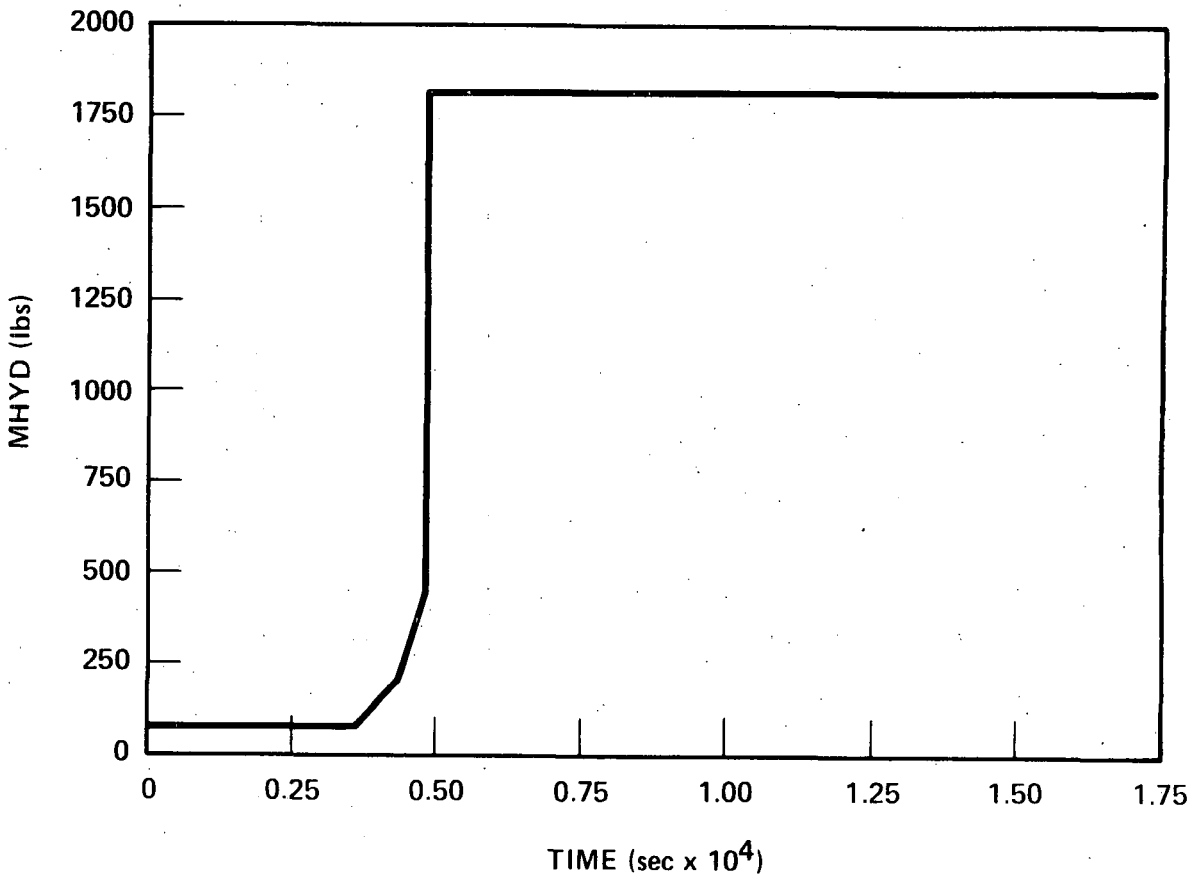


Pressure (in Containment) vs. Time
S2D, W, 80% Dispersive, No Burn
Class III, Case 5A

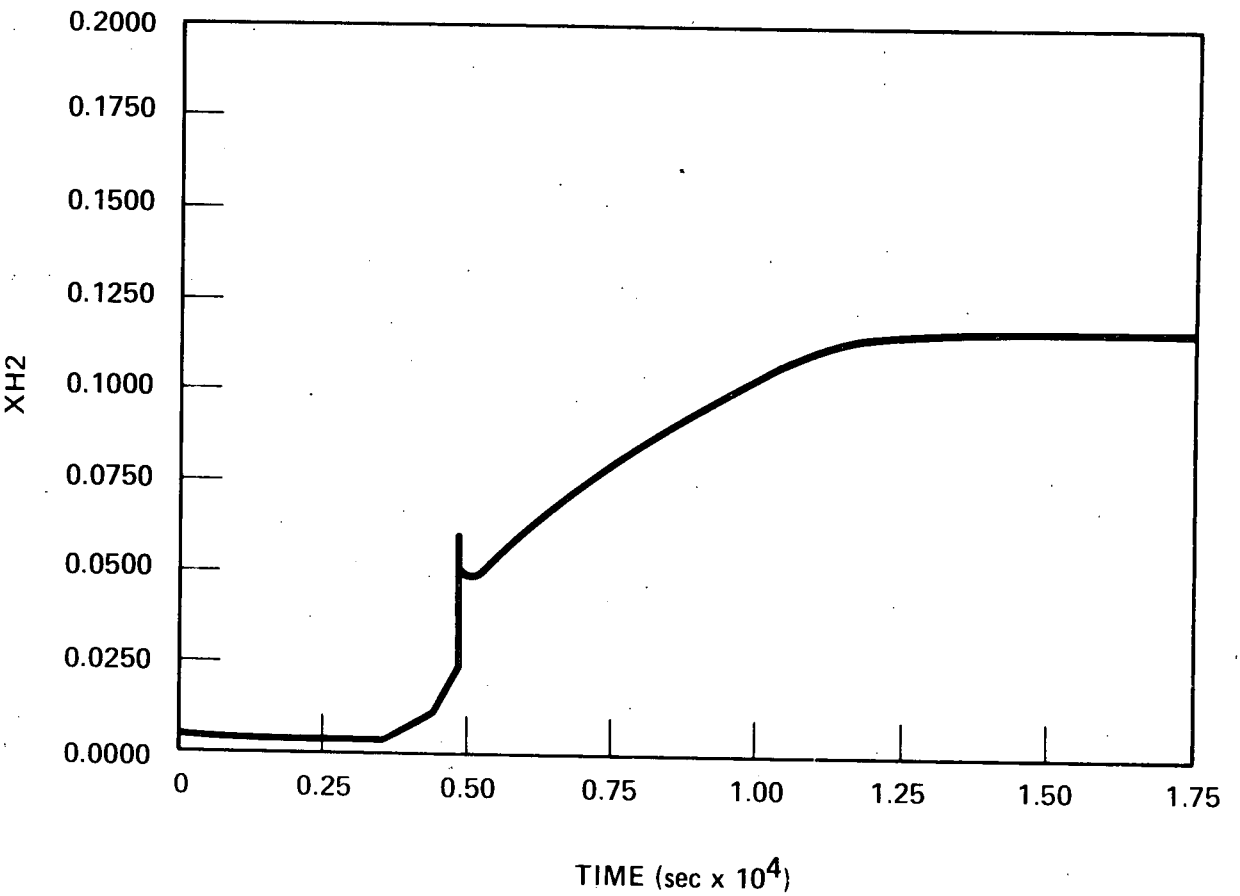
Sheet 2 of 7



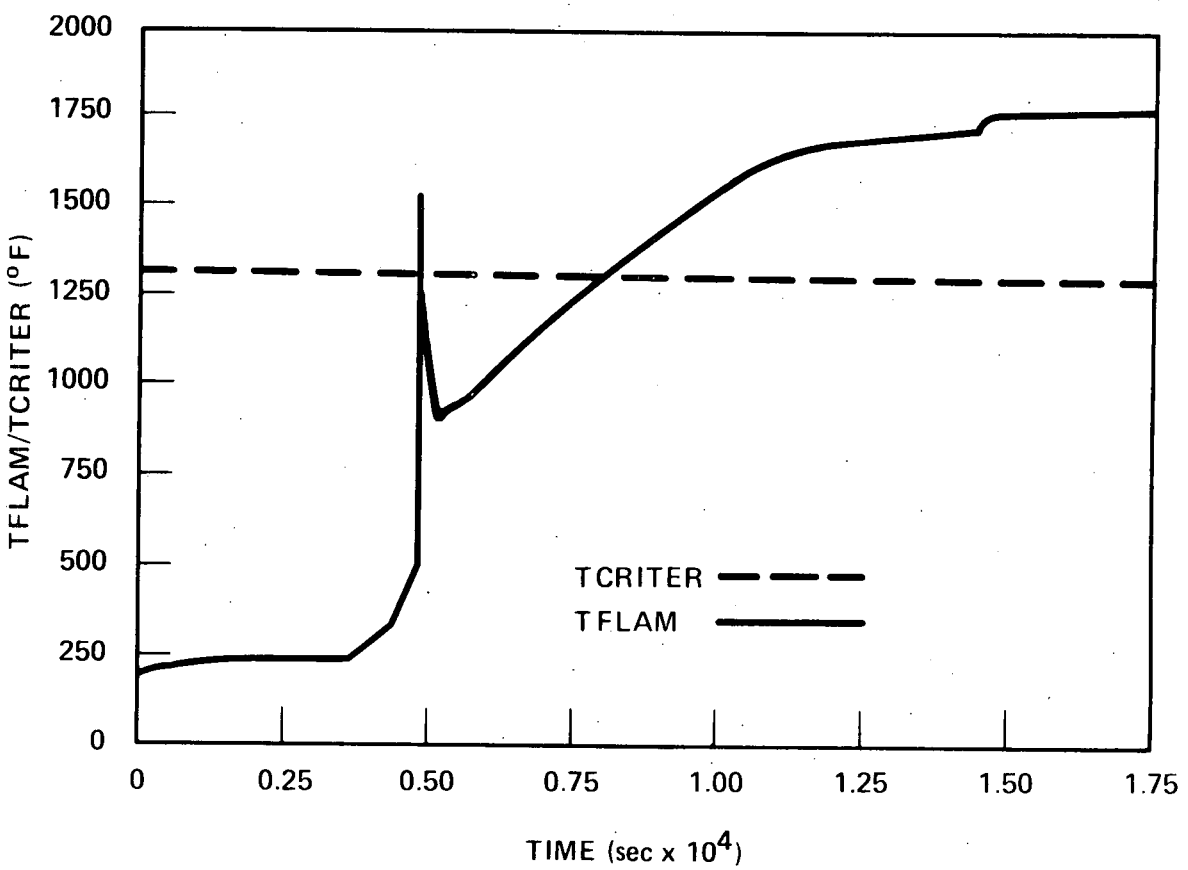
Temperature (in Containment) vs. Time
S2D, W, 80% Dispersive, No Burn
Class III, Case 5A



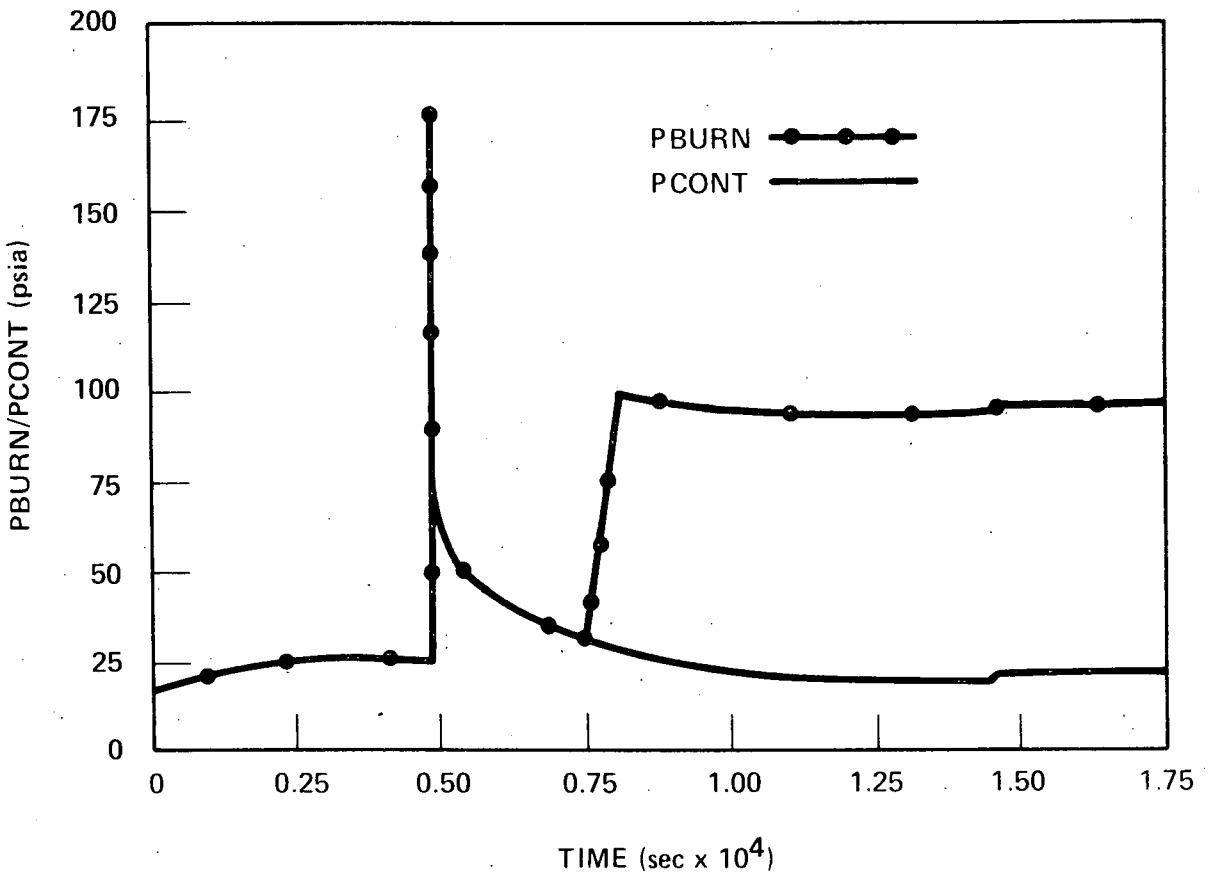
Mass Hydrogen (in Containment) vs. Time
S2D, W, 80% Dispersive, No Burn
Class III, Case 5A



Mole Fraction H_2 (in Containment) vs. Time
S2D, W, 80% Dispersive, No Burn
Class III, Case 5A



Flame Temperature (in Containment) vs. Time
S2D, W, 80% Dispersive, No Burn
Class III, Case 5A



Adiabatic Burn Pressure/Pressure in Containment vs. Time
S2D, W, 80% Dispersive, No Burn
Class III, Case 5A

CASE: CLASS III, CASE 5B, S2D, W, 80% DISPERSIVE, BURN @ VESSEL FAILURE

DISPERSIVE: YES PERCENT CORE: 80 FRACTION IN CAVITY: 0.20

RUN #: AALAAGR DATE: 11/15/80

BLOWDOWN PEAK: _____ PSIA TIME: _____ SEC.

HYDROGEN BURN?: YES CRITERIA: VESSEL FAILURE

TIME @ BURN: 4897.1 SEC, PRESSURE: 101 PSIA, TEMPERATURE: 923 °F

PEAKS:

PRESSURE: 140 PSIA, TIME: 4917.2 SEC,

TEMPERATURE: 1492 °F, TIME: 4917 SEC,

DISPERSIVE: YES

PRESSURE: 140 PSIA, TIME: 4868.3 SEC, WHY?: DISPERSION/BURN

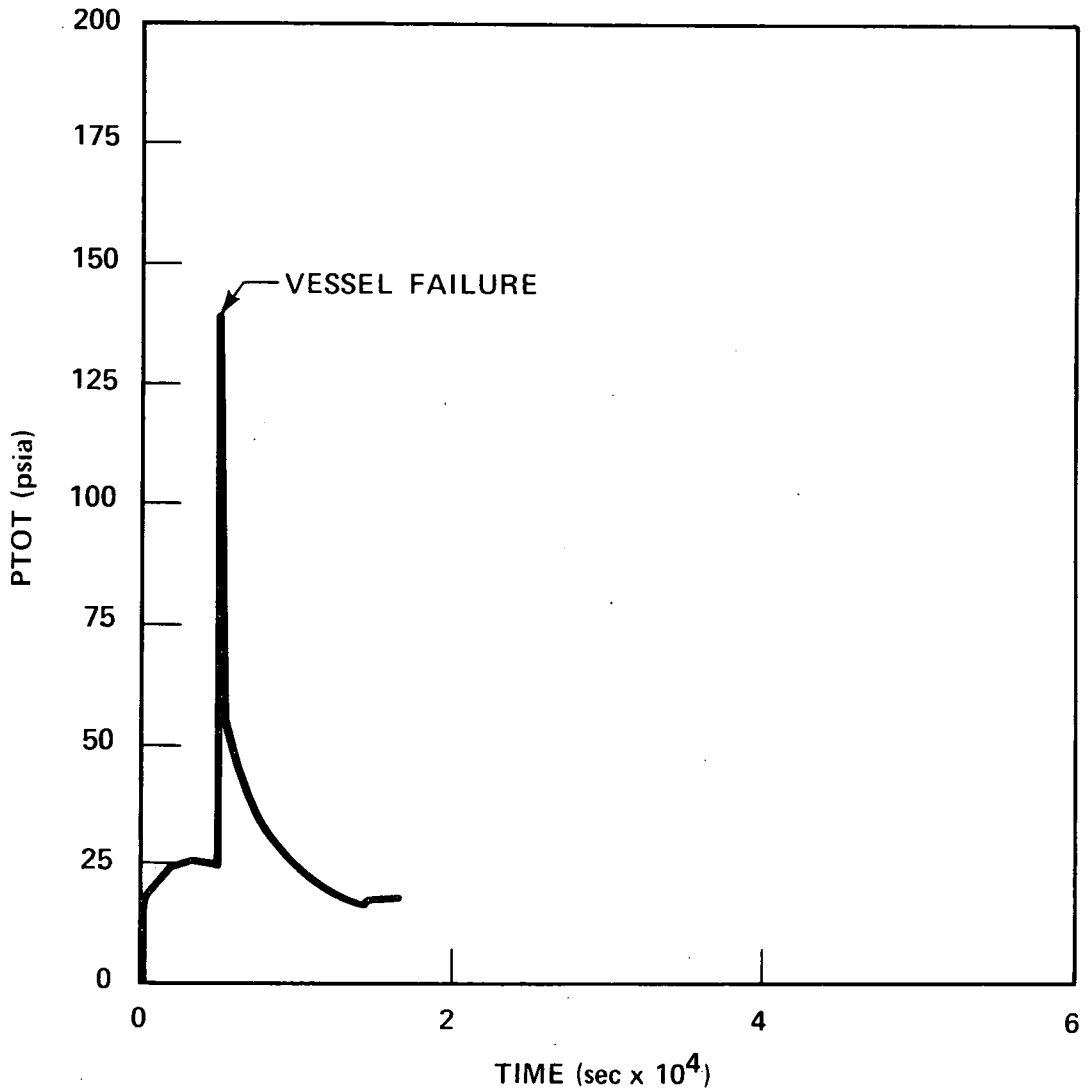
TEMPERATURE: 1492 °F, TIME: 4868.3 SEC, WHY?: DISPERSION/BURN

END OF BOIL: 4865.4 SEC. END OF HEAD: 4868.3 SEC.

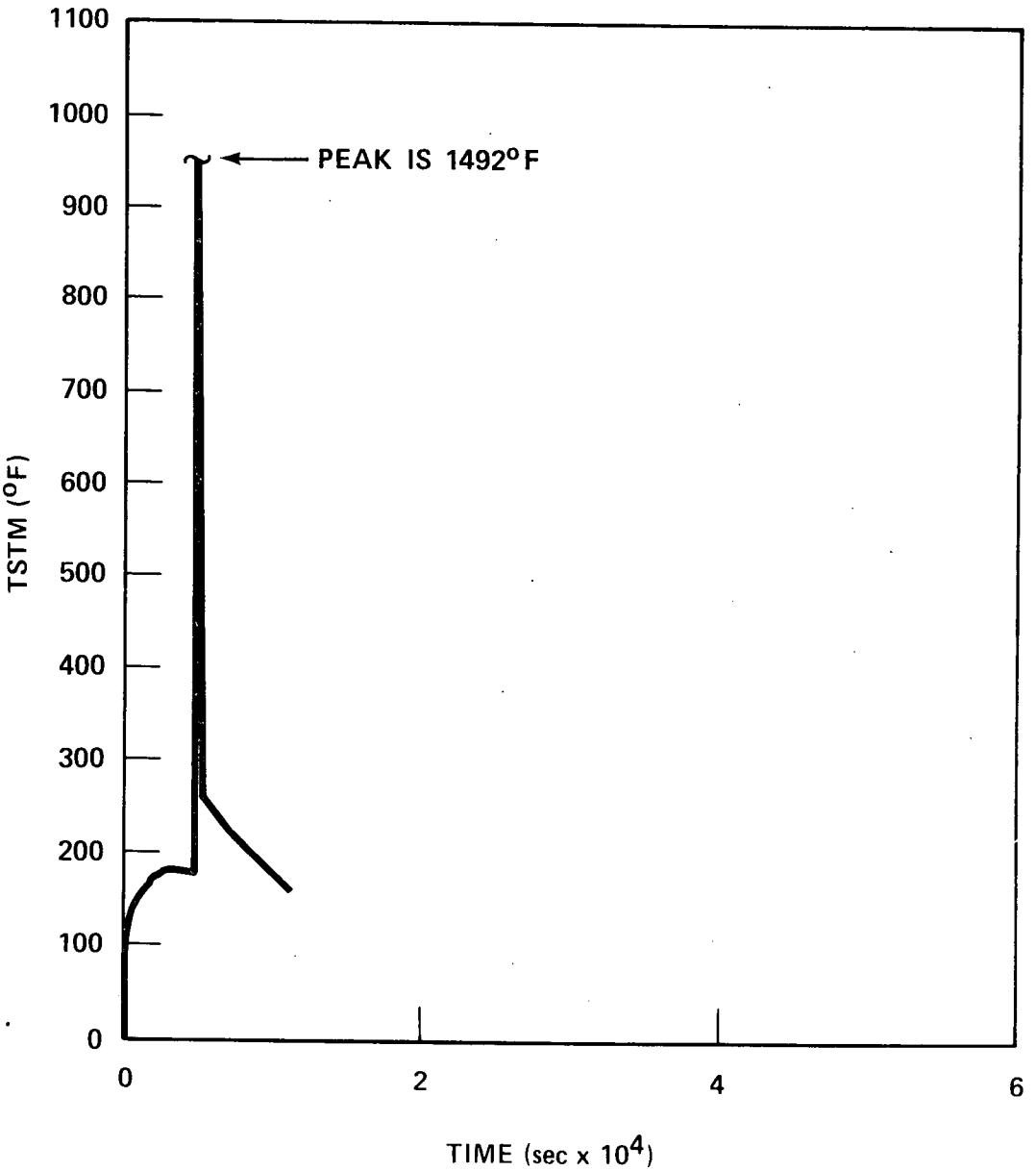
VESSEL FAILURE: 4868.3 SEC. END OF HOTDROP: _____ SEC.

END OF INTER: 86319 SEC.

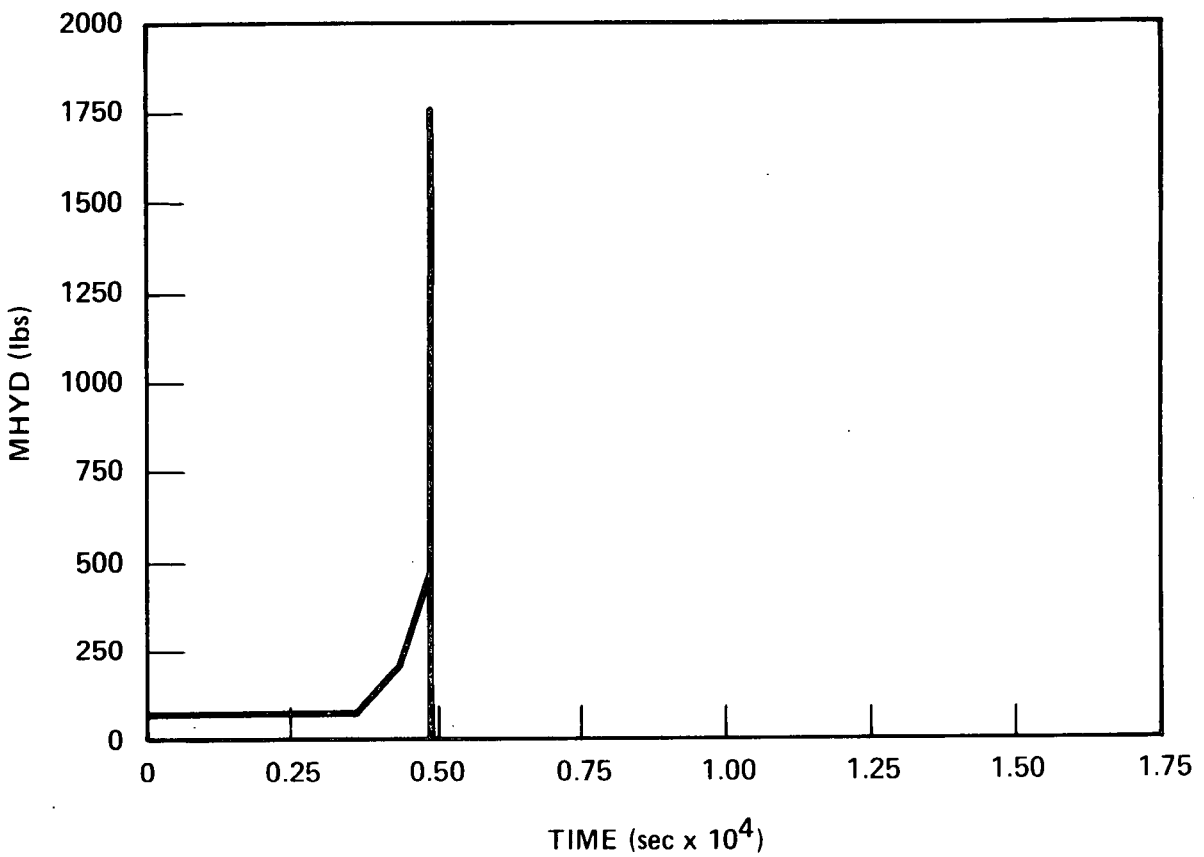
Class III, Case 5B



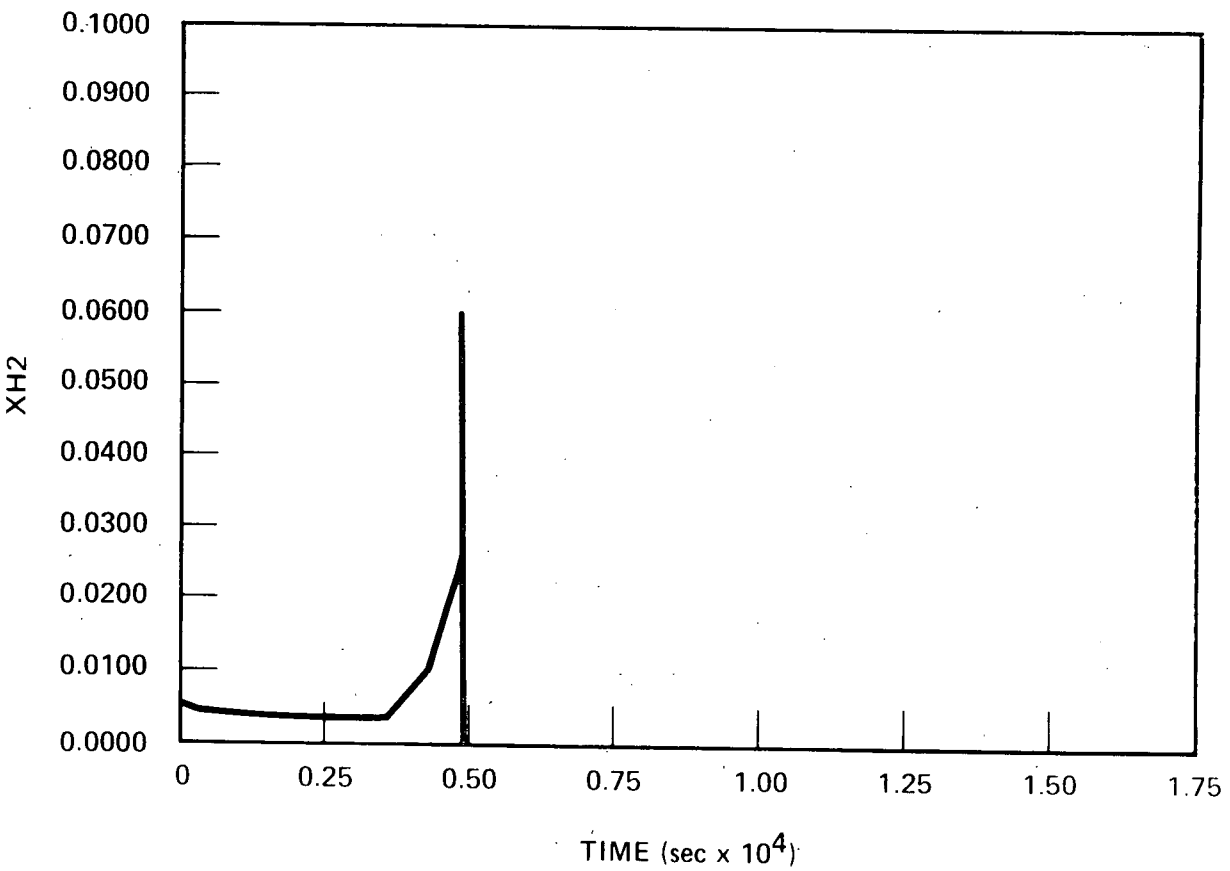
Pressure (in Containment) vs. Time
S2D, W, 80% Dispersive, Burn @ Vessel Failure
Class III, Case 5B



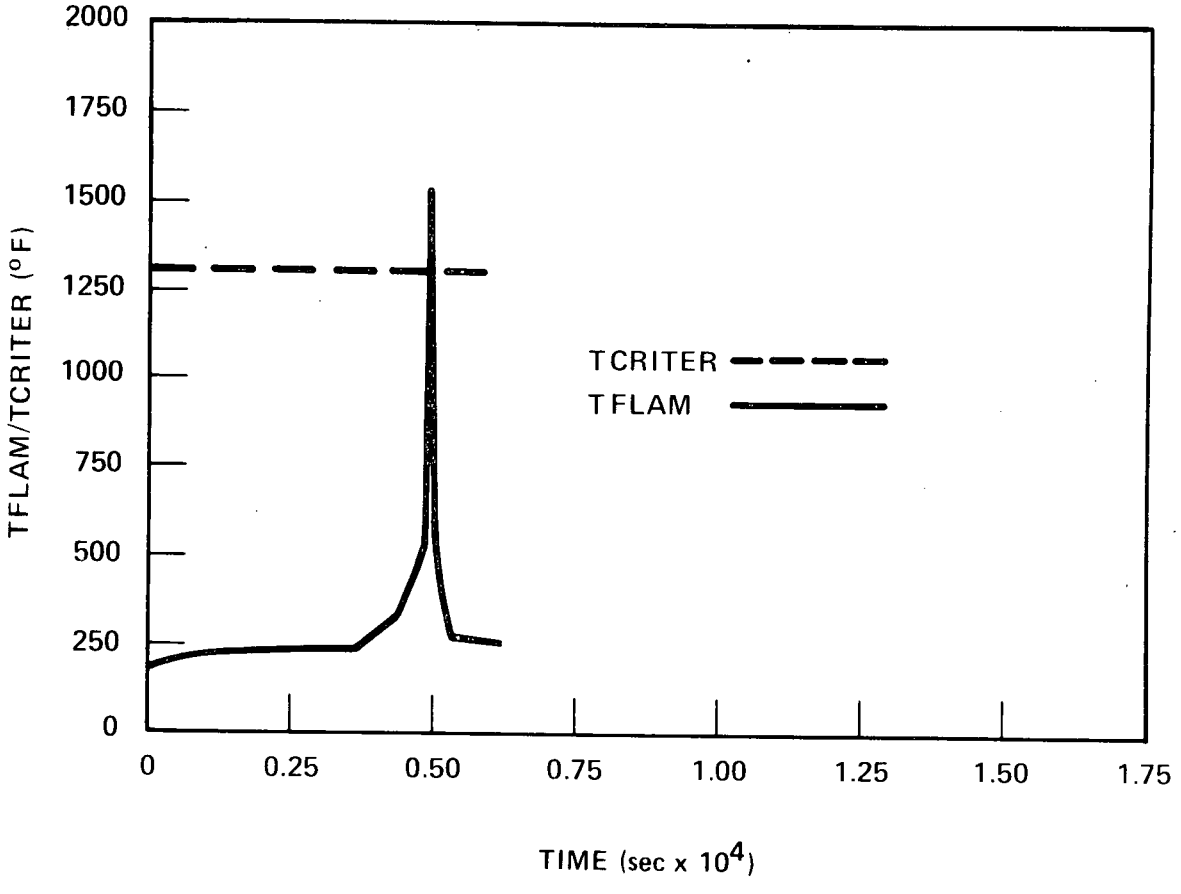
Temperature (in Containment) vs. Time
S2D, W, 80% Dispersive, Burn @ Vessel Failure
Class III, Case 5B



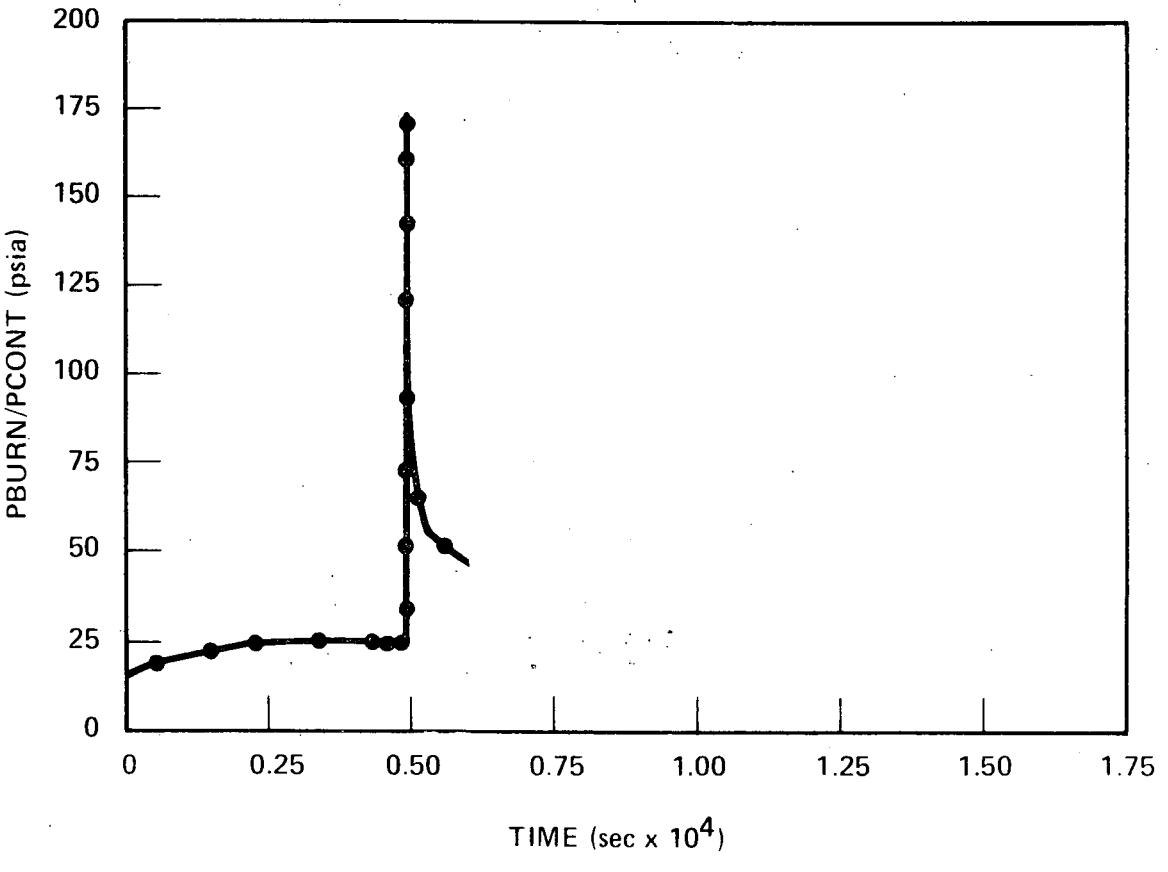
Mass Hydrogen (in Containment) vs. Time
S2D, W, 80% Dispersive, Burn @ Vessel Failure
Class III, Case 5B



Mole Fraction H_2 (in Containment) vs. Time
S2D, W, 80% Dispersive, Burn @ Vessel Failure
Class III, Case 5B



Flame Temperature (in Containment) vs. Time
S2D, W, 80% Dispersive, Burn @ Vessel Failure
Class III, Case 5B



Adiabatic Burn Pressure/Pressure in Containment vs. Time
S2D, W, 80% Dispersive, Burn @ Vessel Failure
Class III, Case 5 B

CASE: CLASS III, CASE 6A, S2D, W, 50% DISPERSIVE, NO BURN

DISPERSIVE: YES PERCENT CORE: 50 FRACTION IN CAVITY: 0.50

RUN #: AALAAGN DATE: 11/15/80

BLOWDOWN PEAK: _____ PSIA TIME: _____ SEC.

HYDROGEN BURN?: NO CRITERIA: _____

TIME @ BURN: _____ SEC, PRESSURE: _____ PSIA, TEMPERATURE: _____ °F

PEAKS:

PRESSURE: 95 PSIA, TIME: 4898.3 SEC, WHY?: END OF DISPERSION

TEMPERATURE: 699 °F, TIME: 4898 SEC, WHY?: END OF DISPERSION

DISPERSION: YES

PRESSURE: 95 PSIA, TIME: 4868.3 SEC, WHY?: VESSEL FAILURE/ BEGINNING OF SPERT

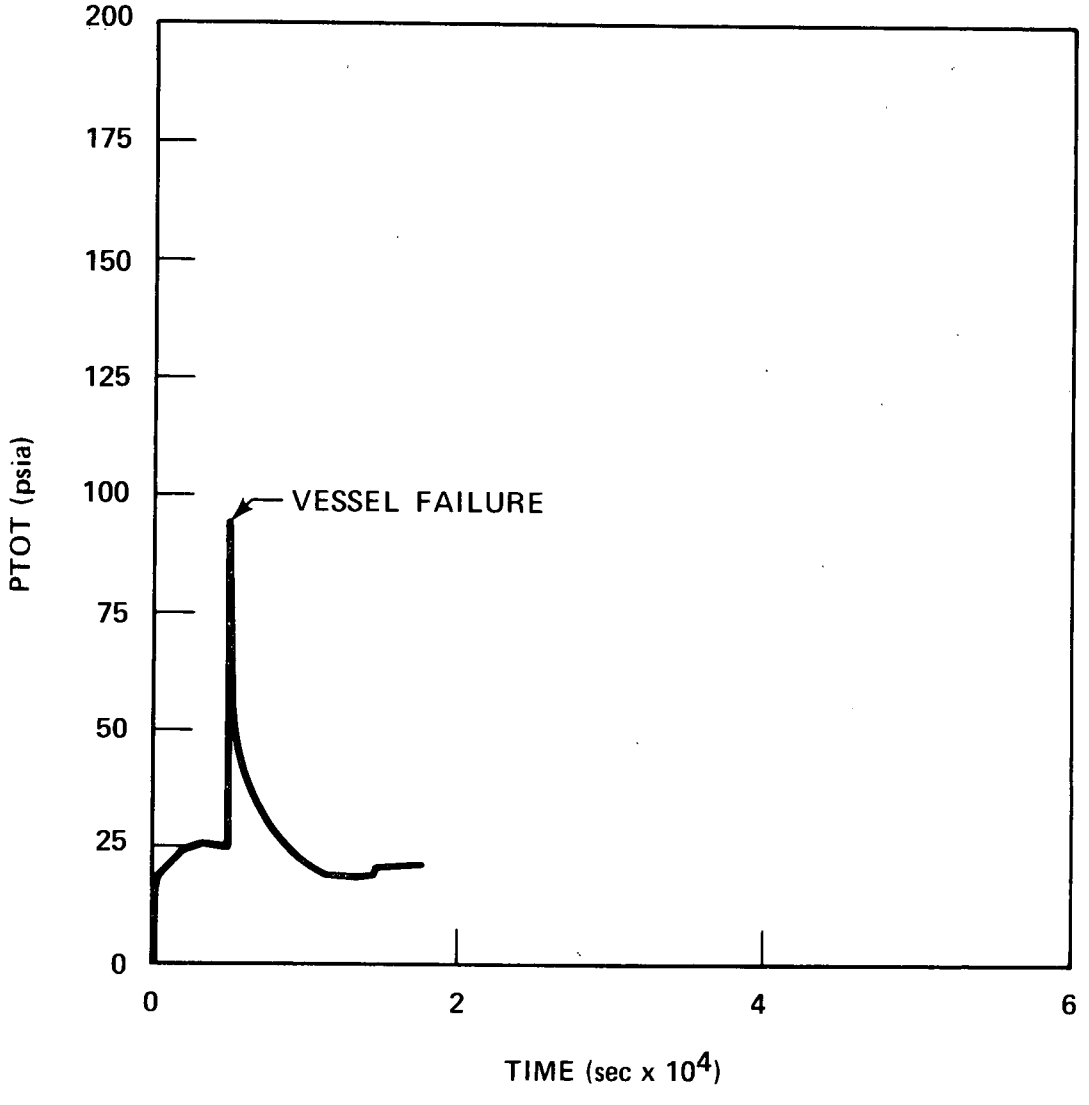
TEMPERATURE: 699 °F, TIME: 4868.3 SEC, WHY?: VESSEL FAILURE/ BEGINNING OF SPERT

END OF BOIL: 4865.4 SEC. END OF HEAD: 4868.3 SEC.

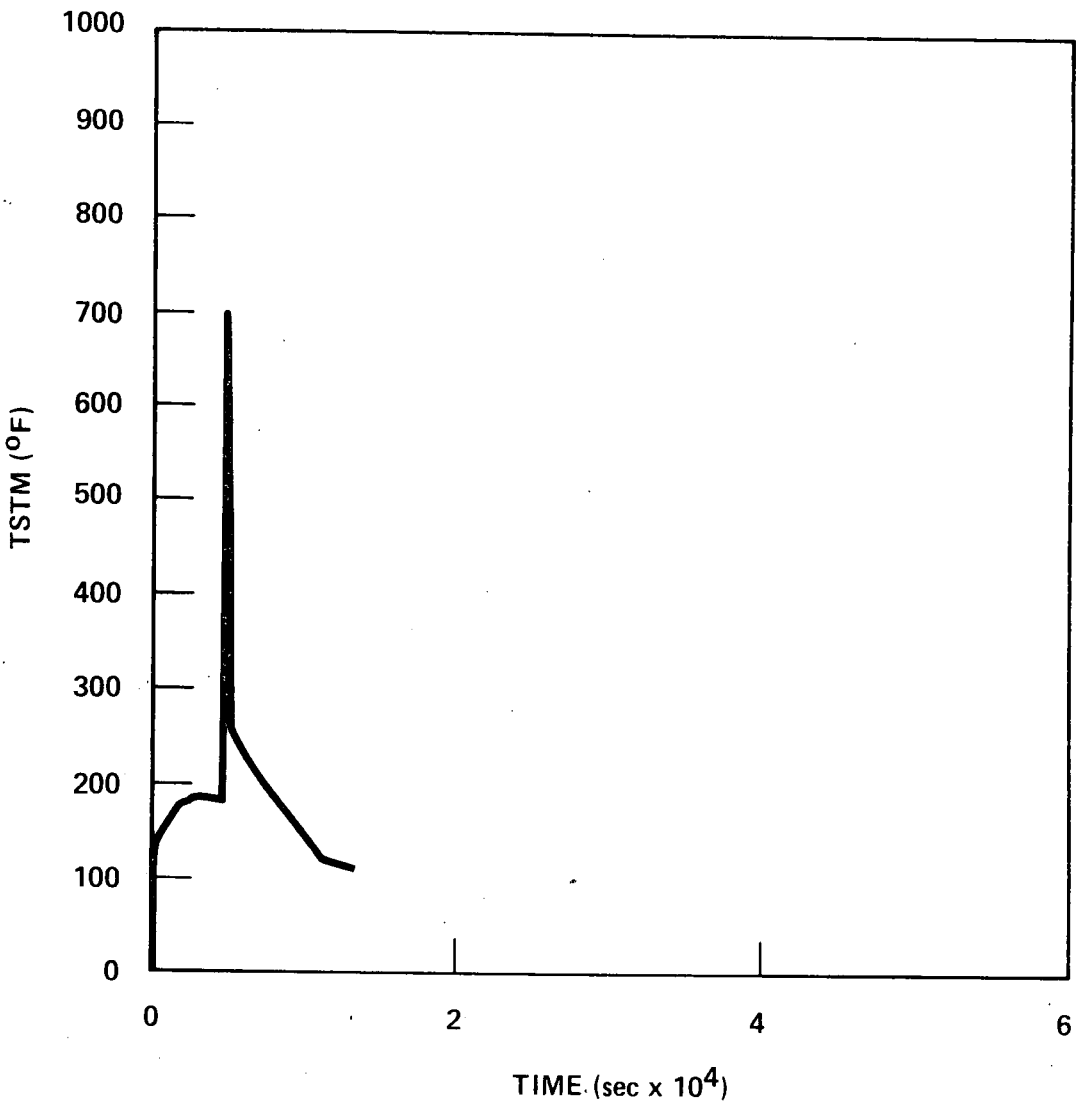
VESSEL FAILURE: 4868.3 SEC. END OF HOTDROP: _____ SEC.

END OF INTER: 8631.9 SEC.

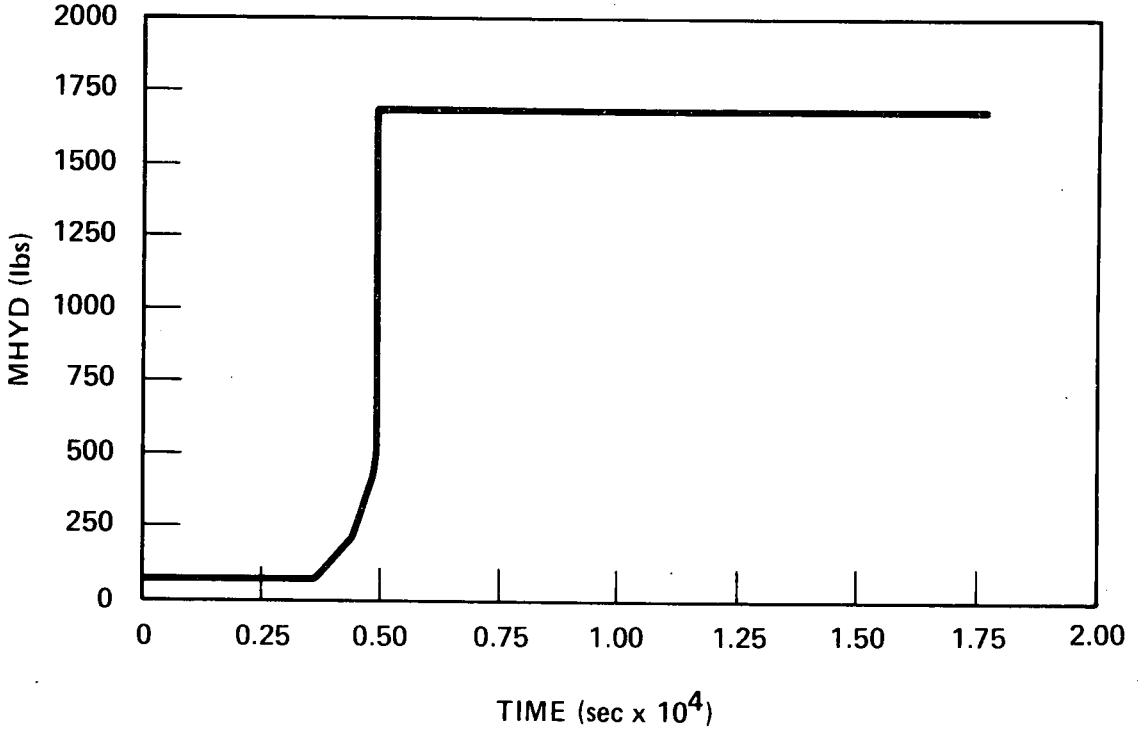
Class III, Case 6A



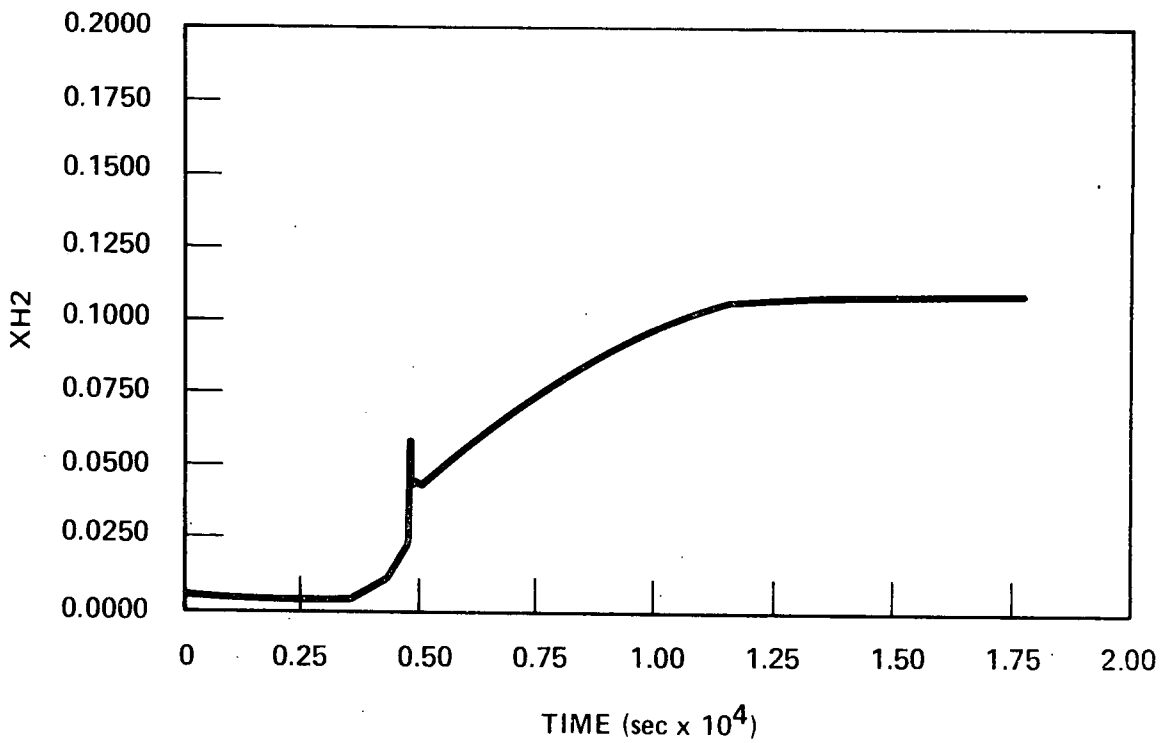
Pressure (in Containment) vs. Time
S2D, W, 50% Dispersive, No Burn
Class III, Case 6A



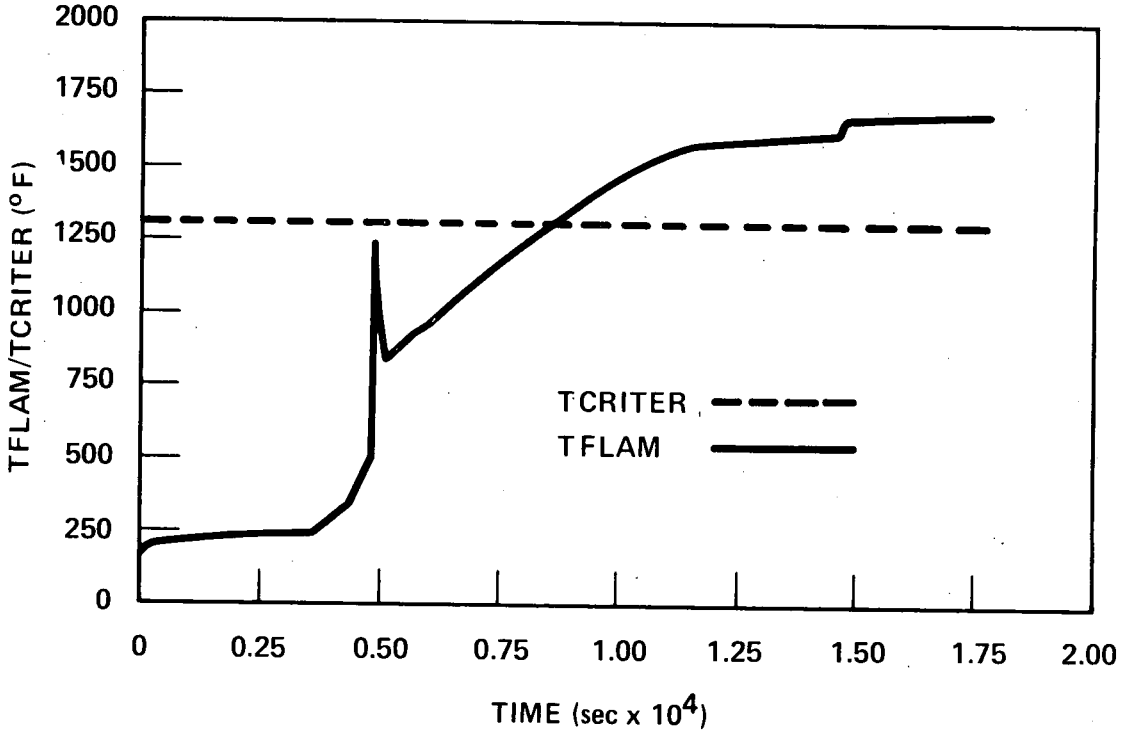
Temperature (in Containment) vs. Time
S2D, W, 50% Dispersive, No Burn
Class III, Case 6A



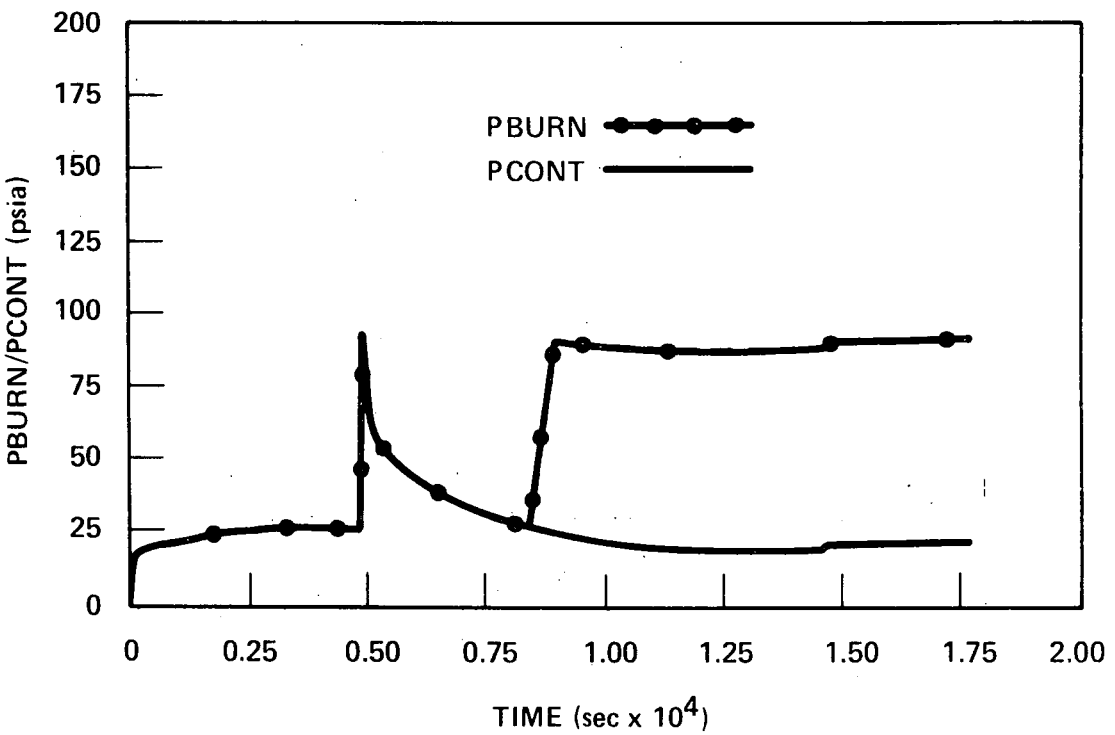
Mass Hydrogen (in Containment) vs. Time
S2D, W, 50% Dispersive, No Burn
Class III, Case 6A



Moel Fraction H_2 (in Containment) vs. Time
S2D, W, 50% Dispersive, No Burn
Class III, Case 6A



Flame Temperature (in Containment) vs. Time
S2D, W, 50% Dispersive, No Burn
Class III, Case 6A



Adiabatic Burn Pressure/Pressure in Containment vs. Time
S2D, W, 50% Dispersive, No Burn
Class III, Case 6A

CASE: CLASS III, CASE 6B, S2D, W, 50% DISPERSIVE, BURN @ VESSEL FAILURE

DISPERSIVE: YES PERCENT CORE: 50 FRACTION IN CAVITY: 0.50

RUN #: AALAAGO DATE: 11/15/80

BLOWDOWN PEAK: _____ PSIA TIME: _____ SEC.

HYDROGEN BURN?: YES CRITERIA: VESSEL FAILURE

TIME @ BURN: 4897.1 SEC, PRESSURE: 93 PSIA, TEMPERATURE: 694 °F

PEAKS:

PRESSURE: 137 PSIA, TIME: 4917.3 SEC, WHY?: VESSEL FAILURE/H_2 BURN @ END OF DISPERSION

TEMPERATURE: 1269 °F, TIME: 4917 SEC, WHY?: VESSEL FAILURE/H_2 BURN @ END OF DISPERSION

DISPERSION: YES

PRESSURE: 137 PSIA, TIME: 4868.3 SEC,

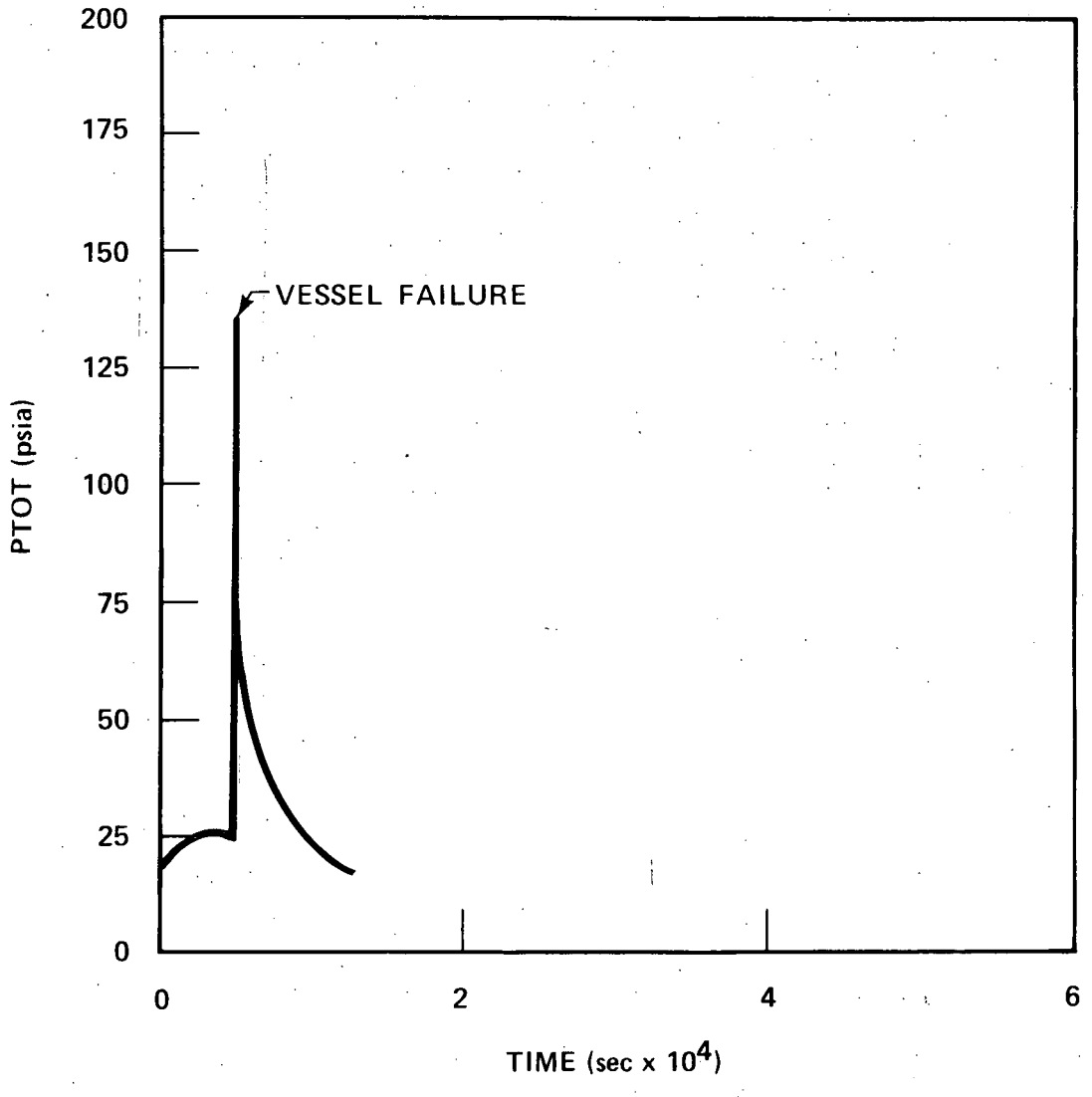
TEMPERATURE: 1269 °F, TIME: 4868.3 SEC,

END OF BOIL: 4865.4 SEC. END OF HEAD: 4868.3 SEC.

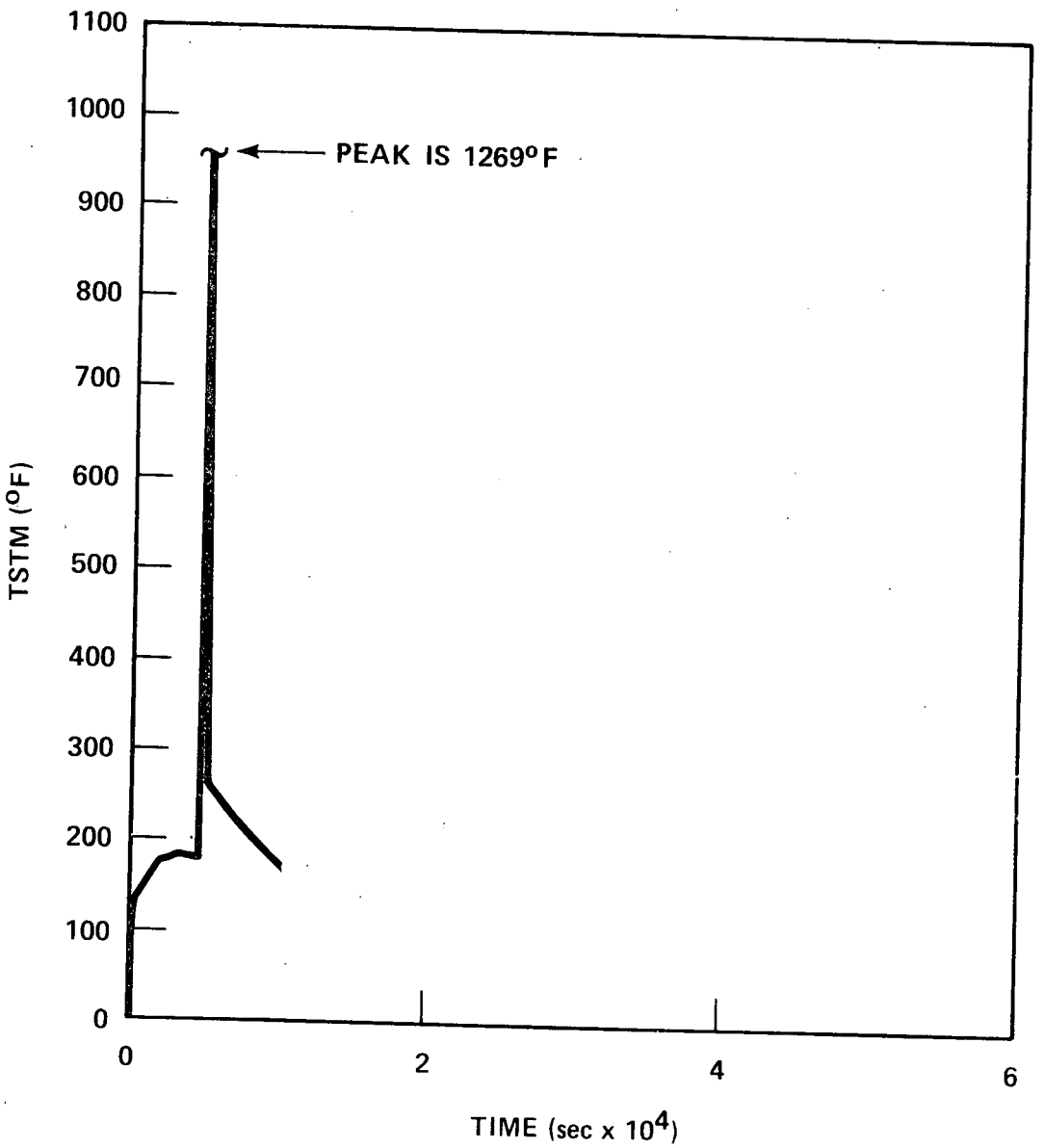
VESSEL FAILURE: 4868.3 SEC. END OF HOTDROP: _____ SEC.

END OF INTER: 86319 SEC.

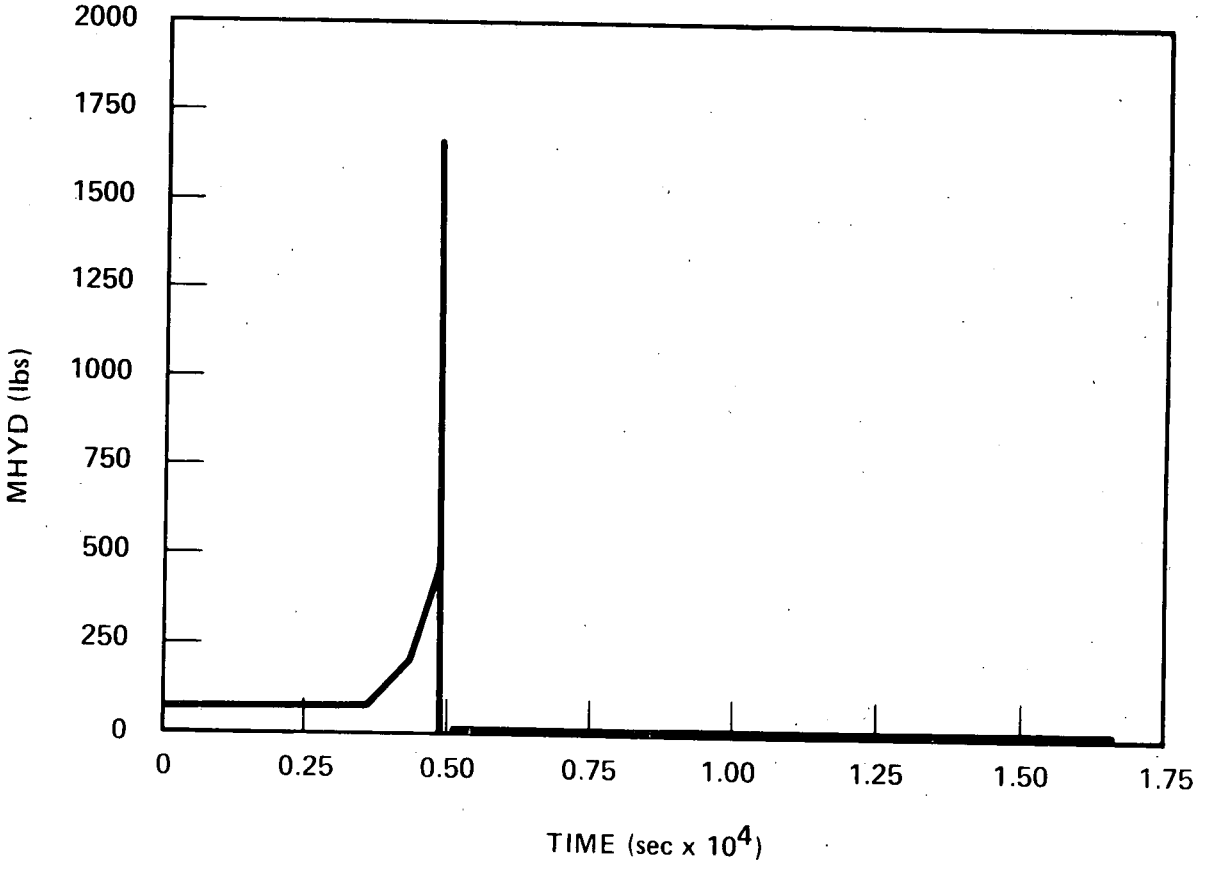
Class III, Case 6B



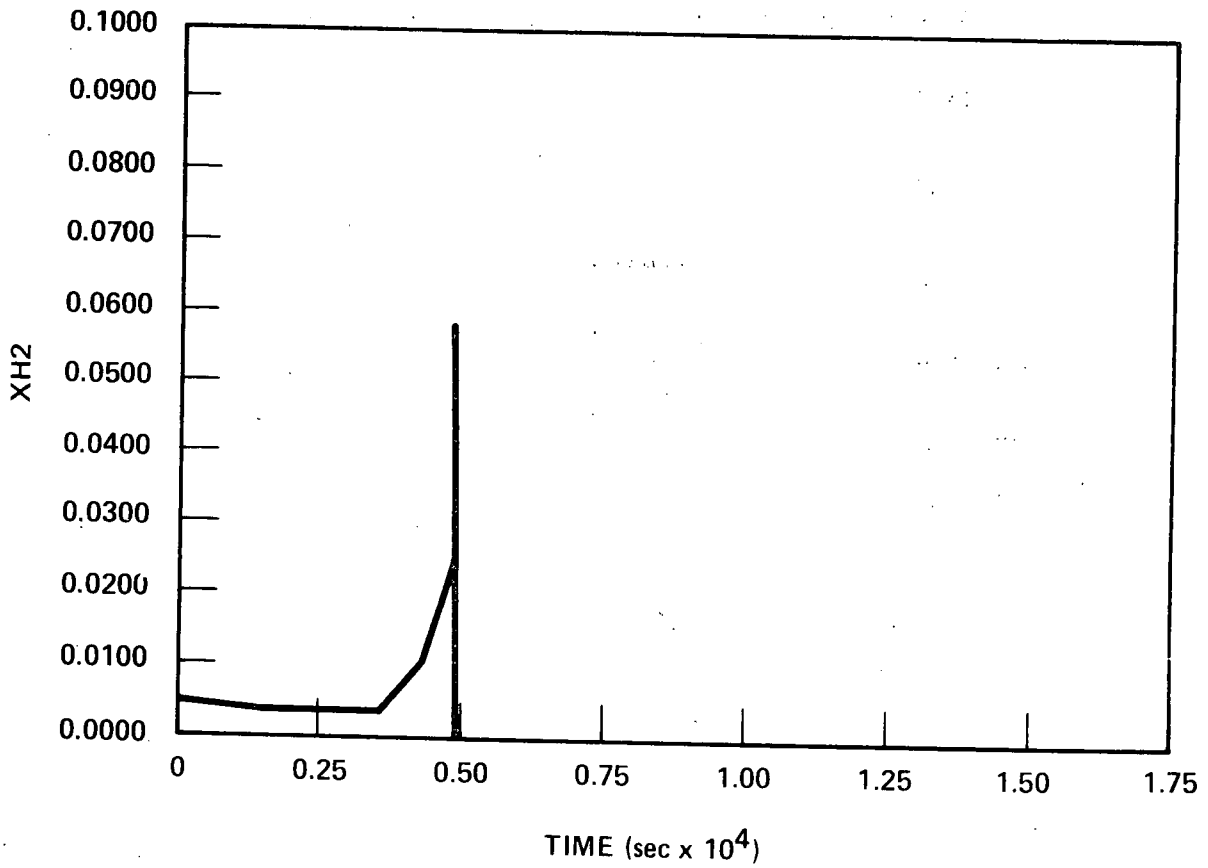
Pressure (in Containment) vs. Time
S2D, W, 50% Dispersive, Burn @ Vessel Failure
Class III, Case 6B



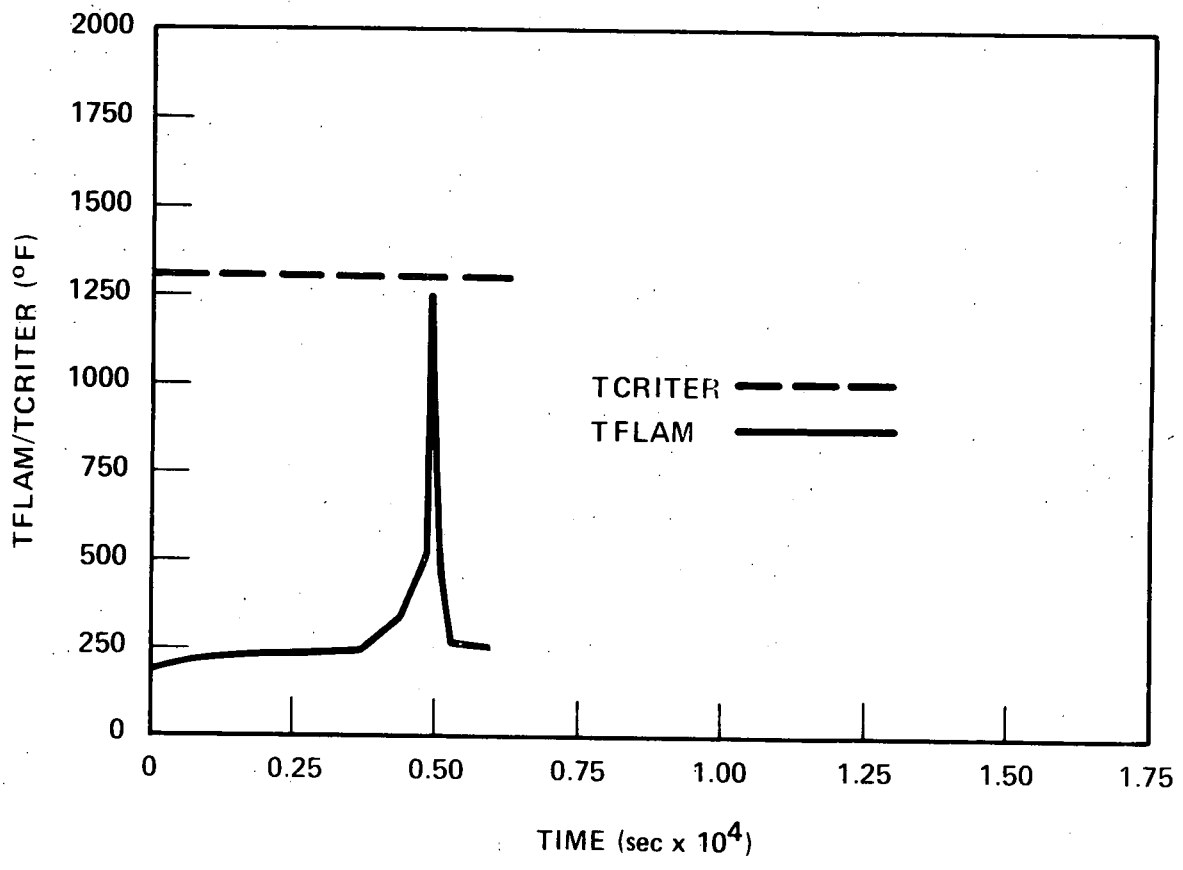
Temperature (in Containment) vs. Time
S2D, W, 50% Dispersive, Burn @ Vessel Failure
Class III, Case 6B



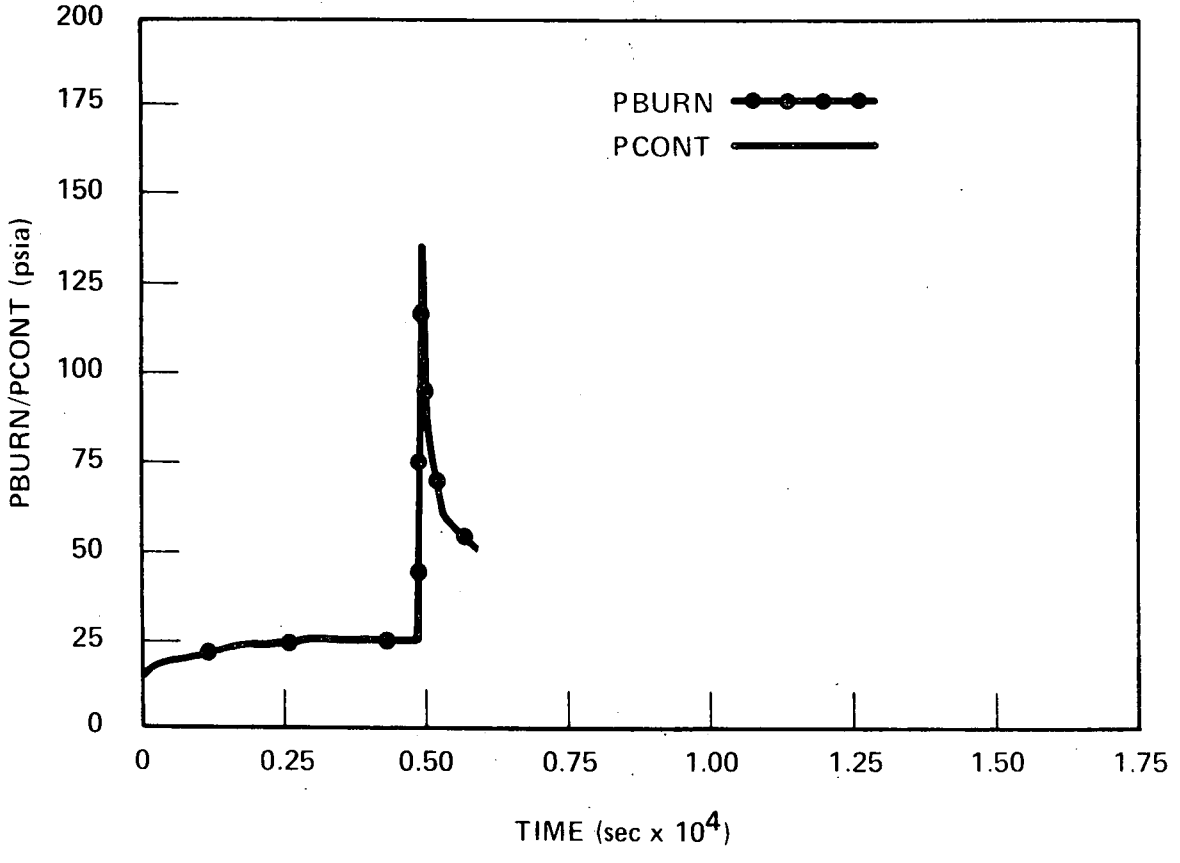
Mass Hydrogen (in Containment) vs. Time
S2D, W, 50% Dispersive, Burn @ Vessel Failure
Class III, Case 6B



Mole Fraction H_2 (in Containment) vs. Time
S2D, W, 50% Dispersive, Burn @ Vessel Failure
Class III, Case 6B



Flame Temperature (in Containment) vs. Time
S2D, W, 50% Dispersive, Burn @ Vessel Failure
Class III, Case 6B



Adiabatic Burn Pressure/Pressure in Containment vs. Time
S2D, W, 50% Dispersive, Burn @ Vessel Failure
Class III, Case 6B

CASE: CLASS III, CASE 7A, S2D, B, 80% DISPERSIVE, NO BURN

DISPERSIVE: YES PERCENT CORE: 80 FRACTION IN CAVITY: 0.20

RUN #: AALAACO DATE: 11/15/80

BLOWDOWN PEAK: N/A PSIA TIME: _____ SEC.

HYDROGEN BURN?: NO CRITERIA: _____

TIME @ BURN: _____ SEC, PRESSURE: _____ PSIA, TEMPERATURE: _____ °F

PEAKS:

PRESSURE: 104 PSIA, TIME: 4897 SEC, WHY?: END OF DISPERSION

TEMPERATURE: 907 °F, TIME: 4897 SEC, WHY?: END OF DISPERSION

DISPERSIVE:

PRESSURE: 104 PSIA, TIME: 4897 SEC,

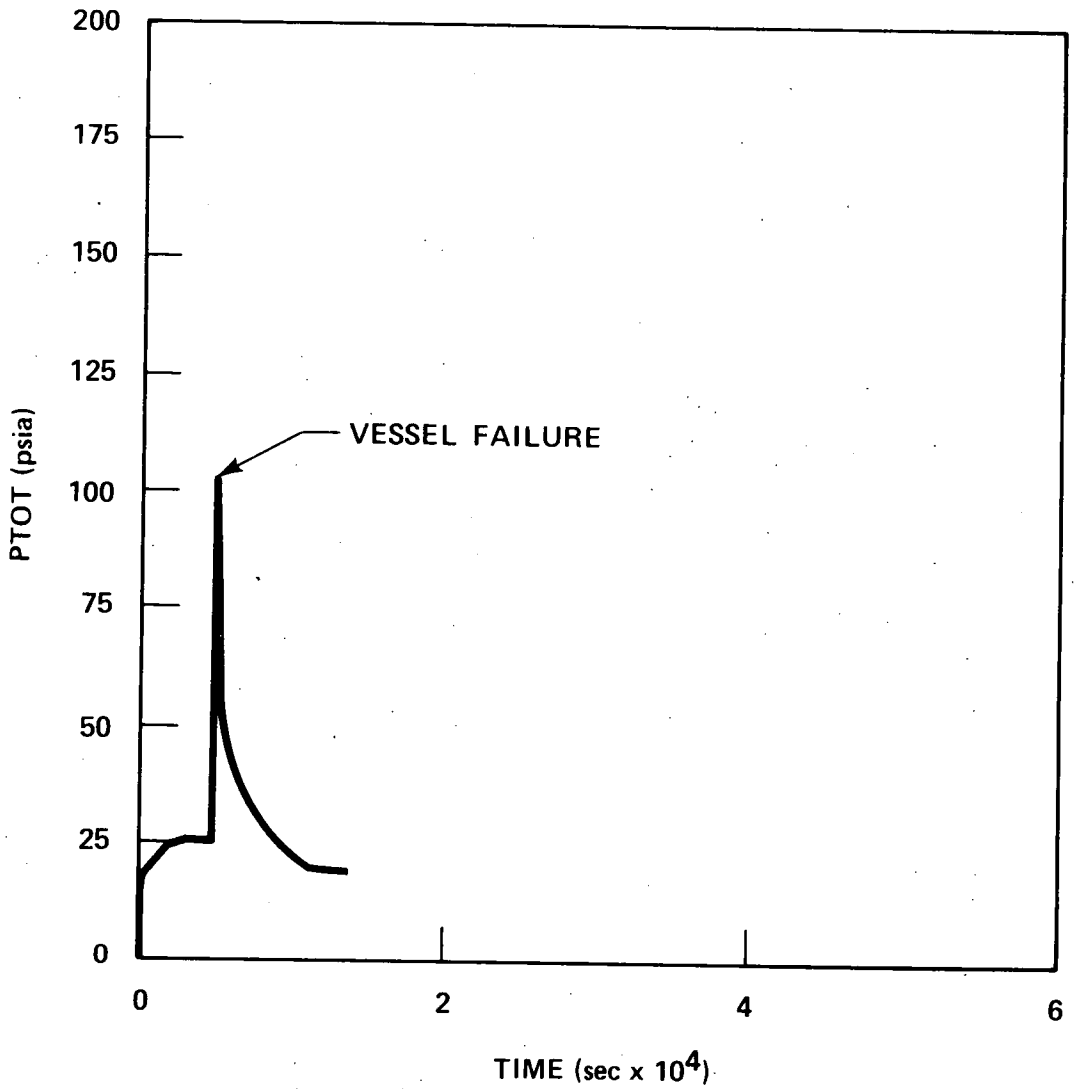
TEMPERATURE: 907 °F, TIME: 4897 SEC,

END OF BOIL: 4864.5 SEC. END OF HEAD: 4867.1 SEC.

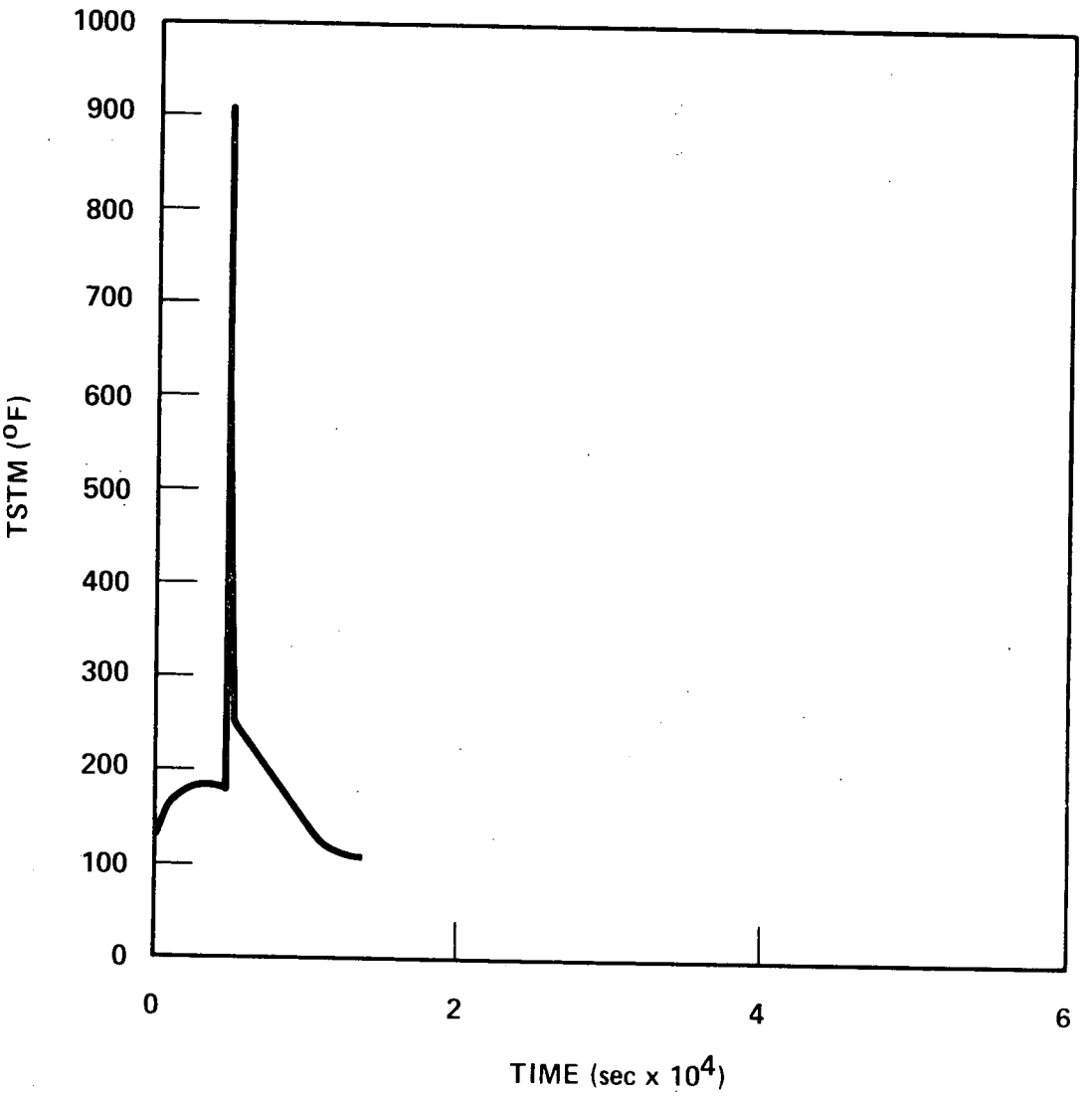
VESSEL FAILURE: 4867.1 SEC. END OF HOTDROP: 10394 SEC.

END OF INTER: 86947 SEC.

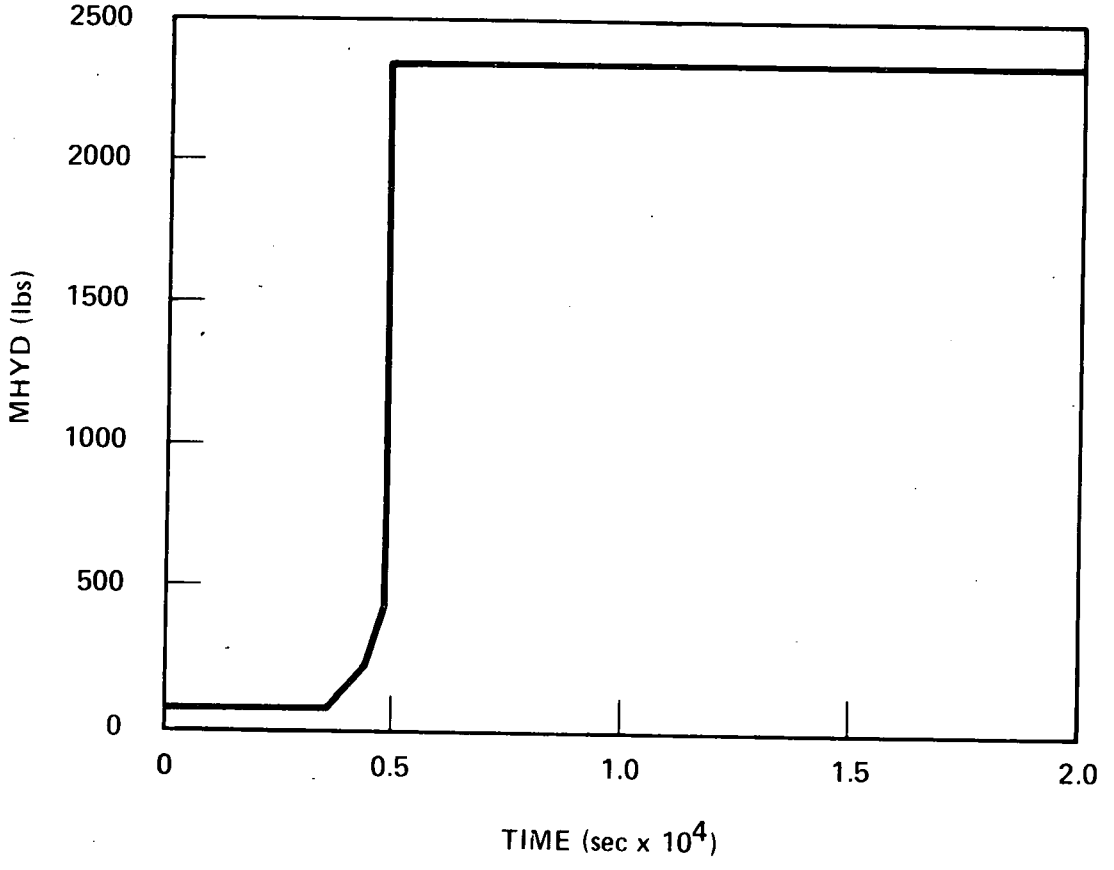
Class III, Case 7A



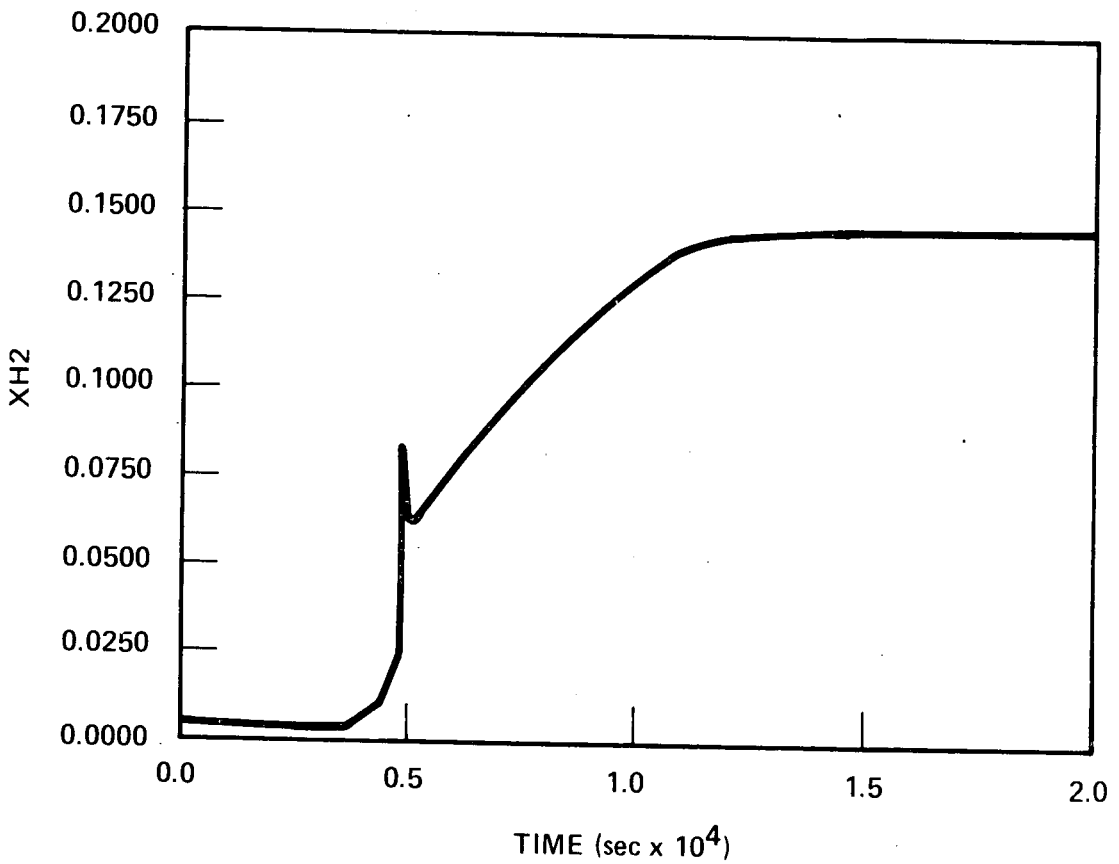
Pressure (in Containment) vs. Time
S2D, B, 80% Dispersive, No Burn
Class III, Case 7A



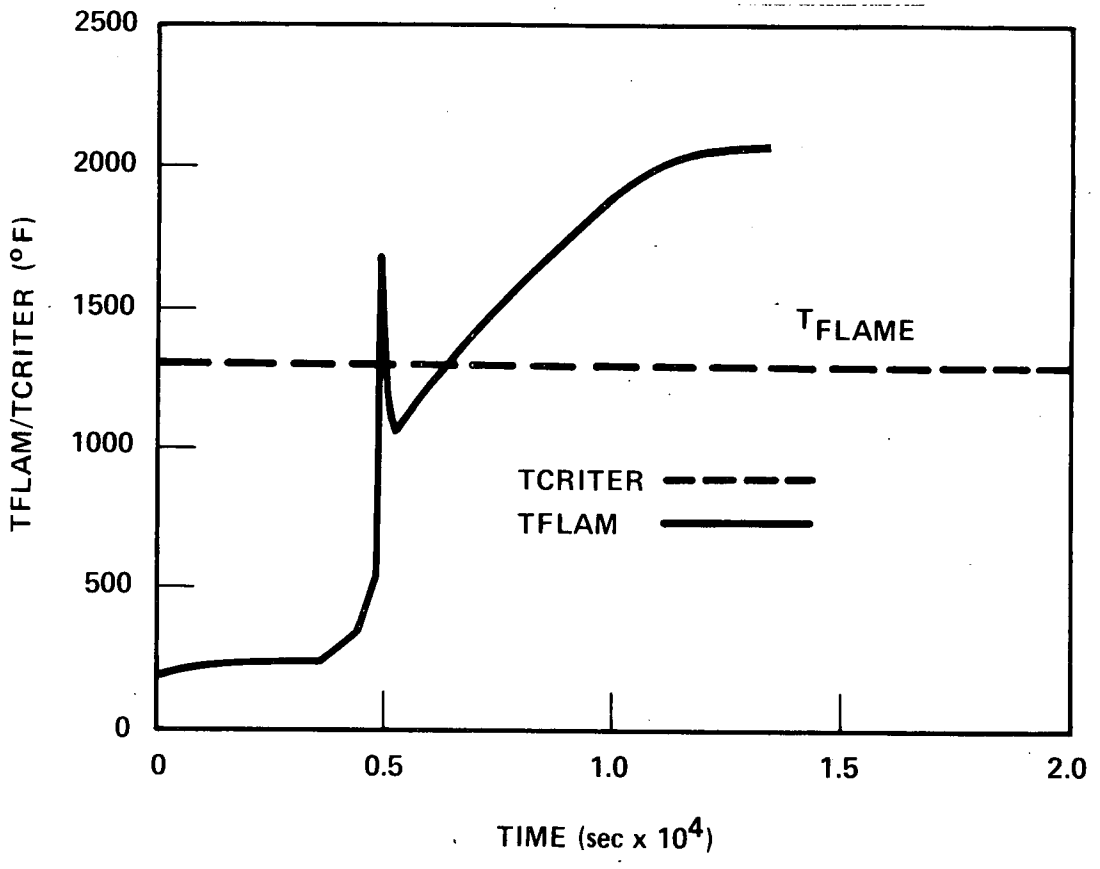
Temperature (in Containment) vs. Time
S2D, 80% Dispersive, No Burn
Class III, Case 7A



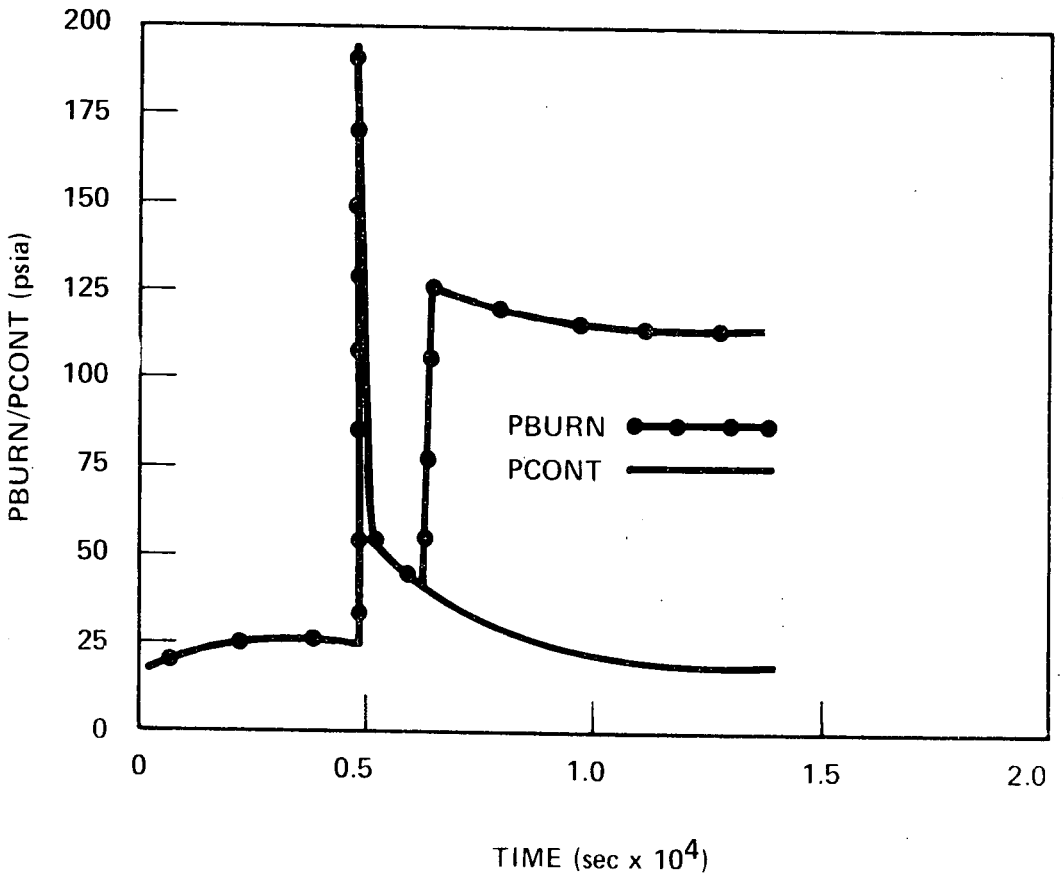
Mass Hydrogen (in Containment) vs. Time
S2D, B, 80% Dispersive, No Burn
Class III, Case 7A



Mole Fraction H_2 (in Containment) vs. Time
S2D, B, 80% Dispersive, No Burn
Class III, Case 7A



Flame Temperature (in Containment) vs. Time
S2D, B, 80% Dispersive, No Burn
Class III, Case 7A



Adiabatic Burn Pressure/Pressure in Containment vs. Time
S2D, B, 80% Dispersive, No Burn
Class III, Case 7A

CASE: CLASS III, CASE 7B, S2D, B, 80% DISPERSIVE, BURN @ VESSEL FAILURE

DISPERSIVE: YES PERCENT CORE: 80 FRACTION IN CAVITY: 0.20

RUN #: AALAACY DATE: 11/15/80

BLOWDOWN PEAK: _____ PSIA TIME: _____ SEC.

HYDROGEN BURN?: YES CRITERIA: VESSEL FAILURE

TIME @ BURN: 4897.1 SEC, PRESSURE: 104 PSIA, TEMPERATURE: 907 °F

PEAKS:

PRESSURE: 155 PSIA, TIME: 4917.2 SEC, WHY?: VESSEL FAILURE/H_2 BURN (END OF DISPERSION)

TEMPERATURE: 1668 °F, TIME: 4917 SEC, WHY?: VESSEL FAILURE/H_2 BURN (END OF DISPERSION)

SPERT: YES

PRESSURE: 155 PSIA, TIME: 4867.1 SEC,

TEMPERATURE: 1668 °F, TIME: 4867.1 SEC,

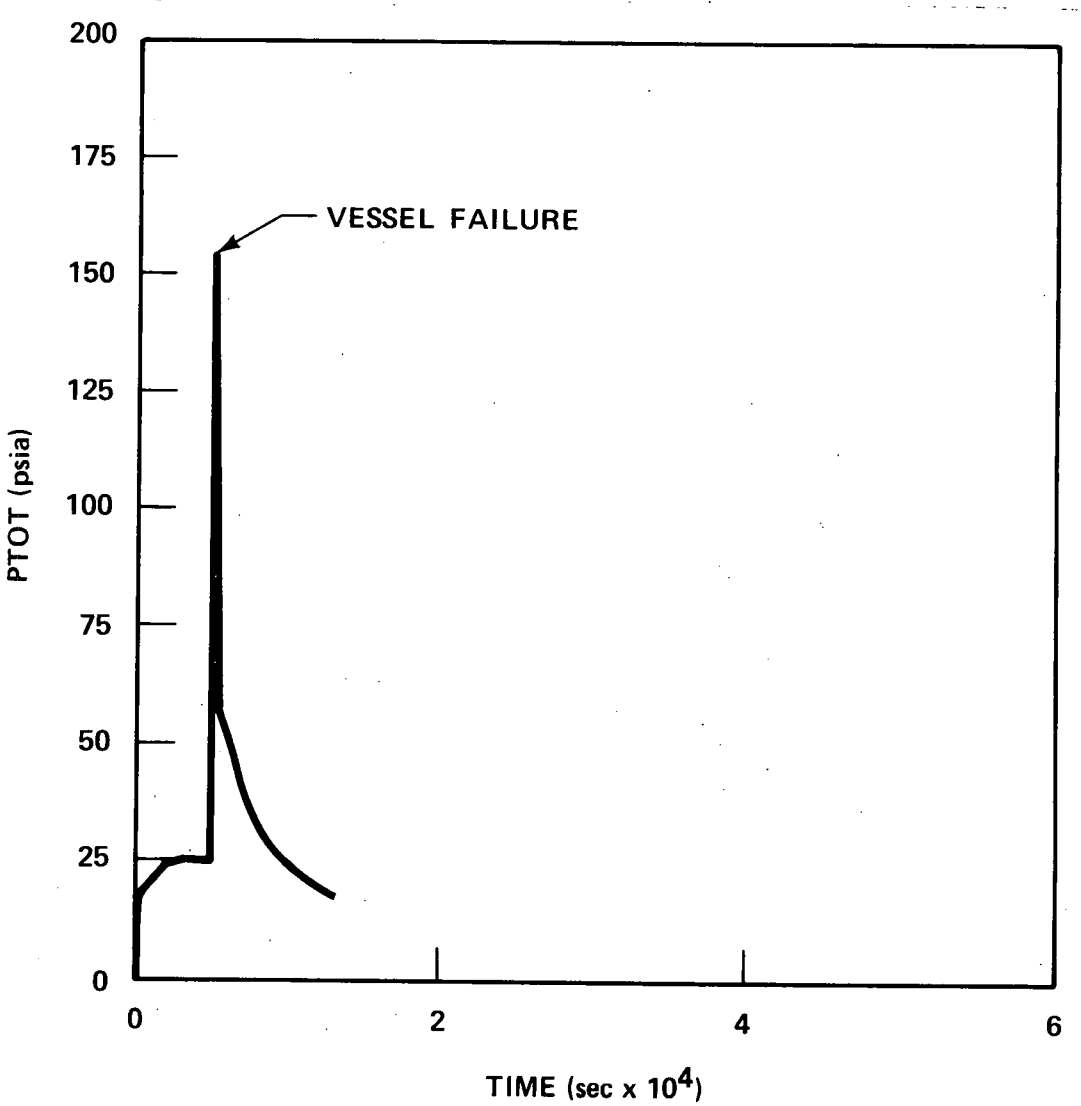
END OF BOIL: 4864.5 SEC. END OF HEAD: 4867.1 SEC.

VESSEL FAILURE: 4867.1 SEC. END OF HOTDROP: 10394 SEC.

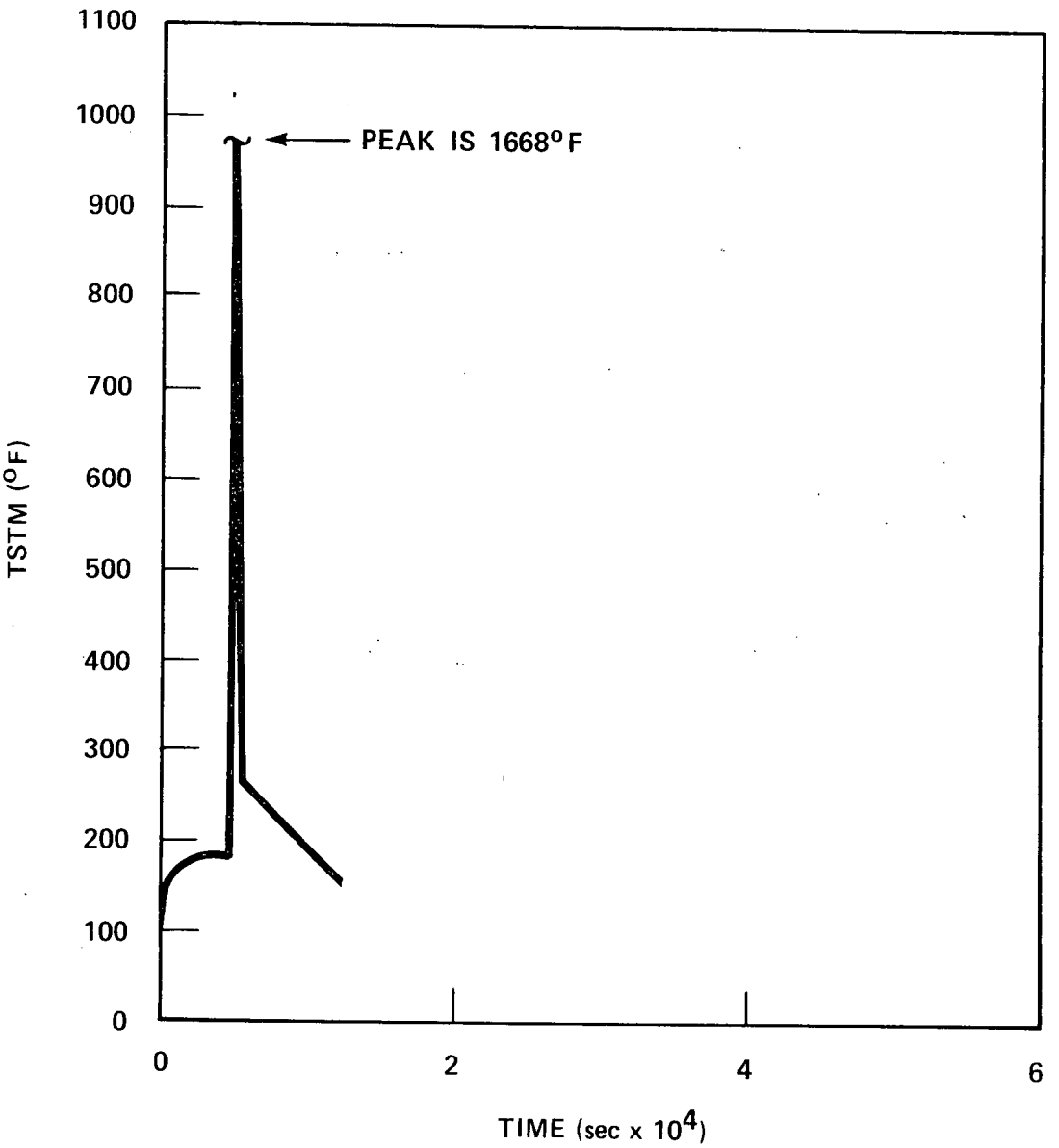
END OF INTER: 86947 SEC.

Class III, Case 7B

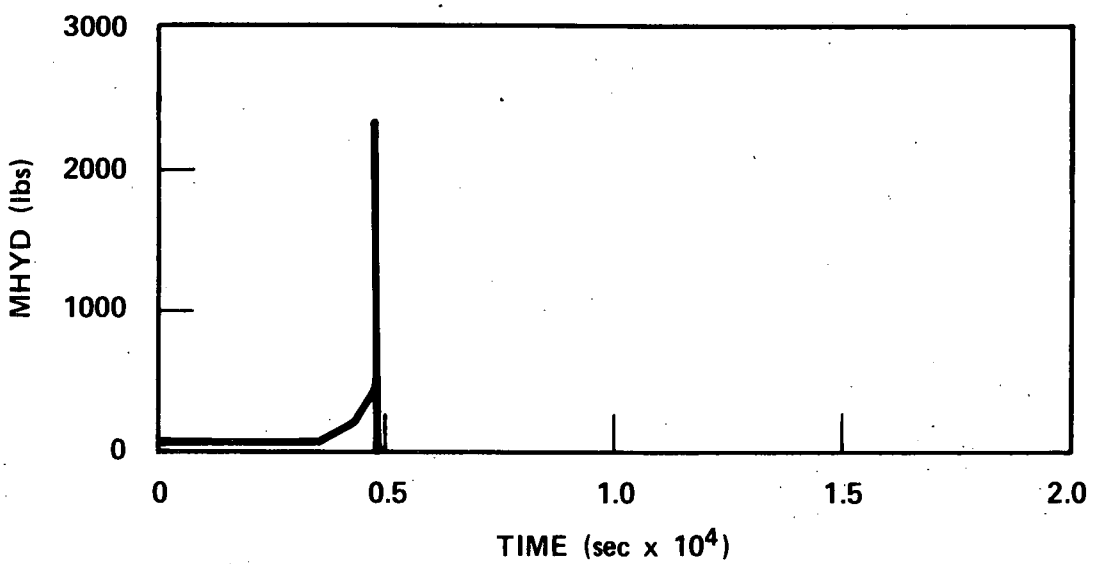
Sheet 1 of 7



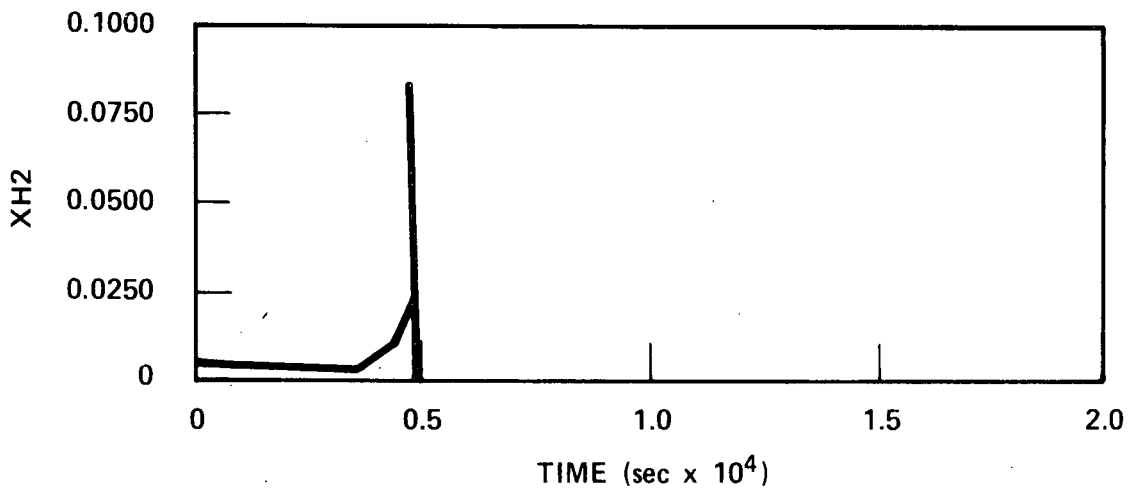
Pressure (in Containment) vs. Time
S2D, B, 80% Dispersive, Burn @ Vessel Failure
Class III, Case 7B



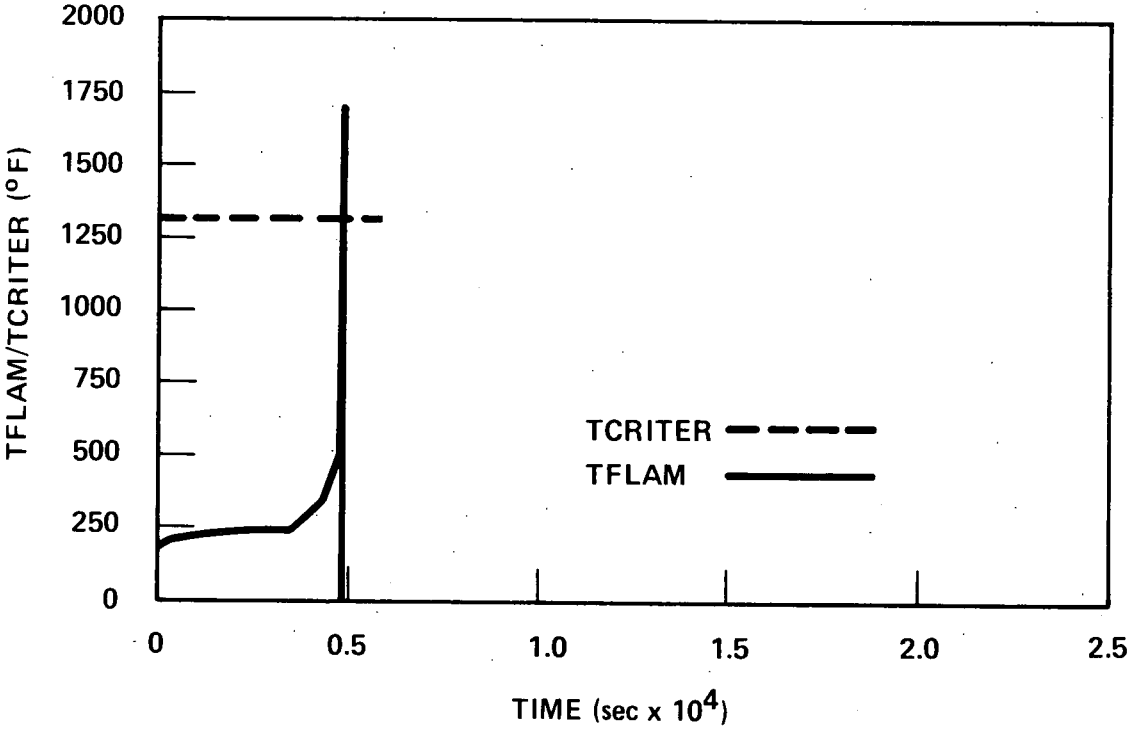
Temperature (in Containment) vs. Time
S2D, B, 80% Dispersive, Burn @ Vessel Failure
Class III, Case 7B



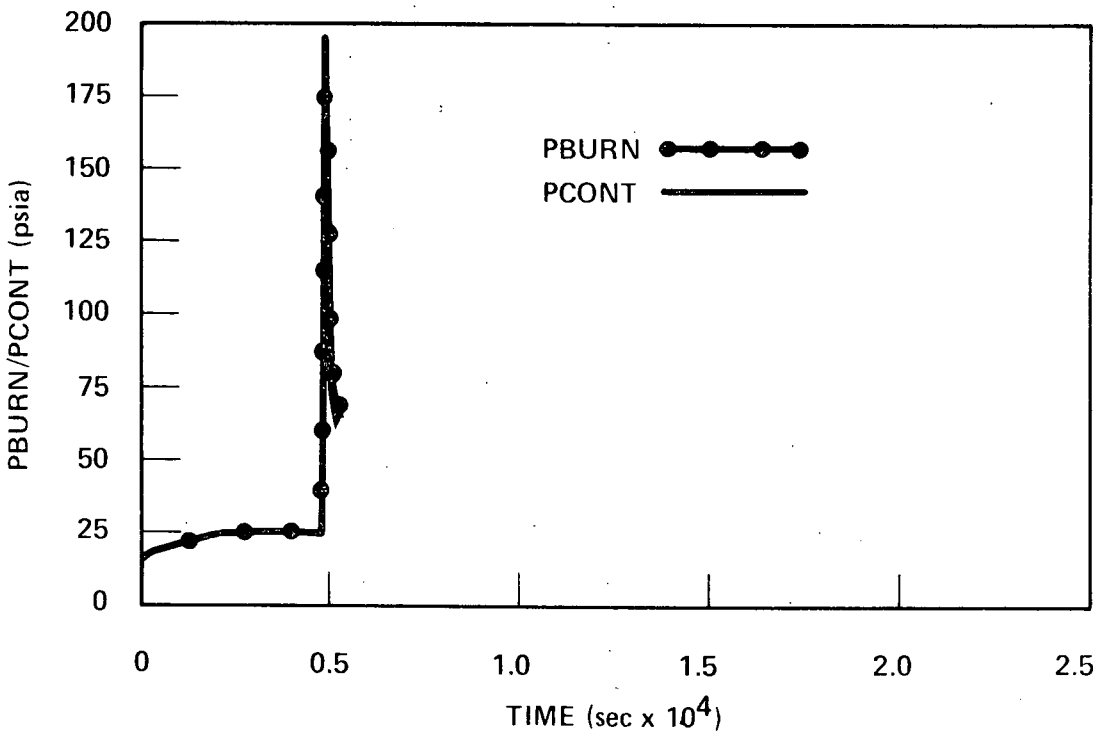
Mass Hydrogen (in Containment) vs. Time
S2D, B, 80% Dispersive, Burn @ Vessel Failure
Class III, Case 7B



Mole Fraction H_2 (in Containment) vs. Time
S2D, B, 80% Dispersive, Burn @ Vessel Failure
Class III, Case 7B



Flame Temperature (in Containment) vs. Time
S2D, B, 80% Dispersive, Burn @ Vessel Failure
Class III, Case 7B



Adiabatic Burn Pressure/Pressure in Containment vs. Time
S2D, B, 80% Dispersive, Burn @ Vessel Failure
Class III, Case 7B

CASE: CLASS IV, CASE 1A, S2HF, B, NO BURN, NON-DISPERSIVE

DISPERSIVE: NO PERCENT CORE: _____ FRACTION IN CAVITY: _____

RUN #: AALABDX DATE: 12/31/80

BLOWDOWN PEAK: N/A PSIA TIME: _____ SEC.

HYDROGEN BURN?: NO CRITERIA: _____

TIME @ BURN: _____ SEC, PRESSURE: _____ PSIA, TEMPERATURE: _____ °F

PEAKS:

PRESSURE: 63 PSIA, TIME: 44822 SEC, WHY?: VESSEL FAILURE

TEMPERATURE: 357 °F, TIME: 44822 SEC, WHY?: VESSEL FAILURE

DISPERSIVE: NO

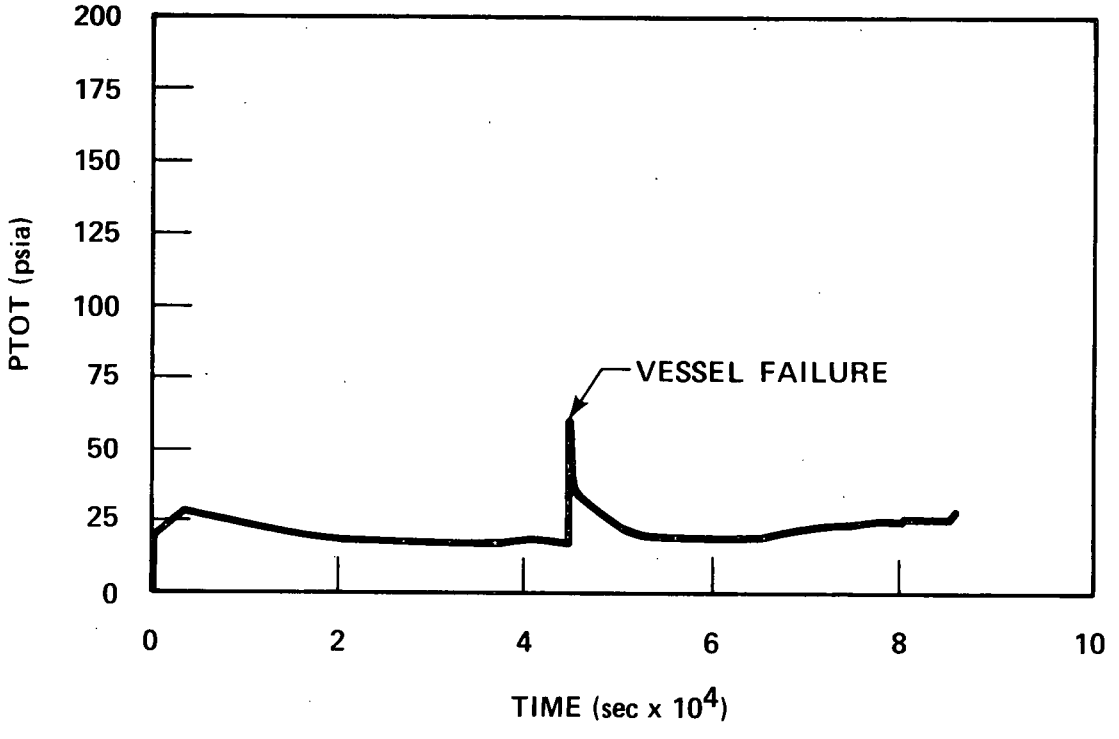
PRESSURE: _____ PSIA, TIME: _____ SEC,

TEMPERATURE: _____ °F, TIME: _____ SEC,

END OF BOIL: 44815 SEC. END OF HEAD: 44816 SEC.

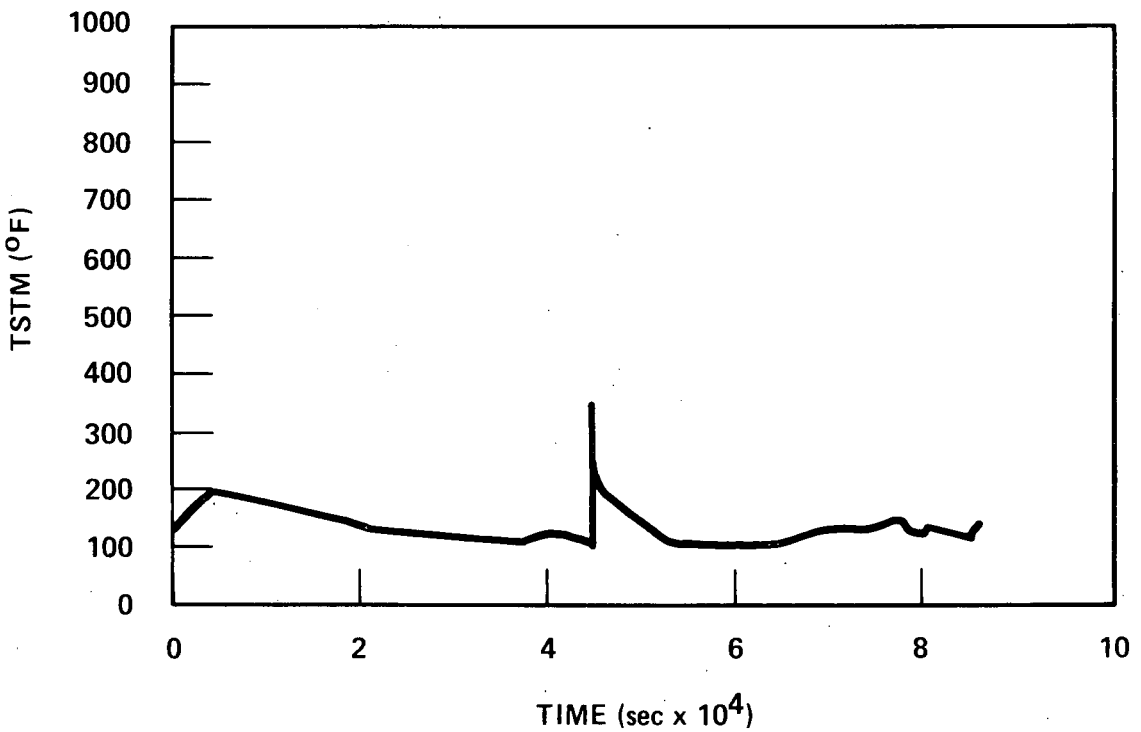
VESSEL FAILURE: 44816 SEC. END OF HOTDROP: 53942 SEC.

END OF INTER: 86037 SEC.

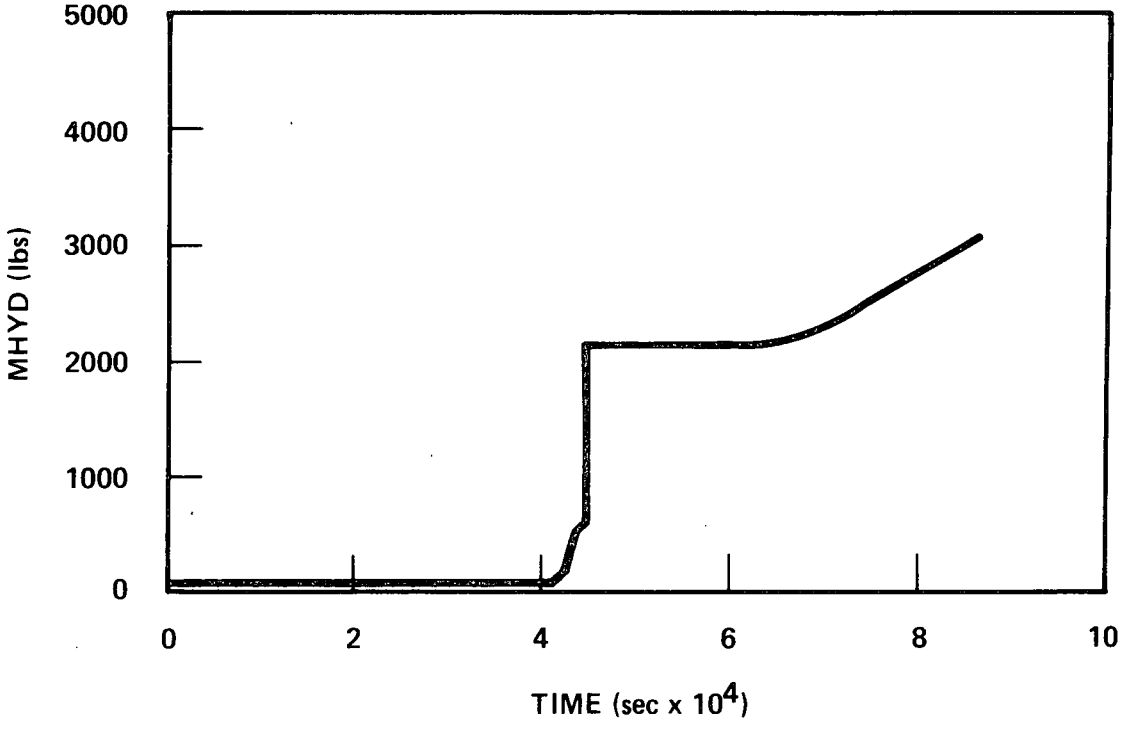


Pressure (in Containment) vs. Time
S2HF, B, No Burn
Class IV, Case 1A

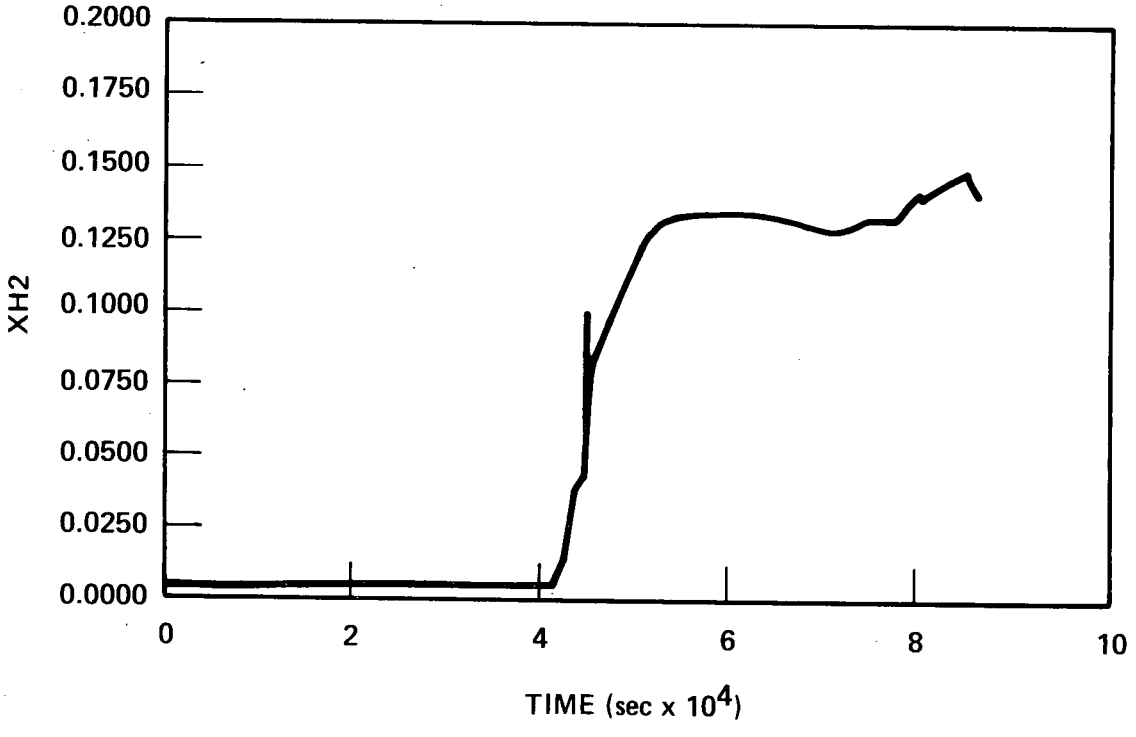
Sheet 2 of 7



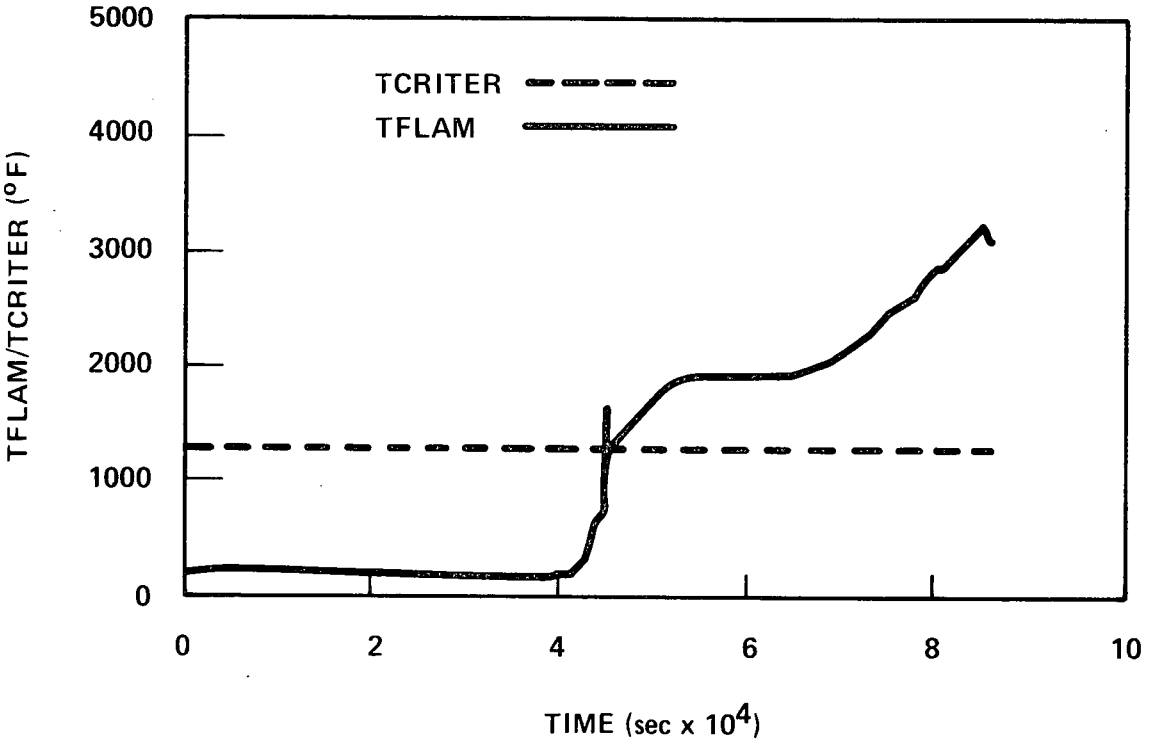
Temperature (in Containment) vs. Time
S2HF, B, No Burn
Class IV, Case 1A



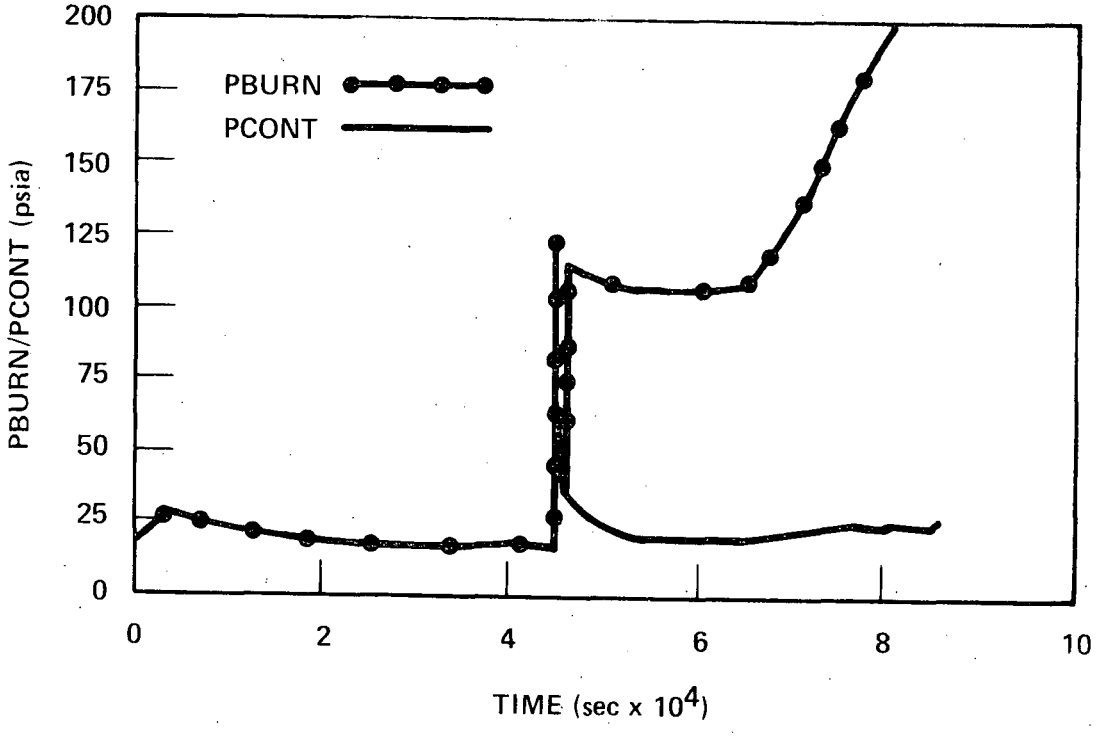
Mass Hydrogen (in Containment) vs. Time
S2HF, B, No Burn
Class IV, Case 1A



Mole Fraction H_2 (in Containment) vs. Time
S2HF, B, No Burn
Class IV, Case 1A



Flame Temperature (in Containment) vs. Time
S2HF, B, No Burn
Class IV, Case 1A



Adiabatic Burn Pressure/Pressure in Containment vs. Time
S2HF, B, No Burn
Class IV, Case 1A

CASE: CLASS IV, CASE 1B, S2HF, B, BURN @ VESSEL FAILURE, NON-DISPERSIVE

DISPERSIVE: NO PERCENT CORE: _____ FRACTION IN CAVITY: _____

RUN #: AALADNO DATE: 12/12/80

BLOWDOWN PEAK: N/A PSIA TIME: _____ SEC.

HYDROGEN BURN?: YES CRITERIA: VESSEL FAILURE

TIME @ BURN: 44816 SEC, PRESSURE: 118 PSIA, TEMPERATURE: >1000 °F

PEAKS:

PRESSURE: 118 PSIA, TIME: 44836.9 SEC, WHY?: BURN @ VESSEL FAILURE

TEMPERATURE: 1167 °F, TIME: 44836.9 SEC, WHY?: BURN @ VESSEL FAILURE

DISPERSIVE: NO

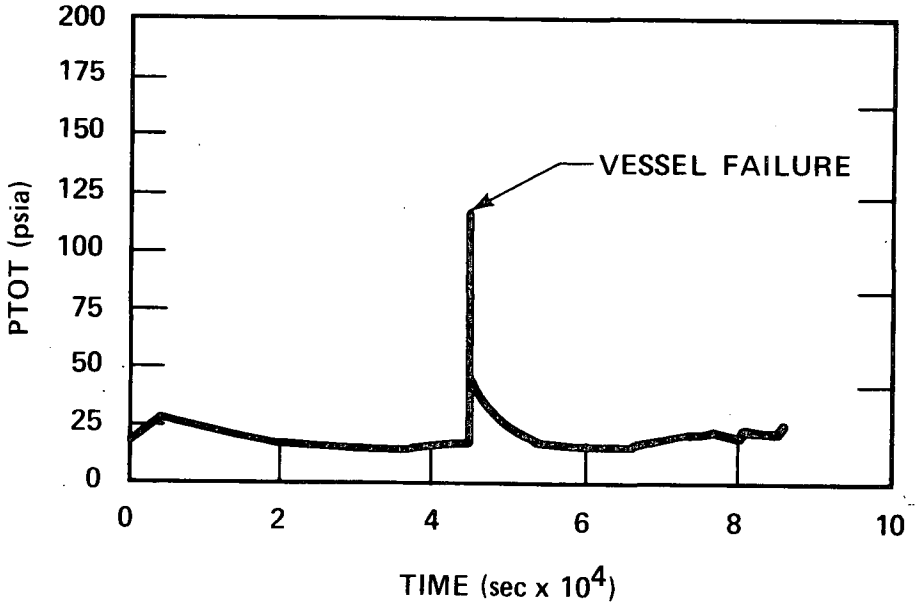
PRESSURE: _____ PSIA, TIME: _____ SEC,

TEMPERATURE: _____ °F, TIME: _____ SEC,

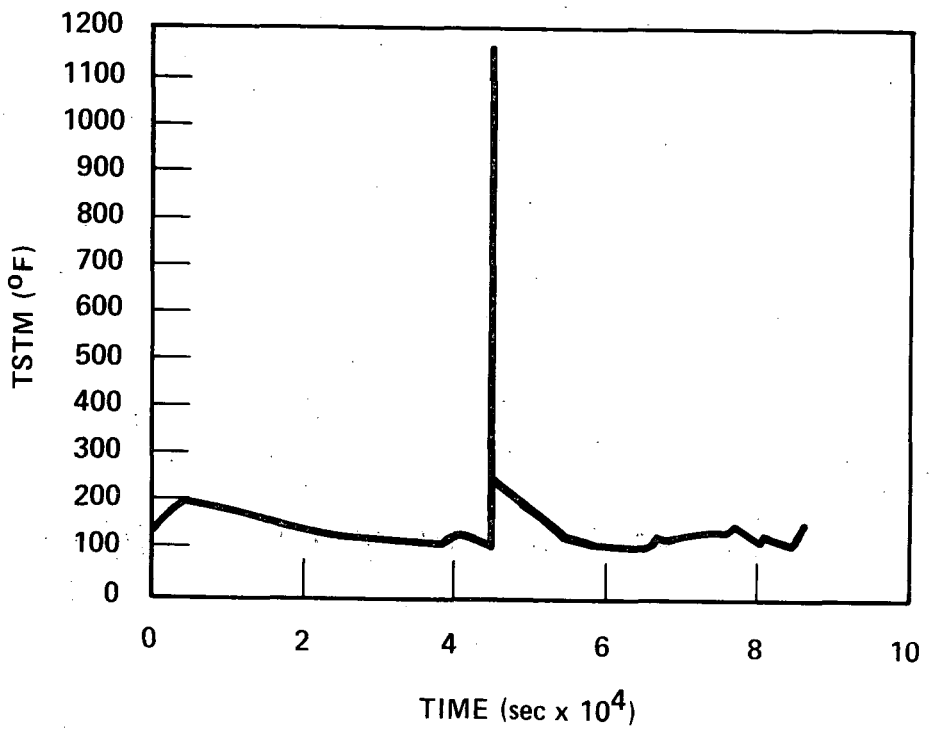
END OF BOIL: 44815 SEC. END OF HEAD: 44816 SEC.

VESSEL FAILURE: 44816 SEC. END OF HOTDROP: 53942 SEC.

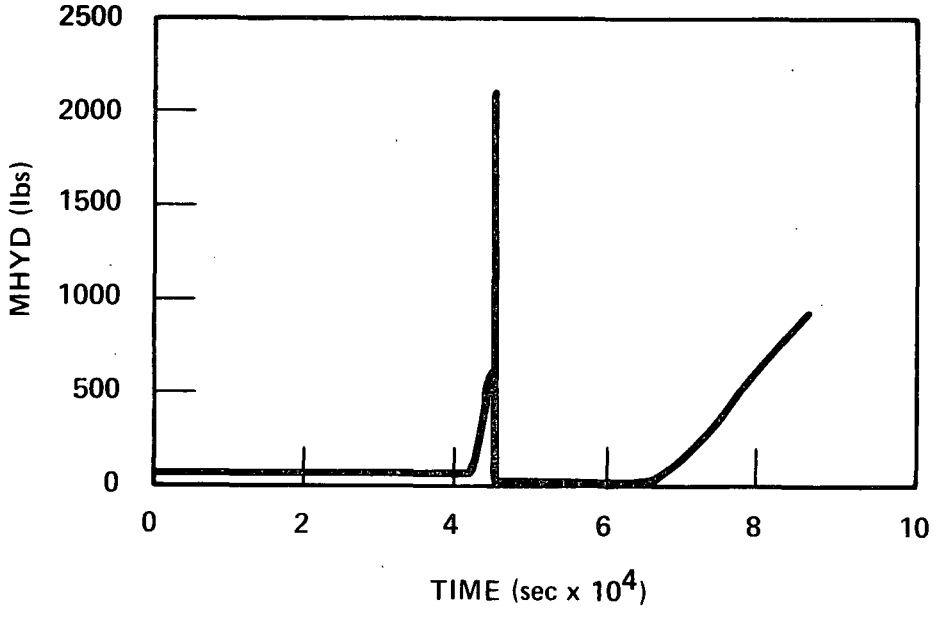
END OF INTER: 86237 SEC.



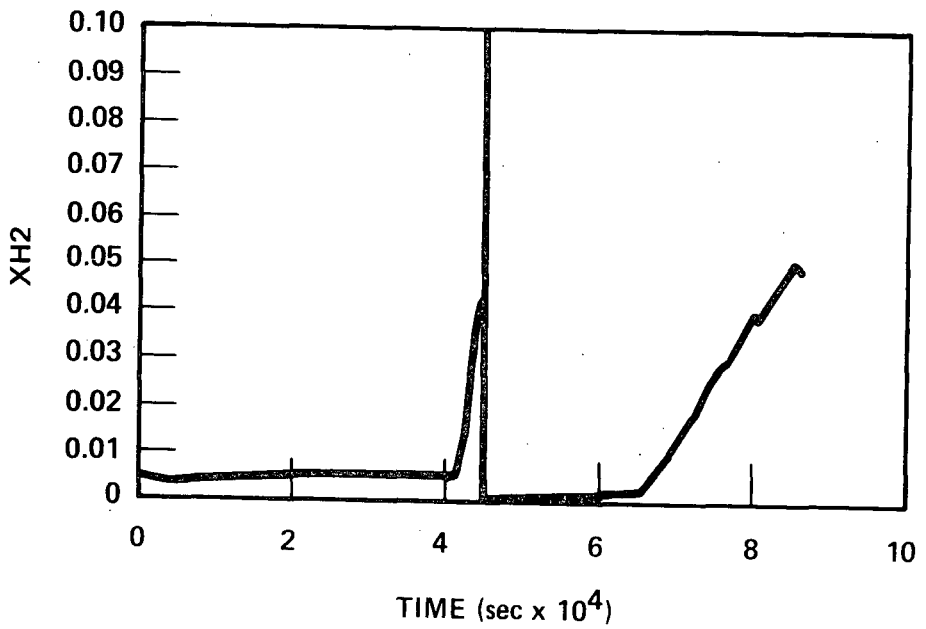
Pressure (in Containment) vs. Time
S2HF, B, Burn @ Vessel Failure
Class IV, Case 1B



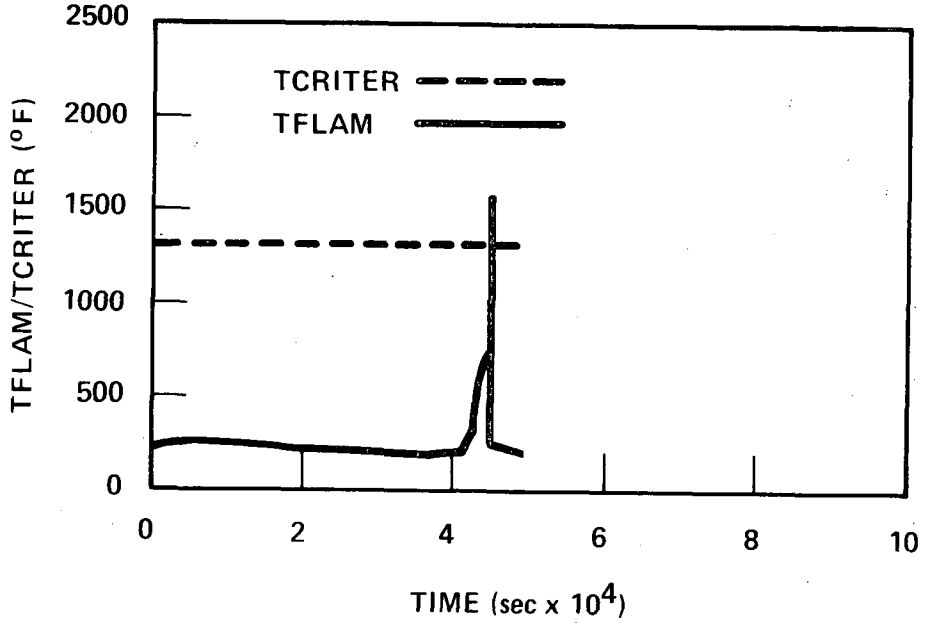
Temperature (in Containment) vs. Time
S2HF, B, Burn @ Vessel Failure
Class IV, Case 1B



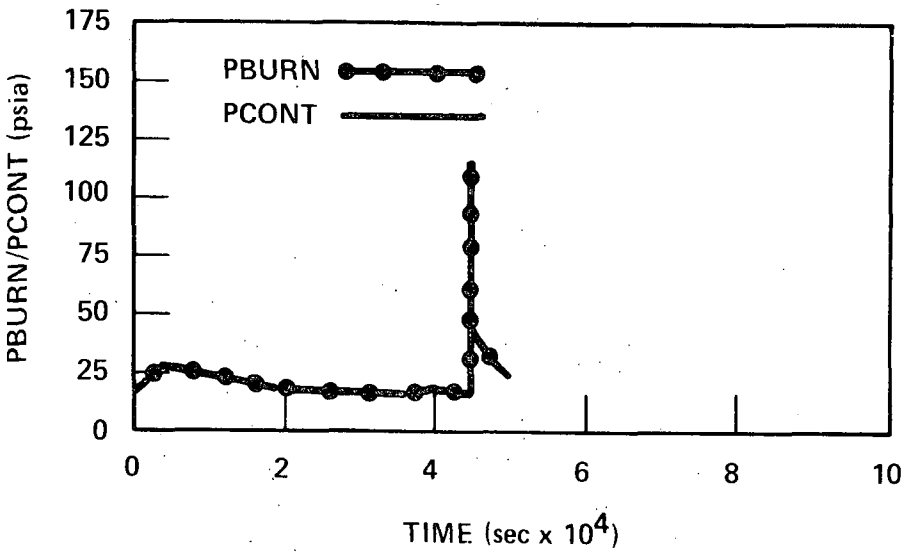
Mass Hydrogen (in Containment) vs. Time
S2HF, B, Burn @ Vessel Failure
Class IV, Case 1B



Mole Fraction H_2 (in Containment) vs. Time
S2HF, B, Burn @ Vessel Failure
Class IV, Case 1B



Flame Temperature (in Containment) vs. Time
S2HF, B, Burn @ Vessel Failure
Class IV, Case 1B



Adiabatic Burn Pressure/Pressure in Containment vs. Time
S2HF, B, Burn @ Vessel Failure
Class IV, Case 1B

CASE: CLASS IV, CASE 1C, S2HF, B, BURN @ T_{MAX}, NON-DISPERSIVE

DISPERSIVE: NO PERCENT CORE: _____ FRACTION IN CAVITY: _____

RUN #: AALAAOL DATE: 12/31/80

BLOWDOWN PEAK: N/A PSIA TIME: _____ SEC.

HYDROGEN BURN?: YES CRITERIA: T_{MAX} FLAME

TIME @ BURN: 85215 SEC, PRESSURE: 127 PSIA, TEMPERATURE: 72500 °F

PEAKS:

PRESSURE: 127 PSIA, TIME: 85235 SEC, WHY?: H_2 BURN

TEMPERATURE: 2880 °F, TIME: 85235 SEC, WHY?: H_2 BURN

DISPERSIVE: NO

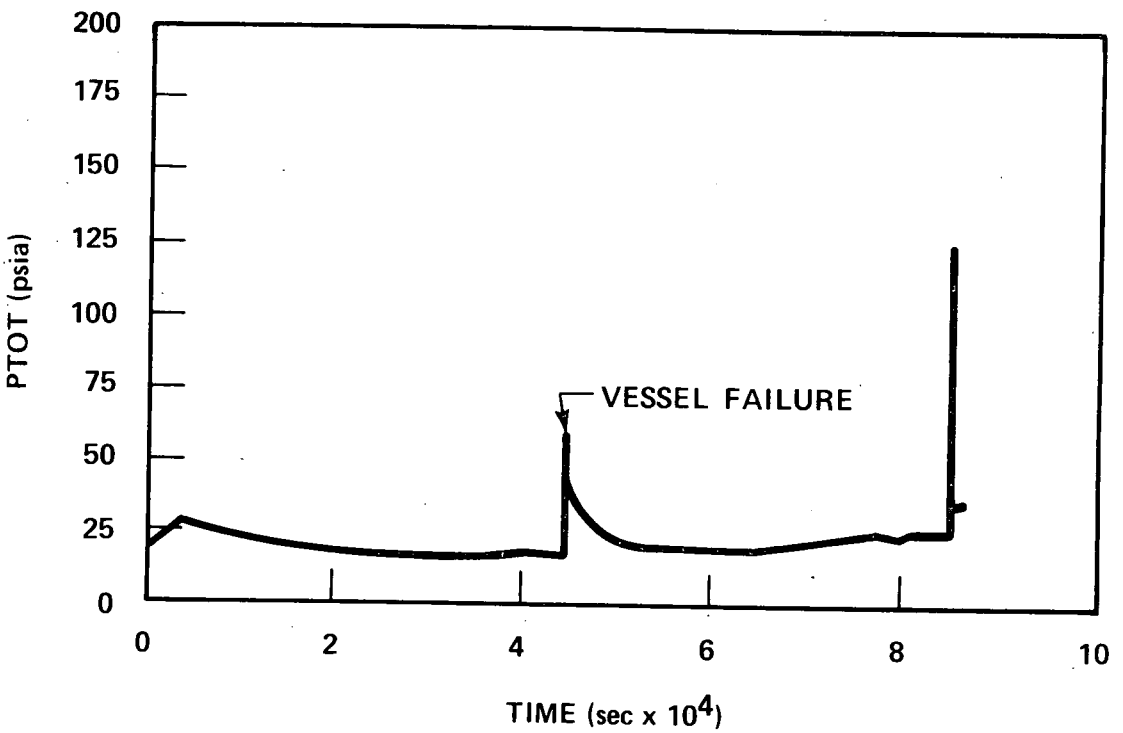
PRESSURE: _____ PSIA, TIME: _____ SEC,

TEMPERATURE: _____ °F, TIME: _____ SEC,

END OF BOIL: 44815 SEC. END OF HEAD: 44816 SEC.

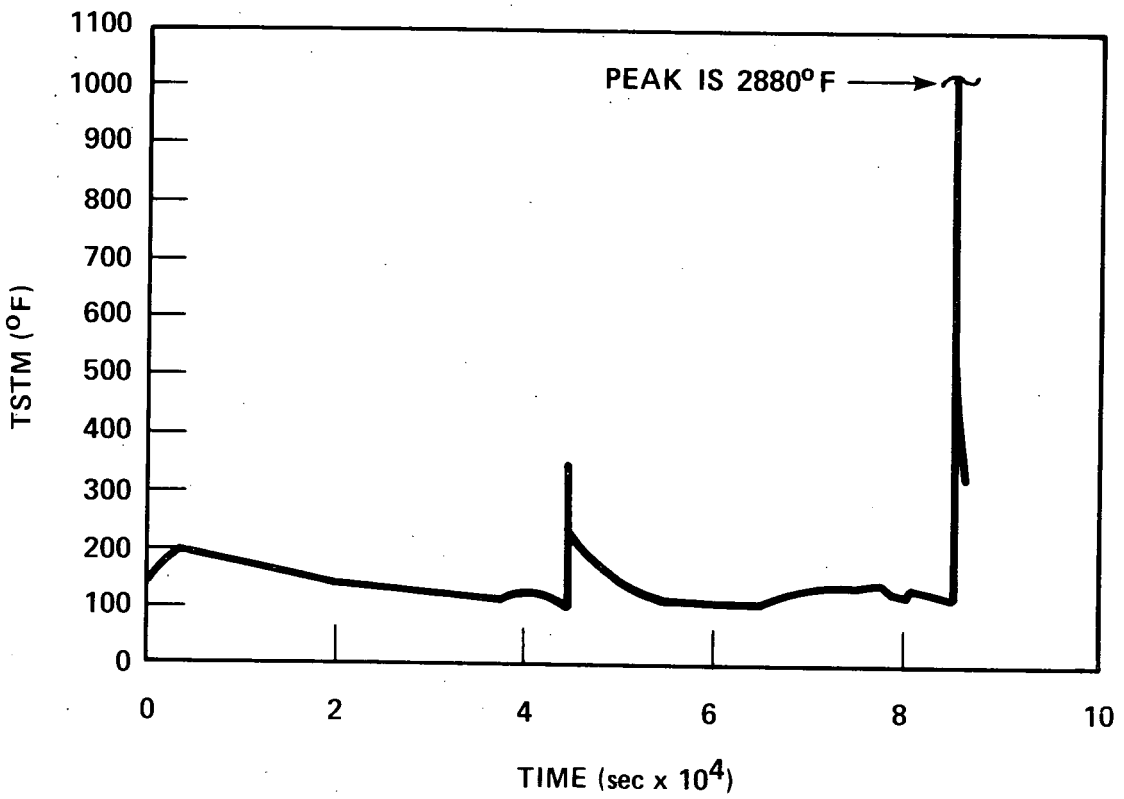
VESSEL FAILURE: 44816 SEC. END OF HOTDROP: 53942 SEC.

END OF INTER: 86237 SEC.

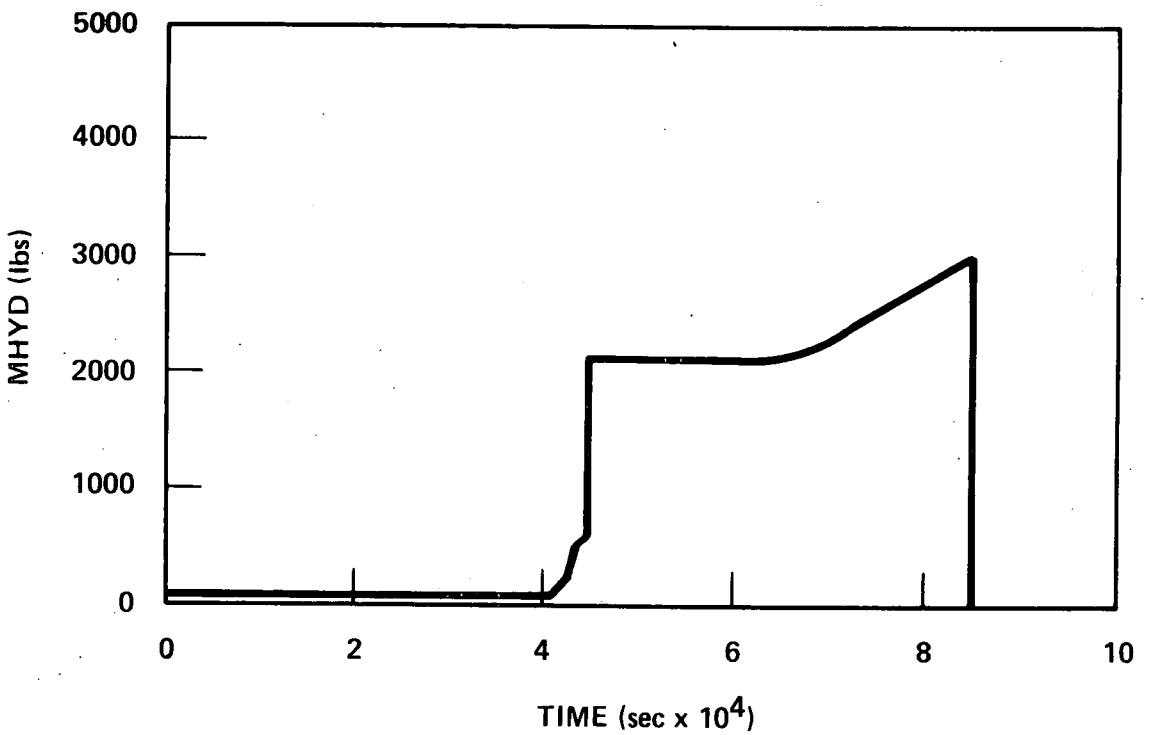


Pressure (in Containment) vs. Time
S2HF, B, Burn @ T_{MAX}
Class IV, Case 1C

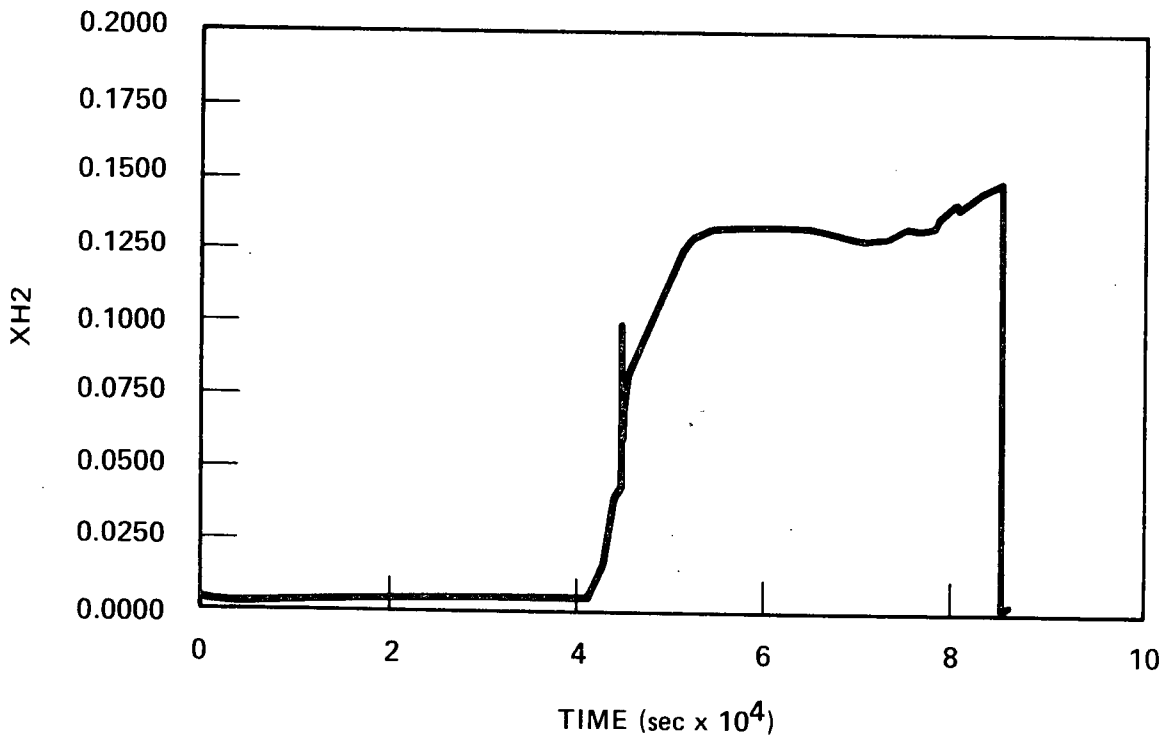
Sheet 2 of 7



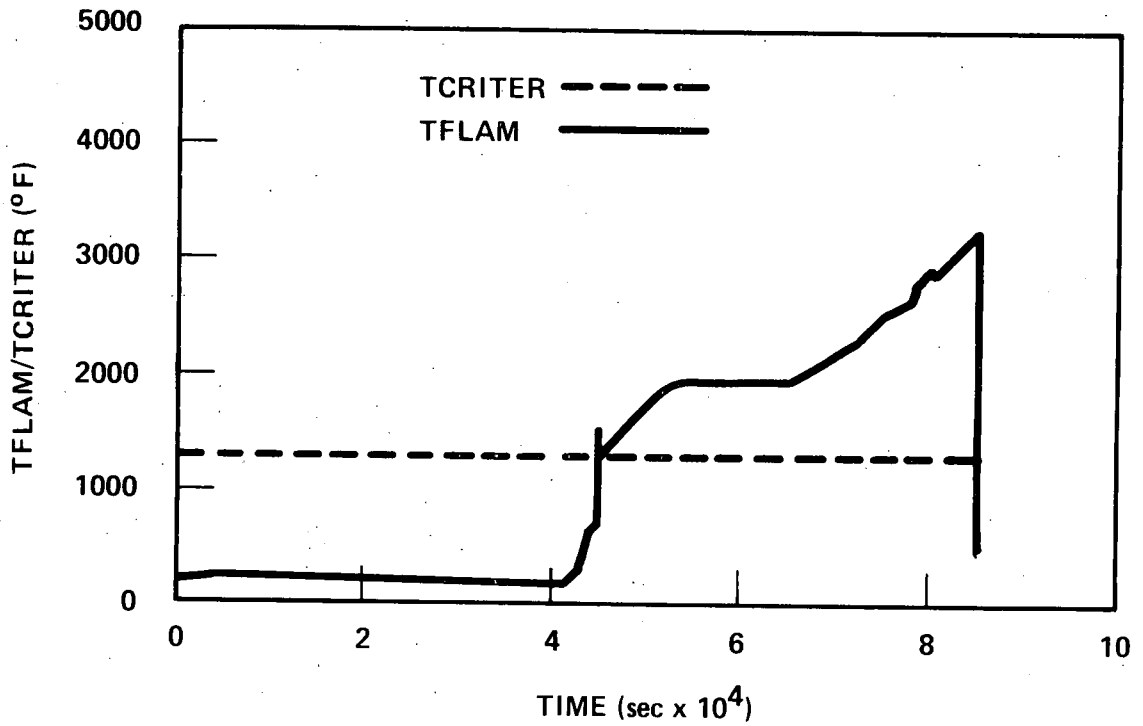
Temperature (in Containment) vs. Time
S2HF, B, Burn @ T_{MAX}
Class IV, Case 1C



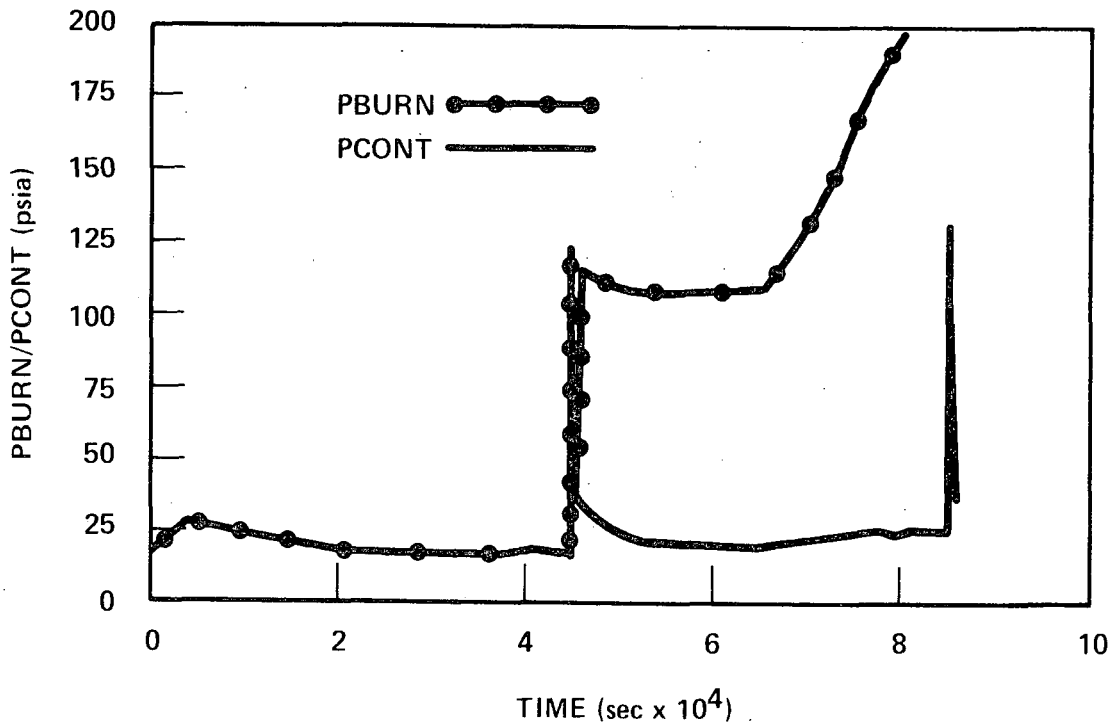
Mass Hydrogen (in Containment) vs. Time
S2HF, B, Burn @ T_{MAX}
Class IV, Case 1C



Mole Fraction H_2 (in Containment) vs. Time
S2HF, B, Burn @ T_{MAX}
Class IV, Case 1C



Flame Temperature (in Containment) vs. Time
S2HF, B, Burn @ T_{MAX}
Class IV, CAse 1C



Adiabatic Burn Pressure/Pressure in Containment vs. Time
S2HF, B, Burn @ T_{MAX}
Class IV, Case 1C

CASE: CLASS IV, CASE 2A, S2HF, W, NO BURN, NON-DISPERSIVE

DISPERSIVE: NO PERCENT CORE: _____ FRACTION IN CAVITY: _____

RUN #: AALABDQ DATE: 12/31/80

BLOWDOWN PEAK: N/A PSIA TIME: _____ SEC.

HYDROGEN BURN?: NO CRITERIA: _____

TIME @ BURN: _____ SEC, PRESSURE: _____ PSIA, TEMPERATURE: _____ °F

PEAKS:

PRESSURE: 33 PSIA, TIME: 46006 SEC, WHY?: _____

TEMPERATURE: 222 °F, TIME: 46006 SEC, WHY?: _____

DISPERSIVE: NO

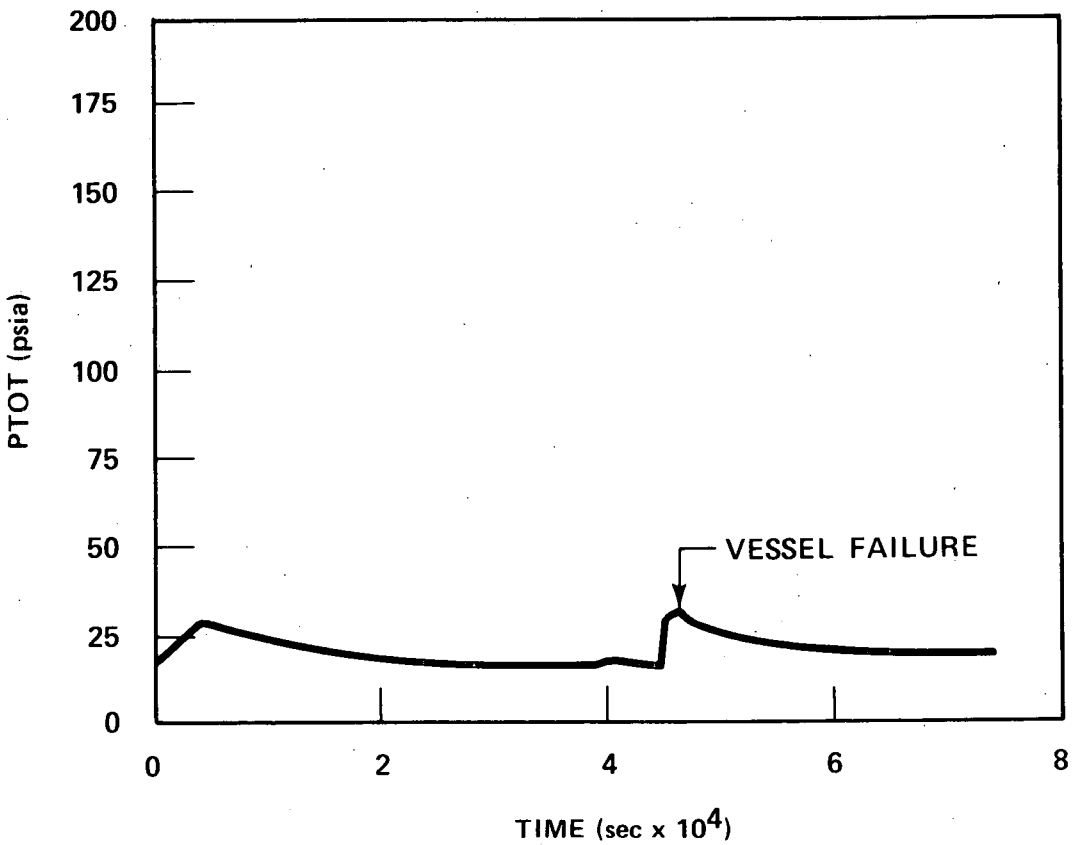
PRESSURE: NO PSIA, TIME: _____ SEC,

TEMPERATURE: _____ °F, TIME: _____ SEC,

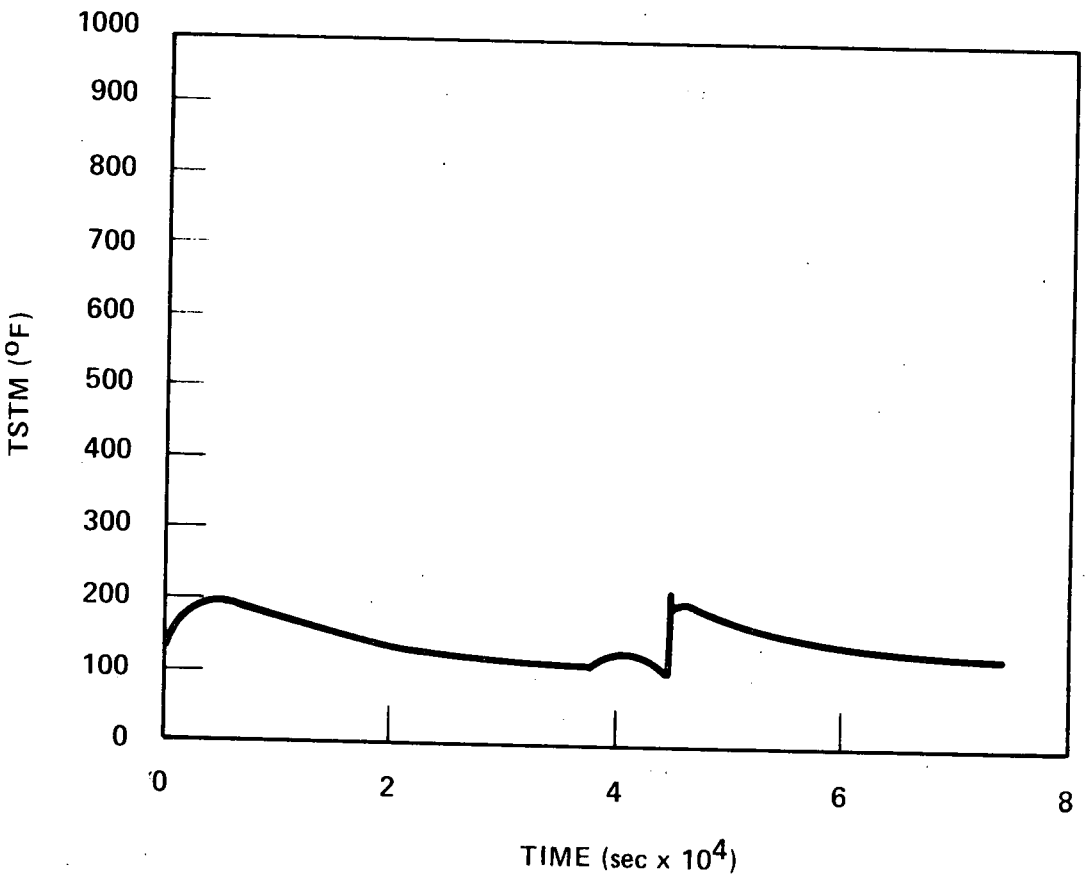
END OF BOIL: 44815 SEC. END OF HEAD: 44816 SEC.

VESSEL FAILURE: 44816 SEC. END OF HOTDROP: _____ SEC.

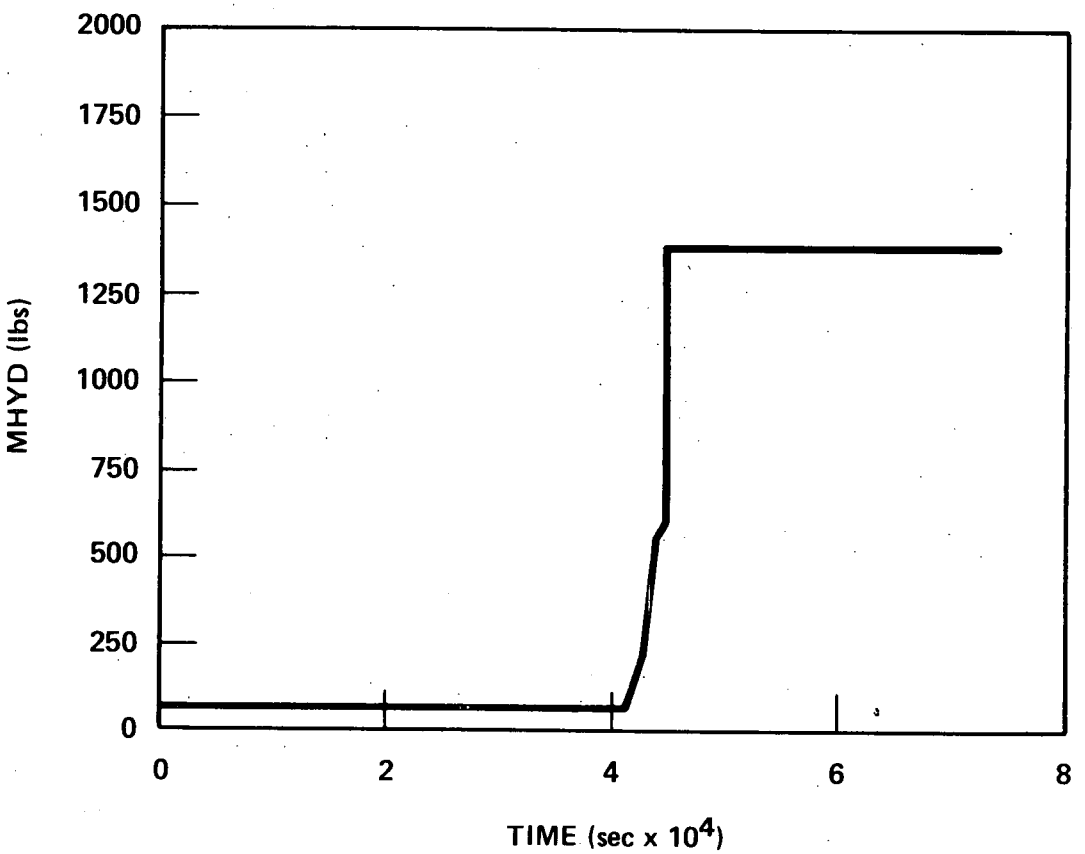
END OF INTER: 86326 SEC.



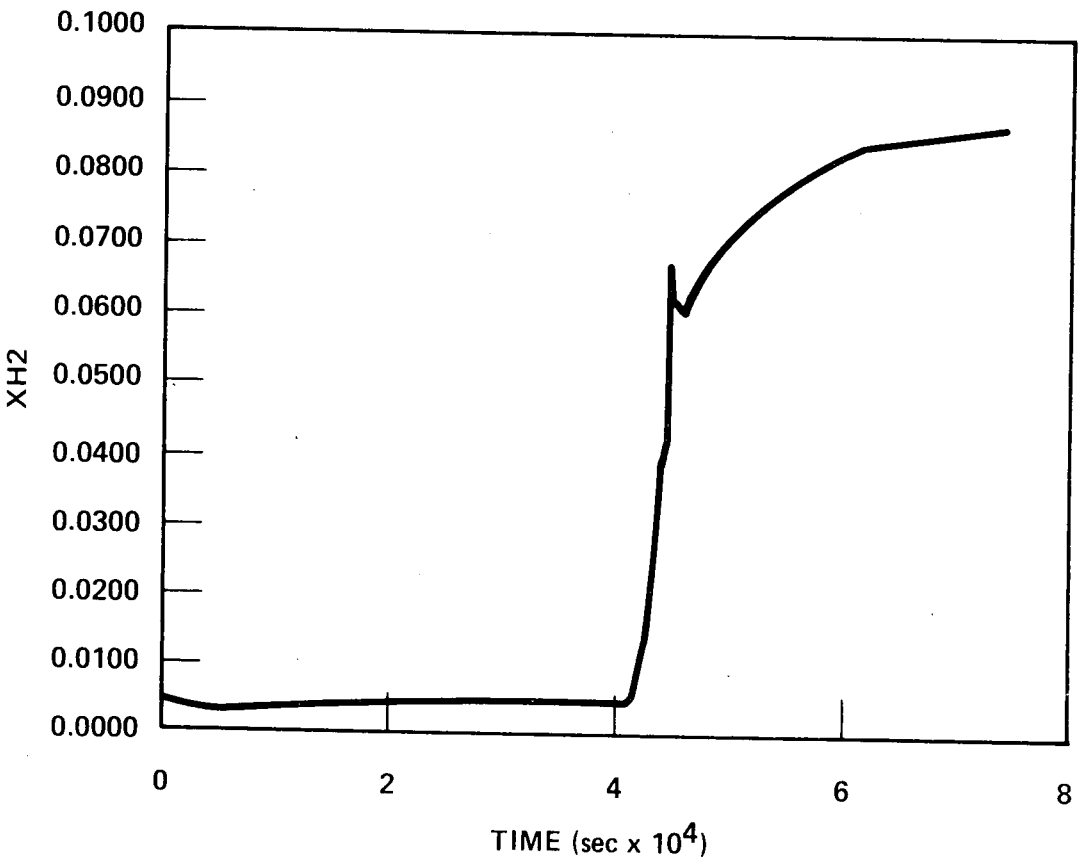
Pressure (in Containment) vs. Time
S2HF, W, No Burn
Class IV, Case 2A



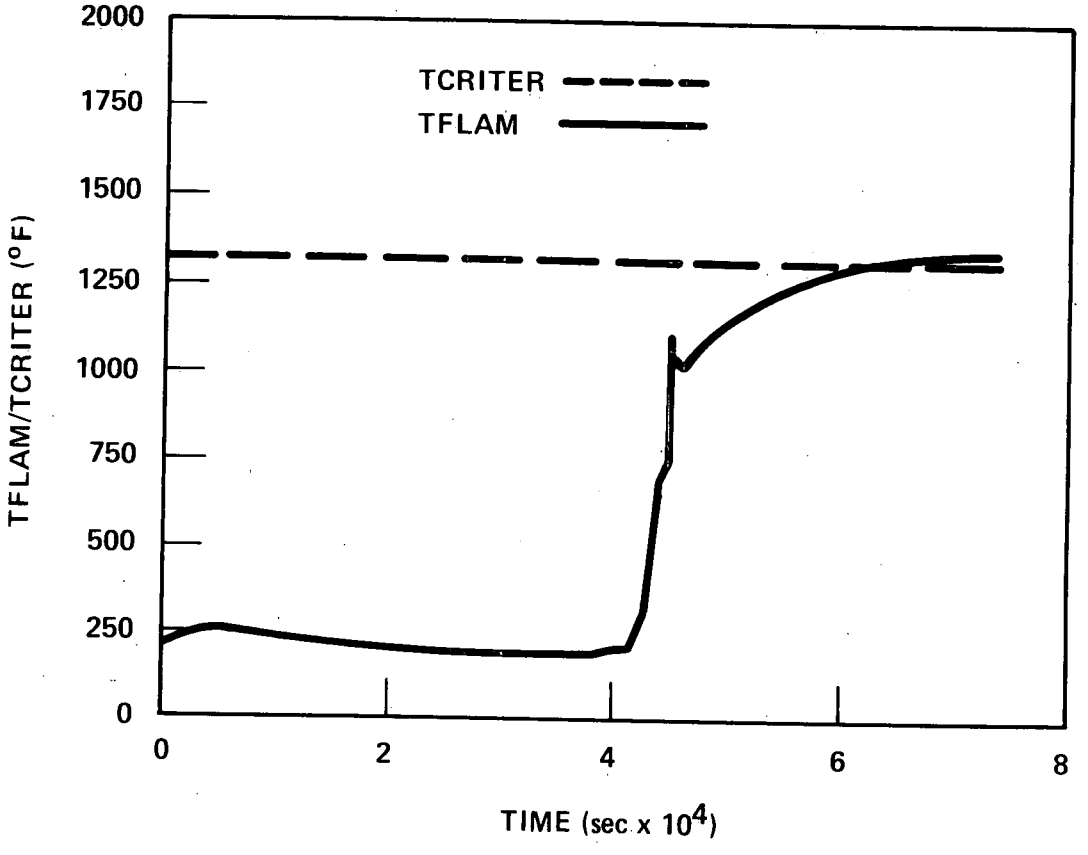
Temperature (in Containment) vs. Time
S2HF, W, No Burn
Class IV, Case 2A



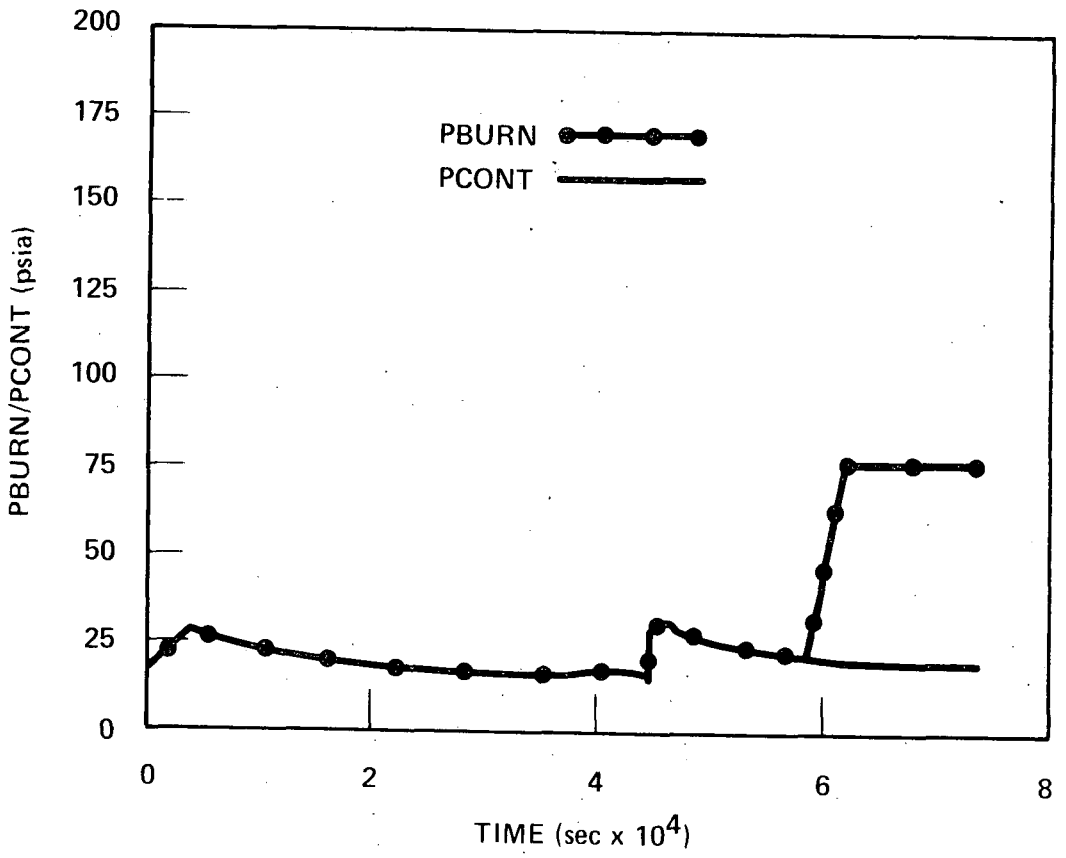
Mass Hydrogen (in Containment) vs. Time
S2HF, W, No Burn
Class IV, Case 2A



Mole Fraction H_2 (in Containment) vs. Time
S2HF, W, No Burn
Class IV, Case 2A



Flame Temperature (in Containment) vs. Time
S2HF, W, No Burn
Class IV, Case 2A



Adiabatic Burn Pressure/Pressure in Containment vs. Time
S2HF, W, No Burn
Class IV, Case 2A

CASE: CLASS IV, CASE 2B, S2HF, W, BURN @ VESSEL FAILURE, NON-DISPERSIVE

DISPERSIVE: NO PERCENT CORE: _____ FRACTION IN CAVITY: _____

RUN #: AALABDP DATE: 12/31/80

BLOWDOWN PEAK: N/A PSIA TIME: _____ SEC.

HYDROGEN BURN?: YES CRITERIA: VESSEL FAILURE

TIME @ BURN: 44816 SEC, PRESSURE: 20 PSIA, TEMPERATURE: >1000 °F

PEAKS:

PRESSURE: 70 PSIA, TIME: 44837 SEC, WHY?: VESSEL FAILURE/H_2 BURN

TEMPERATURE: 1190 °F, TIME: 44837 SEC, WHY?: VESSEL FAILURE/H_2 BURN

DISPERSIVE: NO

PRESSURE: _____ PSIA, TIME: _____ SEC,

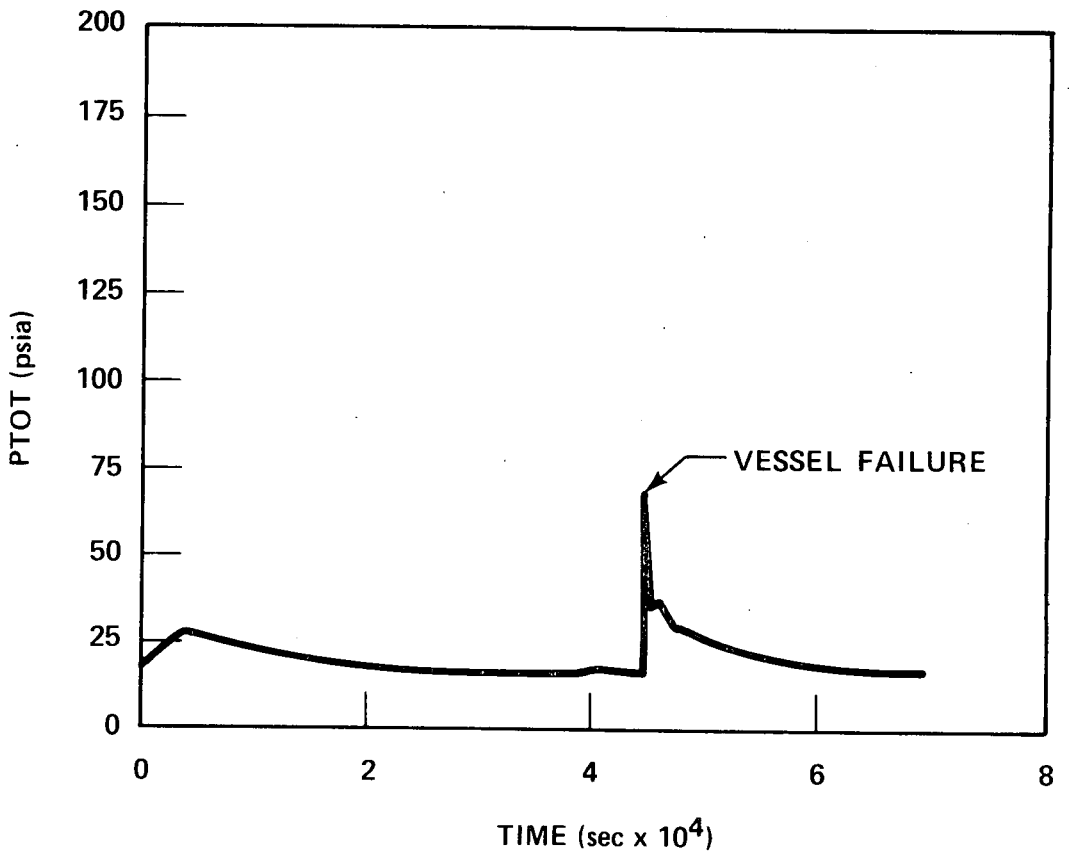
TEMPERATURE: _____ °F, TIME: _____ SEC,

END OF BOIL: 44815 SEC. END OF HEAD: 44816 SEC.

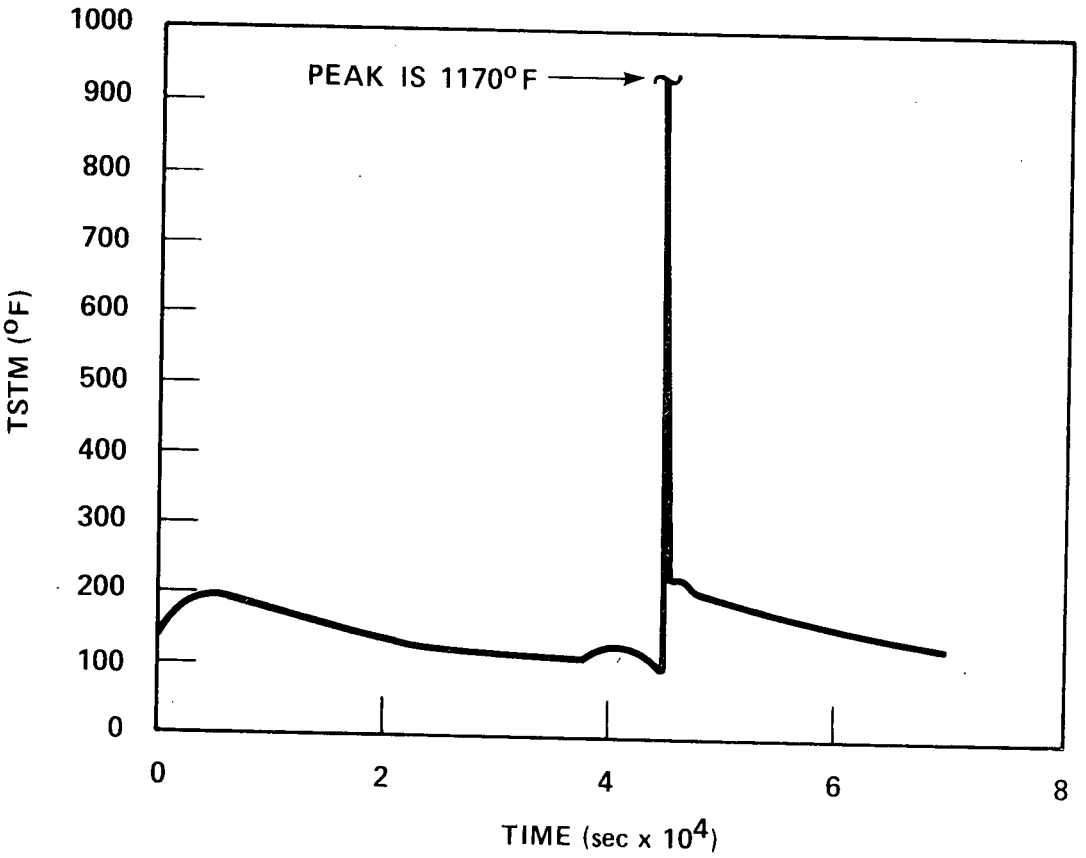
VESSEL FAILURE: 44816 SEC. END OF HOTDROP: _____ SEC.

END OF INTER: 86326 SEC.

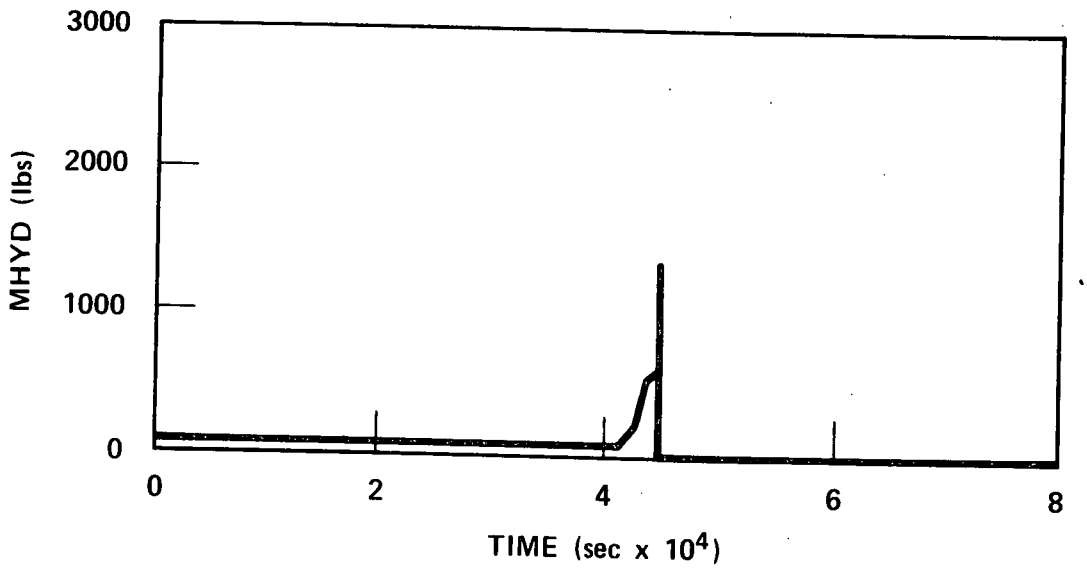
Class IV, Case 2B



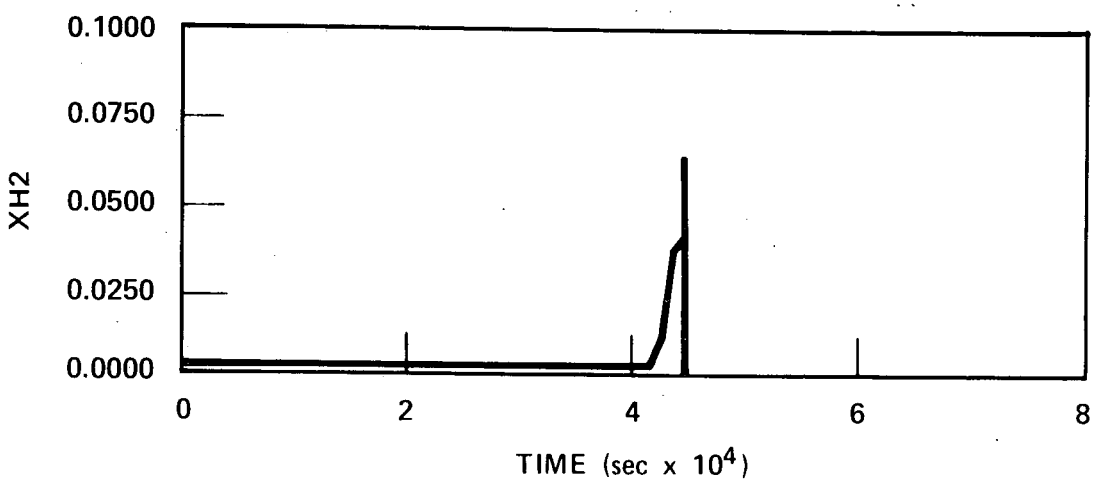
Pressure (in Containment) vs. Time
S2HF, W, Burn @ Vessel Failure
Class IV, Case 2B



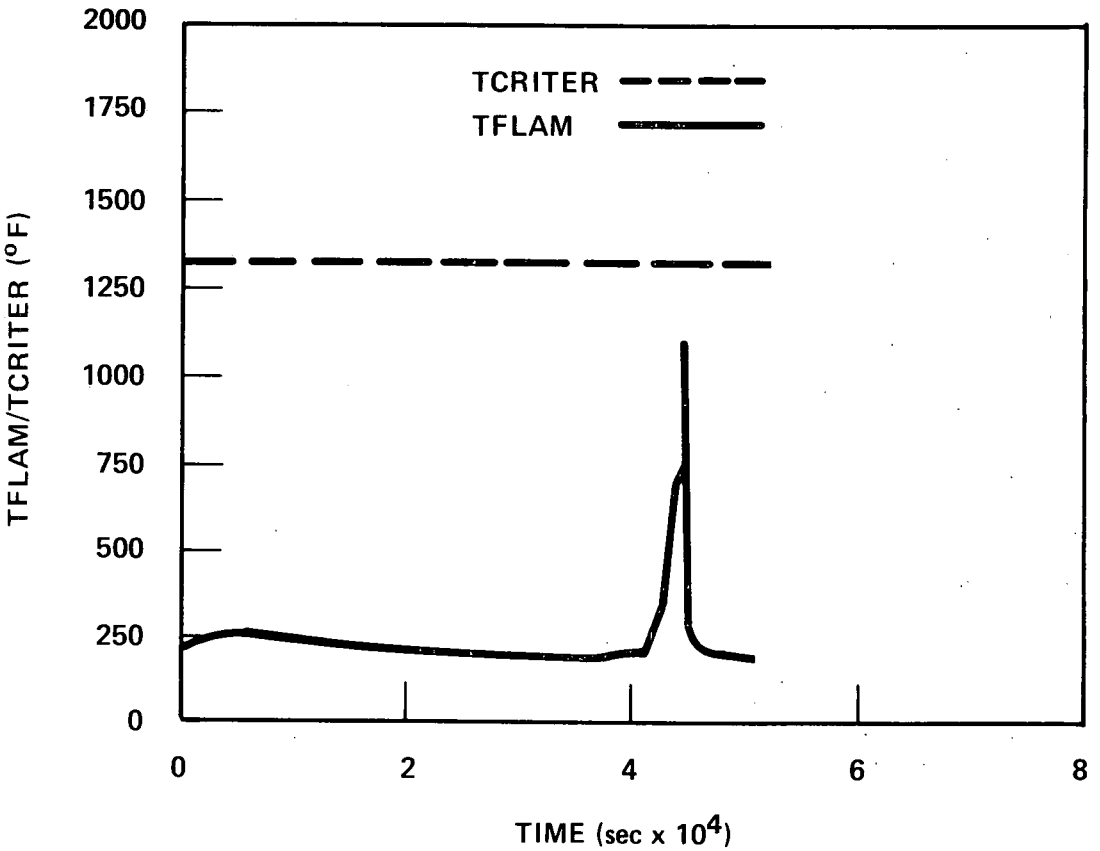
Temperature (in Containment) vs. Time
S2HF, W, Burn @ Vessel Failure
Class IV, Case 2B



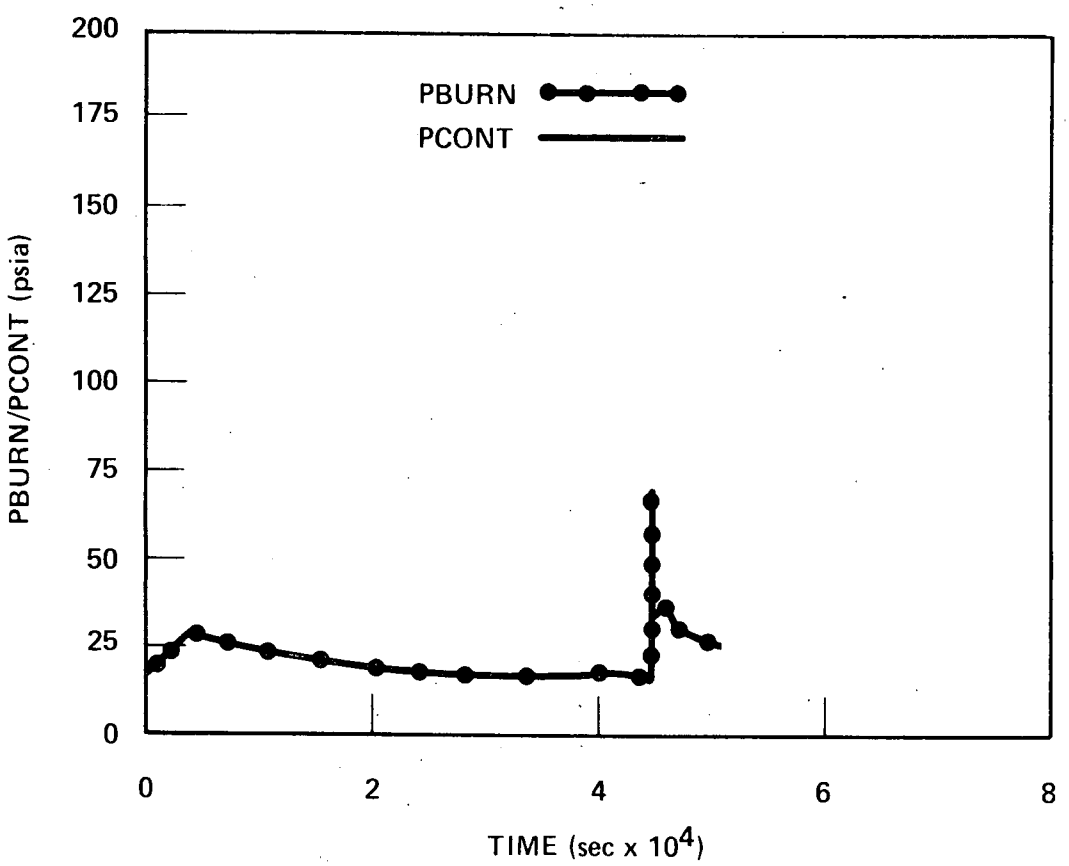
Mass Hydrogen (in Containment) vs. Time
S2HF, W, Burn @ Vessel Failure
Class IV, Case 2B



Mole Fraction H_2 (in Containment) vs. Time
S2HF, W, Burn @ Vessel Failure
Class IV, Case 2B



Flame Temperature (in Containment) vs. Time
S2HF, W, Burn @ Vessel Failure
Class IV, Case 2B



Adiabatic Burn Pressure/Pressure in Containment vs. Time
S2HF, W, Burn @ Vessel Failure
Class IV, Case 2B

CASE: CLASS IV, CASE 3a' S2HF, TIME PHASED 75, NO BURN, F64

DISPERSIVE: YES PERCENT CORE: 75 FRACTION IN CAVITY: _____

RUN #: AB3IBWE DATE: 4/2/81 PERCENT ZR REACTED: 63.5

BLOWDOWN PEAK: NO PSIA TIME: _____ SEC.

HYDROGEN BURN?: NO CRITERIA: _____

TIME @ BURN: _____ SEC, PRESSURE: _____ PSIA, TEMPERATURE: _____ °F

PEAKS:

PRESSURE: 61 PSIA, TIME: 44958 SEC, WHY?: VESSEL FAILURE

TEMPERATURE: 277 °F, TIME: 44958 SEC, WHY?: VESSEL FAILURE

DISPERSIVE:

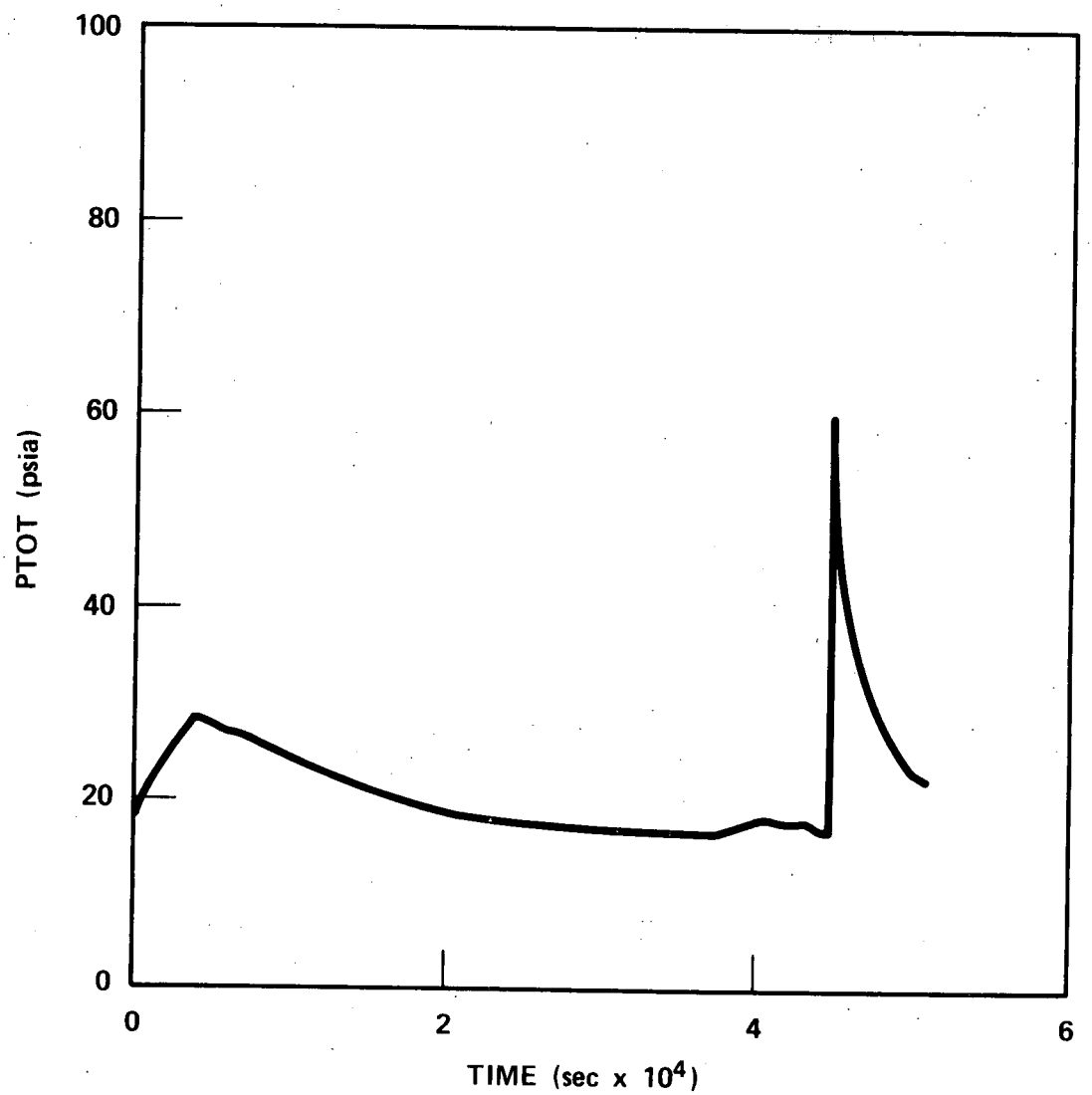
PRESSURE: 61 PSIA, TIME: 44958 SEC,

TEMPERATURE: 277 °F, TIME: 44958 SEC,

END OF BOIL: 44814 SEC. END OF HEAD: _____ SEC.

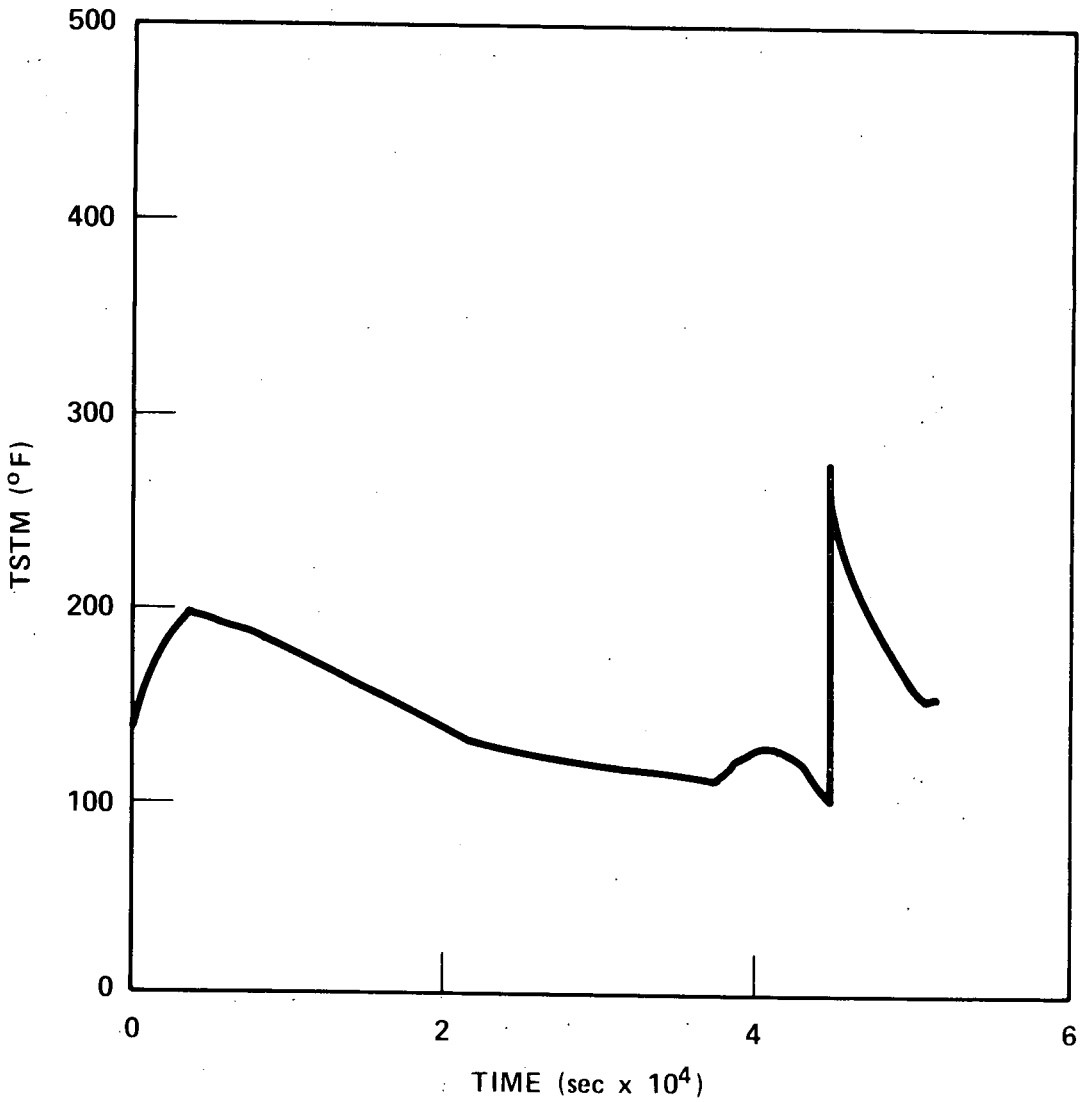
VESSEL FAILURE: 44814 SEC. END OF HOTDROP: _____ SEC.

END OF INTER: _____ SEC.

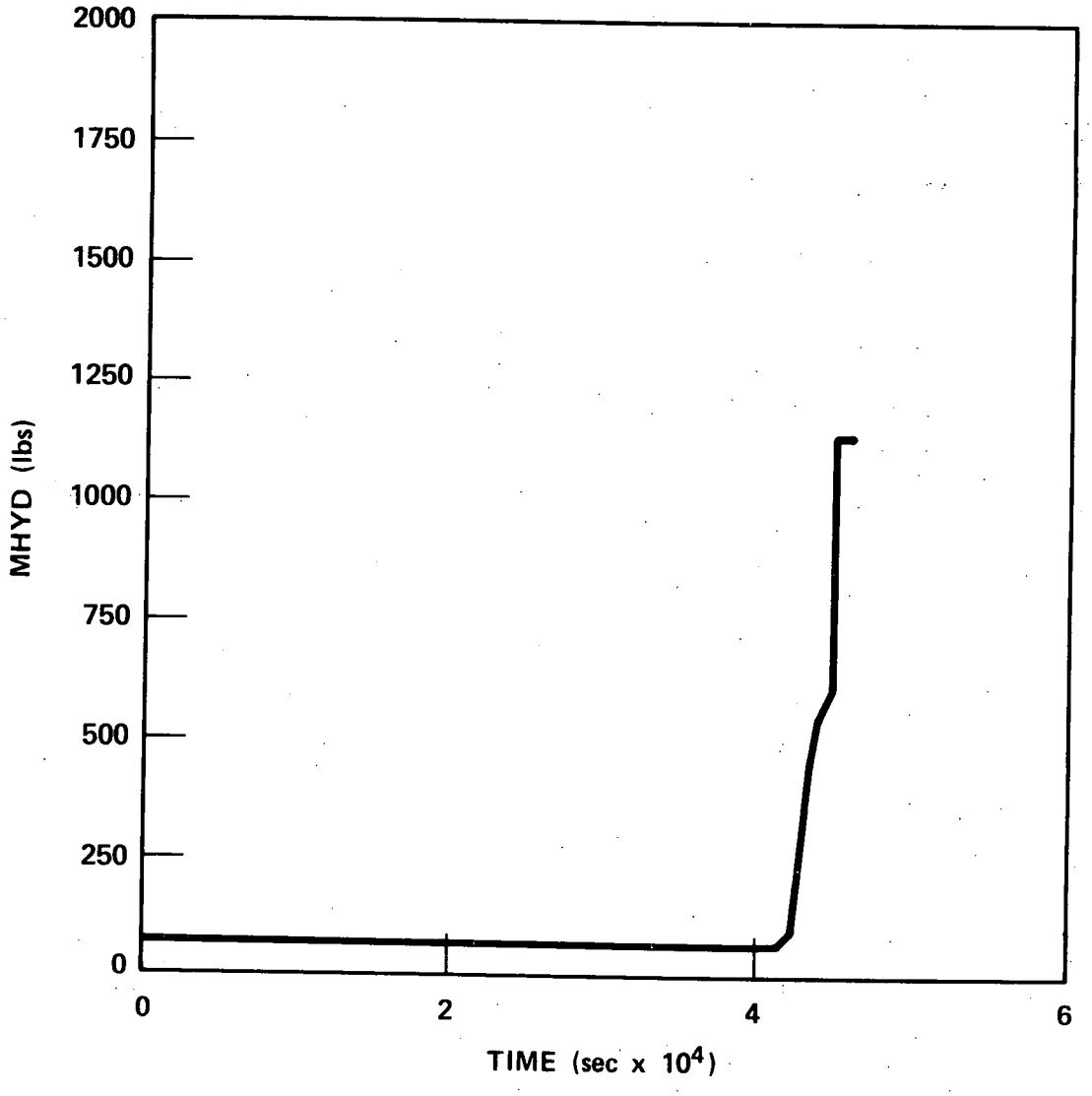


Pressure (in Containment) vs. Time
S2HF, Time Phased 75, No Burn, F64
Class IV, Case 3a'

Sheet 2 of 7

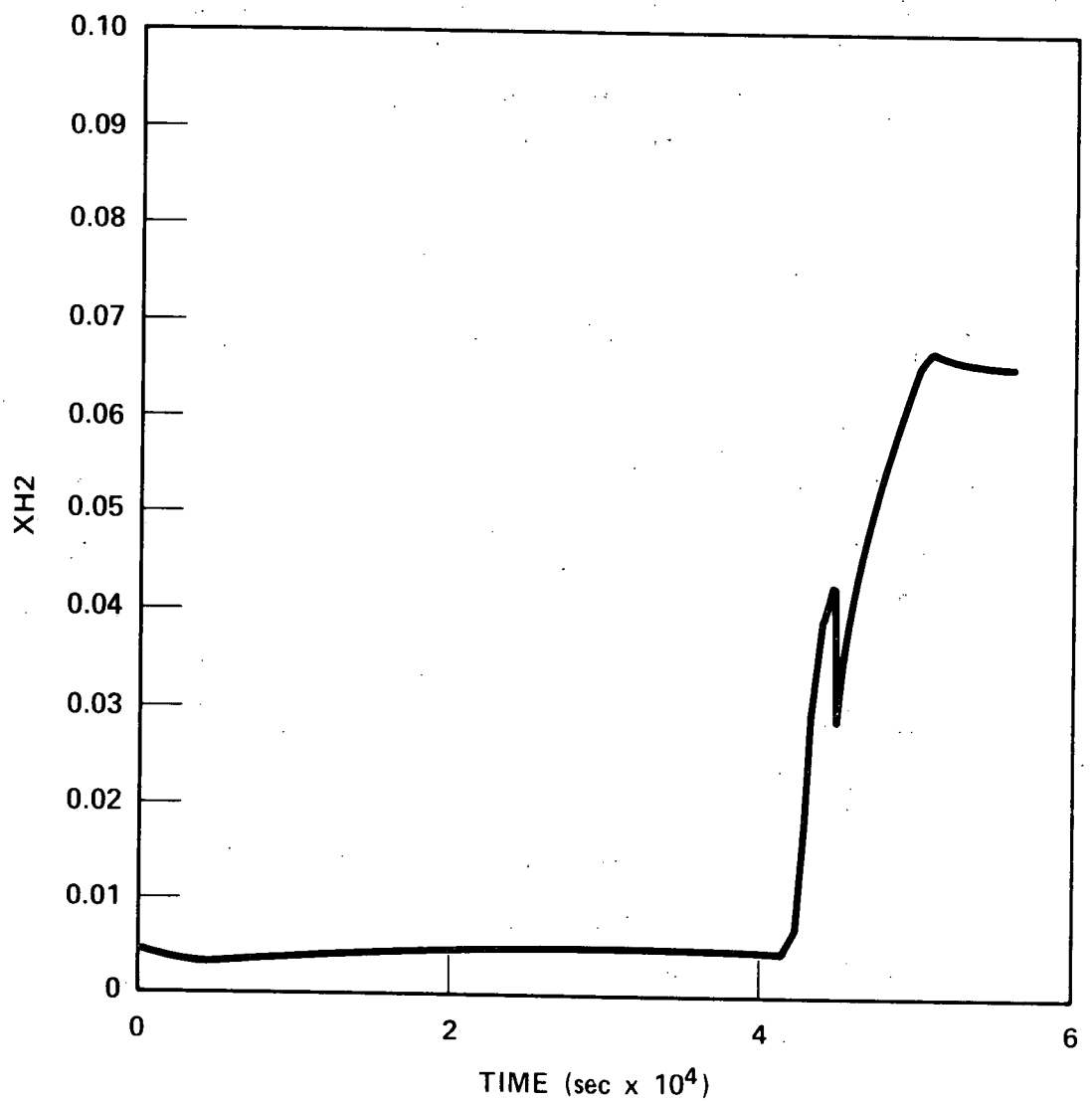


Temperature (in Containment) vs. Time
S2HF, Time Phased 75, No Burn, F64
Class IV, Case 3a'

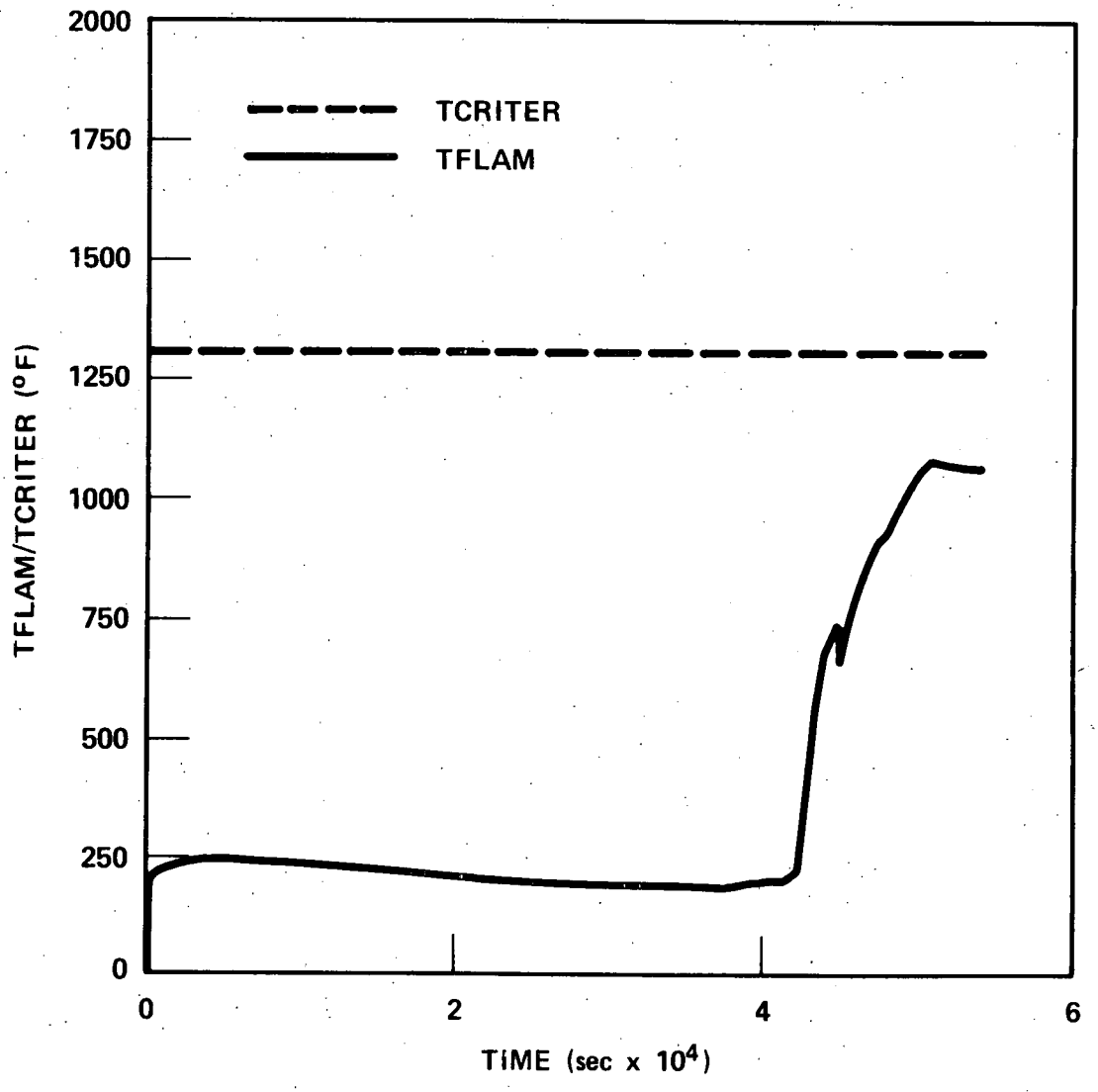


Mass Hydrogen (in Containment) vs. Time
S2HF, Time Phased 75, No Burn, F64
Class IV, Case 3a'

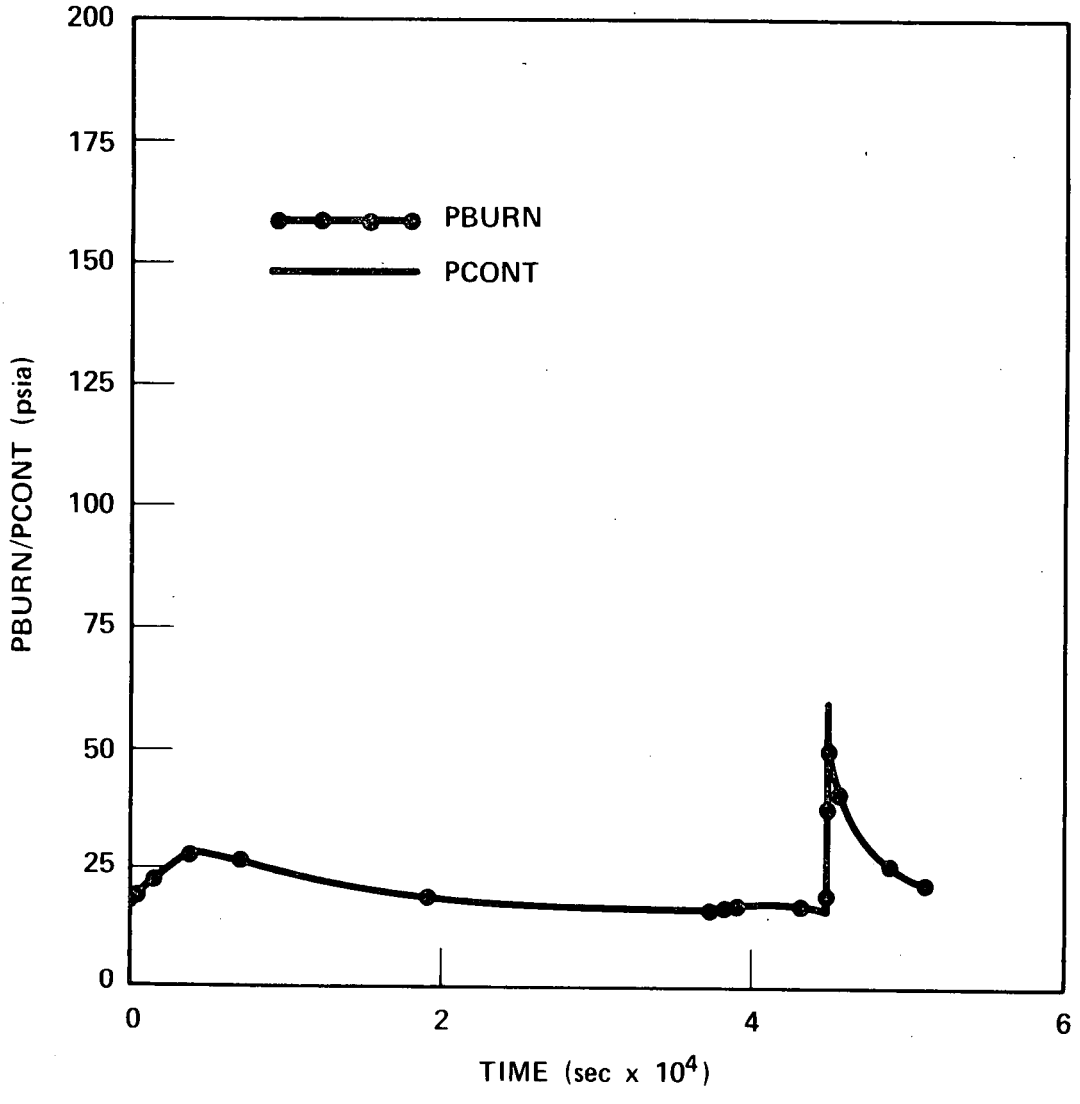
Sheet 4 of 7



Mole Fraction H_2 (in Containment) vs. Time
S2HF, Time Phased 75, No Burn, F64
Class IV, Case 3a'



Flame Temperature (in Containment) vs. Time
S2HF, Time Phased 75, No Burn, F64
Class IV, Case 3a'



Adiabatic Burn Pressure/Pressure in Containment vs. Time
S2HF, Time Phased 75, No Burn, F64
Class IV, Case 3a'

CASE: CLASS IV, CASE 4a', S2HF, TIME PHASED 50, NO BURN, F26

DISPERSIVE: YES PERCENT CORE: 50 FRACTION IN CAVITY: .50

RUN #: AB3IGNC DATE: 4/8/81 PERCENT ZR REACTED: 25.9

BLOWDOWN PEAK: NO PSIA TIME: _____ SEC.

HYDROGEN BURN?: NO CRITERIA: _____

TIME @ BURN: _____ SEC, PRESSURE: _____ PSIA, TEMPERATURE: _____ °F

PEAKS:

PRESSURE: 56 PSIA, TIME: 44425 SEC, WHY?: VESSEL FAILURE

TEMPERATURE: 272 °F, TIME: 44425 SEC, WHY?: VESSEL FAILURE

DISPERSIVE:

PRESSURE: 56 PSIA, TIME: 44425 SEC,

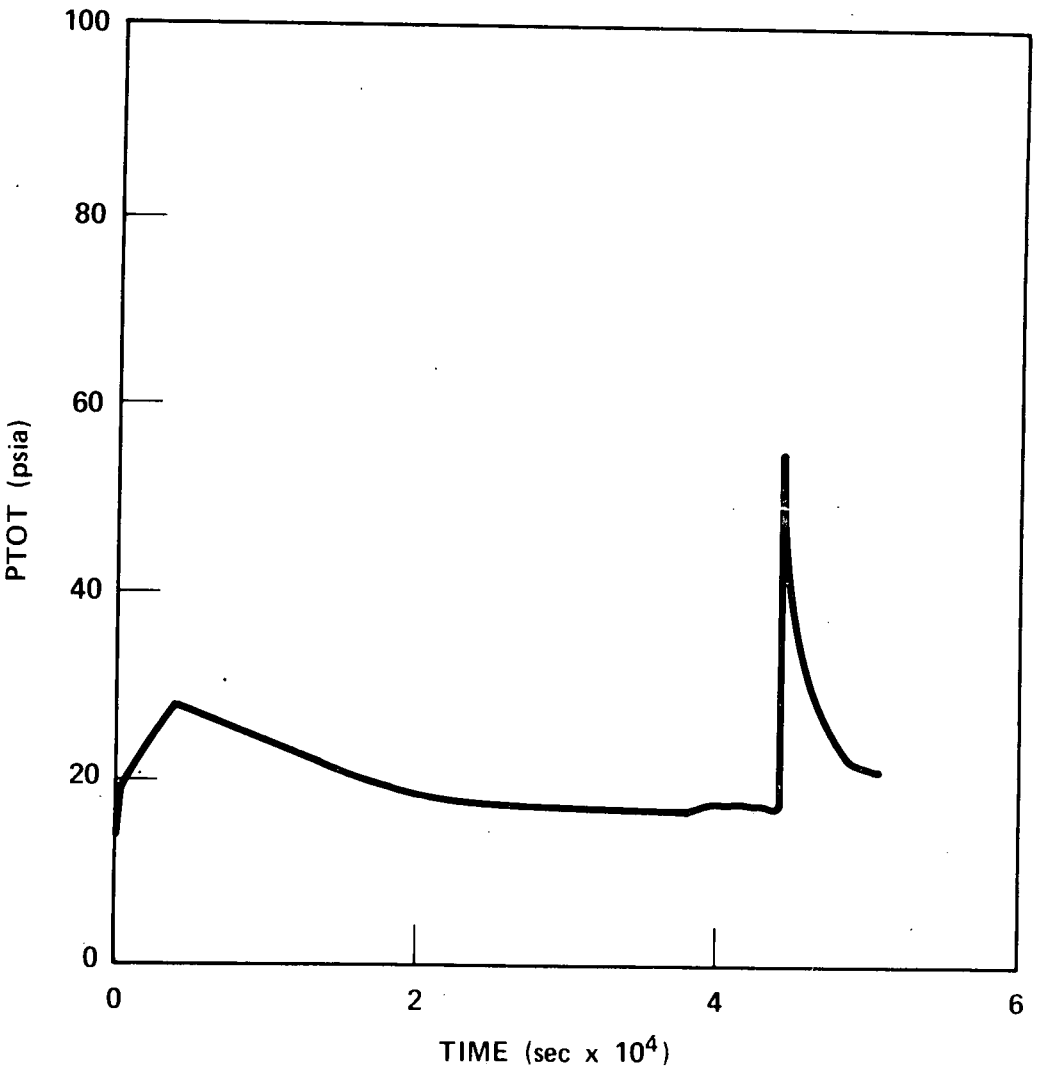
TEMPERATURE: 272.48 °F, TIME: 444.25 SEC,

END OF BOIL: 44334.0 SEC. END OF HEAD: _____ SEC.

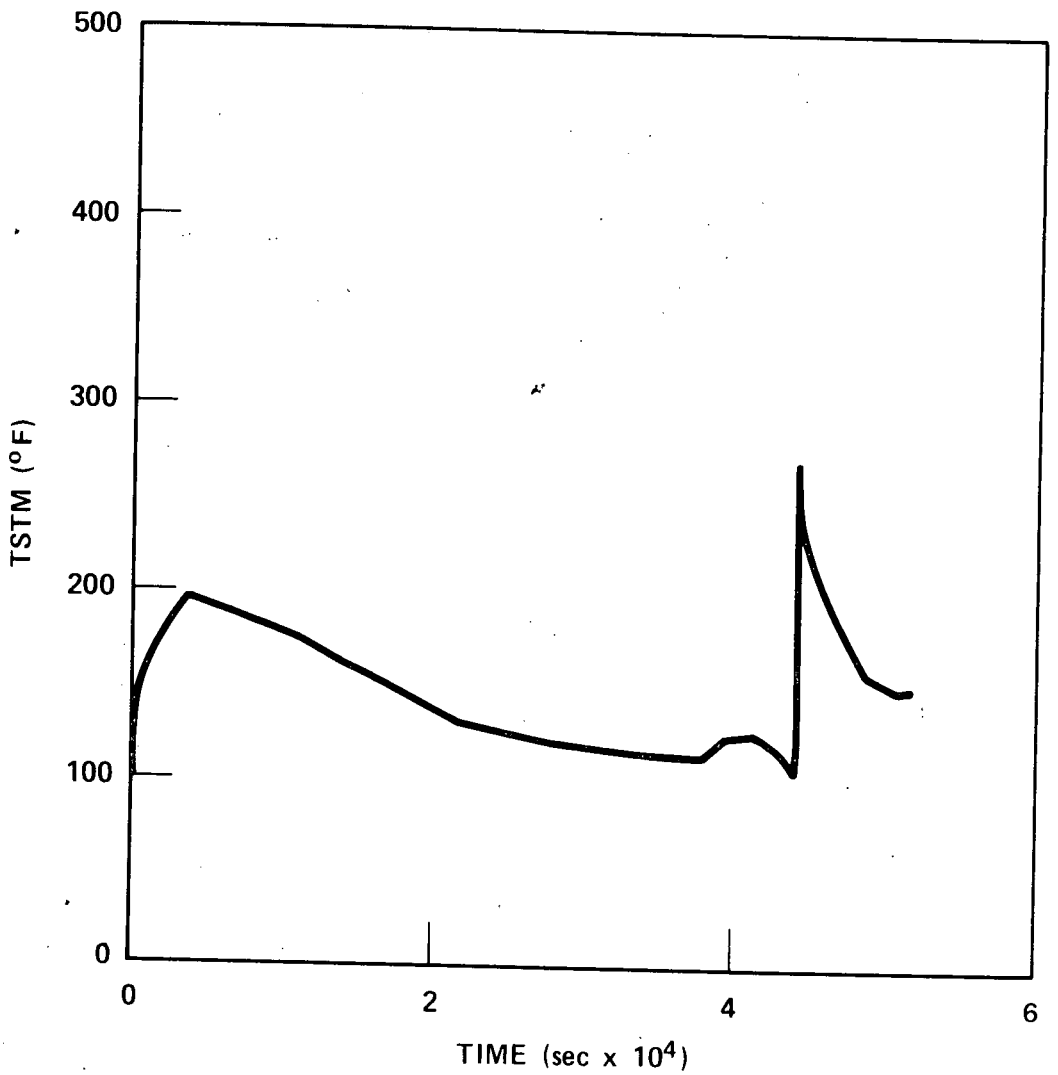
VESSEL FAILURE: 44334.0 SEC. END OF HOTDROP: _____ SEC.

END OF INTER: _____ SEC.

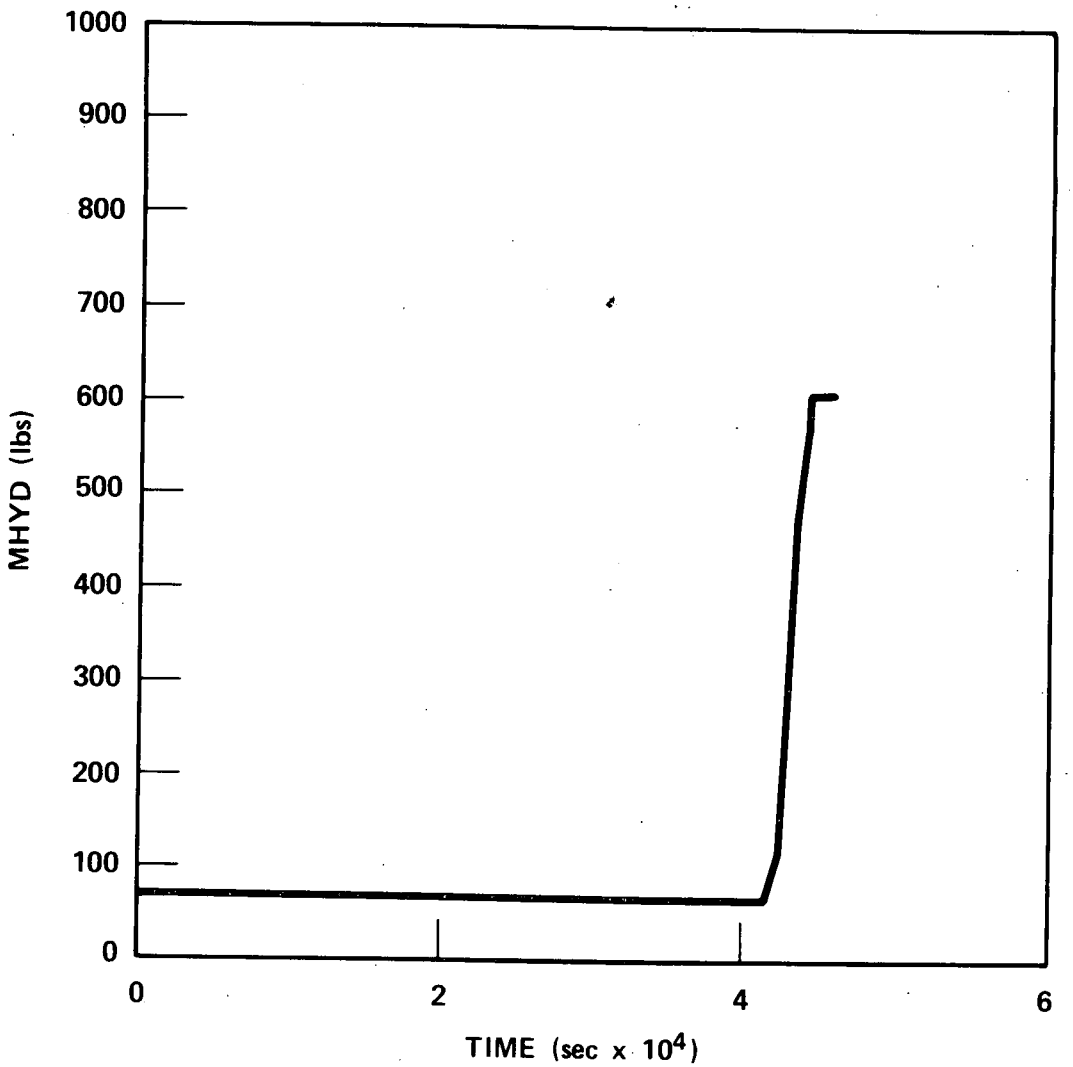
Class IV, Case 4A'



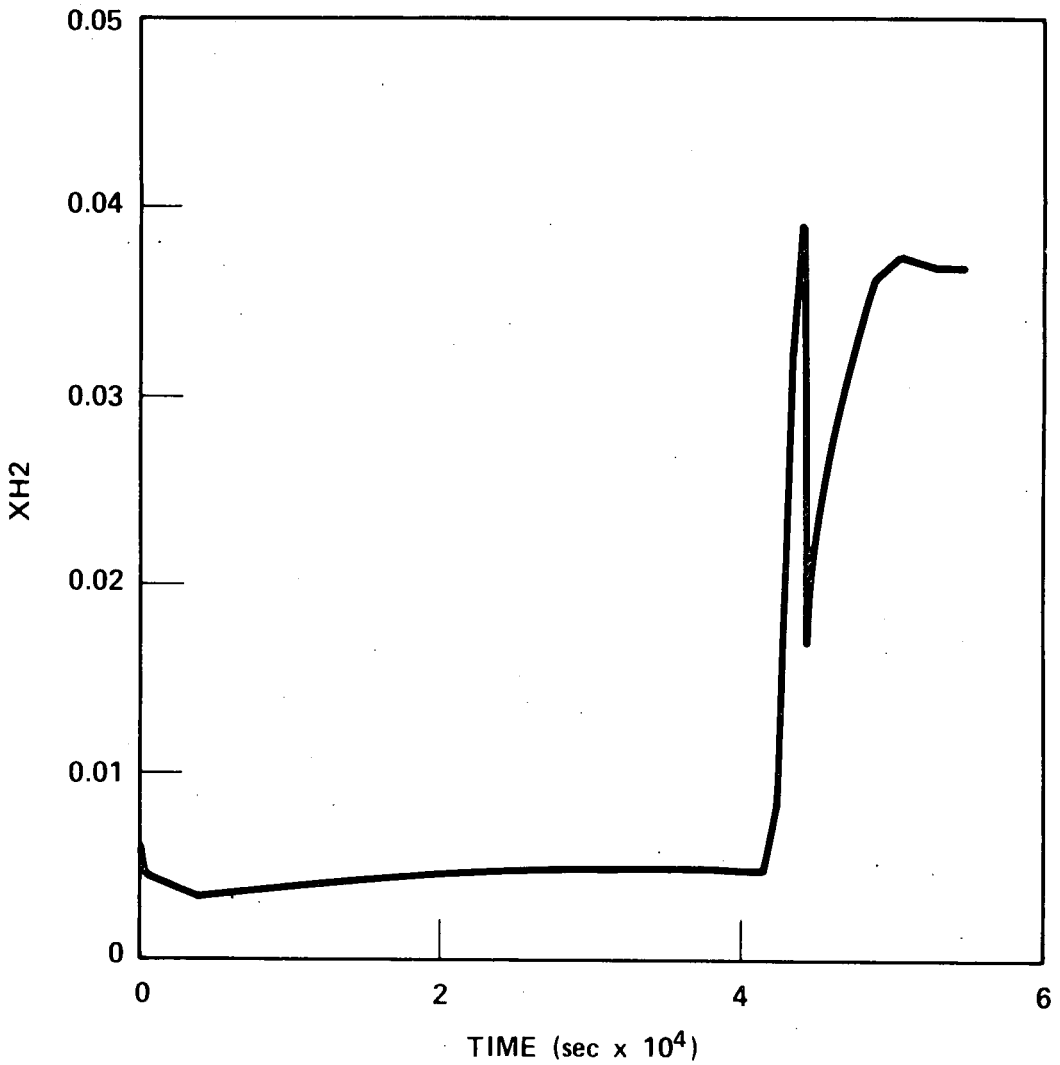
Pressure (in Containment) vs. Time
S2HF, Time Phased 50, No Burn, F26
Class IV, Case 4A'



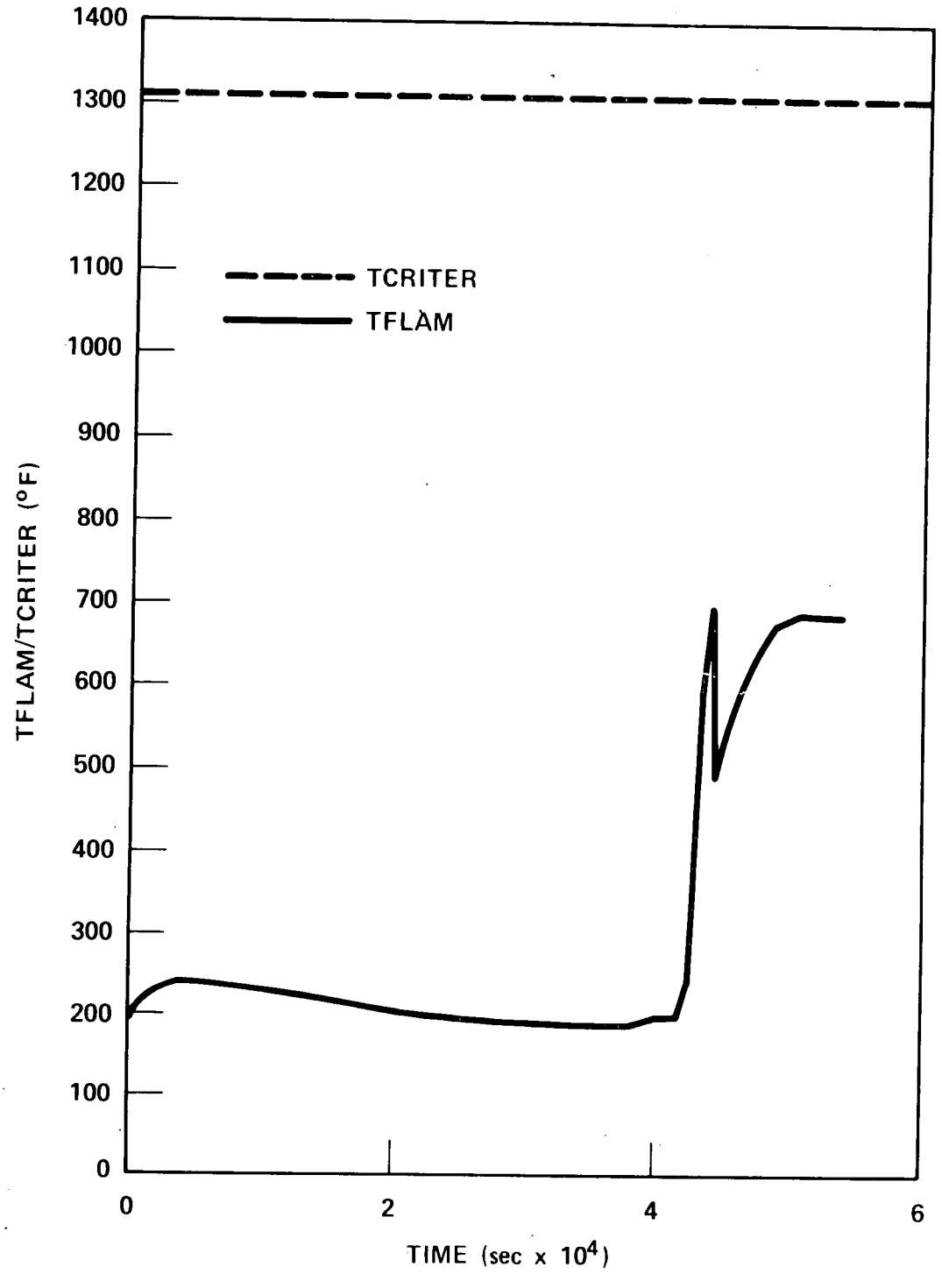
Temperature (in Containment) vs. Time
S2HF, Time Phased 50, No Burn, F26
Class IV, Case 4A'



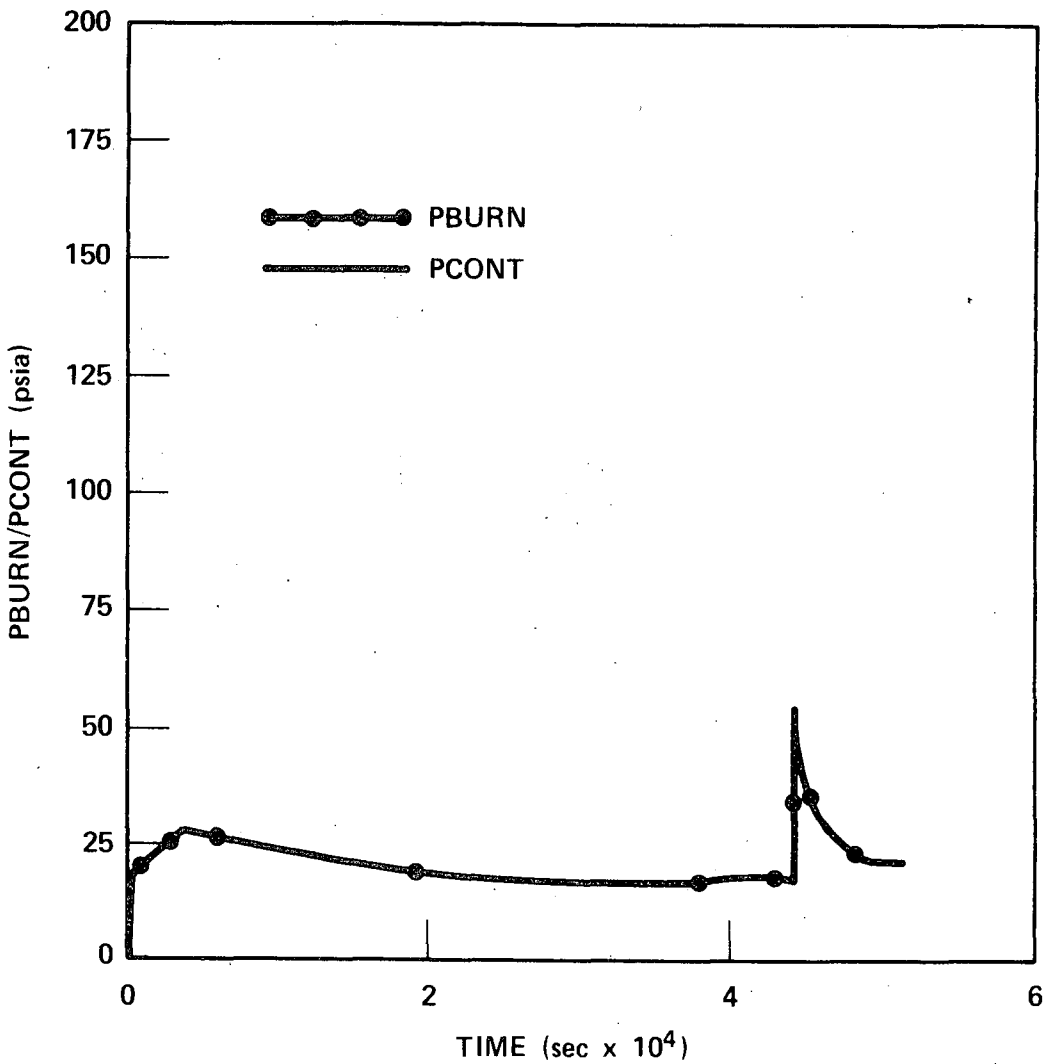
Mass Hydrogen (in Containment) vs. Time
S2HF, Time Phased 50, No Burn, F26
Class IV, Case 4A'



Mole Fraction H_2 (in Containment) vs. Time
S2HF, Time Phased 50, No Burn, F26
Class IV, Case 4A'



Flame Temperature (in Containment) vs. Time
S2HF, Time Phased 50, No Burn, F26
Class IV, Case 4A'



Adiabatic Burn Pressure/Pressure in Containment vs. Time
S2HF, Time Phased 50, No Burn, F26
Class IV, Case 4A'

CASE: CLASS IV, CASE 5A, S2HF, W, 80% DISPERSIVE, NO BURN

DISPERSIVE: YES PERCENT CORE: 80 FRACTION IN CAVITY: 0.20

RUN #: AALABDY DATE: 12/31/80

BLOWDOWN PEAK: N/A PSIA TIME: _____ SEC.

HYDROGEN BURN?: NO CRITERIA: _____

TIME @ BURN: _____ SEC, PRESSURE: _____ PSIA, TEMPERATURE: _____ °F

PEAKS:

PRESSURE: 75 PSIA, TIME: 44846 SEC, WHY?: DISPERSIVE FAILURE

TEMPERATURE: 1235 °F, TIME: 44846 SEC, WHY?: DISPERSIVE FAILURE

DISPERSIVE: YES

PRESSURE: 75 PSIA, TIME: 44846 SEC,

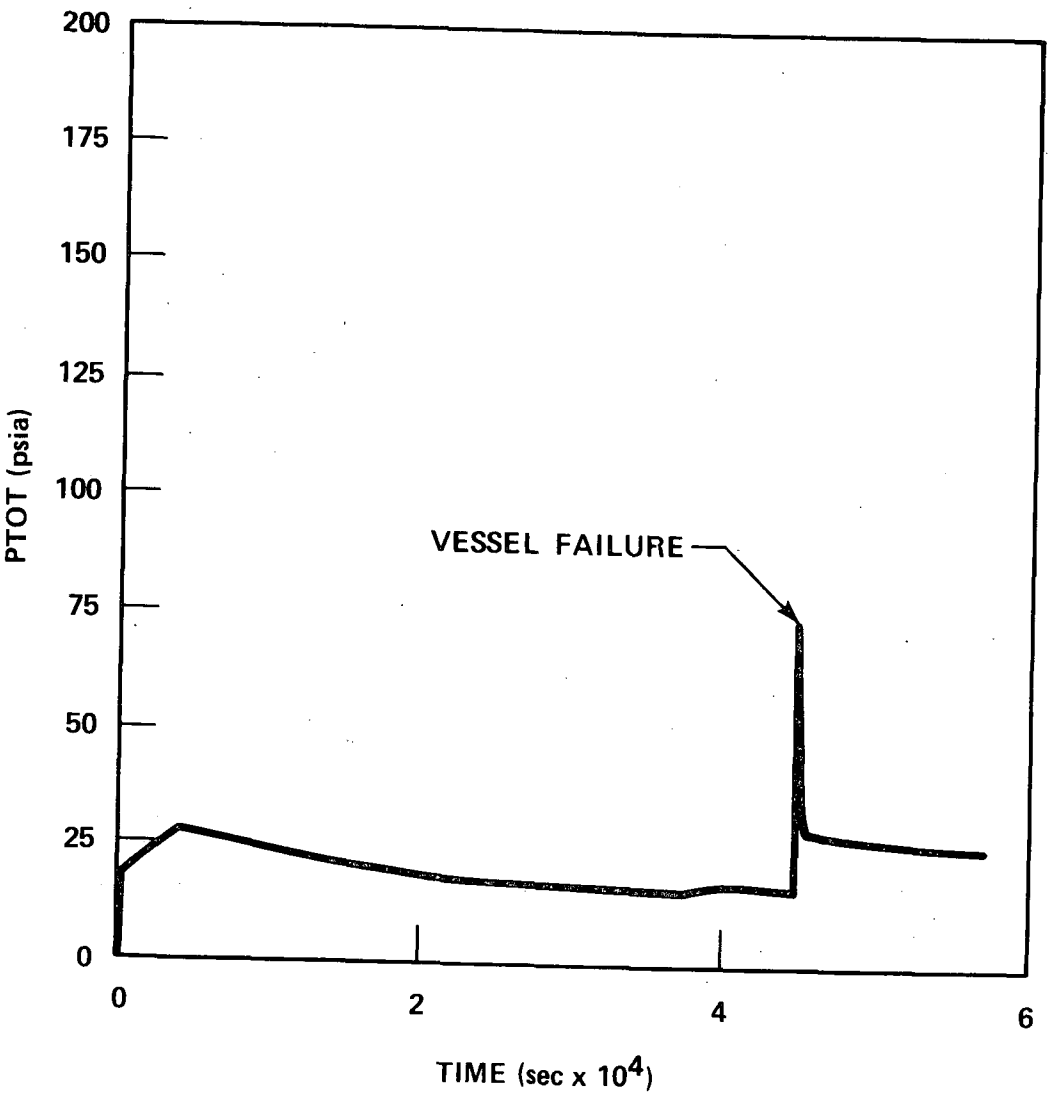
TEMPERATURE: 1235 °F, TIME: 44846 SEC,

END OF BOIL: 44815 SEC. END OF HEAD: 44816 SEC.

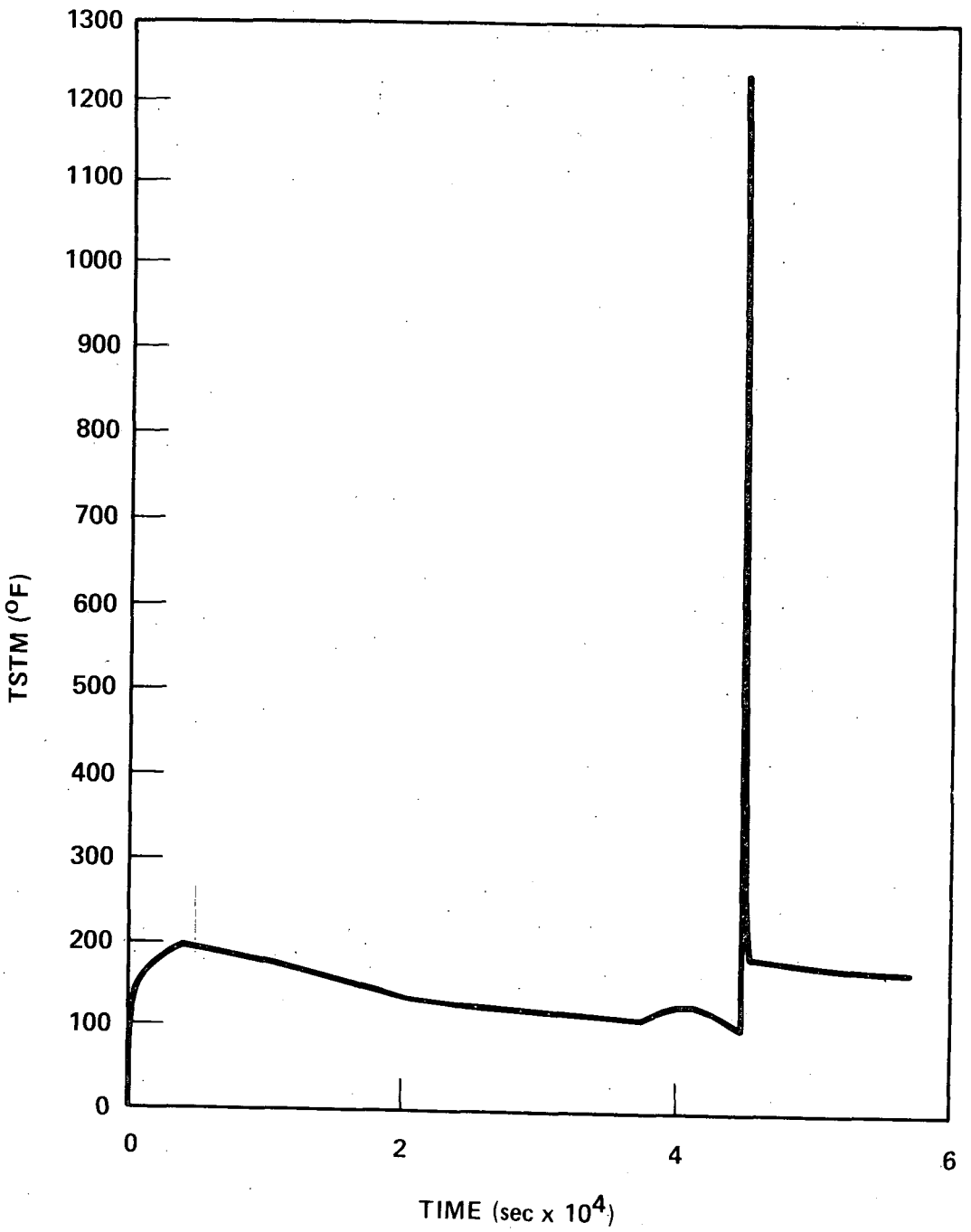
VESSEL FAILURE: 44816 SEC. END OF HOTDROP: _____ SEC.

END OF INTER: 86326 SEC.

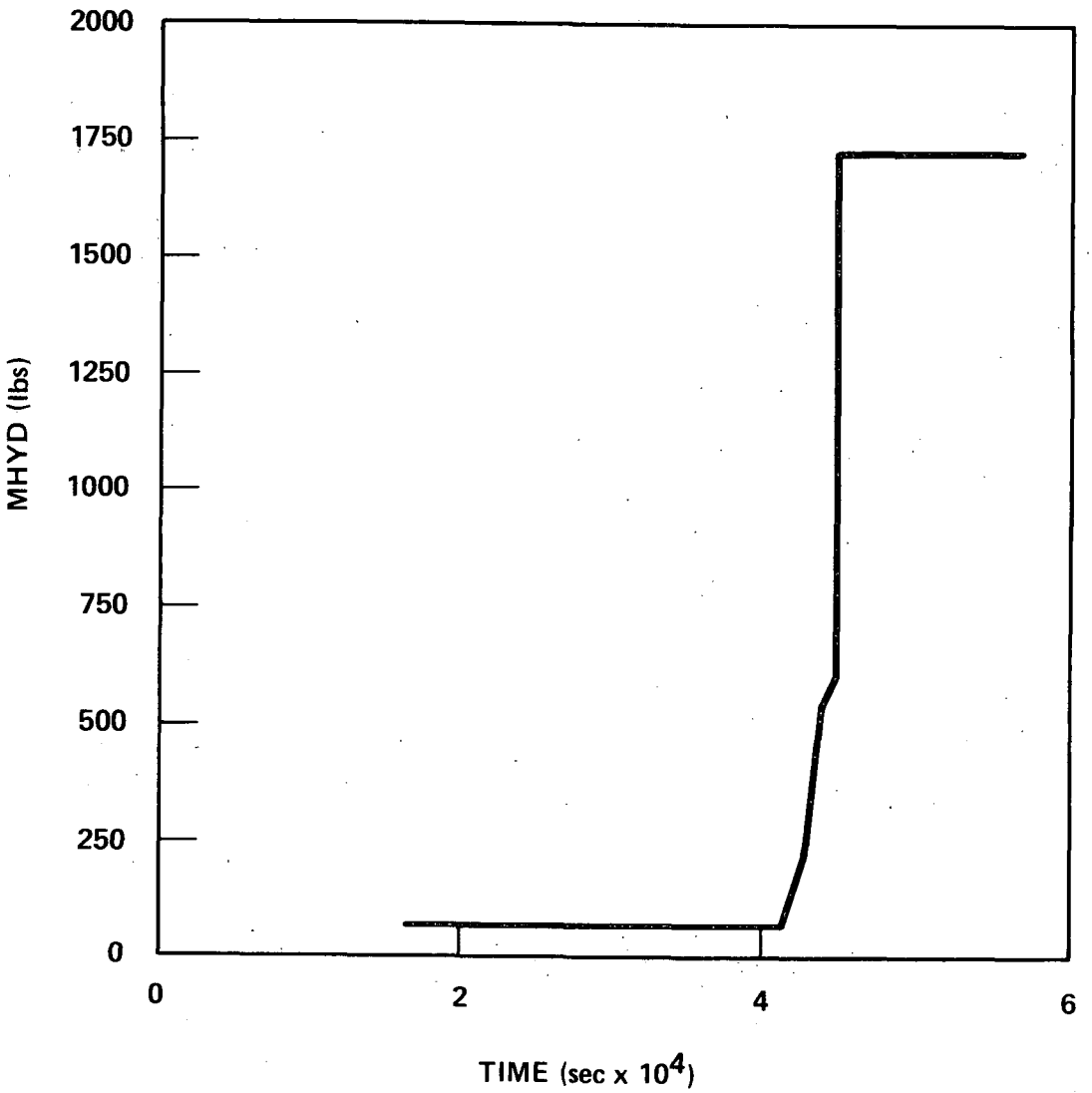
Class IV, Case 5A



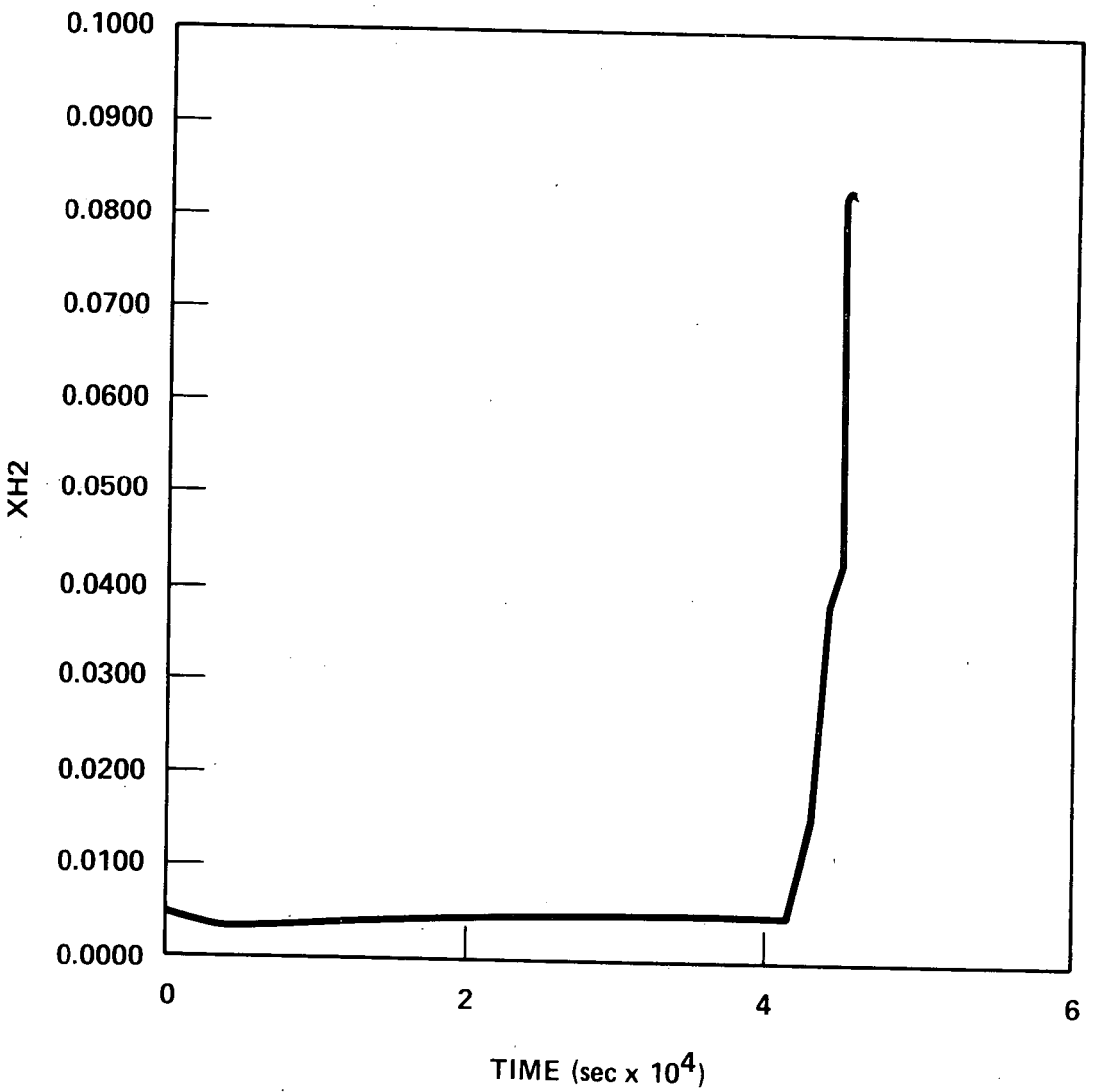
Pressure (in Containment) vs. Time
S2HF, W, 80% Dispersive, No Burn
Class IV, Case 5A



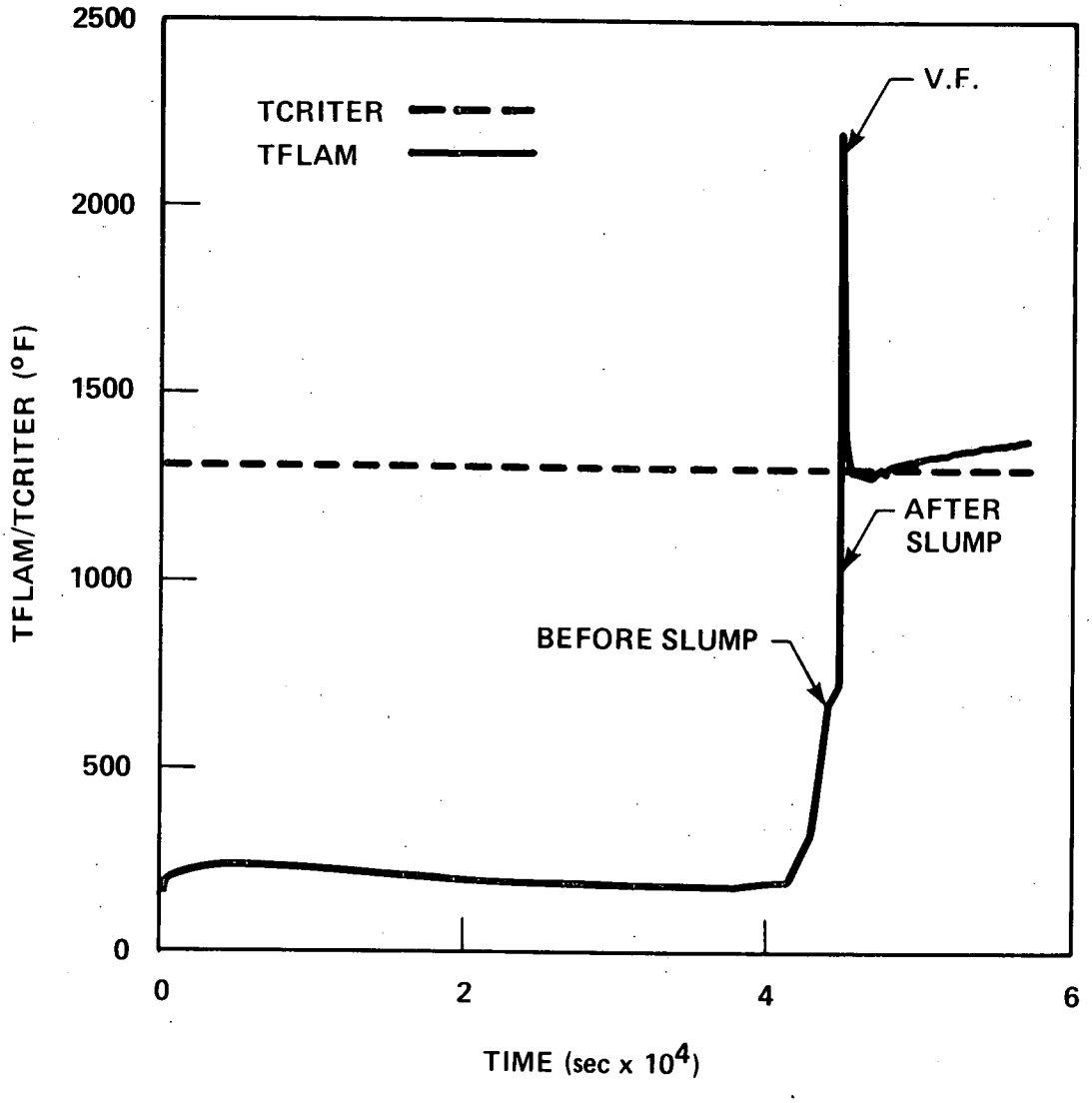
Temperature (in Containment) vs. Time
S2HF, W, 80% Dispersive, No Burn
Class IV, Case 5A



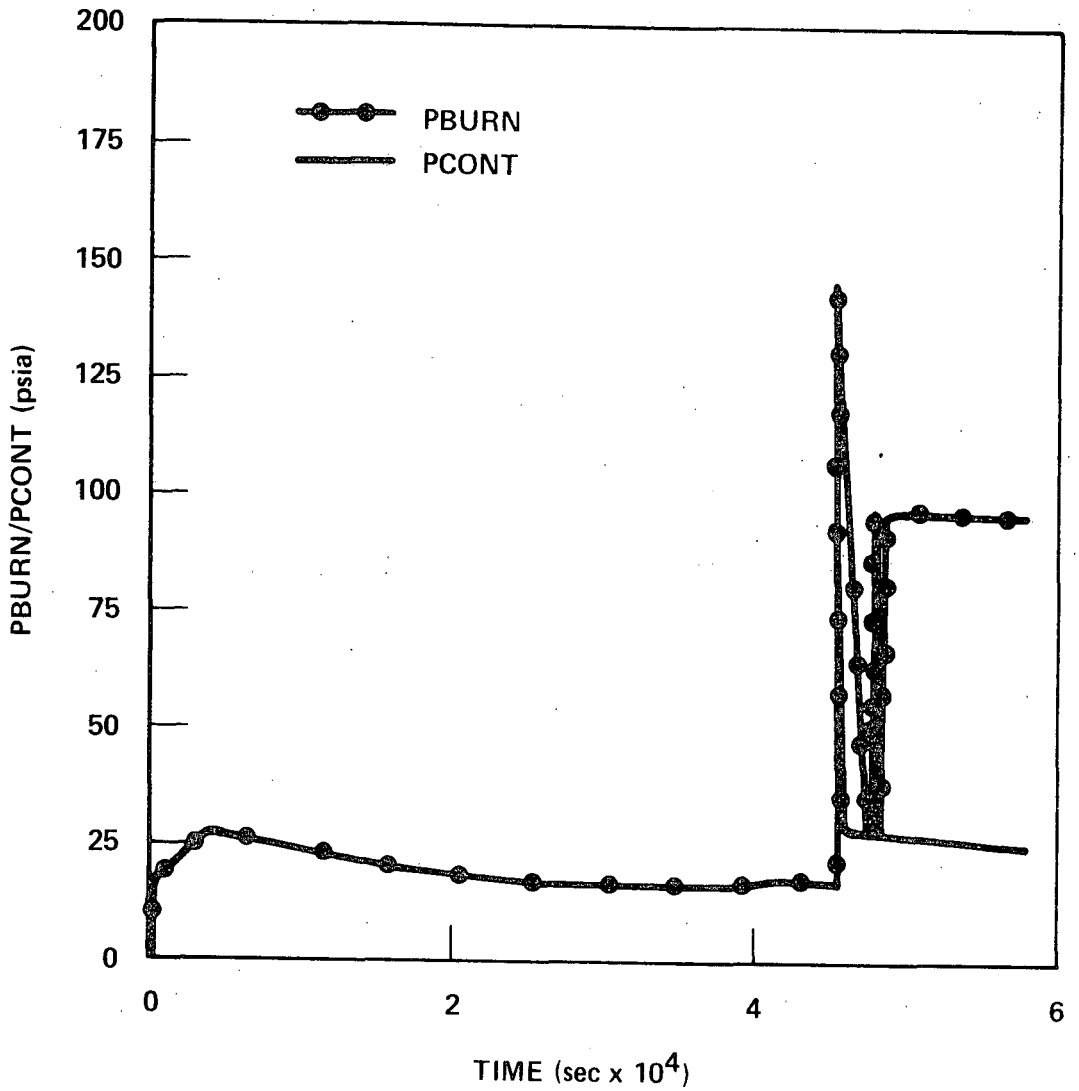
Mass Hydrogen (in Containment) vs. Time
S2HF, W, 80% Dispersive, No Burn
Class IV, Case 5A



Mole Fraction H_2 (in Containment) vs. Time
S2HF, W, 80% Dispersive, No Burn
Class IV, Case 5A



Flame Temperature (in Containment) vs. Time
S2HF, W, 80% Dispersive, No Burn
Class IV, Case 5A



Adiabatic Burn Pressure/Pressure in Containment vs. Time
S2HF, W, 80% Dispersive, No Burn
Class IV, Case 5A

CASE: CLASS IV, CASE 5B, S2HF, W, 80% DISPERSIVE, BURN @ E.S.

DISPERSIVE: YES PERCENT CORE: 80 FRACTION IN CAVITY: 20

RUN #: AALAAMY DATE: 12/31/80

BLOWDOWN PEAK: N/A PSIA TIME: _____ SEC.

HYDROGEN BURN?: YES CRITERIA: END OF DISPERSION

TIME @ BURN: 44846 SEC, PRESSURE: 75 PSIA, TEMPERATURE: 1217 °F

PEAKS:

PRESSURE: 96 PSIA, TIME: 44866 SEC, WHY?: H_2 BURN

TEMPERATURE: 1787 °F, TIME: _____ SEC, WHY?: _____

DISPERSIVE: YES

PRESSURE: 75 PSIA, TIME: 44846.6 SEC, WHY?: _____

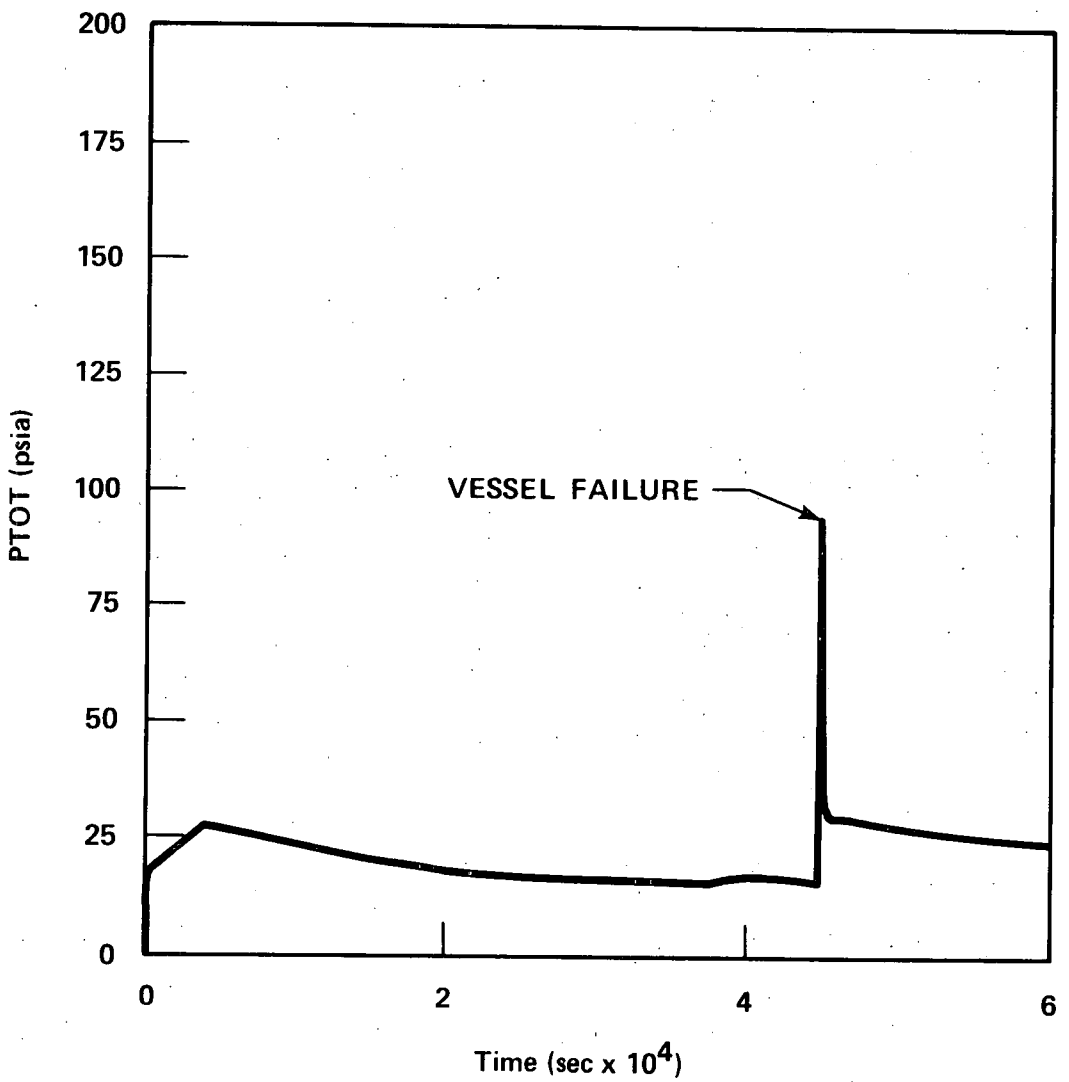
TEMPERATURE: 1235 °F, TIME: 44846.6 SEC, WHY?: _____

END OF BOIL: 44815 SEC. END OF HEAD: 44816 SEC.

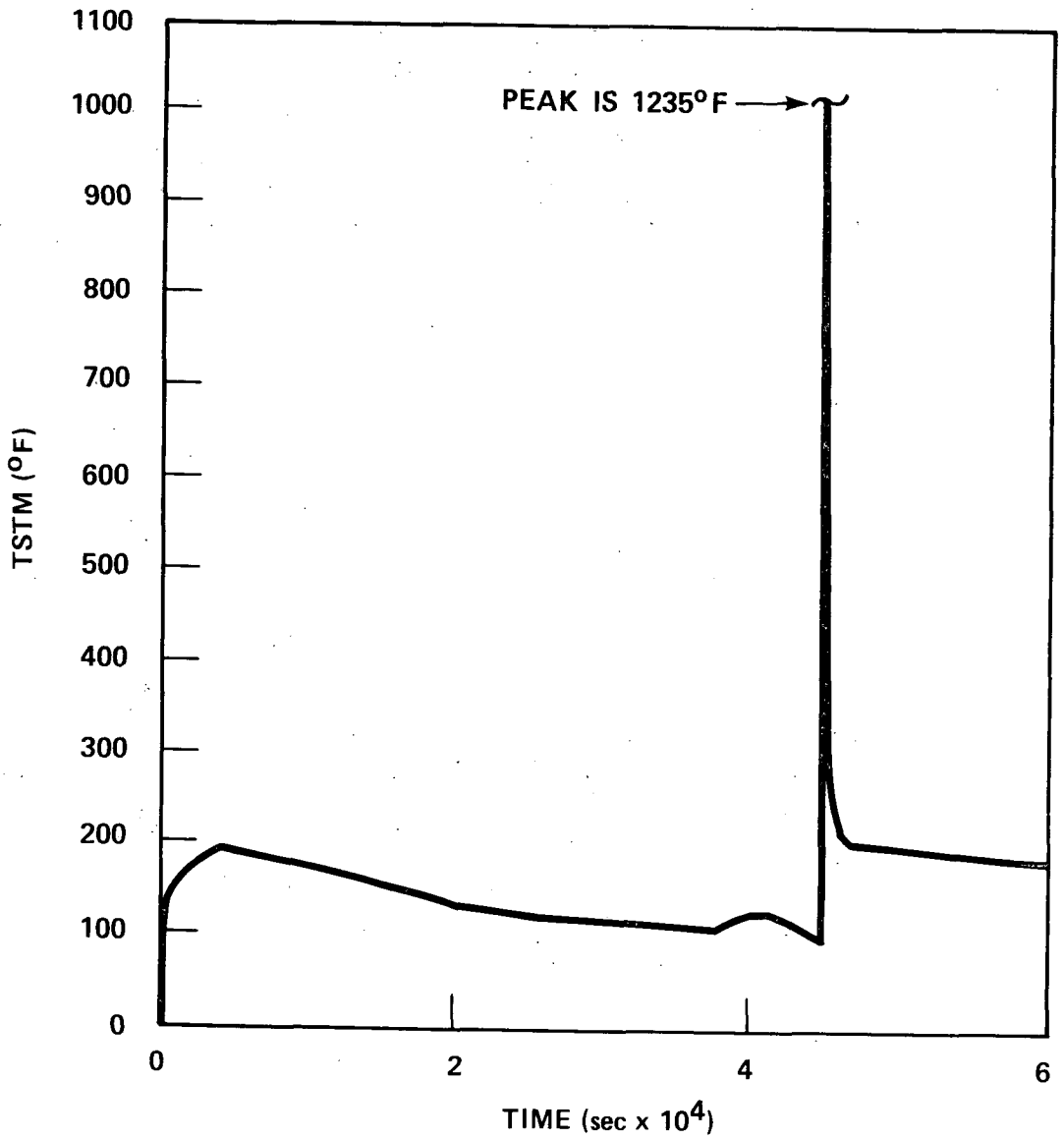
VESSEL FAILURE: 44816 SEC. END OF HOTDROP: _____ SEC.

END OF INTER: 86326 SEC.

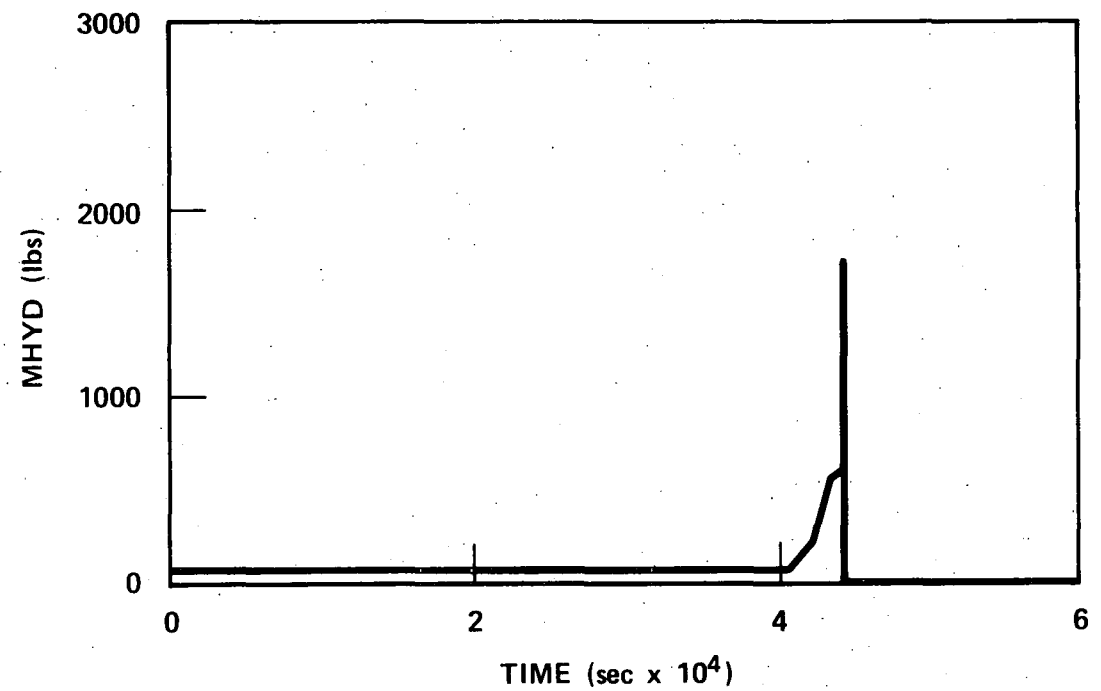
Class IV, Case 5B



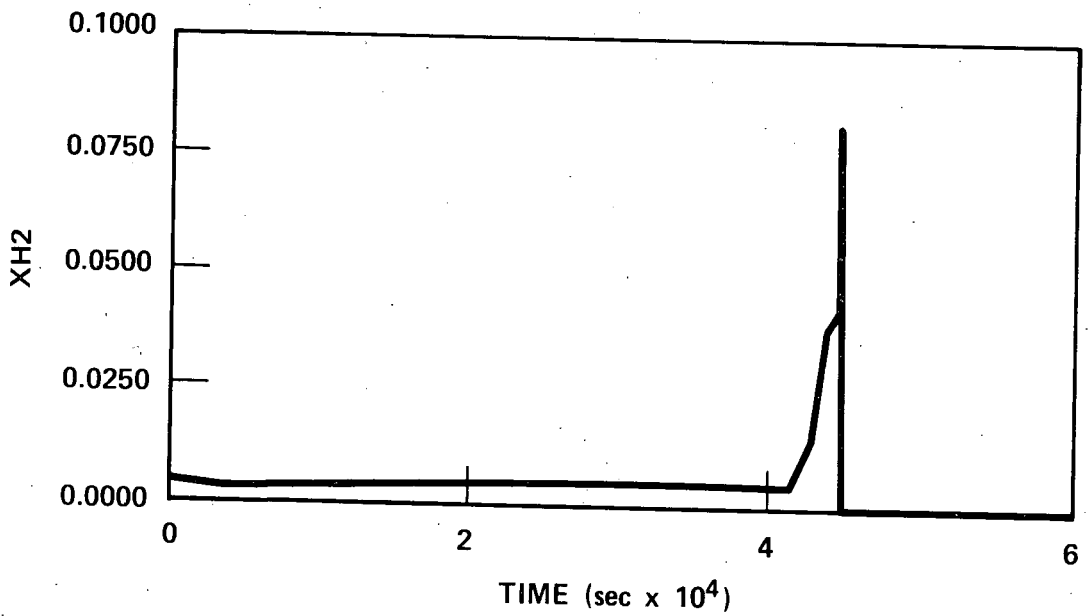
Pressure (in Containment) vs. Time
S2HF, W, 80% Dispersive, Burn @ E.S.
Class IV, Case 5B



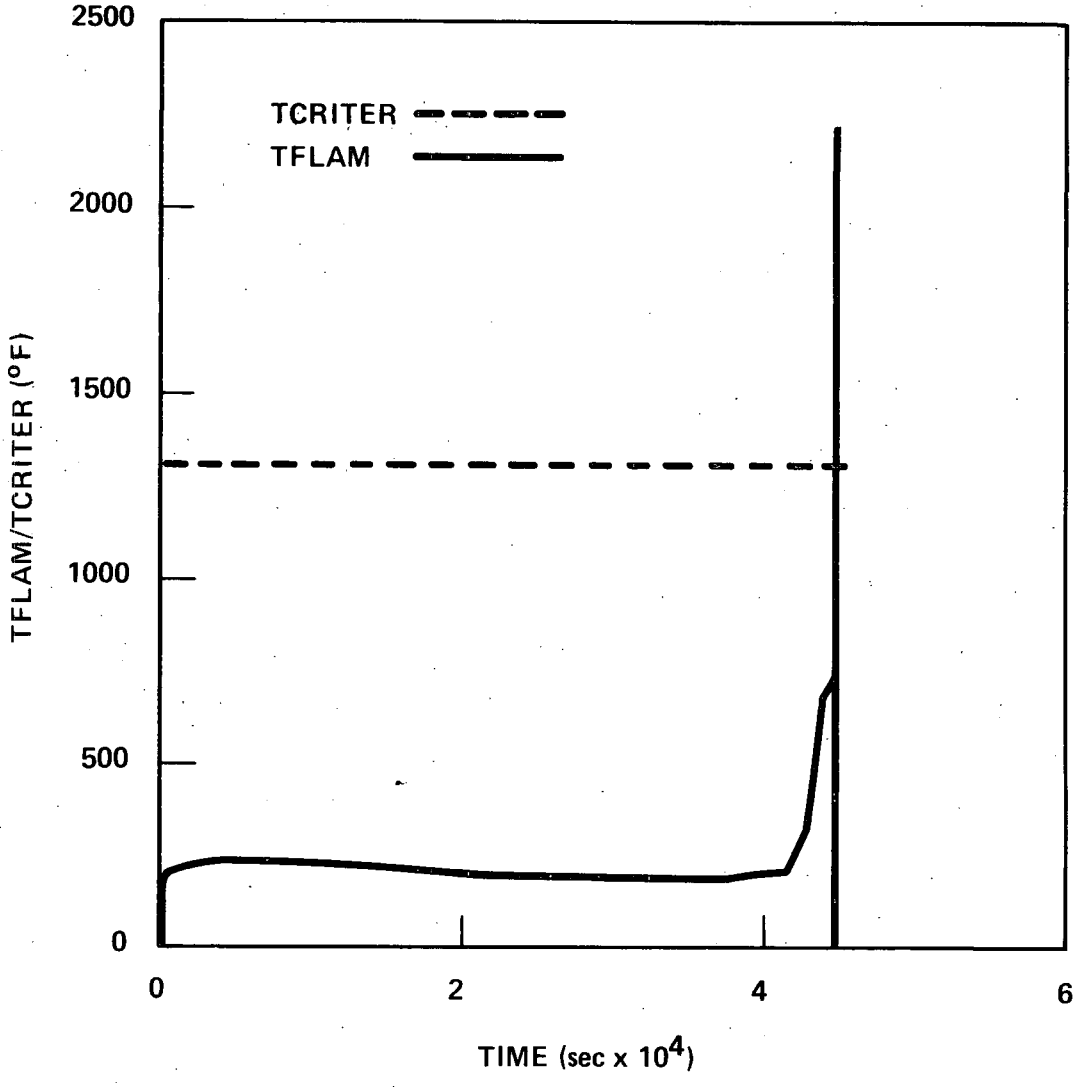
Temperature (in Containment) vs. Time
S2HF, W, 80% Dispersive; Burn @ E.S.
Class IV, Case 5B



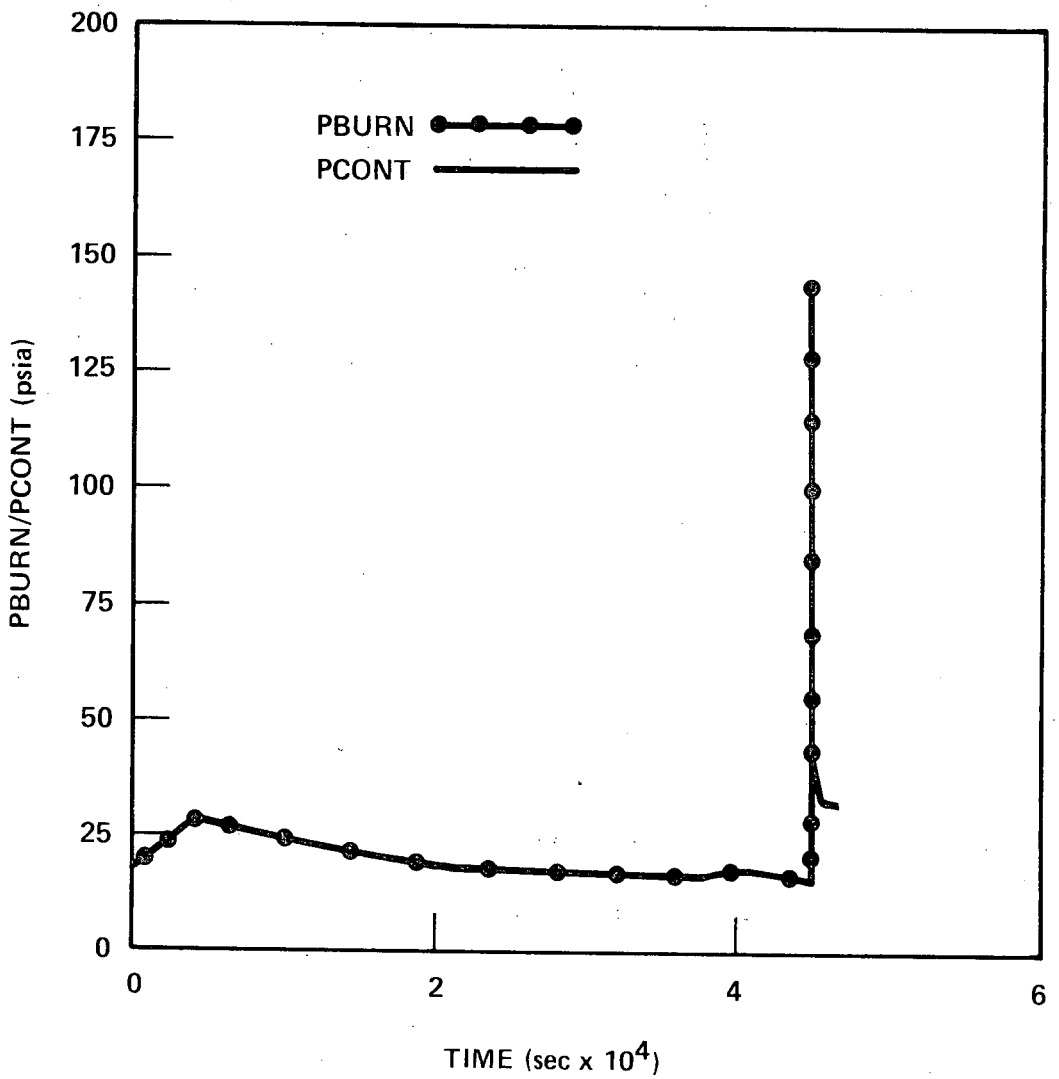
Mass Hydrogen (in Containment) vs. Time
S2HF, W, 80% Dispersive, Burn @ E.S.
Class IV, Case 5B



Mole Fraction H_2 (in Containment) vs. Time
S2HF, W, 80% Dispersive, Burn @ E.S.
Class IV, Case 5B



Flame Temperature (in Containment) vs. Time
S2HF, W, 80% Dispersive, Burn @ E.S.
Class IV, Case 5B



Adiabatic Burn Pressure/Pressure in Containment vs. Time
S2HF, W, 80% Dispersive, Burn @ E.S.
Class IV, Case 5B

CASE: CLASS IV, CASE 7B, S2HF, B, 80% DISPERSIVE, BURN @ E.S.

DISPERSIVE: YES PERCENT CORE: 80 FRACTION IN CAVITY: 0.20

RUN #: AALAAOE DATE: 12/31/80

BLOWDOWN PEAK: N/A PSIA TIME: _____ SEC.

HYDROGEN BURN?: YES CRITERIA: END OF SPERT

TIME @ BURN: 44846 SEC, PRESSURE: 73 PSIA, TEMPERATURE: 1179 °F

PEAKS:

PRESSURE: 105 PSIA, TIME: 44866 SEC, WHY?: BURN @ END OF DISPERSION

TEMPERATURE: 2046 °F, TIME: 44866 SEC, WHY?: BURN @ END OF DISPERSION

DISPERSIVE: YES

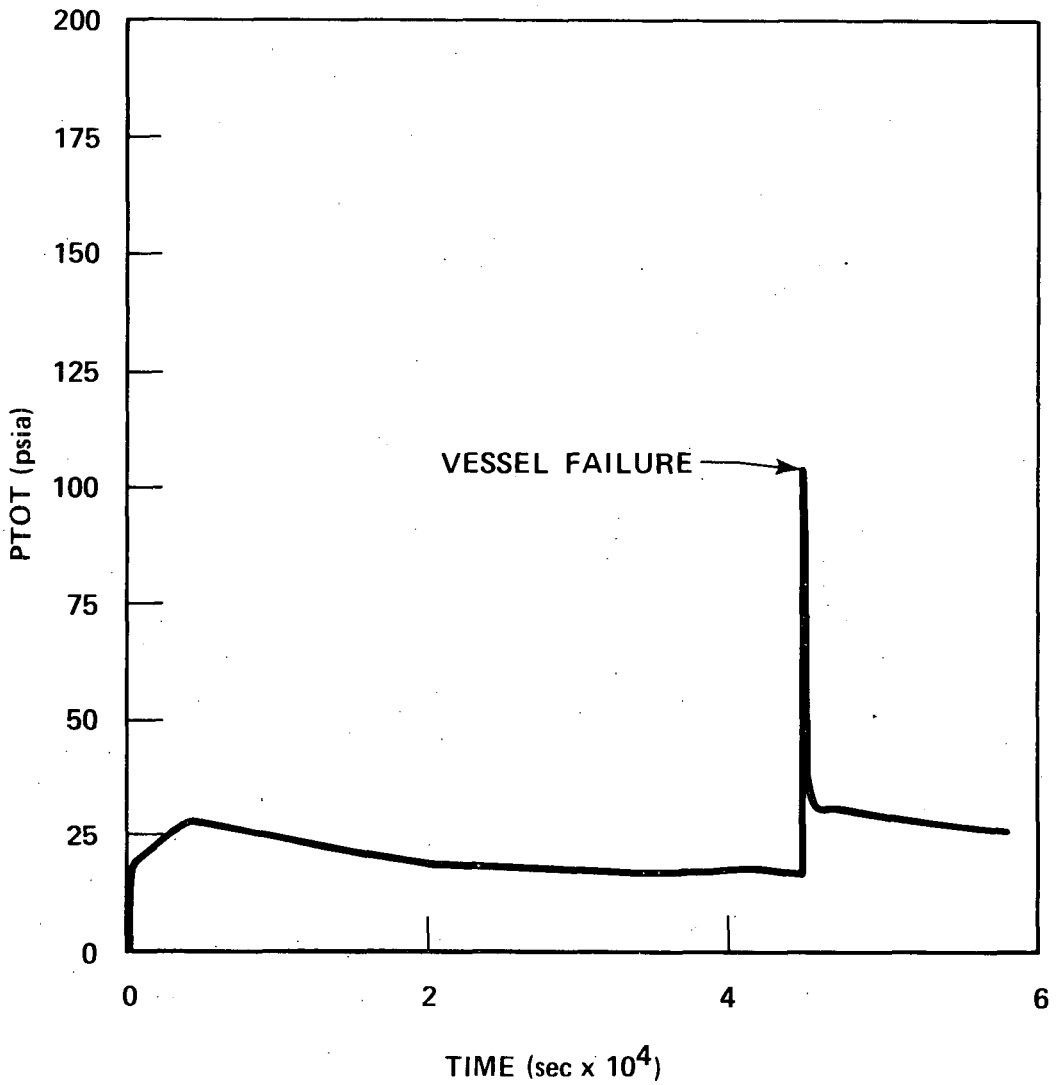
PRESSURE: 73 PSIA, TIME: 44846 SEC,

TEMPERATURE: 1179 °F, TIME: 44846 SEC,

END OF BOIL: 44815 SEC. END OF HEAD: 44816 SEC.

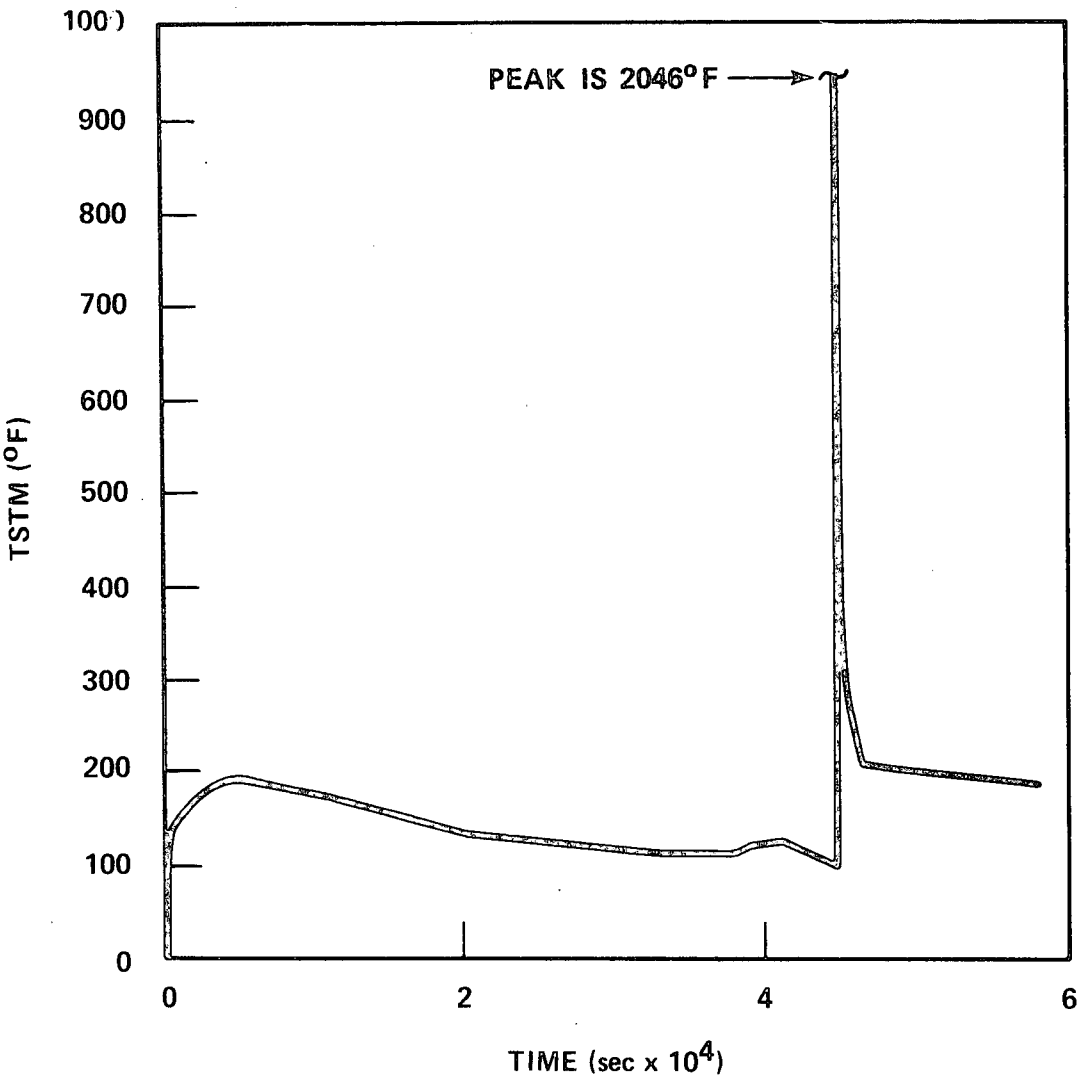
VESSEL FAILURE: 44816 SEC. END OF HOTDROP: 53942 SEC.

END OF INTER: 86237 SEC.

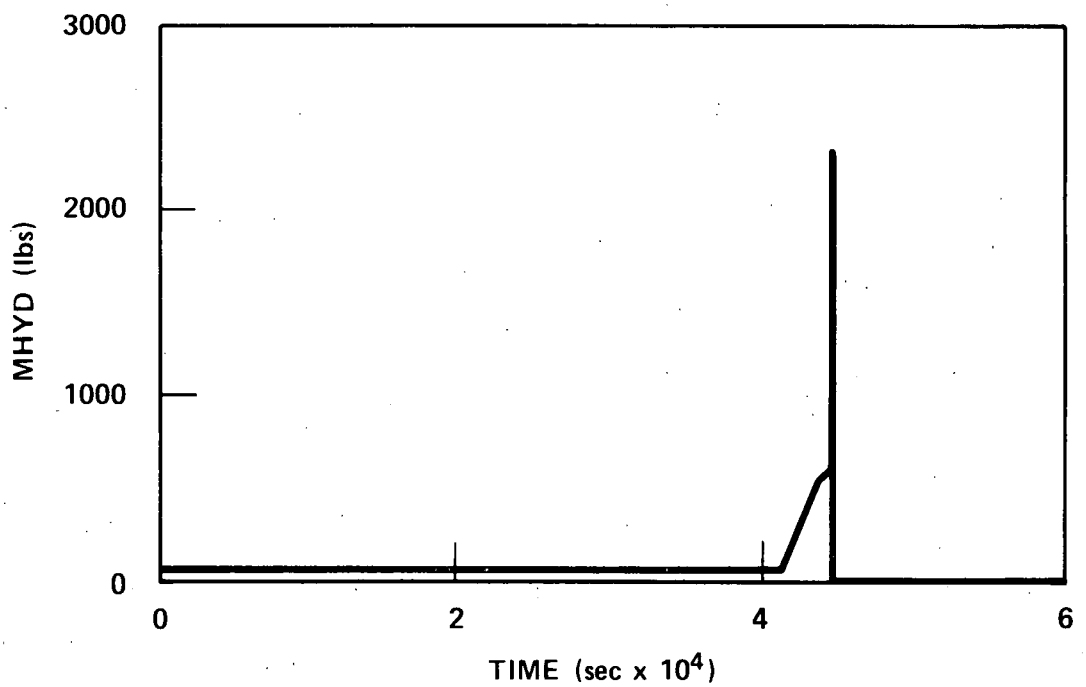


Pressure (in Containment) vs. Time
S2HF, B, 80% Dispersive, Burn @ E.S.
Class IV, Case 7B

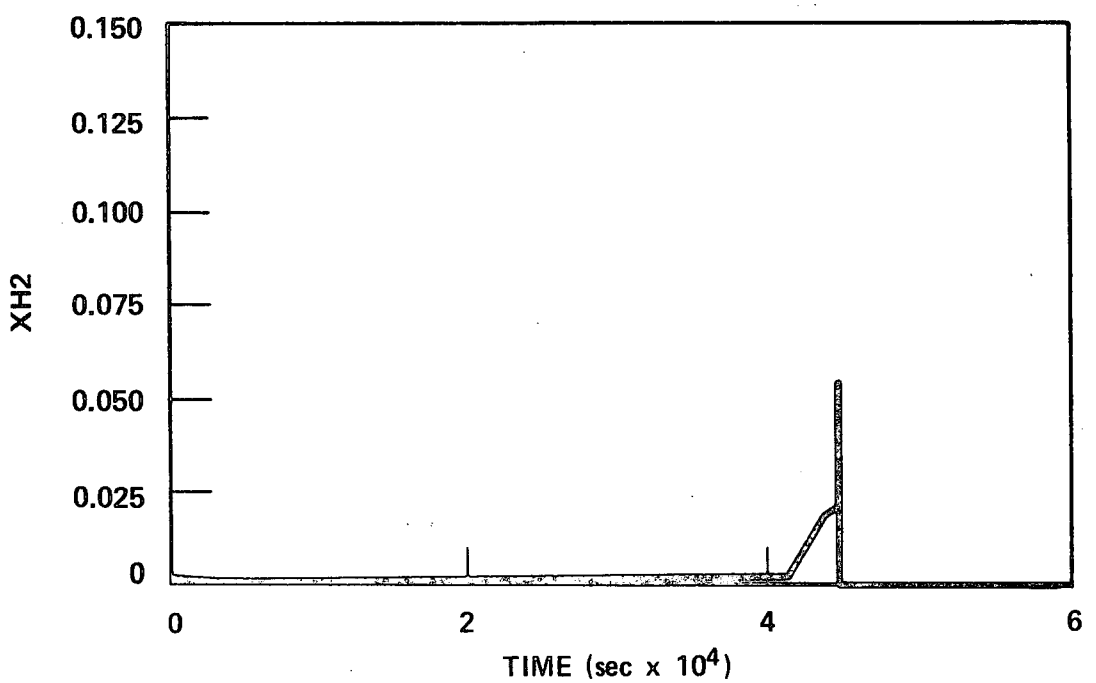
Sheet 2 of 7



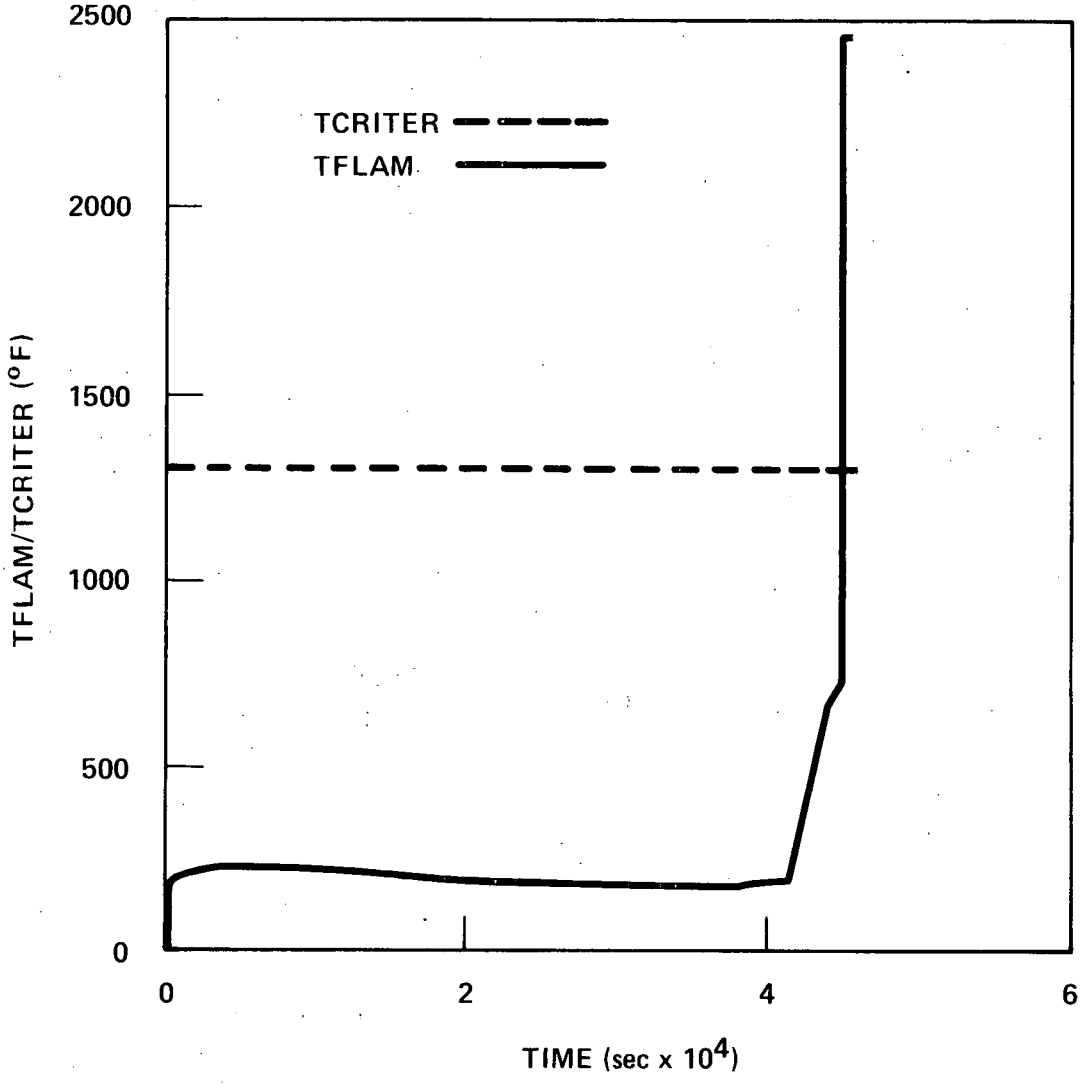
Temperature (in Containment) vs. Time
S2HF, B, 80% Dispersive, Burn @ E.S.
Class IV, Case 7B



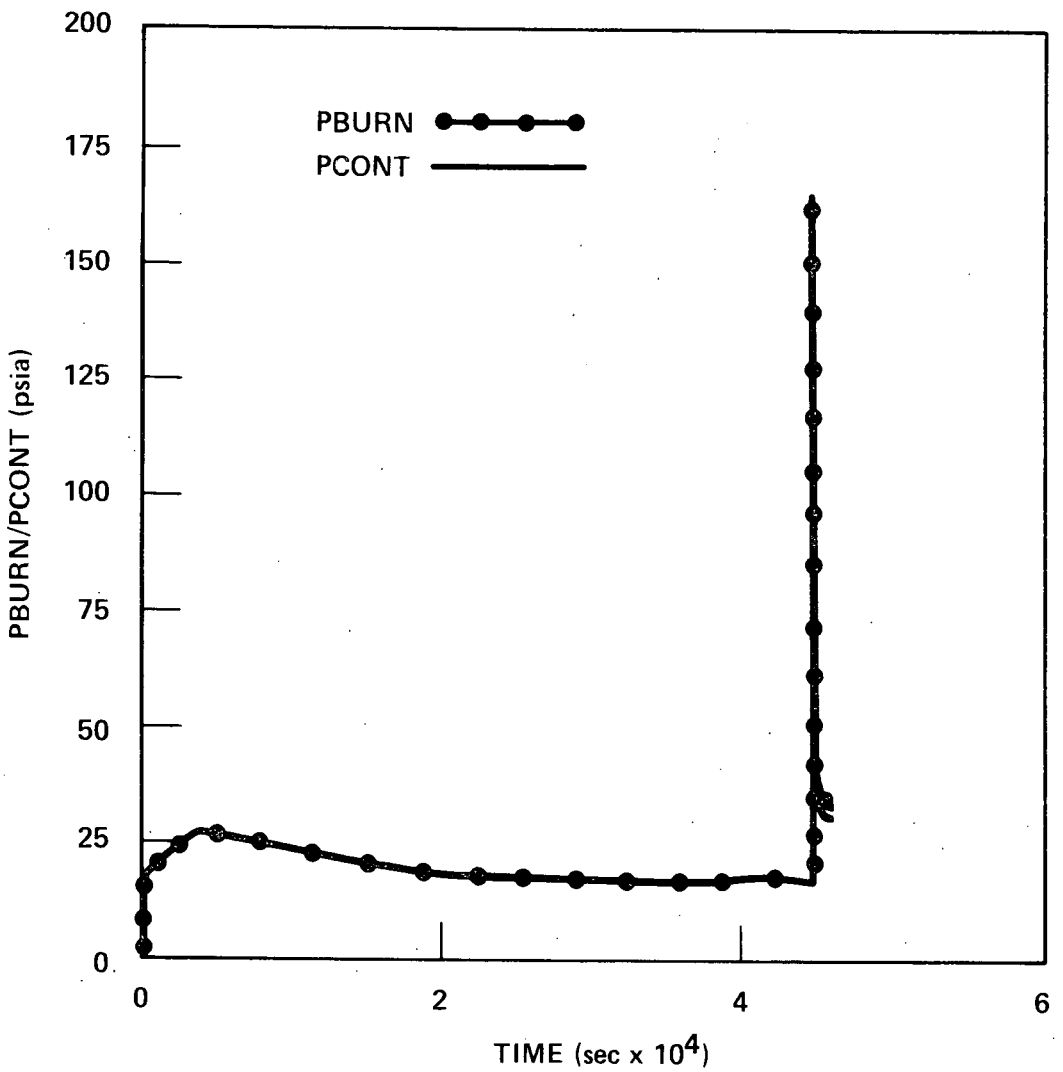
Mass Hydrogen (in Containment) vs. Time
S2HF, B, 80% Dispersive, Burn @ E.S.
Class IV, Case 7B



Mole Fraction H_2 (in Containment) vs. Time
S2HF, B, 80% Dispersive, Burn @ E.S.
Class IV, Case 7B



Flame Temperature (in Containment) vs. Time
S2HF, B, 80% Dispersive, Burn @ E.S.
Class IV, Case 7B



Adiabatic Burn Pressure/Pressure in Containment vs. Time
S2HF, B, 80% Dispersive, Burn @ E.S.
Class IV, Case 7B

CASE: CLASS V, CASE 1A, TMLB, B, NO BURN, NON-DISPERSIVE

DISPERSIVE: NO PERCENT CORE: _____ FRACTION IN CAVITY: _____

RUN #: AALAAGY DATE: 11/15/80

BLOWDOWN PEAK: N/A PSIA TIME: _____ SEC.

HYDROGEN BURN?: NO CRITERIA: _____

TIME @ BURN: _____ SEC, PRESSURE: _____ PSIA, TEMPERATURE: _____ ^{o}F

PEAKS:

PRESSURE: 147 PSIA, TIME: 86420 SEC, WHY?: END OF RUN

TEMPERATURE: 437 ^{o}F, TIME: ~15540 SEC, WHY?: VESSEL FAILURE

SPERT:

PRESSURE: _____ PSIA, TIME: _____ SEC, WHY?: _____

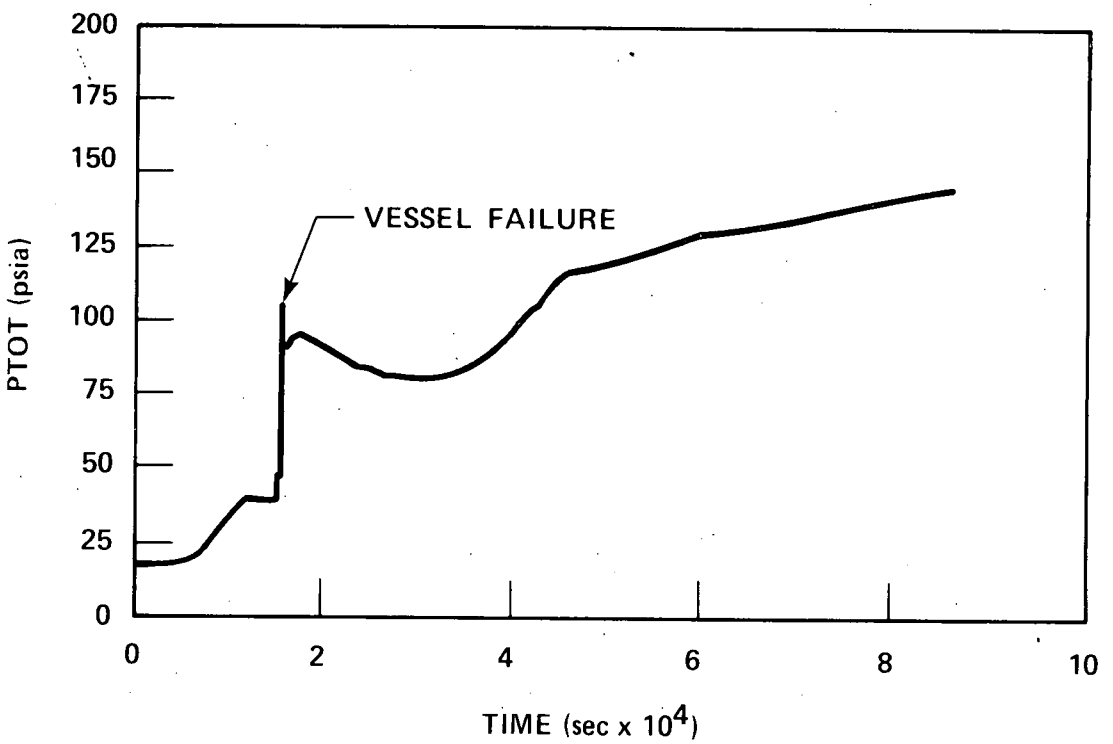
TEMPERATURE: _____ ^{o}F, TIME: _____ SEC, WHY?: _____

END OF BOIL: 15180 SEC. END OF HEAD: 15540 SEC.

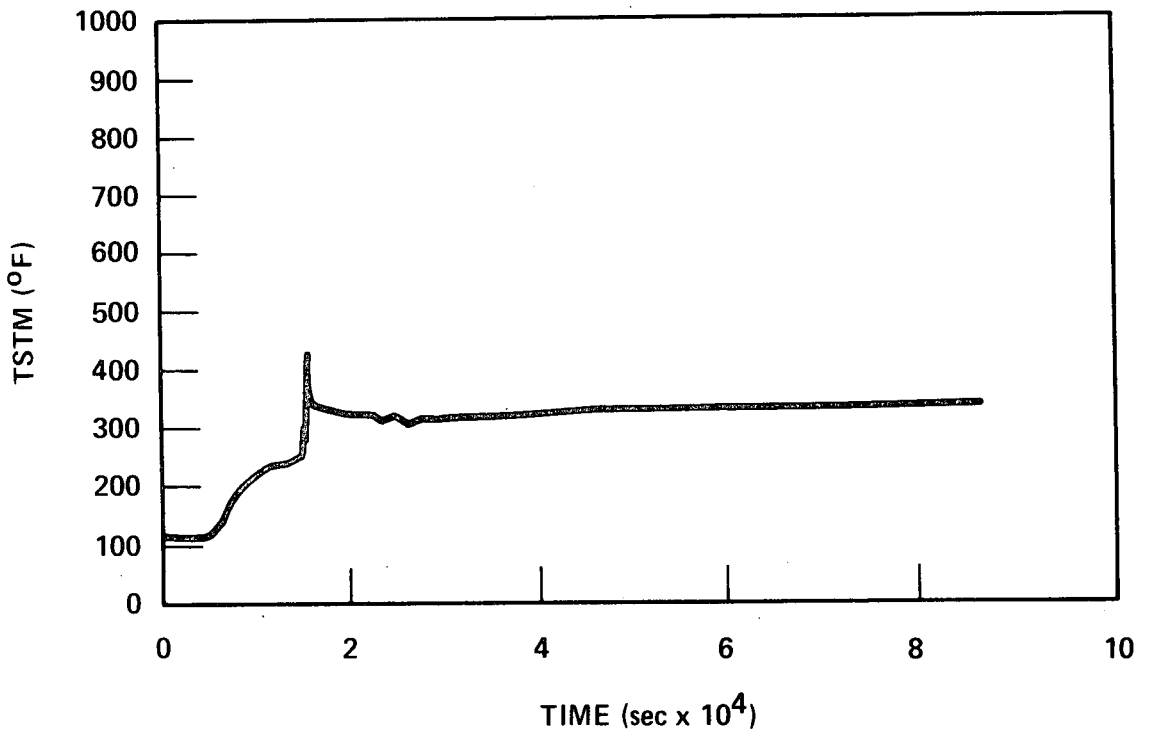
VESSEL FAILURE: 15540 SEC. END OF HOTDROP: 25147 SEC.

END OF INTER: 86420 SEC.

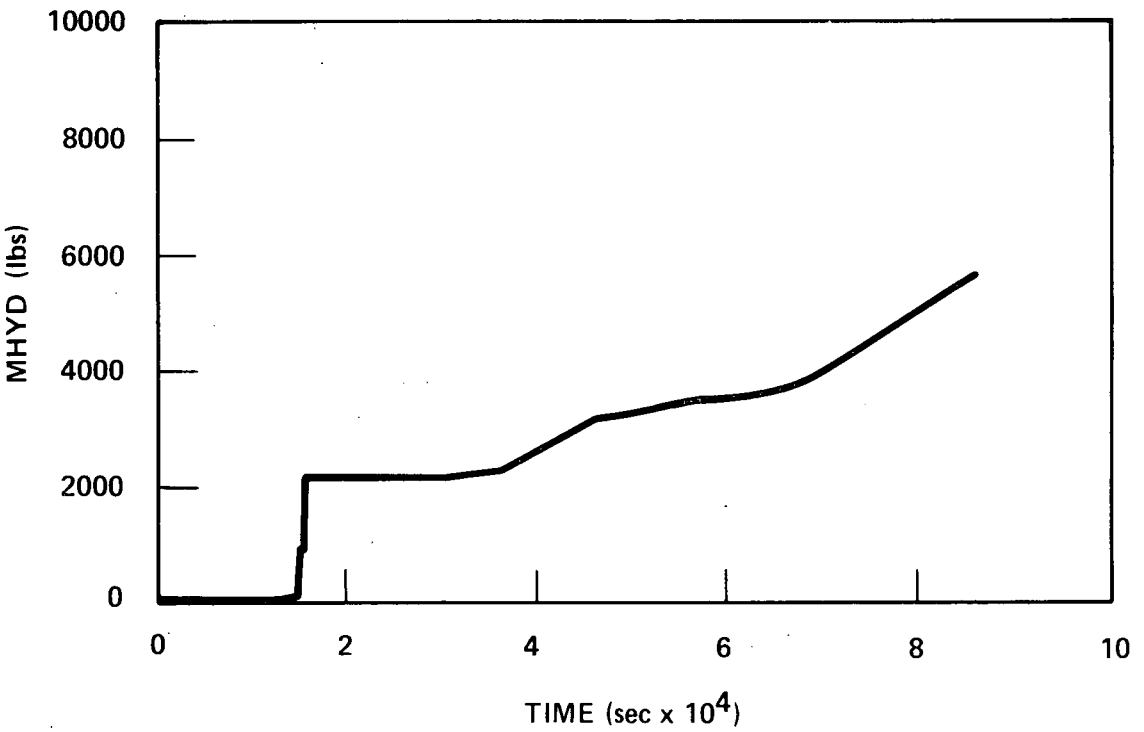
Class V, Case 1A



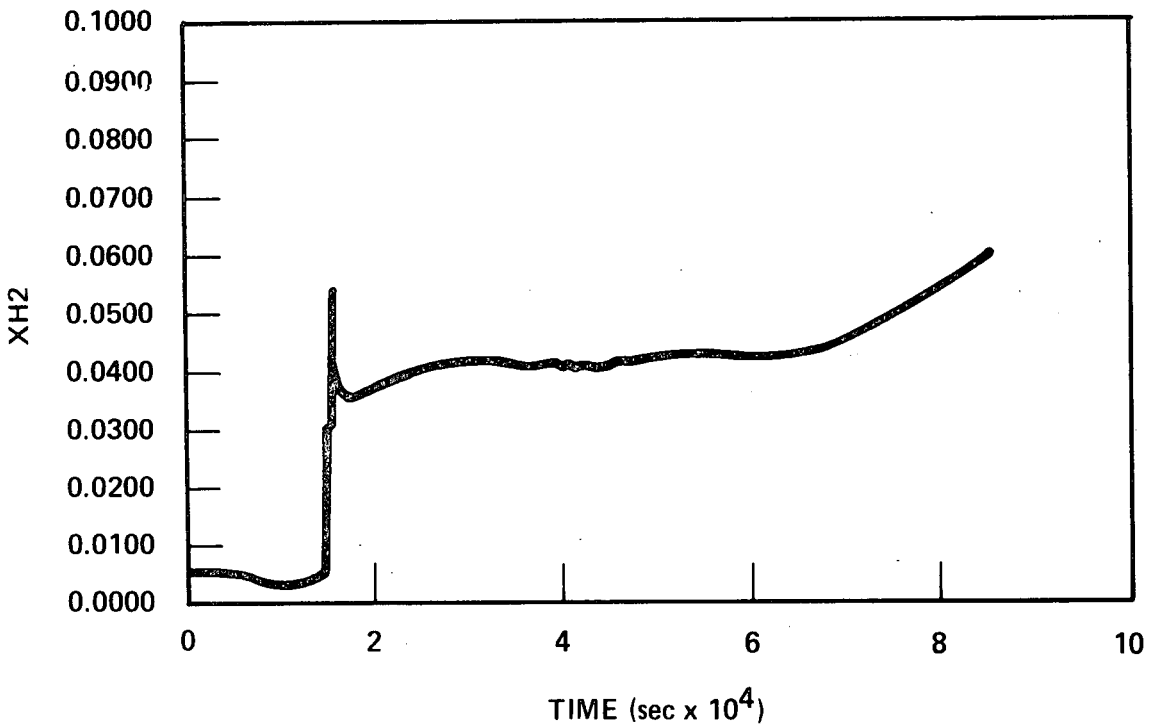
Pressure (in Containment) vs. Time
TMLB, B, No Burn, Non-Dispersive
Class V, Case 1A



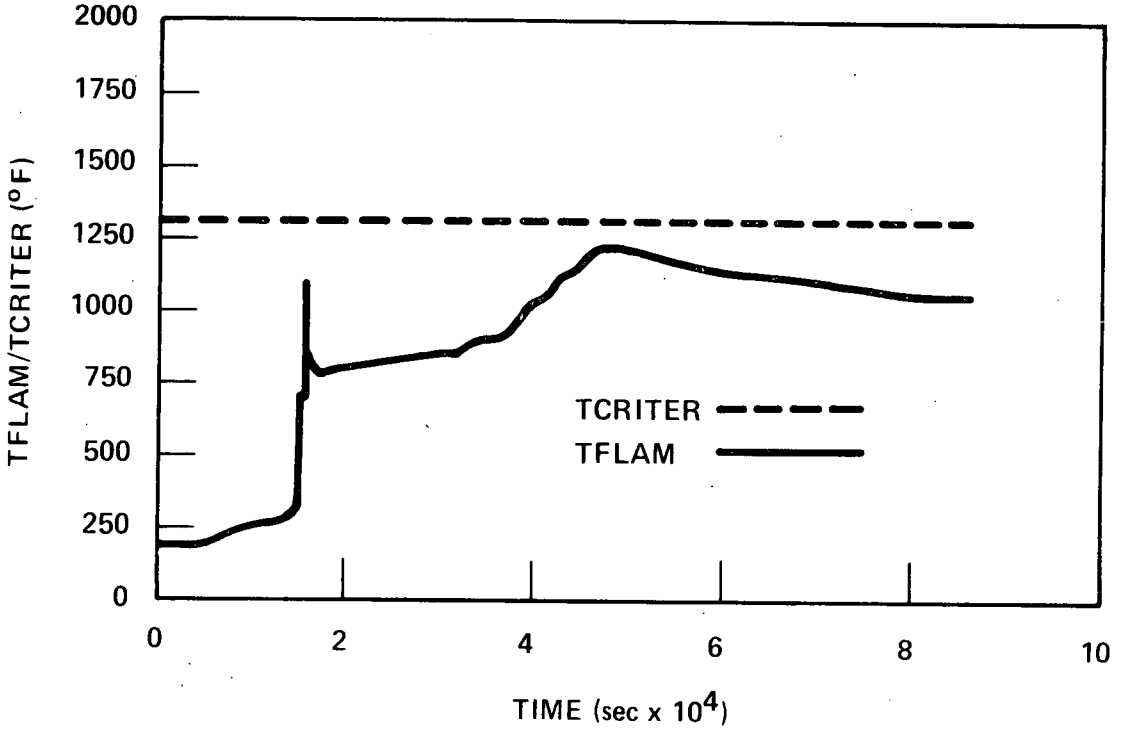
Temperature (in Containment) vs. Time
TMLB, B, No Burn, Non-Dispersive
Class V, Case 1A



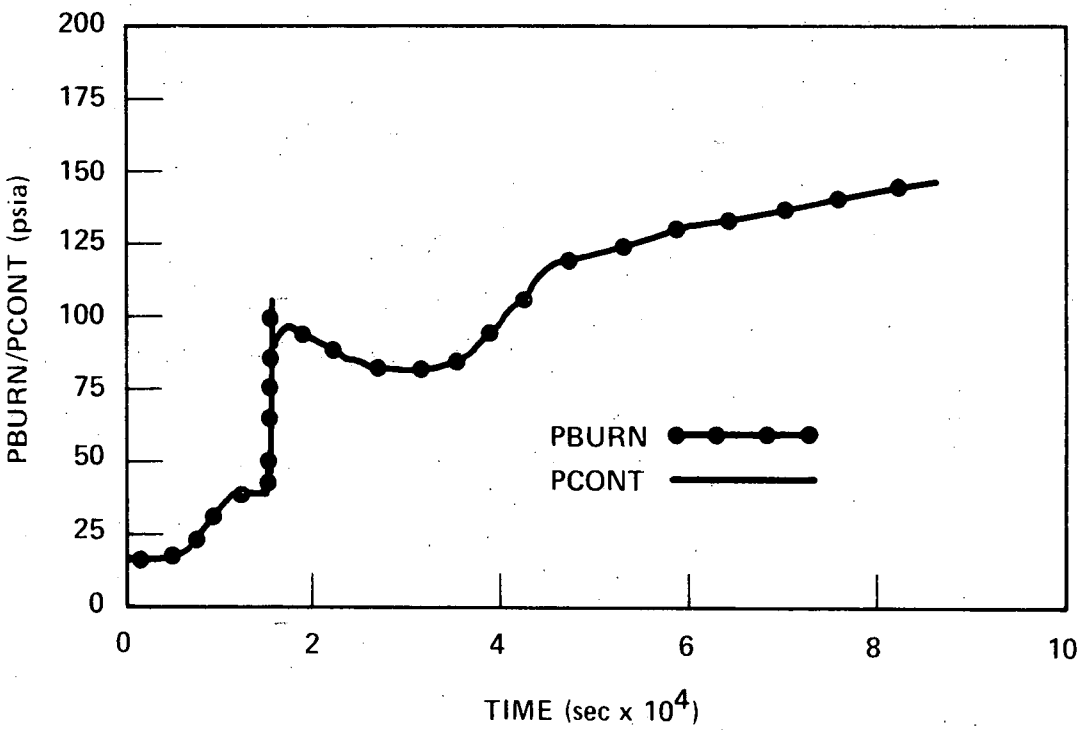
Mass Hydrogen (in Containment) vs. Time
TMLB, B, No Burn, Non-Dispersive
Class V, Case 1A



Mole Fraction H_2 (in Containment) vs. Time
TMLB, B, No Burn, Non-Dispersive
Class V, Case 1A



Flame Temperature (in Containment) vs. Time
TMLB, B, No Burn, Non-Dispersive
Class V, Case 1A



Adiabatic Burn Pressure/Pressure in Containment vs. Time
TMLB, B, No Burn, Non-Dispersive
Class V, Case 1A

CASE: CLASS V, CASE 2A, TMLB, W, NO BURN, NON-DISPERSIVE

DISPERSIVE: NO PERCENT CORE: _____ FRACTION IN CAVITY: _____

RUN #: AALAAJA DATE: 11/15/80

BLOWDOWN PEAK: N/A PSIA TIME: _____ SEC.

HYDROGEN BURN?: NO CRITERIA: _____

TIME @ BURN: _____ SEC, PRESSURE: _____ PSIA, TEMPERATURE: _____ °F

PEAKS:

PRESSURE: 110 PSIA, TIME: 60,000 SEC, WHY?: LONG TERM PRESSURIZATION

TEMPERATURE: 335 °F, TIME: ~15540 SEC, WHY?: VESSEL FAILURE

DISPERSIVE: NO

PRESSURE: _____ PSIA, TIME: _____ SEC, WHY?: _____

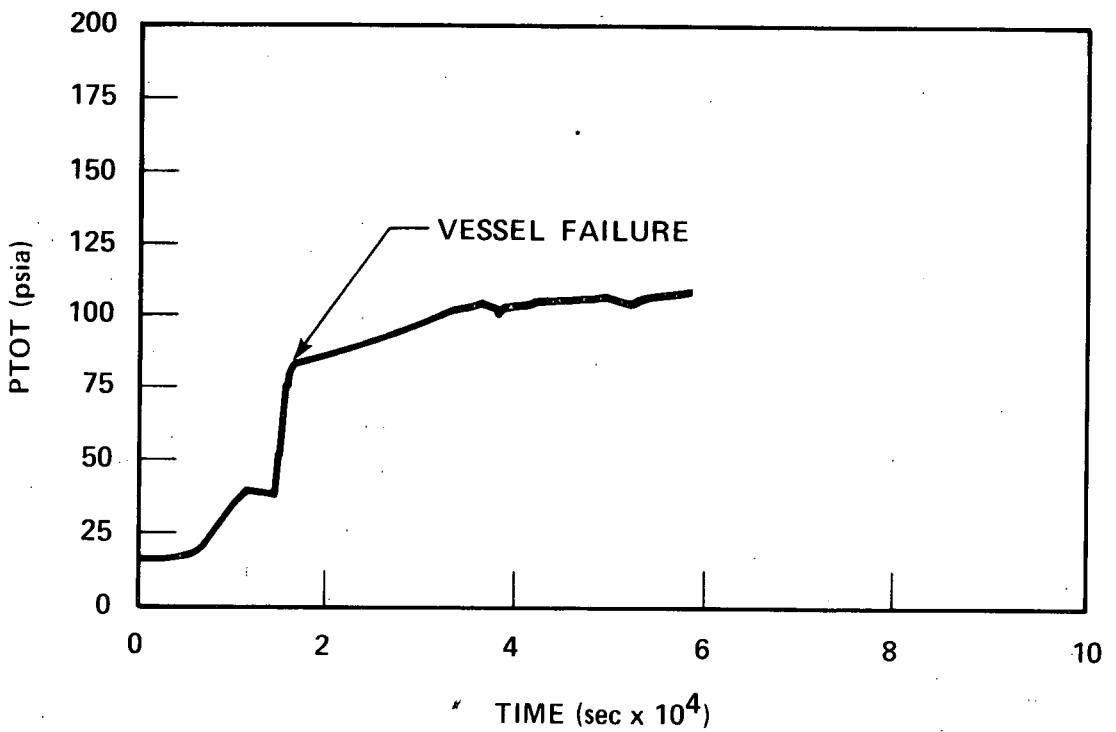
TEMPERATURE: _____ °F, TIME: _____ SEC, WHY?: _____

END OF BOIL: 15180 SEC. END OF HEAD: 15540 SEC.

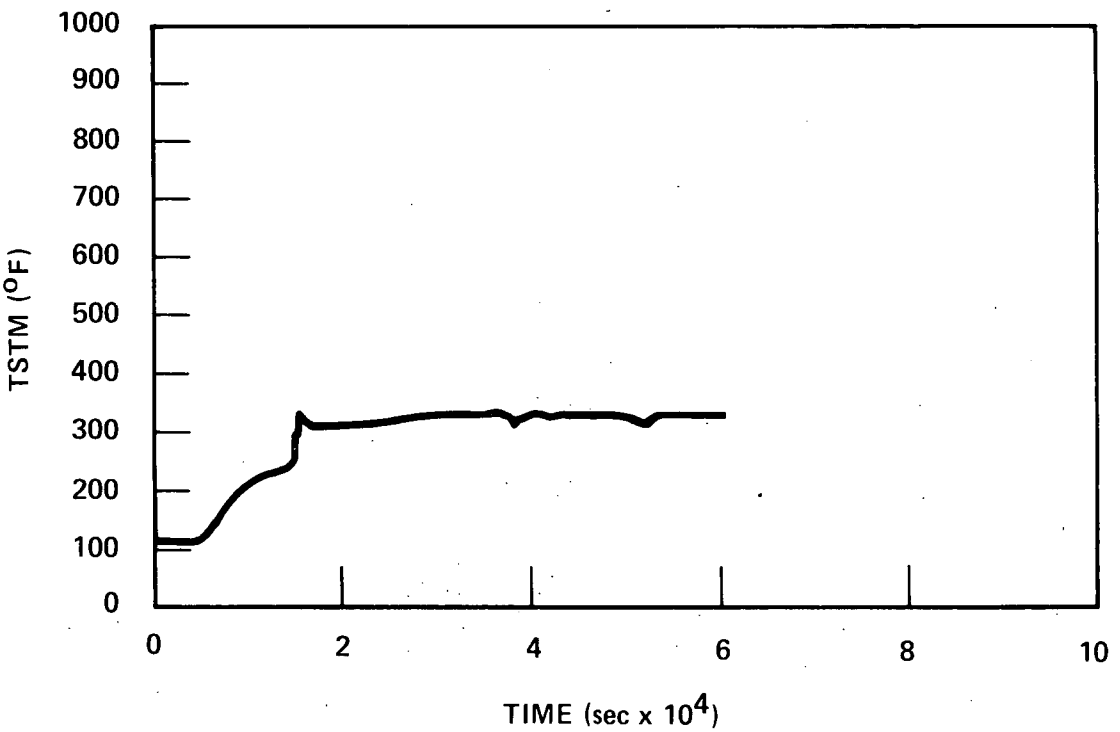
VESSEL FAILURE: 15540 SEC. END OF HOTDROP: 50240 SEC.

END OF INTER: 86753 SEC.

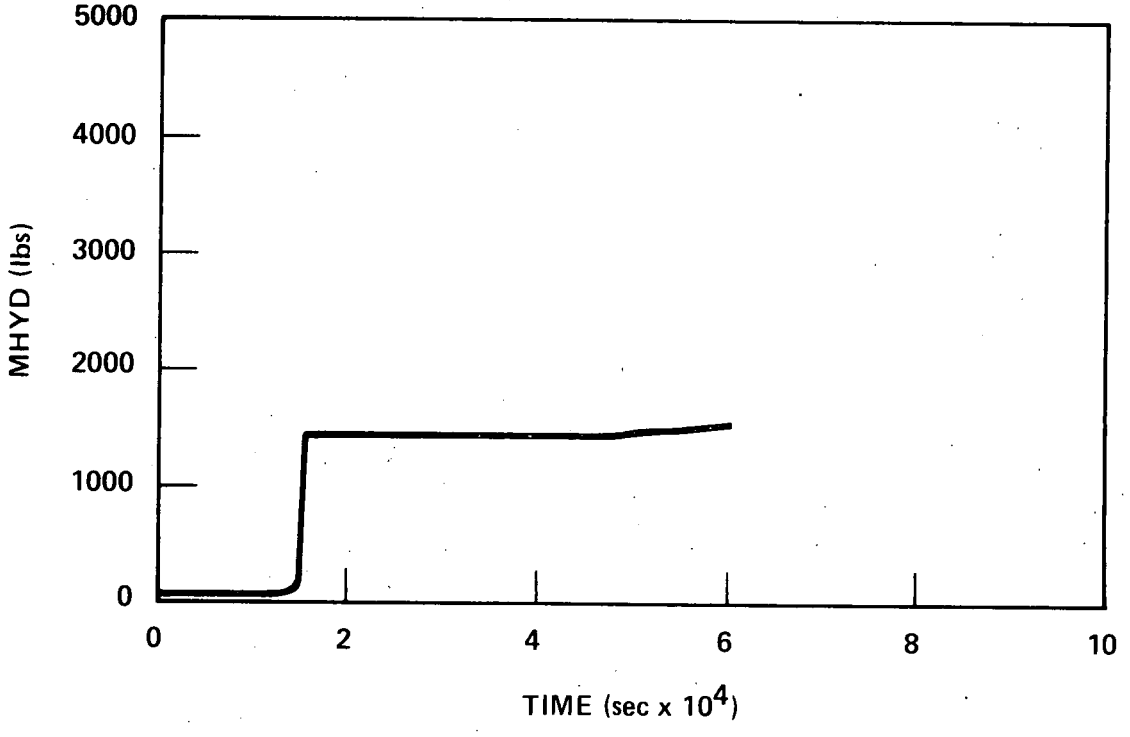
Class V, Case 2A



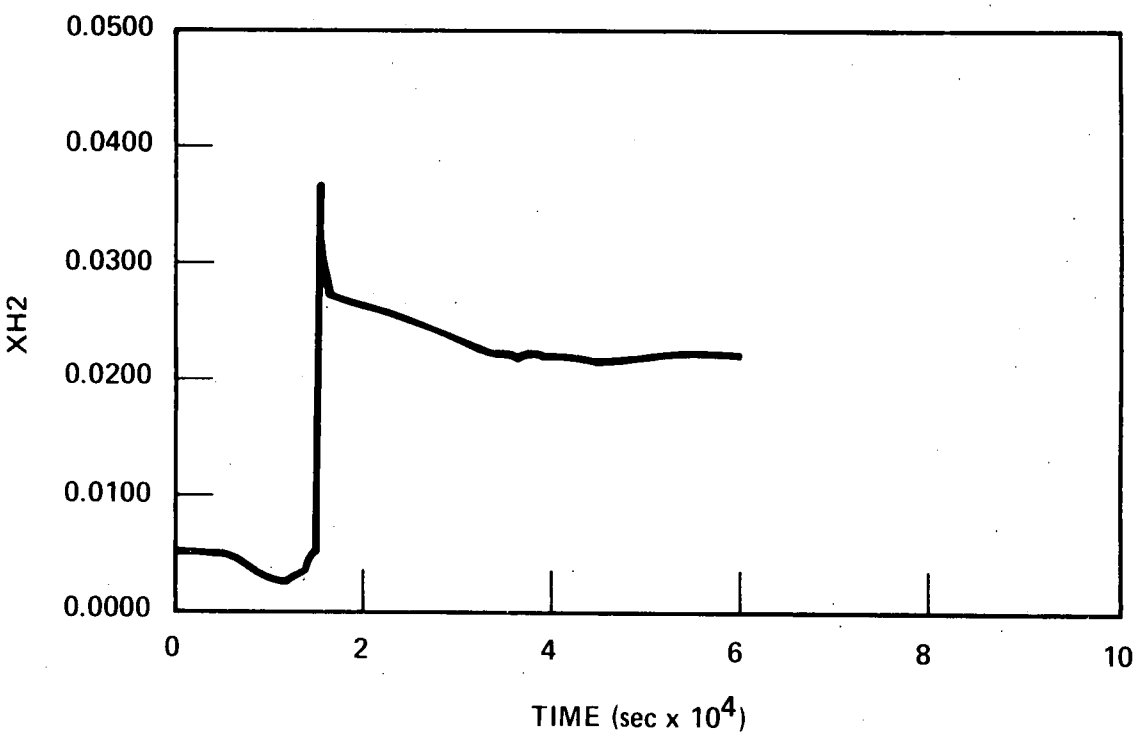
Pressure (in Containment) vs. Time
TMLB, W, No Burn, Non-Dispersive
Class V, Case 2A



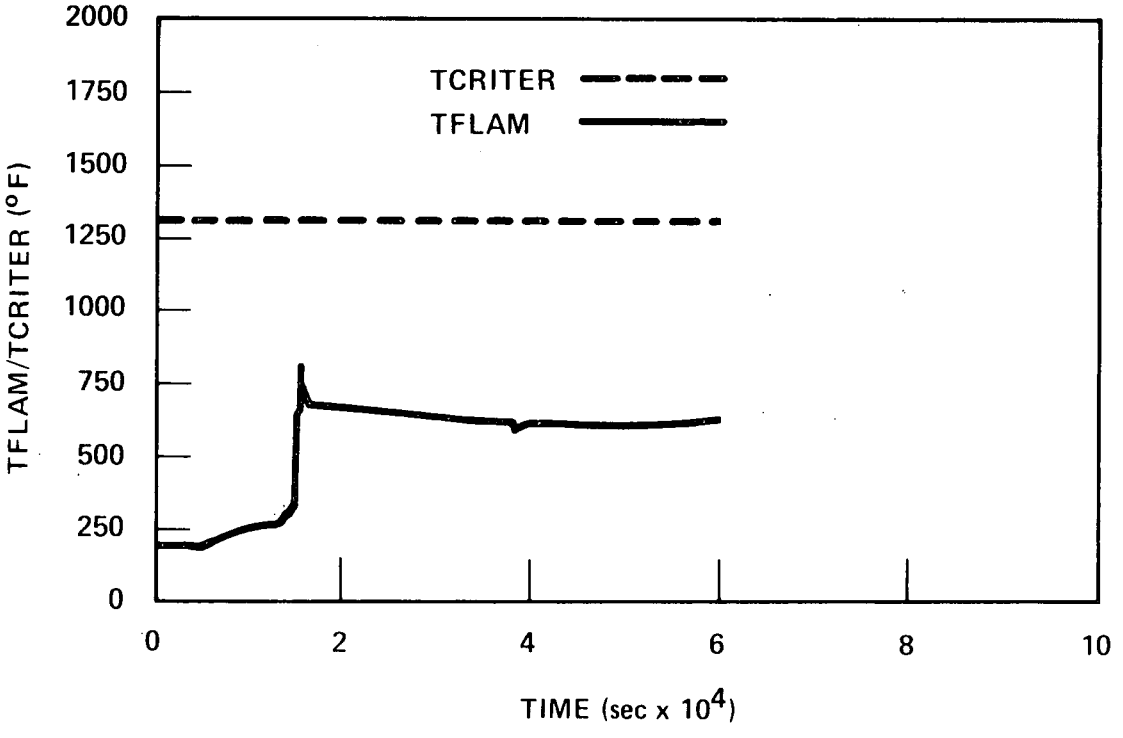
Temperature (in Containment) vs. Time
TMLB, W, No Burn, Non-Dispersive
Class V, Case 2A



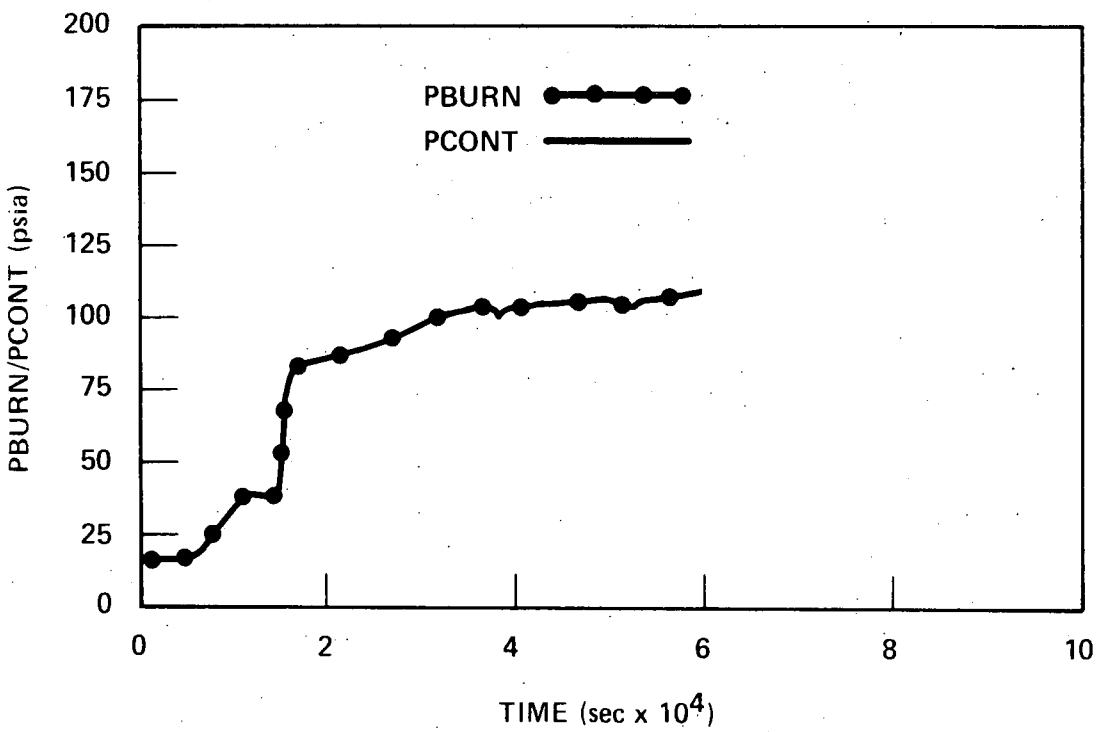
Mass Hydrogen (in Containment) vs. Time
TMLB, W, No Burn, Non-Dispersive
Class V, Case 2A



Mole Fraction H_2 (in Containment) vs. Time
TMLB, W, No Burn, Non-Dispersive
Class V, Case 2A



Flame Temperature (in Containment) vs. Time
TMLB, W, No Burn, Non-Dispersive
Class V, Case 2A



Adiabatic Burn Pressure/Pressure in Containment vs. Time
TMLB, W, No Burn, Non-Dispersive
Class V, Case 2A

CASE: CLASS V, CASE 3a, TMLB, TIME PHASED, 75% DISPERSED, NO BURN, 28% Zr REACTED

DISPERSIVE: YES PERCENT CORE: 75 FRACTION IN CAVITY: 0.25

RUN #: AB3YAWR DATE: 3/8/81 PERCENT ZR REACTED: 28

BLOWDOWN PEAK: N/A PSIA TIME: _____ SEC.

HYDROGEN BURN?: NO CRITERIA: _____

TIME @ BURN: _____ SEC, PRESSURE: _____ PSIA, TEMPERATURE: _____ °F

PEAKS:

PRESSURE: 83 PSIA, TIME: 15129 SEC, WHY?: VESSEL FAILURE

TEMPERATURE: 353 °F, TIME: 15130 SEC, WHY?: VESSEL FAILURE

DISPERSIVE: YES

PRESSURE: 83 PSIA, TIME: 15129 SEC, WHY?: _____

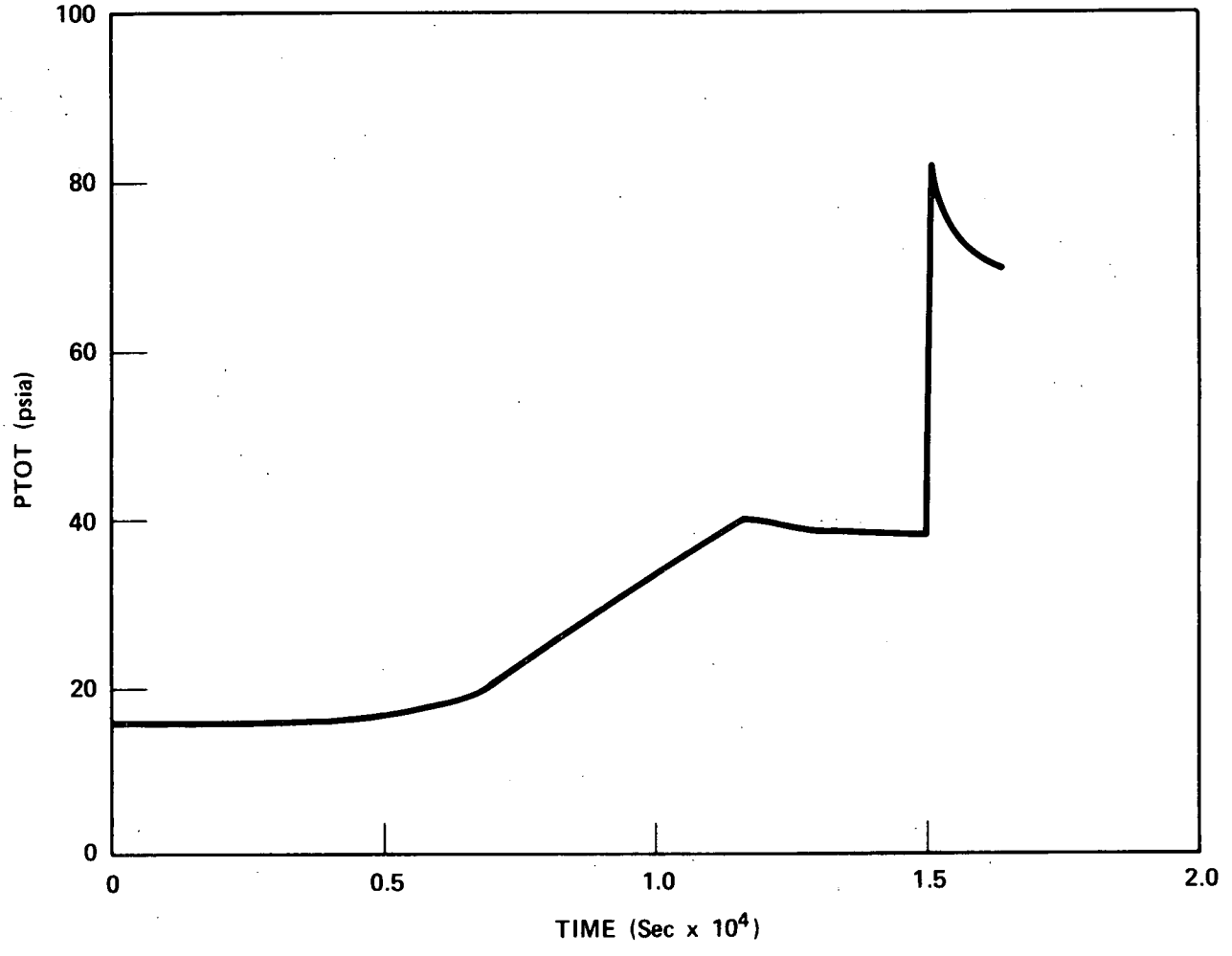
TEMPERATURE: 353 °F, TIME: 15129 SEC, WHY?: _____

END OF BOIL: 15000 SEC. END OF HEAD: _____ SEC.

VESSEL FAILURE: 15000 SEC. END OF HOTDROP: _____ SEC.

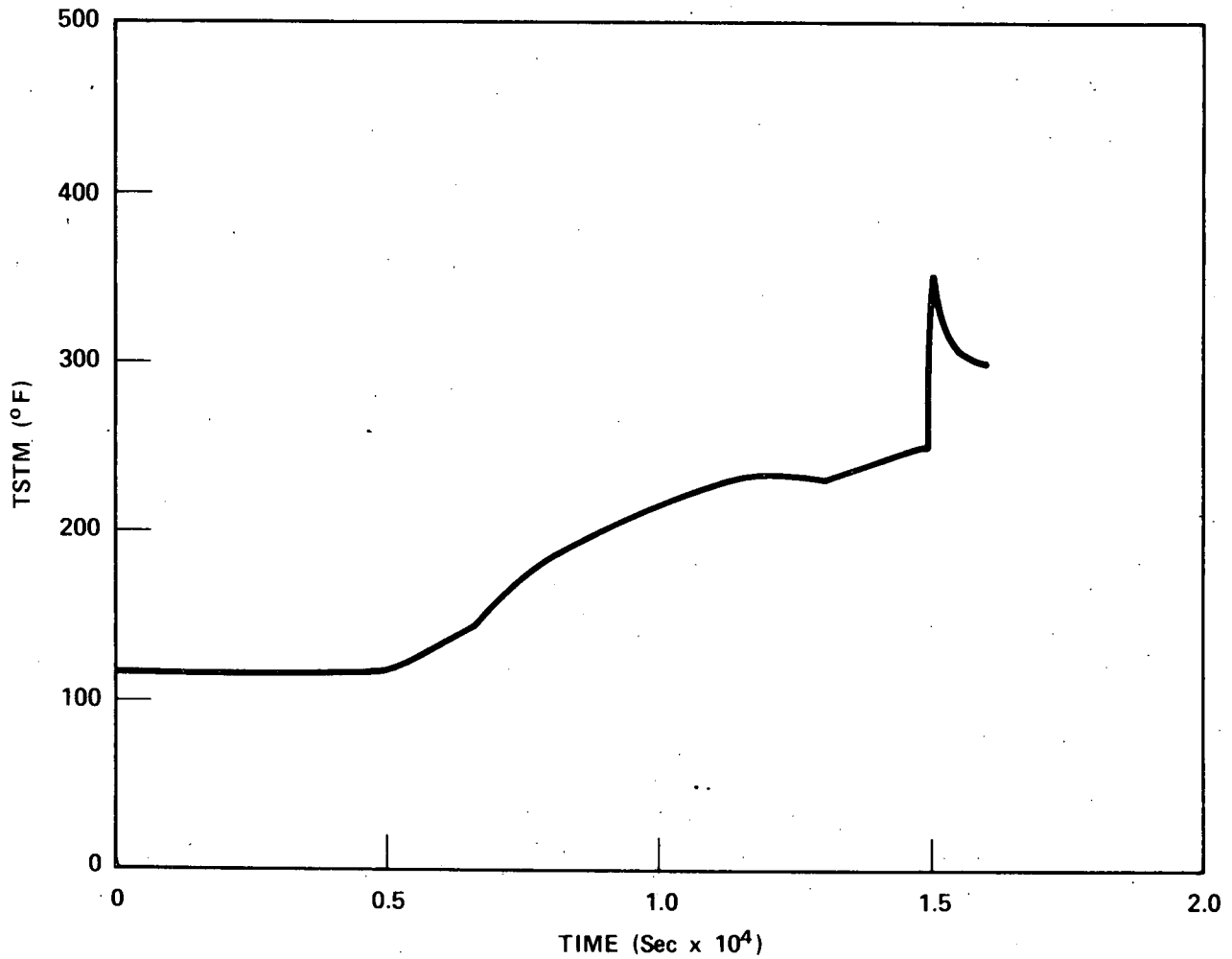
END OF INTER: _____ SEC.

Class V, Case 3a

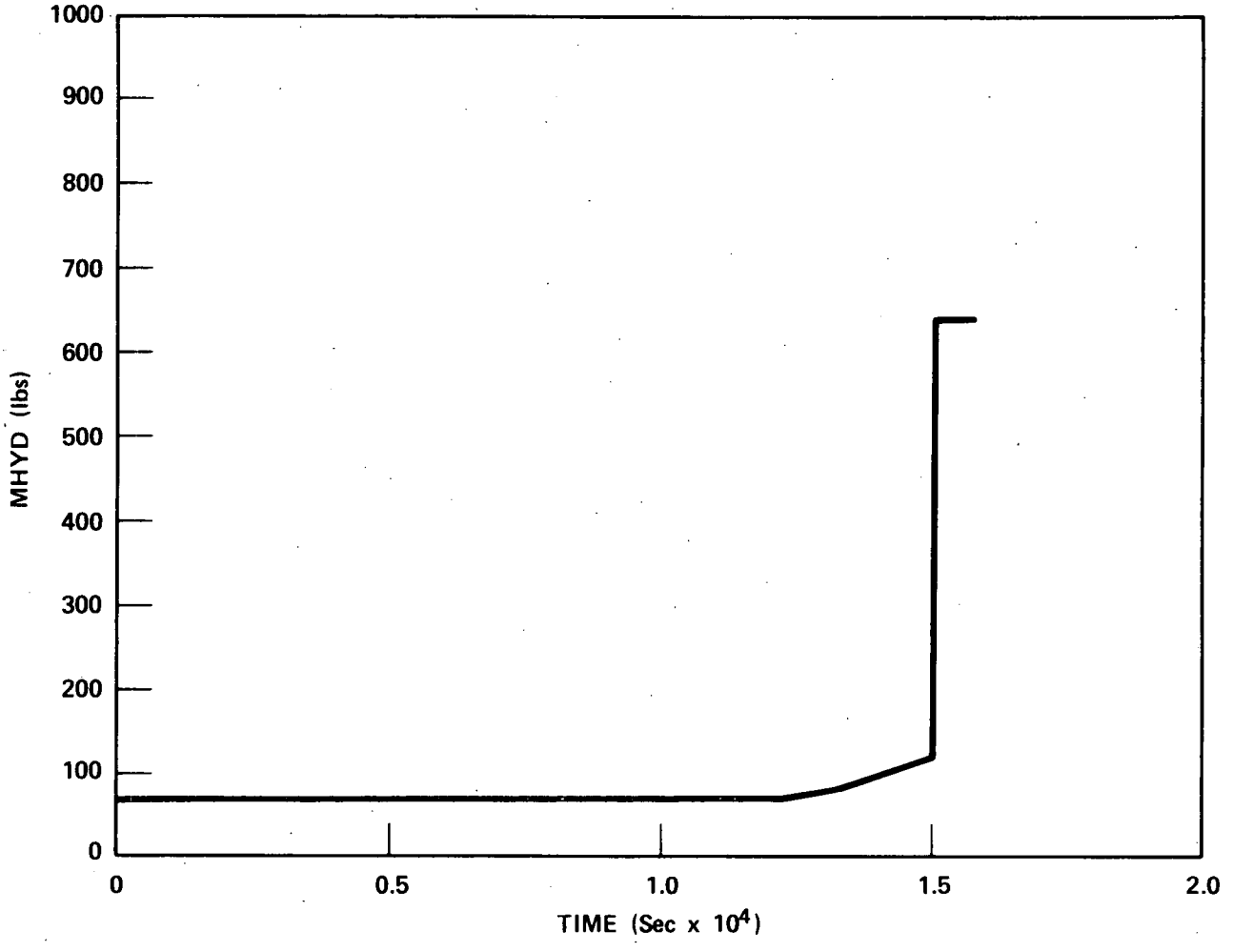


Pressure (in Containment) vs. Time
TMLB, Time Phased, 75% Dispersive, No Burn, 28% Zr Reacted
Class V, Case 3a

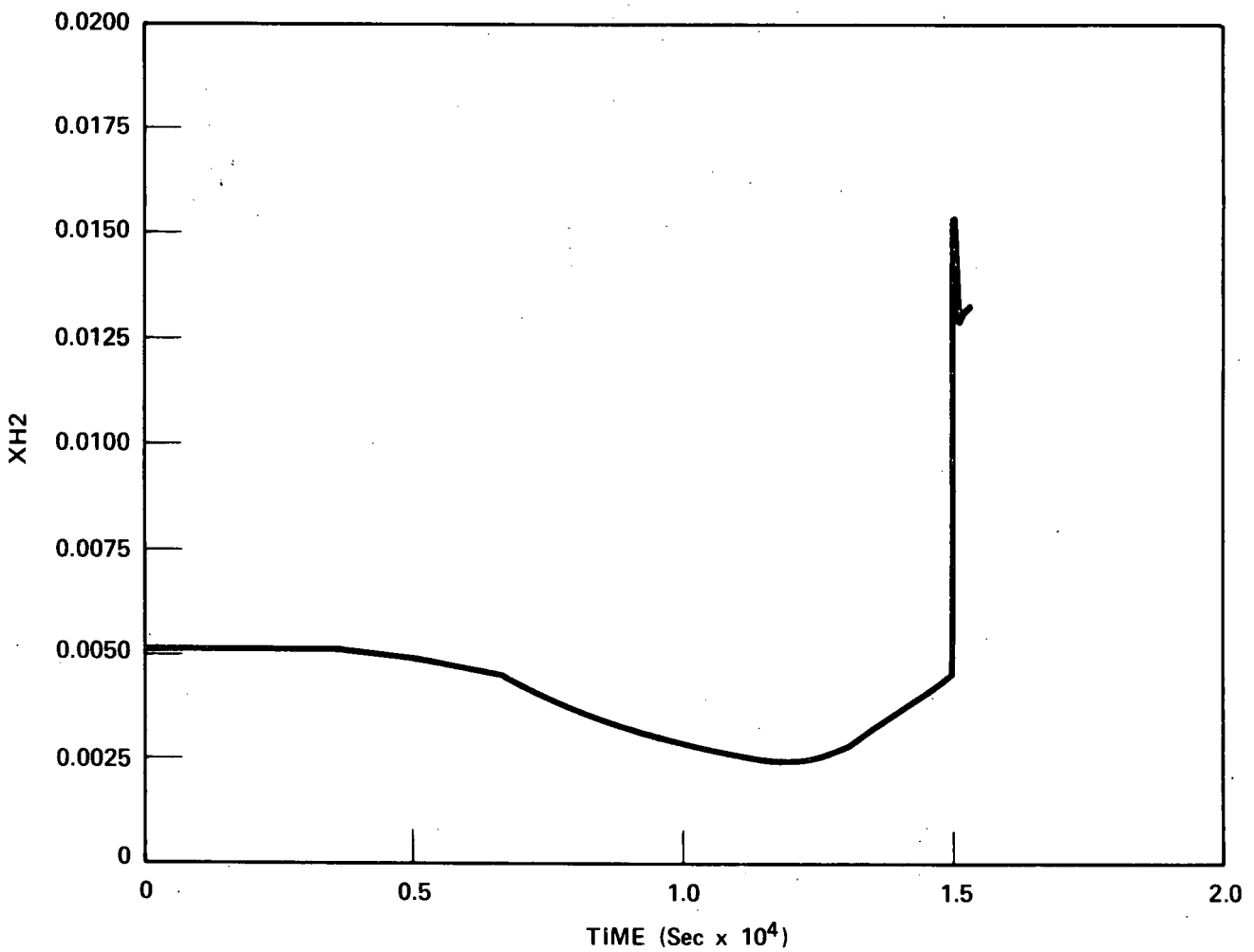
Sheet 2 of 7



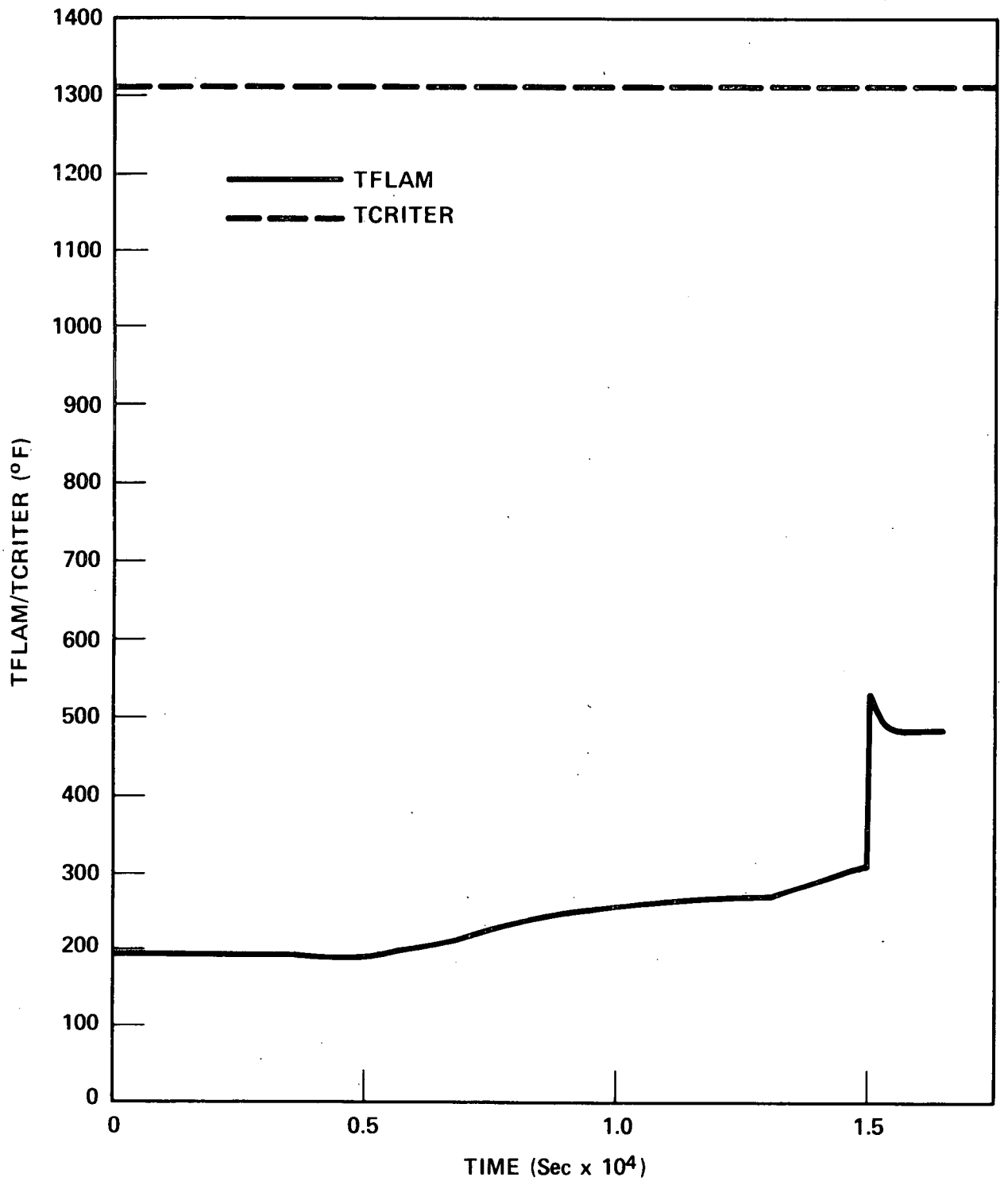
Temperature (in Containment) vs. Time
TMLB, Time Phased, 75% Dispersive, No Burn, 28% Zr Reacted
Class V Case 3a



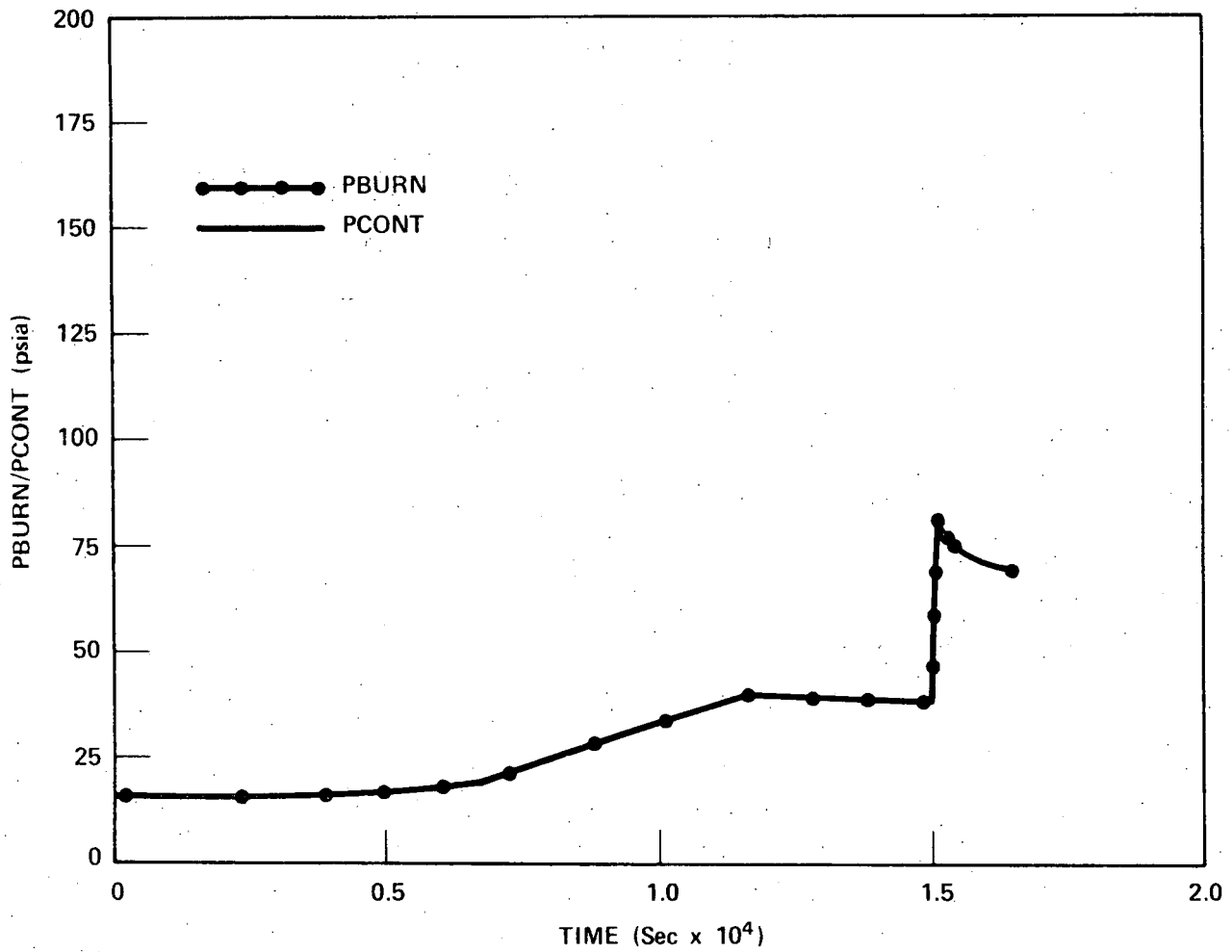
Mass Hydrogen (in Containment) vs. Time
TMLB, Time Phased, 75% Dispersive, No Burn, 28% Zr Reacted
Class V Case 3a



Mole Fraction H_2 (in Containment) vs. Time
TMLB, Time Phased, 75% Dispersive, No Burn 28% Zr Reacted
Class V, Case 3a



Flame Temperature (in Containment) vs. Time
TMLB, Time Phased, 75% Dispersive, No Burn 28% Zr Reacted
Class V, Case 3a



Adiabatic Burn Pressure/Pressure in Containment vs. Time
TMLB, Time Phased, 75% Dispersive, No Burn, 28% Zr Reacted
Class V, Case 3a

CASE: CLASS V, CASE 3a', TMLB, TIME PHASED, 75% DISPERSED, NO BURN, 64% Zr REACTED

DISPERSIVE: YES PERCENT CORE: 75 FRACTION IN CAVITY: 0

RUN #: AB3YALY DATE: 3/9/81 PERCENT ZR REACTED: 64

BLOWDOWN PEAK: N/A PSIA TIME: _____ SEC.

HYDROGEN BURN?: NO CRITERIA: _____

TIME @ BURN: _____ SEC, PRESSURE: _____ PSIA, TEMPERATURE: _____ °F

PEAKS:

PRESSURE: 93 PSIA, TIME: 15169 SEC, WHY?: VESSEL FAILURE

TEMPERATURE: 365 °F, TIME: 15169 SEC, WHY?: VESSEL FAILURE

DISPERSIVE: YES

PRESSURE: 93 PSIA, TIME: 15169 SEC, WHY?: _____

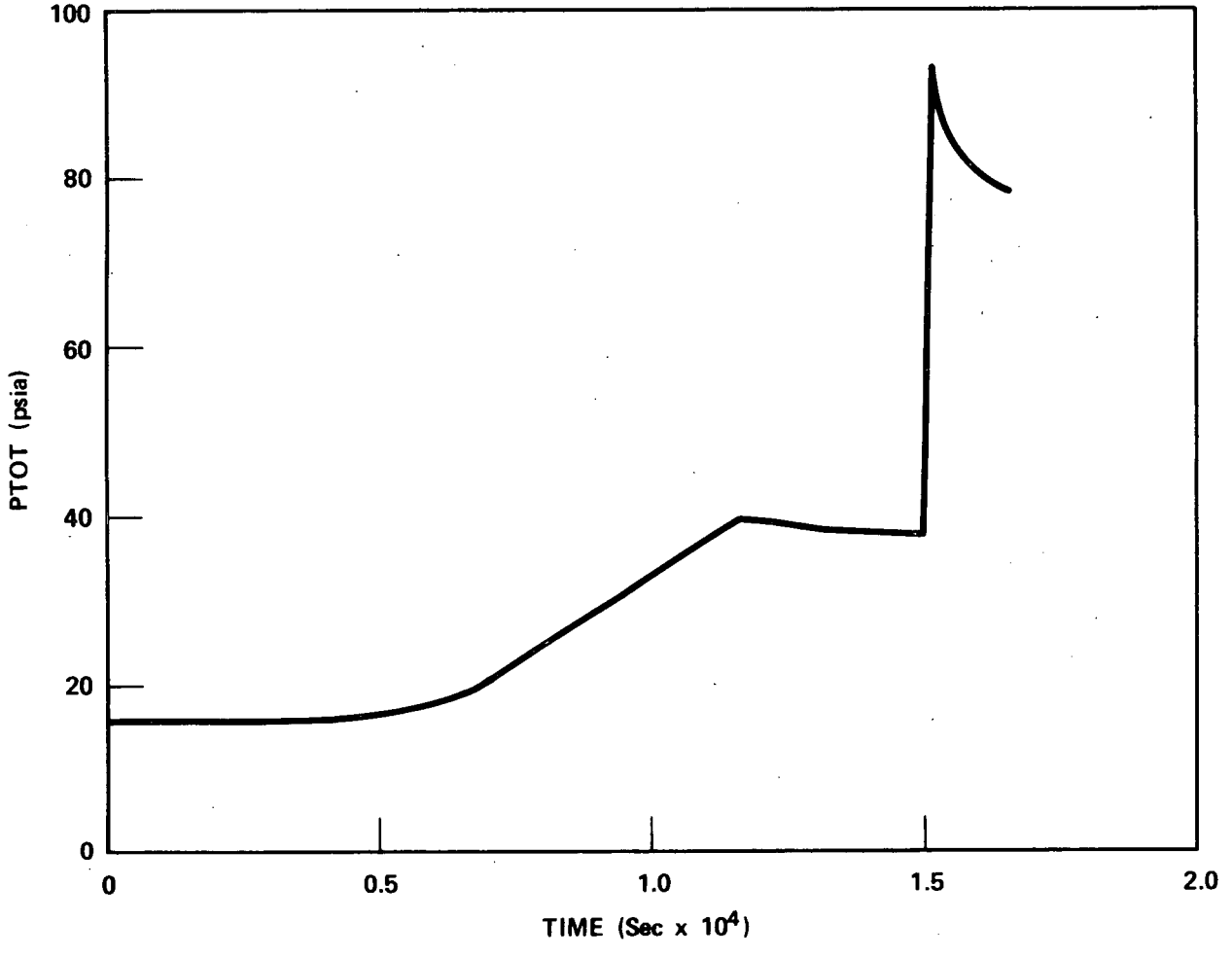
TEMPERATURE: 365 °F, TIME: 15169 SEC, WHY?: _____

END OF BOIL: 15000 SEC. END OF HEAD: _____ SEC.

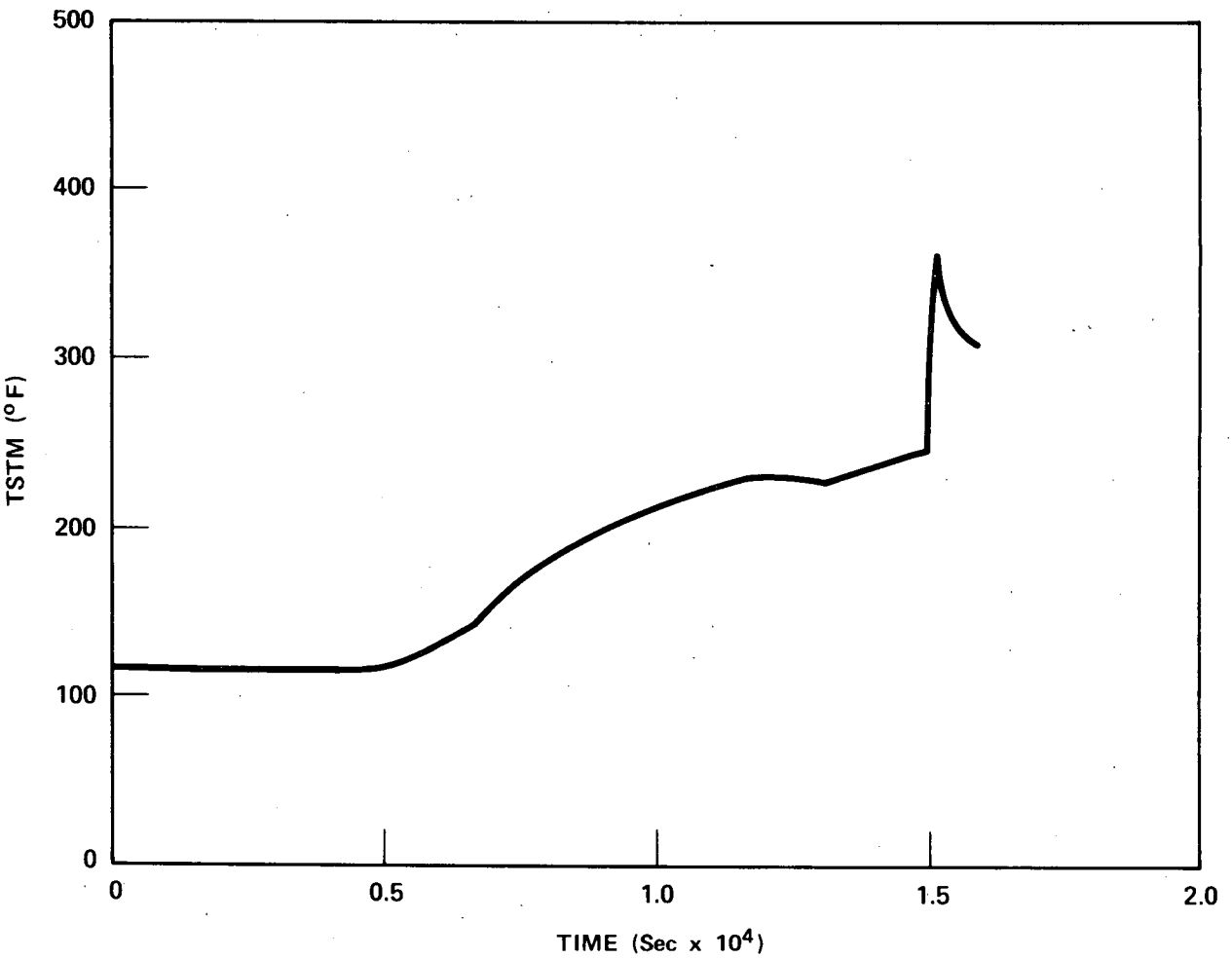
VESSEL FAILURE: 15000 SEC. END OF HOTDROP: _____ SEC.

END OF INTER: _____ SEC.

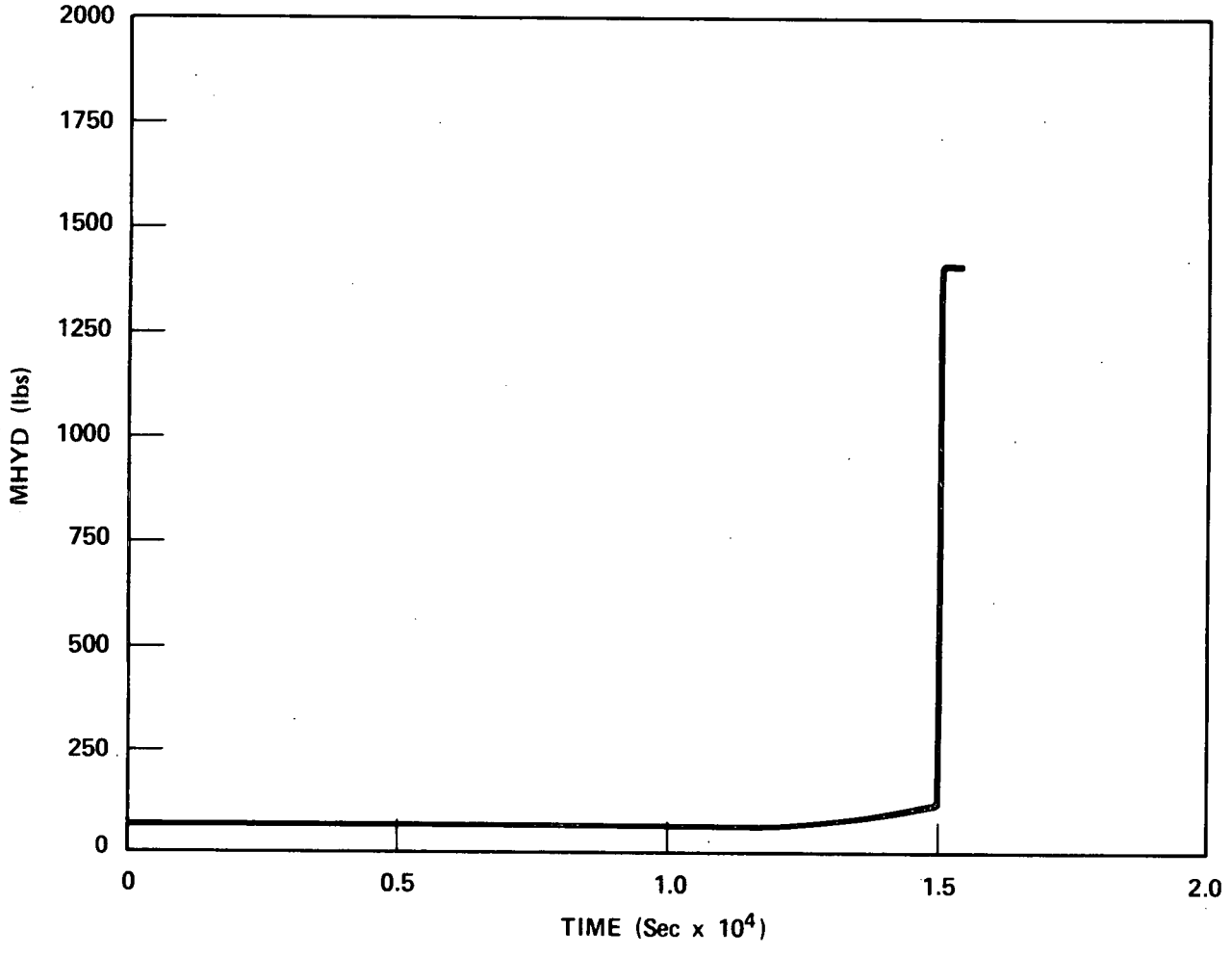
Class V, Case 3a'



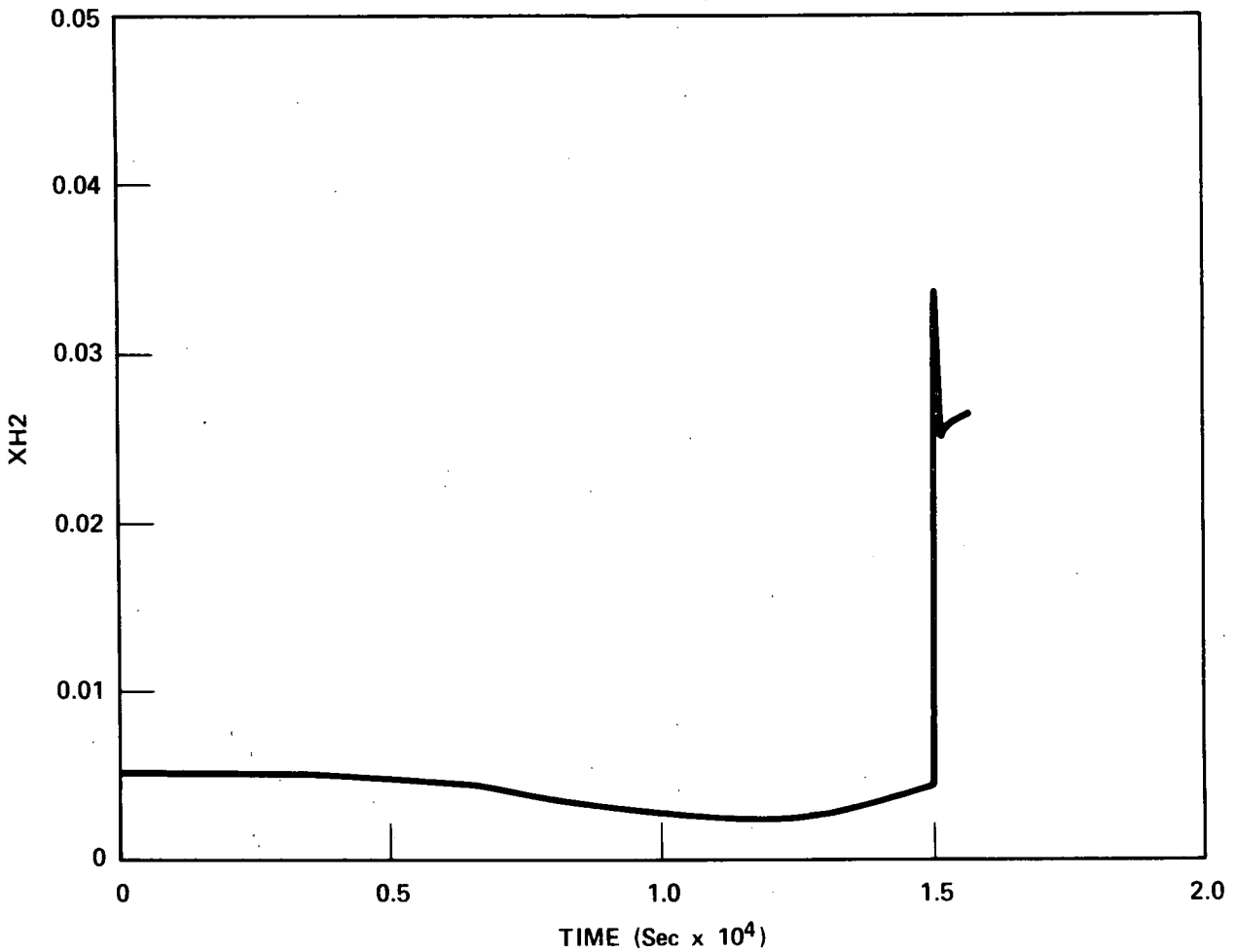
Pressure (in Containment) vs. Time
TMLB, Time Phased, 75% Dispersive, No Burn, 64% Zr Reacted
Class V, Case 3a'



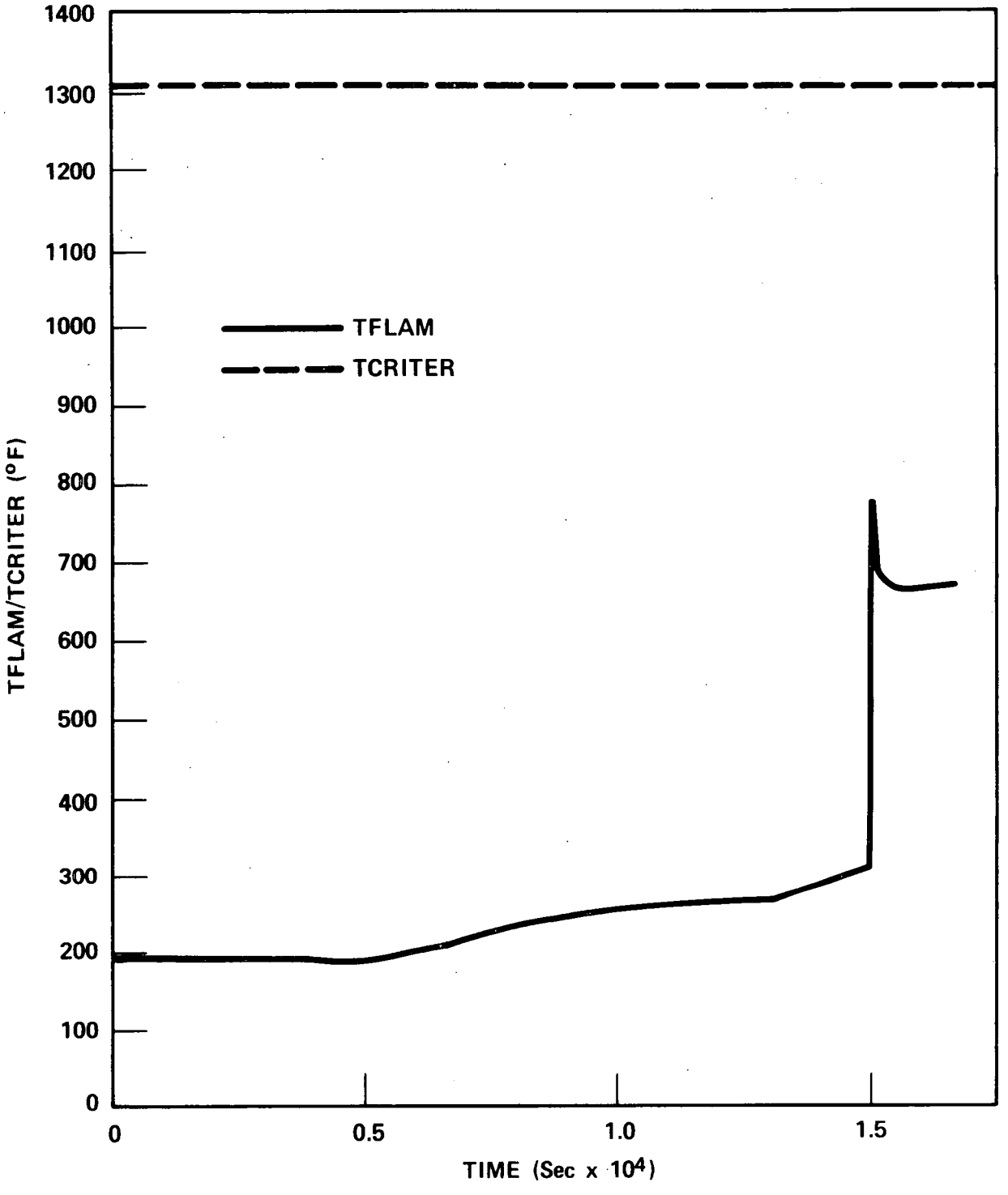
Temperature (in Containment) vs. Time
TMLB, Time Phased, 75% Dispersive, No Burn, 64% Zr Reacted
Class V, Case 3a'



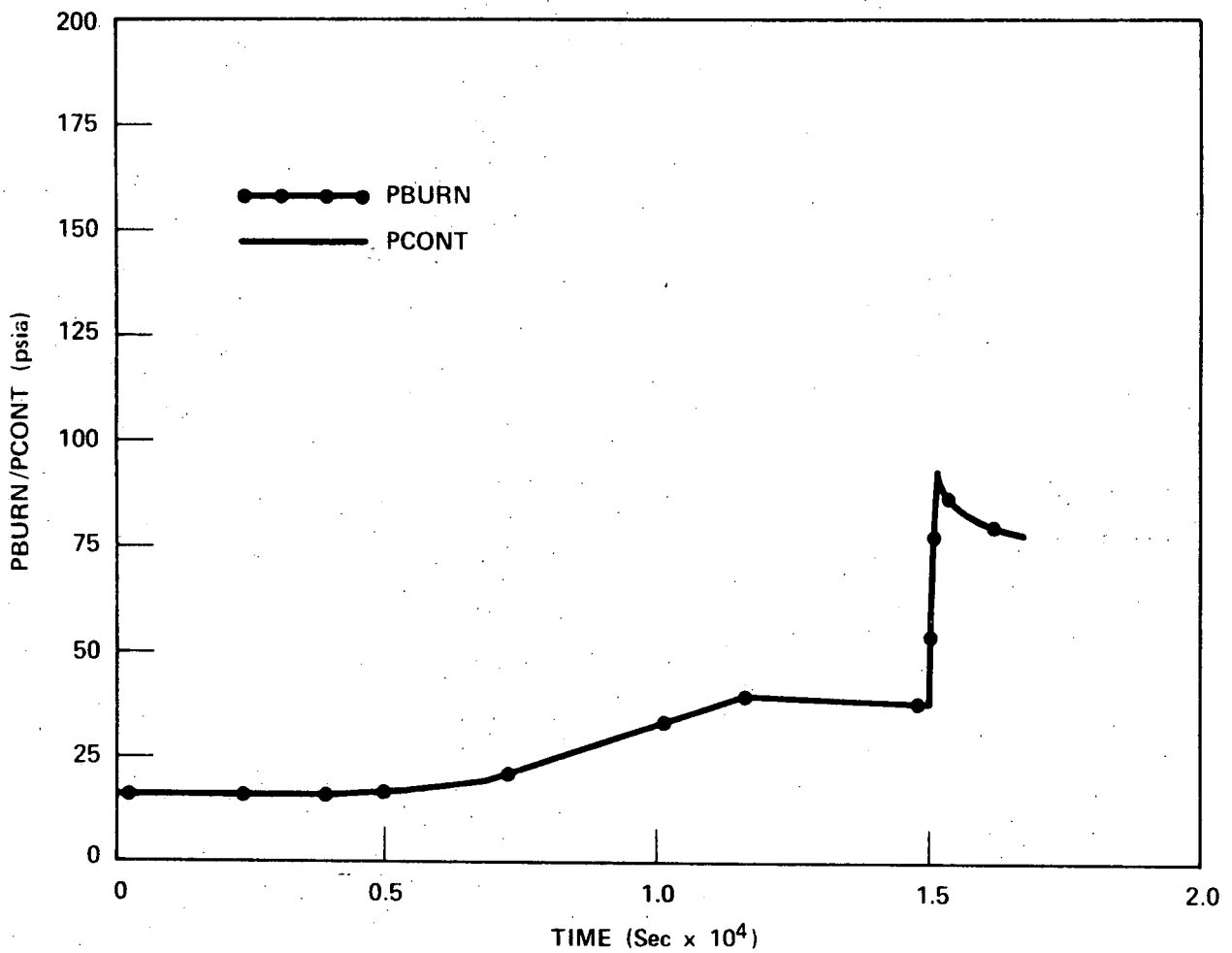
Mass Hydrogen (in Containment) vs. Time
TMLB, Time Phased, 75% Dispersive, No Burn, 64% Zr Reacted
Class V, Case 3a'



Mole Fraction H_2 (in Containment) vs. Time
TMLB, Time Phased, 75% Dispersive, No Burn, 64% Zr Reacted
Class V, Case 3a'



Flame Temperature (in Containment) vs. Time
TMLB, Time Phased, 75% Dispersive, No Burn, 64% Zr Reacted
Class V, Case 3a'



Adiabatic Burn Pressure/Pressure in Containment vs. Time
TMLB, Time Phased, 75% Dispersive, No Burn, 64% Zr Reacted
Class V, Case 3a'

CLASS V, CASE 3a', TMLB, TIME PHASED,

CASE: 75% DISPERSIVE, BURN @ VESSEL FAILURE, F64

DISPERSIVE: YES PERCENT CORE: 75 FRACTION IN CAVITY: 0

RUN #: AB3YAUD DATE: 3/24/81 PERCENT ZR REACTED: 64

BLOWDOWN PEAK: NO PSIA TIME: _____ SEC.

HYDROGEN BURN?: YES CRITERIA: T_{MAX}

TIME @ BURN: 15058 SEC, PRESSURE: 112 PSIA, TEMPERATURE: 818 °F

PEAKS:

PRESSURE: 117 PSIA, TIME: 15169 SEC, WHY?: END OF H_2 BURN

TEMPERATURE: 818 °F, TIME: 15078 SEC, WHY?: END OF H_2 BURN

DISPERSIVE: YES

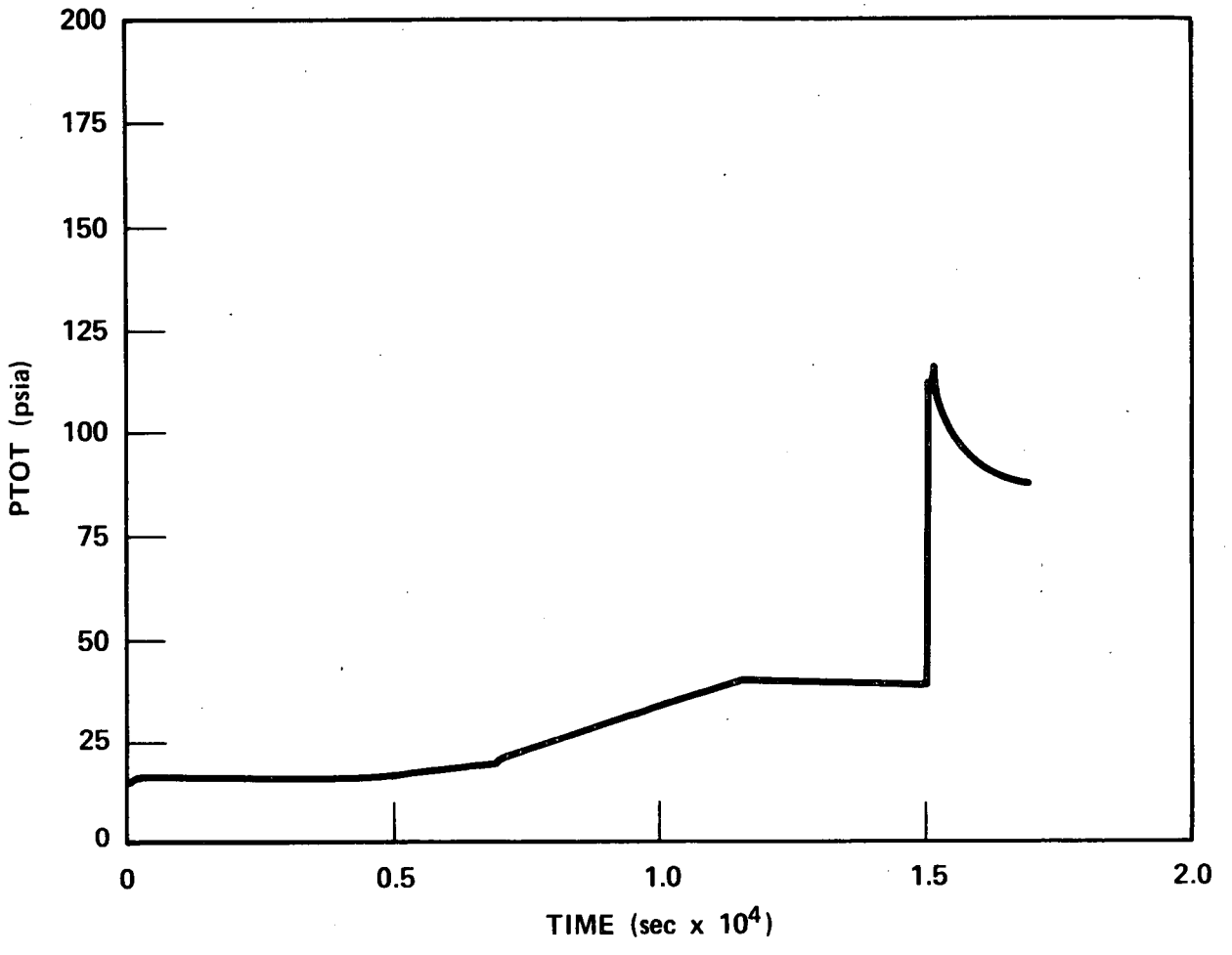
PRESSURE: 117 PSIA, TIME: 15169 SEC,

TEMPERATURE: 549 °F, TIME: 15169 SEC,

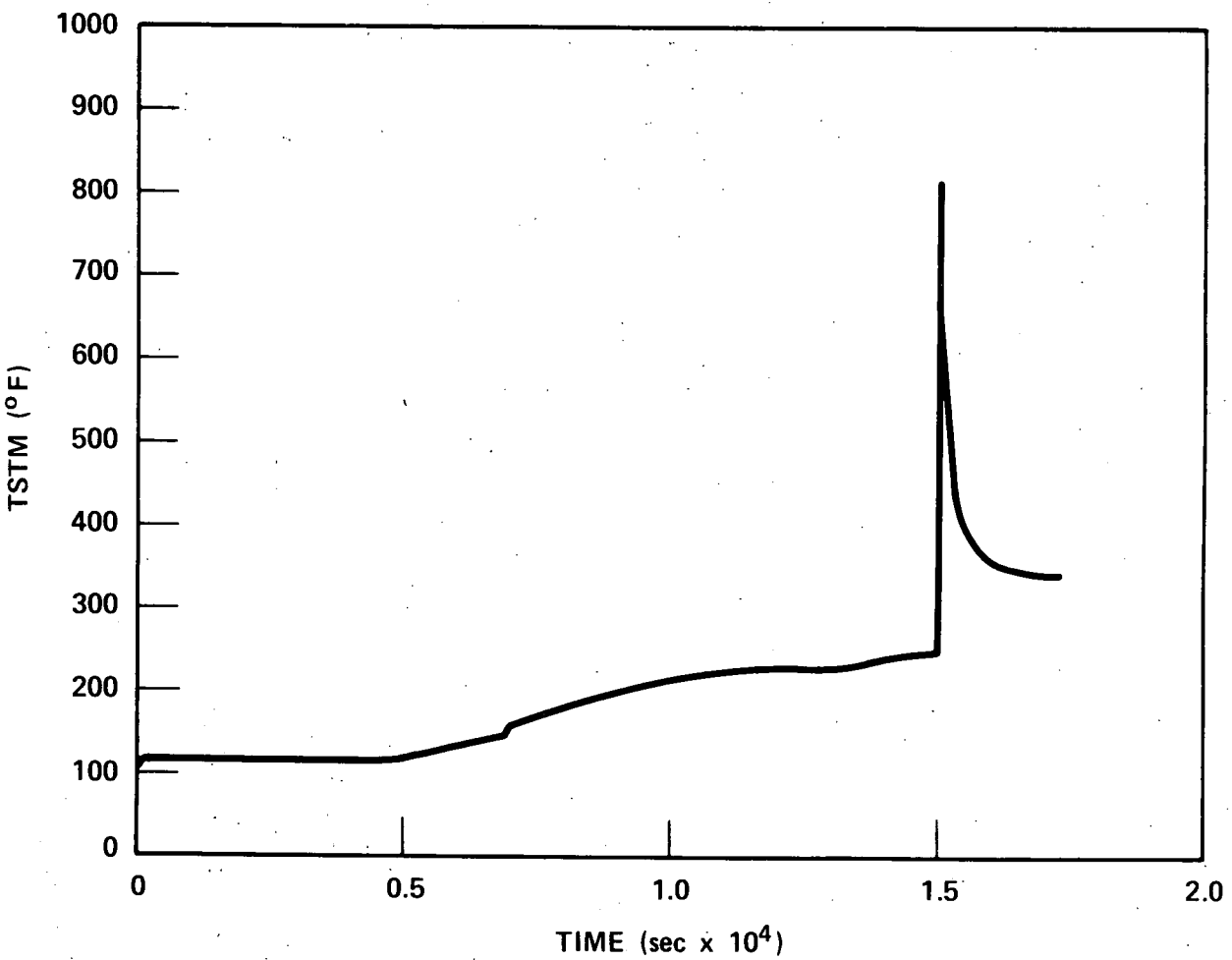
END OF BOIL: 15000 SEC. END OF HEAD: _____ SEC.

VESSEL FAILURE: 15000 SEC. END OF HOTDROP: _____ SEC.

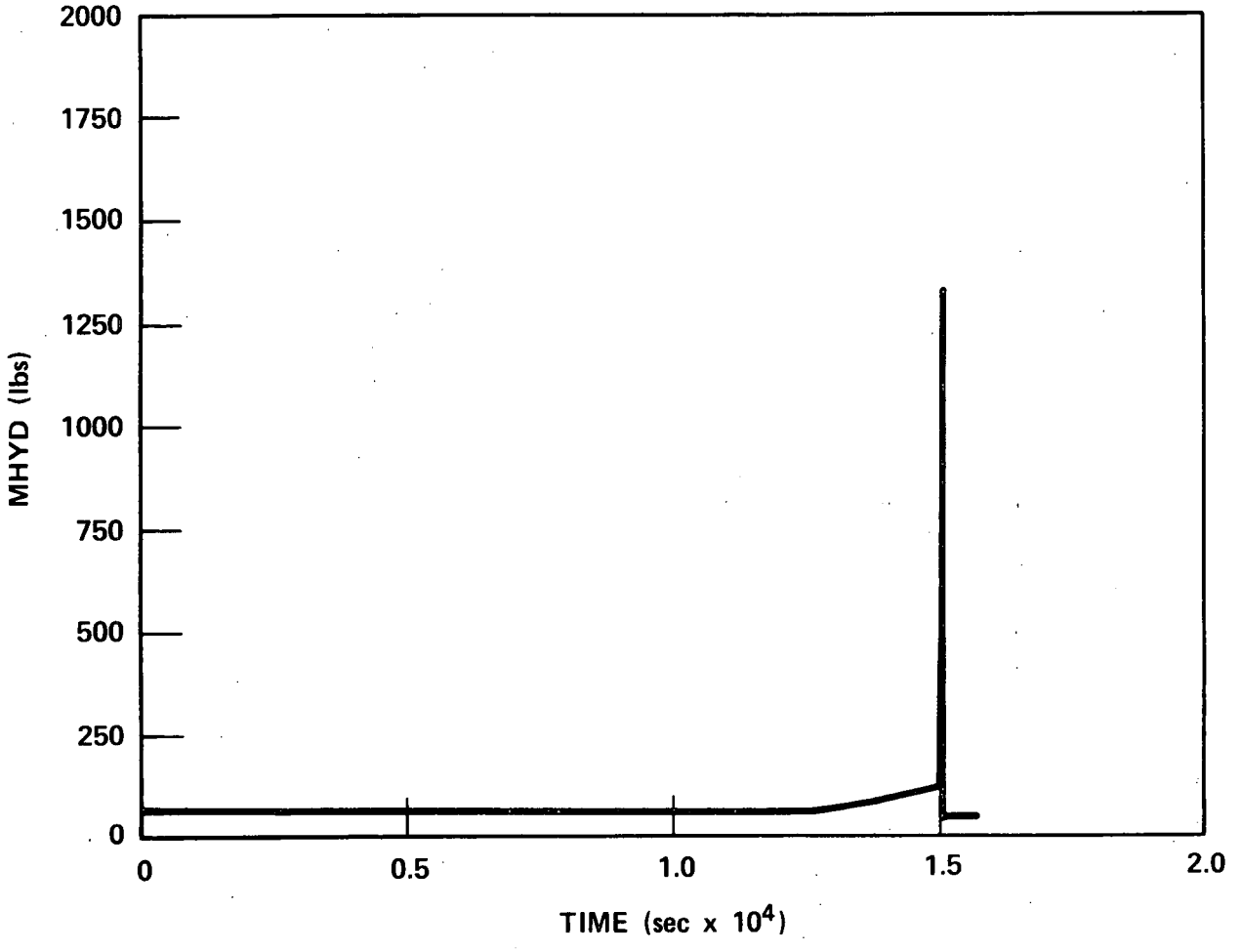
END OF INTER: _____ SEC.



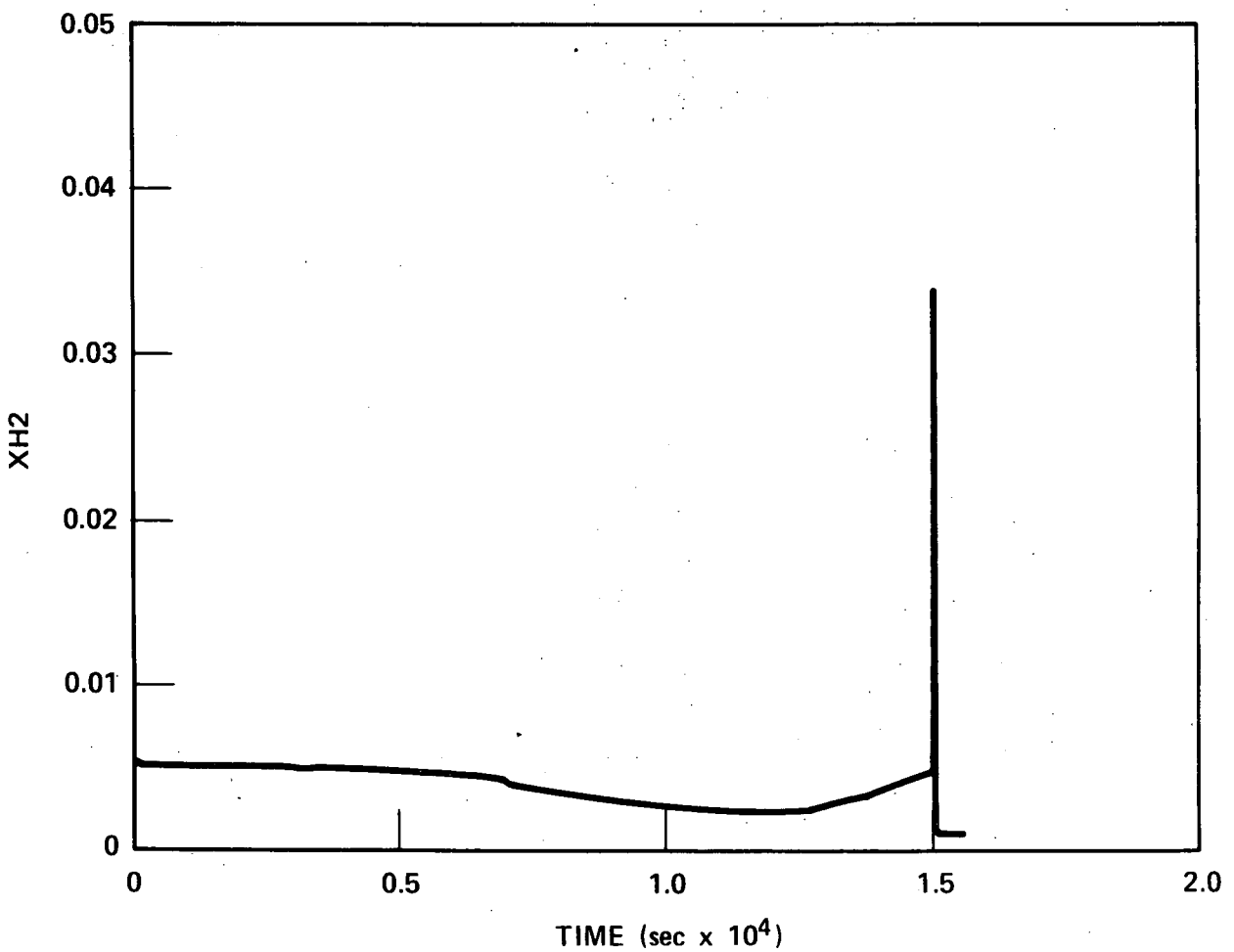
Pressure (in Containment) vs. Time
TMLB, NEWPH 75, Burn @ Vessel Failure, 64% Zr Reacted
Class V, Case 3a'



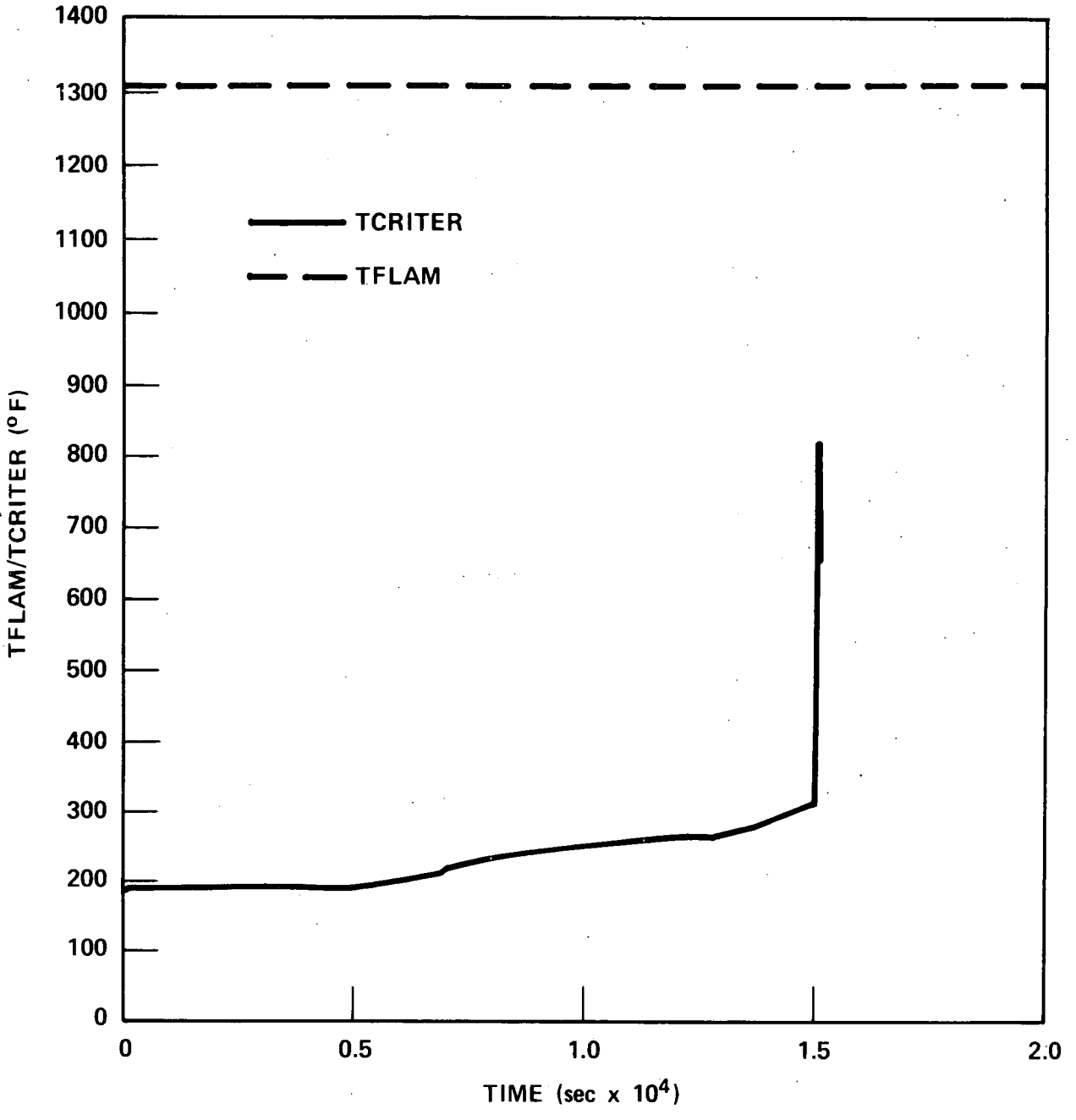
Temperature (in Containment) vs. Time
TMLB, NEWPH 75, Burn @ Vessel Failure, 64% Zr Reacted
Class V, Case 3a'



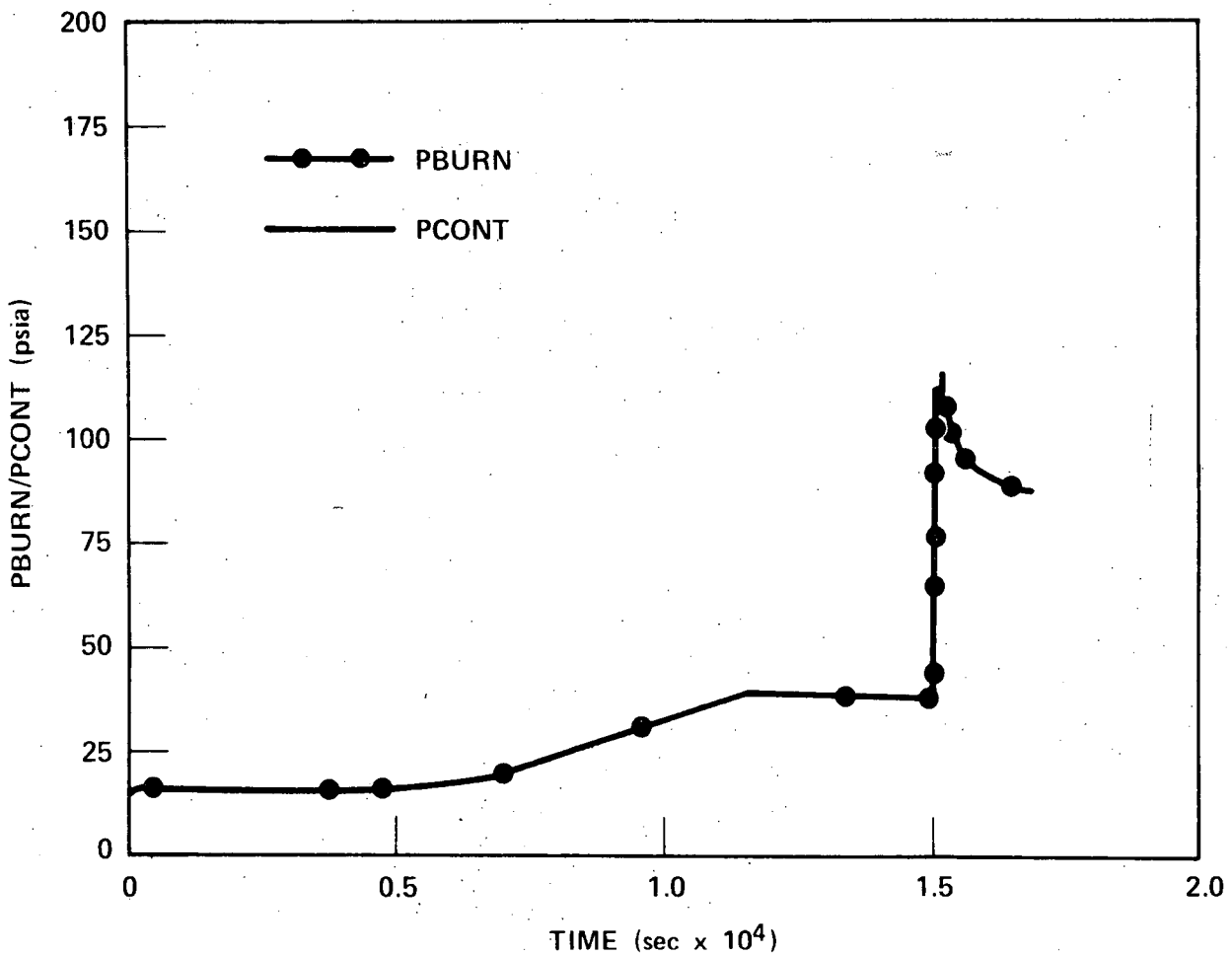
Mass Hydrogen (in Containment) vs. Time
TMLB, NEWPH 75, Burn @ Vessel Failure, 64% Zr Reacted
Class V, Case 3a'



Mole Fraction H_2 (in Containment) vs. Time
TMLB, NEWPH 75, Burn @ Vessel Failure, 64% Zr Reacted
Class V, Case 3a'



Flame Temperature (in Containment) vs. Time
TMLB, NEWPH 75, Burn @ Vessel Failure, 64% Zr Reacted
Class V, Case 3a'



Adiabatic Burn Pressure/Pressure in Containment vs. Time
TMLB, NEWPH 75, Burn @ Vessel Failure, 64% Zr Reacted
Class V, Case 3a'

CASE: CLASS V, CASE 4a, TMLB, TIME PHASED, 50% DISPERSIVE, NO BURN 21% Zr REACTED

DISPERSIVE: YES PERCENT CORE: 50 FRACTION IN CAVITY: 0

RUN #: AB3YCSR DATE: 3/8/81 PERCENT ZR REACTED: 21

BLOWDOWN PEAK: N/A PSIA TIME: _____ SEC.

HYDROGEN BURN?: NO CRITERIA: _____

TIME @ BURN: _____ SEC, PRESSURE: _____ PSIA, TEMPERATURE: _____ °F

PEAKS:

PRESSURE: 75 PSIA, TIME: 14251 SEC, WHY?: VESSEL FAILURE

TEMPERATURE: 354 °F, TIME: 14251 SEC, WHY?: VESSEL FAILURE

DISPERSIVE: YES

PRESSURE: 75 PSIA, TIME: 14251 SEC,

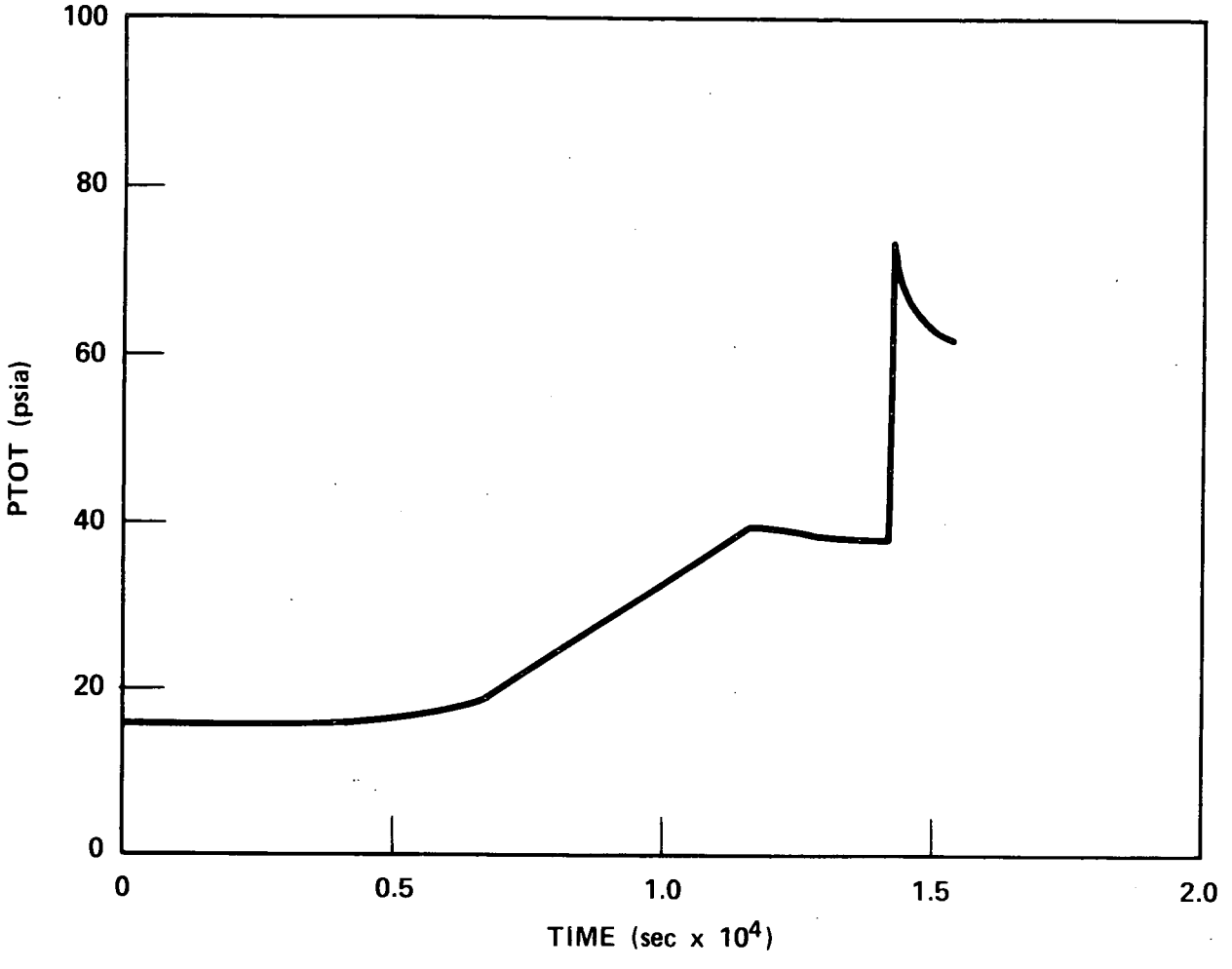
TEMPERATURE: 354 °F, TIME: 14251 SEC,

END OF BOIL: 14160 SEC. END OF HEAD: _____ SEC.

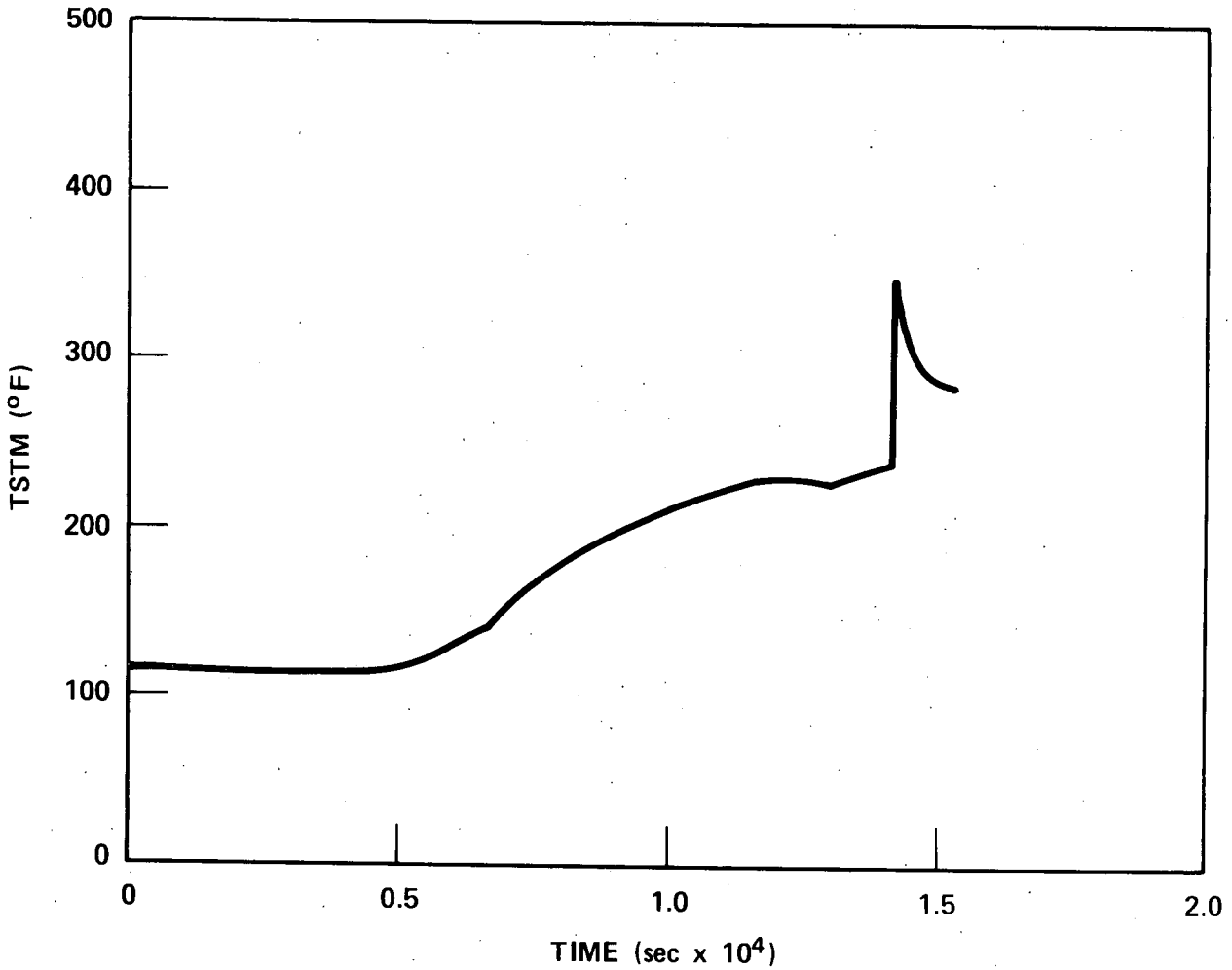
VESSEL FAILURE: 14160 SEC. END OF HOTDROP: _____ SEC.

END OF INTER: _____ SEC.

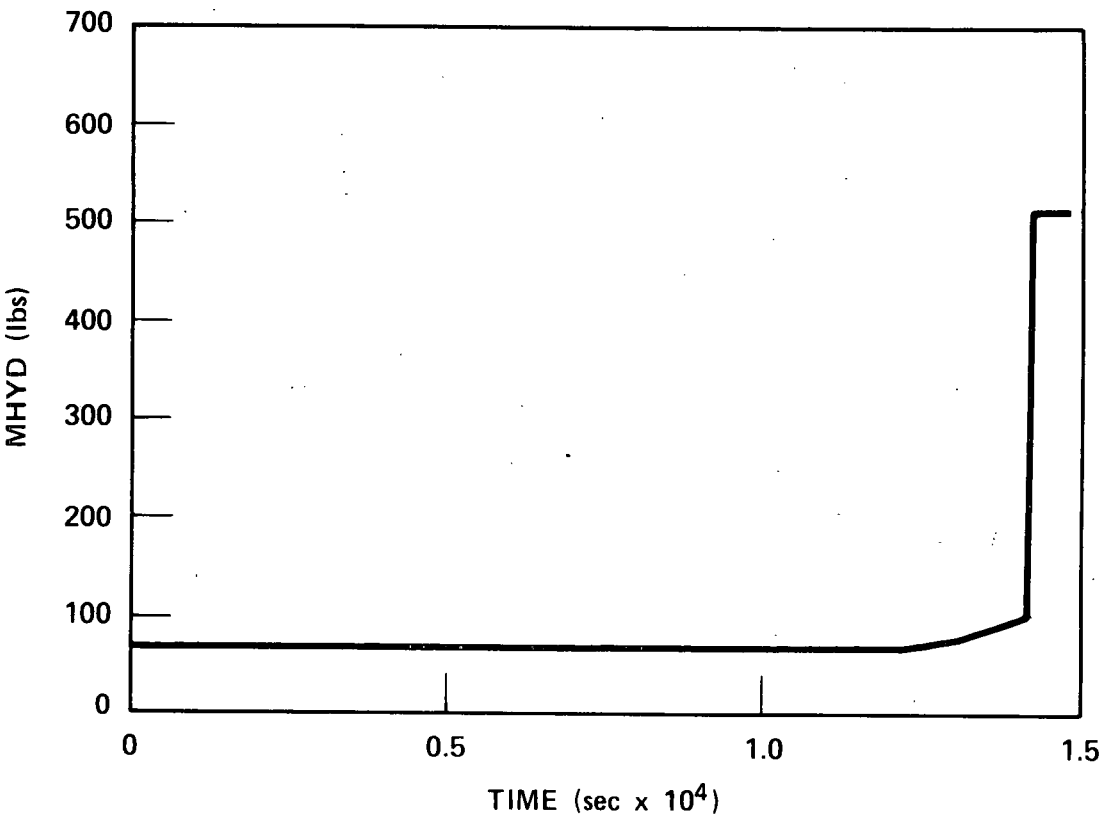
Class V, Case 4a



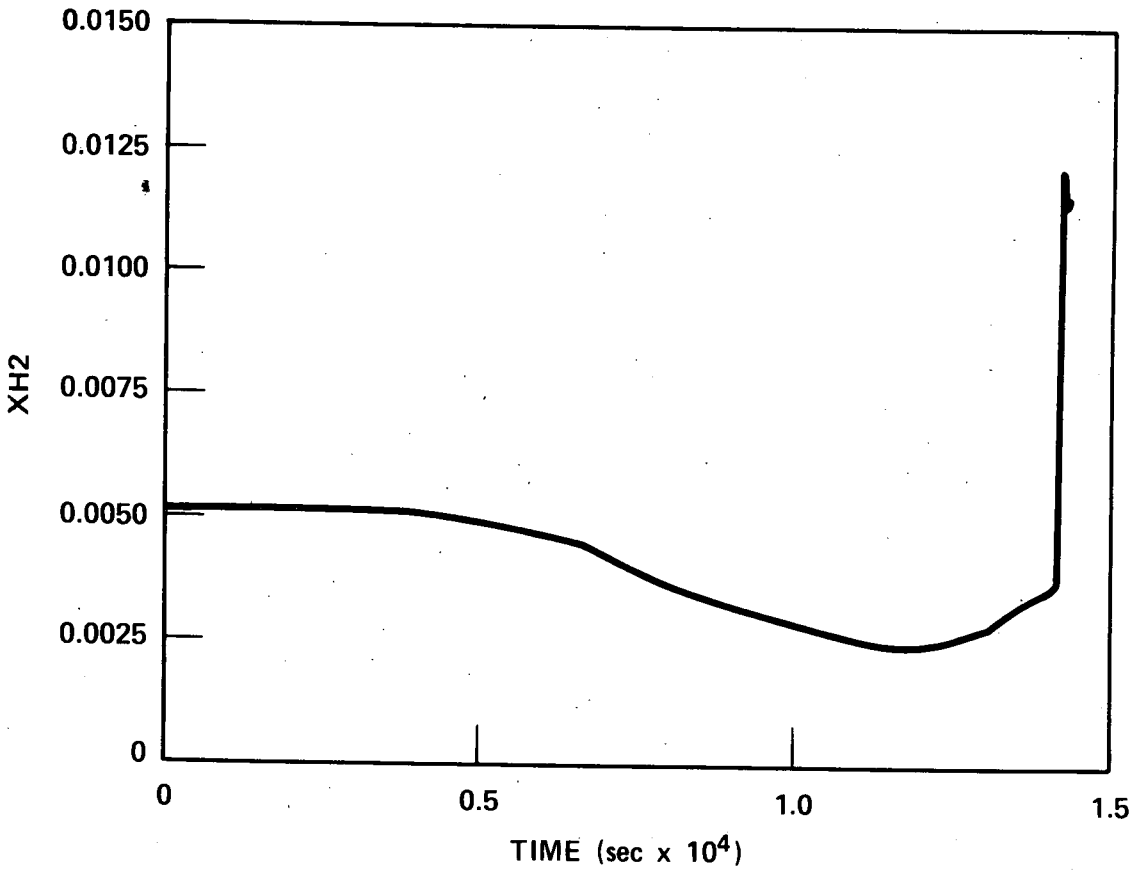
Pressure (in Containment) vs. Time
TMLB, Time Phased, 50% Dispersive, No Burn, 21% Zr Reacted
Class V, Case 4a



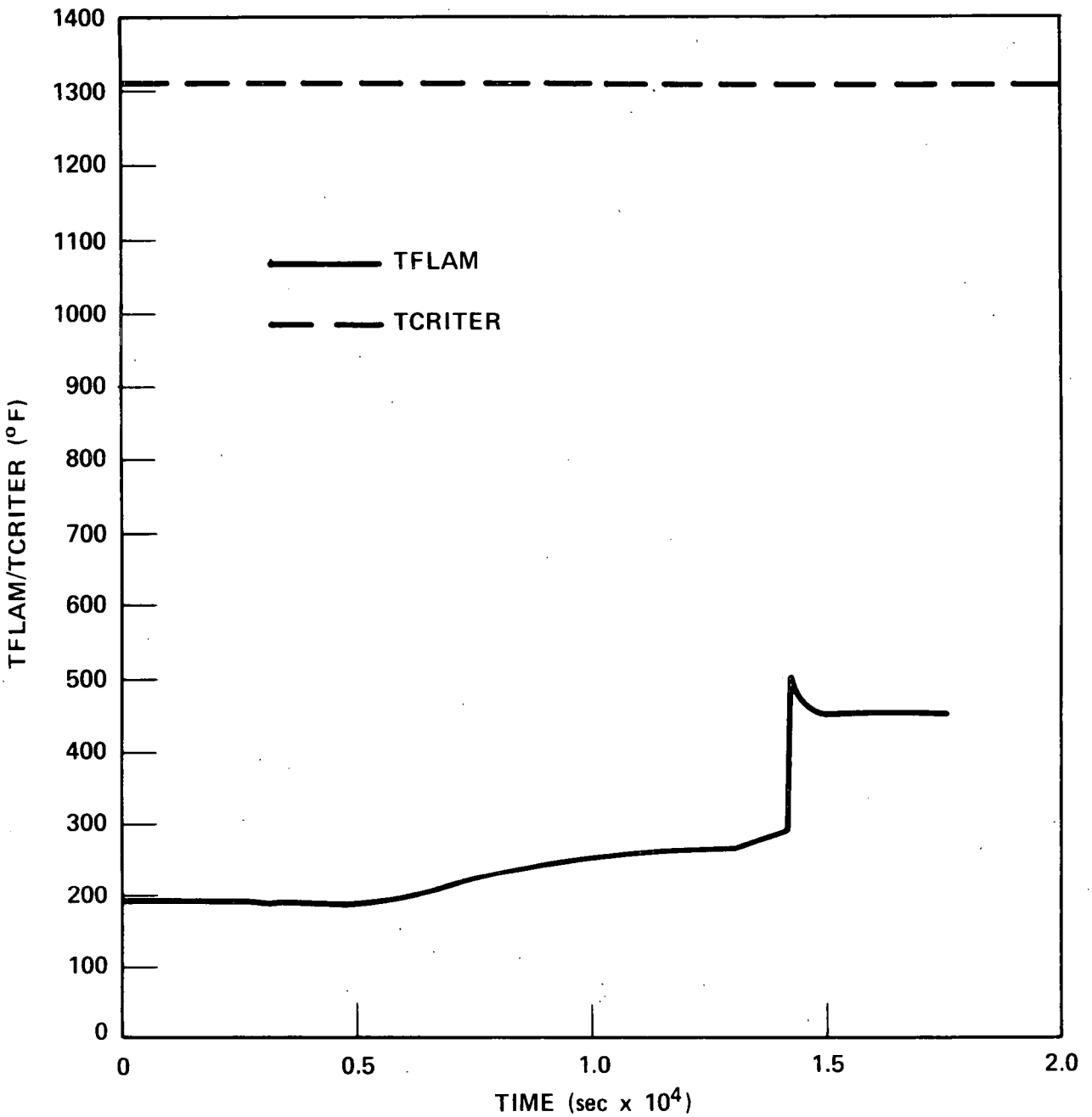
Temperature (in Containment) vs. Time
TMLB, Time Phased, 50% Dispersive, No Burn, 21% Zr Reacted
Class V, Case 4a



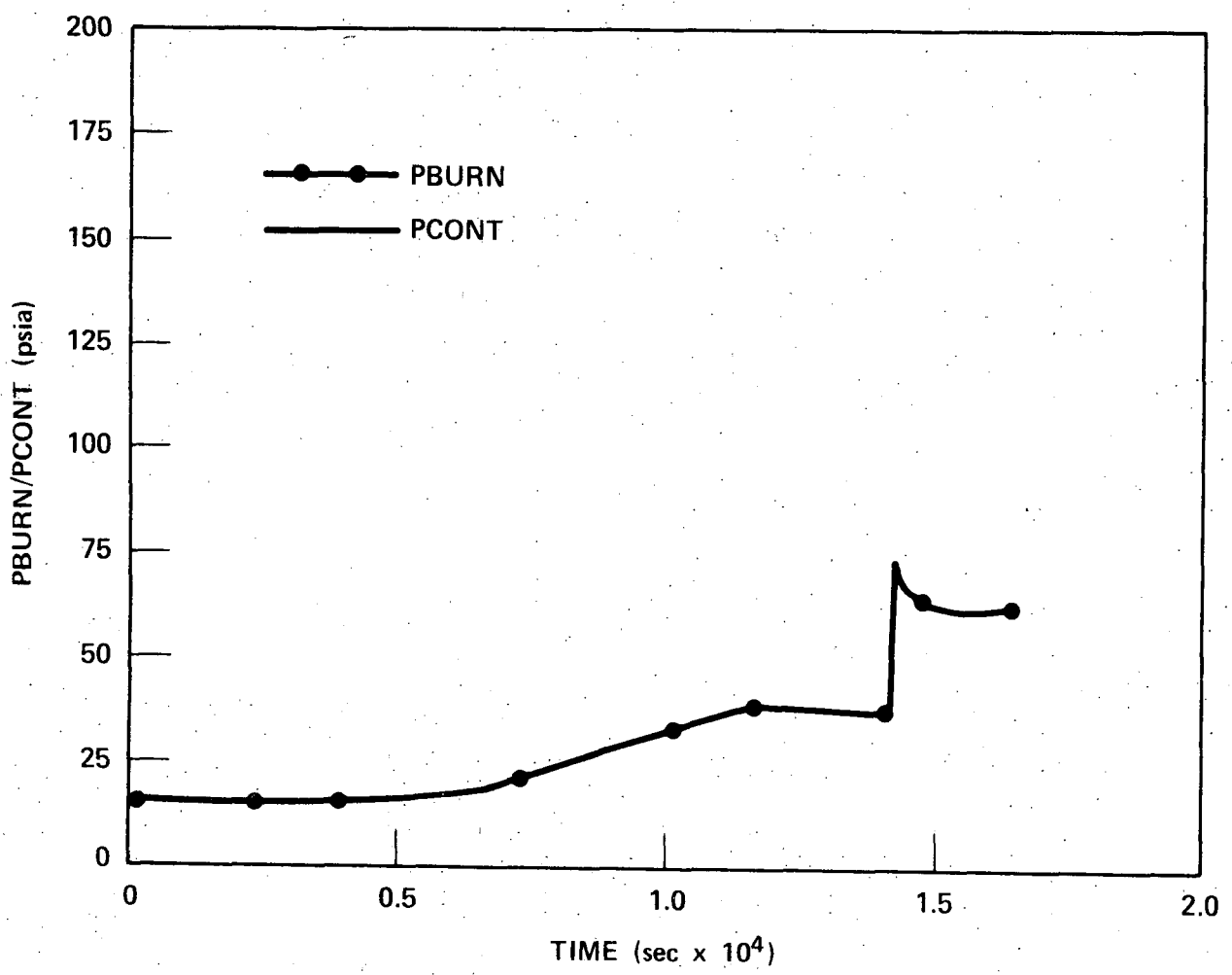
Mass Hydrogen (in Containment) vs. Time
TMLB, Time Phased, 50% Dispersive, No Burn, 21% Zr Reacted
Class V, Case 4a



Mole Fraction H_2 (in Containment) vs. Time
TMLB, Time Phased, 50% Dispersive, No Burn, 21% Zr Reacted
Class V, Case 4a



Flame Temperature (in Containment) vs. Time
TMLB, Time Phased, 50% Dispersive, No Burn, 21% Zr Reacted
Class V, Case 4a



Adiabatic Burn Pressure/Pressure in Containment vs. Time
TMLB, Time Phased, 50% Dispersive, No Burn, 21% Zr Reacted
Class V, Case 4a

CASE: CLASS V, CASE 4a', TMLB, TIME PHASED, 50% DISPERSIVE, NO BURN, 63% Zr REACTED

DISPERSIVE: YES PERCENT CORE: 50 FRACTION IN CAVITY: 0

RUN #: AB3YAWM DATE: 3/8/81 PERCENT ZR REACTED: 63

BLOWDOWN PEAK: N/A PSIA TIME: _____ SEC.

HYDROGEN BURN?: NO CRITERIA: _____

TIME @ BURN: _____ SEC, PRESSURE: _____ PSIA, TEMPERATURE: _____ °F

PEAKS:

PRESSURE: 85 PSIA, TIME: 14291 SEC, WHY?: VESSEL FAILURE

TEMPERATURE: 366 °F, TIME: 14291 SEC, WHY?: VESSEL FAILURE

DISPERSIVE: YES

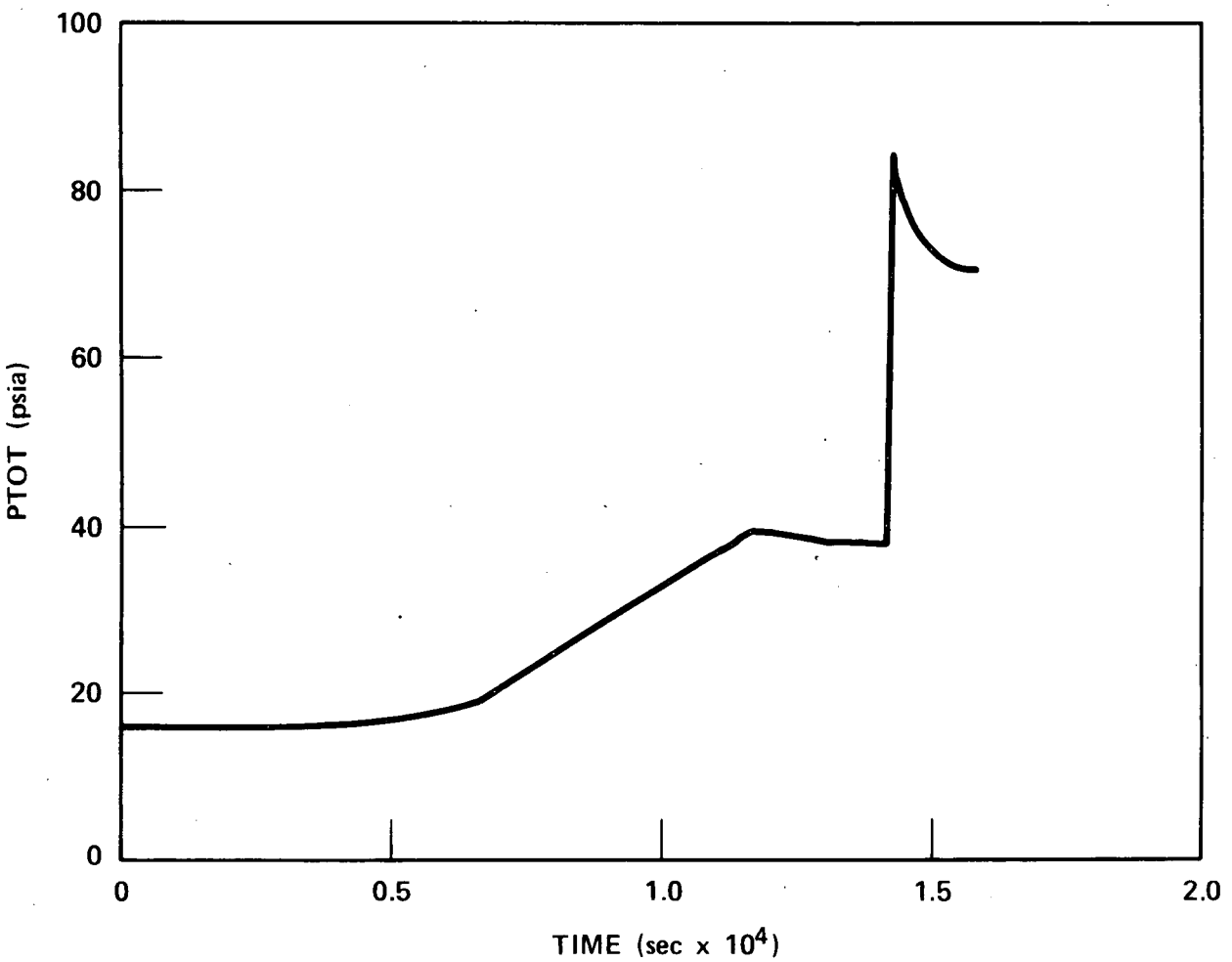
PRESSURE: 85 PSIA, TIME: 14291 SEC,

TEMPERATURE: 366 °F, TIME: 14291 SEC,

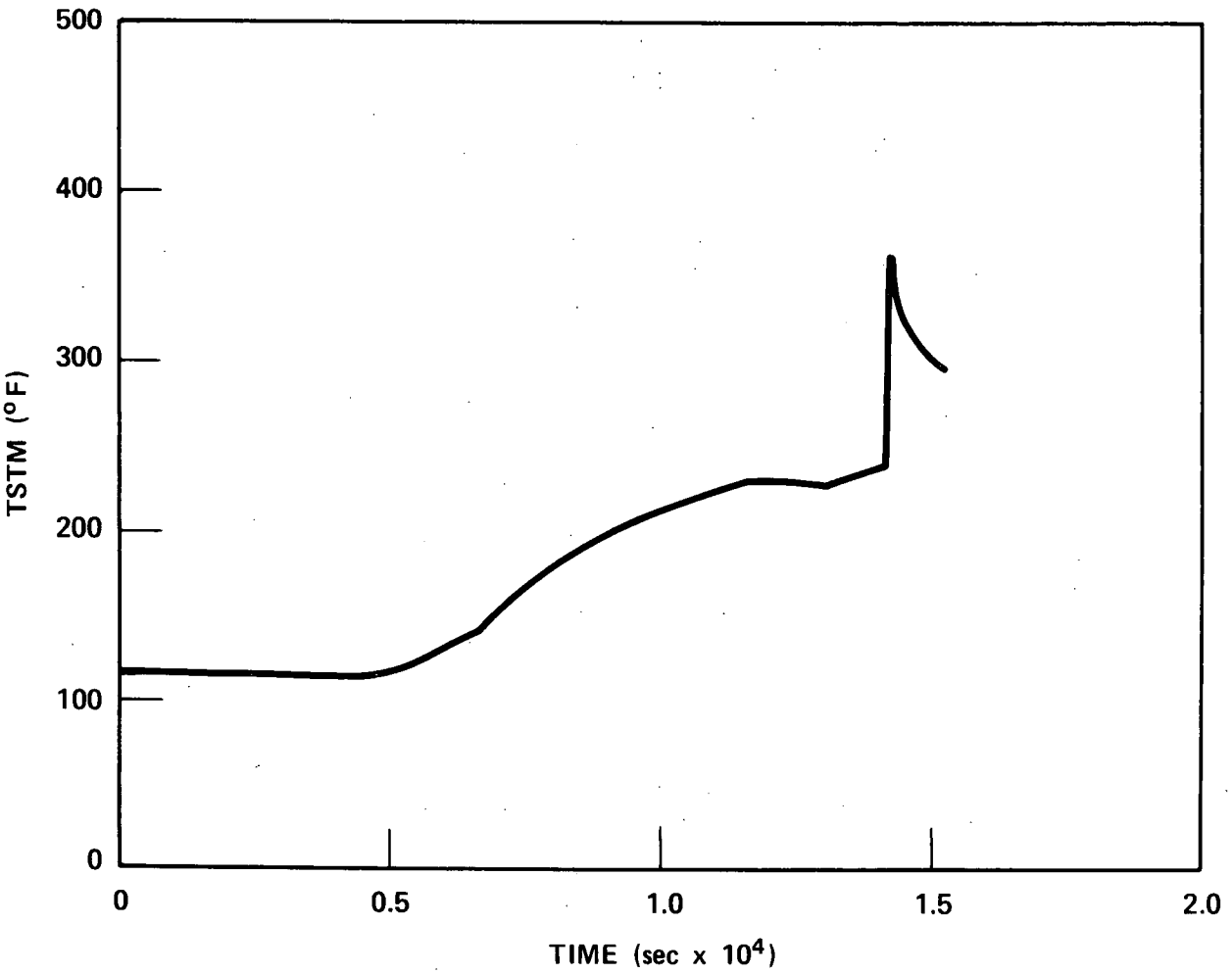
END OF BOIL: 14160 SEC. END OF HEAD: _____ SEC.

VESSEL FAILURE: 14160 SEC. END OF HOTDROP: _____ SEC.

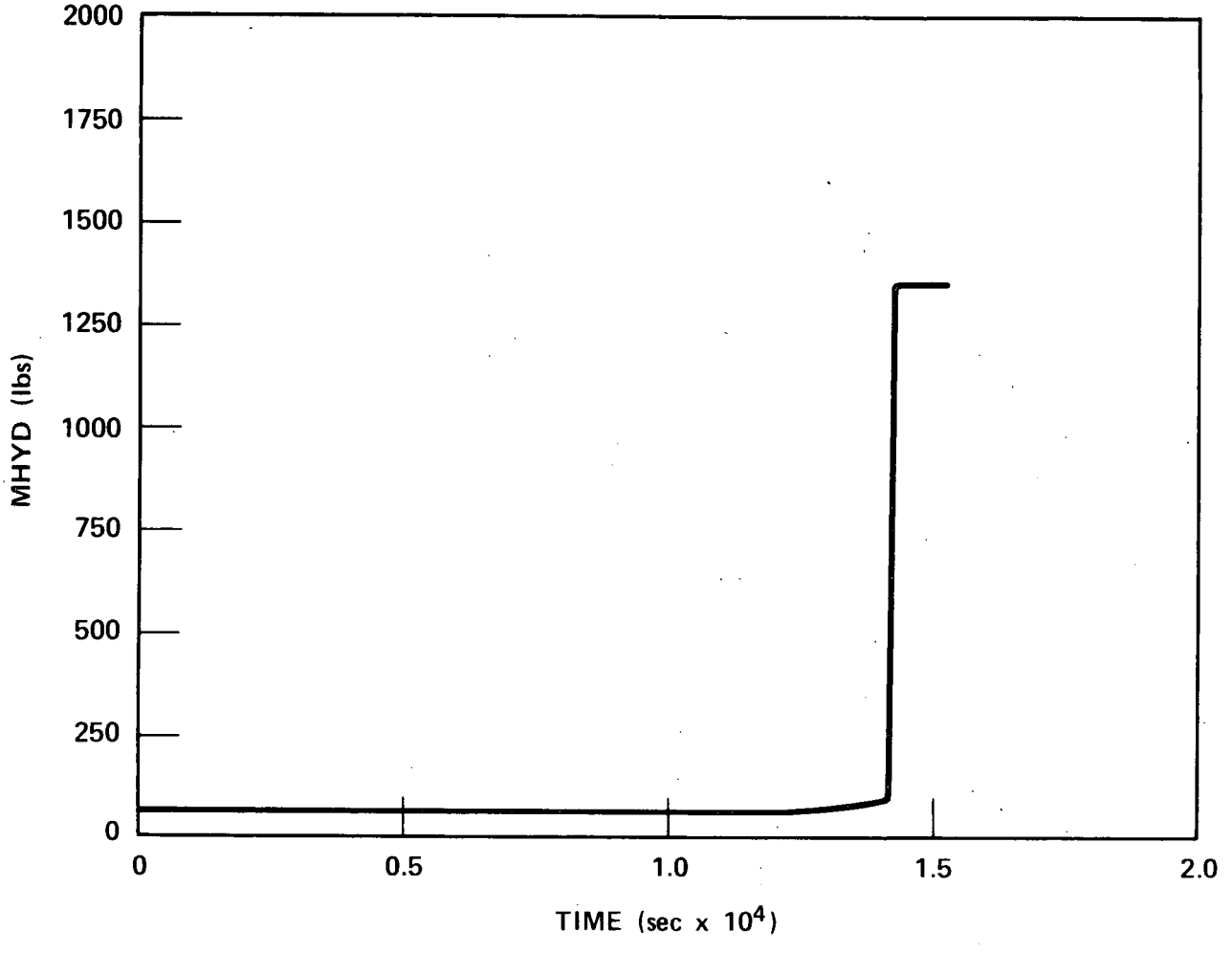
END OF INTER: _____ SEC.



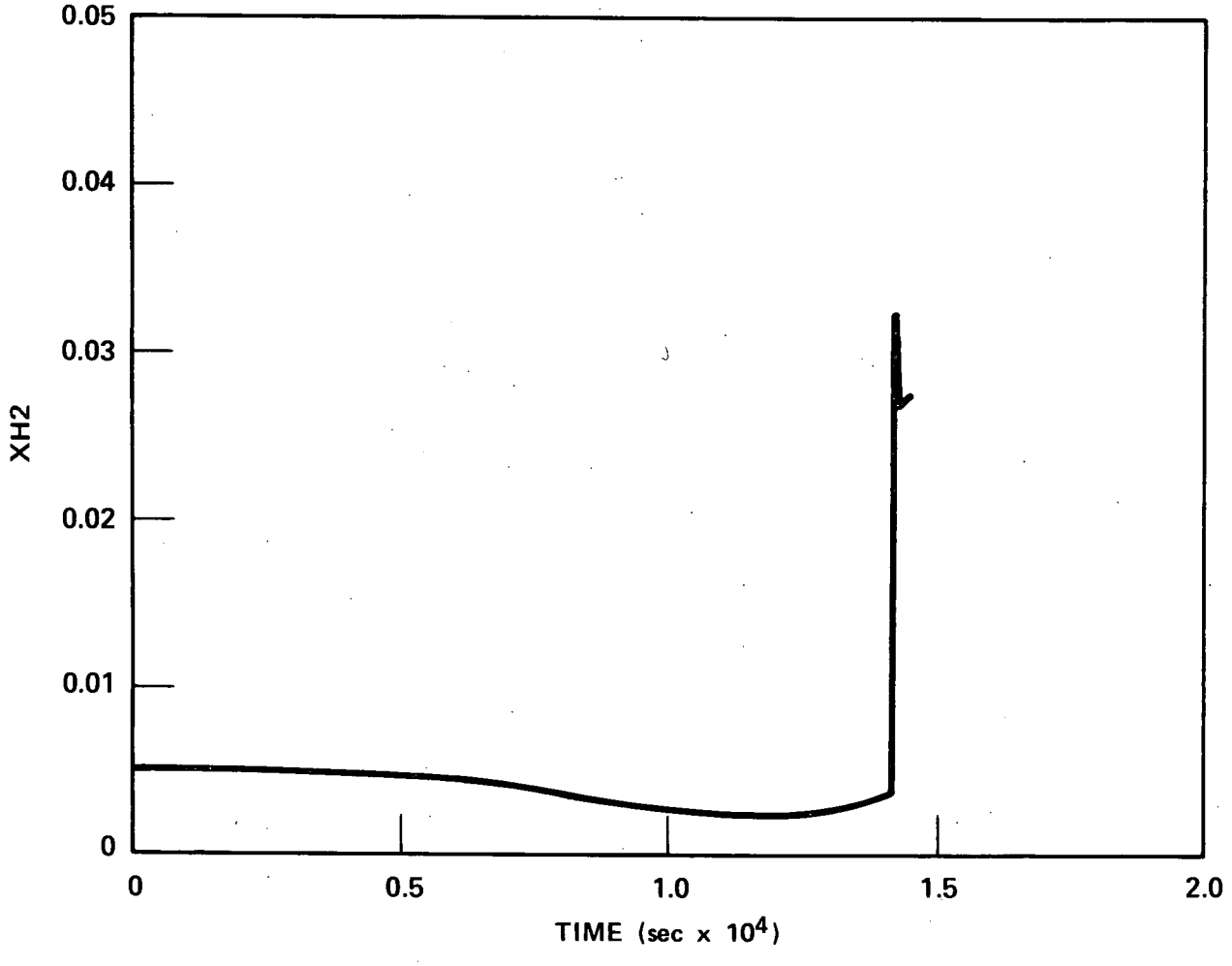
Pressure (in Containment) vs. Time
TMLB, Time Phased, 50% Dispersive, No Burn, 63% Zr Reacted
Class V, Case 4a'



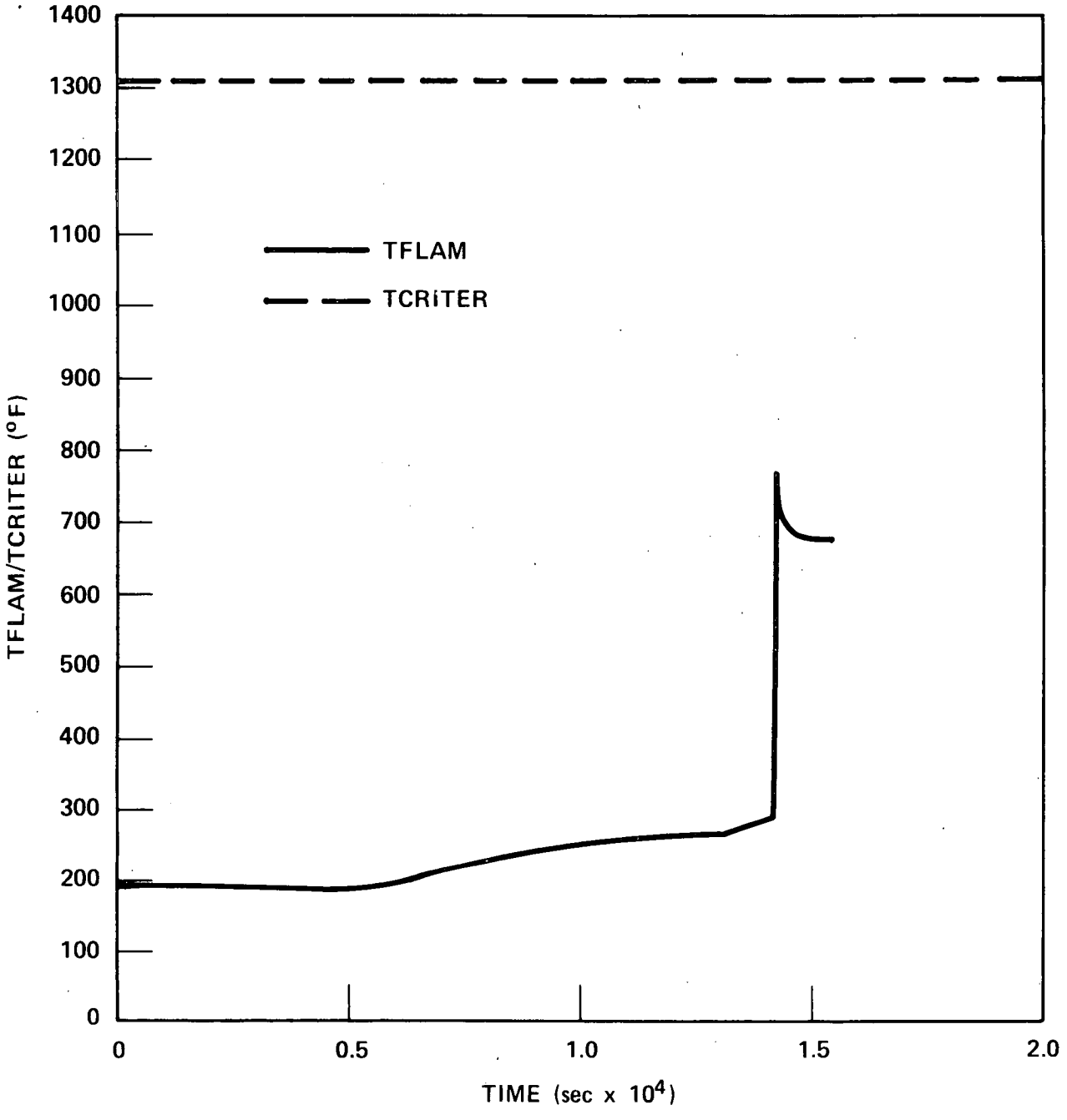
Temperature (in Containment) vs. Time
TMLB, Time Phased, 50% Dispersive, No Burn, 63% Zr Reacted
Class V, Case 4a'



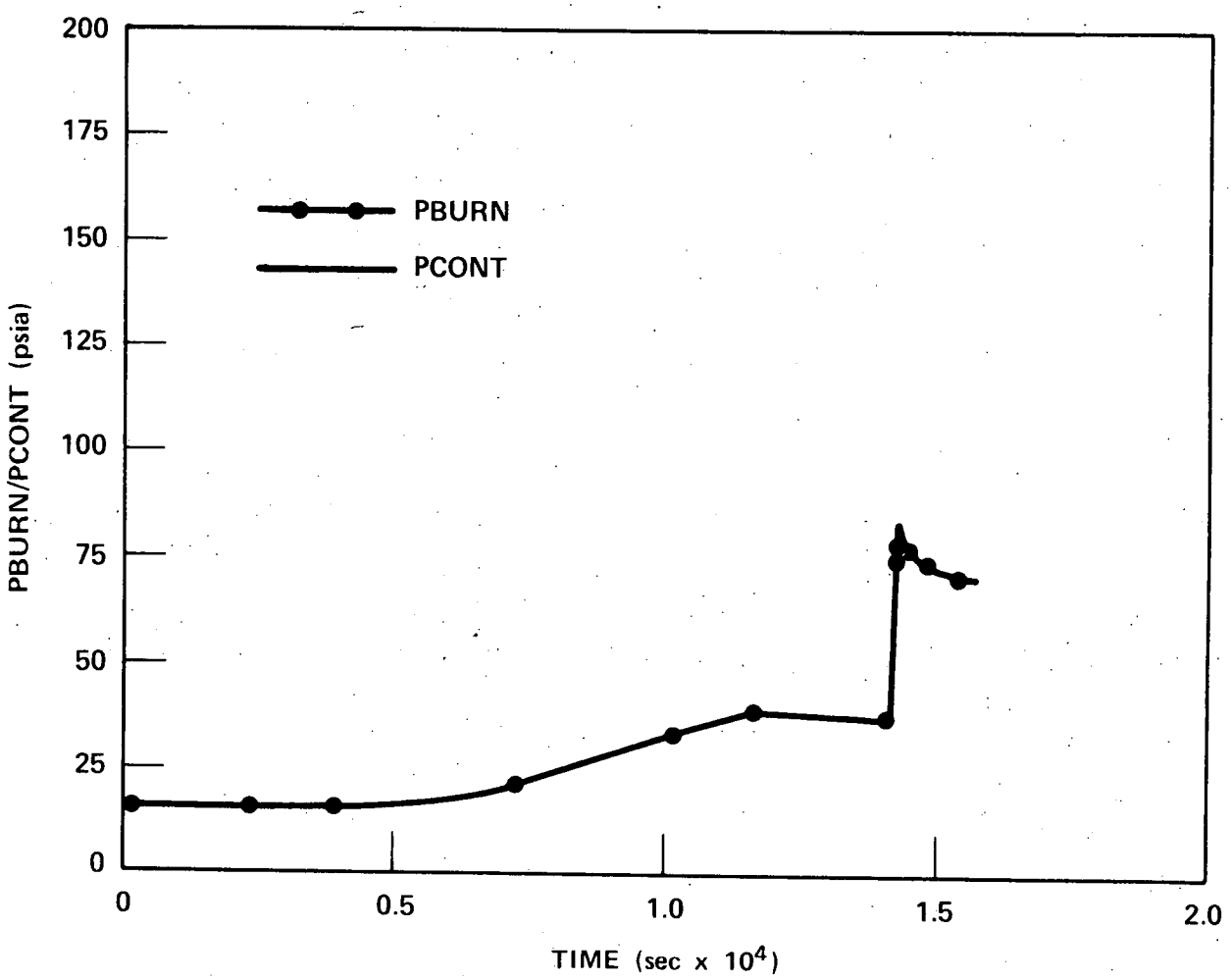
Mass Hydrogen (in Containment) vs. Time
TMLB, Time Phased, 50% Dispersive, No Burn, 63% Zr Reacted
Class V, Case 4a'



Mole Fraction H_2 (in Containment) vs. Time
TMLB, Time Phased, 50% Dispersive, No Burn, 63% Zr Reacted
Class V, Case 4a'



Flame Temperature (in Containment) vs. Time
TMLB, Time Phased, 50% Dispersive, No Burn, 63% Zr Reacted
Class V, Case 4a'



Adiabatic Burn Pressure/Pressure in Containment vs. Time
TMLB, Time Phased, 50% Dispersive, No Burn, 63% Zr Reacted
Class V, Case 4a'

CASE: CLASS V, CASE 5A, TMLB, W, 80% DISPERSIVE, NO BURN

DISPERSIVE: YES PERCENT CORE: 80% FRACTION IN CAVITY: .20

RUN #: AALAAIS DATE: 11/15/80

BLOWDOWN PEAK: N/A PSIA TIME: _____ SEC.

HYDROGEN BURN?: NO CRITERIA: _____

TIME @ BURN: _____ SEC, PRESSURE: _____ PSIA, TEMPERATURE: _____ °F

PEAKS:

PRESSURE: 132 PSIA, TIME: 15570 SEC, WHY?: DISPERSIVE FAILURE

TEMPERATURE: 830 °F, TIME: ~15570 SEC, WHY?: DISPERSIVE FAILURE

SPERT:

PRESSURE: 132 PSIA, TIME: 15570 SEC, WHY?: _____

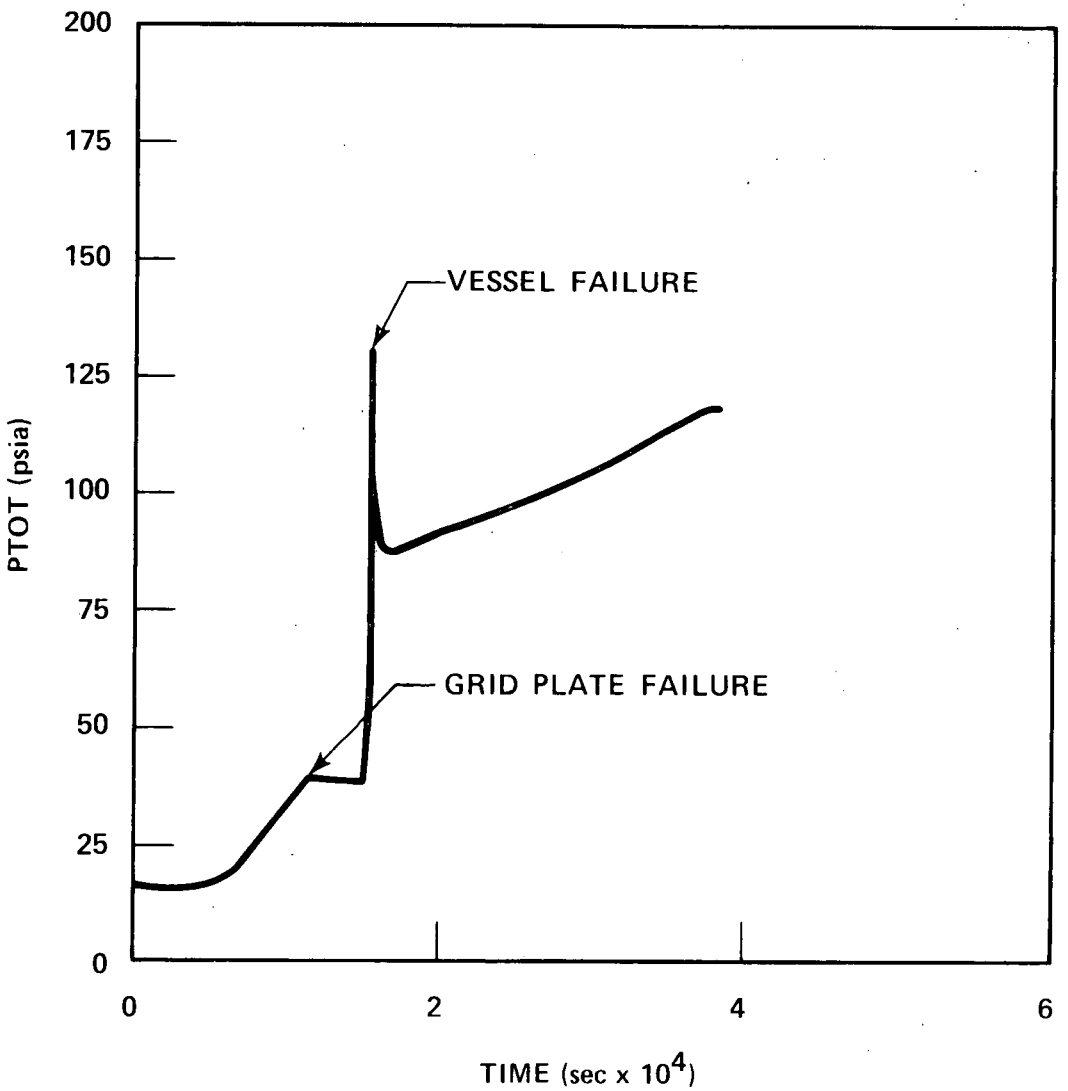
TEMPERATURE: 830 °F, TIME: ~15570 SEC, WHY?: _____

END OF BOIL: 15180 SEC. END OF HEAD: 15540 SEC.

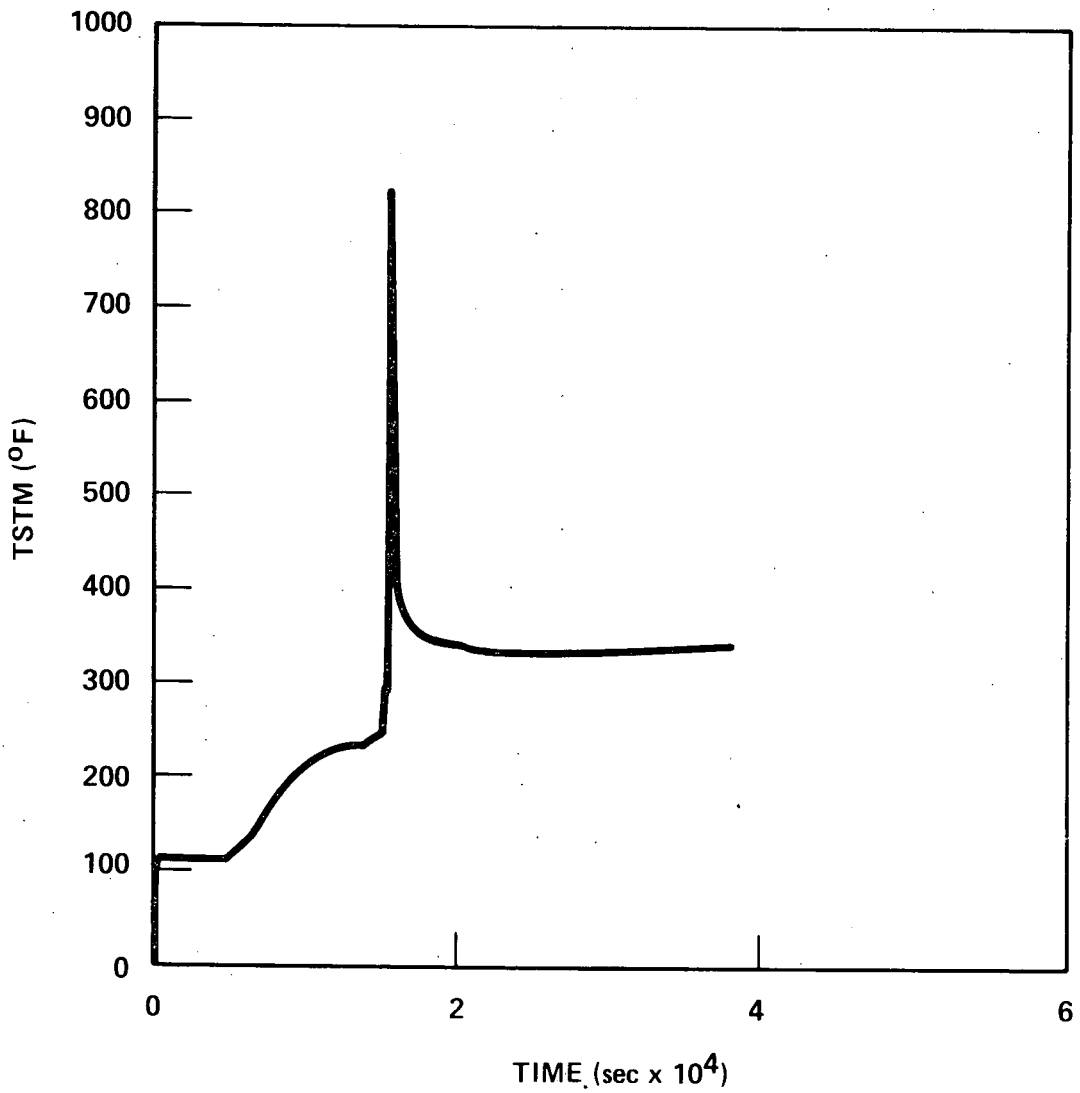
VESSEL FAILURE: 15540 SEC. END OF HOTDROP: 50240 SEC.

END OF INTER: 86753 SEC.

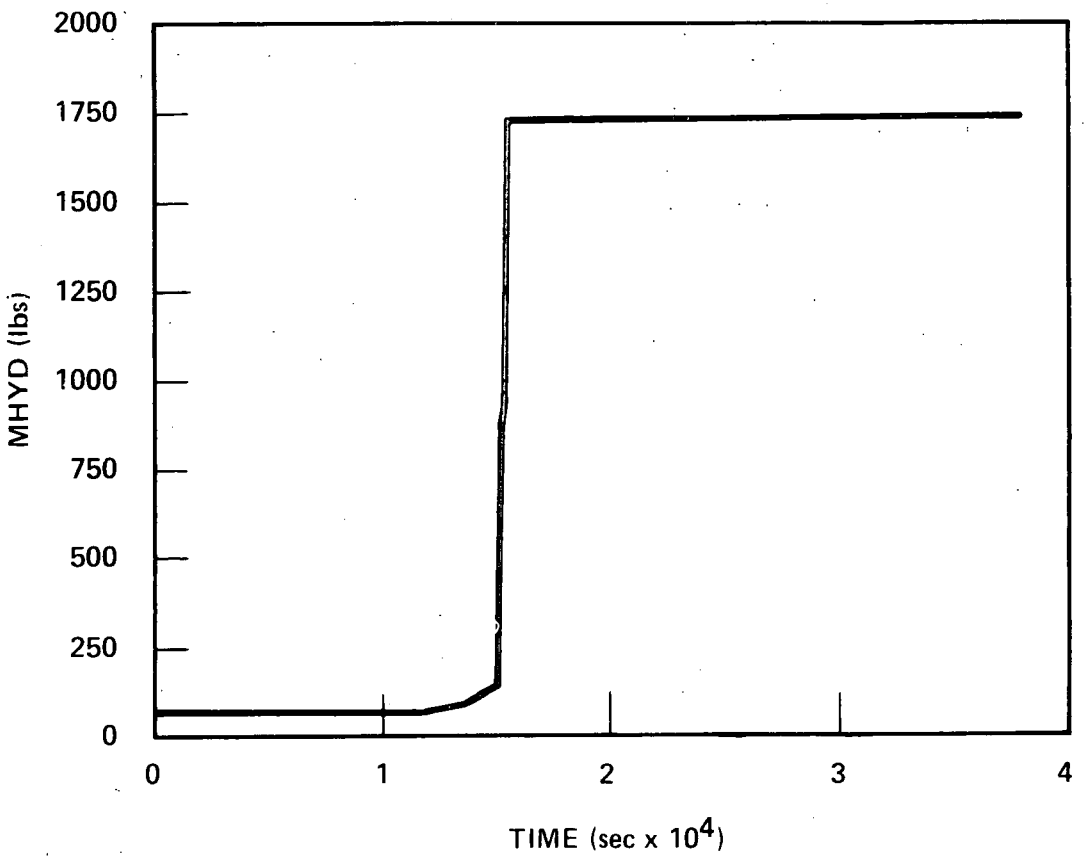
Class V, Case 5A



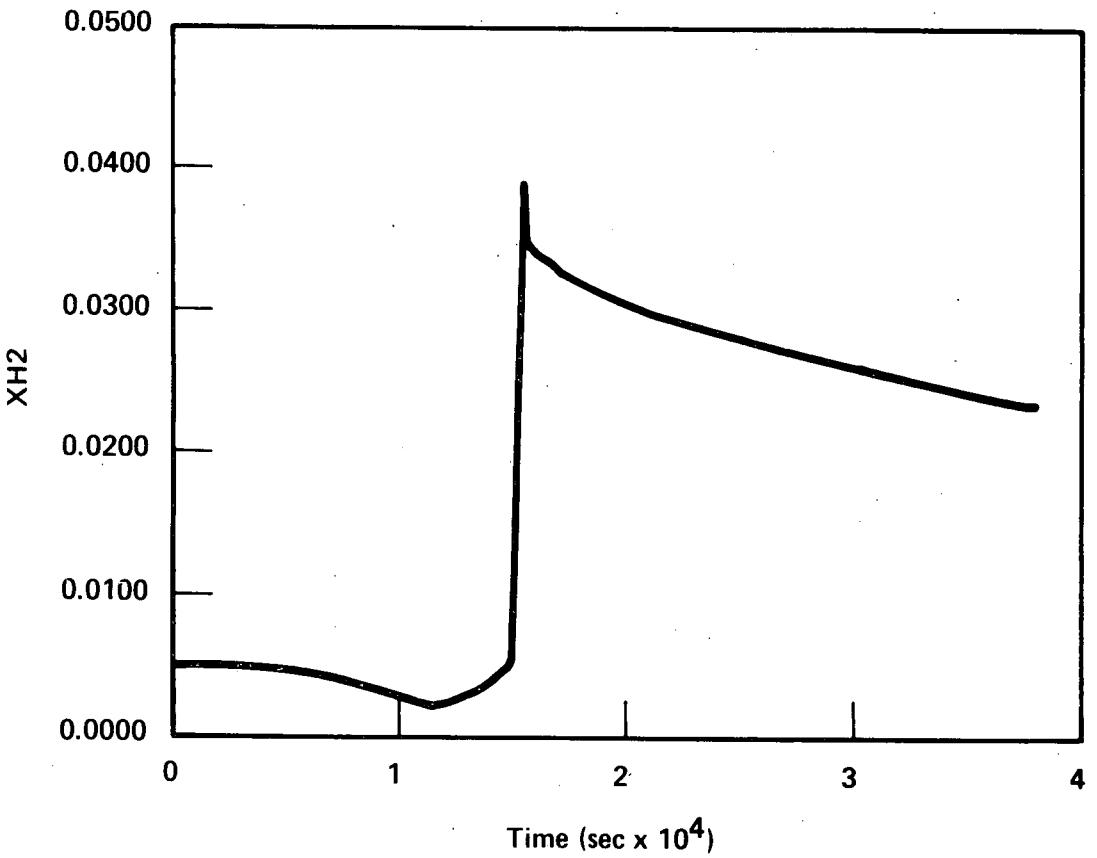
Pressure (in Containment) vs. Time
TMLB, 80% Dispersive, No Burn
Class V, Case 5A



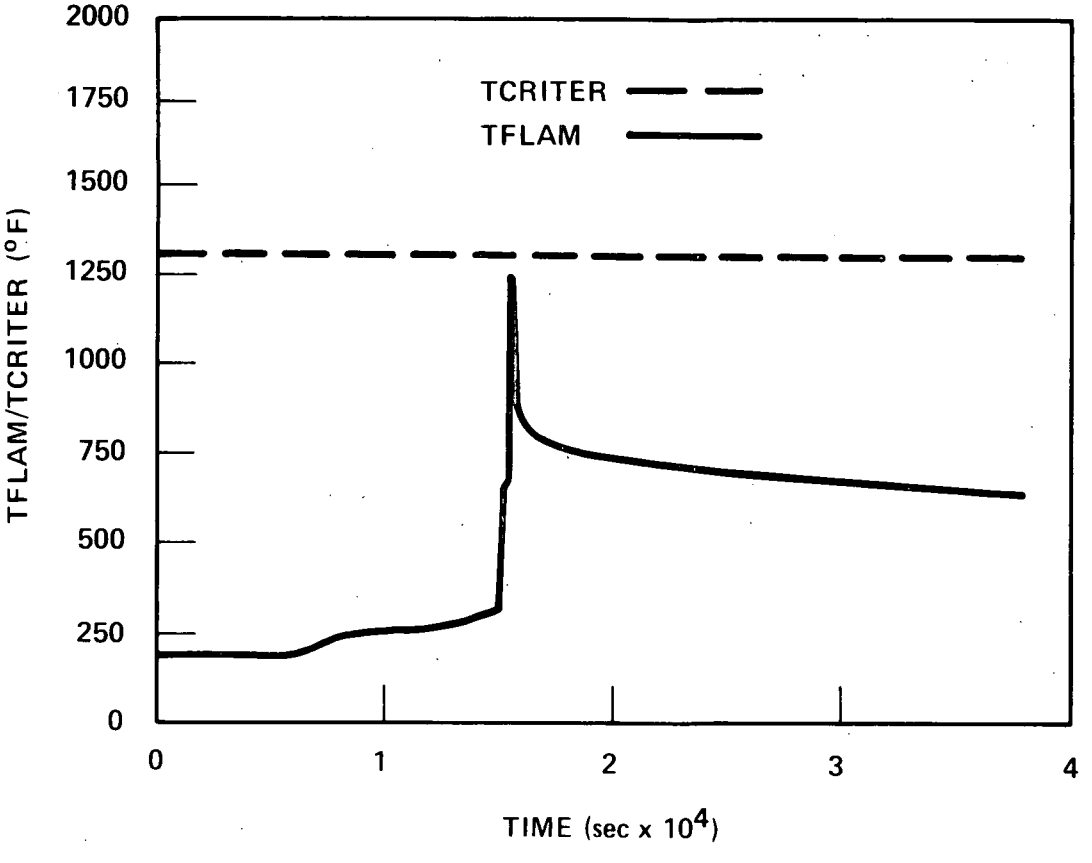
Temperature (in Containment) vs. Time
TMLB, 80% Dispersive, No Burn
Class V, Case 5A



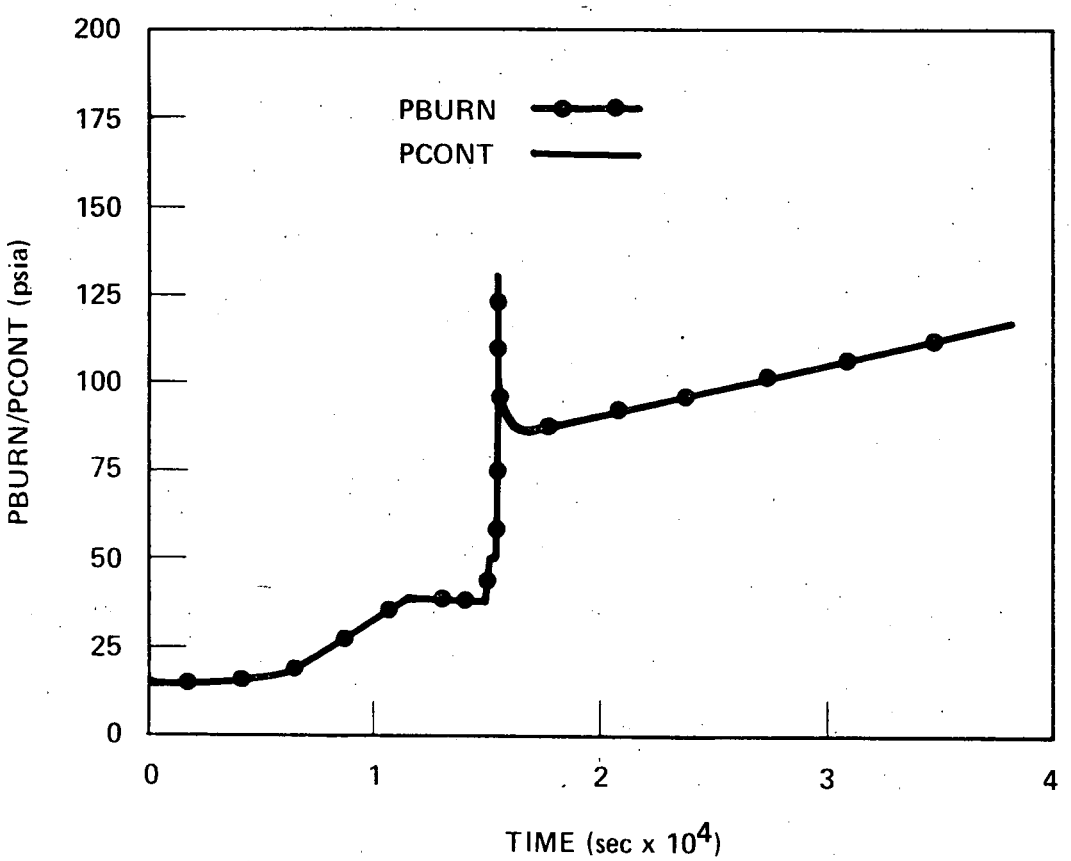
Mass Hydrogen (in Containment) vs. Time
TMLB, 80% Dispersive, No Burn
Class V, Case 5A



Mole Fraction H_2 (in Containment) vs. Time
TMLB, 80% Dispersive, No Burn
Class V, Case 5A



Flame Temperature (in Containment) vs. Time
TMLB, 80% Dispersive, No Burn
Class V, Case 5A



Adiabatic Burn Pressure/Pressure in Containment vs. Time
TMLB, 80% Dispersive, No Burn
Class V, Case 5A

CASE: CLASS V, CASE 5B, TMLB, W, 80% DISPERSIVE, BURN @ END OF DISPERSION

DISPERSIVE: YES PERCENT CORE: 80 FRACTION IN CAVITY: 0

RUN #: AALAAIT DATE: 11/15/80

BLOWDOWN PEAK: N/A PSIA TIME: _____ SEC.

HYDROGEN BURN?: YES CRITERIA: END OF SPERT

TIME @ BURN: 15570 SEC, PRESSURE: 174 PSIA, TEMPERATURE: 1280 °F

PEAKS:

PRESSURE: 174 PSIA, TIME: 15590 SEC, WHY?: DISPERSIVE/BURN

TEMPERATURE: 1280 °F, TIME: ~15590 SEC, WHY?: DISPERSIVE/BURN

DISPERSIVE: YES

PRESSURE: 174 PSIA, TIME: 15590 SEC, WHY?: _____

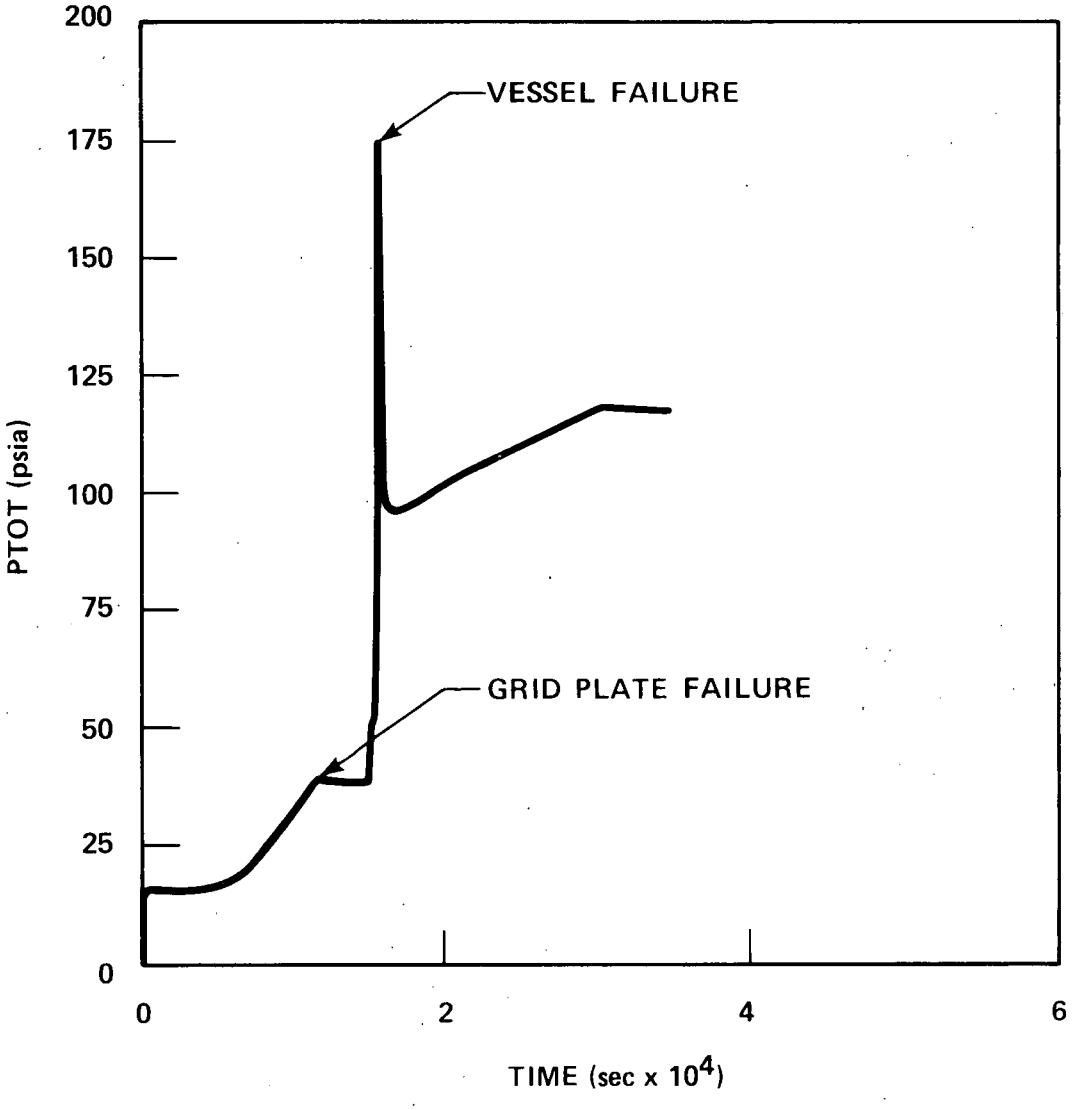
TEMPERATURE: _____ °F, TIME: _____ SEC, WHY?: _____

END OF BOIL: 15180 SEC. END OF HEAD: 15540 SEC.

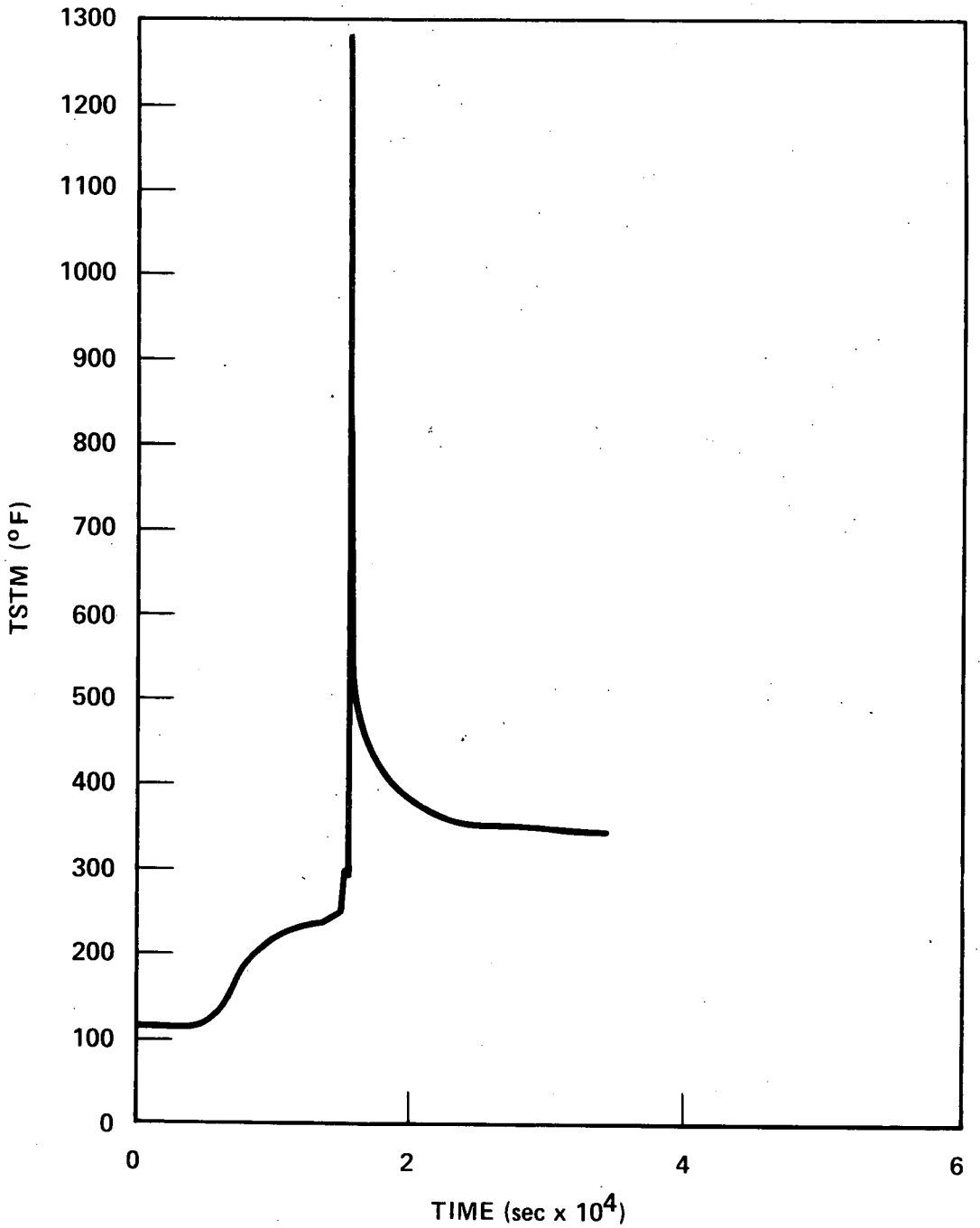
VESSEL FAILURE: 15540 SEC. END OF HOTDROP: _____ SEC.

END OF INTER: _____ SEC.

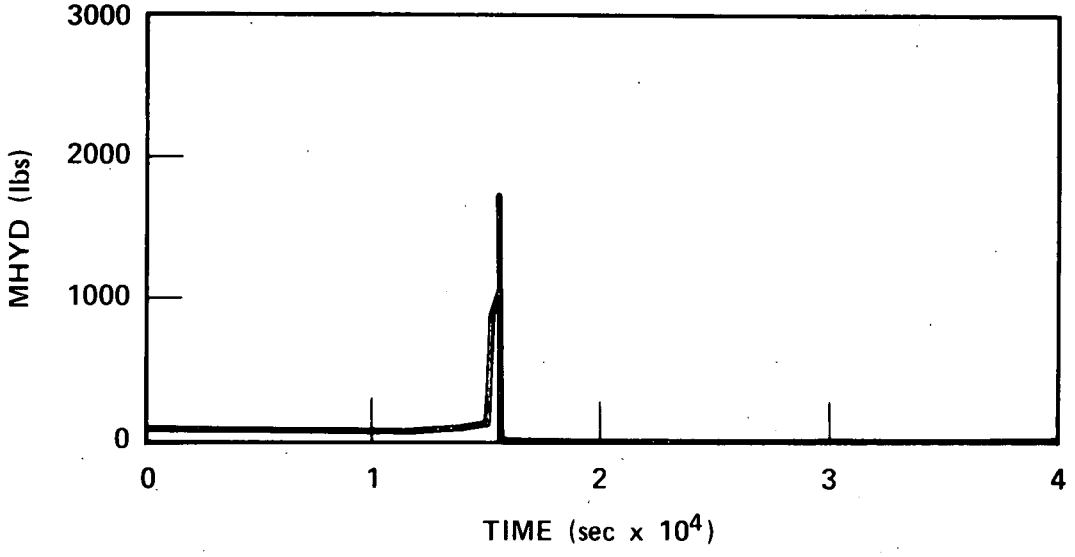
Class V, Case 5B



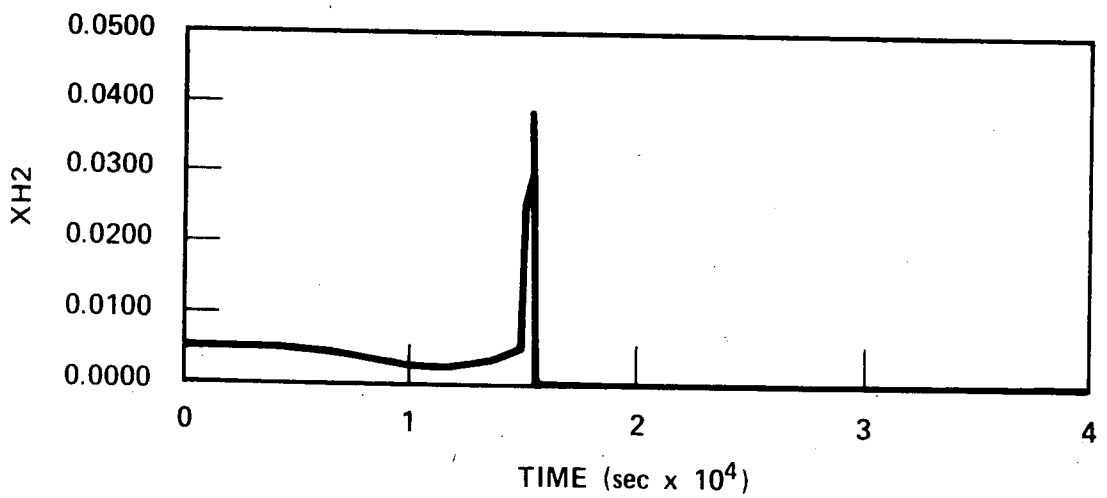
Pressure (in Containment) vs. Time
TMLB, W, 80% Dispersive, Burn @ End of Dispersion
Class V, Case 5B



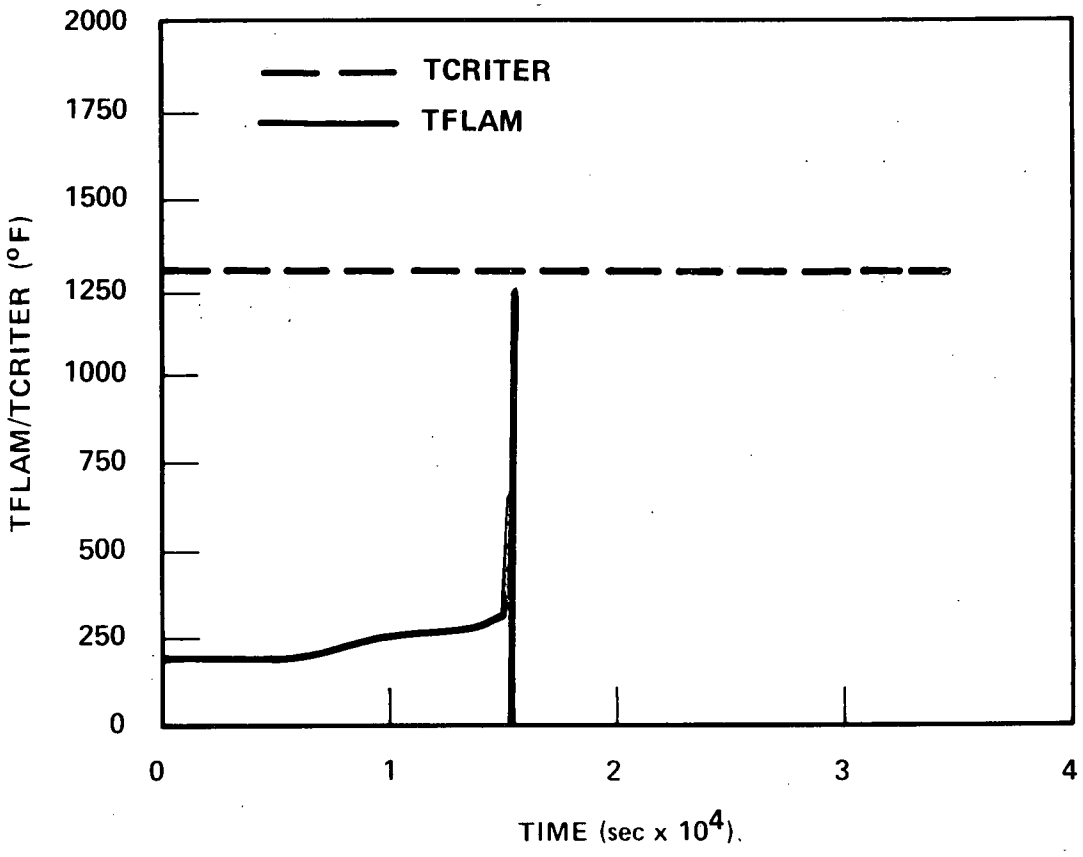
Temperature (in Containment) vs. Time
TMLB, W, 80% Dispersive, Burn @ End of Dispersion
Class V, Case 5B



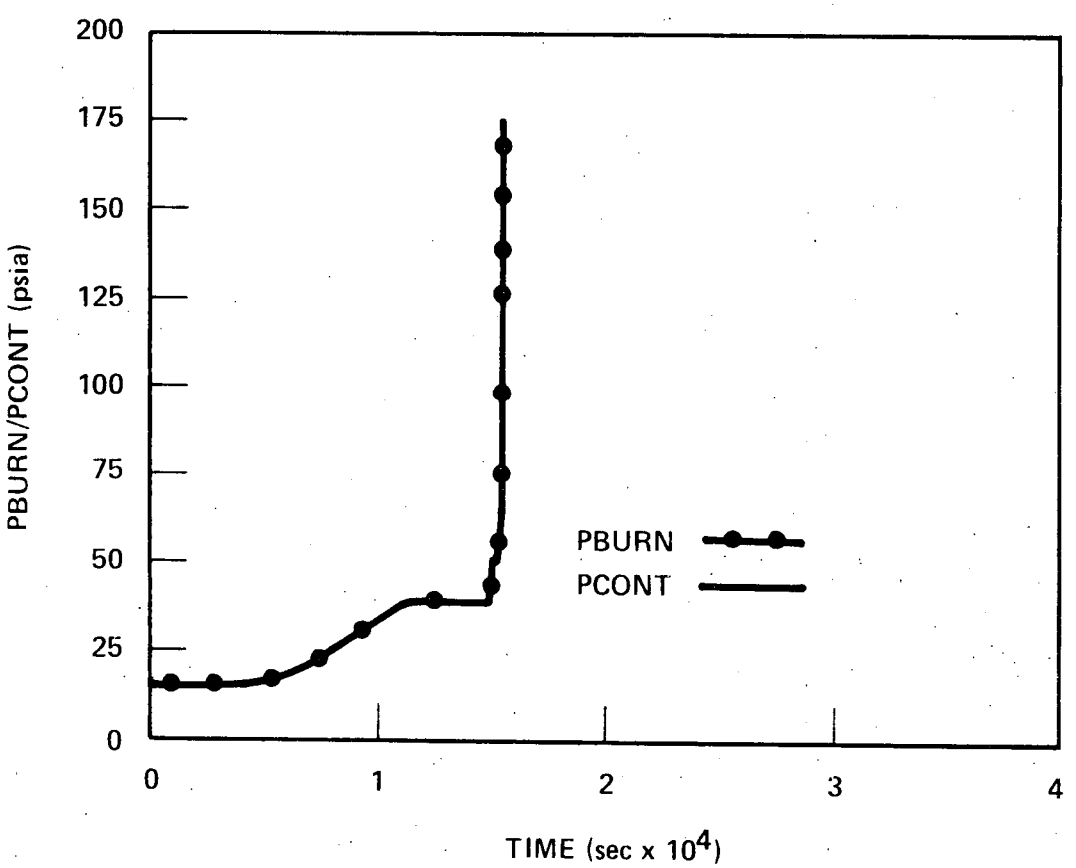
Mass Hydrogen (in Containment) vs. Time
TMLB, W, 80% Dispersive, Burn @ End of Dispersion
Class V, Case 5B



Mole Fraction H_2 (in Containment) vs. Time
TMLB, W, 80% Dispersive, Burn @ End of Dispersion
Class V, Case 5B



Flame Temperature (in Containment) vs. Time
TMLB, W, 80% Dispersive, Burn @ End of Dispersion
Class V, Case 5B



Adiabatic Burn Pressure/Pressure in Containment vs. Time
TMLB', W, 80% Dispersive, Burn @ End of Dispersion
Class V, Case 5B

CASE: CLASS V, CASE 6A, TMLB, W, 50% DISPERSIVE, NO BURN

DISPERSIVE: YES PERCENT CORE: 50 FRACTION IN CAVITY: .50

RUN #: AALAAIZ DATE: 11/15/80

BLOWDOWN PEAK: N/A PSIA TIME: _____ SEC.

HYDROGEN BURN?: NO CRITERIA: _____

TIME @ BURN: _____ SEC, PRESSURE: _____ PSIA, TEMPERATURE: _____ °F

PEAKS:

PRESSURE: 122 PSIA, TIME: 15570 SEC, WHY?: DISPERSIVE FAILURE

TEMPERATURE: 654 °F, TIME: ~15570 SEC, WHY?: DISPERSIVE FAILURE

SPERT:

PRESSURE: 122 PSIA, TIME: 15570 SEC,

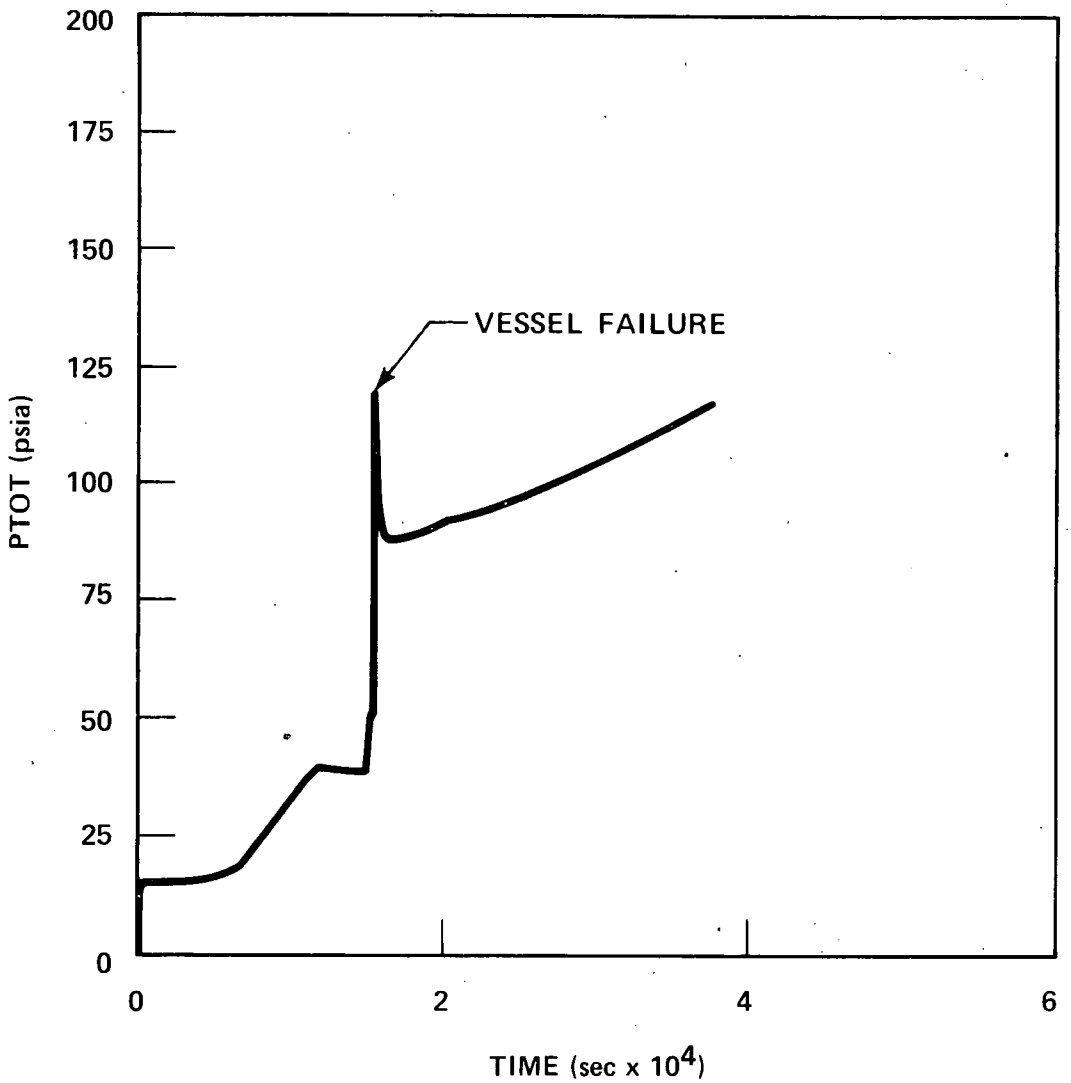
TEMPERATURE: 654 °F, TIME: ~15570 SEC,

END OF BOIL: 15180 SEC. END OF HEAD: 15540 SEC.

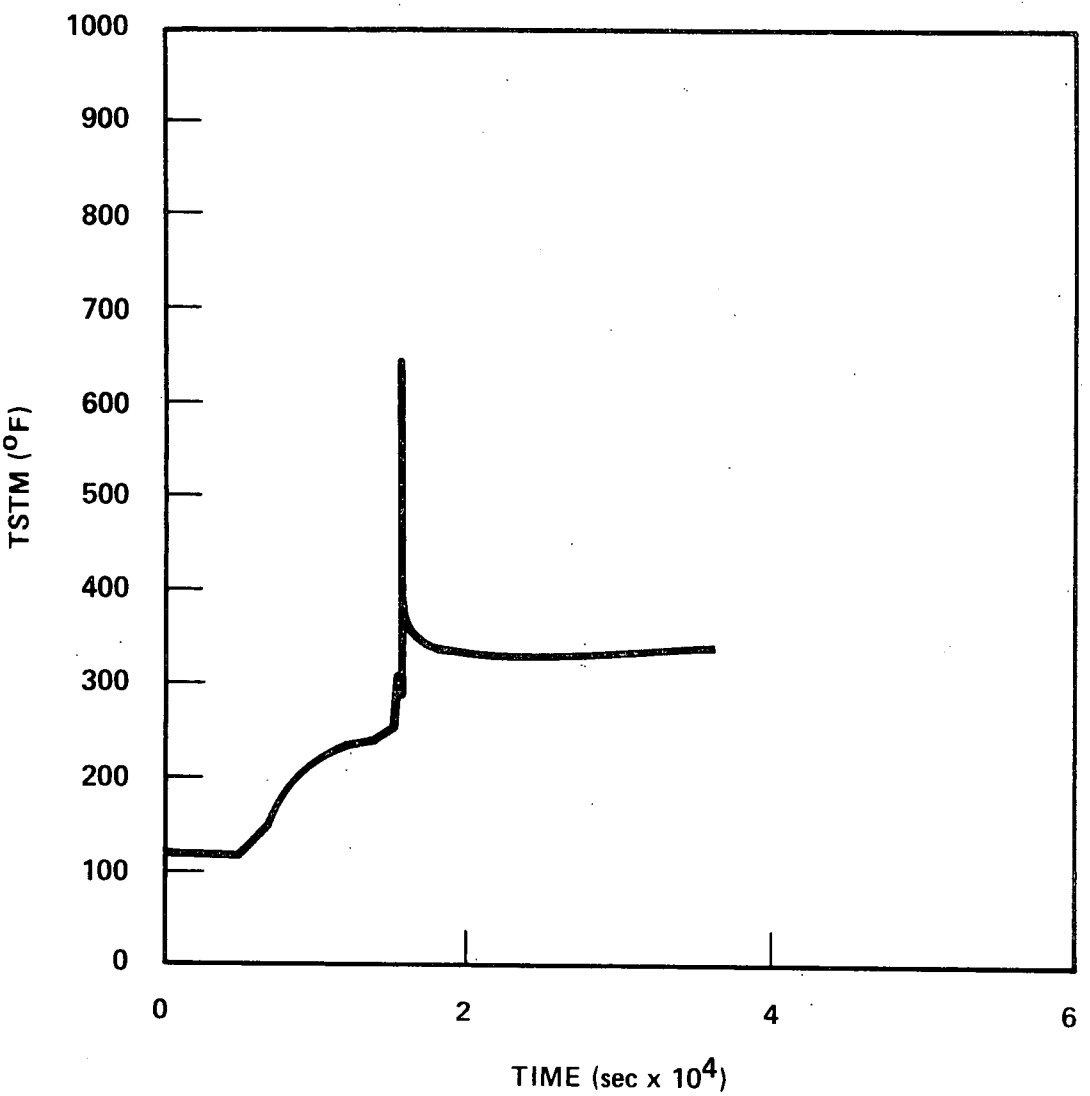
VESSEL FAILURE: 15540 SEC. END OF HOTDROP: 50240 SEC.

END OF INTER: 86753 SEC.

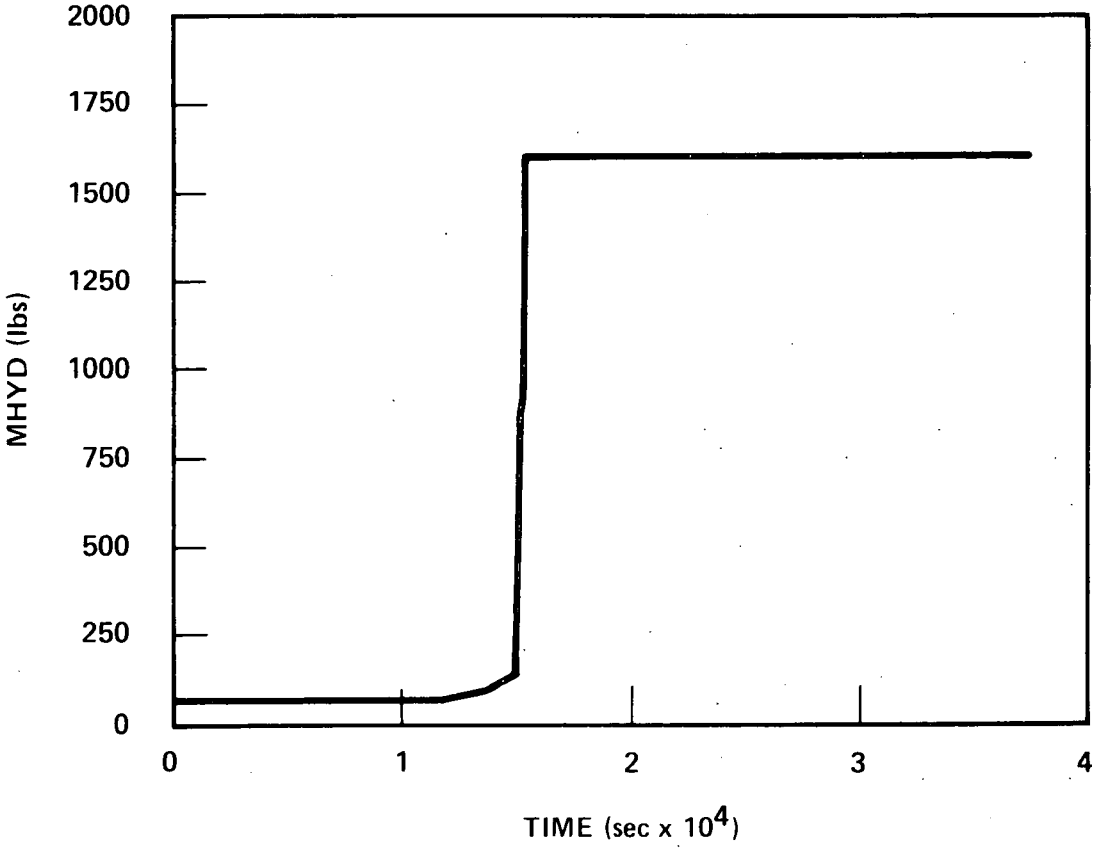
Class V, Case 6A



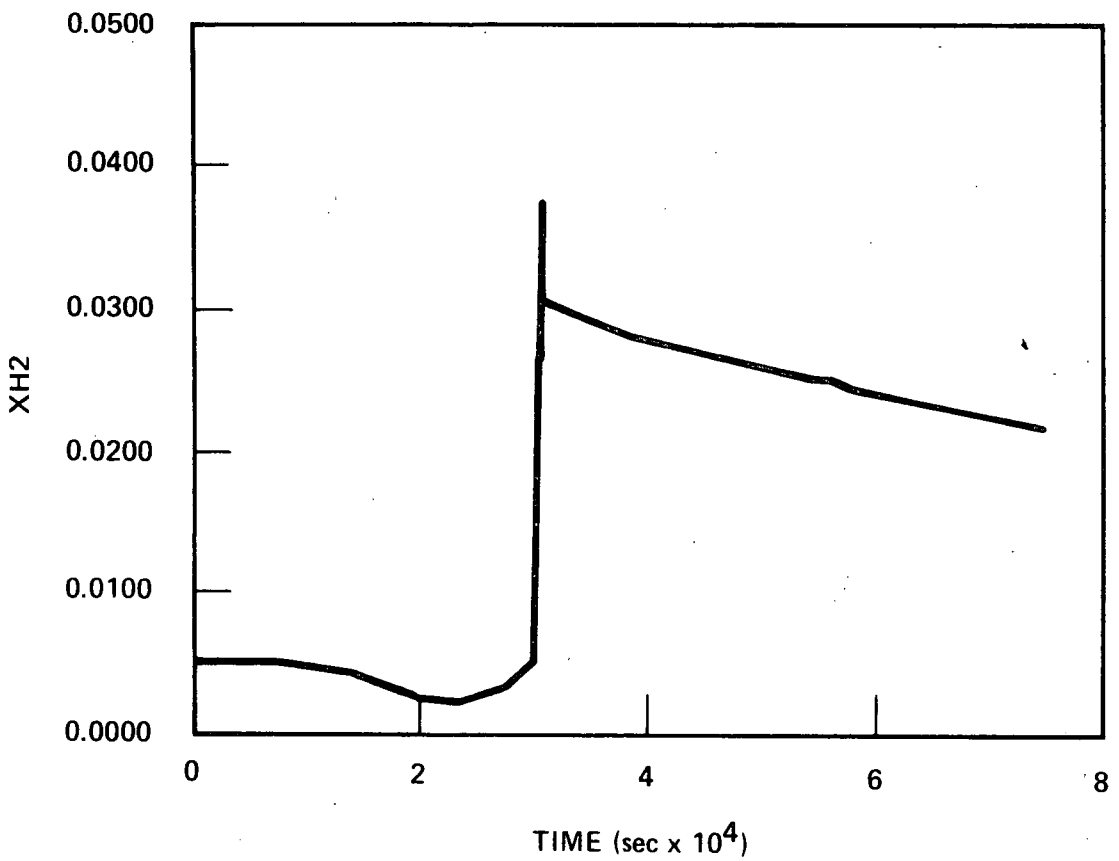
Pressure (in Containment) vs. Time
TMLB, W, 50% Dispersive, No Burn
Class V, Case 6A



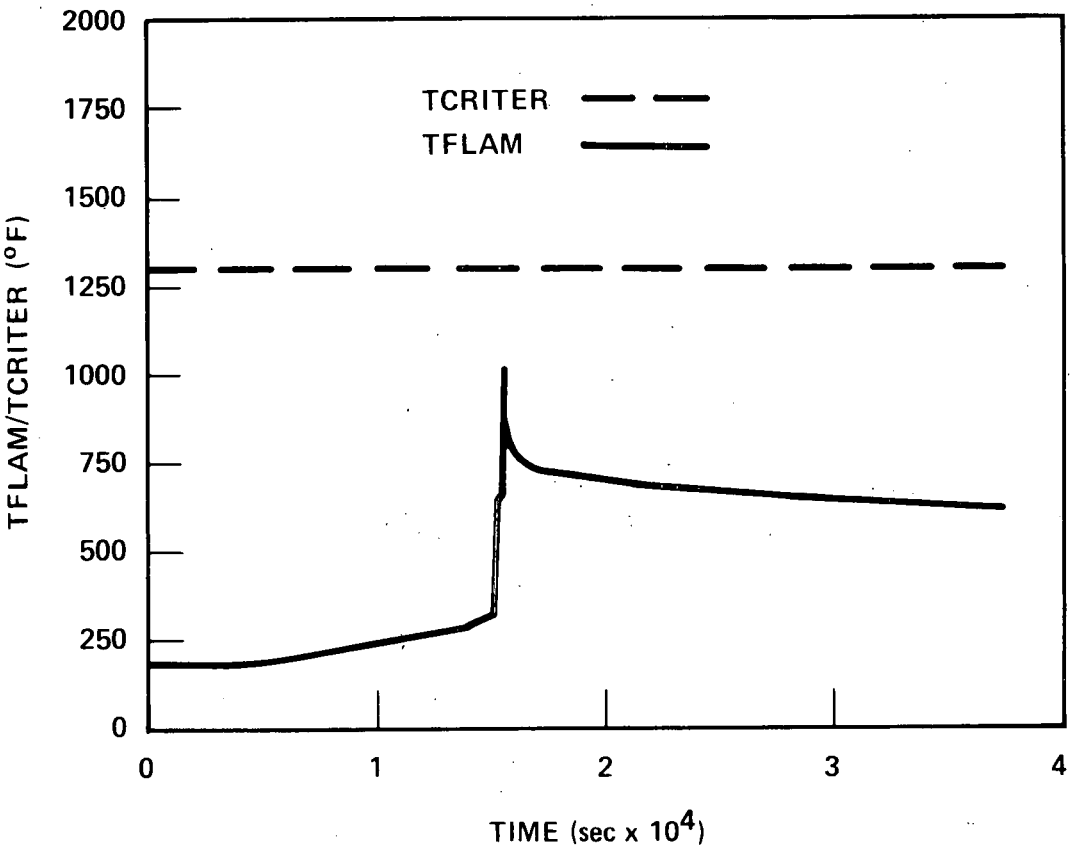
Temperature (in Containment) vs. Time
TMLB, W, 50% Dispersive, No Burn
Class V, Case 6A



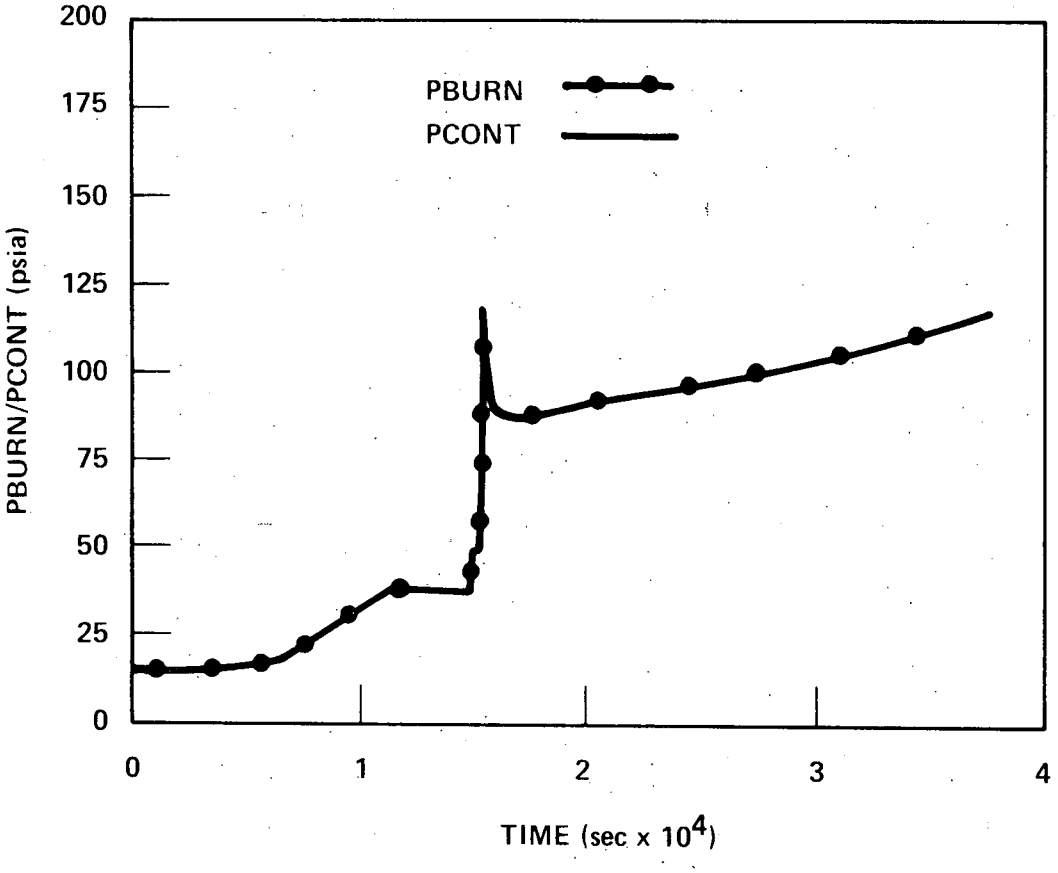
Mass Hydrogen (in Containment) vs. Time
TMLB, W, 50% Dispersive, No Burn
Class V, Case 6A



Mole Fraction H_2 (in Containment) vs. Time
TMLB, W, 50% Dispersive, No Burn
Class V, Case 6A



Flame Temperature (in Containment) vs. Time
TMLB, W, 50% Dispersive, No Burn
Class V, Case 6A



Adiabatic Burn Pressure/Pressure in Containment vs. Time
TMLB, W, 50% Dispersive, No Burn
Class V, Case 6A

CASE: CLASS V, CASE 6B, TMLB, W, 50% DISPERSIVE, BURN @ END OF DISPERSION

DISPERSIVE: YES PERCENT CORE: 50 FRACTION IN CAVITY: .50

RUN #: AALAAIY DATE: 11/15/80

BLOWDOWN PEAK: N/A PSIA TIME: _____ SEC.

HYDROGEN BURN?: YES CRITERIA: END OF DISPERSION

TIME @ BURN: 15570 SEC, PRESSURE: 167 PSIA, TEMPERATURE: >1000 °F

PEAKS:

PRESSURE: 167 PSIA, TIME: 15590 SEC, WHY?: DISPERSION/BURN

TEMPERATURE: 1099 °F, TIME: ~15590 SEC, WHY?: DISPERSION/BURN

DISPERSIVE: YES

PRESSURE: 167 PSIA, TIME: 15590 SEC,

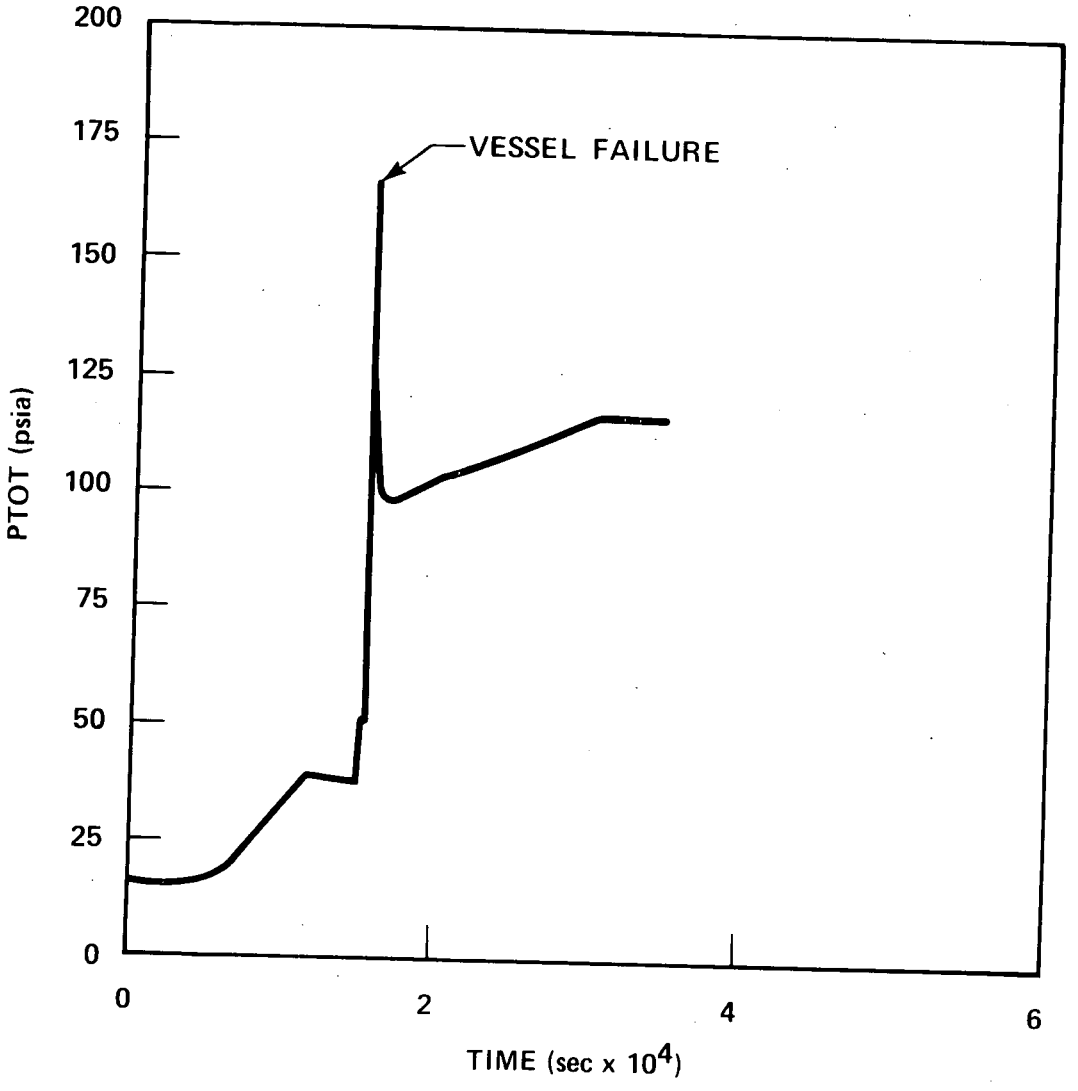
TEMPERATURE: 1099 °F, TIME: 15590 SEC,

END OF BOIL: 15180 SEC. END OF HEAD: 15540 SEC.

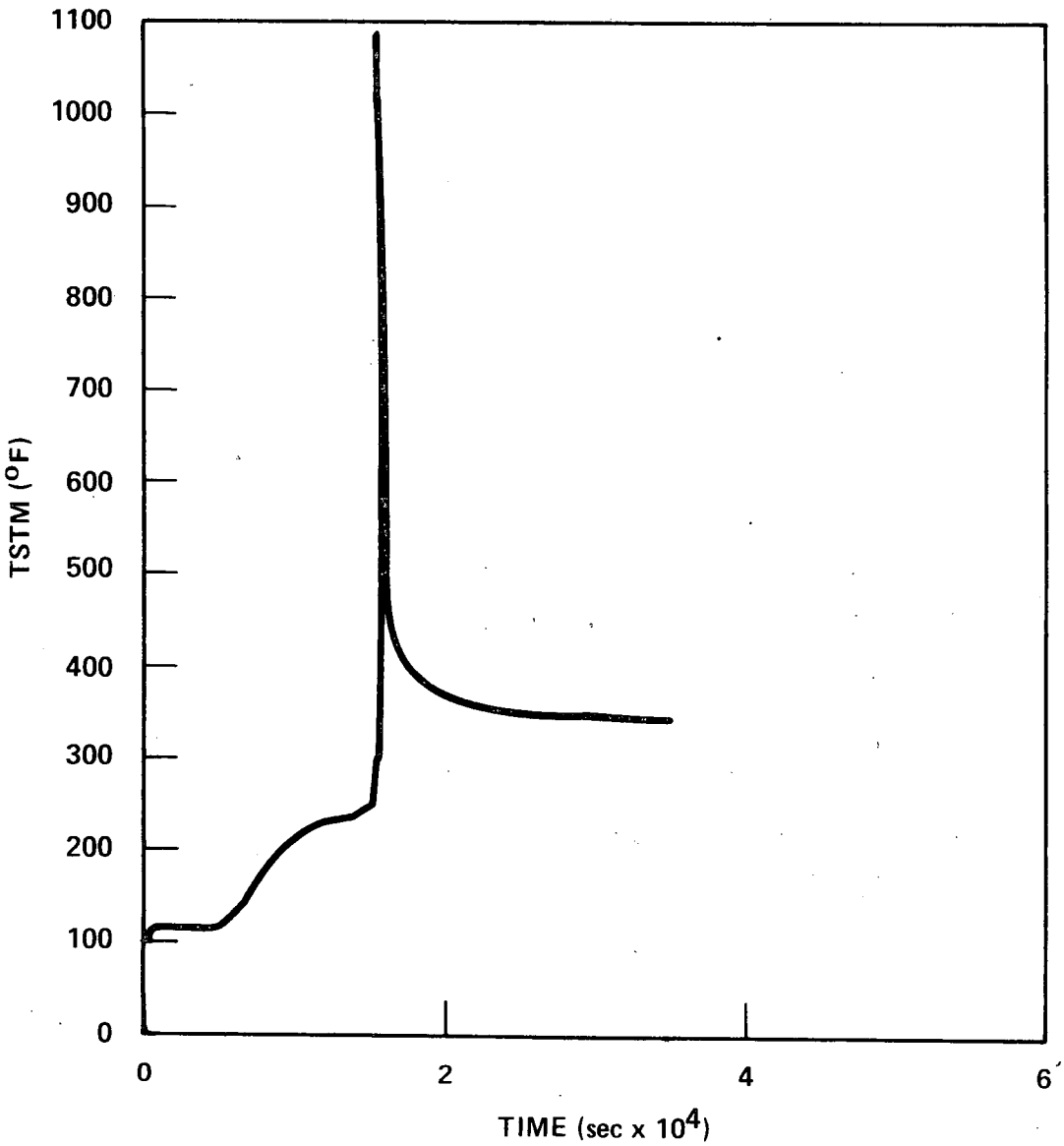
VESSEL FAILURE: 15540 SEC. END OF HOTDROP: 50240 SEC.

END OF INTER: 86753 SEC.

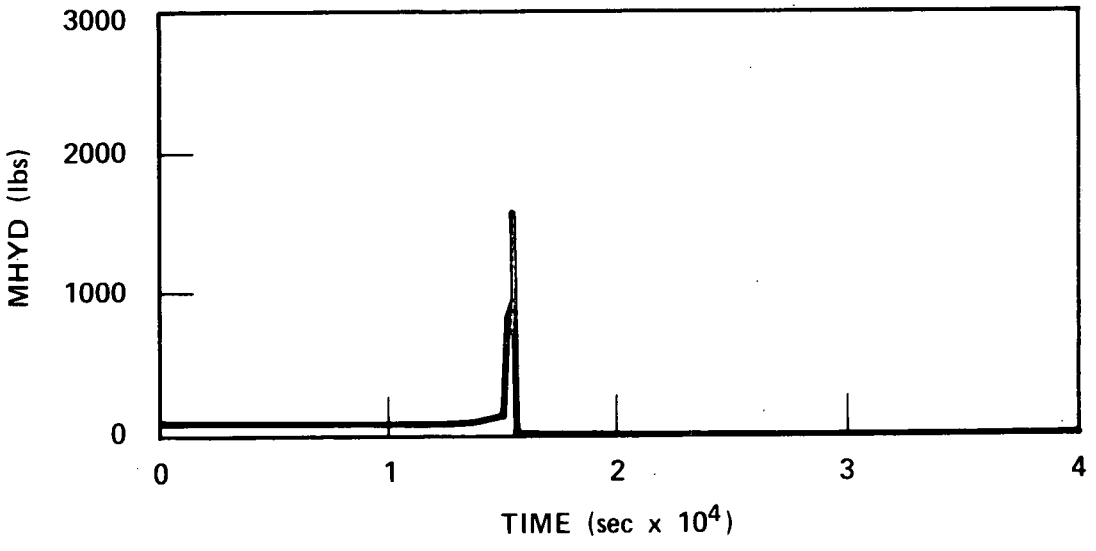
Class V, Case 6B



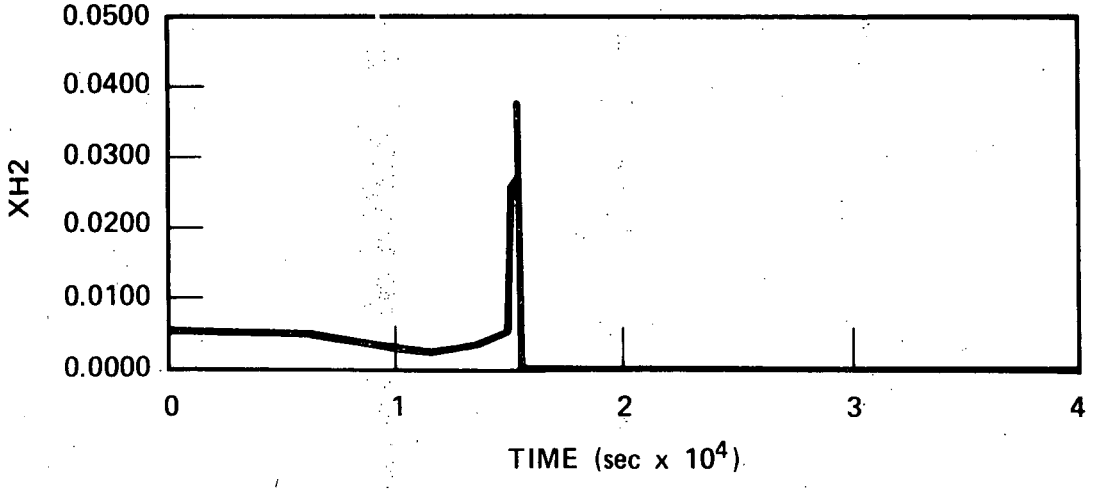
Pressure (in Containment) vs. Time
TMLB, W, 50% Dispersive, Burn @ End of Dispersion
Class V, Case 6B



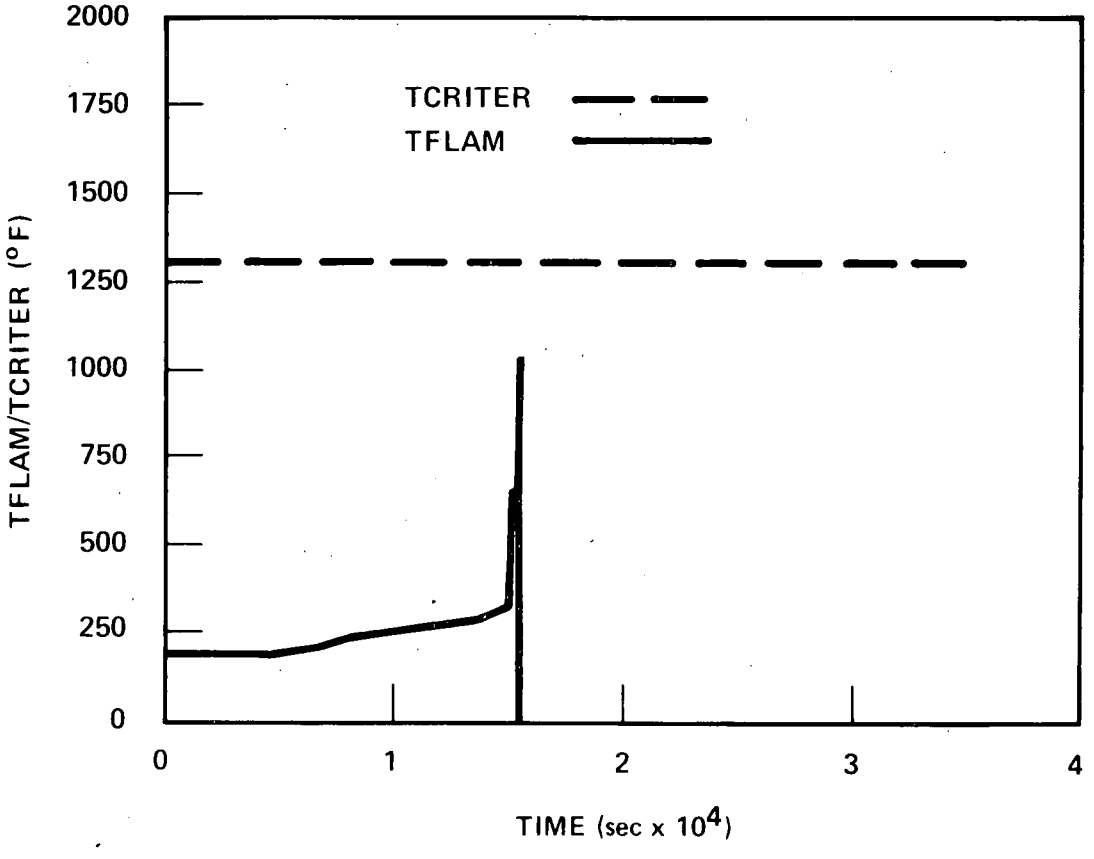
Temperature (in Containment) vs. Time
TMLB, W, 50% Dispersive, Burn @ End of Dispersion
Class V, Case 6B



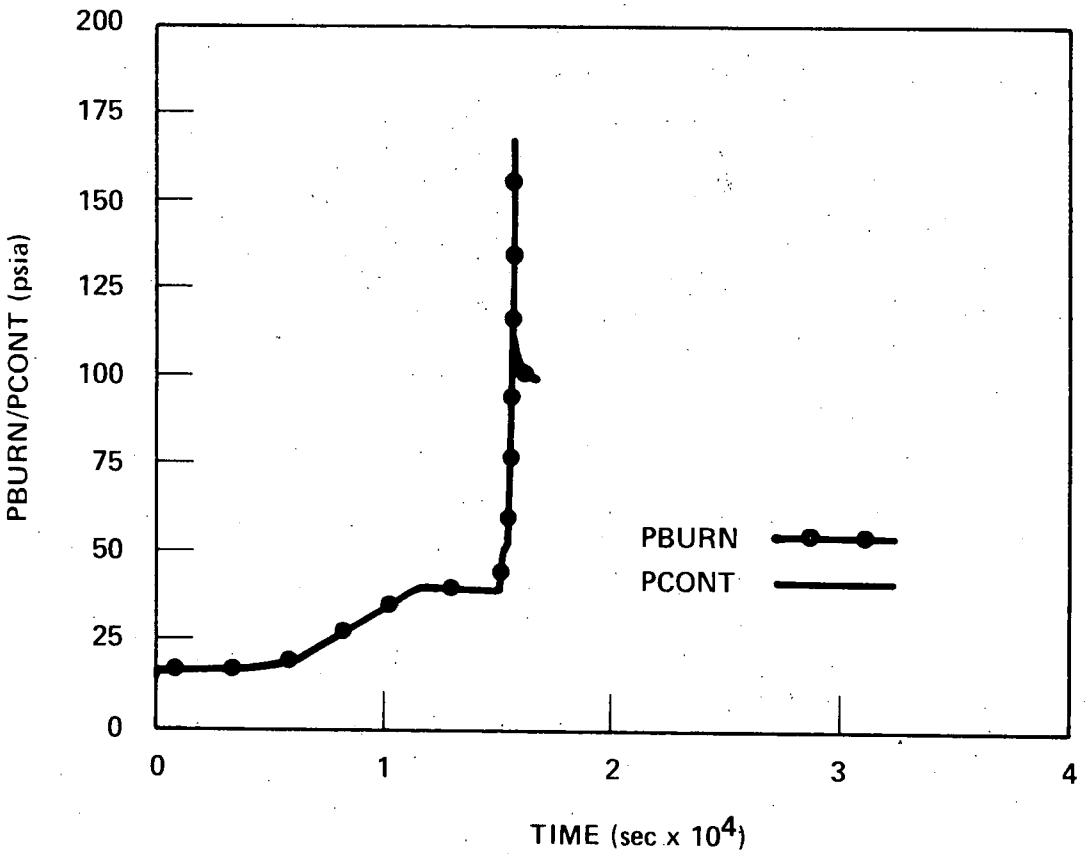
Mass Hydrogen (in Containment) vs. Time
TMLB, W, 50% Dispersive, Burn @ End of Dispersion
Class V, Case 6B



Mole Fraction H_2 (in Containment) vs. Time
TMLB, W, 50% Dispersive, Burn @ End of Dispersion
Class V, Case 6B



Flame Temperature (in Containment) vs. Time
TMLB, W, 50% Dispersive, Burn @ End of Dispersion
Class V, Case 6B



Adiabatic Burn Pressure/Pressure in Containment vs. Time
TMLB; W, 50% Dispersive, Burn @ End of Dispersion
Class V, Case 6B

CASE: CLASS V, CASE 7A, TMLB, B, 80% DISPERSIVE, NO BURN

DISPERSIVE: YES PERCENT CORE: 80 FRACTION IN CAVITY: 0

RUN #: AALAAIQ DATE: 11/15/80

BLOWDOWN PEAK: N/A PSIA TIME: _____ SEC.

HYDROGEN BURN?: NO CRITERIA: _____

TIME @ BURN: _____ SEC, PRESSURE: _____ PSIA, TEMPERATURE: _____ °F

PEAKS:

PRESSURE: 124 PSIA, TIME: 15570 SEC, WHY?: DISPERSIVE FAILURE

TEMPERATURE: 853 °F, TIME: ~15570 SEC, WHY?: DISPERSIVE FAILURE

DISPERSIVE: YES

PRESSURE: 124 PSIA, TIME: 15570 SEC,

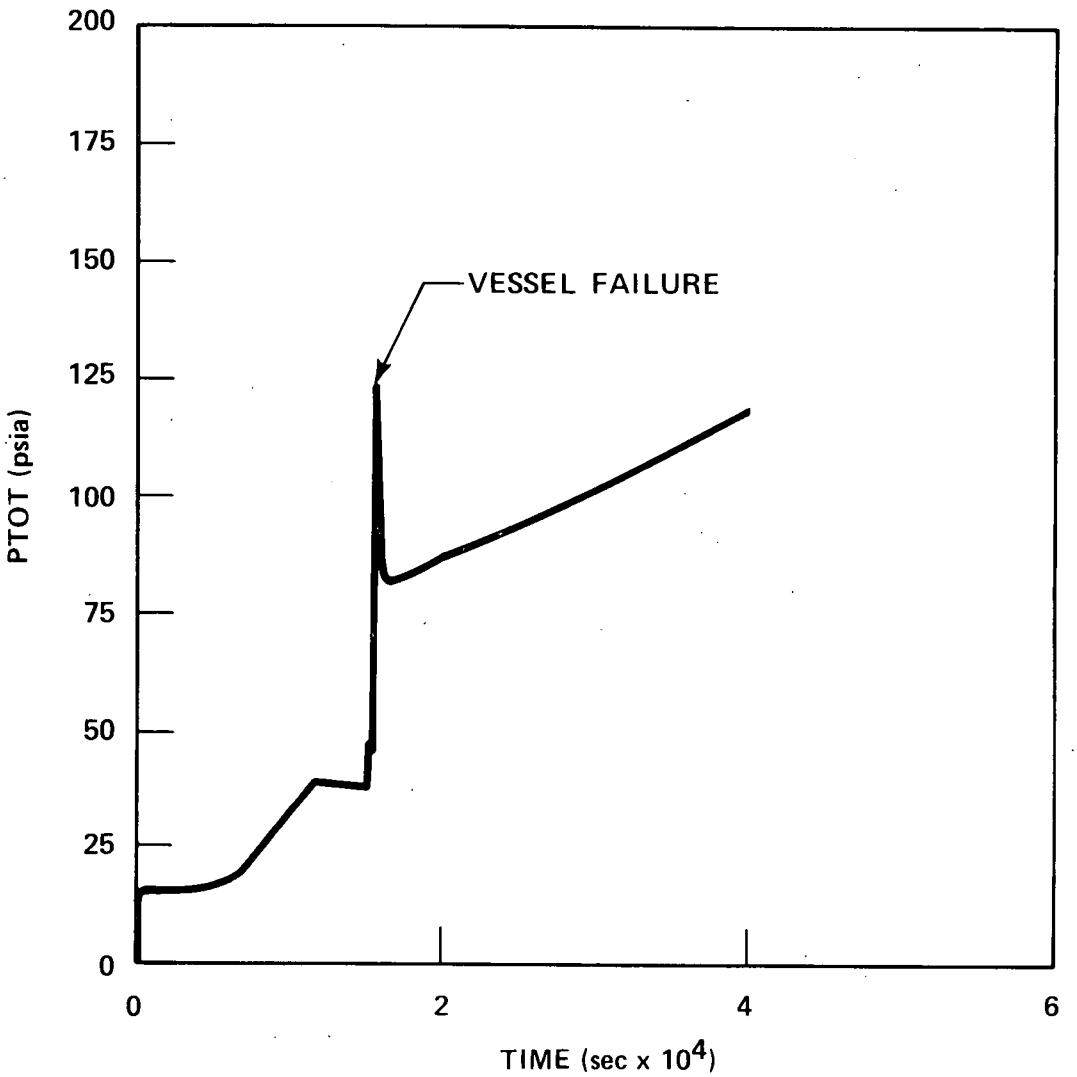
TEMPERATURE: 853 °F, TIME: 15570 SEC,

END OF BOIL: 15180 SEC. END OF HEAD: 15540 SEC.

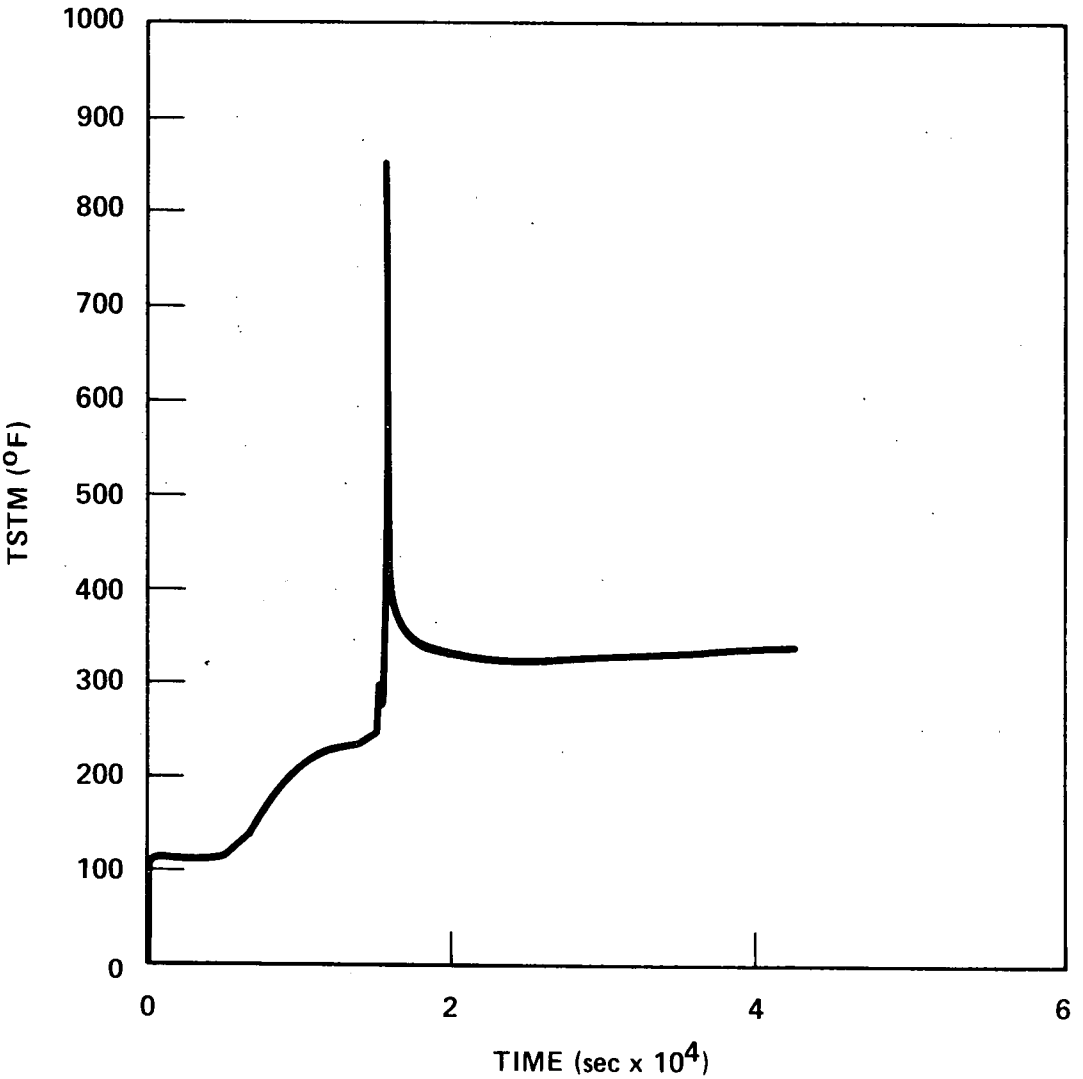
VESSEL FAILURE: 15540 SEC. END OF HOTDROP: 25147 SEC.

END OF INTER: 86419 SEC.

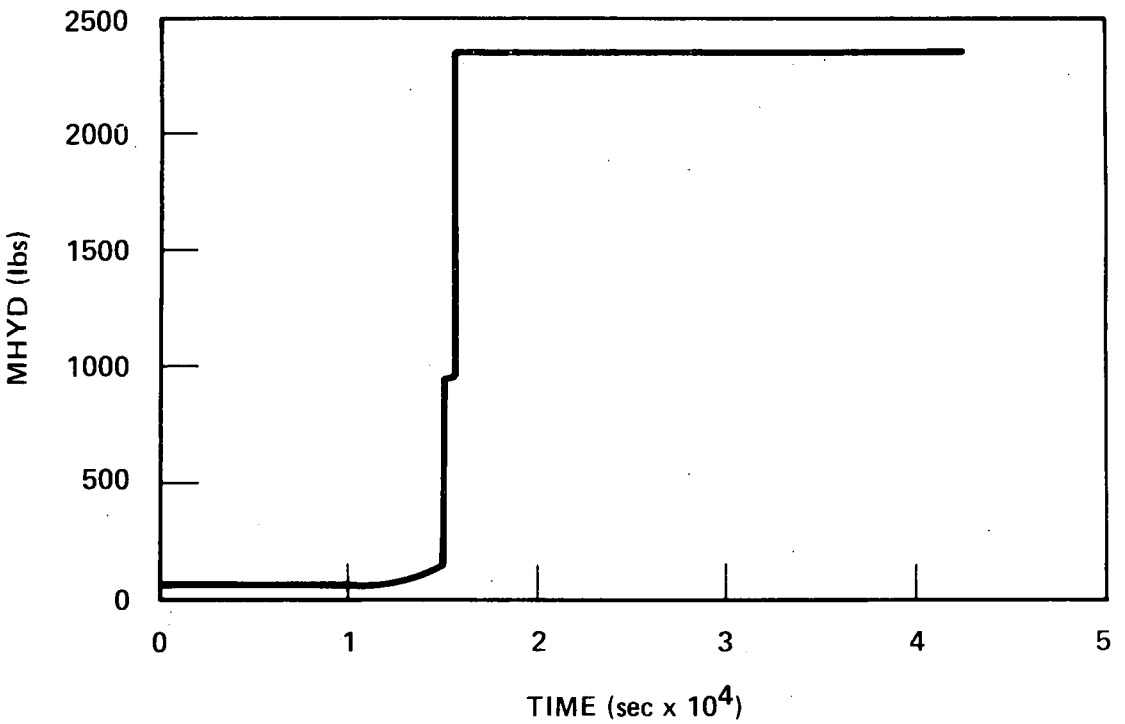
Class V, Case 7A



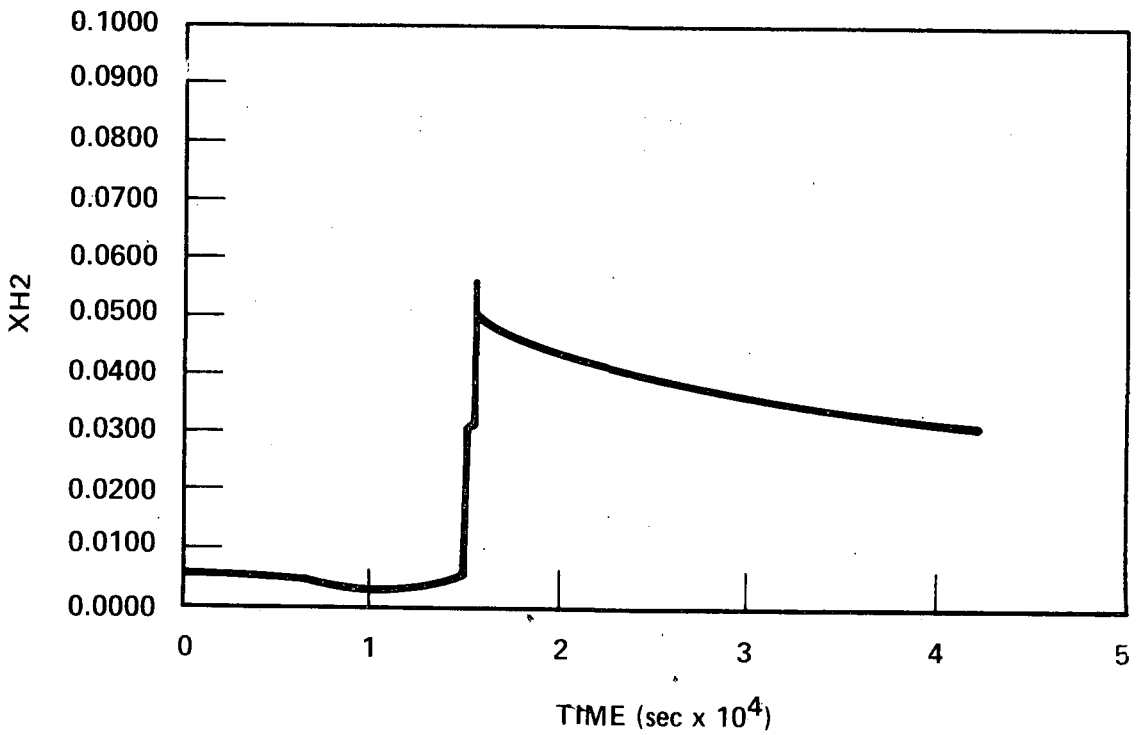
Pressure (in Containment) vs. Time
TMLB, B, 80% Dispersive, No Burn
Class V, Case 7A



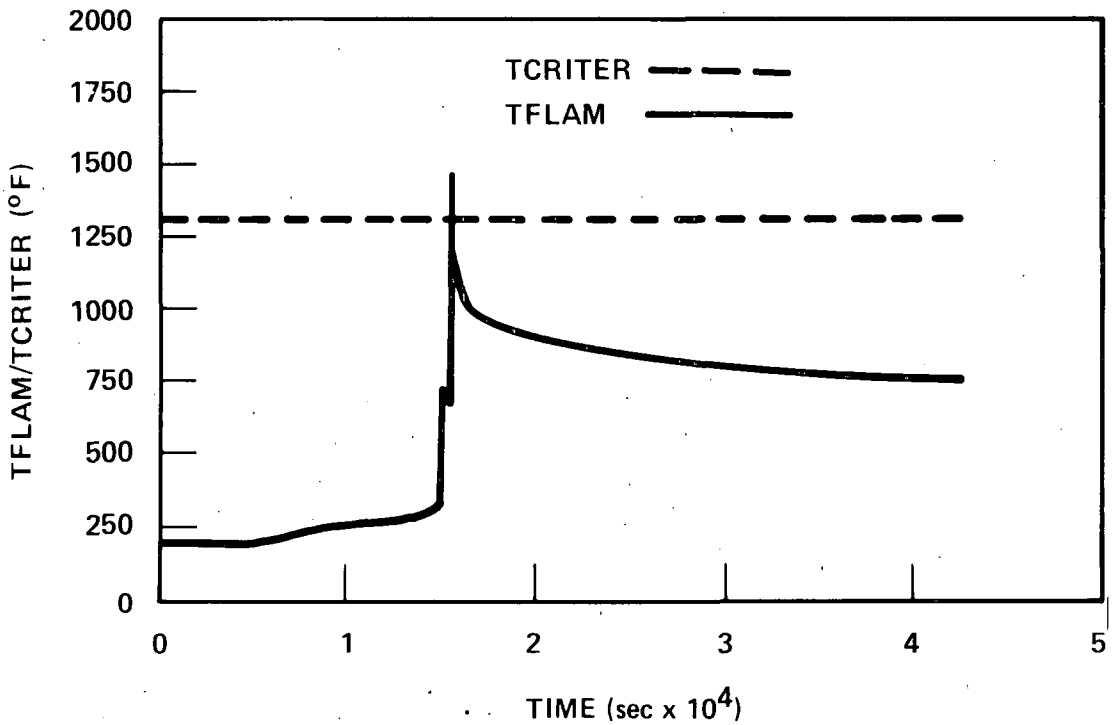
Temperature (in Containment) vs. Time
TMLB, B, 80% Dispersive, No Burn
Class V, Case 7A



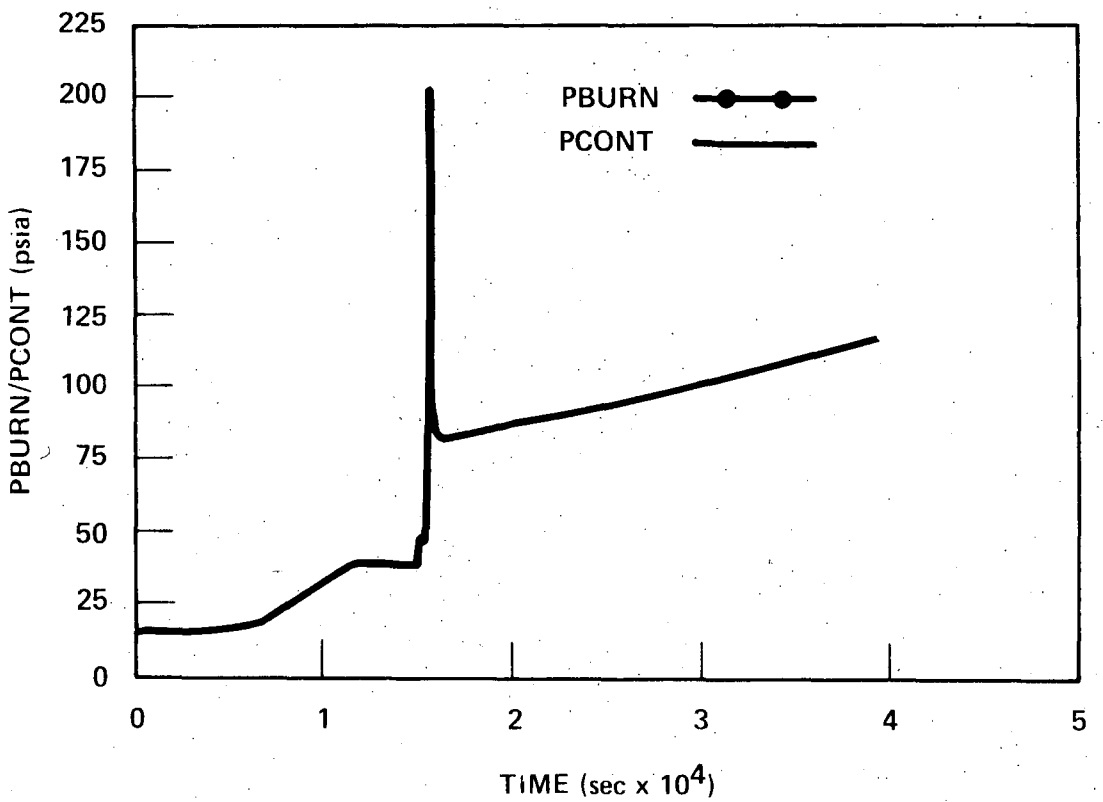
Mass Hydrogen (in Containment) vs. Time
TMLB, B, 80% Dispersive, No Burn
Class V, Case 7A



Mole Fraction H_2 (in Containment) vs. Time
TMLB, B, 80% Dispersive, No Burn
Class V, Case 7A



Flame Temperature (in Containment) vs. Time
TMLB, B, 80% Dispersive, No Burn
Class V, Case 7A



Adiabatic Burn Pressure/Pressure in Containment vs. Time
TMLB, B, 80% Dispersive, No Burn
Class V, Case 7A

CASE: CLASS V, CASE 7B, TMLB, B, 80% DISPERSIVE, BURN @ END OF DISPERSION

DISPERSIVE: YES PERCENT CORE: 80 FRACTION IN CAVITY: 0

RUN #: AALAAIP DATE: 11/15/80

BLOWDOWN PEAK: N/A PSIA TIME: _____ SEC.

HYDROGEN BURN?: YES CRITERIA: END OF DISPERSION

TIME @ BURN: 15570 SEC, PRESSURE: 181 PSIA, TEMPERATURE: ~1000 °F

PEAKS:

PRESSURE: 181 PSIA, TIME: 15590 SEC, WHY?: DISPERSION/BURN

TEMPERATURE: 1517 °F, TIME: 15590 SEC, WHY?: DISPERSION

DISPERSIVE:

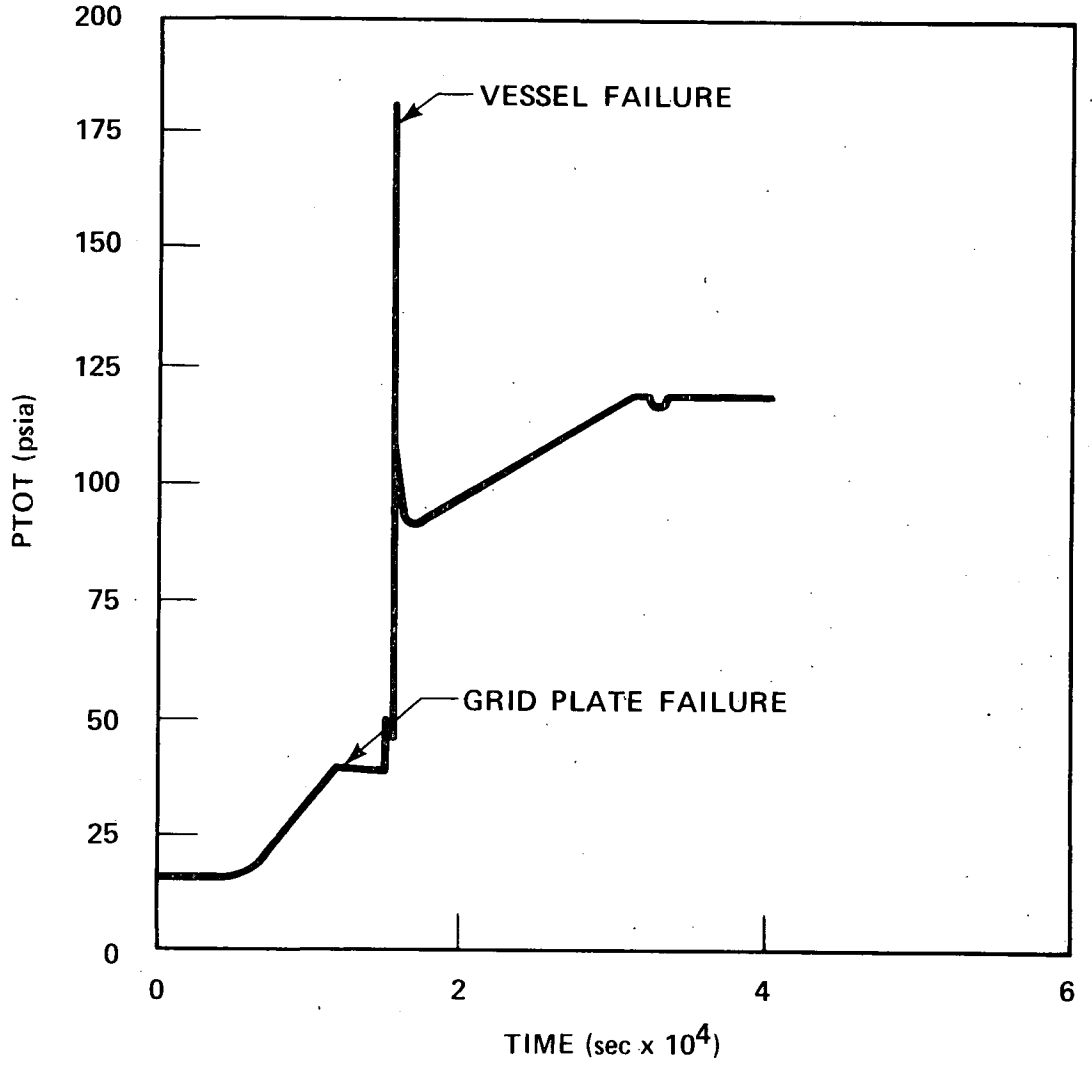
PRESSURE: 181 PSIA, TIME: 15590 SEC,

TEMPERATURE: 1517 °F, TIME: 15590 SEC,

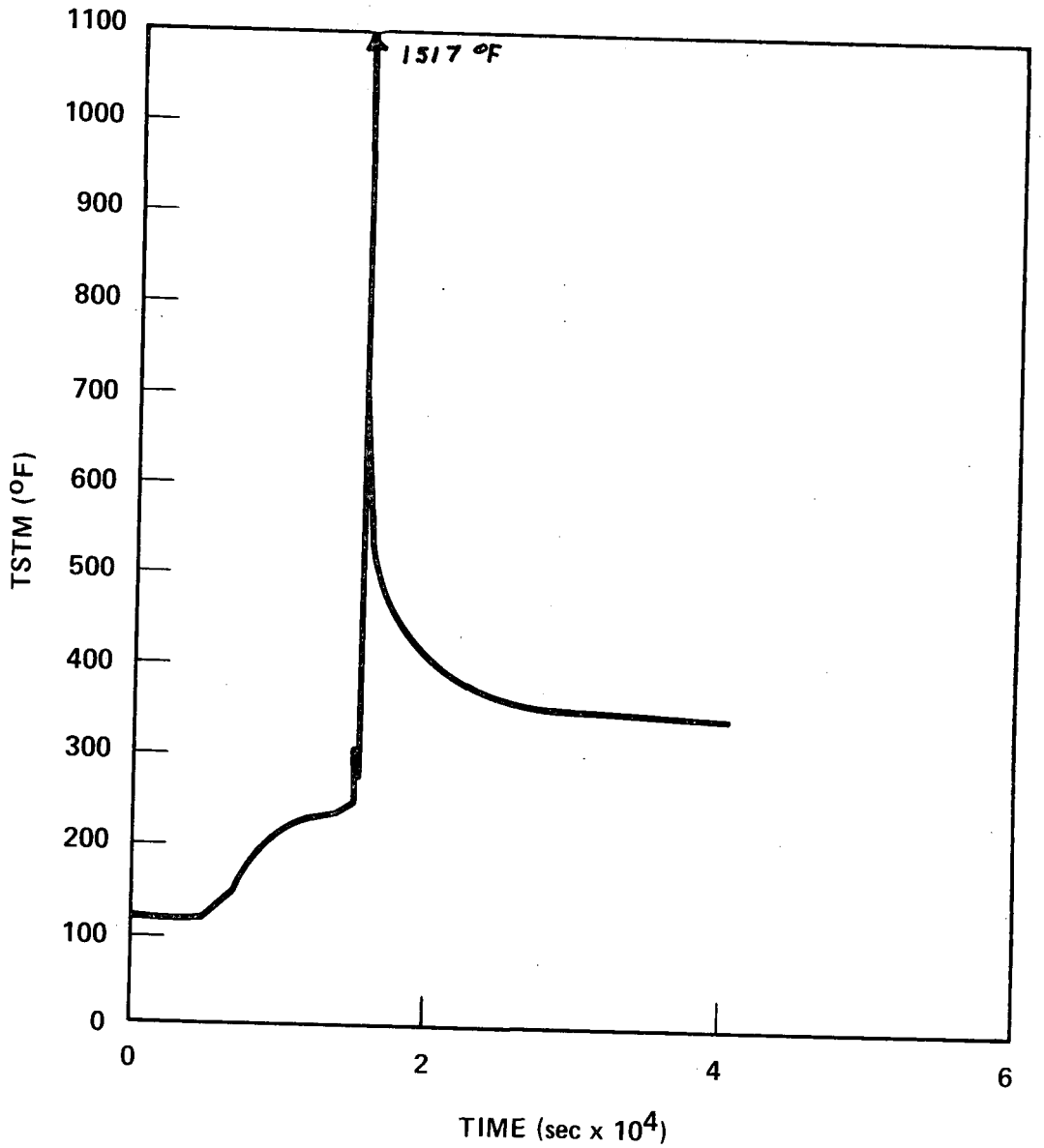
END OF BOIL: 15180 SEC. END OF HEAD: 15540 SEC.

VESSEL FAILURE: 15540 SEC. END OF HOTDROP: 25147 SEC.

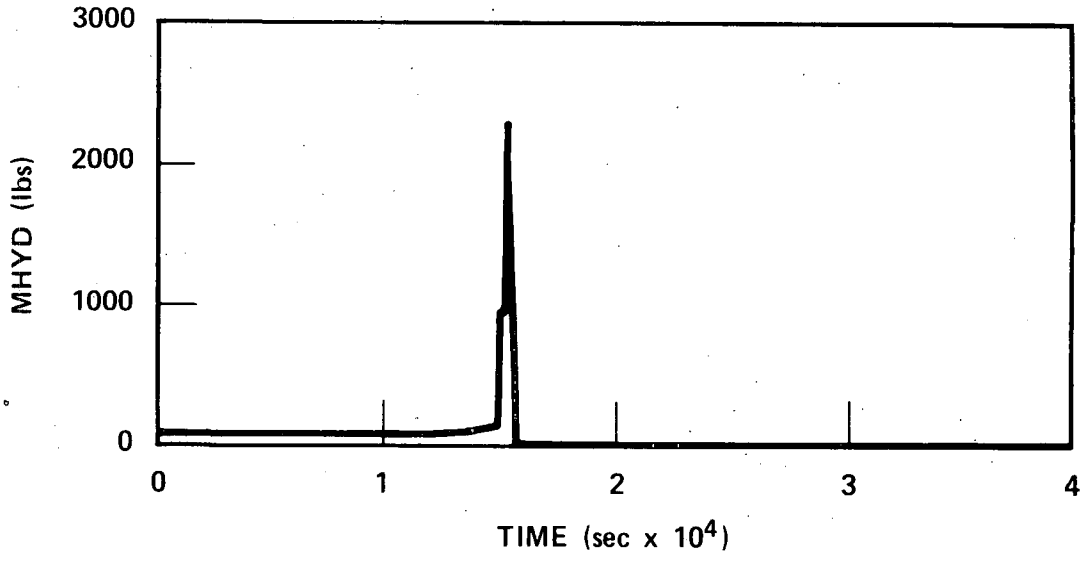
END OF INTER: 86419 SEC.



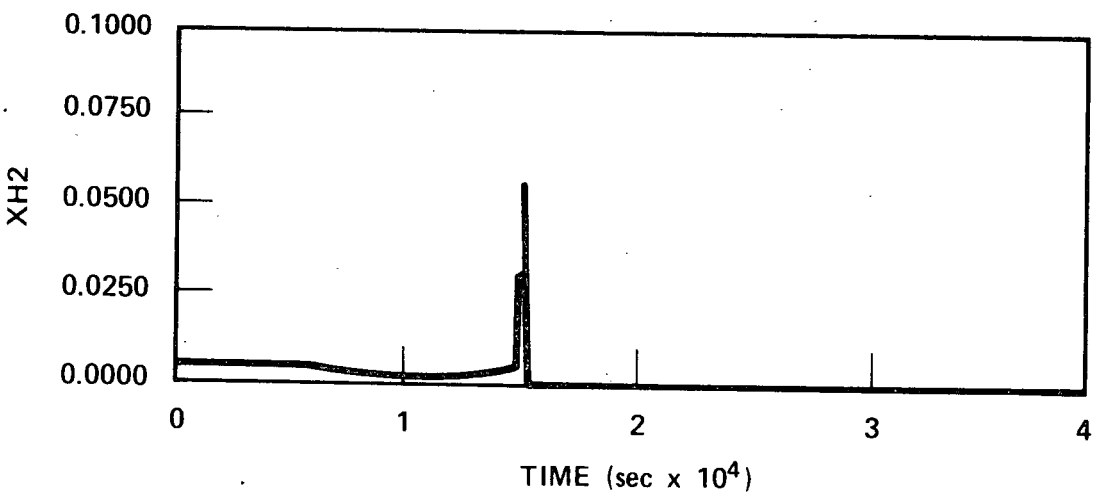
Pressure (in Containment) vs. Time
TMLB, B, 80% Dispersive, Burn @ End of Dispersion
Class V, Case 7B



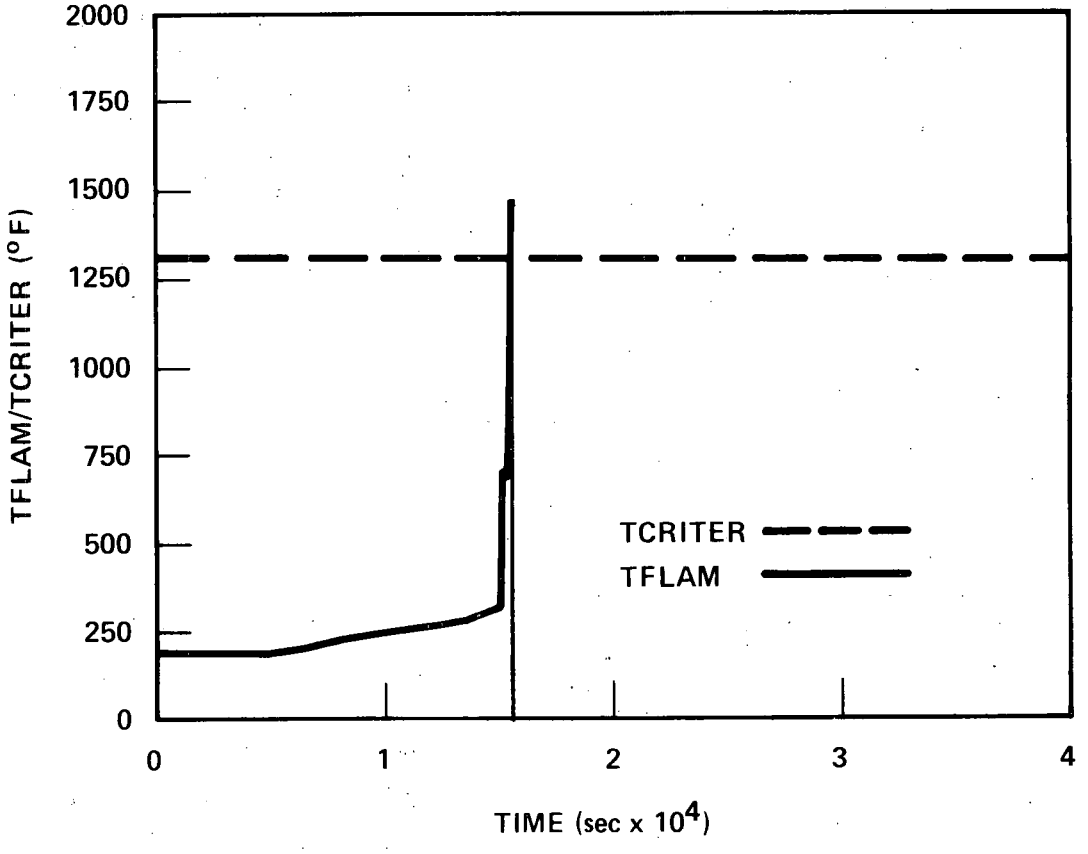
Temperature (in Containment) vs. Time
TMLB, B, 80% Dispersive, Burn @ End of Dispersion
Class V, Case 7B



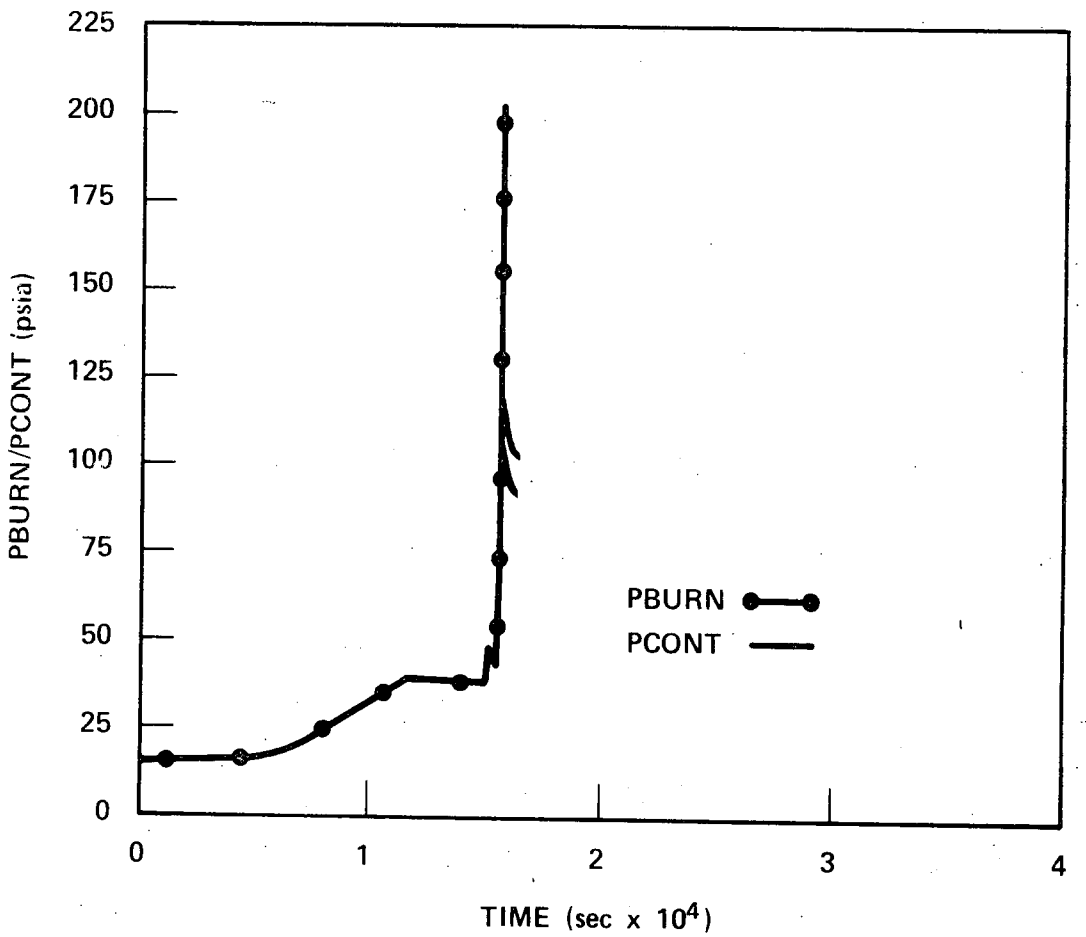
Mass Hydrogen (in Containment) vs. Time
TMLB, B, 80% Dispersive, Burn @ End of Dispersion
Class V Case 7B



Mole Fraction H_2 (in Containment) vs. Time
TMLB, B, 80% Dispersive, Burn @ End of Dispersion
Class V, Case 7B



Flame Temperature (in Containment) vs. Time
TMLB, B, 80% Dispersive, Burn @ End of Dispersion
Class V, Case 7B



Adiabatic Burn Pressure/Pressure in Containment vs. Time
TMLB, B, 80% Dispersive, Burn @ End of Dispersion
Class V, Case 7B

CASE: CLASS VI, CASE 1A, TMLB, B, FANS ONLY, NO BURN

DISPERSIVE: NO PERCENT CORE: _____ FRACTION IN CAVITY: _____

RUN #: AB3ICNW DATE: 3/24/81 PERCENT ZR REACTED:

BLOWDOWN PEAK: NO PSIA TIME: _____ SEC.

HYDROGEN BURN?: NO CRITERIA: _____

TIME @ BURN: _____ SEC, PRESSURE: _____ PSIA, TEMPERATURE: _____ °F

PEAKS:

PRESSURE: 96 PSIA, TIME: 15487 SEC, WHY?: _____

TEMPERATURE: 409. °F, TIME: 15487 SEC, WHY?: _____

DISPERSIVE: NO

PRESSURE: _____ PSIA, TIME: _____ SEC,

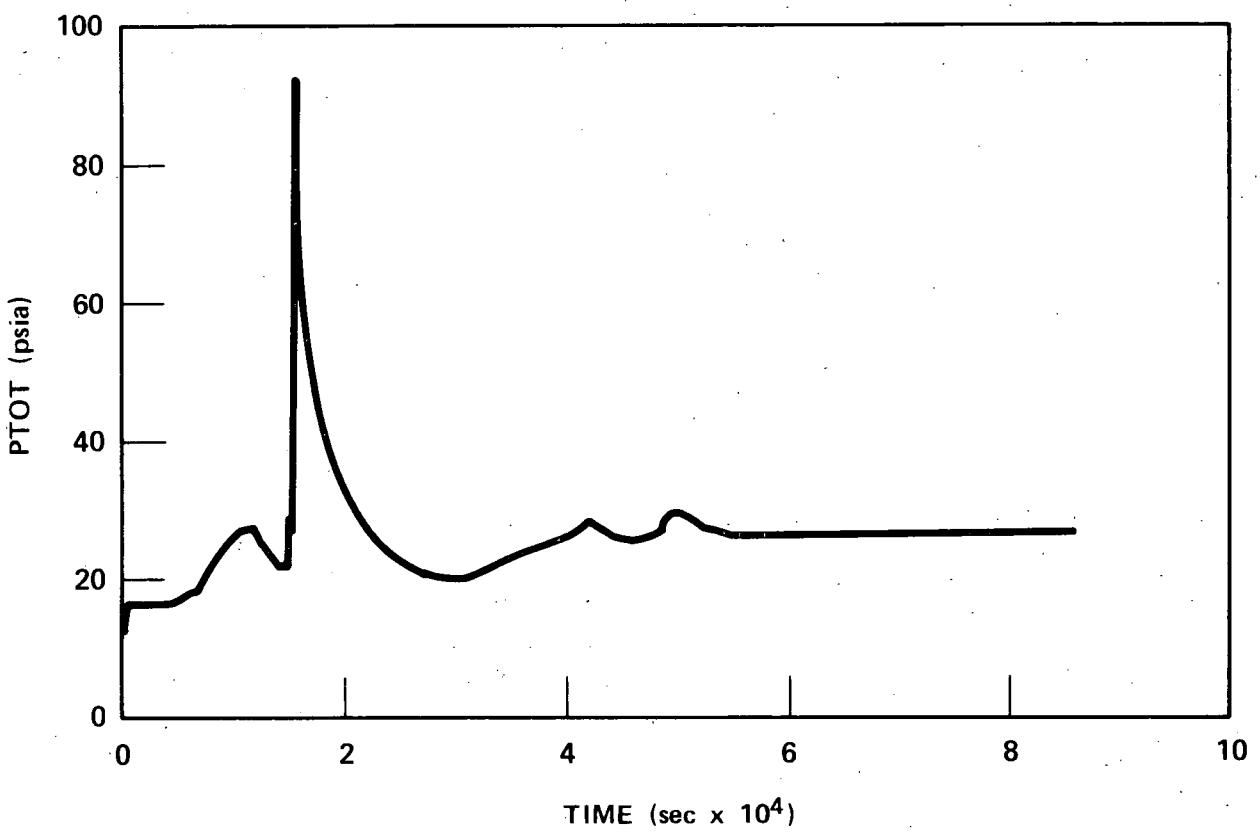
TEMPERATURE: _____ °F, TIME: _____ SEC,

END OF BOIL: 15120 SEC. END OF HEAD: 15480 SEC.

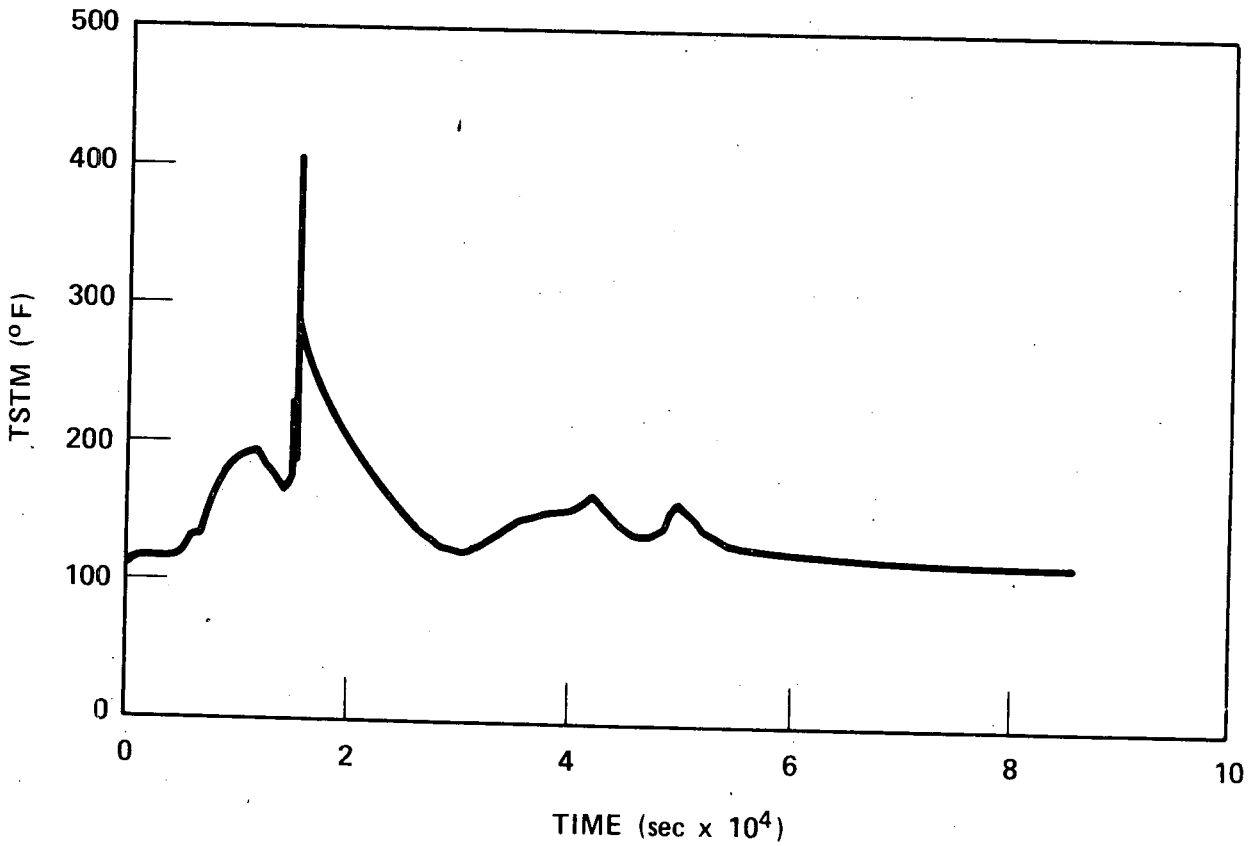
VESSEL FAILURE: 15480 SEC. END OF HOTDROP: 22807 SEC.

END OF INTER: 109260 SEC.

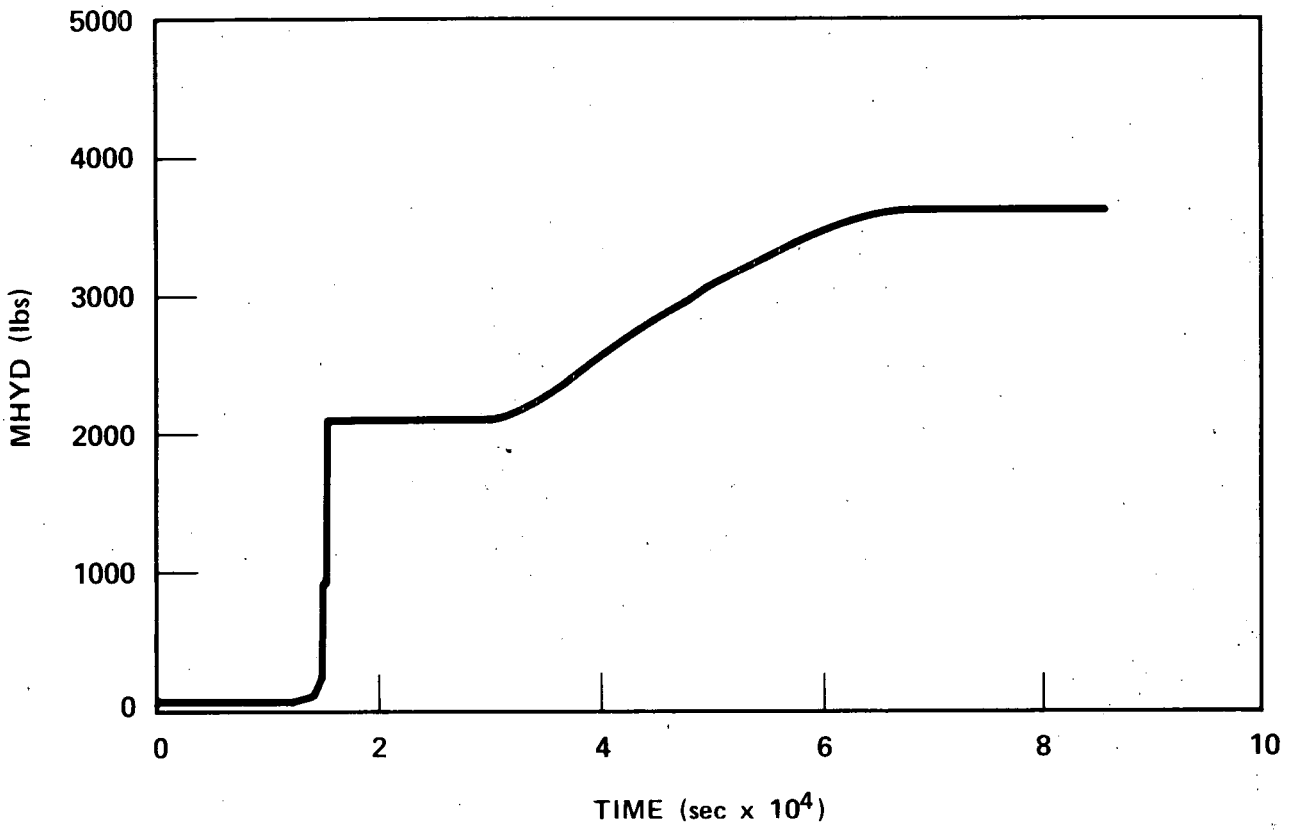
Class VI, Case 1A



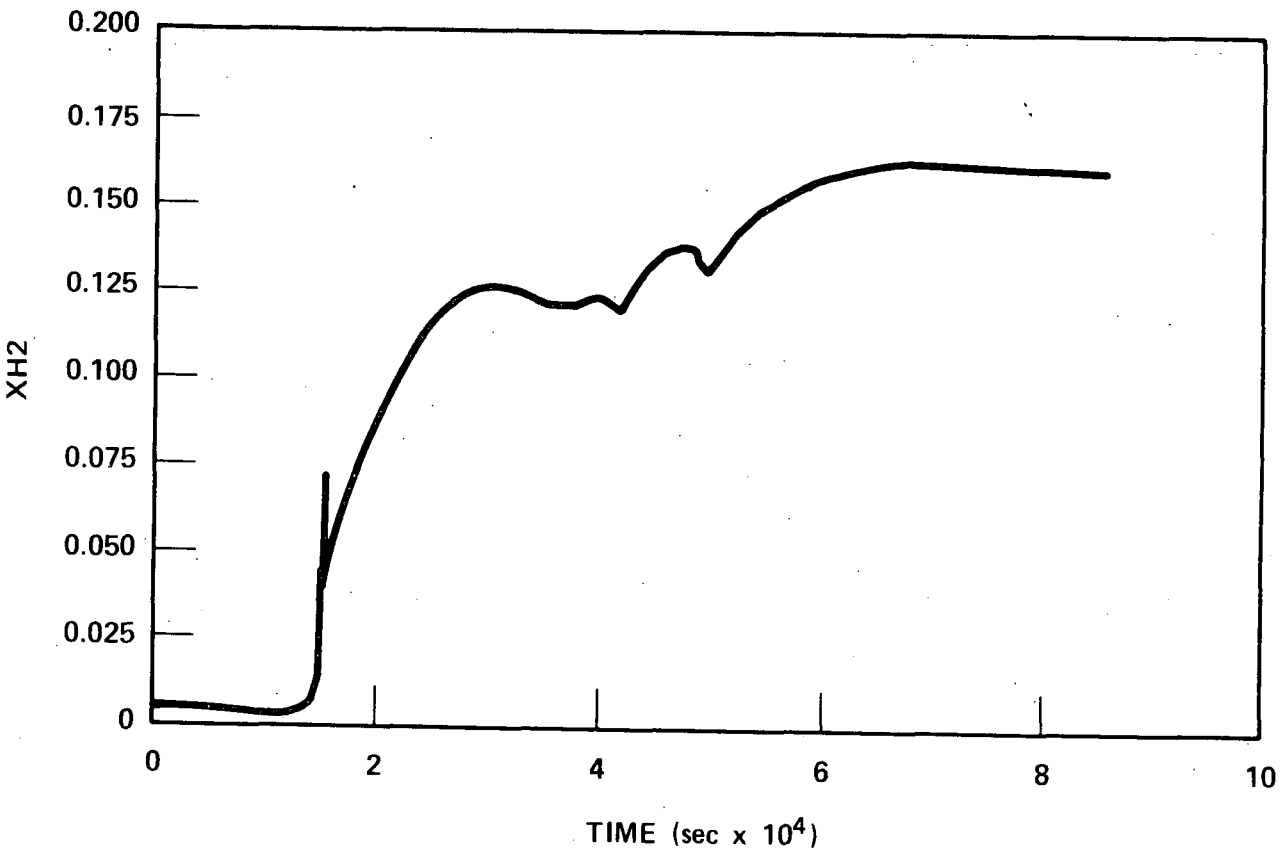
Pressure (in Containment) vs. Time
TMLB, B, Fans Only, No Burn
Class VI, Case 1A



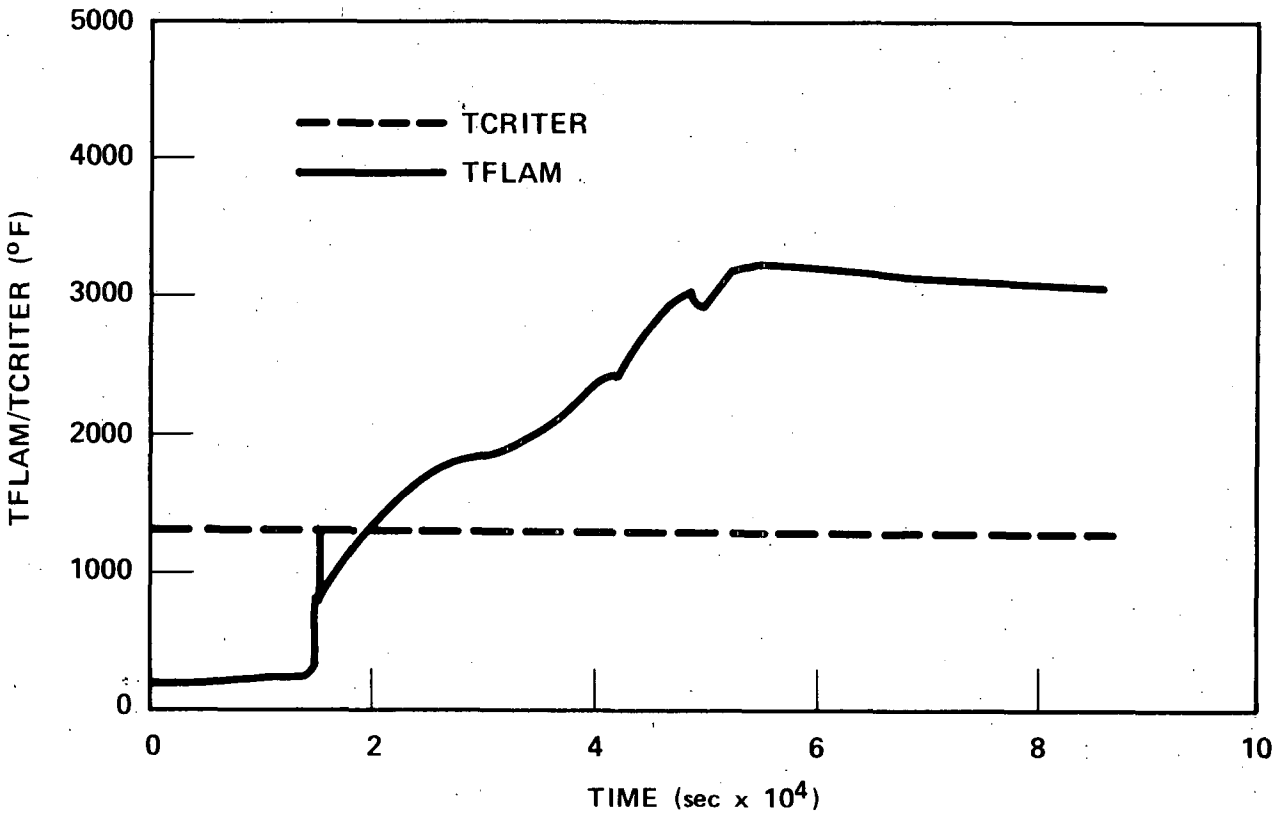
Temperature (in Containment) vs. Time
TMLB', B, Fans Only, No Burn
Class VI, Case 1A



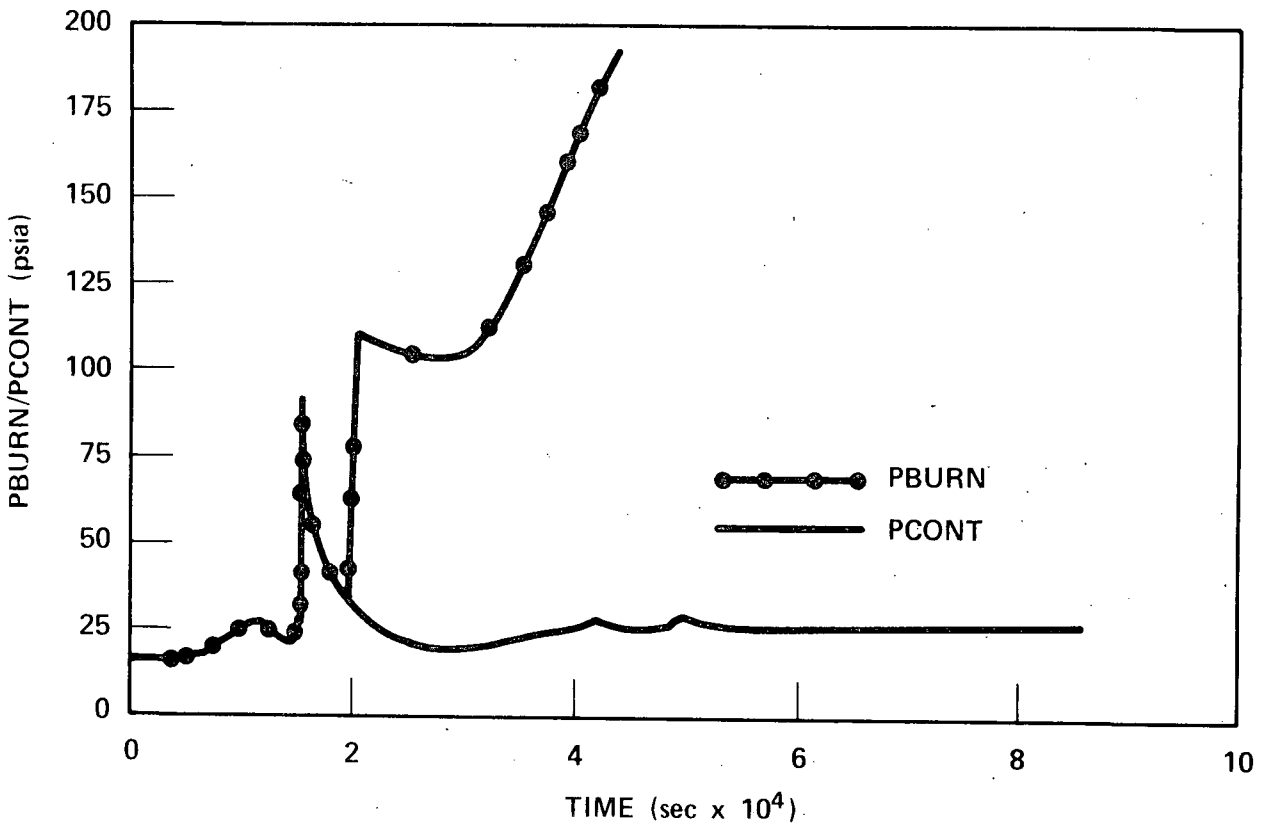
Mass Hydrogen (in Containment) vs. Time
TMLB, B, Fans Only, No Burn
Class VI, Case 1A



Mole Fraction H_2 (in Containment) vs. Time
TMLB, B, Fans Only, No Burn
Class VI, Case 1A



Flame Temperature (in Containment) vs. Time
TMLB, B, Fans Only, No Burn
Class VI, Case 1A



Adiabatic Burn Pressure/Pressure in Containment vs. Time
TMLB, B, Fans Only, No Burn
Class VI, Case 1A

CASE: CLASS VI, CASE 1A', TMLB, B, BURN @ T_{MAX}, FANS + SPRAY

DISPERSIVE: NO PERCENT CORE: _____ FRACTION IN CAVITY: _____

RUN #: AB3YAWB DATE: 1/26/81 PERCENT ZR REACTED:

BLOWDOWN PEAK: NO PSIA TIME: _____ SEC.

HYDROGEN BURN?: YES CRITERIA: T_{MAX}

TIME @ BURN: 54624 SEC, PRESSURE: 27 PSIA, TEMPERATURE: 138 °F

PEAKS:

PRESSURE: 137.6 PSIA, TIME: 54967 SEC, WHY?: H_2 BURN

TEMPERATURE: 2906. °F, TIME: 54967 SEC, WHY?: H_2 BURN

DISPERSIVE: NO

PRESSURE: _____ PSIA, TIME: _____ SEC,

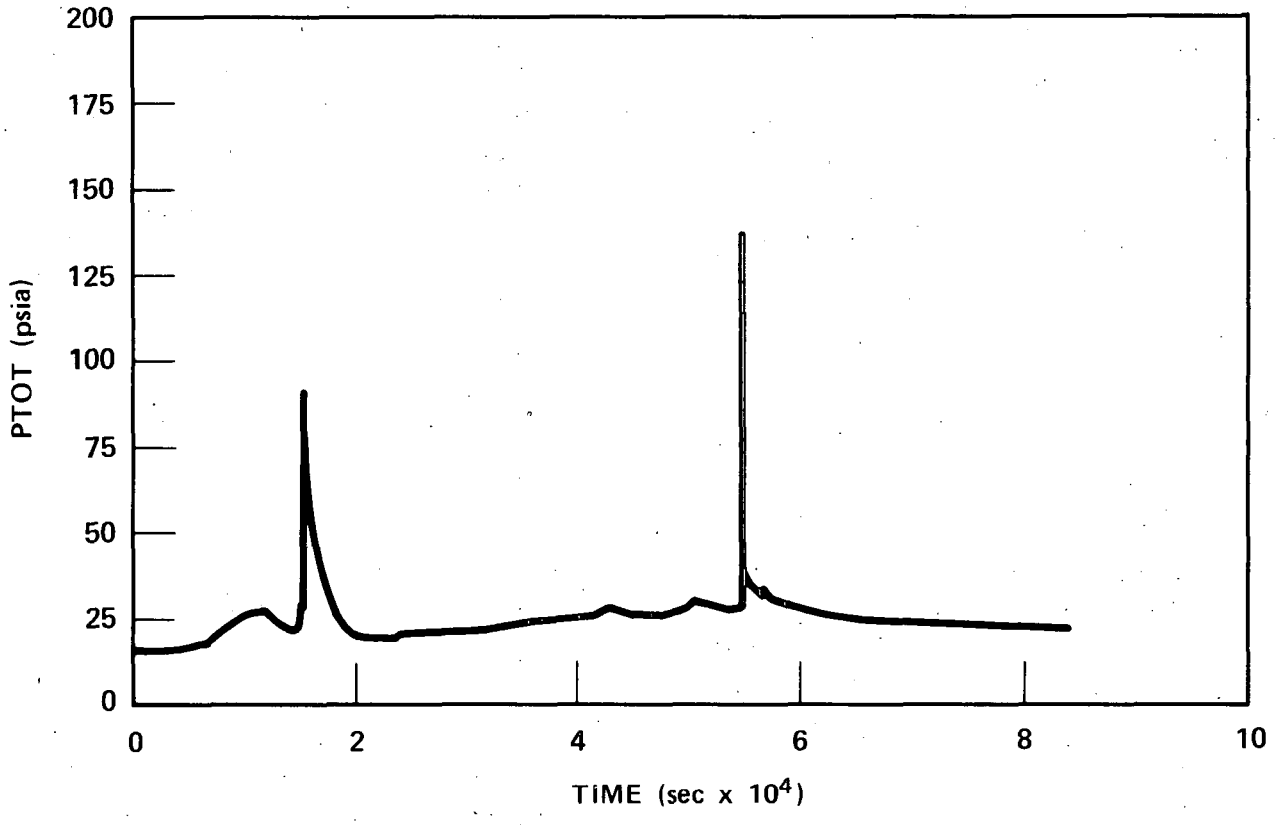
TEMPERATURE: _____ °F, TIME: _____ SEC,

END OF BOIL: 15120 SEC. END OF HEAD: 15480 SEC.

VESSEL FAILURE: 15480 SEC. END OF HOTDROP: 22807 SEC.

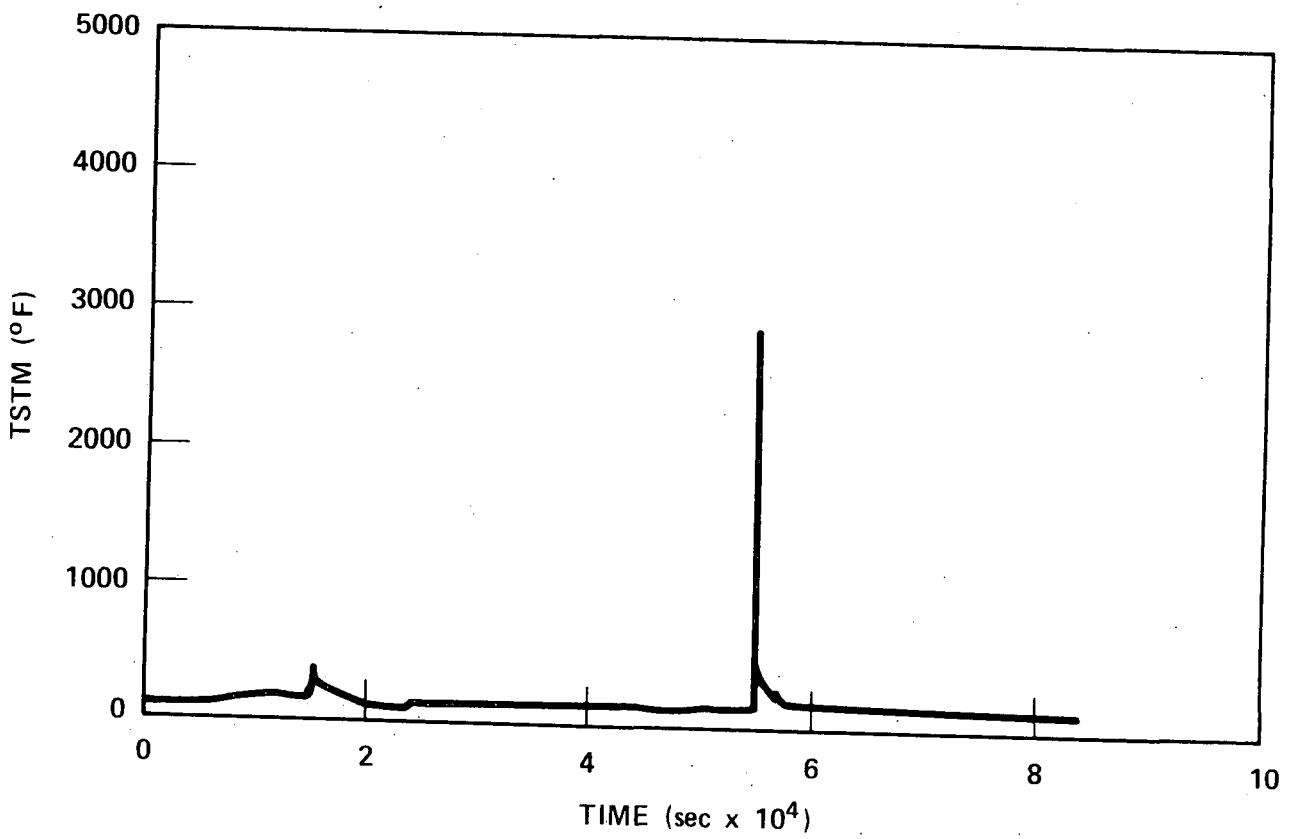
END OF INTER: 109390 SEC.

Class VI, Case 1A'

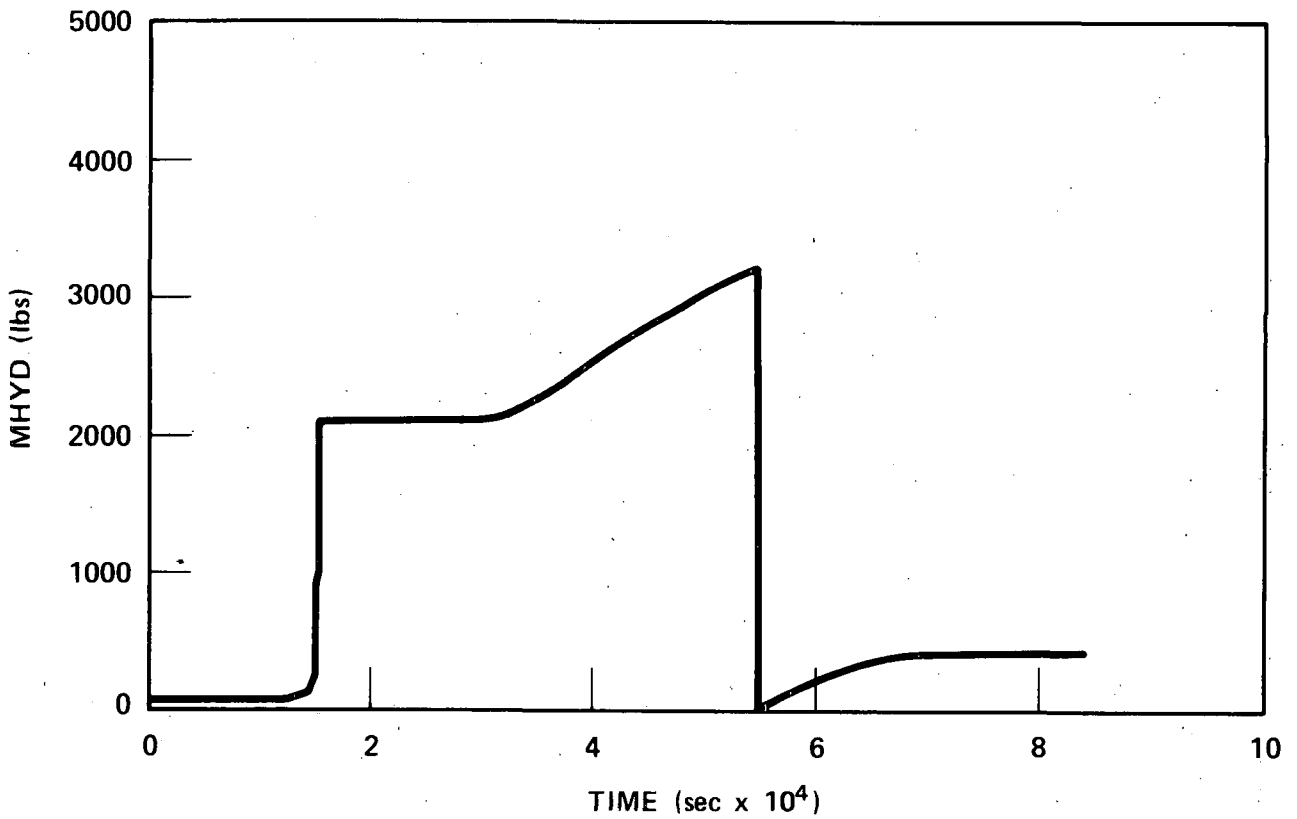


Pressure (in Containment) vs. Time
TMLB, B, Burn @ T_{MAX}, Fans + Spray
Class VI, Case 1A'

Sheet 2 of 7

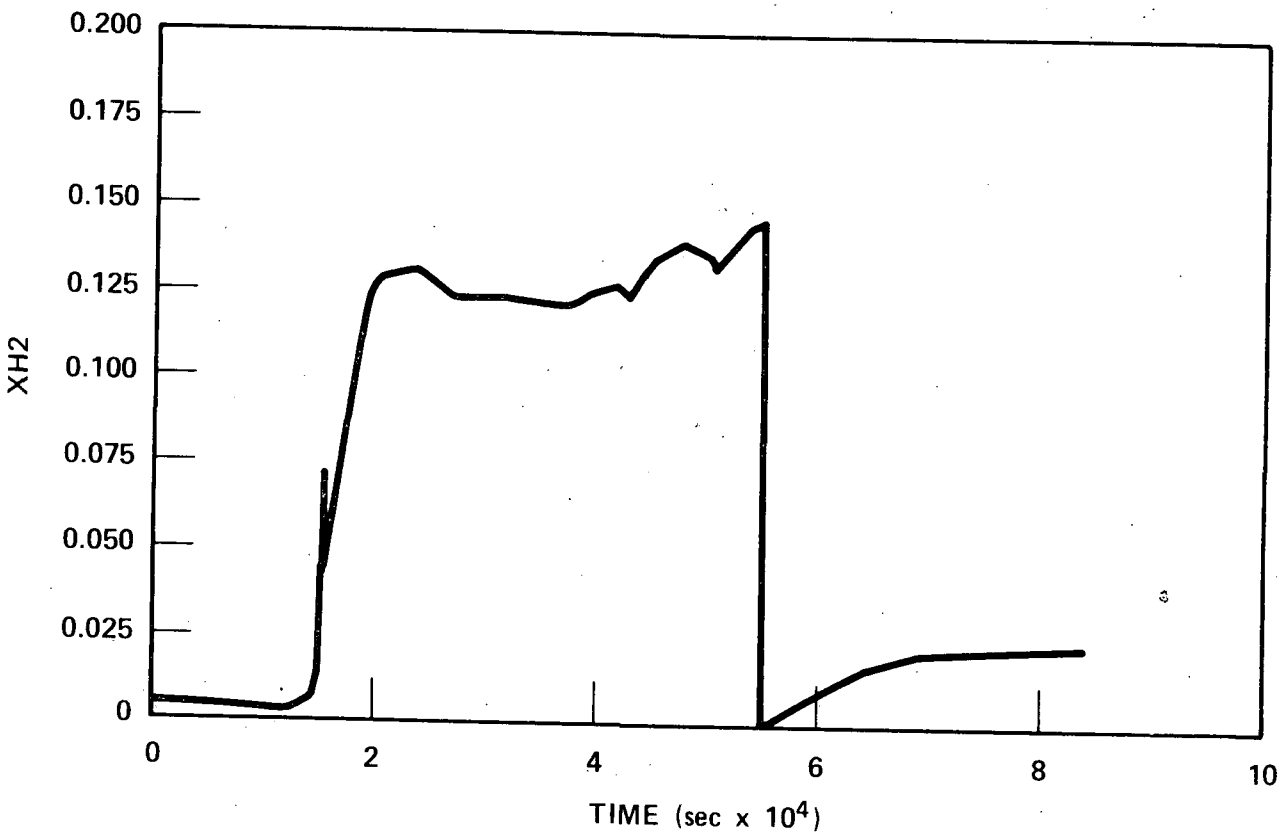


Temperature (in Containment) vs. Time
TMLB, B, Burn @ T_{MAX}, Fans + Spray
Class VI, Case 1A'

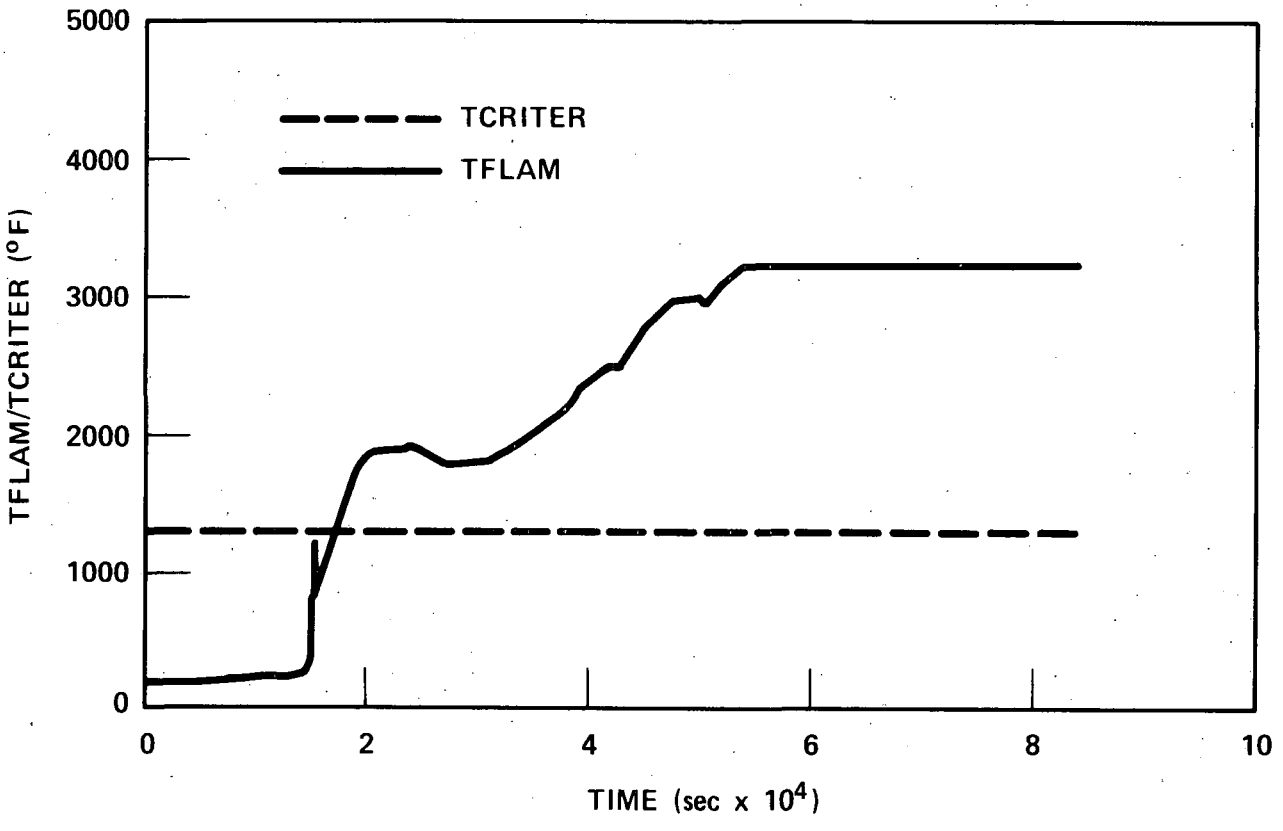


Mass Hydrogen (in Containment) vs. Time
TMLB, B, Burn @ T_{MAX}, Fans + Spray
Class VI, Case 1A'

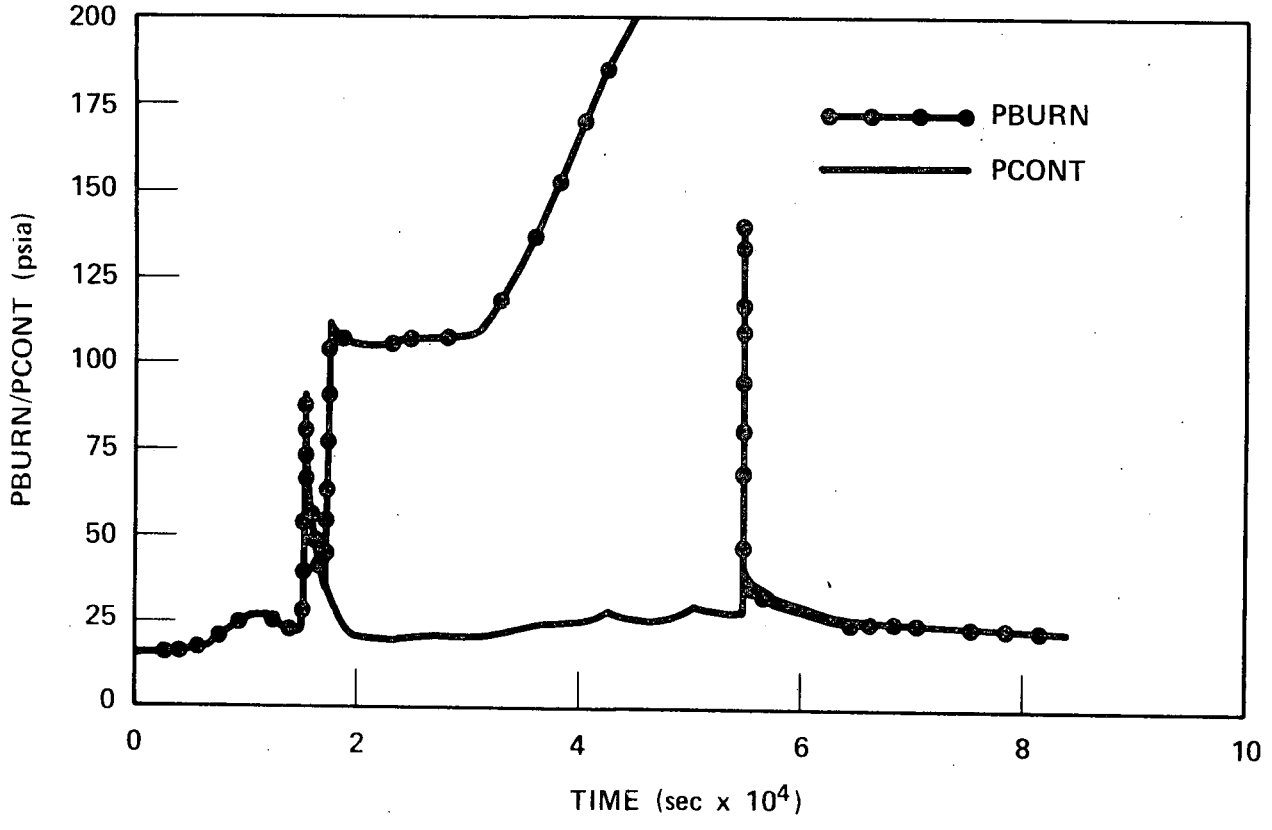
Sheet 4 of 7



Mole Fraction H_2 (in Containment) vs. Time
TMLB, B, Burn @ T_{MAX}, Fans + Spray
Class VI, Case 1A'



Flame Temperature (in Containment) vs. Time
TMLB, B, Burn @ T_{MAX}, Fans + Spray
Class VI, Case 1A'



Adiabatic Burn Pressure/Pressure in Containment vs. Time
TMLB, B, Burn @ T_{MAX}, Fans + Spray
Class VI, Case 1A'

CASE: CLASS VI, CASE 1A", TMLB, B, NO BURN, SPRAYS ONLY

DISPERSIVE: NO PERCENT CORE: _____ FRACTION IN CAVITY: _____

RUN #: ABEIEMY DATE: 3/25/81 PERCENT ZR REACTED:

BLOWDOWN PEAK: NO PSIA TIME: _____ SEC.

HYDROGEN BURN?: NO CRITERIA: _____

TIME @ BURN: _____ SEC, PRESSURE: _____ PSIA, TEMPERATURE: _____ °F

PEAKS:

PRESSURE: 89 PSIA, TIME: 15427 SEC, WHY?: _____

TEMPERATURE: 401 °F, TIME: 15427 SEC, WHY?: _____

DISPERSIVE:

PRESSURE: _____ PSIA, TIME: _____ SEC,

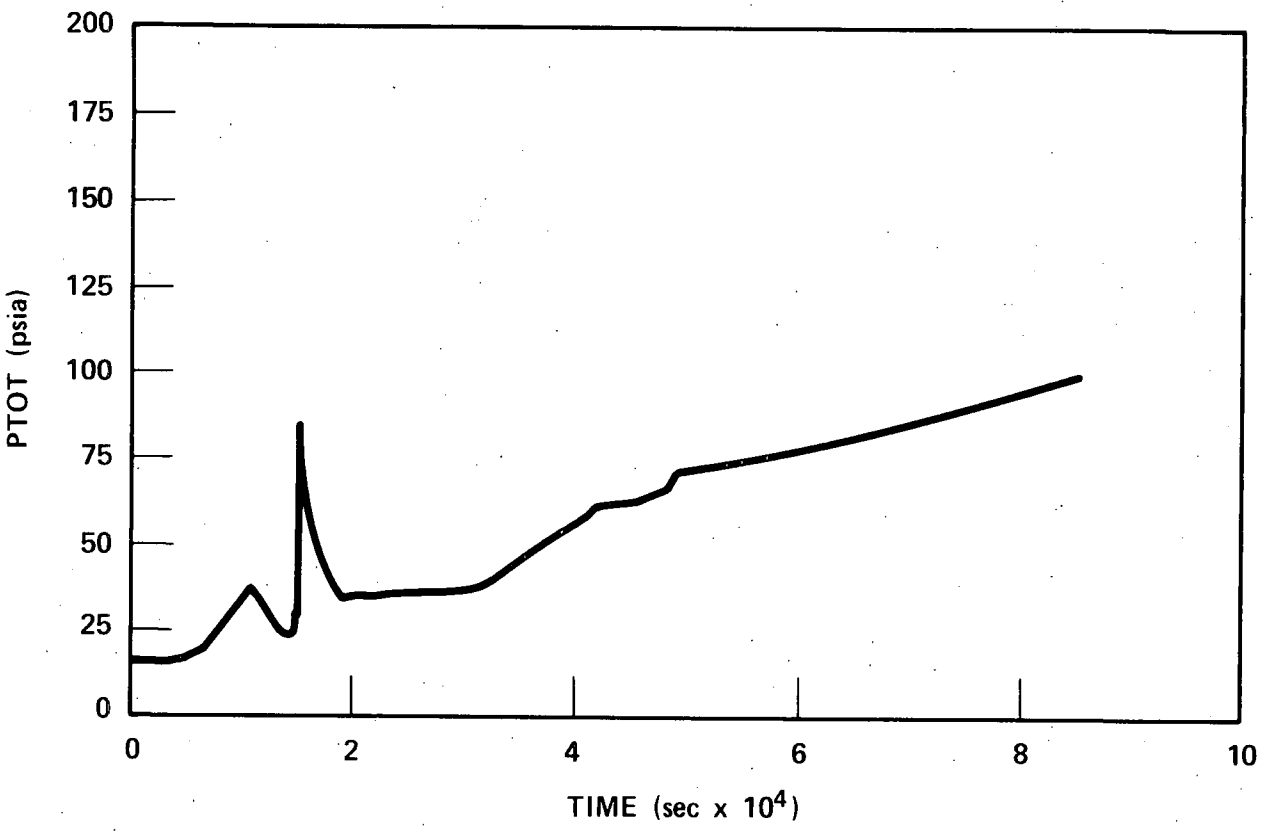
TEMPERATURE: _____ °F, TIME: _____ SEC,

END OF BOIL: 15060 SEC. END OF HEAD: 15420 SEC.

VESSEL FAILURE: 15420 SEC. END OF HOTDROP: 22747 SEC.

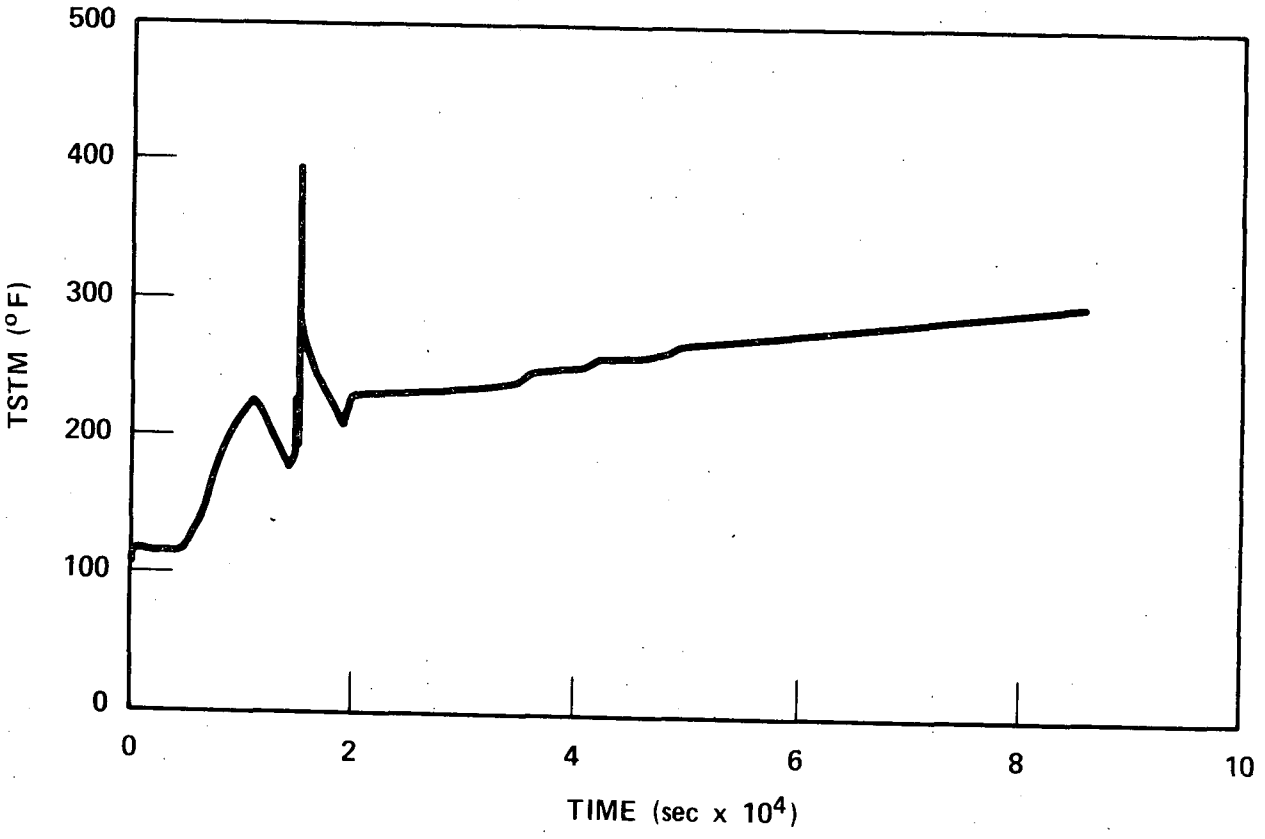
END OF INTER: 109460 SEC.

Class VI, Case 1A"

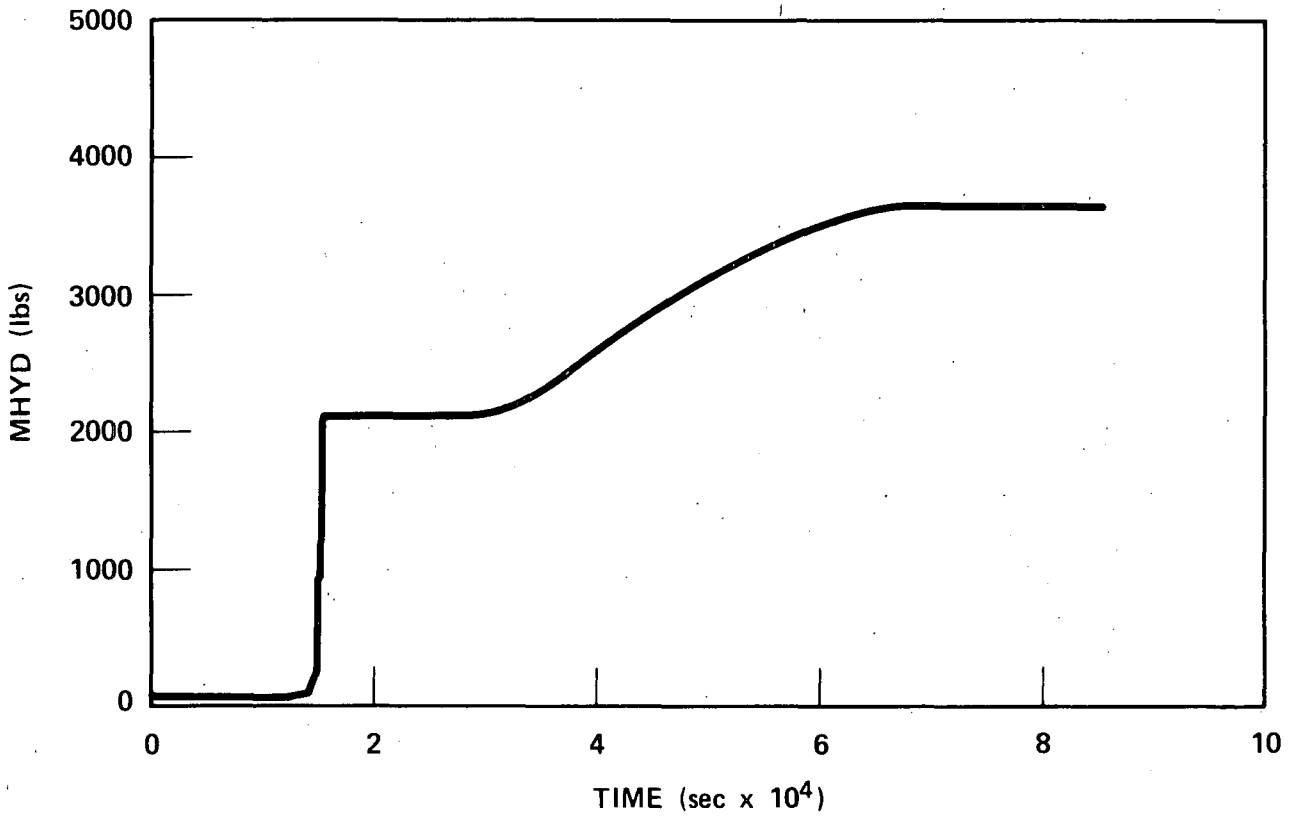


Pressure (in Containment) vs. Time
TMLB, B, No Burn, Sprays Only
Class VI, Case 1A"

Sheet 2 of 7

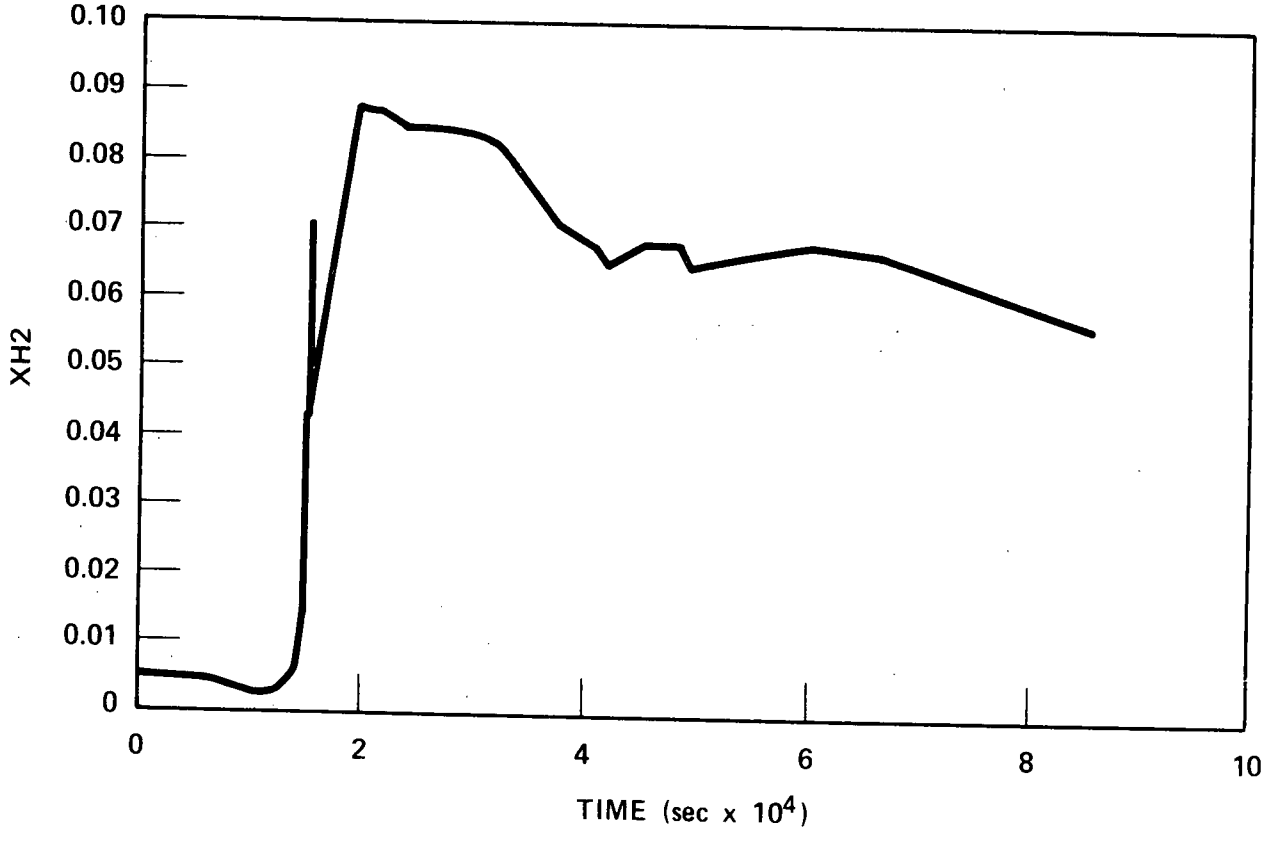


Temperature (in Containment) vs. Time
TMLB, B, No Burn, Sprays Only
Class VI, Case 1A"

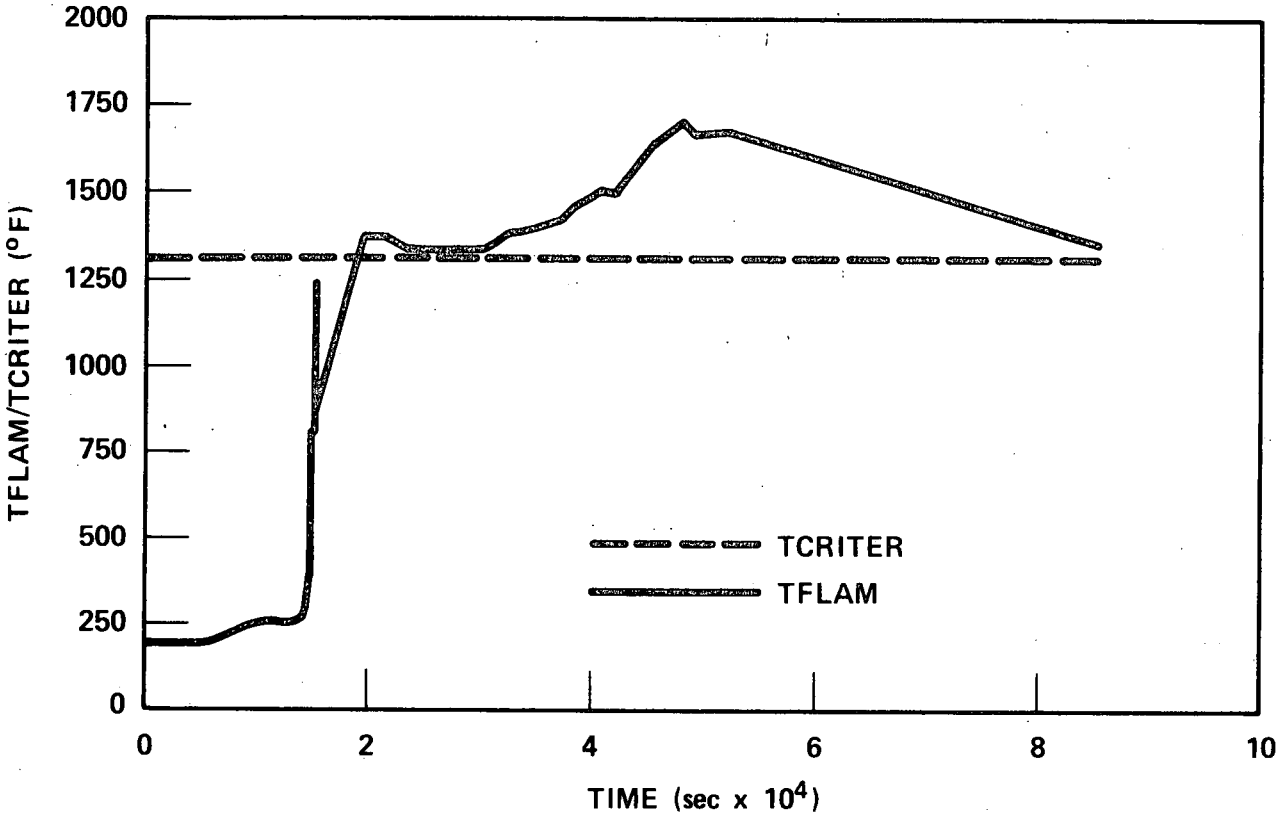


Mass Hydrogen (in Containment) vs. Time
TMLB, B, No Burn, Sprays Only
Class VI, Case 1A"

Sheet 4 of 7

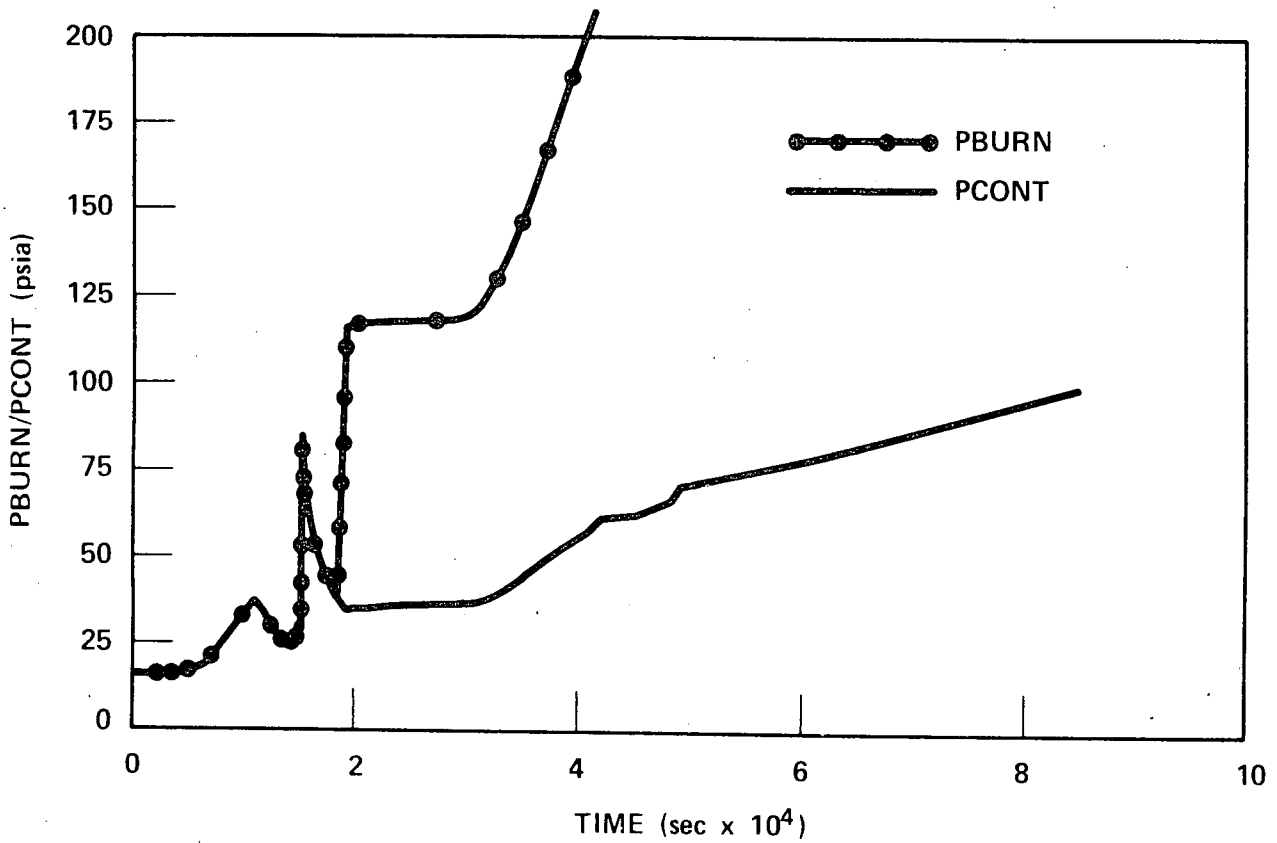


Mole Fraction H_2 (in Containment) vs. Time
TMLB, B, No Burn, Sprays Only
Class VI, Case 1A"



Flame Temperature (in Containment) vs. Time
TMLB, B, No Burn, Sprays Only
Class VI, Case 1A"

Sheet 6 of 7



Adiabatic Burn Pressure/Pressure in Containment vs. Time
TMLB, B, No Burn, Sprays Only
Class VI, Case 1A"

Sheet 7 of 7

Indian Point Probabilistic Safety Study

Power Authority of the State of New York
Consolidated Edison Company of New York, Inc.

— NOTICE —

THE ATTACHED FILES ARE OFFICIAL RECORDS OF THE DIVISION OF DOCUMENT CONTROL. THEY HAVE BEEN CHARGED TO YOU FOR A LIMITED TIME PERIOD AND MUST BE RETURNED TO THE RECORDS FACILITY BRANCH 016. PLEASE DO NOT SEND DOCUMENTS CHARGED OUT THROUGH THE MAIL. REMOVAL OF ANY PAGE(S) FROM DOCUMENT FOR REPRODUCTION MUST BE REFERRED TO FILE PERSONNEL.

Docket # 50-247
Control # 8203110003
DEADLINE RETURN DATE Date 03-06-82 of Document:
REGULATORY DOCKET FILE

REGULATORY DOCKET FILE COPY

RECORDS FACILITY BRANCH

Volume 9

Indian Point Probabilistic Safety Study

Copyright 1982 by
Power Authority of the State of New York
Consolidated Edison Company of New York, Inc.

Volume 9

Copy No. 15

REGULATORY DOCKET FILE COPY

SECTION 5
SOURCE TERMS

TABLE OF CONTENTS

Section			Page
5.0	CORE MELT ACCIDENT SOURCE TERMS		5.1-1
5.1	INTRODUCTION		5.1-1
5.2	BACKGROUND		5.2-1
5.3	RATIONALE AND BASIS FOR INDIAN POINT SOURCE TERMS		5.3-1
	5.3.1	Energetic Debris - Water Interaction	5.3-1
	5.3.2	Early Overpressure Events Leading to Containment Failure	5.3-2
	5.3.3	Late Overpressure Failures	5.3-3
	5.3.4	Containment Isolation Failure	5.3-4
	5.3.5	Basemat Penetration	5.3-4
	5.3.6	Core Melt Events Without Containment Failure	5.3-4
	5.3.7	Venting of Containment Through a Filter	5.3-4
	5.3.8	Containment Spray and Fan Coolers	5.3-5
	5.3.9	Summary	5.3-5
5.4	SOURCE TERMS AND ASSOCIATED RELEASE PARAMETERS		5.4-1
	5.4.1	Source Terms	5.4-1
	5.4.2	Consequence Parameters	5.4-1
	5.4.2.1	Time and Duration of Release	5.4-1
	5.4.2.2	Release Energy	5.4-2
5.5	SOURCE TERM TECHNOLOGY		5.5-1
5.6	PRINCIPLE SOURCE TERM CATEGORIES AND THEIR UNCERTAINTIES		5.6-1
	5.6.1	Principle Source Term Categories	5.6-1
	5.6.2	Uncertainty Estimates	5.6-1
	5.6.2.1	Release Category 2	5.6-2
	5.6.2.2	Release Category Z-1	5.6-2
	5.6.2.3	Release Category 2RW	5.6-3
	5.6.2.4	Release Category 8B	5.6-3
	5.6.2.5	Release Category 2RV	5.6-4
5.7	REFERENCES		5.7-1
5.8	APPENDIX		
	5.8.1	Summary Description of Fission Product Release Categories Employed in the Reactor Safety Study	
	5.8.2	Description of CORRAL Calculations Performed to Estimate Source Terms for Delayed Overpressure Failures (Assumptions and Results)	

SECTION 5
CORE MELT ACCIDENT SOURCE TERMS

TABLE OF CONTENTS (Con't)

Section			Page
5.8	APPENDIX (Con't)		
	5.8.3	Source Reduction by Functional Fan Coolers	
	5.8.4	Multi-Phase Release Source Terms for Release Category 2RW and Release Category 2 (V Sequence)	

LIST OF TABLES

Tables		Page
5.4-1	Summary of Release Category Rationale and Nomenclature	5.4-3
5.4-2	Radioactivity Release Fractions for Source Term Categories	5.4-7
5.4-3	Associated Source Term Release Parameters	5.4-8

LIST OF FIGURES

Figures		Page
5.3-1	Simplified Containment Event Tree for Identifying Release Categories	5.3-6
5.6-1	Release Category 2 & 2RV, Z-1Q & Z-1A, 2RW and 8B Source Terms	5.6-5

SECTION 5

SOURCE TERMS

5.0 CORE MELT ACCIDENT SOURCE TERMS

5.1 INTRODUCTION

This section describes the methology and bases used to estimate the quantity of fission products potentially released from the containment, given the various hypothetical combinations of system and containment failure modes. In general, the approach used in the Reactor Safety Study (RSS) (Ref. 1) has been followed here. Thirteen release categories were initially defined for this study. Parameters for the timing of release and the associated release energy are important for each release category. For some release categories, more than one such set of release parameters were considered and as a result, there were initially 18 release conditions for the study. Phenomenological studies showed some of the release conditions were unlikely to occur. As a result only 12 of the release categories (and 13 release conditions) were considered when calculating release frequencies. Many of these categories were calculated to have very low frequencies and as a result consequence calculations were only performed for an even more limited set of release categories and conditions.

5.2 BACKGROUND

As part of the RSS, the CORRAL code was developed to calculate the fraction of the core inventory of fission products that would be released from the containment as a function of time The results of the MARCH code (see Section 4.1.1) were used for estimating the release of radioactivity from the core to the containment as a function of time and were used as input for the CORRAL analysis. Four basic components of release from the core to the containment were considered: the gap-release component, the core melt release component, the vaporization release component, and the release component associated with steam explosion. Released fission product species were divided into seven groups: the noble gases, the halogens, the alkali metals, the tellurium group, the alkaline earths, the noble metals, and the refractory oxides. Release from the core to the containment and from the containment to the atmosphere was calculated in terms of fraction of core inventory. Processes such as plateout on the containment walls, washout by containment sprays, trapping by filter systems, and settling of aerosols will reduce the fission products in containment as a function of time. The CORRAL code uses this information to calculate the time-dependent containment source inventory, and then the cumulative release fractions to the atmosphere.

In the RSS, CORRAL calculations were performed for about 40 sequences. The results indicated that releases from containment could be grouped into a limited set of release categories. Seven categories with significant releases were considered for PWRs. All potentially significant sequences were assigned to the most appropriate release category, and consequence calculations were performed for this limited set of release categories.

This study uses a similar approach in considering a limited number of release categories. The RSS release categories were used directly in some cases. There were, however, some additional release categories developed for this study (see Section 5.3) as a direct result of the phenomenological and containment response investigation described in Sections 2 and 3.

For the purpose of reference, a brief description of each RSS release category and the type of sequences assigned to each category is presented as Appendix 5.8.1.

5.3 RATIONALE AND BASES FOR INDIAN POINT SOURCE TERMS

Core melt phenomenology, containment processes, containment pressure response, and containment failure modes were considered in developing the source term categories used in this study. Figure 5.3-1 is a simplified containment event tree map for internal events which considers phenomenological and containment processes important to source term categorization. The phenomena of particular interest, which led to development of source term categories not included in the RSS, are early overpressure failure with limited time for spray interaction with the source, late overpressure failures without containment sprays or fan coolers functional where there is significant time for natural processes within the containment to reduce the containment atmosphere source term, and the non-coherency of core melt progression. In addition, source terms were developed for core melt sequences where containment failure does not occur and for a sequence where the containment is vented through a filter.

Following is a discussion of the effect of each of the processes indicated on Figure 5.3-1 upon source term categorization. Section 2 (Containment Event Trees) and Section 3 (Degraded Core Phenomena) contain more detailed discussions of the core melt phenomenological processes referred to in this section.

5.3.1 Energetic Debris-Water Interaction

In the RSS, the containment failure mechanism associated with an energetic debris-water interaction resulted from a steam explosion occurring when molten core debris drops into the reactor vessel lower head which is filled with water. The RSS postulated that this event could produce a missile of sufficient energy to rupture containment and release fission products. Current information, however, indicates that this event cannot occur. (See discussion in Section 3.1.5.)

In this study, a source term similar to the steam explosion source term of the RSS was retained to account for accident sequences with a steam explosion in the reactor cavity. Steam explosion may occur when molten core debris drops into the water after vessel melt-through. Such events are not likely to produce sufficient pressure to cause containment failure. However, if a containment failure had already occurred from an external event (such as earthquake) or if a hydrogen burn were to occur at or very soon after the debris/water interaction the source term available for release would have the characteristic of a steam explosion source term (increased levels of tellurium and ruthenium).

The breakup of a significant fraction of the core debris into fine particulate material (a few hundred microns) and the distribution of that material in the containment atmosphere would produce a fission product source term characteristic of a steam explosion. Under such conditions, ruthenium and tellurium oxidize to more volatile forms, and the fraction of these two species in the containment atmosphere can be increased.

A coherent drop of core debris material into the reactor cavity is necessary for an energetic interaction of significant magnitude to occur.

The analytical studies summarized in Section 3.2 demonstrate that this coherent drop is not expected to involve more than 50 percent of the core debris material rather than the 100 percent assumed in the RSS.

Thus, the fission product source for the steam explosion event was assumed to introduce only one-half as much fine particulate material debris into the containment atmosphere as was assumed in the RSS (e.g., 50 percent of the debris was assumed in the RSS and 25 percent in this study). Tellurium and ruthenium were assumed to be oxidized under these conditions, as in the RSS. The increase in the source terms from these two species over a simple melt source, however, was assumed to be one-half the RSS value. These modified source terms are designated Z-1 or Z-1Q (cases without sprays functional) and Z-3 (cases with sprays functional).

5.3.2 Early Overpressure Events Leading to Containment Failure

Potential overpressure events which lead to containment failure and which occur up to the time of or shortly after reactor vessel failure are considered. With respect to the events identified on the detailed containment event tree of Section 2, Nodes B and C, Nodes F and G, Nodes M and N, and Nodes O and P are potential early overpressure failure events. These events all produce a relatively rapid rise in containment pressure which potentially could lead to containment failure.

A debris dispersion event (Node I) (see Section 2) has the potential for dispersing particulate material into the containment atmosphere in a way similar to a steam explosion. The debris particulate material associated with a dispersive event, however, is likely to be much larger than that associated with an energetic debris-water interaction (range of 0.3 to 3 cm as compared with 300-500 microns, respectively). Thus the rate of oxidation and the release of ruthenium and tellurium from the dispersed debris will be substantially less than for the steam explosion case, and an increase of tellurium and ruthenium source terms was not considered appropriate for these events.

In those cases in which sprays are not functional, containment failure sequences were assigned to Category 2 as in the RSS. For cases where sprays are functional, the relatively rapid pressure rise which has the potential for causing containment failure, and the release of fission products to the containment are likely to occur closely in time. Thus, spray effectiveness will be limited by the short time available for contact between spray and fission products before containment failure and subsequent release of the source from the containment. A new source term category, Z-5, has been defined to account for reduced spray effectiveness for these early overpressure failure events. Source term values were derived from calculations with the CORRAL code, assuming the containment failure was one minute after reactor vessel failure (when most of the fission products are released to the containment).

Whether or not there is a high energy release associated with the escape of radioactive sources from containment is also important. If there is significant energy release, lofting of the source can occur, an effect which influences consequence estimates (see discussion in Section 6.1.1). In this study, overpressure events which produce pressures

exceeding the containment failure pressure of 141 psia by more than 10 psi are assumed to open a large enough hole in the containment to produce a high rate of energy release. Lofting of the plume may result depending on the building geometry and wind speed.

Overpressure events which produce calculated overpressures exceeding the containment failure pressure of 141 psia, but by less than 10 psi are assumed to open small cracks in the containment. Thus, the rate of radioactivity release and the rate of energy release would be low. Source lofting is not assumed for such conditions. Thus, for release Categories 2 and Z-5, there are both low and high energy release cases which are designated 2A, 2B and Z-5A, Z-5B, respectively. Similarly, for events which produce a steam explosion-like source term, both low energy and high energy release cases can occur, and are designated Z-1A and Z-1B.

5.3.3 Late Overpressure Failures

Late overpressure failures are events assumed to occur as a result of long-term steam buildup (loss of containment heat sink), perhaps abetted by long-term non-condensible gas or hydrogen generation from debris concrete interaction. For such events with sprays functional (Node R from the Section 2 event tree) sprays have sufficient time to wash out fission products if sprays are functional. Release Category 5 (for functional sprays) from the RSS was assigned for these sequences. The significant additional time available for evacuation is also important. This additional evacuation time is accounted for in the consequence models. Sequences with this additional time are denoted as 5-R sequences in Sections 2 and 6.

For sequences where sprays are not functional and where late overpressure failures occur, CORRAL calculations were performed to establish source term estimates. In these calculations, reduction of the containment source available for release by natural processes in the containment was accounted for. Two source release categories were identified as follows:

1. Release Category 2R, for which it is assumed that the core melt debris in the reactor cavity remains covered with water. For such a case, the debris does not overheat to a temperature sufficient for vaporization release to occur.

2. Release Category 2RW, for which it is assumed that core melt debris in the reactor cavity eventually boils away all of the water in the cavity. For such a case, overheating of the debris can occur and vaporization release from the debris can result. MARCH calculations indicate that if vaporization release occurs at all, it will be after containment failure. The tellurium release associated with such events will be greater than for 2R events.

Assumptions used and results of CORRAL calculations for the 2R and 2RW categories are presented in more detail in Appendix 5.8.2. The extra time available for evacuation for 2R and 2RW sequences, compared with early overpressure failures, is accounted for in the consequence calculations (see Section 6).

5.3.4 Containment Isolation Failure

Containment isolation failure events were generally assigned to release categories in the same manner as in the RSS. Two types of events are considered: (1) those resulting from failures of penetrations or from failure to isolate small lines penetrating containment, and (2) those resulting from failure of valves separating high pressure and low pressure portions of systems connected to the reactor coolant system, where failure of such valves could lead to blowdown outside of containment. The first type of isolation failures was assigned to Category 5 when sprays are functional. For the no spray cases, they were assigned to Category 4. The second type of isolation failure involving valve failures in interfacing systems (the RSS V failure mode) was assigned to release Category 2, as was done in RSS.

5.3.5 Basemat Penetration

Basemat penetration sequences were assigned to release categories in the same manner as in the RSS. Sequences where sprays are functional were assigned to release Category 7 while cases where sprays are not functional were assigned to release Category 6.

5.3.6 Core Melt Events Without Containment Failure

Unlike the RSS, this study shows that most of the core melt sequences for the Indian Point units will not lead to containment failure. For such sequences the only fission product release will be that which occurs from leakage at the low rates typical of containment design leakage. Releases for these conditions were calculated using the CORRAL code. The calculated releases represent new release categories which were designated 8A for the case in which sprays are not functional and 8B for the case in which sprays are functional. For the calculations a post accident containment leakage rate of 0.1 percent/day was assumed at design basis conditions.

5.3.7 Venting of Containment Through a Filter

An additional source term was developed to assess the benefits that could be gained from a filtered vented containment system. In developing the source term, it was assumed: (1) that the filter would provide a decontamination factor of 50 for iodine and particulate species; (2) that noble gases and organic iodides would not be removed by the filter; and (3) that the source venting to the filter would be from actuation of the system by an early overpressure event in which there was no sprays and hence no containment heat sink. Thus, a Category 2 source term was assumed to vent to the filters. The source exiting these filters was designated as a 2RV source term. For many of the sequences for which a filtered vent system would function, the system would open to prevent a late overpressure failure. For such conditions a 2R or 2RW source would vent to the filters. Assumption of the larger Category 2 source term venting to the filters is, therefore, a conservative approach.

5.3.8 Containment Spray and Fan Coolers

The effect of sprays in reducing sources was discussed in the preceding sections. With respect to fan coolers, no credit was taken for source reduction in deriving the source term values because sequences with fan coolers but not sprays are of low probability compared to sequences with neither the sprays nor fan coolers. The source reduction provided by fan cooler operation only is summarized in Appendix 5.8.3.

5.3.9 Summary

The discussion presented above has been summarized in Table 5.4-1 which contains a description of each release category used in this study.

Source terms for the categories have been obtained in some instances from CORRAL calculations and in some instances from the RSS source term values. Of the dominant categories (in terms of risk), values for release categories Z-1 and 2 were taken from the RSS. Values for release categories 2RW, 8A, and 8B were obtained from plant specific CORRAL calculations.

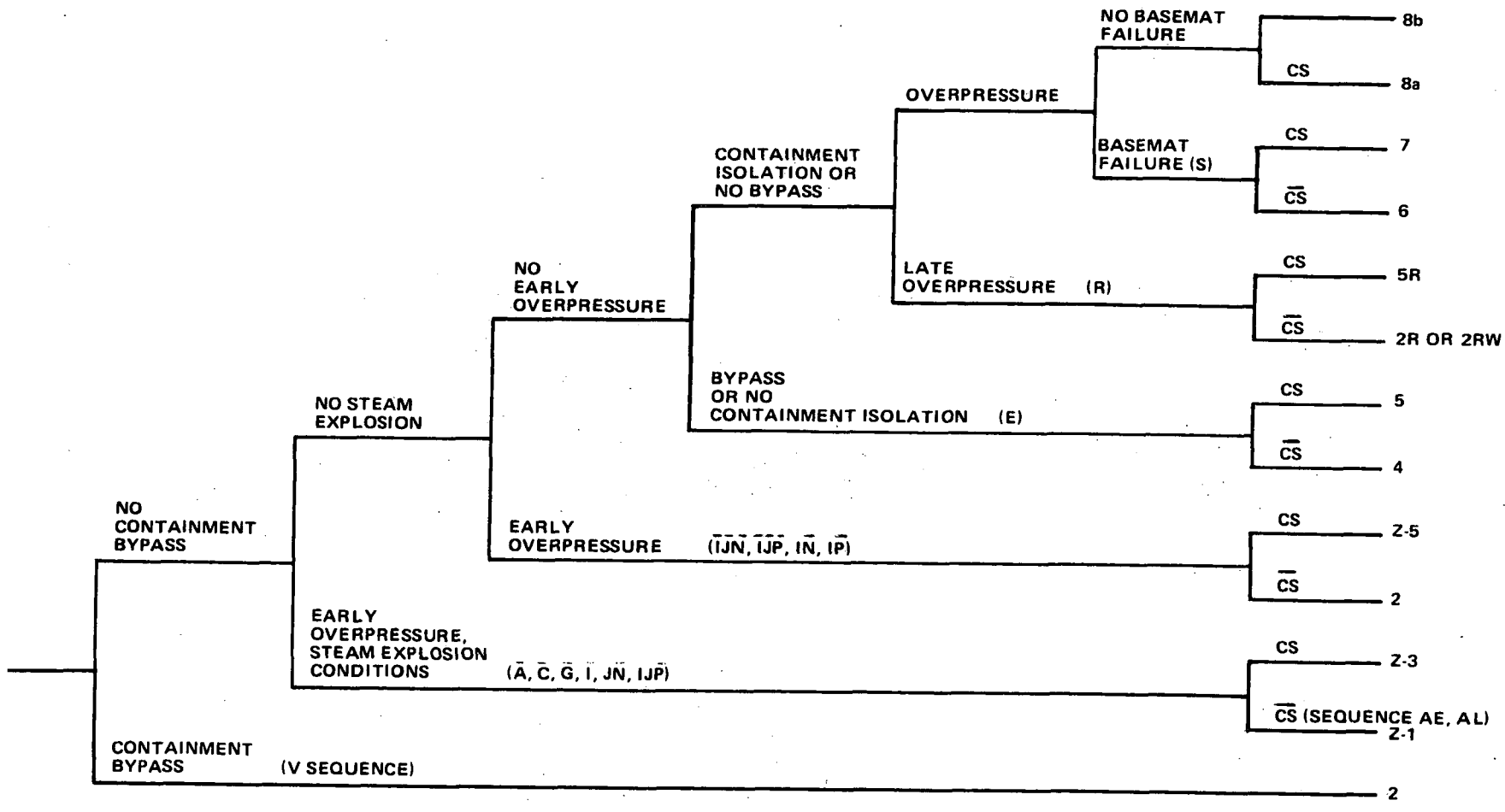


Figure 5.3-1. Simplified Containment Event Tree for Identifying Release Categories

5.4 SOURCE TERMS AND ASSOCIATED RELEASE PARAMETERS

5.4.1 Source Terms

Estimated values for the fraction of core inventory released from the containment for each of the thirteen release categories defined in Table 5.4-1 are presented in Table 5.4-2. Values are tabulated for each release category for each of the seven groups of radioactive fission product species considered in the RSS. In addition, the halogen group has been partitioned into organic and inorganic fractions for use in consequence calculations.

5.4.2 Consequence Parameters

Parameters other than the fractional fission product release are important to the consequence estimates. These parameters include time of release, duration of release, energy associated with the source release process, and the elevation of release. Values for the associated source term release parameters are listed in Table 5.4-3. Release from containment was assumed to occur at an elevation of 10 meters above grade for consequence calculations.

5.4.2.1 Time and Duration of Release

In general, the time and duration of release were derived from the values developed in the RSS. Releases for early overpressure failure cases were assumed to begin after 2.5 hours. Releases for failure to isolate containment and for sequences where the only release mode is containment leakage were assumed to start at 2.0 hours. In this study, steam explosion source terms are also associated with sequences initiated by a seismic event. Such events could lead to release as early as one hour after accident initiation. As a result, an additional release condition was defined for an early release to an already failed containment. This is release condition Z-1Q.

An overpressure failure time value of 2.5 hours was used for Category 5 releases, and represents a departure from the RSS, which used 2.0 hours. For Categories 2R, 2RW, and 5R, late overpressure failures, releases were assumed to be delayed until 12 hours after the start of the accident.

With regard to duration of release, generally the values from the RSS were adopted. A value of 0.5 hours was used for sequences where the failure mechanism produces a large containment hole or opening with high containment pressure, and for sequences where early containment failure (1 hour) can occur. In particular, a duration of 0.5 hours was used for release condition B overpressure events and for release condition Z-1Q. For Categories Z-1A, 2A, 2R, Z3, and Z-5A, (lower pressure failures), a release duration of 3 hours was used. For Categories 5 and 5R, where sprays are functional, a longer release duration of 4 hours was used (the 4 hour duration for Category 5 corresponds to that in the RSS for Category 5). For Categories 8A and 8B (leakage at normal rates) a release duration of 10 hours was assumed.

Category 2RW is a special case for which release fractions for sequential periods were defined. This approach is called a multi-phase release model (see Section 6.1.2.6). For category 2RW, melt release from core debris is followed in time by a vaporization release. The basis for the fractional release values for the four periods is presented in Appendix 5.8.4.

5.4.2.2 Release Energy

The energy associated with the release of radioactivity affects the characteristics of the plume released from the containment and is discussed in Section 6. In particular, if significant energy accompanies the release, the plume may be lofted and the radioactivity may be carried a substantial distance from the plant before it descends to the surface to cause dose effects other than the cloud dose. In general, values for energy associated with release of radioactivity were derived from values developed in the RSS.

Energy release values for steam explosion cases were taken from the RSS. For overpressure sequences without sprays and a large containment opening (Category 2B), the value of the associated energy release was adjusted upward from the RSS value of 170×10^6 to a value of 250×10^6 BTU/hr. This accounts for the higher pressure associated with containment failure (values used for gross containment failure pressure were approximately 110 psia in the RSS and approximately 140 psia in this study). For overpressure failure cases with small containment opening (Categories 2A and Z-5A) or failed containment at the time of source release (Z-1Q), the energy release value associated with Category Z-1A from the RSS (steam explosion with low containment pressure) was assumed. Other energy release values were taken from the RSS. The values for each release category are shown in Table 5.4-3.

TABLE 5.4-1

SUMMARY OF RELEASE CATEGORY RATIONALE AND NOMENCLATURE

Category	Description
Z-1 (Z-1A, Z-1B, and Z-1Q release conditions)*	This release category applies to overpressure failure and seismic induced containment failure sequences. The source term values are similar to the RSS steam explosion source release Category 1, in which containment sprays are not functional. The sources were adjusted, however, for 25% of the core entering the containment atmosphere as fine particles by the steam explosion, rather than the 50% assumed in RSS (see Section 5.3.1). Tellurium and ruthenium are the only radioactive species whose release fractions to the atmosphere are increased by the steam explosion. Values for these species were appropriately adjusted. Both low energy and high energy source release conditions, designated Conditions Z-1A and Z-1B, respectively, are considered for this category, as well as a release condition Z-1Q induced by a seismic event.
2 (2A and 2B release conditions)*	This release category is primarily used for containment bypass failures associated with check valve failures in interfacing systems. It is also used for overpressure failures without functional sprays. Both the dispersive and gravity drop cases are included when they lead to containment failure. Both low energy and high energy source release conditions are considered in this category, designated Conditions 2A and 2B, respectively. Sources for this release category are the same as in the RSS.
2R	This release category applies to late overpressure failures without functional sprays. These failures result from relatively slow pressure buildup due to loss of containment heat removal capability so that only low energy source release conditions are considered. For this release category, an 8 hour delay between the time of reactor vessel failure (when release of most of the fission products to the containment occurs) and containment failure is assumed. During this period natural processes reduce the source term available for release at containment failure. March calculations indicate that reactor vessel failure occurs approximately 4 hours after accident initiation for this sequence so that containment failure occurs approximately 12 hours

TABLE 5.4-1 (Continued)

SUMMARY OF RELEASE CATEGORY RATIONALE AND NOMENCLATURE

Category	Description
	after accident initiation. It is assumed that core melt debris in the cavity remains covered by water so that no vaporization source release occurs. Source estimates are based on CORRAL calculations.
2RW	This release category also applies to late overpressure failures without functional sprays. It differs from Category 2R in that core melt debris is assumed to dry out following containment failure so that a vaporization release from the debris occurs. Failures result from relatively slow pressure buildup due to loss of containment heat removal capability so that only a low energy source release condition is considered. An eight hour delay between reactor vessel failure (when release of most of the fission products to the containment occurs) and containment failure is used. Reactor vessel failure occurs approximately 4 hours after accident initiation for these sequences. During this time natural processes reduce the source term available for release at containment failure. Source estimates are based on CORRAL calculations.
2RV	This release category is used to evaluate mitigating features, particularly a filtered vent system. It is assumed that a Category 2 source term vents from the containment to a filter and that the filter provides a decontamination factor of 50 for iodine and particulate species. Noble gases and organic iodine are assumed not to be absorbed by the filter.
Z-3	This release category applies to overpressure failure events with a source similar to the RSS steam explosion source release Category 3, in which the spray system is functional when the steam explosion occurs. The sources were adjusted, however, for 25% of the core entering the containment atmosphere as fine particles, rather than the 50% assumed in the RSS. Tellurium and ruthenium are the only species whose release fraction into and out of the containment are increased by the steam explosion event. Values for these species were appropriately adjusted. Only a low energy release condition is considered for this release category.

TABLE 5.4-1 (Continued)

SUMMARY OF RELEASE CATEGORY RATIONALE AND NOMENCLATURE

Category	Description
4	This category is used for containment failure modes that involve failure to properly isolate the containment from openings with a hole size equivalent to approximately 4". It is assumed that sprays are not effective in reducing the fission product source term for this mode. The source term for this release category is the same as RSS Category 4. Frequencies for this category were low enough that the category was not carried in the containment matrix evaluations.
Z-5 (Z-5A and Z-5B release conditions)*	This release category applies to overpressure failures where sprays have only a short time to reduce the source term before containment failure permits release. The source term is intermediate between Category 2 and Category 5 of the RSS. This category is used for containment failures which occur at or shortly after reactor vessel failure as a result of a rapid pressure spike and with the spray system functional. Both low energy and high energy source release conditions, designated Conditions Z-5A and Z-5B, respectively, are considered for this category.
5 (5 and 5-R release conditions)*	This release category applies to delayed overpressure failures and for containment isolation failures which occur with the spray system functional The source term used for this release category is the same as that in the RSS. Only low energy source release conditions are considered. A delayed release condition, from long term overpressure failure, however, is considered and is designated Condition 5-R.
6	This release category applies to penetration of the basemat without a functional spray system. It is assumed that a core melt source term is released through the basemat and surrounding soil. The source term for this release category is the same as RSS release Category 6.
7	This release category applies to penetration of the basemat with a functional spray system. It is assumed that a core melt source term is released through the basemat and surrounding soil. The source term for this release category is the same as RSS release Category 7.

TABLE 5.4-1 (Continued)

SUMMARY OF RELEASE CATEGORY RATIONALE AND NOMENCLATURE

Category	Description
8A and 8B	These release categories apply to all damaged or core melt accidents in which the containment remains intact. Radioactivity released from containment would be small, corresponding to that associated with normal levels of containment leakage. Source terms for these release categories were generated with the CORRAL code. Category 8-A is for a core melt sequence without functional sprays and Category 8-B is for a core melt sequence with functional sprays.

---

* All release conditions for a category employ the same fission products release fractions.

TABLE 5.4-2

RADIOACTIVITY RELEASE FRACTIONS FOR SOURCE TERM CATEGORIES
(FRACTION OF CORE INVENTORY RELEASE FROM CONTAINMENT)
FISSION PRODUCT CLASS

Designations For This Study	Organic Iodide	Iodine	Cs-Rb	Te-Sb	Ba-Sr	Ru	La	Xe-Kr
Z-1	6×10^{-3}	0.7	0.4	0.35	0.05	0.21	3×10^{-3}	0.9
2	7×10^{-3}	0.7	0.5	.3	0.06	0.02	4×10^{-3}	0.9
2R	6×10^{-3}	9×10^{-3}	0.2	3×10^{-2}	0.02	7×10^{-3}	7×10^{-4}	0.9
2RW**	7×10^{-3}	0.1	0.3	0.4	0.03	0.03	5×10^{-3}	0.9
2RV	7×10^{-3}	1.4×10^{-2}	1.0×10^{-2}	6×10^{-3}	1.2×10^{-3}	4×10^{-4}	8×10^{-5}	0.9
Z-3	6×10^{-3}	0.2	0.2	0.25	0.02	0.015	3×10^{-3}	0.8
4*	2×10^{-3}	0.09	0.04	0.03	5×10^{-3}	3×10^{-3}	4×10^{-4}	0.6
Z-5	7×10^{-3}	0.2	0.25	0.25	0.025	1.5×10^{-3}	4×10^{-3}	0.8
(5* and 5R)	2×10^{-3}	0.03	9×10^{-3}	5×10^{-3}	1×10^{-3}	6×10^{-4}	7×10^{-5}	0.3
6	2×10^{-3}	8×10^{-4}	8×10^{-4}	1×10^{-3}	9×10^{-5}	7×10^{-5}	1×10^{-5}	0.3
7	2×10^{-5}	2×10^{-5}	1×10^{-5}	2×10^{-5}	1×10^{-6}	1×10^{-6}	2×10^{-7}	6×10^{-3}
8A	1.7×10^{-4}	2.7×10^{-3}	5.0×10^{-6}	1.0×10^{-6}	7×10^{-7}	2×10^{-7}	2×10^{-8}	2.7×10^{-2}
8B	1.9×10^{-4}	1.6×10^{-5}	8×10^{-7}	1.5×10^{-7}	1×10^{-7}	3×10^{-8}	3×10^{-9}	2.7×10^{-2}

Notes:

Z-1 - RSS Category 1 Source Modified for 25% rather than 50% fine particulate generation (affects Te & Ru only)

Z-3 - RSS Category 3 Source Modified for 25% rather than 50% fine particulate generation (affects Te & Ru only)

Z-5 - RSS Category 2 Source Term Modified for Short Term Spray Application.

* - Categories 4 and 5 had low frequencies and therefore were not included in the containment matrix quantification.

** - The total release fractions listed here were split into four multi-phase groups for consequence calculations, see Appendix 5.8.4 and Table 6.2-16.

TABLE 5.4-3

ASSOCIATED SOURCE TERM RELEASE PARAMETERS

Release Conditions	Time Release Begins (hrs)	Duration Release (hrs)	Associated Energy Release BTU/hr
Z-1Q	1.0	0.5	20×10^6
Z-1A	2.5	3	20×10^6
Z-1B*	2.5	0.5	520×10^6
2-A (V sequence)**	2.5	1	20×10^6
2-B*	2.5	0.5	250×10^6
2-R*	12	3	20×10^6
2RV	2.5	0.5	1×10^6
2RW	12	Multi-phase***	6×10^6***
Z-3*	2.5	3.0	6×10^6
4*	2.0	3.0	1×10^6
Z-5A*	2.5	3	20×10^6
Z-5B*	2.5	0.5	250×10^6
5*	2.5	4	0.3×10^6
5-R*	12	4	0.3×10^6
6*	12	10	NA
7*	10	10	NA
8A	2	10	NA
8B	2	10	NA

* These release conditions were determined to have low frequency and were therefore not included in Section 6 consequence calculations. Most however were included in the containment matrix quantification (exceptions are categories 4 and 5).

** The dominant accident sequence in release condition 2-A is the interfacing system failure or V sequence for which release duration is relatively short. A one hour value for release duration was used, see Appendix 5.8.4.

*** A multi-phase release condition was used for category 2RW. See Appendix 5.8.4 and Table 6.2-16. Release energies of 6×10^6 Btu/hr were used except for the last phase of a four phase release.

5.5 SOURCE TERM TECHNOLOGY

The radioactivity release estimates used in the RSS were based on experiment and analytical work conducted before 1974. Since that time additional experiments and analyses have been quite limited. The accident at TMI-2, of course, provided significant data regarding the quantity of the various fission product species released from the core region to the containment, and the quantities available in the containment for potential release to the atmosphere.

One observation at TMI-2 was that the fraction of the core inventory of iodine released from the containment to the environment was orders of magnitude less than the fraction of noble gases released even though significant iodine was released from the core. Both classes of fission products are volatile, and it had been generally assumed that fractional releases to the containment of the two classes should be similar. Because of these observations regarding fission products at TMI-2, various investigators re-examined the fission product source term estimates and the associated assumptions used in the RSS (see, for example, Reference 2). These re-examinations emphasized the substantial conservatism in assumptions used to estimate the fission product source term. These assumptions had been based on the lack of adequate experimental and analytical data regarding the processes which influence the behavior of fission products released in a damaged core or core melt accident. The conservatisms used in fission product source estimates for core melt accidents have been discussed at a meeting of the NRC commissioners (References 3 and 4).

Source terms for accidents like that at TMI-2 were not discussed in the RSS. Estimates made since that accident, however, show that if the RSS data and methodology were applied to the TMI-2 accident, the characteristics of the release observed at TMI-2 would be predicted. That is, the fractional release to containment of noble gas species would be predicted to be orders of magnitude greater than the release to containment of iodine species. Further, the general characteristic of the source distribution within the containment would be predicted (Reference 5). The reduced quantity of iodine available for release in an accident like TMI-2 is largely due to significant contact between the released fission products and reactor coolant before the fission products are released from the reactor system, and to significant contact with containment sprays after release to the containment. Iodine species in a reduced chemical state are readily absorbed and effectively retained by coolant and/or by the spray solution under such conditions. The present study did not revise the RSS source terms to account for the TMI-2 observation. For many of the sequences considered in this study, contact between the released fission products and reactor coolant would be considerably less than was the case at TMI-2; other sequences could be similar to TMI-2 with respect to contact with reactor coolant.

The study team and other investigators who were consulted (References 5 and 6) judge that data available today does not yet provide a sufficient foundation for altering the basis and assumptions of the RSS source term estimates. It is important to recognizes however, that the available data does indicate that the point estimate source term values used in this study (and derived from the RSS) are conservatively high.

Section 5.6 presents estimates of the extent of conservatism in the source term (based on engineering judgement) for those release categories and release conditions which are dominant contributors to overall risk. These estimates are presented in the form of probability distributions and include the 2R and 2RW release categories for which specific CORRAL calculations were performed. Assumptions and approaches used in the CORRAL calculations are basically those of the RSS, and thus also contain significant conservatisms. As new data or calculations related to fission product behavior become available, a re-evaluation of the source term values will be appropriate to define more realistic source terms and/or new fission product release categories.

5.6 PRINCIPLE SOURCE TERM CATEGORIES AND THEIR UNCERTAINTIES

5.6.1 Principle Source Term Categories

Only a limited number of the 13 release categories defined this section were used in the consequence calculations and assembly of the risk curves. Limiting the number of release categories considered was possible because of the low frequencies and/or low consequences for some of the categories. The reduction of categories for consequence calculations was done in two stages. Relatively early in the study, it became apparent that the probability of failure of containment isolation was low so release category 4 was not considered in assembling the containment matrix. Similarly containment response calculations indicated that the probability of containment failure with the spray system functioning was very low so that release category 5 was not considered. As indicated earlier, containment pressure-temperature calculations also showed that pressures substantially in excess of containment failure pressures were unlikely so that B type release conditions were eliminated from consideration.

Scoping consequence calculations were performed for the remaining release conditions and categories and these calculations showed that the contribution to risk of many of the categories was very small (see probability distribution curves for various release conditions in Section 8). As a result only 6 of the release categories/conditions were retained for detailed consequence calculations, these being release conditions Z-1Q and Z-1A, release category 2, release category 2RW, release category 2RV, and release category 8B.

In the section which follows uncertainty for the release category point value estimates are developed in terms of probability distributions. As part of this process, the dominant accident sequences associated with each release category/condition are identified.

5.6.2 Uncertainty Estimates

The source terms used in this study are based on the technology developed in the RSS. The RSS assumed relatively complete release of volatile fission products during core melt followed by essentially complete transport of fission products from the core region to the containment. Processes in the containment atmosphere were described in the RSS using the best available models. Modeling was a relatively realistic treatment of the processes. Physical parameters used in the models were conservatively selected, however. Thus the source terms, although not bounding, were conservative rather than realistic. That is, the probability that the actual source terms will be larger than the value assigned a category is small. Conversely, the probability that the actual source term value will be lower than the selected value is large. In fact, realistic values could be lower by at least one order of magnitude than the values used for certain combinations of system and containment failure. In this section, estimates of uncertainty in terms of probability distribution are developed.

In order to estimate uncertainties in the source term, dominant accident sequences for each category need to be identified. The evaluations reported in Section 2 listed the dominant accident sequences for each release category. Evaluations reported in Section 6 demonstrated that Release Categories Z-1A, Z-1Q, 2, and 2RW are dominant contributors to risk, and that Category 8B is a significant contributor for certain types of damage indices. Hence, simple probability distribution estimates for these release categories and for category 2RV were made in the form of histograms. The probability distribution histograms are based on engineering judgment regarding the effects of accident phenomenology, core melt progression, and containment processes (including safeguards systems) on the source term in the containment atmosphere available for release from containment. Dominant accident sequences within each of the principal release categories, as well as sensitivity studies using the CORRAL code (see Appendix 5.8.3) were used to derive these probability distribution estimates. More experimental data and analysis should provide a basis for improving the source term estimate values and the associated estimates for probability distribution as such data becomes available.

The probability distributions for the release categories are presented as Figure 5.6-1. The distribution for each release category assigns a probability that source terms will be: (1) 2 times the point estimate indicated in Table 5.4-2; (2) equal to the estimates; (3) 0.5 times the point estimate; and (4) 0.1 times the given point estimate. These probability distributions are derived from engineering judgement based on an evaluation of information regarding the transport and deposition of fission products following a core melt accident.

5.6.2.1 Release Category 2

The dominant sequence considered in estimating the probability distribution for release Category 2 was a sequence in which there is failure of the isolation valves between the high pressure and low pressure portions of a system connected to the reactor coolant system. Such an event can lead to a reactor system blowdown and core melt event in which the released source can bypass the containment (the V sequence of the RSS). The Category 2 source term used in this study assumes high release fractions for the transportable fission products. The probability that actual source terms will have a larger value is very low. In fact, some retention of the source in the reactor system and auxiliary building is likely. Hence a condition in which the source is approximately a factor of 2 lower than that assumed in this study is probable; greater source term reduction up to a factor of 10 was assigned a probability value of 0.15.

5.6.2.2 Release Category Z-1

The dominant sequence considered in estimating a probability distribution for the Z-1 release category was the Z-1Q release condition which is a sequence with containment failure prior to core melt caused by an external event such as a seismic event. Core melt is assumed to result from a large LOCA with a steam explosion occurring when melt debris drops into the reactor cavity following vessel melt through. Since the

steam explosion source term is released outside the reactor vessel to a filled containment, escape of much of this source component to the environment is likely. However, the earlier melt release component must be transported from the core region, through the reactor system and to the break locations. Some attenuation of the melt component in the reactor system, which is not accounted for in the models, may occur.

As a result of these considerations, the probability of sources as high as the point source estimate was judged to be reasonably high (0.4) and a source term a factor of 2 lower than the point estimate was also judged to be substantial (0.5). A source a factor of 10 less than the point source value was judged to have a probability of 0.1.

The Z-1Q probability distribution was also applied to the less frequent Z-1A release condition even though this release condition appears to have more uncertainty associated with it than does the Z-1Q release condition.

5.6.2.3 Release Category 2RW

The dominant accident sequence considered in estimating a source probability distribution for release Category 2RW was a core melt sequence initiated by a transient with loss of all AC power and with loss of secondary heat sink. Loss of power continues for the long-term and eventually a delayed containment failure occurs from pressure buildup in containment. Containment failure occurs 10 to 12 hours after accident initiation. Containment sprays are not functional for this sequence. Such a sequence generally corresponds to the TMLB' sequence of the RSS.

In deriving the Category 2RW source term, it was assumed that almost all fission products released from the core are transported to the containment atmosphere. CORRAL is used to calculate the concentration of fission products in the containment atmosphere as a function of time. The substantial period of time between fission product release (at vessel failure) and containment failure will permit much of the iodine to plate out and will also provide time for significant aerosol settling and deposition. These processes are accounted for in the CORRAL calculations. For the 2RW sequence, dry out of the core debris occurs late in the sequence (near to or after containment failure). Dry out is followed by overheating of the core debris and a vaporization release.

A condition in which the source is approximately a factor of 2 lower than the point value listed in Table 5.4-2 is regarded as more probable than is a release of the point value estimate. The probability that the source released will be a factor of 10 lower than the point estimate value is estimated to be 0.15.

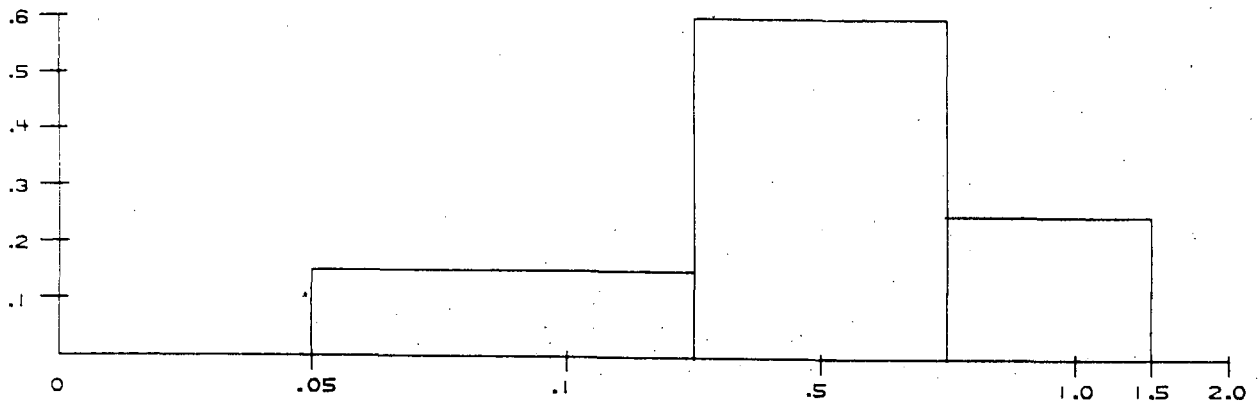
5.6.2.4 Release Category 8B

The dominant accident sequence considered in developing a source term probability distribution for release Category 8B was a core melt sequence initiated by a small pipe break with failure of either ECC injection or ECC recirculation; containment sprays are assumed to be functional. A significant fraction of the fission products released

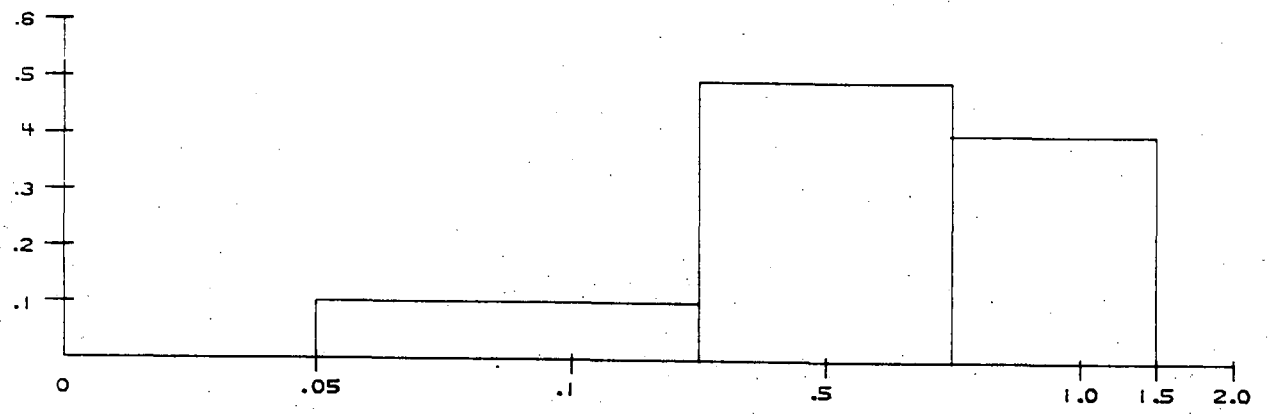
from the core debris are likely to be eventually transported to the containment, but most will be washed out by the sprays. Source term estimates from the CORRAL code are considered to be within a factor of 2 to 4 of the point value source term presented for this release category in Table 5.4-2. Source terms greater than the value used in the study are not likely. This distribution is presented on the histogram of Figure 5.6-1.

5.6.2.5 Release Category 2RV

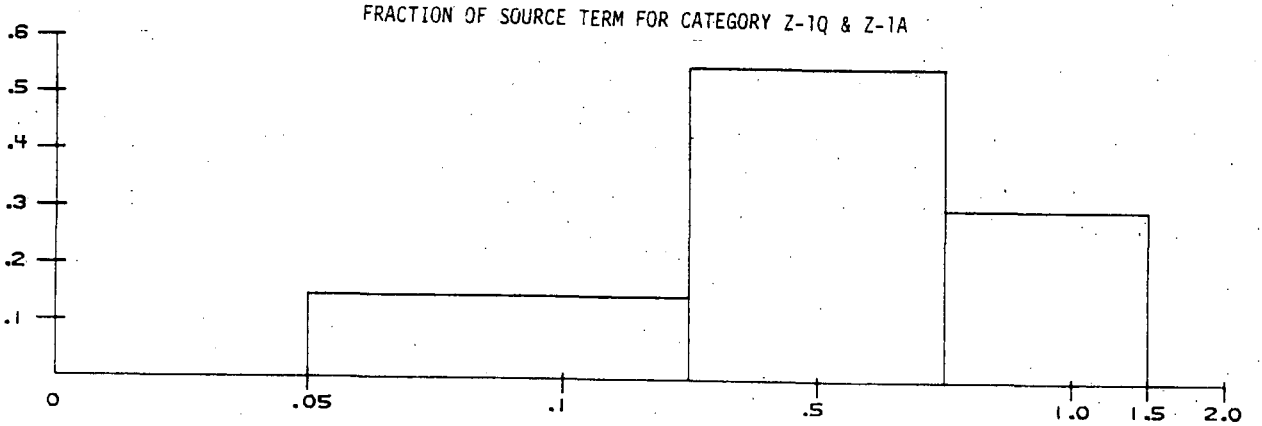
An evaluation of the potential benefit from a filtered containment vent system would use release Category 2RV to characterize the source term released through the system. Source term uncertainty for Category 2 is assumed as input to the system and thus, its probability distribution was assumed in evaluating Category 2RV.



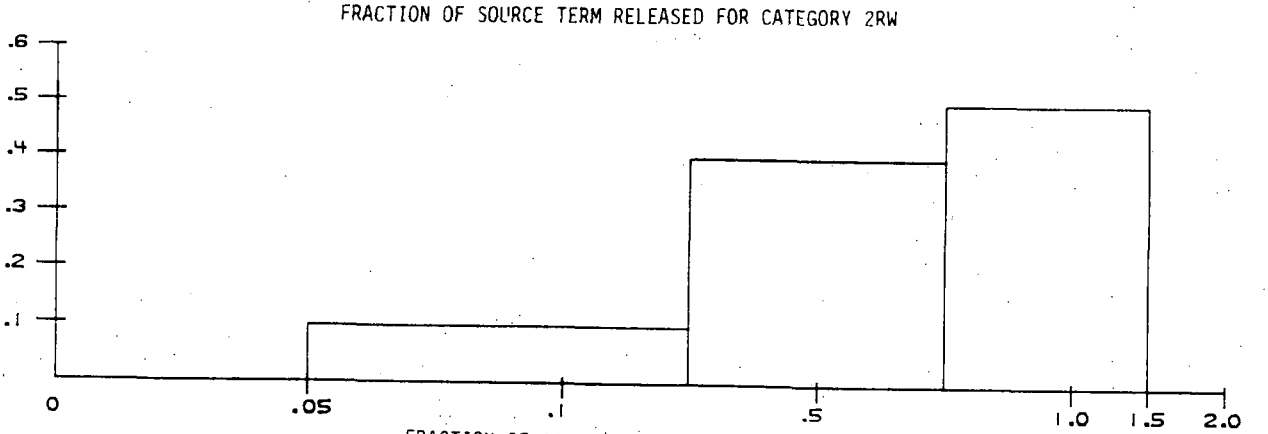
FRACTION OF SOURCE TERM FOR CATEGORIES 2 & 2RV



FRACTION OF SOURCE TERM FOR CATEGORY Z-1Q & Z-1A



FRACTION OF SOURCE TERM RELEASED FOR CATEGORY 2RW



FRACTION OF CATEGORY 8B SOURCE TERM

FIGURE 5.6-1
RELEASE CATEGORY
2 & 2RV, Z-1Q & Z-1A, 2RW AND 8B
SOURCE TERMS

5.7 REFERENCES

1. "Reactor Safety Study, An Assessment of Accident Risks in U.S. Commercial Nuclear Power Plants," WASH-1400, October 1975.

2. M. Levenson & F. Rahn, "Realistic Estimates of the Consequences of Nuclear Accidents", EPRI paper presented at American Nuclear Society Meeting, 11/80.

3. Briefing of NRC Commission on Iodine Release During Reactor Accidents, 11/18/80, included NRC paper SECY-80-504, 11/13/80.

4. Letter from W. R. Stratton, A. P. Malinauskas and D. O. Campbell to Chairman J. Ahearme, NRC, August 14, 1980.

5. Private Communications with R. Ritzman of SAI and H. K. Hilliard of W-HEDL.

6. Meeting at Oak Ridge National Laboratory, 11/6/80. Participants were D. O. Campbell, R. Lorentz, A. P. Malinauskas and G. W. Parker of Oak Ridge National Laboratory and D. H. Walker of Offshore Power Systems.

APPENDIX 5.8.1

SUMMARY DESCRIPTION OF FISSION PRODUCT RELEASE CATEGORIES EMPLOYED IN THE REACTOR SAFETY STUDY

APPENDIX 5.8.1

SUMMARY DESCRIPTION OF FISSION PRODUCT RELEASE CATEGORIES USED IN THE REACTOR SAFETY STUDY

Release Category 1

Sequences in which containment failure resulted from steam explosion, and in which containment spray system is not functional were placed in Category 1. The RSS considered two types of Category 1 releases. Subcategory 1a applies to sequences which occur with reduced containment pressure. Subcategory 1b applies to sequences which occur with the containment at high pressure so that the released source may be lofted after leaving the containment by the high energy release rate.

Release Category 2

Sequences in which containment failure results from overpressure and in which containment spray system is not functional were placed in Category 2 in the RSS. Also placed in this category was the V sequence which was a failure of the interfacing check valves permitting fission product release to bypass containment.

Release Category 3

Sequences in which containment failure results from steam explosion and in which the containment spray system is functional were placed in Category 3.

Release Category 4

The principal sequences in this category involved failure to isolate containment for smaller penetrations (a few inches in diameter) without functional sprays to remove fission products.

Release Category 5

Sequences in which containment failure results from overpressure and in which the containment spray system is functional were placed in Category 5. Also placed here were sequences involving failure to isolate with the sprays functional.

Release Category 6

Sequences in which containment failure results from basemat penetration and in which the containment spray system is not functional were placed in this category.

Release Category 7

Sequences in which containment failure results from basemat penetration and in which the containment spray system is functional were placed in this category.

Release Category 8 and 9

Sequences in which LOCAs did not lead to damaged or melted core conditions were placed in these categories. The contributions of these sequences to risk was negligible.

APPENDIX 5.8.2

DESCRIPTION OF CORRAL CALCULATIONS PERFORMED TO ESTIMATE SOURCE TERMS FOR DELAYED OVERPRESSURE FAILURES (ASSUMPTIONS AND RESULTS)

APPENDIX 5.8.2

DESCRIPTION OF CORRAL CALCULATIONS PERFORMED TO ESTIMATE SOURCE TERMS FOR DELAYED OVERPRESSURE FAILURES (ASSUMPTIONS AND RESULTS)

5.8.2.1 Introduction

This appendix describes the CORRAL code calculations (Reference 1) performed to estimate fission product release from containment for loss of power initiated transient core melt accident sequences in which neither the containment spray system nor the fan cooler system are functional. The CORRAL calculations were performed using Indian Point plant parameters. The two main purposes of the sensitivity calculations reported in this Appendix were to determine the effect of a delay in containment failure time on the magnitude of fission product source released to the environment and to determine the effect of a more realistic iodine deposition rate on release to the environment.

Phenomenological evaluations and containment pressure calculations reported in Sections 3 and 4, respectively, indicate that for such sequences containment failure will most likely not occur until a number of hours after failure of the reactor vessel. Release of most of the fission products to the containment is predicted to occur at reactor vessel failure. However, containment failure will likely not occur until a number of hours after reactor vessel failure. During the period between reactor vessel failure and containment failure, the source term in the containment atmosphere available for release will be significantly reduced as a result of natural processes. These processes include plateout of iodine from atmospheric circulation (induced by temperature differences between the atmosphere and the containment surfaces) and from settling of particulate material to surfaces within the containment.

Source terms were developed for both release Categories 2R and 2RW. Category 2R is a delayed release category which assumes that the core melt debris in the vessel cavity after vessel failure remains covered with water so that no vaporization release component is produced. For Category 2RW, it is assumed that melt debris in the reactor cavity eventually boils away all of the surrounding water so that the debris overheats and vaporization release of the less volatile fission products occurs. Vaporization release is assumed to occur many hours after reactor vessel failure and near to or after containment failure (as predicted by MARCH calculations).

This appendix also includes sensitivity studies which indicate the extent of reduction in release of radioiodine provided by use of more realistic values for the rate of deposition of iodine on containment surfaces. The values for radioiodine deposition used in CORRAL are regarded as conservatively low, as discussed in Section 5.8.2.4

5.8.2.2 Description of the Accident Sequence Considered and of Sensitivities Studied

The core melt accident sequences considered for the calculations reported in this section are sequences initiated by complete loss of AC power to the plant (both offsite and emergency onsite power supplies). The assumed subsequent loss of core decay heat removal capability eventually leads to core melt conditions. For the sequence considered, loss of power is assumed to be long term and to persist over the course of the accident (for at least 12 to 14 hours). As a result, containment sprays and containment fan coolers are not functional during the accident to reduce the fission product concentration in the containment atmosphere. Because the sequence also involves loss of containment heat sink, containment pressure can eventually become high enough to cause containment failure unless a heat sink is restored. The sequence is comparable to the TMLB' sequence of the RSS (Reference 2).

During the time between reactor vessel failure (when most of the fission products are released to the containments) and the time of containment failure, processes which occur naturally within the containment reduce the fission product source in the containment atmosphere. The reduction processes considered in the CORRAL calculations are deposition of iodine on surfaces from containment atmosphere circulation (induced by temperature differences between the atmosphere and the containment surfaces), and the settling and eventual deposition of particulate material on the containment surfaces and floor. In the RSS containment failure was assumed to occur shortly after the fission products were released to the containment; hence most of the source is released from the containment. The present CORRAL calculations indicate the extent to which source term release to the atmosphere is reduced during the period between source release to the containment and containment failure, as well as reduction in source term from use of more realistic values for the iodine deposition rate.

The three cases considered in the study of the effect on source terms of a delay in containment failure time were:

Case 1) Containment failure occurs shortly after reactor vessel melt-through; 1 minute was assumed.

Case 2) Containment failure time is midway between Cases 1 and 3 (as measured from reactor vessel melt-through time), approximately 4 hours.

Case 3) Containment failure occurs approximately 8 hours after reactor vessel melt-through. Eight hours is typical of the time containment pressure calculations indicate that containment failure could occur.

Calculations were performed for the same three cases with the increased, more realistic iodine deposition rate, and these cases were designated cases 1B, 2B, and 3B, respectively. Values for iodine deposition rates and the basis for these values are discussed in Section 5.8.2.4.

5.8.2.3 Reactor System and Containment Response Estimates

A MARCH-COCO code combination, described in Section 4, was used to estimate the thermal response of the core, the thermal-hydraulic responses of the reactor system, and the thermal and pressure history of the containment for a transient initiated core melt accident. The accident sequence considered for these calculations assumed a coherent drop of the core debris into the reactor cavity at reactor vessel melt-through. The accident conditions summarized in Table 5.8.2.3-1 are a chronology of significant events as derived from the MARCH-COCO calculations.

As indicated on Figure 5.8.2.3-1, there are three components of fission product release considered: (1) an initial small gap release, (2) a release during core melt, which is generally the largest release of the components, and (3) a vaporization release which occurs if the core debris can collect, dryout, and overheat at some time following failure of the reactor vessel. For the accident sequence considered here, the gap and melt releases precede both reactor vessel failure and containment failure. Vaporization release, assumed to occur for Category 2RW, will occur later, probably after containment failure.

If vaporization release occurs, fission products will be released to a failed containment at nearly ambient pressure conditions. Gases generated within the containment, from debris-concrete basemat interaction provide the driving force for carrying the fission products from the containment. In the CORRAL calculations, for the period after containment failure, the containment is assumed to be a well mixed tank with a leak rate equivalent to the gas production rate. The MARCH-COCO code combination uses the INTER subroutine for estimating gas generation resulting from debris-concrete interaction. Calculations assumed a concrete with limestone aggregate rather than the largely basaltic aggregate actually used for construction of the Indian Point basemat. Because interaction with basaltic aggregate generates less gas than does interaction with a limestone aggregate, the gas generation rates, the containment leak rates, and the fission product release rates following containment rupture are all conservatively high.

Containment leak rates used in the CORRAL calculations are presented as Figure 5.8.2.3-2 and Figure 5.8.2.3-3. Figure 5.8.2.3-2 is a plot of the leak rate for the period before containment failure and is based on the containment design basis leak rate. Figure 5.8.2.3-3 is the containment leak rate for the period after containment failure derived as indicated above.

5.8.2.4 Iodine Deposition Rate for Sequences Without Containment Safety Systems Operational

5.8.2.4.1 Background

Important variables which affect the rate of iodine loss by surface deposition are:

1. Chemical form of the iodine in the atmosphere,

2. Deposition rate between the atmosphere and surfaces,

3. Time available for deposition, and

4. Chemical conversion on and resuspension from surfaces.

Background data and the basis for assumptions used in the CORRAL code models are discussed below:

1. Certain iodine forms deposit more readily than others. Airborne iodine can be in any combination of the chemical forms: elemental (I_2), particulate, hypoiodous acid (HOI), and organic. Each of these forms has its own rate of deposition. The relative rates are 100, 10, 5, and 1, respectively (see References 3 and 4). In the CORRAL code 99.6% of the iodine released to containment is assumed to be in elemental form when containment sprays are functional. When the sprays are not functional, 99.3% is assumed to be in elemental form. The remaining iodine (0.4% and 0.7%) is assumed to be

organic. In CORRAL, organic iodine is assumed to be non-depositing. Elemental iodine is assumed to deposit at a rate determined mainly by the temperature difference (Δt) between the atmosphere and the containment surfaces.

2. The iodine deposition rate used in CORRAL is based on the assumption that the deposition rate is limited by the diffusion rate across the air-surface boundary layer (Reference 5). This assumption, in turn, is based on iodine deposition experiments in relatively small vessels ($\sim$21,000 ft^3) under natural convection conditions. The deposition rate (cm/sec) multiplied by the surface to volume ratio (cm^{-1}) gives the time constant for removal of iodine by surface deposition. The surface to volume ratio for the Indian Point containment is 0.0023 cm^{-1} (1.8×10^5 $ft^2/2.61 \times 10^6$ ft^3). For cases 1-3, which are transient cases, the time constant for removal by deposition is 0.48 hr^{-1} which represents a half life of 1.4 hours.

3. The reduction of iodine by surface deposition is dependent on the deposition rate and time, and the accident scenario. For a slow deposition rate, there is a longer time available before containment failure and greater source reduction due to deposition. In virtually all experiments involving iodine loss due to surface deposition, the initial rate of reduction of the iodine concentration in air is large. The rate of reduction eventually decreases to zero, so that the concentration remains constant. To account for this, the CORRAL code limits the reduced air concentration of elemental iodine to 0.01 of its original concentration. Organic iodine is assumed to be non-depositing. Therefore, the maximum reduction in iodine without functional sprays is 1/59 and with functional sprays is 1/71.

4. Recent investigations into the phenomenon of iodine deposition have demonstrated that the process is reversible (Reference 6). At least some of the iodine which has deposited on surfaces is available for resuspension into the atmosphere. Resuspension is probably responsible for the slowing down and eventual halt in net deposition.

This resuspension is itself probably caused by the chemical conversion of deposited iodine to less reactive forms (for example, to HOI and organic iodine). These less reactive forms, in turn, resuspend into the atmosphere. Ultimately, equilibrium is reached between deposition and resuspension. At this point the air concentration stays constant.

5.8.2.4.2 Application of Existing Data

The only deposition experiments to be done in a large containment test facility (~250,000 ft^3), measured rates of deposition higher than the value of 0.48 hr^{-1} calculated with the CORRAL models (Reference 7). In fact, rates as high as 3.6 hr^{-1} were measured.

CORRAL calculations were performed for deposition rates of 0.48 hr^{-1} and 3.6 hr^{-1} to estimate the effects that a larger iodine deposition rate would have on the quantity of iodine released. Only values calculated with the lower deposition rate of 0.48 hr^{-1} were used in the consequence calculations discussed in Section 6.

5.8.2.5 Fission Product Release Values

For the three cases discussed in Appendix 5.8.2.2 results of fission product release from the containment are listed in Tables 5.8.2.5-1 through 5.8.2.5-5.

1. Table 5.8.2.5-1 contains a summary of the overall fraction of the core inventory released from containment for the three transient cases assuming there is no vaporization release. Values are tabulated for each of the eight fission product species groups. These releases are for Category 2R (cases 2 and 3) with case 3 used for consequence calculations.

2. Table 5.8.2.5-2 contains a summary of the overall fraction of the core inventory released from containment for the three cases assuming there is vaporization release. These releases are for Category 2RW (cases 2 and 3) with case 3 used in the consequence calculations.

3. Table 5.8.2.5-3 contains a comparison of iodine release from containment for cases with the conservative (slow) iodine deposition rate and the increased iodine deposition for the 3 cases assuming there is no vaporization release. Values calculated with the conservative deposition rate were used in consequence calculations.

4. Table 5.8.2.5-4 presents the ratio of the total fission product release of case 1 to case 2 and case 1 to case 3, respectively, for each of the 8 fission product groups for Categories 2R and 2RW.

5. Table 5.8.2.5-5 lists the ratio of the release from containment for cases with vaporization release to that of a corresponding case without vaporization release. The ratios are indicative of the importantance of the vaporization release component to overall release.

5.8.2.6 Discussion

1. Source Term Reduction from the Delay in Containment Failure Time

The ratios listed in Table 5.8.2.5-4 show that accounting for the delay in containment failure substantially reduces the CORRAL-calculated quantity of iodine released. An 8 hour delay in containment failure reduces iodine by approximately a factor of 80 for no vaporization release and by approximately a factor of 8 for the vaporization release case. The source term for particulates are reduced by approximately a factor of 3 for the cases with no vaporization by delaying containment failure time for 8 hours. As expected, the noble gases and organic iodine release fraction are hardly reduced at all.

Source terms for the Te group, Ru group, and La group are reduced less than a factor of 2 by the delay for vaporization release cases. The smaller reduction for these types of fission products is a result of their relatively large release during the vaporization release period. For vaporization release, the containment failure

has already occurred, so that released fission products species are carried from the containment by generated gases.

2. Limitations in Reduction of Iodine Deposition

Values listed in Table 5.8.2.5-3 show that the increased iodine deposition rate can significantly reduce the released source if containment failure occurs relatively soon (a few hours) after the source is released to the containment. Iodine source reduction in the range of 3 to 4 is calculated. If containment failure is delayed for as long as 8 hours, little further reduction is calculated because iodine levels in the containment atmosphere have been reduced to equilibrium levels by this time, even assuming reduced iodine deposition rates.

3. Effects of Vaporization Release on Short-Term Dose Consequences

Values listed in Table 5.8.2.5-4 and 5.8.2.5-5 show that if the vaporization release does not occur shortly after containment failure, the released source terms for the iodine, the tellurium, and the lanthanum groups are substantially reduced if containment failure is delayed until 8 hours after reactor vessel failure. There is also a substantial reduction in the release of ruthenium. Only the reduction in the tellurim source is significant with respect to short term dose consequences. For the case where containment failure is delayed for 8 hours after vessel failure, iodine in the containment atmosphere is already reduced to a low value by depositional processes before containment failure, so that iodine release at containment failure is small. Even though most of the iodine release for such a case would result from vaporization, the vaporization release component is also small enough so that short-term case consequences are minimal. Hence, addition of the iodine vaporization release component does not have a significant effect on short-term or early dose consequences.

TABLE 5.8.2.3-1

SUMMARY OF CONDITIONS FOR A TRANSIENT-INITIATED CORE MELT ACCIDENT

1) Complete loss of AC power with no power recovery

2) No ECC injection

3) No functional spray

4) No functional fan coolers

5) Core uncovers at 188 minutes (from MARCH calculations)

6) Core melt from 212 to 253 minutes (from MARCH calculations)

7) Reactor vessel failure at 259 minutes (from MARCH calculations)

8) Boil off of cavity water permits debris-concrete interaction to start at 837 minutes (from MARCH calculations)

9) No hydrogen burning during the accident

10) Coherent drop of core debris to reactor cavity after reactor vessel melt-through

TABLE 5.8.2.5-1

FRACTION OF CORE INVENTORY RELEASED FROM CONTAINMENT
FOR TRANSIENT-INITIATED CORE MELT ACCIDENTS

NO VAPORIZATION RELEASE OR CATEGORY

Fission Product Group	Fraction of Core Inventory Released		
	Case 1	Case 2	Case 3
Xe-Kr	9.00 (-1)	9.00 (-1)	9.00 (-1)
OI	6.30 (-3)	6.30 (-3)	6.30 (-3)
I2 - Br	6.91 (-1)	2.90 (-2)	9.00 (-3)
Cs-Rb	5.99 (-1)	2.37 (-1)	1.78 (-1)
Te	1.13 (-1)	4.40 (-2)	3.31 (-2)
Ba-Sr	7.53 (-2)	2.93 (-2)	2.21 (-2)
Ru	2.26 (-2)	8.80 (-3)	6.62 (-3)
La	2.26 (-3)	8.80 (-4)	6.62 (-4)

Note: For all cases the natural deposition of iodine is taken as zero after containment failure. However, for particulates, settling continues after containment failure. Numbers in parentheses refer to power of ten.

TABLE 5.8.2.5-2

FRACTION OF CORE INVENTORY RELEASED FROM CONTAINMENT
FOR TRANSIENT-INITIATED CORE MELT ACCIDENTS
WITH VAPORIZATION RELEASE OR CATEGORY 2RW

Fission Product Group	Case 1	Case 2	Case 3
Kr - Ke	9.9 (-1)	9.9 (-1)	9.9 (-1)
OI	6.9 (-3)	6.9 (-3)	6.9 (-3)
I_2 - Br	7.8 (-1)	1.2 (-1)	9.7 (-2)
Cs - Rb	6.7 (-1)	3.1 (-1)	2.5 (-1)
Te	4.4 (-1)	3.7 (-1)	3.6 (-1)
Ba - Sr	7.9 (-2)	3.3 (-2)	2.6 (-2)
Ru	4.2 (-2)	2.8 (-2)	2.6 (-2)
La	6.1 (-3)	4.7 (-3)	4.5 (-3)

Note: Numbers in parentheses refer to powers of 10.

For all cases the natural deposition of iodine is taken as zero after containment failure. However, for particulates settling is assumed to continue after containment failure.

TABLE 5.8.2.5-3

COMPARISON OF FRACTION OF IODINE CORE INVENTORY RELEASE FROM CONTAINMENT AS CALCULATED USING CONSERVATIVE AND INCREASED IODINE MODEL IN CORRAL

	Deposition (Assuming no vaporization release)		
Case No.	Iodine Release Conservative Deposition	Iodine Release Increased Deposition	Ratio Conservative / Increased
1	6.91 (-1)	1.84 (-1)	3.8
2	2.90 (-2)	9.00 (-3)	3.2
3	9.00 (-3)	8.96 (-3)	1.0

Note: Numbers in parentheses refer to powers of 10.

TABLE 5.8.2.5-4

EFFECT OF DELAY IN CONTAINMENT FAILURE TIME
ON
FISSION PRODUCT RELEASE

Fission Product Group	With Vaporization (2RW)		Without Vaporization (2R)	
	Case 2 / Case 1	Case 3 / Case 1	Case 2 / Case 1	Case 3 / Case 1
Kr-Xe	1.0	1.0	1.0	1.0
OI	1.0	1.0	1.0	1.0
I_2-Br	0.15	0.12	0.042	0.013
Cs-Rb	0.46	0.37	0.40	0.29
Te	0.84	0.82	0.39	0.29
Ba-Sr	0.42	0.33	0.39	0.29
Ru	0.67	0.62	0.39	0.29
La	0.77	0.71	0.39	0.29

Case 1 - Containment failure 1 minute after reactor vessel failure
Case 2 - Containment failure 4 hours after reactor vessel failure
Case 3 - Containment failure 8 hours after reactor vessel failure

TABLE 5.8.2.5-5

COMPARISON OF CASES WITH VAPORIZATION RELEASE (2RW) TO THOSE WITHOUT VAPORIZATION RELEASE (2R) FOR TRANSIENT-INITIATED CORE MELT ACCIDENTS

	Fraction of Core Inventory Released		
Fission Product Group	Case 1 Ratio $\frac{2RW}{2R}$	Case 2 Ratio $\frac{2RW}{2R}$	Case 3 Ratio $\frac{2RW}{2R}$
Kr-Xe	1.1	1.1	1.1
OI	1.1	1.1	1.1
I_2 - Br	1.13	4.05	10.8
Cs - Rb	1.12	1.31	1.41
Te	3.73	8.44	10.9
Ba - Sr	1.05	1.13	1.17
Ru	1.81	3.19	3.91
La	2.64	5.38	6.83

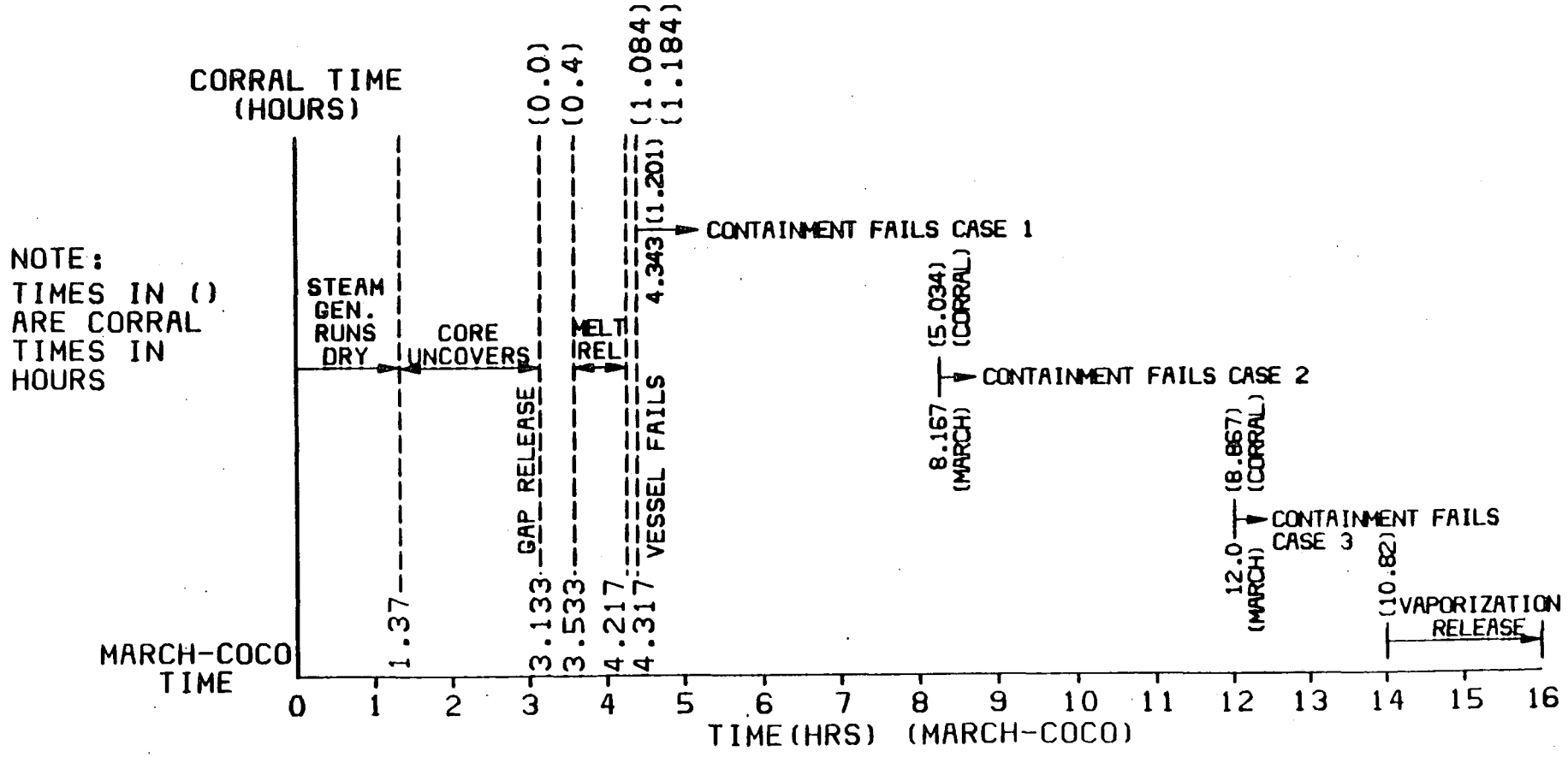
Note: For all cases (with out without vaporization), the natural deposition of iodine is taken as zero after containment failure. However, for particulates, the settling continues after containment failure.

FIGURE 5.8.2.3-1

CHRONOLOGY OF EVENTS FOR TRANSIENT INITIATED CORE MELT ACCIDENT
CASES 1, 2 AND 3

CASE 1 CONTAINMENT FAILS 1.0 MINUTE AFTER VESSEL FAILS
CASE 2 CONTAINMENT FAILS~HALFWAY BETWEEN TIMES FOR CASE 1,&3
CASE 3 CONTAINMENT FAILS 12 HOURS AFTER START OF TRANSIENT

NOTE: VAPORIZATION RELEASE TAKEN AS 2 HOUR DURATION



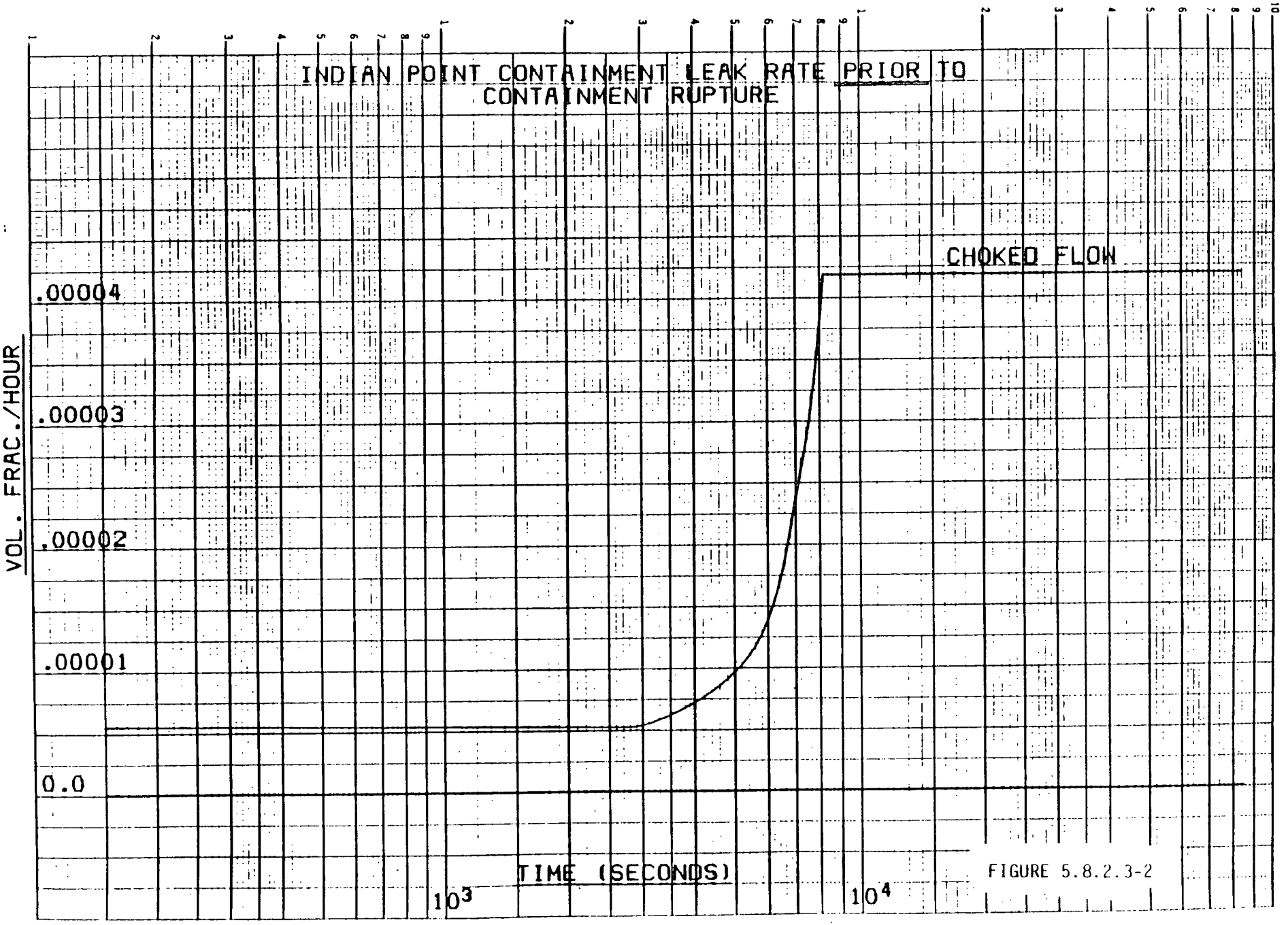
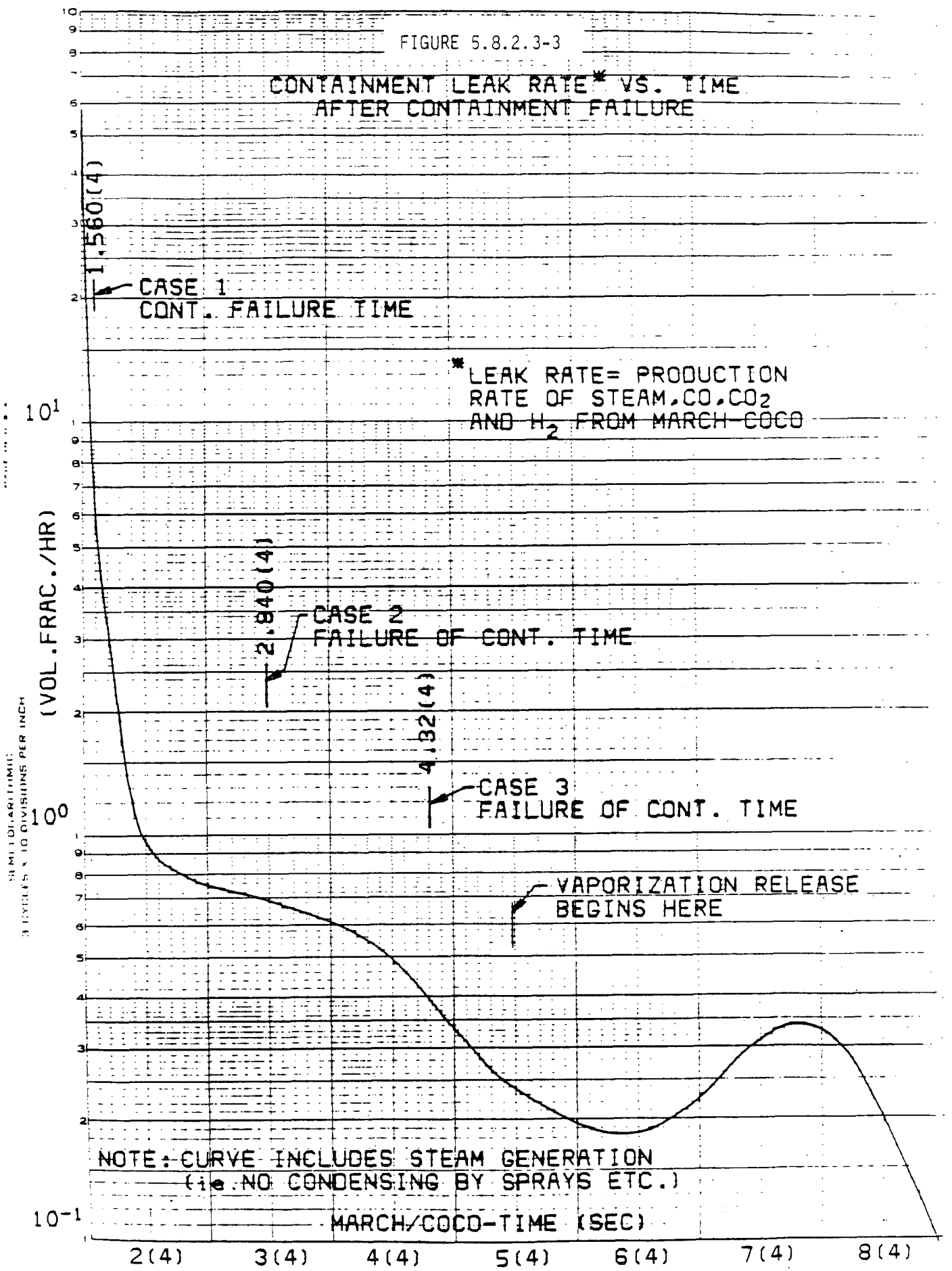


FIGURE 5.8.2.3-2

FIGURE 5.8.2.3-3



APPENDIX 5.8.3

SOURCE REDUCTION BY FUNCTIONAL FAN COOLERS

APPENDIX 5.8.3

SOURCE REDUCTION BY FUNCTIONAL FAN COOLERS

This appendix describes CORRAL code calculations (Reference 1) performed to estimate the reduction in fission product release from containment provided by functional fan coolers for core-melt accident sequences. Source release calculations were performed for both large and small break-initiated accident sequences. Source terms developed in this Appendix were not used in consequence calculations. For all sequences, in which fan coolers but not sprays were functional a source term assuming no operation of containment safety systems was used for consequence calculations (see Section 5.3.8).

5.8.3.1 Description of Accident Sequences Considered

Cases considered in evaluating the source reduction by functional fan coolers are listed in Table 5.8.3.1-1. CORRAL calculations were performed for large and small break-initiated accident sequences. For small breaks, calculations were made for cases with both spray and fan coolers functional (cases 4 and 5), for cases with only fan coolers functional (cases 6 and 7) and for cases with neither sprays nor fan coolers functional (cases 8 and 9). All calculations were performed assuming the conservative iodine deposition rate (see discussion in Appendix 5.8.2.1).

Calculations were performed for small break cases where failure of containment occurs soon after failure of the reactor vessel and for cases where containment does not reach pressures sufficient for containment failure. Containment pressure response calculations in Section 4 demonstrate that containment failure is not likely for sequences with containment safety systems functional (either sprays and/or fan coolers) unless the failure occurs very soon after reactor vessel failure. For sequences where neither sprays nor fan coolers are functional, containment failure may occur sometime after reactor vessel failure due to loss of containment heat removal capability. For this situation, fission product fractional release from containment was calculated for a case

with containment failure soon after reactor vessel failure (case 8) and for a case where containment failure is delayed until four hours after reactor vessel failure (case 9).

For large break events calculations were performed for cases with both sprays and fan coolers functional (cases 10 and 11), for cases with only fan coolers functional (cases 12 and 13) and for a case with neither sprays nor fan coolers functional (case 14).

For large breaks, calculations were performed for cases where containment failure occurs soon after reactor vessel failure and for cases where containment failure does not occur. Containment pressure response calculations in Section 4 demonstrate that containment failure is not likely for sequences with containment safety systems functional (either sprays and/or fan coolers) unless the failure occurs very soon after reactor vessel failure.

5.8.3.2 Reactor System and Containment Response Estimates and CORRAL Input Parameters

A MARCH-COCO code combination, described in Section 4, was used to estimate the thermal response of the core, the thermal-hydraulic response of the reactor system, and the thermal and pressure history of the containment. Results of the MARCH-COCO calculations for small and large break initiated transients are discussed in Section 4. A chronology of events for the specific sequences used in the CORRAL calculations are summarized as Figures 5.8.3.2-1 through Figure 5.8.3.2-6.

Indian Point plant specific data input to the CORRAL code are summarized in Table 5.8.3.2-1. In addition, containment leak rate as a function of time is required as input. The leak rate is assumed to vary linearly with pressure from 0.0 volume percent per hour at 14.7 psia to choked flow, i.e., 4.2×10^{-3} volume percent per hour, at 25 psia. The 4.2×10^{-3} volume percent per hour is equal to a 0.1% per day volumetric leak rate. Above 25 psia, the leak rate is assumed to be constant and equal to the choked flowrate.

In this study it was assumed that after containment failure, containment pressure would rapidly fall to ambient conditions. There would be no more than 10% of the airborne fission product inventory remaining in the containment after the venting which accompanies containment failure. For all cases which had any functional safety systems, it was assumed that any steam produced after containment failure would be condensed, the containment pressure would remain at ambient conditions and no leakage would occur. For those cases having no functional safety systems after containment failure, the leak rate was assumed to be equivalent to the production rate of steam and other gases generated within the containment.

If vaporization release occurs, the fission products are assumed to be released to a failed containment at nearly ambient pressure conditions. Gases generated within the containment, largely from debris-concrete basemat interactions, provide the driving force for carrying the fission products from the containment. In the CORRAL calculations for the period after containment failure, the containment is assumed to be a well mixed tank with a leak rate equivalent to the gas production rate within the containment. The MARCH code uses the INTER subroutine to estimate gas generation resulting from debris-concrete interaction. Calculations for this study assumed a concrete with limestone aggregate rather than the largely basaltic aggregate actually used in the Indian Point basemat. Because interaction with basaltic aggregate concrete generates less gas than does interaction with a limestone aggregate concrete, the gas generation rates, the containment leak rates, and the fission product release rates following containment failure used in this study are all conservatively high.

5.8.3.3 Results

Calculated results for fission product release from the containment are listed in Table 5.8.3.3-1 through 5.8.3.3-3.

1. Table 5.8.3.3-1 contains a summary of the overall fraction of core inventory released for four cases assuming that either sprays and fan coolers or fan coolers only are functional. Calculations are performed for an assumed containment failure time of one minute after reactor vessel failure and for cases where containment failure does not occur.

2. Table 5.8.3.3-2 contains a summary of the overall fraction of core inventory released from the containment for four cases assuming neither the spray or fan cooler systems are functional. Calculations are performed for assumed containment failure times of one minute and of four hours after reactor vessel failure. There are calculations for cases with and without a vaporization release component.

3. Table 5.8.3.3-3 contains a summary of overall fractions of core inventory released from containment for five large break cases. Two cases have sprays and fan coolers functional (10 and 11), two cases have only the fan coolers functional (12 and 13), and for the last case neither sprays or fan coolers are functional (case 14). Values listed are for an assumed containment failure time of one minute after reactor vessel failure and for cases where the containment failure does not occur.

5.8.3.4 Discussion

Table 5.8.3.4-1 presents the ratios of fission product releases for cases with both sprays and fan coolers functional to those with only fan coolers functional. Ratios are listed for sequences initiated by small and large pipe breaks, and assume containment failure one minute after reactor vessel failure. The tabulated ratios are identical for small and large breaks. Source releases for iodine are about a factor of 16 lower for cases with sprays functional. For particulates, releases are approximately a factor of 8 lower for cases with functional sprays and fan coolers than for cases with functional fan coolers only.

Table 5.8.3.4-2 presents values of fission product release for cases with functional sprays and fan coolers to those with only functional fan coolers for sequences where containment failure does not occur. Release values for radioiodine for cases with only functional fan coolers are a factor of 6 to 8 higher than for cases with functional sprays and fan coolers. For particulates, release values with only fans functional are a factor of 2.5 to 3 higher than those for cases with both sprays and fan coolers functional.

5.8.3.4 References

1. Burian, R. J., and Cybulski, P., "Corral II Users Manual," Battelle Columbus Laboratories, January 1977.

2. Reactor Safety Study, "An Assessment of Accident Risks in U.S. Commercial Nuclear Power Plants," WASH-1400, October 1975.

3. H. Deuber and J. G. Wilhelm, "Recent Non-Industrial Research and Development in the Federal Republic of Germany Concerning Exhaust Air Cleaning in Nuclear Power Plants", IAEA Moscow 12-16 June, 1979.

4. P. G. Voilleque and J. H. Keller, "Air-to-Vegetation Transport of ^{131}I as Hypoiodous Acid (HOI)", HEALTH PHYSICS, VOL. 40, No. 1, January, 1981.

5. J. G. Knudsen and R. K. Hilliard, "Fission Product Transport by Natural Processes in Containment Vessels, BNWL-943, January, 1969.

6. Rober T. Hemphill et. al., "Surface Effects in the Transport of Airborne Radiodine at Light Water Nuclear Power Plants", EPRI NP-876, September, 1978.

7. A. C. Chamberlain, et. al., - Physical Chemistry of Iodine and Removal of Iodine from Gas Streams, Reactor Science and Technology, Vol. 17, pp. 519-550, 1963.

TABLE 5.8.3.1-1

CASES CONSIDERED IN EVALUATION
OF SOURCE REDUCTION BY
FUNCTIONAL FAN COOLERS

Case 4)	Small break initiated core melt with one spray pump and three fan coolers functional; containment failure 1 minute after reactor vessel failure.
Case 5)	Small break - initiated core melt with one spray pump and three fan coolers functional; containment failure does not occur.
Case 6)	Small break - initiated core melt with no spray pumps functional and three fan coolers functional; containment failure 1 minute after vessel failure.
Case 7)	Small break-initiated core melt with no spray pumps functional and three fan coolers functional; containment failure does not occur.
Case 8)	Small break-initiated core melt with no spray pumps or fan coolers functional; containment failure 1 minute after vessel failure.
Case 9)	Small break-initiated core melt with neither the spray pumps nor fan coolers functional; containment failure assumed 4 hours after reactor vessel failure.

TABLE 5.8.3.1-1 (Continued)

CASES CONSIDERED IN EVALUATION
OF SOURCE REDUCTION BY
FUNCTIONAL FAN COOLERS

Case 10)	Large break-initiated core melt with one spray pump and three fan coolers functional; containment failure 1 minute after reactor vessel failure.
Case 11)	Large break-initiated core melt with one spray pump and three fan coolers functional; containment failure does not occur.
Case 12)	Large break-initiated core melt with no spray pumps functional and three fan coolers functional; containment failure does not occur.
Case 13)	Large break-initiated core melt with no spray pumps functional and with three fan coolers functional; containment failure 1 minute after reactor vessel failure.
Case 14)	Large break-initiated core melt with neithr spray pumps nor fan coolers functional; containment failure 1 minute after vessel failure.

TABLE 5.8.3.2-1

INDIAN POINT PLANT SPECIFIC DATA
INPUT TO THE CORRAL CODE

Parameters	Value
Containment Free Volume	2.61×10^6 ft^3
Wall Area	1.6×10^5 ft^2
Floor Area	2.01×10^4 ft^2
Containment Height	212.5 ft.
Fall Height for Spray	104 ft.
Spray Pump Flow Rate	2500 gpm
Fan Flow Rate Through Particulate Filter (Per Fan)	65000 cfm
Fan Flow Rate Through Charcoal Filter (Per Fan)	8000 cfm
Particulate Filter Removal Rate (3 fans)	4.5 hr^{-1}
Elemental Iodine Filter Removal Rate (3 Fans)	0.496 hr^{-1}
Organic Iodine Filter Removal Rate (3 Fans)	0.386 hr^{-1}

Note: Spray solution includes sodium hydroxide.

TABLE 5.8.3.3-1

FRACTION OF CORE INVENTORY RELEASE FROM CONTAINMENT
FOR SMALL BREAK-INITIATED CORE MELT ACCIDENTS

(REFER TO BOTTOM OF PAGE FOR DESCRIPTION OF CASES)

Fission Product Group	Case 4	Case 5	Case 6	Case 7
Kr-Xe	8.1(-1)	1.5(-2)	8.1(-1)	1.5(-2)
OI	4.9(-3)	5.0(-7)	4.9(-3)	5.0(-7)
I_2-Br	3.1(-2)	4.6(-6)	5.3(-1)	3.7(-5)
Cs-Rb	2.1(-2)	2.9(-6)	1.6(-1)	6.7(-6)
Te	4.1(-3)	5.0(-7)	3.2(-2)	1.2(-6)
Ba-Sr	2.7(-3)	3.3(-7)	2.1(-2)	8.2(-7)
Ru	8.1(-4)	9.9(-8)	6.4(-3)	2.5(-7)
La	8.1(-5)	9.9(-9)	6.4(-4)	2.5(-8)

Note: Numbers in parentheses refer to powers of 10.

Case 4 - One spray pump and 3 fan coolers functional; containment failure 1 minute after vessel failure.

Case 5 - One spray pump and 3 fan coolers functional; containment failure does not occurred.

Case 6 - No spray pumps functional; 3 fan coolers functional; containment failure 1 minute after vessel failure.

Case 7 - No spray pumps functional; 3 fan coolers functional; containment failure does not occur.

TABLE 5.8.3.3-2

FRACTION OF CORE INVENTORY RELEASED FROM CONTAINMENT
FOR SMALL BREAK-INITIATED CORE MELT ACCIDENTS
NO FUNCTIONAL CONTAINMENT SAFETY SYSTEMS

(REFER TO BOTTOM OF PAGE FOR DESCRIPTION OF CASES)

Vaporization Release Component		No Vaporization Release Component	
Case 8	Case 9	Case 8	Case 9
1.0(0)	1.0(0)	9.0(-1)	9.0(-1)
7.0(-3)	7.0(-3)	6.3(-3)	6.3(-3)
8.0(-1)	3.0(-2)	7.0(-1)	9.8(-3)
7.7(-1)	3.4(-1)	6.7(-1)	2.5(-1)
5.8(-1)	4.6(-1)	1.3(-1)	4.7(-2)
9.0(-2)	3.6(-2)	8.4(-2)	3.1(-2)
5.2(-2)	3.4(-2)	2.5(-2)	9.3(-3)
7.9(-3)	5.8(-3)	2.5(-3)	9.3(-4)

Note: Numbers in parentheses refer to powers of 10.

Case 8: When the spray or fan cooler systems are functional;containment assumed to fail 1 minute after reactor vessel failure.

Case 9: Neither spray or fan cooler systems are functional;containment failure assumed 4 hours after reactor vessel failure.

TABLE 5.8.3.3-3

FRACTION OF CORE INVENTORY RELEASED TO THE ENVIRONMENT
FOR LARGE BREAK INITIATED CORE MELT ACCIDENTS

(REFER TO BOTTOM OF PAGE FOR DESCRIPTION OF CASES)

Fission Product Group	Case 10	Case 11	Case 12	Case 13	Case 14
Kr-Xe	8.1(-1)	1.4(-2)	1.0(-2)	8.1(-1)	9.0(-1)
OI	4.2(-3)	6.4(-7)	4.6(-7)	3.5(-3)	6.3(-3)
I_2-Br	6.3(-3)	2.6(-6)	1.7(-5)	9.9(-2)	3.2(-1)
Cs-Rb	3.4(-4)	1.6(-6)	4.3(-6)	2.6(-3)	4.2(-1)
Te	7.2(-5)	2.9(-7)	8.8(-7)	5.6(-4)	8.3(-2)
Ba-Sr	4.8(-5)	1.9(-7)	5.8(-7)	3.8(-4)	5.5(-2)
Ru	1.4(-5)	5.7(-8)	1.8(-7)	1.1(-4)	1.7(-2)
La	1.4(-6)	5.7(-9)	1.8(-8)	1.1(-5)	1.7(-3)

Note: Numbers in parentheses refer to powers of 10.

Case 10 - One spray pump and 3 fan coolers operating; containment fails 1 minute after failure.

Case 11 - One spray pump and 3 fan coolers operating; containment does not fail.

Case 12 - No spray pump and 3 fan coolers operating; containment does not fail.

Case 13 - No spray pump and 3 fan coolers operating; containment fails 1 minute after failure.

Case 14 - No spray pump or fan coolers operating; containment fails 1 minute after vessel failure.

TABLE 5.8.3.4-1

COMPARISON SHOWING EFFECTIVENESS OF FAN COOLERS RELATIVE TO BOTH FAN COOLERS AND SPRAYS FOR CONTAINMENT FAILURE 1 MINUTE AFTER REACTOR VESSEL FAILURE FOR CASES WITH NO VAPORIZATION RELEASE COMPONENT

Fission Product Group	Small Break Case 4 / Case 6	Large Break Case 10 / Case 13
I2-Br	.06	.06
Cs-Rb	.13	.13
Te	.13	.13
Ba-Sr	.13	.13
Ru	.13	.13
La	.13	.13

Case 4 - One spray pump functional; 3 fan coolers functional.

Case 6 - No spray pumps functional; 3 fan coolers functional.

Case 10 - One spray pump functional; 3 fan coolers functional.

Case 13 - No spray pumps functional; 3 fan coolers functional.

TABLE 5.8.3.4-2

COMPARISON SHOWING EFFECTIVENESS OF FAN COOLERS IN REDUCING FISSION PRODUCT RELEASE FOR CASES WHERE CONTAINMENT FAILURE DOES NOT OCCUR

Fission Product Group	Small Breaks: Ratio of Sprays & Fan Cooler / Fan Coolers Only (Case 5 / Case 7)	Large Breaks: Ratio of Sprays & Fan Coolers / Fan Coolers Only (Case 11 / Case 12)
I_2 - Br	0.12	0.15
Cs - Rb	0.43	0.37
Te	0.40	0.33
Ba - Sr	0.40	0.33
Ru	0.40	0.33
La	0.40	0.33

Case 5 - One spray pump and 3 fan coolers functional

Case 7 - No spray pump and 3 fan coolers functional

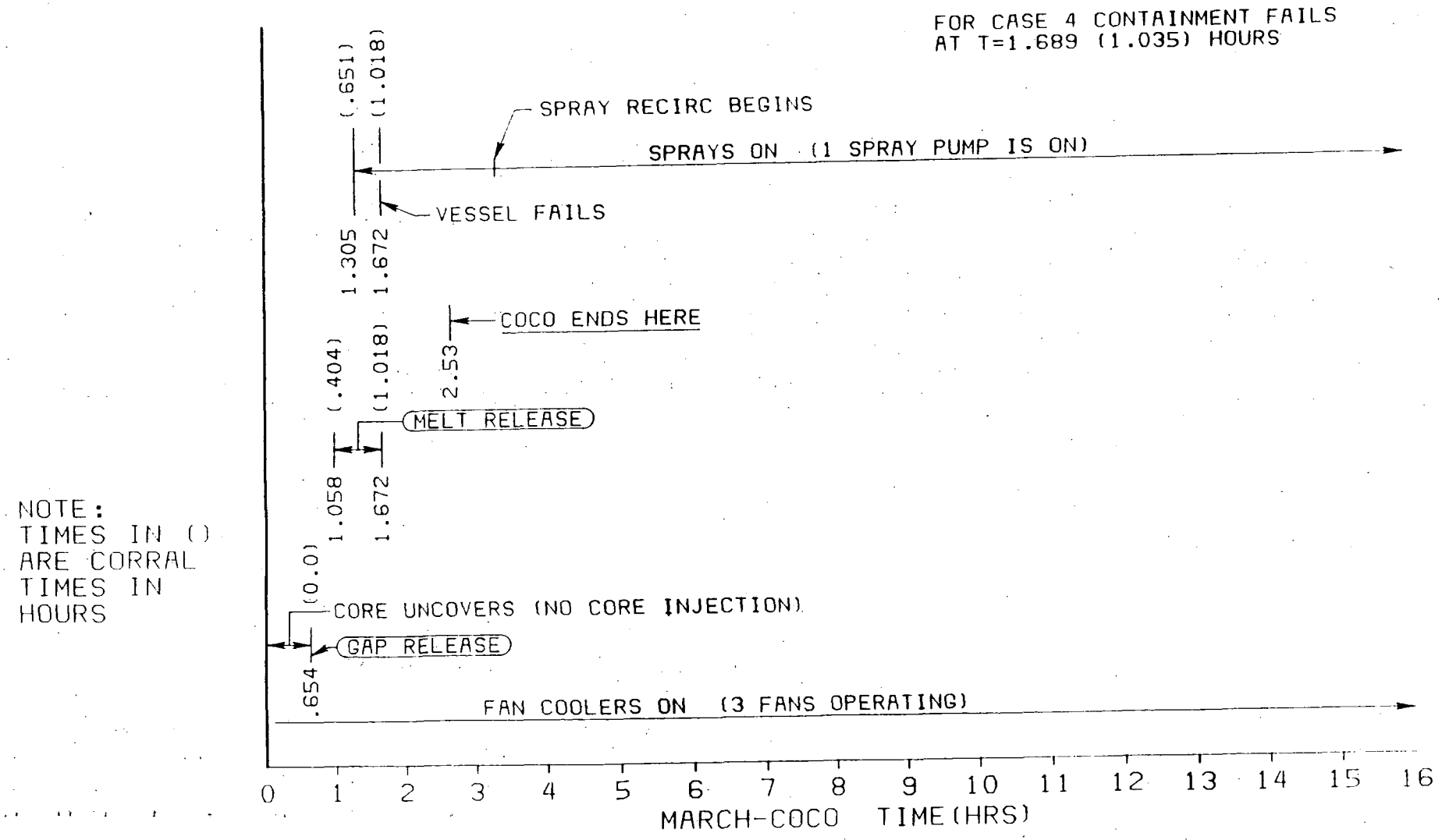
Case 11 - One spray pump and 3 fan coolers functional

Case 12 - No spray pump and 3 fan coolers functional

FIGURE 5.8.3.2-1

CHRONOLOGY OF EVENTS FOR SMALL BREAK INITIATED
CORE MELT ACCIDENT - CASES 4 AND 5

CASE 4 - CONTAINMENT FAILS 1.0 MINUTE AFTER VESSEL FAILS
CASE 5 - CONTAINMENT DOES NOT FAIL

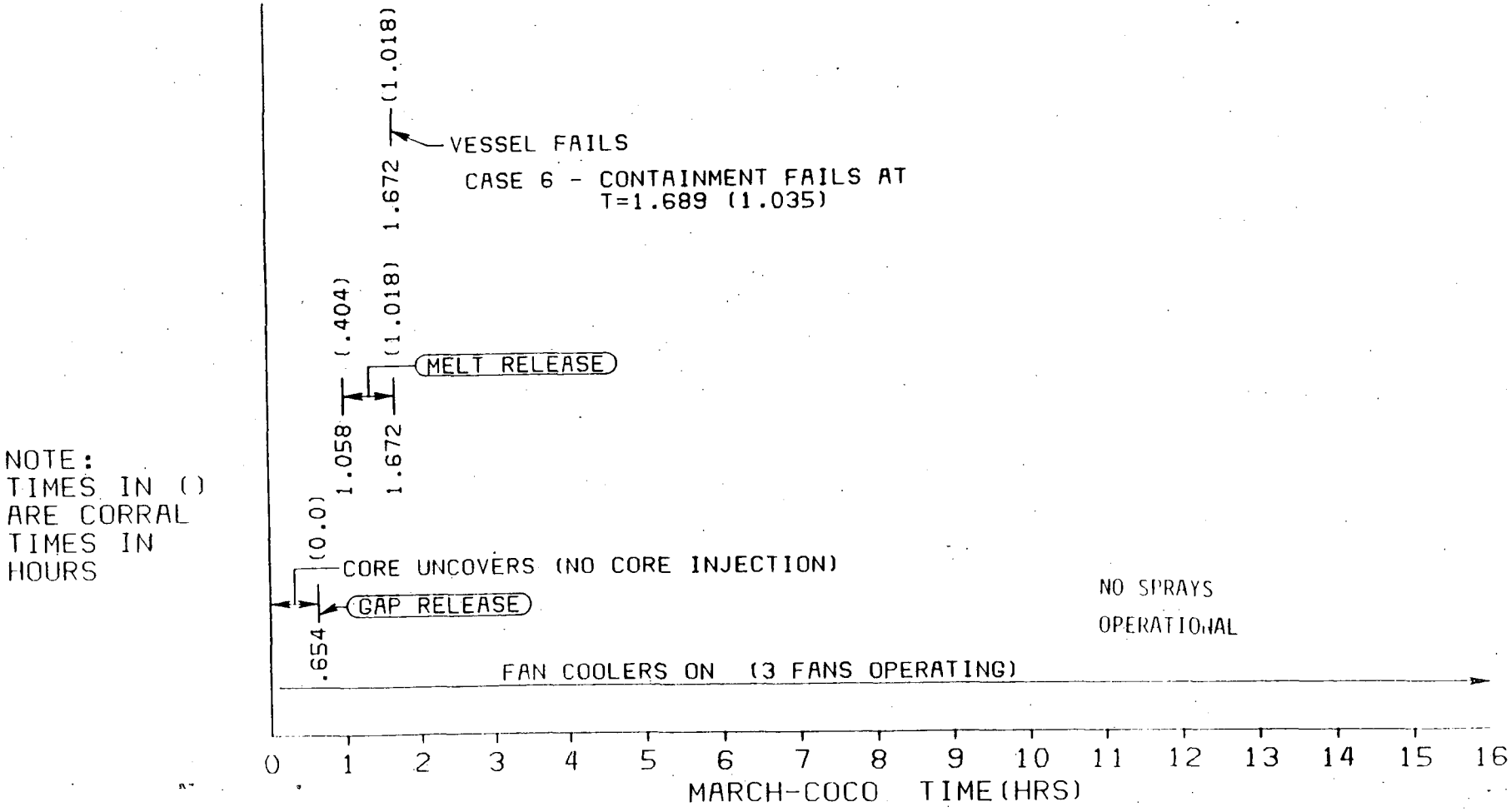


NOTE:
TIMES IN ()
ARE CORRAL
TIMES IN
HOURS

FIGURE 5.8.3.2-2

CHRONOLOGY OF EVENTS FOR SMALL BREAK INITIATED
CORE MELT ACCIDENT - CASES 6 AND 7

CASE 6 - CONTAINMENT FAILS 1.0 MINUTE AFTER VESSEL FAILS
CASE 7 - CONTAINMENT DOES NOT FAIL

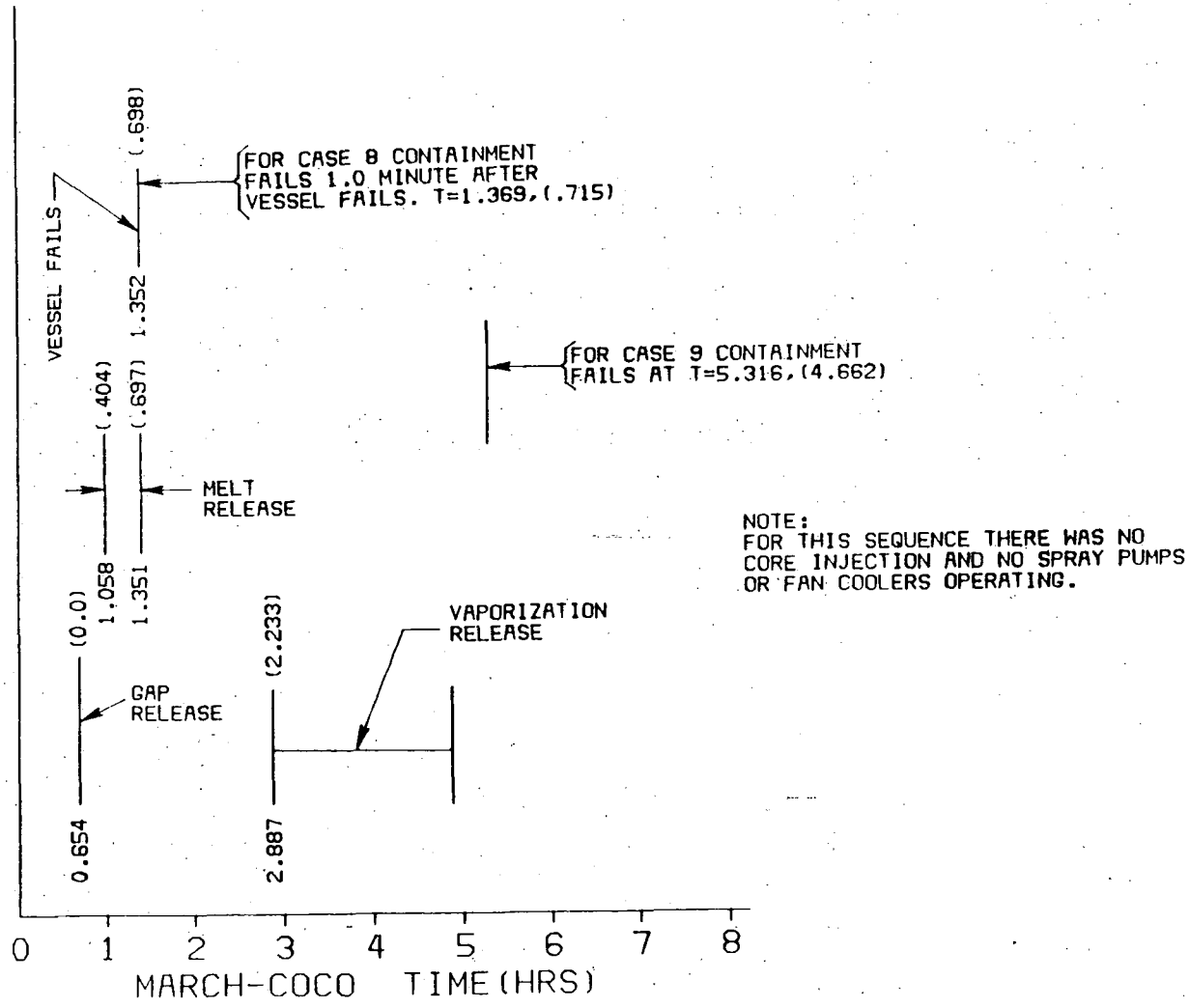


NOTE:
TIMES IN ()
ARE CORRAL
TIMES IN
HOURS

FIGURE 5.8.3.2-3

CHRONOLOGY OF EVENTS FOR SMALL BREAK INITIATED
CORE MELT ACCIDENT - CASES 8 AND 9

CASE 8 - CONTAINMENT FAILS 1.0 MINUTE AFTER VESSEL FAILS
CASE 9 - CONTAINMENT FAILS APPROX 4 HOURS AFTER VESSEL FAILS



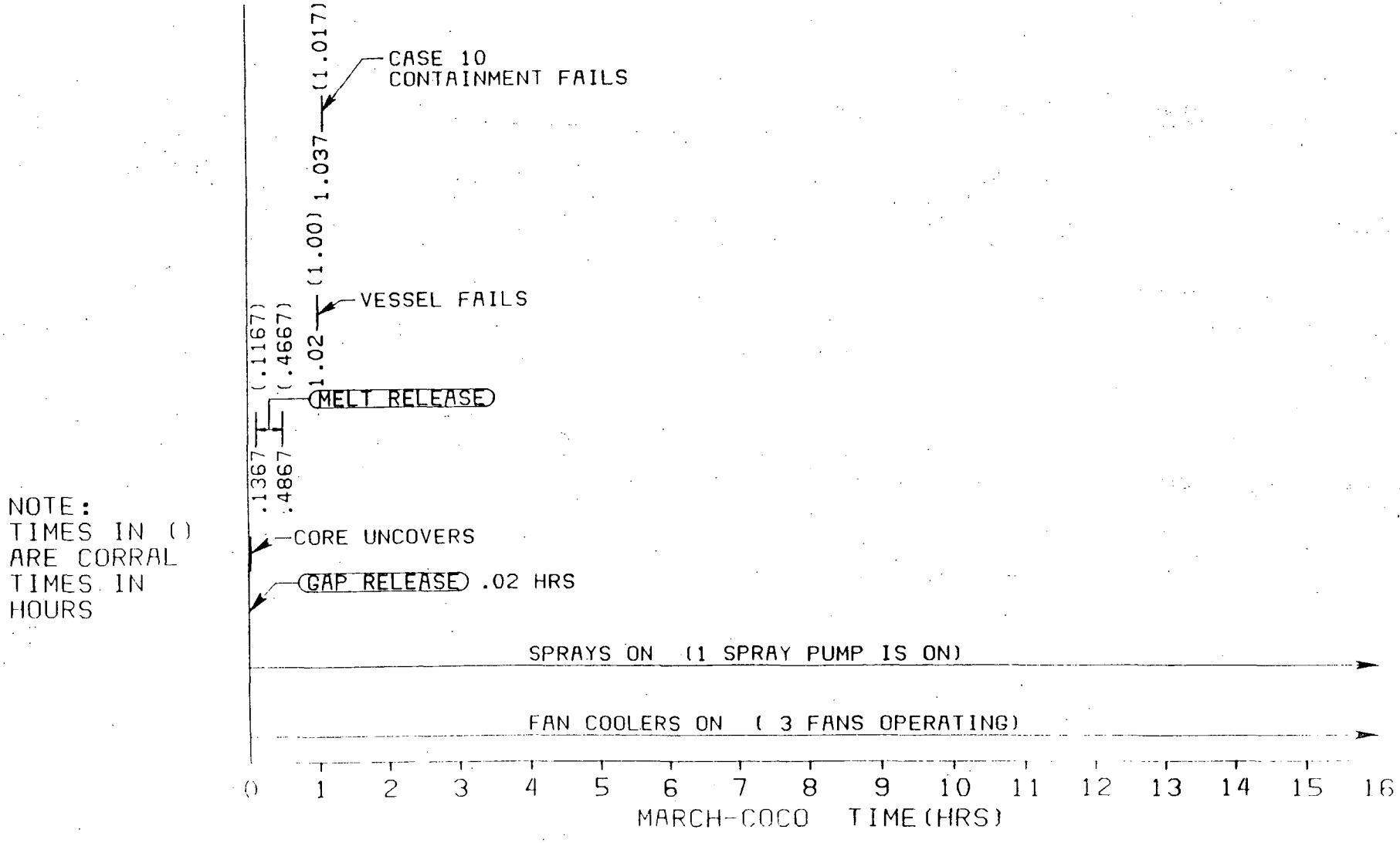
NOTE:
TIMES IN () ARE CORRAL TIMES IN HOURS

NOTE:
FOR THIS SEQUENCE THERE WAS NO CORE INJECTION AND NO SPRAY PUMPS OR FAN COOLERS OPERATING.

FIGURE 5.8.3.2-4

CHRONOLOGY OF EVENTS FOR LARGE BREAK INITIATED
CORE MELT ACCIDENT - CASES 10 AND 11

CASE 10 - CONTAINMENT FAILS 1.0 MINUTE AFTER VESSEL FAILURE
CASE 11 - CONTAINMENT DOES NOT FAIL



NOTE:
TIMES IN ()
ARE CORRAL
TIMES IN
HOURS

FIGURE 5.8.3.2-5

CHRONOLOGY OF EVENTS FOR LARGE BREAK INITIATED
CORE MELT ACCIDENT - CASES 12 AND 13

CASE 12 - CONTAINMENT DOES NOT FAIL
CASE 13 - CONTAINMENT FAILS 1.0 MINUTE AFTER VESSEL FAILS

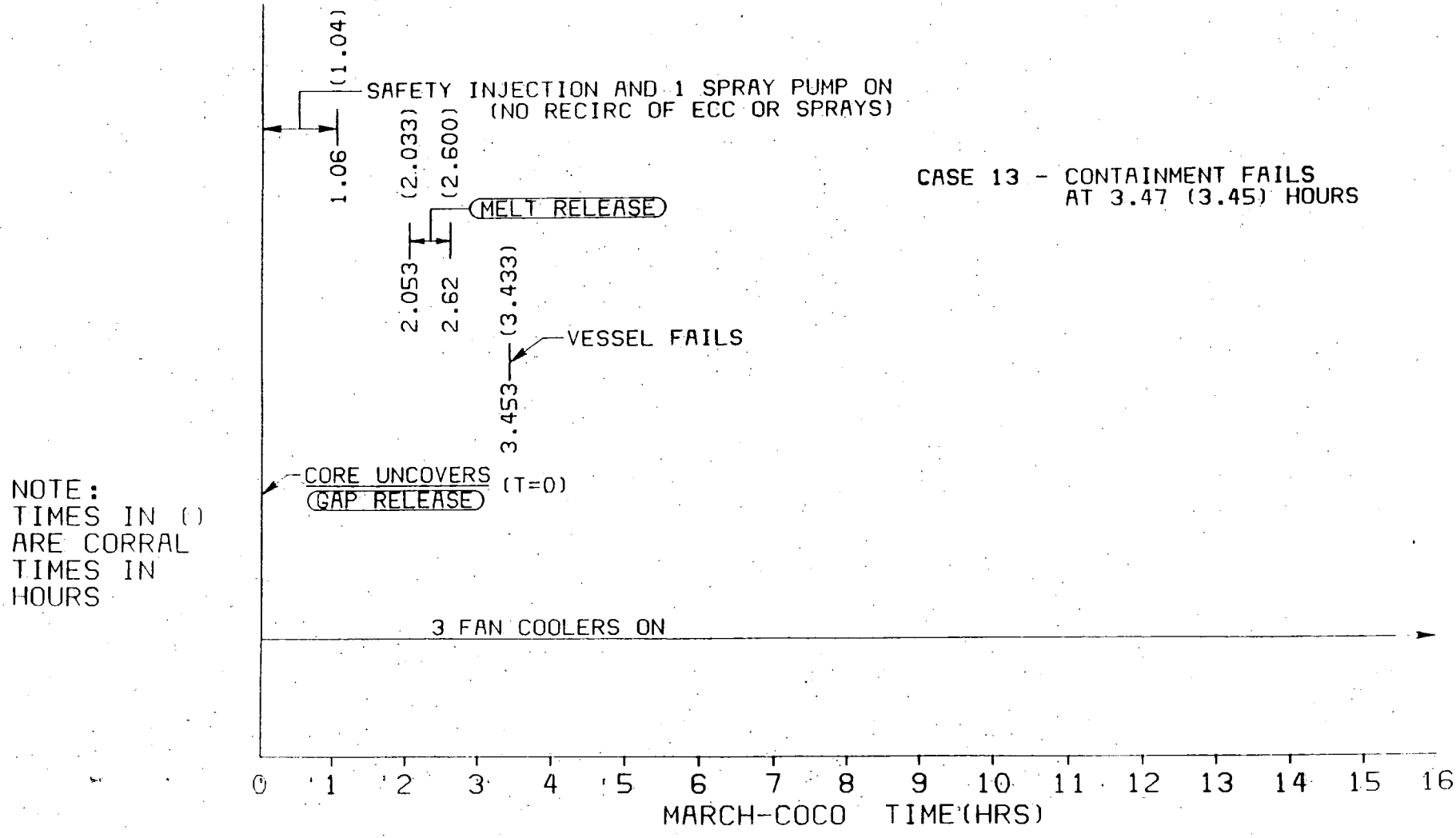
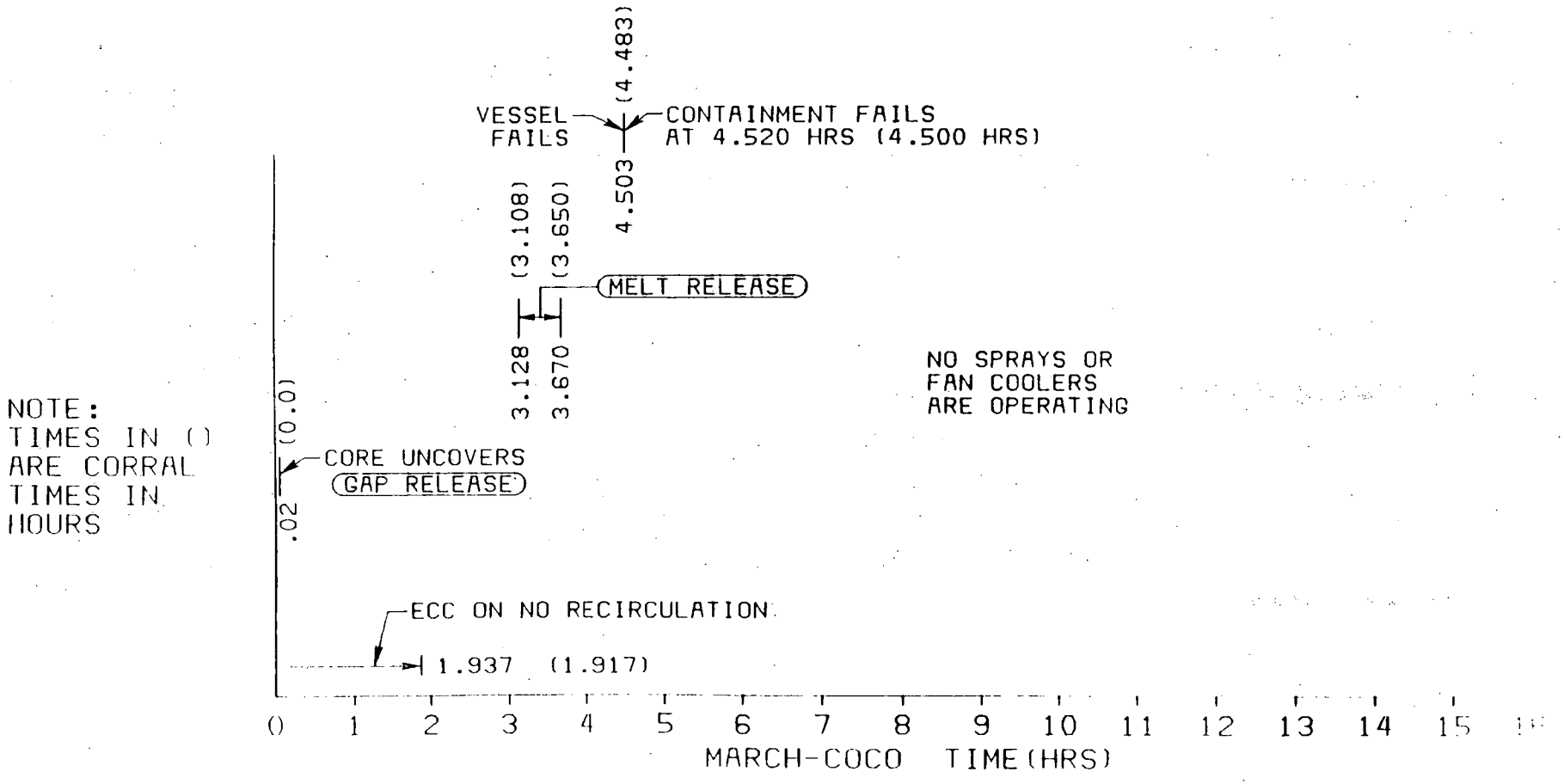


FIGURE 5.8.3.2-6

CHRONOLOGY OF EVENTS FOR LARGE BREAK INITIATED CORE MELT ACCIDENT - CASE 14



APPENDIX 5.8.4

MULTI-PHASE RELEASE SOURCE TERMS FOR RELEASE CATEGORY 2RW AND RELEASE CATEGORY 2 (V SEQUENCE)

APPENDIX 5.8.4

MULTI-PHASE RELEASE SOURCE TERMS FOR RELEASE CATEGORIES 2RW AND 2 (V SEQUENCE)

In performing consequence calculations (with CRAC or CRACIT), it is generally assumed for a particular consequence calculation that the released source is released as a single puff and that the puff follows a single trajectory defined by a single sequence of hourly wind data. The release duration of the puff is taken as one hour in the calculation. Where longer release durations are indicated for a particular release category (as is the case in Table 5.4-3), a plume broadening correction is applied to correct for the additional dispersion but the broadened plume is still assumed to follow a single trajectory for a particular consequence calculation.

As discussed in Section 6.1.2.6, the assumption of a single trajectory is conservatively high for calculating short term consequences (such as early fatalities and early injuries) and particularly so for those weather and wind sequences which lead to higher values for consequences. The higher consequence sequences result from high levels of source deposition on the ground caused by precipitation. If releases actually occur over a number of one hour intervals, there is significant probability the components of the release will follow different trajectories, particularly for the wind and weather sequence which leads to higher values for the early consequence indices.

As a result, a version of CRACIT was developed to permit calculation of consequences for a series of releases that could follow different trajectories. Such source terms were labeled as "multi-phase" source terms and they are used in the "multi-phase" consequence calculations.

Described in this Appendix are multi-phase source terms developed for release category 2RW and for release category 2 assuming a V sequence (failure of valves separating high pressure and low pressure portions of

interfacing systems connected to the reactor coolant system). Calculations and estimates show that enough of the source for the V sequence is released in one hour so that short term consequences calculated assuming either a 1 hour release or a multi-phase release are not significantly different.

5.8.4.1 RELEASE CATEGORY 2RW

CORRAL calculations provide values for source release to the environment as a function of time. These values can be used to specify a multi-phase release source term. For category 2RW, the CORRAL calculation for transient events described in Appendix 5.8.2 was used to derive a multi-phase source. In particular, CORRAL calculations for Case 3 with vaporization release was used for this purpose (see Table 5.8.2.5-2 and Figure 5.8.2.3-1). The data were generated assuming that the containment leak rate is such that containment pressure relief occurs over a period of 3 hours and that vaporization release occurs uniformly over a 2 hour period beginning 2 hours after containment failure. Multi-phase release values are presented in Table 5.8.4-1.

5.8.4.2 RELEASE CATEGORY 2, V SEQUENCE

As part of this study, a set of scoping calculations were performed to determine when loss of cooling capability to the core might occur for a V sequence and to estimate times for onset of melt release and vaporization release from the core melt debris. The calculations were performed with the MARCH code and showed that for a case with all of the low pressure and high pressure injection pumps operating, the water supply in the refueling water storage tank could be exhausted in just less than one hour. For the calculations, it was assumed that the high head pumps delivered water to the reactor vessel while low pressure pumps were discharging out of the broken RHR line. Core melt was calculated to begin in about 105 minutes and to take 20 to 25 minutes so that melt release was completed by about 2 hours into the accident. Sequences with less than a full safeguard complement of pumps operating are, of course, extended in time.

Vaporization release is calculated to begin as early as about 3 hours into the accident and, as for the 2RW sequence, is assumed to occur uniformly over a 2 hour period.

For the purpose of source term estimates, the V sequence which rapidly develops to core melt (maximum safeguards operation) was assumed. Estimates for source term values as a function time developed utilizing the approach described above are presented in Table 5.8.4-2.

TABLE 5.8.4-1

FRACTION OF CORE INVENTORY RELEASED TO ENVIRONMENT IN CONSECUTIVE TIME PERIODS FOR INDIAN POINT

CATEGORY 2RW RELEASE (LATE OVERPRESSURE FAILURE)

	FRACTION OF CORE INVENTORY RELEASED					
ISOTOPE	HOURS* 12-13	HOURS* 13-14	HOURS* 14-15	HOURS* 15-16	HOURS* 16-17	HOURS* 17-21
Kr-Xe	5.06(-1)	2.08(-1)	1.19(-1)	3.14(-2)	2.45(-2)	6.91(-2)
OI	3.54(-3)	1.46(-3)	8.35(-4)	2.20(-4)	1.71(-4)	4.83(-4)
I_2-Br	5.11(-3)	2.42(-3)	2.24(-2)	1.10(-2)	1.02(-2)	2.87(-2)
Cs-Rb	9.97(-2)	3.86(-2)	5.60(-2)	1.94(-2)	1.26(-2)	2.39(-2)
Te	1.85(-2)	9.91(-3)	1.83(-1)	7.43(-2)	4.81(-2)	8.73(-2)
Ba-Sr	1.24(-2)	4.74(-3)	4.08(-3)	1.23(-3)	7.99(-4)	1.60(-3)
Ru	3.71(-3)	1.58(-3)	1.12(-2)	4.45(-3)	2.88(-3)	5.25(-3)
La	3.71(-4)	1.75(-4)	2.17(-3)	8.79(-4)	5.68(-4)	1.03(-3)

* Times are measured from initiation of event. Containment fails at 12 hours. Vaporization begins at 14 hours. Numbers in () refer to powers of 10.

TABLE 5.8.4-2

HOURLY RELEASE ESTIMATES FOR CATEGORY 2(V SEQUENCE)

NORMALIZED TO RSS VALUES

	FRACTION OF CORE INVENTORY RELEASED		
ISOTOPE	HOUR-1	HOUR-2	HOUR-3
Xe-Kr	0.81	0.045	0.045
OI	0.0062	0.00035	0.00035
I2-Br	0.63	0.035	0.035
Cs-Rb	0.405	0.0475	0.0475
Te-Sb	0.0450	0.128	0.128
Ba-Sr	0.0545	0.00273	0.00273
Ru	0.00750	0.00625	0.00625
La	0.000924	0.00154	0.00154

SECTION 6
SITE CONSEQUENCE ANALYSIS

TABLE OF CONTENTS

Section			Page
6.0	OVERVIEW OF SITE CONSEQUENCE ANALYSIS		6.0-1
	6.0.1 Introduction		6.0-1
		6.0.1.1 Atmospheric Pathways	6.0-1
		6.0.1.2 Liquid Pathways	6.0-1
	6.0.2 Summary		6.0.2
6.1	CONSEQUENCE ANALYSIS METHODOLOGY		6.1-1
	6.1.1 Description of Original CRAC Model		6.1-2
		6.1.1.1 Atmospheric Dispersion of Released Material--CRAC	6.1-2
		6.1.1.2 Plume Depletion, Radioactive Decay, and Deposition	6.1-7
		6.1.1.3 Radiation Dose and Health Effects Calculations	6.1-8
		6.1.1.4 Determination of Consequence Frequency Distribution	6.1-13
	6.1.2 Modifications to the CRAC Program		6.1.13
		6.1.2.1 Changes to Site Input Data for CRACIT	6.1-14
		6.1.2.2 Changes to the Spatial Interval Concept for CRACIT	6.1-14
		6.1.2.3 Dispersion Model Changes (DISP and ACTIVE)	6.1-18
		6.1.2.4 Characterization of Plume Trajectory (GRIDOS)	6.1-50
		6.1.2.5 Overlaying the Plume on the Fine Grid (GRIDOS)	6.1-52
		6.1.2.6 Multiple Phase Release Model	6.1-53
		6.1.2.7 Computation of Doses and Health Effects	6.1-53
6.2	SITE SPECIFIC AND PLANT SPECIFIC INPUT INFORMATION		6.2-1
	6.2.1 Site Specific Data		6.2-1
		6.2.1.1 Meteorological Data	6.2-1
		6.2.1.2 Population, Evacuation, and Sheltering Data	6.2-4
		6.2.1.3 Plume Modification Data	6.2-10
		6.2.1.4 Other Site Related Input	6.2-12
	6.2.2 Releases from the Plant		6.2-12
		6.2.2.1 Release Categories	6.2-12
		6.2.2.2 Radioactive Inventory of Reactor Core	6.2-13
6.3	SENSITIVITY STUDIES AND MODEL VERIFICATION		6.3-1
	6.3.1 Model Testing		6.3-1
		6.3.1.1 Straight Line (Single Sequence) Comparisons with CRAC	6.3-1
		6.3.1.2 Selection of Fine Grid Size	6.3-2

TABLE OF CONTENTS (continued)

Section			Page
		6.3.1.3 Determination of Sample Frequency for Meteorological Sequences	6.3-2
		6.3.1.4 Conservation of Plume Area Coverage	6.3-3
	6.3.2	Construction of Risk Curves	6.3-3
		6.3.2.1 Important Parameters	6.3-4
		6.3.2.2 "Tails" Definition	6.3-5
		6.3.2.3 Uncertainty	6.3-6
6.4	RESULTS		6.4-1
6.5	LIQUID PATHWAYS CONSEQUENCES		6.5-1
6.6	REFERENCES		6.6-1
6.7	APPENDIX - ANALYSIS OF LIQUID PATHWAYS CONSEQUENCES DUE TO BASEMAT PENETRATION		6.7-1
	6.7.1	Introduction	6.7-1
	6.7.2	Source Definition and Release Mechanisms	6.7-2
		6.7.2.1 Core Melt and Basemat Penetration	6.7-2
		6.7.2.2 Release Mechanisms	6.7-3
	6.7.3	Groundwater Pathways Analysis	6.7-4
		6.7.3.1 Introduction	6.7-4
		6.7.3.2 Groundwater Hydrology	6.7-4
		6.7.3.3 Analysis of Available Data	6.7-8
		6.7.3.4 Nuclide Release to Groundwater	6.7-11
		6.7.3.5 Summary	6.7-28
	6.7.4	Hudson River Estuary Surface Water Transport	6.7-29
		6.7.4.1 Model Desciption	6.7-29
		6.7.4.2 Solution to Contaminant Transport Model	6.7-32
		6.7.4.3 Data Input to Hudson River Estuary Model	6.7-40
		6.7.4.4 Application of Estuary Model to Indian Point Site	6.7-46
	6.7.5	Pathways Definition	6.7-50
	6.7.6	Dose Assessment	6.7-52
		6.7.6.1 Dosimetry Models and Data	6.7-52
		6.7.6.2 Doses and Health Effects	6.7-52
		6.7.6.3 Sensitivity to Important Parameters	6.7-53
	6.7.7	References	6.7-56

LIST OF TABLES

Table		Page
6.1-1	Classification of Atmospheric Stability Used in Consequence Analysis	6.1-59
6.1-2	Values of Diffusion Coefficients Used in Dispersion Model	6.1-60
6.1-3	Consequence Model Subroutine Inventory	6.1-61
6.1-4	Coarse and Fine Mesh Spacing for Spatial Intervals	6.1-62
6.1-5	Approximate Equivalents to Pasquill-Gifford Stability Classes Used in Numerical Model	6.1-64
6.1-6	Typical Grid Dimensions Used For Numerical Model Calculations	6.1-65
6.1-7	Polar Grid Element Spacing	6.1-66
6.2-1	Meteorological Data Bases--Indian Point	6.2-14
6.2-2	Distribution of Lid Heights from Fort Totten, New York Upper Air Data (1978-1979)	6.2-15
6.2-3A	Joint Frequency Tables--Indian Point, Period of Record from 78080101 to 79073124, Speed and Direction from 122m Level, Temperature Difference Between 122m and 10m for Temperature Difference (Deg F/100 ft) $\leq$ -1.0	6.2-16
6.2-3B	Joint Frequency Tables--Indian Point, Period of Record from 78080101 to 79073124, Speed and Direction from 122m Level, Temperature Difference Between 122m and 10m for Temperature Difference (Deg F/100 ft) > -1.0 but < -0.9	6.2-16
6.2-3C	Joint Frequency Tables--Indian Point, Period of Record from 78080101 to 79073124, Speed and Direction from 122m Level, Temperature Difference Between 122m and 10m for Temperature Difference (Deg F/100 ft) > -0.9 but $\leq$ -0.8	6.2-17
6.2-3D	Joint Frequency Tables--Indian Point, Period of Record from 78080101 to 79073124, Speed and Direction from 122m Level, Temperature Difference Between 122m and 10m for Temperature Difference (Deg F/100 ft) > -0.8 but < -0.3	6.2-17
6.2-3E	Joint Frequency Tables--Indian Point, Period of Record from 78080101 to 79073124, Speed and Direction from 122m Level, Temperature Difference Between 122m and 10m for Temperature Difference (Deg F/100 ft) > -0.3 but $\leq$ -0.8	6.2-18
6.2-3F	Joint Frequency Tables--Indian Point, Period of Record from 78080101 to 79073124, Speed and Direction from 122m Level, Temperature Difference Between 122m and 10m for Temperature Difference (Deg F/100 ft) > -0.8 but < -2.2	6.2-18
6.2-3G	Joint Frequency Tables--Indian Point, Period of Record from 78080101 to 79073124, Speed and Direction from 122m Level, Temperature Difference Between 122m and 10m for Temperature Difference (Deg F/100 ft) > -2.2	6.2-19

LIST OF TABLES (continued)

Table		Page
6.2-4A	Joint Frequency Tables--Indian Point, Period of Record from 78080101 to 79073124, Speed and Direction from 10m Level, Temperature Difference Between 61m and 10m for Temperature Difference (Deg F/100 ft) ≤ -1.0	6.2-20
6.2-4B	Joint Frequency Tables--Indian Point, Period of Record from 78080101 to 79073124, Speed and Direction from 10m Level, Temperature Difference Between 61m and 10m for Temperature Difference (Deg F/100 ft) > -1.0 but ≤ -0.9	6.2-20
6.2-4C	Joint Frequency Tables--Indian Point, Period of Record from 78080101 to 79073124, Speed and Direction from 10m Level, Temperature Difference Between 61m and 10m for Temperature Difference (Deg F/100 ft) > -0.9 but ≤ -0.8	6.2-21
6.2-4D	Joint Frequency Tables--Indian Point, Period of Record from 78080101 to 79073124, Speed and Direction from 10m Level, Temperature Difference Between 61m and 10m for Temperature Difference (Deg F/100 ft) > -0.8 but ≤ -0.3	6.2-21
6.2-4E	Joint Frequency Tables--Indian Point, Period of Record from 78080101 to 79073124, Speed and Direction from 10m Level, Temperature Difference Between 61m and 10m for Temperature Difference (Deg F/100 ft) > -0.3 but ≤ -0.8	6.2-22
6.2-4F	Joint Frequency Tables--Indian Point, Period of Record from 78080101 to 79073124, Speed and Direction from 10m Level, Temperature Difference Between 61m and 10m for Temperature Difference (Deg F/100 ft) > -0.8 but ≤ -2.2	6.2-22
6.2-4G	Joint Frequency Tables--Indian Point, Period of Record from 78080101 to 79073124, Speed and Direction from 10m Level, Temperature Difference Between 61m and 10m for Temperature Difference (Deg F/100 ft) > -2.2	6.2-23
6.2-5	Indian Point--Population (0 - 50 miles), (Weekday, School in Session)	6.2-24
6.2-6	Indian Point--Night Population (0 - 50 miles)	6.2-27
6.2-7	Indian Point--Population Distribution Estimate	6.2-30
6.2-8	Indian Point--Evacuation Vectors (Weekday, School in Session)	6.2-31
6.2-9	Indian Point--Example of Evacuation Speed by Population Grid Element	6.2-40
6.2-10	Indian Point--Example of Average Speed Along Evacuation Paths for Evacuees Starting in Each Population Segment	6.2-41
6.2-11	Indian Point--Example of Time Along Evacuation Path for Evacuees Starting in Each Population Segment	6.2-43

LIST OF TABLES (continued)

Table		Page
6.2-12	Indian Point--Example of Distance Along Evacuation Path for Evacuees Starting in Each Population Segment	6.2-45
6.2-13A	Indian Point--Summary of Evacuation Data (Night)	6.2-47
6.2-13B	Indian Point--Summary of Evacuation Data (Weekday, School in Session)	6.2-48
6.2-13C	Indian Point--Summary of Evacuation Data (Weekday, School Out)	6.2-49
6.2-13D	Indian Point--Summary of Evacuation Data (Winter Holiday)	6.2-50
6.2-13E	Indian Point--Summary of Evacuation Data (Summer Holiday)	6.2-51
6.2-14	Characteristics of the 288 Randomly Selected Meteorological Sequences - Indian Point	6.2-52
6.2-15	Indian Point--Terrain Heights	6.2-53
6.2-16	Indian Point--Source Term Release Categories	6.2-54
6.2-17	Indian Point--Source Term Category Release Fractions	6.2-55
6.3-1	Comparison of Single Sequence Straight-Line-Plume Results from CRACIT Versus CRAC for Five Effects	6.3-8
6.3-2	Comparison of Results Using Three Azimuthal Grid Spacings and 96 Meteorological Sequences	6.3-9
6.7-1	Radionuclide Source Inventories and Release Fractions for Selected Nuclides	6.7-60
6.7-2	Initial Radionuclide Source Inventories and Estimated Distribution Coefficients for Groundwater Transport in Limestone	6.7-61
6.7-3	Values of Log Mean and Log Standard Deviation of Travel Times in Days of Nuclides from Indian Point 3 to the Hudson River for Several Values of Distribution Coefficients and Varying Uncertainty Assumptions About Hydrologic Parameters	6.7-62
6.7-4	Discharge Rates of Selected Nuclides to the River at Various Times Following Sump Water Release	6.7-63
6.7-5	Final Composition of Melts	6.7-67
6.7-6	Summary of Leach Constants and of Parameters by Which They Were Estimated	6.7-68
6.7-7	Discharge Rates of Selected Nuclides to the River at Various Times from Core Melt Leaching	6.7-69
6.7-8	Time and Space Step Criteria for Finite Difference Solution Schemes	6.7-73
6.7-9	Parameter Values for Validation Studies	6.7-74
6.7-10	Hudson River Cross-Sectional Areas	6.7-75
6.7-11	Mean Hudson River Freshwater Flow Rate in CFS	6.7-76
6.7-12	Data for Taylor Dispersion Calculations	6.7-77
6.7-13	Tidally Averaged Diffusivity Data in Square Miles Per Day	6.7-78
6.7-14	Radionuclide Distribution Coefficients for the Hudson River Estuary	6.7-79

LIST OF TABLES (continued)

Table		Page
6.7-15	Results of Steady State, Pu-239 Sensitivity Analysis Calculations for Each Month Table Entries Are Normalized Concentrations in Curies Per Cubic Mile Per CI/Yr Released	6.7-80
6.7-16	Results of Steady State, Pu-239 Sensitivity Analysis Calculations for Special Conditions Table Entries Are Normalized Concentrations in Curies Per Cubic Mile Per CI/Yr Released	6.7-82
6.7-17	Summary of Dissolved Radionuclide Concentration Computer Runs	6.7-84
6.7-18	Hudson River Usage for Drinking Water	6.7-85
6.7-19	Hudson River and Ocean Beach Usage	6.7-86
6.7-20	Population Fed by Hudson River Aquatic Biota	6.7-87
6.7-21	Hudson River Aquatic Finfish and Shellfish Annual Yields	6.7-88
6.7-22	Maximum Doses to Individuals	6.7-89
6.7-23	Population Doses	6.7-90

LIST OF FIGURES

Figure		Page
6.1-1	CRAC and CRACIT Consequence Assessment	6.1-67
6.1-2	Top View of the Straight Line Lateral Plume Dispersion Model--CRAC	6.1-68
6.1-3	Illustration of Vertical Plume Dispersion Model--CRAC	6.1-69
6.1-4	Simplified Illustration of Interdiction Model	6.1-70
6.1-5	Changes in Flow of the Main Routine in the Consequence Model (CRACIT)	6.1-71
6.1-6	Example of Spatial Interval Distances for Typical Weather Sequence	6.1-72
6.1-7	Schematic Flow Diagram for Subroutine SPEDIT	6.1-73
6.1-8	Logic for First Spatial Interval	6.1-74
6.1-9	Schematic of Calculation Approach for Modified Potential Flow Terrain Model	6.1-76
6.1-10	Schematic Representation of Plume Undergoing TIBL Fumigation	6.1-77
6.1-11	Schematic Illustration of Method for Running CRACIT After Completion of Off-Line Plume Editing Process	6.1-78
6.1-12	Schematic Flow Diagram for Subroutine GRIDOS	6.1-79
6.1-13	Illustration of Plume Shape Definition in GRIDOS	6.1-80
6.1-14	Illustration of Plume and Evacuation Paths on Fine Grid	6.1-81
6.1-15	Schematic Flow Diagram of Damage Calculation Subroutines in CRACIT	6.1-82
6.1-16	Relation Between Population Grid Elements and Fine Grid Elements	6.1-83
6.2-1	Indian Point Meteorological Regions	6.2-56
6.2-2	Indian Point 122m Wind Rose	6.2-57
6.2-3	Indian Point 10m Wind Rose	6.2-58
6.2-4	Flow Diagram for Site Meteorological Data Processing Via CRACIN Routine	6.2-59
6.2-5	Model for Estimating Lid Height	6.2-60
6.2-6	Example of Evacuation Vectors--Indian Point	6.2-61
6.2-7	Representation of Terrain Surrounding the Indian Point Site	6.2-62
6.2-8A	Example of Plume Track After Edit (Early Morning, Down River Valley Flow--Low Level Release)	6.2-63
6.2-8B	Example of Plume Track Before Edit (Early Morning, Down River Valley Flow--Low Level Release)	6.2-64
6.2-9A	Example of Plume Track After Edit (Low Wind Speed, Up-Valley Flow Confined by Terrain--Low Level Release)	6.2-65
6.2-9B	Example of Plume Track Before Edit (Low Wind Speed, Up-Valley Flow Confined by Terrain--Low Level Release)	6.2-66
6.2-10A	Example of Plume Track After Edit (Elevated Release Out of Valley Influence)	6.2-67
6.2-10B	Example of Plume Track Before Edit (Elevated Release Out of Valley Influence)	6.2-68

LIST OF FIGURES (continued)

Figure		Page
6.3-1	Comparison of Acute Fatalities from CRACIT Runs Using Three Different Azimuthal Grid Spacings	6.3-10
6.3-2	Comparison of Injuries from CRACIT Runs Using Three Different Azimuthal Grid Spacings	6.3-11
6.3-3	Comparison of Acute Fatalities Results Using Different Sets of Meteorological Sequences--IP Release Category 2	6.3-12
6.3-4	Comparison of Injuries Results Using Different Sets of Meteorological Sequences--IP Release Category 2	6.3-13
6.3-5	Comparison of Whole Body Man-Rem Results Using Different Sets of Meteorological Sequences--IP Release Category 2	6.3-14
6.4-1	Conditional Consequence Curves for Various Release Categories--Damage Index: Acute Fatalities	6.4-2
6.4-2	Conditional Consequence Curves for Various Release Categories--Damage Index: Injuries	6.4-3
6.4-3	Conditional Consequence Curves for Various Release Categories--Damage Index: Thyroid Cancer Cases	6.4-4
6.4-4	Conditional Consequence Curves for Various Release Categories--Damage Index: Cancer Fatalities (other than those from Thyroid Cancers)	6.4-5
6.4-5	Conditional Consequence Curves for Various Release Categories--Damage Index: Whole Body Man-Rem	6.4-6
6.7-1	Indian Point Liquid Pathways Analysis Schematic	6.7-91
6.7-2	Base Map of the Indian Point Reactor Site	6.7-92
6.7-3	Base Map of Indian Point Showing the Extent of the Limestone and the Potentiometric Surface in the Aquifer	6.7-93
6.7-4	Finite-Difference Grid Used to Simulate the Indian Point Flow Field Showing Regions Where Recharge Was Varied	6.7-94
6.7-5	Comparison of Computer Potentiometric Surface with that Observed	6.7-95
6.7-6	Histogram of Travel Times Computed by Monte Carlo Simulation for Known Porosity and Uncertain Hydraulic Conductivity	6.7-96
6.7-7	Histogram of Travel Times Computed by Monte Carlo Simulation for Uncertain Hydraulic Conductivity with Porosity Proportional to the Square Root of Hydraulic Conductivity	6.7-97
6.7-8	Histogram of Travel Times Computed by Monte Carlo Simulation for Uncertain and Independent Hydraulic Conductivity and Porosity	6.7-98
6.7-9A	Distribution of Trace from Sump Water Release in Groundwater (Time = 20 Days and 40 Days)	6.7-99
6.7-9B	Distribution of Trace from Sump Water Release in Groundwater (Time = 80 Days and 126 Days)	6.7-100
6.7-9C	Distribution of Trace from Sump Water Release in Groundwater (Time = 200 Days and 300 Days)	6.7-101

LIST OF FIGURES (continued)

Figure		Page
6.7-9D	Distribution of Trace from Sump Water Release in Groundwater (Time = 400 Days)	6.7-102
6.7-10	Variation of Discharge Rate to the River with Time of a Tracer in Sump Water Release	6.7-103
6.7-11	Discharge Rates of Selected Nuclides to River as Functions of Time Following a Sump Water Release Event	6.7-104
6.7-12	Comparison of Leach Constants Calculated Assuming Different Controlling Mechanisms	6.7-105
6.7-13	Discharge Rates of Selected Nuclides to River as Functions of Time from Core Melt Leaching	6.7-106
6.7-14	Steady State Solution for Pu-239 (No Decay) for Unit Intensity Source at x_0 = 75 Miles	6.7-107
6.7-15A	Steady State Solution for I-131 for Unit Intensity Source at x_0 = 75 Miles	6.7-108
6.7-15B	Steady State Solution for I-131 for Unit Intensity Source at x_0 = 75 Miles	6.7-109
6.7-16	Steady State Solution for SR-89 for Unit Intensity Source at x_0 = 75 Miles	6.7-110
6.7-17A	Transient (Nonsteady State) Solution for Ru-103 at 0.05 Years for Unit Intensity Source at x_0 = 75 Miles	6.7-111
6.7-17B	Transient (Nonsteady State) Solution for Ru-103 at 0.10 Years for Unit Intensity Source at x_0 = 75 Miles	6.7-112
6.7-17C	Transient (Nonsteady State) Solution for Ru-103 at 0.15 Years for Unit Intensity Source at x_0 = 75 Miles	6.7-113
6.7-17D	Transient (Nonsteady State) Solution for Ru-103 at 0.25 Years for Unit Intensity Source at x_0 = 75 Miles	6.7-114
6.7-18	Hudson River Salt Intrusion Curves	6.7-115
6.7-19	Results of Steady State, Pu-239 Sensitivity Analysis Calculations Downstream of Indian Point (MP43) for Each Month	6.7-116
6.7-20	Results of Steady State, Pu-239 Sensitivity Analysis Calculations Downstream of Indian Point (MP43) for Special Conditions	6.7-117
6.7-21	Population Dose (Man-Rem) as a Function of Time Due to a Release to the Liquid Pathways	6.7-118

SECTION 6

SITE CONSEQUENCE ANALYSIS

6.0 OVERVIEW OF SITE CONSEQUENCE ANALYSIS

6.0.1 INTRODUCTION

Each of the major postulated accident scenarios identified in this study has a release of radioactive material associated with its occurrence. Releases were assumed to be to the atmosphere and for "basemat melt through" cases to the ground water. Thus, both atmospheric and liquid pathways were considered. Each atmospheric release scenario was assigned to one of several "release categories" based on the core and containment responses to the accident conditions. The objective of the consequence portion of this analysis is to estimate the potential for health effect impact on the surrounding population due to exposure to the releases assigned to each release category.

6.0.1.1 Atmospheric Pathways

The atmospheric release portion of this section is done in a probabilistic manner. Assuming that an atmospheric release occurs at any random time, a number of factors would cause the consequences to vary. The most important factors affecting this variation are related to the weather conditions that exist during the release. Wind speed, wind direction, atmospheric turbulence, and rainfall dictate the area contaminated and the amount of radioactive material in the plume. Once the distribution of airborne and deposited radioactive material is defined in the environment as a function of time, an estimate of health effects can proceed. Many individual weather condition scenarios were studied to determine the probability of five selected health effects occurring. The calculation procedure shown in the block diagram of Figure 6.1-1 is repeated for each meteorological sequence.

To compute the impact on the health of individuals or population groups, information related to their locations and travel paths during evacuation with respect to the location of the radioactive plume must be characterized. The degree of radiation exposure is dependent not only on time of exposure to the plume or deposited material on the ground but also on the shielding provided by dwellings and/or other protective measures taken.

Once the frequency of occurrence of selected health effects has been established for each atmospheric release category, these results are combined with the frequency of occurrence of the release category. This is done to determine the overall potential impact on health (expressed as risk curves).

6.0.1.2 Liquid Pathways

The liquid pathways analysis was performed to assess the consequences of a release of radioactive material from a postulated failure of the

containment basemat through the local groundwater system and into the Hudson River. Numerical computer models were used to determine the time it takes for the released material to reach the river, the amount of material entering the river as a function of time, and the resulting doses accounting for the dilution and buildup in the environment.

6.0.2 SUMMARY

Calculations using the Calculation of Reactor Accident Consequences Including Trajectories (CRACIT) model were made for all identified atmospheric release categories. Emphasis was placed on those release categories that had a higher frequency of occurrence. Several release categories initially identified in the RSS were determined to have a very low frequency of occurrence and were not used in the final assembly of the total risk curves (see Section 8). The major conditional risk curves are plotted and displayed as part of Section 6.4.

Calculations for liquid pathways were also performed. However, since the atmospheric releases lead to much higher consequences, the results were not presented in a probabilistic manner in Section 8.

The consequence section is divided into six subsections. Details of the atmospheric consequence computer model are found in Section 6.1, and site specific input characteristics for this model are presented in Section 6.2. A series of sensitivity and model tuning studies was made as reported in Section 6.3. Results from this study are presented in Section 6.4. The details of the liquid pathways are presented in Sections 6.5 and 6.7. References are listed in Section 6.6.

6.1 CONSEQUENCE ANALYSIS METHODOLOGY

The principal model used was an extensively modified version of the Calculation of Reactor Accident Consequences (CRAC) computer program developed by the U.S. Nuclear Regulatory Commission during the Reactor Safety Study (RSS). It was reported in the RSS (NUREG-75/014). The CRAC dose model is complex since it is based on many different scientific and medical disciplines. A complete description of the model appears in Appendix VI of the RSS (Reference 6-1). Rather than repeat information already available, program descriptions in this study will be supplemented by frequent references to Appendix VI of the RSS.

The CRAC program, as it existed for the RSS, was intended for use in computing the overall risk from a number of nuclear plants in different regions throughout the United States. However, the present study analyzes consequences specific to the site. Therefore, it was necessary to modify the CRAC program to treat specific site conditions adequately and realistically. The modified version uses variable direction plume trajectories and incorporates a variable direction evacuation scheme. CRAC models both plume travel and evacuation path in straight lines extending radially outward from the plant. The modified version of CRAC, referred to as CRACIT, is detailed in in Section 6.1.2. CRACIT also incorporates processing to compute results for up to four "multi-phased" releases to more realistically estimate consequences for longer duration releases.

A probabilistic approach is used to compute consequences such as early death and early injury, and long term mortality from given hypothetical releases. Meteorological data measured at the site and in the site region were an important input. Assumed accident start dates were selected randomly in sets so that release start times were uniformly distributed over all months. Each month had the same number of day and night samples. The radiation dose calculation portion of the CRACIT consequence model was essentially unchanged from that used in the RSS.

As part of this safety assessment, CRACIT combines a series of mathematical and statistical models. It utilizes an inventory of radioisotopes which are assumed to be released from the plant to the environment for each type of accident release category as input. Basic functions of the program include calculation of meteorological dispersion of the released radioactive material as it travels downwind and estimation of the effects this material could have on the health of the surrounding population. Each CRACIT run uses a continuous series of measured hourly meteorological conditions. A set of runs with randomly selected start times is made to form a probability distribution. Estimated health effects, computed from the simulations of radiation exposure, are combined to form frequency distributions of consequences versus probability for a given hypothetical accident. Program libraries include detailed site specific information on meteorology and seasonal population.

CRACIT calculates health effect consequences for each release category using random samples of sequential meteorological conditions. Each consequence (e.g., health effect) set has a frequency of occurrence

associated with it. In general, this frequency is obtained by multiplying the frequency of occurrence of release category by the frequency of the consequence calculated from meteorological scenario sampling. Details on the determination of risk curves is provided in Section 8. It should be noted that in CRACIT, wind direction frequency is accounted for in each meteorological sequence and is not treated separately as it was in CRAC. Therefore, the term "probability of population" which was dependent on wind direction in CRAC is not included. After the frequencies of all consequence sets have been calculated, they are combined to yield an overall frequency distribution of consequences versus probability. For this study, conditional probability distributions are also given separately for each release category in Section 6.4. Figure 6.1-1 is a schematic flow diagram of the CRAC program.

Section 6.1.1 summarizes the original CRAC program. Section 6.1.2 details the modifications made in developing CRACIT. A description of the CRAC model is presented here, since an understanding of the code is fundamental for evaluation of the modifications made in formulating CRACIT.

6.1.1 DESCRIPTION OF ORIGINAL CRAC MODEL

As discussed in Section 5, the spectrum of postulated releases to the environment is classified into core melt release categories. The frequency of occurrence of each of these release categories has been estimated in Section 8. Uncertainties in the source term are discussed in Section 5.

For a given release, the meteorological model in CRACIT computes near-ground air concentration and ground deposition of released radioactive material by distance and direction from the plant. This information is then used to compute external irradiation from the passing cloud and material deposited on the ground, irradiation from inhaled radionuclides, and from ingestion of radionuclides from contaminated food. These different modes of exposure and the corresponding dosimetric models are discussed in detail in Appendix VI of the RSS.

Summaries of the plume dispersion and depletion and dosimetric models follow in Sections 6.1.1.1 through 6.1.1.3. Determination of consequence frequency distributions is discussed in Section 6.1.1.4.

6.1.1.1 Atmospheric Dispersion of Released Material--CRAC

The plume of radioactive material released from an assumed accident is carried away from the plant by the wind. The volume of air into which the plume is initially diluted and the plume speed are determined by the wind speed at plume level. The amount of turbulence in the atmosphere in which the plume is dispersed determines its dilution and dimensions versus time and distance. In CRAC, plume travel is assumed to be in a straight line. The chance that the plume will be in any one of 16 direction sectors with the corresponding wind speed and stability conditions is taken to be proportional to the fraction of time that the wind blows into that sector based on annual wind rose data. Atmospheric

stability (characterizing air turbulence) is determined from vertical temperature difference data measured at the site and from offsite meteorological observations. Rainfall is important in defining the extent of removal (or washout) of material from the plume. The CRAC program requires only wind speed, stability, and rainfall data as input.

The atmospheric dispersion model is described in Appendix A of Appendix VI to the RSS. An accident starting time is specified for each run. This defines the sequence of precipitation occurrence, stability category, and wind speed necessary to calculate plume movement and dimensions. It also determines values of air concentration and deposition versus time, distance, and direction from the plant. The calculations for each hour apply for one or more spatial intervals (SIs). Spatial intervals in CRAC are fixed at predetermined distances downwind. The spatial interval is converted to a trapezoidal area in which the width is based on atmospheric dispersion conditions and release duration, representing the cloud path segment. The radial dimension of an interval becomes larger with increasing distance from the plant. The plume path is represented by the time it takes to pass through the preselected intervals. The radial boundaries of each spatial interval coincide with those used in defining the population distribution. The air concentrations and ground deposits of the released radioactivity are computed at the midpoint of each spatial interval and are assumed to be uniform within it.

The plume dispersion (X/Q, defined below) is determined for a simple ground level continuous release. Concentrations that allow for building wake effects, buoyant plume rise, differences in release duration for the release category, and depletion by dry and wet deposition as well as radioactive decay are then calculated. At the midpoint of each spatial interval, the ratio of ground level contaminant concentration in the air to the source strength is given by a modified Gaussian plume model derived as follows:

1. Wind speed is steady, unidirectional (in x direction), and independent of spatial coordinates.

2. Dispersion in the direction of the wind is negligible compared to convection in that direction.

3. The origin of coordinates is at the ground and at a point whose crosswind, y, and downwind, x, components are defined to be $(x,y) = (0,0)$.

For a point source of strength Q, the flux, XU, in the downwind direction of a contaminant dispersing in an infinite medium, is given by

$$XU = Q P_y P_z \qquad (6.1\text{-}1)$$

where

X = concentration

U = wind velocity

P_y = the probability density function of particle (fluid point) locations in the crosswind direction

P_z = the probability density function of particle (fluid point) locations in the vertical direction

If the probability densities are assumed to be Gaussian, then

$$P_y = \frac{1}{\sqrt{2\pi}\sigma_y} \exp - \frac{1}{2}\left(\frac{y-\bar{y}}{\sigma_y}\right)^2 \tag{6.1-2}$$

$$P_z = \frac{1}{\sqrt{2\pi}\sigma_z} \exp - \frac{1}{2}\left(\frac{z-\bar{z}}{\sigma_z}\right)^2 \tag{6.1-3}$$

for a point source located at $(x,y,z) = (0,\bar{y},\bar{z})$.

Let us assume that the point source is located at the origin of x and y, but at a distance H above the origin of z, then $\bar{y}=0$, $\bar{z}=H$. Combining Equations (6.1-1), (6.1-2), and (6.1-3) results in

$$XU = \frac{Q}{\sqrt{2\pi}\sigma_y \sqrt{2\pi}\sigma_z} \exp - \frac{1}{2}\left(\frac{y}{\sigma_y}\right)^2 \exp - \frac{1}{2}\left(\frac{z-H}{\sigma_z}\right)^2 \tag{6.1-4}$$

If the point source is diffusing in a semibounded medium such as the atmosphere, with ground defined by z = 0, then H is the emission height above ground. Equation (6.1-4) must be modified to account for reflection at the z = 0 plane. The loss of mass by dispersion in the -z direction through the z = 0 plane can be resupplied by defining an image plume located a distance -H below the z = 0 plane. The transport of mass in the +z direction through the ground plane (z = 0) will equal that in the -z direction through the ground plane from the real plume. This is known as the method of images.

The contribution of the image plume can be determined from Equations (6.1-1), (6.1-2), and (6.1-3) by setting z = -H (y still = 0). Then

$$XU\Big|_{\text{image}} = \frac{Q}{\sqrt{2\pi}\sigma_y \sqrt{2\pi}\sigma_z} \exp - \frac{1}{2}\left(\frac{y}{\sigma_y}\right)^2 \exp - \frac{1}{2}\left(\frac{z+H}{\sigma_z}\right)^2 \tag{6.1-5}$$

The total XU at any point can be determined by adding the contributions from Equations (6.1-4) and (6.1-5). Rearranging results in

$$X = \frac{Q}{2\pi\sigma_y\sigma_z U} \exp - \frac{1}{2}\left(\frac{y}{\sigma_y}\right)^2 \left[\exp - \frac{1}{2}\left(\frac{z-H}{\sigma_z}\right)^2 + \exp - \frac{1}{2}\left(\frac{z+H}{\sigma_z}\right)^2 \right] \tag{6.1-6}$$

This is just the Gaussian dispersion formula.

It is evident from Equations (6.1-1), (6.1-2), (6.1-3), and (6.1-6) that, if P_z is Gaussian as assumed, but P_y is arbitrary, then X is given by

$$X = \frac{Q}{2\pi\sigma_z U} P_y \left[\exp - \frac{1}{2}\left(\frac{z-H}{\sigma_z}\right)^2 + \exp - \frac{1}{2}\left(\frac{z+H}{\sigma_z}\right)^2 \right] \qquad (6.1\text{-}7)$$

Now assume that the contaminant is uniformly distributed in the cross-wind direction over a distance equal to $3\sigma_y$. This is equivalent to

$$P_y = \frac{1}{3\sigma_y} \quad \text{for } -1.5\sigma_y \leq y \leq 1.5\sigma_y \qquad (6.1\text{-}8)$$

and

$$P_y = 0 \text{ for } y < -1.5\sigma_y \text{ and } y > 1.5\sigma_y$$

Substituting Equations (6.1-8) into (6.1-7), results in

$$X = \frac{Q}{3\sigma_y \sqrt{2\pi}\sigma_z U} \left[\exp - \frac{1}{2}\left(\frac{z-H}{\sigma_z}\right)^2 + \exp - \frac{1}{2}\left(\frac{z+H}{\sigma_z}\right)^2 \right] \qquad (6.1\text{-}9)$$

At ground level, z=0, Equation (6.1-9) becomes

$$\frac{X}{Q} = \frac{2}{3\sigma_y \sqrt{2\pi}\sigma_z U} \exp - \frac{1}{2}\left(\frac{H}{\sigma_y}\right)^2 \qquad (6.1\text{-}10)$$

The plume dispersion coefficients, σ_y and σ_z, are each a function of downwind distance and the stability category. The stability category for the site meteorological towers is determined using measured temperature lapse rate data and the stability classification scheme of NRC Regulatory Guide 1.23 (Reference 6-2, as given in Table 6.1-1). For other "satellite" or regional meteorological data sites, the method used is based on cloud cover, wind speed, and other factors. The Pasquill-Gifford category, G, was considered equivalent to F category in this report. This is because the meander condition in the valley situation would tend to cause considerable plume spread during very stable conditions compared with the G stability case. It was assumed that the G category would overpredict doses. The same assumption was made for all sites in the RSS.

Each spatial interval is assigned a stability class and wind speed in subroutine SPADAT. These two parameters determine the amount of plume dispersion. The lateral diffusion is determined by computing a σ_y spread based on the Martin and Tikvart (Reference 6-3) power law relationships to describe the Pasquill-Gifford coefficients as shown in Table 6.1-2.

Figure 6.1-2 shows the model used to determine lateral spread of the plume in subroutine ACTIVE. The accident occurs at point O and has an initial spread of OAOB. Point O is computed as a virtual distance based on the stability at the start of the release and the building dimensions.

The value of σ_y at the endpoint of the first spatial interval, 1A1B, is calculated from the virtual origin 0. The model assumes that the lateral coverage of the cloud extends a distance $y = 1.5\sigma_y$ on both sides of the plume centerline (total plume width = $3\sigma_y$) and has a uniformly distributed crosswind concentration distribution. A purely Gaussian plume would contain 87% of its mass within this width. As implied in Figure 6.1-2, this formulation generates a uniform trapezoidal area of coverage for each spatial interval. The first spatial interval is covered by trapezoid 0A0B1B1A.

The time it takes for the cloud to arrive at the midpoint (indicated by a dashed line) and to traverse each spatial interval is calculated using the average wind speed for that interval. Whenever there is a change in stability, a new virtual distance is computed based on the new stability. The points 2' and 4' are examples of new virtual distances that result from changes in stability.

The vertical dispersion calculation is based on a treatment suggested by Turner (Reference 6-4). Figure 6.1-3 shows the vertical expansion of the cloud as a function of distance from the source. A virtual distance from the origin and the vertical standard deviation, σ_z, is calculated for each stability change. The model uses the Pasquill-Gifford expansion to a distance, SMAX, from the reactor. SMAX is the distance the cloud must travel for σ_z to become 0.465 of the mixing height. The model assumes that a linear expansion of σ_z will occur from SMAX to a distance equal to twice SMAX. This expansion is assumed to be bounded by the mixing height. Once σ_z is equal to the mixing height, it will remain constant. With a change from unstable to stable meteorology, σ_z is not allowed to decrease in value. Figure 6.1-3 represents a "typical" set of meteorological conditions. The accident occurs at X_1 during a stable meteorological configuration. At X_2, the meteorology changes to an unstable condition. Note the recalculation of $SMAX_2$ and the new virtual source, X_2'. The weather changes back to stable at X_3, and no plume growth is allowed since the σ_z is already above the stable layer mixing height. At X_4 a more unstable condition occurs than at X_2, and σ_z reaches the final mixing height. Significant changes have been made to the inversion lid processing in CRACIT as described later. The term "lid" refers to the top of the atmospheric mixing layer.

Buoyant plume rise in CRAC is computed using the recommendations of Briggs (Reference 6-5) as discussed in Appendix A of the RSS. Estimates of plume rise versus distance are based on wind speed, released energy, and stability. The plume centerline height is not allowed to rise above the top of the mixing layer so that no penetration of the mixing layer is allowed. Significant changes have been made to CRACIT in this regard, and are discussed in Section 6.1.2.3.

Allowance for plume spread for release durations in excess of 0.5 hour is made using the following relationship:

$$f_w = \left(\frac{t_r}{0.5}\right)^p \qquad (6.1\text{-}11)$$

where f_w is the factor used to increase plume width, t_r is the duration of release, and p is taken as 1/3. It has been found that p varies between 1/5 and 1/2 depending on stability (Reference 6-4).

Plume depletion by fallout and precipitation removal is accomplished for each spatial interval. Therefore, to ensure a mass balance, the amount of material deposited is subtracted from the plume source.

6.1.1.2 Plume Depletion, Radioactive Decay, and Deposition

As the plume of radioactive material travels away from the plant, airborne concentrations are reduced by radioactive decay, deposition, and turbulence. These processes are taken into account in estimating air concentrations at large distances from the plant and to estimate the amount of deposited radioactivity in the environment. These processes, and the manner in which they are treated in the RSS consequence model, are summarized in this section.

6.1.1.2.1 Radioactive Decay

The time period over which the radioactive material may remain airborne after release from the containment is relatively short. Only radionuclides with half-lives of less than a few hours will decay appreciably in this interval. For each spatial interval outward from the plume origin, the airborne concentration in the model is adjusted for the radioactive decay that occurred during the travel time from the preceding spatial interval. In addition, since some of the radionuclides have daughters that are also radioactive, the buildup of radioactive daughters in the plume is calculated for the travel time in each spatial interval.

6.1.1.2.2 Dry Deposition

Impaction is the dominant mechanism for dry removal of released aerosols (particles and vapors). The mechanism is expressed by a deposition velocity that is defined as the ratio of the deposition flux to the air concentration at a given distance from the surface. In the consequence model, a constant deposition velocity is used. The dry deposition flux of aerosols to the surface is assumed to be $v_d X_o$, where v_d is the deposition velocity, and X_o is the air concentration near ground level. Dry deposition is assumed to proceed at all times and variations in deposition velocity because of precipitation, surface wetting, vegetative cover, desorption, etc., are assumed to be accounted for in the single deposition velocity used. The consequence model uses a deposition velocity of 10^{-2}m/sec for both particulate and halogen aerosols. Noble gases are not removed.

6.1.1.2.3 Wet Deposition

Precipitation washout of airborne material (wet deposition) can occur by in-cloud or below-cloud scavenging. These processes are discussed in Appendix B of the RSS. In-cloud scavenging occurs when the airborne material stimulates or even initiates precipitation by condensation

precipitation. If a convective storm is present, the released aerosols are swept up into the cloud and effectively removed from the atmosphere. In below-cloud scavenging, the precipitation falling through the plume impacts upon and collects the airborne material.

To treat the wet deposition process in the consequence model, a simple exponential formulation is used. The plume concentration is assumed to decrease because of precipitation scavenging according to

$$\exp^{[-\gamma(t - t_0)]}$$

where $(t - t_0)$ is the time since the onset of precipitation at time t_0, and γ is the wet removal rate. The removal rate, γ, is taken to be 10^{-4} sec^{-1} under stable conditions (warm frontal storms) and 10^{-3} sec^{-1} under unstable conditions (convective storms). Particles and gases are treated identically. The noble gases are assumed to be insoluble and are not removed by precipitation scavenging.

Only information on precipitation occurrence within a given hour is available in the meteorological data file. Since rain does not always occur for the entire hour, it was assumed that washout occurs only half the time within any specified hour of precipitation. This hourly fraction was based on the following references: Marshall and Holtz (Reference 6-6), Austin and Houze (Reference 6-7), and Zawadski (Reference 6-8). In CRACIT, the removed fraction is based on the rain rate for the hour as described in Section 6.1.2.3.2. Buildup of radioactive daughters is accounted for in the deposited material for both wet and dry disposition.

6.1.1.3 Radiation Dose and Health Effects Calculations

6.1.1.3.1 Dose Calculations

The dose model used in CRAC was incorporated into CRACIT in this study with only minor modifications. Details of these calculations are included, starting in Section 8 of Appendix VI of the RSS. A brief summary of the dose calculation model follows.

There are two basic elements in the problem of assessing the hazards of radioactive materials entering the environment from a hypothetical accident. First, the concentrations of the radioactive isotopes in the environment (air, soil, water, on and in vegetation, animals, etc.) must be estimated. Second, the absorption in human tissues of radiation emitted by these isotopes must be quantified. This second process involves identifying environmental pathways for human exposure. Exposure may be internal, the result of ingestion of food or inhalation of air containing isotopes. Or it may be external, resulting from isotopes that remain in the environment.

Time is an important variable in the dose assessment. Biological effects depend not only upon the total radiation dose received but its rate as a function of time. The latter, in turn, depends upon environmental concentrations of isotopes and their transport to humans. These also vary as a function of time.

To simplify the assessment in CRAC, exposure is broken into early and chronic phases. The early phase includes all exposure to radioactive isotopes in the environment within a week after their release. The cutoff time for this period is the completion of the evacuation process, the completion of the relocation process, or 7 days following release, whichever comes first. The RSS assumes that within 7 days a decision would be implemented as to whether a resident should be permitted to remain in the areas. The early phase of exposure is marked by concentrations of isotopes in the environment that change rapidly as a function of time due both to environmental transport characteristics and the rapid decay of shortlived isotopes. This phase is also marked by highly variable human exposure pathway characteristics due to mitigative measures. For example, a person evacuating his residence following a large accidental release may be exposed in varying degrees to airborne radioisotopes and isotopes deposited on the ground during passage of the cloud. This depends on the location of the residence, the meteorological conditions during and shortly after the release, and the path followed during evacuation.

The chronic exposure phase begins when land contaminated during passage of the plume is returned to use. This phase is marked by more gradual decreases in environmental concentrations and essentially unvarying human exposure pathway characteristics. It will persist for many years as the radioactive isotopes decay and weather away.

A major distinction between the two phases is that chronic exposure is subject to administrative control. Such measures as interdiction of land could prevent doses that lead to early fatalities or injuries. The interdiction could be permanent if contamination levels are high enough to warrant it. The degree of administrative control in the early phase is more limited and, for a given site, is exercised by mitigative measures.

The physical measure of radiation impact most directly related to biological effects is the dose absorbed in the tissue. This is measured in units of energy deposited per unit mass of tissue (1 rad tissue equals 100 ergs/gram tissue). Given the pattern of an individual's exposure to radioactive isotopes determined in the pathway analysis, doses to certain tissues and organs integrated over specified time periods are assessed for each isotope and results are accumulated. The selection of organs and time periods is made bearing in mind the likely biological effects. For example, if early fatality is the effect of interest, the dose of interest is the marrow dose (accumulated over all pathways and isotopes) integrated over a period of about a month following the release. Conversely, if lung cancer is the effect of interest, the dose of interest is the lung dose integrated over several discrete time intervals that span the range of a lifetime. The dosimetric models used to relate environmental isotope concentrations to organ doses are described in detail in Section 8.4 of Appendix VI of the RSS.

6.1.1.3.2 Health Effects

Once the radiation doses have been computed, the effect on the health of the exposed individual must be estimated. The health effects model in CRAC was used unchanged in the CRACIT calculations. The following summary is brief, but detailed information concerning the clinical and experimental data on which the calculations are based is included in Appendices F, G, H, and I of Appendix VI of the RSS. These appendices include data on the early, continuing, somatic effects, late somatic effects, thyroid and genetic effects.

The health effects that could be associated with a reactor accident are divided into the following categories. Early and continuing somatic effects that include the early mortalities and morbidities that are usually observed after large, acute doses of radiation. They can occur within days to weeks after exposure. They also include illnesses and deaths that can become manifest within a year or so. In general, these early and continuing somatic effects are associated with individual total body doses of 100 rads or more and thus would affect only those persons exposed near the plant following the accident.

The late somatic effects include latent cancer fatalities and morbidities as well as benign thyroid nodules. In radiation effects experience, these are typically observed 2 to 30 years after irradiation. Finally, there are genetic effects that do not manifest themselves in the irradiated individuals, but rather in their descendants. In contrast to the early somatic effects, both latent cancer and genetic diseases are assumed to be random phenomena whose probability of occurrence is some function of the dose magnitude. For this reason, both late somatic and genetic effects are calculated based on the population dose (cases per million man-rem) rather than individual doses. Individuals who receive fatal doses are excluded from latent effects calculations of risk or population exposure.

The underlying objective of this study is to make as realistic an assessment of risk as is possible and to indicate the uncertainties in the estimate. Until recently, the 1972 BEIR report (Reference 6-9) was considered to represent the best authoritative data source for quantifying latent cancer and genetic effects and was used as input data to CRAC. However, experimental evidence suggested that the 1972 BEIR report overestimated cancer risks. The RSS used these experimental data to justify reductions to the BEIR linear risk coefficients for low doses and dose rates. The latest report by the BEIR committee (Reference 6-10) supports the use of reduction factors used in the RSS for certain cancers. Accordingly, the RSS reduction factors have been used in this study, except for thyroid and breast cancers, which are in keeping with BEIR recommendations.

6.1.1.3.3 Mitigation of Radiation Exposure

The preceding sections have described the mechanisms whereby radioactive material released by a reactor accident could reach humans, the methods used to estimate the radiation dose, and the resultant health effects and property damage. This section discusses the actions that could be taken to reduce the radiation exposure and thus health effects.

It is helpful to distinguish between two time periods: (1) immediate actions to reduce early exposure during the passage of the radioactive cloud, and (2) long term actions to reduce chronic exposure from radioactive material deposited on the ground or vegetation. Since an individual's exposure to the cloud would last only about an hour, immediate actions must be taken within hours of the accident if they are to be of any value. Possible actions are evacuation and sheltering (i.e., having the public remain indoors). Sheltering might reduce the dose incurred from both inhalation and external cloud shine.

There are several modes of chronic exposure. The most important is direct irradiation from contaminated ground and ingestion of contaminated milk or crops. Chronic exposure would generally involve lower dose rates than would early exposure. However, the time scales would be several weeks for milk ingestion, one season for crops, and 50 years or more for ground contamination. For these reasons, long term mitigating actions could be delayed for days or weeks while the situation was fully evaluated. Only a marginal increase in exposure would occur in the population dose due to such a delay.

There are two long term mitigating actions: interdiction and decontamination of land. Interdiction prohibits the use of land or food produced on such land for a period of time. This is done either by relocating people or by impounding milk and crops. (Relocation should be distinguished from evacuation. Relocation should be initiated within days or weeks after a release and might continue for months or years, whereas evacuation would be initiated immediately and would last only for a short period.)

To facilitate an understanding of the long term mitigating actions, a simplified interdiction model is shown in Figure 6.1-4. For a ground level release, the degree of ground and vegetation contamination would decrease monotonically with distance from the reactor. The most restrictive health contamination criterion would be applied to milk. Therefore, the largest interdicted area would be associated with milk impoundment. A less restrictive criterion would be applied to the direct contamination of foliage, so the interdicted crop growing area would be smaller. The least restrictive criterion would be applied to the continuing occupancy by people. Decontamination of land can reduce its period of interdiction.

6.1.1.3.3.1 Evacuation Model. The evacuation model used in CRAC is described in detail in Section 11.1 of Appendix VI to the RSS. Evacuees are assumed to move radially outward at a constant "effective" velocity. In the RSS, the "effective" velocity was a probabilistic variable.

The "effective" velocity histogram was determined by statistical analysis of evacuation data compiled by the U.S. Environmental Protection Agency. These data included the total time required for the evacuation and the distance traveled by evacuees. No data were available for estimating delay time. The RSS assumed it to be zero because the estimate of "effective velocity" included delay time. However, the CRAC code can accommodate input of a constant delay time and a constant velocity (that could be a value approximating the actual velocity attained by evacuees).

The CRAC model allows for the evacuation of all residents who live either within a circle centered on the reactor whose radius is specified by the user, or within a 45^0 sector centered on the downwind direction and bounded by a second radius also specified by the user. The radii specified for the RSS were 5 miles for the circle and 25 miles for the sector.

If the plume comes close enough to affect the evacuee, the evacuee is assumed to be exposed to the passage of the entire cloud and to the resulting contaminated ground for 4 hours. Once exposed, it is assumed that the evacuee receives no further dose.

The evacuation model used for this study is a considerable improvement compared with the CRAC model and is described in Section 6.1.2.7.2.

6.1.1.3.3.2 Ventilation. The quantity of radionuclides inhaled may be reduced by remaining indoors during passage of the cloud. This mitigative measure is described in Section 4.1, Appendix VI of the RSS. However, the RSS did not consider any reduction from this measure, and the CRAC code has no provision for including it. A simplified treatment of this effect, involving application of a constant reduction factor for early phase inhalation doses, has been incorporated in CRACIT.

6.1.1.3.3.3 Interdiction and Decontamination. The mitigative measures described previously limit early exposure. Chronic exposure is limited most effectively by either interdiction or decontamination of land affected by the release.

The criterion for requiring land interdiction or decontamination would be a limiting individual dose commitment that could result from unrestricted use of the land. The RSS used criteria adopted from the recommendations of the U.S. Federal Radiation Council and Medical Research Council of Great Britain. The criteria for requiring mitigative measures for human occupation were external irradiation dose commitments of 10 rem in 30 years for sparsely populated areas and 25 rem in 30 years for densely populated areas. The criteria for requiring mitigative measures for land used for milk production were milk ingestion dose commitments limits of 3.3 rem to bone marrow from strontium in the first year, 3.3 rem to the whole body from cesium, and 10 rem to the thyroid from iodine isotopes. The criteria for requiring mitigative measures for other land uses were ingestion dose commitment limits for other food pathways of 2 rem to the bone marrow from strontium in the first year and 2 rem to the whole body from cesium.

Four types of interdiction are modeled:

- Total interdiction for long periods (20 years or more)
- Partial land interdiction for several years
- Crop interdiction for a season
- Milk interdiction for a season

Selection of one of these depends upon conformance with the criteria.

The area of interdicted land decreases with time because of radioactive decay and weathering, but decontamination could return the land to immediate use. The maximum decontamination factor considered practical is 20. Interdiction and decontamination are discussed in Section 11.2, Appendix VI of the RSS. Figure 6.1-4 illustrates the interdiction model.

6.1.1.3.3.4 Shielding. Absorption of radiation by structural materials will reduce doses from exposure to direct radiation from external sources. The shielding factors used in this study are described in Section 6.2.1.2.

6.1.1.4 Determination of Consequence Frequency Distribution

The consequences (health effects) of each meteorological sequence for each release category are combined to form cumulative probability distributions as described in the RSS. Each meteorological sequence has a probability of one divided by the total number of sequences in the calculation. In CRAC, the wind direction frequency is used to determine the probabilities of the effects calculated for population groups in each of the 16 sectors. Since wind direction is fixed within the meteorological sequence in CRACIT, each meteorological sequence is considered separately without regard to the probability of wind being in other direction sectors.

6.1.2 MODIFICATIONS TO THE CRAC PROGRAM

To develop CRACIT for site specific studies, a considerable number of modifications were made to the original CRAC program. With a few exceptions, the basic flow of the program including the input information remains unchanged. A list of subroutines is given in Table 6.1-3.

Section 6.1.1 described the CRAC model in general terms. This section focuses on routines that were modified and fully describes new subroutines. The MAIN routine controls the execution sequence of CRACIT and retains all options originally available in CRAC. Flow of the MAIN routine in the consequence model is shown in Figure 6.1-5.

Few changes to the INPUT routines were necessary. However, the program changes required to read-in detailed site and plant specific input information are discussed in Section 6.1.2.1. The actual data are provided in Section 6.2. The new spatial interval concept is embodied in subroutine SPEDIT which replaces SPADAT as discussed in Section 6.1.2.2. As discussed in Section 6.1.2.3, major changes were made to the dispersion model subroutine, DISP. Sections 6.1.2.4 and 6.1.2.5 describe the new GRIDOS subroutine developed to characterize

plume trajectory on the fine area grid. The development of the PMATCH subroutine that includes the evacuation model and calculation of doses to the evacuating populace is described in Sections 6.1.2.5 and 6.1.2.6. Flow diagrams for the major replacement subroutines are given in the sections that follow. Modifications were also made to enable modification of meteorological sequences so they more accurately represent plume trajectories and dispersion characteristics in the specific site region. These changes are described in Section 6.1.2.4.

6.1.2.1 Changes to Site Input Data for CRACIT

The major differences in site data requirements for CRACIT and CRAC are the need for atmospheric, local dispersion phenomena, seasonal and/or day-night population distributions near the site, hourly meteorological data, including direction and lid height each hour, and evacuation path information.

Hourly meteorological data were obtained from several locations in the plant region. In CRACIT, as the plume crosses certain assumed region boundaries, it is assumed to be influenced by the meteorology. Summaries of the meteorological data are given in Section 6.2. The method used for selecting the appropriate regional data set is included in the SPEDIT routine described in Section 6.1.2.2, and the regions are described in Section 6.2.

Population distributions for the site were prepared based on recreational and other site population factors. The appropriate population is selected depending on time of day or week or based on season. No changes were assumed in the population distributions beyond 50 miles. Actual population data are given in Section 6.2. To provide more accuracy in the evacuation routine, population figures for 32 direction sectors were used. The population data file is read by subroutine PMATCH depending on the time the weather sequence starts. The population data files are created by an evacuation preprocessor routine called PEVAC discussed in Section 6.2.1.2.

Standard input data libraries developed for all parts of the consequence model during the RSS are available for various regions throughout the United States.

6.1.2.2 Changes to the Spatial Interval Concept for CRACIT

The CRAC model assumes a straight line plume trajectory with calculations at fixed distances out to 2,000 miles independent of the sequence of hourly wind speed and direction conditions. This may have been appropriate in the RSS where it was used to determine aggregate risks. However, for a site specific case, more attention was given to predicting and treating changes in plume trajectory with time.

First consider the spatial interval concept in CRAC. This spatial concept is the most important basic computation step in CRAC. It must be understood before modifications made for CRACIT can be fully appreciated. In CRAC, the plume is divided into a series of up to 34 radial segments called spatial intervals as shown for case A on Figures 6.1-2

and 6.1-6. All computations of airborne or deposited concentrations of radioactive material are made at a distance equivalent to the center of each spatial interval. Thus, the area affected by a release is bounded radially by the spatial interval distances and on the azimuth by the width of the plume of radioactive material defined in the dispersion routines. Case A in Figure 6.1-6 is a characterization for a straight line trajectory. However, one of the major modifications to CRAC was to change the trajectory from the straight line to one that follows the measured or predicted changes in wind direction as a function of time and space. As will be explained later, this requires that the spatial intervals be determined separately for each meteoro- logical sequence. An example of spatial interval spacing based on wind speed for the same meteorological sequence is shown in case B on Figure 6.1-6. Case C on Figure 6.1-6 illustrates the effect of direction changes on plume shape and spatial interval boundaries.

In CRAC the spatial intervals are fixed for each run and the meteorological conditions are assigned to each spatial interval based on wind speed. If the speed is fast, several spatial intervals will be crossed during 1 hour. Conversely, if the speed is slow, several hours may be required for the plume to cross one spatial interval. In CRACIT, it is desirable to change direction as frequently as once per hour, or when a new meteorological region is entered. Because of this, it would be impossible to accurately change the direction of the plume if more than 1 hour were needed to cross a spatial interval of fixed length, if averaging were allowed. This led to a major revision to the SPADAT routine to dynamically set spatial interval length for each new weather sequence based on wind speed. The new routine, called SPEDIT, does not allow averaging of weather conditions for the first 31 spatial intervals. This will be discussed further in Section 6.1.2.2.2.

6.1.2.2.1 Criteria for Redefining Spatial Interval Distances

In developing the new approach that could allow plume turning, various techniques for representing the variable plume path were explored with the following criteria in mind:

- Dispersion routines in CRAC should remain compatible with the new spatial interval concept.
- Dispersion calculations must be made at distance intervals that are sufficiently small to assure accuracy.
- Area affected by the plume after turning should approximate that of the straight line model.
- Plume can turn through any angle at the end of any spatial interval.
- Spatial intervals are limited to 34 to be compatible with all other subroutines.
- Averaging of meteorological data within one spatial interval should be avoided for at least the first 20 miles of plume travel.

The plan selected meets these criteria. Dynamic spacing of spatial intervals was readily merged into CRAC by replacing the SPADAT routine with SPEDIT. Not all of the above criteria were met in SPEDIT alone. The GRIDOS routine (see Sections 6.1.2.4 and 6.1.2.5) was used to create the actual plume area of coverage including variable trajectories. Figure 6.1-7 is a functional flow diagram of the SPEDIT subroutine. Spacing of the intervals is not always uniform in this concept because the length is determined by wind speed or the maximum distance allowed between dispersion calculations (a graduated scale becoming larger with distance). Therefore, a spatial interval must end (based on wind speed) before reaching the required maximum distance from the end of the last interval depending on total distance from the plant. Required spatial interval mesh sizes are given in Table 6.1-4. Fixed spatial interval distances used in the RSS are also given in Table 6.1-4 for comparison.

If only 34 spatial intervals are to be used, some averaging of weather within a spatial interval is desirable to follow the plume for at least a thousand miles or for several days to compute the effects of low level exposures to large population groups. Weather conditions are averaged only in the last three spatial intervals that normally represent conditions after the plume has traveled more than 5 hours and more than 30 miles from the plant. At these locations, wind conditions are assumed to have little effect on the accuracy of results (especially early effects). The most important location for having accurate wind direction is near the plant where the potentially highest exposures to evacuees generally occur. Methods for averaging are explained in the following SPEDIT discussion.

6.1.2.2.2 Description of SPEDIT Subroutine

The primary functions of SPEDIT are to compute the distance between spatial intervals, assign the direction of plume travel, and determine the appropriate meteorological data for computing dispersion in the plume region (See Figure 6.1-7). Plume shapes and trajectories are described later. As described in Section 6.1.2.3.8, SPEDIT is also used to determine the possible effect of terrain on plume travel. The sequential progression of SPEDIT calculations is:

- SPEDIT begins with the start date (hour) for the meteorological sequence that is passed from another subroutine. Interval spacing is not fixed as in CRAC and must be determined separately for each new meteorological sequence.

- One hundred hours of meteorological data for each of the meteorological regions in I9 format (see Section 6.2) beginning with the start hour are read into memory from disc files.

- Meteorological data from the site tower are used for the first spatial interval. Thereafter, meteorological data are used from the region in which the last spatial interval plume front existed. The regional boundaries are chosen to account for variations in weather conditions that may occur because of complex terrain and/or interactions of land and water near the site under certain meteorological conditions.

- Subroutine POLYPT determines the meteorological region in which the last plume front is located.

- Meteorological data are packed into an I9 integer word in the computer to save file space (Section 6.2). Subroutine EXTRC converts the I9 integer word into the five meteorological parameters for the hour. These parameters are wind speed, wind direction, atmospheric stability, rainfall rate, and lid height.

- Knowing the speed and direction, a vector calculation is made to estimate the location of the plume front at the end of each spatial interval. This is used primarily to select the meteorological region previously discussed and to determine the average wind direction described later for the 32nd through 34th spatial intervals.

- The next step is a complex one that determines the length of each spatial interval. Basically, there is a check to determine if the speed would cause the plume to travel beyond a certain maximum distance during 1 hour (based on total travel distance from the plant, see Table 6.1-4). If so, the hour is split into more than one spatial interval. For low winds there may be only one spatial interval for the hour, and for high winds there may be many. As the plume travels further from the plant, the likelihood of there being many spatial intervals in 1 hour decreases because maximum allowable interval size becomes larger (see Table 6.1-4).

- Next, the program checks to see if the 31st spatial interval has been processed. If not, another hour of meteorological data are needed and the processing continues with the last spatial interval and adds on the appropriate new intervals for the hour.

- The INCTIM routine, which is called whenever the 34th spatial interval has not been reached in the current hour, increments the last hour by one to determine the next start hour.

- When 31 spatial intervals are complete, a different type of processing is used. The last three spatial intervals are reserved to define meteorological conditions applicable to longer distances and greater time periods. In CRAC, the 34th spatial interval extends from 350 to 2,000 miles. Because the total travel distance to the 31st spatial in SPEDIT is variable, the last three spatial intervals were spaced as follows. The 32nd spatial interval extends from the end of the 31st to one-half the distance to 200 miles, and the 33rd extends out to 200 miles. The 34th ends at 2,000 miles or at the distance traveled in 100 hours. All processing stops after 100 hours.

- Averages of speed, stability, rain, and lid height are computed algebraically for the 32nd through 34th spatial intervals. However, the same procedure cannot be used for direction. Therefore, the average direction is determined by averaging the x-y components over all hours and calculating the average direction trigonometrically.

Because the plume in this spatial interval travels in a straight line in the average direction, the area it covers is represented as being longer and narrower than the zig-zag area actually covered.

- In CRAC, material remaining in the plume at the 34th spatial interval out to 2,000 miles is assumed to be washed out by rain over the area of coverage. In this analysis, the 34th spatial interval could extend less than 2,000 miles. However, the plume would be 100 hours old and all remaining activity is assumed to be washed out in the 34th spatial interval area.

- The final step is to pass to the DISP routine the 34 spatial interval distances, the time it takes to reach and traverse each spatial interval, and meteorological conditions for each spatial interval.

6.1.2.3 Dispersion Model Changes (DISP and ACTIVE)

The original CRAC dispersion model contained in subroutines DISP and ACTIVE (as described in Section 6.1.1.1) was extensively modified to include the use of wind speeds at or near plume height, revised wet deposition input parameters, revised plume rise and lid penetration models, trapping and fumigation models under inversion lids, a turbulent internal boundary layer (TIBL) model for lake sites, and a terrain model. These are described in Sections 6.1.2.3.1 through 6.1.2.3.10. Generalized flow diagrams of the lid processing portions of the DISP routines are shown in Figure 6.1-8.

6.1.2.3.1 Adjustment of Wind Speed With Height

In CRAC, meteorological data from only one level near the ground were used. No increase in winds with height was accounted for in either the plume dispersion transport time or plume rise calculations. For this analysis, however, winds from several levels on the site tower were available. Because certain release categories have considerable release energy and plume rise, the higher level data from the meteorological tower were used for diffusion calculations. All other accident categories used lower level (10m) winds. Data from the other meteorological regions are adjusted to the higher average (plume dispersion) level using the following exponential relationships to approximate wind speeds at higher levels:

$$U_u = U_\ell \left(\frac{H_u}{H_\ell}\right)^n \qquad (6.1\text{-}12)$$

where n is a function of stability as follows:

Stability	n
A	0.20
B	0.20
C	0.20
D	0.30
E	0.40
F	0.40

and

U_u = upper level estimated wind speed at release height or near plume (m/sec)

U_ℓ = lower level measured wind speed (m/sec)

H_u = height of upper level (release height or plume height)

H_ℓ = height of measurement

Several adjustments of wind speed were made from the measured height using Equation (6.1-12). First, the speed is adjusted to the assumed "release height" for the Brigg's plume rise calculations. Second, the speed is adjusted to a height characteristic of the atmospheric volume in which the "average" plume is dispersing. This is referred to as "reference plume height." Third, it is adjusted to a height of 250 feet for use when defining TIBL slope. Assumed values for these heights are given in Section 6.2.

6.1.2.3.2 Deposition Models

Several changes were made to the original CRAC dry and wet deposition models.

6.1.2.3.2.1 Dry Deposition Model - CRACIT. According to the CRAC model the deposition at the middle of the spatial interval is calculated from

$$D = Q_1(X/Q)F_D H_{eff}(1-F_D{}^2F_w)\ T$$

where

D = amount of material deposited per unit area

Q_1 = source strength of plume at beginning of spatial interval

F_D = fraction of source Q_1 remaining after dry deposition over the first half of the spatial interval

F_w = fraction of source Q_1 remaining after wet deposition over the entire spatial interval

T = time for plume front to cross spatial interval

H_{eff} = effective plume height

(X/Q) = normalized ground level concentration at middle of spatial interval

H_{eff} is defined so that

$$X/Q = \frac{1}{WH_{eff}U}$$

$W = 3\sigma_y$ is the plume width at the middle of the spatial interval

U = wind speed

Comparing this equation with the CRAC modified Gaussian diffusion equation, (6.1-10) yields

$$H_{eff} = \sqrt{\frac{\pi}{2}}\sigma_z \exp \frac{1}{2}\left(\frac{H}{\sigma_z}\right)^2$$

where

σ_y = crosswind sigma

σ_z = vertical sigma

H = plume centerline height

F_D and F_W are given by

$$F_D = 1 - \frac{v_d T}{2H_{eff}}$$

$$F_W = e^{-\lambda f_t T}$$

where

v_d = dry deposition velocity

λ = rainout time constant

f_t = fraction of time that plume is in the spatial interval when it is raining

In CRAC, dry deposition is treated as a two step process (evaluated separately for first half and second half of spatial interval), while wet deposition is a one step process (evaluated for the entire spatial interval at once).

The CRAC computer code limits the argument $1/2\ (H/\sigma_z)^2$ in the exponential of the above equation to values less than or equal to 35, leading to a truncation error that is propagated throughout the deposition equation. This causes appreciable roundoff error particularly close to the source under light wind speed conditions when $1/2\ (H/s_z)^2$ often exceeds 35.

To circumvent this problem in CRACIT, the CRAC deposition model was recast in a slightly different way to yield an equivalent formulation. The CRACIT model is

$$D = Q_1 F_d \left[(X/Q) v_a + \frac{(1-F_w)}{1/2WUT} \right]$$

where

$$F_D = 1 - \frac{1}{2} v_d WUT(X/Q)$$

$$F_w = e^{-\frac{1}{2}\lambda f T_t}$$

The new formulation differs in two respects. For consistency, both dry and wet deposition are treated as two step processes and the propagation of truncation errors is elminated. The models are equivalent in all other respects.

6.1.2.3.2.2 Wet Deposition Model - CRACIT. Wet deposition from scavenging of airborne particles is a highly complex phenomenon. Inspection of preliminary calculations showed that the most severe consequences at relatively large distances occur as a result of rainfall. The assumed deposition rate during rain is an important part of this study. As discussed in Section 6.2.1, rainfall data from as many locations as possible in the site region were incorporated into the data base. The measured average rainfall rate over each hour was categorized into five groups, and each group was assigned a washout rate as follows:

Rainfall Rate (in/hr)	Washout Rate (sec^{-1})
0 - 0.02	0
0.03 - 0.06	2.5×10^{-4}
0.07 - 0.1	6.0×10^{-4}
0.11 - 0.25	1.0×10^{-3}
more than 0.26	3.0×10^{-3}

The chosen rainout rates are based on the work by Engleman and reported in Slade (Reference 6-11). Figure 5.10, found in this reference, was used to judge the rates as a function of time. Because these rates are averages for the hour, it was assumed that the appropriate rainout rate applied over the whole hour, and not over half the hour as assumed in CRAC. Some uncertainty is introduced by averaging over the 1-hour intervals. However, this effect should become less significant as the number of weather scenarios with rain increases. Snow is treated the same as rain in this analysis.

6.1.2.3.3 Plume Rise Modifications

A more recent version (References 6-12, 6-13, 6-14, and 6-15) of the Briggs' plume rise relationships was programmed into CRACIT for this study. This change results in a somewhat higher plume rise for the release categories with higher release energies. Plume rise formulae are given below.

For stable atmospheres, three calculations are made. The lowest is added to the release height as follows:

$$\Delta h_1 = 2.6\ (F/US)^{1/3} \qquad (6.1\text{-}13)$$

$$\Delta h_2 = 4.0\ F^{1/4} S^{-3/8} \qquad (6.1\text{-}14)$$

$$\Delta h_3 = 1.6\ F^{1/3}\ x^{2/3}\ U^{-1} \qquad (6.1\text{-}15)$$

$$H = h_s + \text{min of } (\Delta h_1, \Delta h_2, \Delta h_3) \qquad (6.1\text{-}16)$$

H = height of plume centerline above ground, m

h_s = release height, m

U = wind speed, m/sec

x = downwind distance, m

where

$$S = \frac{g}{T}\frac{\partial \theta}{\partial Z} \qquad (6.1\text{-}17)$$

and

S = stability parameter, sec^{-2}

$\partial\theta/\partial Z$ = gradient of potential temperature, $^0K/m$ (assumed $0.02^0K/m$ for Pasquill E and $0.035^0K/m$ for Pasquill F)

T = ambient temperature, ^0K

g = acceleration due to gravity, m/sec^2

$$F = 3.7 \times 10^{-5}\ Q_H \qquad (6.1\text{-}18)$$

F = buoyancy flux, m^4/sec^3

Q_H = energy of release, cal/sec

NOTE: The plume has always reached its equilibrium height by the middle of the first spatial interval.

Neutral and Unstable Atmospheres - Plume Levels Off Well Below the Inversion Layer (LID)

$$H = h_s + \text{min of } (\Delta h_1, \Delta h_2) \qquad (6.1\text{-}19)$$

$$\Delta h_1 = 1.6\ F^{1/3}\ x^{2/3}\ U^{-1} \qquad (6.1\text{-}20)$$

$$\Delta h_2 = 1.6\ F^{1/3}\ (3.5\ X^*)^{2/3}\ U^{-1} \qquad (6.1\text{-}21)$$

If $U < 1.0$ m/sec, set $U = 1.0$ m/sec

$$X^* = 14\ F^{5/8} \quad \text{if} \quad F < 55\ m^4/sec^3 \qquad (6.1\text{-}22a)$$

$$X^* = 34\ F^{2/5} \quad \text{if} \quad F \geq 55\ m^4/sec^3 \qquad (6.1\text{-}22b)$$

6.1.2.3.3.1 Plume Liftoff Criteria. Several researchers have suggested that a buoyant release may become trapped in the reactor building wake during moderate to high wind speed conditions and therefore fail to "lift off" or rise into the atmosphere. The trapped plume will be rapidly brought to ground level and plume rise restricted.

Briggs (Reference 6-16) suggests that the critical wind speed for liftoff is given by

$$U_{crit} = 1.5\ (B/W)^{1/3}$$

where

$$B = \pi F$$
$$F = 3.7 \times 10^{-5}\ Q_H$$
$$W \cong H_b/2$$

and

U_{crit} = critical speed for liftoff, m/sec
F = plume buoyancy flux, m^4/sec^3
H_b = building height, m
Q_H = release energy, cal/sec
W = width of building

This equation is based on experiment and is consistent with other proposals made by Briggs and the Warren Spring Laboratory in Great Britain (Reference 6-17).

If the wind speed at release height is greater then U_{crit}, the plume fails to lift off and is trapped in the reactor building wake. For this case the release energy is assumed equal to zero and no plume rise is allowed. The release height for buoyant plumes that do not lift off is set to 10m, and the reference height for wind speed calculations is set to the original assumed release height.

6.1.2.3.4 Plume Penetration of Elevated Stable Layer (LID)

In CRAC, average seasonal heights are used. However, for this study, the lid height is estimated for each hour. Models for lid penetration and/or trapping and fumigating under the lid as it moves were incorporated. The equations for dispersion above and below the lid are discussed in Section 6.1.2.3.5. A discussion of lid penetration treatment in CRACIT follows.

6.1.2.3.4.1 Criteria for Use of Penetration Equations. For the penetration equations to apply, the atmosphere below the lid must be neutral or unstable and the plume must still be rising as it approaches

the downwind distance, X, of interest. An initial estimate of the plume rise, H_i is obtained from the Briggs plume rise formulas [Equations (6.1-19) to (6.1-22)].

An initial estimate of the vertical dispersion coefficient, σ_{zi}, at the distance X, is obtained for the stability under the lid.

- If $H_i + \sigma_{zi} < L$, the entire plume is below the lid and the penetration equations do not apply.

  $$H = H \ , \ \sigma_z = \sigma_{zi}$$

- If $H_i + \sigma_{zi} \geq L$, the plume is near the lid and the penetration equations must be applied to determine the actual location and condition of the plume.

6.1.2.3.4.2 Penetration Equations for a Buoyant Bent Over Plume. If $U \geq 1$ m/sec, the plume is considered to be bent over and the following equations apply

The plume centerline height is given by the solution of

$$\frac{3F}{\beta'^2 USZ_b^3} = \frac{3}{2}\left(\frac{Z_{eq}}{Z_b}\right)^2\left(\frac{Z_{eq}}{Z_b} - 1\right) + \frac{2}{9} \qquad (6.1\text{-}23)$$

where

$$Z_b = L - h_s$$

$$Z_{eq} = H - h_s$$

$$S = \frac{g}{T}\frac{\partial\theta}{\partial Z}$$

Equation (6.1-23) can be rearranged to yield

$$\left(\frac{Z_{eq}}{Z_b}\right)^2\left[\left(\frac{Z_{eq}}{Z_b}\right) - 1\right] = \frac{2}{3}\left[\frac{3F}{\beta'^2 USZ_b^3} - \frac{2}{9}\right] \qquad (6.1\text{-}24)$$

Let $\alpha = Z_{eq}/Z_b$

$$A = \frac{3F}{\beta'^2 USZ_b^3}$$

With these definitions, Equation (6.1-24) becomes

$$\alpha^2(\alpha-1) = \frac{2}{3}\left[A - \frac{2}{9}\right] \qquad (6.1\text{-}25)$$

The fraction of the plume that penetrates the lid is

$$P = \frac{\text{Depth of Plume Above } Z_b}{\text{Total Depth of Plume}}$$

The plume is assumed to have a width equal to its height so that the height of the top of the plume is $Z_e + 0.5Z_e = 1.5Z_e$ and the height of the bottom of the plume is $Z_e - 0.5Z_e = 0.5Z_e$.

Depth of plume above $Z_b = 1.5Z_{eq} - Z_b$

Total depth of plume = $1.5Z_{eq} - 0.5Z_{eq} = Z_{eq}$

Therefore, $P = (1.5Z_{eq} - Z_b)/Z_{eq}$

$$P = 1.5 - \frac{Z_b}{Z_{eq}} = 1.5 - \left(\frac{1}{\alpha}\right) \qquad (6.1\text{-}26)$$

For total penetration, $Z_{eq} > 2Z_b$

For this to occur, $A = \dfrac{3F}{\beta'^2 USZ_b^3} < 6.222$

In this case, Equation (6.1-24) reduces to

$$\frac{Z_{eq}}{Z_b} = \left[1.8 + \frac{3F}{\beta'^2 USZ_b^3}\right]^{1/3} \qquad (6.1\text{-}27)$$

or

$$\alpha = [1.8 + A]^{1/3}$$

For P = 0, Equation (6.1-26) states that $\frac{1}{\alpha} = 1.5$ or $\alpha = 0.6667$.

Let

$$B = \frac{2}{3}\left[A - \frac{2}{9}\right]$$

so that Equation (6.1-25) becomes $\alpha^2(\alpha-1) = B$. Substituting $\alpha = 0.6667$ into this equation yields $B = -0.1481$. If $B \leq -0.1481$, then $\alpha \leq 0.6667$ and $P = 0$ so that no penetration occurs.

If $A = 6.222$, $B = 4.000$

For $B \geq 4$, $P \geq 1$ and α is calculated from Equation (6.1-27).

For $B \leq -0.1481$, $P \leq 0$ and the plume must be well below the lid.

For $-0.1481 < B < 4$, α must be calculated by direct solution of Equation (6.1-25). This is best done by assuming values of α and

calculating B from Equation (6.1-25). A table of α versus B values is generated. For the conditions of interest

$$B = \frac{2}{3}\left[\frac{3F}{\beta'^2 USZ_b^3} - \frac{2}{9}\right]$$

is calculated and the corresponding value of α is obtained by linear interpolation of the table values. Fortunately, in the range $-0.1481 < B < 4$, Equation (6.1-25) has only one positive real root for any value of B, so this procedure is easily implemented.

The solution to the penetration equation for bent over plume is as follows:

$$\alpha = Z_{eq}/Z_b$$

$$B = \frac{2}{3}\left[\frac{3F}{\beta'^2 USZ_b^3} - \frac{2}{9}\right]$$

$$\alpha^2(\alpha-1) = B$$

Following are the solutions to these relationships:

α	B	α	B
2.00	4.0000	1.30	0.5070
1.95	3.6124	1.25	0.3906
1.90	3.2490	1.20	0.2880
1.85	2.9091	1.15	0.1984
1.80	2.5920	1.10	0.1210
1.75	2.2969	1.05	0.0551
1.70	2.0230	1.00	0
1.65	1.7696	0.95	-0.0451
1.60	1.5360	0.90	-0.0810
1.55	1.3214	0.85	-0.1084
1.50	1.1250	0.80	-0.1280
1.45	0.9461	0.75	-0.1406
1.40	0.7840	0.70	-0.1470
1.35	0.6379	0.6667	-0.1481

Thus, the procedure for calculating $\alpha = Z_{eq}/Z_b$ for a bouyant bent over plume is

- Calculate

$$A = \frac{3F}{\beta'^2 U S Z_b^3}$$

$$B = \frac{2}{3}\left[A - \frac{2}{9}\right]$$

- If $A \geq 6.222$ $(B \geq 4.0)$

$$\alpha = Z_{eq}/Z_b = [1.8 + A]^{1/3}$$

- If $B \leq -0.1481$, $\alpha < 0.6667$, $P < 0$, plume penetration may be indicated when the plume is well below the lid. This condition should be initially checked in a computer program.

- If $-0.1481 < B < 4.000$, $\alpha = Z_{eq}/Z_b$ is determined by linear interpolation of the values in the preceding table. For $B_1 < B < B_2$ where B is the value of interest and B_1 and B_2 are table values, the linear interpolation formula is

$$\alpha = \alpha_1 + \frac{\alpha_2 - \alpha_1}{B_2 - B_1}(B - B_1) \qquad (6.1\text{-}28)$$

Once α is known, the plume centerline height and penetration are given by

$$H = h_s + \alpha Z_b = h_s + \alpha(L - h_s) \qquad (6.1\text{-}29)$$

$$P = 1.5 - (1/\alpha) \qquad (6.1\text{-}30)$$

$$\alpha = Z_{eq}/Z_b = \frac{H - h_s}{L - h_s}$$

NOTE: For a plume of zero buoyancy (F=0),

$$A = 0 \text{ and } B = \frac{2}{3}\left[A - \frac{2}{9}\right] = -0.1481$$

$$H = h_s + 0.6667\,(L - h_s) = 0.3333h_s + 0.6667L$$

The penetration equations do not apply to a plume of zero buoyancy. If applied mistakenly, they will yield the incorrect and misleading result that the plume rises to about two-thirds of the lid height. In general, the penetration equations have a narrow range of conditions over which they apply. Appropriate initial checks are mandatory.

6.1.2.3.4.3 Penetration Equations for a Buoyant Vertical Plume. If $U < 1.0$ m/sec, the plume is considered to be vertical and the following equations apply:

The plume centerline height is given by

$$\alpha = \frac{Z_{eq}}{Z_b} = \left[1 + \frac{37F^{2/3}}{SZ_b^{8/3}}\right]^{3/8} \qquad (6.1\text{-}31)$$

where

$$Z_{eq} = H - h_s$$

$$Z_b = L - h_s$$

$$S = \frac{g}{T}\frac{\partial\theta}{\partial Z}$$

$$P = \frac{\text{Depth of Plume Above Lid}}{\text{Total Depth of Plume}}$$

For a vertical plume, the top, centerline, and bottom of the plume are assumed to be in the ratio 5:4:3.

$$\text{Top of plume} = \frac{5}{4} Z_{eq}$$

$$\text{Bottom of plume} = \frac{3}{4} Z_{eq}$$

$$\text{Depth of plume above lid} = \frac{5}{4} Z_{eq} - Z_b$$

$$\text{Total depth of plume} = \frac{5}{4} Z_{eq} - \frac{3}{4} Z_{eq} = \frac{2}{4} Z_{eq}$$

$$P = \left(\frac{5}{4} Z_{eq} - Z_b\right) \Big/ \frac{2}{4} Z_{eq}$$

$$P = 2.5 - 2\left(\frac{Z_b}{Z_{eq}}\right) = 2.5 - (2/\alpha) \qquad (6.1\text{-}32)$$

For 100% penetration, $\alpha = Z_{eq}/Z_b = 4/3$. Therefore, if $\alpha > 4/3$; then $P \geq 1.0$. Once $\alpha = Z_{eq}/Z_b$ is known, the plume centerline height is given by

$$H = h_s + \alpha Z_b = h_s + \alpha(L - h_s) \qquad (6.1\text{-}33)$$

NOTE: For a plume of zero buoyancy (F=0), Equation (6.1-7) yields

$\alpha = 1$ which results in $H = h_s + L - h_s = L$

The penetration equations do not apply to this case as for the bent over plume case.

Once it is determined that the penetration equations apply and the plume centerline height is calculated according to these equations, the plume is assumed to have attained its equilibrium centerline height.

To ensure consistency and to maintain a smooth transition between different dispersion regimes, a system of checks is applied and the following assumptions are made. The procedure requires the initial estimate, σ_{zi}, of the vertical dispersion coefficient.

- If $P \geq 0.75$ or $H - \sigma_{zi} > L$, the plume is assumed to have entirely penetrated the lid. Since the plume is entirely above the lid, the stability is set to Pasquill-Gifford type C. The sigmas are reevaluated for this stability and the normal diffusion equation is applied to calculate X/Q at the ground.

- If $P \leq 0.25$ or $H + \sigma_{zi} < L$, the plume is assumed to be well below the lid. Since the entire plume is below the lid, the sigmas are given by the stability under the lid and the normal diffusion equation is applied to calculate X/Q at the ground.

- If neither of the above conditions are met, then $0.25 < P < 0.75$ and $H - \sigma_{zi} \leq L \leq H + \sigma_{zi}$. Therefore, the plume is trapped beneath the lid. For $P \geq 0.5$, $\alpha > 1$, which means that $H > L$. To ensure consistency for calculations in subsequent spatial intervals, the plume centerline height is not allowed to be greater than L. Therefore, if $H > L$, then $H = L$.

The sigmas are given by the stability below the lid. The check to determine the trapping condition is as follows:

- If $H > 2.15\,\sigma_z$, then the bottom of the plume is above the ground. Since the plume has not yet reached the ground, the X/Q is calculated using the Bierly and Hewson equation (Reference 6-18).

- If $H \leq 2.15\,\sigma_z$, then the plume has reached the ground. The X/Q is calculated from

$$X/Q = \frac{1}{3\sigma_y LU} \qquad (6.1\text{-}34)$$

  which is the CRAC modified trapping equation for a well mixed layer.

NOTE: The $2.15\sigma_z$ boundary is the plume radius at which the concentration falls off to 10% of its centerline value.

The nomenclature for lid penetration equations is:

F	= flux of buoyancy due to energy of release, m^4/sec^3
g	= acceleration due to gravity, m/sec^2
H	= height of plume centerline above ground, m
h_s	= height of release of contaminant above ground, m
L	= height of inversion layer (lid) above ground, m
P	= mass fraction of plume which penetrates the lid
S	= stability parameter for stable layer above lid, sec^{-2}

T = ambient temperature, ^0K
U = wind speed, m/sec
X = downwind distance, m
Z_b = height of stable layer (lid) above release point, m
Z_{eq} = height of plume centerline above release point, m
β = modified entrainment coefficient = 0.40
σ_z = vertical dispersion coefficient for Gaussian plume model, m
$\partial\theta/\partial Z$ = gradient of potential temperature in stable layer above lid, $^0K/m$ (assumed = $0.02^0K/m$)

Subscript i refers to initial estimate.

6.1.2.3.5 Plume Dispersion for Fumigation and Trapping Under a Lid

Following is the logic programmed into CRACIT to account for changes in the plume dispersion due to the presence of a lid. The logic is complicated by the possibility of changing weather conditions at each spatial interval distance and a changing lid each hour. This treatment is most important during morning hours after sunrise when lids are nearest to the ground. There are five cases of plume versus lid position treated in CRACIT.

- Plume is trapped under the lid but has not yet reached the ground. The ground level X/Q is calculated according to the Bierly and Hewson equation (Reference 6-18). At ground level,

$$X = \frac{2Q}{2\pi\sigma_y\sigma_z U}\left[\exp -\frac{1}{2}\left(\frac{y}{\sigma_y}\right)^2\right]\left\{\exp -\frac{1}{2}\left(\frac{H}{\sigma_z}\right)^2 + \sum_{N=1}^{N=J}\left[\exp -\frac{1}{2}\left(\frac{H-2NL}{\sigma_z}\right)^2 + \exp -\frac{1}{2}\left(\frac{H+2NL}{\sigma_z}\right)^2\right]\right\} \quad (6.1\text{-}35)$$

L = height of lid (inversion layer) above the ground.

According to the CRAC modified dispersion equations

$$\frac{1}{\sqrt{2\pi}}\exp -\frac{1}{2}\left(\frac{y}{\sigma_y}\right)^2$$

is replaced with

$$\frac{1}{3\sigma_y},$$

to obtain

$$\frac{X}{Q} = \frac{2}{3\sigma_y\sqrt{2\pi}\sigma_z U}\left\{\exp -\frac{1}{2}\left(\frac{H}{\sigma_z}\right)^2 + \sum_{N=1}^{N=J}\left[\exp -\frac{1}{2}\left(\frac{H-2NL}{\sigma_z}\right)^2 + \exp -\frac{1}{2}\left(\frac{H+2NL}{\sigma_z}\right)^2\right]\right\} \quad (6.1\text{-}36)$$

NOTE: $\frac{2}{3\sqrt{2\pi}} = 0.265962$

J = 5 provides sufficient accuracy for this application.

- Plume is trapped and has reached the ground by the middle of this spatial interval but not by the end of the previous spatial interval. The plume is assumed to be well mixed in the layer below the lid.

$$X = \frac{Q}{\sqrt{2\pi}\sigma_y L'U} \left[\exp - \frac{1}{2}\left(\frac{y}{\sigma_y}\right)^2\right] \qquad (6.1\text{-}37)$$

Again, according to the CRAC modification,

$$\frac{1}{\sqrt{2\pi}\sigma_y} \exp\left[-\frac{1}{2}\left(\frac{y}{\sigma_y}\right)^2\right]$$

is replaced with

$$\frac{1}{3\sigma_y}$$

Thus,

$$\frac{X}{Q} = \frac{1}{3\sigma_y L'U} \qquad (6.1\text{-}38)$$

where L' = modified lid height.

If the plume has been trapped after reaching its final rise by growth from below the lid, or if it has been trapped during its rise by close approach to or contact with the lid, then L' is set to the actual lid height, L.

If the plume has been trapped after reaching its final rise because the lid has moved down within close proximity to its centerline, then L' = max of (L, H + σ_{z1}) where σ_{z1} is the value of σ_z at of the previous spatial interval. The plume is subsequently treated as a ground level release.

- Plume is trapped and has not reached the ground by the middle of this spatial interval but has reached the ground by the end of this spatial interval. For this spatial interval, the ground level X/Q is calculated using the Bierly and Hewson equation (Reference 6-18) as Equation (6.1-36). The plume is subsequently treated as if at ground level, using Equation (6.1-43).

- Plume has fumigated in this spatial interval. When the plume is fumigated by inversion breakup (i.e., the lid rises above the assumed plume centerline level), the assumption is made that the

plume is brought immediately to the ground. Therefore, it is well mixed in the layer below the lid so that

$$X = \frac{Q}{\sqrt{2\pi}\sigma_y LU}\left[\exp - \frac{1}{2}\left(\frac{y}{\sigma_y}\right)^2\right] \qquad (6.1\text{-}39)$$

According to the CRAC modification (see Section 6.1.1.1),

$$\frac{1}{\sqrt{2\pi}\sigma_y} \exp\left[-\frac{1}{2}\left(\frac{y}{\sigma_y}\right)^2\right]$$

is replaced with

$$\frac{1}{3\sigma_y}:$$

$$\frac{X}{Q} = \frac{1}{3\sigma_y LU} \qquad (6.1\text{-}40)$$

The plume is subsequently treated as if at ground level using Equation (6.1-43).

- Plume that has been trapped and reached the ground, or has been fumigated to the ground, is subsequently treated as a ground level release.

σ_{z2} = value of σ_z at the middle of the spatial interval

σ_{z3} = value of σ_z at the end of the spatial interval

Consider the spatial interval in which the trapped plume reaches the ground or in which the plume has been fumigated. In this spatial interval,

$$\frac{X}{Q} = \frac{1}{3\sigma_y L' U} \qquad (6.1\text{-}41)$$

where $L' = L$
$L' = \max(L, H + \sigma_{z1})$
$L' = L$

For a ground level release,

$$X = \frac{2Q}{2\pi\sigma_y\sigma_z U}\left[\exp - \frac{1}{2}\left(\frac{y}{\sigma_y}\right)^2\right] \text{ at ground} \qquad (6.1\text{-}42)$$

According to the CRAC modification,

$$\frac{1}{\sqrt{2\pi}\sigma_y}\left[\exp - \frac{1}{2}\left(\frac{y}{\sigma_y}\right)^2\right] \text{ is replaced by } \frac{1}{3\sigma_y}$$

to obtain

$$\frac{X}{Q} = \frac{2}{3\sigma_y\sqrt{2\pi}\sigma_z U} \qquad (6.1\text{-}43)$$

To calculate plume growth in subsequent spatial intervals according to a simulated ground level release, the solutions of Equations (6.1-41) and (6.1-43) must be matched at this spatial interval so that an effective σ_z for the simulated ground level release can be defined. Equations (6.1-41) and (6.1-43) give (note that σ_y does not change)

$$\frac{2}{\sqrt{2\pi}\sigma_z} = \frac{1}{L'} \Rightarrow \sigma_z = .7979L' \qquad (6.1\text{-}44)$$

In the case where the plume has fumigated or is trapped on the ground, it has reached the ground at the middle of this spatial interval, $\sigma_{z2} = .7979L'$. Since the ground level plume cannot grow vertically against the lid, it is assumed that $\sigma_{z3} = \sigma_{z2}$ in this spatial interval.

For the case in which the trapped plume is still aloft by the middle of this spatial interval but reaches the ground by the end of this spatial interval, σ_{z2} is not modified and the match is made at the end of this spatial interval. Therefore, $\sigma_{z3} = .7979L$; where $L' = L$.

In all cases, once the plume has reached the ground due to trapping or fumigation, it is considered a ground level release in all remaining spatial intervals. The growth of dispersion coefficients in spatial intervals downwind of the fumigation or trapping interval is determined by the relative magnitudes of σ_{z1} and L as follows:

- If $L = 0$, calculate σ_{z2} and σ_{z3} for the measured stability class, then calculate σ_{y2} and σ_{y3} in similar fashion.
- If $\sigma_{z1} = L$ and $\sigma_{z2} = \sigma_{z1}$ and $\sigma_{z3} = \sigma_{z2}$, then calculate σ_{y2} and σ_{y3} for the measured stability class.
- If $\sigma_{z1} < L$, calculate σ_{z2} and σ_{z3} and set $\sigma_{z2} = \min(\sigma_{z2}, L)$ and $\sigma_{z3} = \min(\sigma_{z3}, L)$. Then calculate σ_{y2} and σ_{y3} for the measured stability class.
- If $\sigma_{z1} > L$, and if $\sigma_{z1} > 2L$, calculate σ_{z2} and σ_{z3} as well as σ_{y2} and σ_{y3} for Pasquill-Gifford E stability.
- If $\sigma_{z1} < 2L$ set $\sigma_{z2} = \sigma_{z1}$ and $\sigma_{z3} = \sigma_{z2}$, then calculate σ_{y2} and σ_{y3} for the measured stability class.

In the above discussion, remember that

- σ_{y1}, σ_{z1} = sigmas at the end of the last spatial interval
- σ_{y2}, σ_{z2} = sigmas at the middle of this spatial interval
- σ_{y3}, σ_{z3} = sigmas at the end of this spatial interval

6.1.2.3.6 Introduction of Terrain Effects in the Straight-Line Gaussian Model

The terrain can significantly influence dispersion calculations at certain sites. For elevated plumes, the presence of high terrain can result in high doses (because the receptor on the terrain is closer to the plume). In addition, for both ground and elevated plumes, terrain can alter the flow patterns so that straight line plume trajectories are not realistic. Modifications to the CRAC program have been made to accommodate both the vertical receptor location and the effects of plume turning (Section 6.1.2.3.7).

A conservative way to account for a receptor being closer to an elevated plume has been to assume that the receptor is closer to the plume in direct proportion to the local terrain height. If the plume strikes the terrain, the receptor is assumed to receive the centerline plume dose. In fact, the plume would have turned or traveled over the terrain since it could not travel "through" it. In stable cases, the air flow is most likely to seek a path around, rather than over, the terrain. Therefore, the conservative convention of subtracting terrain height was adopted for stable conditions. However, for neutral and unstable conditions, the receptor was assumed to be only one-half the terrain height closer to the plume. Terrain for Gaussian plume applications is input in each of 16 directions for 34 distances.

This convention is complicated when lid processing is introduced. The convention chosen was one that effectively maintained the lid height at the same distance above the terrain at all locations. This enabled the lid processing to proceed normally while accounting for terrain effects in the standard Gaussian model.

6.1.2.3.7 Modified Potential Flow Treatment of Terrain

If there are significant terrain features near the site, their effects on plume dispersion should be evaluated. Terrain in the site region may cause the standard Gaussian model to yield inaccurate doses, probably on the high side. To reduce these uncertainties, a modified potential flow model is used. The method for determining which of these models is appropriate for any given spatial interval is discussed in Section 6.1.2.3.8.

Basically, this model uses digitized site terrain to compute a wind flow field in which a dispersion model is introduced. This model is run for each of the 16 wind direction sectors for three stability categories,

and for plumes assumed to be released at 40, 300, 600, and 1,000-foot levels. Results were stored on files. They were then used as "look-up tables" for the appropriate weather sequences to better define plume travel and dispersion in the first 9 miles. A complete description of this numerical model follows. Results of this calculation were used instead of values normally computed in DISP for spatial intervals for which modified potential flow (MPF) applied.

To calculate the dispersion of pollutants in the atmosphere over irregular terrain, a three dimensional spatial distribution of wind velocities (flow field) is calculated first. Then, the dispersion of pollutant within this flow field is calculated to obtain the spatial distribution of pollutant concentration including that at ground level on terrain. Following is a description of the model used.

6.1.2.3.7.1 The Modified Potential Flow Model. A theoretically precise flow field model would calculate a spatial distribution of fluid velocities for a real fluid by the simultaneous solution of the continuity equation, the three components of the equation of motion, the energy equation, and the equation of state. An exact solution to this complete set of equations for arbitrarily prescribed boundary conditions (such as terrain) has not been found. Further, if it were to be found, or even closely approximated (e.g., numerical solutions), it would be too complex for practical use. Consequently, to develop a practical model, simplifications must be made that maintain both theoretical soundness and validity of results to an acceptable degree. Simplification is commonly achieved by assuming either potential flow or Navier-Stokes flow. Potential flow is a simplification that assumes nonviscous, nonturbulent, irrotational, incompressible, and homogeneous flow and requires the solution of only the continuity equation. The potential flow solution is inadequate because it cannot accept the necessary no-slip, zero velocity, solid boundary condition, such as terrain, and so cannot reproduce the atmospheric surface boundary layer. The Navier-Stokes solution is more realistic, being based on the assumptions of incompressibility and hydrostatic equilibrium, generally used for motions in the atmospheric boundary layer with the effect of vertical temperature stratification included as a vertical body force. The Navier-Stokes solution is reliable only to the extent that the eddy diffusivity, viscosity, and thermal input are known. The numerical model used for this evaluation is a practical compromise between these two solutions. It utilizes the modified potential flow concept (References 6-19 and 6-20) and is calibrated to yield results in agreement with both atmospheric observations and Navier-Stokes solutions.

Modified potential flow is an adaptation of classical potential flow in which the continuity equation is written as a modified Laplace equation incorporating direction dependent flow coefficients. Appropriate choices of the forms of the coefficients allow numerical solutions that exhibit the mean velocity profile and the constraints on vertical motions which are characteristic of the atmospheric boundary layer. The MPF approach is best described by reference to classical potential flow.

Classical potential flow is inviscid, nonturbulent, irrotational, incompressible, and homogeneous. The velocity components u, v, and w are defined as gradients of a velocity potential $\phi(x,y,z)$ as follows:

$$u = -\frac{\partial \phi}{\partial x}, \qquad v = -\frac{\partial \phi}{\partial y}, \qquad w = -\frac{\partial \phi}{\partial z} \tag{6.1-45}$$

The flow field is found by solving the continuity equation

$$\frac{\partial u}{\partial x} + \frac{\partial v}{\partial y} + \frac{\partial w}{\partial z} = 0 \tag{6.1-46}$$

which may be rewritten in terms of the velocity potential as

$$\frac{\partial}{\partial x}\left(\frac{\partial \phi}{\partial x}\right) + \frac{\partial}{\partial y}\left(\frac{\partial \phi}{\partial y}\right) + \frac{\partial}{\partial z}\left(\frac{\partial \phi}{\partial z}\right) = 0 \tag{6.1-47}$$

When Equation (6.1-47) together with appropriate boundary conditions is solved for ϕ, the velocity components may be found from Equation (6.1-45).

Potential flow cannot provide a realistic description of the mean flow in the atmospheric boundary layer because it cannot accept the viscous, no-slip solid boundary condition needed to provide zero velocity at the ground, and it cannot provide for vertical suppression of the flow in a stable atmosphere. To introduce these characteristics, the definition of the velocity potential can be modified to include height dependent flow coefficients B_x, B_y, and B_z such that the velocity components are defined in terms of a potential $\phi(x,y,z)$ as follows:

$$u = -B_x \frac{\partial \phi}{\partial x}, \qquad v = -B_y \frac{\partial \phi}{\partial y}, \qquad w = -B_z \frac{\partial \phi}{\partial z} \tag{6.1-48}$$

Combination of Equations (6.1-46) and (6.1-48) produces the MPF equivalent of Equation (6.1-47):

$$\frac{\partial}{\partial x}\left(B_x \frac{\partial \phi}{\partial x}\right) + \frac{\partial}{\partial y}\left(B_y \frac{\partial \phi}{\partial y}\right) + \frac{\partial}{\partial z}\left(B_z \frac{\partial \phi}{\partial z}\right) = 0 \tag{6.1-49}$$

Consider boundary layer flow over level ground. To produce an unaccelerated, horizontally homogeneous boundary layer flow over level ground, let $\phi = ax$, where a is a constant. Using Equation (6.1-48), $v = w = 0$ because $\partial\phi/\partial y = 0$, and u is proportional to B_x. From Equation (6.1-49), $\partial B_x/\partial x = 0$, which means that B_x is invariant with x but may have a dependence on y or z. The former is precluded by the condition of horizontal homogeneity, leaving B_x dependent on z alone. Therefore, u, having the same functional form as B_x, is also dependent on z alone.

The functional form of u(z) in the atmospheric boundary layer may be written as

$$u/u_\infty = (z/z_\infty)^\alpha \tag{6.1-50}$$

where subscript ∞ designates the top of the boundary layer and α is a stability dependent constant. In the free stream above the boundary layer, u is assumed constant and equal to u_∞. Since the functional forms of B_x and u are the same, B_x and B_{x_∞} may be substituted for u and u_∞ in Equation (6.1-50). Also, B_{x_∞} may be set equal to unity for convenience. This leads to the following specification for B_x for the postulated flow:

$$B_x = (z/z_\infty)^\alpha \qquad z \leq z_\infty$$

$$B_x = 1 \qquad z > z_\infty \qquad (6.1\text{-}51)$$

B_y is assumed to have the same functional form as B_x because constraints on horizontal motions over flat ground due to surface friction have no directional preference.

B_z reflects the influence of stratification on vertical velocities. It need not be defined for the postulated flow because the vertical velocity is zero everywhere. However, it is important for flow over irregular ground.

Over irregular terrain, the shape of the velocity profile and the height of the boundary layer vary with ground contours. In the MPF model, B_x as expressed by Equation (6.1-51) is assumed applicable at all horizontal locations, with z = 0 at the local ground surface, and the entire profile displaced vertically a distance equal to the increment in local ground elevation. B_y (= B_x) is treated in the same manner.

B_z is a stability dependent modifier of vertical velocities generated by the impressed horizontal flow around terrain irregularities. Like B_x and B_y, B_z should not vary horizontally, but it could vary vertically. To examine whether a vertical variation is necessary for the MPF model, we may refer to the Froude number, a hydrodynamic criterion which appears in the buoyancy term of the nondimensionalized equation of motion. When applied to a layer of thickness, ΔH, in which the velocity gradient, $\Delta U/\Delta H$, and the temperature gradient, $\Delta T/\Delta H$, are constant, the Froude number (Fr) is expressed as:

$$Fr = (\Delta U/\Delta H)\{(g/T)(\Delta T/\Delta H + \Gamma)\}^{-1/2} \qquad (6.1\text{-}52)$$

where

g = gravitational constant

T = absolute temperature

Γ = adiabatic lapse rate in the atmosphere = 0.01 C/m

In practice, ΔH is taken as the characteristic height of the terrain or the height of the boundary layer, and the velocity and temperature differences are measured over this height. Since the velocity at the ground is zero, ΔU may be replaced by the wind velocity at terrain height or in the free stream.

Parallelism between the behaviors of Fr and B_z as measures of flow stability can be demonstrated. It is generally accepted that vertical motion is suppressed when the temperature gradient is increased (buoyant restoring force is increased) and the horizontal velocity is reduced (inertial forces are weakened), in which case the numerical value of Fr is reduced according to Equation (6.1-52). The MPF model suppresses vertical velocity when B_z is reduced, according to Equation (6.1-48). Therefore, for both indices, a small numerical value is associated with strong stability. This parallelism suggests that, if a single value of Fr has been found to be acceptable as a stability criterion for the entire boundary layer, a single value of B_z should likewise be acceptable. Accordingly, B_z is not given a dependence on z in the MPF model, but its value decreases with increasing stability.

Table 6.1-5 gives values of z_∞, α, and B_z corresponding to each of the Pasquill-Gifford stability classes. The numerical values for z_∞ and α are somewhat subjective because judgment is required in assigning stability classes to atmospheric temperature and wind structures. The B_z values were selected by comparing velocity fields generated by the MPF model and a Navier-Stokes model applied to simple two and three dimensional sharp edged obstacles. A review of the Navier-Stokes modeling technique and several of the velocity field comparisons may be found in Reference 6-21.

The MPF equation is solved numerically to obtain the three dimensional wind field. A three dimensional array of grid blocks is placed over the terrain as shown schematically in Figure 6.1-9 and the lower blocks occupied by the terrain are discarded. The elevation of the bottom surface of each bottom block in a tier is adjusted to the average terrain elevation over the plan area of the block. The top, side, and end surfaces of the array are set at a sufficient distance from the hill to preclude reflection of wall effects into the flow field near the hill. The desired number of blocks is selected on the basis of core storage, and the number of blocks in each direction is specified. The dimensions of each block are selected to provide best resolution near the hill surface (and near the pollutant source when the MPF and dispersion model (discussed below) are to be run sequentially with the same array).

Initially, a unidirectional wind in the x-direction, containing the desired vertical profile of horizontal velocity, is assumed. No-flow boundaries at the horizontal and vertical surfaces of the lowest blocks are created by setting the appropriate flow coefficients to zero. All other boundaries have $v = w = 0$ and $u = u(z)$, with z measured above local terrain. A finite difference representation of Equation (6.1-49) is then solved by the line successive over relaxation (LSOR) method, starting with $\phi = ax$ and ending with a field of $\phi(x,y,z)$ that is compatible with the the terrain. This is an iterative procedure which develops the steady state solution through a reduction of the coefficient matrix to tridiagonal by calculating the vertical direction potentials at the new iterate while the others are at known iterate levels. Iteration proceeds until the material balance error is acceptable. Convergence of the iterative procedure is accelerated by choice of an optimum iteration parameter whose determination depends upon estimating

the spectral radius of the Gauss-Seidel matrix. The final velocity field, calculated by Equation (6.1-48), represents the original boundary layer profile modified by terrain-induced flow changes embodied in $\partial\phi/\partial x$, $\partial\phi/\partial y$, and $\partial\phi/\partial z$.

6.1.2.3.7.2 Turbulent Diffusion Model. After the modified potential flow model has established the wind flow field, turbulent dispersion of the pollutant is calculated within each box of the numerical model grid (see Table 6.1-6 for grid spacing) using the formulations discussed below.

A material balance on the pollutant advecting and diffusing in the atmosphere can be described by the following classical equation:

$$u\frac{\partial X}{\partial x} + v\frac{\partial X}{\partial y} + w\frac{\partial X}{\partial z} + q_s = \frac{\partial}{\partial y}\left(E_y\frac{\partial X}{\partial y}\right) + \frac{\partial}{\partial z}\left(E_z\frac{\partial X}{\partial z}\right) \qquad (6.1\text{-}53)$$

This equation is the well known steady state, advection-diffusion equation with source term q_s. The turbulent fluctuations of wind and concentration have been approximated by diffusion fluxes $E_i \cdot \nabla X$ $(i = y,z)$. This introduces turbulent mass eddy diffusivities E_y and E_z, similar to the eddy viscosity, which should vary with height in the boundary layer.

As discussed in the previous section, the boundary layer approximation produces a power law wind speed variation with height over flat terrain. This occurs because the eddy viscosity is also a power law function of height with an exponent $1 - \alpha$. By the analogy between mass transfer and momentum transfer, the eddy diffusivity would also be expected to vary in about the same manner with height, yielding the following power law variation of diffusivity with height:

$$E_y = E_{y_\infty}\left(\frac{Z}{Z_\infty}\right)^\beta, \qquad E_z = E_{z_\infty}\left(\frac{Z}{Z_\infty}\right)^\beta \qquad (6.1\text{-}54)$$

where E_{y_∞} and E_{z_∞} are the values of E_y and E_z, respectively, at height Z_∞ and β is close to, but not exactly equal to, $1-\alpha$.

The parameters E_{y_∞}, E_z , and β are stability dependent. These were estimated for each Pasquill-Gifford stability category by reference to the Gaussian dispersion model for flat terrain. The Gaussian model was used as a reference standard at ground level because its coefficients have been derived from a large amount of measured ground level concentration data. Equation (6.1-53) was solved numerically with Equation (6.1-54) for the case of flat terrain ($v = w = 0$) and the resulting ground level concentrations for each Pasquill-Gifford stability category were matched to those obtained from the Gaussian model by varying the parameters E_{y_∞}, E_{z_∞}, and β. The optimal values of these parameters needed to bring the two models into agreement were determined as follows:

- The exponent β was varied starting with $1-\alpha$ (α values are given in Table 6.1-5).

- The ratio $E_{y_\infty}/E_{z_\infty}$ was determined from the maximum ground level concentration.

- The value of E_{z_∞} was determined from the downwind distance of the maximum ground level concentration.

Values of E_{y_∞}, E_{z_∞}, and β obtained as discussed above are given in Table 6.1-5. It is assumed that these values also apply to the case of irregular terrain.

As previously discussed, the turbulent diffusion model [Equations (6.1-53) and (6.1-54)] is solved for the case of irregular terrain using the three dimensional wind field obtained from solution of the MPF model. The numerical procedure used is described in Reference 6-19. When both models are used together, they may be conveniently referred to as the modified potential flow-turbulent diffusion (MPF-TD) model.

6.1.2.3.7.3 Comparison with Gaussian Plume Models. A principal difference between the numerical and Gaussian plume models is the specification of the flow field and the variation of turbulent diffusivities with height in the atmosphere. The Gaussian plume models assume uniform wind velocity with height and crosswind spreading rates of pollutant that implies a variation of turbulent diffusivity with downwind distance but not with height. In the numerical model, both wind velocity and turbulent diffusivities are varied with height, as they do in the atmosphere according to a power law.

By using the selected power law models for the variation of velocity and diffusivity with height, ground level concentration estimates generated with the numerical model for flat terrain agree closely with analogous estimates made using the Gaussian model at, and downwind from, the location of maximum ground concentrations. This, and the fact that Gaussian models are calibrated using measured concentrations, implies that the two questionable assumptions in Gaussian models (the invariance of standard deviations with height and the invariance of wind speed with height) may offset each other.

The Gaussian plume models cannot properly account for the influence of variations in terrain elevation on the wind flow field. Although several kinds of nonmechanistic approximations are used to estimate this influence on ground level concentration estimates, none of them adequately represents the real physical situation. On the other hand, in the numerical solution technique, wind velocities and turbulent diffusivities are allowed to vary as they do in the atmosphere, and there is no need for artificial assumptions. The flow of air over and around a terrain feature is calculated in a mechanistic, physical way, and a material balance is accomplished at each grid boundary.

6.1.2.3.7.4 Representation of Vertical Parameters. The meteorological variables used by the program in setting up the boundary layer wind field and performing the diffusion calculations are given in

Table 6.1-5. The parameters used to modify the potential flows are $B_x = B_y = (z/z_\infty)^\alpha$ and B_z = (constant) in the boundary layer, and $B_x = B_y = 1$ and B_z = (same constant) above the boundary layer. The values of α, z_∞, and B_z are directly related to the amount of turbulence in the atmosphere. In a slightly turbulent (stable) atmosphere, the surface boundary layer will be relatively thin because the effect of friction at the surface will not be transferred by turbulent eddies very far up into the atmosphere. This lack of transfer allows the lowest layers to "feel" the surface more than higher levels. The lack of vertical transfer is also reflected in the actual value of the vertical flow coefficient that is small for this case. In the unstable case, characterized by a great deal of turbulence in the atmosphere, the vertical transfer is much more important. As a result, the layer of surface effect is much thicker, and the vertical flow coefficient is not restricted as in the stable case.

The diffusion calculation portion of the model requires three input parameters. These include the power law exponent, β, to be applied to the eddy diffusion coefficient in the surface boundary layer, the absolute value of the horizontal diffusion coefficient at the top of the surface boundary layer, and the ratio of the vertical to horizontal coefficients. Direct measurements of these parameters are rarely available from field data. Therefore, for each Pasquill-Gifford stability category, the values in Table 6.1-5 are used to simulate the turbulence characteristics of the atmosphere.

The diffusion transport in the x direction is neglected. Therefore, the horizontal diffusion coefficient, E_y, only refers to diffusion in the crosswind direction. This approximation is sufficient for all but puff releases or very low wind speed situations in which the diffusion in the horizontal plane would approach the same magnitude downwind as in the crosswind direction.

6.1.2.3.7.5 Model Validation. Model validation studies can be divided into two categories.

The wind flow part of the model has been compared with measurements collected during model experiments. The combined flow and dispersion (MPF-TD) calculations of concentration have been compared with field measurements. Each is discussed separately below.

6.1.2.3.7.5.1 Validation of the MPF Model. The MPF model was used recently in a licensing application involving impingement of a chimney plume on an isolated hill (Potomac Electric Power Company (PEPCO), Reference 6-22). Concurrently, Hunt et al (Reference 6-23) reported results of a physical model test for flow around a three dimensional hill towed in a density stratified water channel. Computer studies were undertaken by PEPCO to determine how flow patterns generated by the MPF model compared with those generated by the physical model under the strongest stability condition (lowest value of Fr) that could be expected with a large hill in the atmosphere. Halitsky (Reference 6-24) used the results of the PEPCO study to show that the MPF model

adequately simulated the results of physical model tests of Hunt et al, and that the MPF model could be adequately applied to a real terrain feature provided that the vertical flow coefficient, B_z, is given by

$$B_z = 0.1\ Fr$$

Furthermore, he concluded that the values of α and B_z given in Table 6.1-5 were adequate for real terrain features in general.

6.1.2.3.7.5.2 Validation of the MPF-TD Model. Concentration data taken in complex terrain at Huntington Canyon, at the Navajo Generating Station, and at Garfield, Utah, were available for comparison with MPF-TD model calculations.

The data collected in Huntington Canyon by the Air Resources Laboratory (Reference 6-25) were intended to provide measurements of plume dispersion in rough, canyon type terrain. The experimental method was to release SF_6 gas tracer and use helicopter sampling for measurements in the plume and canyon wall and floor sampling stations for the ground level measurements.

Tracer releases were made at two points. Elevated releases during unstable to neutral stability conditions (Tests 1-6) were made from the top of the Unit One stack of the Utah Light and Power's Huntington Canyon power plant. During such conditions, wind flows were generally up canyon. The second point of tracer release was from the canyon wall (Test 7) and flow (Tests 8-11) at a distance of about 10 km up the canyon from the power plant stack. These releases were made during strong temperature inversions and were always down canyon flows. Air Research Laboratory personnel classified the stability as Pasquill Category F.

In making the numerical model calculations, the initial atmospheric conditions at the point of tracer release were assumed to be invariant and with wind direction parallel to the valley centerline. This was an attempt to use the model as it would be used to make predictions when measured wind information was not available. More accurate results might be obtained if actual wind data were used as input since it would change the position of the plume centerline with respect to the sensor, with resulting changes in the predicted value. The numerical model overestimates as often as it underestimates the individual measured values within a factor of 3. Comparison of arithmetic means of the calculated and measured concentrations for stable cases is shown in the table that follows.

HUNTINGTON CANYON COMPARISONS FOR STABLE CASES

Test Number	Concentration Mean, $\mu g/m^3$	
	Measured	Calculated
7	0.45	0.73
8	9.8	42.7
9	9.2	15.2
10	10.2	28.9
11	84.6	37.4

The data from the Navajo Station were collected during stable atmospheric conditions when the plume interacted with the Vermillion Cliffs, a broad mesa top, approximately at plume height. A comparison of values computed using the numerical, EPA (Reference 6-26), and NOAA (Reference 6-27) models with the maximum measured ground level concen- trations near the top of Vermillion Cliffs is given in the table that follows.

COMPARISONS FOR NAVAJO POWER PLANT

Date (emission rate, g/sec)	Stability (wind speed m/s)	Peak Hourly Average SO_2 Concentrations, ppm	
		Predicted	Measured
October 16 (583)	F (1.5)	0.11	.102
	F (2.1)	0.08	
	E (1.5)	0.078	
	E (2.1)	0.058	
November 24 (478)	F (1.5)	0.087	.070
	F (2.1)		
	E (1.5)		
	E (2.1)	0.057	
December 2 (376)	F (1.5)	0.066	.069
	F (2.1)		
	E (1.5)		
	E (2.1)	0.048	

The table shows that the peak hourly average SO_2 concentrations could be predicted accurately by the numerical model. The combination of wind speed and stability was presented to cover the variability in measured meteorological conditions on these days. The numerical model predictions are within a factor of two of the measurements regardless of the four conditions selected. For F stability conditions with wind speeds of 1.5 m/sec, numerical model results would be in very close agreement with the measurements.

During June and July of 1973, NOAA Air Resources Laboratory personnel conducted SF_6 tracer tests in the mountainous terrain near Garfield, Utah (Reference 6-25). Sulfur hexafluoride was released from the 122m stack of an operating smelter of Kennecott Copper Corporation. NOAA's airborne helicopter and ground level tracer samples were obtained to evaluate maximum aerial concentrations and ground level concentration distributions. The plume centerline height over rough terrain predicted by the numerical model closely matched the observed location. Therefore, the ground level concentrations computed using the numerical model should be reasonably accurate as shown in the following table.

MODEL COMPARISONS FOR TEST CASES OF TRACER RELEASES AT GARFIELD, UTAH

Test	Ratio Calc/Obs	Pasquill Stability
2	0.90	C
3	0.45	C
7	1.50	B

The validation cases indicate that when the effect of major terrain on the wind flow field is included by using the numerical model, the predictions are within a factor of about 2-1/2 on the average for different complex terrain situations under stable and unstable atmospheric conditions.

The observed differences between the numerical model measured data are not unreasonable. In fact, they are about the same as are characteristically observed in data comparisons with the generally accepted Gaussian models. Comparisons of Gaussian model results often show considerable skew, and in a typical case, about 50% of the measured data fell within a factor of 2.0 of predictions (Reference 6-28).

6.1.2.3.7.6 Grid Specification and Terrain. The basic approach is to use the three separate grid systems as illustrated in Figure 6.1-9. The "Elevation Grid" describes input information prepared by digitizing terrain elevation from a U.S. Geological Survey contour map and translating these elevations at each intersection of a very fine two dimensional grid. The "Calculational Grid" is constructed based on the receptor location, source, terrain, and atmospheric conditions for the

particular run being made. Calculation results are obtained for specified locations within the "Calculational Grid." A grid similar to the master grid is shown at the bottom of Figure 6.1-9.

The grid block sizes selected are not uniform. In the x (downwind) direction and in the y (crosswind) direction, relatively small grid spacing is used around the source, receptors, and important terrain features. In the z (vertical) direction, relatively small grid blocks are used at the ground level and at effective plume height. In general, the z dimension of the grid matrix is usually chosen to be much less than the x and y dimensions. Both the z and y dimensions of the total grid matrix must be chosen so that no pollutant is reflected from the top and side boundary planes of the model. Grid dimensions used in the terrain calculations are given in Table 6.1-6.

6.1.2.3.8 DISP Interdiction with MPF Data

The output from the MPF model includes the velocity and concentration fields and the plume centerline trajectories. Dose calculations require knowledge of the concentration field, the plume centerline height, the plume width, and an effective σ_z for the plume. The last two quantities are not given directly. An effective plume width, W, is calculated from the MPF model concentration field by searching for the 10% concentration boundaries; that is, the distances on either side of the plume centerline where the concentration falls off to 10% of the maximum concentration in the plume cross section. An effective σ_y is then defined from $W = 3\sigma_y$. An effective σ_z is then calculated from the CRAC dispersion formula, Equation (6.1-10), applied at the plume centerline using the effective σ_y and the value of the maximum concentration in the plume cross section. These calculations are made in DISP. The MPF dispersion values are corrected to the wind speed for the hour by ratioing to the measured speed at the appropriate height, used in the MPF offline analysis.

The MPF model solution is assumed to be valid up to a travel distance of 9.0 miles from the source. At this distance, the MPF model output is matched to the DISP dispersion model by considering the relative location of the plume and the inversion lid. Dispersion downwind of this point is calculated using the DISP dispersion model. If there is more than a 45^0 change in the wind direction, use of the MPF results is discontinued and the calculation will revert back to Gaussian dispersion and plume tracking in accordance with regional meteorological data. A virtual source technique is used to match the Gaussian plume segment to the MPF segment.

6.1.2.3.9 Turbulent Internal Boundary Layer (TIBL) Model

This section describes a phenomenon which is not applicable to the Indian Point site but is included in this text for completeness. In certain land/water interface zones, a lid condition can exist that is not parallel to the ground. When relatively cool stable air, that has traversed a large body of water, flows onshore during periods of moderate to strong solar insolation, the air near ground level is heated from below. The degree of vertical penetration of the land-heated air

into the stable cooler air aloft increases with inland distance. An approximately parabolic shaped interface or lid is formed, starting at or near ground at the shore and increasing in height with inland distance. This separates the relatively warm unstable air near the ground from the relatively cooler stable air aloft. The unstable warm air layer near the ground is referred to as a turbulent internal boundary layer (TIBL). The parabolically shaped interface is referred to as the TIBL lid. The height of the lid is often called the TIBL height. Plumes injected above or below this particular type of lid cannot be treated with the conventional lid processing scheme described in previous sections. Therefore, the TIBL model described below was added to CRACIT and is used for daytime onshore flows when the incoming solar insolation is sufficient to lead to TIBL formation.

Since the height of the TIBL increases with distance from the shoreline, the plume from a source located inland can be released below or above the TIBL, depending upon its release height and buoyancy. If the plume is released near ground level and is nonbuoyant or the buoyancy is insufficient to penetrate the TIBL lid, it will eventually become trapped beneath the lid. Its growth and dispersion will be governed by the degree of turbulence (instability) beneath the TIBL lid and the growth rate of the TIBL. If the release is above the TIBL, or is below the lid with buoyancy sufficient to penetrate the lid, the plume will level off (achieve maximum rise) rapidly in the stable air aloft. Plume growth for some distance will be governed by the stability above the lid. Since the TIBL height increases with downwind distance, the plume will eventually intersect the TIBL and begin to fumigate to the ground, becoming uniformly mixed in the unstable layer beneath the lid. The TIBL lid will continue to grow through the plume until it has completely fumigated (Figure 6.1-10). Once fumigation is complete, plume growth is governed by the stability beneath the lid and the rate of growth of the lid.

6.1.2.3.9.1 Calculation of TIBL Lid Height. The height of the TIBL lid at any inland distance is given by Lyons (Reference 6-29).

$$L(x) = h_p + \left[2\gamma^2 \frac{\phi(t) q_{ho} \, SIN\left(\frac{\pi t}{\tau}\right)}{(\partial\theta/\partial z) C_p} \right]^{1/2} \frac{(X + X_s - X_o)^p}{U_u^{1/2}} \qquad (6.1\text{-}55)$$

where

$L(x)$ = height of TIBL lid at downwind distance X

h_p = offset height (height of TIBL lid at shoreline)

γ = site specific constant

$\phi(t)$ = hourly solar insolation factor (ϕ = 1 for zero cloud cover; ϕ = 0 for complete cloud cover)

q_{ho} = solar heat flux constant (= 15% of solar constant)

t = time after sunrise

τ = amount of time (in a day) that it is daylight

$\partial\theta/\partial z$ = gradient of potential temperature above TIBL (stable air)

C_p = heat capacity of air above TIBL

ρ = density of air above TIBL

U_u = wind speed at upper level on meteorological tower

X = downwind distance from source to point of interest

X_o = distance from shoreline at which TIBL growth begins

X_s = distance from shoreline to source in direction of wind

P = distance power law parameter (~0.5)

The precise values of all parameters in Equation (6.1-55) are not always available for each hour of data used in CRACIT. Therefore, for model applications, Equation 6.1-55 is approximated by

$$L(x) = h_p + \left(\frac{\beta}{U_u}\right)^{1/2} (X_1 + X_s + X_o)^P \qquad (6.1\text{-}56)$$

where β is a growth rate parameter which approximates the quantity in brackets in Equation (6.1-55) and is a function of solar intensity and the stability of the air mass over the water body.

6.1.2.3.9.2 Rise, Growth, and Dispersion of Plumes Released Above TIBL. If the release height is greater than the TIBL lid height directly above the source, the plume is released into the stable layer aloft. The plume rise for bouyant releases is given by Equations (6.1-13) to (6.1-18), the Briggs' formulae for stable atmospheres. Plume growth and dispersion is given by a modification of the Lyons and Cole (Reference 6-28) TIBL model which is an adaptation of the Gaussian dispersion model. The model will be presented here by reference to Figure 6.1-10. Before proceeding, the following variables are defined:

f = fraction of plume that has fumigated undet the TIBL lid

H = plume centerline height

U = wind speed at reference height

X_b = downwind distance at which TIBL fumigation begins

X_e = downwind distance at which TIBL fumigation is complete

X/Q = normalized ground level concentration

$\sigma_y(u)$ = crosswind sigma evaluated at stability under TIBL (unstable)

$\sigma_y(s)$ = crosswind sigma evaluated at stability above TIBL (stable)

$\sigma_y(f)$ = crosswind sigma during TIBL fumigation

$\sigma_z(u)$ = vertical sigma evaluated at stability under TIBL (unstable)

$\sigma_z(s)$ = vertical sigma evaluated at stability above TIBL (stable)

The plume sigmas, $\sigma_y(u)$, $\sigma_y(s)$, $\sigma_z(u)$, $\sigma_z(s)$ are evaluated from the Martin and Tikvart expressions (Table 6.1-2) with appropriately defined virtual sources.

The plume first begins to fumigate at X_b defined by $L(X_b) = H - 2.15\sigma_z(s)$. Fumigation is complete at X_e defined by $L(X_e) = H + 2.15\sigma_z(s)$. For $X \leq X_b$ the plume is dispersing freely above the TIBL lid. The normalized ground level concentration (X/Q) is given by the CRAC modified Gaussian diffusion equation (Equation (6.1-10)). For $X_e < x < X_b$, the plume is in the process of fumigating. Lyons (Reference 6-29) gives

$$X/Q = \frac{f}{\sqrt{2\pi}\sigma_y(f)UL(x)} \exp - \frac{1}{2}\left(\frac{Y}{\sigma_y(f)}\right)^2 \qquad (6.1\text{-}57)$$

The plume is assumed to be Gaussian in the crosswind direction. According to the CRAC modification (uniform plume of width $3\sigma_y$ in crosswind direction) developed in Section 6.1.1.1, Equation (6.1-57) becomes

$$(X/Q) = \frac{f}{3\sigma_y(f)L(x)U} \qquad (6.1\text{-}58)$$

The fraction fumigated is given by

$$F = \int_{-\infty}^{P} \frac{1}{\sqrt{2\pi}} \exp\left(-\frac{1}{2}P^2\right)dP \qquad (6.1\text{-}59)$$

where

$$P = \left(L(x) - H\right)/\sigma_z(s) \qquad (6.1\text{-}60)$$

The crosswind sigma for fumigation is modified to account for enhanced growth during fumigation and is given by

$$\sigma_y(f) = \sigma_y(s) + H/8 \qquad (6.1\text{-}61)$$

Once the plume has completely fumigated ($X \geq Xe$, $f = 1$) it becomes trapped under the TIBL lid with uniform concentration in the vertical. Crosswind plume growth is the result of stability under the lid. Therefore, it is necessary to define a virtual source based on the value of $\sigma_y(f)$ at $X = Xe$ so that values of $\sigma_y(u)$ for $X > Xe$ can be evaluated.

For the completely fumigated plume, X/Q is obtained from Equation (6.1-38) applied to the TIBL lid height,

$$\frac{X}{Q} = \frac{1}{3\sigma_y(u)L(x)U} \qquad (6.1\text{-}62)$$

An effective $\sigma_z(U)$ for the completely fumigated plume is defined by analogy to Equation (6.1-44),

$$\sigma_z(U) = .7979\ L(x) \qquad (6.1\text{-}63)$$

6.1.2.3.9.3 Rise, Growth, and Dispersion of Plumes Released Below TIBL. Plumes released below the TIBL lid that are nonbuoyant or have insufficient buoyancy will not penetrate the TIBL lid. Conversely, plumes with considerable buoyant energy may penetrate the TIBL lid. The criteria for plume penetration are as follows:

- An initial estimate of H at the distance X is obtained from the Briggs' formulae Equations (6.1-18) through (6.1-22) for unstable atmospheres.
- If $H + \sigma_z(u) \leq L(X)$ and the plume has achieved its maximum rise, the plume has failed to penetrate the TIBL.
- If $H + \sigma_z(u) > L(X)$ and the plume is still rising, the plume is in the vicinity of the lid. The actual plume rise is calculated from the penetration equations Equations (6.1-23) through (6.1-25).

A plume that has penetrated the TIBL lid is subsequently treated as a plume released above the TIBL with one modification. To account for the initial plume growth in the unstable layer beneath the TIBL, new virtual sources are defined based on the values of $\sigma_y(u)$ and $\sigma_z(u)$ at the point (distance) of penetration and the stability above the TIBL. Subsequent growth in the stable layer $\sigma_y(s)$, $\sigma_z(s)$ is based on these virtual sources. Otherwise the logic of Section 6.1.2.3.9.2, applies.

If the plume fails to penetrate the lid, it eventually becomes trapped beneath the lid. The criteria for trapping are as follows:

- If $L(x) > H + 2.15\sigma_z(u)$, the plume is dispersing freely below the TIBL lid. X/Q is calculated from Equation (6.1-10).
- If $L(x) < H + 2.15\sigma_z(u)$, the plume is trapped. If $H > 2.15\sigma_z(u)$, the plume is trapped aloft. X/Q is obtained from Equation (6.1-36), the CRAC modified Bierly and Hewson equation. If $H \geq 2.15\sigma_z(u)$, the plume is trapped completely on the ground and is well mixed in the layer beneath the lid. The plume condition is exactly the same as if it had been completely fumigated by the TIBL and Equations (6.1-62) and (6.1-63) apply.

The treatment of plumes that have not penetrated the TIBL is very similar to that for dispersion beneath a mixing lid.

6.1.2.3.9.4 TIBL Inland Penetration. After air flowing onshore has traveled a considerable distance inland, it is warmed and mixed to such an extent that a definite TIBL lid interface no longer exists. The TIBL inland penetration distance is a function of solar insolation and the stability of the air over the water body and can only be determined from experimental data. When data are sparse or lacking, an estimate is made based on physical judgment by meteorological data. A distance greater than the TIBL penetration distance, plume growth, and dispersion are treated by the dispersion model previously discussed. This incorporates a lid based on mixing height.

6.1.2.3.9.5 Use of TIBL Equations. The meteorological data stored for each hour in the input data base are insufficient for determining the existence of or extent of a TIBL condition. Therefore, expert judgment is applied to first determine if the equations apply for a given start hour; and, if so, what values of the input parameters are appropriate. The TIBL equations are then used for all start hours that apply. After inspecting of the results, further editing of plume parameters may be necessary as discussed in Section 6.1.2.3.10.

6.1.2.3.10 Offline Plume Processing to Incorporate Expert Judgment

No matter how good the quality or quantity of site data, there are cases in which the models for defining plume dispersion and trajectory are not accurate. Examples of such cases are conditions over large bodies of water where no measurements exist and the influence of complex terrain on plume trajectory. To reduce the uncertainties, a method was devised to enable a pre-edit of the parameters that define plume behavior before performing the dose calculations. A schematic of this procedure is illustrated in Figure 6.1-11.

To accomplish this feature, a minicomputer and a graphics cathode ray tube (CRT) were used. Each plume scenario was displayed on a site map on the CRT along with printed values for pertinent parameters for "before" and "after" edit cases as illustrated in Section 6.2. A team of diffusion meteorologists then inspected the plume characteristics for reasonableness and decided what, if any, changes were necessary. Edits were possible for each of six parameters: wind speed, wind direction, stability, lid height, rainfall, or plume front width. After the editing process, the plume is redrawn for inspection and again changed if necessary. The editing process was repeated until the appropriate plume scenario was achieved. Then, all the parameters normally available after the ACTIVE routine were stored on a file that was available for input to the subsequent CRACIT run. This procedure was done for each of two groups of release categories, one for elevated releases and one for ground level releases. More site specific information on the results of this procedure is contained in Section 6.2.1.3.

6.1.2.4 Characterization of Plume Trajectory (GRIDOS)

Having defined the length and meteorological characteristics for each spatial interval, the program progresses through the DISP and ACTIVE subroutines. After the plume front width is computed in ACTIVE, all the

information necessary to describe plume width is available for each spatial interval. Thus the plume can be characterized by a series of trapezoids (case B, see Figure 6.1-6) that change length according to wind speed (or maximum distance criteria) the width according to stability (stable plumes grow slower than unstable plumes) and duration of release (plumes for longer release times have more time to meander or change direction and cover a wider area). Case B, Figure 6.1-6, characterizes the straight line plume represented by a series of trapezoids based on computations in the SPEDIT, DISP, and ACTIVE subroutines. Case A in Figure 6.1-6, shows the plume shape derived using the original CRAC program for comparison.

Now suppose the wind direction had changed as a result of the plume entering a new meteorological region or because of an hour change. The area covered and population exposed around the site could be considerably different compared to the straight line characterization shown as case C on Figure 6.1-6. Thus, the problem becomes one of representing the plume area of coverage following a trajectory dictated by the local wind direction. This was accomplished in the new routine called GRIDOS, which is flow diagrammed schematically in Figure 6.1-12. The following description discusses each program step in GRIDOS. Refer to Figure 6.1-13 for a graphic description of trajectory development and definition for two typical adjacent spatial intervals.

- First, the centerline direction of the next hour's plume path (16 possible) from the center of the end of the previous hour's plume front is established as in step 1 of Figure 6.1-13.

- If the angle between the centerline angle is less than or equal to 90^0 from the last centerline trajectory, draw the plume front for the last plume as if it bisected the large angle shown in step 1 of Figure 6.1-13.

- If the new centerline angle is greater than 90^0, draw the last plume front as if it bisected the angle opposite to the last case as shown in step 2 of Figure 6.1-13.

- Next, to form the plume area for a wind change less than 90^0, connect the ends of the plume fronts with straight lines (e.g., A to C to E and B to D to F in step 3 of Figure 6.1-13).

- If the plume turns more than 90^0, the edges of the next plume front are reversed to form a trapezoid with no crossovers (e.g., A to C to F and B to D to E in step 4 of Figure 6.1-13). Note that E and F have been reversed and that the same area (marked "area of overlap" on the figure) lies beneath portions of two different spatial interval polygons. Thus, longer plume residence time and higher exposures are accounted for in this area. GRIDOS includes a routine to ensure that crossovers of spatial interval boundaries do not occur (i.e., that a four sided polygon results for each spatial interval after turning).

The technique used here imagines the plume boundaries to be described as the projection on the ground of a puff that expands as it travels downwind and turns, according to wind direction, at the end of any spatial interval. Certain release categories have release durations over relatively long periods of time. These categories generally have considerably lower source terms, and thus, lower consequences than the shorter duration releases. Plume width is increased to account for more plume meander as the release duration increases. The CRACIT program can break the release up into as many as four phases as described in Section 6.1.2.6.

6.1.2.5 Overlaying the Plume on the Fine Grid (GRIDOS)

The new plume area definition and dispersion calculations are not compatible with the CRAC straight line, 16 direction sector grid with fixed downwind distances for meteorology and population data. As soon as the direction changes, the required symmetry about the direction sector centerline and the simple geometry of having the trapezoid side boundaries parallel to the direction sector boundaries are lost. Therefore, it was necessary to abandon the old grid in favor of a more finely spaced grid. A radial grid with 64 direction sectors and 400 meter radial spacing out to 20 miles was chosen with increasingly larger spacing out to 2,000 miles as shown in Table 6.1-7 for the fine grid. This spacing provides adequate resolution for plumes of all stability classes (widths) traversing the grid at any angle. The grid spacing becomes larger at greater distances where plume areas are also larger. It is important to characterize the area receiving the exposure accurately to properly account for threshold effects in the dose model so that if a larger population group received a lower dose, the effect would not necessarily be the same as a larger dose to a smaller group.

An example of the plume overlay on the fine grid is shown in Figure 6.1-14. Calculations of doses to population groups on this grid are discussed in Section 6.1.2.7.

Another very important task performed by GRIDOS involves saving information for each fine grid location to indicate which of the 34 spatial intervals have reached each fine grid location. Referring again to the GRIDOS flow diagram in Figure 6.1-12, the following functions take place:

- Using the locations and boundaries of the nth spatial interval polygon from previous GRIDOS processing, subroutines POLYPT and INTSCT are called to determine which fine grid elements have their centers within the spatial interval boundaries.

- Fine grid elements that are in the spatial interval are identified. Thus, it is known which spatial intervals passed over the fine grid element during the entire pasage of the plume including possible overlaps.

- This process continues until all 34 spatial intervals have been processed and all flags are set on the fine grid for the complete meteorological sequence.

Knowing the spatial interval at the fine grid element also defines the time of plume arrival, speed of plume passage, and dispersion information for later use. Provisions are made to enable more than one spatial interval to reach the same fine grid element. Thus, all plume information is stored in memory for processing in the evacuation and dose computation routines described in the following sections.

6.1.2.6 Multiple Phase Release Model

Releases that are longer than 1-hour duration can be divided into multiple phases of at least 1 hour each up to a maximum of four phases. This facilitates a more realistic assessment of longer releases that are characterized by release rates of each fission product group that vary with time. For example, if a release is 3 hours long, it can be considered to have two phases with source terms for the first hour (first phase) which differ from the source terms for the next 2 hours (second phase). Each phase of the release is treated as a separate plume during the calculations described in the preceding sections. The dose contribution (to effects) to a receptor in each fine grid element from each phase is totaled and used in the compuations (of doses) of health effects described in the following section (6.1.2.7). The meteorological data sequence used for each phase starts on the hour that the phase is released. Therefore, different phases of the release may follow different trajectories, each determined by the meteorological conditions that exist during that phase of the release. Leakage rates for each phase are input to CRACIT using the original CRAC program input structure for multiple leakage categories.

6.1.2.7 Computation of Doses and Health Effects

At the completion of subroutine GRIDOS, plume trajectory segments have been laid out in space on a fine grid and data for each segment (air and ground concentrations by isotope and arrival times) have been stored.

The remaining task is to quantify the impact of the release on public health. The impact on public health results from two exposure phases: early exposure and chronic exposure. Early exposure, exposure that occurs within a short time following release, may be distinctly different for two population groups, people who evacuate immediately upon notification and those who do not. Within both groups there are subgroups whose exposures are distinctly different because of varying radiation conditions at the different residence locations. Exposure is also different for evacuees at points along their different evacuation paths. A minor additional complication is that the numbers of people in each group vary with the start time (season or time of day).

Chronic exposure results from return to normal use of the land contaminated during the passage of the radioactive cloud and accumulates over a period of years following the release. The program has been made flexible to accommodate studies of the effects of different mitigation strategies:

- Public health impacts from early phase exposures received by evacuees.

- Public health impacts from early phase exposures received by people who do not evacuate.

- Public health impacts from chronic exposures received during the years following the release by people who occupy contaminated areas or who consume food grown in those areas.

These problems are solved by a set of subroutines controlled by subroutine DAMG in CRACIT. Program flow through this group of subroutines is shown in Figure 6.1-15. It also shows the position of this group of routines in the overall flow of CRACIT. The functions are described in the following.

6.1.2.7.1 Computation of Doses for Fixed Early Exposures

CRAC and CRACIT use 54 isotopes for computing doses from early exposure. This computation of dose by isotope for each of the large number of population groups in CRACIT is not necessary. For this reason, CRACIT uses the subroutines UDOSE and ERLY (derived from CRAC's EARLY) to compute and store ground, cloud, and inhalation doses summed over all isotopes for hypothetical early exposures to radioactivity in each spatial interval. Doses for each organ of interest are saved to assess acute effects from early exposure and by each organ of interest for latent effects from early exposure. In addition, since it accumulates slowly following exposure, it is computed for a single short period that varies by organ for acute effect computation and for up to 10 multiyear periods for latent effect computation. Exposure during passage of the entire cloud was used as a basis for computing cloud and inhalation doses. Ground doses were computed and saved for two exposure times, 8 hours and 7 days.

In subsequent computations these doses are adjusted by scaling and interpolation to obtain doses for exposure times differing from those used in EARLY. With this approach, the isotopic dose is computed only once for each weather sequence and is a negligible contributor to overall computation time.

6.1.2.7.2 Computation of Exposures, Doses, and Impacts

The major part of the impact computation is performed in a subroutine called PMATCH and a group of five subroutines called from it.

One function of PMATCH is to determine early phase exposure characteristics for individuals representing subgroups within each of the two population groups evaluated for those effects, evacuees and noneva-cuees. The exposure characteristics determined are times of exposure by cloud path spatial interval for exposure to ground contamination and times of exposure by cloud path spatial interval (as a fraction of total cloud passage time) for exposure to airborne radioactivity. These exposure characteristics are used in subroutine EDH that computes total doses by organ and pathway for the representative individual and then computes the probability per person for each type of health effect considered. These probabilities, along with the number of people in the

population subgroup, are used to compute total health effects from the early exposure phase. Subroutine EHTOT performs this totaling operation and accumulates health effects totals over all population subgroups exposed to radiation.

A major function of subroutine PMATCH is to set up the chronic exposure health effects calculations. This function is detailed later in this section.

Subroutine PMATCH first reads in site population and evacuation data. To conserve computation time, the population grid has a "coarser mesh" than the fine grid used for mapping the cloud path but is designed so that an integral number of fine grid elements is contained within each population grid element. The CRACIT population grid structure is shown in Table 6.1-7 and the relation to fine grid structure is shown in Figure 6.1-16. The population grid has 32 direction sectors and 34 distance segments for a total of 1,088 elements. To provide maximum resolution where it is needed most, the length of distance segments are smallest near the plant. Good resolution is required for a clear definition of the population spatial distribution and evacuation paths.

Separate population data files are stored for each evacuation scenario. The appropriate set is selected in PMATCH based on the start date of the weather sequence being evaluated.

The first part of the evacuation data read by PMATCH is a set of data that is used to determine the evacuation path followed by any evacuee. The evacuation path is defined as a sequence of population grid elements through which an evacuee moves. The items read in are: the distance a resident of the grid element travels to leave it, the sector and segment identifiers of the next population grid element in the evacuation path, and the distance traveled while crossing the next element. It is assumed that once an evacuee enters a new population grid element, he follows the path of the evacuee who started from that element. It is further assumed that all evacuees starting from a given element follow the same path. The data input was determined from studies of evacuation routes near the plant. The flexibility of the model is enough to permit simulation of evacuation paths. In some cases, topographic features may dictate that evacuees from certain locations must follow a path that requires them to travel toward the plant before they turn away. These features are simulated in the model. The model does not reflect any capability for evacuees to avoid contaminated areas by changing their paths. To the extent that such capability would exist, the results obtained in this study would be overstated.

The outer limit of the area within which people are evacuated is determined by the user by specifying the subscript of the outermost population grid distance segment evacuated. Thus, the area is always circular. Sufficient data for the site exist on the CRACIT file to simulate evacuation within approximately a 10-mile radius. No one beyond the limiting distance is assumed to be evacuated within the model, and paths followed by evacuees are terminated when they reach the limiting distance.

It is assumed that the same paths would be followed during any of the evacuation scenarios, day, night, seasonal, etc. Evacuation data read by PMATCH can account for different evacuation speeds for each population grid element; one set for each evacuation scenario. Speeds specified for each grid element permit the simulation of "bottlenecks" along the evacuation path. The various speed sets allow for consideration of the effect of population variation on evacuation speed.

The approach used in PMATCH for computing early phase exposures differs for evacuees and nonevacuees. The population that evacuates from a single population grid element is the subgroup considered to be a unit for computation of health effects from early exposure for evacuees. At each fine grid element within each population grid element along the path, the exposures of an individual representative of the population to airborne and ground radioactivity are computed for each cloud path spatial interval that covers the fine grid element. These exposures are accumulated over the entire evacuation path. The early exposure phase for evacuees ends at the termination of the evacuation path after the evacuee has occupied that location for 4 hours. This assumption is equivalent to that made in the RSS and was based on the assumption that persons would not remain in highly contaminated areas. The exposures accumulated over the evacuation path are then used to compute doses and health effects probabilities per person in EDH. The results from EDH and the number of people in the evacuee subgroup are then used in EHTOT to compute total health effects for the subgroup. The results are accumulated over all evacuee population subgroups.

Calculating the exposure of an evacuee at any point is a matter of timing. Evacuee arrival and departure times for every population grid element along the evacuation path are computed from evacuation travel distances and speeds discussed before. Warning and delay times are taken into account. Similarly, cloud front arrival times and cloud departure times are known for each cloud path spatial interval. If the evacuee leaves a population grid element before the arrival of any spatial interval, there is no exposure. If he arrives in a population grid element after the cloud has departed, he receives only ground exposure. If the cloud and the evacuee are present in one population grid element at the same time, the evacuee receives both ground and cloud exposure. Ground exposure time is computed from time spent on contaminated ground. Cloud exposure is estimated as some fraction of full cloud passage determined by the ratio of time spent in the presence of the cloud to the time required for full passage of the cloud.

Allowance is made for the fact that radiological conditions vary between fine grid elements within a population grid element, and for evacuees moving through grid elements (see Figure 6.1-14). Assume an evacuee enters population grid element (10,5) at some time after the departure of the cloud from cloud path spatial intervals 1 and 2, both of which fall within the element. The evacuee receives ground exposure from both spatial intervals. However, it is assumed that his time in the population grid element is evenly distributed between all fine grid elements within it. This means that while he receives ground exposure from spatial interval 1 for the entire time he spends in the population grid

element, he receives ground exposure from spatial interval 2 for half the time in the population grid element since spatial interval 2 covers only half of the fine grid elements within population grid element (10,5).

Thus, the evacuees' exposure is "averaged" over the population grid element. This averaging introduces some error into the analysis. However, this error may be an overestimation or an underestimation. In addition, the exposures accumulated in individual population grid elements are likely to be quite small because of short residence times. It is also likely that the errors introduced in the estimate of exposures accumulated along the entire evacuation path are small.

The population that resides in a single fine grid element and does not evacuate is the subgroup considered to be a unit for computation of health effects from early exposure for nonevacuees. The population distribution in any element is assumed to be uniform. Analysis on a population grid element basis, using radiological conditions averaged over the population grid element, could possibly lead to a significant underestimate of acute injuries and early fatalities. The following points were weighed in opting for the fine grid basis:

- Acute injuries and early fatalities have thresholds with fairly rapid increases in effects with increasing doses. Nonevacuees may be particularly vulnerable to these effects.

- Radiological conditions may vary greatly between fine grid elements within a population grid element.

- The nonevacuee remains stationary in his home fine grid element throughout the entire early phase of exposure. There is no basis for assuming that he moves between fine grid elements thereby encountering radiological conditions averaged over some larger area.

Conversely, assuming radiological conditions for the population grid element to be the same as for the most highly contaminated small grid element could result in significant overestimates of early fatalities and injuries, again largely due to the threshold effect.

So, for each occupied fine grid element in the cloud path, exposures are initially set at full cloud passage for exposure to airborne radioactivity. To simulate exposure at relocation centers, it is assumed that evacuees spend 4 hours in the terminal elements of their evacuation trajectories. These locations are just beyond the evacuation zone. It is also assumed that the resident beyond the evacuation zone would be relocated within 24 hours, and the ground dose is calculated to be equivalent to 24 hours of exposure. This exposure time, along with the assumed factor of 3 reduction in ground dose because of shielding, may result in an overestimate of doses and health effects. Further study of these parameters would be expected to lead to reductions in health effects.

The impact on health from chronic exposure is calculated for each population grid element. During PMATCH processing of health effects from early phase exposures, fine grid elements within a population grid element are examined to see which element has the highest ground concentrations, and indicators for the cloud path spatial intervals set for that fine grid element are set for the population grid element. In addition, the fraction of the area within the population grid element that is contaminated to any extent is saved. In the computation of health effects from chronic exposure it is assumed that only the contaminated area within the population grid element is affected. However, it is assumed that the severity of contamination throughout the area is the same as the most severely contaminated fine grid element within the area. Ground concentrations representative of the contaminated area are computed and passed to subroutine CHRONX. CHRONX computes a contamination severity code, decontamination factors, and decay times. It also determines whether land should be interdicted or decontaminated, and computes chronic exposure health effects probabilities per person. CHTOT then uses affected areas and populations from PMATCH to compute and accumulate health effects from chronic exposure.

TABLE 6.1-1

CLASSIFICATION OF ATMOSPHERIC STABILITY
USED IN CONSEQUENCE ANALYSIS

Stability Classification	Pasquill Categories	Temperature Change With Height (^{o}C/100m)
Unstable	A	< -1.9
Moderately Unstable	B	-1.7 to -1.9
Slightly Unstable	C	-1.7 to -1.5
Neutral	D	-1.5 to -0.5
Slightly Stable	E	-0.5 to 1.5
Moderately Stable	F	> 1.5

TABLE 6.1-2

VALUES OF DIFFUSION COEFFICIENTS
USED IN DISPERSION MODEL

Pasquill Stability Category	Diffusion Coefficients*	
	σ_y	σ_z
A	$0.3658 \times 0.9031^{**}$	$0.00024 \times 2.094_{-9.6}$
B	0.2751×0.9031	$0.05500 \times 1.098_{+2.0}$
C	0.2089×0.9031	0.11300×0.911
D	0.1471×0.9031	$1.26000 \times 0.516_{-13.0}$
E	0.1046×0.9031	$6.73000 \times 0.305_{-34.0}$
F	0.0722×0.9031	$18.05000 \times 0.18_{-48.6}$

*From Reference 6-3.
**The distance (x) is raised to the power 0.9031.

TABLE 6.1-3

CONSEQUENCE MODEL SUBROUTINE INVENTORY

Remaining Original CRAC Subroutines	Deleted Original CRAC Subroutines
MAIN[1]	SITE
INPUT	SPADAT
ISOTOP	EXTRCT
INCORE	DAMAGE
LEAKAG	EARLY
SIT	POPU
SPAT	
SCALE	
RESIN	
OPT	
EVACU[2]	
DISOPT	
ECONOM	
CHRON	
TOPO	
ACUTE	
LATE	
RANDU	
TIMES	
TIMESZ	
INCTIM	
DISP[3]	
ACTIVE[3]	
POL[2]	
SHINCF	
CHRONX[1]	
PROPDAM[1]	
STORE	

1 Some modifications were made.
2 Most population and evacuation data are input from a separate file produced by a separate support program (PEVAC).
3 Extensive modifications were made.

TABLE 6.1-4

COARSE AND FINE MESH SPACING FOR SPATIAL INTERVALS

Spatial Interval	Fixed Spatial Interval Distance in CRAC (Miles)	Targeted Spatial Interval Distance in SPEDIT (Miles)	Targeted Incremental Spacing As A Function Of Distance In SPEDIT (Miles ±50%)	Typical Spacing In SPEDIT for Actual Meteorological Sequence (Miles)	Example of Typical Weather Conditions			
					Hour Number	Wind Speed (m/sec)	Stability	Direction
1	0.5	0.5	0.5	0.45	1	1.0	1	8
2	1.0	1.0	0.5	0.89	1	1.0	6	8
3	1.5	1.5	0.5	1.34	1	1.0	6	8
4	2.0	2.0	0.5	1.79	1	1.0	6	8
5	2.5	2.5	0.5	2.24	1	1.0	6	8
6	3.0	3.0	0.5	2.70	2	2.5	2	7
7	3.5	3.5	0.5	3.16	2	2.5	2	7
8	4.0	4.0	0.5	3.62	2	2.5	2	7
9	4.5	4.5	0.5	4.08	2	2.5	2	7
10	5.0	5.0	0.5	4.54	2	2.5	2	7
11	6.0	6.0	1.0	5.00	2	2.5	2	7
12	7.0	7.0	1.0	5.94	2	2.5	2	7
13	8.5	8.0	1.0	6.89	2	2.5	2	7
14	10.0	9.0	1.0	7.83	2	2.5	2	7
15	12.5	10.0	1.0	8.50	3	0.9	2	9
16	15.0	12.0	2.0	9.17	3	0.9	2	9
17	17.5	14.0	2.0	9.84	3	0.9	2	9
18	20.0	16.0	2.0	10.00	4	1.9	2	4
19	25.0	18.0	1.0	11.37	4	1.9	2	4
20	30.0	20.0	1.0	12.73	4	1.9	2	4
21	35.0	25.0	5.0	14.10	4	1.9	2	4
22	40.0	30.0	5.0	15.59	5	2.0	4	1

TABLE 6.1-4 (continued)

COARSE AND FINE MESH SPACING FOR SPATIAL INTERVALS

Spatial Interval	Fixed Spatial Interval Distance in CRAC (Miles)	Targeted Spatial Interval Distance in SPEDIT (Miles)	Targeted Incremental Spacing As A Function Of Distance In SPEDIT (Miles ±50%)	Typical Spacing In SPEDIT for Actual Meteorological Sequence (Miles)	Example of Typical Weather Conditions			
					Hour Number	Wind Speed (m/sec)	Stability	Direction
23	45.0	35.0	50	17.08	5	2.0	4	1
24	50.0	40.0	10	18.57	5	2.0	4	1
25	55.0	50.0	10	20.00	6	4.1	2	15
26	60.0	60.0	10	23.87	6	4.1	2	15
27	65.0	70.0	10	27.74	6	4.1	2	15
28	70.0	80.0	10	32.44	7	4.2	3	16
29	85.0	90.0	10	37.14	7	4.2	3	16
30	100.0	100.0	10	40.00	8	5.0	5	16
31	150.0	125.0	25	48.33	8	5.0	5	16
32	200.0	150.0	25	126.19	9-21	2.7	4	1
33	350.0	200.0	50	207.86	22-31	3.6	3	1
34	2000.0	2000.0	1800	971.70	32-100	5.0	4	2

TABLE 6.1-5

APPROXIMATE EQUIVALENTS TO PASQUILL-GIFFORD STABILITY CLASSES USED IN NUMERICAL MODEL

Class	z_∞ feet(m)	α Wind	B_z	β/α Diffusion	$E_{z_\infty}/E_{y_\infty}$	$E_{y\infty}$ (feet^2/sec)	$E_{y\infty}$ (m^2/sec)
A	3000 (915)	0.143	1.00	12.6	10.0	2740	625
B	3000 (915)	0.143	0.70	9.6	2.0	1140	257
C	2000 (610)	0.143	0.23	8.0	0.67	545	110
D	2000 (610)	0.20	0.09	5.0	0.17	440	90
E	1000 (305)	0.30	0.02	3.33	0.053	360	75
F	500 (152)	0.40	0.008	1.67	0.0083	310	65

First three related by: $u_x/u_\infty = B_x = B_y = B_\infty(z/z_\infty)^\alpha$ only in flat plate
Last three related by: $E_y = E_{y_\infty}(z/z_\infty)^\beta = E_{y_\infty}(u_x/u_{x\infty})^{\beta/\alpha}$, $E_x = 0$

where:

z = height above ground level in feet or meters
z_∞ = height at the top of the boundary layer in feet or meters
u_x = horizontal wind velocity at z in ft/sec or m/sec
$u_{x\infty}$ = horizontal wind velocity at z_∞ in ft/sec or m/sec
u_z = vertical wind velocity in ft/sec or m/sec
α = nondimensional power law exponent for wind
E_y = horizontal diffusion coefficient at height z, direction function of wind speed in (ft^2/sec) or (m^2/sec)
$E_{y\infty}$ = horizontal diffusion coefficient at height z_∞, E_y varies directly with u_x and is shown for u_{x30} = 1 mph (1.5ft/sec) in the English system and u_{x10} = 1 m/sec in the metric
E_z = vertical diffusion coefficient in (ft^2/sec) or (m^2/sec)
β = nondimensional power law exponent for diffusion
B_z = vertical flow coefficient

TABLE 6.1-6

TYPICAL GRID DIMENSIONS USED FOR NUMERICAL MODEL CALCULATIONS

Block Number	Grid Direction		
	Downwind (x)	Horizontal (y)	Vertical (z)
1	4000	5000	25
2	2000	4000	50
3	1000	2000	100
4	500	1500	100
5	500	1000	100
6	500	1000	100
7	500	750	200
8	500	750	200
9	1000	500	200
10	1000	500	400
11	1500	500	600
12	1500	500	1000
13	2000	500	2000
14	2000	750	
15	3000	750	
16	4000	1000	
17	4000	1000	
18	5000	1500	
19	5000	2000	
20	5000	4000	
21	5000	5000	
22	5000		
23	5000		

TABLE 6.1-7

POLAR GRID ELEMENT SPACING

Grid Type and Use	Downwind Spacing			Angular Spacing	
	Number Before Spacing Changes	Incremental Spacing (Miles)	Distance to Outer Boundary Where Spacing Changes (Miles)	Number of Sectors to Represent Full Circle	Angle of Coverage Per Element (Degrees)
Fine Grid (Early Doses)	80 40 20 28 18	0.25 0.50 1.0 5.0 10.0	20.0 40.0 60.0 200.0 2000.0	64	5.625
Population Grid (Population Distribution, Evacuation Model, and Chronic Doses)	10 5 5 6 1 2 2 1 1 1	0.5 1.0 2.0 5.0 10.0 20.0 50.0 300.0 600.0 900.0	5.0 10.0 20.0 50.0 60.0 100.0 200.0 500.0 1100.0 2000.0	32	11.25

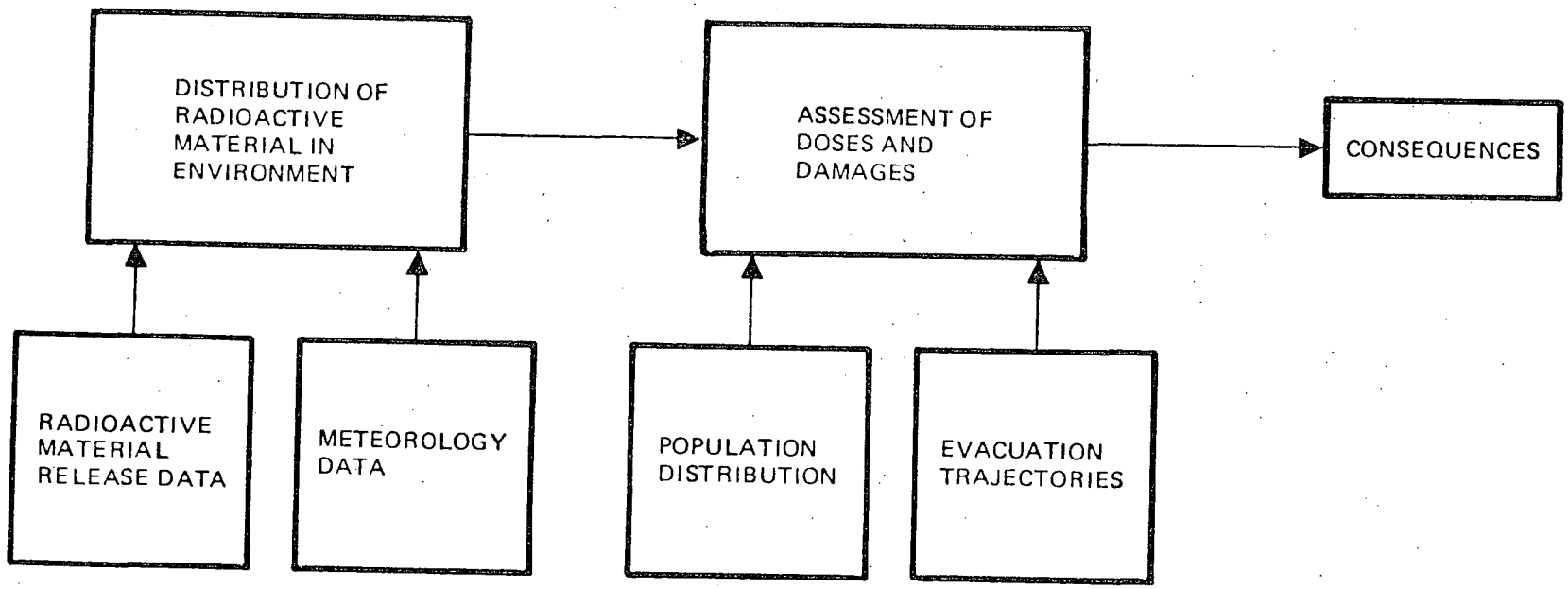


Figure 6.1-1. CRAC and CRACIT Consequence Assessment

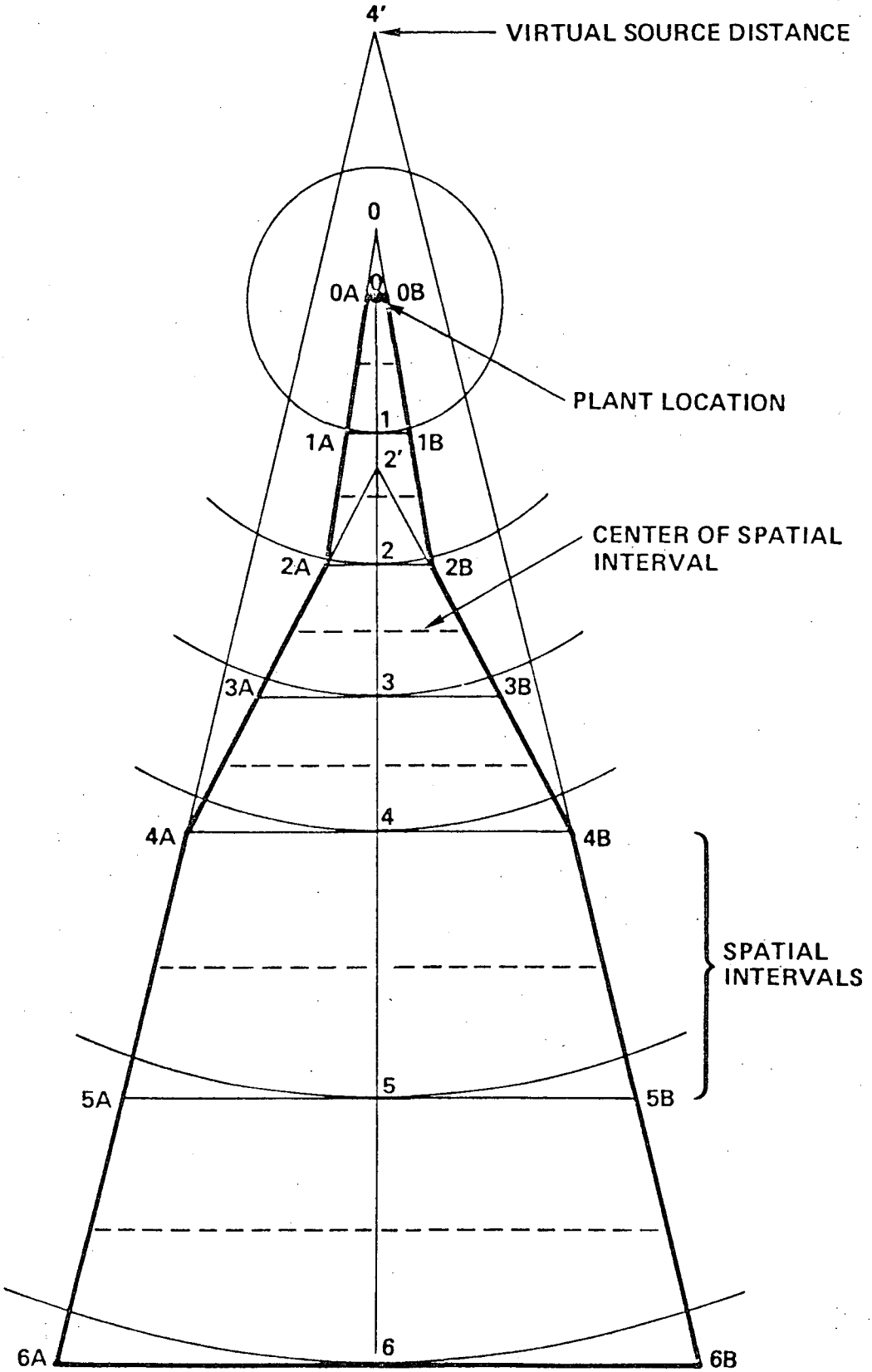


Figure 6.1-2. Top View of the Straight Line Lateral Plume Dispersion Model--CRAC

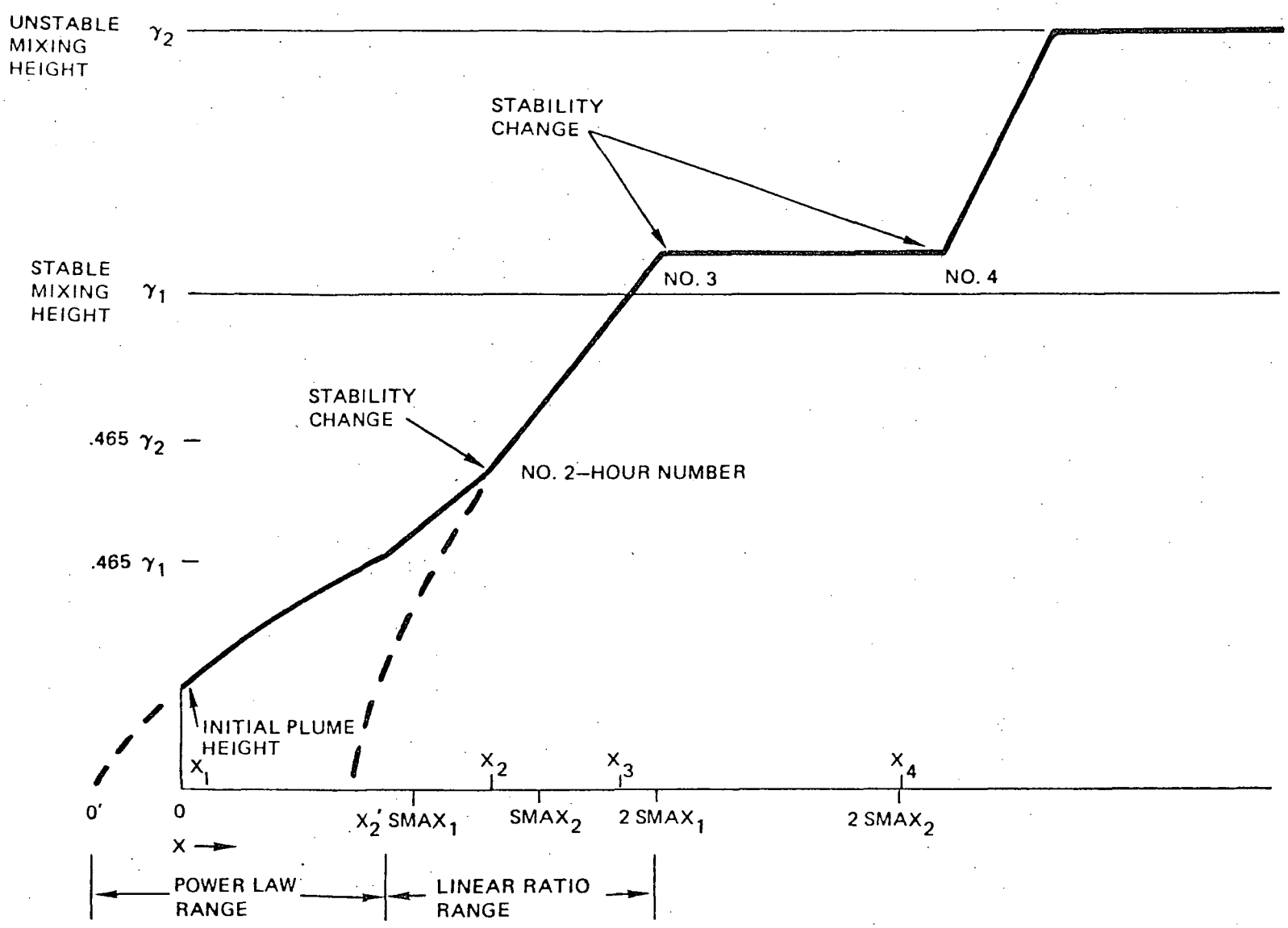


Figure 6.1-3. Illustration of Vertical Plume Dispersion Model--CRAC

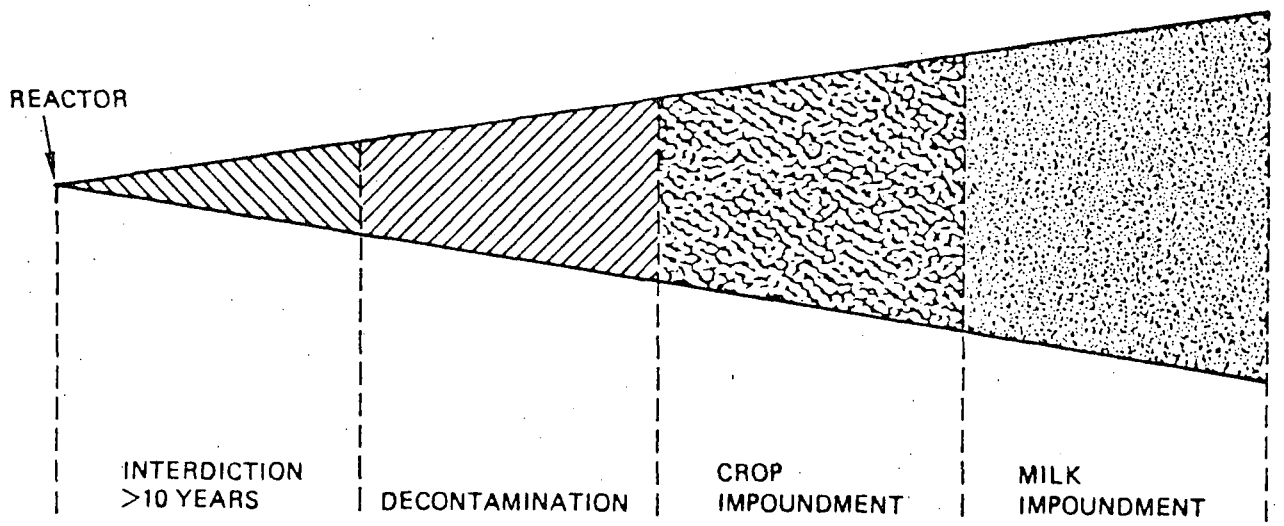


Figure 6.1-4. Simplified Illustration of Interdiction Model

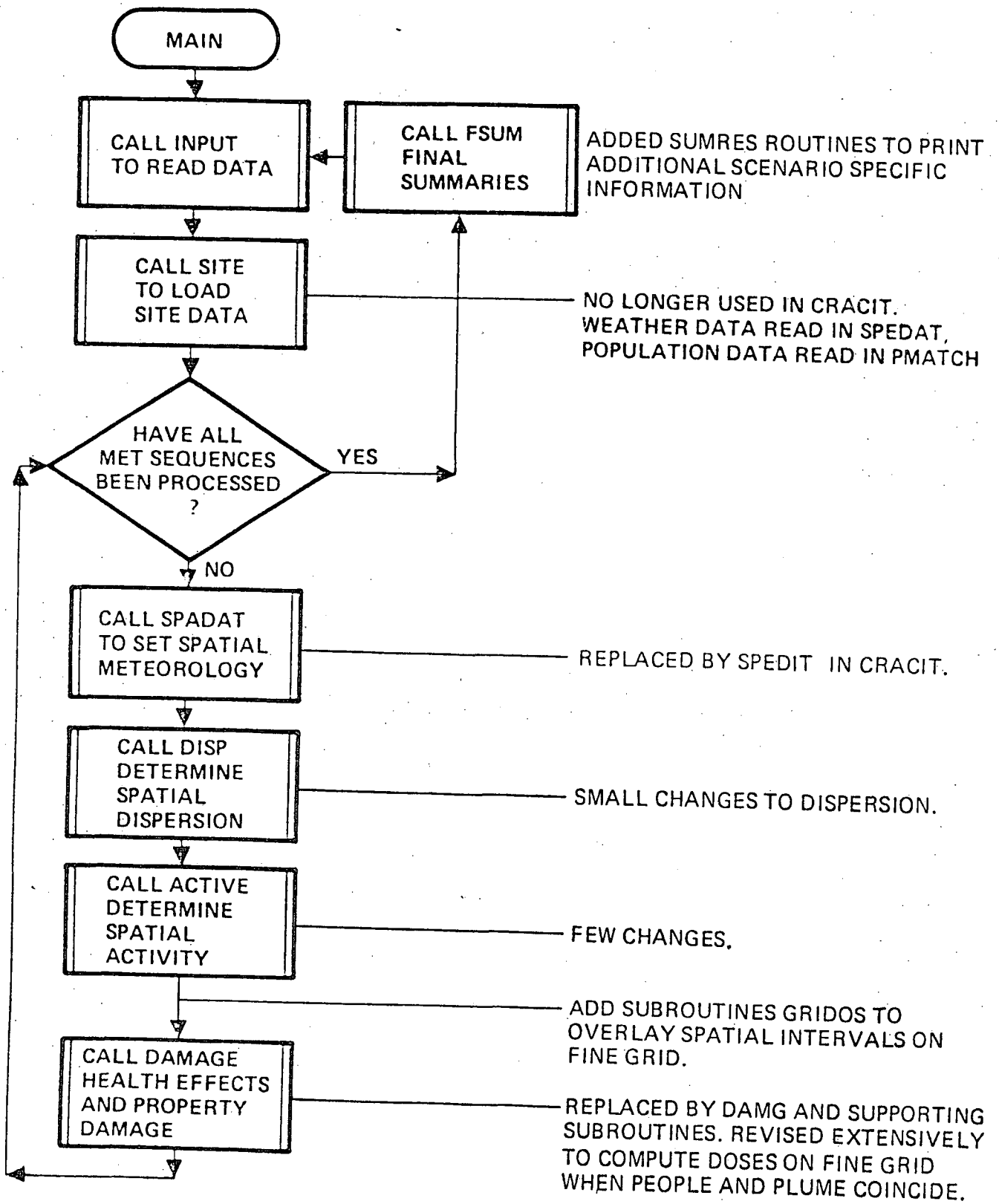
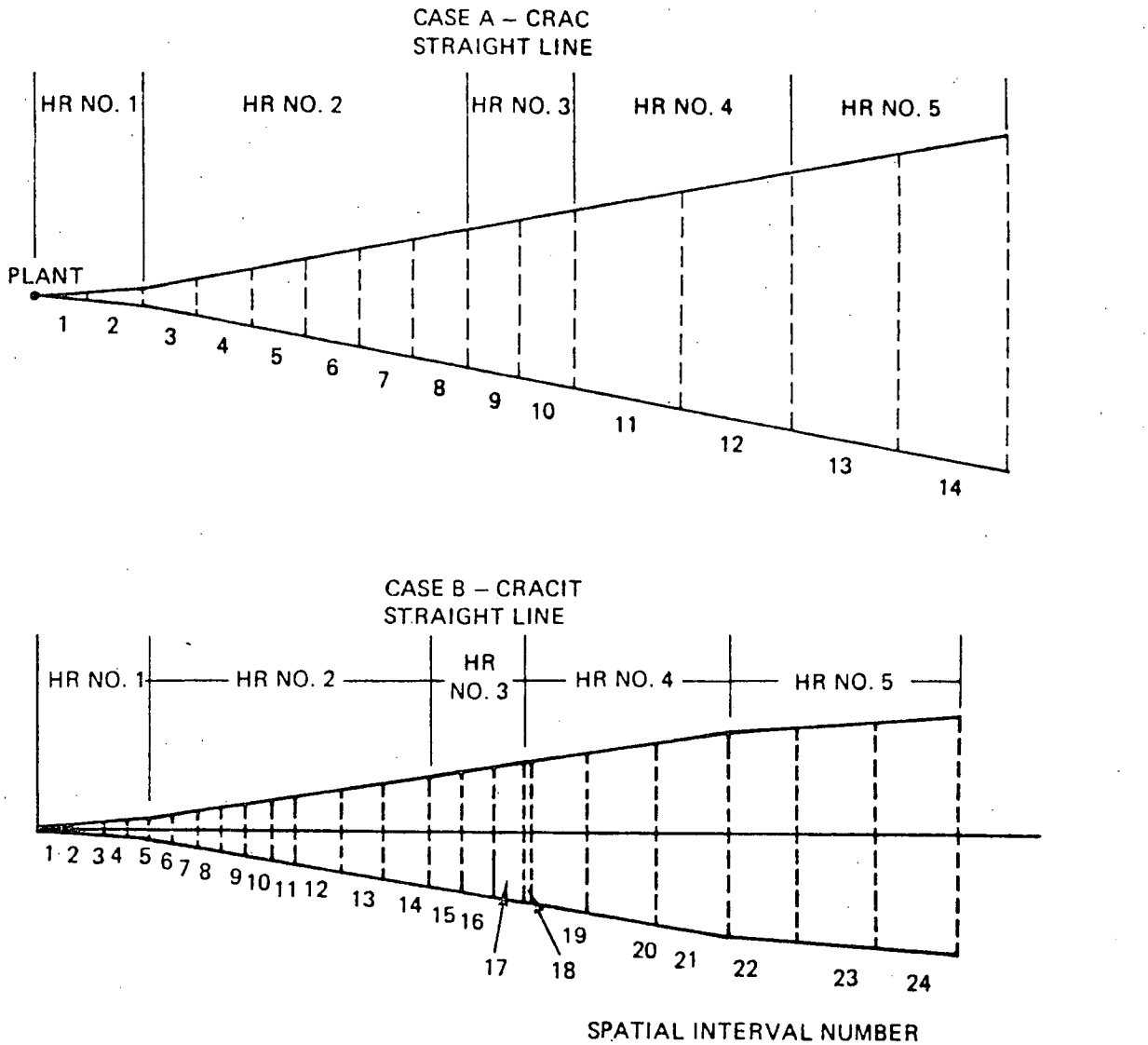


Figure 6.1-5. Changes in Flow of the Main Routine in the Consequence Model (CRACIT)



METEOROLOGICAL SEQUENCE

HR	$\bar{U}$	STABILITY	DIR
1	1.0	6	8
2	2.5	2	7
3	0.9	2	9
4	1.9	2	4
5	2.0	4	1

Figure 6.1-6. Example of Spatial Interval Distances for Typical Weather Sequence

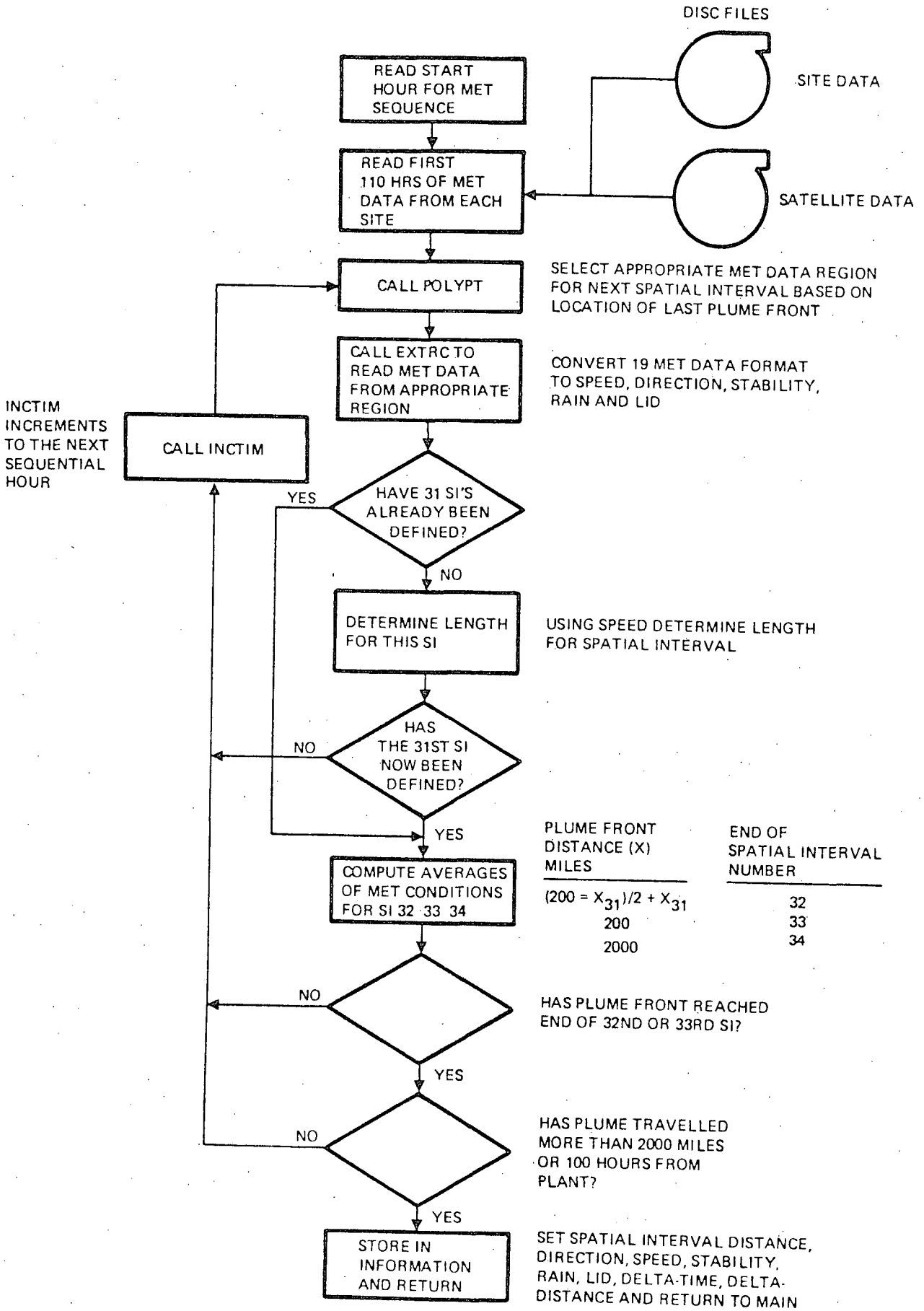


Figure 6.1-7. Schematic Flow Diagram for Subroutine SPEDIT

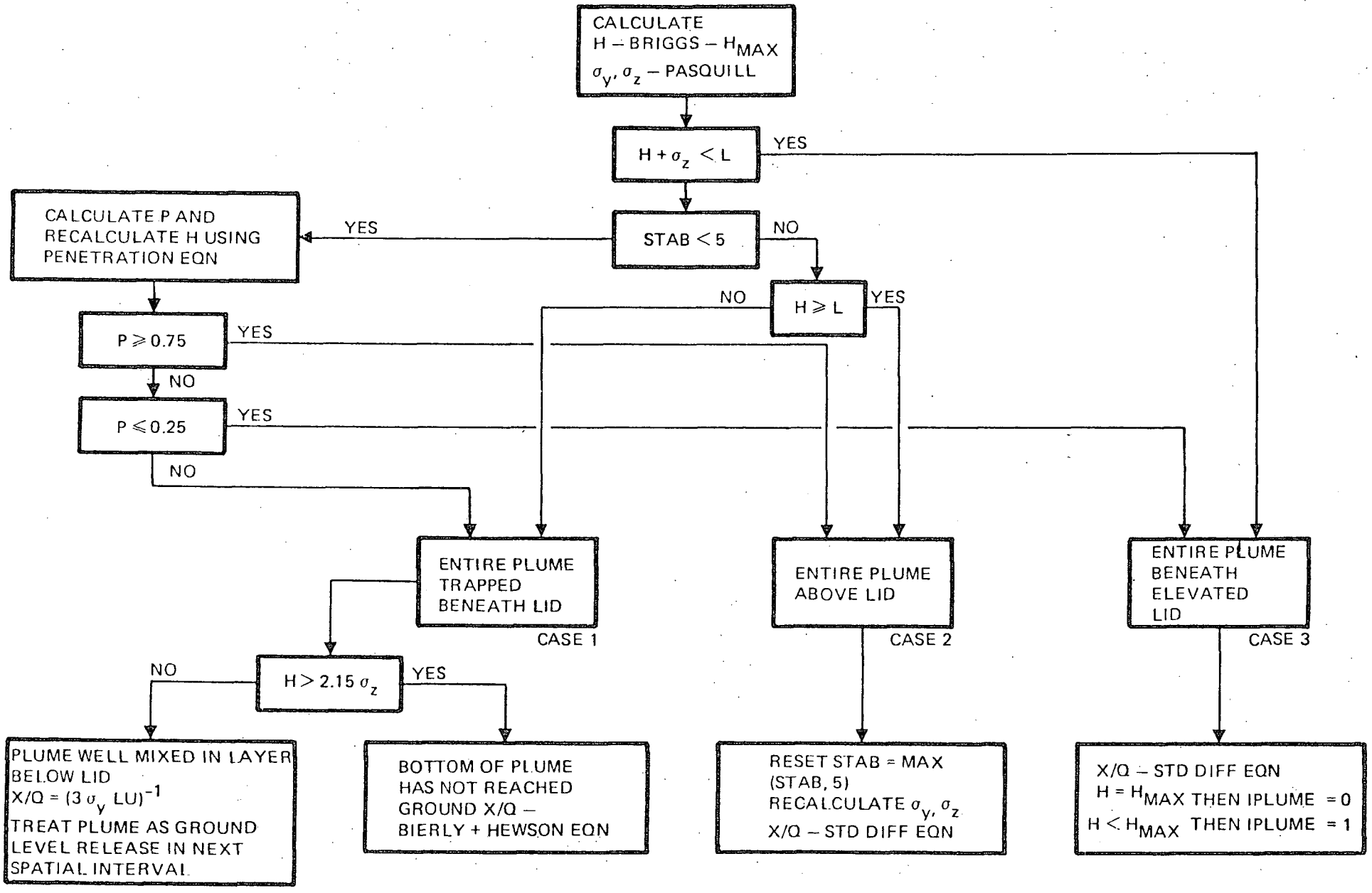
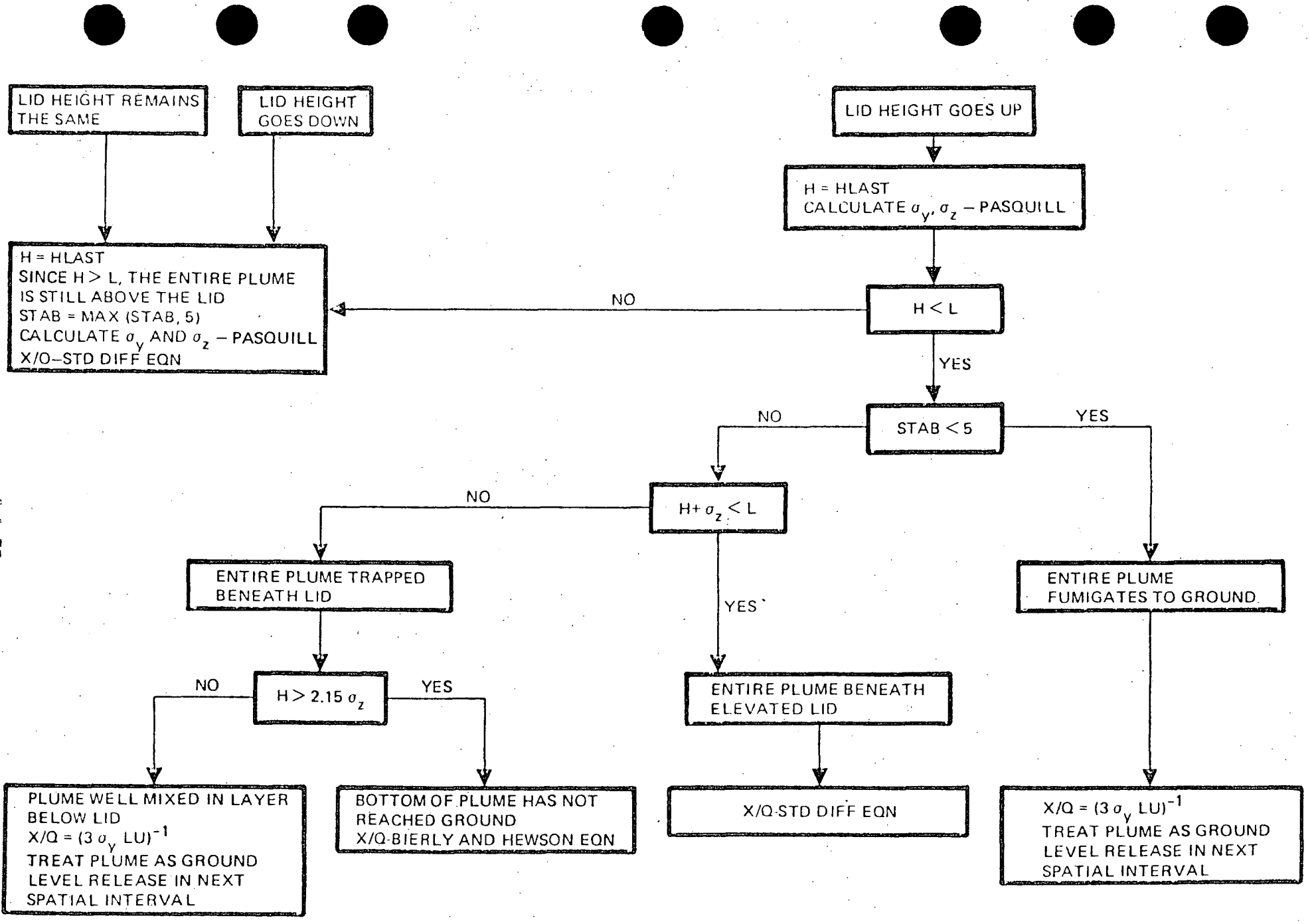


Figure 6.1-8. Logic for First Spatial Interval



6.1-75

Figure 6.1-8 (continued). Logic for First Spatial Interval

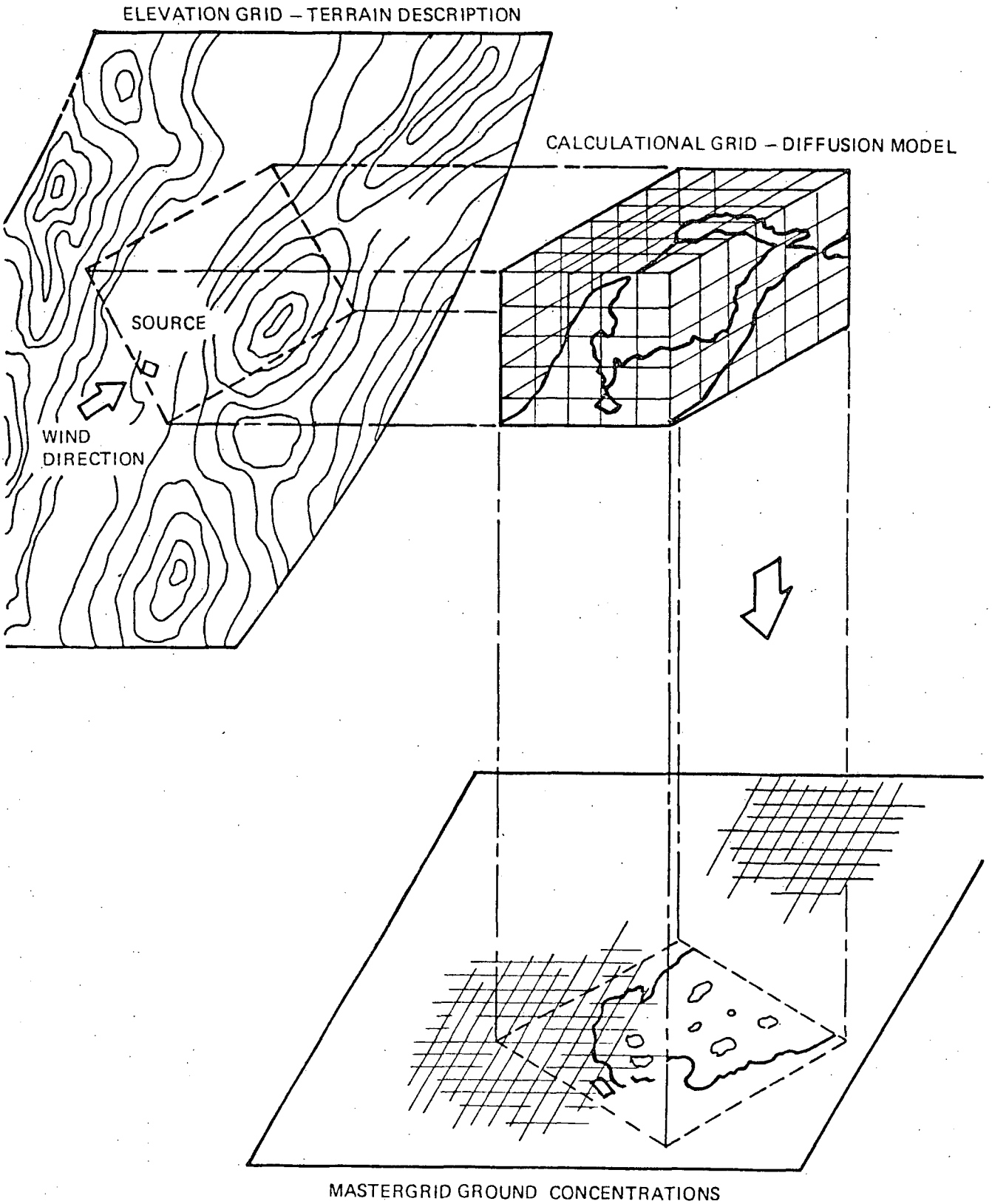


Figure 6.1-9. Schematic of Calculational Approach for Modified Potential Flow Terrain Model

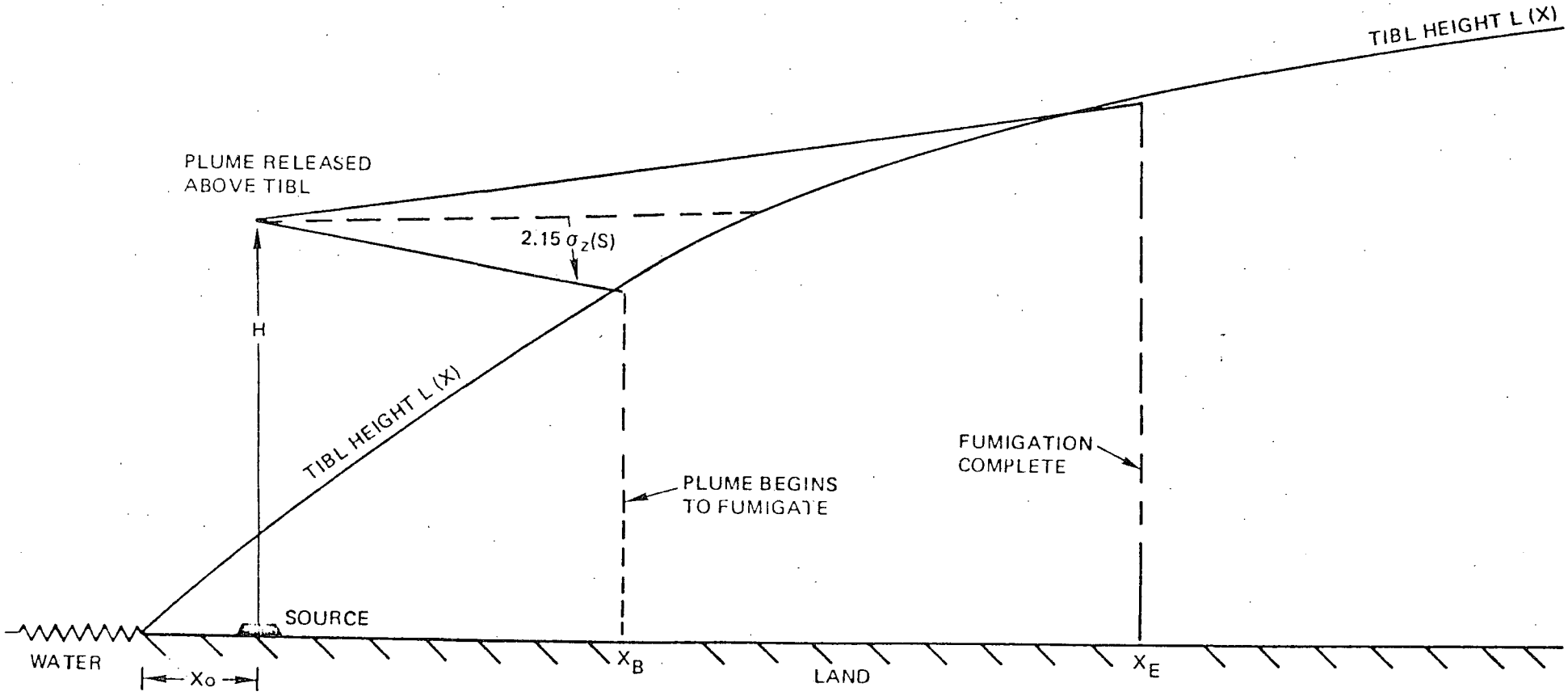


Figure 6.1-10. Schematic Representation of Plume Undergoing TIBL Fumigation

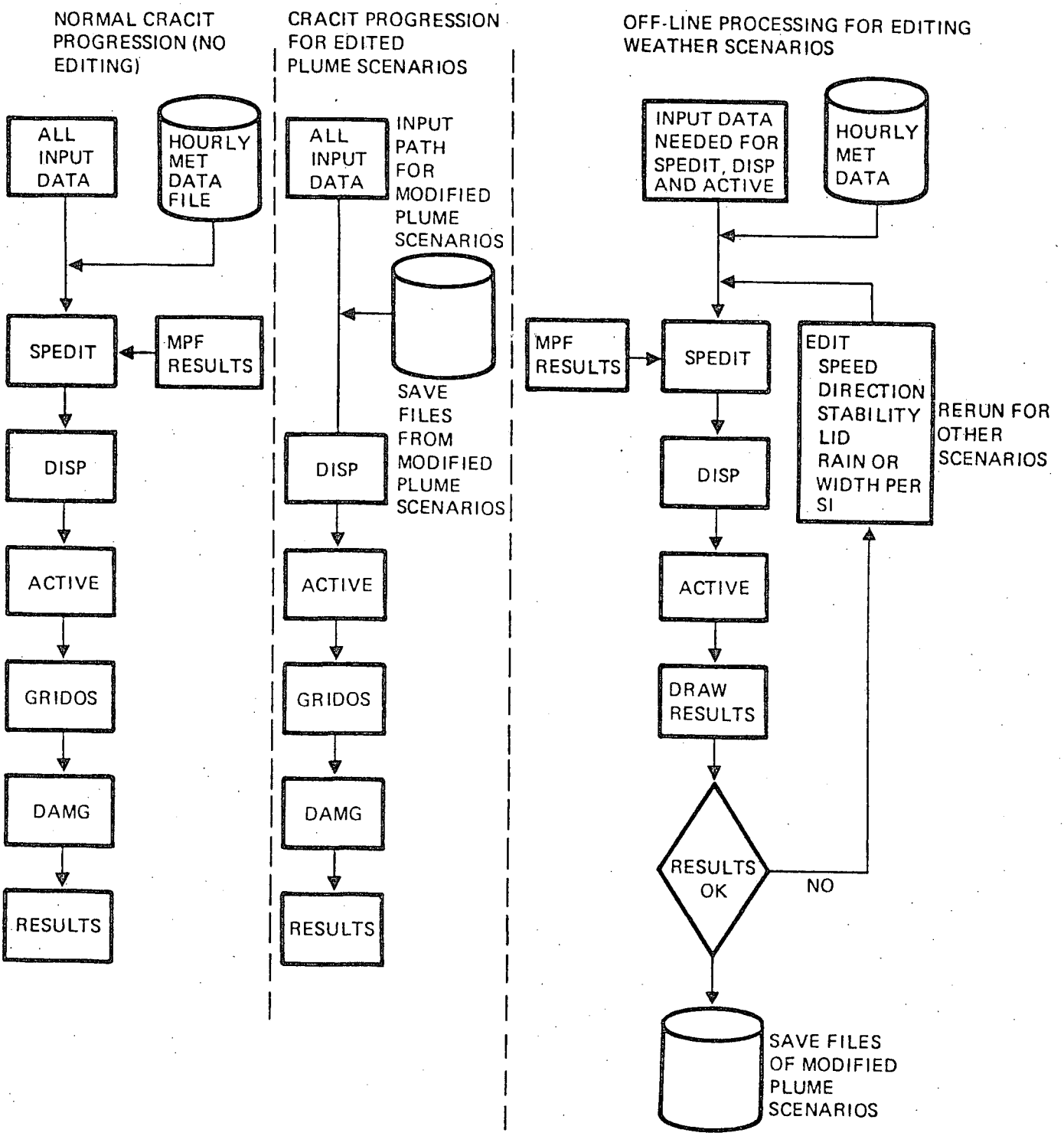


Figure 6.1-11. Schematic Illustration of Method for Running CRACIT After Completion of Off-Line Plume Editing Process

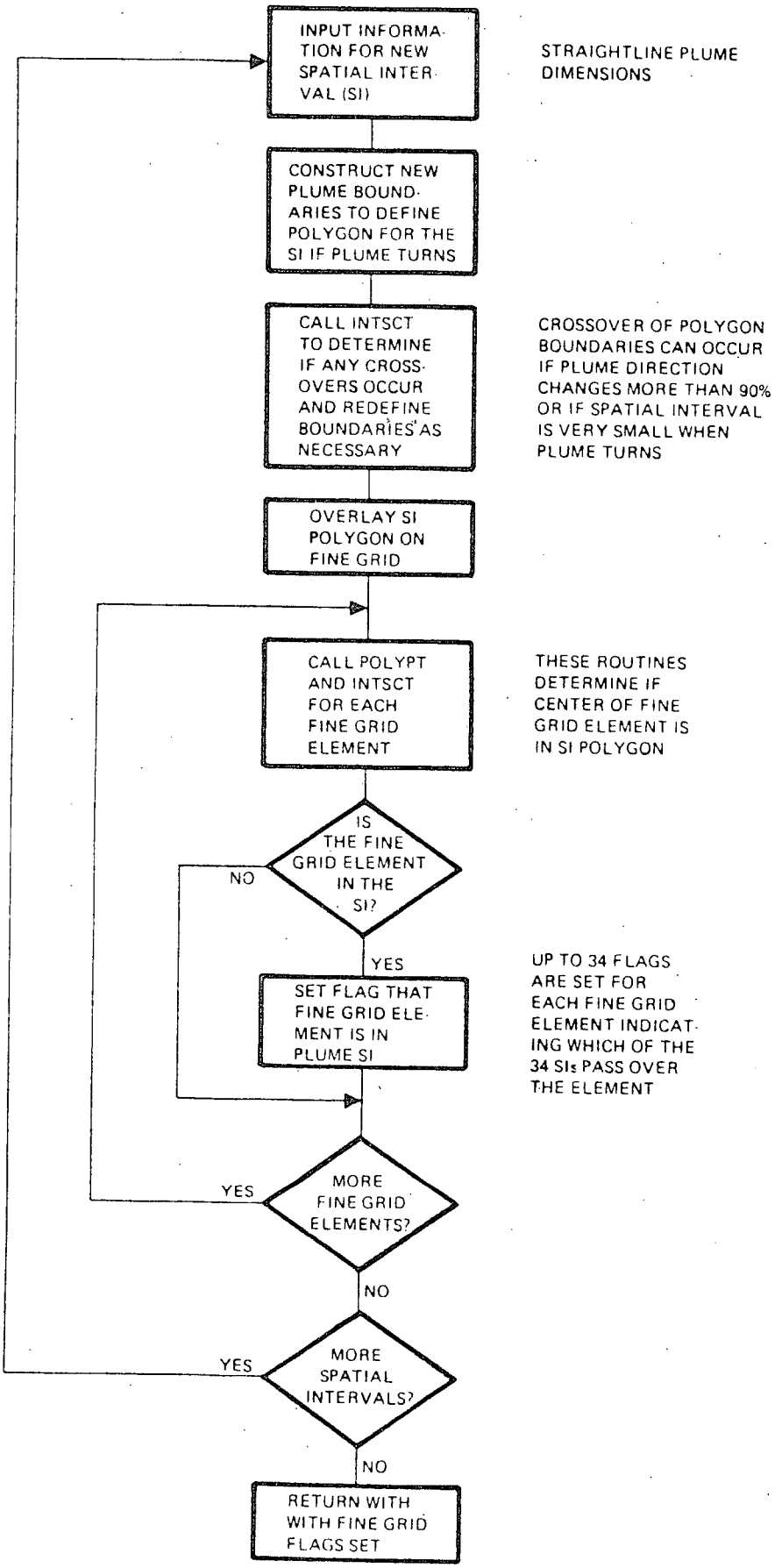


Figure 6.1-12. Schematic Flow Diagram for Subroutine GRIDOS

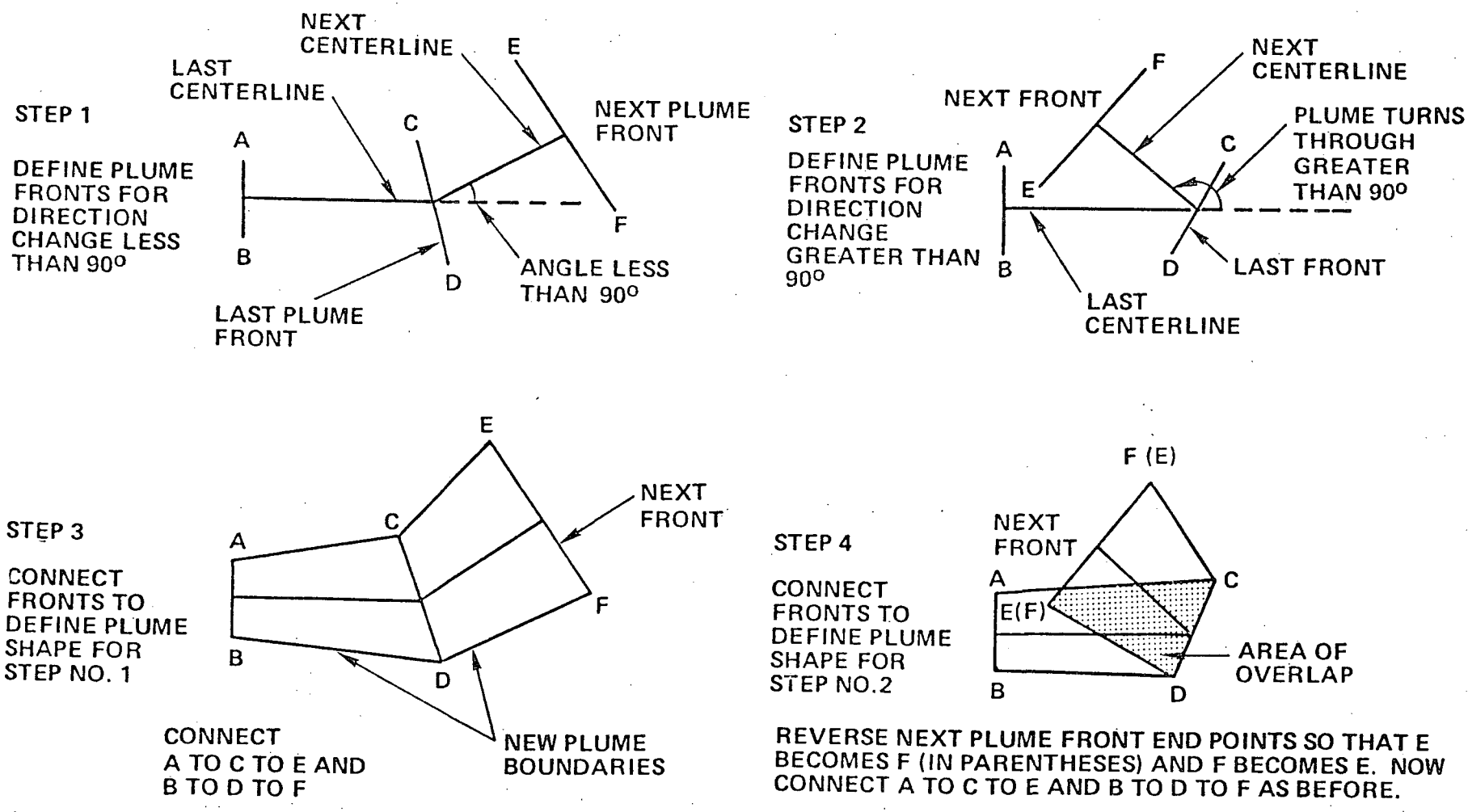


Figure 6.1-13. Illustration of Plume Shape Definition in GRIDOS

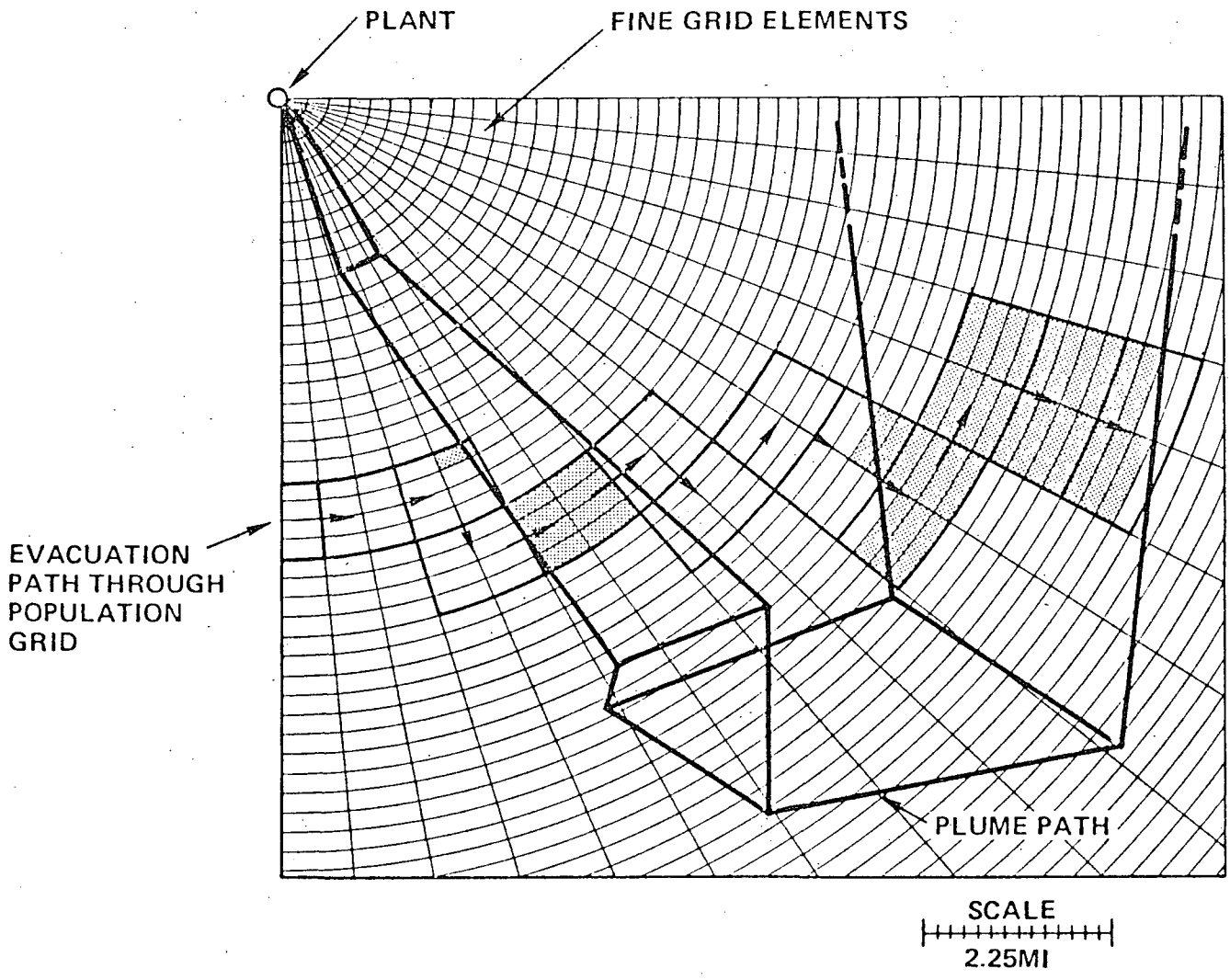


Figure 6.1-14. Illustration of Plume and Evacuation Paths on Fine Grid (Dose Calculations Made in Shaded Fine Grid Areas)

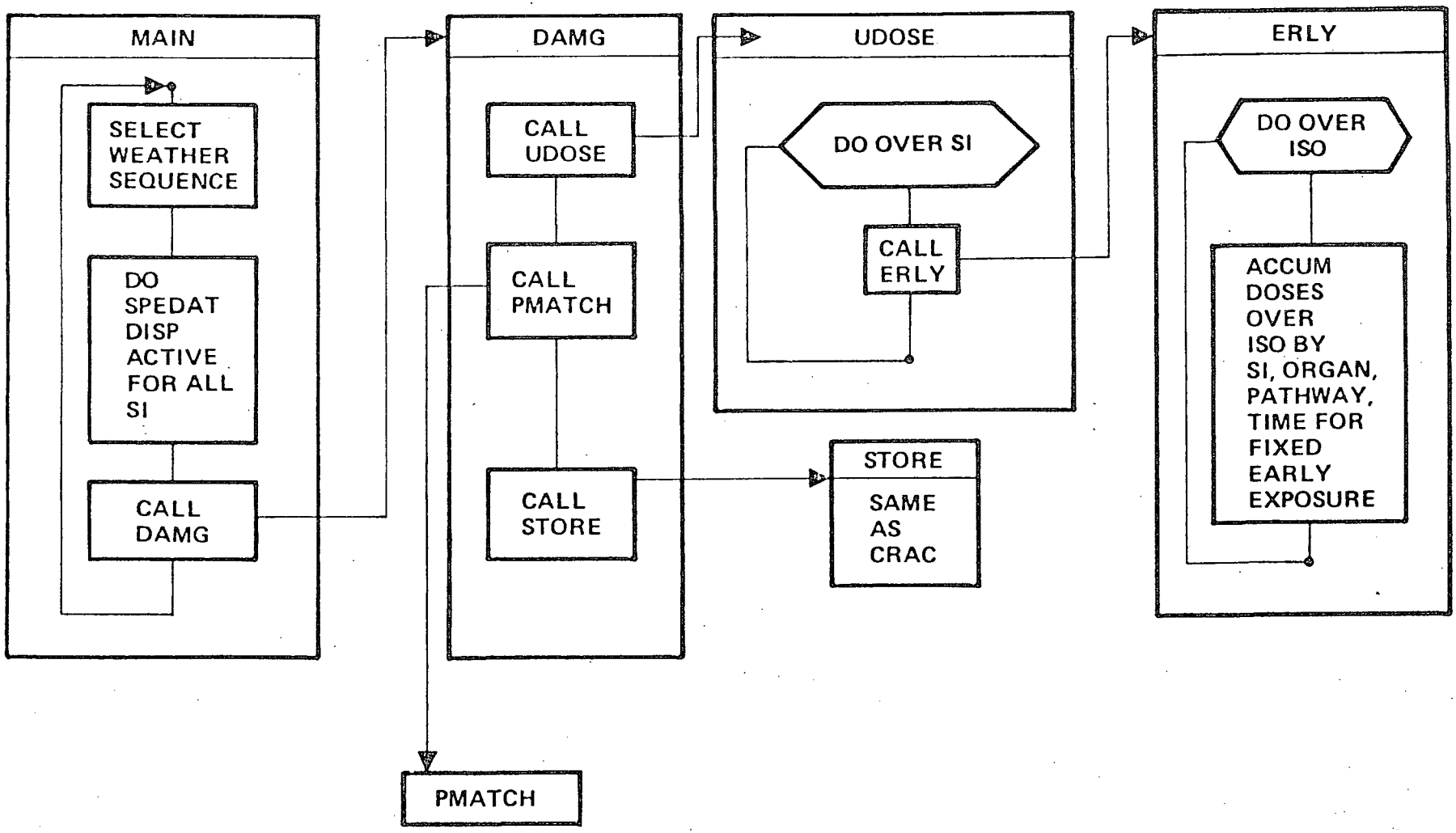
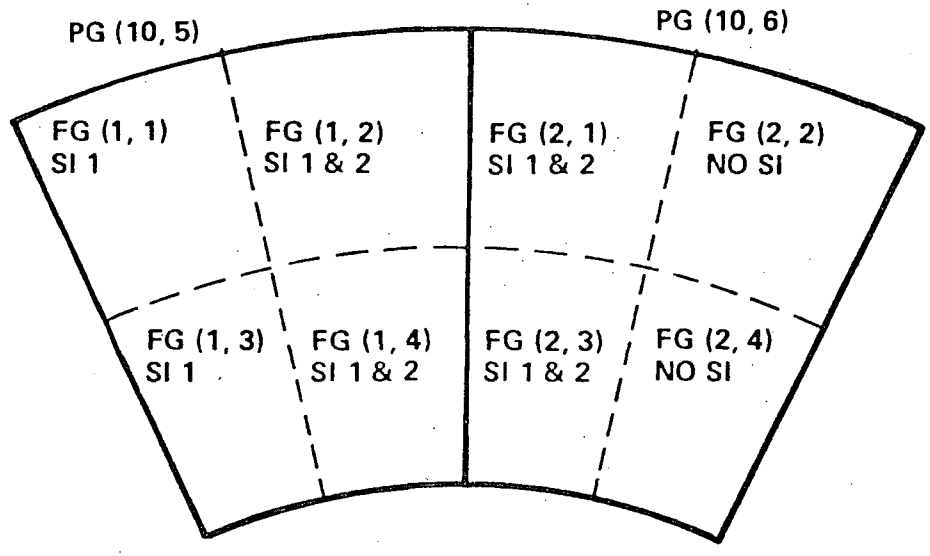


Figure 6.1-15. Schematic Flow Diagram of Damage Calculation Subroutines in CRACIT



TWO OF THE 1088 CRACIT POPULATION GRID ELEMENTS ARE SHOWN ABOVE, PG (10, 5) AND PG (10, 6). EACH CONTAINS AN INTEGRAL NUMBER OF ELEMENTS (BOUNDED BY DASHED LINES) OF THE FINE GRID UPON WHICH THE PATH OF THE RADIOACTIVE CLOUD IS MAPPED. WITHIN THE BOUNDARIES OF EACH FINE GRID ELEMENT APPEAR THE ELEMENT IDENTIFIER, SUCH AS FG (1, 1), AND AN INDICATION OF WHICH SPATIAL INTERVALS (EG: SI 1, 2 OR BOTH) REPRESENTING THE CLOUD PATH FALL UPON THE FINE GRID ELEMENT. EQUIVALENCE IN SPATIAL INTERVAL INDICATORS FOR DIFFERENT FINE GRID ELEMENTS MEANS THAT RADIOLOGICAL CONDITIONS ARE THE SAME IN THOSE ELEMENTS. IT SHOULD BE NOTED THAT RADIOLOGICAL CONDITIONS CAN VARY BETWEEN FINE GRID ELEMENTS WITHIN A POPULATION GRID ELEMENT.

Figure 6.1-16. Relation Between Population Grid Elements and Fine Grid Elements

6.2 SITE SPECIFIC AND PLANT SPECIFIC INPUT INFORMATION

This section describes requirements for input information to the CRACIT consequence program. Input data sets, with a few exceptions, are generally interchangeable between the CRAC and CRACIT programs. Section 6.2.1 describes site specific data while Section 6.2.2 discusses plant related input data.

6.2.1 SITE SPECIFIC DATA

The plant site is located about 2-1/2 miles southwest of Peekskill, New York, and about 40 miles north of New York City as shown in Figure 6.2-1. The terrain is complex and significantly influences flow patterns by channeling and induces turbulence due to surface roughness. This section describes the meteorological and population data used in the consequence analysis.

6.2.1.1 Meteorological Data

The general air flow in the site region, as indicated in the wind roses shown in Figures 6.2-2 and 6.2-3, is from the northwest through southwest. During the fall and winter months, the Eastern United States is generally dominated by high pressure centers from Canada and the Pacific. These high pressure systems and their clockwise flow of air produce west and northwest winds when they are west of the plant region, and south and southwest winds when they are east of the plant region. During the spring and summer months, the predominant flow across the United States is from west to east, resulting in winds from the northwest to the southwest. Low pressure systems move up the East Coast, producing easterly winds in the site region. However, they move rapidly and their duration of influence is short in comparison to the high pressure systems.

During low wind speed, stable conditions, interactions resulting from temperature differences in the river valley cause air flow patterns that result in characteristic changes in wind direction. These phenomena are difficult to model. However, onsite data and concurrent data from two other sites (referred to as satellite sites) were used to characterize the effects as realistically as possible. After these were reviewed, edits were made based on judgment using satellite regional weather station data and other data sources as a basis for modifications to the weather data. The technique for effecting these changes is discussed in Section 6.1.2.3.10.

6.2.1.1.1 Site Meteorological Tower

The primary source of weather data is the 400-foot tower instrumented at three levels in conformance with NRC Regulatory Guide 1.23. A 1-year period of these data, from August 1978 through July 1979, was used. Meteorological tower characteristics are given in Table 6.2-1. Meteorological parameters were stored as sequential hourly values on magnetic tape for use in the CRACIT program runs. Preprocessing of these tapes compressed the necessary information into one integer computer word for

each hour (I9 format). Two additional parameters, wind direction and lid height, were added to the I5 formatted word originally used in CRAC to form the I9 formatted computer word as follows.

Position in I9 Word (left to right)	Spaces	Parameters	Units and Ranges
1st	2	Direction ÷ 2	1-16 (N through NNW clockwise)
2nd	3	Speed x 4	(M/sec)
3rd	1	Stability	(PG 1-7)
4th	1	Rain	0-4 Based on Increasing Intensity
5th	2	Lid Height ÷ 100	(m)

6.2.1.1.2 Satellite Station Meteorological Data

Because of local meteorological effects at the site, any plume that is projected to leave the site area is assumed to be influenced according to weather data measured in an adjacent region. Therefore, separate tapes were prepared in the I9 format for data from 14 sites in the region such that data were available concurrently for each hour from all sites. These sites, referred to as satellites, are listed in Table 6.2-1. As indicated in Table 6.2-1, the STAR stability routine was used to determine stability categories for most of these sites since vertical temperature difference data are not available. For the satellite locations, data were available only from lower elevations (see Table 6.2-1). However, adjustments were made in the speed to account for the difference between "average" plume height and measurement height when an elevated plume entered a satellite region.

6.2.1.1.3 Preprocessing of Weather Data

A routine called CRACIN was used to preprocess available weather data into the appropriate input format. It is shown in the flow diagram in Figure 6.2-4. Basically, this routine computes stability group from temperature difference on the tower, classifies rain intensity into four categories, and estimates lid height.

A procedure generally following that described in the CRSTER User's Guide (Reference 6-30) for rural sites and originally suggested by R. Hrenko (Reference 6-31), was used to provide a rough estimate of the lid height for each hour. It used the nearest upper air radiosonde

data. Although the lid obtained may not always be accurate at the plant site, it should provide a reasonable representation of lid height in the region in which the plume is dispersing. In the step by step procedure outlined below, one 24-hour cycle is developed starting the afternoon of Day 1 and ending on the afternoon of Day 2. A pictorial description of this process is given in Figure 6.2-5.

1. Compute the afternoon mixing height M_a (used from 1400 to sunset every day), by extrapolating from the maximum surface temperature from 1200 to 1600 at Fort Totten along the dry adiabat to the intersection with the morning temperature sounding (see Reference 6-32). The elevation at this intersection is the assumed afternoon lid height.

2. The morning mixing height is not computed for the rural situation since the lid is assumed to be near the ground during stable conditions.

3. Determine whether the early morning conditions of Day 2 are stable by checking for a stability of 5, 6, or 7 during the hour before sunrise at the radiosonde location. Stablity category is calculated using the STAR subroutine (Reference 6-33).

4. Estimate lid height by interpolating between Day 1's afternoon lid height at sunset and Day 2's afternoon lid height at 1400 unless conditions are stable from item 3. If they are stable, follow items 5, 6, and 7.

5. If Day 2's early morning hours are stable, interpolate between Day 1's and Day 2's afternoon lid height as in item 4 until Day 1's midnight (2400).

6. After midnight, continue the interpolation of lid height to Day 1's afternoon lid height as in item 4.

7. From Day 2's sunrise to 1400, interpolate lid height from a height of L = 0 at sunrise to Day 2's afternoon mixing height at 1400.

8. If radiosonde data are missing, set lids to 600 meters.

Under certain atmospheric conditions, this method produces unrealistic results. These can be caused by frontal systems and rainfall that can affect the normal temperature change, making estimates difficult for the hours between soundings. The following adjustments were made to compensate for these effects.

1. If the afternoon surface temperature is below the morning sounding temperature, assume a lid height of 1,200 meters.

2. If the afternoon surface temperature is higher than the morning sounding temperature when extrapolated to all heights, assume a lid height of 3,000 meters.

3. If the lid height for any afternoon hour is less than 240 meters and the surface wind speed at the airport is below 15 mph, assume that the lid is 250 meters.

4. If the lid height for any afternoon hour is less than 250 meters and the surface winds at the airport are greater than 15 mph, assume that the lid height is at an elevation of 700 meters.

Table 6.2-2 summarizes the results of the lid processing and gives the frequency of occurrence of each lid height.

The CRACIT program reads meteorological data sequentially 1 hour at a time. Since some short periods of data were missing from the site weather tower records, an interpolation procedure was used in the preprocessing procedure to "fill in" missing hours. These areas were checked to ensure that the input values were reasonable. Data from other local sources were used to fill in whenever possible. Since most of the satellite data are from continuously attended stations, fill-in procedures were not necessary.

6.2.1.1.4 Data Summaries

A summary of the Indian Point tower data in the form of joint frequency tables including wind speed and direction for each stability class is given in Table 6.2-3 for the 400-foot (122m) level and in Table 6.2-4 for the 33-foot (10m) level. Wind roses for the 400-foot (122m) and 33-foot (10m) levels are given in Figures 6.2-2 and Figure 6.2-3, respectively.

Since certain release categories result in radioactive material emissions at elevated levels, the weather data at the level closest to the release level are needed. Data from two levels on the site tower were available on the input file for use with the appropriate release category in the CRACIT runs. Two separate files are created for this purpose, each of which containes either the upper or lower level data and data from the satellite stations. Input meteorological data files are read by CRACIT in subroutine SPEDIT.

6.2.1.2 Population, Evacuation, and Sheltering Data

At the time this report was prepared, the most up-to-date information concerning evacuation was used to derive the risk curves. As mentioned previously, changes to the evacuation model in CRAC were made to give a more realistic account of exposures received during evacuation. The evacuation model is discussed in detail in Section 6.1.2.7.2. Input data specific to evacuation trajectories are described next along with population data compiled for this study.

Five sets of population and evacuation data were prepared for the 10-mile evacuation zone surrounding the plant. These five evacuation

scenarios were chosen to account for the most probable starting population configurations. They are designated as follows:

- Nighttime
- Weekday, school in session
- Weekday, school out
- Summer holiday
- Winter holiday

The five population distributions were based on estimates for the year 1980. To provide improved resolution of evacuation paths, the population was subdivided on a more detailed grid (32 sectors) than that normally used in safety analyses (16 sectors). The sectors are numbered 1 to 32 clockwise starting at north. Intervals of 0.5 miles are used from 0 to 5 miles, 1 mile from 5 to 10 miles, 2 miles from 10 to 20 miles, 5 miles from 20 to 50 miles as shown in Tables 6.2-5 through 6.2-7. These intervals are numbered, moving outward. Therefore, each location can be referred to by a doublet (sector number, interval number). For example, (1, 5) is located between 0^0 and $11\text{-}1/4^0$ and between 2.0 and 2.5 miles from the reactor.

Two of the five population distributions are illustrated in Table 6.2-5, which gives the weekday, school in session population distribution. Table 6.2-6 gives the nighttime population distribution. The start date and time of the meteorological sequence determine which of the five population distributions is to be used.

As previously discussed, population doses resulting from low levels of radiation at large distances are estimated in these calculations. Therefore, estimates of population distribution out to 2,000 miles were made as described below.

Residential population estimates within a 2,000-mile radius of the Indian Point Nuclear Power Plant were prepared for the year 1980. The 2,000-mile radius encompassed varying portions of the United States and Canada. Different units of measurement, ranging from block statistics within the 10-mile radius to less exact measures further from the plant, were used to determine the population estimates.

The population estimates for each element within the 10-mile radius were derived by first determining the 1970 population for each of these elements. The 1970 population was determined by plotting a polar grid which showed the elements within the 10-mile radius on a composite map made from New York State Department of Transportation (NYSDOT) Planimetric charts at a scale of 1:24000, and then allocating population to each of the elements using census tract and block statistics from the 1970 U.S. Department of Commerce Bureau of the Census. Where block statistics were not available, population by element was estimated by applying a household size factor obtained from the census to house counts made from the NYSDOT planimetric maps. The 1970 populations were then used as the basis for proportionally allocating the 1980 population estimate. Projections by municipality for each of the counties are included in the plume exposure pathway emergency planning zone; i.e., Orange, Putnam, Rockland, and Westchester Counties.

The population for the elements beyond the 10-mile radius, but within the 50-mile radius, was determined by plotting the element grid on a map of New York, New Jersey, and Connecticut featuring all cities, towns, villages, counties, and townships. Population was then allocated to each of the elements using individual town populations based on population estimates and projections by county for the year 1980.

For the elements within the United States which were beyond the 50-mile radius and within the 2,000-mile radius, a map of the United States showing all counties was used as the base for a plot of the element grid. The population was allocated proportionally by area to each element based on population projections by county, which were issued individually by each of the states within the area, for the year 1980.

A map of Canada showing provinces and territories was used to plot the elements and to proportionally allocate to each element the 1980 population projections.

To accommodate these estimates, the population grid was extended from 50 miles to 2,000 miles with values given in Table 6.2-7. Seasonal or time of day changes are not considered beyond the 10-mile radius emergency planning zone.

With the exception of travel paths, the evacuation parameter estimates were made separately for each of the five population configurations using a detailed link analysis that accounts for road capacity and population in the site area out to 10 miles. The first step involved locating major evacuation routes and determining which of the 32 direction and 34 radial distance segments was traversed along each route. A series of evacuation direction vectors was established as shown in Figure 6.2-6. After determining the direction of each vector, the distance from the center of each segment to the center of the next segment along the vector was estimated. These values are shown in Table 6.2-8. Knowing the distance and speed, the time in the segment is easily determined and is used in the dose calculations.

Diagonal evacuations across segments were allowed only when the speed was such that the evacuee would spend only a short period of time in adjacent segments. The speeds along the vector in each segment were estimated based on an evacuation time study. The study provided estimates of speed along each route for each of five scenarios.

The calculation of average travel speed for the first evacuation wave was based on results obtained from a static traffic assignment model developed by Parsons Brinckerhoff specifically for evacuation planning. The model, which is described below in more detail, was used to determine the roadway evacuation time for each element in the 10-mile plume exposure pathway emergency planning zone (EPZ) radius. In addition, the model indicated locations where significant travel delays would be experienced by evacuees. These data were analyzed manually using the element length data to estimate average vehicle operating speeds for the duration of the evacuation in each individual element throughout the EPZ.

For subsequent evacuation waves, vehicles were assumed to travel at free flow speeds out of the EPZ. Subsequent evacuation waves were assumed to begin only after preceding waves were completed. Therefore, the second trip for any vehicle began after the entire first wave of evacuating vehicles had cleared the 10-mile area.

The static traffic assignment process developed to estimate roadway travel and delay times required three basic types of input. The first type is related to the characteristics of the evacuation roadway network, which was comprised of unidirectional links, each having its own attributes. The links were described in terms of their capability to accommodate evacuating traffic (evacuation capacity), length, and free-flow speed (posted speed limit).

The second type of input required for this assignment process was vehicle trip generation data. The 10-mile EPZ was disaggregated into elements, and the number of trips by each vehicle type (e.g., autos, buses, ambulances) was estimated in terms of passenger car equivalents (PCEs) for each element. Buses were weighted as the equivalent of two passenger cars in this analysis. In addition, a terminal time for all trip types for each element was input. The terminal time for autos represented the time to drive from homes within the element via feeder streets to the first link of the primary evacuation route. For buses and special vehicles, terminal time represented the total of loading time, circulation time (multiple pickups), and the time to travel to the first link on the evacuation path.

The third input type used in the static assignment process was evacuation path data. Evacuation routes were designated as fixed paths extending from the origin element to the EPZ boundary via specific roadways. Paths were developed for each trip type and were expressed in terms of connecting link numbers. The paths were chosen to correspond as much as possible to the evacuation routes specified in the actual evacuation plan, given the restriction that each element was only allowed one evacuation path.

A computer program was written to process the above data and compute roadway evacuation times for each trip type by element. Initially, the program calculated the total vehicular demand volume (in PCEs) on each link in the network by aggregating the vehicle trips generated by each element along the evacuation path. Implicit in this assignment was the assumption what all vehicles from all elements using a given evacuation route were on each link along the designated route concurrently. The assignment process was thus considered "static," because the spatial movement of vehicles across the network as a function of time was not explicitly recognized.

For each link in the network, three additional computations were performed. First, the free-flow travel time was calculated as the quotient of the link length and the free-flow speed. Second, the total vehicular demand volume was divided by the hourly evacuation capacity of the link to obtain the volume capacity (V/C) relationship for the link. Finally, the evacuation speed or delay time was computed for each link, depending on the valued formula contained in the Federal Highway

Administration August 1973 Traffic Assignment Manual was adopted and modified as follows for use in computing the speed at which evacuees would travel:

$$\text{Evacuation Speed} = \frac{\text{Free Flow Speed}}{0.25\left(\frac{\text{Demand}}{\text{Capacity}}\right)^4 + 1}, \text{ for capacity} > \text{demand}$$

Following these calculations, the model computed the roadway travel time for each element's evacuation route by scanning the links comprising the evacuation route to determine the maximum V/C ratio along the route.

When the hourly evacuation capacity exceeded the total demand volume (V/C ratio less than 1.0) for all links along the route, the link evacuation speeds were used to compute link travel time, and the travel times for each link along the path were summed to obtain the element to EPZ boundary roadway travel time for the route.

When the traffic volume exceeded the hourly evacuation capacity (V/C greater than 1.0) along any link of an element's evacuation route, the route and the roadway travel time were represented by the maximum link delay time incurred along the route. Link delay time was calculated as the maximum volume/capacity ratio in hours along the route.

The roadway travel time as determined above was added to the terminal time and the free-flow travel time for each element trip type to determine the total roadway evacuation time. The total roadway evacuation time resulting from this analysis represented the time for the last vehicle in the element to clear the EPZ.

The computer program developed for the static assignment process provided two basic reports which were used in the determination of element travel speeds. The reports are described below:

- Summary of link statistics including link number, description, length, free flow speed and time, vehicular demand, evacuation capacity, and demand capacity ratio.

- Summary of element statistics including number of trips, evacuation route, destination element, terminal time, free flow travel time, roadway travel time, total evacuation time, and bottleneck link, for each trip type.

After converting the results of the link analysis to CRACIT compatible input, a program called TRACK was used to summarize evacuation characteristics used by CRACIT. Table 6.2-9 provides a summary of the evacuation path speed data. The longest evacuation scenarios occurred for weekday, school in session conditions (Table 6.2-10). Evacuation times are shown in Table 6.2-11. Travel distances for each start location are summarized in Table 6.2-12, and the average speed for each start location is given in Table 6.2-10. Table 6.2-13 summarizes evacuation data for all five scenarios. From discussions with evacuation planners, it was learned that certain areas would be evacuated in two phases. The affected population segment was assumed to start late. The method used

for this purpose in the program was to artificially increase the distance traveled in the affected population segment. Thus, the normal speed with an exaggerated large travel distance (for the nonmoving "resident" population) effectively delayed the occupants in the segment. These large distances explain apparent anomalies in Table 6.2-13.

The anticipated delay in evacuation due to variables such as evacuee preparation and limited transportation availability is considered for each population grid location. An anticipated evacuation delay time of 1 hour is assigned to all locations for all population evacuation scenarios except the weekday, school in session scenario. In this scenario, some sections of the population will be delayed for 5.5 hours. These are identified by direction sector and distance in the following table:

ANTICIPATED WEEKDAY, SCHOOL IN SESSION EVACUEE DELAY

Direction Sector	Population Grid Distance (miles)
11	1.0 - 1.5
12	2.0 - 2.5
13	1.0 - 1.5
14	0.5 - 1.0
14	2.0 - 2.5
15	1.0 - 1.5
16	1.0 - 1.5
17	0.5 - 1.0
18	0.5 - 1.0
19	2.0 - 2.5
20	1.0 - 1.5
21	2.0 - 2.5

There is some probability that any portion of the population may be delayed for more or less time. This is accounted for by assuming a probability distribution of factors which are applied (as multipliers) to the anticipated delay times. The probability distribution assumed for each multiplying factor in this study is as follows:

Assumed (Multiplier) Change in Evacuation Delay Time	0.5	0.7	1.0	1.5	2.0
Probability	0.05	0.15	0.5	0.15	0.15

For example, if the assumed delay time for a given population grid element is 5.5 hours, there is a 15% chance that the delay would be 0.7 times 5.5 hours, or 3.8 hours. During any given weather scenario computation, a multiplier is selected probabilistically for each population grid element. Thus, a multiplier of 1.0 occurs 50% of the time for a large number of samples. The result is that different grid elements have different anticipated delay times in any accident scenario.

The evacuation distance of 10 miles conforms with the plume exposure pathway emergency planning zone specified in NUREG-0654 and NUREG-0396. The evacuation time estimates are also in conformance with methodology provided in Appendix 4 of NUREG-0654.

The possibility exists that the entire evacuation may be delayed beyond the time assumed. Examples include a communications failure that results in a delay of the evacuation order to all locations or severe weather. The additional delay times were factored into this analysis probabilistically by assuming the following probability distribution for additional delay:

Additional Delay Time (hours)	0	1.0	2.0
Probability	0.9	0.07	0.03

These additional delay times were selected probabilistically and added to the delay times of the entire population grid. As a result, for any accident scenario, the selected delay time applies to the entire population. The probability values in this table reflect the high degree of emergency planning which should result in proper notification. Longer delays due to severe weather are very unlikely.

Shielding dose reduction factors (see Section 6.1.1.3.3.4) were used for nonevacuees participating in normal activities and for evacuees. The shielding factors for these sections of the population were the same as those used in the RSS. The RSS factors were 1.0 and 0.5 for evacuees exposed to the cloud and contaminated soil, and 0.75 and 0.33 for people who are not evacuated (Section 11.3, Appendix VI of the RSS). Beyond the evacuation zone out to 50 miles from the plant, 90% of the population was assumed to have basements and be sheltered in them. The shielding dose reduction factors used for this section of the population were 0.5 for cloud dose and 0.08 for ground dose (see Reference 6-34). The remaining 10% was assumed to have shielding factors (i.e., 0.75 and 0.33 for nonevacuees) as modeled in the RSS.

6.2.1.3 Plume Modification Data

As discussed in Sections 6.1.2.3.8 and 6.1.2.3.9, two models are available to account for terrain effects. Both models rely on terrain height as a function of distance and direction around the site. For the Indian Point site, the terrain significantly influences local dispersion.

Studies were made using site data to determine the expected frequency of conditions that could be difficult to model using the Gaussian and possibly MPF terrain plume models. The basic problem arises from the lack of available meteorological data from more than one location within 5 miles of the site for determining flow conditions during periods of low wind speed. These studies showed that possibly as many as 20% of the scenarios required modification. One such study used hodographs to identify the diurnal flow up and down the river valley. A hodograph was prepared for each day that wind speeds were less than 4 mph.

Based on these studies, about 50 start hours from the 288 scenario random sample were chosen for further study. Plume trajectory plots were made on site maps. Of the 50, about 15 scenarios were actually edited to ensure that the best characterization of the plume was achieved. Meteorological conditions for both ground level and elevated releases were edited separately. Examples of plumes before and after modification are given in Figures 6.2-8A through 6.2-12A.

Atmospheric data to support those judgments included surface data from several airports in the region. The 288 meteorological sequences were classified into several types of meteorological scenarios to determine how frequently diurnal valley effect conditions would be expected. The percentages of each type of event in the 288-sequence sample were compared with the percentages determined for the entire year. This comparison, shown in Table 6.2-14, indicates that the 288 scenarios provide a good sample of the actual conditions that existed throughout the year.

The results of the offline numerical MPF computer runs described in Section 6.1.2.3.6 were stored on tape for eventual input into the Indian Point CRACIT computer runs. Data stored for each downwind, x, MPF numerical grid location and for each of three stabilities, B, D, and F included the following:

- x, y, and z - the location of the maximum concentration.
- z_{max} and z_{min} - the heights of the bottom and top of the plume where the concentration is 10% of the maximum.
- y_{min} and y_{max} - the lateral edges of the plume at 10% of the maximum concentration.
- X/Q_G - the maximum X/Q at ground level.
- X/Q_{max} - the maximum X/Q value at any height.
- H_{terr} - the terrain height.

The potential flow model applied in this report assumes that local phenomena that may alter local flow patterns (e.g., drainage winds) do not affect the plume path. The situation is similar to that in a tank test in which the motion of the test apparatus is responsible for perturbations to the flow field. This is justified since highest concentrations are expected to occur for plume trajectories unperturbed by such effects and any local anomalies would probably act to lower concentrations. In addition, diffusion in the downwind, x, direction is neglected. In this case, because steady state flow conditions are assumed for all conditions, neglecting downwind diffusion does not reduce the accuracy of the estimate. The same limitations generally apply to all but the most complex diffusion models and are within the state of the art for application to atmospheric dispersion modeling.

6.2.1.3.1 Characterization of Terrain Surrounding Indian Point

To accurately represent the terrain input to the numerical model, a U.S. geological survey map of the area with a scale of 1 inch = 610m was digitized at 50-foot contour intervals with more accuracy (e.g., at 20-foot intervals) in areas of elevated terrain. These results were then transferred to a rectangular grid with 0.2-inch (122m) spacing between grid lines for an area of about 7 miles square in each direction from the plant. This information was stored on magnetic tape and served as direct input to the numerical model calculations. Figure 6.2-7 is a printer map showing terrain for each x-y grid location. A less detailed grid is used for the Gaussian terrain height (used when conditions do not support use of the MPF model) correction and assumed values are given in Table 6.2-15.

6.2.1.3.2 Grid Selections

Grid sizing was selected to provide accuracy in critical areas in accordance with the guidance of Section 6.1.2.3.7. Smaller spacing was used during initial plume dispersion and near ground level on terrain. Therefore, different grid spacing was required for each major terrain feature, and in some cases, had to be adjusted vertically for the different stability and power level cases. The plume is assumed to be inserted in block x=4, y=11, and at one of four heights (z boxes) depending on the height of the plume rise. This would characterize the plume as having a uniform distribution with a y-z dimension of 500 feet at the source. This initial assumed plume expansion is considerably less than would be expected due to the turbulence in the buoyant jet above the plant.

6.2.1.4 Other Site Related Input

Other than meteorological, population, and certain geographical data, the CRACIT program uses the same input as CRAC.

6.2.2 RELEASES FROM THE PLANT

In the RSS, nine release categories were identified for the pressurized water reactor (PWR) plant. Each had similar characteristics important to dispersion and dose calculations. In this study, several additional categories were identified with new ones added as shown in Tables 6.2-16 and 6.2-17. The logic for these selections is explained in Section 5. Only those categories associated with core melt were used in this consequence analysis.

6.2.2.1 Release Categories

Separate CRACIT runs are made for each release category with the probability of each release category set to 1.0. The magnitudes of radioactive releases are input as fractions of the initial core radioactivity that might leak from the containment structure. In addition to release magnitude, the parameters that characterize the various hypothetical accident sequences are time of release, duration of release, warning time for evacuation, height of release and energy content of the released plume.

The time of release is the time interval between the start (core shutdown) of the hypothetical accident and the release of radioactive material to the atmosphere. It is used to calculate the initial decay of radioactivity. The release duration is the total time during which radioactive material is released and is used to adjust the horizontal dispersion resulting from wind meander during releases longer than one-half hour. The warning time for evacuation is defined as the interval between awareness of impending core melt and the release of radioactive material to the atmosphere. The height of release and the energy content of the released plume (which causes buoyancy) are used to compute plume height. Table 6.2-16 lists the leakage parameters that are assumed to characterize the 11 release categories. These categories are composites of numerous accident sequences with similar characteristics as discussed in Section 6.1. To operate CRACIT in multiphase mode, these leakage data are input separately for each phase.

6.2.2.2 Radioactive Inventory of Reactor Core

The CRACIT program contains a library of isotopes resident in the reactor core. This inventory was developed using the ORIGEN program for a 3,200 Mwt core as discussed in Section 3.2, Appendix VI of the RSS. Indian Point Unit 3 operates at a maximum core power level of 3,025 Mwt and Unit 2 operates at a power level of 2,758 Mwt. Therefore, the CRAC inventory was ratioed downward by a small fraction to represent the Unit 3 power level for all consequence calculations at the site.

The ORIGEN program calculates the time dependent concentration of a large number of nuclides. Although many of these nuclides are not radioactive, the total number of radionuclides is quite large. The number of radionuclides considered can be reduced considerably without affecting the precision of the dose calculations. The elimination of radionuclides from consideration in radiation dose calculations was based on studies conducted during preparation of the RSS. Radionuclides used for this study included the 54 normally used in the CRAC program.

One other related parameter, the heat of release, is important in dispersion calculations. The greater the heat content of the released plume, the higher the plume rise will be. This results in lower ground level concentrations. The estimated energies for this study have been made based on a detailed containment response study as discussed in Section 5. In some cases, they are different than those used in the RSS for PWRs. One case, 2RV, assumes the use of a filtered vent system.

TABLE 6.2-1

METEOROLOGICAL DATA BASES--INDIAN POINT

Site Number	Name	Level of Speed and Direction Measurement (m)	Stability Based on	Location of Rain Data	Lid Height Based on
1	Indian Point	10	Site ΔT (60-10)	Yorktown Heights	Fort Totten upper air data with LaGuardia surface data
2	Indian Point	122	Site ΔT (122-10)	Yorktown Heights	"
3	Bowline	10	Site ΔT (40-10)	Yorktown Heights	"
4	Teterboro	10	LaGuardia Star	Central Park	"
5	Poughkeepsie	10	"	Yorktown Heights	"
6	Allentown	7	"	Newark	"
7	Newark	6	"	Newark	"
8	JFK	6	"	JFK	"
9	Bridgeport	26	"	Bridgeport	"
10	Westchester	6	"	Yorktown Heights	"
11	Central Park	19	"	Central Park	"
12	Hartford	19	"	Hartford	"
13	LaGuardia	6	"	LaGuardia	"
14	Albany	19	"	Yorktown Heights	"

TABLE 6.2-2

DISTRIBUTION OF LID HEIGHTS FROM
FORT TOTTEN, NEW YORK
UPPER AIR DATA (1978-1979)

Lid Height Between	Number of Hours	Percent of Total Hours
0 and 100	121	1.4
100 and 150	26	0.3
150 and 200	44	0.5
200 and 250	126	1.5
250 and 300	228	2.7
300 and 350	166	2.0
350 and 400	168	2.0
400 and 450	211	2.5
450 and 500	210	2.5
500 and 600	504	6.0
600 and 700	683	8.1
700 and 800	678	8.0
800 and 900	606	7.2
900 and 1000	656	7.8
1000 and 1200	1502	17.8
1200 and 1400	911	10.8
1400 and 1600	590	7.0
1600 and 1800	426	5.0
1800 and 2000	142	1.7
2000 and 2500	122	1.4
2500 and 3000	333	3.9
Greater than 3000	0	0.0

TABLE 6.2-3A

JOINT FREQUENCY TABLES--INDIAN POINT, PERIOD OF RECORD FROM 78080101 TO 79073124, SPEED AND DIRECTION FROM 122m LEVEL, TEMPERATURE DIFFERENCE BETWEEN 122m AND 10m FOR TEMPERATURE DIFFERENCE (DEG F/100 FT) ≤ -1.0

DIRECTIONS

SPEED(MPH)	N	NNE	NE	ENE	E	ESE	SE	SSE	S	SSW	SW	WSW	W	WNW	NW	NNW	TOTAL	PERCENT	GEO MEAN SPD(MPH)
CALM	0	0	0	0	0	0	0	0	0	0	0	0	0	0	0	0	0	0.0	0.00
CALM+ - 3.5	12	12	2	2	0	1	1	4	58	21	8	1	1	2	9	6	140	34.0	2.71
3.6 - 7.5	53	11	1	0	0	1	5	4	67	10	10	0	0	15	46	19	242	58.7	5.25
7.6 - 12.5	7	1	0	0	0	0	0	0	6	1	0	0	0	0	10	5	30	7.3	8.42
12.6 - 18.5	0	0	0	0	0	0	0	0	0	0	0	0	0	0	0	0	0	0.0	0.00
18.6 - 24.5	0	0	0	0	0	0	0	0	0	0	0	0	0	0	0	0	0	0.0	0.00
24.6 - 32.5	0	0	0	0	0	0	0	0	0	0	0	0	0	0	0	0	0	0.0	0.00
32.6+	0	0	0	0	0	0	0	0	0	0	0	0	0	0	0	0	0	0.0	0.00
TOTAL	72	24	3	2	0	2	6	8	131	32	18	1	1	17	65	30	412	0.0	4.07
PERCENT	17.5	5.8	.7	.5	0.0	.5	1.5	1.9	31.8	7.8	4.4	.2	.2	4.1	15.8	7.3	100.0		
AV SPD	5.3	4.2	3.6	2.1	0.0	3.6	4.8	3.8	4.5	3.9	4.1	2.5	3.5	5.6	5.7	5.4			

AVERAGE SPEED FOR THIS TABLE EQUALS 4.8
HOURS IN ABOVE TABLE WITH VARIABLE DIRECTION = 0

TABLE 6.2-3B

JOINT FREQUENCY TABLES--INDIAN POINT, PERIOD OF RECORD FROM 78080101 TO 79073124, SPEED AND DIRECTION FROM 122m LEVEL, TEMPERATURE DIFFERENCE BETWEEN 122m AND 10m FOR TEMPERATURE DIFFERENCE (DEG F/100 FT) > -1.0 BUT < -0.9

WIND DIRECTION

SPEED(MPH)	N	NNE	NE	ENE	E	ESE	SE	SSE	S	SSW	SW	WSW	W	WNW	NW	NNW	TOTAL	PERCENT	GEO MEAN SPD(MPH)
CALM	0	0	0	0	0	0	0	0	0	0	0	0	0	0	0	0	0	0.0	0.00
CALM+ - 3.5	10	11	5	2	0	1	1	3	28	18	5	6	4	4	7	5	110	47.6	2.25
3.6 - 7.5	35	16	0	0	0	1	1	1	18	6	4	1	0	4	13	6	106	45.9	5.26
7.6 - 12.5	0	1	0	0	0	0	0	0	7	1	0	0	0	0	4	1	14	6.1	8.97
12.6 - 18.5	0	0	0	0	0	0	0	0	0	0	0	0	0	0	1	0	1	.4	13.50
18.6 - 24.5	0	0	0	0	0	0	0	0	0	0	0	0	0	0	0	0	0	0.0	0.00
24.6 - 32.5	0	0	0	0	0	0	0	0	0	0	0	0	0	0	0	0	0	0.0	0.00
32.6+	0	0	0	0	0	0	0	0	0	0	0	0	0	0	0	0	0	0.0	0.00
TOTAL	45	28	5	2	0	2	2	4	53	25	9	7	4	8	25	12	231	0.0	3.27
PERCENT	19.5	12.1	2.2	.9	0.0	.9	.9	1.7	22.9	10.8	3.9	3.0	1.7	3.5	10.8	5.2	100.0		
AV SPD	5.1	4.1	2.1	2.8	0.0	3.9	4.3	3.3	4.6	3.2	3.4	2.5	2.5	4.3	5.6	4.7			

AVERAGE SPEED FOR THIS TABLE EQUALS 4.3
HOURS IN ABOVE TABLE WITH VARIABLE DIRECTION = 0

TABLE 6.2-3C

JOINT FREQUENCY TABLES--INDIAN POINT, PERIOD OF RECORD FROM 78080101 TO 79073124, SPEED AND DIRECTION FROM 122m LEVEL, TEMPERATURE DIFFERENCE BETWEEN 122m AND 10m FOR TEMPERATURE DIFFERENCE (DEG F/100 FT) > -0.9 BUT ≤ -0.8

WIND DIRECTION

SPEED(MPH)	N	NNE	NE	ENE	E	ESE	SE	SSE	S	SSW	SW	WSW	W	WNW	NW	NNW	TOTAL	PERCENT	GEO MEAN SPD(MPH)
CALM	0	0	0	0	0	0	0	0	0	0	0	0	0	0	0	0	0	0.0	0.00
CALM* - 3.5	12	26	4	2	1	1	4	7	58	34	19	6	7	6	10	8	205	52.8	2.11
3.6 - 7.5	27	23	0	0	1	1	1	1	25	10	9	3	5	7	30	14	157	40.5	5.20
7.6 - 12.5	2	3	0	0	0	0	0	0	4	0	1	0	1	1	10	3	25	6.4	9.42
12.6 - 18.5	0	0	0	0	0	0	0	0	0	0	0	0	1	0	0	0	1	.3	13.50
18.6 - 24.5	0	0	0	0	0	0	0	0	0	0	0	0	0	0	0	0	0	0.0	0.00
24.6 - 32.5	0	0	0	0	0	0	0	0	0	0	0	0	0	0	0	0	0	0.0	0.00
32.6*	0	0	0	0	0	0	0	0	0	0	0	0	0	0	0	0	0	0.0	0.00
TOTAL	41	52	4	2	2	2	5	8	87	44	29	9	14	14	50	25	388	0.0	2.98
PERCENT	10.6	13.4	1.0	.5	.5	.5	1.3	2.1	22.4	11.3	7.5	2.3	3.6	3.6	12.9	6.4	100.0		
AV SPD	4.8	4.0	1.9	1.5	3.1	4.3	2.2	2.4	3.7	3.0	3.3	2.6	4.3	4.6	6.2	5.1			

AVERAGE SPEED FOR THIS TABLE EQUALS 4.1
HOURS IN ABOVE TABLE WITH VARIABLE DIRECTION = 0

TABLE 6.2-3D

JOINT FREQUENCY TABLES--INDIAN POINT, PERIOD OF RECORD FROM 78080101 TO 79073124, SPEED AND DIRECTION FROM 122m LEVEL, TEMPERATURE DIFFERENCE BETWEEN 122m AND 10m FOR TEMPERATURE DIFFERENCE (DEG F/100 FT) > -0.8 BUT ≤ -0.3

WIND DIRECTION

SPEED(MPH)	N	NNE	NE	ENE	E	ESE	SE	SSE	S	SSW	SW	WSW	W	WNW	NW	NNW	TOTAL	PERCENT	GEO MEAN SPD(MPH)
CALM	2	2	1	2	1	3	1	2	1	3	1	4	2	1	1	1	28	.6	.50
CALM* - 3.5	112	213	131	98	80	55	74	74	283	161	107	64	73	79	59	65	1728	39.6	1.91
3.6 - 7.5	285	364	78	16	11	13	36	26	161	106	88	53	74	151	338	215	2015	46.2	5.36
7.6 - 12.5	65	53	2	0	1	0	0	2	20	3	3	3	10	44	238	107	551	12.6	9.11
12.6 - 18.5	1	1	0	0	0	0	0	0	0	0	0	0	4	1	28	6	41	.9	14.05
18.6 - 24.5	0	0	0	0	0	0	0	0	0	0	0	0	0	0	0	0	0	0.0	0.00
24.6 - 32.5	0	0	0	0	0	0	0	0	0	1	0	0	0	0	0	0	1	.0	24.75
32.6*	0	0	0	0	0	0	0	0	0	0	0	0	0	0	0	0	0	0.0	0.00
TOTAL	465	633	212	116	93	71	111	104	465	274	199	124	163	276	664	394	4364	0.0	3.12
PERCENT	10.7	14.5	4.9	2.7	2.1	1.6	2.5	2.4	10.7	6.3	4.6	2.8	3.7	6.3	15.2	9.0	100.0		
AV SPD	5.4	4.7	3.3	2.5	2.6	2.8	3.2	3.0	3.6	3.5	3.5	3.5	4.4	5.2	7.3	6.4			

AVERAGE SPEED FOR THIS TABLE EQUALS 4.8
HOURS IN ABOVE TABLE WITH VARIABLE DIRECTION = 0

TABLE 6.2-3E

JOINT FREQUENCY TABLES--INDIAN POINT, PERIOD OF RECORD FROM 78080101 TO 79073124, SPEED AND DIRECTION FROM 122m LEVEL, TEMPERATURE DIFFERENCE BETWEEN 122m AND 10m FOR TEMPEATURE DIFFERENCE (DEG F/100 FT) > -0.3 BUT ≤ 0.8

WIND DIRECTION

SPEED(MPH)	N	NNE	NE	ENE	E	ESE	SE	SSE	S	SSW	SW	WSW	W	WNW	NW	NNW	TOTAL	PERCENT	GEO MEAN SPD(MPH)
CALM	8	6	2	1	5	2	4	5	24	9	16	15	20	10	8	11	146	5.0	.50
CALM* - 3.5	149	134	87	37	34	40	42	93	256	241	175	117	82	46	59	90	1682	58.1	1.65
3.6 - 7.5	103	120	32	14	4	4	11	16	166	171	93	32	44	26	38	39	913	31.6	5.00
7.6 - 12.5	20	22	1	2	7	1	0	3	26	15	11	2	4	8	13	6	141	4.9	9.09
12.6 - 18.5	2	0	0	0	3	0	0	0	1	2	0	0	0	1	2	0	11	.4	14.91
18.6 - 24.5	0	0	0	0	0	0	0	0	0	0	0	0	0	0	0	0	0	0.0	0.00
24.6 - 32.5	0	0	0	0	0	0	0	0	0	0	0	0	0	0	0	0	0	0.0	0.00
32.6*	0	0	0	0	0	0	0	0	0	0	0	0	0	0	0	0	0	0.0	0.00
TOTAL	282	282	122	54	53	47	57	117	473	438	295	166	150	91	120	146	2893	0.0	1.92
PERCENT	9.7	9.7	4.2	1.9	1.8	1.6	2.0	4.0	16.3	15.1	10.2	5.7	5.2	3.1	4.1	5.0	100.0		
AV SPD	3.8	4.0	3.1	3.2	3.8	2.0	2.3	2.4	3.6	3.6	3.2	2.4	2.8	3.5	4.2	3.1			

AVERAGE SPEED FOR THIS TABLE EQUALS 3.4
HOURS IN ABOVE TABLE WITH VARIABLE DIRECTION = 0

TABLE 6.2-3F

JOINT FREQUENCY TABLES--INDIAN POINT, PERIOD OF RECORD FROM 78080101 TO 79037124, SPEED AND DIRECTION FROM 122m LEVEL, TEMPERATURE DIFFERENCE BETWEEN 122m AND 10m FOR TEMPERATURE DIFFERENCE (DEG F/100 FT) > 0.8 BUT ≤ 2.2

WIND DIRECTION

SPEED(MPH)	N	NNE	NE	ENE	E	ESE	SE	SSE	S	SSW	SW	WSW	W	WNW	NW	NNW	TOTAL	PERCENT	GEO MEAN SPD(MPH)
CALM	3	1	2	1	2	2	0	3	6	5	4	1	9	3	3	3	48	10.5	.50
CALM* - 3.5	56	39	17	3	11	4	6	0	28	37	31	32	27	12	20	38	361	79.2	1.45
3.6 - 7.5	5	8	3	0	0	1	0	1	3	12	5	2	3	2	2	0	47	10.3	4.68
7.6 - 12.5	0	0	0	0	0	0	0	0	0	0	0	0	0	0	0	0	0	0.0	0.00
12.6 - 18.5	0	0	0	0	0	0	0	0	0	0	0	0	0	0	0	0	0	0.0	0.00
18.6 - 24.5	0	0	0	0	0	0	0	0	0	0	0	0	0	0	0	0	0	0.0	0.00
24.6 - 32.5	0	0	0	0	0	0	0	0	0	0	0	0	0	0	0	0	0	0.0	0.00
32.6*	0	0	0	0	0	0	0	0	0	0	0	0	0	0	0	0	0	0.0	0.00
TOTAL	64	48	22	4	13	7	6	4	37	54	40	35	39	17	25	41	456	0.0	1.28
PERCENT	14.0	10.5	4.8	.9	2.9	1.5	1.3	.9	8.1	11.8	8.8	7.7	8.6	3.7	5.5	9.0	100.0		
AV SPD	2.4	2.6	2.3	.9	.9	1.4	1.8	1.4	2.0	2.4	1.9	1.7	1.3	1.9	1.9	1.7			

AVERAGE SPEED FOR THIS TABLE EQUALS 2.0
HOURS IN ABOVE TABLE WITH VARIABLE DIRECTION = 0

TABLE 6.2-3G

JOINT FREQUENCY TABLES--INDIAN POINT, PERIOD OF RECORD FROM 78080101 TO 79073124, SPEED AND DIRECTION FROM 122m LEVEL, TEMPERATURE DIFFERENCE BETWEEN 122m AND 10m FOR TEMPERATURE DIFFERENCE (DEG F/100 FT) > 2.2

WIND DIRECTION

SPEED(MPH)	N	NNE	NE	ENE	E	ESE	SE	SSE	S	SSW	SW	WSW	W	WNW	NW	NNW	TOTAL	PERCENT	GEO MEAN SPD(MPH)
CALM	0	0	0	0	0	0	0	0	0	0	0	0	0	0	0	0	0	0.0	0.00
CALM+ - 3.5	3	1	0	0	0	0	0	0	1	1	3	2	1	1	0	1	14	87.5	1.52
3.6 - 7.5	1	0	0	0	0	0	0	0	0	0	1	0	0	0	0	0	2	12.5	4.62
7.6 - 12.5	0	0	0	0	0	0	0	0	0	0	0	0	0	0	0	0	0	0.0	0.00
12.6 - 18.5	0	0	0	0	0	0	0	0	0	0	0	0	0	0	0	0	0	0.0	0.00
18.6 - 24.5	0	0	0	0	0	0	0	0	0	0	0	0	0	0	0	0	0	0.0	0.00
24.6 - 32.5	0	0	0	0	0	0	0	0	0	0	0	0	0	0	0	0	0	0.0	0.00
32.6+	0	0	0	0	0	0	0	0	0	0	0	0	0	0	0	0	0	0.0	0.00
TOTAL	4	1	0	0	0	0	0	0	1	1	4	2	1	1	0	1	16	0.0	1.66
PERCENT	25.0	6.3	0.0	0.0	0.0	0.0	0.0	0.0	6.3	6.3	25.0	12.5	6.3	6.3	0.0	6.3	100.0		
AV SPD	2.7	2.8	0.0	0.0	0.0	0.0	0.0	0.0	.8	1.8	2.8	1.6	2.0	1.0	0.0	2.0			

AVERAGE SPEED FOR THIS TABLE EQUALS 2.2

HOURS IN ABOVE TABLE WITH VARIABLE DIRECTION = 0

TABLE 6.2-4A

JOINT FREQUENCY TABLES--INDIAN POINT, PERIOD OF RECORD FROM 78080101 TO 79073124, SPEED AND DIRECTION FROM 10m LEVEL, TEMPERATURE DIFFERENCE BETWEEN 61m AND 10m FOR TEMPERATURE DIFFERENCE (DEG F/100 FT) ≤ -1.0

DIRECTIONS

SPEED(MPH)	N	NNE	NE	ENE	E	ESE	SE	SSE	S	SSW	SW	WSW	W	WNW	NW	NNW	TOTAL	PERCENT	GEO MEAN SPD(MPH)
CALM	0	0	0	0	0	0	0	3	5	4	1	1	2	0	0	1	17	1.3	.50
CALM+ - 3.5	194	133	31	8	6	2	7	19	254	297	98	32	46	32	57	79	1295	96.6	1.50
3.6 - 7.5	10	3	3	0	0	0	0	0	0	1	1	0	1	1	0	8	28	2.1	4.62
7.6 - 12.5	0	0	0	0	0	0	0	0	0	0	0	0	0	0	0	0	0	0.0	0.00
12.6 - 18.5	0	0	0	0	0	0	0	0	0	0	0	0	0	0	0	0	0	0.0	0.00
18.6 - 24.5	0	0	0	0	0	0	0	0	0	0	0	0	0	0	0	0	0	0.0	0.00
24.6 - 32.5	0	0	0	0	0	0	0	0	0	0	0	0	0	0	0	0	0	0.0	0.00
32.6+	0	0	0	0	0	0	0	0	0	0	0	0	0	0	0	0	0	0.0	0.00
TOTAL	204	136	34	8	6	2	7	22	259	302	100	33	49	33	57	88	1340	0.0	1.48
PERCENT	15.2	10.1	2.5	.6	.4	.1	.5	1.6	19.3	22.5	7.5	2.5	3.7	2.5	4.3	6.6	100.0		
AV SPD	2.0	2.2	2.5	1.4	1.3	1.9	1.6	1.1	1.5	1.6	1.6	1.5	1.5	2.1	2.1	2.2			

AVERAGE SPEED FOR THIS TABLE EQUALS 1.8
HOURS IN ABOVE TABLE WITH VARIABLE DIRECTION = 0

TABLE 6.2-4B

JOINT FREQUENCY TABLES--INDIAN POINT, PERIOD OF RECORD FROM 78080101 TO 79073124, SPEED AND DIRECTION FROM 10m LEVEL, TEMPERATURE DIFFERENCE BETWEEN 61m AND 10m FOR TEMPERATURE DIFFERENCE (DEG F/100 FT) > -1.0 BUT < -0.9

WIND DIRECTION

SPEED(MPH)	N	NNE	NE	ENE	E	ESE	SE	SSE	S	SSW	SW	WSW	W	WNW	NW	NNW	TOTAL	PERCENT	GEO MEAN SPD(MPH)
CALM	0	0	0	0	0	0	0	0	1	1	0	1	0	0	0	0	3	1.8	.50
CALM+ - 3.5	30	19	13	1	0	1	2	1	11	24	18	5	8	11	4	11	159	93.5	1.50
3.6 - 7.5	1	1	2	0	0	0	0	0	0	0	1	0	0	0	2	1	8	4.7	4.41
7.6 - 12.5	0	0	0	0	0	0	0	0	0	0	0	0	0	0	0	0	0	0.0	0.00
12.6 - 18.5	0	0	0	0	0	0	0	0	0	0	0	0	0	0	0	0	0	0.0	0.00
18.6 - 24.5	0	0	0	0	0	0	0	0	0	0	0	0	0	0	0	0	0	0.0	0.00
24.6 - 32.5	0	0	0	0	0	0	0	0	0	0	0	0	0	0	0	0	0	0.0	0.00
32.6+	0	0	0	0	0	0	0	0	0	0	0	0	0	0	0	0	0	0.0	0.00
TOTAL	31	20	15	1	0	1	2	1	12	25	19	6	8	11	6	12	170	0.0	1.49
PERCENT	18.2	11.8	8.8	.6	0.0	.6	1.2	.6	7.1	14.7	11.2	3.5	4.7	6.5	3.5	7.1	100.0		
AV SPD	1.9	2.1	2.4	1.8	0.0	1.0	1.1	1.0	1.1	1.6	1.7	1.4	1.9	2.4	2.8	2.0			

AVERAGE SPEED FOR THIS TABLE EQUALS 1.9
HOURS IN ABOVE TABLE WITH VARIABLE DIRECTION = 0

TABLE 6.2-4C

JOINT FREQUENCY TABLES--INDIAN POINT PERIOD OF RECORD FROM 78080101 TO 79073124, SPEED AND DIRECTION FROM 10m LEVEL, TEMPERATURE DIFFERENCE BETWEEN 61m AND 10m FOR TEMPERATURE DIFFERENCE (DEG F/100 FT) > -0.9 BUT ≤ -0.8

WIND DIRECTION

SPEED(MPH)	N	NNE	NE	ENE	E	ESE	SE	SSE	S	SSW	SW	WSW	W	WNW	NW	NNW	TOTAL	PERCENT	GEO MEAN SPD(MPH)
CALM	0	0	0	1	0	0	0	0	3	3	1	0	1	0	0	0	9	2.7	.50
CALM* - 3.5	35	24	31	8	3	5	2	4	35	41	21	19	16	15	27	21	307	92.7	1.44
3.6 - 7.5	5	0	0	0	0	0	0	0	0	0	0	1	0	4	1	4	15	4.5	4.75
7.6 - 12.5	0	0	0	0	0	0	0	0	0	0	0	0	0	0	0	0	0	0.0	0.00
12.6 - 18.5	0	0	0	0	0	0	0	0	0	0	0	0	0	0	0	0	0	0.0	0.00
18.6 - 24.5	0	0	0	0	0	0	0	0	0	0	0	0	0	0	0	0	0	0.0	0.00
24.6 - 32.5	0	0	0	0	0	0	0	0	0	0	0	0	0	0	0	0	0	0.0	0.00
32.6*	0	0	0	0	0	0	0	0	0	0	0	0	0	0	0	0	0	0.0	0.00
TOTAL	40	24	31	9	3	5	2	4	38	44	22	20	17	19	28	25	331	0.0	1.42
PERCENT	12.1	7.3	9.4	2.7	.9	1.5	.6	1.2	11.5	13.3	6.6	6.0	5.1	5.7	8.5	7.6	100.0		
AV SPD	2.6	2.0	1.8	1.2	1.4	1.2	1.1	1.0	1.3	1.3	1.8	1.4	1.7	2.7	2.8	2.3			

AVERAGE SPEED FOR THIS TABLE EQUALS 1.9
HOURS IN ABOVE TABLE WITH VARIABLE DIRECTION = 0

TABLE 6.2-4D

JOINT FREQUENCY TABLES--INDIAN POINT, PERIOD OF RECORD FROM 78080101 TO 79073124, SPEED AND DIRECTION FROM 10m LEVEL, TEMPERATURE DIFFERENCE BETWEEN 61m AND 10m FOR TEMPERATURE DIFFERENCE (DEG F/100 FT) > -0.8 BUT ≤ -0.3

WIND DIRECTION

SPEED(MPH)	N	NNE	NE	ENE	E	ESE	SE	SSE	S	SSW	SW	WSW	W	WNW	NW	NNW	TOTAL	PERCENT	GEO MEAN SPD(MPH)
CALM	5	3	3	9	7	12	6	20	39	24	11	6	10	3	4	5	167	7.2	.50
CALM* - 3.5	253	329	229	77	38	19	17	50	163	180	120	44	76	94	136	105	1930	83.4	1.56
3.6 - 7.5	29	18	4	1	0	0	0	0	0	1	0	0	3	23	69	68	216	9.3	4.49
7.6 - 12.5	0	0	0	0	0	0	0	0	0	0	0	0	0	0	0	0	0	0.0	0.00
12.6 - 18.5	0	0	0	0	0	0	0	0	0	0	0	0	0	0	0	0	0	0.0	0.00
18.6 - 24.5	0	0	0	0	0	0	0	0	0	0	0	0	0	0	0	0	0	0.0	0.00
24.6 - 32.5	0	0	0	0	0	0	0	0	0	0	0	0	0	0	0	0	0	0.0	0.00
32.6*	0	0	0	0	0	0	0	0	0	0	0	0	0	0	0	0	0	0.0	0.00
TOTAL	287	350	236	87	45	31	23	70	202	205	131	50	89	120	209	178	2313	0.0	1.43
PERCENT	12.4	15.1	10.2	3.8	1.9	1.3	1.0	3.0	8.7	8.9	5.7	2.2	3.8	5.2	9.0	7.7	100.0		
AV SPD	2.6	2.3	1.8	1.3	1.0	1.0	1.1	1.0	1.2	1.4	1.4	1.4	1.8	2.7	3.3	3.4			

AVERAGE SPEED FOR THIS TABLE EQUALS 2.1
HOURS IN ABOVE TABLE WITH VARIABLE DIRECTION = 0

TABLE 6.2-4E

JOINT FREQUENCY TABLES--INDIAN POINT, PERIOD OF RECORD 78080101 TO 79073124, SPEED AND DIRECTION FROM 10m LEVEL, TEMPERATURE DIFFERENCE BETWEEN 61m AND 10m FOR TEMPERATURE DIFFERENCE (DEG F/100 FT) > -0.3 BUT ≤ 0.8

	WIND DIRECTION																		
SPEED(MPH)	N	NNE	NE	ENE	E	ESE	SE	SSE	S	SSW	SW	WSW	W	WNW	NW	NNW	TOTAL	PERCENT	GEO MEAN SPD(MPH)
CALM	40	36	30	19	23	26	26	61	118	66	37	35	37	22	15	16	607	16.4	.50
CALM+ - 3.5	274	412	336	144	64	31	28	75	297	361	142	81	171	120	139	142	2817	76.1	1.36
3.6 - 7.5	13	41	23	7	1	0	0	0	2	0	1	1	4	24	119	39	275	7.4	4.78
7.6 - 12.5	0	0	0	0	0	0	0	0	0	0	0	0	0	1	3	0	4	.1	8.12
12.6 - 18.5	0	0	0	0	0	0	0	0	0	0	0	0	0	0	0	0	0	0.0	0.00
18.6 - 24.5	0	0	0	0	0	0	0	0	0	0	0	0	0	0	0	0	0	0.0	0.00
24.6 - 32.5	0	0	0	0	0	0	0	0	0	0	0	0	0	0	0	0	0	0.0	0.00
32.6+	0	0	0	0	0	0	0	0	0	0	0	0	0	0	0	0	0	0.0	0.00
TOTAL	327	489	389	170	88	57	54	136	417	427	180	117	212	167	276	197	3703	0.0	1.11
PERCENT	8.8	13.2	10.5	4.6	2.4	1.5	1.5	3.7	11.3	11.5	4.9	3.2	5.7	4.5	7.5	5.3	100.0		
AV SPD	1.8	2.0	1.9	1.3	1.0	.7	.8	.8	1.1	1.3	1.2	1.1	1.5	2.4	3.6	2.6			

AVERAGE SPEED FOR THIS TABLE EQUALS 1.7
HOURS IN ABOVE TABLE WITH VARIABLE DIRECTION = 0

TABLE 6.2-4F

JOINT FREQUENCY TABLES--INDIAN POINT, PERIOD OF RECORD 78080101 TO 79073124, SPEED AND DIRECTION FROM 10m LEVEL, TEMPERATURE DIFFERENCE BETWEEN 61m AND 10m FOR TEMPERATURE DIFFERENCE (DEG F/100 FT) > 0.8 BUT ≤ 2.2

	WIND DIRECTION																		
SPEED(MPH)	N	NNE	NE	ENE	E	ESE	SE	SSE	S	SSW	SW	WSW	W	WNW	NW	NNW	TOTAL	PERCENT	GEO MEAN SPD(MPH)
CALM	34	18	19	4	0	2	6	12	27	24	9	13	17	6	3	9	203	26.0	.50
CALM+ - 3.5	35	149	163	59	20	11	6	10	37	26	14	15	12	9	4	7	577	74.0	1.08
3.6 - 7.5	0	0	0	0	0	0	0	0	0	0	0	0	0	0	0	0	0	0.0	0.00
7.6 - 12.5	0	0	0	0	0	0	0	0	0	0	0	0	0	0	0	0	0	0.0	0.00
12.6 - 18.5	0	0	0	0	0	0	0	0	0	0	0	0	0	0	0	0	0	0.0	0.00
18.6 - 24.5	0	0	0	0	0	0	0	0	0	0	0	0	0	0	0	0	0	0.0	0.00
24.6 - 32.5	0	0	0	0	0	0	0	0	0	0	0	0	0	0	0	0	0	0.0	0.00
32.6+	0	0	0	0	0	0	0	0	0	0	0	0	0	0	0	0	0	0.0	0.00
TOTAL	69	167	182	63	20	13	12	22	64	50	23	28	29	15	7	16	780	0.0	.83
PERCENT	8.8	21.4	23.3	8.1	2.6	1.7	1.5	2.8	8.2	6.4	2.9	3.6	3.7	1.9	.9	2.1	100.0		
AV SPD	.8	1.1	1.3	1.3	1.0	.9	.7	.7	.8	.7	.8	.8	.8	.8	.9	.6			

AVERAGE SPEED FOR THIS TABLE EQUALS 1.0
HOURS IN ABOVE TABLE WITH VARIABLE DIRECTION = 0

TABLE 6.2-4G

JOINT FREQUENCY TABLES--INDIAN POINT, PERIOD OF RECORD 78080101 TO 79073124, SPEED AND DIRECTION FROM 10m LEVEL, TEMPERATURE DIFFERENCE BETWEEN 61m AND 10m FOR TEMPERATURE DIFFERENCE (DEG F/100 FT) > 2.2

WIND DIRECTION

SPEED(MPH)	N	NNE	NE	ENE	E	ESE	SE	SSE	S	SSW	SW	WSW	W	WNW	NW	NNW	TOTAL	PERCENT	GEO MEAN SPD(MPH)
CALM	2	1	3	0	0	0	0	0	4	1	0	2	4	0	2	3	22	17.9	.50
CALM+ - 3.5	7	21	31	28	3	2	1	1	3	0	0	0	1	1	0	2	101	82.1	1.23
3.6 - 7.5	0	0	0	0	0	0	0	0	0	0	0	0	0	0	0	0	0	0.0	0.00
7.6 - 12.5	0	0	0	0	0	0	0	0	0	0	0	0	0	0	0	0	0	0.0	0.00
12.6 - 18.5	0	0	0	0	0	0	0	0	0	0	0	0	0	0	0	0	0	0.0	0.00
18.6 - 24.5	0	0	0	0	0	0	0	0	0	0	0	0	0	0	0	0	0	0.0	0.00
24.6 - 32.5	0	0	0	0	0	0	0	0	0	0	0	0	0	0	0	0	0	0.0	0.00
32.6+	0	0	0	0	0	0	0	0	0	0	0	0	0	0	0	0	0	0.0	0.00
TOTAL	9	22	34	28	3	2	1	1	7	1	0	2	5	1	2	5	123	0.0	.98
PERCENT	7.3	17.9	27.6	22.8	2.4	1.6	.8	.8	5.7	.8	0.0	1.6	4.1	.8	1.6	4.1	100.0		
AV SPD	.8	1.0	1.6	1.7	1.3	1.1	.8	.8	.9	.5	0.0	.5	.6	1.0	.5	.7			

AVERAGE SPEED FOR THIS TABLE EQUALS 1.3

HOURS IN ABOVE TABLE WITH VARIABLE DIRECTION = 0

TABLE 6.2-5

INDIAN POINT--POPULATION (0 - 50 MILES), (WEEKDAY, SCHOOL IN SESSION)

Direction Sector*	Distance Segment 1	2	3	4	5	6	7	8	9
1	0.	0.	0.	0.	1350.	0.	0.	16.	73.
2	0.	0.	0.	17.	65.	9.	41.	24.	44.
3	0.	0.	0.	17.	23.	19.	20.	21.	258.
4	0.	0.	0.	741.	1314.	2975.	774.	1618.	326.
5	0.	0.	345.	3551.	4321.	3335.	667.	1117.	1462.
6	0.	167.	172.	2677.	1149.	1213.	599.	915.	658.
7	0.	0.	459.	730.	312.	217.	144.	571.	808.
8	0.	23.	601.	0.	0.	0.	41.	33.	38.
9	0.	34.	73.	0.	0.	0.	729.	148.	33.
10	0.	57.	106.	41.	0.	24.	425.	131.	16.
11	0.	112.	57.	41.	41.	131.	31.	491.	91.
12	0.	290.	510.	295.	8.	61.	65.	131.	122.
13	0.	328.	480.	480.	216.	612.	268.	180.	41.
14	24.	57.	365.	780.	408.	571.	530.	70.	219.
15	0.	31.	118.	510.	245.	0.	0.	0.	0.
16	0.	121.	86.	122.	24.	0.	0.	0.	0.
17	0.	474.	532.	0.	0.	0.	109.	12.	144.
18	0.	73.	877.	0.	0.	0.	674.	121.	1971.
19	0.	75.	635.	0.	65.	1134.	1274.	1927.	3174.
20	0.	0.	24.	0.	61.	1316.	1207.	1920.	1435.
21	0.	0.	0.	0.	143.	202.	194.	344.	36.
22	0.	0.	0.	208.	117.	12.	182.	24.	121.
23	0.	0.	24.	121.	109.	0.	126.	24.	0.
24	0.	0.	49.	79.	121.	77.	17.	0.	0.
25	0.	0.	12.	73.	87.	0.	0.	0.	0.
26	0.	0.	43.	0.	0.	0.	0.	0.	0.
27	0.	0.	61.	0.	0.	57.	0.	0.	945.
28	0.	0.	13.	0.	0.	69.	141.	0.	0.
29	0.	0.	0.	0.	0.	12.	0.	0.	0.
30	0.	0.	0.	0.	0.	36.	4325.	224.	150.
31	0.	0.	61.	0.	0.	0.	0.	0.	24.
32	0.	0.	139.	0.	0.	0.	0.	0.	224.

*Sector 1 is wind toward sector between 0 and 11.25 degrees. Sector number increases clockwise.

TABLE 6.2-5 (continued)

INDIAN POINT--POPULATION (0 - 50 MILES), (WEEKDAY, SCHOOL IN SESSION)

Direction Sector*	Distance Segment 10	11	12	13	14	15	16	17	18
1	0.	73.	250.	1212.	540.	105.	1965.	1965.	1965.
2	102.	261.	218.	218.	508.	145.	1965.	1965.	1965.
3	643.	580.	470.	393.	1500.	1060.	1965.	1965.	1965.
4	841.	2172.	1750.	1542.	350.	600.	1965.	1965.	1965.
5	2637.	2336.	3373.	631.	276.	790.	1965.	1965.	1965.
6	82.	1946.	1482.	5761.	2345.	2551.	1675.	3640.	2970.
7	911.	569.	1094.	5220.	2805.	2023.	5025.	5025.	6832.
8	1347.	87.	1367.	4758.	4255.	2431.	5025.	5025.	1837.
9	65.	122.	140.	970.	1304.	2089.	2001.	3115.	3260.
10	8.	75.	757.	67.	271.	426.	1630.	10645.	3260.
11	82.	556.	121.	949.	2650.	1039.	4075.	4075.	2875.
12	131.	6444.	326.	402.	790.	1953.	4015.	6605.	4520.
13	161.	2637.	2430.	1935.	6761.	6483.	5587.	7020.	3690.
14	16.	0.	108.	87.	8001.	6495.	3798.	12040.	19280.
15	0.	0.	0.	0.	50.	50.	0.	2920.	5750.
16	0.	0.	551.	2563.	5897.	6346.	9464.	10863.	3259.
17	4164.	4974.	2866.	1989.	5525.	2547.	2912.	3802.	8690.
18	3583.	3139.	1592.	2480.	7049.	6566.	8008.	10146.	24190.
19	3534.	4885.	1021.	858.	3355.	4038.	8443.	8443.	15500.
20	3535.	493.	1321.	375.	4374.	3821.	8443.	8443.	880.
21	426.	1322.	1420.	446.	807.	300.	8443.	8443.	17325.
22	40.	187.	85.	22.	230.	0.	4221.	4221.	8563.
23	0.	0.	0.	0.	66.	2185.	123.	613.	196.
24	0.	0.	1134.	143.	0.	0.	735.	123.	123.
25	0.	0.	0.	647.	885.	42.	884.	1401.	480.
26	0.	28.	20.	35.	188.	2263.	2571.	7609.	478.
27	10.	5.	0.	1461.	283.	2769.	1448.	959.	1901.
28	17.	0.	0.	89.	19.	536.	1650.	1281.	3650.
29	17.	0.	13.	150.	0.	49.	2311.	475.	5471.
30	449.	135.	0.	28.	19.	0.	769.	4571.	4520.
31	727.	1147.	0.	0.	0.	0.	0.	2311.	4520.
32	87.	103.	4972.	6059.	1873.	819.	328.	4816.	2214.

*Sector 1 is wind toward sector between 0 and 11.25 degrees. Sector number increases clockwise.

TABLE 6.2-5 (continued)

INDIAN POINT--POPULATION (0 - 50 MILES), (WEEKDAY, SCHOOL IN SESSION)

Direction Sector*	Distance Segment 19	20	21	22	23	24	25	26
1	2214.	2214.	6642.	11070.	8856.	11070.	13284.	13284.
2	2214.	2214.	6642.	11070.	8856.	11070.	13284.	13284.
3	1965.	2214.	6642.	6642.	8856.	11070.	13715.	8220.
4	1965.	1965.	6642.	6642.	8856.	2585.	4164.	4164.
5	1965.	1965.	6550.	9027.	14808.	14808.	4882.	6604.
6	1965.	1965.	6550.	14808.	14808.	6738.	37987.	37987.
7	1100.	1100.	11465.	16452.	14808.	17717.	37987.	37987.
8	1806.	1900.	10068.	14808.	14808.	90433.	56083.	37937.
9	2665.	1703.	3820.	42461.	67241.	90433.	90433.	57430.
10	3175.	2236.	43341.	42461.	42461.	0.	0.	0.
11	2575.	9361.	42461.	42461.	0.	0.	13560.	54240.
12	8846.	8846.	42461.	0.	13560.	67800.	67800.	67800.
13	5059.	19930.	61586.	0.	111120.	152460.	151800.	123360.
14	13450.	21350.	69425.	10050.	138900.	208350.	208350.	138900.
15	14400.	20850.	236760.	443000.	508260.	540810.	471540.	180390.
16	14195.	24800.	93400.	733700.	787700.	714750.	1015050.	229500.
17	31000.	32750.	105252.	141175.	502321.	500120.	723500.	319500.
18	31000.	18673.	76600.	150412.	92836.	165120.	221140.	234960.
19	32560.	19140.	34550.	51029.	148608.	165120.	200200.	200200.
20	16380.	1320.	65949.	24018.	24018.	48036.	48036.	48036.
21	440.	23635.	53509.	51029.	24018.	48036.	48036.	48036.
22	23195.	23195.	51029.	51029.	24018.	4767.	9767.	9767.
23	2424.	441.	51029.	3446.	3446.	9767.	9767.	9767.
24	881.	441.	4406.	3446.	3446.	9767.	9767.	10070.
25	459.	1101.	5507.	5948.	5500.	19391.	303.	1209.
26	1912.	556.	3958.	4082.	2995.	3273.	2586.	1663.
27	3335.	2523.	12471.	32175.	3704.	3251.	3350.	2010.
28	2053.	1819.	2533.	6796.	3719.	3350.	3350.	5360.
29	4520.	2405.	5402.	5802.	4125.	4125.	4125.	3660.
30	2260.	2495.	10732.	4874.	4125.	4125.	4125.	4125.
31	31090.	2495.	12455.	4125.	4125.	4125.	4125.	4125.
32	2214.	3602.	7465.	4125.	4125.	4125.	4125.	4125.

*Sector 1 is wind toward sector between 0 and 11.25 degrees. Sector number increases clockwise.

TABLE 6.2-6

INDIAN POINT--NIGHT POPULATION (0 - 50 MILES)

Distance Segment

Direction Sector*	1	2	3	4	5	6	7	8	9
1	0.	0.	0.	0.	1000.	0.	0.	16.	73.
2	0.	0.	0.	17.	65.	9.	41.	24.	44.
3	0.	0.	0.	17.	23.	19.	20.	21.	258.
4	0.	0.	0.	574.	890.	2672.	774.	949.	286.
5	0.	0.	345.	3533.	2671.	2671.	667.	1117.	1462.
6	0.	34.	172.	1500.	1149.	1213.	400.	647.	658.
7	0.	0.	459.	230.	312.	217.	144.	571.	808.
8	0.	23.	402.	0.	0.	0.	41.	33.	38.
9	0.	34.	73.	0.	0.	0.	33.	148.	33.
10	0.	57.	106.	41.	0.	24.	114.	131.	16.
11	0.	112.	57.	41.	41.	131.	31.	286.	91.
12	0.	290.	510.	295.	8.	61.	65.	131.	122.
13	0.	328.	480.	480.	216.	612.	268.	180.	41.
14	24.	57.	365.	780.	1521.	571.	530.	70.	25.
15	0.	31.	118.	510.	245.	0.	0.	0.	0.
16	0.	121.	86.	122.	24.	0.	0.	0.	0.
17	0.	474.	532.	0.	0.	0.	109.	12.	144.
18	0.	73.	877.	0.	0.	0.	364.	121.	1686.
19	0.	75.	635.	0.	65.	1134.	285.	1041.	2071.
20	0.	0.	24.	0.	61.	1316.	1207.	911.	1251.
21	0.	0.	0.	0.	143.	202.	194.	344.	36.
22	0.	0.	0.	208.	117.	12.	182.	24.	121.
23	0.	0.	24.	121.	109.	0.	126.	24.	0.
24	0.	0.	49.	79.	121.	12.	17.	0.	0.
25	0.	0.	12.	73.	87.	0.	0.	0.	0.
26	0.	0.	43.	0.	0.	0.	0.	0.	0.
27	0.	0.	61.	0.	0.	57.	0.	0.	15.
28	0.	0.	13.	0.	0.	69.	141.	0.	0.
29	0.	0.	0.	0.	0.	12.	0.	0.	0.
30	0.	0.	0.	0.	0.	36.	85.	86.	150.
31	0.	0.	61.	0.	0.	0.	0.	0.	24.
32	0.	0.	139.	0.	0.	0.	0.	0.	209.

*Sector 1 is wind toward sector between 0 and 11.25 degrees. Sector number increases clockwise.

TABLE 6.2-6 (continued)

INDIAN POINT--NIGHT POPULATION (0 - 50 MILES)

Direction Sector*	Distance Segment 10	11	12	13	14	15	16	17	18
1	0.	73.	250.	330.	337.	116.	1965.	1965.	1965.
2	102.	261.	217.	218.	508.	145.	1965.	1965.	1965.
3	863.	580.	470.	393.	1500.	1060.	1965.	1965.	1965.
4	861.	2172.	1750.	480.	350.	600.	1965.	1965.	1965.
5	2637.	1469.	2166.	631.	276.	790.	1965.	1965.	1965.
6	82.	1804.	1262.	1948.	2345.	1865.	1675.	3640.	2970.
7	245.	569.	1094.	2524.	2805.	2023.	5025.	5025.	6832.
8	33.	87.	1367.	320.	2805.	1792.	5025.	5025.	1837.
9	65.	122.	140.	834.	1125.	1462.	2001.	3115.	3260.
10	8.	75.	757.	67.	271.	426.	1630.	10645.	3260.
11	82.	441.	121.	321.	638.	1039.	4075.	4075.	2875.
12	131.	3923.	326.	402.	790.	910.	4015.	6605.	4520.
13	91.	2637.	2580.	1856.	5140.	5529.	5587.	7020.	3690.
14	16.	0.	41.	87.	4680.	5529.	3798.	12040.	19280.
15	0.	0.	0.	0.	50.	50.	0.	2920.	5750.
16	0.	0.	451.	2000.	2998.	4161.	9464.	10863.	3259.
17	1185.	4477.	2866.	1989.	2626.	1800.	2912.	3802.	8690.
18	2089.	1620.	1300.	1700.	5000.	5251.	8008.	10146.	24190.
19	2783.	2733.	1021.	966.	1741.	3658.	8443.	8443.	15500.
20	573.	3055.	1321.	375.	2862.	3821.	8443.	8443.	880.
21	426.	1322.	1420.	446.	176.	300.	8443.	8443.	17325.
22	40.	187.	85.	22.	95.	0.	4221.	4221.	8563.
23	0.	0.	0.	0.	66.	583.	123.	613.	196.
24	0.	0.	144.	143.	0.	0.	735.	123.	123.
25	0.	0.	0.	47.	315.	42.	884.	1401.	480.
26	0.	28.	20.	35.	23.	71.	2571.	7609.	478.
27	10.	5.	0.	552.	283.	1921.	1448.	959.	1901.
28	17.	0.	0.	89.	19.	536.	1650.	1281.	3650.
29	17.	0.	13.	150.	0.	49.	2311.	475.	5471.
30	449.	135.	0.	28.	19.	0.	769.	4571.	4520.
31	787.	278.	0.	0.	0.	0.	0.	2311.	4520.
32	87.	154.	4888.	5243.	1873.	819.	328.	4816.	2214.

*Sector 1 is wind toward sector between 0 and 11.25 degrees. Sector number increases clockwise.

TABLE 6.2-6 (continued)

INDIAN POINT--NIGHT POPULATION (0 - 50 MILES)

Direction Sector*	Distance Segment							
	19	20	21	22	23	24	25	26
1	2214.	2214.	6642.	11070.	8856.	11070.	13284.	13284.
2	2214.	2214.	6642.	11070.	8856.	11070.	13284.	13284.
3	1965.	2214.	6642.	6642.	8856.	11070.	13715.	8220.
4	1965.	1965.	6642.	6642.	8856.	2585.	4164.	4164.
5	1965.	1965.	6550.	9027.	14808.	14808.	4882.	6604.
6	1965.	1965.	6550.	14808.	14808.	6738.	37987.	37987.
7	1100.	1100.	11465.	16452.	14808.	17717.	37987.	37987.
8	1806.	1900.	16068.	14808.	14808.	90433.	56083.	37937.
9	2665.	1703.	3820.	42461.	67241.	90433.	90433.	57430.
10	3175.	2236.	43341.	42461.	42461.	0.	0.	0.
11	2575.	9361.	42461.	42461.	0.	0.	13560.	54240.
12	8846.	8846.	42461.	0.	13560.	67800.	67800.	67800.
13	5050.	19930.	61586.	0.	111120.	152460.	151800.	123360.
14	13450.	21350.	69825.	10050.	138900.	208350.	208350.	138900.
15	14400.	20850.	236760.	443000.	508260.	540810.	471540.	180390.
16	14195.	24800.	93400.	733700.	787700.	714750.	1015050.	229500.
17	31000.	32750.	105252.	141175.	502321.	500120.	723500.	319500.
18	31000.	18673.	76600.	150412.	92836.	165120.	221140.	234960.
19	32560.	19140.	34550.	51029.	148608.	165120.	200200.	200200.
20	16380.	1320.	65949.	24018.	24018.	48036.	48036.	48036.
21	440.	23635.	53509.	51029.	24018.	48036.	48036.	48036.
22	23195.	23195.	51029.	51029.	24018.	4767.	9767.	9767.
23	2424.	441.	51029.	3446.	3446.	9767.	9767.	9767.
24	881.	441.	4406.	3446.	3446.	9767.	9767.	10070.
25	459.	1101.	5507.	5948.	5500.	19391.	303.	1209.
26	1912.	956.	3958.	4082.	2995.	3273.	2586.	1663.
27	3335.	2523.	12471.	32175.	3704.	3251.	3350.	2010.
28	2053.	1819.	2533.	6796.	3719.	3350.	3350.	5360.
29	4520.	2405.	5402.	5802.	4125.	4125.	4125.	3660.
30	2260.	2495.	10732.	4874.	4125.	4125.	4125.	4125.
31	31090.	2495.	12455.	4125.	4125.	4125.	4125.	4125.
32	2214.	3602.	7465.	4125.	4125.	4125.	4125.	4125.

*Sector 1 is wind toward sector between 0 and 11.25 degrees. Sector number increases clockwise.

TABLE 6.2-7

INDIAN POINT--POPULATION DISTRIBUTION ESTIMATE (BEYOND 50 MILES)
Distance Segment

Direction Sector*	27	28	29	30	31	32	33	34
1	11800.0	21900.0	170200.0	236584.0	71535.0	1592486.0	300000.0	4704.0
2	8850.0	137502.0	161752.0	149213.0	70104.0	788798.0	277500.0	19100.0
3	142156.0	119802.0	179703.0	165602.0	161966.0	385943.0	385200.0	17100.0
4	82255.0	261958.0	299505.0	369774.0	303730.0	906670.0	418500.0	17100.0
5	82255.0	183284.0	460435.0	479208.0	413164.0	419790.0	764000.0	0.0
6	82255.0	164510.0	185074.0	1057423.0	1198016.0	290000.0	308500.0	0.0
7	82255.0	164510.0	185074.0	1107198.0	599009.0	0.0	0.0	0.0
8	61692.0	143947.0	164510.0	265992.0	299505.0	0.0	0.0	0.0
9	20564.0	20564.0	54240.0	27120.0	0.0	0.0	0.0	0.0
10	0.0	122040.0	189840.0	0.0	0.0	0.0	0.0	0.0
11	135600.0	216960.0	0.0	0.0	0.0	0.0	0.0	0.0
12	135600.0	27120.0	0.0	0.0	0.0	0.0	0.0	0.0
13	40680.0	0.0	0.0	0.0	0.0	0.0	0.0	0.0
14	0.0	0.0	0.0	0.0	0.0	0.0	0.0	0.0
15	0.0	0.0	0.0	0.0	0.0	0.0	0.0	0.0
16	0.0	0.0	0.0	0.0	0.0	0.0	0.0	0.0
17	0.0	297360.0	70320.0	105480.0	0.0	0.0	0.0	0.0
18	415240.0	349070.0	210660.0	462000.0	105705.0	393874.0	545395.0	2689250.0
19	198640.0	322580.0	231205.0	870125.0	231020.0	1572310.0	6794055.0	392922.0
20	83680.0	145810.0	271692.0	3052779.0	638419.0	4814115.0	4748106.0	3149193.0
21	80060.0	59880.0	207819.0	719686.0	1030179.0	3380740.0	9767265.0	4563811.0
22	25620.0	121896.0	264690.0	411153.0	541134.0	2324673.0	6645344.0	15404599.0
23	5642.0	35313.0	42369.0	289563.0	262006.0	2629768.0	6965953.0	10893118.0
24	3430.0	16395.0	134073.0	299204.0	120103.0	2932706.0	10012677.0	5609854.0
25	3430.0	8910.0	198520.0	83337.0	102002.0	9047815.0	17185335.0	6398780.0
26	7370.0	8633.0	37656.0	51933.0	112944.0	3030041.0	9656521.0	2252298.0
27	7370.0	14011.0	34085.0	253235.0	196950.0	2099829.0	2048189.0	2666784.0
28	8040.0	12090.0	15510.0	137110.0	362650.0	3192464.0	172989.0	1874896.0
29	19850.0	18540.0	18150.0	177250.0	362850.0	2923707.0	211639.0	591316.0
30	16500.0	15930.0	13280.0	116050.0	146750.0	1432218.0	289232.0	137614.0
31	15750.0	17900.0	19200.0	104350.0	33100.0	975073.0	315000.0	3744.0
32	13200.0	14700.0	173400.0	210650.0	27250.0	1587413.0	315000.0	5704.0

*Sector 1 is wind toward sector between 0 and 11.25 degrees. Sector number increases clockwise.

TABLE 6.2-8

INDIAN POINT--EVACUATION VECTORS
(WEEKDAY, SCHOOL IN SESSION)

START ELEMENT SECTOR	START ELEMENT SEGMENT	DISTANCE TRAVELED IN START ELEMENT (MI)	DESTINATION ELEMENT SECTOR	DESTINATION ELEMENT SEGMENT	DISTANCE TRAVELED IN DESTINATION ELEMENT (MI)
1	1	0.00	0	0	0.00
1	2	0.00	0	0	0.00
1	3	0.00	0	0	0.00
1	4	.30	1	5	.60
1	5	.60	32	5	.50
1	6	.60	32	6	.50
1	7	.70	2	7	.60
1	8	.80	32	9	.80
1	9	.90	32	9	.80
1	10	1.00	32	10	.50
1	11	1.20	1	12	1.00
1	12	1.00	1	13	1.10
1	13	1.10	1	14	1.00
1	14	1.00	1	15	1.20
1	15	1.20	1	16	0.00
2	1	0.00	0	0	0.00
2	2	0.00	0	0	0.00
2	3	0.00	0	0	0.00
2	4	.20	2	5	.40
2	5	.40	3	5	.60
2	6	.50	2	7	.60
2	7	.60	2	8	.50
2	8	.50	2	9	.50
2	9	.50	2	10	.50
2	10	.50	2	11	1.10
2	11	1.10	2	12	1.00
2	12	1.00	2	13	1.00
2	13	1.00	2	14	1.10
2	14	1.10	2	15	1.00
2	15	1.00	2	16	0.00
3	1	.10	4	1	.10
3	2	0.00	0	0	0.00
3	3	0.00	0	0	0.00
3	4	.30	3	5	.60
3	5	.60	3	6	.50
3	6	.50	2	7	.60
3	7	.50	3	8	.50
3	8	.50	3	9	.50
3	9	.50	3	10	.50
3	10	.50	3	11	.90
3	11	.90	3	12	1.00
3	12	1.00	3	13	1.60
3	13	1.60	3	14	1.40
3	14	1.40	3	15	1.10
3	15	1.10	3	16	0.00
4	1	.10	5	1	.10
4	2	.10	5	2	.10
4	3	.10	5	3	.50
4	4	.40	5	5	.60
4	5	.50	4	6	.10
4	6	.10	3	6	.50
4	7	.50	4	8	.50
4	8	.50	4	9	.50
4	9	.50	4	10	.50

TABLE 6.2-8 (continued)

INDIAN POINT--EVACUATION VECTORS
(WEEKDAY, SCHOOL IN SESSION)

START ELEMENT SECTOR	START ELEMENT SEGMENT	DISTANCE TRAVELED IN START ELEMENT (MI)	DESTINATION ELEMENT SECTOR	DESTINATION ELEMENT SEGMENT	DISTANCE TRAVELED IN DESTINATION ELEMENT (MI)
4	10	.50	4	11	1.00
4	11	1.00	4	12	.30
4	12	.30	5	12	.70
4	13	1.10	4	14	2.60
4	14	2.60	4	15	1.10
4	15	1.10	4	16	0.00
5	1	.10	6	1	.10
5	2	.10	5	3	.50
5	3	.50	5	4	.50
5	4	.50	5	5	.60
5	5	.60	6	6	.50
5	6	.50	5	7	.60
5	7	.60	5	8	.50
5	8	.50	6	9	.50
5	9	.90	6	9	.50
5	10	.30	6	10	.50
5	11	.70	4	11	1.00
5	12	.70	5	13	1.50
5	13	1.50	4	14	2.60
5	14	.90	4	15	1.10
5	15	1.20	5	16	0.00
6	1	.10	7	1	.10
6	2	.50	6	3	.50
6	3	.50	6	4	.50
6	4	.50	6	5	.50
6	5	.50	7	6	.60
6	6	.50	6	7	.60
6	7	.60	7	8	.50
6	8	.50	7	9	.50
6	9	.50	6	10	.50
6	10	.50	6	11	1.00
6	11	1.00	6	12	1.00
6	12	1.00	6	13	1.00
6	13	1.00	6	14	.80
6	14	.80	5	15	1.20
6	15	1.50	6	16	0.00
7	1	.10	8	1	.50
7	2	.20	8	2	.30
7	3	.20	6	3	.50
7	4	.30	6	4	.50
7	5	.50	7	6	.60
7	6	.60	8	6	.30
7	7	.70	8	7	.60
7	8	.50	7	9	.50
7	9	.50	7	10	.50
7	10	.50	7	11	1.10
7	11	1.10	7	12	1.60
7	12	1.60	8	13	1.70
7	13	1.20	6	13	1.00
7	14	.70	7	15	1.20
7	15	1.20	7	16	0.00
8	1	.50	8	2	.30
8	2	.30	9	2	.20
8	3	.20	9	3	.20

TABLE 6.2-8 (continued)

INDIAN POINT--EVACUATION VECTORS
(WEEKDAY, SCHOOL IN SESSION)

START ELEMENT SECTOR	START ELEMENT SEGMENT	DISTANCE TRAVELED IN START ELEMENT (MI)	DESTINATION ELEMENT SECTOR	DESTINATION ELEMENT SEGMENT	DISTANCE TRAVELED IN DESTINATION ELEMENT (MI)
8	4	.50	9	3	.20
8	5	.50	8	6	.30
8	6	.30	8	7	.60
8	7	.60	8	8	.40
8	8	.40	9	9	.50
8	9	1.10	9	9	.50
8	10	.50	8	11	1.20
8	11	1.20	7	11	1.10
8	12	.70	8	13	1.70
8	13	1.70	9	13	2.00
8	14	1.80	8	15	1.00
8	15	1.00	8	16	0.00
9	1	.50	9	2	.20
9	2	.20	10	3	.20
9	3	.20	10	3	.20
9	4	.50	9	5	.50
9	5	.50	9	6	.60
9	6	.60	8	6	.30
9	7	.80	8	8	.40
9	8	.50	9	9	.50
9	9	.50	9	10	.50
9	10	.50	9	11	1.40
9	11	1.40	9	12	1.00
9	12	1.00	9	13	2.00
9	13	2.00	10	13	1.60
9	14	1.20	8	14	1.80
9	15	1.80	9	16	0.00
10	1	.50	10	2	.20
10	2	.20	9	2	.20
10	3	.20	11	3	.30
10	4	.40	11	4	.40
10	5	.50	10	6	.60
10	6	.60	11	6	.40
10	7	.70	9	8	.50
10	8	.80	9	8	.50
10	9	.90	9	8	.50
10	10	1.00	9	11	1.40
10	11	1.00	10	12	1.80
10	12	1.80	9	13	2.00
10	13	1.60	11	14	1.80
10	14	1.00	10	15	1.00
10	15	1.00	10	16	0.00
11	1	****	11	2	.20
11	2	****	10	2	.20
11	3	****	12	4	.50
11	4	****	12	4	.50
11	5	****	11	6	.40
11	6	****	12	7	.70
11	7	.70	12	7	.70
11	8	.40	12	8	.50
11	9	.90	12	9	.50
11	10	.50	11	11	1.60
11	11	1.60	10	12	1.80
11	12	.90	11	11	1.60

TABLE 6.2-8 (continued)

INDIAN POINT--EVACUATION VECTORS
(WEEKDAY, SCHOOL IN SESSION)

START ELEMENT SECTOR	START ELEMENT SEGMENT	DISTANCE TRAVELED IN START ELEMENT (MI)	DESTINATION ELEMENT SECTOR	DESTINATION ELEMENT SEGMENT	DISTANCE TRAVELED IN DESTINATION ELEMENT (MI)
11	13	1.00	11	14	1.80
11	14	1.80	12	15	2.00
11	15	2.30	11	16	0.00
12	1	****	12	2	.20
12	2	****	11	2	.20
12	3	****	13	4	.30
12	4	****	12	5	.50
12	5	****	12	6	.50
12	6	****	13	7	.50
12	7	.70	12	8	.50
12	8	.50	12	9	.50
12	9	.50	12	10	.80
12	10	.80	11	11	1.60
12	11	2.40	11	11	1.60
12	12	.90	11	12	.90
12	13	.50	12	14	1.80
12	14	1.80	11	15	2.30
12	15	2.00	12	16	0.00
13	1	****	13	2	.30
13	2	****	12	2	.20
13	3	****	13	4	.30
13	4	****	13	5	.60
13	5	****	13	6	.50
13	6	****	13	7	.50
13	7	.50	13	8	.30
13	8	.30	14	8	.30
13	9	.30	14	9	.50
13	10	.50	13	11	1.00
13	11	1.00	13	12	1.00
13	12	1.00	13	13	1.30
13	13	1.30	13	14	1.30
13	14	1.30	13	15	1.00
13	15	1.00	13	16	0.00
14	1	****	14	2	.20
14	2	****	13	2	.30
14	3	****	13	4	.30
14	4	****	13	4	.30
14	5	****	13	5	.60
14	6	****	14	7	.70
14	7	.70	13	7	.50
14	8	.30	14	9	.50
14	9	.50	14	10	.40
14	10	.40	13	11	1.00
14	11	0.00	0	0	0.00
14	12	1.20	13	12	1.00
14	13	.40	13	13	1.30
14	14	.40	14	15	1.20
14	15	1.20	14	16	0.00
15	1	****	15	2	.50
15	2	****	15	3	.50
15	3	****	15	4	.70
15	4	****	15	5	.30
15	5	****	14	5	.40
15	6	****	14	6	.50

TABLE 6.2-8 (continued)

INDIAN POINT--EVACUATION VECTORS
(WEEKDAY, SCHOOL IN SESSION)

START ELEMENT SECTOR	START ELEMENT SEGMENT	DISTANCE TRAVELED IN START ELEMENT (MI)	DESTINATION ELEMENT SECTOR	DESTINATION ELEMENT SEGMENT	DISTANCE TRAVELED IN DESTINATION ELEMENT (MI)
15	7	0.00	0	0	0.00
15	8	0.00	0	0	0.00
15	9	0.00	0	0	0.00
15	10	0.00	0	0	0.00
15	11	0.00	0	0	0.00
15	12	0.00	0	0	0.00
15	13	.30	16	13	1.10
15	14	.60	16	14	1.00
15	15	.60	16	15	1.10
16	1	****	16	2	.50
16	2	****	16	3	.30
16	3	****	15	4	.70
16	4	****	15	4	.70
16	5	****	15	5	.30
16	6	0.00	0	0	0.00
16	7	0.00	0	0	0.00
16	8	0.00	0	0	0.00
16	9	0.00	0	0	0.00
16	10	0.00	0	0	0.00
16	11	0.00	0	0	0.00
16	12	1.30	16	13	1.10
16	13	1.10	16	14	1.00
16	14	1.00	16	15	1.10
16	15	1.10	16	16	0.00
17	1	****	17	2	.50
17	2	****	17	3	.30
17	3	****	16	3	.30
17	4	0.00	0	0	0.00
17	5	0.00	0	0	0.00
17	6	0.00	0	0	0.00
17	7	.10	18	7	.50
17	8	.20	18	9	.90
17	9	.40	18	9	.90
17	10	.50	17	11	1.60
17	11	1.60	16	12	1.30
17	12	1.70	17	13	1.40
17	13	1.40	17	14	1.40
17	14	1.40	17	15	1.00
17	15	1.00	17	16	0.00
18	1	****	18	2	.50
18	2	****	18	3	.20
18	3	****	17	3	.30
18	4	0.00	0	0	0.00
18	5	0.00	0	0	0.00
18	6	0.00	0	0	0.00
18	7	.50	18	8	.50
18	8	.50	18	9	.90
18	9	.90	19	9	.90
18	10	1.00	19	11	1.40
18	11	1.10	19	11	1.40
18	12	1.00	18	13	1.20
18	13	1.20	18	14	2.50
18	14	2.50	18	15	1.40
18	15	1.40	18	16	0.00

TABLE 6.2-8 (continued)

INDIAN POINT--EVACUATION VECTORS
(WEEKDAY, SCHOOL IN SESSION)

START ELEMENT SECTOR	START ELEMENT SEGMENT	DISTANCE TRAVELED IN START ELEMENT (MI)	DESTINATION ELEMENT SECTOR	DESTINATION ELEMENT SEGMENT	DISTANCE TRAVELED IN DESTINATION ELEMENT (MI)
19	1	****	19	2	.50
19	2	****	19	3	.30
19	3	****	18	3	.20
19	4	0.00	0	0	0.00
19	5	****	20	5	.50
19	6	****	20	6	.70
19	7	.70	20	7	.70
19	8	.80	20	9	.70
19	9	.90	20	9	.70
19	10	.80	20	11	1.40
19	11	1.40	19	12	1.40
19	12	1.40	19	13	1.10
19	13	1.10	19	14	1.30
19	14	1.30	18	15	1.40
19	15	1.20	19	16	0.00
20	1	****	20	2	0.00
20	2	0.00	0	0	0.00
20	3	****	19	3	.30
20	4	0.00	0	0	0.00
20	5	****	21	6	.50
20	6	****	21	6	.50
20	7	.70	21	7	.60
20	8	.50	20	9	.70
20	9	.70	21	10	1.00
20	10	1.00	21	11	1.50
20	11	1.40	21	12	1.40
20	12	1.10	20	13	1.00
20	13	1.00	19	14	1.30
20	14	1.00	20	15	1.00
20	15	1.00	20	16	0.00
21	1	****	20	1	.50
21	2	0.00	0	0	0.00
21	3	0.00	0	0	0.00
21	4	****	21	5	.40
21	5	****	21	6	.50
21	6	****	21	7	.60
21	7	.60	21	8	.70
21	8	.70	22	9	.90
21	9	.50	21	10	1.00
21	10	1.00	22	11	.90
21	11	1.50	20	12	1.10
21	12	1.40	21	13	.90
21	13	.90	21	14	1.20
21	14	1.20	21	15	1.00
21	15	1.00	21	16	0.00
22	1	0.00	0	0	0.00
22	2	0.00	0	0	0.00
22	3	0.00	0	0	0.00
22	4	.60	21	5	.40
22	5	.50	21	5	.40
22	6	.60	21	6	.50
22	7	.70	21	7	.60
22	8	.50	22	9	.90
22	9	.90	23	10	.70

TABLE 6.2-8 (continued)

INDIAN POINT--EVACUATION VECTORS
(WEEKDAY, SCHOOL IN SESSION)

START ELEMENT SECTOR	START ELEMENT SEGMENT	DISTANCE TRAVELED IN START ELEMENT (MI)	DESTINATION ELEMENT SECTOR	DESTINATION ELEMENT SEGMENT	DISTANCE TRAVELED IN DESTINATION ELEMENT (MI)
22	10	.50	22	9	.90
22	11	.90	22	12	1.40
22	12	1.40	22	13	.60
22	13	.60	23	13	1.00
22	14	.80	22	15	1.60
22	15	1.60	22	16	0.00
23	1	0.00	0	0	0.00
23	2	0.00	0	0	0.00
23	3	.30	22	4	.60
23	4	.40	22	4	.60
23	5	.50	22	5	.50
23	6	.50	23	7	.50
23	7	.50	23	8	.80
23	8	.80	22	9	.90
23	9	.50	23	10	.70
23	10	.70	24	10	.70
23	11	1.00	23	10	.70
23	12	1.00	23	13	1.00
23	13	1.00	24	13	1.70
23	14	1.00	23	15	1.10
23	15	1.10	23	16	0.00
24	1	0.00	0	0	0.00
24	2	0.00	0	0	0.00
24	3	.30	23	3	.30
24	4	.40	23	4	.40
24	5	.50	23	5	.50
24	6	.50	24	7	.70
24	7	.70	23	7	.50
24	8	.80	23	8	.80
24	9	.60	25	9	.80
24	10	.70	24	9	.60
24	11	1.00	24	12	1.00
24	12	1.00	24	13	1.70
24	13	1.70	23	14	1.00
24	14	1.40	23	14	1.00
24	15	1.00	24	16	0.00
25	1	0.00	0	0	0.00
25	2	0.00	0	0	0.00
25	3	.30	24	3	.30
25	4	.40	24	4	.40
25	5	.50	24	5	.50
25	6	.60	24	6	.50
25	7	.70	24	7	.70
25	8	.80	26	8	.80
25	9	.80	26	9	.90
25	10	.50	25	11	1.00
25	11	1.00	25	12	.60
25	12	.60	24	13	1.70
25	13	.60	24	13	1.70
25	14	1.00	25	15	1.00
25	15	1.00	25	16	0.00
26	1	0.00	0	0	0.00
26	2	0.00	0	0	0.00
26	3	.30	25	3	.30

TABLE 6.2-8 (continued)

INDIAN POINT--EVACUATION VECTORS
(WEEKDAY, SCHOOL IN SESSION)

START ELEMENT SECTOR	START ELEMENT SEGMENT	DISTANCE TRAVELED IN START ELEMENT (MI)	DESTINATION ELEMENT SECTOR	DESTINATION ELEMENT SEGMENT	DISTANCE TRAVELED IN DESTINATION ELEMENT (MI)
26	4	.40	25	4	.40
26	5	.50	25	5	.50
26	6	.60	27	6	.60
26	7	.70	27	8	.50
26	8	.80	27	9	.50
26	9	.90	27	9	.50
26	10	1.00	27	10	.60
26	11	1.00	26	12	1.20
26	12	1.20	25	12	.60
26	13	1.30	27	13	1.20
26	14	.80	26	15	1.20
26	15	1.20	26	16	0.00
27	1	0.00	0	0	0.00
27	2	0.00	0	0	0.00
27	3	.30	26	3	.30
27	4	.50	28	5	.50
27	5	.50	28	6	.30
27	6	.60	28	6	.30
27	7	.50	27	8	.50
27	8	.50	27	9	.50
27	9	.50	27	10	.60
27	10	.60	27	11	1.00
27	11	1.00	27	12	1.00
27	12	1.00	27	13	1.20
27	13	1.20	27	14	.80
27	14	.80	26	14	.80
27	15	1.00	27	16	0.00
28	1	0.00	0	0	0.00
28	2	0.00	0	0	0.00
28	3	.30	29	2	.20
28	4	.50	28	5	.50
28	5	.50	28	6	.30
28	6	.30	29	7	.70
28	7	.50	28	6	.30
28	8	.70	28	9	.50
28	9	.50	29	10	.90
28	10	1.00	27	11	1.00
28	11	1.10	29	11	1.00
28	12	1.20	29	12	1.00
28	13	1.30	27	13	1.20
28	14	1.00	28	13	1.30
28	15	1.00	28	16	0.00
29	1	0.00	0	0	0.00
29	2	.20	30	2	.20
29	3	.50	29	2	.20
29	4	.50	29	5	.50
29	5	.50	29	6	.60
29	6	.60	28	6	.30
29	7	.70	28	8	.70
29	8	.80	28	8	.70
29	9	.90	28	9	.50
29	10	.90	28	10	1.00
29	11	1.00	29	12	1.00
29	12	1.00	29	13	1.30

TABLE 6.2-8 (continued)

INDIAN POINT--EVACUATION VECTORS
(WEEKDAY, SCHOOL IN SESSION)

START ELEMENT SECTOR	START ELEMENT SEGMENT	DISTANCE TRAVELED IN START ELEMENT (MI)	DESTINATION ELEMENT SECTOR	DESTINATION ELEMENT SEGMENT	DISTANCE TRAVELED IN DESTINATION ELEMENT (MI)
29	13	1.30	28	13	1.30
29	14	1.00	29	13	1.30
29	15	1.00	29	16	0.00
30	1	0.00	0	0	0.00
30	2	.20	31	2	.10
30	3	.50	30	2	.20
30	4	.50	29	5	.50
30	5	.50	29	5	.50
30	6	.50	29	6	.60
30	7	.30	29	7	.70
30	8	.50	30	9	1.10
30	9	1.10	29	10	.90
30	10	.50	30	9	1.10
30	11	1.00	30	10	.50
30	12	1.00	30	13	1.30
30	13	1.30	29	13	1.30
30	14	1.40	31	14	1.40
30	15	1.00	30	16	0.00
31	1	0.00	0	0	0.00
31	2	.10	32	3	.50
31	3	.30	32	3	.50
31	4	.50	30	4	.50
31	5	.10	31	6	.60
31	6	.60	31	7	.80
31	7	.80	31	8	.80
31	8	.80	32	9	.80
31	9	.30	30	9	1.10
31	10	1.00	30	9	1.10
31	11	1.10	32	12	.80
31	12	1.20	32	12	.80
31	13	.60	31	14	1.40
31	14	1.40	31	15	1.00
31	15	1.00	31	16	0.00
32	1	0.00	0	0	0.00
32	2	0.00	0	0	0.00
32	3	.50	31	4	.50
32	4	.10	32	5	.50
32	5	.50	31	6	.60
32	6	.50	32	7	.50
32	7	.50	32	8	.50
32	8	.50	32	9	.80
32	9	.80	32	10	.50
32	10	.50	32	11	1.00
32	11	1.00	1	12	1.00
32	12	.80	32	13	.60
32	13	.60	31	14	1.40
32	14	1.40	31	14	1.40
32	15	1.10	31	16	0.00

Note: Artificially high distances used to simulate delay.

TABLE 6.2-9

INDIAN POINT--EXAMPLE OF EVACUATION SPEED BY POPULATION GRID ELEMENT (Weekday, School in Session)

Outer Distance (mi)	(Miles/Hour), Direction Sector 1-32*							
0.5	0.00	0.00	35.00	35.00	35.00	35.00	25.00	25.00
	25.00	25.00	25.00	25.00	25.00	25.00	25.00	25.00
	25.00	25.00	25.00	35.00	25.00	0.00	0.00	0.00
	0.00	0.00	0.00	0.00	0.00	0.00	0.00	0.00
1.0	0.00	0.00	0.00	35.00	25.00	15.00	25.00	29.00
	29.00	29.00	29.00	29.00	29.00	25.00	25.00	25.00
	15.00	25.00	25.00	0.00	0.00	0.00	0.00	0.00
	0.00	0.00	0.00	0.00	35.00	35.00	35.00	0.00
1.5	0.00	0.00	0.00	25.00	25.00	25.00	25.00	15.00
	25.00	49.00	49.00	25.00	25.00	25.00	25.00	29.00
	29.00	29.00	15.00	25.00	0.00	0.00	25.00	25.00
	35.00	25.00	25.00	35.00	35.00	35.00	35.00	35.00
2.0	35.00	35.00	15.00	15.00	15.00	15.00	35.00	35.00
	35.00	25.00	35.00	49.00	6.60	25.00	29.00	35.00
	0.00	0.00	0.00	0.00	25.00	30.00	25.00	25.00
	25.00	35.00	35.00	35.00	35.00	35.00	35.00	35.00
2.5	24.00	24.00	15.00	15.00	3.80	15.00	35.00	35.00
	35.00	35.00	35.00	49.00	6.60	29.00	29.00	35.00
	0.00	0.00	35.00	25.00	25.00	25.00	25.00	25.00
	35.00	35.00	35.00	35.00	35.00	35.00	35.00	24.00
3.0	35.00	25.00	15.00	30.00	36.00	3.80	3.80	3.80
	35.00	35.00	30.00	49.00	6.60	25.00	25.00	0.00
	0.00	0.00	25.00	30.00	5.00	25.00	35.00	35.00
	35.00	35.00	35.00	40.00	35.00	35.00	24.00	35.00
3.5	35.00	15.00	35.00	30.00	36.00	3.80	25.00	3.80
	0.00	35.00	35.00	30.00	25.00	25.00	0.00	0.00
	25.00	25.00	15.00	15.00	5.00	25.00	35.00	35.00
	35.00	35.00	35.00	25.00	40.00	35.00	24.00	35.00
4.0	35.00	15.00	35.00	3.10	36.00	3.80	25.00	3.80
	25.00	35.00	30.00	30.00	3.20	3.20	0.00	0.00
	35.00	35.00	15.00	15.00	5.00	35.00	35.00	35.00
	35.00	35.00	35.00	40.00	35.00	35.00	24.00	35.00
4.5	35.00	15.00	29.00	3.10	25.00	3.40	3.80	3.80
	3.80	35.00	35.00	30.00	35.00	3.20	0.00	0.00
	25.00	15.00	15.00	2.70	35.00	19.00	35.00	47.00
	47.00	47.00	47.00	40.00	35.00	46.00	35.00	24.00
5.0	35.00	15.00	29.00	3.10	3.40	3.40	3.80	35.00
	3.80	35.00	35.00	30.00	25.00	3.20	0.00	0.00
	25.00	15.00	17.00	25.00	2.70	35.00	47.00	47.00
	35.00	35.00	40.00	46.00	46.00	35.00	25.00	24.00
6.0	24.00	15.00	29.00	3.10	3.10	3.40	3.80	25.00
	3.80	35.00	18.00	14.00	3.20	0.00	0.00	0.00
	2.20	25.00	4.50	3.50	49.00	2.70	35.00	35.00
	35.00	35.00	2.10	35.00	35.00	35.00	35.00	24.00
7.0	24.00	15.00	29.00	3.10	3.10	3.40	3.80	30.00
	3.80	2.00	30.00	30.00	3.20	35.00	0.00	2.10
	2.20	25.00	4.50	49.00	3.50	2.70	35.00	25.00
	49.00	35.00	2.10	35.00	35.00	35.00	35.00	13.00
8.0	2.20	15.00	29.00	2.40	3.50	4.20	4.80	3.80
	17.00	4.40	35.00	13.00	3.20	35.00	35.00	15.00
	2.20	4.60	3.70	49.00	3.50	2.70	2.70	40.00
	46.00	35.00	2.10	35.00	25.00	35.00	13.00	13.00
9.0	2.60	15.00	2.90	4.50	3.10	3.60	2.00	1.10
	24.00	25.00	2.00	13.00	3.20	1.00	35.00	15.00
	2.25	4.60	1.60	25.00	3.50	30.00	2.70	35.00
	35.00	2.10	2.10	35.00	35.00	35.00	13.00	25.00
10.0	2.60	15.00	2.90	4.50	3.40	14.00	2.00	1.10
	10.00	10.00	13.00	2.00	3.20	1.00	35.00	15.00
	2.20	1.60	1.60	25.00	3.50	35.00	2.70	35.00
	35.00	2.10	25.00	25.00	35.00	35.00	35.00	13.00
12.0	0.00	0.00	0.00	0.00	0.00	0.00	0.00	0.00
	0.00	0.00	0.00	0.00	0.00	0.00	0.00	0.00
	0.00	0.00	0.00	0.00	0.00	0.00	0.00	0.00
	0.00	0.00	0.00	0.00	0.00	0.00	0.00	0.00
14.0	0.00	0.00	0.00	0.00	0.00	0.00	0.00	0.00
	0.00	0.00	0.00	0.00	0.00	0.00	0.00	0.00
	0.00	0.00	0.00	0.00	0.00	0.00	0.00	0.00
	0.00	0.00	0.00	0.00	0.00	0.00	0.00	0.00
16.0	0.00	0.00	0.00	0.00	0.00	0.00	0.00	0.00
	0.00	0.00	0.00	0.00	0.00	0.00	0.00	0.00
	0.00	0.00	0.00	0.00	0.00	0.00	0.00	0.00
	0.00	0.00	0.00	0.00	0.00	0.00	0.00	0.00

*Direction sector 1 is wind toward sector between 0^{o} and 11.25^{o}. Sector numbers increase clockwise.

TABLE 6.2-10

INDIAN POINT--EXAMPLE OF
AVERAGE SPEED ALONG EVACUATION PATHS FOR EVACUEES STARTING IN EACH POPULATION SEGMENT
(Weekday, School in Session)

SPD (M/H)

SECTOR ACROSS,1=TOWARD N-NNE,CLOCKWISE,DISTANCE SEGMENT DOWN

	1	2	3	4	5	6	7	8
1	0.	0.	0.	0.	0.	0.	0.	0.
2	0.	0.	0.	0.	0.	3.970E+00	0.	4.397E+00
3	0.	0.	0.	0.	3.874E+00	3.870E+00	3.916E+00	4.346E+00
4	0.	1.545E+01	1.500E+01	3.753E+00	3.772E+00	3.754E+00	3.827E+00	0.
5	8.019E+00	1.526E+01	1.500E+01	1.509E+01	3.680E+00	3.651E+00	3.670E+00	0.
6	0.	1.539E+01	1.500E+01	1.510E+01	4.368E+00	3.675E+00	3.545E+00	0.
7	0.	1.500E+01	7.650E+00	3.939E+00	4.113E+00	3.671E+00	3.705E+00	3.527E+00
8	6.608E+00	1.500E+01	7.271E+00	3.656E+00	3.802E+00	3.556E+00	3.665E+00	3.513E+00
9	6.680E+00	1.500E+01	6.881E+00	3.696E+00	3.925E+00	3.539E+00	3.547E+00	3.529E+00
10	0.	1.500E+01	6.500E+00	3.743E+00	3.544E+00	3.552E+00	3.537E+00	3.961E+00
11	5.232E+00	1.500E+01	6.105E+00	3.794E+00	3.723E+00	3.568E+00	3.527E+00	3.831E+00
12	4.295E+00	1.500E+01	5.359E+00	3.941E+00	3.996E+00	3.612E+00	3.501E+00	3.686E+00
13	3.439E+00	1.500E+01	4.470E+00	3.749E+00	4.157E+00	3.689E+00	3.950E+00	3.453E+00
14	2.500E+00	1.500E+01	2.900E+00	4.500E+00	3.740E+00	3.477E+00	2.000E+00	1.100E+00
15	2.600E+00	1.500E+01	2.900E+00	4.500E+00	3.400E+00	1.400E+01	2.000E+00	1.100E+00

SECTOR ACROSS,1=TOWARD N-NNE,CLOCKWISE,DISTANCE SEGMENT DOWN

	9	10	11	12	13	14	15	16
1	0.	0.	0.	0.	0.	1.895E+01	0.	0.
2	4.286E+00	4.360E+00	2.177E+01	2.177E+01	2.178E+01	1.894E+01	1.856E+01	1.855E+01
3	4.284E+00	4.211E+00	3.538E+01	1.841E+01	1.941E+01	1.841E+01	1.854E+01	2.134E+01
4	0.	4.310E+00	2.586E+01	3.586E+01	5.280E+00	1.841E+01	2.132E+01	2.539E+01
5	0.	0.	2.341E+01	3.584E+01	5.257E+00	2.129E+01	2.131E+01	2.538E+01
6	0.	4.346E+00	2.045E+01	3.582E+01	5.238E+00	1.876E+01	0.	0.
7	3.531E+00	3.843E+00	4.268E+00	4.080E+00	3.395E+00	3.662E+00	0.	0.
8	3.642E+00	3.871E+00	4.000E+00	3.893E+00	3.200E+00	3.200E+00	0.	0.
9	3.504E+00	3.900E+00	4.005E+00	3.758E+00	3.598E+00	3.200E+00	0.	0.
10	3.490E+00	3.792E+00	3.541E+00	3.621E+00	3.446E+00	3.200E+00	0.	0.
11	3.476E+00	3.273E+00	3.400E+00	3.942E+00	3.200E+00	0.	0.	0.
12	3.427E+00	2.979E+00	3.649E+00	3.843E+00	3.200E+00	3.941E+00	0.	5.406E+00
13	3.382E+00	2.608E+00	2.489E+00	1.300E+01	3.200E+00	3.520E+00	0.	1.500E+01
14	1.550E+00	1.429E+01	2.000E+00	1.300E+01	3.200E+00	1.000E+00	1.718E+01	1.500E+01
15	1.000E+01	1.000E+01	1.300E+01	2.000E+00	3.200E+00	1.000E+00	1.879E+01	1.500E+01

TABLE 6.2-10 (continued)

INDIAN POINT--EXAMPLE OF
AVERAGE SPEED ALONG EVACUATION PATHS FOR EVACUEES STARTING IN EACH POPULATION SEGMENT
(Weekday, School in Session)

SPD (MPH)

SECTOR ACROSS,1=TOWARD N-NNE,CLOCKWISE,DISTANCE SEGMENT DOWN

	17	18	19	20	21	22	23	24
1	0.	0.	0.	0.	0.	0.	0.	0.
2	1.174E+01	1.858E+01	1.857E+01	0.	0.	0.	0.	0.
3	2.051E+01	2.136E+01	1.172E+01	1.457E+01	0.	0.	4.331E+00	4.404E+00
4	0.	0.	0.	0.	0.	4.259E+00	4.356E+00	4.452E+00
5	0.	0.	2.333E+01	1.701E+01	1.701E+01	4.229E+00	4.351E+00	4.470E+00
6	0.	0.	1.704E+01	1.897E+01	4.766E+00	4.156E+00	0.	4.610E+00
7	4.029E+00	4.002E+00	4.283E+00	4.132E+00	3.977E+00	4.155E+00	4.268E+00	4.468E+00
8	3.775E+00	3.863E+00	3.460E+00	3.382E+00	3.938E+00	4.036E+00	4.123E+00	0.
9	3.828E+00	3.716E+00	3.486E+00	3.248E+00	3.473E+00	3.888E+00	0.	0.
10	4.172E+00	2.843E+00	3.867E+00	4.053E+00	3.302E+00	4.036E+00	0.	0.
11	3.911E+00	2.905E+00	2.532E+00	3.500E+00	3.578E+00	3.400E+00	0.	0.
12	2.200E+00	3.548E+00	2.265E+00	2.774E+00	3.500E+00	3.521E+00	0.	5.580E+00
13	2.200E+00	3.037E+00	1.915E+00	2.166E+00	3.500E+00	3.822E+00	0.	4.633E+00
14	2.200E+00	2.749E+00	1.600E+00	2.500E+01	3.500E+00	3.316E+01	2.700E+00	0.
15	2.200E+00	1.600E+00	1.600E+00	2.500E+01	3.500E+00	0.	2.700E+00	0.

SECTOR ACROSS,1=TOWARD N-NNE,CLOCKWISE,DISTANCE SEGMENT DOWN

	25	26	27	28	29	30	31	32
1	0.	0.	0.	0.	0.	0.	0.	0.
2	0.	0.	0.	0.	0.	0.	0.	0.
3	4.490E+00	4.551E+00	4.622E+00	4.425E+00	0.	0.	4.282E+00	4.195E+00
4	4.547E+00	0.	0.	0.	0.	0.	0.	0.
5	4.596E+00	0.	0.	0.	0.	0.	0.	0.
6	0.	0.	3.602E+00	3.420E+00	3.602E+00	3.752E+00	0.	0.
7	0.	0.	0.	3.565E+00	0.	3.418E+00	0.	0.
8	0.	0.	0.	0.	0.	3.235E+00	0.	0.
9	0.	0.	2.463E+00	0.	0.	3.080E+00	3.173E+00	6.016E+00
10	0.	0.	2.298E+00	2.431E+00	2.726E+00	3.235E+00	3.376E+00	5.453E+00
11	0.	7.349E+00	2.100E+00	0.	0.	3.541E+00	1.779E+01	5.082E+00
12	0.	6.440E+00	0.	0.	3.758E+00	0.	0.	1.558E+01
13	5.268E+00	2.729E+00	2.100E+00	2.729E+00	3.310E+00	3.890E+00	0.	1.645E+01
14	3.500E+01	2.100E+00	2.100E+00	3.197E+00	0.	2.156E+01	0.	1.976E+01
15	3.500E+01	2.100E+00	2.500E+01	2.500E+01	3.500E+01	0.	0.	1.300E+01

TABLE 6.2-11

INDIAN POINT--EXAMPLE OF
TIME ALONG EVACUATION PATH FOR EVACUEES STARTING IN EACH POPULATION SEGMENT
(Weekday, School in Session)

TIME (HR)

SECTOR ACROSS,1=TOWARD N-NNE,CLOCKWISE,DISTANCE SEGMENT DOWN

	1	2	3	4	5	6	7	8
1	0.	0.	0.	0.	0.	0.	0.	0.
2	0.	0.	0.	0.	0.	3.703E+00	0.	2.297E+00
3	0.	0.	0.	0.	4.130E+00	3.669E+00	3.677E+00	2.301E+00
4	0.	5.824E-01	5.800E-01	4.103E+00	4.110E+00	3.649E+00	3.658E+00	0.
5	1.235E+00	5.767E-01	5.600E-01	5.567E-01	4.076E+00	3.616E+00	3.597E+00	0.
6	0.	5.067E-01	5.200E-01	5.233E-01	1.740E+00	3.918E+00	3.583E+00	0.
7	0.	4.467E-01	1.046E+00	2.396E+00	1.726E+00	3.787E+00	3.374E+00	3.346E+00
8	1.120E+00	4.467E-01	1.032E+00	2.380E+00	1.710E+00	3.740E+00	3.629E+00	3.188E+00
9	1.123E+00	4.133E-01	1.017E+00	2.219E+00	1.732E+00	1.696E+00	3.609E+00	3.372E+00
10	0.	3.800E-01	1.000E+00	2.057E+00	1.637E+00	1.549E+00	3.477E+00	3.408E+00
11	1.051E+00	3.467E-01	9.828E-01	1.896E+00	2.122E+00	1.401E+00	3.346E+00	3.394E+00
12	1.001E+00	2.733E-01	9.517E-01	1.573E+00	1.477E+00	1.107E+00	3.056E+00	2.659E+00
13	9.596E-01	2.067E-01	9.172E-01	1.281E+00	1.251E+00	8.133E-01	1.063E+00	2.635E+00
14	8.662E-01	1.400E-01	8.621E-01	8.222E-01	5.348E-01	5.752E-01	9.500E-01	2.545E+00
15	4.615E-01	6.667E-02	3.793E-01	2.444E-01	3.529E-01	1.071E-01	6.000E-01	9.091E-01

SECTOR ACROSS,1=TOWARD N-NNE,CLOCKWISE,DISTANCE SEGMENT DOWN

	9	10	11	12	13	14	15	16
1	0.	0.	0.	0.	0.	7.805E+00	0.	0.
2	2.286E+00	2.293E+00	7.811E+00	7.817E+00	7.824E+00	7.797E+00	7.954E+00	7.944E+00
3	2.288E+00	2.280E+00	7.780E+00	7.931E+00	7.931E+00	7.931E+00	7.934E+00	7.971E+00
4	0.	2.297E+00	7.698E+00	7.769E+00	5.436E+00	7.931E+00	7.947E+00	7.882E+00
5	0.	0.	8.702E+00	7.759E+00	5.345E+00	7.923E+00	7.936E+00	7.858E+00
6	0.	3.291E+00	8.760E+00	7.749E+00	5.269E+00	7.747E+00	0.	0.
7	3.398E+00	3.123E+00	3.260E+00	3.260E+00	2.239E+00	2.267E+00	0.	0.
8	3.103E+00	3.125E+00	3.250E+00	3.237E+00	2.219E+00	2.125E+00	0.	0.
9	3.083E+00	3.128E+00	3.246E+00	3.220E+00	2.057E+00	2.031E+00	0.	0.
10	2.951E+00	2.848E+00	3.191E+00	3.203E+00	1.770E+00	1.875E+00	0.	0.
11	2.819E+00	3.116E+00	3.177E+00	3.348E+00	1.750E+00	0.	0.	0.
12	2.451E+00	3.048E+00	3.207E+00	3.237E+00	1.438E+00	1.472E+00	0.	8.324E-01
13	2.188E+00	2.070E+00	1.929E+00	3.538E-01	1.125E+00	1.136E+00	0.	2.133E-01
14	2.581E+00	1.400E-01	1.900E+00	3.154E-01	7.188E-01	1.600E+00	1.571E-01	1.400E-01
15	1.900E-01	1.000E-01	1.769E-01	1.000E+00	3.125E-01	1.200E+00	9.048E-02	7.333E-02

TABLE 6.2-11 (continued)

INDIAN POINT--EXAMPLE
TIME ALONG EVACUATION PATH FOR EVACUEES STARTING IN EACH POPULATION SEGMENT
(Weekday, School in Session)

TIME (HR)

SECTOR ACROSS,1=TOWARD N-NNE,CLOCKWISE,DISTANCE SEGMENT DOWN

	17	18	19	20	21	22	23	24
1	0.	0.	0.	0.	0.	0.	0.	0.
2	8.141E+00	7.961E+00	7.981E+00	0.	0.	0.	0.	0.
3	7.148E+00	7.992E+00	8.015E+00	7.981E+00	0.	0.	3.417E+00	3.429E+00
4	0.	0.	0.	0.	0.	3.405E+00	3.421E+00	3.437E+00
5	0.	0.	8.960E+00	8.849E+00	8.849E+00	3.405E+00	3.425E+00	3.445E+00
6	0.	0.	8.872E+00	7.936E+00	1.427E+01	3.393E+00	0.	3.080E+00
7	3.053E+00	3.049E+00	3.362E+00	3.316E+00	3.269E+00	3.297E+00	3.046E+00	3.066E+00
8	3.030E+00	3.024E+00	2.949E+00	2.923E+00	3.149E+00	3.023E+00	3.032E+00	0.
9	3.030E+00	3.014E+00	2.954E+00	2.894E+00	2.649E+00	3.009E+00	0.	0.
10	1.580E+00	2.674E+00	1.733E+00	1.801E+00	2.635E+00	3.023E+00	0.	0.
11	1.560E+00	2.651E+00	2.607E+00	1.686E+00	1.761E+00	2.265E+00	0.	0.
12	2.500E+00	1.719E+00	2.296E+00	1.730E+00	1.286E+00	1.931E+00	0.	8.603E-01
13	1.727E+00	1.679E+00	1.985E+00	1.708E+00	8.857E-01	1.413E+00	0.	8.203E-01
14	1.091E+00	1.418E+00	1.688E+00	8.000E-02	6.286E-01	7.238E-02	7.778E-01	0.
15	4.545E-01	8.750E-01	7.500E-01	4.000E-02	2.857E-01	0.	4.074E-01	0.

SECTOR ACROSS,1=TOWARD N-NNE,CLOCKWISE,DISTANCE SEGMENT DOWN

	25	26	27	28	29	30	31	32
1	0.	0.	0.	0.	0.	0.	0.	0.
2	0.	0.	0.	0.	0.	0.	0.	0.
3	3.437E+00	3.449E+00	3.461E+00	3.051E+00	0.	0.	3.036E+00	3.028E+00
4	3.453E+00	0.	0.	0.	0.	0.	0.	0.
5	3.459E+00	0.	0.	0.	0.	0.	0.	0.
6	0.	0.	2.971E+00	2.953E+00	2.971E+00	2.985E+00	0.	0.
7	0.	0.	0.	2.973E+00	0.	2.955E+00	0.	0.
8	0.	0.	0.	0.	0.	2.937E+00	0.	0.
9	0.	0.	2.843E+00	0.	0.	2.922E+00	2.931E+00	1.097E+00
10	0.	0.	2.872E+00	2.879E+00	2.898E+00	2.937E+00	2.962E+00	1.064E+00
11	0.	8.981E-01	2.857E+00	0.	0.	2.965E+00	2.754E-01	1.043E+00
12	0.	8.696E-01	0.	0.	2.022E+00	0.	0.	2.440E-01
13	8.353E-01	1.942E+00	1.905E+00	1.942E+00	1.894E+00	2.031E+00	0.	1.824E-01
14	5.714E-02	9.524E-01	1.333E+00	1.970E+00	0.	1.763E-01	0.	1.923E-01
15	2.857E-02	5.714E-01	4.000E-02	4.000E-02	2.857E-02	0.	0.	8.462E-02

TABLE 6.2-12

INDIAN POINT--EXAMPLE OF
DISTANCE ALONG EVACUATION PATH FOR EVACUEES STARTING IN EACH POPULATION SEGMENT*
(Weekday, School in Session)

DIST (MI)

SECTOR ACROSS,1=TOWARD N-NNE,CLOCKWISE,DISTANCE SEGMENT DOWN

	1	2	3	4	5	6	7	8
1	0.	0.	0.	0.	0.	0.	0.	0.
2	0.	0.	0.	0.	0.	1.470E+01	0.	1.010E+01
3	0.	0.	0.	0.	1.600E+01	1.420E+01	1.440E+01	1.000E+01
4	0.	9.000E+00	8.700E+00	1.540E+01	1.550E+01	1.370E+01	1.400E+01	0.
5	9.900E+00	8.800E+00	8.400E+00	8.400E+00	1.500E+01	1.320E+01	1.320E+01	0.
6	0.	7.800E+00	7.800E+00	7.900E+00	7.400E+00	1.440E+01	1.270E+01	0.
7	0.	7.300E+00	8.000E+00	9.200E+00	7.100E+00	1.390E+01	1.250E+01	1.180E+01
8	7.400E+00	6.700E+00	7.500E+00	8.700E+00	6.500E+00	1.330E+01	1.330E+01	1.120E+01
9	7.500E+00	6.200E+00	7.000E+00	8.200E+00	6.900E+00	6.000E+00	1.240E+01	1.190E+01
10	0.	5.700E+00	6.500E+00	7.700E+00	5.800E+00	5.500E+00	1.230E+01	1.350E+01
11	5.500E+00	5.200E+00	6.000E+00	7.200E+00	7.900E+00	5.000E+00	1.180E+01	1.300E+01
12	4.300E+00	4.100E+00	5.100E+00	6.200E+00	5.900E+00	4.000E+00	1.070E+01	9.800E+00
13	3.300E+00	3.100E+00	4.100E+00	4.800E+00	5.200E+00	3.000E+00	4.200E+00	9.100E+00
14	2.200E+00	2.100E+00	2.500E+00	3.700E+00	2.000E+00	2.000E+00	1.900E+00	2.800E+00
15	1.200E+00	1.000E+00	1.100E+00	1.100E+00	1.200E+00	1.500E+00	1.200E+00	1.000E+00

SECTOR ACROSS,1=TOWARD N-NNE,CLOCKWISE,DISTANCE SEGMENT DOWN

	9	10	11	12	13	14	15	16
1	0.	0.	0.	0.	0.	1.479E+02	0.	0.
2	9.800E+00	1.000E+01	1.700E+02	1.702E+02	1.704E+02	1.477E+02	1.476E+02	1.474E+02
3	9.800E+00	9.600E+00	2.791E+02	1.460E+02	1.460E+02	1.460E+02	1.471E+02	1.701E+02
4	0.	9.900E+00	1.991E+02	2.785E+02	2.870E+01	1.460E+02	1.694E+02	2.001E+02
5	0.	0.	2.037E+02	2.781E+02	2.810E+01	1.687E+02	1.691E+02	1.994E+02
6	0.	1.430E+01	1.743E+02	2.776E+02	2.760E+01	1.453E+02	0.	0.
7	1.200E+01	1.200E+01	1.400E+01	1.330E+01	7.600E+00	8.300E+00	0.	0.
8	1.130E+01	1.210E+01	1.300E+01	1.260E+01	7.100E+00	6.800E+00	0.	0.
9	1.090E+01	1.220E+01	1.300E+01	1.210E+01	7.400E+00	6.500E+00	0.	0.
10	1.030E+01	1.050E+01	1.130E+01	1.160E+01	6.100E+00	6.000E+00	0.	0.
11	9.800E+00	1.020E+01	1.080E+01	1.320E+01	5.600E+00	0.	0.	0.
12	8.400E+00	9.200E+00	1.170E+01	1.260E+01	4.600E+00	5.800E+00	0.	4.500E+00
13	7.400E+00	5.400E+00	4.800E+00	4.500E+00	3.600E+00	4.000E+00	0.	3.200E+00
14	4.000E+00	2.000E+00	3.800E+00	4.100E+00	2.300E+00	1.600E+00	2.700E+00	2.100E+00
15	1.800E+00	1.000E+00	2.300E+00	2.000E+00	1.000E+00	1.200E+00	1.700E+00	1.100E+00

*Note: Distances in some elements are artificially high to simulate delay.

TABLE 6.2-12 (continued)

INDIAN POINT--EXAMPLE OF
DISTANCE ALONG EVACUATION PATH FOR EVACUEES STARTING IN EACH POPULATION SEGMENT*
(Weekday, School in Session)

DIST (MI)

SECTOR ACROSS,1=TOWARD N-NNE,CLOCKWISE,DISTANCE SEGMENT DOWN

	17	18	19	20	21	22	23	24
1	0.	0.	0.	0.	0.	0.	0.	0.
2	9.570E+01	1.479E+02	1.482E+02	0.	0.	0.	0.	0.
3	1.474E+02	1.707E+02	9.390E+01	1.482E+02	0.	0.	1.480E+01	1.510E+01
4	0.	0.	0.	0.	0.	1.450E+01	1.490E+01	1.530E+01
5	0.	0.	2.090E+02	1.505E+02	1.505E+02	1.440E+01	1.490E+01	1.540E+01
6	0.	0.	1.512E+02	1.505E+02	6.300E+01	1.410E+01	0.	1.420E+01
7	1.230E+01	1.220E+01	1.440E+01	1.370E+01	1.300E+01	1.370E+01	1.300E+01	1.370E+01
8	1.140E+01	1.170E+01	1.020E+01	9.900E+00	1.240E+01	1.220E+01	1.250E+01	0.
9	1.160E+01	1.120E+01	1.030E+01	6.400E+00	9.200E+00	1.170E+01	0.	0.
10	6.400E+00	7.600E+00	6.700E+00	7.300E+00	8.700E+00	1.220E+01	0.	0.
11	6.100E+00	7.700E+00	6.600E+00	5.900E+00	6.300E+00	7.700E+00	0.	0.
12	5.500E+00	6.100E+00	5.200E+00	4.800E+00	4.500E+00	6.800E+00	0.	4.800E+00
13	3.800E+00	5.100E+00	3.800E+00	3.700E+00	3.100E+00	5.400E+00	0.	3.800E+00
14	2.400E+00	3.900E+00	2.700E+00	2.000E+00	2.200E+00	2.400E+00	2.100E+00	0.
15	1.000E+00	1.400E+00	1.200E+00	1.000E+00	1.000E+00	0.	1.100E+00	0.

SECTOR ACROSS,1=TOWARD N-NNE,CLOCKWISE,DISTANCE SEGMENT DOWN

	25	26	27	28	29	30	31	32
1	0.	0.	0.	0.	0.	0.	0.	0.
2	0.	0.	0.	0.	0.	0.	0.	0.
3	1.540E+01	1.570E+01	1.600E+01	1.350E+01	0.	0.	1.300E+01	1.270E+01
4	1.570E+01	0.	0.	0.	0.	0.	0.	0.
5	1.590E+01	0.	0.	0.	0.	0.	0.	0.
6	0.	0.	1.070E+01	1.010E+01	1.070E+01	1.120E+01	0.	0.
7	0.	0.	0.	1.060E+01	0.	1.010E+01	0.	0.
8	0.	0.	0.	0.	0.	9.500E+00	0.	0.
9	0.	0.	7.100E+00	0.	0.	9.000E+00	9.300E+00	6.600E+00
10	0.	0.	6.600E+00	7.000E+00	7.900E+00	9.500E+00	1.000E+01	5.800E+00
11	0.	6.600E+00	6.000E+00	0.	0.	1.050E+01	4.900E+00	5.300E+00
12	0.	5.600E+00	0.	0.	7.600E+00	0.	0.	3.800E+00
13	4.400E+00	5.300E+00	4.000E+00	5.300E+00	6.600E+00	7.900E+00	0.	3.000E+00
14	2.000E+00	2.000E+00	2.800E+00	6.300E+00	0.	3.800E+00	0.	3.800E+00
15	1.000E+00	1.200E+00	1.000E+00	1.000E+00	1.000E+00	0.	0.	1.100E+00

TABLE 6.2-13A

INDIAN POINT--SUMMARY OF EVACUATION DATA
(NIGHT)

EVACUATION PATH SUMMARY DATA

DIST (MI)		PATHS	TIME (HOURS)			DISTANCE (MILES)			SPEED (MPH)		
			MAX	MIN	AVG	MAX	MIN	AVG	MAX	MIN	AVG
1	.5	1	2.218E+00	2.218E+00	2.218E+00	1.140E+01	1.140E+01	1.140E+01	5.140E+00	5.140E+00	5.140E+00
2	1.0	13	2.533E+00	2.159E+00	2.315E+00	1.470E+01	9.800E+00	1.101E+01	6.416E+00	4.368E+00	4.765E+00
3	1.5	24	2.772E+00	2.148E+00	2.351E+00	1.600E+01	9.400E+00	1.223E+01	6.932E+00	3.770E+00	5.230E+00
4	2.0	17	2.752E+00	5.771E-01	2.157E+00	1.570E+01	8.700E+00	1.201E+01	1.559E+01	3.600E+00	6.449E+00
5	2.5	20	2.719E+00	5.130E-01	1.925E+00	1.590E+01	8.400E+00	1.199E+01	1.930E+01	3.600E+00	7.831E+00
6	3.0	20	2.606E+00	5.067E-01	1.838E+00	1.470E+01	7.600E+00	1.123E+01	1.539E+01	3.600E+00	7.238E+00
7	3.5	23	2.511E+00	2.671E-01	1.855E+00	1.440E+01	7.100E+00	1.147E+01	2.995E+01	3.600E+00	7.460E+00
8	4.0	22	2.472E+00	2.528E-01	1.708E+00	1.330E+01	6.500E+00	1.033E+01	2.967E+01	3.600E+00	7.826E+00
9	4.5	24	2.378E+00	2.385E-01	1.587E+00	1.300E+01	6.000E+00	9.329E+00	2.935E+01	3.504E+00	7.899E+00
10	5.0	25	2.231E+00	2.213E-01	1.573E+00	1.350E+01	5.500E+00	8.360E+00	2.938E+01	3.275E+00	6.900E+00
11	6.0	24	2.183E+00	2.040E-01	1.327E+00	1.320E+01	4.900E+00	7.700E+00	2.941E+01	3.000E+00	8.320E+00
12	7.0	25	2.011E+00	1.730E-01	1.128E+00	1.260E+01	3.800E+00	6.464E+00	2.948E+01	2.735E+00	7.730E+00
13	8.0	29	1.757E+00	1.385E-01	9.357E-01	9.100E+00	3.000E+00	4.655E+00	2.960E+01	2.307E+00	7.386E+00
14	9.0	29	2.200E+00	5.714E-02	6.755E-01	6.300E+00	1.600E+00	2.766E+00	3.500E+01	1.000E+00	1.061E+01
15	10.0	28	1.200E+00	2.857E-02	2.743E-01	2.300E+00	1.000E+00	1.229E+00	3.500E+01	1.000E+00	1.216E+01

TABLE 6.2-13B

INDIAN POINT--SUMMARY OF EVACUATION DATA*
(WEEKDAY, SCHOOL IN SESSION)

--EVACUATION PATH SUMMARY DATA

DIST	(MI)	PATHS	TIME (HOURS) MAX	TIME (HOURS) MIN	TIME (HOURS) AVG	DISTANCE (MILES) MAX	DISTANCE (MILES) MIN	DISTANCE (MILES) AVG	SPEED (MPH) MAX	SPEED (MPH) MIN	SPEED (MPH) AVG
1	.5	1	7.805E+00	7.805E+00	7.805E+00	1.479E+02	1.479E+02	1.479E+02	1.895E+01	1.895E+01	1.895E+01
2	1.0	13	8.141E+00	2.286E+00	6.293E+00	1.704E+02	9.600E+00	1.069E+02	2.178E+01	3.970E+00	1.441E+01
3	1.5	24	8.015E+00	2.280E+00	5.138E+00	2.791E+02	9.600E+00	7.436E+01	3.588E+01	3.870E+00	1.095E+01
4	2.0	17	7.987E+00	5.800E-01	4.550E+00	2.786E+02	8.700E+00	6.874E+01	3.586E+01	3.753E+00	1.174E+01
5	2.5	20	8.960E+00	5.567E-01	5.007E+00	2.781E+02	8.400E+00	8.473E+01	3.584E+01	3.651E+00	1.359E+01
6	3.0	20	1.427E+01	5.067E-01	4.652E+00	2.776E+02	7.600E+00	5.710E+01	3.582E+01	3.420E+00	1.028E+01
7	3.5	23	3.787E+00	4.867E-01	2.831E+00	1.440E+01	7.100E+00	1.147E+01	1.500E+01	3.395E+00	4.547E+00
8	4.0	22	3.740E+00	4.467E-01	2.653E+00	1.330E+01	6.500E+00	1.033E+01	1.500E+01	3.200E+00	4.486E+00
9	4.5	24	3.609E+00	4.133E-01	2.472E+00	1.300E+01	6.000E+00	9.329E+00	1.500E+01	2.463E+00	4.383E+00
10	5.0	25	3.477E+00	3.800E-01	2.336E+00	1.350E+01	5.500E+00	8.360E+00	1.500E+01	2.298E+00	4.109E+00
11	6.0	24	3.394E+00	2.754E-01	2.055E+00	1.320E+01	4.900E+00	7.700E+00	1.779E+01	2.100E+00	4.907E+00
12	7.0	25	3.237E+00	2.440E-01	1.731E+00	1.260E+01	3.800E+00	6.464E+00	1.558E+01	2.200E+00	4.762E+00
13	8.0	29	2.635E+00	1.824E-01	1.351E+00	9.100E+00	3.000E+00	4.655E+00	1.645E+01	1.915E+00	4.926E+00
14	9.0	29	2.581E+00	5.714E-02	8.712E-01	6.300E+00	1.600E+00	2.766E+00	3.500E+01	1.000E+00	8.868E+00
15	10.0	28	1.200E+00	2.857E-02	3.522E-01	2.300E+00	1.000E+00	1.229E+00	3.500E+01	1.000E+00	1.036E+01

*Note: Distance in some trajectories are artificially high to simulate delay.

TABLE 6.2-13C

INDIAN POINT--SUMMARY OF EVACUATION DATA
(WEEKDAY, SCHOOL OUT)

EVACUATION PATH SUMMARY DATA

DIST	(MI)	PATHS	TIME (HOURS) MAX	TIME (HOURS) MIN	TIME (HOURS) AVG	DISTANCE (MILES) MAX	DISTANCE (MILES) MIN	DISTANCE (MILES) AVG	SPEED (MPH) MAX	SPEED (MPH) MIN	SPEED (MPH) AVG
1	.5	2	2.771E+00	2.464E+00	2.618E+00	1.160E+01	1.140E+01	1.150E+01	4.626E+00	4.186E+00	4.406E+00
2	1.0	13	2.945E+00	2.405E+00	2.592E+00	1.470E+01	9.800E+00	1.101E+01	4.992E+00	3.975E+00	4.242E+00
3	1.5	24	3.562E+00	2.394E+00	2.880E+00	1.600E+01	9.400E+00	1.223E+01	4.933E+00	3.434E+00	4.214E+00
4	2.0	17	3.542E+00	5.790E-01	2.555E+00	1.570E+01	6.700E+00	1.201E+01	1.554E+01	3.277E+00	5.507E+00
5	2.5	20	3.508E+00	5.600E-01	2.515E+00	1.590E+01	8.400E+00	1.199E+01	1.535E+01	3.267E+00	6.175E+00
6	3.0	20	3.351E+00	5.067E-01	2.486E+00	1.470E+01	7.600E+00	1.123E+01	1.539E+01	3.245E+00	5.822E+00
7	3.5	23	3.222E+00	4.867E-01	2.604E+00	1.440E+01	7.100E+00	1.147E+01	1.500E+01	3.224E+00	4.877E+00
8	4.0	22	3.173E+00	4.467E-01	2.425E+00	1.330E+01	6.500E+00	1.033E+01	1.500E+01	3.200E+00	4.886E+00
9	4.5	24	3.041E+00	4.133E-01	2.270E+00	1.300E+01	6.000E+00	9.329E+00	1.500E+01	2.463E+00	4.811E+00
10	5.0	25	3.013E+00	3.800E-01	2.153E+00	1.350E+01	5.500E+00	8.360E+00	1.500E+01	2.298E+00	4.460E+00
11	6.0	24	2.965E+00	2.754E-01	1.863E+00	1.320E+01	4.900E+00	7.700E+00	1.779E+01	2.100E+00	5.308E+00
12	7.0	26	2.663E+00	2.440E-01	1.555E+00	1.260E+01	3.800E+00	6.438E+00	1.558E+01	2.265E+00	5.115E+00
13	8.0	29	2.196E+00	1.824E-01	1.252E+00	9.100E+00	3.000E+00	4.655E+00	1.645E+01	1.915E+00	5.219E+00
14	9.0	29	2.592E+00	5.714E-02	8.461E-01	6.300E+00	1.600E+00	2.766E+00	3.500E+01	1.000E+00	8.952E+00
15	10.0	28	1.200E+00	2.857E-02	3.212E-01	2.300E+00	1.000E+00	1.229E+00	3.500E+01	1.000E+00	1.079E+01

TABLE 6.2-13D

INDIAN POINT--SUMMARY OF EVACUATION DATA
(WINTER HOLIDAY)

EVACUATION PATH SUMMARY DATA

DIST	(MI)	PATHS	TIME (HOURS) MAX	TIME (HOURS) MIN	TIME (HOURS) AVG	DISTANCE (MILES) MAX	DISTANCE (MILES) MIN	DISTANCE (MILES) AVG	SPEED (MPH) MAX	SPEED (MPH) MIN	SPEED (MPH) AVG
1	.5	1	2.159E+00	2.159E+00	2.159E+00	1.140E+01	1.140E+01	1.140E+01	5.280E+00	5.280E+00	5.280E+00
2	1.0	13	2.424E+00	2.100E+00	2.247E+00	1.470E+01	9.800E+00	1.101E+01	6.208E+00	4.567E+00	4.897E+00
3	1.5	24	2.425E+00	2.089E+00	2.295E+00	1.600E+01	9.400E+00	1.223E+01	6.878E+00	3.962E+00	5.330E+00
4	2.0	17	2.405E+00	5.771E-01	2.092E+00	1.570E+01	8.700E+00	1.201E+01	1.559E+01	3.785E+00	6.574E+00
5	2.5	20	2.372E+00	5.529E-01	1.918E+00	1.590E+01	8.400E+00	1.199E+01	1.791E+01	3.769E+00	7.708E+00
6	3.0	20	2.269E+00	5.067E-01	1.861E+00	1.470E+01	7.600E+00	1.123E+01	1.539E+01	3.735E+00	7.066E+00
7	3.5	23	2.299E+00	4.867E-01	1.921E+00	1.440E+01	7.100E+00	1.147E+01	1.500E+01	3.703E+00	6.315E+00
8	4.0	22	2.174E+00	4.383E-01	1.768E+00	1.330E+01	6.500E+00	1.033E+01	1.689E+01	3.500E+00	6.594E+00
9	4.5	24	2.137E+00	4.133E-01	1.661E+00	1.300E+01	6.000E+00	9.329E+00	1.700E+01	3.500E+00	6.647E+00
10	5.0	25	2.151E+00	3.800E-01	1.634E+00	1.350E+01	5.500E+00	8.360E+00	1.518E+01	3.275E+00	5.779E+00
11	6.0	24	2.231E+00	2.754E-01	1.413E+00	1.320E+01	4.900E+00	7.700E+00	1.779E+01	3.000E+00	6.960E+00
12	7.0	25	2.391E+00	2.440E-01	1.213E+00	1.260E+01	3.800E+00	6.464E+00	1.558E+01	2.300E+00	6.464E+00
13	8.0	29	1.652E+00	1.824E-01	9.781E-01	9.100E+00	3.000E+00	4.655E+00	1.645E+01	2.300E+00	6.398E+00
14	9.0	29	1.908E+00	5.714E-02	6.859E-01	6.300E+00	1.600E+00	2.766E+00	3.500E+01	1.000E+00	9.647E+00
15	10.0	28	1.200E+00	2.857E-02	2.903E-01	2.300E+00	1.000E+00	1.229E+00	3.500E+01	1.000E+00	1.120E+01

TABLE 6.2-13E

INDIAN POINT--SUMMARY OF EVACUATION DATA
(SUMMER HOLIDAY)

EVACUATION PATH SUMMARY DATA

DIST	(MI)	PATHS	TIME (HOURS) MAX	TIME (HOURS) MIN	TIME (HOURS) AVG	DISTANCE (MILES) MAX	DISTANCE (MILES) MIN	DISTANCE (MILES) AVG	SPEED (MPH) MAX	SPEED (MPH) MIN	SPEED (MPH) AVG
1	.5	1	2.327E+00	2.327E+00	2.327E+00	1.140E+01	1.140E+01	1.140E+01	4.900E+00	4.900E+00	4.900E+00
2	1.0	13	4.007E+00	2.268E+00	2.541E+00	1.470E+01	9.800E+00	1.101E+01	4.726E+00	3.669E+00	4.371E+00
3	1.5	24	5.210E+00	2.257E+00	3.572E+00	1.600E+01	9.400E+00	1.223E+01	4.394E+00	2.654E+00	3.611E+00
4	2.0	17	5.201E+00	5.800E-01	3.348E+00	1.570E+01	8.700E+00	1.201E+01	1.519E+01	2.814E+00	4.867E+00
5	2.5	20	5.208E+00	5.567E-01	3.377E+00	1.590E+01	8.400E+00	1.199E+01	1.662E+01	2.708E+00	5.677E+00
6	3.0	20	5.161E+00	5.067E-01	3.537E+00	1.470E+01	7.600E+00	1.123E+01	1.539E+01	2.144E+00	4.898E+00
7	3.5	23	6.673E+00	4.867E-01	3.889E+00	1.440E+01	7.100E+00	1.147E+01	1.500E+01	1.829E+00	3.755E+00
8	4.0	22	6.649E+00	4.467E-01	3.759E+00	1.330E+01	6.500E+00	1.033E+01	1.603E+01	1.512E+00	4.185E+00
9	4.5	24	6.650E+00	4.133E-01	3.559E+00	1.300E+01	6.000E+00	9.329E+00	1.615E+01	1.443E+00	4.507E+00
10	5.0	25	6.210E+00	3.800E-01	2.950E+00	1.350E+01	5.500E+00	8.360E+00	1.500E+01	1.401E+00	4.174E+00
11	6.0	24	5.775E+00	2.754E-01	2.525E+00	1.320E+01	4.900E+00	7.700E+00	1.779E+01	1.300E+00	5.275E+00
12	7.0	26	5.384E+00	2.440E-01	2.356E+00	1.260E+01	3.800E+00	6.438E+00	1.558E+01	1.250E+00	4.422E+00
13	8.0	29	4.775E+00	1.824E-01	1.861E+00	9.100E+00	3.000E+00	4.655E+00	1.645E+01	1.000E+00	4.479E+00
14	9.0	29	3.143E+00	5.714E-02	9.104E-01	6.300E+00	1.600E+00	2.766E+00	3.500E+01	1.000E+00	8.403E+00
15	10.0	28	1.200E+00	2.857E-02	3.473E-01	2.300E+00	1.000E+00	1.229E+00	3.500E+01	1.000E+00	1.001E+01

TABLE 6.2-14

CHARACTERISTICS OF THE 288 RANDOMLY SELECTED METEOROLOGICAL SEQUENCES--INDIAN POINT

Parameters	Percent of Occurrences in 288 Sequences	Expected Percent of Annual Period
Rain in first 5 hours	12	10
Speed slowdown in first 5 hours (more than 2m/sec)	46	Unknown
Speed at 33 feet less than 5m/sec	98	98
Start Hour		
Stability A,B,C	23	21
Stability D	24	26
Stability E,F	53	53
Direction Trajectory Changes of 45^0 or more within 45 miles	32	28
Wind Direction for Start Hour Toward		
SSE-SSW	34	26
NE-E	13	16
Lid Below 700m for Start Hour	20	23

TABLE 6.2-15

INDIAN POINT--TERRAIN HEIGHTS(1)

	DISTANCE	HEIGHT BY SECTOR AND DISTANCE															
		1	2	3	4	5	6	7	8	9	10	11	12	13	14	15	16
1	.5	0.	80.	80.	100.	120.	120.	140.	140.	120.	120.	100.	0.	0.	0.	0.	0.
2	1.0	0.	0.	60.	40.	80.	80.	80.	60.	100.	100.	30.	0.	0.	0.	0.	0.
3	1.5	200.	0.	120.	140.	140.	160.	100.	100.	60.	60.	0.	0.	360.	520.	720.	720.
4	2.0	20.	260.	200.	280.	320.	300.	140.	140.	110.	0.	0.	500.	540.	980.	1060.	900.
5	2.5	460.	360.	300.	380.	580.	500.	250.	120.	150.	0.	208.	720.	1000.	1120.	1086.	200.
6	3.0	780.	280.	403.	436.	680.	560.	340.	150.	0.	0.	360.	793.	846.	1100.	500.	600.
7	3.5	840.	460.	540.	440.	380.	440.	350.	150.	0.	100.	300.	600.	900.	1257.	560.	780.
8	4.0	867.	520.	600.	640.	600.	400.	450.	0.	0.	103.	290.	840.	920.	1146.	1200.	900.
9	4.5	780.	580.	480.	600.	780.	550.	603.	0.	0.	100.	600.	1023.	940.	949.	1284.	400.
10	5.0	860.	580.	400.	580.	760.	750.	600.	0.	0.	220.	580.	900.	1100.	1200.	1000.	520.
11	6.0	916.	640.	480.	500.	540.	630.	500.	0.	0.	720.	600.	1022.	1171.	1140.	941.	940.
12	7.0	900.	740.	660.	600.	500.	450.	250.	0.	800.	730.	600.	1100.	1195.	1060.	1075.	1000.
13	8.5	885.	800.	660.	660.	613.	430.	500.	20.	530.	640.	600.	1160.	1200.	1232.	1157.	1200.
14	10.0	740.	820.	600.	720.	608.	550.	550.	30.	573.	700.	900.	1260.	1247.	1300.	1060.	1260.
15	12.5	1000.	1020.	980.	720.	820.	800.	650.	100.	510.	600.	1100.	1283.	1380.	1384.	1414.	1300.
16	15.0	1000.	900.	1040.	760.	701.	600.	600.	300.	330.	600.	1100.	1260.	1367.	1420.	1438.	1463.
17	17.5	0.	0.	0.	0.	0.	0.	0.	0.	0.	0.	0.	0.	0.	0.	0.	0.
18	20.0	0.	0.	0.	0.	0.	0.	0.	0.	0.	0.	0.	0.	0.	0.	0.	0.
19	25.0	0.	0.	0.	0.	0.	0.	0.	0.	0.	0.	0.	0.	0.	0.	0.	0.
20	30.0	0.	0.	0.	0.	0.	0.	0.	0.	0.	0.	0.	0.	0.	0.	0.	0.
21	35.5	0.	0.	0.	0.	0.	0.	0.	0.	0.	0.	0.	0.	0.	0.	0.	0.
22	40.0	0.	0.	0.	0.	0.	0.	0.	0.	0.	0.	0.	0.	0.	0.	0.	0.
23	45.5	0.	0.	0.	0.	0.	0.	0.	0.	0.	0.	0.	0.	0.	0.	0.	0.
24	50.0	0.	0.	0.	0.	0.	0.	0.	0.	0.	0.	0.	0.	0.	0.	0.	0.
25	55.0	0.	0.	0.	0.	0.	0.	0.	0.	0.	0.	0.	0.	0.	0.	0.	0.
26	60.0	0.	0.	0.	0.	0.	0.	0.	0.	0.	0.	0.	0.	0.	0.	0.	0.
27	65.0	0.	0.	0.	0.	0.	0.	0.	0.	0.	0.	0.	0.	0.	0.	0.	0.
28	70.0	0.	0.	0.	0.	0.	0.	0.	0.	0.	0.	0.	0.	0.	0.	0.	0.
29	85.0	0.	0.	0.	0.	0.	0.	0.	0.	0.	0.	0.	0.	0.	0.	0.	0.
30	100.0	0.	0.	0.	0.	0.	0.	0.	0.	0.	0.	0.	0.	0.	0.	0.	0.
31	150.0	0.	0.	0.	0.	0.	0.	0.	0.	0.	0.	0.	0.	0.	0.	0.	0.
32	200.0	0.	0.	0.	0.	0.	0.	0.	0.	0.	0.	0.	0.	0.	0.	0.	0.
33	350.0	0.	0.	0.	0.	0.	0.	0.	0.	0.	0.	0.	0.	0.	0.	0.	0.
34	500.0	0.	0.	0.	0.	0.	0.	0.	0.	0.	0.	0.	0.	0.	0.	0.	0.

THE INPUT WAS IN FEET
THE REACTOR ELEVATION WAS 40. FEET

(1) Note: Beyond 15 miles, the terrain was assumed equal to the value at 15 miles.

TABLE 6.2-16

INDIAN POINT--SOURCE TERM RELEASE PARAMETERS

Designation for This Study	Phase Number	Time of Release (hours)	Duration of Release (hours)	Warning Time (hours)	Release Energy ($\times 10^6$ Btu/hr)	Reference Height (feet)	Assumed Release Height (feet)	Meteorological Tower Level (feet)
Z-1Q	1	1.0	0.5	0.5	20	33	33	33
2 and Z-1	1	2.5	1.0	1.0	20	33	33	33
2RW	1	12.0	2.0	11.0	6	33	33	33
2RW	2	14.0	1.0	13.0	6	33	33	33
2RW	3	15.0	2.0	14.0	6	33	33	33
2RW	4	17.0	4.0	16.0	1	33	33	33
2RV	1	2.5	3.0	1.0	1	33	33	33
8A	1	2.0	10.0	1.0	0	33	33	33
8B	1	2.0	10.0	1.0	0	33	33	33

TABLE 6.2-17

INDIAN POINT--SOURCE TERM CATEGORY RELEASE FRACTIONS

Designations For This Study	Phase Number	Fractional Releases							
		Xe-Kr	Org I	Iodine	Cs-Rb	Te-Sb	Ba-Sr	Ru	La
Z-1Q	1	0.9	6.0×10^{-3}	0.7	0.4	0.35	0.05	0.21	3.0×10^{-3}
2 and Z-1	1	0.9	7.0×10^{-3}	0.7	0.5	0.3	0.06	0.02	4.0×10^{-3}
2RW	1	0.75	5.0×10^{-3}	7.3×10^{-3}	1.4×10^{-1}	2.8×10^{-2}	1.7×10^{-2}	5.3×10^{-3}	5.4×10^{-3}
2RW	2	0.12	8.0×10^{-4}	2.1×10^{-2}	5.4×10^{-2}	1.7×10^{-1}	4.0×10^{-3}	1.0×10^{-2}	2.0×10^{-3}
2RW	3	0.06	4.0×10^{-4}	2.3×10^{-2}	3.6×10^{-2}	1.4×10^{-1}	2.2×10^{-3}	8.2×10^{-3}	1.6×10^{-3}
2RW	4	0.08	6.0×10^{-4}	3.5×10^{-2}	2.8×10^{-2}	1.0×10^{-1}	1.9×10^{-3}	6.2×10^{-3}	1.2×10^{-3}
2RV	1	0.8	7.0×10^{-3}	1.4×10^{-2}	1.0×10^{-2}	6.0×10^{-3}	1.2×10^{-3}	4×10^{-4}	8.0×10^{-5}
8A	1	2.7×10^{-2}	1.7×10^{-4}	2.7×10^{-3}	5.0×10^{-6}	1.0×10^{-6}	7×10^{-7}	2×10^{-7}	2.0×10^{-8}
8B	1	2.7×10^{-2}	1.9×10^{-4}	1.6×10^{-5}	8.0×10^{-7}	1.5×10^{-7}	1×10^{-7}	3×10^{-8}	3.0×10^{-9}

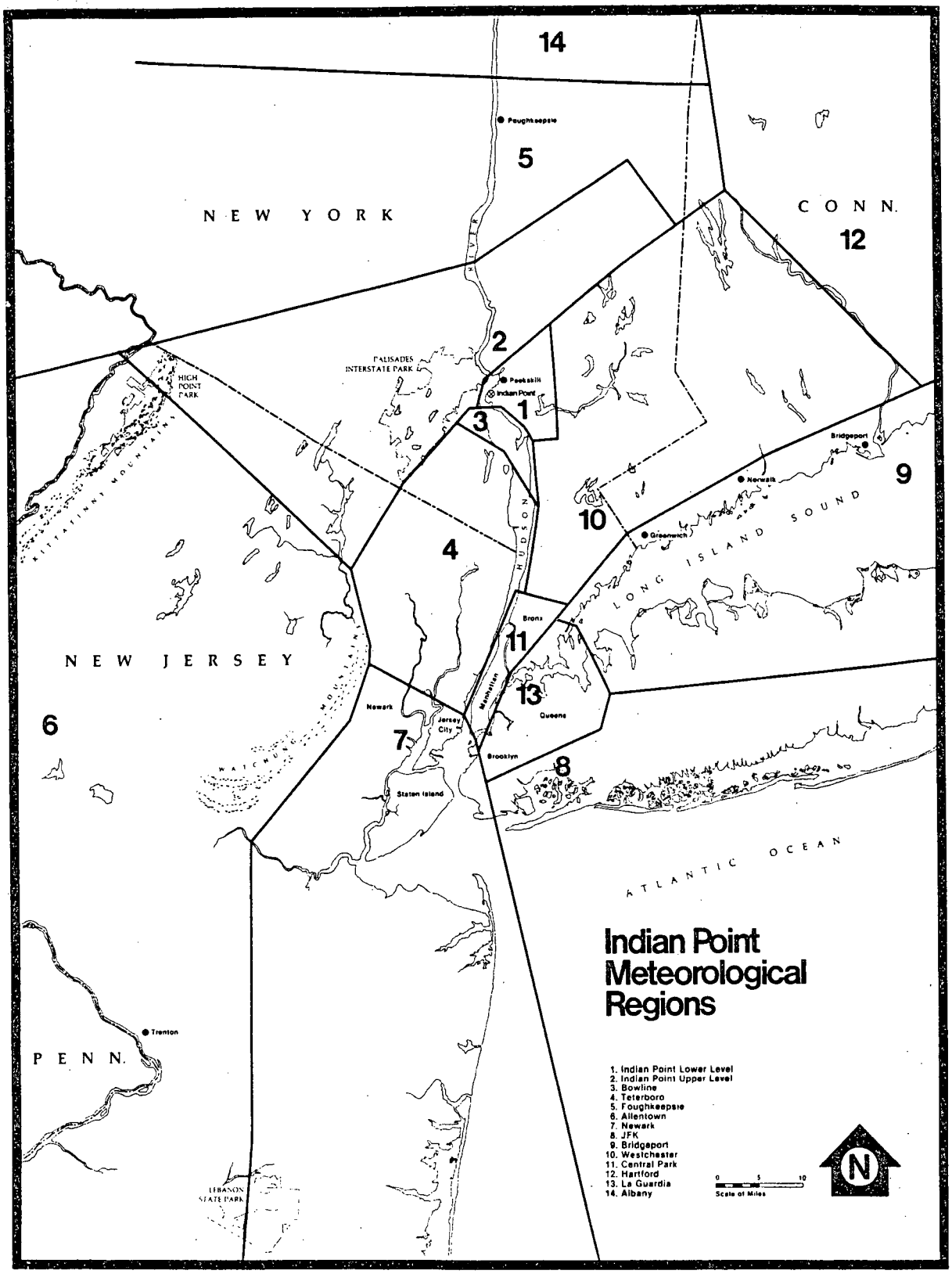
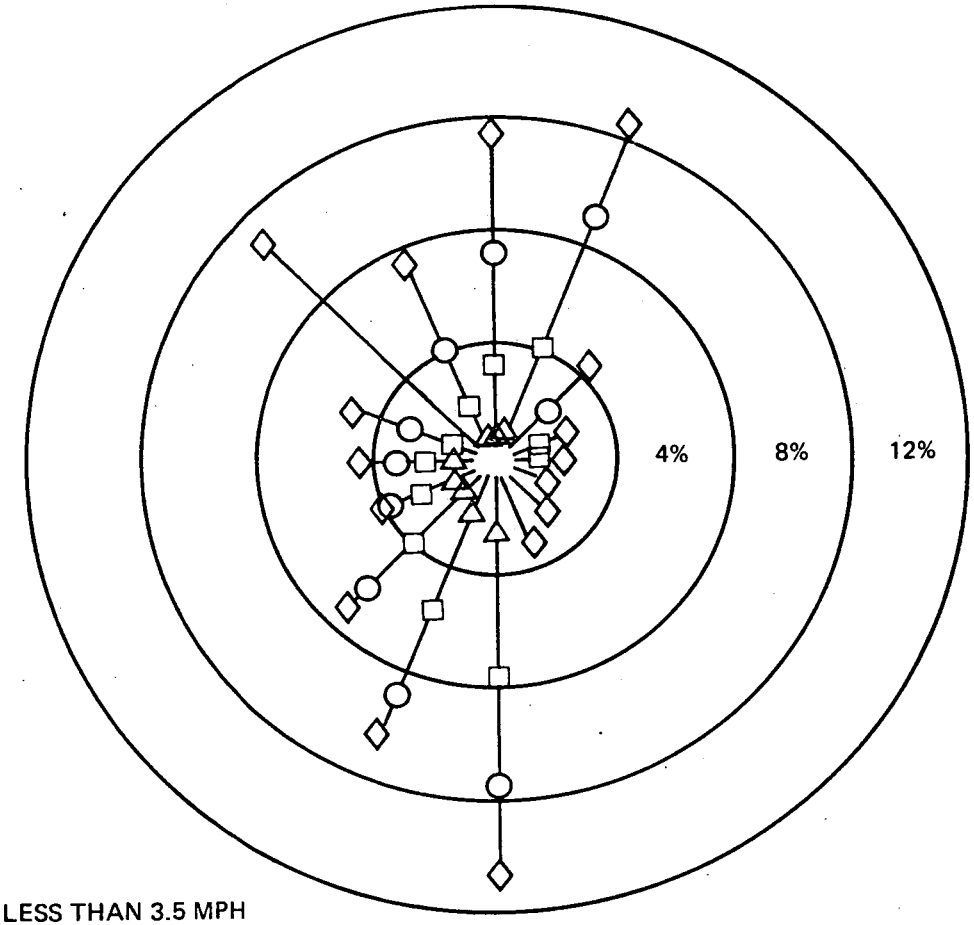


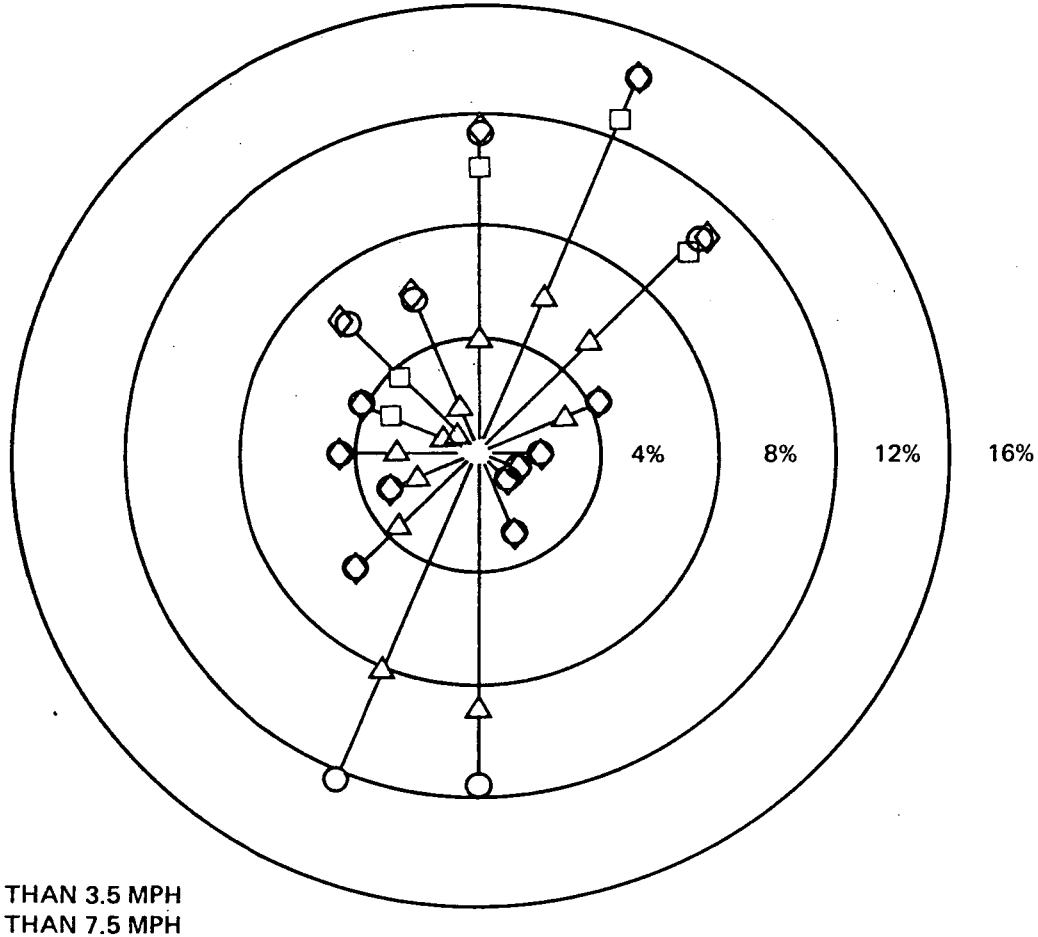
Figure 6.2-1. Indian Point Meteorological Regions



△ WIND SPEED LESS THAN 3.5 MPH
□ WIND SPEED LESS THAN 7.5 MPH
○ WIND SPEED LESS THAN 12.5 MPH
◇ WIND SPEED GREATER THAN 12.5 MPH

0.2 PERCENT CALMS
(CALMS DEFINED AS SPEED LESS THAN 0.5)

Figure 6.2-2. Indian Point 122m Wind Rose



△ WIND SPEED LESS THAN 3.5 MPH
□ WIND SPEED LESS THAN 7.5 MPH
○ WIND SPEED LESS THAN 12.5 MPH
◇ WIND SPEED GREATER THAN 12.5 MPH

0.3 PERCENT CALMS
(CALMS DEFINED AS SPEED LESS THAN 0.5)

Figure 6.2-3. Indian Point 10m Wind Rose

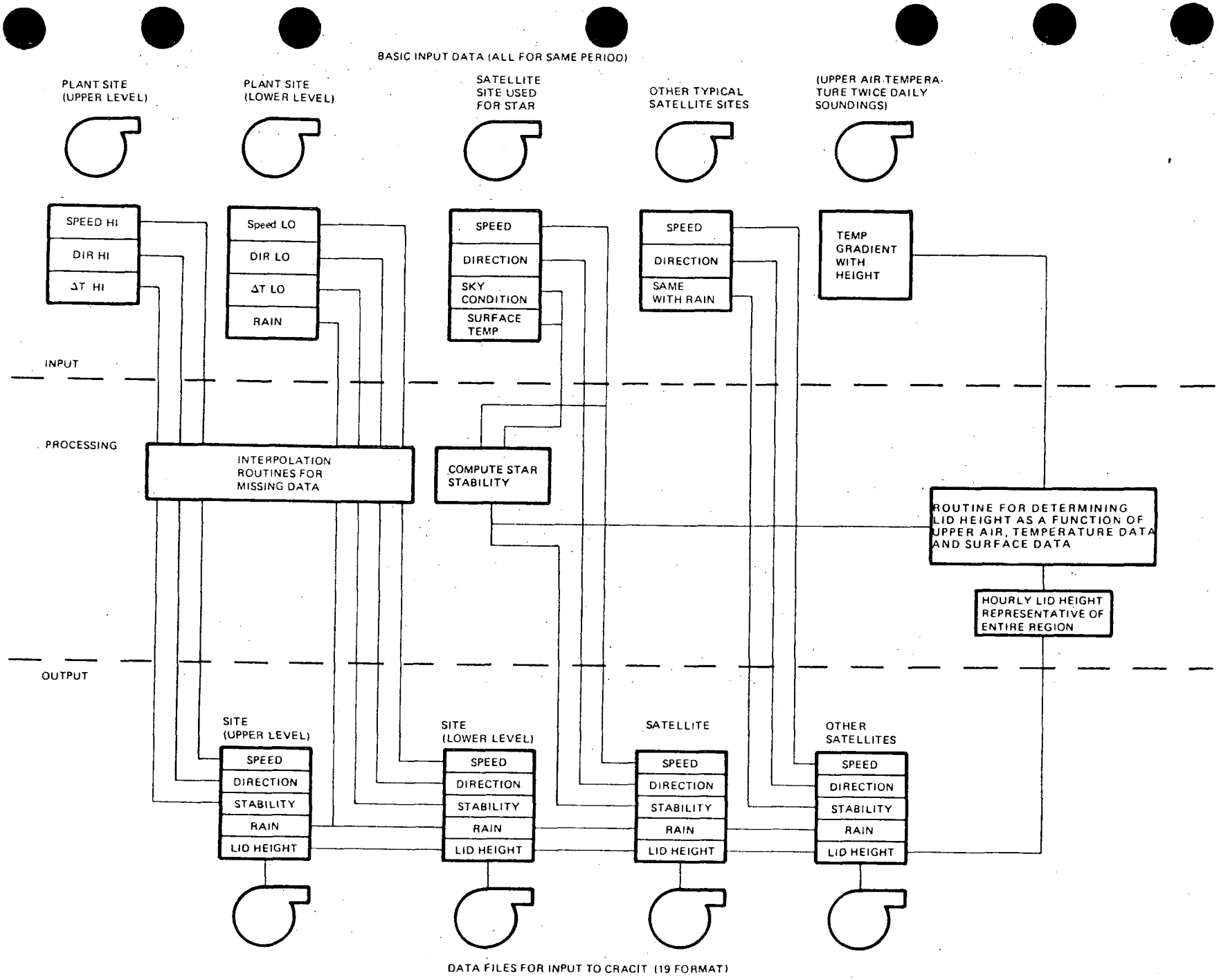


Figure 6.2-4. Flow Diagram for Site Meteorological Data Processing Via CRACIN Routine

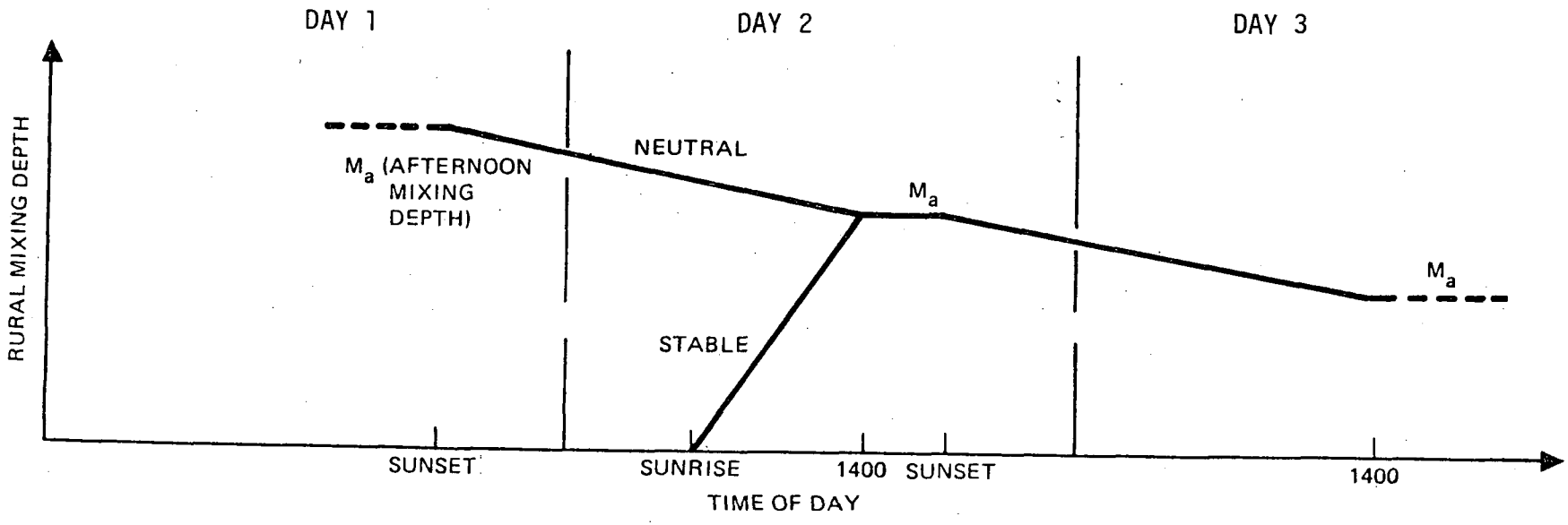


Figure 6.2-5. Model for Estimating Lid Height

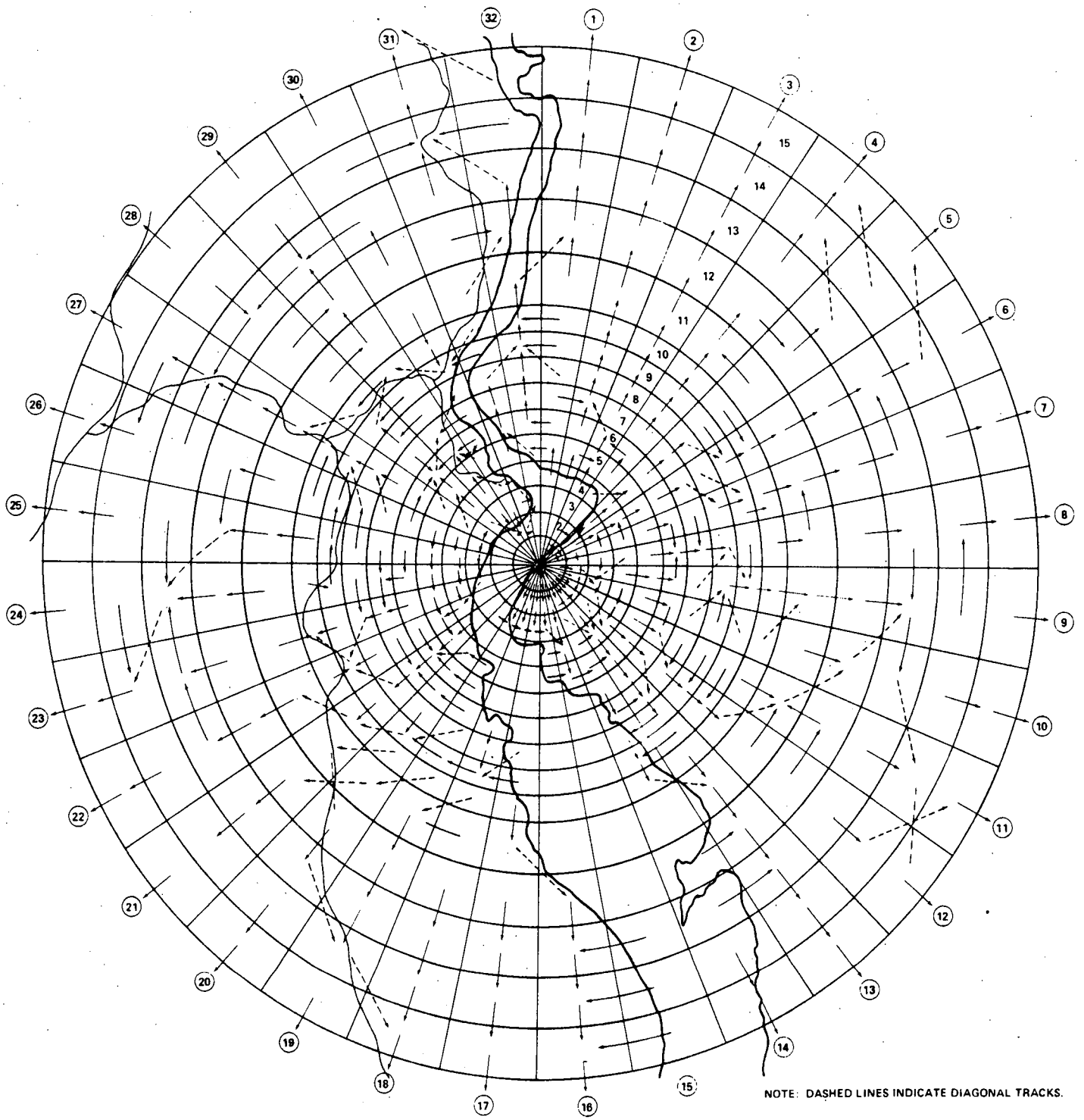


Figure 6.2-6. Example of Evacuation Vectors--Indian Point (Daytime--School in Session)

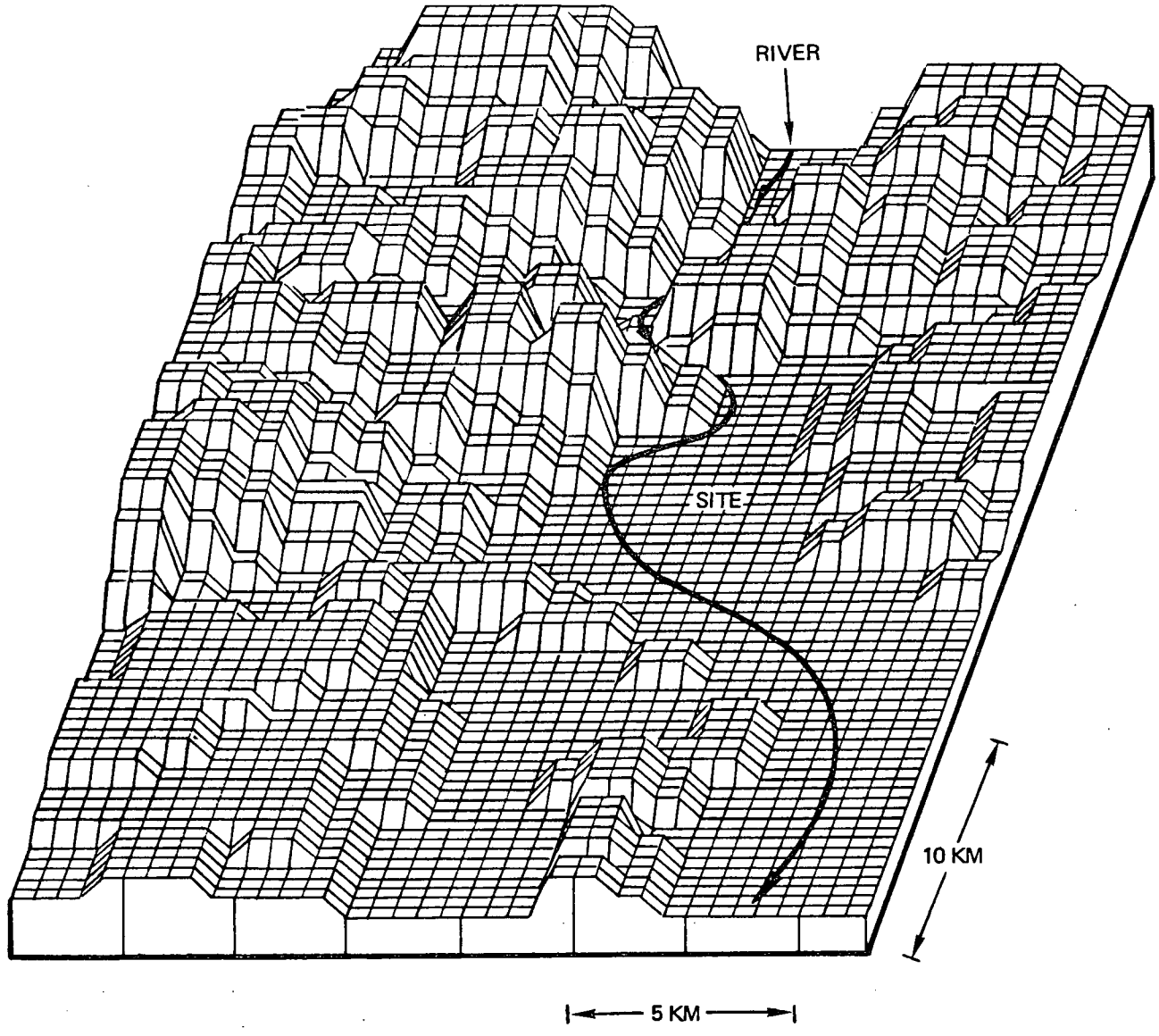


Figure 6.2-7. Representation of Terrain Surrounding the Indian Point Site

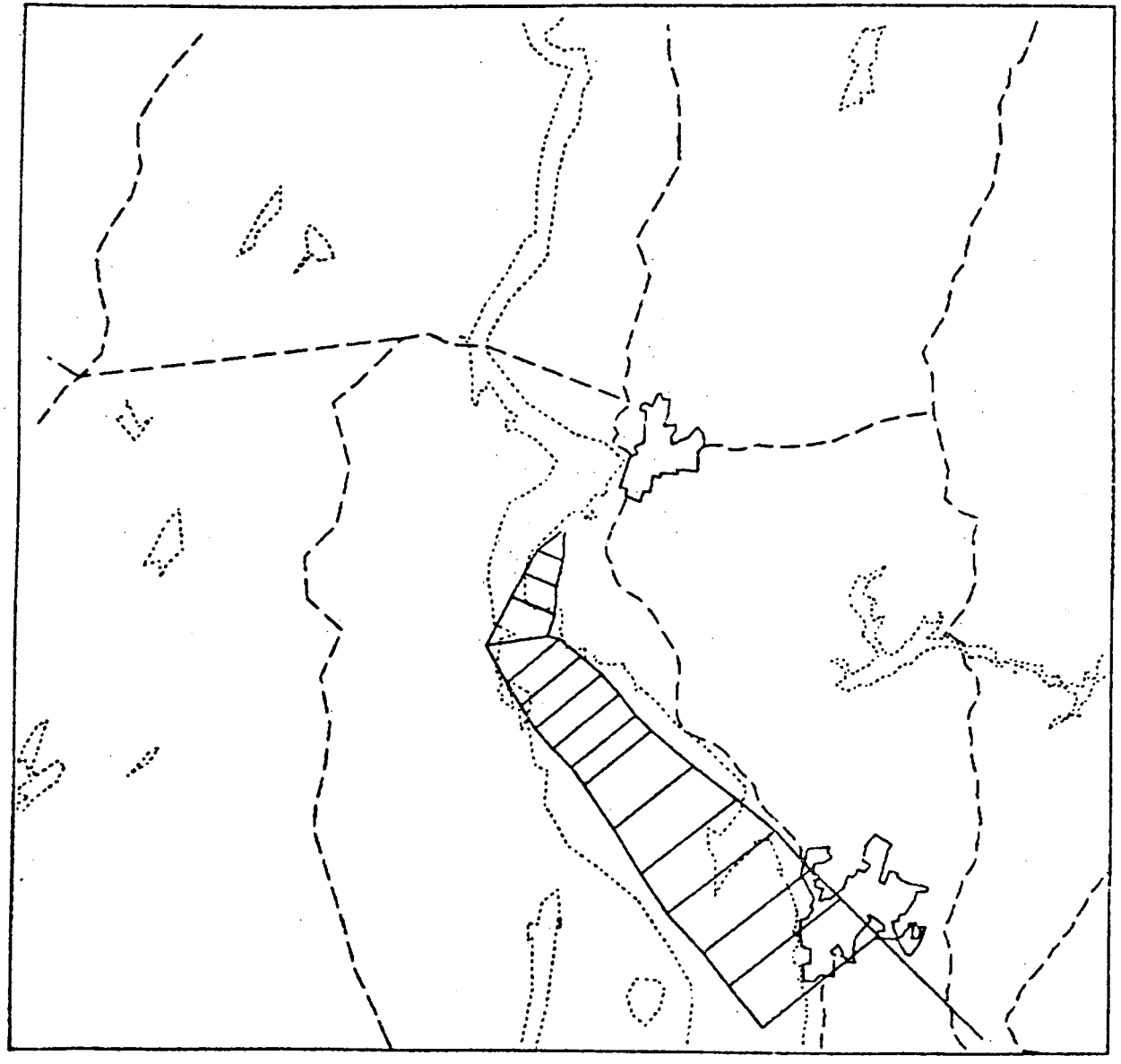


Figure 6.2-8A. Example of Plume Track After Edit
(Early Morning, Down River Valley Flow--Low Level Release)

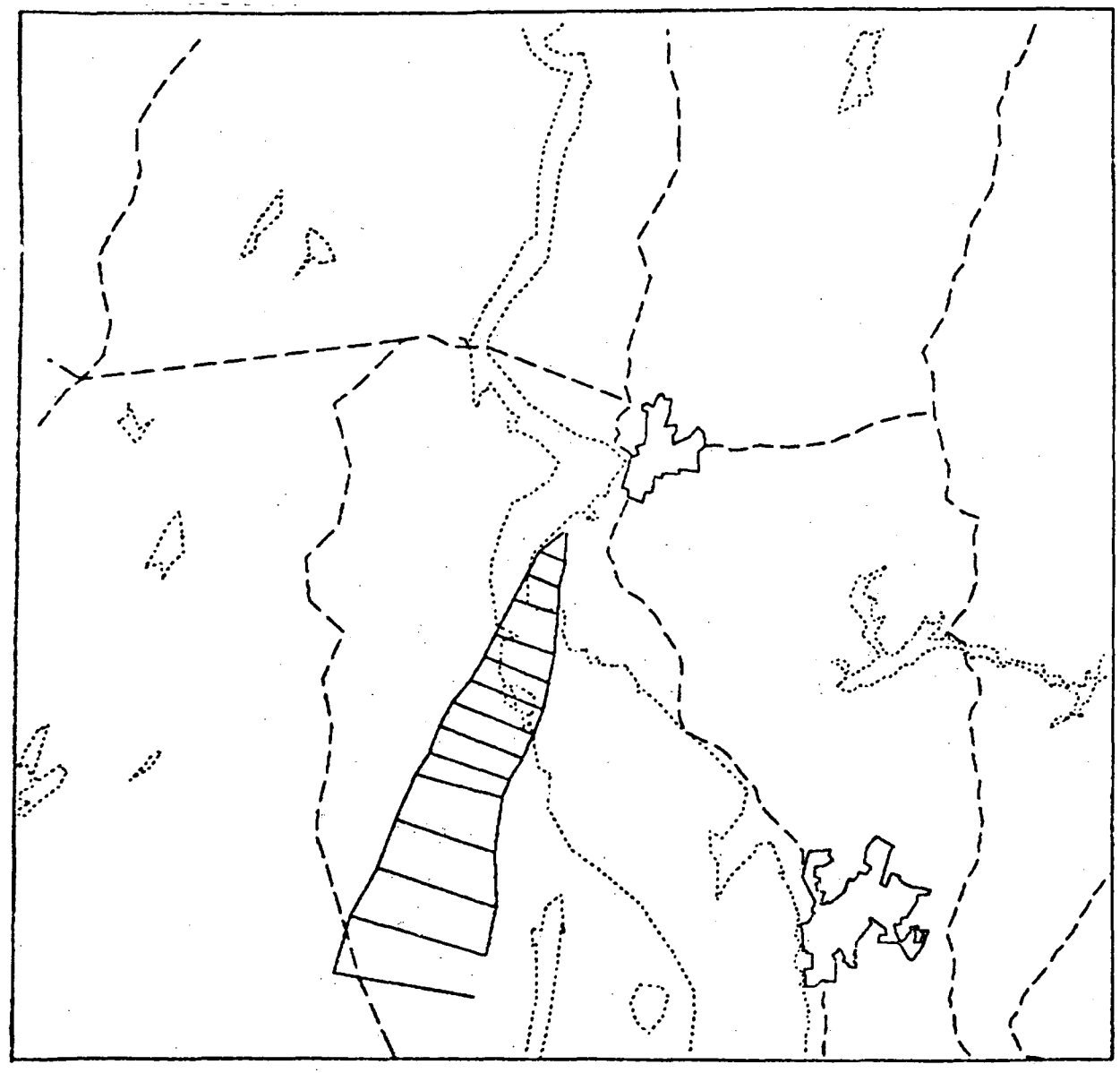


Figure 6.2-8B. Example of Plume Track Before Edit
(Early Morning, Down River Valley Flow--Low Level Release)

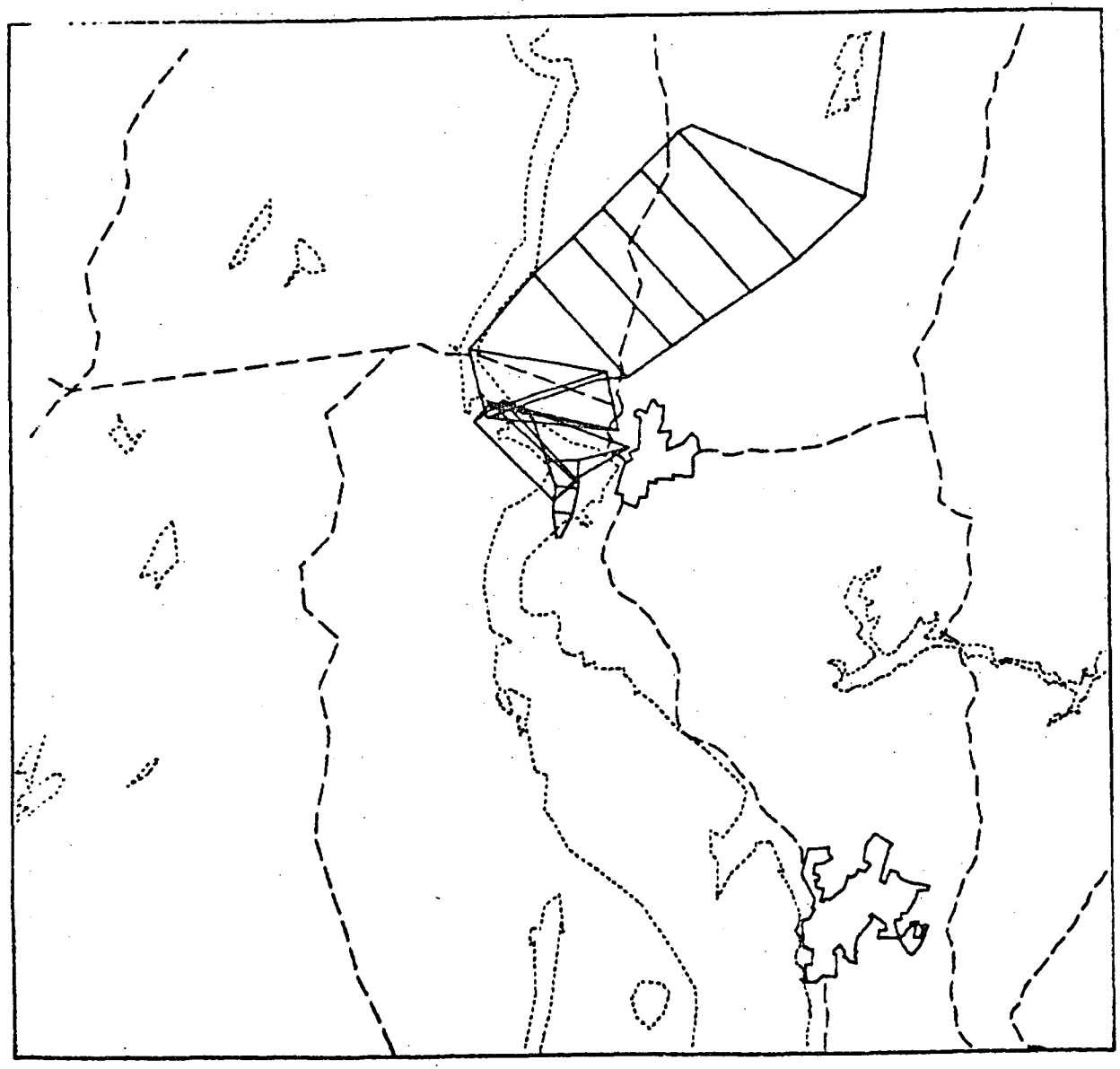


Figure 6.2-9A. Example of Plume Track After Edit
(Low Wind Speed, Up-Valley Flow Confined by Terrain--Low Level Release)

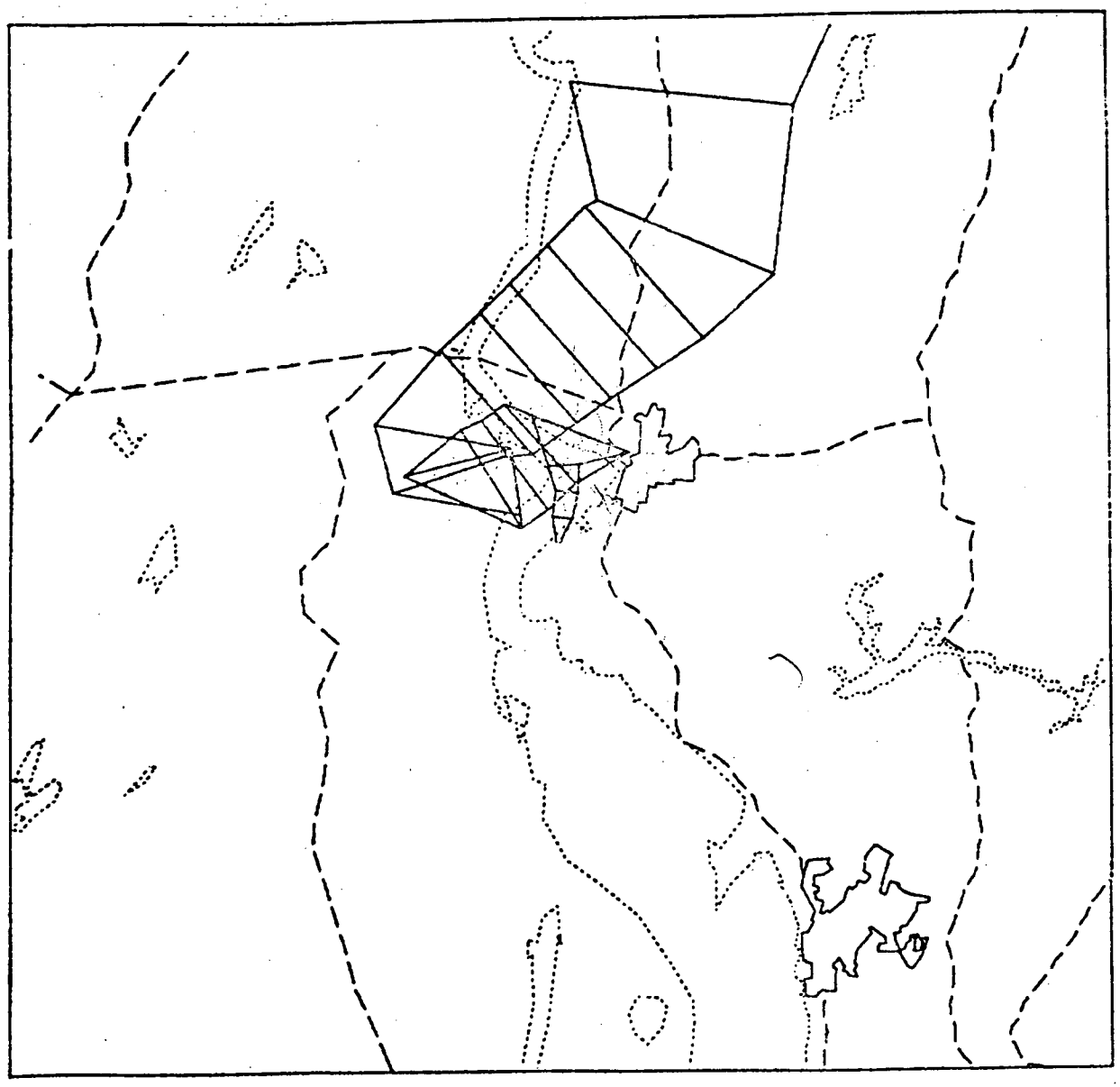


Figure 6.2-9B. Example of Plume Track Before Edit
(Low Wind Speed, Up-Valley Flow Confined by Terrain--Low Level Release)

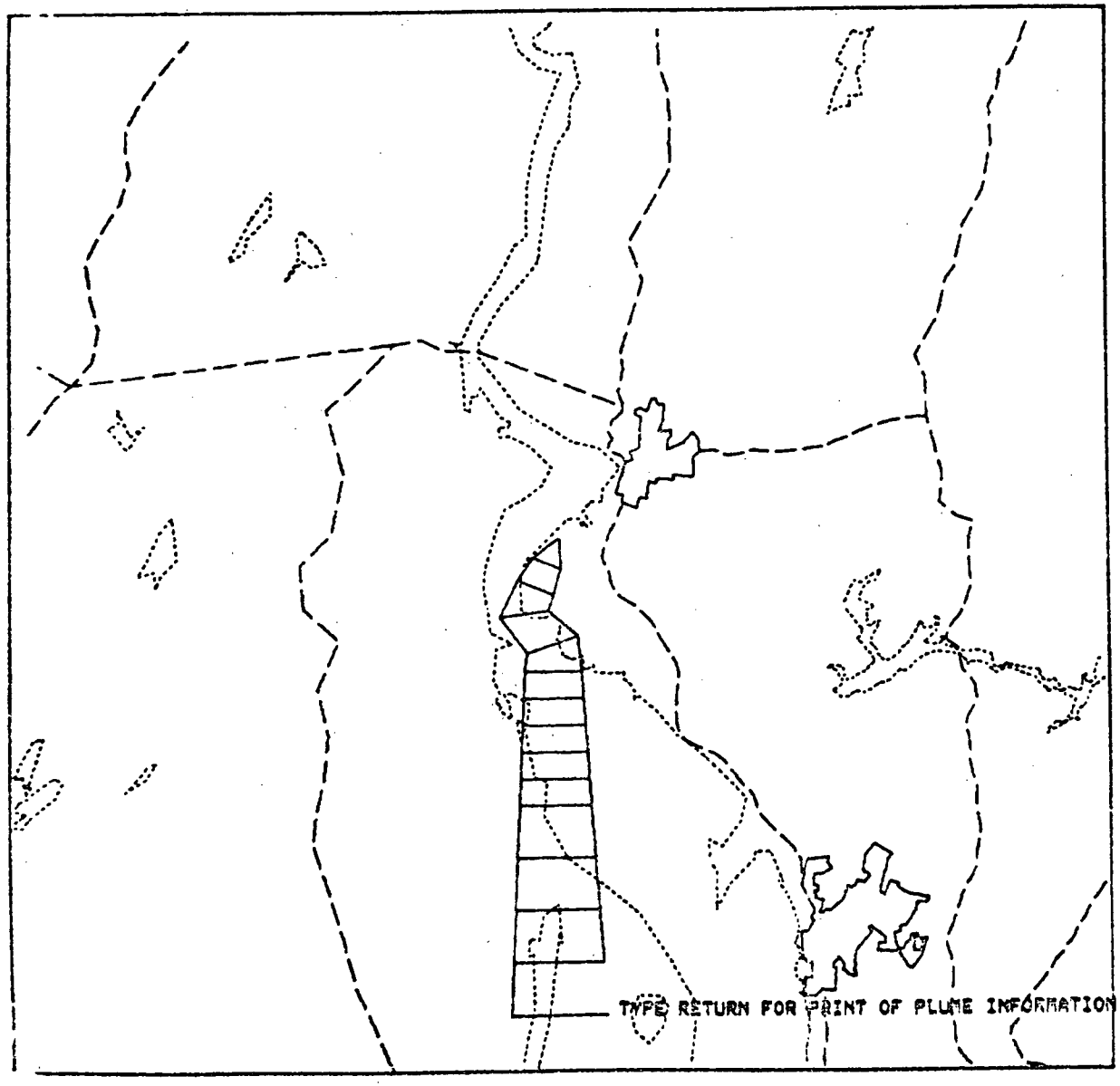


Figure 6.2-10A. Example of Plume Track After Edit
(Elevated Release Out of Valley Influence)

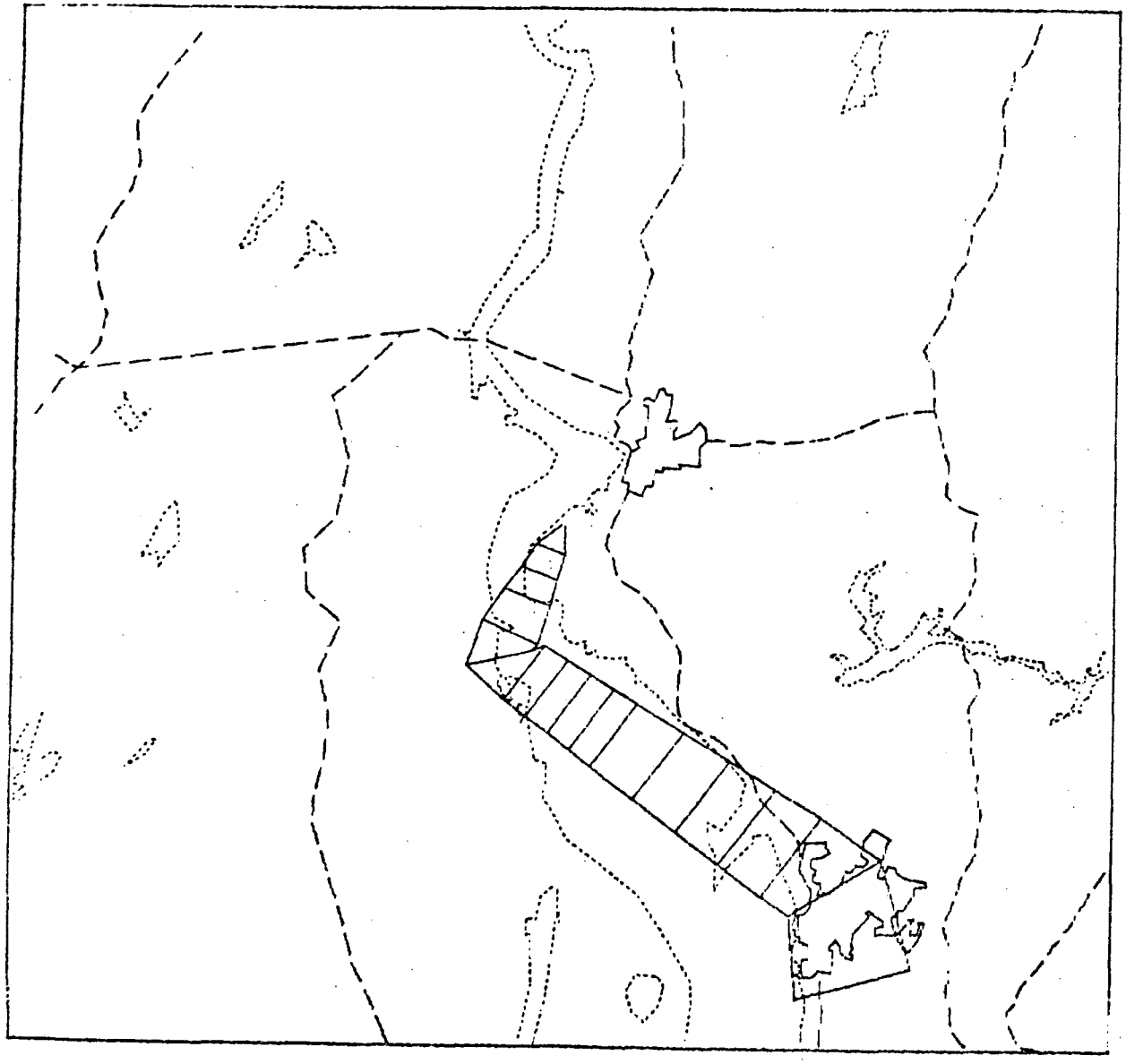


Figure 6.2-10B. Example of Plume Track Before Edit
(Elevated Release Out of Valley Influence)

6.3 SENSITIVITY STUDIES AND MODEL VERIFICATION

After CRAC modifications were completed, a series of CRACIT test runs was made and the results were compared with similar runs using the CRAC program to verify the correctness of the modified version. These test runs, other sensitivity runs, and runs to characterize uncertainty are described in this section.

6.3.1 MODEL TESTING

During the development of the CRACIT routine, results obtained from hand calculations were compared with CRACIT results in a step by step manner whenever possible. The completed version was then run and compared with CRAC runs using similar input assumptions. This section details the test comparison runs used to confirm the validity of the CRACIT program and concepts.

Although this study is for a large PWR-type reactor system, the initial tests used the BWR-1 release category from the RSS with a power level of 1,930 Mwt. This category is very similar to the PWR-2 category in the RSS which has dominated the risk curves in the past. Therefore, the test runs presented here should be applicable to PWRs and BWRs.

6.3.1.1 Straight Line (Single Sequence) Comparisons with CRAC

The first and most critical test of the CRACIT program was the duplication of the CRAC results using straight line plumes for both CRAC and CRACIT. This provided a good check of the fine grid area coverage, dose calculations, and diffusion conditions for stationary receptors. Since the evacuation models are completely different, no comparison tests with CRAC were possible and proper program operation was verified using hand checks and sensitivity tests (Section 6.3.2). The single sequence test consisted of a series of runs using one set of meteorological conditions for both CRAC and CRACIT. Thus, wind speed and stability conditions were assumed to be the same for all hours and spatial intervals were forced to be the same size. This resulted in the plume traveling in a straight trajectory with its lateral boundaries growing at the same rate as it traveled downwind. Results for five effects categories expressed as numbers of effects are given in Table 6.3-1.

Each case was run assuming three different azimuthal grid sizes for a release category with a 30-minute release duration since duration affects plume width. As shown for the 64 and 128 sector cases, the results differ by 30% to 40% compared with CRAC results for certain stability classes. This may be attributed to the radial fine grid used to approximate plume dimensions in CRACIT (CRAC does not use a grid approach to determine areas of coverage). As expected, the 192 sector case appears to be most comparable, since the finer resolution can best represent the plume dimensions for all stabilities. However, the plume width increases for other release categories (depending on the meander factor assigned as a function of release duration) thereby improving the comparability of CRACIT results using 64 sectors.

Comparison of intermediate results including air and ground concentrations, individual doses by organ and pathway, and health effect probability per person showed numerically identical results. This verified that CRACIT was operating correctly.

6.3.1.2 Selection of Fine Grid Size

To determine the appropriate radial grid size, small distances were selected radially downwind since the basic dispersion calculation is very sensitive to distance from the source. The selected radial spacing is given in Table 6.1-7.

Although the 64 sector single sequence test appeared to give reasonable resolution, it was expected that considerable improvement would result when a number of meteorological sequences and other categories were run. Therefore, as will be discussed later, CRACIT runs were made using 96 real meteorological sequences (a multiple sequence test) to select the appropriate azimuthal grid sizes.

The azimuthal grid spacing primarily determines the resolution of plume coverage area, and thus the size of the population group affected. Therefore, after it was established that the CRACIT model was functioning properly (Section 6.3.1.1), a series of runs was made on a representative sample of 96 meteorological sequences. These used real meteorology and trajectories for each of three azimuthal grid spacings of 64, 128, and 192 direction sectors. Results are given in Table 6.3-2 for five effects categories and in Figures 6.3-1 and 6.3-2 for early fatalities and acute injuries. As shown, there was very little difference between results using any of the three azimuthal grid spacings in the CRACIT model. This being the case, production runs were made using the 64-sector grid to conserve computer time. Multiple sequence comparisons of CRACIT and CRAC for verification purposes are not feasible because significant inherent differences in the evacuation and plume trajectory portions of the two models lead to differences in results.

6.3.1.3 Determination of Sample Frequency for Meteorological Sequences

As discussed in Section 6.1, CRACIT determines the start date for each meteorological sequence using a stratified random sample technique on 1 year of hourly meteorological data. In the RSS, the NRC based its calculations on 91 sequences that had been shown to adequately define the risk curve using the CRAC model and the RSS input assumptions. However, for this study, input assumptions and plume and evacuation trajectories are different. Therefore, it was necessary to establish the number of samples required to adequately define the consequence curves.

CRACIT computer runs were made for release category 2 (since only ground level releases contribute significantly to the risk curves) using up to 288 randomly selected meteorological sequence start hours. Results were then separated into three sets of 96 sequences each, and risk curves showing the probability of exceeding a given number of effects were plotted as shown in Figures 6.3-3, 6.3-4, and 6.3-5. As shown in Figure 6.3-3 for early fatalities, there are some differences for small samples. Results are in closer agreement for the acute injury and

man-rem effect curves shown in Figures 6.3-4 and 6.3-5, respectively. The screening process describedin Section 6.3.2.2 was used to select scenarios (in addition to the standard 96) for use in achieving greater definition in the tails of the distributions.

6.3.1.4 Conservation of Plume Area Coverage

When the plume trajectory is allowed to deviate from a straight line, as is the case in the CRACIT model, the area covered by each spatial interval is often different than that computed for the trapezoidal shaped spatial intervals in CRAC. Since one objective was to preserve as much of the area of plume coverage that exists for the straight line plumes in CRAC as practical, several area checks were made for different meteorological sequences that resulted in plume turning. Inspection of these runs indicated that for certain spatial intervals area differences of as much as 25% occurred if the plume had undergone considerable turning. This discrepancy was not considered serious since areas for some spatial intervals would be high while others would be low compared with CRAC plume areas. In addition, they could vary from sequence to sequence.

Having been satisfied that the direction dependent plume area representation was proper, and after overlaying the plume on the fine grid, another check was made. All fine grid box areas that were under the plume were added and the total of these areas was compared with the exact areas computed before overlaying on the grid. Again, the areas varied considerably (by factors in the range 0.5 to 2.0) for certain spatial intervals. However, the agreement was good for the entire plume as a whole. The multisequence test described in Section 6.3.1.3 also showed that consequences (all of which are plume area dependent) do not change appreciably when the number of azimuthal sectors, which affects the accuracy of plume area coverage, is varied. Based on these results it was concluded that the fine grid representation of area with 64 azimuthal sectors was sufficiently accurate.

6.3.2 CONSTRUCTION OF RISK CURVES

Risk curves were constructed directly from CRACIT production run results for all effects except early fatalities and injuries. Construction of the curves for these two effects is complicated by several factors:

1. Large numbers of effects are usually associated with ground dose from rain-deposited material over densely populated areas, events that occur infrequently.

2. The dose-response curves for these effects are very sharp. For example, the probability of a fatality from a marrow dose of 400 rem is near 0, but the probability climbs rapidly to 1.0 at a dose of 620 rem. A similar situation exists for injuries. All other effects have essentially a linear response to dose.

3. In rare, worst case scenarios, ground concentrations are usually only slightly higher than those necessary to exceed the upper end of the dose-response curve. Scenarios that lead to much higher concentrations necessarily affect smaller areas and fewer people.

Parameters that can make factors of two differences in dose can make large differences in early fatality or injury consequences. Further, since the phenomena leading to large consequences are rare, a comprehensive search is required to ensure that they are identified so that the high consequence end of the risk curve is adequately defined. Therefore, an investigation of the effect was conducted as described below.

6.3.2.1 Important Parameters

Analysis of intermediate results indicated the importance of consequence analysis variables in determining the characteristics of the conditional risk curves for early fatalities. These parameters included the atmospheric dispersion model variables, the definition of the zone within which people were evacuated, the length of delay time between release and the start of the evacuation, duration of release, dose reduction due to shielding, and time of exposure to ground radiation for persons not evacuated.

The values of evacuation parameters selected for production runs are based primarily on the site emergency plan. However, they are also consistent with values derived from an evacuation data base compiled by the U.S. Environmental Protection Agency (EPA) and used to develop the RSS evacuation model. These are summarized in Appendix VI of the RSS. The EPA data included numbers of people evacuated, distances moved, time required for evacuations in response to transportation accidents, and flood and hurricane warnings.

Although delay times are not specifically identified in the EPA data, the fact that most operations were completed within 5 hours, and rarely required more than 10 hours, suggested that delay times could be limited to less than a few hours. One hour was selected as the base case value for the time between warning and the start of evacuation. In some scenarios, residents are assumed to remain for several hours before evacuating (see Section 6.2.1.2). Since it is assumed that warnings are issued prior to a release, evacuation may occur before releases begin. Observed dose distributions indicate that greater delay times could increase the probability of fatalities at the lower (less severe) end of the consequence curve because some evacuees would be exposed to radioactive material during the mobilization period. For people near the plant, this incremental exposure could raise the doses over the fatality or injury thresholds. Because relatively few people would be affected, the impact would appear in the lower consequence end of the curve.

Evacuation speed may also be important, but it should be noted that speeds assumed are quite low. Results indicated that fatal doses are particularly infrequent for moving evacuees. Therefore, increases in speed, while leading to lower doses, would not be expected to change the fatality or injury risk curves substantially.

Current NRC recommendations for emergency response call for evacuation from a downwind area within about 10 miles of the plant if the situation warrants. Thus, for this analysis, a value of about 10 miles is used as the radius of the evacuation zone.

6.3.2.2 "Tails" Discussion

Studies of sample size showed that variations in all but the extreme "tails" of the curve could be stabilized if at least 96 samples were taken. Therefore, to define the low consequence end of the curve, 96 samples were used for the release categories dominating risk. It is expected that considerable uncertainties would exist in the high consequence "tails" of the early fatality and injury risk curves if only 96 samples were used. Therefore, a screening study was made to search for additional meteorological scenarios that could lead to high ground level concentrations. Tails of the other health effect curves are fairly well defined without using the screening methodology.

The screening study consisted of running every possible meteorological scenario in the 1-year data base through the dispersion model in CRACIT. Release category 2 source term characteristics were used to represent categories that dominate risk. Since it is known that the highest number of effects is likely to result from fission products deposited over densely poplulated areas, sequences with high ground concentrations beyond the evacuation zone were identified. Out of these sequences, about 200 start times were selected as potential candidates for large numbers of fatalities within 20 miles south of the site. Additionally, 20 sequences were selected that had high concentrations in the densely populated areas further south. Every 6th one of the 200 "close in" (making 35) and all 20 of the "far out" start times identified were then run through CRACIT. The sequences with the highest consequences were determined and used to define the high consequence "tails" of the early fatality risk curves or S matrices (see Section 8.0). The scenario with the highest number of effects from the 20-sample group was used to define the "highest" consequence value on the risk curve. Results from the 35-sample group was used to "fill-in" the risk curve between the end of the 96-sample group and the "highest" consequence value.

An upward bias in dose and consequence estimates exists for releases longer than about 1 hour. The CRAC model includes an implicit assumption that all radioactive material released during the course of an accident follows the same trajectory. As described in Section 6.1.2.6, CRACIT has been programmed to include processing of multiphased releases. The concentration reductions that accrued from multiphased releases in CRACIT were associated with the spread of the release over a longer period. Thus, the fact that different portions of the releases are allowed to follow entirely different trajectories is accommodated in CRACIT.

For latent effects that depend on doses aggregated over the entire population and are not strongly sensitive to doses received by individuals, the single release assumption does not affect results compared with multiphased release assumptions. For early fatalities and injuries,

however, threshold effects are important and, as a result, doses received by individuals are important. If the hourly portions of a multihour release follow different trajectories, as is likely, the doses received by any individual would be less than the maximum dose estimated using the CRAC or CRACIT model in the conventional manner. The more accurate treatment leads to reductions in levels below the early fatality threshold for these high consequence scenarios. Thus, the multiphased CRACIT processing has reduced the uncertainty originally introduced by the single plume assumption.

6.3.2.3 Uncertainty

The consequence analysis models used in this study incorporate a large number of variables. Examples include meteorological conditions, factors affecting plume dispersion, evacuation assumptions, shielding assumptions, dose conversion factors, and health effect factors. For most of these parameters, a single value or point estimate was assigned. The intent was to assign a best estimate value, but there is a tendency to assign conservative values as uncertainty increases. Thus, the consequences computed for this study are based on point estimates for each parameter with recognition that some uncertainty exists. The effort made in this study to reduce uncertainties by improving the physical models that describe the dispersion (or transport) of released material in the atmosphere is important. The use of extensive amounts of meteorological data from 14 sites in this study, the use of a modified potential flow, three dimensional terrain model, and the use of a multiphased release model are examples of attempts to improve the ability to predict plume location. Associated with the improved modeling and data activities was the incorporation of expert judgment, based on many years of actual experience with local conditions, concerning transport of the released material. Another example of model improvements lies in the evacuation model that simulated realistic evacuation times and paths for five evacuation scenarios.

These activities were designed to improve the accuracy of the analysis. The result is a state of the art assessment, but uncertainties remain. The remaining uncertainties are of two types, those related to parameters used in the model and those related to the inherent limitations in the model. Given that the dispersion model uses hourly meteorological data to determine the trajectory and dispersion of released radioactive material, even if the data and dispersion estimates were perfect, there is some uncertainty about the accuracy of the estimated trajectory. The implications of an error in trajectory are substantial. A scenario which, in the model, deposits a large amount of radioactive material over a densely populated area could, in fact, develop with a trajectory that misses the populated area entirely, or vice versa. The fact that the uncertainty could go either way is important, because in the relatively high frequency, low severity range of the risk curve, there are opportunities for errors to offset one another. These would reduce the importance of uncertainties of this type. Opportunities for offsetting errors at the low level, high severity end of the curve are rare; however, there are upper bounds, such as the population in a given area, that cannot physically be exceeded. Uncertainties of this type are minimized by the screening process and multiphased release modeling described previously.

The uncertainties estimated quantitatively in this analysis are those resulting from uncertainties in model parameters. They do not fully address trajectory uncertainties. The largest uncertainties of this type are those related to the determination of dose. The uncertainties related to the estimate of health effects from dose are relatively small for early fatalities and injuries. They are somewhat larger for latent effects, but are still considered small relative to those in the estimate of dose.

After quantitative consideration of the net effect of uncertainties in many aspects of the dose calculations, such as mitigation assumptions, rainfall washout, and release durations, it was judged that there is a small chance that doses are underestimated by a factor greater than 2 (S2 matrix), a reasonable chance that the doses computed are correct (S1 matrix), a lower chance that the doses are overestimated by a factor of 2 (S3 matrix), and a small chance that doses are overestimated by a factor of 10 (S4 matrix). The 2RW release category frequency which used the multiphased release was assigned a higher probability of being correct. Since 2RV and 8B have very low source terms which do not generally lead to doses above the 50 rem threshold for injuries, the uncertainties are considered to be less. A zero probability was assigned to the S4 matrix. Latent effects were assumed to have a higher probability of being overestimated by a factor of 2 due to the fact that an end of life core inventory was used.

Effect	Release Category	Site Matrix			
		(S4)	(S3)	(S1)	(S2)
Acute Fatalities and Injuries	Z-1Q	10	25	50	15
	2 and Z-1	10	25	50	15
	2RW	10	20	60	10
	2RV	0	40	50	10
	8A	0	40	50	10
	8B	0	40	50	10
All Others	Z-1Q	10	50	30	10
	2 and Z-1	10	50	30	10
	2RW	10	50	30	10
	2RV	10	50	30	10
	8A	10	50	30	10
	8B	10	50	30	10

These uncertainties were expressed as probabilities for each frequency versus health effect distribution for the significant release categories (S matrices) used in assembling the final risk curves in Section 8.0. Separate CRACIT runs were made as necessary for dominant release categories to define risk curves with the source term artificially increased or decreased. This was done to simulate uncertainty in the model or input assumptions.

TABLE 6.3-1

COMPARISON OF SINGLE SEQUENCE STRAIGHT-LINE-PLUME RESULTS FROM CRACIT VERSUS CRAC FOR FIVE EFFECTS*

(30-Minute Release Duration)

Stability	Number of Azimuthal Direction Sectors	Early Fatalities		Acute Injuries		Initial Leukemia		Total Whole Body		Total Man-Rem	
		CRACIT	CRAC	CRACIT	CRAC	CRACIT	CRAC	CRACIT	CRAC	CRACIT	CRAC
B	64	1,030	1,250	1,130	1,210	27	29	168	180	1.4E6	1.5E6
C		1,190	1,080	1,430	1,160	28	25	170	150	1.4E6	1.2E6
D		670	945	508	863	12	19	68	116	5.7E5	9.6E5
E		810	1,070	3,970	4,300	118	120	662	868	5.5E6	7.2E6
F		1,260	1,130	5,490	4,180	134	100	754	707	6.3E6	5.9E6
B	128	1,170	1,250	1,320	12,109	31	29	187	180	1.5E6	1.5E6
C		1,030	1,080	1,190	1,160	23	25	142	150	1.2E6	1.2E6
D		827	945	762	863	17	19	102	116	8.5E5	9.6E5
E		1,200	1,070	5,960	4,300	150	120	861	868	7.2E6	7.2E6
F		780	1,130	2,740	4,180	67	100	380	707	3.2E6	5.9E6
B	192	1,220	1,250	1,190	1,210	28	29	172	180	1.4E6	1.5E6
C		1,070	1,080	1,110	1,160	22	25	133	150	1.1E6	1.2E6
D		878	945	847	863	19	19	114	116	9.5E5	9.6E5
E		1,000	1,070	3,970	4,300	118	120	664	868	5.5E6	7.2E6
F		1,260	1,130	5,490	4,180	132	100	809	707	6.7E6	5.9E6

*All results are for a wind speed of 4.4m/sec with no rain.

TABLE 6.3-2

COMPARISON OF RESULTS USING THREE AZIMUTHAL GRID SPACINGS AND 96 METEOROLOGICAL SEQUENCES

(30-Minute Release Duration)

Effect	Number of Azimuthal Direction Grids					
	192		128		64	
	Mean	Peak	Mean	Peak	Mean	Peak
Early Fatality	3.35×10^{-1}	1.48×10^{-3}	3.47×10^{-1}	1.42×10^{-3}	3.54×10^{-1}	1.38×10^{-3}
Acute Injury	5.04×10^{-3}	7.71×10^{-4}	4.58×10^{-3}	8.46×10^{-4}	4.93×10^{-3}	8.74×10^{-4}
Initial Leukemia	4.33×10^{-2}	3.64×10^{-3}	4.20×10^{-2}	3.20×10^{-3}	4.02×10^{-2}	3.18×10^{-3}
Total Leukemia	1.71×10^{-3}	2.34×10^{-4}	1.70×10^{-3}	2.32×10^{-4}	1.65×10^{-3}	2.28×10^{-3}
Total Man-Rem	5.33×10^{-7}	7.14×10^{-8}	5.32×10^{-7}	7.09×10^{-8}	5.16×10^{-7}	6.94×10^{-8}

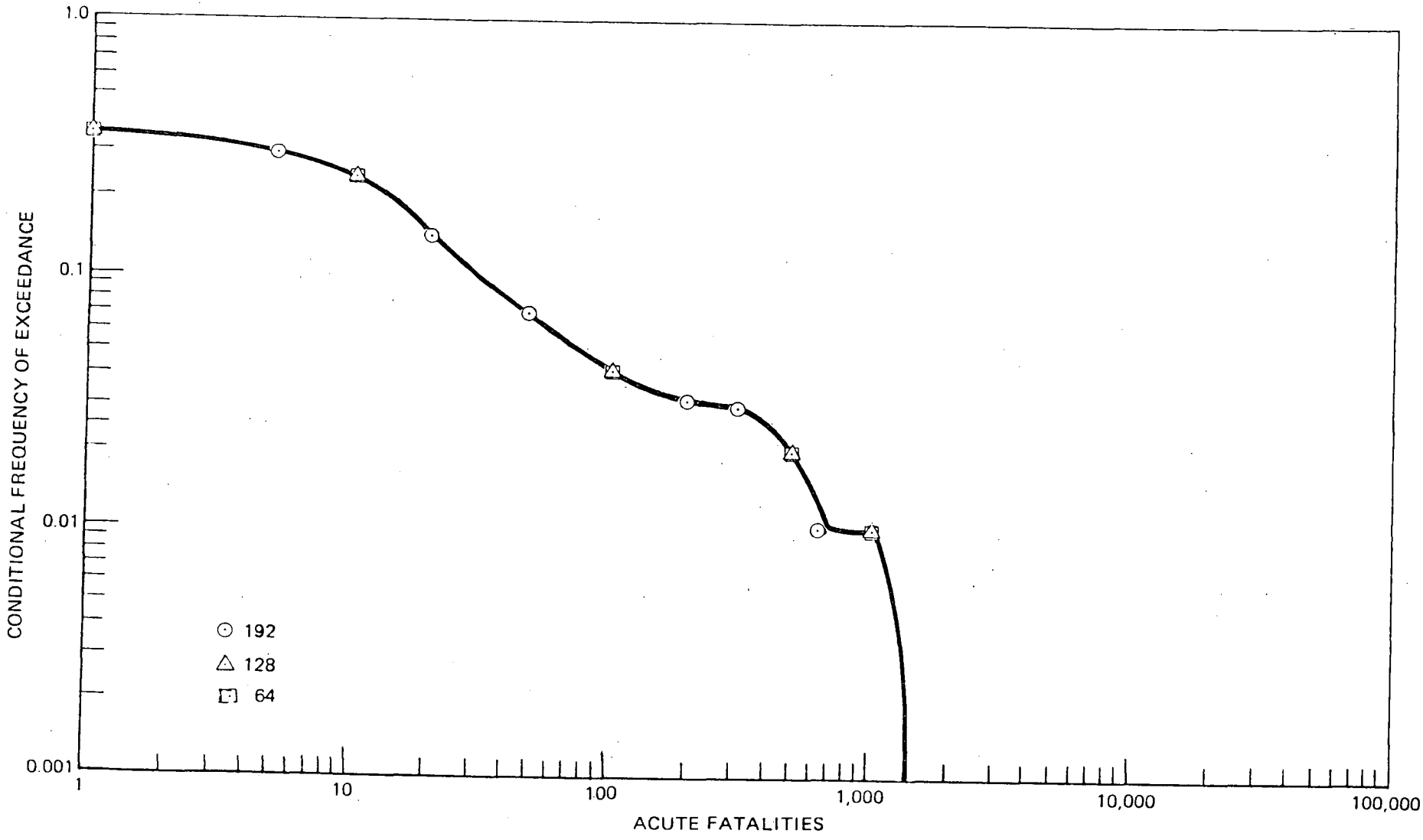


Figure 6.3-1. Comparison of Acute Fatalities from CRACIT Runs Using Three Different Azimuthal Grid Spacings (30-Minute Duration, 96 Meteorological Sequences)

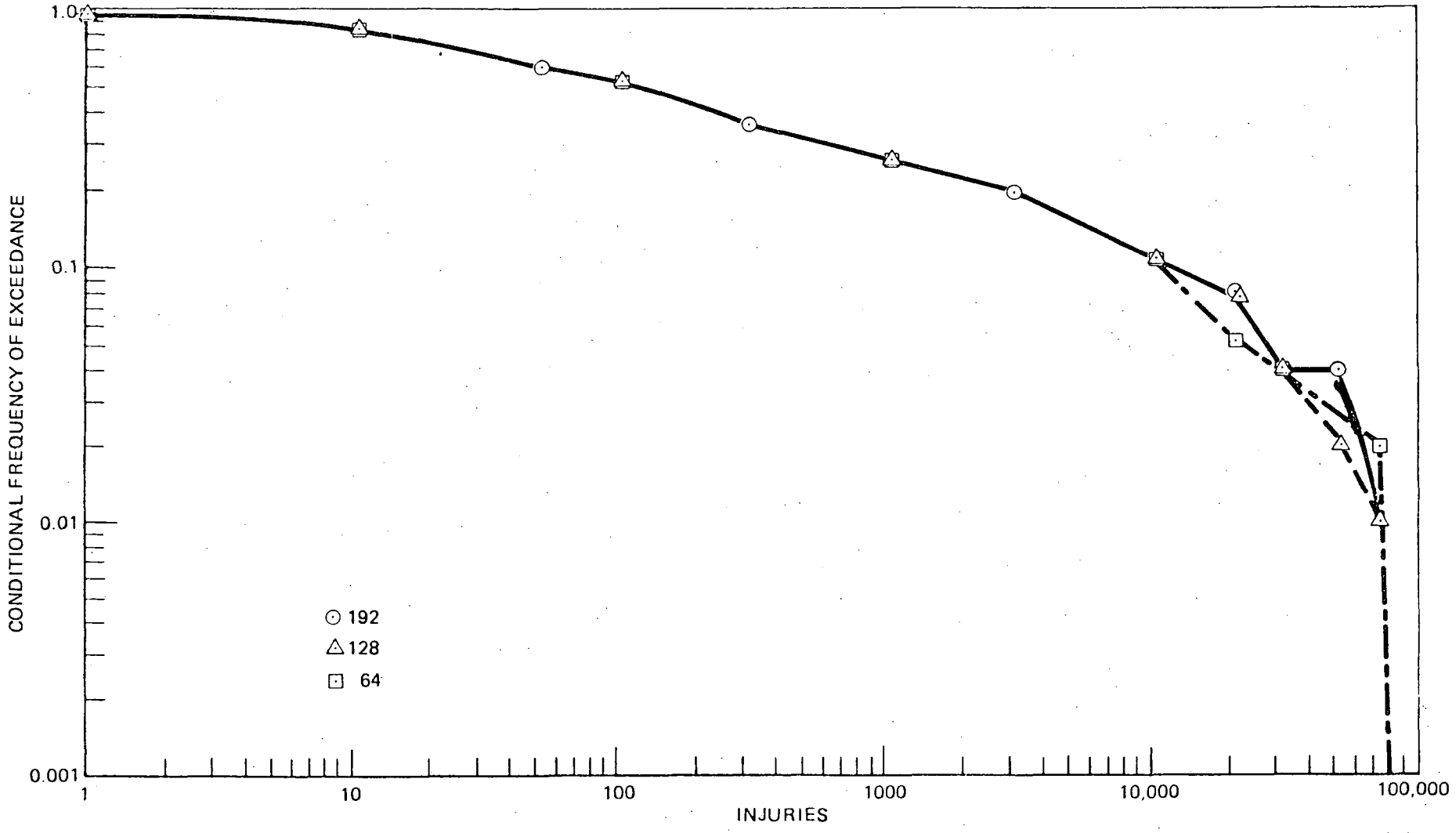


Figure 6.3-2. Comparison of Inuries from CRACIT Runs Using Three Different Azimuthal Grid Spacings (30-Minute Duration, 96 Meteorological Sequences)

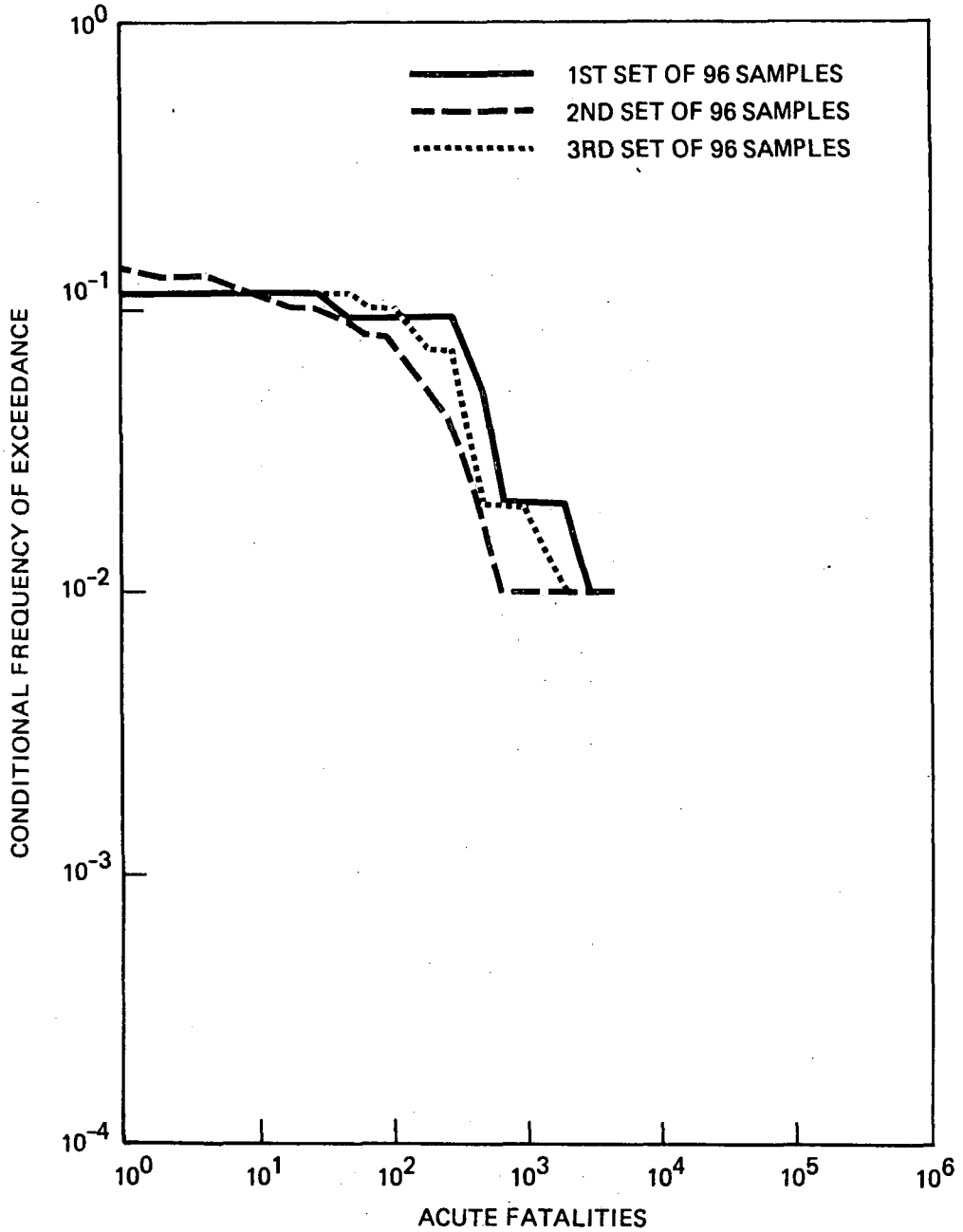


Figure 6.3-3. Comparison of Acute Fatalities Results Using Different Sets of Meteorological Sequences--IP Release Category 2

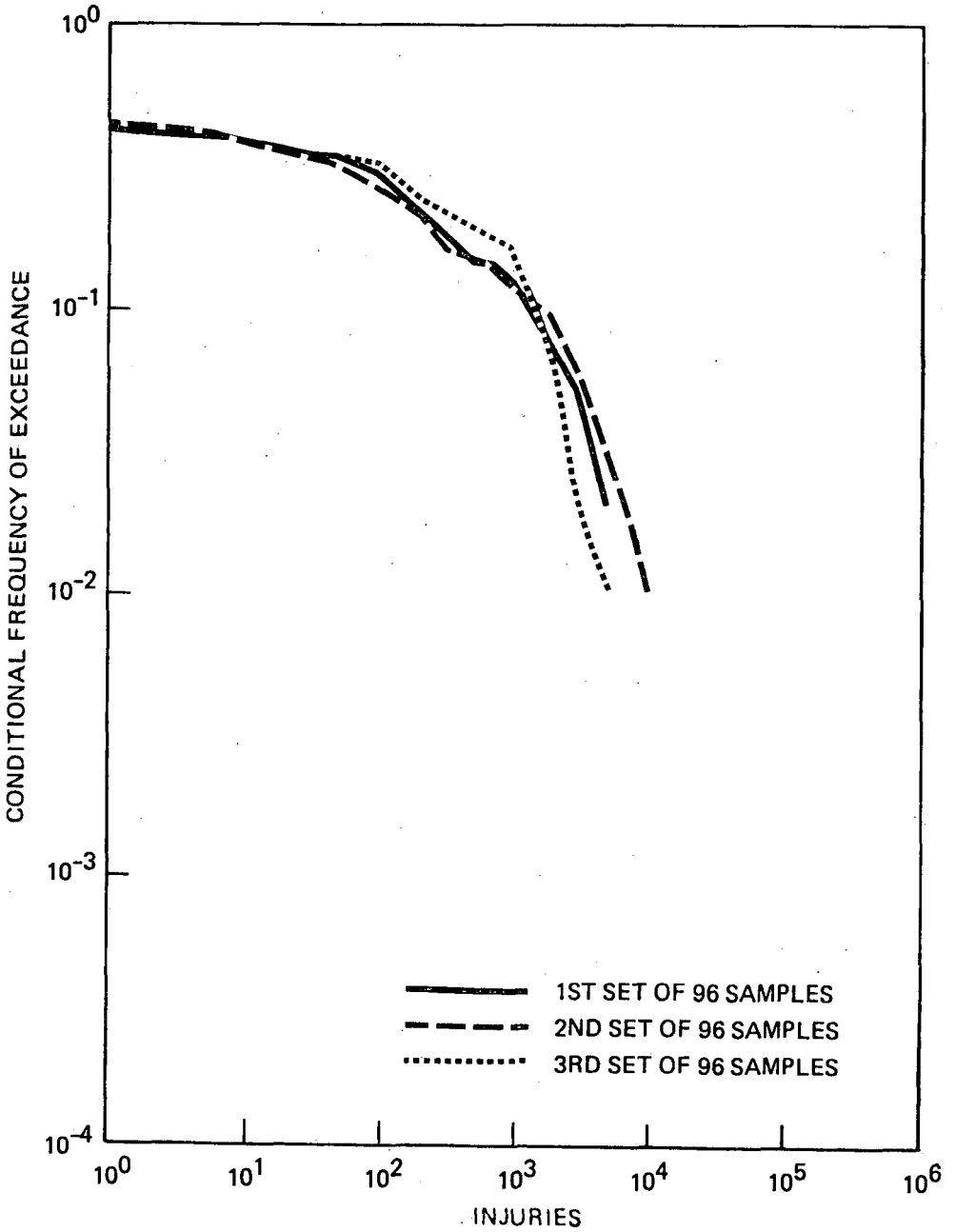


Figure 6.3-4. Comparison of Injuries Results Using Different Sets of Meteorological Sequences--IP Release Category 2

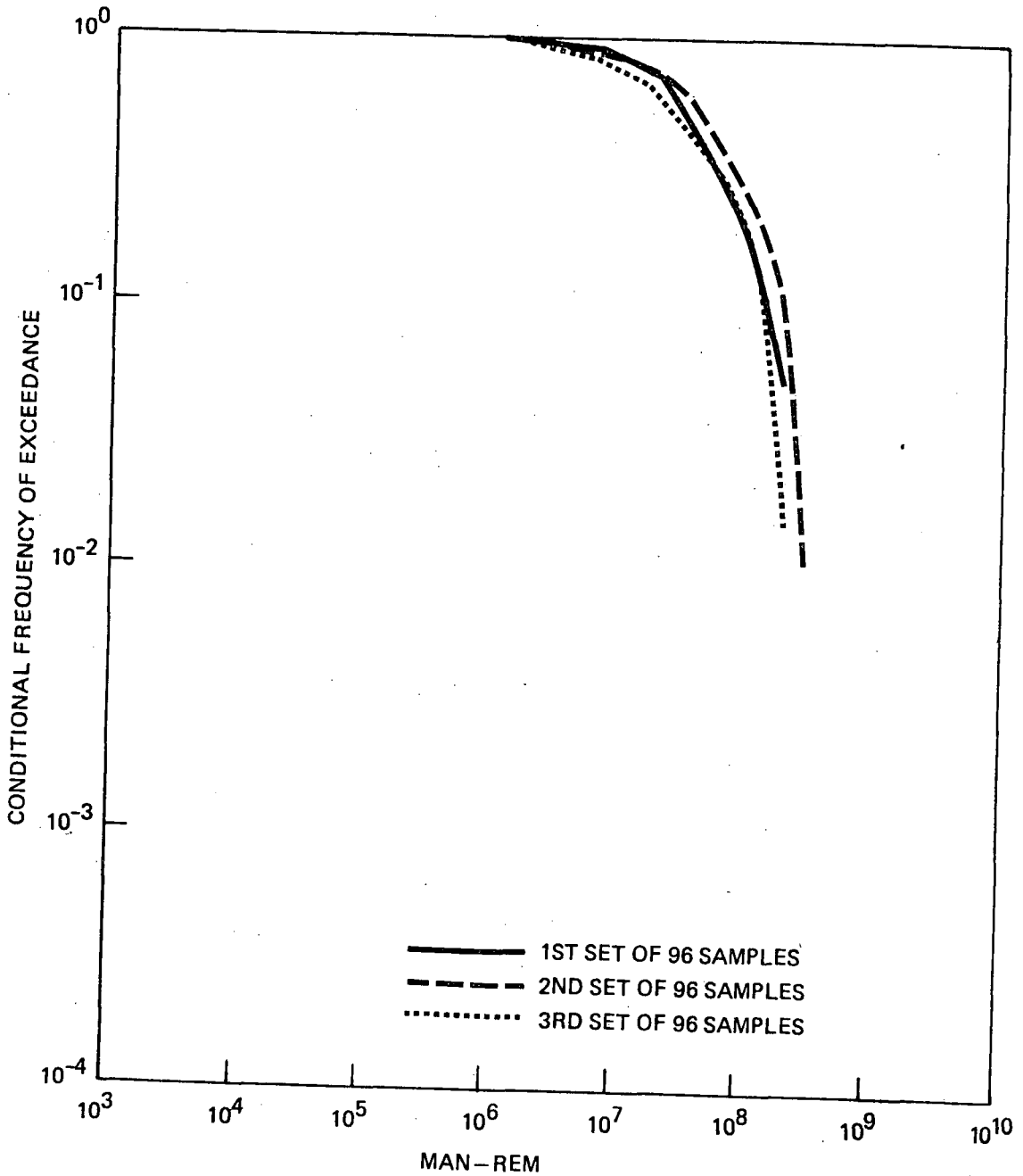


Figure 6.3-5. Comparison of Whole Body Man-Rem Results Using Different Sets of Meteorological Sequences--IP Release Category 2

6.4 RESULTS

The results of site consequence analyses can best be presented as a set of conditional consequence curves. Each release category (from Section 5) could result in a set of such curves, one for each damage index (or health effect) considered. As a matter of practicality, however, some release categories do not result in some health effects (or do so with such very low frequency that they may be deleted from consideration). Figures 6.4-1 through 6.4-5 display the conditional consequence curves resulting from this analysis. In practice, these curves are constructed from the values in the S1 site matrix. The S1 matrix is carried forward to Section 8.0 and is used along with the other three site matrices as an input to the [MCS] matrix multiplication used for risk integration.

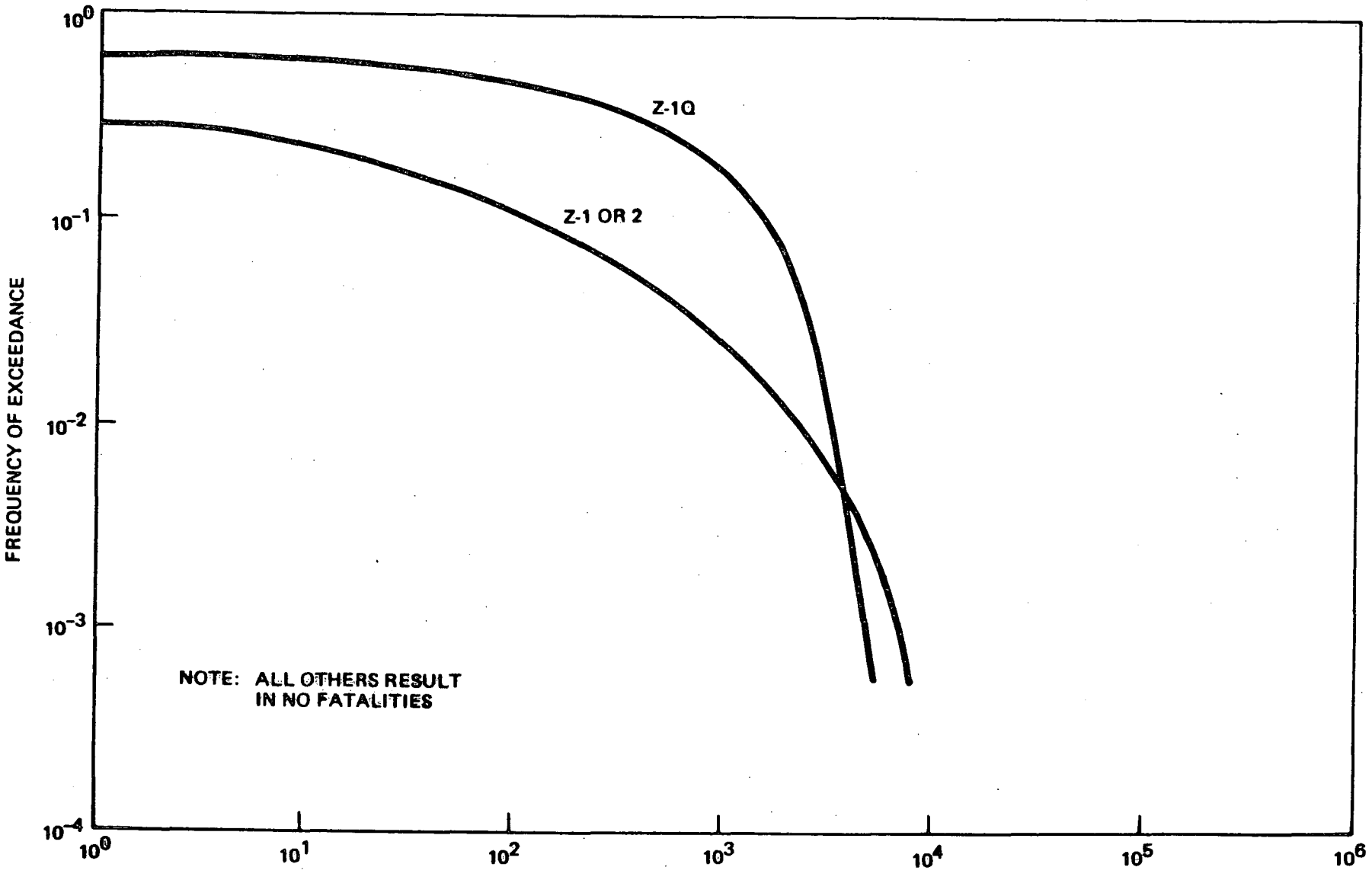


Figure 6.4-1. Conditional Consequence Curves for Various Release Categories--Damage Index: Acute Fatalities

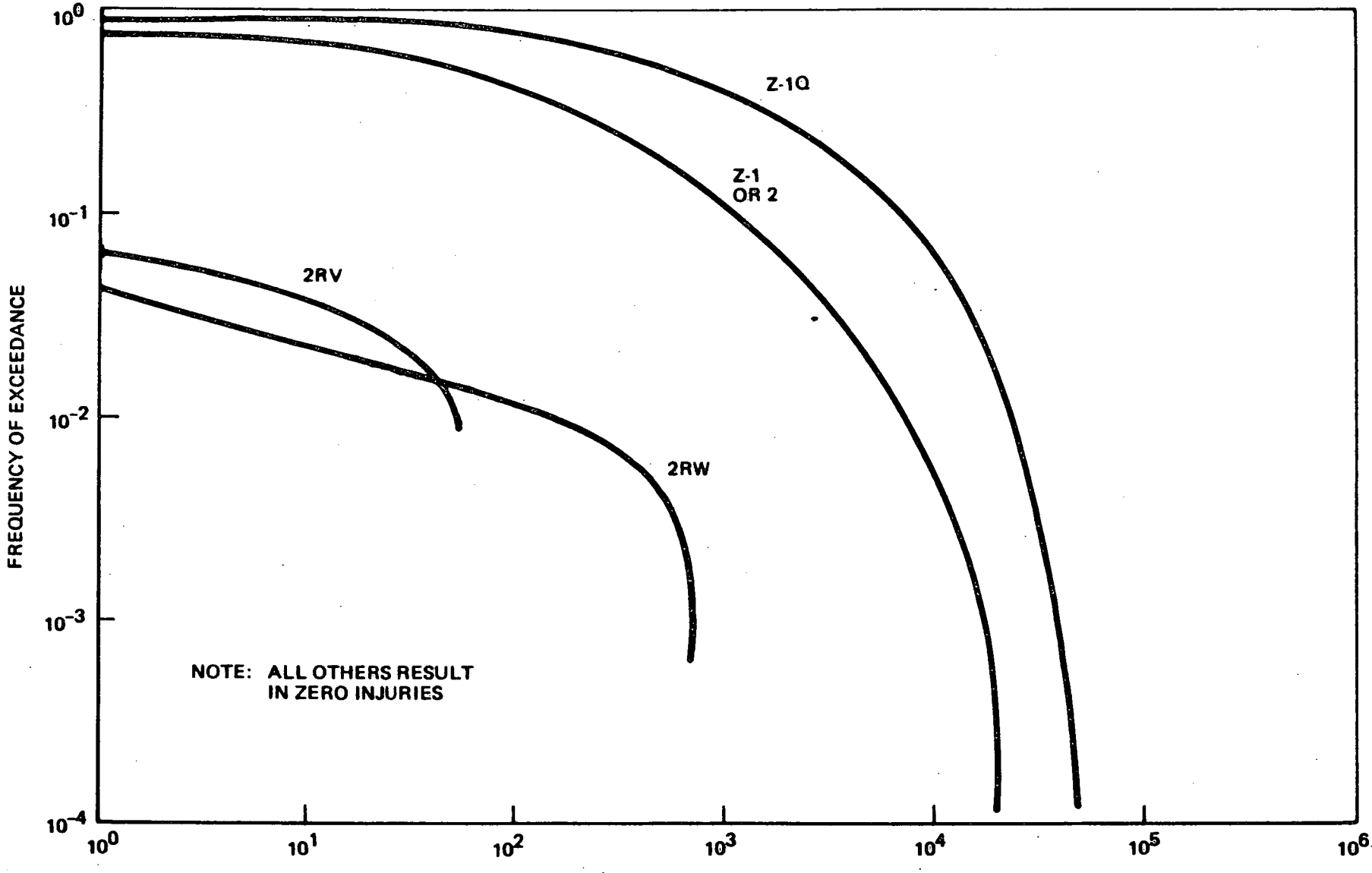


Figure 6.4-2. Conditional Consequence Curves for Various Release Categories --Damage Index: Injuries

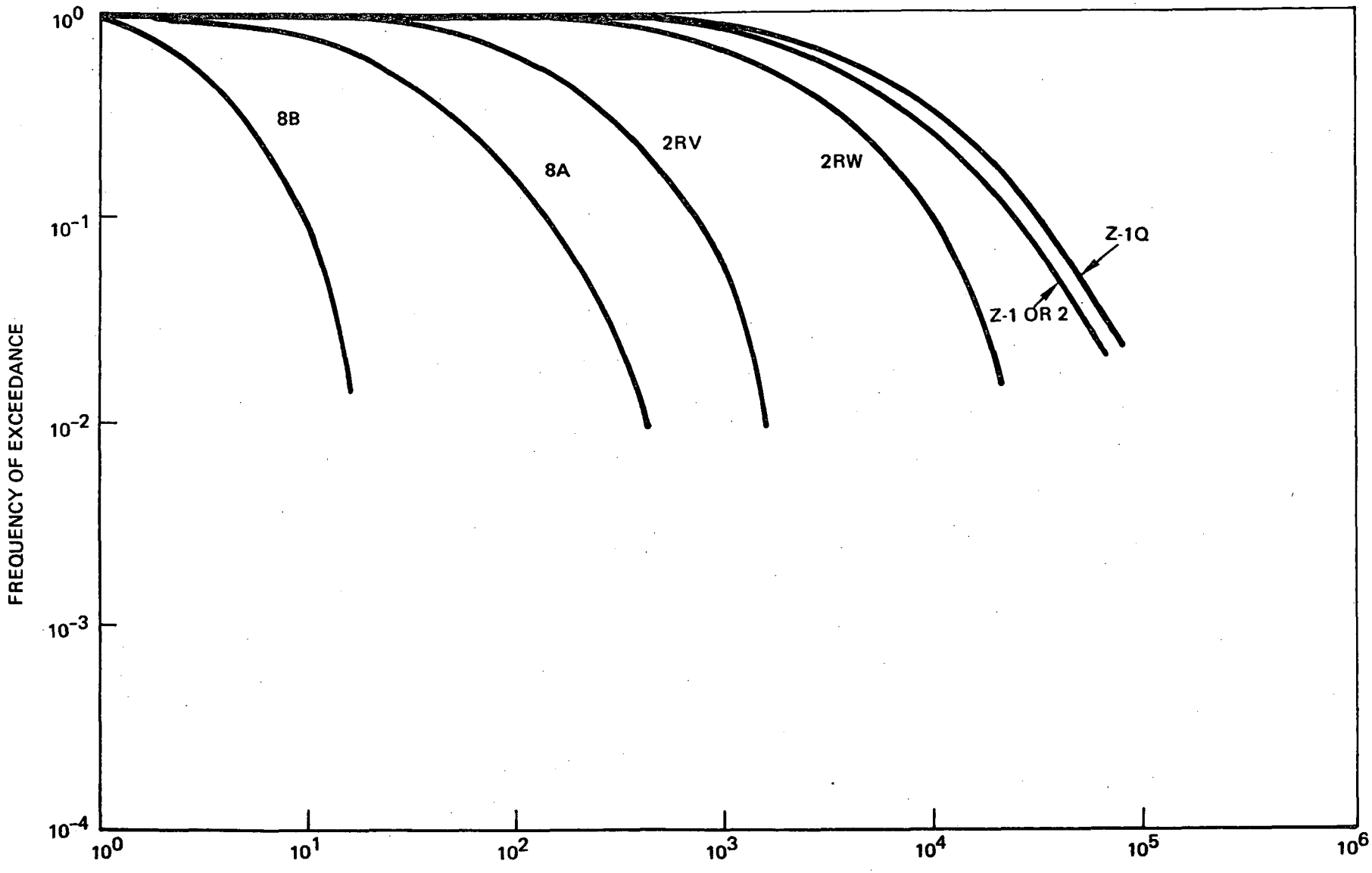


Figure 6.4-3. Conditional Consequence Curves for Various Release Categories--Damage Index: Thyroid Cancer Cases

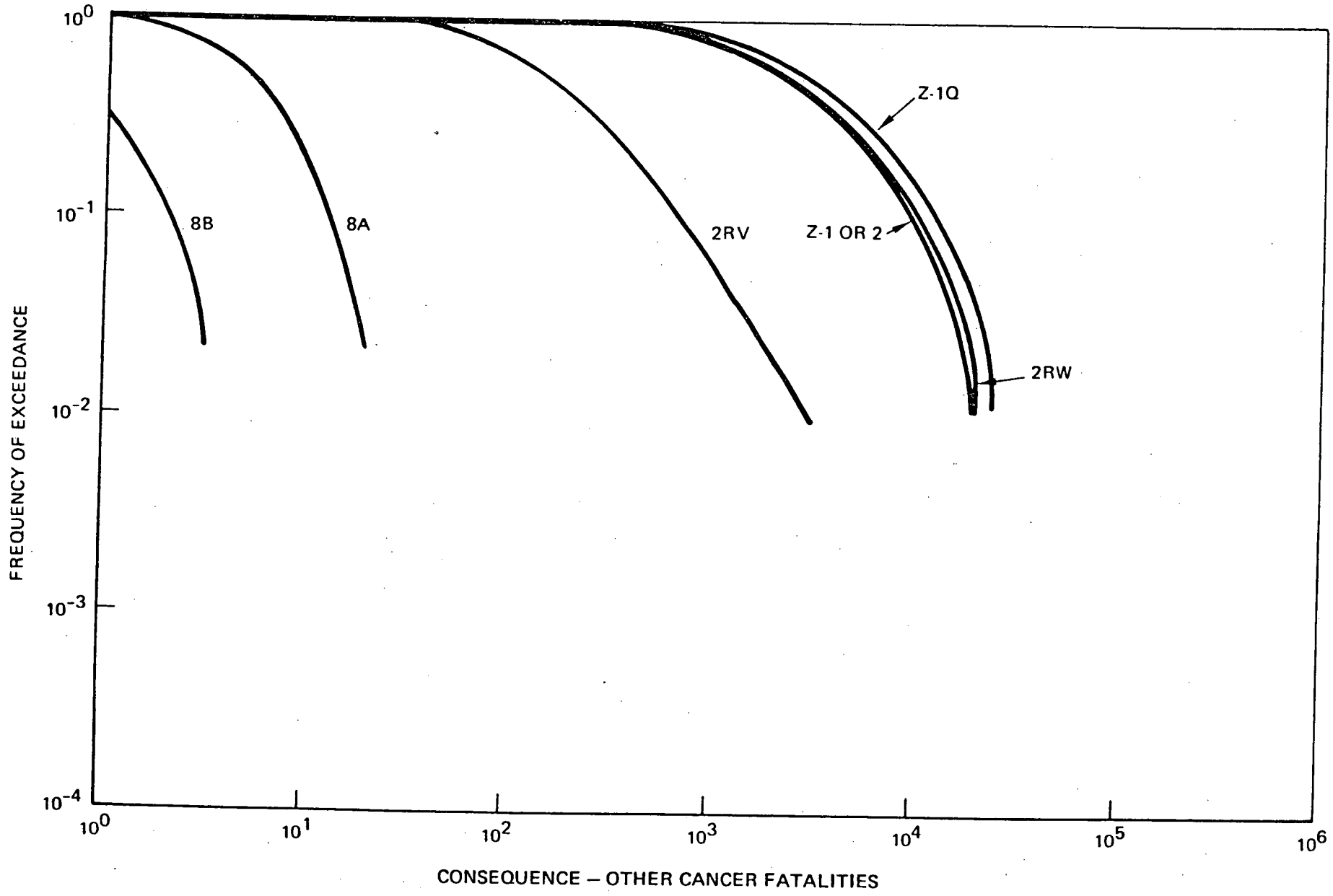


Figure 6.4-4. Conditional Consequence Curves for Various Release Categories--Damage Index: Cancer Fatalities (Other Than Those from Thyroid Cancers)

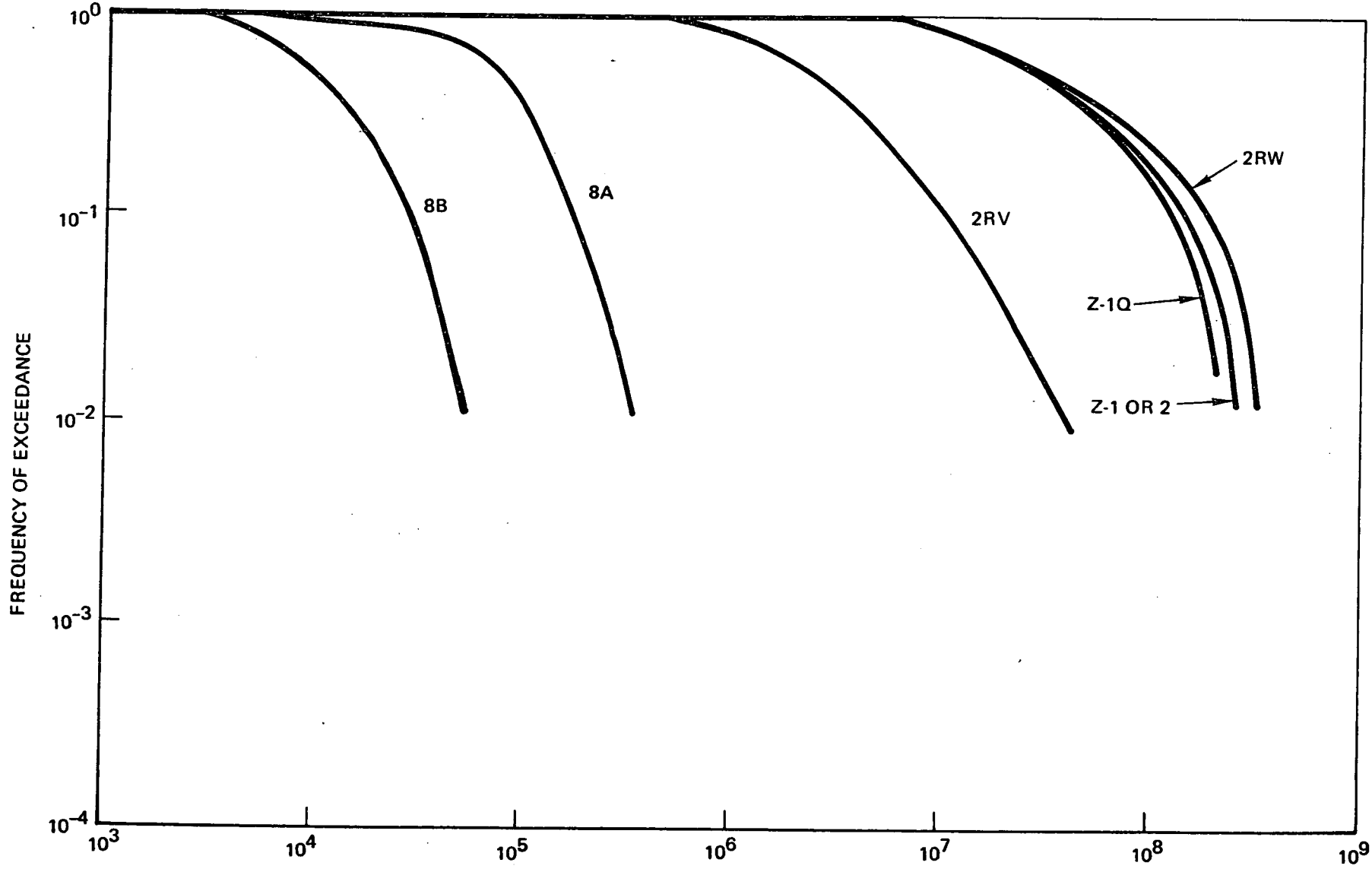


Figure 6.4-5. Conditional Consequence Curves for Various Release Categories--Damage Index: Whole Body Man-Rem

6.5 LIQUID PATHWAYS CONSEQUENCES

The sequences of events leading to failure of the containment via interaction between the basemat and molten core debris have been identified in Section 2. The frequencies of such postulated occurrences have been found to be exceedingly small; however, they were carried forward in the event trees to preserve the scenarios. An atmospheric release pathway has been assigned to these scenarios when appropriate.

Due to the proximity of the plant to the Hudson River, an analysis was performed to determine the amount of radioactive material transported to the river as a function of time, given a theoretically assumed failure of the containment basemat. Although previous studies have shown that the liquid releases contribute little to overall risk, for completeness, a liquid pathways analysis was performed and is included as Appendix 6.7.

The analysis assumed two types of source releases after basemat failure. The first type of source release postulated a long term leaching by groundwater of radionuclide from the core debris embedded in the substrata. The second type postulated direct release of sump water to the groundwater. The discussion of phenomena associated with core melt progression in Section 2 shows that release of sump water through the failed basemat is particularly unlikely. If sump water is present in the reactor cavity region at or soon after the core melt debris enters the cavity, in-place cooling of the debris is likely. Dry conditions in the cavity are necessary for significant penetration of the basemat concrete by the debris. Thus, while the release of any radioactive material to the groundwater is considered very unlikely, release via leaching of the melt debris is considered the more likely of the two release modes.

The impact of containment basemat penetration and subsequent radionuclide release through liquid pathways from sump water or long term leaching is not significant when compared with the impact from atmospheric releases. The imbalance is even more pronounced when the very low likelihood of sump water release is considered.

6.6 REFERENCES

6-1 U.S. Nuclear Regulatory Commission, "Calculation of Reactor Accident Consequences," Reactor Safety Study, WASH-1400, 1975.

6-2 U.S. Nuclear Regulatory Commission, "Onsite Meteorological Programs," Regulatory Guide 1.23, 1972.

6-3 Martin, D. O., and J. A. Tikvart, "A General Atmospheric Diffusion Model for Estimating the Effects on Air Quality of One or More Sources," paper presented at 61st Annual Meeting of the Air Pollution Control Association, 1968.

6-4 Turner, D. B., "Workbook of Atmospheric Dispersion Estimates," U.S. Department of Health, Education and Welfare, Public Health Service, Publication No. 999-AP-26, 1969.

6-5 Briggs, G. A., "Plume Rise", U.S. Atomic Energy Commission, Critical Review Series, Pub. No TID-25075, 1969.

6-6 Marshall, J. S., and C. D. Holtz, "Pattern Analysis of One Summer's Multilevel Maps of Montreal Rain," Monthly Weather Review, 98, pp. 335-345, 1970.

6-7 Austin, P. M., and R. A. Houze, "Analysis of the Structure of Precipitation Patterns in New England," J. Appl. Meteorol., 11, pp. 926-935, 1972.

6-8 Zawadski, I. I., "Statistical Properties of Precipitation Patterns," J. Appl. Meteorol. pp. 459-472, 1973.

6-9 U.S. Department of Health, Education and Welfare and Environmental Protection Agency, "Effects on Populations of Exposure to Low Levels of Ionizing Radiation," NTIS PB-239735, November 1972.

6-10 Beir, "The Effects on Populations of Exposure to Low Levels of Ionizing Radiation," 1980.

6-11 Slade, D. H., "Meteorology and Atomic Energy," 1968.

6-12 Briggs, G. A., "Some Recent Analyses of Plume Rise Observation," Proc, 2nd Int. Clean Air Congress, H. M. Englund and W. T. Berry, Editors, Academic Press, New York, pp 1029-1032, 1971.

6-13 Briggs, G. A., "Discussion on Chimney Plume in Neutral and Stable Surroundings," Atm. Env., 6, 507-510, 1972.

6-14 Briggs, G. A., "Plume Rise Predictions," Chapt. 3 in Lectures on Air Pollution and Environmental Impact Analyses, D. A. Haugen, Editor, Am. Met. Soc., Boston, MA, 1975.

6-15 Turner, D. B., "Dispersion Estimate Suggestion No. 2 (Revised)," NOAA, Model Applications Branch, 1973.

6-16 Briggs, G. A., Letter to Dr. Ian B. Wall of NRC, 4-10-78, 1978.

6-17 Kaiser, "Discussion of Plume Lift at OECD Benchmark Model Conference held in Paris, October 1980," 1980.

6-18 Bierly, E. W., and E. W. Hewson, "Some Restrictive Meteorological Conditions to be Considered in the Design of Stacks", Journal of Applied Meteorology, Volume 1, No. 3, pp. 283-290, 1962.

6-19 Lantz, "Environmental Modeling System," Air Quality Model (A Three-Dimensional Finite Difference Solution of the Boundary Layer Wind Flow and Plume Dispersion), Program User Documentation, 1974.

6-20 Lantz, R. B., K. H. Coats, and C. V. Kloepfer, "A Three-Dimensional Model for Calculating the Spread and Dilution of Air Pollutants," Proceedings, Air Pollution, Turbulence and Diffusion Symposium, New Mexico State University, Las Cruces, New Mexico, December 7-10, 1971 (Proceedings edited by H. W. Church and R. E. Luna, Atmospheric Fluid Dynamics Division 5644, Sandia Laboratories, Albuquerque, New Mexico, published March 1972).

6-21 Settari, A., and R. B. Lantz, "A Turbulent Flow Model for Use in Numerical Evaluation of Air Quality," Journal of Canadian Petroleum Technology, October-December 1974, Montreal, Canada.

6-22 Potomac Electric Power Company, "Diffusion Analysis and Ground Level Concentration Estimates for Dickerson Power Plant of the Potomac Electric Power Company," prepared by Pickard, Lowe and Garrick, Inc., in association with Intera Environmental Consultants, Inc., and Dr. James Halitsky, February 24, 1978, Revised September 4, 1979.

6-23 Hunt, J. C. R., W. H. Snyder, and R. E. Lawson, Jr., "Flow Structure and Turbulent Diffusion Around a Three-Dimensional Hill. Fluid Modeling Study on Effects of Stratification," Part 1, Flow Structure, EPA-600/4-78-041, U.S. EPA Environmental Sciences Research Laboratory, July 1978.

6-24 Halitsky, J., "Modified Potential Flow Solutions for Stratified Flow Over Irregular Terrain," Symposium on Physical Modeling and Simulation in Technics, Universita degli Studi di Trieste, Instituto di Fisica Tecnica, Trieste, Italia, June 1980.

6-25 Start, G., et al, "Diffusion in a Canyon within Rough Mountainous Terrain," NOAA Tech Memo ERLTM-ARL 38, 1974.

6-26 U.S. Environmental Protection Agency, "User's Guide to the Valley Model," Office of Air Quality Planning and Standards, Research Triangle Park, NC, 1977.

6-27 Van der Hoven, I., et al, "Report of Meteorology," SW Energy Study, Appendix E, 1972.

6-28 Weil, J. C., "Evaluation of the Gaussian Plume Model at Maryland Power Plants," presented at the Joint Conference on Applications of Air Pollution Meteorology, Salt Lake City, UT, 1977.

6-29 Lyons, W. A., and H. S. Cole, "Fumigation and Plume Trapping on the Shores of Lake Michigan During Stable Onshore Flow," J. Appl. Met., 12 (3), 494-510, 1973, Lyons, W. A., Personal Communication, 1980.

6-30 U.S. Environmental Protection Agency, "User's Manual for Single-Source (CRSTER) Model," EPA-450/2-77-013, 1977.

6-31 Hrenko, J., B. Turner, and J. Zimmerman, "Interim User's Guide to a Computational Technique to Estimate Maximum 24-Hour Concentrations from Single Sources," Environmental Protection Agency, 1972.

6-32 Holzworth, G. C., "Mixing Heights, Wind Speeds, and Potential for Urban Air Pollution Throughout the Contiguous United States," Environmental Protection Agency, Office of Air Programs, Publication No. AP-101, 1972.

6-33 National Climatic Center, "Procedure for Running STAR Program," 1976.

6-34 Aldrich, D. C., D. M. Ericson, Jr., and J. D. Johnson, "Public Protection Strategies for Potential Nuclear Reactor Accidents: Sheltering Concepts with Existing Public and Private Structures," Sandia Laboratories, SAND77-1725, February 1978.

6.7 APPENDIX - ANALYSIS OF LIQUID PATHWAYS CONSEQUENCES DUE TO BASEMAT PENETRATION

6.7.1 INTRODUCTION

As part of the overall probabilistic risk assessment being performed for Indian Point Units 2 and 3, a consequence analysis was undertaken to examine a postulated release of radionuclides through the liquid pathways following a core melt accident.

In the past, generic investigations of the above postulated release of radioactive material through the liquid pathways have been performed on several occasions. The first was the RSS (NUREG-75/014, Reference 6.7-1), which was primarily a scoping study. This was followed by the "Liquid Pathway Generic Study Topical Report," (Reference 6.7-2), and USNRC NUREG-0440 Study (Reference 6.7-3) in February 1978 which addressed the impact of accidental radioactive releases to the hydrosphere from both land based and floating nuclear power plants. In January 1980, a preliminary draft of a more detailed liquid pathways report being prepared by Sandia Laboratories was released for review (Reference 6.7-4).

These studies had a common conclusion: the consequences from a release through the liquid pathways for land based plants were small compared to consequences due to releases through the atmospheric pathways. The dominance of the consequences associated with the atmospheric pathways over the liquid pathways is expected for at least two reasons. First, there is a contrast between the time scales over which radioactivity is transported to the receptor. The atmospheric transport and contact with nearby populations can begin in a period of hours, whereas for the liquid pathways, transport and contact with the population would be measured in days, weeks, and years. Second, while initial population exposure to atmospheric releases cannot always be avoided, contact with radioactive contaminants in the liquid pathways can usually be avoided because there is sufficient time to apply interdictive measures.

The starting point for this liquid pathways analysis assumed that a core melt accident occurs in which the melt penetrates the basemat and settles into the limestone substrata below it. The source terms associated with both sump water release and leaching of the melt debris were adopted directly from the 1980 draft of the Sandia liquid pathways report (Reference 6.7-4). The times at which these sources initially enter the groundwater system were also adopted from the Sandia report. These times are 1 day for the sump water release and 1 year for the leaching of the melt debris.

As discussed in Sections 2 and 3 of this report, the probability of basemat penetration following a core melt accident is extremely low. In addition, the use of the source terms with the times at which these sources initially enter the groundwater system, as adopted from the Sandia report (Reference 6.7-4), are generally considered conservative. The effect these conservatisms have on the consequences of a postulated release through the liquid pathways will be addressed later.

The consequence analysis associated with a postulated release of radionuclides through the liquid pathways at Indian Point can be divided into five distinct parts, which are illustrated in Figure 6.7-1. They are: (1) source definition and release mechanisms, (2) site hydrology and groundwater transport, (3) Hudson River estuary and surface water transport, (4) pathways definition, and (5) dose assessment.

Each aspect of the analysis is developed individually in the following sections. Specifically, Section 6.7.2, Source Definition and Release Mechanisms, describes the assumptions regarding the radionuclide source term and the timing of its introduction into the groundwater system. Section 6.7.3, Groundwater Pathways Analysis, addresses the subject of site hydrology and groundwater transport. This section was prepared by INTERA Environmental Consultants, Inc., and GeoTrans, Inc. The results of the groundwater analysis are the radionuclide release rates to the Hudson River. Section 6.7.4, Hudson River Estuary and Surface Water Transport, discusses the river, the surface water transport phenomena in the estuary, and the model which was developed to analyze this aspect of the study. Given the source terms based on the groundwater analysis of Section 6.7.3, the associated time dependent radionuclide concentration profiles throughout the estuary are developed. Section 6.7.5, Pathways Definition, discusses the radionuclide pathways and population distribution that provide the basis for the dose assessment. Finally, Section 6.7.6, Dose Assessment, describes the dose assessment that is based on the work performed in Sections 6.7.2 through 6.7.5 and presents the results.

6.7.2 SOURCE DEFINITION AND RELEASE MECHANISMS

The radionuclide inventory used in this analysis has been adopted from the Sandia draft report (Reference 6.7-4) to maintain consistency with the generic liquid pathways analyses performed previously by the USNRC (Reference 6.7-3) and the more recent report by Sandia Laboratories for the USNRC (Reference 6.7-4).

This inventory was based on the ORIGEN computer code model of a 3,200 MW(t) Westinghouse pressurized water reactor. This is slightly conservative for the Indian Point units, but is fairly consistent with the inventory used to develop the source terms for the Indian Point atmospheric analysis, and with the results for the RSS (Reference 6.7-1).

The isotopes actually considered in this analysis are presented in Table 6.7-1. They represent the more significant radionuclides for liquid pathways, and are taken from Table A.1 of Appendix A of the Sandia draft report (Reference 6.7-4). The isotopes of elements such as xenon and krypton, which essentially all enter the gas phase and are considered in the atmospheric consequence analysis, are not included in the Sandia table.

6.7.2.1 Core Melt and Basemat Penetration

The interaction of the molten core with the containment basemat is addressed at great length in Section 3 of this report and in Appendix A of the Sandia draft report (Reference 6.7-4). In both discussions, it

is clear that the probability of basemat penetration by the melt debris following a postulated core melt accident is extremely small. The purpose of the present analysis, however, is to estimate the potential impact on the health of the surrounding population, which is conditional on a core melt accident taking place and then being followed by basemat penetration and release through the liquid pathways.

6.7.2.2 Release Mechanisms

Given the above stated assumption, it is necessary to partition those radionuclides that do not enter the gas phase into fractions that would dissolve in the water which comes into contact with the melt, and fractions that remain with the melt debris.

For many core melt scenarios, fission products released from the damaged or melted core to the containment subsequently end up in a dissolved state as a result of containment sprays and/or other sources of water, such as the primary system and accumulator tanks. This water is commonly referred to as the "sump" water since it covers the containment building and reactor cavity floors under a number of scenarios. For purposes of this analysis, sump water volume is assumed to be 40,000 feet^3, which is a representative fraction of the primary coolant volume, the accumulator tanks, and the containment sprays. The resulting fractions of each radionuclide associated with the sump water are presented in Table 6.7-1. The remaining fractions of the inventories listed in this table are associated with the melt debris and are potentially available for leaching as a function of time. These fractions are consistent with assumptions used in previous liquid pathways analysis and in particular can be found in Table 2.2 of the Sandia draft report (Reference 6.7-4).

The distinction made here is important in that once basemat penetration is postulated, there is the possibility for early introduction of radionuclide loaded sump water directly into the established groundwater system. However, delay is likely because of steam phase blockage as sump water contacts the hot melt debris beneath the basemat. Sandia postulates for calculational purposes that the sump water could be released immediately or that it could take as long as 6 months for it to begin to enter the groundwater system. The groundwater analysis, as presented in Section 6.7.3, calculates that the sump water would take approximately 4 months to drain completely if it begins to drain immediately into the groundwater system. It is again important to reemphasize that it is highly unlikely that basemat penetration would occur in the presence of sump water, which provides cooling of core melt debris.

In this analysis, the radionuclides associated with the melt debris are treated as a separate source term. The melt is assumed to have reacted with and penetrated the basemat and to have penetrated into the soil beneath. At some time after melt-through, the melt debris will have cooled sufficiently to allow the groundwater to begin leaching of radionuclides. The composition of the melt, postulated dimensions, and other details are based on Appendix A of Reference 6.7-3, and on Chapter 2 and

Appendix A of the Sandia draft report (Reference 6.7-4). These details are presented in the following sections. Leaching is assumed to begin 1 year after the core melt has taken place. This assumption is also consistent with the assumptions made in the Sandia draft report (Reference 6.7-4) and one which we believe is reasonable.

6.7.3 GROUNDWATER PATHWAYS ANALYSIS

6.7.3.1 Introduction

To evaluate the potential for radionuclide transport by groundwater beneath Indian Point, it was necessary to proceed in three stages. The first was to develop a description of the regional flow system at Indian Point. This flow system is the baseline on which any perturbations because of reactor events would be superimposed. Available data were collected from a variety of sources and were synthesized using a steady state groundwater flow model to give a consistent regional description of groundwater flow.

The second stage was to characterize scenarios that would lead to the introduction of radionuclides into the groundwater system. Several previous analyses of liquid pathways were available (References 6.7-3 and 6.7-4). From these, it was apparent that two end-member scenarios should be considered. One is the sump water release scenario in which it is assumed that the containment building basemat has been ruptured, leading to the discharge of sump water directly to the groundwater system. In this scenario, the core itself is not explicitly considered other than as the source of radionuclides to the sump water. The second is the core melt-through scenario, in which it is assumed that the core and entrained material actually enter the groundwater system, and nuclides are then leached from the core by moving groundwater. The leaching source is considered to be more likely in the event of melt-through (see the discussion in Section 2).

The third stage was to calculate the consequences of these scenarios, expressed as nuclide fluxes into the river. In all cases, an attempt was made to choose models that were consistent with the available data to analyze the various scenarios. Uncertainties in the calculated consequences were also addressed, based on estimates of the uncertainties inherent in the hydrologic information available.

6.7.3.2 Groundwater Hydrology

6.7.3.2.1 General

In this section an overview of groundwater hydrology is presented. Common terminology is discussed in Section 6.7.3.2.2. For more details, a text on groundwater hydrology, such as that by Freeze and Cherry (Reference 6.7-5) should be consulted. Data sources are discussed in Section 6.7.3.2.3 and the site geology is summarized in Section 6.7.3.2.4. Finally, existing groundwater hydrologic data are reviewed in Section 6.7.3.2.5.

6.7.3.2.2 Review of Basic Concepts

Groundwater is the water below the land surface that fills pores or fractures in soil and rock. This water filled space is generally measured as a volumetric percentage of the total volume and is labeled porosity (dimensionless). Just as the water level of a river can be measured and used to partially determine the flow of the river, groundwater levels can also be measured and used to help determine flow. Groundwater levels, generally measured in wells, are expressed relative to a datum of mean sea level elevation and are called hydraulic heads (length). The three dimensional surface that hydraulic-head measurements produce is called the potentiometric surface. Groundwater also flows from a higher to a lower hydraulic head, just as water in a river flows downhill (that is, from a higher water level to a lower water level).

Groundwater, unlike river water, has to overcome the resistance to flow by rocks or soil. Hydraulic conductivity (length per unit time) is a measure of how well a rock or soil transmits water. The direction of groundwater flow is determined by the hydraulic-head gradient (changes in head with distance), whereas groundwater flow rates are determined by both hydraulic conductivity and the hydraulic-head gradient. Wells are again required, along with pumping tests, to determine hydraulic conductivity. In a pumping test, one well is pumped and the decline in water level in nearby observation wells or in the pumping well itself is measured. Using the pumping as the forcing function and the water level measurements as the response, hydraulic conductivity may be "backed out." The parameter's porosity, hydraulic gradient, and hydraulic conductivity are especially important in groundwater contamination problems since they determine the convective flow rates of the fluid transporting agent. They also determine travel times of the contaminant.

The term "aquifer" is used to indicate a layer of rock and/or soil that can transport reasonable amounts of water; that is, a layer with significant hydraulic conductivity. Often, aquifers are found to have sufficient uniformity with depth so that their properties can be described as averages over thickness. Transmissivity (length squared per unit time) is the product of hydraulic conductivity and the aquifer thickness. It represents the ability of the entire thickness of the aquifer to transmit water.

In addition to their ability to transmit water, aquifers are reservoirs that store water. Their storage properties (over the entire thickness) are described by the storage coefficient (dimensionless). The value of this coefficient varies widely depending on whether or not the aquifer is entirely saturated. This parameter is also determined from pumping tests, but only enters into an analysis when transient groundwater flow is considered. Transient, as opposed to steady state flow, implies that hydraulic head varies with time. Steady state implies that there is no net change in storage. That is, recharge, such as infiltration from rainfall, equals discharge, such as seepage to a river.

The flow of water through the rock or soil can be described by using the equation for fluid flow in porous media. This is a partial differential equation with appropriate boundary and initial conditions. The parameters are source/sink terms, transmissivity multiplying the space derivative, and storage coefficient multiplying the time derivative in which the dependent variable is hydraulic head. For steady state flow the time derivative is zero and the parameters reduce to source/sink terms, such as recharge and transmissivity.

Boundary conditions are generally of the specified head or the specified flux type. An example of a specified head boundary is the intersection of an aquifer and a large river or lake which holds the water level in the aquifer at a relatively constant level. In the special case of a specified flux boundary the flux is zero, a condition used to represent the contact of an aquifer with a unit of low permeability. Given boundary conditions and equation parameters, the partial differential equation may be solved to obtain the hydraulic head distribution and, in turn, to compute groundwater velocities. For contamination problems, these velocities are used in an additional partial differential equation that describes the transport of solutes. The solution to this equation provides concentration distributions.

6.7.3.2.3 Data Sources

Data sources on the groundwater hydrology of the Indian Point region considered in this study included: (1) county groundwater reports published by the U.S. Geological Survey; (2) environmental impact statements prepared for the site; (3) base maps and boring information from Consolidated Edison Company of New York, Inc., and the Power Authority of the State of New York; and (4) discussions with personnel from these companies.

6.7.3.2.4 Geology

The Indian Point Reactor site is located in Westchester County, New York, southwest of Peekskill and about 40 miles north of New York City. It is situated approximately 500 feet from the east bank of the Hudson River. In this vicinity, the Hudson River ranges from 4,500 to 5,000 feet in width and has maximum depths from 55 to 75 feet. On the side away from the river, the ground rises 600 to 1,000 feet above sea level (see Figure 6.7-2).

The geology of the site consists of fractured limestone covered by a thin veneer of unconsolidated deposits. The limestone is bounded to the east and north by hills and ridges of phyllite and schist. According to Metcalf & Eddy Engineers (Reference 6.7-6), "Unconsolidated deposits cover most of the bedrock in this area and range in thickness from a few feet in the hills to several hundred feet in the larger valleys. Unconsolidated deposits range from clays, which produce only meager quantities of water, to coarse sand and gravel capable of yielding several hundred gallons per minute (gpm) to a well." The phyllite and schist are the uppermost formation of sedimentary origin (Reference 6.7-6).

These rocks yield very little groundwater as shown by a well drilled for the Indian Point Park. The well was drilled into the schist and, even following blasting, the yield was only 3.75 gpm (Reference 6.7-7).

Indian Point Units 2 and 3 are founded in the limestone. Therefore, this geologic rock formation is discussed in more detail than the other geological material. According to Thomas W. Fluhr (Reference 6.7-6),

> Beneath the phyllite or schist, and apparently conformable with it, is a limestone. The limestone has a well-defined layered structure, believed to be original bedding, which strikes N to NE and dips to the east at 45 to 65 degrees. This layered structure is marked by shear planes and, rarely, thin shaley layers. The notable feature of the limestone is its extremely jointed condition. A major joint system extends at about right angles to the bedding structure but, in addition, there are also many irregular joints. The jointing has an intensity which might almost be described as brecciation. The joints are open but few display decay. This limestone formation is not cavernous.

Fluhr goes on to say, "When test borings are made into the limestone there is no return of drill water; it all runs away into the limestone."

Because the limestone and phyllite or schist are probably conformable, and the bedding planes in the limestone are dipping easterly at 45 to 65 degrees, the contact between the limestone and phyllite or schist is probably also dipping similarly. Other structural features at the site including several faults passing through the site are discussed by Dames & Moore (Reference 6.7-8). It is interesting to note that some of the faults examined were "characterized by discontinuous healed breccias" and "filled with deformed calcite."

Based on these descriptions of the limestone, it is difficult to qualitatively ascertain whether the hydraulic conductivity is high or low. The loss of drill water would indicate a relatively high hydraulic conductivity, whereas the description of the healed breccias and calcite fillings tend to support a low hydraulic conductivity. This topic is discussed further in Section 6.7.3.3.3.

6.7.3.2.5 Existing Data

Existing data consisted of that published in the site reports referenced previously. These reports represent work that emphasized foundation engineering (groundwater concerns were minor). Therefore, no pumping tests were made to determine hydraulic conductivity and no potentiometric surface maps were included in the site reports.

Borings were made at the site and water levels were taken. Boring logs were made available by Consolidated Edison Company of New York and by the Power Authority of the State of New York. From the water level measure- ments included in these logs, a potentiometric surface map was constructed. This map is discussed later in Section 6.7.3.3.3 and shown in Figure 6.7-3. As will be seen, the map provides only partial coverage of the site.

6.7.3.3 Analysis of Available Data

6.7.3.3.1 General

This section describes the analysis of the available water level data. Numerical results that provide a two dimensional match to the water level data are presented in Section 6.7.3.3.3. The purpose of this section is to assess the groundwater properties and conditions at Indian Point. The results from this section will be used to help analyze what might occur in the groundwater in the event of a release of radionuclides. Before proceeding to the analysis, we first discuss the basic approach used.

6.7.3.3.2 Approach

Because the limestone is jointed and fractured, a general discussion concerning flow in fractured media is appropriate. Two approaches for simulating flow in fractured media have been used: discontinuum and continuum. The discontinuum approach treats each fracture discretely, and requires a geometrical description of the fracture surface and its width. In the continuum approach, the scale of the problem is assumed to be large enough that meaningful averages of fluid pressures and velocities in fractures can be defined. Regional aquifer studies show that porous media models can be applied with good results.

While groundwater flow in fractured media is an area of current research, chemical transport processes in such media are understood even less. For this reason and because of the limited data, it is assumed the problem can be averaged and treated using an equivalent porous media model. Perhaps the most important implication of this assumption is that computed velocities and travel times are taken as the values for average fractures. If the transmissive characteristics of individual fractures vary over a wide range, they may lead to overestimates of travel times.

Once an equivalent porous medium is assumed, the next step is to formulate a conceptual model to provide boundaries and boundary conditions for the mathematical model. The aquifer under the Indian Point reactor site is assumed to be composed of a thin veneer of soil (a few feet to tens of feet thick) overlying fractured limestone. Although no data are available for modeling purposes, the limestone is assumed to extend to 100 feet below mean sea level. This provides a depth below which the conductivity of fractures is substantially reduced.

Figure 6.7-3 shows the boundaries chosen for the problem. The lower boundary of the limestone is assumed to follow the river and the head is assumed to be zero. Although the stage of the river at this location varies by several feet with the tide, the assumption of zero head represents an approximate time average. As Figure 6.7-3 shows, the limestone is bounded to the north and east by the phyllite or schist. Because these are known to conduct very little water, the contact between the limestone and phyllite or schist (which dips steeply) is treated as a no

flow boundary. To the south in Figure 6.7-3, the flow is expected to follow the topography. Therefore, the south boundary is considered to follow a flow line and is also treated as no flow.

It is also assumed that the flow field at Indian Point does not vary with time and, therefore, is at steady state. The construction at the site was carried out in phases over a period of time. Available water level measurements were taken at different times during construction. This is an important factor because the magnitude and spatial distribution of the recharge would depend on the existence of buildings, parking lots and drainage systems at any given time. Accordingly, it was decided to investigate and to simulate steady state flow for the two endpoints of this period: first, with no buildings on the site and, second, with all construction features in place as the site exists today.

6.7.3.3.3 Two Dimensional Match

A two dimensional, numerical match to the water level data available for the aquifer under the Indian Point site was undertaken, using the boundary conditions outlined in Section 6.7.3.3.2. As discussed, the available potentiometric heads are confined to a limited area around Unit 3. As shown in Figure 6.7-3 the hydraulic head gradient is high. The parameters manipulated to obtain the match were recharge and hydraulic conductivity.

The system is treated as a two dimensional, areal flow problem. A finite difference numerical model was constructed using a version of the SWIFT code (Reference 6.7-9). The finite difference grid used is shown in Figure 6.7-4. The model has the facility to input variable recharge into selected grid blocks and, depending on the boundary conditions, yields a steady state head surface. The boundary condition at the river corresponds to zero head at the river. The entire system was divided into a rectangular grid of 29 by 19 blocks. The impermeable phyllite boundary was defined by assigning very small transmissivities to the blocks outside this boundary. The grid is aligned with the river and limestone outcrop; this also aligns with many of the regional structural features.

Because of a lack of data on the geologic properties, the two dimensional system was assumed homogeneous and isotropic, i.e., with hydraulic conductivity uniform in all directions. Therefore, a single value of conductivity was determined for reasonable values of recharge in order to obtain a potentiometric match. Because the simulations were at steady state, there was no accumulation within the system and the porosity did not enter the computations. Porosity would, however, directly affect the travel time as discussed below.

Groundwater recharge values are difficult to measure directly. Of the few reported, many were found by water balance studies. No measured recharge values are available for the Indian Point site, nor is there enough information to construct a groundwater balance for the site and thus obtain recharge by difference. Therefore, it has been necessary to estimate a site recharge value based on results reported for similar geographic and geologic terrains (Reference 6.7-10).

From these results, the site average recharge is estimated as 5 inches per year. This is not distributed evenly over the total site area but will vary locally because of topography and such man-made features as drainage structures, buildings, and pavement. The local effects of these features have been taken into account, but the site wide area average of 5 inches per year has been maintained.

To simulate the recharge over the system, the area was divided into four major regions, A, B, C, and D, of Figure 6.7-4. The recharge values used in these four areas were adjusted to match the observed hydraulic heads and were consistent with the local topography. The inclination of the entire terrain is downward from left to right in the direction of flow of the Hudson River. Figure 6.7-3 shows that area A is relatively high (90 feet) and slopes down to the system boundaries nearby. Area B is much flatter and would lose precipitation by runoff less rapidly and therefore, would have higher recharge. Another reason for this higher recharge is the soil cover of about 7 to 15 feet above the phyllite. Although the phyllite is treated as impermeable, there is probably some flow across the uphill boundary that recharges area B through the soil cover. Area C is the lowest part of the terrain, but it also includes a valley with a gutter that would provide substantial surface runoff. The remaining grid blocks are the fourth region, D. The final values of recharge in these four areas (A, B, C, and D) were 10, 25, 2, and 5 inches per year, respectively.

With these recharge values, the best match to the 40-foot contour is achieved with a hydraulic conductivity, K, of 0.2 feet per day. The shape of the other contours agree; however, their locations do not match. A more accurate match could be made by locally varying both recharge and conductivity; however, this would be justifiable only if more data were available over a greater part of the area. The final match between observed and numerical contours is shown in Figure 6.7-5. This match corresponds to the site with no buildings.

Finally, calculations were made that removed all the recharge from area D, which is now covered by buildings and paving, but with conductivity left unchanged. This was done to assess the effect of the buildings and their associated drainage systems which prevent recharge into the blocks of area D on the groundwater flow system. The shape of the contours did not change perceptibly, but the hydraulic gradient was reduced by roughly a factor of 40% in the region of interest. Therefore, a better match to the 20-foot and 10-foot contours was obtained, but the observed 40-foot contour was about 26 feet in the numerical simulation.

The bottom of the aquifer was assumed to be at 100 feet below sea level. This assumption affects the value for the aquifer's saturated thickness. This, in turn, affects the value of transmissivity used in the model. As discussed in Section 6.7.3.2.2, transmissivity is the product of thickness and hydraulic conductivity. Therefore, if the saturated thickness were reduced by a factor of 2 to 50 feet instead of 100 feet to maintain the same transmissivity used to match the measured

potentiometric surface, the hydraulic conductivity would need to be increased by a factor of 2 to 0.4 feet per day, which is still relatively low. Thus, it appears that the water level data tend to support the observations of low values of hydraulic conductivity discussed in Section 6.7.3.2.4.

6.7.3.4 Nuclide Release to Groundwater

6.7.3.4.1 General

In this section, two scenarios by which radionuclides could be introduced to groundwater are discussed and their consequences analyzed. The first involves the discharge of sump water directly to the groundwater through a rupture in the basemat of the containment building. The second scenario is the one in which the core and entrained material actually enter the groundwater system, and nuclides are then leached from the core by moving groundwater.

To analyze the consequences of the two scenarios, it is necessary to determine the nuclides present at the time of release. These data are provided in Section 6.7.3.4.2. In Section 6.7.3.4.3 the uncertainty associated with the analysis of travel times to the Hudson River is addressed. In Sections 6.7.3.4.4 and 6.7.3.4.5, the analyses of the two release scenarios are discussed.

6.7.3.4.2 Nuclide Source Inventory

The radionuclide inventory of a reactor depends on the length of time the reactor has been operating and its power. For conservatism, it is assumed that at the time of a hypothetical accident the reactor has been operating for its entire design life at its maximum power. The nuclide inventories are calculated using the code ORIGEN. No ORIGEN runs were made by INTERA for this study; however, the results of such runs made by Sandia Laboratories (Reference 6.7-4) were available. From Table A1 of the Sandia report, the initial core inventory given in Table 6.7-2 was selected.

While all these nuclides will be present in the core at the time the postulated core-melt accident begins, the temperature would be so great that the nuclides will be partitioned into several different phases. In particular, the gaseous nuclides, especially those of Kr and Xe, will enter the gas phase in the containment vessel and will not enter the liquid pathways calculations at all. Therefore, no isotopes of these elements are listed in Table 6.7-2. Other normally nongaseous isotopes will also be volatile at the temperatures attained by the melting core. It is likely that the water flooding the system will dissolve these elements. The amount of each nuclide which ends up in the sump water is the sump water source fraction shown in Table 6.7-2. This source fraction was evaluated by Ritzman and others (Reference 6.7-1) as part of the RSS. Their values form the basis for subsequent studies such as those by the USNRC (Reference 6.7-3) and Sandia Laboratories (Reference 6.7-4).

It is also necessary to estimate how the various elements will behave once they have entered the groundwater system. Such an estimate can be made if all reactions between dissolved elements and the rock in which the groundwater is flowing are considered to be simple sorption reactions. Then the amount of nuclide present on the rock will be directly proportional to the amount present in the fluid. This proportionality constant is called the distribution coefficient, K_d. From it one can calculate the rate of movement of an element in a flowing groundwater system relative to the rate of flow of the transporting water itself according to the expression

$$\frac{\text{Water Velocity}}{\text{Nuclide Velocity}} = 1 + \frac{\rho}{\phi} K_d \qquad (6.7\text{-}1)$$

where

ρ = aquifer bulk density

ϕ = aquifer porosity (Section 6.7.3.2.2)

The values of the distribution coefficient for the Indian Point system are given in Table 6.7-2. Only a few distribution coefficients for the various elements have been measured in a limestone matrix and it has been necessary, therefore, to estimate the distribution coefficients of most of the elements. These estimates assume that sorption behavior is based largely on electrostatic attraction between a positively charged species in solution and negatively charged solid rock surface. Thus, elements whose dominant solution species is unchanged or negatively charged are likely to be considerably less sorbed than elements with positively charged solution species. When measured distribution coefficients are not available, Table 6.7-2 lists the solution species likely to be dominant in the groundwater system at Indian Point considering the hydrolysis behavior of the several elements.

Distribution coefficient values reported in the literature vary widely, even for a single element. For example, Table A1 of the Sandia draft (Reference 6.7-4) lists k_d values from 0 ml/gm for Ru through 20 ml/gm for Sr to 2,000 ml/gm for Pu. The nonzero values are considerably larger than those appropriate for use in calculations specific to the Indian Point site that are listed in Table 6.7-2. From this table, for example, the k_d for Sr is 0.5 ml/gm, while that for Pu is 10 ml/gm. Both are considerably smaller than the Sandia values.

For the nuclide travel times needed for the consequence calculations, the k_d value is less important than the retardation resulting from it. As Equation (6.7-1) shows, the retardation also depends on the bulk density, ρ, and porosity, ϕ, of the aquifer. The Sandia report (Reference 6.7-4) chose a value of ρ/ϕ of 5 for its generic calculations. Using this with the Sandia k_d values in Equation (6.7-1) leads to retardation factor values of 101 for Sr and 10,001 for Pu. For Indian Point, however, the proper ρ/ϕ value is 540 (see

Section 6.7.3.4.4). Using this value with the k_d values of Table 6.7-2 in Equation (6.7-2) leads to retardation factor values of 271 for Sr and 5,401 for Pu. These agree more closely with the Sandia report values than do the raw k_d values. That they do not agree more closely is a result of the consideration of recent laboratory data on k_d values for limestone (Seitz, and others, Reference 6.7-11) that apparently were not yet available to the authors of the Sandia report.

6.7.3.4.3 Travel Times and Uncertainty Analysis. The interstitial velocity of flowing groundwater can be written

$$v_i = \frac{K}{\phi} \frac{\partial h}{\partial s} \qquad (6.7\text{-}2)$$

where

v_i = interstitial velocity (ft/day)

K = hydraulic conductivity

ϕ = porosity (dimensionless)

$\frac{\partial h}{\partial s}$ = hydraulic gradient (dimensionless)

This section focuses on the travel time, a parameter that is computed based on almost all the physical characteristics of the system and contaminant, except the half-life of the radionuclide. The radionuclide half-life, however, is what makes the travel time a significant parameter. If the contaminant were nondecaying, its impact at the discharge point would be independent of the travel time. Assigning a particular travel time renders the highly radioactive isotopes least hazardous, i.e., the threat posed by any isotope is described by the relation between its half-life and the travel time.

Travel time, t, is simply distance, L, divided by interstitial velocity, v_i. These velocities and travel times must be adjusted for the retardation effects described in the preceding section. The complete expression for nuclide travel times is

$$t = \frac{L\phi}{K\frac{\partial h}{\partial s}} \times \left(1 + \frac{\rho}{d} k_d\right) \qquad (6.7\text{-}3)$$

Considerable uncertainties are associated with ϕ, K, and k_d, which lead to uncertainties in the resulting calculated travel time. In this section, a best estimate travel time to the river is calculated for nuclides with various properties without regard to the scenario by which they entered the groundwater system. The uncertainty of this estimate is then evaluated for three cases, each representing a different set of assumptions regarding the relationship between porosity and hydraulic conductivity, using Monte Carlo simulation techniques.

From the preceding sections, the following parameters were selected for evaluating t in Equation (6.7-3):

L = 475-foot distance from containment (IP-3) to river, (Figure 6.7-2)

K = 0.2 feet per day (Section 6.7.3.3.3)

$\frac{\partial h}{\partial s}$ = 0.062 (from two dimensional match)

ρ = 2.7 gm/ml; common limestone density (Reference 6.7-14)

ϕ = 0.005 effective porosity (typical of fractured limestones, Reference 6.7-15)

k_d = 0 to 10 ml/gm (See Table 6.7-2)

There is a discharge canal between Indian Point Unit 3 and the river (Figure 6.7-2). The canal bottom elevation is reported to be 20 feet below mean sea level, relatively shallow compared to the estimated depth of groundwater circulation (100 feet). Therefore, dominant nuclide flow will be beneath the canal to the river, and a larger distance was chosen for evaluating t. If travel times to the canal are desired, however, they will be 300/475 or approximately 63% of those to the river, because by Equation (6.7-3), travel time, t, is directly proportional to distance, L.

These values are best estimates from the base map, potentiometric surface, steady state simulation, and hydrologic judgment. Using these values, Equation (6.7-3) gives a travel time for a perfect tracer ($k_d = 0$) or for the water alone of 190 ($= 10^{2.28}$) days.

Freeze (Reference 6.7-16) presents a large body of direct and indirect evidence supporting a lognormal frequency distribution for hydraulic conductivity. If hydraulic conductivity is assumed to be lognormally distributed, a new parameter $y = \log K$ can be defined that is normally distributed and can be described by a mean value, μ_y, and a standard deviation, σ_y; that is,

$$N[\mu_y, \sigma_y]$$

For this application, $\mu_y = -0.70$ and $\sigma_y = 0.5$; that is,

$$K = 10^{-0.7 \pm 0.5} \text{ ft/day}$$

This is the value obtained from the steady state match of the potentiometric surface with the standard deviation of one-half log unit, which is the average value for the limestone data presented in Freeze (Reference 6.7-16).

For the first simulation, Case 1, the best estimate for porosity, $\phi = 0.005$, is used, and values of K are chosen from a lognormal probability distribution. This is done by recognizing that the values of $y = \log K_i$ come from a normal probability distribution. The normal generator is

$$y = \sigma_y S_n + \mu_y \qquad (6.7\text{-}4)$$

where S_n is a random number taken from a normal distribution with a zero mean and a standard deviation of one, N[0,1]. To obtain S_n, we use a random number, R_n^*, uniformly distributed on the interval (0,1). R_n^* is used to compute S_n (also called the random normal deviate) by

$$S = (-2 \ln R_n^*)^{1/2} \sin 2\pi R_n^* + 1 \qquad (6.7\text{-}5)$$

(see Reference 6.7-17). Using the value of y from Equation (6.7-4), hydraulic conductivity is computed from

$$K = 10^y \qquad (6.7\text{-}6)$$

and is used in Equation (6.7-3) to compute the travel time to the Hudson River. To check convergence, the Monte Carlo simulations were run for 100, 200, 400, 800, 1,600, 3,200, and 6,400 events. A convergence appeared to exist and the 6,400 event distribution was used.

A plot of the fraction of events in each interval versus the logarithm of travel time for a perfect tracer ($k_d = 0$) is shown in Figure 6.7-6. Case 1 is where the "best estimate" for porosity is used. Note that if porosity were decreased by an order of magnitude, the plot would shift one log unit to the left.

The spread of the plotted travel times reflects the confidence with which one is able to specify them, given the precision of our estimate of the hydraulic conductivity, K. A range of 2σ on each side of the mean groundwater travel time of 190 days ($10^{2.28}$) encompasses the 95% confidence interval and is shaded in Figure 6.7-6. Based on the tabulated mean and standard deviation (Table 6.7-3), this means that there is a probability of less than 0.05 that the travel time of a tracer (nonretarded element) will be greater than

$$1{,}900 \text{ days } (10^{2.28 + 2 \times 0.50})$$

or less than

$$19 \text{ days } (10^{2.28 - 2 \times 0.50})$$

In Case 2, constant porosity is not assumed, but rather, following Maini (Reference 6.7-18) porosity is assumed proportional to the square root of hydraulic conductivity

$$\phi = a \sqrt{K}$$

Assuming also that the mean porosity (0.005) is proportional to the square root of the mean conductivity, this gives a value of

$$0.005/\sqrt{0.2} = 0.011$$

for the proportionality constant a.

Using this assumption, an analysis similar to that for Case 1 was made and the results are shown in Figure 6.7-7. The equation that we used to find porosity from hydraulic conductivity assumes that they are perfectly correlated and their relationship is completely known. This assumed knowledge is evident from the narrow spread shown in the figure. For this case, the mean travel time was also

$$190 \text{ days } (10^{2.28})$$

with a standard deviation in log units of 0.25 (Table 6.7-3). For Case 2 there is a probability of less than 0.05 that the travel time of a tracer will be greater than

$$600 \text{ days } (10^{2.28 + 2 \times .25})$$

or less than

$$60 \text{ days } (10^{2.28 - 2 \times .25})$$

Case 3 tries to account for the uncertainty in both hydraulic conductivity and porosity, but assume they are uncorrelated. The same lognormal distribution for hydraulic conductivity is used, but now we assume that porosity is also lognormally distributed with a standard deviation of 0.75 log units. That is,

$$x = \log \phi$$

where

$$N[\mu_x, \sigma_x]$$

with

$$\mu_x = -2.3$$

and

$$\sigma_x = 0.75$$

This corresponds to a mean porosity of 0.005. The values of porosity are chosen from a lognormal probability distribution as described earlier for the K values. Monte Carlo simulations for Case 3 produced the results shown in Figure 6.7-8. The most probable travel time again is

$$190 \text{ days } (10^{2.28})$$

but the standard deviation in log units now is 0.90. For this case then, the probability is less than 0.05 that the travel time of a tracer will be greater than

$$12{,}000 \text{ days } (10^{2.28 + 2 \times .9})$$

or less than

$$3.0 \text{ days } (10^{2.28 - 2 \times .9})$$

The broad spread in travel times in Case 3 ($\sigma = 10^{0.90}$) is a result of the assumption that porosity and hydraulic conductivity are completely uncorrelated, while the narrow spread of Case 2 ($\sigma = 10^{0.25}$) follows from the assumption that they are perfectly correlated. There is unquestionably some correlation between porosity and conductivity at the Indian Point site, as there is everywhere. We will assume that the travel time standard deviation is adequately represented by that resulting from uncertainty in the conductivity alone, $10^{0.50}$, as for Case 1. While this is merely an assumption for tracer travel times, its correctness for elements which are retarded will be demonstrated.

The preceding discussion and the results displayed in Figures 6.7-6, 6.7-7, and 6.7-8 were restricted to elements that are tracers. Such elements have k_d values of zero, so that the parenthetic expression within Equation (6.7-3) equals one. As shown in Table 6.7-2, many of the nuclides of interest are of elements likely to be retarded with nonzero k_d values.

To account for retardation, additional sets of Monte Carlo simulations were made using Equation (6.7-1) and fixed k_d value of 0.5, 1.0, 3.0, and 10.0 for the elements of Table 6.7-2. Three runs were made for each k_d value, corresponding to the conductivity and porosity choices of the three cases described above. The results are given in the form of tabulated log means and standard deviations of travel time in Table 6.7-3.

Table 6.7-3 shows how retardation increases travel time, from mean values of

$$10^{2.28} \text{ (190 days)}$$

for a tracer, to

$$10^{6.02} \text{ (1,050,000 days)}$$

for an element of $k_d = 10$. It is of particular interest that the standard deviation associated with all retarded travel times is the same, $10^{0.5}$.

The Monte Carlo calculations thus confirm what could have been deduced from Equation (6.7-3). The differences among Cases 1, 2, and 3 that lead to the varying standard deviations of tracer travel times are the

result of different assumptions about the uncertainty associated with the porosity estimates. In Equation (6.7-3), when k_d is nonzero, porosity is important in the denominator of the parenthetic term, and in the numerator of the other part of the equation. The uncertainties in the porosity values, therefore, tend to cancel. This leaves the input standard deviation associated with the conductivity estimate as the residual travel time uncertainty. This is 0.5 log units, the value produced by the Monte Carlo calculations.

In the following sections, consequences of the sump water release and core melt leaching scenarios are discussed. These are reported as nuclide amounts entering the river as functions of time. The uncertainties in the estimates are not explicitly discussed; however, they are available by simply combining the travel time uncertainty estimates of this section with the results of the following discussions.

6.7.3.4.4 Sump Water Release Scenario

Many core meltdown event scenarios result in the containment building sump and the floor cavity being covered with a considerable amount of water. This water would have picked up the relatively volatile nuclides from the melted core in amounts corresponding to the sump water fractions of Table 6.7-2. The groundwater transport scenario of this section assumes that the containment building basemat had been breached and that this radioactive sump water entered the groundwater system beneath.

Given the discussion in Section 2 regarding the phenomena associated with core melt progression in the presence of sump water, this scenario is considered to be a worst case leading to an early release of nuclides to the groundwater system under conditions which would allow them to travel to the river with maximum velocity. By neglecting the core melt as well as the possible delays in escape of the sump water associated with steam phase blockage due to the presence of the core melt beneath the containment, it is possible to introduce nuclide laden groundwater into the groundwater system at as early a time as possible after the event.

To calculate the consequences of this scenario requires estimates of the sump water volume involved, and the time and characteristics of the basemat breach. A 40,000 ft^3 sump water volume was assumed, which is a representative fraction of the primary coolant volume, accumulator tanks, and containment sprays. The release is conservatively assumed to begin at a time of 1 day. This is based on characteristic melt-through times for various event scenarios as given in Table A6 of the Sandia draft (Reference 6.7-4). For the purposes of our analysis, the association of the breach with melt-through is not explicitly assumed.

The character of the breach is unimportant to the groundwater transport calculations unless it restricts the flow of sump water into the groundwater system. Because there seems to be no reason for assuming that the breach would restrict flow, the modeling has proceeded, assuming that

the rate of sump water release is equal to the underlying aquifer's ability to accept it. Based on the aquifer properties, this rate corresponds to 3.2×10^2 ft^3/day so that the duration of a release of $4 \times 10^4 ft^3$ is 125 days.

As the released sump water enters the aquifer, it mixes with the groundwater and moves toward the natural discharge area at the Hudson River. The appearance of this mixing and movement is shown in Figures 6.7-9A through 6.7-9D, which map the concentrations in the aquifer at various times during and after a sump water release. These maps show the groundwater concentrations as proportions of an initial sump water concentration of one for an idealized tracer which does not decay, has a k_d of zero, and so is not retarded.

Forty days after the start of the release, the 5% concentration line has not yet reached the river. By 80 days, concentrations of between 10% and 15% of the sump water concentration have begun to appear there. All the sump water has been released after 125 days, and the maximum concentrations begin to decrease as the flow of normal groundwater reasserts itself. Still, even after 400 days, concentrations of between 5% and 10% of that of the sump water are entering the river.

Figure 6.7-10 shows the discharge to the Hudson as a function of time, expressed in concentration units of grams/year. Based on a unit tracer input rate in the sump water of 1 lb/day for 125 days, 4.7×10^4 gms of tracer entered the aquifer. The integral under the breakthrough curve of Figure 6.7-10 reflects this total.

The maximum discharge rate to the river is about 0.5 lb/day ($10^{4.9}$ gm/yr), or about half of the sump water input concentration of radionuclides. This rate occurs for a period of about 130 days, beginning about 130 days after the release begins. The length of the duration of the maximum discharge is essentially the length of the duration of the sump water release itself (125 days) and would vary directly with changes in release duration. The 130-day time to peak concentration, though, is a function of the groundwater hydrology of the system and its equivalence to the release duration is merely coincidental.

Table 6.7-4 gives the discharge rates to the river at various times for the nuclides listed in Table 6.7-2. The important nuclides are plotted versus time in Figure 6.7-11. The first nuclides to appear are the isotopes of I and Ru which are not retarded ($k_d = 0$). The Ru-106 peak occurs at about 180 days, while I-131 peaks at about 110 days. The I-131 peak leads that of Ru-106 because of its more rapid decay. Sr-90 ($k_d = 0.5$) peaks at about 70 years ($10^{4.4}$ days). This is somewhat shorter than the travel time for a nondecaying tracer of the same k_d (Table 6.7-3), and results from the Sr-90 decay.

The Pu-239 peak occurs at approximately 2,000 years ($10^{5.9}$ days), the same time as calculated for a nondecaying tracer of equivalent k_d (Table 6.7-3). The half-life of Pu-239 is long ($10^{6.95}$ days) compared to the 10^6 day travel time. Therefore, no decay effects for that isotope should have been expected.

One effect of the sump water release is a decrease in the travel time (increase in the groundwater velocity) from the containment building to the river during the release itself. This is because the water standing in the sump and draining into the aquifer is at a higher potential than the natural groundwater under the building. This higher head increases the gradient to the river and, therefore, increases the flow rate. The travel time during the sump water release is about 120 days, while that of the natural groundwater system, which is assumed to hold at all times other than during the sump water release, is about 190 days (Table 6.7-3).

The choice of several parameters affects the results of the simulation. As described, the rate of sump water release is likely to be set by the parameters of the groundwater system. Using the best hydraulic conductivity estimate of 0.2 ft/day leads to the sump water input rate of $3.2 \times 10^{-2} ft^3/day$, given earlier. The standard deviation of one-half log unit for the conductivity used in Section 6.7.3.4.3 would also lead to a $10^{2.5 \pm 0.5} ft^3/day$ sump water input rate. Input rate variations change the amount of mixing between sump water and natural groundwater and, therefore, change the nuclide concentrations in the mix that discharges to the river. An input rate standard deviation of one-half log unit will produce the same uncertainty in the concentrations. Thus, the 95% confidence interval (two standard deviations) associated with the peak concentrations, C, of Figure 6.7-11 is $10^{\log C \pm 1.0}$ Ci/yr.

Variation in the hydraulic conductivity will also affect the travel time as discussed in Section 6.7.3.4.3. From that section, the 95% confidence interval in the peak arrival time, T, is also $10^{\log T \pm 1.0}$ years.

An obvious area of uncertainty is in the initial sump water nuclide concentrations. The amount of a nuclide available for sump water solution (mass x sump water source fraction, Table 6.7-5) is assumed to be fixed; therefore, the sump water concentration will vary inversely with sump water volume. For uncertainties expressed as standard deviations,

$$\sigma \text{ concentration} = \sigma \text{ volume}$$

A second potential effect of a sump water volume change is in the rate of sump water input to the groundwater system. If a change in sump water volume significantly changed the elevation of the sump water level in the containment building, the gradient of the flow to the river would also change. Because of the large diameter of the containment building, it is not likely that large head changes will result even from large sump water volume differences.

The third effect of a sump water volume change is to vary the duration of sump water release. This was discussed earlier.

A groundwater transport parameter (that has not been previously discussed) is dispersion, a measure of the smoothing of sharp concentration gradients that might be expected as a result of groundwater flow. The values used in this analysis were 50 feet and 5 feet longitudinal

and transverse dispersivity, respectively. Varying the dispersion parameters changes the shapes of the toes and tails of breakthrough curves. Reasonable dispersion variations in this system are unlikely to change toe and tail concentrations by amounts that even approach the uncertainties resulting from hydraulic conductivity uncertainties and, therefore, the effects of dispersion variation have not been explicitly investigated. Expected values of dispersivity and the effects of varying them on transport are discussed by Freeze and Cherry (Reference 6.7-5) or in other treatises on groundwater hydrology.

The results shown in Figure 6.7-11 assume a release initiation time of 1 day. Changing this initiation time will simply change the initial and subsequent nuclide concentrations by the amount appropriate to the radioactive decay of the nuclides.

6.7.3.4.5 Core Melt Leaching Scenario

6.7.3.4.5.1 Mass, Volume, and Groundwater Flow Parameters. This scenario assumes that the entire core has melted through the reactor vessel, reacted with and penetrated the concrete of the containment building, and lodged in the soil beneath. At some time after melt-through the mass will have lost enough heat so that groundwater can encroach on it and begin to leach it. Nuclides so leached will be transported in the regional groundwater flow to the Hudson River. This section develops estimates of the times and rates of discharge to the river for selected radioisotopes as a result of core leaching.

Many of the parameters used in the calculations described here are from Appendix A of the Liquid Pathways Generic Study (LPGS, Reference 6.7-3), and Chapter 2 and Appendix A of the Sandia Laboratories draft report on liquid pathways (Reference 6.7-4).

The melt lodged beneath the containment building will have a complex chemical composition because of its varied history. The core includes the reactor fuel, taken as 118 tons of UO_2 (Reference 6.7-4, Section A3.1 and Table A3), and zirconium cladding material. It will also contain a variety of fission products and other radionuclides. Although these may dominate the problem from the health standpoint, they are of negligible mass compared to the uranium and zirconium. The melt will also contain a significant amount of iron plus subsidiary chromium and nickel from the reactor vessel steel, but will consist overwhelmingly of light metal oxides (SiO_2,CaO,Al_2O_3), which are the products of the reactions between the molten core and the concrete of the containment building.

The core-concrete chemical reactions are extremely complex and have not yet been described in detail. Early calculations were made for the LPGS (Reference 6.7-3, Appendix A) using a Sandia code, INTER. In the Sandia draft (Reference 6.7-4), these results are supplemented using a more advanced code WECHSL. In addition, experimental work has been reported by Peehs, Skohan, and Reimann, (Reference 6.7-19), and by Skohan, Holleck, and Peehs, (Reference 6.7-20).

Both the calculations and the experimental work suggest that the composition of the concrete of the containment building will affect the final melt composition. Two end-member compositions are considered in the Sandia work (Reference 6.7-4) and in the other two papers cited above. One end-member considers an aggregate of carbonate rock composition and limestone concrete, while the other considers a siliceous rock aggregate and silica concrete. The compositions of the resulting melts are given in Table 6.7-5 in terms of the weight percents of the constituents and of their total masses. The weight percents are from Table A7 of the Sandia draft (Reference 6.7-4). The masses have been calculated assuming a UO_2 mass of 118 tons, equivalent to that initially present in the core. Both have been modified to reflect the fact that CaO is highly reactive and is therefore likely to be found reacted with atmospheric CO_2 as $CaCO_3$. The masses given include atmospheric CO_2 as $CaCO_3$.

The totals of the masses resulting from reactions with the two types of concrete and gravels are significantly different. The core (UO_2 and ZrO_2) and reactor vessel bottom head ($FeO + Ni + Cr_2O_3$) contributions are the same in each case, but the amounts of concrete and soil derived material are not. This is because less limestone than siliceous concrete and less limestone gravel than siliceous gravel are required to cool the molten core to below its melting point, so the final limestone associated mass is smaller than the siliceous mass.

The masses and volume of the core melt residual matter are important, not only in determining the total leach time of the residual matter, but in estimating the leach rate itself. The composition of the concrete in the containment buildings of IP-2 and IP-3 is reported in Reference 6.7-21 to be intermediate between those given in Table 6.7-5. Therefore, for the Indian Point calculations, some intermediate mass, 4×10^3 tons, for example, might be chosen. Considerable uncertainty exists, however, in the calculations which lead to the values in Table A7 of the Sandia draft (Reference 6.7-4), which were adopted for Table 6.7-5. To allow for these uncertainties, the mass used for the calculations has been permitted to range from 2.8×10^3 to 4.9×10^3 tons, the values for entirely limestone and entirely siliceous concrete, respectively.

In the Sandia draft (Reference 6.7-4, Figure 2.3) schematic diagrams of the final configurations of melt debris from both siliceous and limestone aggregates are given. The siliceous debris is shown assuming a roughly spherical shape, 17.6 meters in diameter. This sphere is filled with melt debris to a height of 10.5 meters, which gives the debris a volume of $1.8 \times 10^3 m^3$. For a mass of 4.9×10^3 tons, this requires a density of 2.7 gm/cm^3. Daly, Manger, and Clark (Reference 6.7-14, Table 4-2) show that the densities of a number of natural siliceous glasses range from 2.4 to 2.8 gm/cm^3. The higher densities are characteristic of glasses of iron contents and are similar to that of the siliceous melt debris of Table 6.7-5. Therefore, the siliceous melt debris volume and mass figures of the Sandia report (Reference 6.7-4) are consistent and lead to acceptable melt debris densities.

The limestone debris is shown (Sandia, Reference 6.7-4, Figure 2.3) assuming a flat cylindrical shape with 10 meter radius and 1.9 meter height, with a volume of $0.6 \times 10^3 m^3$. Using Table 6.7-5, the mass of 2.8×10^3 tons gives a density of $4.7\ gm/cm^3$. This is a higher density than one expects from material of similar composition (Reference 6.7-14) and suggests that the volume estimate in the Sandia report may be low. Debris dimensions of 11 meter radius by 1.9 meter height, or of 10 meter radius and 2.2 meter height would give volumes of $0.7 \times 10^3 m^3$. This volume leads to a density of $4.0\ gm/cm^2$, a more acceptable value for material of that composition.

The actual leaching of melt residuum will be by groundwater and, therefore, the cross-sectional area of the melt is important because it determines the amount of groundwater intercepted and available to leach the melt. The area of the siliceous melt, from the dimensions given above, is $1.5 \times 10^2 m^2$, while the area of the limestone melt debris, assuming a volume of $0.7 \times 10^3 m^3$ is $0.4 \times 10^2 m^2$. To combine these areas with other leach parameters, they must be expressed as means and deviations rather than as ranges. Thus, it is assumed that the possible range of areas follows a lognormal distribution and that the two areas calculated are one standard deviation above and below the mean, respectively. The melt debris area is taken as $10^{1.9 \pm 0.3} m^2$.

The specific water discharge across the section of melt residuum is given by the hydrologic calculations previously described as 9.5×10^{-3} ft/day, with a standard deviation of 0.5 log units. The latter is based on the standard deviation of the hydraulic conductivity of the groundwater system. In the metric units of this section, the flow is $10^{-2.5 \pm 0.5}$ m/day. This rate times the cross-sectional area of the melt equals the groundwater flux available to leach the melt, $10^{-0.6 \pm 0.6}\ m^3$/day. The variance of the flux is simply the sum of the variances of the area and flow rate terms. Combining the uncertainties in this way implies no correlation between the phenomena.

6.7.3.4.5.2 Leach Rates and Times. There are two approaches to leaching calculations. The first, which is common to the nuclear waste industry, is based on specific leach rates. This approach assumes that the transfer of nuclides across the solid-liquid interface to the liquid phase is the rate-controlling step. This leach rate is expressed by

$$R\ \frac{gm}{da} = \left(K_e\ \frac{gm}{da\text{-}cm^2}\right) \times SA \left(\frac{cm^2}{gm}\right) \times M(gm) \qquad (6.7\text{-}7)$$

where

R = leach rate at some time, t,

M = mass of the solid being leached, also at t,

K_e = specific leach rate constant, and

SA = specific surface area of the solid.

This can also be expressed as a leach constant with units of reciprocal time as

$$\frac{R}{M}\left(\frac{1}{da}\right) = K_e \times SA \qquad (6.7\text{-}8)$$

This leach rate approach implies that as leaching occurs, the material leached is immediately removed from the leach site and has no further effect on the leaching process. Such conditions adequately describe cases such as the scenario in which the core melt residue of a floating nuclear plant reaches the ocean, or many laboratory experiments in which relatively large ratios of water to solid are used. It may not be a correct physical representation of leaching by relatively small groundwater volumes.

The second approach to leaching calculations assumes that the rate controlling step is the mass transport of leached material away from the leaching site; that is

$$R\left(\frac{gm}{da}\right) = C\left(\frac{gm}{m^3}\right) \times F\left(\frac{m^3}{da}\right) \qquad (6.7\text{-}9)$$

where

R = the rate of removal,

C = the concentration of leached material in solution, and

F = the flux of leaching fluid (groundwater) passing the solid being leached.

In terms of a leach constant

$$\frac{R}{M}\left(\frac{1}{da}\right) = \frac{C \times F}{M} \qquad (6.7\text{-}10)$$

This approach implies that the flow of water past the leaching solid is slow relative to the rate of transfer of material from the solid to the liquid. Therefore, the concentrations of material in solution reach their solubility limits so that the solution concentrations can no longer increase. The rate of removal of material from the system reaches a steady state that depends on fluid flow rate and material solubility, as described by the equations above. Such a physical model has been found to be adequate in accounting for many solution and reaction processes in natural groundwater systems.

The melt debris leach rate, regardless of the two mechanisms used to describe it, dominates the rate of nuclide release to the river and the concentration. Therefore, it has been necessary to carefully consider both mechanisms and to evaluate a considerable amount of data leading to estimates of their characteristic rates. As the remainder of this

section shows, leach constants calculated from either mechanism broadly overlap, a result which supports the estimate chosen for use in the release calculations.

The approach used to estimate leach rates from groundwater fluxes and melt debris solubilities will be considered first. In the preceding section, the flux was estimated to be $10^{-0.6 \pm 0.6}$ m^3/day, but solubility estimates are also required before leach rate calculations can be made.

Many of the potentially hazardous radioisotopes in the core material are of elements such as iodine and cesium, which are highly soluble in water under most conditions. These soluble elements, however, also tend to be relatively volatile and to partition into a gas phase (iodine) or the sump water (cesium) during a melting event. This partitioning was discussed in the preceding section that described the sump water release scenario calculations. The only nuclides that will remain with the core melt residuum and be available for leaching will be those with low sump water source fractions, as given in Table 6.7-2. The elements remaining in the core melt residuum are those such as strontium, transition metals, and rare earth and actinide elements with relatively low solubilities in natural groundwaters.

The amount of segregation of various elements within the cooling core melt is unknown, but could affect the melt solution behavior. At one extreme, the melt could be considered to be homogeneous so that it all dissolves together at a rate controlled by the solubility of the least soluble major constituent. Alternatively, if segregation occurred during cooling, more soluble parts of the melt could be leached more rapidly than less soluble segments. While estimates for both situations will be made, the latter is the more probable case, and gives more conservative (higher leach rate) results.

If the melt cools and dissolves homogeneously, it can be assumed that leach rate will be set by the removal rate of the major constituent. As Table 6.7-5 shows, the major component of a siliceous concrete melt is $10^{3.6}$ tons of SiO_2, and for a limestone concrete melt it is $10^{3.4}$ tons of $CaCO_3$. Silica (SiO_2) is relatively insoluble in water. Even for its most soluble amorphous form, saturation occurs at $10^{2.3}$ gm/m^3 of water at 100°C or at $10^{2.0}$ gm/m^3 of water at 25°C (Reference 6.7-13). The groundwater flux has already been given as $10^{-0.6 \pm 0.6}$ m^3/day.

Adopting a saturation concentration value of $10^{2.3 \pm 0.3}$ gm/m^3, in which the spread is taken as a one standard deviation error and accounts for uncertainty in the temperature of leaching, leads to a leach rate of

$$10^{1.6 \pm 0.6} \frac{gm}{da} \text{ or a leach constant of } 10^{-8.0 \pm 0.6} \text{ per day}$$

The major constituent of a core melt-through limestone concrete will be $CaCO_3$. The solubility of this substance is strongly dependent on the partial pressure of CO_2 on the system, because high CO_2 pressures promote greater $CaCO_3$ solution according to the reaction

$$CaCO_3 + CO_2 + H_2O = Ca^{+2} + 2HCO_3$$

Natural CO_2 partial pressures range from $10^{-3.5}$ bars in the atmosphere to 10^{-1} bar in some soil and groundwater systems. CO_2 pressures between these limits give $CaCO_3$, solubilities of $10^{2.2 \pm 0.5}$ gm/m^3 (Reference 6.7-22). This solubility with the flux above gives a leach rate of $10^{1.5 \pm 0.7}$ gm/day, and a leach constant of $10^{-7.9 \pm 0.7}$ per day for $10^{9.4}$gm $CaCO_3$. A summary of these calculations appears in Table 6.7-6.

Leach rate estimates must also be made based on the assumption that the core melt residuum is not homogeneous, but is segregated into several chemically distinct phases, each of which leaches independently of the others. Two potential segregation product types can be considered. One is dominated by the UO_2 of the original core, and the other by the FeO and allied oxides of the pressure vessel bottom. Solubilities of these constituents and the leach constants they lead to are given in Table 6.7-6.

The other approach to estimating core leach times uses specific leach rate constants and surface areas. Specific leach rates, using recent experimental data appropriate to the core melt problem, have been discussed at length in the LPGS (Reference 6.7-3, p. A-45) and in the Sandia draft report (Reference 6.7-4). Recent experimental data which had been developed by D. A. Powers (private communication, 1980) were reviewed. From these and other studies, it is possible to draw only very broad conclusions regarding appropriate values for specific leach rate constants (K_e), and surface areas (SA), and of the leach constants derived from them.

Compilations of specific leach rate constants for various elements in a number of nuclear waste product types are given in the LPGS (Reference 6.7-3). Elements such as the rare earth and actinide groups that are less easily leached have specific rate constants that range from 10^{-8}gm/cm^{2}day or less in glasses to 10^{-3}gm/cm^{2}day in calcines.

Powers' results are meant to be directly applicable to the core melt leach problem because they were obtained with realistic core melt concrete matrix materials in fluids similar to natural groundwaters and at elevated temperatures. These results are within the lower range of the global constants quoted in the preceding paragraph, and extend from 10^{-9} to 10^{-5}gm/cm^{2}day. Powers' work shows, and as pointed out in the Sandia report (Reference 6.7-4), that under these experimental conditions, some elements leach more rapidly than others. The $10^{-7 \pm 2}$gm/cm^{2}day range includes this interelement variation.

To calculate leach rates from specific leach rate constants also requires the specific area of the leaching solid. Estimates of this parameter appearing in LPGS (Reference 6.7-3, p. A-34) range from 10^{-1} to 10^{3} cm^2/gm. Powers suggested a value of $10^{2.1}$ cm^2/gm for his experiments. A value of $10^{1 \pm 2}$ adequately reflects specific area estimates. When combined with the data of the preceding paragraph, this leads to a leach constant of $10^{-6 \pm 2.8}$ per day.

Table 6.7-6 and Figure 6.7-12 summarize these leach constant estimates. The several solubility flux limited estimates are similar and overlap the lower end of the range of values estimated using conventional specific leach rate constants. As described earlier, the operation of the two processes are such that the slower of the two (the one with the smaller leach constant) controls the overall rate of core melt debris leaching. In this case, because of the limited groundwater flow available, the solubility flux controlled means are below the solid-liquid interface transfer value, and the former processes appear to control. In the leach calculations, the UO_2 controlled rate, $10^{-6.7 \pm 1.2}$ per day, has been used.

6.7.3.4.5.3 Nuclide Discharge Rates. Discharge rates to the river of the nuclides in Table 6.7-2 are given as functions of time in Table 6.7-7 and displayed in Figure 6.7-13. These results are based on the following assumed parameter values:

- Core leaching begins at 1 year.
- Leaching occurs at constant rate of $10^{-6.7 \pm 1.2}$ per day.
- Nuclide contents of core melt at time zero are those of Table 6.7-2.
- The flow field in which transport occurs is the natural groundwater system as described in Section 6.7.3.3. The travel times of the several nuclides depend on this flow and their respective K_d values, and have the mean values given in Table 6.7-3. The actual discharge will occur along some length of river, as shown in Figure 6.7-9. The values in Figure 6.7-13 and Table 6.7-7 are the same over the entire discharge length and are total discharge rates (in Ci/yr) to the river.

As Figure 6.7-13 shows, three nuclides dominate the discharge. Ru-106, which is important from approximately 1 to 180 years; Sr-90, from 180 to 500 years; and Pu-239 beyond 500 years. For the sump water release, the breakthrough times are in the same sequence as the nuclide k_d values.

At times up to 1,000 years, the discharges resulting from the sump water release are larger than those from the core melt leaching. This is expected because of the higher input rate of nuclides in the sump water. At longer times, though, the Pu-239 leached from the core melt dominates and continues long after all effects of the sump water release have passed.

The major uncertainties associated with these core melt leach discharges are the travel time (Section 6.7.3.4.3) and the leach times. Travel time uncertainties will be directly reflected in the peak arrival times, modulated slightly by radionuclide decay effects. The 95% confidence interval associated with the peak time, T, will be $10^{\log T \pm 1.0}$ years.

Leach time uncertainty will be reflected in the discharge concentrations at peak heights, again with a secondary effect of radionuclide decay. Peak concentrations will be inversely proportional to leach time, and can be assumed to have the same associated uncertainty. Based on the results of the previous section, the 95% confidence interval on peak concentration, C, can be taken as $10^{\log C \pm 2.2}$ Ci/yr.

6.7.3.5 Summary

Groundwater flows beneath the reactors at Indian Point and discharges into the Hudson River. This flow is mainly within a fractured limestone system. A limited number of head measurements were available to characterize the flow properties of the limestone. A two dimensional, areal numerical groundwater model was used to simulate these head data, based on the site physiography and rainfall. The best match was achieved with a hydraulic conductivity of 0.2 ft/day.

Given a core melt event, nuclides can enter the groundwater system in solution if there is a sump water release through the containment building basemat and/or by leaching of core melt debris, if there is melt-through. Nuclides, which are assumed to result from maximum power reactor operation for full fuel life, are partitioned into the sump water or core melt, depending on their volatility.

Uncertainty in nuclide travel time depends on uncertainties in hydraulic conductivity, porosity, and k_d. For typical k_d values, uncertainty in porosity cancels and uncertainty in conductivity ($\pm 10^{0.5}$) dominates. For a nonretarded (tracer) nuclide, the expected travel time is 190 days and there is a 95% probability that the travel time is between 19 and 1,900 days.

The sump water release calculations assume a volume of 40,000 ft^3 that enters the groundwater system at 3.2×10^2 ft^3/da, beginning at 1 day. Peak nuclide discharge rates reach 4×10^6 Ci/yr for Ru-106 at 0.5 year, 3×10^2 Ci/yr for Sr-90 at 70 years, and 6×10^{-2} Ci/yr for Pu-239 at 2,000 years. The 95% confidence interval of both the peak arrival times, T, and concentrations, C, is plus or minus one log unit (i.e., $10^{\log T \pm 1.0}$ years and $10^{\log C \pm 1.0}$ Ci/yr, respectively).

The core melt leaching calculations assume a constant leach rate of $10^{-6.7 \pm 1.2}$ per day, based on core residue size calculations and solubility considerations. Peak nuclide discharge rates vary from 6×10^2 Ci/yr for Ru-106 at 1.8 years, through 4.0 Ci/yr for Sr-90 at 100 years, to 1.0 Ci/yr for Pu-239 at 6,500 years. The 95% probability ranges of the peak arrival times, T, are ±1.0 log units and of the peak concentrations, C, are 2.2 log units (i.e., $10^{\log T \pm 1.0}$ years and $10^{\log C \pm 2.2}$ Ci/yr, respectively).

6.7.4 HUDSON RIVER ESTUARY SURFACE WATER TRANSPORT

Transport of contaminants in tidal estuaries, such as the lower Hudson River basin, is significantly affected by downstream convection due to freshwater flow, oscillatory tidal advection, and nontidal gravitational circulation induced by salinity gradients. As a result, there is transport of material both upstream and downstream from the discharge point, with the maximum upstream contaminant penetration being limited to the general region of the oceanic salt intrusion and/or tidal penetration.

6.7.4.1 Model Description

Tidal advection and salinity induced circulation tend to reduce concentration gradients in lateral and vertical directions relative to those in the longitudinal direction. Therefore, for radionuclide transport prediction, reducing the estuarine transport problem to a single dimension (longitudinal) produces satisfactory results over most of the estuary reach (Reference 6.7-23). The one dimensional simplification is accomplished by averaging all transport coefficients over the river cross-section. The resulting constituent transport equation is

$$\frac{\partial}{\partial t}(AC) + \frac{\partial}{\partial x}(Q_V C) = \frac{\partial}{\partial x}\left(AK \frac{\partial C}{\partial x}\right) - \lambda_d AC + F_s A \qquad (6.7\text{-}11)$$

$$- \sum_i \delta(x_i) \frac{A_i}{V_i} q_{si}$$

where

x = longitudinal distance, L

t = time, T

$C(x,t)$ = radionuclide concentration, M/L^3 (mass/length^3)

$A(x,t)$ = cross-sectional area, L^2

$Q_V(x,t)$ = river volumetric flow rate, L^3/T

$K(x,t)$ = longitudinal eddy diffusivity, L^2/T

λ_D = isotope decay constant = $\ln 2/T_{1/2}$, T^{-1}

$T_{1/2}$ = isotope half-life, T

F_s = sediment interaction parameter, $\frac{M}{L^3 T}$

$q_s(t)$ = source (positive) or sink (negative) of radionuclides M/T

δ = dirac delta function

x_i = longitudinal position at which source/sink i is introduced, L

A_i = river cross-sectional area at longitudinal distance x_i, L^2

V_i = volume of water into which source/sink i is introduced L^3

6.7.4.1.1 "Tidally Averaged" Approximation

Solution of Equation (6.7-11) with appropriate boundary conditions requires knowledge of the distance dependent coefficients A, Q_v, and K as a function of time within a tidal cycle, and for each tidal cycle for the time period of interest. These coefficients can vary significantly from one tidal cycle to another because of the influence of freshwater flow from tributaries and runoff. Such detailed data are not available for the time scale of this problem (about 1 year for I-131 to about 15,000 years for Pu-239).

An acceptable alternative (Reference 6.7-23) is to invoke the "tidally averaged" approximation in which the tidal oscillations and salinity induced circulation cells are not included explicitly. Instead, they are considered to be responsible for large scale longitudinal dispersion. These phenomena are incorporated into the dispersion term of Equation (6.7-11) by replacing K with a tidally averaged effective eddy diffusivity, K_{eff}, which accounts for all contributions to contaminant transport except for convection resulting from freshwater flow. Consequently, Q_v, the instantaneous river volumetric flow rate, is replaced by Q_f, the freshwater flow rate. With these assumptions, A becomes the effective river cross-sectional area averaged over a complete tidal cycle. The resulting tidally averaged transport equation applies only to problems for which the time scale of transport is large compared to that for a single tidal cycle. Such is the case here. The predicted concentrations represent averages over a complete tidal cycle and not instantaneous concentrations within the tidal cycle.

6.7.4.1.2 Sediment Radionuclide Interactions

Radionuclides are known to have a high affinity for certain types of sediments found suspended in the river flow and deposited on the river bottom. Therefore, radionuclides are sorbed onto the surface of suspended and deposited sediments. Suspended sediments are deposited on the river bottom during periods of low freshwater flow and are reentrained during periods of high freshwater flow. Detailed modeling of sediment radionuclide interactions, even within the framework of the one dimensional, tidally averaged approach, is complex. It requires

detailed knowledge of suspended sediment fluxes and deposition and reentrainment rates for each sediment type as a function of time and longitudinal distance. These detailed data are not available.

A conservative alternative compatible with the overall degree of uncertainty of this study is to treat sediment-radionuclide sorption, desorption, deposition, and reentrainment approximate by introducing a first order radionuclide depletion factor into Equation (6.7-11). This is done by proposing that

$$F_s = -\lambda_s C \qquad (6.7\text{-}12)$$

where

$\lambda_s(x,t)$ = sediment depletion factor, T^{-1}

λ_s is positive for sediment depletion and negative for reentrainment. This approach was used by Sandia (Reference 6.7-4). Approximate values of λ_s can be obtained from known sediment deposition and reentrainment rates for various reaches of the estuary and from measured distribution coefficients for radionuclide sorption into various sediment types. With this approximation, predicted concentrations represent the average radionuclide content of river water contained in both the dissolved and suspended (within sediment) state. Modifications of this approach and its implications to dose calculations will be discussed later.

6.7.4.1.3 Sources and Sinks of Radionuclides

A single time varying source term is used to describe a hypothetical release of a given radionuclide into the Hudson River at Indian Point. The model, however, has the capability of handling multiple sources if desired. For example, additional source terms can be used to describe sediment reentrainment by a zero order rate process for short or extended periods of time. In some river reaches, this may be more desirable than the first order process discussed in Section 6.7.4.1.2. Multiple time dependent sinks are included, if desired, to simulate zero order sediment deposition or flow of contaminated water out of the Hudson River into a confluent tributary.

6.7.4.1.4 Final Expression for Transport Equation

In light of the discussion in the preceding subsections, the form of Equation (6.7-11) as applied to this study is given by

$$\frac{\partial}{\partial t}(AC) + \frac{\partial}{\partial x}(Q_f C) = \frac{\partial}{\partial x}\, AK_{eff}\frac{\partial C}{\partial x} - \lambda_D AC - \lambda_s AC \qquad (6.7\text{-}13)$$

$$- \sum_i \delta(x_i)\,\frac{A_i}{V_i}\, q_{source_i} + \sum_j \delta(x_j)\,\frac{A_j}{V_j}\, q_{sink_j}$$

where

$Q_f(x,t)$ = river freshwater flow rate, L^3/T

$K_{eff}(x,t)$ = one dimensional, tidally averaged effective longitudinal eddy diffusivity, L^2/T

λ_s = first order sediment depletion factor, T^{-1} (deposition, λ_s = positive; reentrainment, λ_s = negative)

q_{source_i} = radionuclide source at distance x_i, M/T

q_{sink_j} = radionuclide sink at distance x_j, M/T

In Equation (6.7-13), sources and sinks are given by separate terms to reflect the fact that both a source and sink can exist in the same river reach.

6.7.4.2 Solution to Contaminant Transport Model

It is not possible to obtain an analytical solution to Equation (6.7-13) for the general case in which A, Q_f, K_{eff} and λ_s are functions of time and position and for source and sink terms that vary arbitrarily with time. The transport coefficients in the Hudson River vary significantly with distance and season (time) because of geometry, varying freshwater flow rates and the variable extent of the salt intrusion. Therefore, Equation (6.7-13) is solved numerically using a finite difference approximation.

6.7.4.2.1 Finite Difference Approximation

In using the finite difference approximation, the river is segmented into reaches or grid blocks of varying size. The finite difference approximation to Equation (6.7-13) is written for each grid block. The time dependency is approximated using a constant time step size. The finite difference equations are generalized to allow for both upstream (backward in space, (BIS)) and central (centered in space, (CIS)) weighting of the convective derivative. Time variations can be approximated by backward in time (BIT) or central in time (CIT) weighting. As a result, four solution options exist. These are:

1. CIT - CIS
2. CIT - BIS
3. BIT - CIS
4. BIT - BIS

Because of the one dimensional nature of Equation (6.7-13), all of these schemes result in a tridiagonal matrix of coefficients that is easily inverted by standard techniques (Reference 6.7-24).

Each of the four solution options have advantages and disadvantages. Table 6.7-8 gives time and space step criteria for the four schemes. BIT and BIS weighting of the time and convective space derivatives, respectively, introduces numerical artifacts (truncation errors) that are revealed as a fictitious enhanced dispersion. This results in a loss of accuracy that is equivalent to the exact solution that would be obtained by solving the model with larger dispersion coefficients. In theory, the numerical dispersion error can be eliminated by modifying the eddy diffusivity. However, in practice this is difficult since the coefficients vary from grid block to grid block and are functions of time. The stability of the solution scheme depends on the accuracy of the spatial and temporal resolution process resulting in an "overshoot" or discretization error. The magnitude of the error depends on the size of the space and time steps. Each of the four solution options generates differing amounts of dispersion and overshoot error depending on the magnitude of the transport coefficients, the grid block size, and the time step size. CIS schemes minimize dispersion errors, but result in large overshoot errors. The opposite is true for BIS solutions. CIT solutions are more accurate than BIT solutions, but require more computer time. Selection of the optimal scheme requires a balance between accuracy and computer costs and depends on the numerical values of the transport coefficients and their space and time variation. For this study, several of the schemes are used depending on the time scale of the problem. This is necessary since the duration of the source release under consideration varies from about 1 year for I-131 to over about 15,000 years for Pu-239.

6.7.4.2.2 Initial and Boundary Conditions

The finite difference approximation of Equation (6.7-13) is solved in conjunction with an initial condition and upstream and downstream boundary conditions. The initial condition states that at time zero, the radionuclide concentration in the river is a function of longitudinal distance only. In principle, the numerical model is capable of accommodating any initial condition. For this study, the initial concentration in each grid block was assumed to be zero.

At the upstream boundary, designated as $x = 0$, the appropriate boundary condition is that the total flux of radionuclides is zero. That is,

$$\text{at } x = 0;\ -K_{eff}\frac{\partial C}{\partial x} + Q_f C = 0 \qquad \text{(for all t)} \qquad (6.7\text{-}14)$$

This is accomplished in the numerical solution by zeroing out the convection and dispersion terms at the upstream face of the first (furthest upstream) grid block. This boundary condition requires that the first grid block be placed far enough upstream to be beyond the tidal penetration. In reality, sufficient accuracy results if the first grid block is either placed upstream of the salt intrusion or at the furthest upstream point of interest, whichever is the greater distance from the source.

The downstream boundary condition can be specified in several ways, depending on the spatial extent of the numerical computations. For a tidal estuary discharging at its mouth into an ocean, sea, or bay, the contaminant concentration seaward of the mouth is approximately zero. This occurs since the ocean serves as total sink because of contaminant dilution and enhanced tidal mixing in the large volume of seawater. In some cases, however, the estuary mouth may be located at a large distance from the contaminant release point, and it may not be desirable to carry the computation all the way to the mouth. This is particularly true if the stability criteria limit the maximum grid block and time step size and concentration predictions are only required at considerable distances upstream of the mouth. As a result, two optional downstream boundary conditions are incorporated into the numerical model.

The first downstream boundary condition option specifies that the contaminant concentration is zero at the estuary mouth or at some relatively small distance seaward of the mouth. This is accomplished in the numerical algorithm by assuming that the concentration is zero in a hypothetical grid block that is the same size as, adjacent to, and downstream of the last (farthest downstream) grid block. The coefficients for the last grid block in the tridiagonal matrix representing the solution are modified to give a concentration of zero at the center of the hypothetical grid block. Use of this downstream boundary condition option requires that the numerical computations be carried out all the way to the estuary mouth. Henceforth, it will be referred to as the "zero concentration downstream boundary condition."

The second downstream boundary condition option is an approximation that allows the numerical solution to be terminated upstream of the estuary mouth (but downstream of the source) with little loss of accuracy. It assumes that in the last grid block (farthest downstream), the total contaminant flux is removed by the freshwater flow. This is accomplished by zeroing out the dispersion and convection terms at the downstream face of the last grid block. They are then replaced by a total sink equal to the product of the freshwater flow rate and concentration in the last grid block. Therefore, the last grid block only has to be located a few grid blocks after that, corresponding to the farthest downstream point of interest. This downstream boundary condition option will be called the "freshwater convection downstream boundary condition."

The two downstream boundary condition options were incorporated into the numerical solution algorithm since it was originally thought that it would not be possible to solve Equation (6.7-13) numerically for all relevant reaches of the Hudson estuary, simultaneously. This notion was based on the fact that large spatial and temporal variations in freshwater velocity and eddy diffusivity made it impossible to satisfy the stability criteria of Table 6.7-8 at reasonable computer cost without considering locations upstream and downstream of the source (Indian Point) separately. However, sensitivity analyses showed that with reasonable modifications, the entire estuary could be modeled conservatively in one computer simulation. As a result, the zero concentration downstream boundary condition was used exclusively in the "production runs."

6.7.4.2.3 Pseudo Steady State Approximation

For the shorter lived isotopes, the time scale for radioactive decay is small compared to the residence time in the river. In addition, the magnitude of the source term varies rapidly with time. Therefore, it is necessary to solve Equation (6.7-13) as written. Long lived isotopes decay very little during their residence time in the river. The source term is of long duration, and its magnitude varies slowly with time. Therefore, the magnitude of the source term changes very little during the isotope's residence time in the river. Since the numerical solution requires very small time steps (approximately 0.002 year) to meet the criteria of Table 6.7-8, a nonsteady state or transient solution is impractical. Fortunately, the pseudo steady state approximation can be invoked for these isotopes with very little loss of accuracy. Since the source term varies slowly, the steady state version of Equation (6.7-13) can be solved for a constant source of unit intensity. The resulting normalized concentration field is converted to actual concentrations by multiplying the normalized steady state concentration by the average source term over a reasonable time period. The pseudo steady state approximation can be represented by

$$C(x,t) = \left[\frac{C}{q}(x)\right] q_{source}(t) \qquad (6.7\text{-}15)$$

where

$\frac{C}{q}(x)$ = normalized steady state concentration

$q_{source}(t)$ = average source strength over the time period t to $t + \Delta t$

It should be noted that solution of the steady state problem (Equation (6.7-13) with $\partial/\partial t(AC) = 0$) can only be accomplished numerically using BIT-CIS and BIT-BIS solution schemes with the time step set to infinity.

6.7.4.2.4 Radionuclide Concentrations in Sediment

Radionuclides dissolved in estuarine waters interact with dissolved and bottom sediments and are sorbed onto their surfaces. The degree of sorption (or desorption) is characterized by a distribution coefficient defined by

$$k_D = C_S/C_D \qquad (6.7\text{-}16)$$

where

k_D = sediment distribution coefficient, cm^3/gm

C_S = concentration of radionuclide in sediment, Ci/gm

C_D = concentration of dissolved radionuclide in water, Ci/cm^3

The distribution coefficient is usually defined at equilibrium; that is, C_S is a sediment concentration in thermodynamic equilibrium with estuarine water with dissolved radionuclide concentration, C_D. For a given radionuclide, k_D is actually a complex function of water salinity, sediment composition (i.e., sand, silt, clay), the nature of the sediment surface, the type and concentration of other dissolved cations and anions, and the magnitude of the dissolved radionuclide concentration. Radionuclides are held to sediment surfaces by physical and/or chemical bonds. These factors vary both spatially and temporally in the estuary and, with the exception of salinity, are difficult to quantify. As a result, one must rely on long term average, site specific measurements to obtain order of magnitude estimates of k_D.

For this study, it is assumed that for a given radionuclide, k_D is a function of annual average salinity only, and that instantaneous equilibrium is achieved between dissolved and sediment phases. With these assumptions, the sediment concentration is given by

$$C_S(x,t) = k_D(x)\, C_D(x,t) \qquad (6.7\text{-}17)$$

where $C_D(x,t)$ is approximately equal to $C(x,t)$ as obtained from the solution of Equation (6.7-13). Since the annual average salinity is a function of distance along the river, the distribution coefficient can also be characterized as a function of distance. The approach of Equation (6.7-17) is conservative in that the quantity of dissolved radionuclide is not depleted because of sediment adsorption except as prescribed by the sediment interaction parameter, λ_S. To properly deplete the dissolved concentration resulting from sediment sorption, one must have detailed knowledge of the spatial and temporal variation of the quantity and composition of dissolved and bottom sediments, and sediment deposition and reentrainment rates. Equation (6.7-13) must then be solved in conjunction with appropriate sediment mass balances. These results in a significant increase in the complexity and cost of the numerical simulation. This approach cannot be justified given the project scope and the lack of detailed sediment-radionuclide interaction data.

6.7.4.2.5 Numerical Model Validation--Match to Known Analytical Solutions

The accuracy of the numerical model was validated by matching its results to known or developed analytical solutions. Both steady state and transient models with constant transport coefficients were considered. For the case of constant coefficients with no depletion by sedimentation, no sinks, and a single constant source, Equation (6.7-13) is reduced to

$$\frac{\partial C}{\partial t} + \frac{Q_f}{A}\frac{\partial C}{\partial X} = K\frac{\partial^2 C}{\partial x^2} - \lambda_D C + \delta(x_o)\,\frac{A}{V}\,q_{source} \qquad (6.7\text{-}18)$$

Equation (6.7-18) applies to a channel of constant cross-sectional area and velocity with the velocity given by $U = Q_f/A$. Note that the subscript "eff" has been dropped from K for convenience. Therefore, the one dimensional, tidally averaged effective longitudinal diffusivity will henceforth be referred to as the eddy diffusivity and will be represented by K.

For a source at $x = x_o$, the source term in Equation (6.7-18) can be removed and replaced by a boundary condition at x_o. This yields

$$\frac{\partial C}{\partial t} + U\frac{\partial C}{\partial x} = K\frac{\partial^2 C}{\partial x^2} - \lambda_D C \qquad (6.7\text{-}19a)$$

with boundary conditions

$$\text{at } x = x_o;\ -KA\frac{\partial c}{\partial x}^{I} + Q_f C^{I} + q_{source} = -KA\frac{\partial C}{\partial x}^{II} + Q_f C^{II} \qquad (6.7\text{-}19b)$$

$$\text{at } x = x_o;\ C^{I} = C^{II} \qquad (6.7\text{-}19c)$$

where superscripts I and II refer to the regions upstream and downstream of the source, respectively. Equation (6.7-19) is solved separately for each region, and the solutions are matched at $x = x_o$.

6.7.4.2.5.1 Steady State Solutions. A steady state solution to Equations (6.7-19a) through (6.7-19c) was developed with the following additional boundary conditions:

at

$$x = 0;\ -KA\frac{\partial C}{\partial x}^{I} + Q_f\, C^{I} = 0 \quad \text{(upstream boundary)} \qquad (6.7\text{-}20a)$$

at

$$x = \infty;\ C^{II} = 0 \quad \text{(downstream boundary)} \qquad (6.7\text{-}20b)$$

The numerical solution was generated using the freshwater convection downstream boundary condition so it was replaced by Equation (6.7-20b). The numerical solution is expected to match the analytical solution, except in the last few downstream grid blocks. The analytical solution to Equations (6.7-19) and (6.7-20) is

$$C^{I} = \frac{q_{source}}{UA\alpha}\, e^{-(1-\alpha)\frac{U}{2K}x_o}\left[e^{(1+\alpha)\frac{U}{2K}x} - \frac{(1-\alpha)}{(1+\alpha)}\, e^{(1-\alpha)\frac{U}{2K}x}\right] \qquad (6.7\text{-}21a)$$

$$C^{II} = \frac{q_{source}}{UA\alpha}\left[e^{-(1-\alpha)\frac{U}{2K}X_o} - \frac{(1-\alpha)}{(1+\alpha)}e^{-(1+\alpha)\frac{U}{2K}X_o}\right]e^{(1-\alpha)\frac{U}{2K}X} \quad (6.7\text{-}21b)$$

$$\alpha = \left[1 + \frac{\lambda_D K}{U^2}\right]^{1/2} \quad (6.7\text{-}22)$$

Equation (6.7-21a) applies upstream of the source and Equation (6.7-21b) applies downstream. Analytical versus numerical model comparisons are given in Figures 6.7-14 through 6.7-16 for Pu-239, I-131, and SR-89, respectively. The parameter values used were typical of the Hudson River Estuary. These and other pertinent information are given in Table 6.7-9. The solid lines of the figures represent the analytical solution. Circles represent the BIT-CIS numerical solution and squares represent the BIT-BIS numerical solution.

As expected, the BIT-CIS numerical solutions match the analytical solution almost exactly, except near to the downstream boundary (x = 120 miles). BIT-BIS numerical solutions deviate from the analytical solutions because of a numerical dispersion error. If this error is accounted for, the match is excellent. Concentrations fall off much more rapidly upstream than downstream. This occurs since transport upstream is by dispersion only while transport downstream results from both dispersion and freshwater flow convection. The BIT-CIS solutions tend to deviate slightly from the analytical solutions far upstream because of overshoot error. Figure 6.7-14 shows that the Pu-239 concentration is constant downstream of the source. This occurs since the decay constant for Pu-239 is so small that Pu-239 behaves essentially like a conservative contaminant.

6.7.4.2.5.2 Nonsteady State Solutions. A nonsteady state solution to Equation (6.7-19) for a source of constant intensity is given by the USNRC (Reference 6.7-23). The solution conforms to the following boundary conditions:

at $x' = -\infty$; $C = 0$ (upstream boundary)

at $x' = +\infty$; $C = 0$ (downstream boundary) (6.7-23)

at $x' = 0$ q_{source} = constant for $t \geq 0$ (source location)

The analytical solution is

$$C = \frac{q_{source}}{2A\gamma}\exp\left(\frac{Ux'}{2K}\right)g(x',t) \quad (6.7\text{-}24)$$

where

$$\gamma = \left[U^2 + 4\lambda_D K\right]^{1/2} \quad (6.7\text{-}25)$$

$$g(x',t) = \left[\operatorname{erfc}\left\{\frac{x'+\gamma t}{\sqrt{4Kt}}\right\} \pm 1\right] \exp\frac{\gamma x'}{2K} \qquad (6.7\text{-}26)$$

$$\left[-\operatorname{erfc}\left\{\frac{x'-\gamma t}{\sqrt{4Kt}}\right\} \pm 1\right] \exp\frac{-\gamma x'}{2K}$$

The sign within the brackets of Equation (6.7-26) is chosen negative downstream of the source (positive x') and a positive upstream of the source (negative x'). By defining $x' = x - x_0$, the distance parameter x' of this solution can be made to conform to the distance x of the numerical solution. In comparing the analytical to the numerical solution, the match will not be exact near the upstream and downstream boundaries of the numerical grid because of differing boundary conditions. For long times, the transient solution to Equations (6.7-24) through (6.7-26) approaches a steady state solution since the source is of constant (unit) intensity. The analytical solution is compared to the numerical predictions for Ru-103 in Figure 6.7-17 for times of 0.05, 0.10, 0.15, and 0.25 years. Again, Table 6.7-9 parameters were used with a time-step of $\Delta t = 0.0005$ years. The spatial variation of Ru-103 concentrations has essentially reached steady state by 0.25 years. As expected, the CIT-CIS solution match is very good except near the boundaries where only slight deviations exist. The BIT-CIS solution match is also quite good. It is essentially the same as the CIT-CIS solution except close to the upstream boundary at $t = 0.05$ years. Therefore, unless indicated by open circles on Figure 6.7-15, the BIT-CIS solution falls on top of the CIT-CIS solution (solid circles) and could not be plotted separately on the same figure.

A similar relation exists between the BIT-BIS (closed squares) and CIT-BIS (open squares) solutions. Therefore, only the BIT-BIS solution was plotted except where indicated. However, the BIT-BIS and CIT-BIS solutions show substantial deviations from the analytical solution upstream of the source. This is because of substantial dispersion error (approximately 35% of K). Deviations are small in the downstream direction since grid blocks are smaller and freshwater convection partially negates the dispersion effect. All four numerical solution schemes gave approximately the same result downstream of the source, except close to the downstream boundary. The dispersion error inherent in the CIT-BIS and BIT-BIS solutions can be reduced substantially by choosing smaller grid block sizes and time steps at the cost of increased computer time. A CIT-CIS numerical solution with a larger time step of Wt = 0.001 year was also compared to the analytical solution. The match was quite good although the overshoot criteria of Table 6.7-8 was violated, slightly.

The numerical model predictions were also compared with the transient analytical solutions given by the USNRC (Reference 6.7-23) for a constant intensity step input of short duration and a spike input. The matches were comparable to those already discussed.

6.7.4.2.5.3 Comments. For the cases considered in the validation study, the CIT-CIS and BIT-CIS solution schemes gave good matches to the analytical solutions. The CIT-BIS and BIT-BIS solution schemes provided

only approximate matches, particularly upstream from the source. This is because of the numerical dispersion error inherent in BIS solution schemes. However, it should not be inferred that CIS solution schemes are always preferred. For the parameters used in the validation studies (see Table 6.7-9), the overshoot criteria of Table 6.7-8 are easily met for all solution schemes. If the overshoot criteria are violated significantly, the numerical solution becomes unstable resulting in unacceptable predictions. If the dispersion criteria of Table 6.7-8 are violated, the solution remains stable but artificial numerical dispersion is generated. When the model is applied to a real estuary, it may not always be possible to satisfy the overshoot stability criteria, unless extremely small grid block sizes and time steps are used. This is because of large variations in K and Q_f along the estuary. It is easier to satisfy the overshoot criteria for CIT-BIS and BIT-BIS solutions than for CIT-CIS and BIT-CIS solutions. Therefore, it may be more practical to use a BIS solution scheme and accept some dispersion error to keep computer costs reasonable.

6.7.4.3 Data Input to Hudson River Estuary Model

The Hudson River cross-sectional area, freshwater flow rate and eddy diffusivity data used in the model will be presented here. Data values are given versus mile point (MP). Mile point 0 is taken at Battery Park with MP distances increasing upstream. The Indian Point site is at MP 43, and the dam at Troy, New York, is MP 153.7. The numerical model automatically converts MP distance to the distance configuration of the calculational grid.

6.7.4.3.1 Hudson River Cross-Sectional Areas

Cross-sectional area data were taken from Consolidated Edison Company files. The data were discretized at 1-mile intervals and are given in Table 6.7-10. As required by the model, these are tidally averaged values. The cross-sectional areas were assumed to be independent of time since normally encountered changes in freshwater flow rate should not contribute significantly to changes in tidally-averaged cross-sectional area, and because cross-sectional area versus freshwater flow rate data were not available. In the model simulations, the discretized data were used to calculate an average cross-sectional area for each grid block.

6.7.4.3.2 Hudson River Freshwater Flow Rates

Since tidal volumetric flow rates are at least an order of magnitude larger than freshwater flow rates in the lower Hudson River, it is not possible to directly measure freshwater flow rates in the lower Hudson. Freshwater flow rates above the tidal penetration have been measured for more than 50 years at Green Island, New York. To estimate monthly average freshwater flow rates at various locations in the Hudson, south of Green Island, the customary practice has been to use monthly average freshwater flow rates measured at Green Island and at each of the major tributaries in the lower Hudson River basin. Using this approach,

Texas Instruments (Reference 6.7-25) has developed correlations, based on monthly average data from 1946 to 1966, that relate the freshwater flow rates in New York at Poughkeepsie and Manhattan to those at Green Island. These correlations are:

- Poughkeepsie, New York

$$Q_p = (1.1101 + 0.0207\ Q_g)\ Q_g;\ \text{all months except April and May}$$
$$Q_p = (0.9541 + 0.0103\ Q_g)\ Q_g;\ \text{April and May}$$

- Manhattan, New York

$$Q_m = (1.2078 + 0.0277\ Q_g)\ Q_g;\ \text{all months except April and May}$$
$$Q_m = (1.0445 + 0.0114\ Q_g)\ Q_g;\ \text{April and May}$$

where

Q_g = monthly average freshwater flow rate at Green Island, thousands of cfs

Q_p = monthly average freshwater flow rate at Poughkeepsie, thousands of cfs

Q_m = monthly average freshwater flow rate at Manhattan, thousands of cfs

These correlations were used with mean, monthly average freshwater flow rate data measured at Green Island from 1918 to 1975 to obtain mean monthly averages at Poughkeepsie and Manhattan. Poughkeepsie is located at MP 75. Manhattan freshwater flow rates were assumed to apply at MP 13, just south of the confluence of the Hudson River with the Harlem River.

In addition to monthly average freshwater flow rates, the special case of a persistent drought was considered. It was assumed that during drought conditions, the freshwater flow rate is constant everywhere in the Hudson north of Manhattan and is equal to 3,500 cfs. This assumption was used by Quirk, Lawler, and Matusky (Reference 6.7-26) in their study of possible contamination of drinking water drawn from the Hudson at Poughkeepsie resulting from routine releases of radionuclides at Indian Point.

In this study, the Hudson River estuary is assumed to include New York Bay. Therefore, it extends southward to the Rockaway-Sandy Hook transect. Fresh water enters Upper New York Bay with sewage discharged from the various municipalities bordering on it and from the Passaic and Hackensack Rivers through Newark Bay. Fresh water enters lower New York Bay from the Raritan River through Raritan Bay. Monthly average freshwater flow rate data for these sources were not available, so it was necessary to make estimates as discussed below.

According to Reference 6.7-27, an annual average of 2,120 cfs of water is discharged into New York Bay from municipal sewage systems. It was assumed that the sewage discharge rate remained constant throughout the year and that the discharge point was located approximately at the confluence of the Hudson River with the East River (MP -1.4). Therefore, 2,120 cfs were added to each of the monthly average and drought flow rates at Manhattan, and the updated flow rates were applied at MP -1.4.

The freshwater flow entering Upper New York Bay from Newark Bay was estimated from the ratio of the drainage area of the Passaic and Hackensack Rivers to that of the Hudson River north of Manhattan. According to Reference 6.7-27 the Hudson River drainage basin is 13,500 square miles and the combined Passaic-Hackensack River drainage basin is 463 square miles. Therefore, the contribution of the Newark Bay tributaries was calculated for each month and for drought conditions using the drainage area ratio and the appropriate freshwater flow rates at Manhattan. The freshwater flow contribution from the Raritan River was estimated in the same manner. According to Reference 6.7-27, the Raritan River drainage basin is also 463 square miles. Newark Bay is located at MP -3.8. Raritan Bay is located at MP -17.

Monthly average and drought condition freshwater flow rates at Green Island, Poughkeepsie, Manhattan, East River, Newark Bay, and Raritan Bay are given in Table 6.7-11. Mean annual averages, calculated from the monthly averages, are also given. In the numerical model simulations, the freshwater flow rates at the known locations were interpolated linearly to the middle of each grid block since tributaries entering the Hudson estuary are somewhat evenly distributed.

6.7.4.3.3 Tidally Averaged Eddy Diffusivities

An approximation for the tidally averaged, longitudinal eddy diffusivity that is applicable to the whole length of the estuary can be obtained by a modification of the method suggested by USNRC (Reference 6.7-23). The approach is based on a combination of Taylor's dispersion formula, applicable to the well-mixed portion of the estuary, and an estimate for mixing in the salinity intrusion region that is based on observed steady state, tidally averaged, salinity distributions. The effective eddy diffusivity, K, may be written as

$$K = E_S + E_T \qquad (6.7\text{-}27)$$

where

E_S = contribution because of the salinity intrusion

E_T = contribution because of Taylor dispersion

Consider the contribution to eddy diffusivity because of the salinity intrusion. For a conservative substance such as salt, the one dimensional steady state continuity equation is

$$Q_f \frac{dS}{dx} = \frac{d}{dx}\left(E_S A \frac{dS}{dx}\right) \qquad (6.7\text{-}28)$$

where S is the salinity or salt concentration in ppm. Since S is zero far upstream of the salt intrusion, Equation (6.7-28) can be integrated once and rearranged to yield

$$E_S = \frac{Q_f}{A}\left[\frac{d \ln S}{dx}\right]^{-1} \qquad (6.7\text{-}29)$$

Equation (6.7-29) can be approximated by

$$E_S = \frac{Q_f}{A}\left[\frac{\Delta \ln S}{\Delta x}\right]^{-1} \qquad (6.7\text{-}30)$$

where Q_f and A are averaged values over the spatial region Δx. Equation (6.7-30) can be used with observed steady state, tidally averaged, salinity profile data to obtain estimates of E_S that are applicable to a reach of length Δx. Essentially, the procedure requires differentiation of data and, therefore, leads to order of magnitude estimates of E_S. This is the conventional approach taken in previous thermal mixing studies.

Measured salinity versus freshwater flow rate data for various MPs along the Hudson River are given in Figure 6.7-18. These were obtained from Consolidated Edison Company files. The end of the salt intrusion region, which depends upon freshwater flow rate, is taken as the location where the salinity falls off to 100 ppm. The curves of the semi-logarithmic plot of Figure 6.7-18 were fit to analytical (exponential) functions to minimize error in reading the plot. These were then interpolated to obtain analytical expressions at MPs 5, 15, 35, 55, 75, and 85. With these expressions it was possible to apply Equation (6.7-30) to 5-mile segments using the cross-sectional area and freshwater flow rate data given in Tables 6.7-10 and 6.7-11, respectively. This allowed calculation of monthly, drought, and annual average values of E_S at 13 locations along the estuary. These values were assumed to apply at the middle of the applicable segment.

The contribution to the eddy diffusivity, because of Taylor dispersion, is given by

$$E_T = 77 n U_t R_h^{5/6} \qquad (6.7\text{-}31)$$

where

E_T = Taylor diffusivity, ft^2/sec

n = Manning coefficient $\cong$ 0.025 $sec/ft^{1/3}$ for the Hudson River

U_t = root-mean-square tidal velocity, ft/sec

R_h = hydraulic radius, feet

For an open channel of large width to depth ratio, such as the Hudson River, the hydraulic radius is equal to the mean depth. Root mean square tidal velocities depend on freshwater flow rate, and the distance from the river mouth. These data are generally not available. One set of data, measured during a 1929 United States Geologic Survey study, is available for a freshwater flow rate of 6,000 cfs at Green Island. These data are given in Table 6.7-12. Mean depth data are also given. Since E_T is small compared to E_S in the salinity intrusion region, this single set of data was used to calculate E_S for all months of the year and for drought conditions. Above the salinity intrusion region it is known that the Taylor formula predicts values of E_T that are low by a factor of 5 to 10. For these regions, the total diffusivity was set equal to 1.0 mi^2/day or $10 \cdot E_T$, whichever is less. A similar approach has been taken in previous one dimensional thermal mixing studies of the Hudson River near Indian Point.

Mean monthly, annual average, and drought period eddy diffusivities versus MP are given in Table 6.7-13. The major contribution to K in the salt intrusion region comes from E_S. Since E_S values were obtained by data differentiation, some very large values resulted, particularly in the vicinity of New York Bay. Therefore, the maximum value of K was, limited to 40 mi^2/day.

The salinity and tidal velocity data used to estimate eddy diffusivities were available only as far south as MP -2.5. That is, these data did not extend south into New York Bay. Because of the geometrical complexity of Upper and Lower New York Bay and the number of large tributaries entering it, it is extremely difficult to estimate eddy diffusivities in this region, particularly in the absence of detailed salinity data. As a result, it was assumed that eddy diffusivities in New York Bay are spatially invariant and equal to those estimated for MP -2.5 (see Table 6.7-13).

In the numerical model calculations, the tidally averaged eddy diffusivities of Table 6.7-13 were interpolated linearly to the middle of each grid block.

6.7.4.3.4 Sediment Distribution Coefficients

Numerous experimental studies have been conducted in the Hudson River estuary to determine the distribution of radionuclides in water and sediment resulting from past releases at Indian Point and deposition of bomb blast fallout. Many of these studies have been supported by the Consolidated Edison Company. The more relevant studies are cited in References 6.7-28 to 6.7-33. Most of them have focused on the area near the Indian Point site. Several isotopes were considered but simultaneous measurements of dissolved and sediment concentrations, needed to determine distribution coefficients, K_D, were obtained mostly for

radioactive cesium. Since the sediment composition varies significantly within the estuary, researchers found it difficult to correlate measured distribution coefficients with any parameter except salinity. A correlation of K_D versus salinity is given for Cs-137 in Reference 6.7-28. However, the correlation is based on limited data. As a result, the cesium data of References 6.7-29 through 6.7-32 were analyzed and used with the Reference 6.7-28 data to develop the following correlation based on nonlinear least squares regression analysis:

$$K_D = 12{,}300\ [Cl^-]^{-0.533} \qquad (6.7\text{-}32)$$

where

K_D = Cs-137 distribution coefficient, cm^3/gm

$[Cl^-]$ = dissolved chloride concentration, gm/l

Equation (6.7-32) is in agreement with the correlation of Reference 6.7-28 and is based on all Cs-137 measurements obtained to date in the Hudson by New York University researchers.

Application of Equation (6.7-32) to this study is difficult because of large temporal variations in salinity in the lower Hudson. However, on an annual average basis, the Hudson River north of Indian Point approaches a freshwater river. The salinity in the New York Bay area is close to that of sea water. The salinity in the river south of Indian Point is between fresh and sea water. Based on Equation (6.7-32) and these considerations, the annual average values of the distribution coefficients for cesium were assumed to be 3,000, 5,000, and 50,000 cm^3/g for the New York Bay area, the river south of Indian Point, and the river north of Indian Point, respectively. These values are in agreement with those reported for other estuaries in References 6.7-4 and 6.7-34.

Onishi et al (Reference 6.7-34), present a critical review of radionuclide distribution coefficient measurements obtained in freshwater rivers, estuaries, and sea water. Table 8.96 of their report gives the median and range of measured distribution coefficients for fresh and sea water for 25 different radionuclides. According to this table, K_D is the same for all isotopes of the same element (i.e., Ru-103 and Ru-106). These data were used to estimate distribution coefficients for the radionuclides considered in this study (other than Cs) by reference to the Hudson River cesium measurements. The procedure used is as follows. The river north of Indian Point was considered to be fresh water, New York Bay was assumed to contain sea water, and the river between Indian Point and Manhattan was assumed to be of intermediate salinity. For each region, the median value for cesium reported by Onishi, et al, was ratioed to that determined from the Hudson River data. The ratio was used with median values for the other radionuclides of interest, reported by Onishi et al, to estimate K_D values specific to the Hudson River estuary. The results were checked to ensure that they fell within the range of values reported by Onishi, et al, and were

consistent with those used in the Sandia study (Reference 6.7-4). Adjustments were made for consistency and to ensure that the resulting K_D values contained some margin of conservatism. The distribution coefficients that resulted are reported in Table 6.7-14.

6.7.4.4 Application of Estuary Model to Indian Point Site

The Indian Point site is located on the east bank of the Hudson River estuary at MP 43. Postulated releases of radionuclides into the estuary at Indian Point may affect drinking water drawn from the river as far north as Poughkeepsie (MP 75) and bathers as far south as Rockaway Beach (MP -25). Therefore, it is necessary to model at least a 100 mile segment of the estuary. All of the pathways to man considered in this study are discussed in detail in Section 6.7.5.

Table 6.7-8 shows that in order to meet the numerical model stability criteria, the grid block and/or time step size must decrease as the freshwater velocity increases or as the eddy diffusivity decreases. Far south of the Indian Point site, the eddy diffusivity is relatively large (see Table 6.7-13). Therefore, accurate and stable numerical solutions are readily obtained for the range of freshwater flow rates considered (see Table 6.7-11) using reasonable grid block and time step sizes. North of the salt intrusion, eddy diffusivities are low. The extent of the salt intrusion decreases as the freshwater flow rate increases. Because monthly variations in freshwater flow rates are large, the extent of the salt intrusion varies significantly as far north as MP 80 during assumed drought conditions and as far south as MP 25 during April. This has serious implications to numerical model stability because during periods of high freshwater flow rates, the freshwater velocity is high and the eddy diffusivity is low in the vicinity of, and north of, Indian Point. Unreasonably small grid block sizes and time steps are needed to model the estuary north of about MP 25 during high freshwater months. Ideally, a transient numerical solution to Equation (6.7-13) would account for monthly variations in freshwater flow rate and eddy diffusivity, to do so however, it would be necessary to employ a grid block system and time step size that would satisfy the stability criteria for all months. Such a system would require inordinate computation time and cost, considering the number of isotopes and release types examined in this study. Therefore, a model sensitivity analysis was performed to determine if approximations could be made that would still yield reasonably accurate results.

Another question which had to be resolved before production runs could be made pertains to pseudo-steady state applications of the model. The pseudo-steady state approximation applies to long lived isotopes whose release rates into the estuary do not vary significantly with time. To obtain a steady state solution, it is necessary to specify time averaged eddy diffusivities and freshwater flow rates. It is not clear, however, that a steady state solution based on annual average flow conditions would yield the same spatial concentration distribution as would be obtained by calculating monthly average steady state concentrations and averaging these over the year. In fact, preliminary calculations showed

that use of annual average flow conditions could yield considerably different results than the average of concentrations based on monthly flow conditions, particularly upstream of the site. Therefore, a second consideration in the sensitivity analysis was to determine if data for a particular month could be used to simulate annual average concentrations.

6.7.4.4.1 Sensitivity Analysis

To determine the effect of monthly variations in freshwater flow rate and eddy diffusivity on radionuclide concentrations in the Hudson River estuary, the numerical model was run at steady state for each month and for drought and annual average flow conditions. The isotope considered was Pu-239 because it behaves as a conservative contaminant during its residence time in the estuary. A source of unit intensity (i.e., 1 Ci/yr) was specified at Indian Point so that normalized concentrations, which could later be scaled to actual release rates, would result.

A 110-mile segment of the estuary was simulated, extending from MP +80 (5 miles north of Poughkeepsie) to MP -30 (Rockaway-Sandy Hook transect). The zero concentration downstream boundary condition was used so that the Pu-239 concentration was held at zero at the estuary-ocean boundary. A special grid block system consisting of 200 grid blocks in all was developed so that the stability criteria for the BIT-CIS solution scheme could be met everywhere along the river with negligible dispersion error. The size of the grid blocks, beginning at the upstream boundary (MP 80), and running in order to the downstream boundary, were

Size of Grid Block Δx, Miles	Number of This Size (in order)
0.3	178
0.5	4
1.0	2
2.0	2
3.0	9
4.0	5

It was further assumed that no radionuclide sinks were present in the estuary and that no sediment depletion of radionuclide occurred (i.e., $\lambda_s = 0$ in all grid blocks). As previously mentioned, a single source of unit intensity was placed in the grid block representing the Indian Point site.

The results of the sensitivity analysis are summarized in Tables 6.7-15 and 6.7-16. In interpreting these results, recall that the Indian Point site is located at MP 43. Table 6.7-15 reports the results for each

month of the year. Table 6.7-16 gives the average of the monthly results at each MP, the results based on use of annual average freshwater flow rate and eddy diffusivities, and the results for the assumed drought conditions. The results of Table 6.7-15 at locations downstream of Indian Point are summarized in graphical form in Figure 6.7-19. The results of Table 6.7-16 at locations downstream of Indian Point are summarized in graphical form in Figure 6.7-20.

Considering normalized PU-239 concentrations downstream of Indian Point, Table 6.7-15 and Figure 6.7-19 show that downstream concentrations for August and April vary by approximately a factor of 5 at Indian Point decreasing to approximately a factor of 3 in the New York Bay area. All other months lie in between. April exhibits the highest freshwater flow rates and August exhibits the lowest freshwater flow rates (except for drought). Figure 6.7-20 shows that the average of monthly concentrations is slightly higher than those based on annual average flow conditions. The average of monthly values is, however, a better estimate of actual annual average concentrations. If Figure 6.7-20 is superimposed on Figure 6.7-19, it can be seen that the average of monthly concentrations is adequately represented by the June results, indicating that use of June freshwater flow rates and eddy diffusivities may be used exclusively to predict annual average concentration in the estuary downstream of Indian Point. Drought conditions produce higher concentrations than would normally occur in any month.

Considering normalized Pu-239 concentrations upstream of the Indian Point site, wide variations occur from month to month (Table 6.7-15), particularly far upstream. For instance, near Poughkeepsie (MP 75), the April and August concentrations vary by many orders of magnitude. This occurs since the salt intrusion extends far upstream during August (low freshwater flow), but does not even reach the Indian Point area in April. Table 6.7-16 shows that the average of monthly concentrations is significantly higher than those predicted using annual average flow conditions, indicating that use of annual average flow conditions in the model would lead to erroneous results far upstream. A comparison of the average of monthly values with the values for the individual months shows that, far upstream, all months exhibit lower concentrations than average except for August, which is higher by a factor of 10. No single month adequately represents the annual average conditions. However, use of August would lead to conservative upstream concentration estimates. Concentrations during drought conditions are much higher than for any normal month due to the large range of the salt intrustion.

For the entire estuary, the sensitivity analysis results show that the use of August eddy diffusivities and freshwater flow rates would produce conservative estimates of annual average Pu-239 concentrations. The results would be conservative by a factor of 2 in the New York Bay area, increasing to a factor of 10 in the Poughkeepsie area. This conclusion can be extended to the other isotopes of this study because even after their decay is considered, the results for these isotopes would be qualitatively similar to those for Pu-239. The results reported here

are for steady state conditions. Short lived isotopes (i.e., I-131 and Ru-103) exhibit large temporal variations in release rate and must be simulated by transient (nonsteady state) solutions to Equation (6.7-13). The duration of the release for these isotopes, however, is on the order of a year or longer. Exclusive use of August flow conditions, instead of monthly updating, would not allow realistic estimation of monthly variations in concentration but would allow conservative predictions averaged over the course of a year or more. Because the reason for estimating dissolved radionuclide concentrations is to predict doses to man by various pathways for periods of one year to thousands of years, use of August flow conditions would not present any difficulties, particularly since August results would be conservative when applied to any other month. An additional advantage of using August flow conditions exclusively in transient simulations is that it is then not necessary to specify the month in which the accident begins.

The use of August freshwater flow rates and eddy diffusivities as representative of the entire year greatly reduces the amount of computer computation time needed to perform the analysis for all isotopes because the numerical stability criteria can be met for the entire estuary at one time using about 100 grid blocks and reasonable time step sizes.

6.7.4.4.2 Prediction of Radionuclide Concentrations - Production Runs

The numerical model was run for each isotope of interest for both sump water and core melt leach release scenarios. The source terms (discharge rates) for sump water releases are given in Table 6.7-4. The source terms for core melt leach releases are given in Table 6.7-7. Based on the results of the sensitivity analysis, freshwater flow rates and eddy diffusivities for August were used as representative of average conditions in the estuary. These are given in Tables 6.7-11 and 6.7-13, respectively. The cross-sectional areas used to convert volumetric flow rates to linear velocities are given in Table 6.7-10.

A 110-mile segment of the estuary was simulated beginning upstream at MP 80 and extending downstream to the Rockaway-Sandy Hook transect (MP -30). The zero concentration downstream boundary condition was used. A grid block system consisting of 100 grid blocks was used. The size of the grid blocks, beginning at the upstream boundary and running in order to the downstream boundary were:

Size of Grid Block Δx, Miles	Number of This Size (in order)
0.44	2
0.50	42
1.0	37
1.5	1
2.0	10
3.0	5
4.0	3

For pseudo-steady state solutions the BIT-CIS solution scheme was employed. For transient solutions, the CIT-BIS solution scheme was used with a time step size of 0.0025 years. No credit was taken for radionuclide sinks or sediment depletion (λ_S = 0 in all grid blocks). Sediment concentrations were calculated from predicted dissolved concentrations using the distribution coefficients of Table 6.7-14.

The duration of sump water and core melt leach releases at Indian Point vary from about 1.5 years for I-131 to 15,000 years for Pu-239. For dose prediction, therefore, it was necessary to "break up" the releases into various time segments. The production runs for the various isotope release type time span combinations are summarized in Table 6.7-17. The solution type (i.e., transient or steady state) and times at which results were stored are also given in the table. The results of each computer run were output onto tape; therefore, they could be input to the model used to obtain dose estimates for the various pathways to man. For most of the runs, the output consisted of a 100 by 100 array of concentrations corresponding to distances at the center of each of the 100 grid blocks and 100 time intervals.

6.7.5 PATHWAYS DEFINITION

Existing data on uses of the Hudson River below the dam at Troy, New York, were reviewed to determine the pathways by which release of radioactive materials at the Indian Point site could lead to radiation doses to humans. The important pathways are:

1. Ingestion of water.

2. Ingestion of fish.

3. Ingestion of shellfish (invertebrates).

4. Exposure to direct radiation from sediment deposited on the river and ocean shoreline.

Other pathways were excluded because of their negligible contribution to the dose. For example, boating and swimming could result in doses, but other studies have shown that doses from these pathways would only be a fraction of 1% of the dose resulting from shoreline exposure (Reference 6.7-3).

Interdiction was considered for each pathway. However, it was only included in the dose assessment for those pathways that exhibited a potential for significant health effects. Data were also reviewed to determine the distribution of pathway locations along the river and to estimate the population using each pathway at each location. The primary source of data was a study of the value of the Hudson River fishing resource (Reference 6.7-36). This review was required to estimate both the maximum individual annual doses and the population dose (the sum of the doses received by each individual in the exposed population). Tables 6.7-18 through 6.7-20 show the results for the water,

shoreline, and food pathways. Actual uses for the shoreline pathway and both actual and potential uses for the water and aquatic food pathways are shown. For this analysis, it has been assumed that increases in shoreline use in the future will be small relative to present use and that substantial increases in water use will be limited to emergency operation of the Chelsea pumping station. As shown in Table 6.7-20, the increase in use of the aquatic food pathway could be substantial, but those quantities must be regarded as speculative since massive cleanup of the Hudson River for reasons unrelated to operation of Indian Point Units 2 and 3 would be required to achieve any increase in food pathway use. Supporting data used in estimating aquatic food pathway usage are given in Table 6.7-21.

The data for actual water, shoreline, and fish pathways are judged to be reasonably accurate for use in this analysis. However, only limited data are available for estimating the population exposed through the ingestion of crabs. Since crabs are presently taken mainly by those fishing for recreation, it has been assumed that the recreational crab catch is 10% of the recreational fish catch. A spot survey of fishermen indicates that this assumption is reasonable (Reference 6.7-37).

As shown in Table 6.7-18, the actual water ingestion pathway is presently limited to one location, Poughkeepsie at MP 75, approximately 32 miles upstream from the Indian Point plant. It serves 60,000 people. The potential use, in addition to Poughkeepsie, is the Chelsea pumping station, which serves about 300,000 people as an emergency supply, and is located at MP 60, 17 miles upstream from the Indian Point plant. The station is operable, but has not been used in 13 years.

The shoreline pathway use, shown in Table 6.7-19 is dominated by ocean beaches more than 50 miles downstream from Indian Point. Nearly all of the annual beach visits occur there. But significant uses occur along the river as well. The location of maximum water and sediment concentration, is adjacent to the plant, and has been used to estimate maximum individual annual doses for shoreline exposure.

The annual fish catch, Table 6.7-20, presently serves 67,000 people at average consumption rates and could potentially serve 310,000 with river cleanup. The same table shows that the saltwater invertebrate catch, crabs only at present, serves 14,000 people at average consumption rates. Harvest of clams and oysters has been prohibited since 1925. The catch could be expanded to include enough oysters and clams to serve 10,000,000 people (100,000 from crabs, 4,700,000 from oysters, and 5,200,000 from clams) if the river could be cleaned up. The clam pathway use is assumed to be confined to the mouth of the estuary where they are most numerous, and the other food pathway uses are assumed to be uniformly distributed along the river. Maximum individual annual doses to individuals from food pathways are estimated based on an assumption that the catch is taken at the location of maximum water concentration, adjacent to the plant.

6.7.6 DOSE ASSESSMENT

6.7.6.1 Dosimetry Models and Data

The dosimetry models described in Regulatory Guide 1.109, Revision 1 (Reference 6.7-39), were used to estimate population doses and maximum doses to individuals. The water and sediment isotope concentrations used as input were described in Section 6.7-4. Isotope data for use in the model were given in Regulatory Guide 1.109, Revision 1, for all isotopes except Pu-239 which is not included in that document. Ingestion dose factors for Pu-239 were obtained from NUREG-0172 (Reference 6.7-40). Other data for Pu-239 were obtained from the original version of Regulatory Guide 1.109 (Reference 6.7-41). Values for consumption rates, delay times, and all other parameters used in the model were the default values given in Regulatory Guide 1.109, Revision 1. Saltwater bioaccumulation factors were assumed for fish and shellfish based on studies conducted near the site (Table 6.7-21). The pathway data input to the model is described in Section 6.7.5.

Doses were computed for the eight standard organs: total body, skin, bone, liver, kidney, thyroid, gastro-intestinal tract, and lung. Doses were computed for adults, teenagers, children, and infants. Population doses were estimated using the Regulatory Guide 1.109, Revision 1 age distribution--71% adults, 11% teenagers, and 18% children (including about 2% infants).

6.7.6.2 Doses and Health Effects

Maximum dose estimates to individuals and exposed population for actual pathway uses are summarized in Tables 6.7-22 and 6.7-23.

For reasons explained later, the invertebrate pathway was assumed to be interdicted for a period of 2 years. As shown in Table 6.7-22, the maximum dose to individuals from other pathways would not exceed 6 rem per year for the gastro-intestinal tract or 0.8 rem per year for any other organ for the first 2 years. In addition, they would not exceed 0.03 rem per year for any organ beyond the first 2 years. These doses would not lead to any acute health effects and would cause only a slight increase in the risk of long latency somatic effects or genetic effects in offspring. As a comparison, 6 rem per year only slightly exceeds the present 5 rem limit that applies to occupational radiation exposure. The doses after 2 years, which are less than 0.03 rem per year, are well below those each person receives from natural background radiation, about 0.1 rem per year.

Long term population doses integrated over all releases during the period of time that releases occur, are about 100,000 man-rem for each organ as shown in Table 6.7-23. The shoreline pathway contributes at least half of this in all cases. Almost all of the shoreline population dose is accumulated along ocean beaches. Other pathways contribute significantly only to bone, kidney, and gastro-intestinal tract doses.

Since most of the population dose is uniform whole body dose, a risk conversion factor of 0.0001 cancer fatalities per man-rem can be used to estimate the number of cancer fatalities that could ultimately occur in the exposed population (Reference 6.7-42). The total body population dose of 76,000 man-rem, which assumes that the invertebrate pathway is interdicted for the first 2 years, results in a prediction of less than 10 cancer fatalities. Cancer fatality risk from internal doses to organs would not add significantly to this number.

Figure 6.7-21 shows the accumulation of population dose as a function of time. The doses are accumulated in two time periods. Roughly half of the dose is accumulated in the first 2 years following the release of sump water from the containment. The remainder is accumulated over a period from 50 years to 200 years because of leaching of radionuclides from the debris bed. Short lived isotopes are the major contributors to dose in the first period while longer lived isotopes, Sr-90 and Cs-137, contribute in the second. There is negligible contribution from Pu-239.

The results presented are based on an assumption that only the invertebrate pathway (crabs) is interdicted for 2 years. There are two bases for this assumption. First, without this interdiction, the maximum individual dose to the gastro-intestinal tract in the first 2 years would be about 400 rem per year. Although this dose rate is not high enough to cause immediate physical harm, interdiction would undoubtedly be desirable. The second reason is that implementation of a 2-year prohibition of crabbing would clearly be feasible. Harvesting of clams and oysters from the Hudson River is now and has been prohibited for over 50 years. A 2-year extension of the existing prohibition to recreational crabbing would not seem to be unreasonable.

Because of the nature of the pathways associated with liquid releases and the substantial time between the accident and release to the river, the potential for mitigation of doses from liquid release is much higher than for atmospheric releases. Thus, it is possible that interdiction of other pathways could be assumed for this analysis. However, no other interdiction was assumed because individual doses from other pathways were low enough that it could be considered unnecessary. Of course, any interdiction beyond that assumed would further reduce the severity of the consequences.

6.7.6.3 Sensitivity to Important Parameters

Analyses were performed to determine sensitivity of results to changes in key parameters. The key parameters considered in these analyses were isotope release quantity, groundwater travel time, river flow rate, and pathway usage.

As shown in Figures 6.7-11 and 6.7-13, most of the radioactive material assumed to be released to the river in this analysis comes from the sump water source. It is possible, and perhaps likely that only the leach source would be present in the case of penetration of the containment basemat (see Section 3). That is, if sump water were present, it would

prevent basemat penetration. If only the leach component was presumed to be available for transport to surface waters, the consequences of such an accident through the liquid pathways would almost be eliminated. Even without any mitigation, no individual dose rates would exceed 0.1 rem per year in the first 2 years, 0.02 rem per year in the period 2 to 10 years, or 0.001 rem per year thereafter. The maximum population dose would be 1,800 man-rem to bone. This would be mostly from the water pathway. Population doses for other organs would not exceed 500 man-rem each. No health effects would be expected from these doses.

The concentrations used in the dose assessment are based on the assumption that the river flow rate over the entire period is that for an average August. The August condition was selected as representative of low flow conditions that could occur with reasonable frequency and last for reasonably long periods of time. If the releases occurred over a period of a year or more, in which flows are typical of all of the months of the year, doses would be overestimated. However, if releases occurred during a drought condition, doses would be underestimated. The assessment was not based on the drought condition since droughts are rare and are unlikely to last for periods comparable to the periods during which the most significant releases occur (a minimum of 2 years). For locations downstream from the Indian Point site or a few miles upstream, the effects of using these alternate assumptions on dose results would be a factor of about 2. That is, the drought assumption would lead to a factor of 2 increase in dose, and the average condition assumption would lead to a factor of 2 decrease. Further upstream, the situation is different because of the greater differences in upstream penetration of tidal flow and the greater importance of fresh water flow for dilution. The maximum change in concentrations at locations of pathway usage is at MP 75, the Poughkeepsie water intake. At that point, concentrations in the drought condition could exceed those for the assumed August condition by a factor of 40. Concentrations based on the average condition would be a factor of 10, lower than those based on the August condition. However, the impact on population doses would be relatively small (a factor of about 2) because these doses are dominated by downstream exposures. Only the water pathway population doses would be significantly affected by changes in the flow condition assumption.

The dose assessment is based upon actual pathway usage. If the assessment were based on potential rather than actual pathway usage, no changes would result for maximum individual dose rates. However, higher population doses would be estimated for the water, fish, and shellfish pathways. Significant increases would be limited to population doses for bone, total body, kidney and gastro-intestinal tract. The population doses based on potential use would be 490,000 man-rems for bone, 150,000 for total body, 93,000 for kidney, and 480,000 for gastro-intestinal tract. The health risk would be about double that of estimated actual use statistics.

Finally, this dose assessment is based on a mean travel time of 190 days for a nonretarded (tracer) nuclide through the groundwater system to the river. Section 6.7.3 indicates that there is a 95% probability that the

travel time will be in the range from 19 days to 1,900 days. A dose assessment based on travel times of less than the mean would lead to slight increases in individual dose rates and population doses. An assessment based on travel times at the higher end of the range (longer travel times) would yield lower doses. In this case, interdiction times for invertebrates might be extended, but would not exceed 10 years.

6.7.7 REFERENCES

6.7-1 Ritzman, R. L., et al, "Release of Radioactivity in Reactor Accidents," Appendix VII to Reactor Safety Study, U.S. Nuclear Regulatory Commission (WASH-1400), NUREG-74/014, 1975.

6.7-2 Offshore Power Systems, "Liquid Pathway Generic Study Topical Report," No. 22A60, June 1977.

6.7-3 U.S. Nuclear Regulatory Commission, Liquid Pathway Generic Study, NUREG-0440, 1978.

6.7-4 Sandia Laboratories, "Preliminary Draft of Sandia Report on Effect of Liquid Pathways on RSS Consequence Calculations," Draft, January 1980.

6.7-5 Freeze, R. A., and J. A. Cherry, Groundwater, Prentice-Hall, Englewood Cliffs, New Jersey, 1979, p. 604.

6.7-6 U.S. Atomic Energy Commission, "Consolidated Edison Company of New York, Inc., Indian Point Nuclear Generating Unit No. 3, Final Facility Description and Safety Analysis Report," Docket No. 50-286, Exhibit B-12, Volume 1.

6.7-7 Asselstine, E. S., and I. G. Grossman, "The Groundwater Resources of Westchester County, New York, Part 1, Records of Wells and Test Holes," New York Water and Power Control Commission Bulletin GW-35, 1955, p. 79.

6.7-8 Dames & Moore, "Supplemental Geological Investigation of the Indian Point Generating Station," prepared for Consolidated Edison Company of New York, Inc., 1975.

6.7-9 INTERCOMP, "A Model for Calculating Effects of Liquid Waste Disposal in Deep Saline Aquifers," U.S. Geological Survey Water Resources Inv., 1976, p. 76-61.

6.7-10 Walton, William C., Groundwater Resource Evaluation, McGraw-Hill Book Company, New York, 1970, p. 664.

6.7-11 Seitz, M. G., P. G. Rickert, S. M. Fried, A. M. Friedman, and M. J. Steindler, "Studies of Nuclear-Water Migration in Geological Media," Argonne National Laboratory Report ANL-79-30, 1979, p. 62.

6.7-12 Apps, J. A., J. Lucas, A. K. Mathur, and L. Tsao, "Theoretical and Experimental Evaluation of Waste Transport in Selected Rocks," 1977 Annual Report of LBL Contract No. 45901 AK, Lawrence Berkeley Laboratory, Berkeley, California, Report LBL-6022, 1977, p. 139.

6.7-13 Baes, C. F., Jr., and R. E. Mesmer, The Hydrolosis of Cations, Wiley-Interscience, New York, 1976, p. 489

6.7-14 Daly, R. A., G. E. Manager, and S. P. Clark, Jr., "Density of Rocks" Sydney P. Clark, Jr., Ed., Handbook of Physical Constants, Revised Edition, Geological Society of America Memoir 97, 1966, pp.19-26.

6.7-15 Winograd, I. J., and W. Thordarson, "Hydrogeologic and Hydrochemical Framework, South-Central Great Basin, Nevada-California," with Special Reference to the Nevada Test Site: U.S. Geological Survey Professional Paper 712-C, 1975, pp. C1-C126.

6.7-16 Freeze, R. A., "A Stochastic-Conceptual Analysis of One-Dimensional Groundwater Flow in Nonuniform Homogeneous Media," Water Resources Research, 1975, Vol. 11, pp. 725-741.

6.7-17 Ralston, A., and H. S. Wilf, Mathmatical Methods for Digital Computers, Vol. II, John Wiley & Sons, Inc., New York, 1979, p. 287.

6.7-18 Maini, Y. N. T., "In Situ Hydraulic Parameters in Jointed Rock--Their Measurement and Interpretation," Ph.D. Thesis, Imperial College, University of London, 1971.

6.7-19 Peehs, M., A. Skohan, and M. Reimann, "The Behavior of Concrete in Contact with Molten Corium in the Case of a Hypothetical Core Melt Accident," Nuclear Technology, Vol. 46, 1979, pp. 192-198.

6.7-20 Skohan, A., H. Holleck, and M. Peehs, "Chemical Reactions Between Light Water Reactor Core Melt and Concrete," Nuclear Technology, Vol. 46, 1979, pp. 255-262.

6.7-21 Letter from H. T. Keller of Westinghouse Electric Corporation, to William Bennett of Consolidated Edison Company of New York, Inc., June 9, 1980.

6.7-22 Hem, J. D., "Study and Interpretation of the Chemical Characteristics of Natural Water," Second Edition, U.S. Geological Survey Water Supply Paper 1473, 1970, p. 363.

6.7-23 U.S. Nuclear Regulatory Commission, "Estimating Aquatic Dispersion of Effluents from Accidental and Routine Reactor Releases for the Purpose of Implementing," Appendix I, Regulatory Guide 1.113, 1977.

6.7-24 Carnahan, B., H. A. Luther, and J. O. Wilkes, Applied Numerical Methods, John Wiley and Sons, Inc., New York, 1969.

6.7-25 Texas Instruments, Consolidated Edison Company files.

6.7-26 Quirk, Lawler, and Matusky Engineers, "Transport of Contaminants in the Hudson River Above Indian Point Station," New York, New York.

6.7-27 Duedall, I. W., H. B. O'Connors, R. E. Wilson, and J. H. Parker, "The Lower Bay Complex," MESA New York Bight Atlas Monograph No. 29, New York Sea Grant Institute, Albany, New York, May 1979.

6.7-28 Jinks, S. M., and M. E. Wrenn, "Radiocesium Transport in the Hudson River Estuary," Chapter 11 in Environmental Toxicity of Aquatic Radionuclides: Models and Mechanisms, edited by M. W. Miller and J. N. Stannard, Ann Arbor Science Publishers, Ann Arbor, Michigan, 1975.

6.7-29 Wrenn, M. E., N. P. Singh, N. Cohen, M. Eisenbud, P. Linsalata, S. Schaffer, and G. B. Cook, "Radioecological Studies of the Hudson River, Volume 1: The Distribution of BETA-GAMMA-Emitting Radionuclides, 1976 and 1977," Progress Report to Consolidated Edison Company of New York, Inc., January 29, 1979.

6.7-30 Eisenbud, M., N. Cohen, M. E. Wrenn, P., Linslata, S. Schaffer, M. Maiello, and L. Ayres, "Radioecological Studies of the Hudson River, 1978," Progress Report to Consolidated Edison Company of New York, Inc., March 28, 1980.

6.7-31 Hairr, L. M., "An Investigation of Factors Influencing Radiocesium Cycling in Estuarine Sediments of the Hudson River," Ph.D. Dissertation, New York University, New York, New York, 1974.

6.7-32 Wrenn, M. E., J. W. Lentsch, M. Eisenbud, G. J. Laver, and G. P. Howells, "Radiocesium Distribution in Water, Sediment and Biota in the Hudson River Estuary from 1964 through 1970," Procedures, 3rd National Symposium on Radioecology, USAEC CONF-710501-P1, pp. 334-343, 1971.

6.7-33 Wrenn, M. E., S. M. Jinks, N. Cohen, and L. M. Hairr, "^{137}Cs and ^{134}Cs Distribution in Sediment, Water and Biota of the Lower Hudson River and Their Dosimetric Implications for Man," Procedures, 3rd International Congress of the International Radiation Protection Association, Washington, D.C., September 9-14, 1973.

6.7-34 Onishi, Y., R. J. Serne, E. M. Arnold, C. E. Cowan, and F. L. Thompson, "Critical Review: Radionuclide Transport, Sediment Transport, and Water Quality Mathematical Modeling; and Radionuclide Adsorption/Desorption Mechanisms," USNRC, PNL, NUREG/CR-1322, PNL-2901, August 1980.

6.7-35 Abood, F. A., "Evaluation of Circulation in Partially Stratified Estuary Typified by the Hudson River," Ph.D. Thesis, Rutgers University, June 1977, p. 301.

6.7-36 Sheppart, J.D., "Valuation of the Hudson River Fishery Resources: Past, Present, and Future," Bureau of Fisheries, New York State Department of Environmental Conservation, Albany, New York, 1976.

6.7-37 "Lower Hudson River Creel Survey Report, Summer 1980," New York State Department of Environmental Conservation.

6.7-38 Wrenn, et al, "Radiocesium Distribution in Water, Sediment, and Biota in the Husdon River Estuary from 1964 through 1970," Proceedings of the Third National Syumposium on Radioecology, USAED CONF-710501, pp. 334-343, 1971.

6.7-39 Regulatory Guide 1.109, "Calculation of Annual Doses to Man from Routine Releases of Reactor Effluents for the Purpose of Evaluating Compliance with 10 CFR Part 50, Appendix I, USNRC, Revision 1, October 1977.

6.7-40 "Age-Specific Radiation Dose Commitment Factors for a One-Year Chronic Intake," NUREG-0172, Battelle Pacific Northwest Laboratory, November 1977.

6.7-41 Regulatory Guide 1.109, "Calculation of Annual Doses to Man from Routine Releases of Reactor Effluents for the Purpose of Evaluating Compliance with 10 CFR Part 50, Appendix I, USNRC, Revision 0, March 1976.

6.7-42 "Recommendation of the International Commission on Radiological Protection, ICRP Publication 26, January 1977.

TABLE 6.7-1

RADIONUCLIDE SOURCE INVENTORIES AND RELEASE FRACTIONS FOR SELECTED NUCLIDES

Nuclide[a]	Core Inventory At Melt-Through		Core Inventory After 1 Year		Half Life (days)	Release Fractions	
	(Curies)[a]	(Kilograms)	(Curies)[a]	(Kilograms)		Leach	Sump Water
Co-60	2.90E + 5[c]	2.56E - 1	2.54E + 5	2.24E - 1	1.92E + 3	0.92	0.08
Sr-89	9.41E + 7	3.33E + 0	7.24E + 5	2.56E - 2	5.20E + 1	0.89	0.11
Sr-90	3.71E + 6	2.63E + 1	3.62E + 6	2.54E + 1	1.03E + 4	0.89	0.11
Ru-103	1.08E + 8	3.37E + 0	1.80E + 5	5.62E - 3	3.96E + 1	0.92	0.08
Ru-106	2.48E + 7	7.43E + 0	1.24E + 7	3.71E + 0	3.69E + 2	0.92	0.08
I-131	8.48E + 7	6.84E - 1	-	-	8.04E + 0	0.00	1.00
Cs-134	7.49E + 6	5.78E + 0	5.34E + 6	4.12E + 0	7.52E + 2	0.00	1.00
Cs-137	4.67E + 6	5.39E + 1	4.56E + 6	5.26E + 1	1.10E + 4	0.00	1.00
Pu-239	2.13E + 4	3.47E + 2	2.17E + 4	3.54E + 2	8.91E + 6	0.99	0.01

(a) Selected from Table A1 of Reference 6.7-4
(b) From Table 2.2 of Reference 6.7-4
(c) 2.90E + 5 denotes $2.90 * 10^5$

TABLE 6.7-2

INITIAL RADIONUCLIDE SOURCE INVENTORIES AND ESTIMATED DISTRIBUTION COEFFICIENTS FOR GROUNDWATER TRANSPORT IN LIMESTONE

Nuclide a/	Initial Core Inventory		Half-Life (days) a/	Sump Water Source Fraction b/	Limestone k_d (ml/gm) c/	Dominant Solution Species c/
	Curies a/	Kilograms				
Co-60	2.90E+5	0.3	1.92E+3	0.08	3.0	Unknown
Sr-89	9.41E+7	3.3	5.20E+1	0.11	0.5	Meas k_d
Sr-90	3.71E+6	26.3	1.03E+4	0.11	0.5	Meas k_d
Ru-103	1.08E+8	3.4	3.96E+1	0.08	0.0	Unknown
Ru-106	2.48E+7	7.4	3.69E+2	0.08	0.0	Unknown
I-131	8.48E+7	0.7	8.04E+0	1.00	0.0	I^- or I_2
Cs-134	7.49E+6	5.8	7.52E+2	1.00	3.0	Meas k_d
Cs-137	4.67E+6	53.9	1.10E+4	1.00	3.0	Meas k_d
Pu-239	2.13E+4	347.3	8.91E+6	0.01	13.0	Meas k_d

a/ Selected from Table A.1 of Reference 6.7-4 (Sandia), 2.90E+5 denotes 2.90×10^5

b/ From Table 2.2 of Reference 6.7-4 (Sandia)

c/ Measured: Seitz, and others, (Reference 6.7-11)
Apps, and others, (Reference 6.7-12)
Others: Estimated assuming dominance of hydrolysis product shown (Reference 6.7-13). See text.

TABLE 6.7-3

VALUES OF LOG MEAN AND LOG STANDARD DEVIATION OF TRAVEL TIMES IN DAYS OF NUCLIDES FROM INDIAN POINT 3 TO THE HUDSON RIVER FOR SEVERAL VALUES OF DISTRIBUTION COEFFICIENTS AND VARYING UNCERTAINTY ASSUMPTIONS ABOUT HYDROLOGIC PARAMETERS

Distribution Coefficient, k_d (ml/gm)	0.0		0.5		1.0		3.0		10.0	
	Mean	Sigma	Mean	Sigma	Mean	Sigma	Mean	Sigma	Mean	Sigma
Case 1	2.28	0.50	4.71	0.50	5.02	0.51	5.49	0.49	6.02	0.50
Case 2	2.28	0.25	4.73	0.50	5.02	0.50	5.48	0.49	6.03	0.50
Case 3	2.27	0.90	4.71	0.50	5.01	0.49	5.49	0.50	6.01	0.50

Note: Values of K_d for each nuclide of interest are provided in Table 6.7-2. Corresponding travel times, T, at the mean and 2 sigma (2σ) level (95%) are calculated as:

$$T_{mean} = 10^{(Mean)} \text{ days}$$

$$T_{2\sigma} = 10^{(Mean \pm 2\ Sigma)} \text{ days}$$

TABLE 6.7-4

DISCHARGE RATES OF SELECTED NUCLIDES TO THE RIVER AT VARIOUS TIMES FOLLOWING SUMP WATER RELEASE

Source Terms in Curies Per Year for Sump Water Release											
	Time-Year	Ru-106	Ru-103	Pu-239	SR-90	CO-60	SR-89	I-131	CS-134	CS-137	Total
1	2.00E-02	7.39E+01	1.16E+02	6.39E-23	1.15E-08	1.83E-16	2.13E-13	2.23E+02	4.13E-14	4.47E-14	4.10E+02
2	1.00E-01	8.06E+04	9.21E+04	1.31E-22	3.36E-08	4.32E-16	1.80E-12	6.45E+04	9.71E-14	1.06E-13	2.37E+05
3	2.00E-01	1.07E+06	7.13E+05	1.78E-22	5.33E-08	6.26E-16	6.96E-11	4.21E+04	1.40E-13	1.54E-13	1.83E+06
4	3.00E-01	2.95E+06	1.11E+06	2.13E-22	6.98E-08	7.77E-16	9.49E-10	5.14E+03	1.74E-13	1.91E-13	4.07E+06
5	4.00E-01	3.42E+06	7.26E+05	4.73E-23	1.27E-07	1.41E-15	2.44E-09	2.66E+02	1.99E-13	3.68E-13	4.15E+06
6	5.00E-01	3.87E+06	4.63E+05	2.05E-21	3.88E-07	4.45E-15	4.16E-09	1.34E+01	3.11E-13	1.26E-12	4.33E+06
7	6.00E-01	3.71E+06	2.51E+05	6.81E-21	9.72E-07	1.14E-14	6.57E-09	5.69E-01	5.23E-13	3.45E-12	3.96E+05
8	7.00E-01	3.10E+06	1.18E+05	1.88E-20	2.12E-06	2.52E-14	9.62E-09	2.09E-02	9.25E-13	8.10E-12	3.22E+05
9	8.00E-01	2.34E+06	5.00E+04	4.53E-20	4.16E-06	5.01E-14	1.31E-08	6.91E-04	1.52E-12	1.70E-11	2.39E+06
10	9.00E-01	1.64E+06	1.97E+04	9.83E-20	7.56E-06	9.19E-14	1.66E-08	2.12E-05	2.15E-12	3.26E-11	1.66E+06
11	1.00E-00	1.10E+06	7.44E+03	1.97E-19	1.29E-05	1.58E-13	1.99E-08	6.23E-07	3.47E-12	5.84E-11	1.11E+06
12	1.10E-00	7.14E+05	2.72E+03	3.69E-19	2.10E-05	2.59E-13	2.26E-08	1.78E-08	4.97E-12	9.91E-11	7.17E+05
13	1.20E+00	4.55E+05	9.76E+02	6.55E-19	3.27E-05	4.06E-13	2.44E-08	4.98E-10	7.80E-12	1.61E-10	4.56E+05
14	1.30E+00	2.88E+05	3.47E+02	1.11E-18	4.53E-05	6.14E-13	2.53E-08	1.38E-11	1.18E-11	2.51E-10	2.88E+05
15	1.40E+00	1.81E+05	1.23E+02	1.81E-18	7.20E-05	9.00E-13	2.53E-08	3.83E-11	1.74E-11	3.79E-10	1.81E+05
16	1.50E+00	1.14E+05	4.35E+01	2.85E-18	1.03E-04	1.29E-12	2.45E-08	1.06E-14	2.49E-11	5.56E-10	1.14E+05
17	1.60E+00	7.16E+04	1.54E+01	4.37E-18	1.43E-04	1.80E-12	2.31E-08	2.95E-16	3.48E-11	7.96E-10	7.16E+04
18	1.70E+00	4.58E+04	5.49E+00	6.52E-18	1.95E-04	2.46E-12	2.12E-08	0	4.77E-11	1.12E-09	4.58E+04
19	1.80E+00	2.88E+04	1.96E+00	9.51E-18	2.62E-04	3.31E-12	1.90E-08	0	6.43E-11	1.53E-09	2.88E+04
20	1.90E+00	1.84E+04	7.07E-01	1.36E-17	3.46E-04	4.38E-12	1.67E-08	0	8.51E-11	2.07E-09	1.84E+04
21	2.00E+00	1.18E+04	2.56E-01	1.91E-17	4.51E-04	5.72E-12	1.44E-08	0	1.11E-10	2.76E-09	1.18E+04
22	2.10E+00	7.67E+03	9.36E-02	2.63E-17	5.81E-04	7.36E-12	1.22E-08	0	1.43E-10	3.63E-09	7.67E+03
23	2.20E+00	5.01E+03	3.44E-02	3.58E-17	7.39E-04	9.37E-12	1.02E-08	0	1.82E-10	4.70E-09	5.01E+03
24	2.30E+00	3.29E+03	1.28E-02	4.81E-17	9.30E-04	1.18E-11	8.36E-09	0	2.25E-10	6.03E-09	3.29E+03
25	2.60E+00	9.80E+02	6.78E-04	1.08E-16	1.76E-03	2.23E-11	4.31E-09	0	4.03E-10	1.20E-08	9.80E+02

TABLE 6.7-4 (continued)

DISCHARGE RATES OF SELECTED NUCLIDES TO THE RIVER AT VARIOUS TIMES FOLLOWING SUMP WATER RELEASE

	Source Terms in Curies Per Year for Sump Water Release										
	Time-Year	Ru-106	Ru-103	Pu-239	SR-90	CO-60	SR-89	I-131	CS-134	CS-137	Total
26	2.80E+00	4.53E+02	0	1.77E-16	2.52E-03	3.21E-11	0	0	5.73E-10	1.77E-08	4.53E+02
27	3.00E+00	2.16E+02	0	2.79E-16	3.33E-03	4.27E-11	0	0	7.96E-10	2.40E-08	2.16E+02
28	3.50E+00	3.85E+01	0	7.76E-16	6.18E-03	8.06E-11	0	0	1.67E-09	4.76E-08	3.85E+01
29	4.00E+00	8.16E+00	0	1.88E-15	1.06E-02	1.40E-10	0	0	3.20E-09	8.62E-08	8.17E+00
30	4.50E+00	2.01E+00	0	4.10E-15	1.70E-02	2.27E-10	0	0	5.70E-09	1.46E-07	2.03E+00
31	5.00E+00	5.51E-01	0	8.31E-15	2.60E-02	3.51E-10	0	0	9.55E-09	2.33E-07	5.77E-01
32	5.50E+00	1.63E-01	0	1.57E-14	3.83E-02	5.21E-10	0	0	1.52E-08	3.56E-07	2.01E-01
33	6.30E+00	2.53E-02	0	3.88E-14	7.01E-02	9.73E-10	0	0	2.93E-08	7.09E-07	9.54E-02
34	1.50E+01	0	0	1.33E-11	3.80E+00	6.10E-08	0	0	8.13E-07	1.85E-04	3.80E+00
35	2.00E+01	0	0	9.40E-11	1.35E+01	2.26E-07	0	0	1.22E-06	1.45E-03	1.35E+01
36	2.50E+01	0	0	4.34E-10	3.29E+01	5.53E-07	0	0	1.12E-06	5.89E-03	3.29E+01
37	3.00E+01	0	0	1.53E-09	6.25E+01	1.01E-06	0	0	7.40E-07	1.28E-02	6.25E+01
38	3.50E+01	0	0	4.44E-09	9.99E+01	1.49E-06	0	0	3.94E-07	2.45E-02	9.99E+01
39	4.00E+01	0	0	1.13E-08	1.42E+02	1.88E-06	0	0	1.78E-07	4.33E-02	1.42E+02
40	4.50E+01	0	0	2.57E-08	1.83E+02	2.11E-06	0	0	0	7.18E-02	1.83E+02
41	5.00E+01	0	0	5.40E-08	2.21E+02	2.15E-06	0	0	0	1.13E-01	2.21E+02
42	5.50E+01	0	0	1.05E-07	2.53E+02	2.03E-06	0	0	0	1.69E-01	2.53E+02
43	6.00E+01	0	0	1.41E-07	2.76E+02	1.80E-06	0	0	0	2.42E-01	2.76E+02
44	6.50E+01	0	0	1.87E-07	2.91E+02	1.51E-06	0	0	0	3.37E-01	2.91E+02
45	7.00E+01	0	0	2.41E-07	2.98E+02	1.21E-06	0	0	0	4.53E-01	2.98E+02
46	7.50E+01	0	0	3.06E-07	2.97E+02	9.37E-07	0	0	0	5.87E-01	2.98E+02
47	8.00E+01	0	0	3.83E-07	2.90E+02	7.01E-07	0	0	0	7.48E-01	2.91E+02
48	8.50E+01	0	0	4.72E-07	2.78E+02	5.10E-07	0	0	0	9.31E-01	2.79E+02
49	9.00E+01	0	0	5.75E-07	2.62E+02	3.61E-07	0	0	0	1.12E+00	2.63E+02
50	9.50E+01	0	0	6.94E-07	2.43E+02	2.50E-07	0	0	0	1.34E+00	2.44E+02

TABLE 6.7-4 (continued)

DISCHARGE RATES OF SELECTED NUCLIDES TO THE RIVER AT VARIOUS TIMES FOLLOWING SUMP WATER RELEASE

	Source Terms in Curies Per Year for Sump Water Release										
	Time-Year	Ru-106	Ru-103	Pu-239	SR-90	CO-60	SR-89	I-131	CS-134	CS-137	Total
51	1.00E+02	0	0	8.29E-07	2.23E+02	1.70E-07	0	0	0	1.57E+00	2.25E+02
52	1.10E+02	0	0	1.21E-06	1.83E+02	7.43E-08	0	0	0	2.04E+00	1.85E+02
53	1.20E+02	0	0	1.78E-06	1.45E+02	3.07E-08	0	0	0	2.52E+00	1.48E+02
54	1.30E+02	0	0	2.52E-06	1.11E+02	1.21E-08	0	0	0	2.98E+00	1.14E+02
55	1.40E+02	0	0	3.49E-06	8.37E+01	0	0	0	0	3.36E+00	8.71E+01
56	1.50E+02	0	0	4.73E-06	6.18E+01	0	0	0	0	3.67E+00	6.55E+01
57	1.60E+02	0	0	6.39E-06	4.50E+01	0	0	0	0	3.91E+00	4.89E+01
58	1.70E+02	0	0	8.56E-06	3.24E+01	0	0	0	0	4.03E+00	3.64E+01
59	1.80E+02	0	0	1.13E-05	2.30E+01	0	0	0	0	4.06E+00	2.71E+01
60	1.90E+02	0	0	1.46E-05	1.62E+01	0	0	0	0	4.04E+00	2.02E+01
61	2.00E+02	0	0	1.88E-05	1.14E+01	0	0	0	0	3.92E+00	1.53E+01
62	2.10E+02	0	0	2.39E-05	7.92E+00	0	0	0	0	3.74E+00	1.17E+01
63	2.20E+02	0	0	3.01E-05	5.49E+00	0	0	0	0	3.55E+00	9.04E+00
64	2.30E+02	0	0	3.76E-05	3.78E+00	0	0	0	0	3.29E+00	7.07E+00
65	2.40E+02	0	0	4.64E-05	2.60E+00	0	0	0	0	3.03E+00	5.63E+00
66	2.50E+02	0	0	5.70E-05	1.78E+00	0	0	0	0	2.77E+00	4.55E+00
67	2.60E+02	0	0	6.91E-05	1.22E+00	0	0	0	0	2.49E+00	3.71E+00
68	2.70E+02	0	0	8.31E-05	8.33E-01	0	0	0	0	2.23E+00	3.06E+00
69	2.80E+02	0	0	9.95E-05	5.68E-01	0	0	0	0	1.98E+00	2.55E+00
70	2.90E+02	0	0	1.18E-04	3.87E-01	0	0	0	0	1.74E+00	2.13E+00
71	3.00E+02	0	0	1.40E-04	2.63E-01	0	0	0	0	1.52E+00	1.78E+00
72	3.10E+02	0	0	1.65E-04	1.79E-01	0	0	0	0	1.32E+00	1.50E+00
73	3.20E+02	0	0	1.94E-04	1.22E-01	0	0	0	0	1.14E+00	1.26E+00
74	3.30E+02	0	0	2.25E-04	8.27E-02	0	0	0	0	9.81E-01	1.06E+00
75	3.40E+02	0	0	2.60E-04	5.62E-02	0	0	0	0	8.41E-01	8.97E-01

TABLE 6.7-4 (continued)

DISCHARGE RATES OF SELECTED NUCLIDES TO THE RIVER AT VARIOUS TIMES FOLLOWING SUMP WATER RELEASE

	Source Terms in Curies Per Year for Sump Water Release										
	Time-Year	Ru-106	Ru-103	Pu-239	SR-90	CO-60	SR-89	I-131	CS-134	CS-137	Total
76	3.50E+02	0	0	3.00E-04	3.82E-02	0	0	0	0	7.14E-01	7.53E-01
77	3.60E+02	0	0	3.44E-04	2.60E-02	0	0	0	0	6.05E-01	6.31E-01
78	3.70E+02	0	0	3.93E-04	1.77E-02	0	0	0	0	5.11E-01	5.29E-01
79	3.80E+02	0	0	4.46E-04	1.20E-02	0	0	0	0	4.29E-01	4.41E-01
80	3.90E+02	0	0	5.04E-04	8.20E-03	0	0	0	0	3.59E-01	3.68E-01
81	4.00E+02	0	0	5.68E-04	5.59E-03	0	0	0	0	3.00E-01	3.05E-01
82	4.10E+02	0	0	6.38E-04	3.81E-03	0	0	0	0	2.49E-01	2.53E-01
83	4.20E+02	0	0	7.14E-04	2.60E-03	0	0	0	0	2.07E-01	2.10E-01
84	4.30E+02	0	0	7.95E-04	1.78E-03	0	0	0	0	1.71E-01	1.74E-01
85	4.40E+02	0	0	8.83E-04	1.22E-03	0	0	0	0	1.41E-01	1.43E-01
86	4.50E+02	0	0	9.77E-04	8.32E-04	0	0	0	0	1.16E-01	1.18E-01
87	4.60E+02	0	0	1.08E-03	5.70E-04	0	0	0	0	9.55E-02	9.72E-02
88	4.70E+02	0	0	1.19E-03	3.91E-04	0	0	0	0	7.81E-02	7.97E-02
89	4.80E+02	0	0	1.31E-03	2.68E-04	0	0	0	0	6.38E-02	6.54E-02
90	4.90E+02	0	0	1.43E-03	1.84E-04	0	0	0	0	5.21E-02	5.37E-02
91	5.00E+02	0	0	1.56E-03	1.27E-04	0	0	0	0	4.23E-02	4.40E-02
92	6.00E+02	0	0	3.34E-03	0	0	0	0	0	4.93E-03	8.27E-03
93	7.00E+02	0	0	6.02E-03	0	0	0	0	0	5.09E-04	6.53E-03
94	8.00E+02	0	0	9.60E-03	0	0	0	0	0	4.84E-05	9.65E-03
95	9.00E+02	0	0	1.40E-02	0	0	0	0	0	4.35E-06	1.40E-02
96	1.00E+03	0	0	1.90E-02	0	0	0	0	0	3.75E-07	1.90E-02
97	2.00E+03	0	0	6.16E-02	0	0	0	0	0	0	6.16E-02
98	3.00E+03	0	0	5.47E-02	0	0	0	0	0	0	5.47E-02
99	4.90E+03	0	0	1.75E-02	0	0	0	0	0	0	1.75E-02

TABLE 6.7-5

FINAL COMPOSITION OF MELTS

Compound	Silica Concrete and Silica Gravel		Limestone Concrete and Limestone Gravel	
	Weight %	10^3 Tons	Weight %	10^3 Tons
SiO_2	84.6	4.200	5.3	0.100
$CaCo_3$	3.0	0.100	81.2	2.300
Al_2O_3	6.3	0.300	3.9	0.100
UO_2	2.4	0.118	4.2	0.118
ZrO_2	1.0	0.100	1.7	0.100
FeO+NiO +Cr_2O_3	2.7	0.100	3.7	0.100
Total	100.0	4.9×10^3	100.0	2.8×10^3

Note: Recalculated from Sandia Draft (Reference 6.7-4). Table A.7 assuming CaO present as $CaCO_3$, and the UO_2 present eauals 118 tons initially present in core.

TABLE 6.7-6

SUMMARY OF LEACH CONSTANTS AND OF PARAMETERS BY WHICH THEY WERE ESTIMATED

Assumptions and Parameter Values Leading to Tabulated Leach Constants	Leach Constant (Equations 6.7-8, and 6.7-9) Per Day ± Standard Deviations
I. Rates of solid to liquid transfer are high so that elemental solubilities and rate of groundwater flow control the leach constant, i.e.:	
$\frac{R}{M}\ \frac{1}{da} = F\ \frac{m^3}{da} \times C\ \frac{gm}{m^3}\ /\ M(gms)$	
$F = 10^{-0.6 \pm 0.6} m^3/da$	
A. Homogeneous melt with major constituent:	
SiO_2; $C = 10^{2.3 \pm 0.3}\ \frac{gm}{m^3}$; $M = 10^{9.6} gm$	$10^{-7.9 \pm 0.7}$
$CaCO_3$; $C = 10^{2.2 \pm 0.5}\ \frac{gm}{m^3}$; $M = 10^{9.4} gm$	$10^{-7.8 \pm 0.8}$
B. Heterogeneous melt with major constituent:	
UO_2; $C = 10^{2.0 \pm 1.0}\ \frac{gm}{m^3}$; $M = 10^{8.1} gm$	$10^{-6.7 \pm 1.2}$
FeO; $C = 10^{0 \pm 2}\ \frac{gm}{m^3}$; $M = 10^{8} gm$	$10^{-8.6 \pm 2.1}$
II. Solubilities and groundwater flow rates are high, so that the rate of solid to liquid transfer controls the leach constant, i.e.:	
$\frac{R}{M}\ \frac{1}{day} = KE\ \frac{gm}{cm^2\text{-}da} \times SA\ \frac{cm^2}{gm}$	
$k_e = 10^{-7 \pm 2}\ \frac{gm}{cm^2\text{-}da}$;	
$SA = 10^{1 \pm 2}\ \frac{cm^2}{gm}$	$10^{-6 \pm 2.8}$

TABLE 6.7-7

DISCHARGE RATES OF SELECTED NUCLIDES TO THE RIVER AT VARIOUS TIMES FROM CORE MELT LEACHING

Source Terms in Curies Per Year for Core Leach Release								
	Time-Year	Ru-106	Ru-103	Pu-239	SR-90	CO-60	SR-89	Total
1	1.00E+00	0	0	0	0	0	0	0
2	1.20E+00	3.33E+01	7.45E-02	0	0	0	3.34E-19	3.34E+01
3	1.40E+00	2.83E+02	2.04E-01	0	0	0	1.74E-17	2.84E+02
4	1.60E+00	5.27E+02	1.20E-01	0	0	0	1.82E-16	5.27E+02
5	1.80E+00	6.18E+02	4.48E-02	0	0	0	8.08E-16	6.18E+02
6	2.00E+00	6.08E+02	1.40E-02	0	3.46E-23	0	2.11E-15	6.08E+02
7	2.20E+00	5.58E+02	4.08E-03	0	3.18E-21	0	3.86E-15	5.58E+02
8	2.40E+00	4.98E+02	1.16E-03	0	1.94E-19	1.21E-22	5.50E-15	4.98E+02
9	2.60E+00	4.38E+02	3.24E-04	0	8.53E-18	3.93E-21	6.26E-15	4.38E+02
10	2.80E+00	3.83E+02	0	0	2.85E-16	9.53E-20	0	3.83E+02
11	3.00E+00	3.35E+02	0	0	7.52E-15	1.86E-18	0	3.35E+02
12	4.00E+00	1.69E+02	0	0	6.51E-09	3.50E-14	0	1.69E+02
13	5.00E+00	8.49E+01	0	0	1.83E-05	1.03E-13	0	8.49E+01
14	6.00E+00	4.27E+01	0	2.40E-26	4.08E-05	2.48E-13	0	4.27E+01
15	7.00E+00	2.15E+01	0	3.41E-25	8.07E-05	5.52E-13	0	2.15E+01
16	8.00E+00	1.08E+01	0	3.28E-24	1.46E-04	1.15E-12	0	1.08E+01
17	9.00E+00	5.43E+00	0	2.42E-23	2.56E-04	2.21E-12	0	5.43E+00
18	1.00E+01	2.73E+00	0	1.45E-22	4.36E-04	4.06E-12	0	2.73E+00
19	1.10E+01	1.37E+00	0	7.33E-22	7.06E-04	7.10E-12	0	1.37E+00
20	1.20E+01	6.90E-01	0	3.22E-21	1.10E-03	1.18E-11	0	6.91E-01
21	1.30E+01	3.47E-01	0	1.26E-20	1.68E-03	1.81E-11	0	3.48E-01
22	1.40E+01	1.74E-01	0	4.45E-20	2.50E-03	2.97E-11	0	1.77E-01
23	1.50E+01	8.77E-02	0	1.44E-19	3.61E-03	4.48E-11	0	9.13E-02
24	1.60E+01	4.41E-02	0	4.34E-19	5.11E-03	6.55E-11	0	4.92E-02

TABLE 6.7-7 (continued)

DISCHARGE RATES OF SELECTED NUCLIDES TO THE RIVER AT VARIOUS TIMES FROM CORE MELT LEACHING

	Source Terms in Curies Per Year for Core Leach Release							
	Time-Year	Ru-106	Ru-103	Pu-239	SR-90	CO-60	SR-89	Total
25	1.70E+01	2.22E-02	0	1.22E-18	7.09E-03	9.38E-11	0	2.93E-02
26	1.80E+01	1.11E-02	0	3.24E-18	9.65E-03	1.31E-10	0	2.08E-02
27	1.90E+01	5.61E-03	0	8.16E-18	1.29E-02	1.78E-10	0	1.85E-02
28	2.00E+01	2.82E-03	0	1.96E-17	1.70E-02	2.39E-10	0	1.98E-02
29	4.00E+01	0	0	2.76E-12	4.79E-01	5.16E-09	0	4.79E-01
30	6.00E+01	0	0	2.88E-09	1.85E+00	8.69E-09	0	1.85E+00
31	8.00E+01	0	0	1.68E-07	3.28E+00	5.06E-09	0	3.28E+00
32	1.00E+02	0	0	3.92E-07	3.95E+00	1.67E-09	0	3.95E+00
33	1.20E+02	0	0	7.83E-07	3.80E+00	3.90E-10	0	3.80E+00
34	1.40E+02	0	0	1.41E-06	3.19E+00	0	0	3.19E+00
35	1.60E+02	0	0	2.49E-06	2.45E+00	0	0	2.45E+00
36	1.80E+02	0	0	4.32E-06	1.76E+00	0	0	1.76E+00
37	2.00E+02	0	0	7.09E-06	1.22E+00	0	0	1.22E+00
38	2.20E+02	0	0	1.11E-05	8.15E-01	0	0	8.15E-01
39	2.40E+02	0	0	1.73E-05	5.35E-01	0	0	5.35E-01
40	2.60E+02	0	0	2.61E-05	3.45E-01	0	0	3.45E-01
41	2.80E+02	0	0	3.83E-05	2.20E-01	0	0	2.20E-01
42	3.00E+02	0	0	5.49E-05	1.40E-01	0	0	1.40E-01
43	3.20E+02	0	0	7.76E-05	8.81E-02	0	0	8.81E-02
44	3.40E+02	0	0	1.07E-04	5.53E-02	0	0	5.54E-02
45	3.60E+02	0	0	1.46E-04	3.46E-02	0	0	3.47E-02
46	3.80E+02	0	0	1.96E-04	2.16E-02	0	0	2.18E-02
47	4.00E+02	0	0	2.58E-04	1.35E-02	0	0	1.37E-02
48	4.20E+02	0	0	3.36E-04	8.37E-03	0	0	8.71E-03

TABLE 6.7-7 (continued)

DISCHARGE RATES OF SELECTED NUCLIDES TO THE RIVER AT VARIOUS TIMES FROM CORE MELT LEACHING

Source Terms in Curies Per Year for Core Leach Release								
	Time-Year	Ru-106	Ru-103	Pu-239	SR-90	CO-60	SR-89	Total
49	4.40E+02	0	0	4.33E-04	5.21E-03	0	0	5.64E-03
50	4.60E+02	0	0	5.49E-04	3.24E-03	0	0	3.79E-03
51	4.80E+02	0	0	6.90E-04	2.01E-03	0	0	2.70E-03
52	5.00E+02	0	0	8.58E-04	1.25E-03	0	0	2.11E-03
53	5.20E+02	0	0	1.06E-03	7.76E-04	0	0	1.84E-03
54	5.40E+02	0	0	1.29E-03	4.82E-04	0	0	1.77E-03
55	5.60E+02	0	0	1.56E-03	0	0	0	1.56E-03
56	5.80E+02	0	0	1.88E-03	0	0	0	1.88E-03
57	6.00E+02	0	0	2.24E-03	0	0	0	2.24E-03
58	1.00E+03	0	0	2.52E-02	0	0	0	2.52E-02
59	1.50E+03	0	0	1.17E-01	0	0	0	1.17E-01
60	2.00E+03	0	0	2.72E-01	0	0	0	2.72E-01
61	2.50E+03	0	0	4.49E-01	0	0	0	4.49E-01
62	3.00E+03	0	0	6.12E-01	0	0	0	6.12E-01
63	3.50E+03	0	0	7.43E-01	0	0	0	7.43E-01
64	4.00E+03	0	0	8.40E-01	0	0	0	8.40E-01
65	4.50E+03	0	0	9.07E-01	0	0	0	9.07E-01
66	5.00E+03	0	0	9.49E-01	0	0	0	9.49E-01
67	5.50E+03	0	0	9.74E-01	0	0	0	9.74E-01
68	6.00E+03	0	0	9.87E-01	0	0	0	9.87E-01
69	6.50E+03	0	0	9.91E-01	0	0	0	9.91E-01
70	7.00E+03	0	0	9.89E-01	0	0	0	9.89E-01
71	7.50E+03	0	0	9.83E-01	0	0	0	9.83E-01
72	8.00E+03	0	0	9.75E-01	0	0	0	9.75E-01

TABLE 6.7-7 (continued)

DISCHARGE RATES OF SELECTED NUCLIDES TO THE RIVER AT VARIOUS TIMES FROM CORE MELT LEACHING

Source Terms in Curies Per Year for Core Leach Release								
	Time-Year	Ru-106	Ru-103	Pu-239	SR-90	CO-60	SR-89	Total
73	8.50E+03	0	0	9.65E-01	0	0	0	9.65E-01
74	9.00E+03	0	0	9.54E-01	0	0	0	9.54E-01
75	9.50E+03	0	0	9.42E-01	0	0	0	9.42E-01
76	1.00E+04	0	0	9.30E-01	0	0	0	9.30E-01
77	1.05E+04	0	0	9.17E-01	0	0	0	9.17E-01
78	1.10E+04	0	0	9.05E-01	0	0	0	9.05E-01
79	1.15E+04	0	0	8.92E-01	0	0	0	8.92E-01
80	1.20E+04	0	0	8.80E-01	0	0	0	8.80E-01
81	1.25E+04	0	0	8.68E-01	0	0	0	8.68E-01
82	1.30E+04	0	0	8.56E-01	0	0	0	8.56E-01
83	1.35E+04	0	0	8.43E-01	0	0	0	8.43E-01
84	1.40E+04	0	0	8.32E-01	0	0	0	8.32E-01
85	1.45E+04	0	0	8.20E-01	0	0	0	8.20E-01
86	1.50E+04	0	0	0	0	0	0	0

TABLE 6.7-8

TIME AND SPACE STEP CRITERIA FOR FINITE DIFFERENCE SOLUTION SCHEMES

Scheme	Dispersion	Overshoot
CIT-CIS	--------	$\frac{U\Delta t}{2\Delta x} + \frac{K\Delta t}{(\Delta x)^2} \leq 1$ $\frac{U\Delta x}{2K} \leq 1$
CIT-BIS	$\frac{U\Delta x}{2K} << 1$	$\frac{U\Delta t}{2\Delta x} \leq 1$
BIT-CIS	$\frac{U^2\Delta t}{2K} << 1$	$\frac{U\Delta x}{2K} \leq 1$
BIT-BIS	$\frac{U\Delta x}{2K} + \frac{U^2\Delta t}{2K} << 1$	--------

Nomenclature:

U = freshwater velocity in grid block = Q_f/A
K = eddy diffusivity in grid block
Δx = grid block length
Δt = size of time step

TABLE 6.7-9

PARAMETER VALUES FOR VALIDATION STUDIES

Constant Coefficients	
*Velocity	$U = 600$ mi/yr
*Freshwater Flow Rate	$Q_f = 3$ mi^3/yr
*Cross-Sectional Area	$A = 5 \times 10^{-3}$ mi^2
*Eddy Diffusivity	$K = 3{,}500$ mi^2/day
Source Strength	$q_{source} = 1$ Ci/yr
Source Location	$x_o = 75$ mi
Numerical Model Grid Block Sizes**	
$x < 40$ mi,	$\Delta x = 4$ mi
$x > 40$ mi,	$\Delta x = 2$ mi
Isotope Decay Constants	
Pu-239	$\lambda_D = 2.84 \times 10^{-5}$ yr^{-1}
I-131	$\lambda_D = 31.46$ yr^{-1}
SR-89	$\lambda_D = 4.864$ yr^{-1}
Ru-103	$\lambda_D = 6.388$ yr^{-1}

*These values are typical for the Hudson River Estuary.
**The numerical model was run with the freshwater convection downstream boundary condition option.

TABLE 6.7-10

HUDSON RIVER CROSS-SECTIONAL AREAS

Battery = MP 0

Mile Point	Area 1,000 ft^3	Mile Point	Area 1,000 ft^3	Mile Point	Area 1,000 ft^2	Mile Point	Area 1,000 ft^2	Mile Point	Area 1,000 ft^2	Mile Point	Area 1,000 ft^2
-30	755	2	199	34	186	66	149	98	90	130	35
-29	755	3	180	35	207	67	140	99	89	131	31
-28	755	4	160	36	245	68	131	100	88	132	80
-27	755	5	150	37	279	69	153	101	82	133	28
-26	755	6	130	38	255	70	149	102	75	134	27
-25	755	7	125	39	200	71	124	103	62	135	25
-24	755	8	124	40	185	72	122	104	66	136	23
-23	755	9	126	41	175	73	134	105	68	137	20
-22	755	10	128	42	167	74	122	106	68	138	23
-21	755	11	125	43	175	75	124	107	70	139	24
-20	755	12	124	44	171	76	128	108	94	140	21
-19	755	13	124	45	137	77	123	109	85	141	20
-18	755	14	128	46	138	78	124	110	60	142	19
-17	755	15	135	47	142	79	120	111	50	143	20
-16	755	16	139	48	135	80	113	112	43	144	25
-15	755	17	139	49	131	81	113	113	35	145	18
-14	650	18	137	50	125	82	112	114	32	146	15
-13	575	19	140	51	125	83	115	115	31	147	17
-12	635	20	145	52	129	84	118	116	40	148	15
-11	635	21	147	53	165	85	124	117	50	149	13
-10	580	22	184	54	182	86	109	118	54	150	8
- 9	530	23	183	55	145	87	96	119	50	151	7
- 8	425	24	190	56	127	88	120	120	43	152	6
- 7	335	25	198	57	150	89	110	121	42	153	5
- 6	308	26	202	58	167	90	110	122	40	153.7	3
- 5	330	27	204	59	162	91	106	123	34		
- 4	408	28	203	60	158	92	102	124	28		
- 3	390	29	215	61	154	93	122	125	28		
- 2	345	30	225	62	150	94	120	126	35		
- 1	275	31	220	63	150	95	115	127	34		
0	208	32	209	64	150	96	109	128	33		
1	203	33	200	65	151	97	100	129	34		

TABLE 6.7-11

MEAN HUDSON RIVER FRESHWATER FLOW RATE IN CFS

Month	Green Island MP + 153.7	Poughkeepsie MP + 75	Manhattan MP + 13	East River MP - 1.4	Newark Bay MP - 3.8	Raritan Bay MP - 17
January	12,833	17,655	20,061	21,079	21,937	23,558
February	12,199	16,623	18,856	19,874	20,691	22,271
March	22,190	34,826	40,440	41,458	43,015	45,335
April	31,060	39,571	43,440	44,458	46,118	48,541
May	19,028	21,884	24,002	25,020	26,013	27,769
June	9,684	12,691	14,294	15,312	15,972	17,395
July	6,900	8,645	9,653	10,671	11,172	12,436
August	5,446	6,660	7,399	8,417	8,841	10,028
September	6,231	7,721	8,601	9,619	10,084	11,312
October	7,772	9,878	11,060	12,078	12,627	13,939
November	12,200	16,624	18,858	19,876	20,693	22,273
December	13,771	19,213	21,886	22,904	23,825	25,509
Annual	13,268	17,666	19,879	20,897	21,749	23,364
Drought	3,500	3,500	3,500	4,518	4,808	5,861

TABLE 6.7-12

DATA FOR TAYLOR DISPERSION CALCULATIONS

Segment Number	Mile Point (miles)	Segment Length (miles)	Mean Depth (feet)	Tidal Velocity (fps)
1	153-130	23	6.0	0.50
2	130-120	10	20.0	1.50
3	120-110	10	12.0	1.80
4	110-100	10	16.0	1.80
5	100-95	5	21.0	1.60
6	95-90	5	28.0	1.25
7	90-85	5	34.0	1.10
8	85-80	5	32.0	1.00
9	80-75	5	62.0	1.00
10	75-70	5	52.0	1.05
11	70-68	2	50.0	1.10
12	68-66	2	58.0	1.10
13	66-64	2	47.0	1.05
14	64-62	2	33.0	1.00
15	62-60	2	34.0	1.00
16	60-58	2	26.0	0.95
17	58-56	2	20.0	0.95
18	56-53	3	50.0	0.90
19	53-50	3	88.0	0.90
20	50-47	3	78.0	0.92
21	47-44	3	75.0	1.00
22	44-42	2	50.0	1.00
23	42-40	2	45.0	0.95
24	40-38	2	36.0	0.90
25	38-36	2	22.0	0.85
26	36-34	2	17.0	0.85
27	34-32	2	29.0	0.85
28	32-30	2	19.0	0.90
29	30-25	5	18.0	0.90
30	25-20	5	26.0	1.05
31	20-15	5	29.0	1.25
32	15-10	5	27.0	1.50
33	10-5	5	27.0	2.10
34	5-0	5	46.0	2.20
35	0-(-5)	5	33.0	2.20

Taken from Reference 6.7-35.

TABLE 6.7-13

TIDALLY AVERAGED DIFFUSIVITY DATA IN SQUARE MILES PER DAY

Mile Point	Jan	Feb	March	April	May	June	July	Aug	Sept	Oct	Nov	Dec	Annual	Drought
-02.5	40.000	40.000	40.000	40.000	40.000	32.342	24.572	20.932	22.172	27.742	40.000	40.000	40.000	11.662
02.5	40.000	40.000	40.000	40.000	40.000	32.419	24.649	21.009	22.249	27.819	40.000	40.000	40.000	11.739
07.5	40.000	40.000	40.000	40.000	40.000	40.000	34.365	29.275	31.005	38.835	40.000	40.000	40.000	16.235
12.5	20.899	21.589	19.189	18.929	19.969	23.499	27.449	25.639	26.849	25.419	21.389	20.569	20.999	15.559
17.5	19.113	19.753	17.553	17.323	18.273	21.493	25.113	23.453	24.573	23.253	19.573	18.813	19.213	14.233
22.5	6.385	6.940	5.233	5.080	5.726	8.857	15.855	16.505	17.345	11.485	6.774	6.139	6.466	9.768
27.5	4.042	4.437	0.600	0.600	3.583	5.839	12.110	13.220	13.940	8.004	4.319	3.870	4.099	7.624
32.5	17.750	16.220	0.700	0.700	0.700	13.400	10.460	9.800	9.940	11.680	16.620	0.700	17.490	8.143
37.5	16.150	14.770	0.800	0.800	0.800	12.200	9.529	8.930	9.058	10.640	15.130	0.800	15.920	7.425
42.5	6.707	7.110	1.000	1.000	1.000	8.340	11.634	12.464	12.464	9.789	6.992	1.000	6.768	12.464
47.5	1.000	3.570	1.000	1.000	1.000	4.721	10.393	13.093	13.093	6.579	3.474	1.000	1.000	13.093
52.5	1.000	1.000	1.000	1.000	1.000	1.794	6.316	11.061	11.391	2.805	1.000	1.000	1.000	7.840
57.5	0.910	0.910	0.910	0.910	0.910	0.910	5.960	10.511	10.821	2.593	0.910	0.910	0.910	7.421
62.5	1.000	1.000	1.000	1.000	1.000	1.000	3.722	2.996	2.882	1.000	1.000	1.000	1.000	7.168
67.5	1.000	1.000	1.000	1.000	1.000	1.000	3.944	3.185	3.066	1.000	1.000	1.000	1.000	7.547
72.5	1.000	1.000	1.000	1.000	1.000	1.000	2.296	2.446	2.387	1.000	1.000	1.000	1.000	3.862
77.5	1.000	1.000	1.000	1.000	1.000	1.000	1.000	2.565	1.000	1.000	1.000	1.000	1.000	4.046
82.5	1.000	1.000	1.000	1.000	1.000	1.000	1.000	1.000	1.000	1.000	1.000	1.000	1.000	2.320
87.5	1.000	1.000	1.000	1.000	1.000	1.000	1.000	1.000	1.000	1.000	1.000	1.000	1.000	2.423
92.5	1.000	1.000	1.000	1.000	1.000	1.000	1.000	1.000	1.000	1.000	1.000	1.000	1.000	1.000
97.5	1.000	1.000	1.000	1.000	1.000	1.000	1.000	1.000	1.000	1.000	1.000	1.000	1.000	1.000
105.5	1.000	1.000	1.000	1.000	1.000	1.000	1.000	1.000	1.000	1.000	1.000	1.000	1.000	1.000
115.0	0.850	0.850	0.850	0.850	0.850	0.850	0.850	0.850	0.850	0.850	0.850	0.850	0.850	0.850
125.0	1.000	1.000	1.000	1.000	1.000	1.000	1.000	1.000	1.000	1.000	1.000	1.000	1.000	1.000
140.0	0.130	0.130	0.130	0.130	0.130	0.130	0.130	0.130	0.130	0.130	0.130	0.130	0.130	0.130

TABLE 6.7-14

RADIONUCLIDE DISTRIBUTION COEFFICIENTS FOR THE HUDSON RIVER ESTUARY

Radionuclide	K_D, cm^3/g New York Bay	K_D, cm^3/gm River South of Indian Point	K_D, cm^3/gm River North of Indian Point
Iodine	30	50	500
Ruthenium	300	500	5,000
Strontium	500	850	8,500
Cesium	3,000	5,000	50,000
Plutonium	30,000	50,000	500,000

TABLE 6.7-15

RESULTS OF STEADY STATE, PU-239 SENSITIVITY ANALYSIS CALCULATIONS FOR EACH MONTH
TABLE ENTRIES ARE NORMALIZED CONCENTRATIONS IN CURIES PER CUBIC MILE PER CI/YR RELEASED

Mile Point (MP)	Jan	Feb	Mar	Apr	May	Jun	Jul	Aug	Sep	Oct	Nov	Dec
80.	1.314E-34	2.805E-29	1.104E-83	3.341-100	1.347E-46	1.189E-20	1.704E-06	4.898E-04	9.786E-06	9.746E-14	2.443E-29	7.997E-41
78.	1.962E-32	3.052E-27	1.324E-78	1.021E-93	8.348E-44	4.034E-19	1.832E-05	1.176E-03	8.136E-05	1.482E-12	2.660E-27	1.946E-38
76.	2.405E-30	2.764E-25	8.535E-74	1.022E-87	3.853E-41	1.195E-17	1.377E-04	2.343E-03	4.852E-04	2.028E-11	2.409E-25	3.803E-36
74.	3.053E-28	2.583E-23	6.405E-69	1.178E-81	1.821E-38	3.611E-16	5.548E-04	4.717E-03	1.629E-03	2.815E-10	2.252E-23	7.743E-34
72.	4.234E-26	2.619E-21	6.530E-64	2.048E-75	9.579E-36	1.157E-14	1.620E-03	9.697E-03	4.116E-03	4.081E-09	2.284E-21	1.740E-31
70.	4.625E-24	2.127E-19	3.205E-59	1.167E-69	3.641E-33	3.150E-13	3.600E-03	1.837E-02	8.827E-03	5.225E-08	1.856E-19	3.000E-29
68.	2.901E-22	1.032E-17	3.007E-55	6.174E-65	6.614E-31	5.876E-12	6.359E-03	3.056E-02	1.627E-02	5.014E-07	9.003E-18	2.791E-27
66.	2.246E-20	6.084E-16	5.173E-51	7.130E-60	1.569E-28	1.264E-10	1.077E-02	5.045E-02	2.976E-02	5.364E-06	5.310E-16	3.281E-25
64.	1.292E-18	2.722E-14	3.854E-47	2.593E-55	2.512E-26	2.220E-09	1.778E-02	8.139E-02	5.297E-02	4.911E-05	2.377E-14	2.777E-23
62.	7.652E-17	1.250E-12	3.133E-43	1.025E-50	4.142E-24	3.970E-08	2.963E-02	1.313E-01	9.417E-02	4.355E-04	1.092E-12	2.426E-21
60.	4.615E-15	5.842E-11	2.706E-39	4.253E-46	6.950E-22	7.186E-07	4.562E-02	1.748E-01	1.313E-01	1.941E-03	5.104E-11	2.165E-19
58.	2.671E-13	2.626E-09	2.103E-35	1.493E-41	1.098E-19	1.263E-05	6.417E-02	2.072E-01	1.593E-01	5.191E-03	2.295E-09	1.845E-17
56.	2.632E-11	1.934E-07	8.253E-31	4.558E-36	3.443E-17	2.366E-04	8.942E-02	2.396E-01	1.876E-01	1.244E-02	1.691E-07	2.846E-15
54.	2.201E-09	1.223E-05	2.075E-26	7.597E-31	8.683E-15	2.154E-03	1.235E-01	2.759E-01	2.200E-01	2.883E-02	1.069E-05	3.661E-13
52.	1.175E-07	4.447E-04	1.383E-22	2.070E-26	1.216E-12	1.053E-02	1.656E-01	3.141E-01	2.546E-01	6.107E-02	3.907E-04	2.891E-11
50.	1.835E-05	6.429E-03	2.503E-17	4.647E-20	6.792E-10	3.927E-02	2.262E-01	3.666E-01	3.035E-01	1.216E-01	5.889E-03	7.384E-09
48.	2.441E-03	3.203E-02	2.632E-12	4.541E-14	3.051E-07	9.495E-02	2.902E-01	4.217E-01	3.567E-01	1.970E-01	3.052E-02	1.595E-06
46.	5.574E-02	9.325E-02	1.009E-07	1.058E-08	9.083E-05	1.774E-01	3.560E-01	4.786E-01	4.131E-01	2.815E-01	9.135E-02	2.437E-04
44.	1.760E-01	1.985E-01	2.278E-03	1.208E-03	2.114E-02	2.834E-01	4.292E-01	5.417E-01	4.769E-01	3.759E-01	1.976E-01	3.031E-02
43.	2.435E-01	2.585E-01	1.236E-01	1.122E-01	2.030E-01	3.355E-01	4.633E-01	5.712E-01	5.072E-01	4.192E-01	2.585E-01	2.264E-01
42.	2.426E-01	2.575E-01	1.234E-01	1.121E-01	2.027E-01	3.339E-01	4.597E-01	5.660E-01	5.031E-01	4.164E-01	2.575E-01	2.260E-01
40.	2.409E-01	2.557E-01	1.228E-01	1.117E-01	2.021E-01	3.308E-01	4.516E-01	5.545E-01	4.937E-01	4.105E-01	2.557E-01	2.250E-01
38.	2.399E-01	2.545E-01	1.222E-01	1.114E-01	2.015E-01	3.283E-01	4.433E-01	5.422E-01	4.836E-01	4.051E-01	2.545E-01	2.240E-01
36.	2.392E-01	2.537E-01	1.216E-01	1.111E-01	2.009E-01	3.263E-01	4.356E-01	5.305E-01	4.740E-01	4.005E-01	2.537E-01	2.232E-01
34.	2.385E-01	2.528E-01	1.211E-01	1.108E-01	2.004E-01	3.238E-01	4.253E-01	5.150E-01	4.611E-01	3.944E-01	2.528E-01	2.223E-01
32.	2.378E-01	2.518E-01	1.205E-01	1.104E-01	1.996E-01	3.210E-01	4.133E-01	4.974E-01	4.462E-01	3.873E-01	2.519E-01	2.211E-01
30.	2.370E-01	2.507E-01	1.199E-01	1.101E-01	1.987E-01	3.176E-01	4.016E-01	4.814E-01	4.327E-01	3.794E-01	2.509E-01	2.193E-01
28.	2.356E-01	2.487E-01	1.194E-01	1.098E-01	1.975E-01	3.119E-01	3.891E-01	4.657E-01	4.195E-01	3.686E-01	2.489E-01	2.173E-01
26.	2.319E-01	2.439E-01	1.186E-01	1.094E-01	1.959E-01	3.020E-01	3.754E-01	4.496E-01	4.060E-01	3.540E-01	2.442E-01	2.144E-01
24.	2.262E-01	2.370E-01	1.178E-01	1.089E-01	1.931E-01	2.900E-01	3.612E-01	4.331E-01	3.921E-01	3.383E-01	2.374E-01	2.102E-01
22.	2.184E-01	2.278E-01	1.168E-01	1.084E-01	1.888E-01	2.762E-01	3.462E-01	4.157E-01	3.772E-01	3.214E-01	2.282E-01	2.040E-01
20.	2.088E-01	2.170E-01	1.155E-01	1.075E-01	1.828E-01	2.613E-01	3.300E-01	3.966E-01	3.608E-01	3.037E-01	2.174E-01	1.961E-01
18.	1.994E-01	2.066E-01	1.141E-01	1.065E-01	1.765E-01	2.475E-01	3.136E-01	3.769E-01	3.437E-01	2.871E-01	2.069E-01	1.882E-01
16.	1.886E-01	1.948E-01	1.120E-01	1.050E-01	1.687E-01	2.327E-01	2.966E-01	3.564E-01	3.258E-01	2.699E-01	1.951E-01	1.789E-01
14.	1.767E-01	1.820E-01	1.092E-01	1.028E-01	1.597E-01	2.173E-01	2.792E-01	3.356E-01	3.074E-01	2.523E-01	1.822E-01	1.685E-01
12.	1.622E-01	1.667E-01	1.051E-01	9.940E-02	1.482E-01	1.999E-01	2.603E-01	3.130E-01	2.874E-01	2.331E-01	1.668E-01	1.554E-01
10.	1.473E-01	1.510E-01	9.983E-02	9.489E-02	1.359E-01	1.828E-01	2.408E-01	2.896E-01	2.665E-01	2.143E-01	1.510E-01	1.418E-01
8.	1.330E-01	1.360E-01	9.414E-02	8.991E-02	1.238E-01	1.664E-01	2.216E-01	2.663E-01	2.456E-01	1.963E-01	1.360E-01	1.286E-01
6.	1.196E-01	1.219E-01	8.797E-02	8.441E-02	1.123E-01	1.509E-01	2.020E-01	2.422E-01	2.240E-01	1.788E-01	1.219E-01	1.161E-01
4.	1.066E-01	1.085E-01	8.129E-02	7.834E-02	1.009E-01	1.352E-01	1.813E-01	2.167E-01	2.009E-01	1.605E-01	1.085E-01	1.039E-01

TABLE 6.7-15 (continued)

RESULTS OF STEADY STATE, PU-239 SENSITIVITY ANALYSIS CALCULATIONS FOR EACH MONTH
TABLE ENTRIES ARE NORMALIZED CONCENTRATIONS IN CURIES PER CUBIC MILE PER CI/YR RELEASED

Mile Point (MP)	Jan	Feb	Mar	Apr	May	Jun	Jul	Aug	Sep	Oct	Nov	Dec
2.	9.481E-02	9.624E-02	7.467E-02	7.225E-02	9.035E-02	1.203E-01	1.614E-01	1.924E-01	1.788E-01	1.429E-01	9.624E-02	9.271E-02
0.	8.429E-02	8.540E-02	6.819E-02	6.621E-02	8.078E-02	1.066E-01	1.426E-01	1.696E-01	1.580E-01	1.263E-01	8.540E-02	8.263E-02
- 2.	7.541E-02	7.630E-02	6.241E-02	6.077E-02	7.261E-02	9.514E-02	1.270E-01	1.508E-01	1.406E-01	1.125E-01	7.630E-02	7.410E-02
- 4.	6.752E-02	6.822E-02	5.703E-02	5.569E-02	6.529E-02	8.497E-02	1.132E-01	1.342E-01	1.253E-01	1.003E-01	6.822E-02	6.647E-02
- 6.	6.008E-02	6.063E-02	5.174E-02	5.065E-02	5.832E-02	7.544E-02	1.003E-01	1.187E-01	1.111E-01	8.889E-02	6.063E-02	5.926E-02
- 8.	5.328E-02	5.371E-02	4.668E-02	4.580E-02	5.191E-02	6.677E-02	8.865E-02	1.048E-01	9.818E-02	7.857E-02	5.371E-02	5.264E-02
-10.	4.719E-02	4.753E-02	4.202E-02	4.133E-02	4.613E-02	5.904E-02	7.828E-02	9.246E-02	8.669E-02	6.938E-02	4.753E-02	4.669E-02
-12.	4.189E-02	4.215E-02	3.778E-02	3.722E-02	4.105E-02	5.233E-02	6.932E-02	8.182E-02	7.677E-02	6.144E-02	4.215E-02	4.150E-02
-14.	3.718E-02	3.739E-02	3.396E-02	3.352E-02	3.653E-02	4.639E-02	6.140E-02	7.241E-02	6.800E-02	5.441E-02	3.739E-02	3.688E-02
-16.	3.241E-02	3.257E-02	2.994E-02	2.960E-02	3.191E-02	4.039E-02	5.342E-02	6.296E-02	5.917E-02	4.734E-02	3.257E-02	3.218E-02
-18.	2.824E-02	2.836E-02	2.639E-02	2.613E-02	2.787E-02	3.516E-02	4.646E-02	5.473E-02	5.146E-02	4.117E-02	2.836E-02	2.807E-02
-20.	2.338E-02	2.346E-02	2.209E-02	2.191E-02	2.312E-02	2.907E-02	3.840E-02	4.520E-02	4.253E-02	3.402E-02	2.346E-02	2.326E-02
-22.	1.933E-02	1.938E-02	1.846E-02	1.834E-02	1.916E-02	2.401E-02	3.169E-02	3.729E-02	3.511E-02	2.808E-02	1.938E-02	1.925E-02
-24.	1.389E-02	1.392E-02	1.342E-02	1.335E-02	1.380E-02	1.724E-02	2.273E-02	2.673E-02	2.519E-02	2.014E-02	1.392E-02	1.385E-02
-26.	9.947E-03	9.961E-03	9.721E-03	9.688E-03	9.903E-03	1.233E-02	1.625E-02	1.910E-02	1.801E-02	1.440E-02	9.961E-03	9.927E-03

TABLE 6.7-16

RESULTS OF STEADY STATE PU-239 SENSITIVITY ANALYSIS CALCULATIONS FOR SPECIAL CONDITIONS TABLE ENTRIES ARE NORMALIZED CONCENTRATIONS IN CURIES PER CUBIC MILE PER CI/YR RELEASED

Mile Point (MP)	Average of Monthly Results	Productions Based On Annual Average Conditions	Productions for Drought Conditions
80.	4.178E-05	1.503E-34	9.377E-02
78.	1.063E-04	2.269E-32	1.233E-01
76.	2.472E-04	2.799E-30	1.552E-01
74.	5.750E-04	3.565E-28	1.959E-01
72.	1.286E-03	4.951E-26	2.482E-01
70.	2.566E-03	5.406E-24	2.974E-01
68.	4.432E-03	3.384E-22	3.360E-01
66.	7.582E-03	2.610E-20	3.750E-01
64.	1.268E-02	1.495E-18	4.160E-01
62.	2.129E-02	8.795E-17	4.624E-01
60.	2.947E-02	5.264E-15	5.124E-01
58.	3.632E-02	3.018E-13	5.642E-01
56.	4.411E-02	2.938E-11	6.260E-01
54.	5.420E-02	2.425E-09	6.927E-01
52.	6.723E-02	1.278E-07	7.593E-01
50.	8.913E-02	1.957E-05	8.364E-01
48.	1.188E-01	2.552E-03	9.030E-01
46.	1.623E-01	5.708E-02	9.623E-01
44.	2.278E-01	1.778E-01	1.024E-00
43.	3.102E-01	2.449E-01	1.051E-00
42.	3.084E-01	2.440E-01	1.043E-00
40.	3.046E-01	2.424E-01	1.025E-00
38.	3.009E-01	2.414E-01	1.006E-00
36.	2.975E-01	2.408E-01	9.863E-01
34.	2.932E-01	2.401E-01	9.611E-01
32.	2.882E-01	2.394E-01	9.335E-01
30.	2.833E-01	2.386E-01	9.063E-01
28.	2.777E-01	2.371E-01	8.759E-01
26.	2.704E-01	2.333E-01	8.420E-01
24.	2.621E-01	2.276E-01	8.078E-01
22.	2.524E-01	2.196E-01	7.723E-01
20.	2.415E-01	2.100E-01	7.341E-01
18.	2.306E-01	2.005E-01	6.956E-01
16.	2.187E-01	1.895E-01	6.563E-01
14.	2.061E-01	1.775E-01	6.166E-01
12.	1.915E-01	1.629E-01	5.741E-01
10.	1.763E-01	1.478E-01	5.298E-01
8.	1.615E-01	1.335E-01	4.856E-01

TABLE 6.7-16 (continued)

RESULTS OF STEADY STATE PU-239 SENSITIVITY ANALYSIS CALCULATIONS FOR SPECIAL CONDITIONS TABLE ENTRIES ARE NORMALIZED CONCENTRATIONS IN CURIES OER CUBIC MILE PER CI/YR RELEASED

Mile Point (MP)	Average of Monthly Results	Productions Based On Annual Average Conditions	Productions for Drought Conditions
6.	1.468E-01	1.199E-01	4.397E-01
4.	1.319E-01	1.069E-01	3.920E-01
2.	1.178E-01	9.503E-02	3.467E-01
0.	1.047E-01	8.445E-02	3.049E-01
-2.	9.365E-02	7.554E-02	2.705E-01
-4.	8.386E-02	6.762E-02	2.404E-01
-6.	7.465E-02	6.016E-02	2.126E-01
-8.	6.623E-02	5.335E-02	1.876E-01
-10.	5.869E-02	4.724E-02	1.653E-01
-12.	5.212E-02	4.193E-02	1.463E-01
-14.	4.629E-02	3.721E-02	1.295E-01
-16.	4.037E-02	3.244E-02	1.126E-01
-18.	3.520E-02	2.826E-02	9.794E-02
-20.	2.916E-02	2.339E-02	8.093E-02
-22.	2.412E-02	1.934E-02	6.679E-02
-24.	1.735E-02	1.390E-02	4.791E-02
-26.	1.243E-02	9.949E-02	3.424E-02

TABLE 6.7-17

SUMMARY OF DISSOLVED RADIONUCLIDE CONCENTRATION COMPUTER RUNS

Computer Run	Isotope	Release Type	Time Span years	Time Intervals at Which Results Were Saved years	Solution Type
1	Ru-106	Sump	0 to 1	0.05	Transient
2	Ru-103	Sump	0 to 1	0.05	Transient
3	I-131	Sump	0 to 1	0.05	Transient
4	Ru-106	Sump	0 to 15	0.20	Transient
5	Ru-106	Core Leach	0 to 15	0.20	Transient
6	Ru-103	Sump	0 to 15	0.20	Transient
7	Ru-103	Core Leach	0 to 15	0.20	Transient
8	Sr-90	Sump	0 to 15	0.20	Transient
9	Sr-90	Core Leach	0 to 15	0.20	Transient
10	I-131	Sump	0 to 15	0.20	Transient
11	Sr-90	Sump	0 to 100	1.00	Steady State
12	Sr-90	Core Leach	0 to 100	1.00	Steady State
13	Cs-137	Sump	0 to 100	1.00	Steady State
14	Pu-239	Sump	0 to 1,000	10.00	Steady State
15	Pu-239	Core Leach	0 to 1,000	10.00	Steady State
16	Sr-90	Sump	0 to 1,000	10.00	Steady State
17	Sr-90	Core Leach	0 to 1,000	10.00	Steady State
18	Cs-137	Sump	0 to 1,000	10.00	Steady State
19	Pu-239	Sump	0 to 15,000	150.00	Steady State
20	Pu-239	Core Leach	0 to 15,000	150.00	Steady State

TABLE 6.7-18

HUDSON RIVER USAGE FOR DRINKING WATER

Actual	Potential
1. Poughkeepsie, 60,000 people, Mile Point 75	1. Poughkeepsie, 60,000 people, Mile Point 75 2. Chelsea, 300,000 people, Mile Point 60*

*The Chelsea station is used for emergencies only. Though operable, it has not been used for 13 years. Since it is only used for emergencies, it has been assumed in estimating doses from potential uses that it would operate only 10% of the time over each year--effectively serving 30,000 people at full-time operation.

TABLE 6.7-19

HUDSON RIVER AND OCEAN BEACH USAGE

	Annual Visits[d] (Bathers)	Number of People Served[e]	Mile Point[f]
Bear Mountain	63,671[a]	21,223	47
High Tor	19,587[a]	6,529	34
Georges Island	3,300[c]	1,100	32
Croton Point	11,300[c]	3,766	32
Croton Gorge	700[c]	233	32
Rockland N	56,882[a]	18,960	30
Rockland S	59,907[a]	19,969	28
Kingsland	13,000[c]	4,333	27
Tallman Mountain	14,301[a]	4,767	22
Coney Island	9,000,000[b]	3,040,000	-9.5
Rockaway	72,018,000[b]	24,370,000	-25

(a) From specific statistics on bathers.

(b) All visits assumed to be beach users.

(c) Assumed that 25% of visits were bathers.

(d) Attendance records for state parks along the Hudson River prepared by the New York State Department of Parks and Recreation and same for ocean beaches provided by the New York City Department of Parks and Recreation.

(e) Population weighted average usage of beach for RG 1.109 is 12.8 hr/yr

$$\text{Persons Served} = \frac{\text{No. of Visits} * 4 \text{ hr/visit}}{12.8}$$

(f) Indian Point site is at Mile Point 43.

TABLE 6.7-20

POPULATION FED BY HUDSON RIVER AQUATIC BIOTA[a]

	Actual[b]	Potential[c]
Saltwater Fish	6.7E4[d]	3.1E5[e]
Saltwater Invertebrates	1.4E4[f]	1.0E7[g]
Freshwater Fish	0[h]	0[h]

Note: 6.7E4 is read as 6.7×10^4

[a] See Table 6.7-21 for derivation of catch statistics.

[b] Based upon current use.

[c] Implies potential given cleanup of Hudson River estuary.

[d] 8.7E5 lb/yr commercial and sport fishing yield ÷ 13 lb/yr-person RG 1.109 (Rev. 1) age-weighted average consumption rate (distributed along river).

[e] 4.0E6 lb/yr commercial and sport fishing yield ÷ 13 lb/yr-person RG 1.109 (Rev. 1).

[f] 2.7E4 lb/yr crabs from sport fishing ÷ 1.9 lb/yr-person RG 1.109 (Rev. 1) age-weighted average consumption rate (distributed along river).

[g] 2.0E5 lb/yr crabs, 9.0E6 lb/yr oysters, 1.0E7 lb/yr clams ÷ 1.9 lb/yr-person (clams confined to mouth of estuary, others distributed uniformly along river).

[h] Concentrations of Cs-137 in Hudson River fish indicate that salt-water bioaccumulation factors are more appropriate for dose estimates than fresh water (Reference 6.7-38).

TABLE 6.7-21

HUDSON RIVER ESTUARY AQUATIC FINFISH AND SHELLFISH ANNUAL YIELDS[a]

	Actual (Current Use)	Potential (Requires Cleanup of Hudson)
Commercial Fish	6.0E5 lb (1.6E6 lb ocean)[b]	2.0E6 lb (g)
Sport Fish	2.7E5 lb (2.8E6 lb ocean)[c]	2.0E6 lb (h)
Clams	None[d]	1.0E7 lb (i)
Oysters	None[e]	9.0E6 lb (j)
Crabs	2.7E4 lb[f]	2.0E5 lb (k)

Note: 6.0E5 is read as 6.0×10^5

(a) Except as noted, all data and page numbers are from Reference 6.7-36.

(b) P. 41-42 (ocean figure refers to ocean catch of fish which used Hudson).

(c) 1.35E5 angler-days (p.42b) at 2 lb/angler-day (p. 27) (Poughkeepsie-Tappan Zee only) ocean figure from p. 42b.

(d) P. 42, closed since 1925.

(e) P. 41, closed since 1925.

(f) No quantification available - assumed 10% of sport fish.

(g) P. 42, (ocean figure is 1,400,000 angler-day at 2 lb/angler-day).

(h) 1.0E6 angler-days (p. 42b) at 2 lb/angler-day (p. 27).

(i) P. 42, 1.0E6 bushels standing population in Raritan Bay; assumed 10%/yr yield, 40 lb bushel including shells, 25% meat.

(j) P. 41, 14.8E6 lb pre-1925 minus 5.4E6 lb post-1925 for NY state - difference due to Hudson closing.

(k) No quantification available - assumed 10% of sport fish.

TABLE 6.7-22

MAXIMUM DOSES TO INDIVIDUALS
(rem/yr)

Pathway	Zero to 2 Years After Accident	Greater Than 2 Years After Accident
Fish	6.0 (GI) <0.5 (other organs)	<0.010 (any organ)
Shore	River Parks <0.76 (any organ) Ocean Beaches <0.077 (any organ)	<0.001 (any organ) <0.001 (any organ)
Water	0.43 (GI) <0.03 (other organs)	<0.001 (any organ)
Shellfish	Interdicted	<0.030 (any organ)

TABLE 6.7-23

POPULATION DOSES[1]
(man-rem)

Organ	Pathway				Total
	Water	Shoreline	Fish	Shellfish	
Bone	4.0E3	7.2E4	1.2E4	4.0E3	9.2E4
Liver	1.5E1	7.2E4	1.6E2	1.2E2	7.2E4
Total Body	9.4E2	7.2E4	2.8E3	8.2E2	7.6E4
Thyroid	2.9E1	7.2E4	6.3E2	0.	7.3E4
Kidney	3.5E2	7.2E4	1.1E3	7.3E4	1.5E5
Lung	1.9E1	7.2E4	1.1E1	2.1E1	7.2E4
GI-LLI	8.8E3	7.2E4	3.1E4	9.7E2	1.1E5
Skin	0.	8.6E4	0.	0.	8.6E4

Note: 4.0E3 is read as 4.0×10^3.

(1) Integrated over all releases for all time. Interdiction of shellfish pathway assumed for first two years.

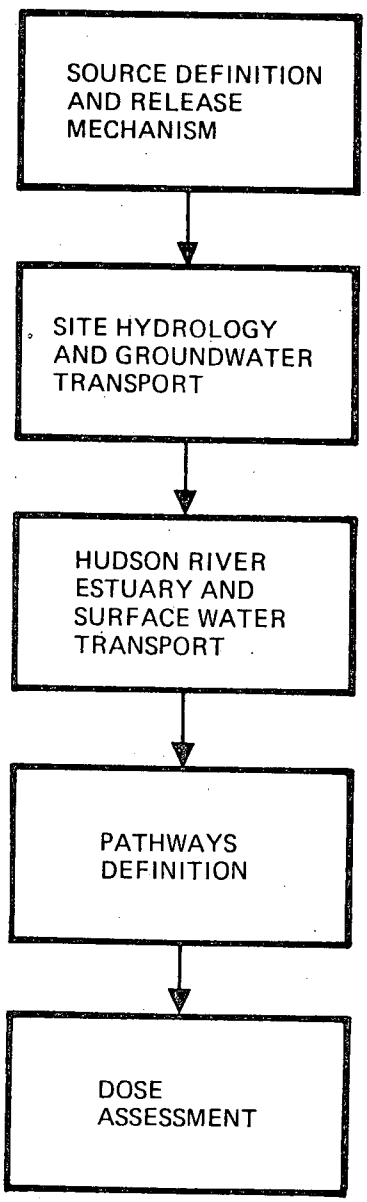


Figure 6.7-1. Indian Point Liquid Pathways Analysis Schematic

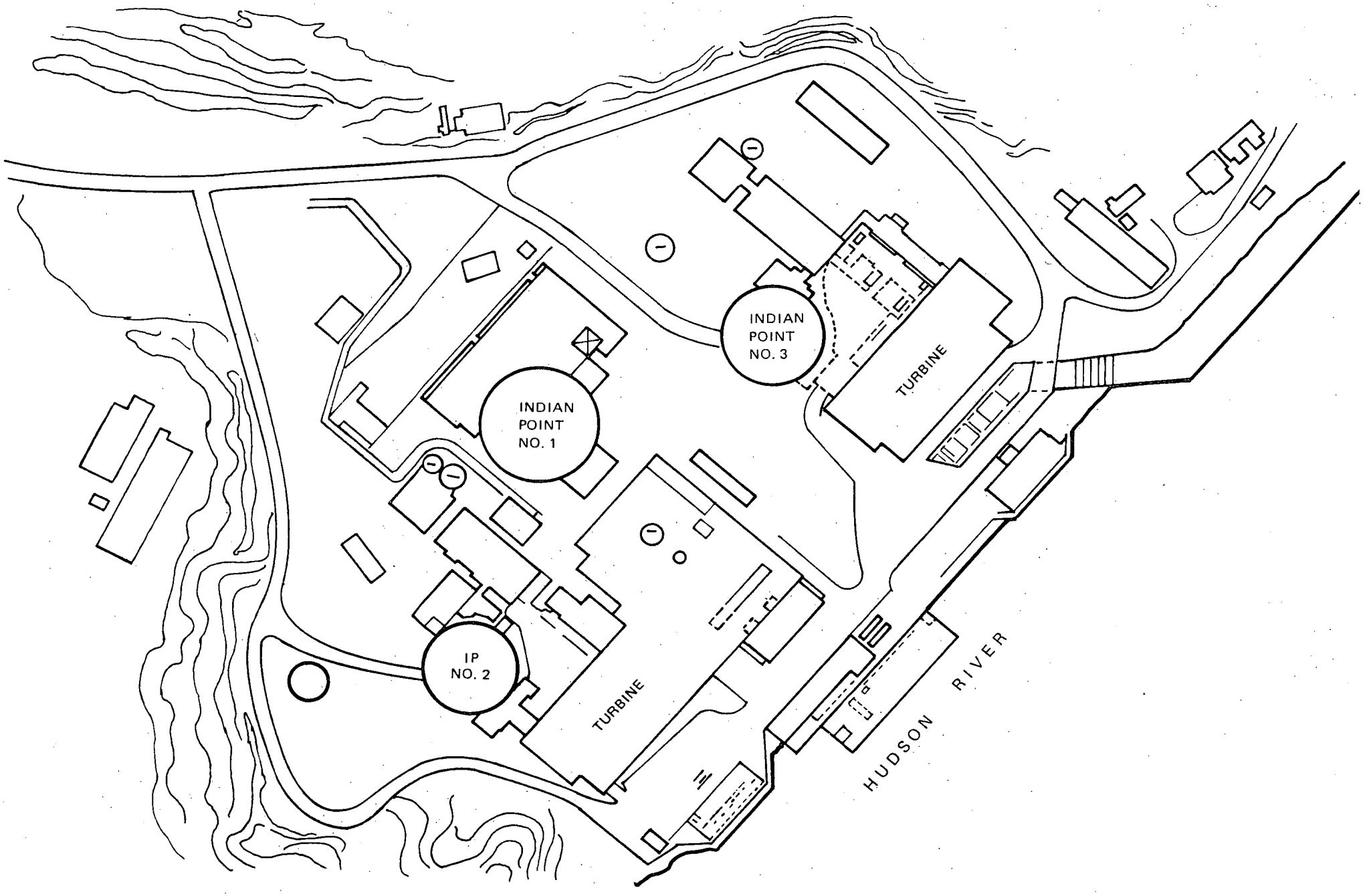


Figure 6.7-2. Base Map of the Indian Point Reactor Site

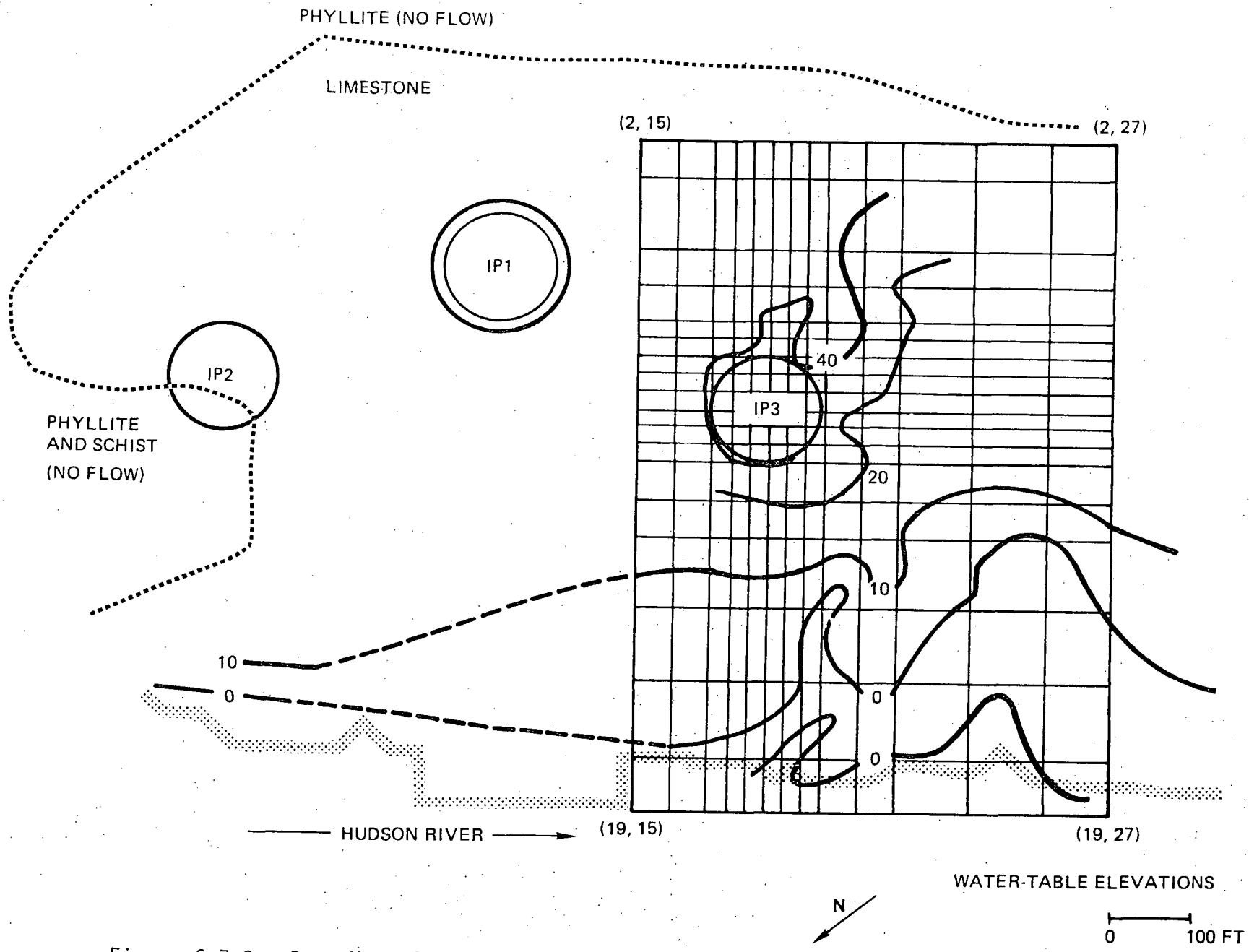


Figure 6.7-3. Base Map of Indian Point Showing the Extent of the Limestone and the Potentiometric Surface in the Aquifer

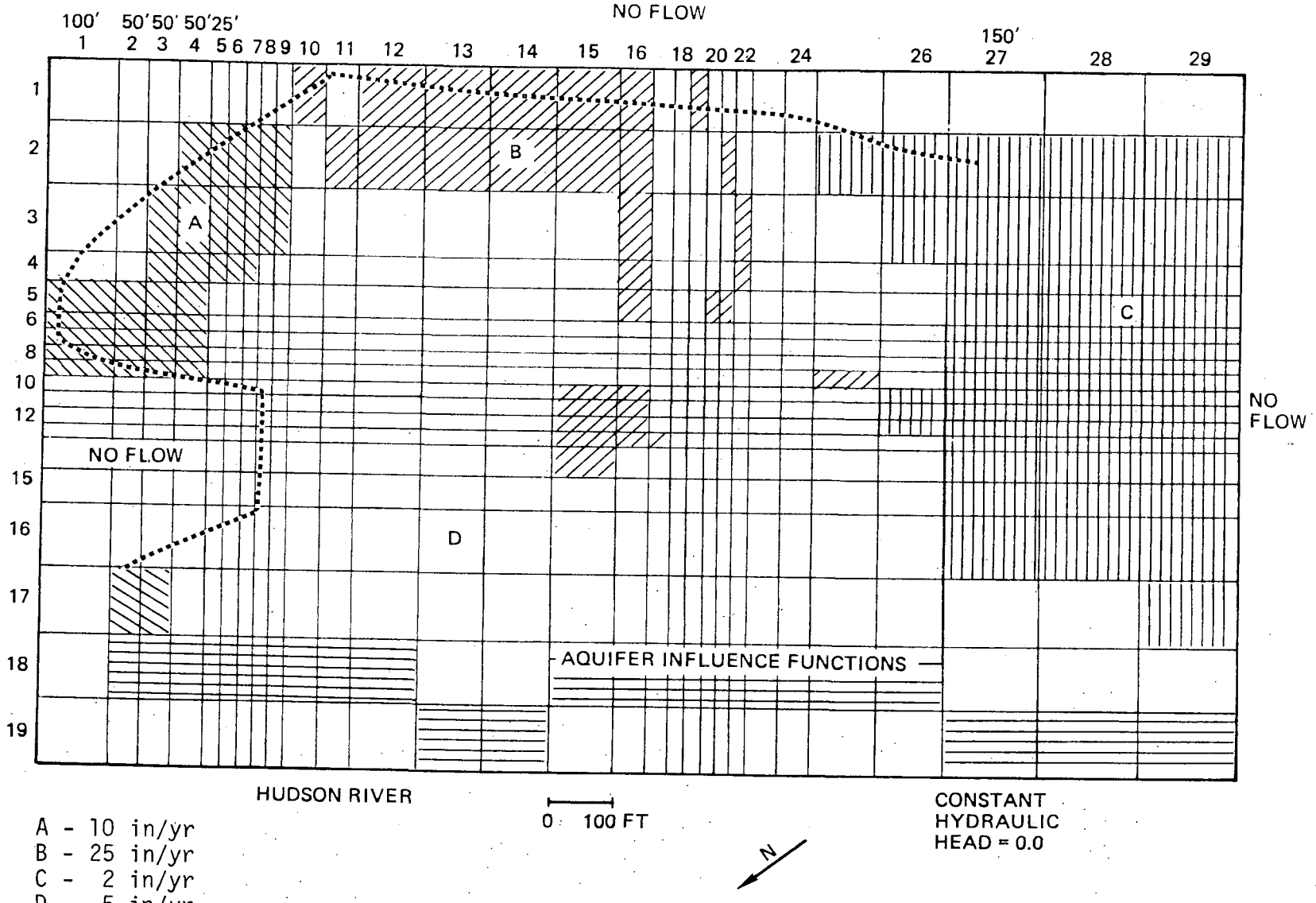


Figure 6.7-4. Finite-Difference Grid Used to Simulate the Indian Point Flow Field Showing Regions Where Recharge Was Varied

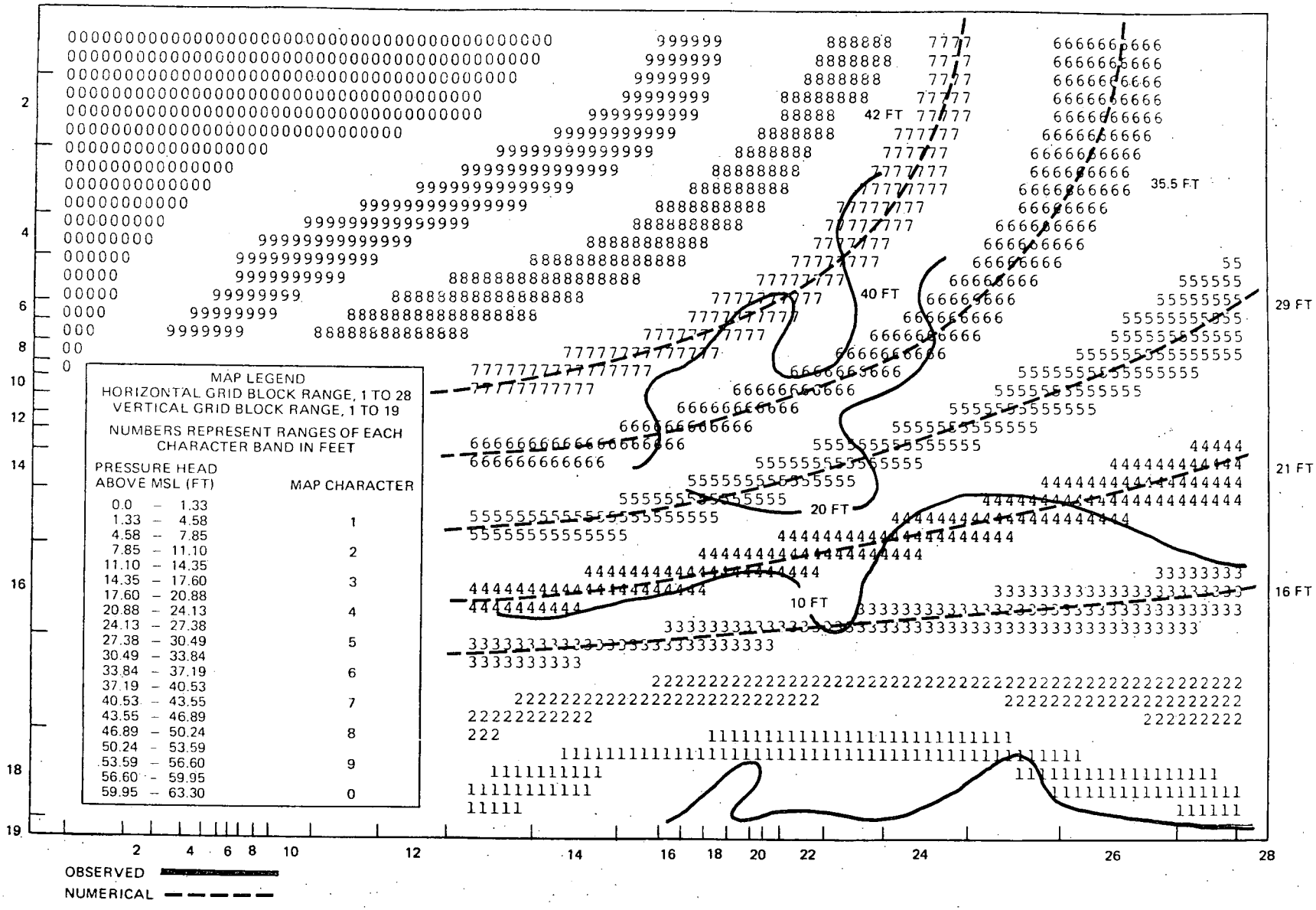


Figure 6.7-5. Comparison of Computer Potentiometric Surface with that Observed

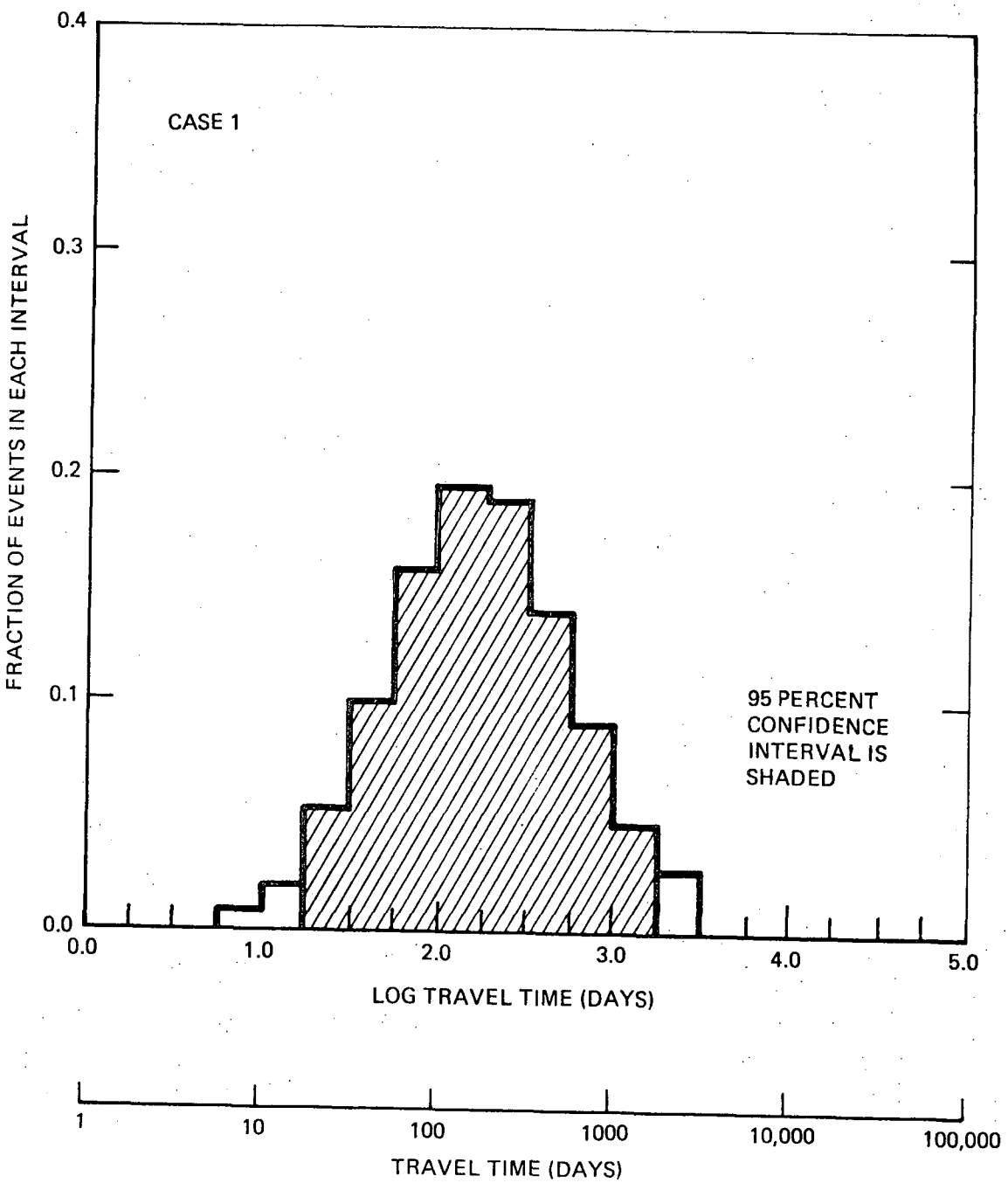


Figure 6.7-6. Histogram of Travel Times Computed by Monte Carlo Simulation for Known Porosity and Uncertain Hydraulic Conductivity

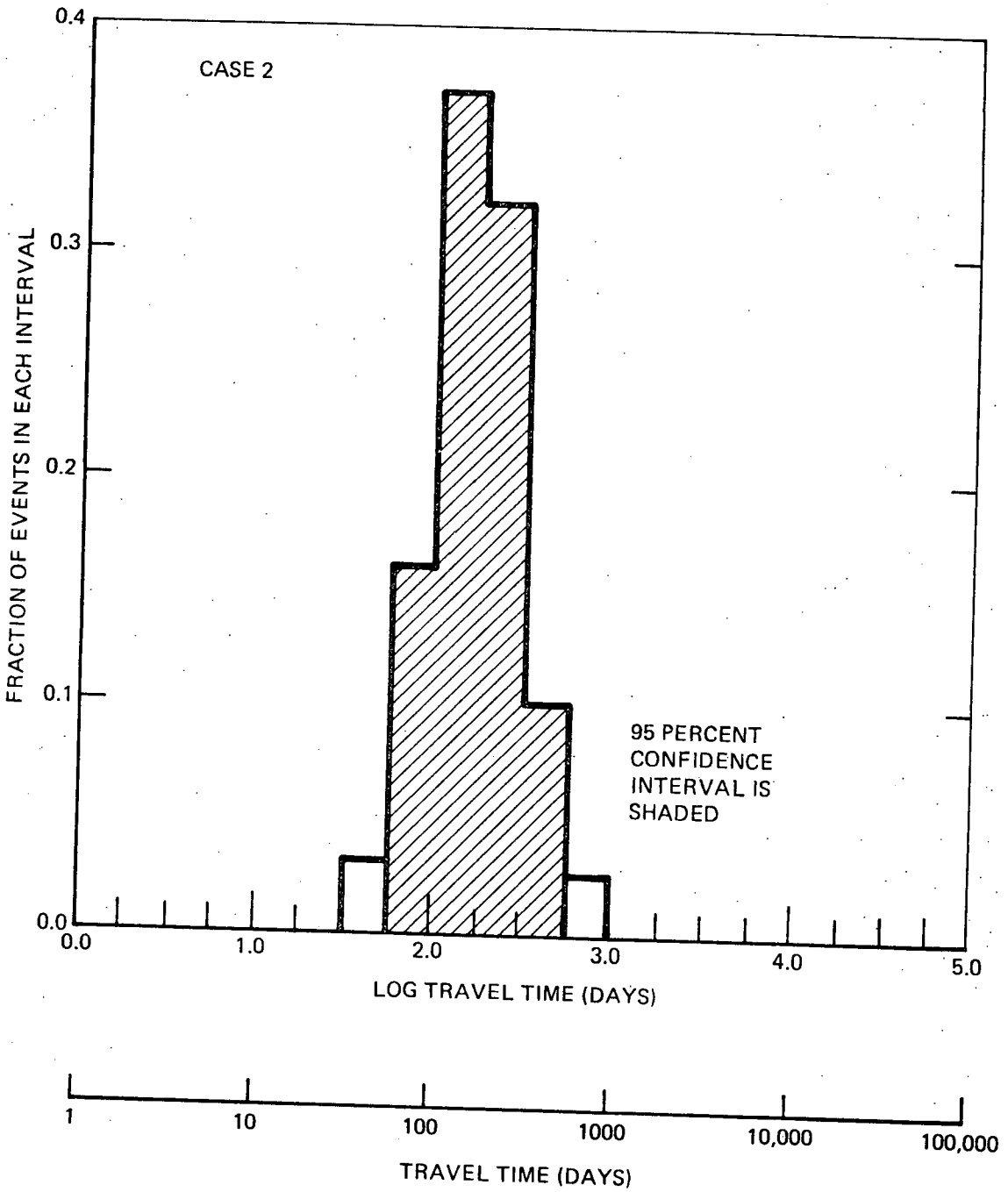


Figure 6.7-7. Histogram of Travel Times Computed by Monte Carlo Simulation for Uncertain Hydraulic Conductivity with Porosity Proportional to the Square Root of Hydraulic Conductivity

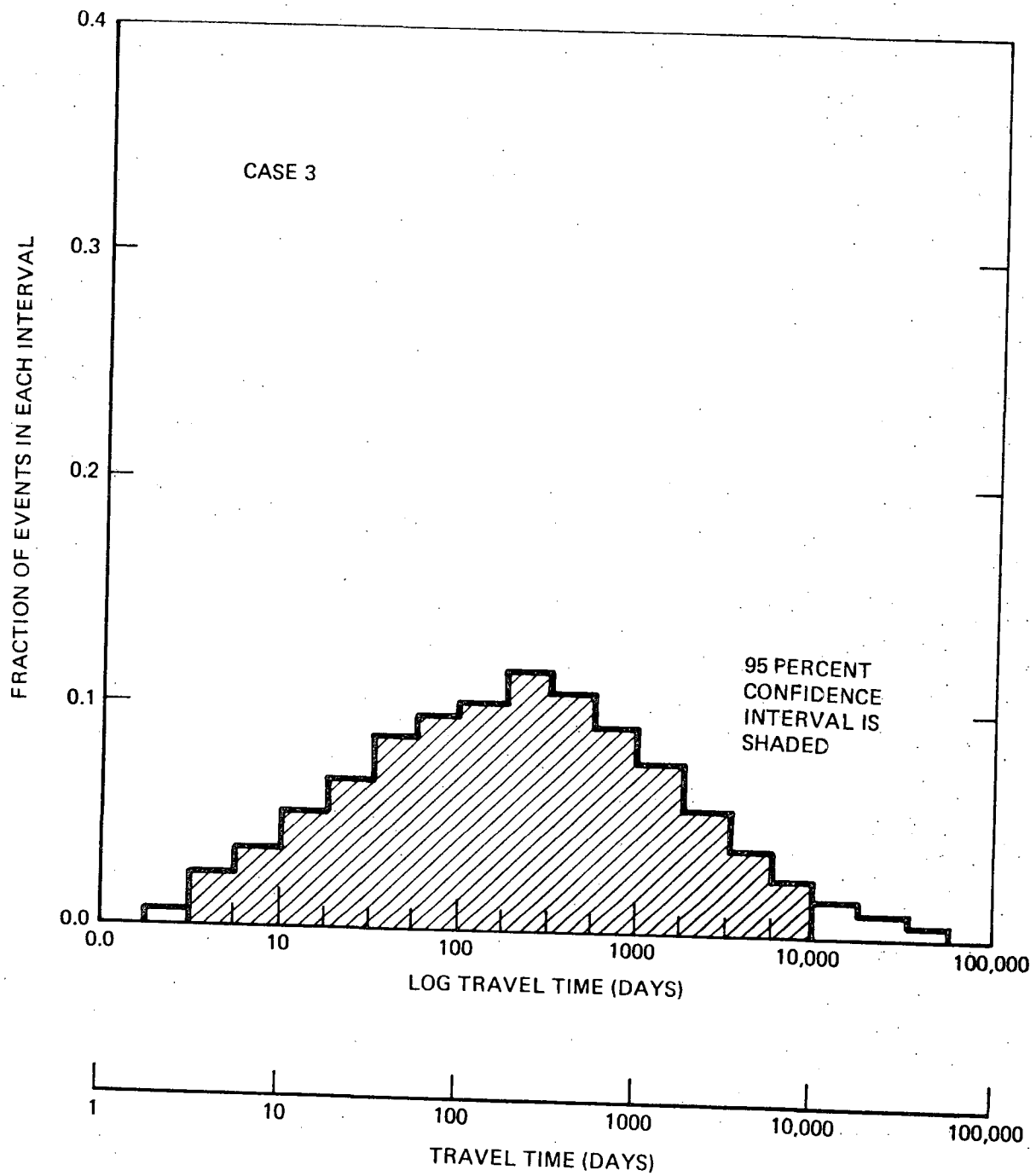
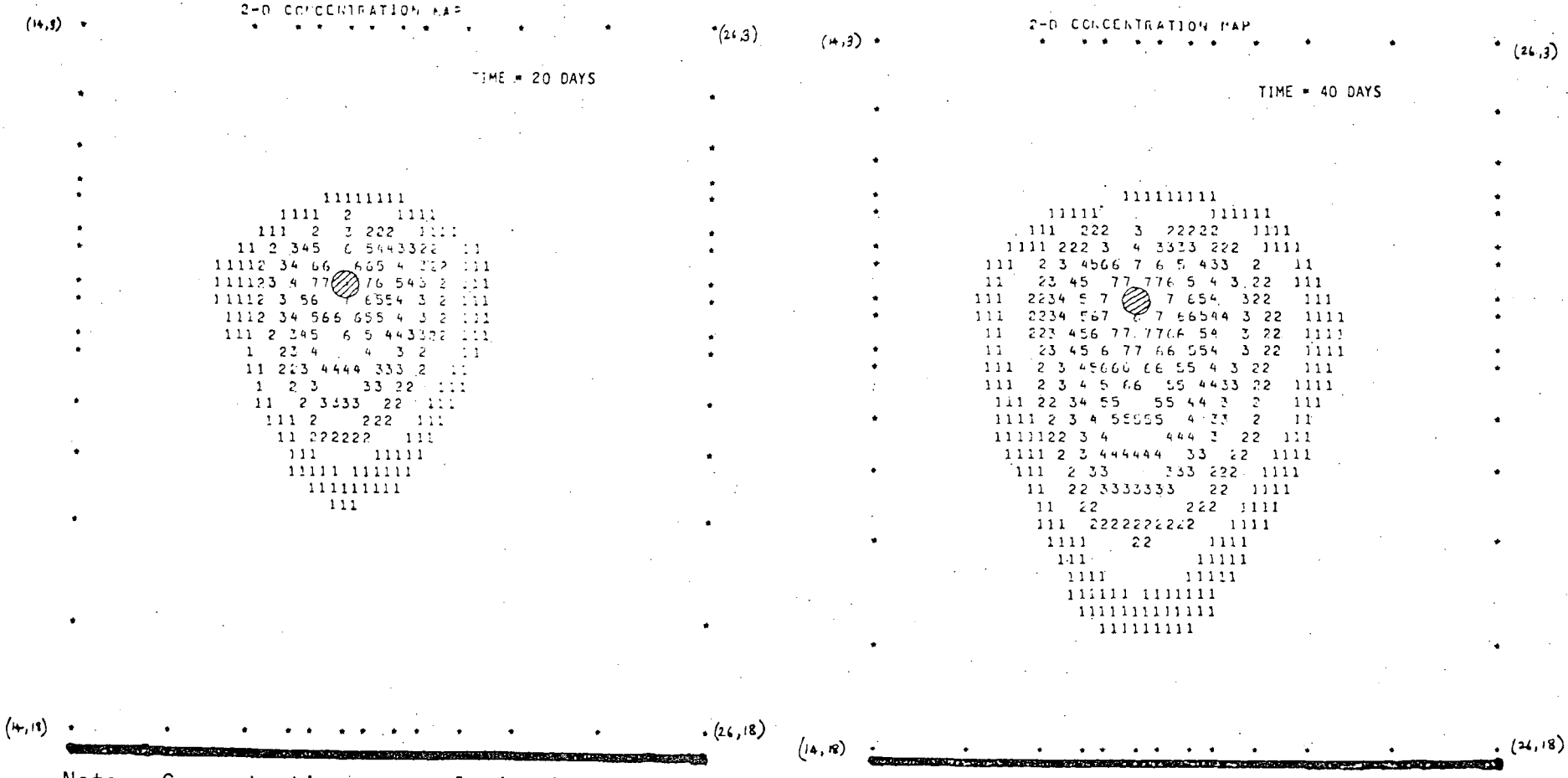
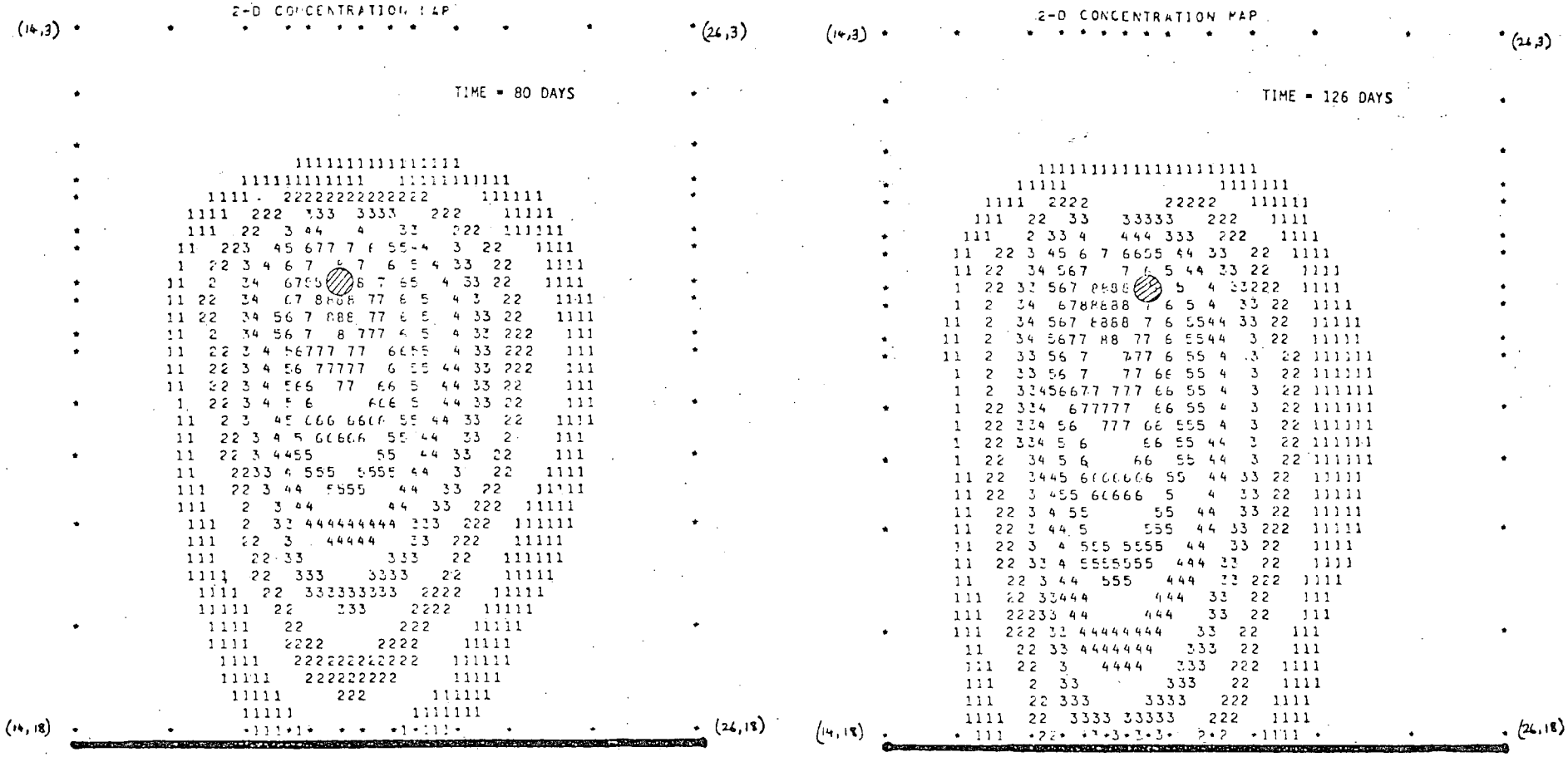


Figure 6.7-8. Histogram of Travel Times Computed by Monte Carlo Simulation for Uncertain and Independent Hydraulic Conductivity and Porosity



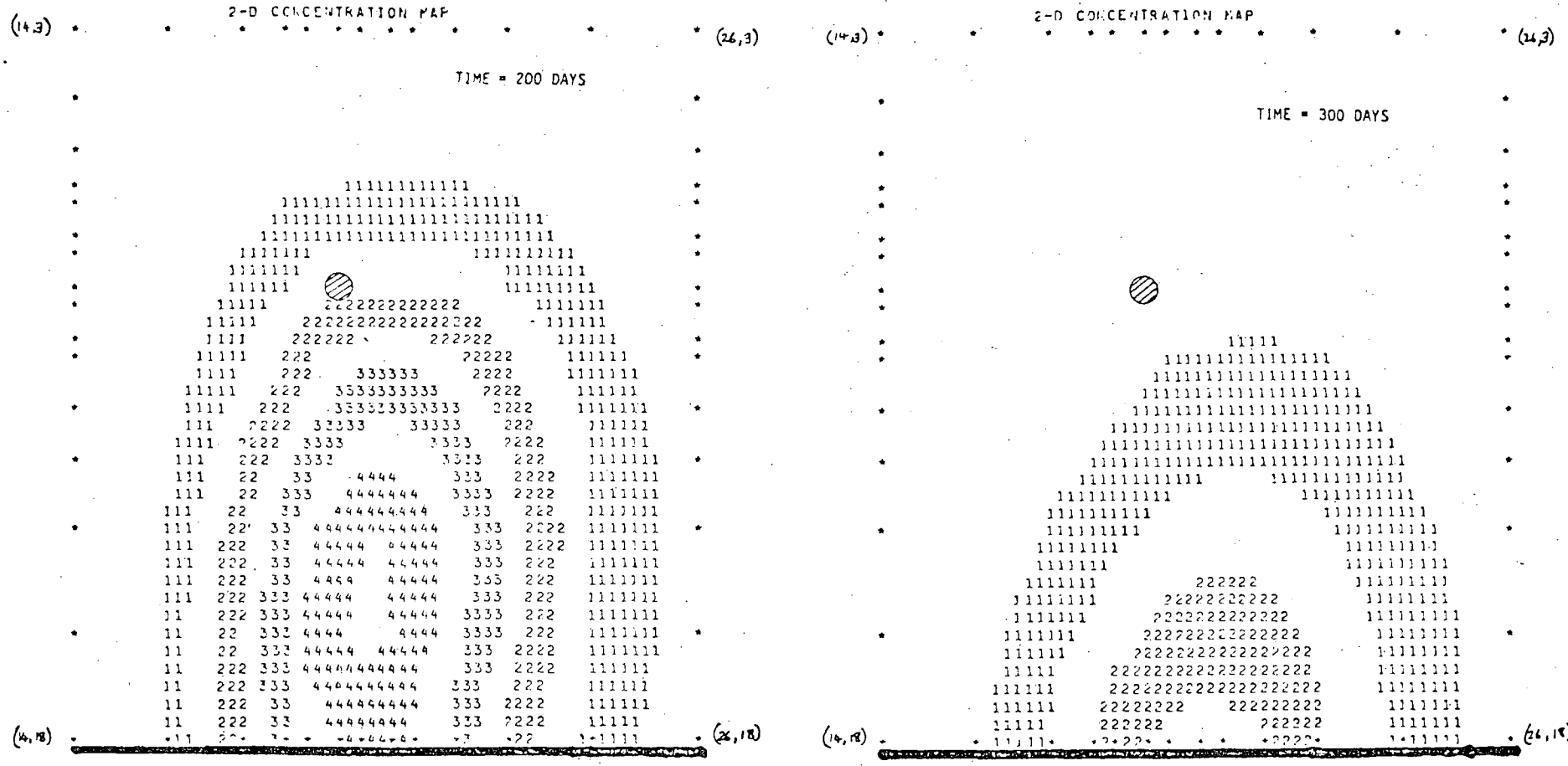
Note: Concentrations are relative based on sump water concentration of one. Shaded circle represents sump of IP-3. Heavy line at bottom represents Hudson River. Numbers at edges are model block numbers. See Figure 6.7-4.

Figure 6.7-9A. Distribution of Trace from Sump Water Release in Groundwater (Time = 20 Days and 40 Days)



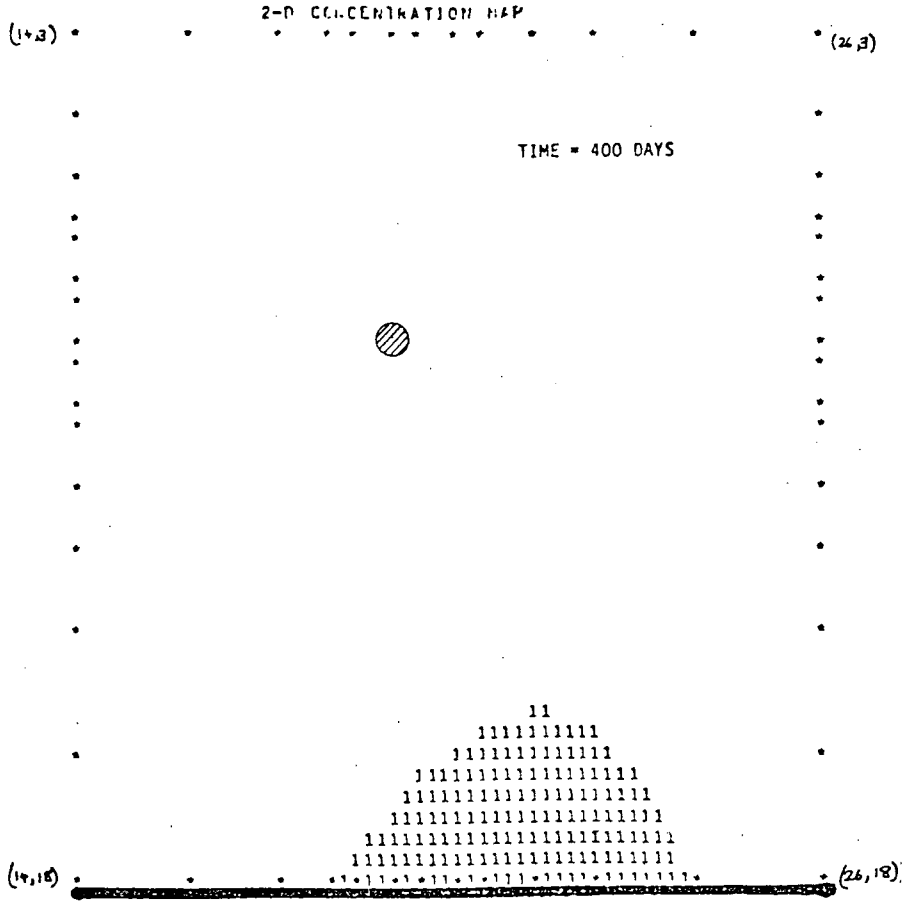
Note: Concentrations are relative based on sump water concentrations of one. Shaded circle represents sump of IP-3. Heavy line at bottom represents Hudson River. Numbers at edges are model block numbers. See Figure 6.7-4.

Figure 6.7-9B. Distribution of Trace from Sump Water Release in Groundwater (Time = 80 Days and 126 Days)



Note: Concentrations are relative based on sump water river concentrations of one. Shaded circle represents sump of IP-3. Heavy line at bottom represents Hudson River. Numbers at edges are model block numbers. See Figure 6.7-4.

Figure 6.7-9C. Distribution of Trace from Sump Water Release in Groundwater (Time = 200 Days and 300 Days)



Note: Each character corresponds to a percentage interval of 5.0E-5 lb/lb as indicated.

MAP LEGEND
HORIZONTAL GRID BLOCK RANGE, FROM 1 TO 13
VERTICAL GRID BLOCK RANGE, FROM 3 TO 18

DEPENDENT VARIABLE RANGE			MAP CHARACTER (%)	
0.	-	.250E-05		
.250E-05	-	.500E-05	1	(5-10)
.500E-05	-	.750E-05		
.750E-05	-	.100E-04	2	(15-20)
.100E-04	-	.125E-04		
.125E-04	-	.150E-04	3	(25-30)
.150E-04	-	.175E-04		
.175E-04	-	.200E-04	4	(35-40)
.200E-04	-	.225E-04		
.225E-04	-	.250E-04	5	(45-50)
.250E-04	-	.275E-04		
.275E-04	-	.300E-04	6	(55-60)
.300E-04	-	.325E-04		
.325E-04	-	.350E-04	7	(65-70)
.350E-04	-	.375E-04		
.375E-04	-	.400E-04	8	(75-80)
.400E-04	-	.425E-04		
.425E-04	-	.450E-04	9	(85-90)
.450E-04	-	.475E-04		
.475E-04	-	.500E-04	0	(95-100)

Note: Concentrations are relative based on sump water river concentrations of one. Shaded circle represents sump of IP-3. Heavy lines at bottom represents Hudson River. Numbers at edges are model block numbers. See Figure 6.7-4.

Figure 6.7-9D. Distribution of Trace from Sump Water Release in Groundwater (Time = 400 Days)

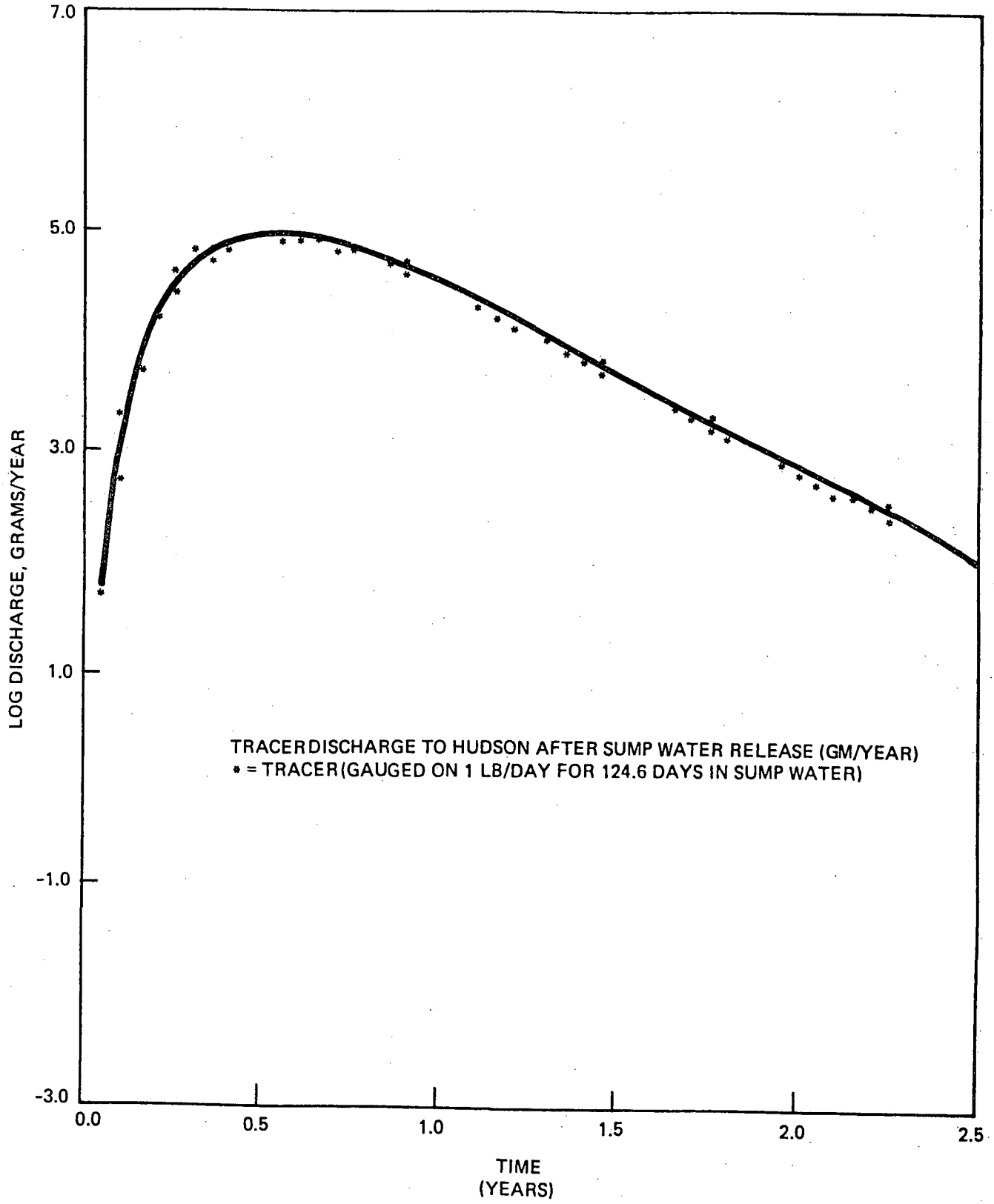


Figure 6.7-10. Variation of Discharge Rate to the River with Time of a Tracer in Sump Water Release

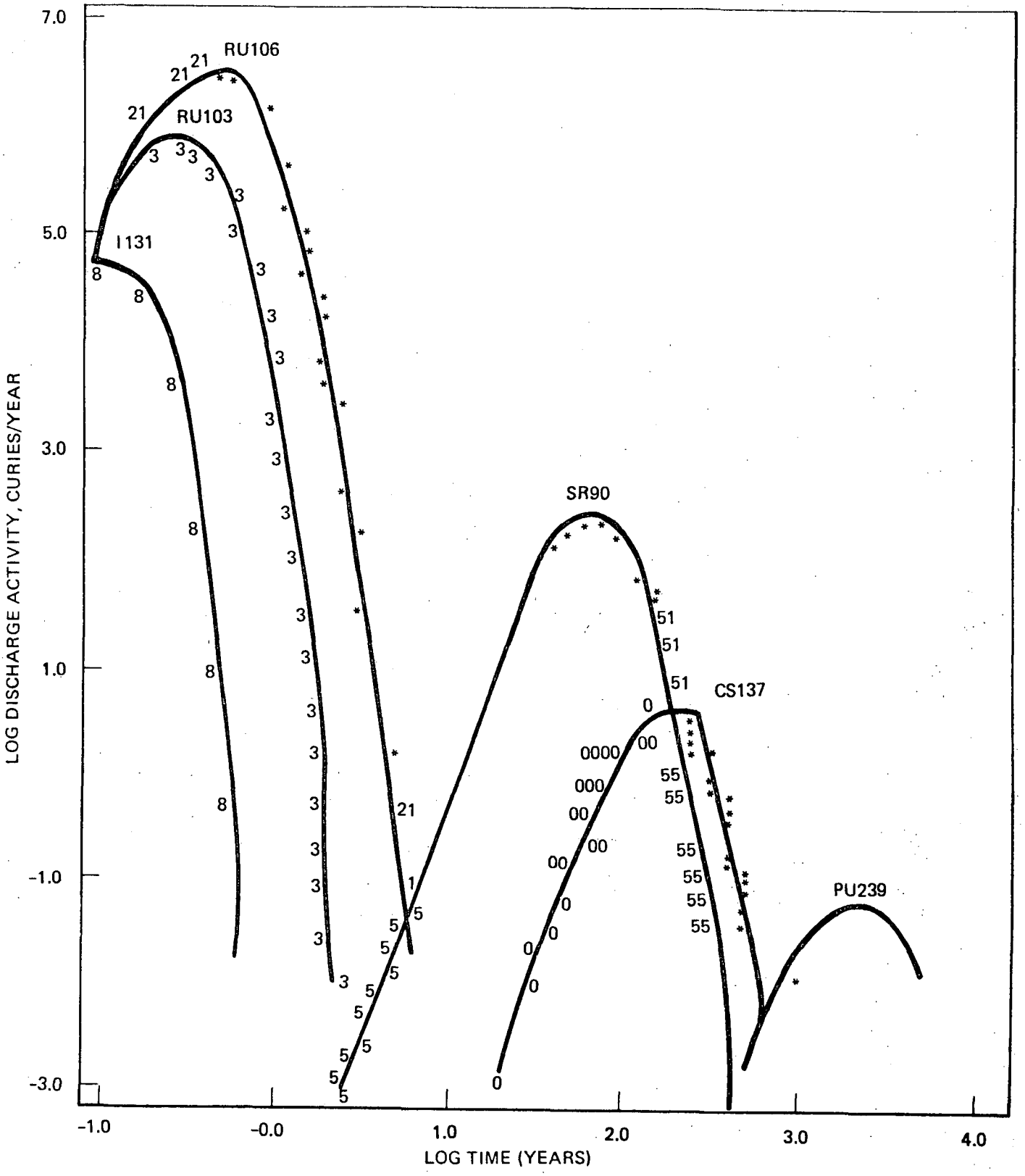


Figure 6.7-11. Discharge Rates of Selected Nuclides to River as Functions of Time Following a Sump Water Release Event

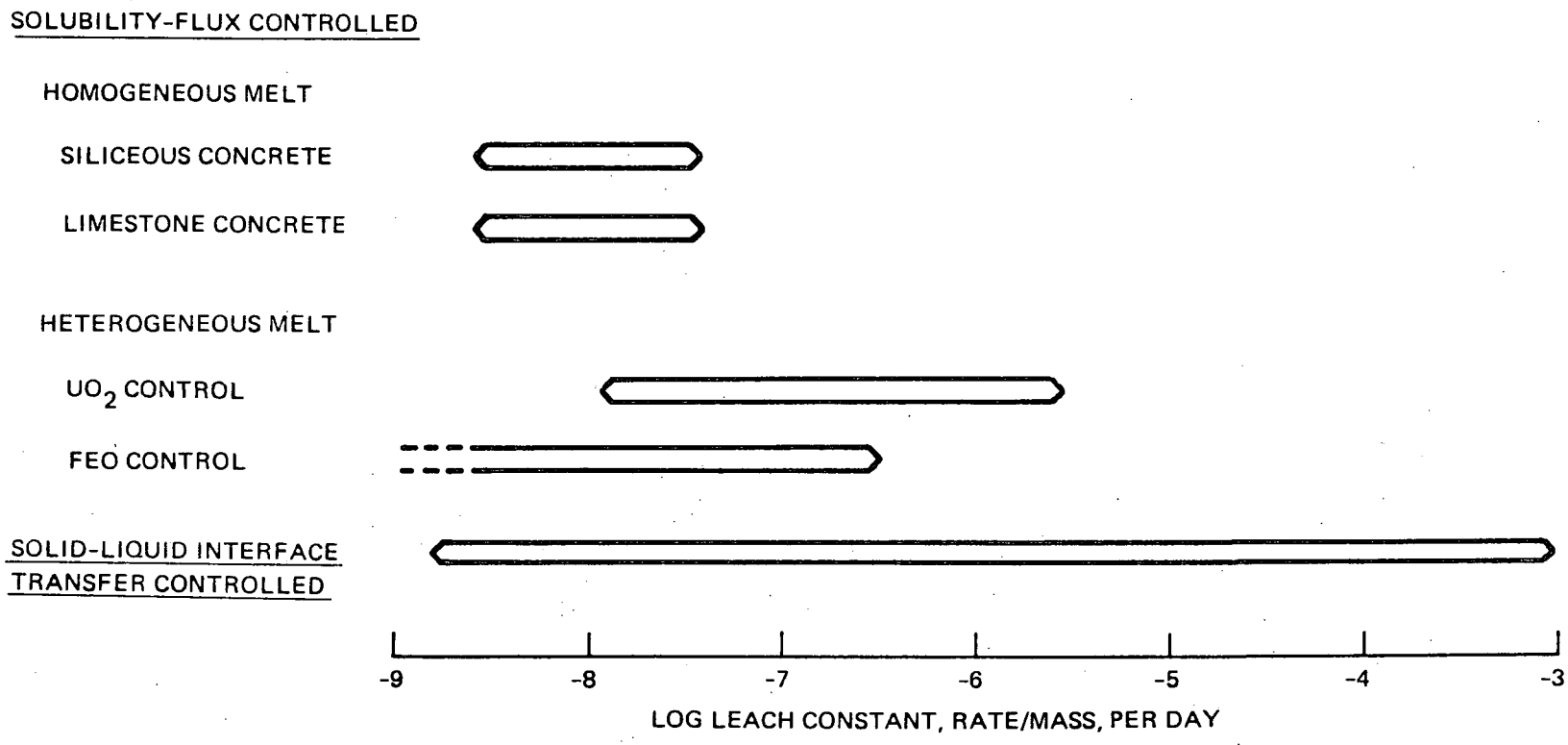


Figure 6.7-12. Comparison of Leach Constants Calculated Assuming Different Controlling Mechanisms

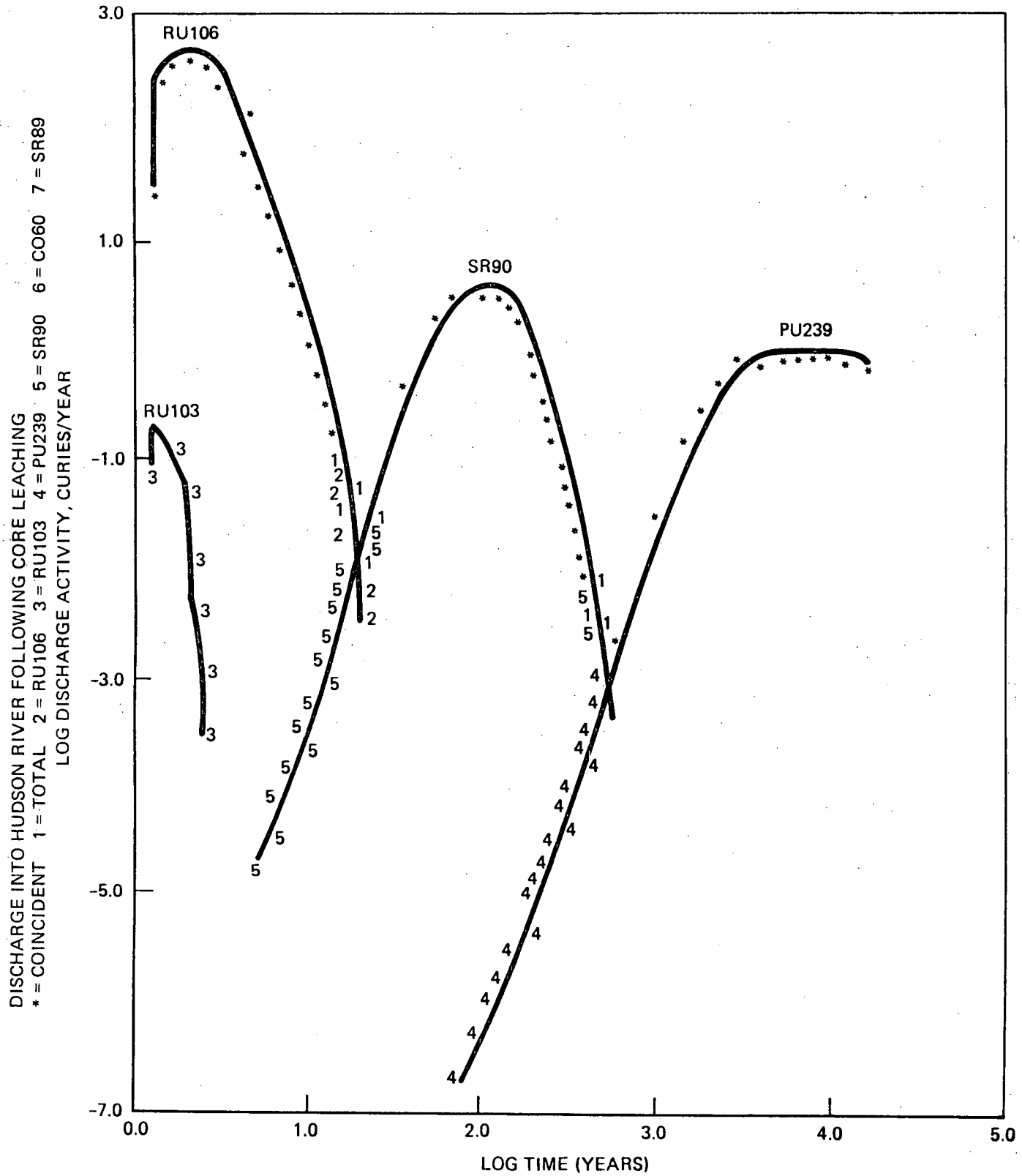


Figure 6.7-13. Discharge Rates of Selected Nuclides to River as Functions of Time from Core Melt Leaching

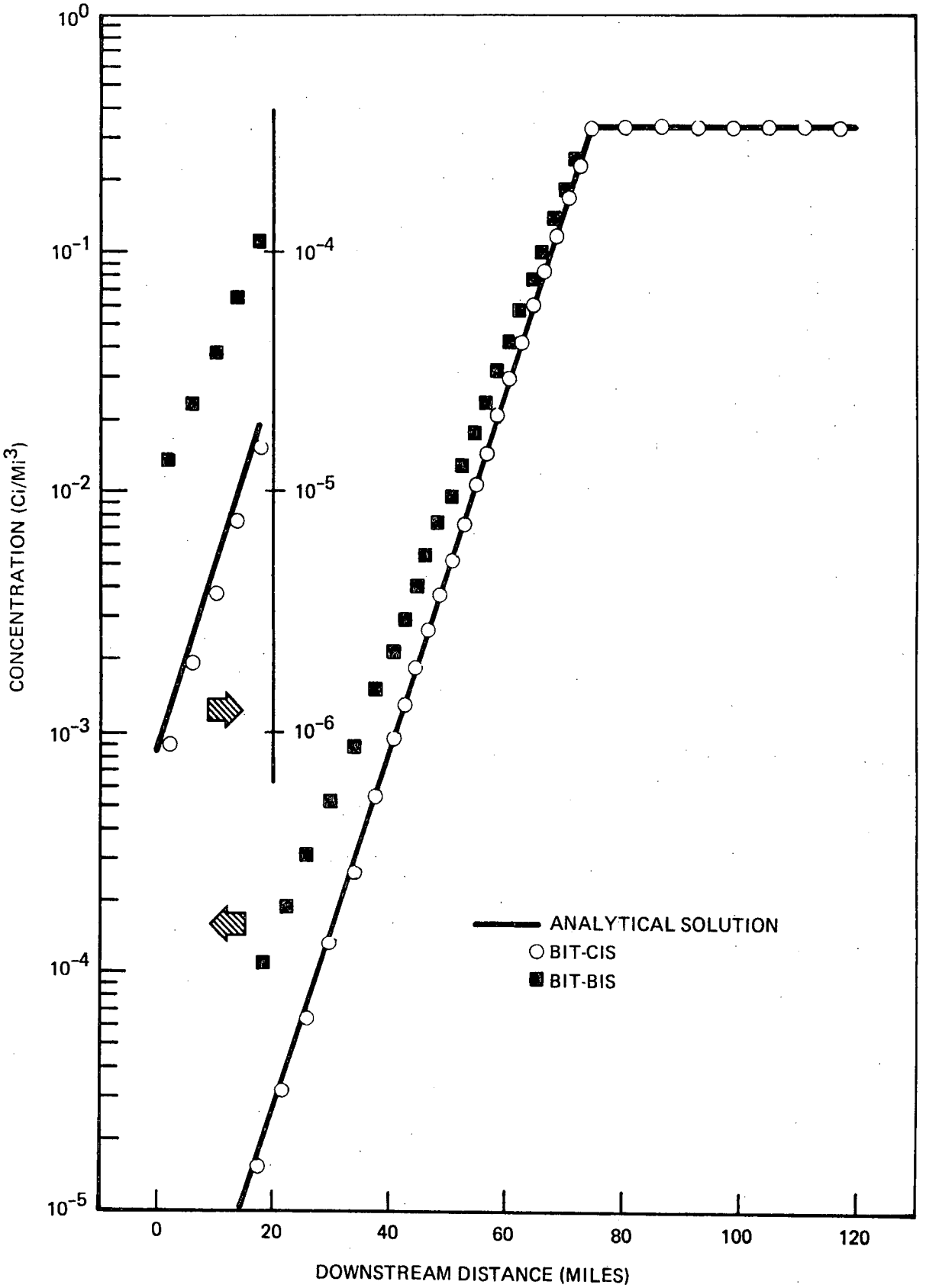


Figure 6.7-14. Steady State Solution for Pu-239 (No Decay) for Unit Intensity Source at x_0 = 75 Miles

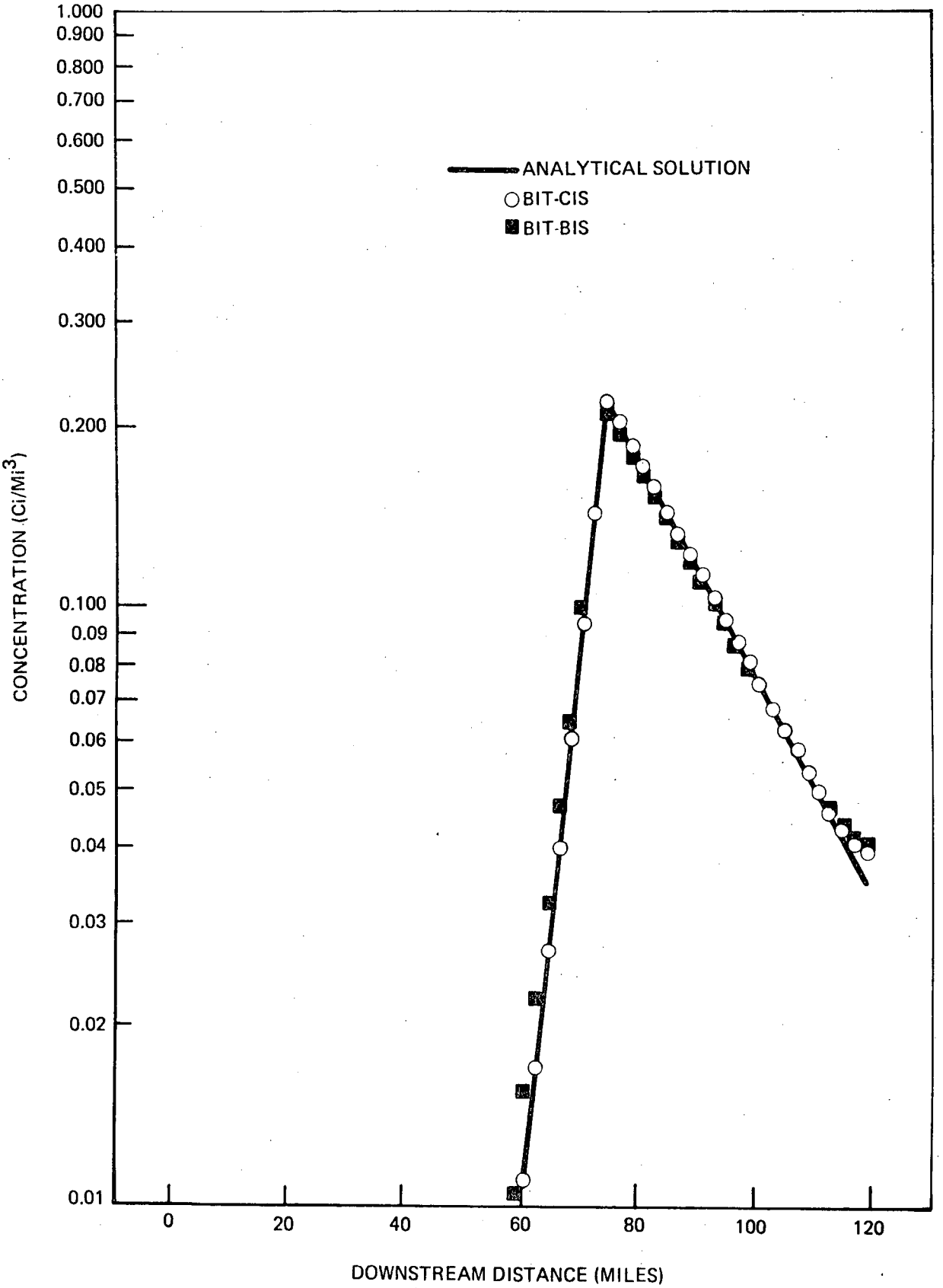


Figure 6.7-15A. Steady State Solution for I-131 for Unit Intensity Source at x_o = 75 Miles

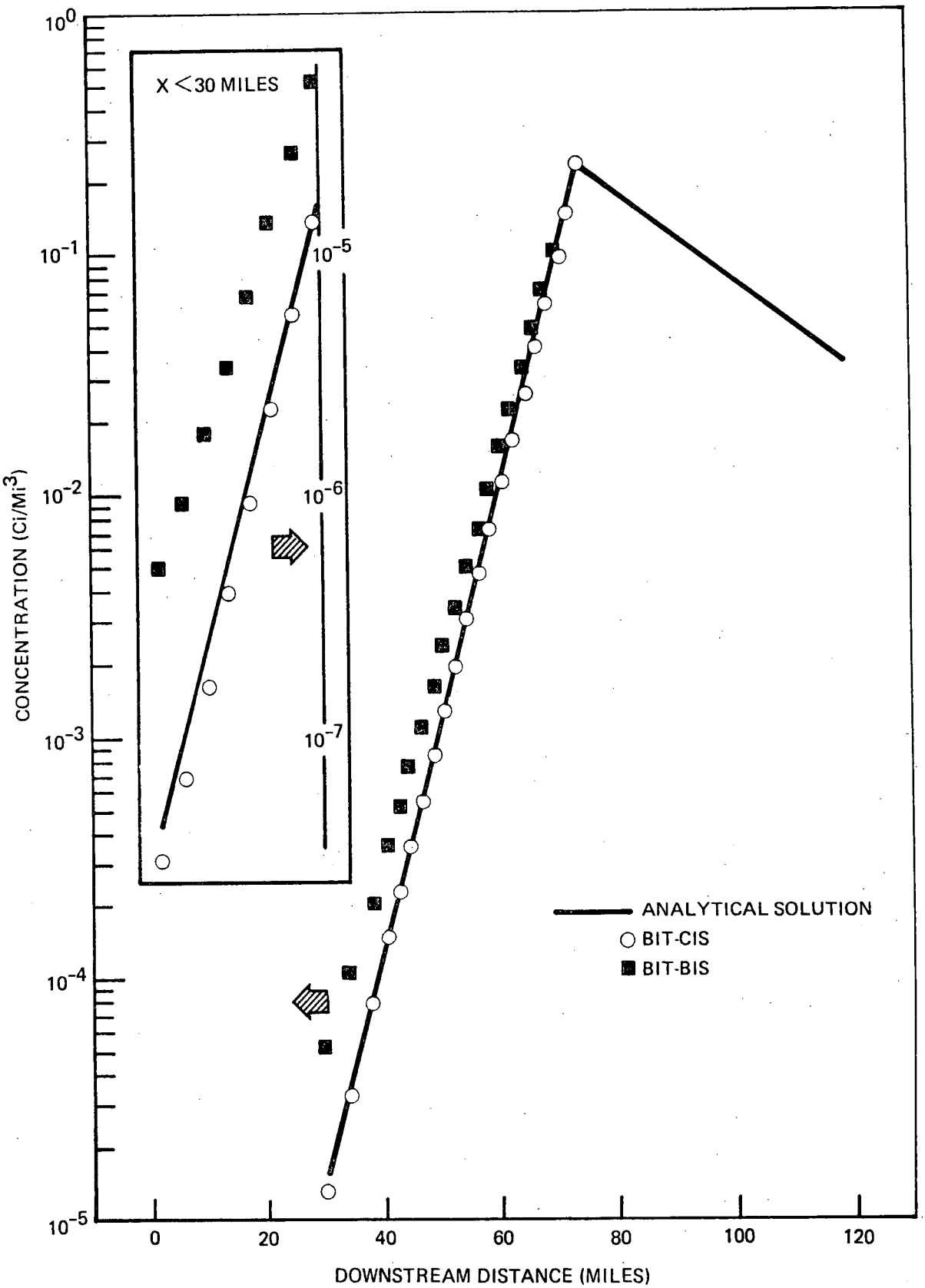


Figure 6.7-15B. Steady State Solution for I-131 for Unit Intensity Source at x_0 = 75 Miles

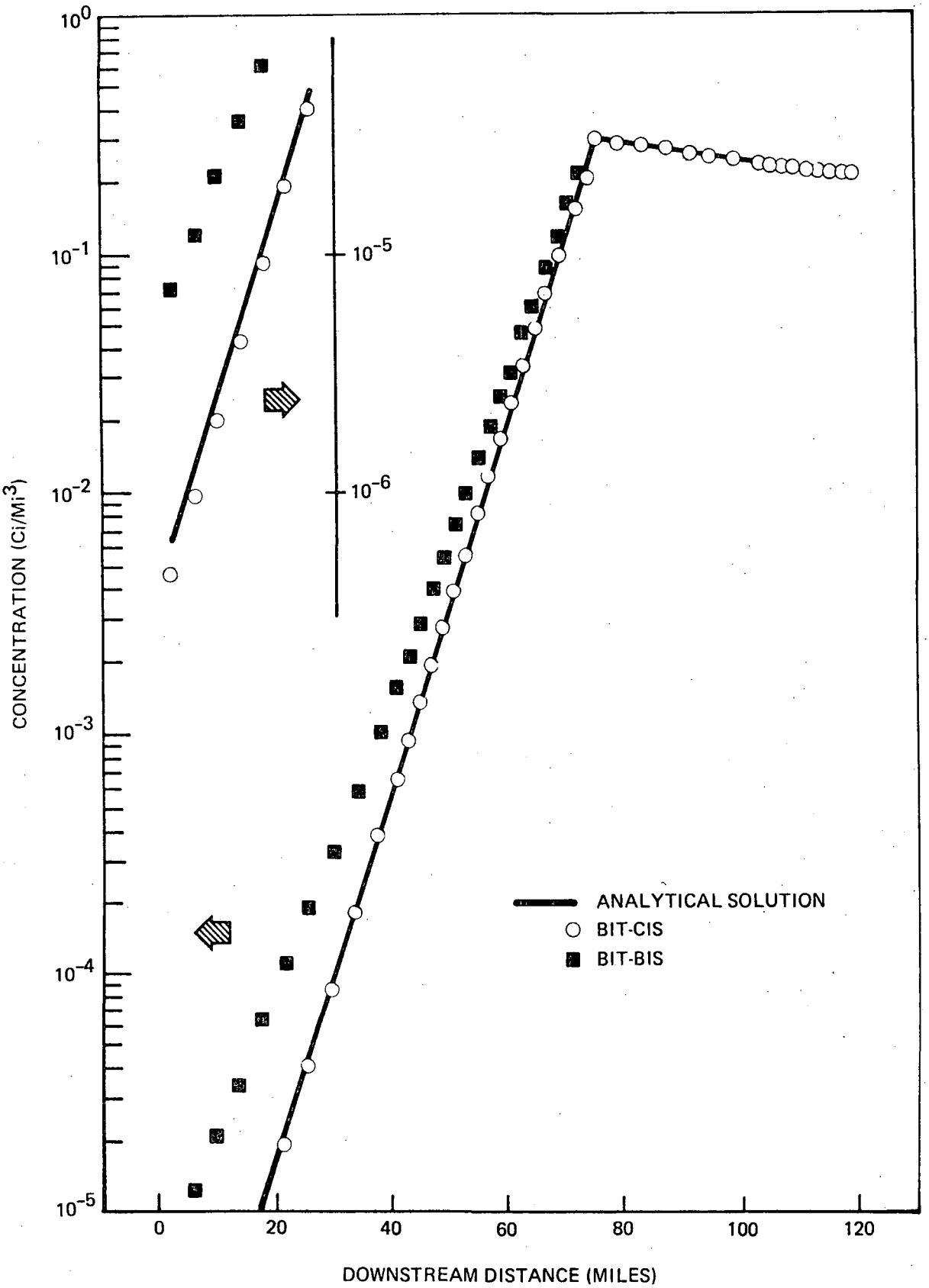


Figure 6.7-16. Steady State Solution for SR-89 for Unit Intensity Source at x_0 = 75 Miles

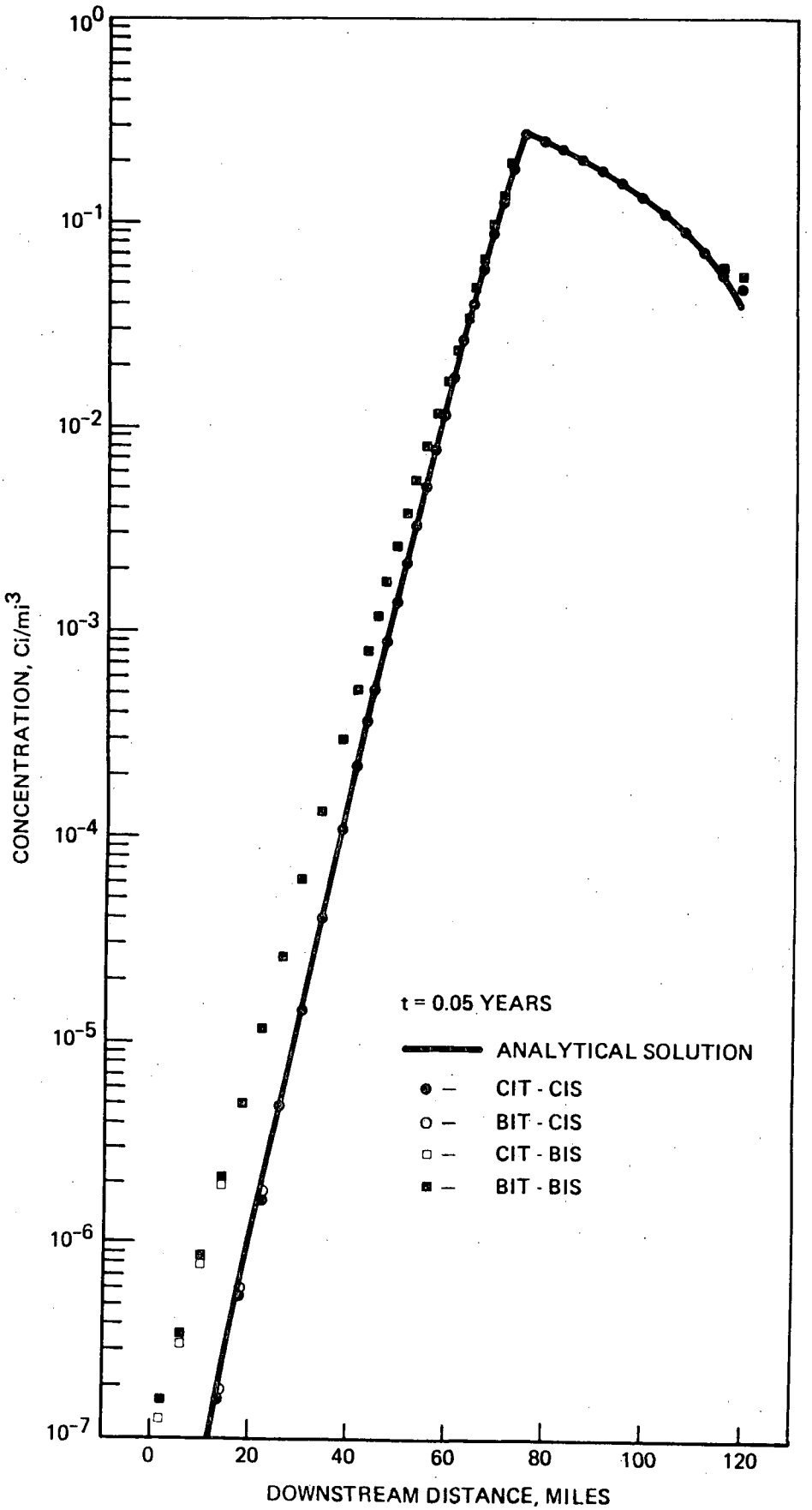


Figure 6.7-17A. Transient (Nonsteady State) Solution for Ru-103 at 0.05 Years for Unit Intensity Source at x_o = 75 Miles

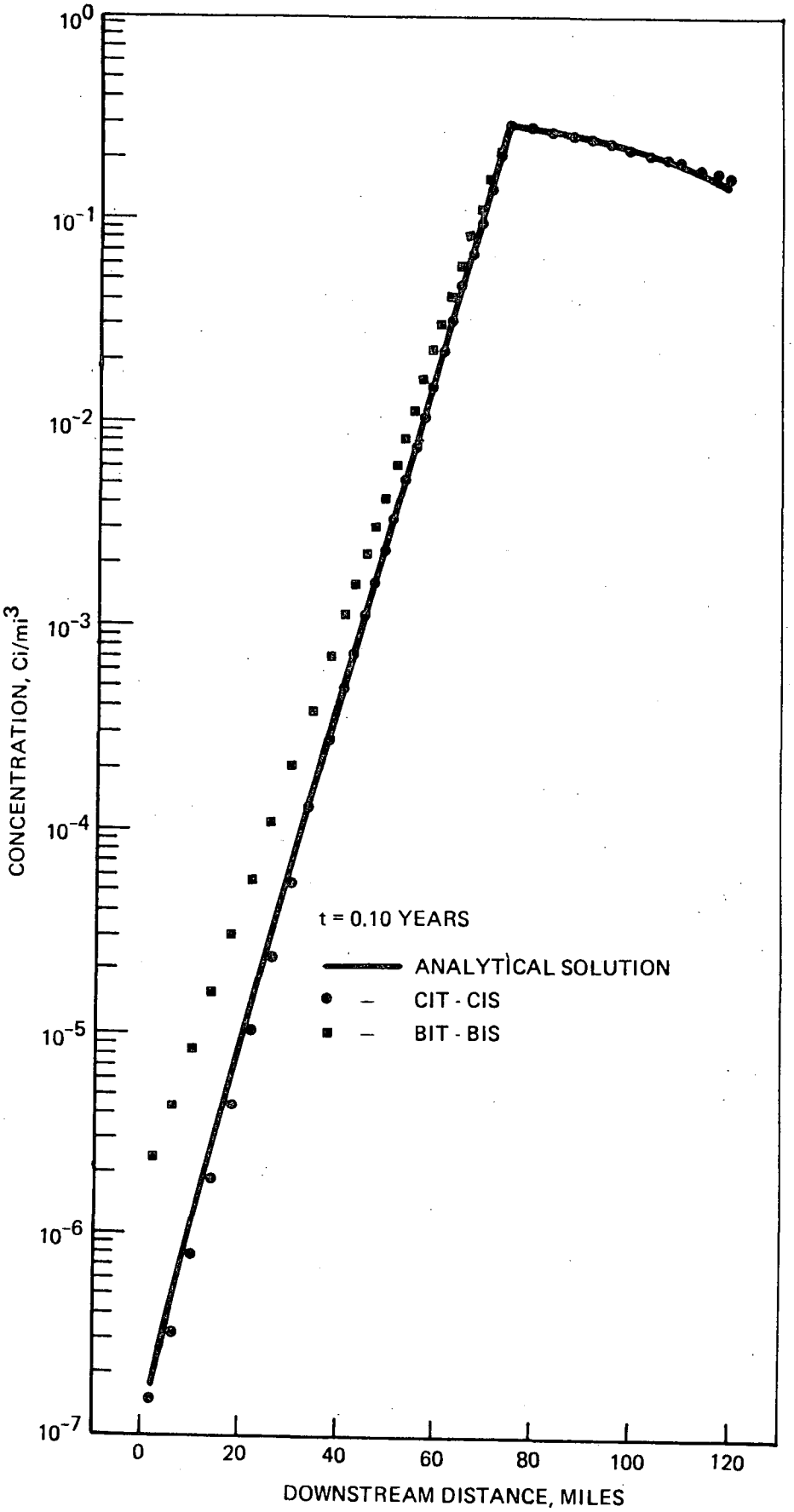


Figure 6.7-17B. Transient (Nonsteady State) Solution for Ru-103 at 0.10 Years for Unit Intensity Source at x_o = 75 Miles

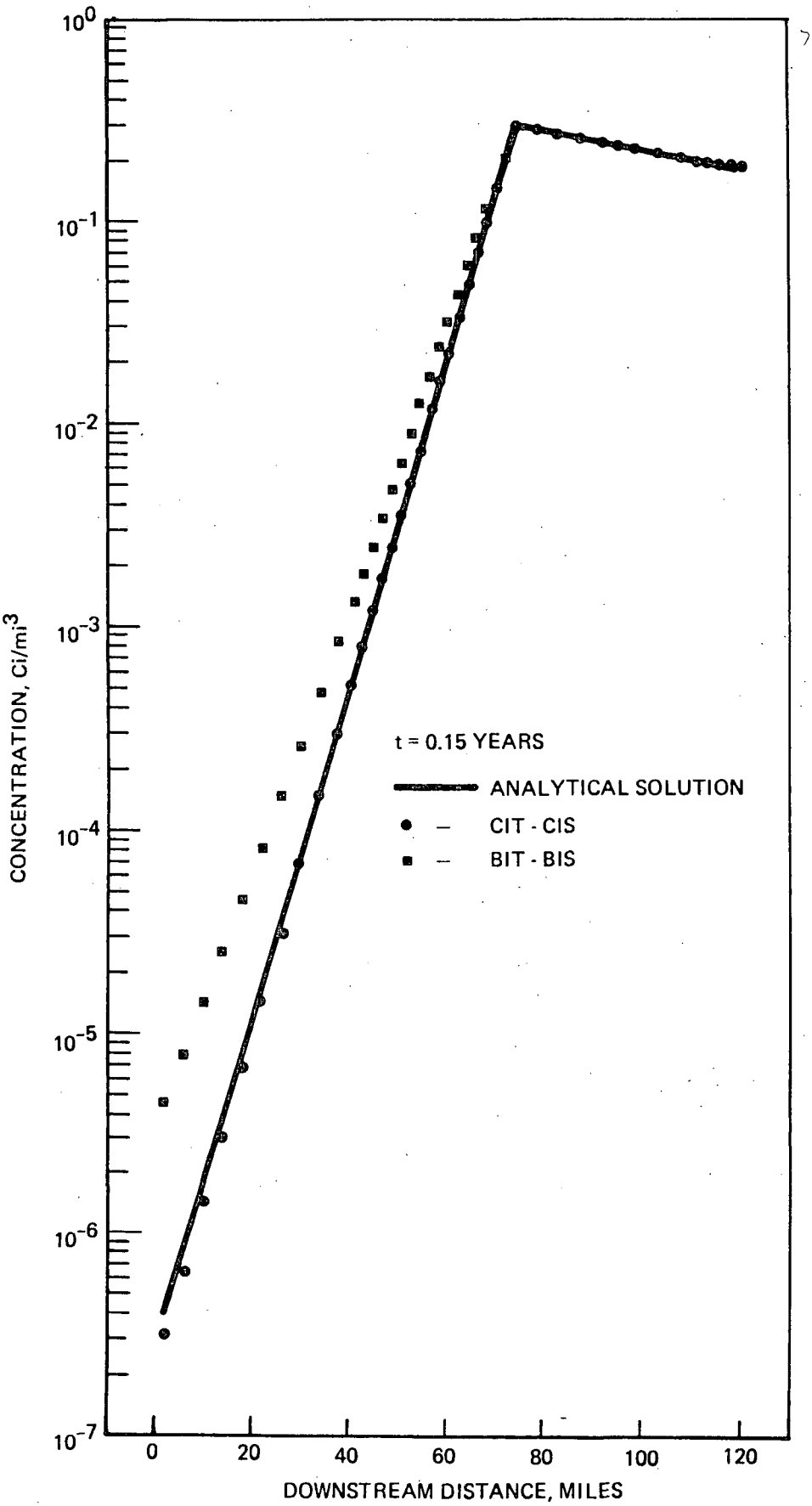


Figure 6.7-17C. Transient (Nonsteady State) Solution for Ru-103 at 0.15 Years for Unit Intensity Source at x_o = 75 Miles

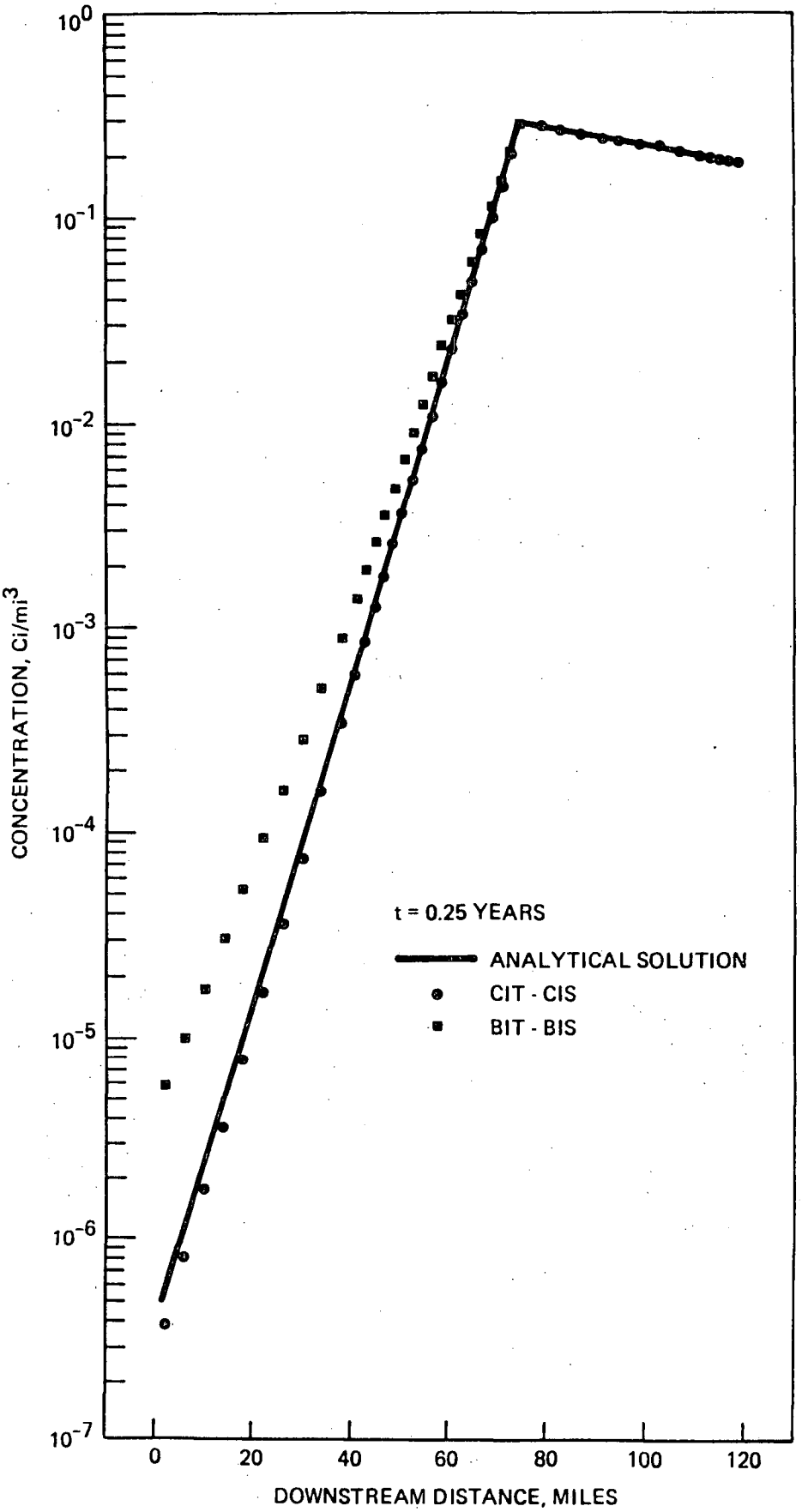


Figure 6.7-17D. Transient (Nonsteady State) Solution for Ru-103 at 0.25 Years for Unit Intensity Source at x_o = 75 Miles

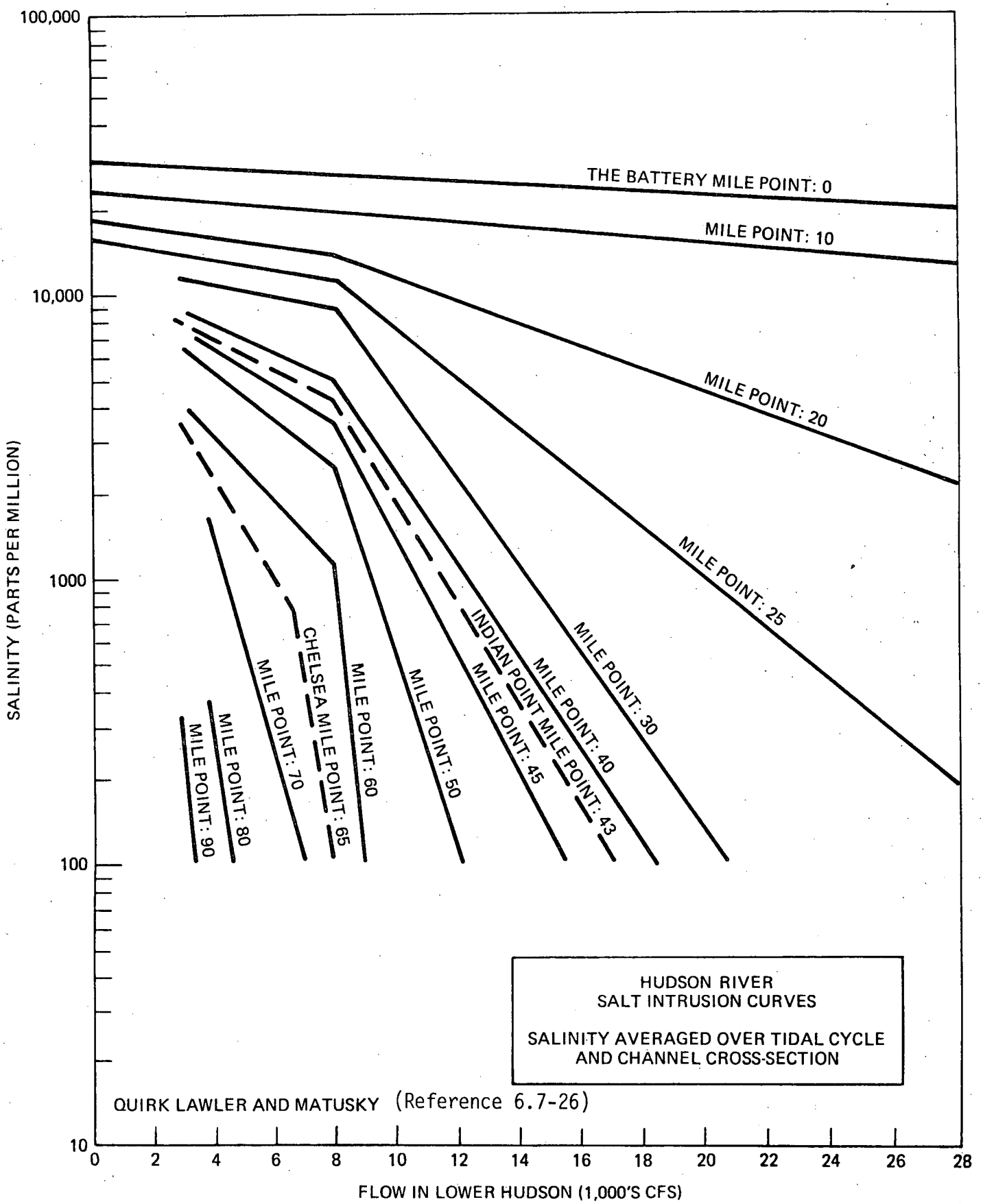


Figure 6.7-18. Hudson River Salt Intrusion Curves

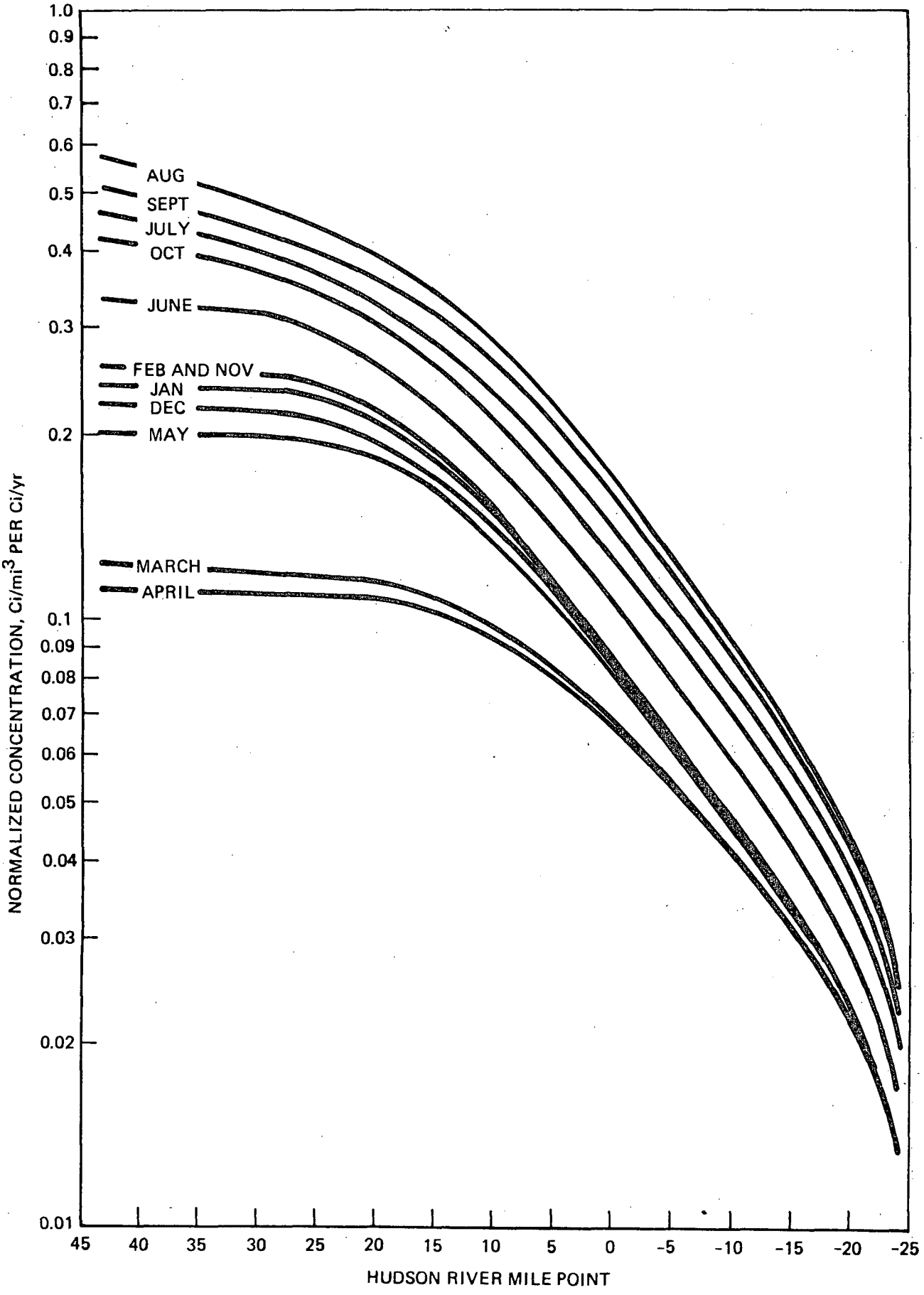


Figure 6.7-19. Results of Steady State, Pu-239 Sensitivity Analysis Calculations Downstream of Indian Point (MP43) for Each Month

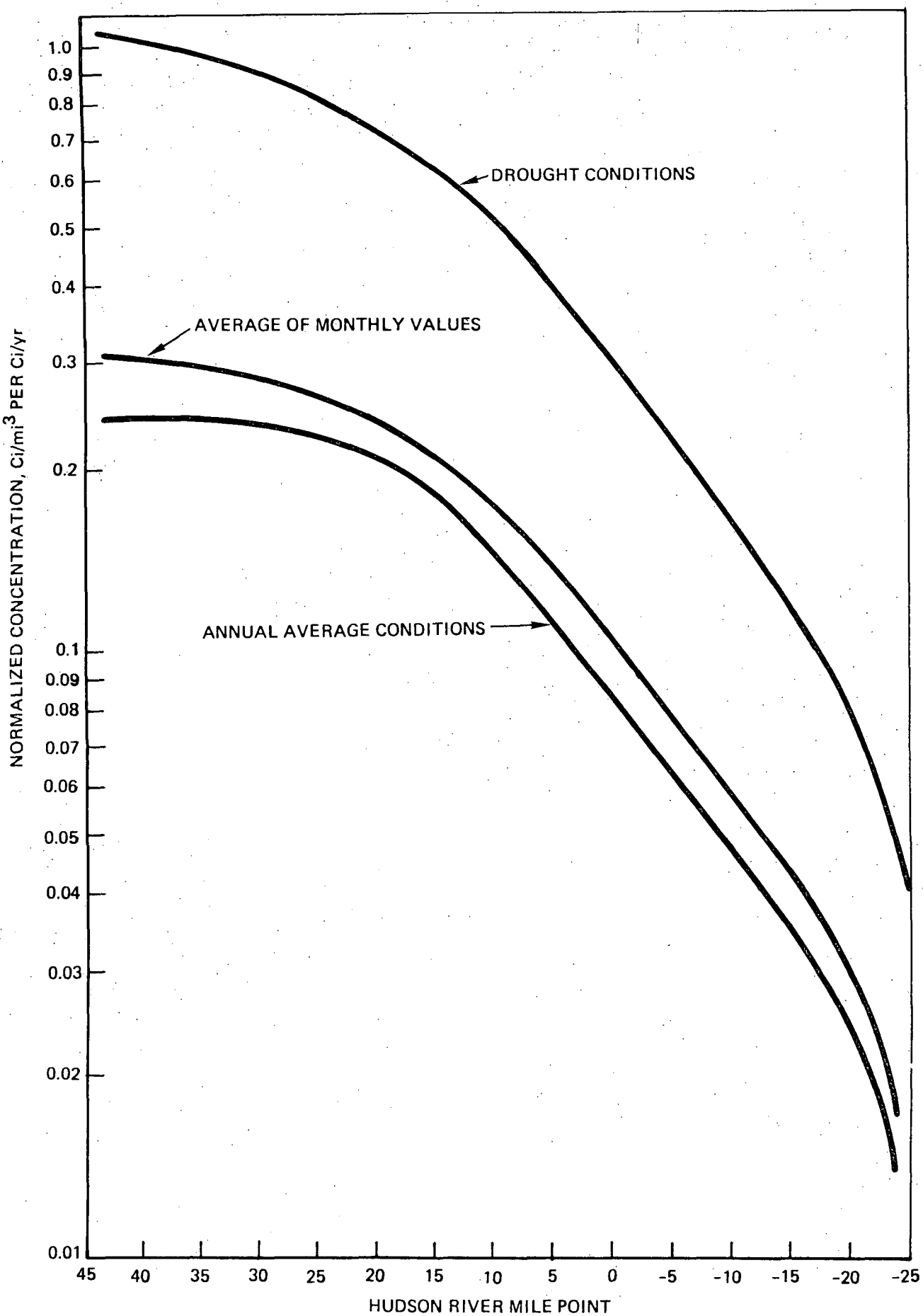


Figure 6.7-20. Results of Steady State, Pu-239 Sensitivity Analysis Calculations Downstream of Indian Point (MP43) for Special Conditions

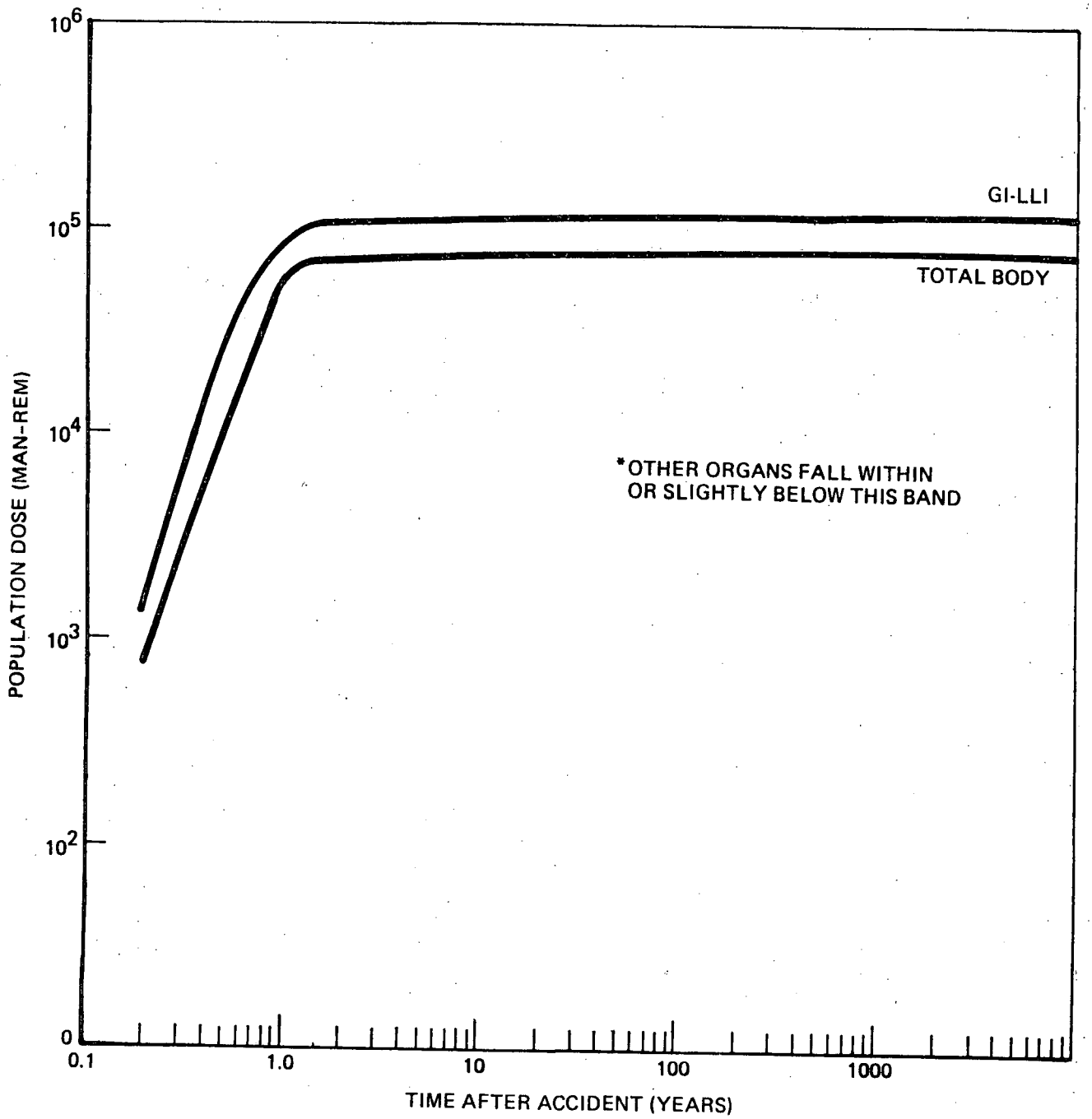


Figure 6.7-21. Population Dose (Man-Rem) as a Function of Time Due to a Release to the Liquid Pathways (Shellfish Interdiction Assumed for First 2 Years)

Indian Point Probabilistic Safety Study

Power Authority of the State of New York
Consolidated Edison Company of New York, Inc.

— NOTICE —

THE ATTACHED FILES ARE OFFICIAL RECORDS OF THE DIVISION OF DOCUMENT CONTROL. THEY HAVE BEEN CHARGED TO YOU FOR A LIMITED TIME PERIOD AND MUST BE RETURNED TO THE RECORDS FACILITY BRANCH 016. PLEASE DO NOT SEND DOCUMENTS CHARGED OUT THROUGH THE MAIL. REMOVAL OF ANY PAGE(S) FROM DOCUMENT FOR REPRODUCTION MUST BE REFERRED TO FILE PERSONNEL.

Docket # 50-247
Control # 8203110003
DEADLINE RETURN DATE Date 03-05-82 of Document
REGULATORY DOCKET FILE

REGULATORY DOCKET FILE COPY

RECORDS FACILITY BRANCH

Volume 10

Indian Point Probabilistic Safety Study

Copyright 1982 by
Power Authority of the State of New York
Consolidated Edison Company of New York, Inc.

Volume 10

Copy No. 15

REGULATORY DOCKET FILE COPY

SECTION 7

TABLE OF CONTENTS

Section			Page
7.1	INTRODUCTION		7.1-1
7.2	SEISMIC		7.2-1
	7.2.1	Methodology	7.2-1
	7.2.2	Seismicity	7.2-1
		7.2.2.1 Dames & Moore Study	7.2-1
		7.2.2.2 Woodward-Clyde Consultants Study	7.2-3
		7.2.2.3 Seismicity Summary	7.2-4
	7.2.3	Fragility	7.2-5
		7.2.3.1 Definition of Failure	7.2-5
		7.2.3.2 Fragility Curve Formulation	7.2-6
	7.2.4	Indian Point Unit 2	7.2-7
		7.2.4.1 Systems and Plant Logic	7.2-7
		7.2.4.2 Seismic Core Melt Frequencies	7.2-11
		7.2.4.3 Initial Assembly Leading to Release Category Frequencies	7.2-11
	7.2.4A	Additional Seismic Analysis, Indian Point Unit 2	7.2-14
		7.2.4A.1 Control Building Seismic Bumpers	7.2-14
		7.2.4A.2 Control Room Ceiling	7.2.14A-1
		7.2.4A.3 Containment Structure	7.2-14A-2
		7.2.4A.4 Revised Fragilities	7.2-14A-3
		7.2.4A.5 Results	7.2-14A-3
	7.2.5	Indian Point Unit 3	7.2-14A-4
		7.2.5.1 Systems and Plant Logic	7.2-14A-4
		7.2.5.2 Seismic Core Melt Frequencies	7.2-17
		7.2.5.3 Initial Assembly Leading to Release Category Frequencies	7.2-18
	7.2.5A	Additional Seismic Analysis, Indian Point Unit 3	7.2-21
		7.2.5A.1 Control Room Ceiling	7.2-21
		7.2.5A.2 Containment Structure	7.2-21A-1
		7.2.5A.3 Revised Fragilities and Results	7.2-21A-1
7.3	FIRE		7.3-1
	7.3.1	Indian Point 2 Fire Analysis	7.3-1
		7.3.1.1 Summary	7.3-1
		7.3.1.2 Cable Spreading Room (Fire Zone 11, Control Building)	7.3-4
		7.3.1.3 Some Areas in the Primary Auxiliary Building, the Fan House, and the Control Building	7.3-16
		7.3.1.4 Fire Zone 1A (Electrical Tunnel, PAB Side)	7.3-18
		7.3.1.5 Switchgear Room (Fire Zone 14)	7.3-29
		7.3.1.6 Corridor (Fire Zone 27A)	7.3-34
		7.3.1.7 Electrical Tunnel, CB Side (Fire Zone 32A)	7.3-34
		7.3.1.8 Electrical Penetration Area (Fire Zone 74A)	7.3-36

TABLE OF CONTENTS (continued)

Section			Page
	7.3.1.9	Diesel Generator Building	7.3-37
	7.3.1.10	Smoke Propagation	7.3-41
	7.3.1.11	Flooding Due to Suppression Activities	7.3-43
	7.3.1.12	Core Melt Frequency Due to Fires at Indian Point 2	7.3-43
	7.3.1.13	Frequencies of Containment Event Tree Entry States Due to Fires at Indian Point 2	7.3-44
	7.3.1.14	Frequencies of Release Categories from Fires at Indian Point 2	7.3-46
7.3.1A	Additional Features, Indian Point Unit 2		7.3-47A-1
	7.3.1A.1	Introduction	7.3-47A-1
	7.3.1A.2	Fire Risk Before the Modification	7.3-47A-1
	7.3.1A.3	Basis for Modification	7.3-47A-2
	7.3.1A.4	Description of Modification	7.3-47A-3
	7.3.1A.5	Fire Risk After the Modification	7.3-47A-4
7.3.1B	Changes to Fire Analysis, Indian Point 2		7.3-47A-20
	7.3.1B.1	Introduction	7.3-47A-20
	7.3.1B.2	Electrical Penetration Area (Fire Zone 74A)	7.3-47A-20
	7.3.1B.3	Auxiliary Feedwater Pump Room	7.3-47A-21
	7.3.1B.4	Overall Impact of Requantification	7.3-47A-24
7.3.2	Indian Point 3 Fire Analysis		7.3-75
	7.3.2.1	Summary	7.3-75
	7.3.2.2	Cable Spreading Room (Fire Zone 11, Control Building)	7.3-77
	7.3.2.3	Some Areas in the Primary Auxiliary Building, the Fan House, and the Control Building	7.3-95
	7.3.2.4	Fire Zone 60A (Upper Electrical Tunnel)	7.3-97
	7.3.2.5	Switchgear Room (Fire Zone 14)	7.3-100
	7.3.2.6	Corridor (Fire Zone 27A)	7.3-106
	7.3.2.7	Upper Electrical Penetration Area (Fire Zone 73A)	7.3-106
	7.3.2.8	Smoke Propagation	7.3-107
	7.3.2.9	Flooding Due to Extinguishing Activities	7.3-108
	7.3.2.10	Core Melt Frequency Due to Fires at Indian Point 3	7.3-109
	7.3.2.11	Frequencies of Containment Event Tree Entry States Due to Fires at Indian Point 3	7.3-109
	7.3.2.12	Frequencies of Release Categories Due to Fires at Indian Point 3	7.3-111
7.3.2A	Additional Features, Indian Point Unit 3		7.3-111A-1
	7.3.2A.1	Introduction	7.3-111A-1
	7.3.2A.2	Fire Risk Before Modification	7.3-111A-1
	7.3.2A.3	Description of the Modification	7.3-111A-2

TABLE OF CONTENTS (continued)

Section			Page
		7.3.2A.4 Impact of the Modification	7.3-111A-4
		7.3.2A.5 Highlights of Base Case Quantification	7.3-111A-11
	7.3.3	References	7.3-133
		7.3.3A.1 References for Section 7.3.1A	7.3-133A-1
		7.3.3A.2 References for Section 7.3.2A	7.3-133A-1
	7.3.4	Appendix I -- Fire Propagation Model	7.3-134
		7.3.4.1 The Physical Model	7.3-134
		7.3.4.2 Uncertainties in Modeling	7.3-137
		7.3.4.3 Code Benchmarking	7.3-139
		7.3.4.4 Development of Fire Propagation Histograms	7.3-140
		7.3.4.5 References	7.3-145
	7.3.5	Appendix II -- A Simple Cabinet Air Temperature Model	7.3-163
	7.3.6	Appendix III -- Heat Fluxes from an Oil Pool Fire	7.3-166
7.4	FLOODING		7.4-1
	7.4.1	External Flooding	7.4-1
	7.4.2	Internal Flooding	7.4-2
		7.4.2.1 NonCategory I Systems	7.4-2
		7.4.2.2 Category I Systems	7.4-4
	7.4.3	Conclusions	7.4-7
	7.4.4	References	7.4-7
7.5	WINDS AND WIND INDUCED MISSILES		7.5-1
	7.5.1	Wind Events	7.5-1
	7.5.2	Tornado Missiles and Winds on Concrete Structures	7.5-1
	7.5.3	Tornado Missiles and Winds on Metal Structures	7.5-3
	7.5.4	Indian Point Unit 2	7.5-10
		7.5.4.1 Plant Logic	7.5-10
		7.5.4.2 Wind Core Melt Frequencies	7.5-12
		7.5.4.3 Initial Assembly Leading to Release Category Frequencies	7.5-13
	7.5.4A	Additional Analyses Unit 2	7.5-15
		7.5.4A.1 Wind Hazard	7.5-15
		7.5.4A.2 Structure Wind Fragilities	7.5-15A-2
		7.5.4A.3 Structure Tornado Missile Fragilities	7.5-15A-4
		7.5.4A.4 Plant Logic	7.5-15A-5
		7.5.4A.5 Wind Core Melt Frequencies	7.5-15A-8
		7.5.4A.6 Wind Release Category Frequencies	7.5-15A-8
	7.5.5	Indian Point Unit 3	7.5-15A-9
		7.5.5.1 Plant Logic	7.5-15A-9
		7.5.5.2 Wind Core Melt Frequencies	7.5-16
		7.5.5.3 Initial Assembly Leading to Release Category Frequencies	7.5-17

TABLE OF CONTENTS (continued)

Section		Page
	7.5.6 Summary	7.5-19
	7.5.7 References	7.5-19
7.6	AIRCRAFT ACCIDENTS	7.6-1
	7.6.1 Airports and Airways	7.6-1
	7.6.2 Aircraft Hazards Analysis	7.6-2
	7.6.3 Conclusions	7.6-5
	7.6.4 References	7.6-6
7.7	TRANSPORTATION AND STORAGE OF HAZARDOUS MATERIALS	7.7-1
	7.7.1 Rail Transportation	7.7-1
	7.7.2 Road Transportation	7.7-1
	7.7.3 Barge and Ship Traffic	7.7-1
	7.7.4 Gas Transmission Lines	7.7-3
	7.7.5 Stationary Sources of Hazardous Materials	7.7-5
	7.7.6 Analysis of Hazards Effects	7.7-6
	7.7.7 References	7.7-6
7.8	TURBINE MISSILES	7.8-1
	7.8.1 References	7.8-1
7.9	APPENDICES	7.9-1
	7.9.1 Dames & Moore Seismicity Study	
	7.9.2 Woodward Clyde Seismicity Study	
	7.9.3 Structural Mechanics Associates, Inc. Fragility Study	
	7.9.3.1 Indian Point Unit 2, Control Building Seismic Improvement Analysis	
	7.9.3.2 Seismic Capacity of Indian Point Containments	
	7.9.4 Structural Mechanics Associates, Inc. Damage - Effective Ground Acceleration	
	7.9.5 Research Triangle Institute. Windspeed Risk Analysis of the Indian Point Nuclear Generating Station	
	7.9.5.1 Extreme Wind Risk Analysis of the Indian Point Nuclear Generating Station, Addendum.	
	7.9.6 Structural Mechanics Associates, Inc., Conditional Probabilities of Wind Induced Failures for Selected Structures	

LIST OF TABLES

Table		Page
7.2-1	Structure Capacity - Indian Point 2	7.2-22
7.2-2	Summary of Equipment Capacities for Indian Point 2	7.2-23
7.2-3	Fragility of Key Structures and Equipment - Indian Point 2	7.2-25
7.2-4	Indian Point 2 Seismic Conditional Release Frequency - Matrix MC^S	7.2-26
7.2-4A-1	Revised Fragilities of Key Structures and Equipment - Indian Point 2	7.2-26A-1
7.2-5	Structure Capacity - Indian Point 3	7.2-27
7.2-6	Summary of Equipment Capacities for Indian Point 3	7.2-28
7.2-7	Fragility of Key Structures and Equipment - Indian Point 3	7.2-30
7.2-8	Indian Point 3 Seismic Conditional Release Frequency - Matrix MC^S	7.2-31
7.2-9	Revised Fragilities of Key Structures and Equipment - Indian Point 3	7.3-31A-1
7.3.1-1	Histogram of the Mean Extinguishing Time for Large Fires	7.3-48
7.3.1-2	Histogram of the Frequency of Containment Event Tree Entry State TEFC or Release Category 8B from a Fire in the Cable Spreading Room	7.3-49
7.3.1-3	Histogram of the Frequency of Containment Event Tree Entry State TE from a Fire in the Cable Spreading Room	7.3-50
7.3.1-4	Histogram of the Mean Extinguishing Time for Cable Tray Fires	7.3-51
7.3.1-5	Conditional Frequencies of Containment Event Tree Entry States Given a Fire That Has Caused Failure of the Power Cables of the Right Stack of Trays	7.3-52
7.3.1-6	Histogram of the Frequency of Containment Event Tree Entry State SLF from a Fire in Fire Zone 1A	7.3-53
7.3.1-7	Histogram of the Frequency of Containment Event Tree Entry State SEF from a Fire in Fire Zone 1A	7.3-54
7.3.1-8	Histogram of the Frequency of Containment Event Tree Entry State SE from a Fire in Fire Zone 1A	7.3-55
7.3.1-9	Histogram of the Frequency of Containment Event Tree Entry State SE fron a Fire in the Switchgear Room	7.3-56
7.3.1-10	Histogram of the Frequency of Containment Event Tree Entry State SE from a Fire in the Electrical Tunnel, CB Side	7.3-57
7.3.1-11	Histogram of the Frequency of Containment Event Tree Entry State SLF	7.3-58
7.3.1-12	Histogram of the Frequency of Containment Event Tree Entry State SEF	7.3-59
7.3.1-13	Histogram of the Frequency of Containment Event Tree Entry State SE	7.3-60
7.3.1-14	Histogram of the Frequency of Release Category 8A	7.3-61
7.3.1-15	Histogram of the Frequency of Release Category 2RW	7.3-62
7.3.1-16	Histogram of the Total Frequency of Core Melt	7.3-63

LIST OF TABLES (continued)

Table		Page
7.3.1A-17	Characteristic Values of the Frequencies of Release Categories and Core Melt Due to Fire After the Modification of Indian Point 2	7.3-63A-1
7.3.1A-18	Mean Frequencies of Fire Contributors Before the Modification	7.3-63A-2
7.3.1A-19	Mean Frequencies of Fire Contributors After the Modification	7.3-63A-3
7.3.1A-20	Frequencies of Several Parameters Used in Section 7.3.1A.5	7.3-63A-5
7.3.1A-21	Fire Contributions Before the Modification	7.3-63A-6
7.3.1B-22	Indian Point 2 - Characteristic Values of the Frequencies of Release Categories and Core Melt Due to Fire After the Alternate Shutdown System Modifications and the Requantification of Fire Zones 74A and 23	7.3-63A-19
7.3.1B-23	Mean Frequencies of Fire Contributors After the Alternate Shutdown System Modifications and the Requantification of Fire Zones 74A and 23	7.3-63A-20
7.3.2-1	Histogram of the Mean Extinguishing Time for Large Fires	7.3-112
7.3.2-2	Histogram of the Mean Extinguishing Time for Cable Tray Fires	7.3-113
7.3.2-3	Histogram of the Frequency of Containment Event Tree Entry State TEFC or Containment Event Tree Entry State 8B from a Fire at the Center of the Northern Wall	7.3-114
7.3.2-4	Histogram of the Frequency of Containment Event Tree Entry State TE from a Fire at the Center of the Northern Wall	7.3-115
7.3.2-5	Histogram of the Frequency of Containment Event Tree Entry State SE from a Fire at the Power Cables in the Cable Spreading Room	7.3-116
7.3.2-6	Histogram of the Frequency of Containment Event Tree Entry State TE from a Fire in Fire Zone 60A	7.3-117
7.3.2-7	Histogram of the Frequency of Containment Event Tree Entry State TE from a Fire in the Switchgear Room	7.3-118
7.3.2-8	Histogram of the Frequency of Containment Event Tree Entry State SE from a Fire in the Switchgear Room	7.3-119
7.3.2-9	Histogram of the Frequency of Containment Event Tree Entry State TE from a Fire in Indian Point 3	7.3-120
7.3.2-10	Histogram of the Frequency of Containment Event Tree Entry State SE from a Fire in Indian Point 3	7.3-121
7.3.2-11	Histogram of the Frequency of Release Category 2RW	7.3-122
7.3.2-12	Histogram of the Frequency of Core Melt	7.3-123
7.3.2A-13	Characteristic Values of the Frequencies of Release Categories and Core Melt Due to Fire After the Appendix R Modification to Indian Point 3	7.3-123A-1
7.3.2A-14	Mean Frequencies of Fire Contributors for Indian Point 3 Before the Modification	7.3-123A-2

LIST OF TABLES (continued)

Table		Page
7.3.2A-15	Mean Frequencies of Fire Contributors After Appendix R Modification is Implemented	7.3-123A-3
7.3.2A-16	Frequencies of Several Parameters Used in the Study	7.3-123A-4
7.3.2A-17	Histogram of the Frequency of Core Melt in Indian Point 3 Due to Fire After the Modification	7.3-123A-5
7.3.2A-18	Histogram of Release Category 8B in Indian Point 3 Due to Fire	7.3-123A-6
7.3.2A-19	Histogram of the Frequency of Release Category 8A in Indian Point 3 Due to Fire	7.3-123A-7
7.3.2A-20	Histogram of the Frequency of Release Category 2RW in Indian Point 3 Due to Fire After the Modification	7.3-123A-8
7.3.2A-21	Fire Area Analysis	7.3-123A-9
7.3.2A-22	Characteristic Values of Several Parameters Used in the Quantification of Base Case Fire Risk	7.3-123A-24
7.3.4-1	Histogram of the Predicted Vertical Spread Fire Propagation Time ($\tau_{V,DRM}$), No Barrier, Q_p = 400 Btu, Including Parameter Uncertainties Only	7.3-147
7.3.4-2	Histogram of the Predicted Vertical Spread Fire Propagation Time ($\tau_{V,DRM}$), No Barrier, Q_p = 4,000 Btu, Including Parameter Uncertainties Only	7.3-148
7.3.4-3	Histogram of the Predicted Vertical Spread Fire Propagation Time ($\tau_{V,DRM}$), No Barrier, Q_p = 40,000 Btu, Including Parameter Uncertainties Only	7.3-149
7.3.4-4	Histogram of the Vertical Spread Fire Propagation Time (τ_V*), No Barrier, Q_p = 400 Btu, Including Modeling Uncertainties	7.3-150
7.3.4-5	Histogram of the Vertical Spread Fire Propagation Time (τ_V*), No Barrier, Q_p = 4,000 Btu, Including Modeling Uncertainties	7.3-151
7.3.4-6	Histogram of the Vertical Spread Fire Propagation Time (τ_V*), No Barrier, Q_p = 40,000 Btu, Including Modeling Uncertainties	7.3-152
7.3.4-7	Histogram of the Predicted Horizontal Spread Fire Propagation Time ($\tau_{H,DRM}$), No Barrier, Q_p = 400 Btu, Including Modeling Uncertainties	7.3-153
7.3.4-8	Histogram of the Predicted Horizontal Spread Fire Propagation Time ($\tau_{H,DRM}$), No Barrier, Q_p = 4,000 Btu, Including Modeling Uncertainties	7.3-154
7.3.4-9	Histogram of the Predicted Horizontal Spread Fire Propagation Time ($\tau_{H,DRM}$), No Barrier, Q_p = 40,000 Btu, Including Modeling Uncertainties	7.3-155
7.3.4-10	Histogram of the Horizontal Spread Fire Propagation Time (τ_H*), No Barrier, Q_p = 400 Btu, Including Modeling Uncertainties	7.3-156

LIST OF TABLES (continued)

Table		Page
7.3.4-11	Histogram of the Horizontal Spread Fire Propagation Time (τ_H*), No Barrier, Q_p = 4,000 Btu, Including Modeling Uncertainties	7.3-157
7.3.4-12	Histogram of the Horizontal Spread Fire Propagation Time (τ_H*), No Barrier, Q_p = 40,000 Btu, Including Modeling Uncertainties	7.3-158
7.3.4-13	Histogram of the Predicted Spread Time to Tray C ($\tau_{C,DRM}$), Including Parameter Uncertainties Only	7.3-159
7.3.4-14	Histogram of the Spread Time to Tray C (τ_C*), Including Modeling Uncertainties	7.3-160
7.5-1	Variability for Extra-Tropical Cyclones and Hurricane Wind Loading - Indian Point Units 2 and 3	7.5-20
7.5-2	Structure Capacities for Tornado Winds - Indian Point Units 2 and 3	7.5-21
7.5-3	Structure Capacities for Extra-Tropical Cyclone and Hurricane Winds - Indian Point Units 2 and 3	7.5-22
7.5-4	Indian Point 2 Conditional Release Frequencies - Extra-Tropical Cyclone and Hurricane Wind Matrix MC^W	7.5-23
7.5-5	Indian Point 2 Conditional Release Frequencies - Tornado Wind Matrix MC^W	7.5-24
7.5-6	Indian Point 3 Conditional Release Frequencies - Tornado Wind Matrix MC^W	7.5-25
7.5-7	Unit 2 Building Wind Fragility	7.5-25A-1
7.5-8	Unit 2 Building Tornado Missile Fragilities	7.5-25A-4
7.5-9	Conditional Probability of Impact	7.5-25A-5
7.5-10	Unit 2 Component Booleans	7.5-25A-6
7.6-1	Number of Flights on Airways Within 12 Miles of Indian Point	7.6-7
7.6-2	Airways Traffic Hit Probabilities	7.6-8
7.7-1	Offsite Rail/Barge Transportation of Hazardous Chemicals	7.7-7
7.7-2	Chemical Storage at Indian Point	7.7-8
7.7-3	Toxic Chemicals Hazards to be Analyzed	7.7-9

LIST OF FIGURES

Figure		Page
7.2-1	Seismicity Family Dames & Moore (NE Zones)	7.2-32
7.2-2	Seismicity Family Dames & Moore (Piedmont Zones)	7.2-33
7.2-3	Seismicity Family Woodward-Clyde	7.2-34
7.2-4	Seismicity Family Summary	7.2-35
7.2-5	Fragility Families for Key Indian Point 2 Components	7.2-36
7.2-6a	Indian Point Unit 2 Seismic Core Melt Fault Tree	7.2-41
7.2-6b	Indian Point Unit 2 Seismic Core Melt Fault Tree (continued)	7.2-42
7.2-6c	Indian Point Unit 2 Seismic Core Melt Fault Tree (continued)	7.2-43
7.2-6d	Indian Point Unit 2 Seismic Core Melt Fault Tree (continued)	7.2-44
7.2-6e	Indian Point Unit 2 Seismic Core Melt Fault Tree (continued)	7.2-45
7.2-6f	Indian Point Unit 2 Seismic Core Melt Fault Tree (continued)	7.2-46
7.2-7	Indian Point Unit 2 Seismic Core Melt Frequency	7.2-47
7.2-8	Indian Point Unit 2 Seismic Fan Coolers Fault Tree	7.2-48
7.2-9	Indian Point Unit 2 Seismic Containment Spray Fault Tree	7.2-49
7.2-10	Release Frequency from Seismic Events - Indian Point Unit 2	7.2-50
7.2-10A-1	Existing Configuration of Control Building and Superheater Building at Elevation 72'-0" (Indian Point 2)	7.2-50A-1
7.2-10A-2	Method for Adding Rubber Pads Between Control Building and Superheater Building (Indian Point 2)	7.2-50A-2
7.2-10A-3	Release Frequency from Seismic Events, Indian Point 2 (After Modification to the Control Building)	7.2-50A-3
7.2-11	Fragility Families for Key Indian Point 3 Components	7.2-51
7.2-12a	Indian Point Unit 3 Seismic Core Melt Fault Tree	7.2-56
7.2-12b	Indian Point Unit 3 Seismic Core Melt Fault Tree (continued)	7.2-57
7.2-12c	Indian Point Unit 3 Seismic Core Melt Fault Tree (continued)	7.2-58
7.2-12d	Indian Point Unit 3 Seismic Core Melt Fault Tree (continued)	7.2-59
7.2-12e	Indian Point Unit 3 Seismic Core Melt Fault Tree (continued)	7.2-60
7.2-12f	Indian Point Unit 3 Seismic Core Melt Fault Tree (continued)	7.2-61
7.2-13	Indian Point Unit 3 Seismic Core Melt Frequency	7.2-62
7.2-14	Indian Point Unit 3 Seismic Fan Coolers Fault Tree	7.2-63
7.2-15	Indian Point Unit 3 Seismic Containment Spray Fault Tree	7.2-64
7.2-16	Release Frequency from Seismic Events - Indian Point Unit 3	7.2-65

LIST OF FIGURES (continued)

Figure		Page
7.2-17	Revised Release Frequency from Seismic Events - Indian Point 3	7.2-66
7.3.1-1	The Cable Spreading Room of Indian Point 2, as Viewed from the Top	7.3-64
7.3.1-2	Cable Routing in Cable Tunnel	7.3-65
7.3.1-3	Simplified Diagram of the Control Circuitry for Opening an RHR Isolation MOV (730 or 731)	7.3-66
7.3.1-4	Valves with the Potential of Causing a Small LOCA	7.3-67
7.3.1-5	Normal and Excess Letdown Lines in Indian Point 2	7.3-68
7.3.1-6	Simplified Event Tree for a Small LOCA	7.3-69
7.3.1-7	Simplified Event Tree for Transient Events	7.3-70
7.3.1-8	Recirculation System Simplified P&ID	7.3-71
7.3.1-9	Top View of the Switchgear Room in Indian Point 2	7.3-72
7.3.1-10	Layout of the Diesel Generator Building	7.3-73
7.3.1-11	Side View of the Diesel Generator Building	7.3-74
7.3.1-12	Schematics of the Transfer Switch Installed for AFWS Pump 21	7.3-74A-1
7.3.2-1	The Cable Spreading Room of Indian Point 3, as Viewed from the Top	7.3-124
7.3.2-2	View Looking East into Cable Tunnel	7.3-125
7.3.2-3	Typical Section in Tunnel Looking from Control Building, Indian Point 3	7.3-126
7.3.2-4	Simplified Diagram of the Control Circuitry for Opening an RHR Isolation MOV (731 or 730)	7.3-127
7.3.2-5	Valves with the Potential of Causing a Small LOCA	7.3-128
7.3.2-6	Normal and Excess Letdown Lines in Indian Point 3	7.3-129
7.3.2-7	Simplified Event Tree for a Small LOCA	7.3-130
7.3.2-8	Simplified Event Tree for Transient Events	7.3-131
7.3.2-9	Simplified Top View of the Switchgear Room in Indian Point 3	7.3-132
7.3.2-10	Schematic of Appendix R Modification	7.3.132A-1
7.3.2-11	Cable Routing of the Alternate Feed System	7.3.132A-2
7.3.4-1	Cable Tray Configuration in the Indian Point 2 Cable Spreading Room	7.3-161
7.3.4-2	Fire Spread Through Elevated Trays	7.3-162
7.3.5-1	Problem Setup	7.3-165
7.3.5-2	Hot Wall Heat Balance	7.3-165
7.3.5-3	Cold Wall Heat Balance	7.3-165
7.3.6-1	Model for Computing Heat Fluxes from a Pool Fire	7.3-168
7.5-1	Hurricane and Extra-Tropical Cyclone Windspeed Exceedance Probabilities at Elevation 33' (Fastest Mile)	7.5-26
7.5-2	Tornado Windspeed Exceedance Probabilities at Elevation 33' (Fastest Quarter Mile)	7.5-27
7.5-3	Structure Tornado Missile Capacities	7.5-28
7.5-4	Structure Hurricane and Extra-Tropical Cyclone Wind Capacities	7.5-29
7.5-5	Structure Tornado Wind Capacities	7.5-30

LIST OF FIGURES (continued)

Figure		Page
7.5-6a	Indian Point Unit 2 Wind and Tornado Missile Core Melt Fault Tree	7.5-31
7.5-6b	Indian Point Unit 2 Wind and Tornado Missile Core Melt Fault Tree (continued)	7.5-32
7.5-6c	Indian Point Unit 2 Wind and Tornado Missile Core Melt Fault Tree (continued)	7.5-33
7.5-6d	Indian Point Unit 2 Wind and Tornado Missile Core Melt Fault Tree (continued)	7.5-34
7.5-6e	Indian Point Unit 2 Wind and Tornado Missile Core Melt Fault Tree (continued)	7.5-35
7.5-6f	Indian Point Unit 2 Wind and Tornado Missile Core Melt Fault Tree (continued)	7.5-36
7.5-7	Core Melt Frequency from Wind Events - Indian Point 2	7.5-37
7.5-8	Indian Point Unit 2 Wind and Tornado Missile Fault Tree for Failure of Fan Coolers	7.5-38
7.5-9	Indian Point Unit 2 Wind and Tornado Missile Fault Tree for Failure of Containment Spray	7.5-39
7.5-10	Release Frequency from Wind Events - Indian Point Unit 2	7.5-40
7.5-11a	Indian Point Unit 3 Wind and Tornado Missile Missile Core Melt Fault Tree	7.5-41
7.5-11b	Indian Point Unit 3 Wind and Tornado Missile Missile Core Melt Fault Tree (continued)	7.5-42
7.5-11c	Indian Point Unit 3 Wind and Tornado Missile Missile Core Melt Fault Tree (continued)	7.5-43
7.5-11d	Indian Point Unit 3 Wind and Tornado Missile Missile Core Melt Fault Tree (continued)	7.5-44
7.5-11e	Indian Point Unit 3 Wind and Tornado Missile Missile Core Melt Fault Tree (continued)	7.5-45
7.5-12	Core Melt Frequency from Wind Events - Indian Point Unit 3	7.5-46
7.5-13	Indian Point Unit 3 Wind and Tornado Missile Fault Tree for Failure of Fan Coolers	7.5-47
7.5-14	Indian Point Unit 3 Wind and Tornado Missile Fault Tree for Failure of Containment Spray	7.5-48
7.5-15	Release Frequency from Wind Events - Indian Point Unit 3	7.5-49
7.5-16	Plant North Combined Windspeed Exceedance Probabilities	7.5-49A-1
7.5-17	Plant South Combined Windspeed Exceedance Probabilities	7.5-49A-2
7.5-18	Plant East Combined Windspeed Exceedance Probabilities	7.5-49A-3
7.5-19	Plant West Combined Windspeed Exceedance Probabilities	7.5-49A-4
7.5-20a	Indian Point Unit 2 Wind and Tornado Transient with Loss of Cooling Fault Tree	7.5-49A-5

LIST OF FIGURES (continued)

Figure		Page
7.5-20b	Indian Point Unit 2 Wind and Tornado Small LOCA with Loss of Injection of Cooling	7.5-49A-6
7.5-20c	Indian Point Unit 2 Wind and Tornado Loss of AC Power	7.5-49A-7
7.5-20d	Indian Point Unit 2 Wind and Tornado Loss of Control	7.5-49A-8
7.5-21	Core Melt Frequency from Wind Events - Indian Point 2	7.5-49A-9
7.5-22	Indian Point Unit 2 Wind and Tornado Missile Fault Tree for Failure of Fan Coolers	7.5-49A-10
7.5-23	Indian Point Unit 2 for Wind and Tornado Missile Failure of Containment Spray	7.5-49A-11
7.5-24	Release Frequency from Wind Events - Indian Point Unit 2	7.5-49A-12
7.6-1	Peekskill Seaplane Base	7.6-9
7.6-2	Airways in Vicinity of Indian Point	7.6-10

SECTION 7

EXTERNAL EVENTS

7.1 INTRODUCTION

Before a location for a nuclear power plant is chosen, engineers and other experts conduct a detailed site investigation which considers all potential external events that could damage the plant. Plants are designed to withstand any event with a significant frequency of occurrence. In this section, external events which could exceed this design basis are discussed. Events analyzed include potential turbine missiles, aircraft and other transportation accidents, accidents associated with the storage of hazardous materials, near proximity gas line accidents, earthquakes, floods, tornadoes, and fires. Uncertainties were placed on event occurrence and component failure estimates so that the results encompass those from more detailed evaluation techniques. The potential for damage is quantified along with the uncertainties associated with these estimates. Generally, uncertainties are expressed at the estimated 5% and 95% confidence levels.

External events can be thought of as additional initiating events. They can therefore expand the $[\phi]$ matrix and can be treated like any other class of initiating events. In practice, a parallel path was indeed employed. Because of the nature of these events, however, and the manner of analysis described herein, full integration with the work in earlier sections takes place in Section 8. The approach for each external event will be clear in the individual descriptions in this section.

7.2 SEISMIC

This section describes the analysis of the probabilities and consequences of seismically initiated events at the plant site. The general methodology presented in Section 7.2.1 provides an overview of the approach. Subsequent sections apply the methodology to the Indian Point site. Reports by seismicity and structural mechanics consultants are included in Section 7.9 and contribute to the information presented here.

7.2.1 METHODOLOGY

A seismic risk analysis consists of five main steps:

1. Seismicity: determination of the frequency of various sized ground motions at the site.

2. Fragility: determination of the inability of plant structures and components to withstand various seismically initiated ground accelerations.

3. Plant Logic: determination of the effect of various combinations of structural and equipment failures on the behavior of the plant.

4. Initial Assembly: combination of the seismicity, component fragility, plant logic, and the containment model to obtain the frequencies of various release categories as a result of the ground motion.

5. Final Assembly: further combination of these with the site specific release consequences model to obtain the final seismic risk curve.

7.2.2 SEISMICITY

Earthquakes can be characterized by a single parameter, the effective peak ground acceleration, a, which structures and equipment might experience. The seismicity of a site is characterized here by a curve relating effective peak ground acceleration to annual exceedance frequency, $\phi(a)$, at the site.

Site seismicity studies have been completed; one by Dames & Moore, and the other by Woodward-Clyde Consultants. These are provided in Section 7.9 as Appendices 7.9.1 and 7.9.2, respectively. Analysis technique and results of each study are presented in the following sections. The two studies were integrated to obtain a common set of seismicity data for further use in the seismic analysis.

7.2.2.1 Dames & Moore Study

This study makes extensive use of tectonic provinces described in earlier Dames & Moore work for Indian Point, as well as the work of TERA Corporation (1979) in which a number of nationally recognized seismicity experts made judgments of the seismicity in various regions

of the United States. Two hypotheses for seismogenic zones were examined. The first, based on the earlier Dames & Moore work, was comprised of relatively small northeast tectonic zones. The second, based on the TERA work, considers either of two larger zones, the Piedmont or Piedmont-Cape Ann. The majority of the experts in the TERA work consider the Piedmont Zone to be the most appropriate of the two for the Indian Point region; however, to include the minority opinion of the experts, it was considered desirable to also include the Piedmont-Cape Ann Zone, but with lesser weight than the Piedmont.

In the absence of instrumentation, most historical earthquakes have been reported in terms of the structural damage they caused. This information has been subsequently converted to the Modified Mercalli Intensity, I_0. In the current study, these intensity values were converted to body wave magnitudes, m_b, using the relation

$$m_b = 0.5\ (I_0 + 3.5)$$

Interest is limited to earthquakes where $m_b \geq 4.0$ because earthquakes of smaller magnitude rarely cause structural damage. The annual number, n, of earthquakes of various magnitudes was expressed by the logarithmic form

$$\log_{10} n(m_b) = a - bm_b$$

where a and b are parameters fit to available seismicity data and m_b is the earthquake magnitude of interest. Inasmuch as a precise value of maximum body wave magnitude cannot be established with absolute certainty, the uncertainty in maximum m_b was provided by assigning a probability P_i to each of several hypothesized maxima such that

$$\sum_i P_i = 1.0$$

The maximum historical earthquake intensity corresponds to Modified Mercalli level VII. To be conservative, the most probable (largest P_i) value of m_b was chosen for each of the tectonic zones examined to correspond to a seismic event of intensity VIII. This represents the mean value of maximum body wave magnitude for which the highest probability was assigned. Lower probabilities have been assigned for the maximum magnitude being above or below this mean value and will be seen on the curves which follow.

Seismic ground motion at the site was estimated for a_s, the sustained acceleration, using the relationship

$$a_s = 0.584 \exp -0.711 \exp(-.444m_b) + 1.098m_b$$

where epicentral distance < 10km, and

$$a_s = 3.98\ \Delta^{-5/6} \exp\ -0.0711 \exp(-.444m_b) + 1.098m_b$$

where epicentral distance $\Delta \geq$ 10km.

This sustained level of acceleration, a_s, corresponds to the third highest peak in the acceleration time history (i.e., the oscillation history of a single seismic event) and is representative of several cycles of ground acceleration to which structures and components must be subjected in order to experience damage. However, the Dames & Moore study results were finally tabulated in terms of sustained-based peak accelerations, a_{ps}, which were derived from $a_{ps} = 1.23a_s$, where the factor 1.23 is approximated (values are actually variable depending on earthquake magnitudes and horizontal component orientations).

Using the results of Dames & Moore's table of sustained-based peak ground acceleration, curves of annual exceedance frequency for sustained-based peak ground acceleration were developed and are presented in Figures 7.2-1 and 7.2-2 based on the Northeast Tectonic Zones and the Piedmont Zones, respectively. In each figure, the curves are weighted so that their sum equals 1.0.

Plant fragility is based on effective or sustained, rather than sustained-based, peak ground accelerations and, because the Dames & Moore curves reflect sustained-based peak ground accelerations, the curves were divided by 1.23 (as derived in the reference) to obtain the peak ground acceleration values shown later in the curves of Figure 7.2-4.

7.2.2.2 Woodward-Clyde Consultants Study

To assess the importance of various parameters in the assumptions that could be made and to obtain a better understanding of the uncertainties in the study, Woodward-Clyde first performed a parametric analysis. Sensitivity studies were conducted and, where variations in assumed values were found to affect study results, probabilities were assigned to the alternative assumed values. Preferred choices were made by Woodward-Clyde from among the technological approach options.

The study indicated that the assumptions made with respect to the intensity-magnitude relationships, attenuation approach, and methods for converting to the ground motion at the site caused significant differences in the annual frequency of predicted peak ground accelerations, varying from 1 to 2 orders of magnitude. Arguing that there would be less error in their approach, Woodard-Clyde attenuated historical epicentral intensity, I_o, according to distance to the site to obtain the site intensity, I_s. Then, site intensity was converted to peak ground acceleration (in g's) from which sustained peak ground acceleration was estimated.

The study indicated that varying the source geometry has minimal impact on the probabilities of exceeding the frequency of various earthquakes at the plant site, ranging from a factor of approximately 2 to 5. Assumptions of larger seismogenic zones imply lower probabilities of occurrence per unit area.

At lower accelerations, which are of greatest interest, exceedance frequencies based on assumed maximum intensities of VII or VIII vary by a factor of 2 to 3. Frequency divergence increases at higher accelerations. To accommodate this variability, a smaller seismogenic zone was

selected with an 80% probability of intensity VII and a 20% probability of intensity VIII as the maximum assumed future earthquake intensity.

Figure 7.2-3 presents the results of the Woodward-Clyde study. The figure indicates, by the dashed curves, the results with upper bound earthquake intensities of VII and VIII, respectively, if there were no constraints on the maximum sustained peak ground acceleration at the site. However, the study indicates that there are upper bounds on the site ground accelerations as a function of the epicentral maximum intensities; these cannot be precisely defined. Estimates were available (from Nuttli data referenced in the study) of mean values for the upper bound values. Using these mean values, Woodward-Clyde estimated maximum sustained peak ground accelerations for each of the assumed maximum earthquake intensities. The results are the solid curves in Figure 7.2-3, to which the study assigned a 95% probability that the maximum sustained peak ground acceleration is less than 0.25g or 0.30g for upper bounds on epicentral intensity of VII and VIII, respectively, and a 100% probability that it is less than 0.35g or 0.5g, respectively, for these two intensities. The curves are weighted accordingly so that their sum is equal to 1.0.

7.2.2.3 Seismicity Summary

The results of the two seismicity studies differ in some respects. There are differences in the selection of the probable upper bound earthquake intensity and in the assumed relationships between earthquake intensity and magnitude to attenuated ground motion at the site; however, the results of each study overlap. Because the consultants who prepared these studies have equal expertise and experience in probabilistic seismicity analysis, the results of each study are integrated with equal weight, thereby reflecting the range of views in present practice.

Many seismologists believe that there is an upper bound to the sustained ground acceleration that an earthquake of given intensity or magnitude can cause at a distant location. There is, however, uncertainty about this maximum value. Because intensity is a measure of potential damage to structures resulting from an earthquake, we can look to the structural analyst to assess the relationship between the upper bound of intensity and structure damage experience. This subject is discussed in a brief report by Structural Mechanics Associates, Inc., (Section 7.9.4). The report indicates that a correlation exists between the energy and frequency content of the maximum earthquake source intensity and the maximum damage that could potentially be experienced by structures at a point of interest. Upper bounds on effective ground accelerations were estimated for various maximum source intensities. These upper bounds were used in this study to truncate the seismicity hazard curves provided by the seismicity consultants.

Figure 7.2-4 presents the curves developed in the two seismicity studies. For each curve, the termination occurs at an upper bound ground acceleration corresponding to the maximum earthquake as discussed in Section 7.9.4. These curves were used to assemble the seismic analysis.

The Dames & Moore and Woodward-Clyde studies are given equal weight, and each curve in Figure 7.2-4 is weighted such that the sum of the curve weights is equal to 1.0.

7.2.3 FRAGILITY

As indicated in the fragility analysis report by Structural Mechanics Associates, Inc. (Appendix 7.9.3), the approach adopted in assigning capacities (failure fraction as a function of effective peak ground acceleration) for the structures, equipment, and other components, was to first determine the median factor of safety against failure and its statistical variability under the design basis or safe shutdown earthquake (SSE). From this safety factor, the median effective ground acceleration causing failure was estimated.

In general, the factor of safety against failure of a structure or component from seismically initiated ground motion can be defined as the ratio of the ground motion at its failure to the maximum ground motion used in design to maintain acceptable elastic stress limits in the component's materials. For the Indian Point site, the SSE ground motion used in design of the facility was 0.15g peak ground acceleration. The overall safety factor was determined by evaluating the safety factors for a number of parameters, which fell into two categories: structural capacity and structural response. Parameters influencing the factor of safety on structural capacity include the strength of the structure compared to the design stress level and the inelastic energy absorption capacity (ductility) of a structure to carry load beyond yield. The parameters in structural response for a given ground acceleration are made up of many factors. The most significant of these include: (1) ground motion and the associated ground response spectra for a given peak free field ground acceleration, (2) energy dissipation (damping), (3) structural modeling, (4) method of analysis, (5) combination of dynamic response modes, and (6) combination of earthquake components. The response of piping and mounted equipment depends on the particular building and the location within the building. The ratio between the best estimate of limiting value of each of these factors and the value used in design of the plant (by analysis or qualification test), or effects on response was quantitatively estimated for each critical plant component. A combination of generic and plant specific information was used for these estimates.

The derivation of each factor of safety considered variability. Section 7.2.3.2 discusses how, in each case, a median safety factor was assigned along with a variability. When combining the median safety factors of contributing parameters, their variabilities were also combined to define the overall safety factor. From this overall safety factor, the effective or sustained peak ground acceleration at failure was determined.

7.2.3.1 Definition of Failure

For purposes of this study, Class I structures are considered to fail when inelastic deformations of the structure under seismic load potentially interfere with the operability of safety related equipment

attached to the structure. These limits on inelastic energy absorption capability (ductility limits) chosen for Class I structures are estimated to correspond to the onset of significant structural damage, not necessarily corresponding to structure collapse.

Piping, electrical, mechanical, and electromechanical equipment vital to a safe shutdown of the plant are considered to fail when they can no longer perform their designated functions. Rupture of the pressure boundary on mechanical components is also considered a failure. Depending upon the equipment type, one or the other failure mode will govern. In most cases, however, function failure will govern as equipment pressure boundaries are usually very conservatively designed for equipment such as pumps and valves.

7.2.3.2 Fragility Curve Formulation

Seismically induced failure data are generally unavailable for specific plant components and are unavailable for structures. Thus, fragility curves which plot the fraction of expected failures versus effective peak ground acceleration must be developed primarily from analysis and engineering judgment supported by limited test data. Such fragility curves will contain a good deal of uncertainty and, therefore, great precision in attempting to define the shape of these curves is unwarranted.

The entire fragility curve for any component and its uncertainty can be expressed in terms of the best estimate of the median ground acceleration capacity, $\tilde{\tilde{a}}$, and the random variables, ϵ_R and ϵ_U. ϵ_R expresses the inherent randomness of the earthquake and response characteristics that affect structures or equipment, and ϵ_U expresses our uncertainty about those and other characteristics. Thus, the ground acceleration, a, corresponding to failure of a component is given by

$$a = \tilde{\tilde{a}}\epsilon_R\epsilon_U$$

The statistical variations of many material properties and seismic response variables are reasonably represented by logarithmic distributions. Therefore, it is assumed that both ϵ_R and ϵ_U are lognormally distributed with logarithmic standard deviations of β_R and β_U, respectively. This representation is reasonable so long as one is not primarily concerned with the contributions near the tails of the distributions. Plots such as the solid curves in Figure 7.2-5, depict the random variability about a median acceleration capacity, $\tilde{\tilde{a}}$, (failure fraction = 0.50) where any value, a, of the random variable is expressed by

$$a = \tilde{\tilde{a}} \cdot \exp(f \cdot \beta_R)$$

and f is the standardized Gaussian random variable. The curve is, effectively, the median fragility curve. The left and right dashed curves as shown in Figure 7.2-5 represent the 5th and 95th percentile curves,

respectively, reflecting the uncertainty in the median curve. Here, any value a' on the curves is expressed by

$$a' = a \cdot \exp(f \cdot \beta_U)$$

In the following sections, the application of the fragility analysis approach and the results of the seismic analysis are presented for Indian Point Units 2 and 3.

7.2.4 INDIAN POINT UNIT 2

7.2.4.1 Systems and Plant Logic

The results of the fragility analysis for the structures of Unit 2 are tabulated in Table 7.2-1. The results of the fragility analysis for key equipment and other mechanical and electrical components in systems, which are part of the accident initiation or safeguards processes, are tabulated in Table 7.2-2.

Recall from the seismicity curves of Figure 7.2-4 that the upper bound on damage effective ground acceleration is about 0.8g. Next, delete from the lists of Tables 7.2-1 and 7.2-2 the structures and equipment that, even considering the uncertainty, have almost no chance of failure at 0.8g. The result is Table 7.2-3 which is a summary of the key plant components having the lower median acceleration capacities. The table lists the components in order of increasing $\tilde{a}$ and includes the random and uncertainty variables, β_R and β_U, respectively.

Several structures and equipment items included in Table 7.2-3 have not been further incorporated in the analyses which follow because their failure or failure mode is not critical in the accident sequence scenarios. For example, as discussed in Appendix 7.9.3, the collapse of the control room nonbearing masonry walls would only affect equipment, piping, or conduits which are either mounted on the wall or which are adjacent to the wall because failure would essentially be vertical collapse of the wall. Control cabinets in the control room are several feet from the wall and might be subject to being dented, but their contents would continue to function. The walls in battery rooms 21 and 22 are scheduled to be reinforced, increasing their seismic capacity to the values shown in the table. These two rooms are capable of supplying all the DC power required for a safe shutdown.

Table 7.2-3 indicates that some of the electrical components fail at relatively low effective peak ground accelerations. Examples are the diesel generators (control cabinets) and distribution panels. These failures, however, are either chatter or relay trip and are automatically or manually recoverable. As indicated in Appendix 7.9.3, the capacity of these components to resist nonrecoverable failure is about three times the indicated values. These components, therefore, are not considered further because the nonrecoverable failures would not occur within the range of possible seismic events.

The failure of the containment fan cooler system duct work is not further included in the analysis because risers and portions of the circular duct and their supports would fail only when their orientation is consistent with the dominant direction of the earthquake force. Because only three out of five fan coolers and duct risers need to be operable for the system to be effective, it is improbable that all could fail from the same earthquake. Even if all the ducts were to fail, the fan coolers would still be capable of cooling a large portion of the containment atmosphere, although less effectively.

The only containment related item in Table 7.2-3 is item (14) -- containment building shear failure of the containment wall. Unlike shear wall failures for other Seismic Category I structures, where failure is defined as severe cracking and loss of supported equipment anchors and equipment function, failure of the containment wall means structural collapse. This is because the containment structure has no other shear walls that are capable of absorbing redistributed shear loads from the failed wall.

Note that the independent seismic capacity of the auxiliary feed pump building is higher than the indicated capacity in Table 7.2-3. It is limited by the capacity of the adjacent containment building. This is because collapse of the containment building is presumed to cause failure of the adjacent auxiliary feed pump building.

The capacities of several of the components, such as the pressurizer, diesel fuel oil tanks, battery racks, and cable trays, were determined from generic information. With specific design review or dynamic analysis, their median capacity might be modified and the uncertainty variability narrowed.

Consideration has been given to the fragility of the 26-inch and 30-inch diameter gas lines crossing the plant property, and the potential for hazard to the plant during a seismic event. These buried lines have an estimated mean fragility value of 1.4g, similar to the other large diameter buried pipes in the plant. With an upper bound of damage-effective ground acceleration set at 0.8g, as previously discussed, the gas lines have little chance for failure due to seismic events. Because they pose negligible hazard to the plant, they have not been included further in the seismic analysis.

The fragility curves for most of the critical components of Table 7.2-3 are seen in Figure 7.2-5 where the 5th, median, and 95th percentile fragility curves are shown. Assembly calculations, however, are actually based on a family of five curves representing the 10th, 30th, 50th, 70th, and 90th percentiles, each curve given a 20% probability.

A large seismic initiating event could cause more than one of the plant initiating event categories to occur. While the exact sequence of events can become very complicated, only a limited number of key functions must be examined. Review of the transient event trees in Section 1 will confirm that as long as turbine trip due to loss of offsite power occurs, ET-11b asks all the required functional questions. Therefore, no matter how many transient initiating event categories occur, the same requirements exist to avoid core damage. We

designate the failures that start with a seismically initiated transient followed by a loss of cooling, M_1. However, a seismic event may induce a reactor coolant system rupture and failure of safeguards systems that could also lead to core melt. We designate the failures starting with a small LOCA followed by a loss of safety injection or cooling, M_2, and those starting with a large LOCA followed by a loss of safety injection, M_3. Thus, we can expect core melt if either M_1, M_2, or M_3 occurs.

The plant logic is developed using a seismic fault tree whose basic events correspond to, and are coded identically with, the key component failures in Table 7.2-3. Each such component failure is denoted by a circle symbol, ①, ②, etc. The fault tree is given in Figure 7.2-6, where Figure 7.2-6a is the master tree, 7.2-6b, 7.2-6c, and 7.2-6d are expansions of the tree for each of the three contributors, and 7.2-6e, and 7.2-6f are branch expansions where referenced. Recirculation component failures are not reflected in the fault trees per se because there are none which have a likelihood of failure that are not represented by the components already in the trees. These trees are summarized below using the Boolean algebra symbols

$\wedge$ = "and"
$\vee$ = "or"

From the fault tree in Figure 7.2-6a, core melt occurs for

$$M_S = M_1 \vee M_2 \vee M_3$$

This condition for core melt is expressed in terms of the basic component failures using the remaining fault trees. Beginning with the fault tree in Figure 7.2-6b, we have

$$M_1 = ① \wedge \{[⑭ \vee \hat{②} \vee \hat{⑯} \vee ㉘ \vee ⑧] \wedge [\hat{②} \vee ㉕ \vee (⑥ \wedge ⑦) \vee ⑭]\}$$

where from Figure 7.2-6f, loss of control is $\hat{②}$ and

$$\hat{②} = ② \vee (0.13 \times ⑤) \vee ㉖ \vee ㉙ \vee ⑬ \vee ⑳ \vee ⑲$$

$0.13 \times ⑤$ = frequency of the Unit 1 superheater stack collapsing onto the control building (see Section 7.9.3, paragraph 4.6)

and from Figure 7.2-6e, loss of AC power is $\hat{⑯}$ and

$$\hat{⑯} = ① \wedge (⑯ \vee ㉞ \vee ㉔ \vee ⑬ \vee ⑲ \vee ⑳ \vee ② \vee 0.13 \times ⑤ \vee ㉗ \vee 0.05 \times ⑤)$$

$0.05 \times ⑤$ = frequency of the Unit 1 superheater stack collapsing onto the diesel generator building (see Section 7.9.3, paragraph 4.6)

Note that in this instance, the unavailability of gas turbine power is conservatively assumed for several reasons. While two gas turbines which are located up the hill and to the east of the plant can be started from the control room, the operator must access the Buchanan substation to perform local switching operations before either of these gas turbines can be placed online. GT-1, which is located adjacent to the Unit 1 turbine building, however, can be started and placed online from the control room. Under normal operations, each gas turbine has a probability of failing to start on demand of approximately 0.15, not considering operator actions under the conditions of the external event or turbine unavailability due to maintenance. Further, even under the most optimistic conditions, a gas turbine would not normally supply power for at least 30 minutes following a loss of offsite and plant power. This would not be soon enough after a large LOCA. Therefore, gas turbine unavailability is assumed to be 1.0.

Using the rules of Boolean algebra, we may simplify the above expressions to:

$$M_1 = ① \wedge \{\hat{②} \vee ⑭ \vee [(⑧ \vee \hat{⑯} \vee ㉘) \wedge (\{⑦ \wedge ⑥\} \vee ㉕)]\}$$

with

$$\hat{②} = ② \vee ⑬ \vee ⑲ \vee ⑳ \vee ㉖ \vee ㉙ \vee 0.13 \times ⑤$$

$$\hat{⑯} = ① \wedge (② \vee ⑬ \vee ⑯ \vee ⑲ \vee ⑳ \vee ㉔ \vee ㉗ \vee ㉞ \vee 0.05 \times ⑤ \vee 0.13 \times ⑤)$$

Similarly, from the tree in Figure 7.2-6c, we obtain for M_2

$$M_2 = \{\hat{⑯} \vee [① \wedge ⑫ \wedge (\hat{②} \vee \hat{⑯} \vee M_{1B})]\} \wedge [M_{1A} \vee \hat{②} \vee \hat{⑯} \vee ⑧]$$

where M_{1A} and M_{1B} represent branch points in Figure 7.2-6b. Then,

$$M_2 = \hat{⑯} \vee [① \wedge ⑫ \wedge M_{1B} \wedge (⑧ \vee M_{1A})]$$

From the tree in Figure 7.2-6d, we obtain for M_3

$$M_3 = (㉝ \vee ⑨ \vee ⑭) \wedge (\hat{②} \vee \hat{⑯} \vee ⑧ \vee ⑭)$$

which reduces to

$$M_3 = ⑭ \vee [(⑨ \vee ㉝) \wedge (\hat{②} \vee ⑧ \vee \hat{⑯})]$$

Finally, conceding ①, the core melt expression

$$M_S = M_1 \vee M_2 \vee M_3$$

becomes

$$M_S = \hat{(2)} \vee (14) \vee \hat{(16)} \vee [(8) \wedge ((9) \vee (33))] \vee \{((8) \vee (28)) \wedge [((7) \wedge (6)) \vee (25)]\}$$

This Boolean equation expresses the logical relationship between the occurrence of melt and the failure of various components. The probability of failure of each individual component, as a function of acceleration, is described by its family of fragility curves. These individual families of fragility curves are combined through the logic of the Boolean equation to obtain a plant level family of fragility curves for the occurrence of core melt.

7.2.4.2 Seismic Core Melt Frequencies

The fragility families are combined with the seismicity family to obtain a probability curve showing our state of knowledge about the frequency of core melt due to seismicity. The result is shown in Figure 7.2-7. From the cumulative probability curve it is seen that the median annual frequency of core melt due to seismic events is about 9.3×10^{-5} with a 90% confidence that core melt frequency is between 5.3×10^{-4} and 6.9×10^{-6}. The mean annual frequency of core melt is 1.4×10^{-4}.

7.2.4.3 Initial Assembly Leading to Release Category Frequencies

In the previous section, we developed a Boolean expression for the state "core melt" in terms of plant components. Now, in order to develop risk curves and integrate seismic analysis with the rest of the study, we need to know which type of core melt and release category occurs. That is, we need to develop Boolean expressions for each of the plant states defined in Section 1 and then aggregate them according to the containment state and release category to which they contribute. For this purpose, we introduce two new expressions:

x = failure of fan coolers
y = failure of containment spray

The fault trees of Figure 7.2-8 and 7.2-9 give the logic for x and y. Summarizing,

$$x = (17) \vee \hat{(16)} \vee \hat{(2)} \vee \hat{(16)} \vee (24) \vee (34) \vee \hat{(2)} \vee (14)$$

which reduces to

$$x = \hat{(2)} \vee (14) \vee \hat{(16)} \vee (17) \vee (24) \vee (34)$$

Then,

$$y = \hat{(16)} \vee (23) \vee (8) \vee \hat{(2)} \vee (14)$$

or

$$y = \hat{(2)} \vee (8) \vee (14) \vee \hat{(16)} \vee (23)$$

From the definitions of the plant states in Section 1, only the following plant states might occur from a seismic initiating event:

Plant State	Boolean Expression
AEFC	$M_3 \wedge \bar{x} \wedge \bar{y}$
AEF	$M_3 \wedge \bar{x} \wedge y$
AEC	$M_3 \wedge x \wedge \bar{y}$
AE	$M_3 \wedge x \wedge y$
SEFC	$M_2 \wedge \overline{M_3} \wedge \bar{x} \wedge \bar{y}$
SEF	$M_2 \wedge \overline{M_3} \wedge \bar{x} \wedge y$
SEC	$M_2 \wedge \overline{M_3} \wedge x \wedge \bar{y}$
SE	$M_2 \wedge \overline{M_3} \wedge x \wedge y$
TEFC	$M_1 \wedge \overline{M_2} \wedge \overline{M_3} \wedge \bar{x} \wedge \bar{y}$
TEF	$M_1 \wedge \overline{M_2} \wedge \overline{M_3} \wedge \bar{x} \wedge y$
TEC	$M_1 \wedge \overline{M_2} \wedge \overline{M_3} \wedge x \wedge \bar{y}$
TE	$M_1 \wedge \overline{M_2} \wedge \overline{M_3} \wedge x \wedge y$

Bars used over the symbols denote negation. Thus, $\bar{x}$ means that fan coolers do not fail, and so on.

Next, similar Boolean equations can be written for the various release categories. In doing this, for the sake of scrutability, in the equations below only those terms which are numerically significant are included.

Consider first Release Category Z-1Q which is a Z-1 type release category but caused by an early seismic failure of containment. Because failure of containment (item (14)) leads to large LOCA, M_3, with failure of safeguards, x and y, we have assigned all occurrences of (14) to Category Z-1Q. Therefore, Z-1Q = (14).

Secondly, as shown in the containment analysis of Section 2, the only one of the above plant states contributing significantly to Z-1 is state AE. Thus, we write the Boolean for seismic occurrence of Release Category Z-1 as

$$Z\text{-}1 = \overline{(14)} \wedge \{(M_3 \wedge x \wedge y) \wedge C_{AE,Z\text{-}1}\}$$

Superseded

where $C_{AE,Z-1}$ is the term from the C matrix governing the transitions from AE to Z-1. As indicated in Section 2, our state of knowledge of this term is given by the following DPD:

	probability	0.01	0.05	0.30	0.30	0.25	0.09
$C_{AE,Z-1}$ =	fraction of AE to Release Category Z-1	0.05	0.02	0.01	0.002	0.001	0.0001

Note that the bar over item (14) denotes negation. Substituting the components for M_3, x, and y, and reducing, we have

$$Z\text{-}1 = \overline{(14)} \wedge \{((9) \vee (33)) \wedge [\hat{(2)} \vee \hat{(16)} \vee ((8) \wedge \{(17) \vee (24) \vee (34)\})] \wedge C_{AE,Z-1}\}$$

Similarly, omitting minor terms, the occurrence of Release Category 2RW is described by the Boolean

$$2RW = \overline{(14)} \wedge (AE \vee SE \vee TE)$$
$$= \overline{(14)} \wedge (M_1 \vee M_2 \vee M_3) \wedge x \wedge y$$

In this case, the complement of the fraction $C_{AE,Z-1}$ which determines the contribution to 2RW is assumed to be 1.0. Thus, Category 2RW occurs if the core melts ($M_1 \vee M_2 \vee M_3$) and the fan coolers and containment sprays fail ($x \wedge y$), and the containment does not fail. If the containment does fail, we have Release Category Z-1.

Substituting in here the components for M_1, M_2, M_3, x, and y, assuming that, because of its low capacity, (1) fails if any other component fails, and reducing, we obtain the simplified form:

$$2RW = \overline{(14)} \wedge \{\hat{(2)} \vee \hat{(16)} \vee [((17) \vee (24) \vee (34)) \wedge (\{(8) \wedge [(\{(7) \wedge (6)\} \vee (25)) \vee (9) \vee (33)]\} \vee \{(28) \wedge (23) \wedge [((7) \wedge (6)) \vee (25)]\})]\}$$

Similarly,

$$8B = \overline{(14)} \wedge (AEFC \vee AEC \vee SEFC \vee SEC \vee TEFC \vee TEC)$$
$$= \overline{(14)} \wedge (M_1 \vee M_2 \vee M_3) \wedge \bar{y}$$
$$= \overline{\hat{(2)}} \wedge \overline{(8)} \wedge \overline{(14)} \wedge \overline{\hat{(16)}} \wedge \overline{(23)} \wedge \{(28) \wedge [((7) \wedge (6)) \vee (25)]\}$$

$$8A = \overline{(14)} \wedge (AEF \vee SEF \vee TEF)$$
$$= \overline{(14)} \wedge (M_1 \vee M_2 \vee M_3) \wedge \bar{x} \wedge y$$
$$= \hat{(2)} \wedge \overline{(14)} \wedge \overline{\hat{(16)}} \wedge \overline{(17)} \wedge \overline{(24)} \wedge \overline{(34)} \wedge [\{[(8) \vee ((28) \wedge (23))] \wedge [((7) \wedge (6)) \vee (25)]\} \vee [(8) \wedge ((9) \vee (33))]]$$

These Boolean equations express the logical relationships between component failures and occurrence of the various release categories. Using these expressions and the fragility families for the components, the plant level fragility family for each release category is obtained. This family, in numerical form, constitutes the seismic MC^S matrix. The uncertainties in the component fragility curves translate through this process into uncertainty in the MC^S matrix. This uncertainty is represented in Table 7.2-4 by showing five different values of the MC^S matrix with 20% probability assigned to each. This table, thus, is an example of the DPD process applied at the matrix level as discussed in Section 0.8.4.2. The numbers entered in Table 7.2-4, are elements of the MC^S matrix and give the conditional frequencies of occurrence of the various release categories, given an earthquake of the acceleration specified in the left column. The MC^S matrix, when combined with the seismicity hazard curves, gives the frequency of seismically initiated release categories. Figure 7.2-10 presents the resultant probability of frequency curves.

The dominant contributors to Release Categories 2RW and Z-1 are:

- Failure of the control room, control cable trays, and batteries for control power.
- Loss of offsite power and failure of the switchgear room in the control building, cable trays, diesel fuel oil tanks, and battery room masonry walls and battery racks affecting batteries for starting the diesel generators.
- Failure of refueling water, condensate storage and city water storage tanks, pressurizer, and fan coolers.

The containment building failure is the contributor to Release Category Z-1Q. The dominant contributors to Release Category 8A are the loss of offsite power and the failure of the refueling water storage tank, condensate storage tank, city water tank, and pressurizer. For Release Category 8B, the dominant contributors are loss of offsite power and failure of the condensate storage and city water storage tanks and power-actuated relief valve.

7.2.5 INDIAN POINT UNIT 3

7.2.5.1 Systems and Plant Logic

The results of the fragility analysis for the structures of Unit 3 are tabulated in Table 7.2-5. The results of the fragility analysis for key equipment and other mechanical and electrical components in systems which are part of the accident mitigation process are tabulated in Table 7.2-6.

Table 7.2-7 is a summary of the key plant components having the lower seismic capacities. The table lists the components in ascending order of capacity, $\tilde{a}$, and indicates the random and uncertainty variables, β_R and β_U, respectively.

where $C_{AE,Z-1}$ is the term from the C matrix governing the transitions from AE to Z-1. As indicated in Section 2, our state of knowledge of this term is given by the following DPD:

	probability	0.01	0.05	0.30	0.30	0.25	0.09
$C_{AE,Z-1}$ =	fraction of AE to Release Category Z-1	0.05	0.02	0.01	0.002	0.001	0.0001

Note that the bar over item (14) denotes negation. Substituting the components for M_3, x, and y, and reducing, we have

$$Z\text{-}1 = \overline{(14)} \wedge \{((9) \vee (33)) \wedge [\hat{(2)} \vee \hat{(16)} \vee ((8) \wedge \{(17) \vee (24) \vee (34)\})] \wedge C_{AE,Z-1}\}$$

Similarly, omitting minor terms, the occurrence of Release Category 2RW is described by the Boolean

$$2RW = \overline{(14)} \wedge (AE \vee SE \vee TE)$$
$$= \overline{(14)} \wedge (M_1 \vee M_2 \vee M_3) \wedge x \wedge y$$

In this case, the complement of the fraction $C_{AE,Z-1}$ which determines the contribution to 2RW is assumed to be 1.0. Thus, Category 2RW occurs if the core melts ($M_1 \vee M_2 \vee M_3$) and the fan coolers and containment sprays fail ($x \wedge y$), and the containment does not fail. If the containment does fail, we have Release Category Z-1.

Substituting in here the components for M_1, M_2, M_3, x, and y, assuming that, because of its low capacity, (1) fails if any other component fails, and reducing, we obtain the simplified form:

$$2RW = \overline{(14)} \wedge \{\hat{(2)} \vee \hat{(16)} \vee [((17) \vee (24) \vee (34)) \wedge (\{(8) \wedge [(\{(7) \wedge (6)\} \vee (25)) \vee (9) \vee (33)]\} \vee \{(28) \wedge (23) \wedge [((7) \wedge (6)) \vee (25)]\})]\}$$

Similarly,

$$8B = \overline{(14)} \wedge (AEFC \vee AEC \vee SEFC \vee SEC \vee TEFC \vee TEC)$$
$$= \overline{(14)} \wedge (M_1 \vee M_2 \vee M_3) \wedge \bar{y}$$
$$= \overline{\hat{(2)}} \wedge \overline{(8)} \wedge \overline{(14)} \wedge \overline{\hat{(16)}} \wedge \overline{(23)} \wedge \{(28) \wedge [((7) \wedge (6)) \vee (25)]\}$$

$$8A = \overline{(14)} \wedge (AEF \vee SEF \vee TEF)$$
$$= \overline{(14)} \wedge (M_1 \vee M_2 \vee M_3) \wedge \bar{x} \wedge y$$
$$= \overline{\hat{(2)}} \wedge \overline{(14)} \wedge \overline{\hat{(16)}} \wedge \overline{(17)} \wedge \overline{(24)} \wedge \overline{(34)} \wedge [([[(8) \vee ((28) \wedge (23))] \wedge [((7) \wedge (6)) \vee (25)]\} \vee [(8) \wedge ((9) \vee (33))]]$$

These Boolean equations express the logical relationships between component failures and occurrence of the various release categories. Using these expressions and the fragility families for the components, the plant level fragility family for each release category is obtained. This family, in numerical form, constitutes the seismic MC^S matrix. The uncertainties in the component fragility curves translate through this process into uncertainty in the MC^S matrix. This uncertainty is represented in Table 7.2-4 by showing five different values of the MC^S matrix with 20% probability assigned to each. This table, thus, is an example of the DPD process applied at the matrix level as discussed in Section 0.8.4.2. The numbers entered in Table 7.2-4, are elements of the MC^S matrix and give the conditional frequencies of occurrence of the various release categories, given an earthquake of the acceleration specified in the left column. The MC^S matrix, when combined with the seismicity hazard curves, gives the frequency of seismically initiated release categories. Figure 7.2-10 presents the resultant probability of frequency curves.

The dominant contributors to Release Categories 2RW and Z-1 are:

- Failure of the control room, control cable trays, and batteries for control power.

- Loss of offsite power and failure of the switchgear room in the control building, cable trays, diesel fuel oil tanks, and battery room masonry walls and battery racks affecting batteries for starting the diesel generators.

- Failure of refueling water, condensate storage and city water storage tanks, pressurizer, and fan coolers.

The containment building failure is the contributor to Release Category Z-1Q. The dominant contributors to Release Category 8A are the loss of offsite power and the failure of the refueling water storage tank, condensate storage tank, city water tank, and pressurizer. For Release Category 8B, the dominant contributors are loss of offsite power and failure of the condensate storage and city water storage tanks and power-actuated relief valve.

7.2.4A ADDITIONAL SEISMIC ANALYSIS, INDIAN POINT UNIT 2

7.2.4A.1 Control Building Seismic Bumpers

The results of the seismic analysis in Section 7.2.4.3 indicated that the dominant contributor to seismically initiated core melt and release is the failure of the Unit 2 control building. This building had a seismic acceleration capacity with a median value of 0.27g. With the exception of the offsite power transformer insulators, which have a median acceleration capacity of 0.2g and whose failure could initiate a loss of power event, the control building had the lowest seismic capacity of all the key plant structures and equipment. This building contains the control room, cable spreading room, DC batteries and panels for control power to safety related equipment, and switchgear supplying AC power to critical equipment.

The control building is adjacent to the Unit 1 superheater building. At the control building roof line there was about a 1-1/2-inch space between the two buildings (see Figure 7.2.10A-1) and about a 3-1/2-inch space between the roof framing of the two buildings.

During a large seismic event, the flexibility of the upper story of the Unit 2 control building could result in deflections that would close these gaps at the roof line. The resulting impact loads at the roof structure could cause distortion of the Unit 2 steel roof and decking at ground accelerations much less than those that would fail other portions of the building. Such roof line impacts could conceivably cause the steel roof structure and decking to fall into the top story which contains the control room. The plant logic indicates that loss of the control room leads to loss of control and core melt. Because of the relative frequency of this scenario, potential changes were considered to increase control building seismic capacity and, therefore, reduce core melt frequency.

Several building modifications were considered. In each case, the 1-1/2-inch roof gap was to be increased to at least 3 inches and rubber material provided in a portion of the gap to absorb the shock of the impact. The selected solution is shown in Figure 7.2.10A-2. An analysis of the control building acceleration capacity was performed for the modification. The results of the analysis are documented in a report by Structural Mechanics Associates, Inc., Section 7.9.3.1. The analysis indicates that the modification will increase the acceleration capacity of the control building, item (2) in Table 7.2-3, as follows:

$\approx{a} = 1.0g \qquad \beta_R = 0.3 \qquad \beta_U = 0.3$

7.2.4A.2 Control Room Ceiling

The Unit 2 control room in the control building is open to the Unit 1 control room located in the adjacent superheater building. Light fixtures for the control room are hung from the room framing by 1-1/2-inch x 1-1/2-inch x 1/8-inch angles. Transite panels 3 feet x 10 feet x 1/4-inch thick are supported along their length by flanges of the light fixtures. An egg crate panel ceiling below is supported by an aluminum tee-bar grid which, in turn, is hung from the light fixture supports by 1/4-inch diameter rods. Perforated aluminum acoustical end panels typically span between the tee-bar grid and the structure. Other light fixtures located flush with the egg crate ceiling are hung from the roof framing by 2-inch x 2-inch x 1/4-inch angles.

At the interface between the Unit 1 and 2 control rooms, there is a row of transite panels supported on one side by hangers to the Unit 2 control building roof framing and on the other side by hangers to the Unit 1 superheater building floor framing. The two structures are separated by a 3-1/2-inch thick expansion joint partially filled by rubber pads. This expansion joint permits the structures to displace relative to each other under seismic response. The light fixture supports at the opposing edges of the transite panels at the structures' interface are constrained to

displace with the structures to which they are connected. The transite panels were cut and installed in the field so that the gap between the panel edges and the vertical faces of the light fixtures does not exceed the overlap between the panel and the light fixture flange. An observed sampling of the panels confirms this. Therefore, the transite panel could only fall if the space between adjacent fixtures was to increase through deflection of many fixtures so that their gaps would accumulate sufficiently to allow a given panel to fall. If sufficient relative displacement between the transite panel edge supports occurs, certain panels would drop through and impact upon the egg crate ceiling below. The egg crate ceiling system probably does not have adequate stability to restrain the transite panels once the panels have been dislocated from their supports.

Based on an observed sampling of the transite panels, the amount of overlap between representative transite panels and their light fixture flange supports is approximately 0.5 to 0.75 inches per edge, while the gaps between the fixtures and edges of transite panels are less than 1/4-inch.

The control room ceiling was found in Amendment 1 to increase the seismic initiated core melt frequency by a factor of 1.7. As a result, the utility designed an interconnection of the eggcrate ceiling panels whereby adjacent panels are attached in multiple locations by a looped wire that interconnects the adjacent panels with their supporting T-bar. These connections of panels form a net that is capable of retaining any of the transite panels above from falling onto control room equipment or operators during an earthquake.

The consequence of the ceiling modification is that the results of Section 7.2.4, as modified by Sections 7.2.4A.1, 7.2.4A.3, 7.2.4A.4, and 7.2.4A.5, apply.

7.2.4A.3 Containment Structure

Additional structural design calculations and a dynamic analysis not previously available in the earlier fragility analysis and additional structural drawings not previously requested due to the relatively large seismic capacity of the structures were the basis for a reanalysis of the Unit 2 containment. This additional analysis is summarized in Structural Mechanics Associates' report contained in Section 7.9.3.2. The new information revealed large conservatisms used in the seismic design. These were not explicit in the summary design report information used in the earlier fragility analysis. These conservatisms include:

1. Method for determining mode shape and frequency and base shear loads.

2. Greater amount of reinforcing steel designed and installed in the walls than considered in the design stress calculations.

3. Greater soil loading area assumed in design of the Unit 2 wall than is possible from the as-built condition where the earth ramp load is a more localized condition.

The results of the analysis indicate that the median acceleration capacity of the Unit 2 containment increases to 2.7g.

The impact of the increased fragility is that the possibility of containment failures from earthquakes is essentially eliminated since, even with uncertainty on the containment capacity, the containment would not fail at accelerations up to 0.8g, the upper bound acceleration at Indian Point. The result is that release category Z-1Q no longer applies. The effect of this change on early fatalities is discussed further in Section 8.

7.2.4A.4 Revised Fragilities

Since the time of the initial publication of the IPPSS, revisions have been made to the fragilities of a number of key structures and components as seen in Table 7.2-4A-1. Noteworthy in the table are changes in the fragilities of the condensate storage, city water, and refueling water storage tanks; the control building; the cable trays; the containment building; and the PORV.

7.2.4A.5 Results

The effect of the control building seismic modification is shown in Figure 7.2-10A-3 which shows the frequency distributions of the various release categories coming from seismic events. The mean annual core melt frequency from seismic events is reduced from 1.4×10^{-4} to 7.7×10^{-6}. A similar reduction is achieved in the seismic contribution to category 2RW since it is the control building interaction which is the dominant cause of seismic release. The mean frequency of 2RW release from seismic events is reduced to 7.2×10^{-6} after the modification. A reduction is also evident in early overpressure release type Z-1. Category Z-1Q, which was caused by failure of the containment structure, is now no longer possible due to the increased capacity of item (14), the containment building. Category 8A becomes slightly more frequent, reflecting the fact that some seismically initiated melts which would previously have resulted in release 2RW or Z-1 are now, because of the modification, converted to the more benign category, 8A. Category 8B is no longer possible with the higher capacity of item (28), the reactor coolant system power-actuated relief valve, as seen in Table 7.2-4A-1.

7.2.5 INDIAN POINT UNIT 3

7.2.5.1 Systems and Plant Logic

The results of the fragility analysis for the structures of Unit 3 are tabulated in Table 7.2-5. The results of the fragility analysis for key equipment and other mechanical and electrical components in systems which are part of the accident mitigation process are tabulated in Table 7.2-6.

Table 7.2-7 is a summary of the key plant components having the lower seismic capacities. The table lists the components in ascending order of capacity, $\bar{a}$, and indicates the random and uncertainty variables, β_R and β_U, respectively.

is expected that the heavy gauge electronic cabinets may be dented from an impact, but their contents would not be adversely affected.

In addition to the core melt logic and frequency presented in Section 7.2.4, consideration is now also given to core melt resulting from the loss of control by incapacitation of all three operators due to control room ceiling failure.

Let (C_1) represent the failure of ceiling panels at the building line between Units 1 and 2 and (C_2) represent the failure of the ceiling panels in the balance of the control room (it is conservatively assumed that the capacity of all these other panels is the same as for the weaker panels at the lighting fixtures mounted over operator positions).

The fraction of time any one operator is likely to be underneath the panels between Units 1 and 2 is judged to be less than 5×10^{-2}. The probability that an operator would be under the other panels is then very nearly 1.0.

It is highly unlikely that if one panel of a given fragility fails, all panels of that fragility will fail. Yet, there is some likelihood that if one fails, several might fail. It is judged that if panels in an area fail, considering some dependency of panel failures, the probability of an operator in the area being under a failed panel is 0.6.

Let us consider that an operator is either beneath the most fragile panels or under those adjacent to the lighting fixtures over operator positions, but never under the other panels with the higher capacity. Conservatively, consider also that any impact of a panel on an operator will incapacitate him. Then, the conditional probability of operators being under those panels at the Unit 1/Unit 2 building line and being incapacitated is:

$$5.0 \times 10^{-2} \times 0.6 = 3.0 \times 10^{-2} \text{ for 1 operator}$$
$$9.0 \times 10^{-4} \text{ for 2 operators}$$
$$2.7 \times 10^{-5} \text{ for 3 operators}$$

Similarly, the conditional probability of operators being under the other panels and being incapacitated is:

0.60 for 1 operator
0.36 for 2 operators
0.22 for 3 operators

Therefore, we can express core melt, M_4, from loss of control due to control room ceiling failure as

$$M_4 = 0.35 \left[2.7 \times 10^{-5} (C_1) \vee (9.0 \times 10^{-4} (C_1) \wedge 0.6 (C_2)) \right.$$
$$\left. \vee (3.0 \times 10^{-2} (C_1) \wedge 0.36 (C_2)) \vee 0.22 (C_2) \right]$$

$$= 9.4 \times 10^{-6} \text{ (C}_1\text{)} \vee (3.2 \times 10^{-4} \text{ (C}_1\text{)} \wedge 2.1 \times 10^{-1} \text{ (C}_2\text{)})$$

$$\vee (1.0 \times 10^{-2} \text{ (C}_1\text{)} \wedge 1.2 \times 10^{-1} \text{ (C}_2\text{)}) \vee 7.7 \times 10^{-2} \text{ (C}_2\text{)}$$

We add M_4 to the core melt expression M_S, using the ceiling fragilities as follows:

(C$_1$): $\tilde{\tilde{a}} = 0.15g$, $\beta_R = 0.31$, $\beta_U = 0.41$

(C$_2$): $\tilde{\tilde{a}} = 0.40g$, $\beta_R = 0.30$, $\beta_U = 0.45$

The annual frequency for core melt due to seismic events is recalculated in the manner presented in Section 7.2.4. The mean value for annual core melt frequency is 1.3×10^{-5}. Comparing this value to the mean frequency of 7.9×10^{-6} previously determined as a result of the control building seismic bumper modification, core melt frequency increases by a factor of 1.70 for seismic events from considering control room ceiling failures. Logically, the same can be stated for the impact on release category 2RW. Thus, the increase is not significant.

7.2.5 INDIAN POINT UNIT 3

7.2.5.1 Systems and Plant Logic

The results of the fragility analysis for the structures of Unit 3 are tabulated in Table 7.2-5. The results of the fragility analysis for key equipment and other mechanical and electrical components in systems which are part of the accident mitigation process are tabulated in Table 7.2-6.

Table 7.2-7 is a summary of the key plant components having the lower seismic capacities. The table lists the components in ascending order of capacity, a, and indicates the random and uncertainty variables, β_R and β_U, respectively.

Several structures and equipment items included in Table 7.2-7 have not been further incorporated in the analyses which follow because their failure or failure mode is not critical in the accident scenarios. For example, as discussed in Appendix 7.9.3, the collapse of the control room nonbearing masonry walls would only affect equipment, piping, or conduits which are either mounted on the wall, or are adjacent to the wall because failure would essentially be vertical collapse of the wall. Control cabinets in the control room are several feet from the wall and might be subject to being dented, but they would continue to function.

Some of the electrical components are indicated as having failures at relatively low capacities. Examples are the diesel generators (control cabinets) and distribution panels. These failures, however, are either chatter or relay trip and are automatically or easily recoverable. As indicated in Appendix 7.9.3, the capacity of these components for nonrecoverable failure is about three times the indicated values. These components, therefore, are not considered further because the nonrecoverable failures would not occur within the range of possible seismic events.

The only containment related item in Table 7.2-7 is item (32) -- containment building shear failure of containment wall. Unlike shear wall failures for other Seismic Category I structures where failure is defined as severe cracking and loss of supported equipment anchors and equipment function, failure of the containment wall means structural collapse. This is because the containment structure has no other shear walls that are capable of absorbing redistributed shear loads from the failed wall.

It is noted that the independent seismic capacity of the auxiliary feed pump building is sufficiently high that its indicated capacity is determined by the capacity of the adjacent containment building.

The capacities of several of the components such as the pressurizer, diesel fuel oil tanks, and battery racks were determined from generic information. With specific design review or dynamic analysis, their median capacity might be modified and the uncertainty variability narrowed.

The fragility curve for each of the key critical components of Table 7.2-7 is seen in Figure 7.2-11 where the 5th, median, and 95th percentile fragility curves are shown. Assembly calculations, however, are actually based on a family of five curves representing the 10th, 30th, 50th, 70th, and 90th percentiles, each curve given a 20% probability.

The plant logic is developed using a seismic fault tree whose basic events correspond to, and are coded identically with, the key component failures in Table 7.2-7. Each such component failure is denoted by a circle symbol, (1), (2), etc. The fault tree is given in Figure 7.2-12, where Figure 7.2-12a is the master tree, 7.2-12b, 7.2-12c, and 7.2-12d are expansions of the tree for each of the three contributors,

and 7.2-12e and 7.2-12f, are branch expansions where referenced. The results of these trees are summarized below using the Boolean algebra symbols:

$\wedge$ = "and"
$\vee$ = "or"

From the fault tree in Figure 7.2-12a, core melt occurs for

$$M_s = M_1 \vee M_2 \vee M_3$$

This condition for core melt is expressed in terms of the basic component failures using the remaining fault trees. Recirculation component failures are not reflected in the fault trees per se because there are none which have a probability of failure that are not represented by the components already on the tree. Beginning with the fault tree in Figure 7.2-12b, we have

$$M_1 = (1) \wedge \{((32) \vee (\hat{18}) \vee (\hat{15}) \vee (27) \vee (6)) \wedge ((\hat{18}) \vee (23) \vee (26) \vee [(5) \wedge ((4) \vee 0.05 \times (3))] \vee (32))\}$$

where, from Figure 7.2-12f,

$$(\hat{15}) = (1) \wedge \{(15) \vee (35) \vee (24) \vee [((13) \vee (11) \vee (18)) \wedge ((19) \vee (28))] \vee (28)\}$$

Note that in this instance, the unavailability of gas turbine power is conservatively assumed for several reasons. While two gas turbines which are located up the hill and to the east of the plant can be started from the control room, the operator must access the Buchanan substation to perform local switching operations before either of these gas turbines can be placed online. GT-1 which is located adjacent to the Unit 1 turbine building, however, can be started and placed online from the control room. Under normal operations, each gas turbine has a probability of failing to start on demand of approximately 0.15, not considering operator actions under the conditions of the external event or turbine unavailability due to maintenance. Further, even under the most optimistic conditions, a gas turbine would not normally supply power for at least 30 minutes following a loss of offsite and plant power. This would not be soon enough after a large LOCA. Therefore, gas turbine unavailability is assumed to be 1.0.

From Figure 7.2-12e,

$$(\hat{18}) = (18) \vee [((11) \vee (13) \vee (18)) \wedge ((19) \vee (28))]$$

and $0.05 \times (3)$ = probability of the Unit 1 superheater stack collapsing onto the condensate storage tank (Section 7.9.3, paragraph 4.6).

Using the rules of Boolean algebra, we may simplify the above expressions to

$$M_1 = (1) \wedge \{(18) \vee (32) \vee [((6) \vee \hat{(15)} \vee (27)) \wedge [(23) \vee (26) \vee ((5) \wedge \{(4) \vee .05 \times (3)\})]]\}$$

with

$$\hat{(15)} = (1) \wedge \{(15) \vee (24) \vee (28) \vee (35) \vee [((11) \vee (13) \vee (18)) \wedge (19)]\}$$

and

$$\hat{(18)} = (18) \vee [((19) \vee (28)) \wedge ((11) \vee (13))]$$

Similarly, from the tree in Figure 7.2-12c, we obtain for M_2

$$M_2 = \{\hat{(15)} \vee [((1) \wedge (10)) \wedge (\hat{(18)} \vee \hat{(15)} \vee M_{1B})]\} \wedge (M_{1A} \vee \hat{(18)} \vee \hat{(15)} \vee (6))$$

where M_{1A} and M_{1B} represent branch points in Figure 7.2-12b. Then,

$$M_2 = \hat{(15)} \vee ((10) \wedge M_1)$$

From the tree in Figure 7.2-12d, we obtain for M_3

$$M_3 = ((32) \vee (33) \vee (7)) \wedge (\hat{(18)} \vee \hat{(15)} \vee (6) \vee (31) \vee (32))$$

which reduces to

$$M_3 = (32) \vee [((7) \vee (33)) \wedge ((6) \vee \hat{(15)} \vee \hat{(18)} \vee (31))]$$

Finally, conceding (1), the expression for core melt becomes

$$M_s = M_1 \vee M_2 \vee M_3$$
$$= \hat{(15)} \vee \hat{(18)} \vee (32) \vee \{((6) \vee (27)) \wedge [(23) \vee (26) \vee ((5) \wedge \{(4) \vee 0.05 \times (3)\})]\} \vee [((7) \vee (33)) \wedge ((6) \vee (31))]$$

The capacity of each component in the Boolean expression can now be aggregated to obtain the plant level fragility.

7.2.5.2 Seismic Core Melt Frequencies

The fragility families are combined with the seismicity families to obtain a probability curve showing our state of knowledge about the frequency of core melt due to seismicity. The result is seen in Figure 7.2-13. From the cumulative probability curve, it is seen that the median annual frequency of core melt due to seismic events is about

2.4×10^{-8} and, with a 90% confidence, the core melt frequency is between 2.3×10^{-5} and 4.3×10^{-12}. The mean annual frequency of core melt is 3.1×10^{-6}.

7.2.5.3 Initial Assembly Leading to Release Category Frequencies

In the previous section, we developed a Boolean expression for the state "core melt" in terms of plant components. Now, in order to develop risk curves and to integrate the seismic analysis with the rest of the study, we need to know which type of core melt and release category occurs. That is, we need to develop Boolean expressions for each of the plant states defined in Section 1 and then group them with according to the containment state and release category to which they contribute. For this purpose, we introduce two new expressions:

x = failure of fan coolers
y = failure of containment spray

The fault trees of Figures 7.2-14 and 7.2-15 give the logic for x and y. Summarizing,

$$x = \hat{15} \vee \hat{18} \vee \hat{15} \vee 24 \vee 35 \vee \hat{18} \vee 32$$

$$y = 21 \vee \hat{15} \vee 25 \vee 34 \vee 6 \vee \hat{18} \vee 32$$

These simplify to

$$x = \hat{15} \vee \hat{18} \vee 24 \vee 32 \vee 35$$

and

$$y = 6 \vee \hat{15} \vee \hat{18} \vee 21 \vee 25 \vee 32 \vee 34$$

Now, from the definitions of the plant states in Section 1, only the following plant states might occur from a seismic initiating event:

Plant State	Boolean Expression
AEFC	$M_3 \wedge \bar{x} \wedge \bar{y}$
AEF	$M_3 \wedge \bar{x} \wedge y$
AEC	$M_3 \wedge x \wedge \bar{y}$
AE	$M_3 \wedge x \wedge y$
SEFC	$M_2 \wedge \overline{M_3} \wedge \bar{x} \wedge \bar{y}$
SEF	$M_2 \wedge \overline{M_3} \wedge \bar{x} \wedge y$
SEC	$M_2 \wedge \overline{M_3} \wedge x \wedge \bar{y}$
SE	$M_2 \wedge \overline{M_3} \wedge x \wedge y$

Plant State	Boolean Expression
TEFC	$M_1 \wedge \overline{M_2} \wedge \overline{M_3} \wedge \overline{x} \wedge \overline{y}$
TEF	$M_1 \wedge \overline{M_2} \wedge \overline{M_3} \wedge \overline{x} \wedge y$
TEC	$M_1 \wedge \overline{M_2} \wedge \overline{M_3} \wedge x \wedge \overline{y}$
TE	$M_1 \wedge \overline{M_2} \wedge \overline{M_3} \wedge x \wedge y$

Bars over the symbols denote negation. Thus, $\overline{x}$ means that fan coolers do not fail, and so on.

Next, similar Boolean equations can be written for the various release categories. In doing this, for the sake of scrutability, in the equation below only those terms which are numerically significant are included.

Consider first Release Category Z-1Q which is a Z-1 type release category but caused by an early seismic failure of containment. Because failure of containment, item (32), leads to large LOCA, M_3, with failure of safeguards, x and y, we have assigned all occurrences of (32) to Category Z-1Q. Therefore, Z-1Q = (32).

Secondly, from the containment analysis of Section 2, the only one of the above plant states contributing significantly to Z-1 is state AE. Thus, we write the Boolean for seismic occurrence of Release Category Z-1 as

$$Z\text{-}1 = \overline{(32)} \wedge \{(M_3 \wedge x \wedge y) \wedge C_{AE,Z\text{-}1}\}$$

where $C_{AE,Z-1}$ is the term from the C matrix governing the transitions from AE to Z-1. As indicated in Section 2, our state of knowledge of this term is given by the following DPD:

	probability	0.01	0.05	0.30	0.30	0.25	0.09
$C_{AE,Z-1}$ =	fraction of AE to Release Category Z-1	0.05	0.02	0.01	0.002	0.001	0.0001

Note that the bar over item (32) denotes negation. Substituting the components for M_3, x, and y, and reducing, we have

$$Z\text{-}1 = \overline{(32)} \wedge ((7) \vee (33)) \wedge [\hat{(15)} \vee \hat{(18)} \vee \{[(6) \wedge ((24) \vee (35))] \vee [(31) \wedge ((21) \vee (25) \vee (34)) \wedge ((24) \vee (35))]\}] \wedge C_{AE,Z\text{-}1}$$

Similarly, omitting minor terms, the occurrence of Release Category 2RW is described by the Boolean:

$$2RW = \overline{(32)} \wedge (AE \vee SE \vee TE)$$

$$= \overline{(32)} \wedge (M_1 \vee M_2 \vee M_3) \wedge x \wedge y$$

In this case, the complement of the fraction $C_{AE,Z-1}$ which determines the contribution to 2RW is assumed to be 1.0. Thus, Category 2RW occurs if the core melts ($M_1 \vee M_2 \vee M_3$) and the fan coolers and containment sprays fail ($x \wedge y$), and the containment does not fail. If the containment does fail, we have Release Category Z-1.

Substituting in here the components for M_1, M_2, M_3, x, and y, assuming, because of its low capacity that (1) fails if any other component fails, and reducing, results in the simplified form:

$$2RW = \overline{(32)} \wedge [\hat{(15)} \vee \hat{(18)} \vee \{((6) \vee (27) \vee (31)) \wedge ((7) \vee (33)) \wedge [(23) \vee (26) \vee ((5) \wedge \{(4) \vee 0.05 \times (3)\})]\}] \wedge ((24) \vee (35)) \wedge ((6) \vee (21) \vee (25) \vee (34))$$

Similarly,

$$8B = \overline{(32)} \wedge (AEFC \vee AEC \vee SEFC \vee SEC \vee TEFC \vee TEC)$$

$$= \overline{(32)} \wedge (M_1 \vee M_2 \vee M_3) \wedge \bar{y}$$

$$= \overline{(6)} \wedge \hat{\overline{(15)}} \wedge \hat{\overline{(18)}} \wedge \overline{(21)} \wedge \overline{(25)} \wedge \overline{(32)} \wedge \overline{(34)} \wedge \{[(27) \wedge ((23) \vee (26) \vee \{(5) \wedge [(4) \vee 0.05 \times (3)]\})] \vee [((7) \vee (33)) \wedge (31)]\}$$

$$8A = \overline{(32)} \wedge (AEF \vee SEF \vee TEF)$$

$$= \overline{(32)} \wedge (M_1 \vee M_2 \vee M_3) \wedge \bar{x} \wedge y$$

$$= \hat{\overline{(15)}} \wedge \hat{\overline{(18)}} \wedge \overline{(24)} \wedge \overline{(32)} \wedge \overline{(35)} \wedge ((6) \vee (21) \vee (25) \vee (34)) \wedge \{[((6) \vee (27)) \wedge ((23) \vee (26) \vee [(5) \wedge \{(4) \vee 0.05 \times (3)\}])] \vee [((7) \vee (33)) \wedge ((6) \vee (31))]\}$$

These Boolean equations express the logical relationships between component failures and occurrence of the various release categories. Using these expressions and the fragility families for the components, the fragility family for each release category is obtained. This family, in numerical form, constitutes the seismic MC^S matrix. The uncertainties in the component fragility curves translate through this process into uncertainty in the MC^S matrix. This uncertainty is represented in Table 7.2-8 by showing five different values of the MC^S matrix with 20% probability assigned to each. This table, thus, is an example of the DPD process applied at the matrix level as discussed in Section 0.8.4.2. The numbers entered in Table 7.2-8 are elements of the MC^S matrix and give the conditional frequencies of occurrence of the various release categories, given an earthquake of the acceleration specified in the left column. The MC^S matrix, when combined with the seismicity hazard curves, gives us the frequency of seismically initiated release categories. Figure 7.2-16 presents the resultant probability of frequency curves.

The dominant contributors to release categories 2RW and Z-1 are:

- Failure of the control building, and battery racks and masonry walls at batteries for control power.

- Loss of offsite power and failure of the diesel fuel oil tanks, battery room masonry walls and battery racks affecting batteries for starting the diesel generators, and control building failure affecting the switchgear room.

The dominant contributor to release category Z-1Q is containment failure.

The dominant contributors to release category 8A are the loss of offsite power and failure of the condensate storage and city water tanks, or pressurizer, and the refueling water storage tank. For release category 8B, the dominant contributors are the loss of offsite power and the failure of the condensate storage tank, city water tank, and poweractuated relief valve.

7.2.5A ADDITIONAL SEISMIC ANALYSIS, INDIAN POINT UNIT 3

7.2.5A.1 Control Room Ceiling

The Unit 3 control room ceiling system utilizes light fixture hangers typically consisting of Unistrut channels bolted to continuous Unistrut concrete inserts embedded in the slab above. One-quarter inch thick transite panels are supported by flanges of the light fixtures. The eggcrate panel ceiling below is supported by an aluminum tee-bar grid which, in turn, is hung from the light fixture supports by 1/4-inch diameter rods. Perforated aluminum acoustical end panels typically span between the tee-bar grid and the structure. The light fixtures which support the 1/4-inch thick transite panels are bolted to the hangers. Other light fixtures located flush with the eggcrate ceiling are hung from the Unistrut concrete inserts by Unistrut channel sections.

The transite panels bear on the light fixture flanges without any positive, mechanical connections. The transite panels were cut and installed in the field so that the gap between the panel edges and the vertical faces of the light fixtures does not exceed the overlap between the panel and the light fixture flange. An observed sampling of the panels confirms this. Therefore, the transite panels could only fall if the space between adjacent fixtures was to increase through deflection of many fixtures so that their gaps would accumulate sufficiently to allow a given panel to fall.

The control room ceiling was found in Amendment 1 to increase the seismic initiated core melt frequency by a factor of 3. As a result, the utility designed an interconnection of the eggcrate ceiling panels whereby adjacent panels are attached in multiple locations by a looped wire that interconnects the adjacent panels with their supporting T-bar. These connections of panels form a net that is capable of

retaining any of the transite panels above from falling onto control room equipment or operators during an earthquake.

The consequence of the ceiling modification is that the results of Section 7.2.5, as modified by Sections 7.2.5A.2 and 7.2.5A.3, apply.

7.2.5A.2 Containment Structure

Additional structural design calculations and a dynamic analysis not previously available in the earlier fragility analysis were the basis for a reanalysis of the Unit 3 containment. This additional analysis is summarized in Structural Mechanics Associates' report contained in Section 7.9.3.2.

The new information revealed large conservatisms used in the seismic design. These were not explicit in the summary design report information used in the earlier fragility analysis. The most prominent conservatism was in the method for determining mode shape and frequency and base shear loads. The results of the current analysis indicate that the median acceleration capacity of the Unit 3 containment increases to 2.4g.

The impact of the decreased fragility is that the possibility of containment failures from earthquakes is essentially eliminated since, even with uncertainty on the containment capacity, the containment would not fail at accelerations up to 0.8g, the upper bound acceleration at the Indian Point site. The result is that release category Z-1Q no longer applies. The effect of this change on early fatalities is discussed further in Section 8.

7.2.5A.3 Revised Fragilities and Results

Table 7.2-9 presents seismic fragilities of key structures and equipment revised since the initial IPPSS publication. Noteworthy in the table are changes in the fragility of the condensate storage, city water, and refueling water storage tanks; masonry walls enclosing the battery rooms; RCS power actuated relief valves; and the containment building.

Using the revised fragilities, the median annual core melt frequency due to seismic events is about 5.4×10^{-8}. With a 90% confidence, the annual core melt frequency is between 2.6×10^{-5} and 5.0×10^{-12}. The mean annual frequency is 3.6×10^{-6}.

The effect of the revised fragilities on the distribution of release category annual frequencies is shown in Figure 7.2-17. The mean annual frequency from seismic events of release category 2RW is 2.9×10^{-6}, of Z-1 is 3.0×10^{-9}, of 8A is 7.0×10^{-7}, and of release category 8B is 1.2×10^{-10}. The major influence on the revised frequencies is from the reduced capacity of the battery room masonry walls and the increased capacity of the power actuated relief valves and containment building.

The major contributors to core melt and release categories 2RW and Z-1 are the loss of offsite power and failure of the battery room masonry walls and battery racks affecting the batteries for controlling the start of the diesel generators, and control building failure affecting the switchgear room.

The major contributors to release category 8A are the failure of the pressurizer and refueling water storage tank. The major contributors to release category 8B are the loss of offsite power and failure of the RHR pumps.

TABLE 7.2-1

STRUCTURE CAPACITY - INDIAN POINT 2

Structure	Critical Component/Mode	Median Acceleration Capacity (g)	Variability	
			β_R	β_U
Containment Building	Shear Failure of Containment Wall	1.1	0.31	0.26
Primary Auxiliary Building	Collapse of Removable Wall Panels	2.2	0.12	0.26
Control Building	Impact with Superheater Building	0.27	0.25	0.24
	Buckling of Superheater Stack	0.72*	0.34	0.26
	Failure of Masonry Walls			
	- Unreinforced	0.35	0.29	0.24
	- Reinforced	1.3	0.28	0.36
Diesel Generator Building	Failure of Steel Framing	1.4	0.30	0.26
	Buckling of Superheater Stack	0.72*	0.34	0.26
Unit 2 Turbine Building	Failure of Steel Framing onto Control Building	1.4	0.30	0.26
Buried Concrete Structures	Failure of Walls	1.9	0.23	0.24
Fuel Storage Building	Failure of Steel Framing	0.92	0.30	0.26
Auxiliary Feed Pump Building	Containment Building Failure	1.1	0.31	0.26

*Applicable only with probability of stack failure in direction of structure.

TABLE 7.2-2

SUMMARY OF EQUIPMENT CAPACITIES FOR INDIAN POINT 2

SYSTEM & COMPONENT	LOCATION IN STRUCTURE	INDEPENDENT /DEPENDENT	EQUIPMENT CHARACTERISTICS	SEISMIC QUAL. METHOD	REFERENCE SEISMIC DESIGN LOADING	BASIS FOR FRAGILITY	STRUCTURAL RESPONSE FACTOR	β, STRUCTURAL RESPONSE	EQUIPMENT RESPONSE FACTOR	β, EQUIPMENT RESPONSE	EQUIPMENT CAPACITY FACTOR	β, EQUIPMENT CAPACITY	MEDIAN GROUND ACCELERATION CAPACITY G's	COMPOSITE β_C	RANDOM β_R	UNCERTAINTY β_U
Main Steam System																
1)Main Steam Isolation Valve	Outside Cont. 63'	Independent	Rigid, Active	Static Analysis	SSE	Generic	1.20	0.20	1.84	0.30	18.25	0.60	6.04	0.70	0.31	0.63
2)Main Steam Safety Valves	Outside Cont. 63'	Independent	Rigid, Active	Static Analysis	SSE	Generic	1.20	0.20	1.84	0.30	18.25	0.60	6.04	0.70	0.31	0.63
3)Piping (Supported) 3" - 12"	Outside Cont. 63'	Independent	Rigid, Active	Static Analysis	SSE	Generic	1.20	0.20	1.84	0.30	18.25	0.60	6.04	0.70	0.31	0.63
4)Active Valves 6", 8", 12"	Cont. Bldg. 63'-143'	Independent	Flexible, Passive	Static Analysis	OBE	Generic	1.20	0.20	1.66	0.23	11.20	0.51	2.23	0.59	0.23	0.54
Boiler Feedwater System																
1)Feedwater Level Control Valves	Aux. F.P. Bldg, 18'	Independent	Rigid, Active	Static Analysis	SSE	Generic	1.20	0.20	1.84	0.30	33.18	0.6	10.99	0.70	0.33	0.62
2)Piping 18"	Cont. Bldg. 57.5'-105'	Independent	Flexible, Passive	Static Analysis	OBE	Generic	1.20	0.20	2.15	0.23	11.20	0.51	2.89	0.59	0.23	0.54
Service Water System																
1)Service Water Pumps (6)	Int. Str. 15'	Dependent	Flexible, Active	Response Spectrum	SSE	Generic	1.60	0.39	0.87	0.66	11.86	0.18	2.47	0.79	0.40	0.68
2)Piping, 18"	Aux. Bldg. 68'	Independent	Flexible, Passive	Static Analysis	OBE	Generic	0.88	0.16	2.56	0.27	11.20	0.51	2.52	0.60	6.23	0.55
3)Active Service Water Valves (2)	Diesel Gen. Bldg. 72'	Independent	Rigid, Active	Static Analysis	SSE	Generic	0.93	0.16	1.09	0.36	26.07	0.60	3.96	0.72	0.32	0.64
4)Active Service Water Valves (2)	Aux. Bldg. 68'	Independent	Rigid, Active	Static Analysis	SSE	Generic	1.20	0.20	1.30	0.33	18.25	0.60	4.27	0.71	0.27	0.66
5)Piping, Buried, 24"	Int. Str. to Turbine	Dependent	Flexible, Passive	Static Analysis	SSE	Generic	NA	NA	NA	NA	9.33	0.61	1.40[1]	0.61	0.20	0.57
6)Piping, 3"	Control Bldg. 15'	Independent	Flexible, Passive	Static Analysis	OBE	Generic	1.10	0.29	9.39	0.35	16.10	0.46	16.62	0.65	0.32	0.57
7)Piping, 20"	Aux. Bldg. 80'	Independent	Flexible, Passive	Static Analysis	OBE	Generic	0.88	0.16	2.56	0.27	11.20	0.51	2.52	0.60	0.23	0.55
8)Piping, 10"	Diesel Gen. 72'	Independent	Flexible, Passive	Static Analysis	OBE	Generic	0.93	0.16	3.13	0.35	11.20	0.51	3.26	0.64	0.23	0.60
9)Piping, 3" & 10"	Cont. Bldg. 68'	Independent	Flexible, Passive	Static Analysis	OBE	Generic	1.20	0.20	2.15	0.23	11.20	0.51	2.89	0.59	0.23	0.54
Condensate Storage System																
1)Condensate Storage Tank	Outside, grade	NA	Flexible, Passive	Response Spectrum	SSE	Generic	NA	NA	NA	NA	8.53	0.33	1.28	0.33	0.22	0.25
2)Piping (Buried) 12"	Cond. tank to Aux. F.P.	NA	Flexible, Passive	Static Analysis	SSE	Generic	NA	NA	NA	NA	9.33	0.61	1.40[1]	0.61	0.20	0.57
3)Piping (Supported) 3"-12"	Aux. F.P. Bldg. 18'	Independent	Flexible, Passive	Static Analysis	OBE	Generic	1.20	0.20	8.1	0.31	11.20	0.51	10.9	0.63	0.26	0.57
4)Active Valves 6", 8", 12"	Aux. F.P. Bldg. 18'	NA	Rigid, Active	Static Analysis	SSE	Generic	1.20	0.20	2.45	0.32	26.07	0.60	11.50	0.71	0.37	0.61
Diesel Fuel Oil																
1)Fuel Oil Tanks (3)	Buried, Elev. 66'	Dependent	Flexible, Passive	Static Analysis	SSE	Generic	NA	NA	1.04	0.02	11.00	0.58	1.14	0.58	0.26	0.52
2)Fuel Oil Transfer Pumps (3)	Diesel Bldg. 75'	Dependent	Rigid, Active	Static Analysis	SSE	Generic	0.93	0.16	2.39	0.11	19.04	0.50	6.35	0.54	0.26	0.47
Containment Spray System																
1)Containment Spray Pumps (2)	Aux. Bldg. 68'	Dependent	Rigid, Active	Static Analysis	SSE	Generic	0.88	0.16	2.17	0.11	23.05	0.50	6.60	0.54	0.26	0.47
2)Motor Operated Valves (4) (866A-D)	Aux. Bldg. 68'	Independent	Rigid, Active	Static Analysis	SSE	Generic	0.88	0.16	1.09	0.25	26.07	0.60	3.75	0.67	0.32	0.59
3)Spray Headers (6") (2)	Cont. Bldg. 200'	Independent	Flexible, Passive	Static Analysis	OBE	Generic	1.20	0.20	1.51	0.23	11.20	0.51	2.03	0.59	0.23	0.54
4)Refueling Water Storage Tank	Outdoors, 70'	NA	Flexible, Passive	Response Spectrum	SSE	Generic	NA	NA	NA	NA	4.67	0.36	0.70	0.36	0.22	0.28
5)Piping, Buried (12")	RWST To Aux. Bldg.	NA	Flexible, Passive	Static Analysis	SSE	Generic	NA	NA	NA	NA	9.33	0.61	1.40[1]	0.61	0.20	0.57
6)Piping, Supported (3"-8")	Aux. Bldg. 68'	Independent	Flexible, Passive	Static Analysis	OBE	Generic	0.88	0.16	2.32	0.24	11.20	0.46	2.29	0.54	0.25	0.48
7)Piping, Supported (8")	Cont. Bldg. 68'-200'	Independent	Flexible, Passive	Static Analysis	OBE	Generic	1.20	0.20	1.51	0.23	11.20	0.46	2.03	0.55	0.25	0.49
8)Sprav Additive Tank	Aux. Bldg. 68'	NA	Rigid, Passive	Static Analysis	OBE	Generic	0.88	0.16	1.04	0.02	11.00	0.58	1.01	0.60	0.29	0.53
Reactor Coolant System																
1)Reactor Vessel	Cont. Bldg. 62'	NA	Flexible, Passive	Response Spectrum	SSE	Plant Specific	1.20	0.20	1.99	0.31	10.60	0.41	3.80	0.55	0.30	0.46
2)Core Geometry	Cont. Bldg. 62'	NA	Flexible, Passive	Response Spectrum	SSE	Plant Specific	1.20	0.20	3.47	0.34	1.66	0.24	1.04	0.45	0.21	0.40
3)Steam Generator (4)	Cont. Bldg. 92'	Dependent	Flexible, Passive	Response Spectrum	SSE	Plant Specific	1.20	0.20	1.99	0.31	5.13	0.34	1.84	0.50	0.26	0.43
4)Reactor Coolant Pumps (4)	Cont. Bldg. 62'	Dependent	Flexible, Passive	Response Spectrum	SSE	Plant Specific	1.20	0.20	1.99	0.31	8.49	0.34	3.04	0.50	0.26	0.43
5)Pressurizer	Cont. Bldg. 68'	NA	Flexible, Passive	Static Analysis	SSE	Plant Specific	1.20	0.20	2.29	0.28	2.10	0.31	0.87	0.46	0.23	0.40
6)Power Actuated Relief Valves (2)	Cont. Bldg. 120'	NA	Rigid, Active	Static Analysis	SSE	Generic	1.20	0.20	2.22	0.30	7.93	0.60	3.17	0.70	0.35	0.61
7)Motor Operated Block Valves (2)	Cont. Bldg. 120'	NA	Rigid, Active	Static Analysis	SSE	Generic	1.20	0.20	2.22	0.30	7.93	0.60	3.17	0.70	0.35	0.61
8)Pressurizer Safety Valves (3)	Cont. Bldg. 120'	Dependent	Rigid, Active	Static Analysis	SSE	Generic	1.20	0.20	1.66	0.47	7.93	0.60	2.37	0.79	0.38	0.69
9)Relief Tank	Cont. Bldg. 46'	NA	Rigid, Passive	Static Analysis	OBE	Generic	1.20	0.20	1.04	0.02	11.00	0.58	1.37	0.61	0.30	0.53
10)Piping, 27.5"-31"	Cont. Bldg. 62'	Independent	Flexible, Passive	Response Spectrum	SSE	Plant Specific	1.20	0.20	2.22	0.30	16.90	0.41	6.75	0.55	0.30	0.46
11)Piping, 1"-4"	Cont. Bldg. 62'-120'	Independent	Flexible, Passive	Static Analysis	OBE	Generic	1.20	0.20	4.58	0.27	16.10	0.46	8.85	0.57	0.26	0.51
12)Piping, 6"-14"	Cont. Bldg. 62'-120'	Independent	Flexible, Passive	Static Analysis	OBE	Generic	1.20	0.20	4.58	0.27	11.20	0.51	6.16	0.61	0.24	0.56
Residual Heat Removal																
1)RHR Pumps (2)	Aux. Bldg. 15'	Dependent	Flexible, Active	Response Spectrum	SSE	Plant Specific	0.88	0.16	8.83	0.31	1.46	0.11	1.70	0.37	0.15	0.34
2)RHR Heat Exchangers (2)	Cont. Bldg. 66'	Dependent	Flexible, Passive	Response Spectrum	SSE	Plant Specific	1.20	0.20	10.31	0.26	5.69	0.34	10.56	0.47	0.22	0.42
3)MOV's Outside Containment	Outside Cont. 60'	Independent	Rigid, Active	Static Analysis	SSE	Generic	1.20	0.20	1.84	0.30	15.87	0.60	5.26	0.70	0.31	0.63
Active (882, 885A, 885B) (12", 14")																
Passive (all others - 2) (8", 12")																
4)MOV's Inside Containment	Cont. Bldg. 66'	Independent	Rigid, Active	Static Analysis	SSE	Generic	1.20	0.20	1.30	0.33	18.25	0.60	4.27	0.71	0.27	0.66
Active (746, 747, 1802A, 1802B) (8",10")																
Passive (all others - 8) (8", 12", 14")																
5)Piping (8"-12")	Aux. Bldg. 15'-60'	Independent	Flexible, Passive	Static Analysis	OBE	Generic	0.88	0.16	2.32	0.24	11.20	0.51	2.29	0.59	0.22	0.55
6)Piping (8"-12", 14")	Cont. Bldg. 60'-60'	Independent	Flexible, Passive	Static Analysis	OBE	Generic	1.20	0.20	2.15	0.23	11.20	0.51	2.89	0.59	0.23	0.54

TABLE 7.2-2 (continued)

SUMMARY OF EQUIPMENT CAPACITIES FOR INDIAN POINT 2

SYSTEM & COMPONENT	LOCATION IN STRUCTURE	INDEPENDENT /DEPENDENT	EQUIPMENT CHARACTERISTICS	SEISMIC QUAL. METHOD	REFERENCE SEISMIC DESIGN LOADING	BASIS FOR FRAGILITY	STRUCTURAL RESPONSE FACTOR	β, STRUCTURAL RESPONSE	EQUIPMENT RESPONSE FACTOR	β, EQUIPMENT RESPONSE	EQUIPMENT CAPACITY FACTOR	β, EQUIPMENT CAPACITY	MEDIAN GROUND ACCELERATION CAPACITY G's	COMPOSITE β_C	RANDOM β_R	UNCERTAINTY β_U
[illegible]y Injection System																
[illegible]afety Injection Pumps (3)	Aux. Bldg. 59'	Dependent	Rigid, Active	Static Analysis	SSE	Plant Specific	0.88	0.16	6.39	0.15	2.84	0.35	2.40	0.41	0.17	0.37
2)MOV's Inside Containment	Cont. Bldg. 46'	Independent	Rigid, Active	Static Analysis	SSE	Generic	1.20	0.16	1.09	0.25	18.25	0.60	4.27	0.71	0.30	0.64
Active (none)																
Passive (all others - 10) (2", 10")																
3)MOV's Outside Containment																
Active (1810,887A,887B,1821,1831,1822A, 1822B, 888A, 888B) (6", 8")	Aux. Bldg. 60'	Independent	Rigid, Active	Static Analysis	SSE	Generic	0.88	0.16	1.09	0.25	26.07	0.60	3.75	0.67	0.28	0.61
Passive (all others - 4) (2", 6")																
[illegible]ecirculation Pumps (2)	Cont. Bldg. 46'	Dependent	Rigid, Active	Static Analysis	SSE	Generic	1.20	0.20	1.91	0.11	23.00	0.50	7.90	0.55	0.31	0.42
[illegible]Boron Injection Tank	Aux. Bldg. 80'	NA	Flexible, Passive	Response Spectrum	SSE	Plant Specific	0.88	0.16	13.84	0.23	1.37	0.37	2.53	0.46	0.23	0.40
6)Accumulators	Cont. Bldg. 46'	Dependent	Flexible, Passive	Response Spectrum	SSE	Plant Specific	1.20	0.20	9.29	0.17	8.20	0.37	13.71	0.45	0.18	0.41
7)Piping, 6" to 8"	Aux. Bldg. 59'-80'	Independent	Flexible, Passive	Static Analysis	OBE	Generic	0.88	0.16	2.32	0.24	11.20	0.46	2.29	0.54	0.23	0.49
8)Piping, 2" to 6"	Cont. Bldg. 46'-60'	Independent	Flexible, Passive	Static Analysis	OBE	Generic	1.20	0.20	7.68	0.27	16.10	0.46	14.85	0.57	0.26	0.51
Component Cooling System																
1)Component Cooling Pumps (3)	Aux. Bldg. 68'	Dependent	Rigid, Active	Static Analysis	SSE	Generic	0.88	0.16	2.17	0.11	23.00	0.50	6.60	0.54	0.25	0.48
2)CCW Heat Exchangers (2)	Aux. Bldg. 80'	Dependent	Flexible, Passive	Response Spectrum	SSE	Plant Specific	0.88	0.16	8.89	0.19	4.63	0.24	5.43	0.35	0.19	0.29
3)MOV's, 12" (2)	Cont. Bldg. 66'	Independent	Rigid, Active	Static Analysis	SSE	Generic	1.20	0.20	1.30	0.33	18.25	0.60	4.27	0.71	0.31	0.64
4)MOV's, 3" & 6" (6)	Aux. Bldg. 68'	Independent	Rigid, Active	Static Analysis	SSE	Generic	0.88	0.16	1.09	0.25	26.07	0.60	3.75	0.67	0.29	0.60
5)Piping, 3" to 8"	Aux. Bldg. 68'-80'	Independent	Flexible, Passive	Static Analysis	OBE	Generic	0.88	0.16	2.32	0.24	11.2	0.46	2.29	0.54	0.23	0.49
6)Piping, 12", 16"	Cont. Bldg.46'-66'	Independent	Flexible, Passive	Static Analysis	OBE	Generic	1.20	0.20	2.15	0.23	11.20	0.51	2.89	0.59	0.23	0.64
7)Aux. Component Cool. Pumps (2)	Aux. Bldg. 68'	Dependent	Rigid, Active	Static Analysis	SSE	Generic	0.88	0.16	2.40	0.11	21.54	0.50	6.83	0.54	0.24	0.48
8)Piping, 10" to 20"	Aux. Bldg. 68'-80'	Independent	Flexible, Passive	Static Analysis	OBE	Generic	0.88	0.16	2.32	0.24	11.20	0.51	2.29	0.59	0.21	0.55
Containment Ventilation System																
1)Containment Fan Coolers (5)	Cont. Bldg. 68'	pairs are depend.	Flexible, Active	Response Spectrum	SSE	Plant Specific	1.20	0.20	2.06	0.31	3.12	0.23	1.16	0.43	0.20	0.38
2)Ductwork & Dampers	Cont. Bldg. 68'	Independent	Flexible, Passive	Static Analysis	OBE	Generic	1.20	0.20	1.04	0.02	9.00	0.57	1.12	0.60	0.23	0.55
[illegible]iary Feedwater System																
1)Motor Driven Pumps (2)	Aux. FP Bldg. -18'6"	Dependent	Rigid, Active	Static Analysis	SSE	Generic	1.20	0.20	3.62	0.11	23.00	0.50	15.00	0.55	0.20	0.51
2)Turbine Driven Pumps (1)	Aux. FP Bldg. -18'6"	NA	Rigid, Active	Static Analysis	SSE	Generic	1.20	0.20	3.62	0.11	23.00	0.50	15.00	0.55	0.20	0.51
3)Piping, 3"-6"	Aux. FP Bldg. -18'-62'	Independent	Flexible, Passive	Static Analysis	OBE	Generic	1.20	0.20	6.45	0.23	16.10	0.46	12.45	0.55	0.25	0.49
4)Valves (air operated)	Aux. FP Bldg. -18'6"	Independent	Rigid, Active	Static Analysis	SSE	Generic	1.20	0.20	1.09	0.32	26.07	0.60	5.11	0.71	0.31	0.64
Reactor Protection System																
1)Logic Panels (Relays) (2)	Control Bldg. 53'	Dependent	Flexible, Active	Test	SSE	Plant Specific	1.10	0.29	1.43	0.47	20.13	0.35	4.75	0.65	0.35	0.55
2)Reactor Trip Breakers (2)	Control Bldg. 53'	Dependent	Flexible, Active	Test	SSE	Plant Specific	1.10	0.29	1.43	0.47	20.13	0.35	4.75	0.65	0.35	0.55
3)SIS Logic Panel (Relays)	Control Bldg. 53'	Dependent	Flexible, Active	Test	SSE	Plant Specific	1.10	0.29	1.43	0.47	20.13	0.35	4.75	0.65	0.35	0.55
4)Inst.& Process Panels	Control Bldg. 53'	Dependent	Flexible, Active	Test	SSE	Plant Specific	1.10	0.29	1.43	0.47	20.13	0.35	4.75	0.65	0.35	0.55
5)Control Rod Drive Mech.	Cont. Bldg. 75'	Dependent	Flexible, Active	Response Spectrum	SSE	Plant Specific	1.20	0.20	2.87	0.26	5.50	0.24	2.84	0.41	0.20	0.36
Electric Power (480 VAC)																
1)Switchgear Incl. Station Service Transformers	Cont. Bldg. 15'	Dependent	Flexible, Active	Test	SSE	Generic	1.10	0.29	1.04	0.23	14.53	0.50	2.49[2]	0.62	0.38	0.49
2)Diesel and Gas Turbine Generators	Grade	Dependent	Flexible, Active	None	SSE	Generic	0.93	0.16	0.81	0.23	11.53	0.50	1.30[2]	0.57	0.24	0.52
3)Motor Control Centers	Various Bldgs.	Dependent	Flexible, Active	Test	SSE	Generic	1.10	0.29	1.59	0.33	6.30	0.50	1.65[2]	0.67	0.41	0.53
4)Cable Trays	Various Bldgs.	Independent	Flexible, Passive	None	SSE	Generic	1.10	0.29	1.08	0.11	6.20	0.55	1.10	0.63	0.30	0.55
Electric Power (6900 VAC)																
[illegible]1)Switchgear	Turbine Bldg. 15'	Dependent	Flexible, Acitve	Test	SSE	Generic	1.60	0.39	1.02	6.22	11.51	0.50	2.81[2]	0.67	0.29	0.60
[illegible]2)Station Aux. Transformer	Outside, Grade Elev.	NA	Flexible, Passive	Static Analysis	OBE	Generic	1.00	0.00	1.54	0.26	11.00	0.58	1.69	0.64	0.20	0.61
[illegible]ctric Power (125 VDC)																
1)Batteries & Racks (4)	Control Bldg., Unit 1 Turb. Bldg. 33'	Dependent	Flexible, Passive	Static Analysis	OBE	Generic	1.10	0.29	1.38	0.29	9.00	0.57	1.37	0.70	0.30	0.63
Electric Power (120 VAC)																
1)Inverters (4)	Control Bldg. 33'	Dependent	Flexible, Passive	Test	SSE	Plant Specific	1.10	0.29	1.30	0.39	30.38	0.35	6.52	0.60	0.35	0.49
[illegible]2)Distribution Panels	Control Bldg. 53'	Dependent	Flexible, Active	Test	SSE	Generic	1.10	0.29	1.59	0.33	6.30	0.50	1.65[2]	0.67	0.41	0.53
[illegible]ite Power																
1)Ceramic Insulators	Outside	Dependent	Flexible, Passive	None	NA	Generic	NA	NA	NA	NA	NA	NA	0.20[3]	0.32	0.20	0.25

Notes:
1 Assumed to be the same capacity as Zion components
2 Failure mode is electrical malfunctions due to relay chatter or breaker trip. Malfunction is recoverable. Permanent damage level estimated at 3 times value stated
3 From historical data

TABLE 7.2-3

FRAGILITY OF KEY STRUCTURES AND EQUIPMENT - INDIAN POINT 2

Symbol	Structure/Equipment	$\bar{a}$	β_R	β_U
(1)	Offsite Power Transformer Ceramic Insulators	.20	.20	.25
(2)	Control Building Unit 2 (Impact with Unit 1 Control Building)	.27	.25	.24
(3)	Control Room Masonry Walls	.35	.29	.24
(4)	Masonry Walls at Battery Rooms No. 23 and 24	.35	.29	.24
(5)	Superheater Stack	.72	.34	.26
(6)	Condensate Storage Tank	.83	.28	.29
(7)	City Water Storage Tank	.83	.28	.29
(8)	Refueling Water Storage Tank	.83	.28	.29
(9)	Reactor Coolant System Pressurizer	.87	.23	.40
(10)	Fuel Storage Building Failure of Steel Frame	.92	.30	.26
(11)	Containment Spray System (CSS) Spray Additive Tank	1.01	.29	.53
(12)	Reactor Core Geometry	1.04	.21	.40
(13)	Cable Trays	1.10	.30	.55
(14)	Containment Building Shear Failure Containment Wall/ Auxiliary Feedwater Pump Building	1.10	.31	.26
(15)	Containment Ductwork and Dampers	1.12	.23	.55
(16)	Diesel Generator Fuel Oil Tanks	1.14	.26	.52
(17)	Containment Fan Coolers	1.16	.20	.38
(18)	Diesel Generators, Gas Turbines (Controls)*	1.30	.24	.52
(19)	Masonry Walls at Battery Rooms No. 21 and 22	1.30	.28	.36
(20)	125 VDC Batteries and Racks	1.37	.30	.63
(21)	120 VAC Transformers	1.37	.30	.63
(22)	RCS Relief Tank	1.37	.30	.53
(23)	CSS Buried Pipe 12"	1.40	.20	.57
(24)	SWS Buried 24" Piping	1.40	.20	.57
(25)	CST Buried 12" Piping	1.40	.20	.57
(26)	Turbine Building Steel Frame/ Control Building	1.40	.30	.26
(27)	Diesel Generator Building Failure of Steel Building	1.40	.30	.26
(28)	RCS Power-Actuated Relief Valve	1.48	.35	.64
(29)	Superheater Building Steel Framing/Control Building	1.50	.30	.26
(30)	120 VAC Distribution Panels*	1.65	.41	.53
(31)	480 VAC Motor Control Centers*	1.65	.41	.53
(32)	6,900 VAC Station Auxiliary Transformer	1.69	.20	.61
(33)	Steam Generators	1.84	.26	.43
(34)	Buried Concrete Structures	1.90	.23	.24

*Fragility values indicated are for chatter, relay trip, or other intermittent or easily recoverable conditions. Nonrecoverable failure is expected to occur at about three times the indicated fragility value.

TABLE 7.2-4A-1

REVISED FRAGILITIES OF KEY STRUCTURES AND EQUIPMENT - INDIAN POINT 2

Symbol	Structure/Equipment	$\hat{a}$	β_R	β_U
(1)	Offsite Power Transformer Ceramic Insulators	.20	.20	.25
(2)*	Control Building Unit 2 (Impact with Unit 1 Control Building)	1.00	.30	.30
(3)	Control Room Masonry Walls	.35	.29	.24
(4)	Masonry Walls at Battery Rooms No. 23 and 24	.35	.29	.24
(5)	Superheater Stack	.72	.34	.26
(6)*	Condensate Storage Tank	1.28	.22	.25
(7)*	City Water Storage Tank	.25	.25	.30
(8)*	Refueling Water Storage Tank	.70	.22	.28
(9)	Reactor Coolant System Pressurizer	.87	.23	.40
(10)	Fuel Storage Building Failure of Steel Frame	.92	.30	.26
(11)	Containment Spray System (CSS) Spray Additive Tank	1.01	.29	.53
(12)	Reactor Core Geometry	1.04	.21	.40
(13)*	Cable Tray Increment	1.54	.37	.61
(14)*	Containment Building Shear Failure Containment Wall/ Auxiliary Feedwater Pump Building	2.70	.35	.38
(15)	Containment Ductwork and Dampers	1.12	.23	.55
(16)	Diesel Generator Fuel Oil Tanks	1.14	.26	.52
(17)	Containment Fan Coolers	1.16	.20	.38
(18)**	Diesel Generators, Gas Turbines (Controls)	1.30	.24	.52
(19)	Masonry Walls at Battery Rooms No. 21 and 22	1.30	.28	.36
(20)	125 VDC Batteries and Racks	1.37	.30	.63
(21)*	120 VAC Transformers	1.07	.30	.60
(22)	RCS Relief Tank	1.37	.30	.53
(23)	CSS Buried Pipe 12"	1.40	.20	.57
(24)	SWS Buried 24" Piping	1.40	.20	.57
(25)	CST Buried 12" Piping	1.40	.20	.57
(26)	Turbine Building Steel Frame/ Control Building	1.40	.30	.26
(27)	Diesel Generator Building Failure of Steel Building	1.40	.30	.26
(28)*	RCS Power-Actuated Relief Valve	3.17	.35	.61
(29)	Superheater Building Steel Framing/Control Building	1.50	.30	.26
(30)**	120 VAC Distribution Panels	1.65	.41	.53
(31)**	480 VAC Motor Control Centers	1.65	.41	.53
(32)*	6,900 VAC Station Auxiliary Transformer	.30	.30	.46
(33)	Steam Generators	1.84	.26	.43
(34)	Buried Concrete Structures	1.90	.23	.24

*Revised since initial publication of the IPPSS.
**Fragility values indicated are for chatter, relay trip, or other intermittent or easily recoverable conditions. Nonrecoverable failure is expected to occur at about three times the indicated fragility value.

TABLE 7.2-5

STRUCTURE CAPACITY - INDIAN POINT 3

Structure	Critical Component/Mode	Median Acceleration Capacity (g)	Variability	
			β_R	β_U
Containment Building	Shear Failure of Containment Wall	1.7	0.31	0.26
Primary Auxiliary Building	Collapse of Removable Wall Panels	2.2	0.12	0.26
	Failure of Shear Walls	3.3	0.13	0.47
Control Building	Failure of Masonry Walls			
	Elevation 53' - Unreinforced	0.33	0.27	0.24
	- Reinforced	1.0	0.21	0.29
	Elevation 33' - Unreinforced	0.35	0.29	0.24
	- Reinforced	1.3	0.28	0.36
	Shear Failure of N-S Walls	1.2	0.16	0.23
Diesel Generator Building	Flexural Failure of Roof Diaphragm	1.5	0.25	0.35
	Failure of Shear Walls	7.5	0.13	0.31
Buried Concrete Structures	Failure of Walls	1.9	0.23	0.24
Fuel Storage Building	Failure of Steel Framing	0.92	0.30	0.26
Condensate Storage Tank	Buckling of Superheater Stack	0.72*	0.34	0.26
Auxiliary Feed Pump Building	Containment Building Failure	1.7	0.31	0.26

*Applicable only with probability of stack failure in direction of tank.

TABLE 7.2-6

SUMMARY OF EQUIPMENT CAPACITIES FOR INDIAN POINT 3

SYSTEM & COMPONENT	LOCATION IN STRUCTURE	INDEPENDENT /DEPENDENT	EQUIPMENT CHARACTERISTICS	SEISMIC QUAL. METHOD	REFERENCE SEISMIC DESIGN LOADING	BASIS FOR FRAGILITY	STRUCTURAL RESPONSE FACTOR	β STRUCTURAL RESPONSE	EQUIPMENT RESPONSE FACTOR	β EQUIPMENT RESPONSE	EQUIPMENT CAPACITY FACTOR	ϵ EQUIPMENT CAPACITY	MEDIAN GROUND ACCELERATION CAPACITY G's	COMPOSITE β_C	RANDOM β_R	UNCERTAINTY β_U
Main Steam System																
1) Main Steam Isolation Valve (4)	Outside Cont. 63'	Independent	Rigid, Active	Static Analysis	SSE	Generic	1.20	0.20	1.84	0.30	18.25	0.60	6.04	0.70	0.31	
2) Main Steam Safety Valves (20)	Outside Cont. 63'	Independent	Rigid, Active	Static Analysis	SSE	Generic	1.20	0.20	1.84	0.30	18.25	0.60	6.04	0.70	0.31	0.63
3) Power Actuated Relief Valves (4)	Outside Cont. 63'	Independent	Rigid, Active	Static Analysis	SSE	Generic	1.20	0.20	1.84	0.30	18.25	0.60	6.04	0.70	0.31	0.63
4) Piping (28")	Cont. Bldg. 63'-143'	Independent	Flexible, Passive	Response Spectrum	OBE	Generic	1.20	0.20	1.51	0.25	11.20	0.51	2.03	0.60	0.23	0.55
Boiler Feedwater System																
1) Feedwater Level Control Valves	Aux. F.P. Bldg. 18'	Independent	Rigid, Active	Static Analysis	SSE	Generic	1.20	0.20	1.84	0.30	33.18	0.60	10.99	0.70	0.33	0.62
2) Piping 18"	Cont. Bldg. 58'-105'	Independent	Flexible, Passive	Response Spectrum	OBE	Generic	1.20	0.20	1.96	0.31	11.20	0.51	2.63	0.63	0.28	0.56
Service Water System																
1) Service Water Pumps (9)	Int. Str. Elev. 15'	Dependent	Flexible, Active	Response Spectrum	SSE	Generic	1.60	0.39	0.87	0.66	11.86	0.18	2.47	0.79	0.40	0.68
2) Piping, 18"	Aux. Bldg. 68'	Independent	Flexible, Passive	Response Spectrum	OBE	Generic	0.88	0.16	2.33	0.28	11.20	0.51	2.30	0.60	0.25	0.55
3) Active Service Water Valves (2)	Diesel Gen. Bldg. 15'	Independent	Rigid, Active	Static Analysis	SSE	Generic	0.93	0.16	1.09	0.36	26.07	0.60	3.96	0.72	0.32	0.64
4) Active Service Water Valves (2)	Aux. Bldg. 68'	Independent	Rigid, Active	Static Analysis	SSE	Generic	1.20	0.20	1.30	0.33	18.25	0.60	4.27	0.71	0.27	0.66
5) Piping, Buried, 24"	Int. Str. to Turbine	Dependent	Flexible, Passive	Static Analysis	SSE	Generic	NA	NA	NA	NA	9.33	0.61	1.40[1]	0.61	0.20	0.57
6) Piping, 3"	Control Bldg. 15'	Independent	Flexible, Passive	Static Analysis	OBE	Generic	0.86	0.19	6.26	0.35	16.10	0.46	8.67	0.61	0.18	0.58
7) Piping, 20"	Aux. Bldg. 55'	Independent	Flexible, Passive	Response Spectrum	OBE	Generic	0.88	0.16	2.33	0.28	11.20	0.51	2.30	0.60	0.25	0.55
8) Piping, 10"	Diesel Gen. 15'	Independent	Flexible, Passive	Response Spectrum	OBE	Generic	0.93	0.16	2.85	0.41	11.20	0.51	2.97	0.67	0.28	0.61
9) Piping, 3" & 10"	Cont. Bldg. 68'	Independent	Flexible, Passive	Response Spectrum	OBE	Generic	1.20	0.20	1.96	0.31	11.20	0.51	2.63	0.63	0.28	0.56
Condensate Storage System																
1) Condensate Storage Tank	Outside, Grade Level	NA	Flexible, Passive	Response Spectrum	SSE	Generic	NA	NA	NA	NA	8.53	0.33	1.28	0.33	0.22	0.25
2) Piping (Buried) 12"	Cond. Tank to Aux. F.P.	NA	Flexible, Passive	Static Analysis	SSE	Generic	NA	NA	NA	NA	9.33	0.61	1.40[1]	0.61	0.20	0.57
3) Valves, 6", 8", 12"	Aux. F.P. Bldg. 18.5'	Independent	Rigid, Active	Static Analysis	SSE	Generic	1.20	0.20	2.45	0.32	26.07	0.60	11.50	0.71	0.37	0.61
4) Piping (Supported) 3"-12"	Aux. F.P. Bldg. 18.5'	Independent	Flexible, Passive	Response Spectrum	OBE	Generic	1.20	0.20	1.09	0.32	11.20	0.51	1.46	0.63	0.29	0.56
Diesel Fuel Oil System																
1) Fuel Oil Tanks (3)	Below Grade	Dependent	Flexible, Passive	Static Analysis	OBE	Generic	NA	NA	1.04	0.02	11.00	0.58	1.14	0.58	0.26	0.52
2) Fuel Oil Transfer Pumps (3)	Diesel Gen.Bldg. 38'	Dependent	Rigid, Active	Static Analysis	SSE	Generic	0.93	0.16	2.39	0.11	19.0	0.50	6.35	0.54	0.26	0.47
Containment Spray System																
1) Containment Spray Pumps (2)	Aux. Bldg. 41'	Dependent	Rigid, Active	Static Analysis	SSE	Generic	0.88	0.16	2.17	0.11	23.05	0.50	6.60	0.54	0.26	0.47
2) Motor Operated Valves (2) (866A, B)	Aux. Bldg. 41'	Independent	Rigid, Active	Static Analysis	SSE	Generic	0.88	0.16	1.09	0.25	26.07	0.60	3.75	0.67	0.32	0.59
3) Spray Headers (6") (2)	Cont. Bldg.200'	Dependent	Flexible, Passive	Response Spectrum	OBE	Generic	0.86	0.19	1.37	0.28	11.20	0.51	1.32	0.61	0.29	0.54
4) Refueling Water Storage Tank	Outdoors, Grade Level	NA	Flexible, Passive	Response Spectrum	SSE	Generic	NA	NA	NA	NA	4.67	0.36	0.7	0.36	0.22	0.28
5) Piping, Buried (12")	RWST To Aux. Bldg.	NA	Flexible, Passive	Static Analysis	SSE	Generic	NA	NA	NA	NA	9.33	0.61	1.40[1]	0.61	0.20	0.57
6) Piping, 3"-4"	Aux. Bldg. 41'-60'	Independent	Flexible, Passive	Static Analysis	OBE	Generic	0.88	0.16	4.64	0.24	16.10	0.46	6.57	0.54	0.27	0.47
7) Piping, 8"	Cont. Bldg. 68'-200'	Independent	Flexible, Passive	Response Spectrum	OBE	Generic	1.20	0.20	1.37	0.28	11.20	0.51	1.84	0.62	0.30	0.54
8) Spray Additive Tank	Aux. Bldg. 41'	NA	Rigid, Passive	Static Analysis	OBE	Generic	0.88	0.16	1.04	0.02	11.00	0.58	1.01	0.60	0.29	0.53
9) Piping, 6"-8"	Aux. Bldg. 41'-60'	Independent	Flexible, Passive	Response Spectrum	OBE	Generic	0.88	0.16	2.11	0.34	16.10	0.46	2.99	0.59	0.28	0.52
Reactor Coolant System																
1) Reactor Vessel	Cont. Bldg. 62'	NA	Flexible, Passive	Response Spectrum	SSE	Plant Specific	1.20	0.20	1.99	0.31	10.60	0.41	3.80	0.55	0.30	0.46
2) Core Geometry	Cont. Bldg. 62'	NA	Flexible, Passive	Response Spectrum	SSE	Plant Specific	1.20	0.20	3.47	0.32	1.66	0.24	1.04	0.45	0.21	0.40
3) Steam Generator (4)	Cont. Bldg. 90'	Dependent	Flexible, Passive	Response Spectrum	SSE	Plant Specific	1.20	0.20	1.99	0.31	5.13	0.34	1.84	0.50	0.26	0.43
4) Reactor Coolant Pumps (4)	Cont. Bldg. 62'	Dependent	Flexible, Passive	Response Spectrum	SSE	Plant Specific	1.20	0.20	1.99	0.31	8.49	0.34	3.04	0.50	0.26	0.43
5) Pressurizer	Cont. Bldg. 68'	NA	Flexible, Passive	Static Analysis	SSE	Plant Specific	1.20	0.20	2.29	0.28	2.10	0.31	0.87	0.46	0.23	0.40
6) Power Actuated Relief Valves (2)	Cont. Bldg. 120'	NA	Rigid, Active	Static Analysis	SSE	Generic	1.20	0.20	2.22	0.30	7.93	0.60	3.17	0.70	0.35	0.61
7) Motor Operated Block Valves (2)	Cont. Bldg. 120'	NA	Rigid, Active	Static Analysis	SSE	Generic	1.20	0.20	2.22	0.30	7.93	0.60	3.17	0.70	0.35	0.61
8) Pressurizer Safety Valves (3)	Cont. Bldg. 120'	Independent	Rigid, Active	Static Analysis	SSE	Generic	1.20	0.20	1.66	0.47	7.93	0.60	2.37	0.79	0.38	0.69
9) Pressurizer Relief Tank	Cont. Bldg. 46'	NA	Rigid, Passive	Static Analysis	OBE	Generic	1.20	0.20	1.04	0.02	11.00	0.58	1.37	0.61	0.30	0.53
10) Main Coolant Piping, 27.5"-31"	Cont. Bldg. 62'	Independent	Flexible, Passive	Response Spectrum	SSE	Plant Specific	1.20	0.20	2.22	0.30	16.90	0.41	6.75	0.55	0.30	0.46
11) Piping, 1"-4"	Cont. Bldg. 62'-120'	Independent	Flexible, Passive	Static Analysis	OBE	Generic	1.20	0.20	9.16	0.27	16.10	0.46	17.70	0.57	0.26	0.51
12) Piping, 6"-14"	Cont. Bldg. 62'-120'	Independent	Flexible, Passive	Response Spectrum	OBE	Generic	1.20	0.20	4.16	0.26	11.20	0.51	5.59	0.61	0.20	0.57
Residual Heat Removal System																
1) RHR Pumps (2)	Aux. Bldg. 15'	Dependent	Flexible, Active	Response Spectrum	SSE	Plant Specific	0.88	0.16	8.83	0.31	1.46	0.11	1.70	0.37	0.15	0.34
2) RHR Heat Exchangers (2)	Cont. Bldg. 66'	Dependent	Flexible, Passive	Response Spectrum	SSE	Plant Specific	1.20	0.20	10.31	0.26	5.69	0.34	10.56	0.47	0.22	0.42
3) MOV's Outside Containment Active (882, 885A, 885B) (12", 14") Passive (all others - 2) (8"-12")	Outside Cont. 60'	Independent	Rigid, Active	Static Analysis	SSE	Generic	1.20	0.20	1.84	0.30	15.87	0.60	5.26	0.70	0.31	0.63
4) MOV's Inside Containment Active (1802A, 1802B) (10") Passive (all others - 14) (6"-14")	Cont. Bldg. 66'	Independent	Rigid, Active	Static Analysis	SSE	Generic	1.20	0.20	1.30	0.33	18.25	0.60	4.27	0.71	0.27	0.66
5) Piping (8"-12")	Aux. Bldg. 15'-60'	Independent	Flexible, Passive	Response Spectrum	OBE	Generic	0.88	0.16	2.11	0.34	11.20	0.51	2.08	0.63	0.28	0.56
6) Piping (8"-12", 14")	Cont. Bldg. 60'-66'	Independent	Flexible, Passive	Response Spectrum	OBE	Generic	1.20	0.20	1.96	0.31	11.20	0.51	2.63	0.63	0.28	0.56

TABLE 7.2-6 (continued)

SUMMARY OF EQUIPMENT CAPACITIES FOR INDIAN POINT 3

SYSTEM & COMPONENT	LOCATION IN STRUCTURE	INDEPENDENT /DEPENDENT	EQUIPMENT CHARACTERISTICS	SEISMIC QUAL. METHOD	REFERENCE SEISMIC DESIGN LOADING	BASIS FOR FRAGILITY	STRUCTURAL RESPONSE FACTOR	β STRUCTURAL RESPONSE	EQUIPMENT RESPONSE FACTOR	β EQUIPMENT RESPONSE	EQUIPMENT CAPACITY FACTOR	β EQUIPMENT CAPACITY	MEDIAN GROUND ACCELERATION CAPACITY G's	COMPOSITE β_C	RANDOM β_R	UNCERTAINTY β_U
Safety Injection System																
1)Safety Injection Pumps (3)	Aux. Bldg. 34'	Dependent	Rigid, Active	Static Analysis	SSE	Plant Specific	0.88	0.16	5.78	0.10	2.84	0.35	2.17	0.40	0.22	0.33
2)MOV's Inside Containment	Cont. Bldg. 46'	Independent	Rigid, Active	Static Analysis	SSE	Generic	1.20	0.20	1.30	0.33	18.25	0.60	4.27	0.71	0.30	0.64
Active (none)																
Passive (all others - 10) (1-1/2",2",10")																
3)MOV's Outside Containment	Aux. Bldg. 34'	Independent	Rigid, Active	Static Analysis	SSE	Generic	0.88	0.16	1.09	0.25	26.07	0.60	3.75	0.67	0.29	0.61
Active (1810, 887A, 887B, 1852A, 1852B, 1835A, 1835B, 888A, 888B (4", 6", 8")																
Passive (all others - 4) (2"-4")																
4)Recirculation Pumps (2)	Cont. Bldg. 46'	Dependent	Rigid, Active	Static Analysis	SSE	Generic	1.20	0.20	1.91	0.11	23.0	0.50	7.90	0.55	0.31	0.45
5)Boron Injection Tank	Aux. Bldg. 35'	NA	Flexible, Passive	Response Spectrum	SSE	Plant Specific	0.88	0.16	15.50	0.25	2.42	0.37	4.95	0.47	0.22	0.42
6)Accumulators	Cont. Bldg. 46'	Dependent	Flexible, Passive	Response Spectrum	SSE	Plant Specific	1.20	0.20	10.41	0.22	8.20	0.37	15.37	0.47	0.22	0.42
7)Piping, 6" to 8"	Aux. Bldg. 34'-60'	Independent	Flexible, Passive	Response Spectrum	OBE	Generic	0.88	0.16	2.11	0.34	16.10	0.46	2.99	0.59	0.27	0.52
8)Piping, 2" to 4"	Cont. Bldg. 46'-60'	Independent	Flexible, Passive	Static Analysis	OBE	Generic	1.20	0.20	4.65	0.27	16.10	0.46	8.98	0.57	0.25	0.51
9)Piping, 6"	Cont. Bldg. 60'	Independent	Flexible, Passive	Response Spectrum	OBE	Generic	1.20	0.20	2.33	0.26	16.10	0.46	4.50	0.56	0.25	0.50
Component Cooling System																
1)Component Cooling Pumps (3)	Aux. Bldg. 41'	Dependent	Rigid, Active	Static Analysis	SSE	Generic	0.88	0.16	2.17	0.11	23.0	0.50	6.60	0.54	0.25	0.48
2)CCW Heat Exchangers (2)	Aux. Bldg. 55'	Dependent	Flexible, Passive	Response Spectrum	SSE	Plant Specific	0.88	0.16	10.03	0.21	4.63	0.24	6.13	0.36	0.20	0.30
3)MOV's, 12" (2)	Aux. Bldg. 66'	Independent	Rigid, Active	Static Analysis	SSE	Generic	1.20	0.20	1.30	0.33	18.25	0.60	4.27	0.71	0.31	0.64
4)MOV's, 3" & 6" (6)	Aux. Bldg. 41'	Independent	Rigid, Active	Static Analysis	SSE	Generic	0.88	0.16	1.09	0.25	26.07	0.60	3.75	0.67	0.29	0.60
5)Piping, 3" to 4"	Aux. Bldg. 41'-60'	Independent	Flexible, Passive	Static Analysis	OBE	Generic	0.88	0.16	4.65	0.24	16.10	0.46	6.59	0.54	0.25	0.48
6)Piping, 12"	Cont. Bldg. 46'-66'	Independent	Flexible, Passive	Response Spectrum	OBE	Generic	1.20	0.20	1.96	0.31	11.20	0.51	2.63	0.63	0.28	0.56
7)Aux. Component Cool. Pumps (4)	Aux. Bldg. 55'	Dependent	Rigid, Active	Static Analysis	SSE	Generic	0.88	0.16	2.40	0.11	21.54	0.50	6.83	0.54	0.24	0.48
8)Piping, 6" to 20"	Aux. Bldg. 41'-60'	Independent	Flexible, Passive	Response Spectrum	OBE	Generic	0.88	0.16	2.11	0.34	11.20	0.51	2.08	0.63	0.29	0.56
Containment Ventilation System																
1)Containment Fan Coolers (5)	Cont. Bldg. 68'	pairs are depend.	Flexible, Active	Response Spectrum	SSE	Plant Specific	1.20	0.20	5.17	0.34	2.33	0.23	2.17	0.46	0.20	0.41
2)Ductwork & Dampers	Cont. Bldg. 68'	Independent	Flexible, Passive	Static Analysis	OBE	Generic	1.20	0.20	1.04	0.02	9.00	0.57	1.12	0.60	0.23	0.55
Auxiliary Feedwater System																
1)Motor Driven Pumps (2)	Aux. FP Bldg. 18'6"	Dependent	Rigid, Active	Static Analysis	SSE	Generic	1.20	0.20	3.62	0.11	23.0	0.50	15.0	0.55	0.20	0.51
2)Turbine Driven Pumps (1)	Aux. FP Bldg. 18'6"	NA	Rigid, Active	Static Analysis	SSE	Generic	1.20	0.20	3.62	0.11	23.0	0.50	15.0	0.55	0.20	0.51
3)Piping, 3"-4"	Aux. FP Bldg. 18'-62'	Independent	Flexible, Passive	Static Analysis	OBE	Generic	1.20	0.20	4.31	0.23	16.10	0.46	8.33	0.55	0.20	0.51
4)Valves (air operated)	Aux. FP Bldg. 18'6"	Independent	Rigid, Active	Static Analysis	SSE	Generic	1.20	0.20	1.09	0.32	26.07	0.60	5.11	0.71	0.31	0.64
5)Piping, 3'-6"	Aux. FP Bldg. 18'- 62'	Independent	Flexible, Passive	Response Spectrum	OBE	Generic	1.20	0.20	2.45	0.32	11.20	0.51	3.29	0.63	0.28	0.56
Reactor Protection System																
1)Logic Panels (Relays) (2)	Control Bldg. 53'	Dependent	Flexible, Active	Test	SSE	Plant Specific	0.86	0.19	0.66	0.27	59.60	0.35	5.07	0.48	0.22	0.43
2)Reactor Trip Breakers (2)	Control Bldg. 53'	Dependent	Flexible, Active	Test	SSE	Plant Specific	0.86	0.19	0.66	0.27	59.60	0.35	5.07	0.48	0.22	0.43
3)SIS Logic Panel (Relays)	Control Bldg. 53'	Dependent	Flexible, Active	Test	SSE	Plant Specific	0.86	0.19	0.66	0.27	59.60	0.35	5.07	0.48	0.22	0.43
4)Inst.& Process Panels	Control Bldg. 53'	Dependent	Flexible, Active	Test	SSE	Plant Specific	0.86	0.19	0.66	0.27	59.60	0.35	5.07	0.48	0.22	0.43
5)Control Rod Drive Mechanism	Cont. Bldg. 75'	Dependent	Flexible, Active	Response Spectrum	SSE	Plant Specific	1.20	0.20	2.87	0.26	5.50	0.24	2.84	0.41	0.20	0.36
Electric Power (480 VAC)																
1)Switchgear Incl. Station Serv. Transf. (4)	Control Bldg. 15'	Dependent	Flexible, Active	Test	SSE	Generic	0.86	0.19	1.02	0.22	11.51	0.50	1.51[2]	0.58	0.25	0.52
2)Diesel and Gas Turbine Generators	Grade	Dependent	Flexible, Active	None	SSE	Generic	0.93	0.16	0.81	0.23	11.51	0.50	1.30[2]	0.57	0.24	0.52
3)Motor Control Centers	Various Bldgs.	Dependent	Flexible, Active	Test	SSE	Generic	0.86	0.19	0.92	0.20	9.82	0.50	1.17[2]	0.57	0.24	0.52
4)Cable Trays	Various Bldgs.	Independent	Flexible, Passive	Static Analysis	SSE	Generic	0.86	0.19	1.08	0.11	15.8	0.55	2.20	0.59	0.27	0.52
Electric Power (6900 VAC)																
1)Switchgear (6 Buses, 2 Structures)	Turbine Bldg. 15'	Dependent	Flexible, Active	Test	SSE	Generic	1.60	0.39	1.02	0.22	11.51	0.50	2.82[2]	0.67	0.29	0.60
2)Station Aux. Transformer	Outdoors, at Grade	NA	Flexible, Active	Static Analysis	OBE	Generic	NA	NA	1.54	0.26	11.00	0.58	1.69	0.64	0.28	0.57
Electric Power (125 VDC)																
1)Batteries (2 Rooms)	Control Bldg. 33'	Dependent	Flexible, Passive	Test & Analysis	OBE	Generic	0.86	0.19	1.38	0.29	9.00	0.57	1.07	0.67	0.30	0.60
2)Batteries (1 Room)	Diesel Gen. Bldg. 15'	Dependent	Flexible, Passive	Static Analysis	OBE	Generic	0.93	0.16	1.54	0.26	9.00	0.57	1.29	0.65	0.28	0.59
Electric Power (120 VAC)																
1)Inverters (3)	Control Bldg. 33'	Dependent	Flexible, Active	Test	SSE	Plant Specific	0.86	0.19	0.66	0.27	47.30	0.35	4.03	0.48	0.29	0.38
2)Transformers	Control Bldg. 33'	Dependent	Flexible, Passive	Static Analysis	OBE	Generic	0.86	0.19	1.38	0.29	9.00	0.57	1.07[2]	0.67	0.30	0.60
3)Distribution Panels	Control Bldg. 53'	Dependent	Flexible, Active	Test	SSE	Generic	0.86	0.19	1.30	0.16	7.10	0.50	1.19[2]	0.56	0.28	0.48
Offsite Power																
Ceramic Insulators	Outside	Dependent	Flexible, Passive	No Qualification	NA	Generic	NA	NA	NA	NA	NA	NA	0.20[3]	0.32	0.20	0.25

Notes:

[1] Assumed to have the same capacity as Zion Components.

[2] Failure Mode is electrical malfunction due to relay chatter or breaker trip. Malfunction is recoverable. Permanent damage level estimated at 3 times value stated.

[3] From historical data.

TABLE 7.2-7

FRAGILITY OF KEY STRUCTURES AND EQUIPMENT - INDIAN POINT 3

Symbol	Structure/Equipment	$\bar{a}$	β_R	β_U
①	Offsite Power Transformer Ceramic Insulators	.20	.20	.25
②	Control Room Masonry Walls at Elevation 53'-0"	.33	.27	.24
③	Superheater Stack	.72	.34	.26
④	Condensate Storage Tank	.83	.28	.29
⑤	City Water Storage Tank	.83	.28	.29
⑥	Refueling Water Storage Tank	.83	.28	.29
⑦	Reactor Coolant System Pressurizer	.87	.23	.40
⑧	Fuel Storage Building Failure of Steel Frame	.92	.30	.26
⑨	Containment Spray System (CSS) Spray Additive Tank	1.01	.29	.53
⑩	Reactor Core Geometry	1.04	.21	.40
⑪	125 VDC Batteries in Control Building	1.07	.30	.60
⑫	120 VAC Transformers	1.07	.30	.60
⑬	Control Building Masonry Walls Enclosing Battery Rooms	1.10	.22	.29
⑭	Containment Ventilation System Duct Work and Dampers	1.12	.23	.55
⑮	Diesel Generator Fuel Oil Tanks	1.14	.26	.52
⑯	480V Motor Control Centers*	1.17	.24	.52
⑰	120 VAC Distribution Panels*	1.19	.28	.48
⑱	Control Building Shear Failure N-S Wall	1.20	.16	.23
⑲	125 VDC Batteries (in Diesel Generator Building)	1.29	.28	.59
⑳	Diesel Generators, Gas Turbines (Controls)*	1.30	.24	.52
㉑	CSS Spray Headers	1.32	.29	.54
㉒	RCS Relief Tank	1.37	.30	.53
㉓	CST Buried Piping 12"	1.40	.20	.57
㉔	Service Water System Buried 24" Piping	1.40	.20	.57
㉕	CSS Buried Piping 12"	1.40	.20	.57
㉖	CST Piping 6"-12"	1.46	.29	.56
㉗	RCS Power-Actuated Relief Valve	1.48	.35	.67
㉘	Diesel Generator Building Flexural Failure of Concrete Roof Diaphragm	1.50	.25	.35
㉙	480 VAC Switchgear Including Station Service Transformer*	1.51	.25	.52
㉚	6,900 VAC Station Auxiliary Transformer	1.69	.28	.57
㉛	RHR Pumps	1.70	.15	.34
㉜	Containment Building Shear Failure Containment Wall/Auxiliary Feed Pump Building	1.70	.31	.26
㉝	RCS Steam Generator	1.84	.26	.43
㉞	CSS Pipe 6"	1.84	.30	.54
㉟	Buried Concrete Structures	1.90	.23	.24

*Fragility values indicated are for chatter, relay trip, or other intermittent or easily recoverable conditions. Nonrecoverable failure is expected to occur at about three times the indicated fragility value.

TABLE 7.2-8

INDIAN POINT 3 SEISMIC CONDITIONAL RELEASE FREQUENCY - MATRIX MC^S

20% Probability Each Table

Acceleration (g)	Release Category				
	Z-1Q	Z-1	2RW	8A	8B
.125	0	0	0	0	0
.175	0	0	0	0	0
.225	0	0	0	0	0
.275	0	0	0	2.71E-11	0
.35	0	0	7.11E-08	1.02E-07	0
.45	0	2.22E-12	2.02E-05	2.60E-05	0
.55	1.22E-06	3.24E-09	7.91E-04	7.62E-04	8.05E-08
.65	1.49E-05	1.76E-07	8.35E-03	5.83E-03	3.44E-06
.75	1.02E-04	2.58E-06	3.99E-02	1.42E-02	8.78E-06
.85	4.67E-04	1.60E-05	1.23E-01	1.06E-02	7.68E-06

Acceleration (g)	Release Category				
	Z-1Q	Z-1	2RW	8A	8B
.125	0	0	0	0	0
.175	0	0	0	0	0
.225	0	0	0	4.34E-13	0
.275	0	0	4.27E-10	3.75E-09	0
.35	0	0	1.18E-05	1.44E-06	0
.45	1.16E-06	6.28E-10	6.61E-04	2.34E-04	5.72E-07
.55	2.29E-05	1.18E-07	8.26E-03	4.75E-03	1.45E-05
.65	2.02E-04	3.37E-06	4.96E-02	2.49E-02	1.10E-04
.75	1.05E-03	2.94E-05	1.74E-01	4.56E-02	3.19E-04
.85	3.77E-03	1.20E-04	3.82E-01	3.99E-02	2.20E-04

Acceleration (g)	Release Category				
	Z-1Q	Z-1	2RW	8A	8B
.125	0	0	0	0	0
.175	0	0	0	0	0
.225	0	0	0	1.41E-10	0
.275	0	0	2.72E-06	3.90E-08	0
.35	0	6.05E-12	1.80E-04	9.88E-06	3.20E-07
.45	9.03E-06	1.80E-08	4.94E-03	1.01E-03	3.10E-05
.55	1.36E-04	1.51E-06	3.91E-02	1.52E-02	4.55E-04
.65	9.63E-04	2.42E-05	1.50E-01	6.28E-02	1.83E-03
.75	4.15E-03	1.41E-04	3.57E-01	1.07E-01	2.51E-03
.85	1.27E-02	4.30E-04	6.05E-01	1.05E-01	1.59E-03

Acceleration (g)	Release Category				
	Z-1Q	Z-1	2RW	8A	8B
.125	0	0	0	0	0
.175	0	0	1.86E-10	6.45E-18	0
.225	0	0	1.34E-07	2.49E-09	1.03E-09
.275	0	1.93E-14	1.43E-05	3.87E-07	1.16E-07
.35	1.57E-06	6.66E-10	9.80E-04	6.49E-05	1.54E-05
.45	5.87E-05	3.67E-07	2.80E-02	4.06E-03	7.35E-04
.55	6.78E-04	1.47E-05	1.76E-01	4.28E-02	6.20E-03
.65	3.85E-03	1.37E-04	4.63E-01	1.37E-01	1.58E-02
.75	1.38E-02	5.36E-04	7.32E-01	2.20E-01	1.50E-02
.85	3.59E-02	1.17E-03	8.58E-01	2.56E-01	8.69E-03

Acceleration (g)	Release Category				
	Z-1Q	Z-1	2RW	8A	8B
.125	0	0	0	0	3.24E-13
.175	0	1.86E-15	1.68E-06	1.25E-10	1.43E-09
.225	0	1.61E-11	1.16E-04	9.13E-08	3.56E-07
.275	0	5.35E-09	1.81E-03	9.25E-06	1.86E-05
.35	2.85E-05	1.15E-06	2.40E-02	8.90E-04	9.87E-04
.45	6.55E-04	5.98E-05	1.61E-01	2.71E-02	1.94E-02
.55	5.13E-03	5.17E-04	4.31E-01	1.51E-01	8.02E-02
.65	2.13E-02	1.79E-03	7.00E-01	3.43E-01	1.31E-01
.75	5.87E-02	3.78E-03	8.68E-01	4.92E-01	1.28E-01
.85	1.23E-01	6.11E-03	9.47E-01	5.24E-01	9.06E-02

TABLE 7.2-9

REVISED FRAGILITIES OF KEY STRUCTURES AND EQUIPMENT - INDIAN POINT 3

Symbol	Structure/Equipment	$\bar{a}$	β_R	β_U
(1)	Offsite Power Transformer Ceramic Insulators	.20	.20	.25
(2) *	Control Room Masonry Walls at Elevation 53'-0"	.48	.30	.40
(3)	Superheater Stack	.72	.34	.26
(4) *	Condensate Storage Tank	1.28	.22	.25
(5) *	City Water Storage Tank	.25	.25	.30
(6) *	Refueling Water Storage Tank	.70	.22	.28
(7)	Reactor Coolant System Pressurizer	.87	.23	.40
(8)	Fuel Storage Building Failure of Steel Frame	.92	.30	.26
(9)	Containment Spray System (CSS) Spray Additive Tank	1.01	.29	.53
(10)	Reactor Core Geometry	1.04	.21	.40
(11)	125 VDC Batteries in Control Building	1.07	.30	.60
(12)	120 VAC Transformers	1.07	.30	.60
(13) *	Control Building Masonry Walls Enclosing Battery Rooms	.48	.30	.40
(14)	Containment Ventilation System Duct Work and Dampers	1.12	.23	.55
(15)	Diesel Generator Fuel Oil Tanks	1.14	.26	.52
(16) **	480V Motor Control Centers	1.17	.24	.52
(17) **	120 VAC Distribution Panels	1.19	.28	.48
(18)	Control Building Shear Failure N-S Wall	1.20	.16	.23
(19)	125 VDC Batteries (in Diesel Generator Building)	1.29	.28	.59
(20) **	Diesel Generators, Gas Turbines (Controls)	1.30	.24	.52
(21)	CSS Spray Headers	1.32	.29	.54
(22)	RCS Relief Tank	1.37	.30	.53
(23)	CST Buried Piping 12"	1.40	.20	.57
(24)	Service Water System Buried 24" Piping	1.40	.20	.57
(25)	CSS Buried Piping 12"	1.40	.20	.57
(26)	CST Piping 6"-12"	1.46	.29	.56
(27)	RCS Power-Actuated Relief Valve	3.17	.35	.61
(28)	Diesel Generator Building Flexural Failure of Concrete Roof Diaphragm	1.50	.25	.35
(29) **	480 VAC Switchgear Including Station Service Transformer	1.51	.25	.52
(30)	6,900 VAC Station Auxiliary Transformer	1.69	.28	.57
(31)	RHR Pumps	1.70	.15	.34
(32)	Containment Building Shear Failure Containment Wall/Auxiliary Feed Pump Building	2.40	.34	.33
(33)	RCS Steam Generator	1.84	.26	.43
(34)	CSS Pipe 6"	1.84	.30	.54
(35)	Buried Concrete Structures	1.90	.23	.24

*Corrected or revised in accordance with information determined since the IPPSS NRC review.

**Fragility values indicated are for chatter, relay trip, or other intermittent or easily recoverable conditions. Nonrecoverable failure is expected to occur at about three times the indicated fragility value.

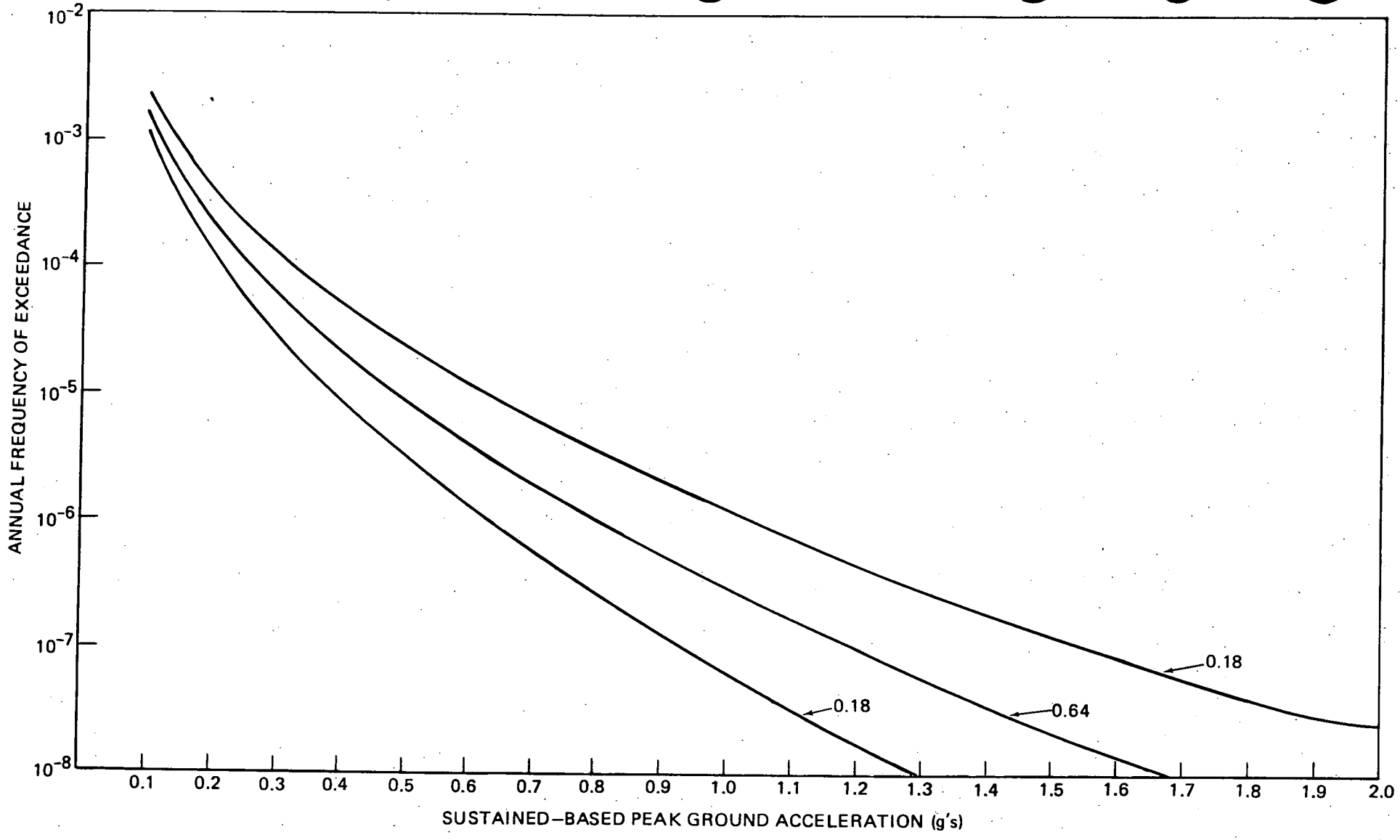


Figure 7.2-1. Seismicity Family Dames & Moore (NE Zones)

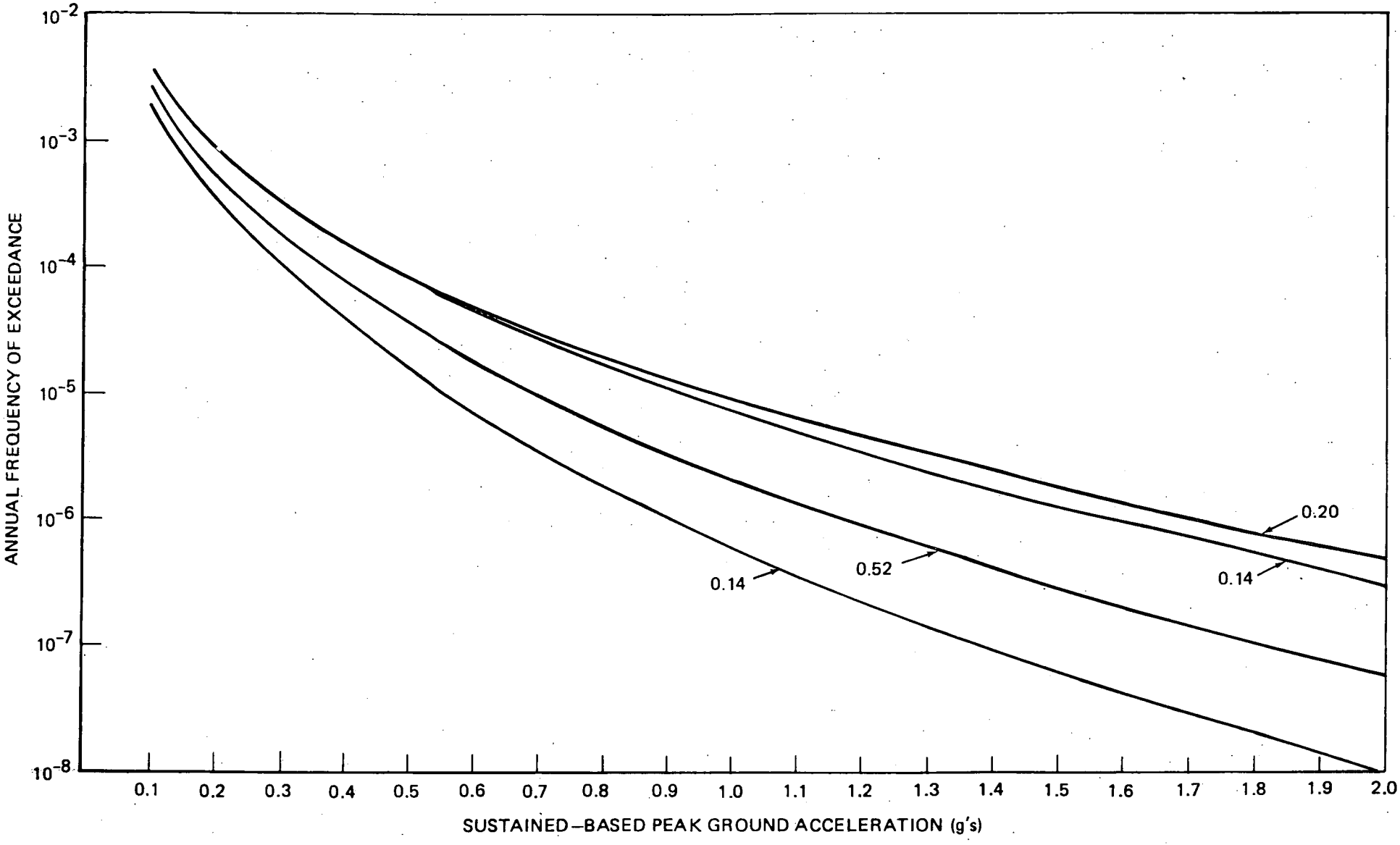


Figure 7.2-2. Seismicity Family Dames & Moore (Piedmont Zones)

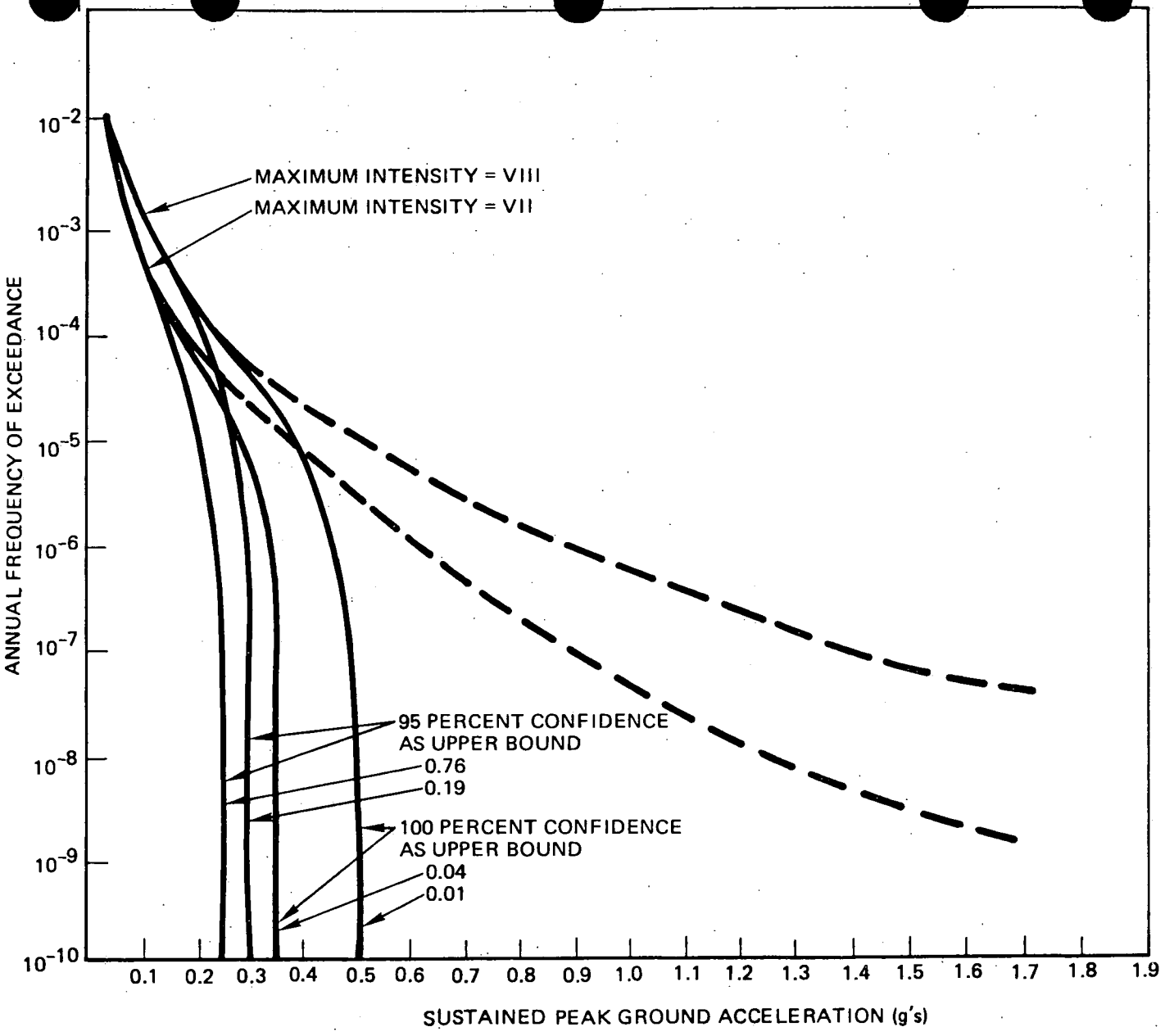


Figure 7.2-3. Seismicity Family Woodward-Clyde

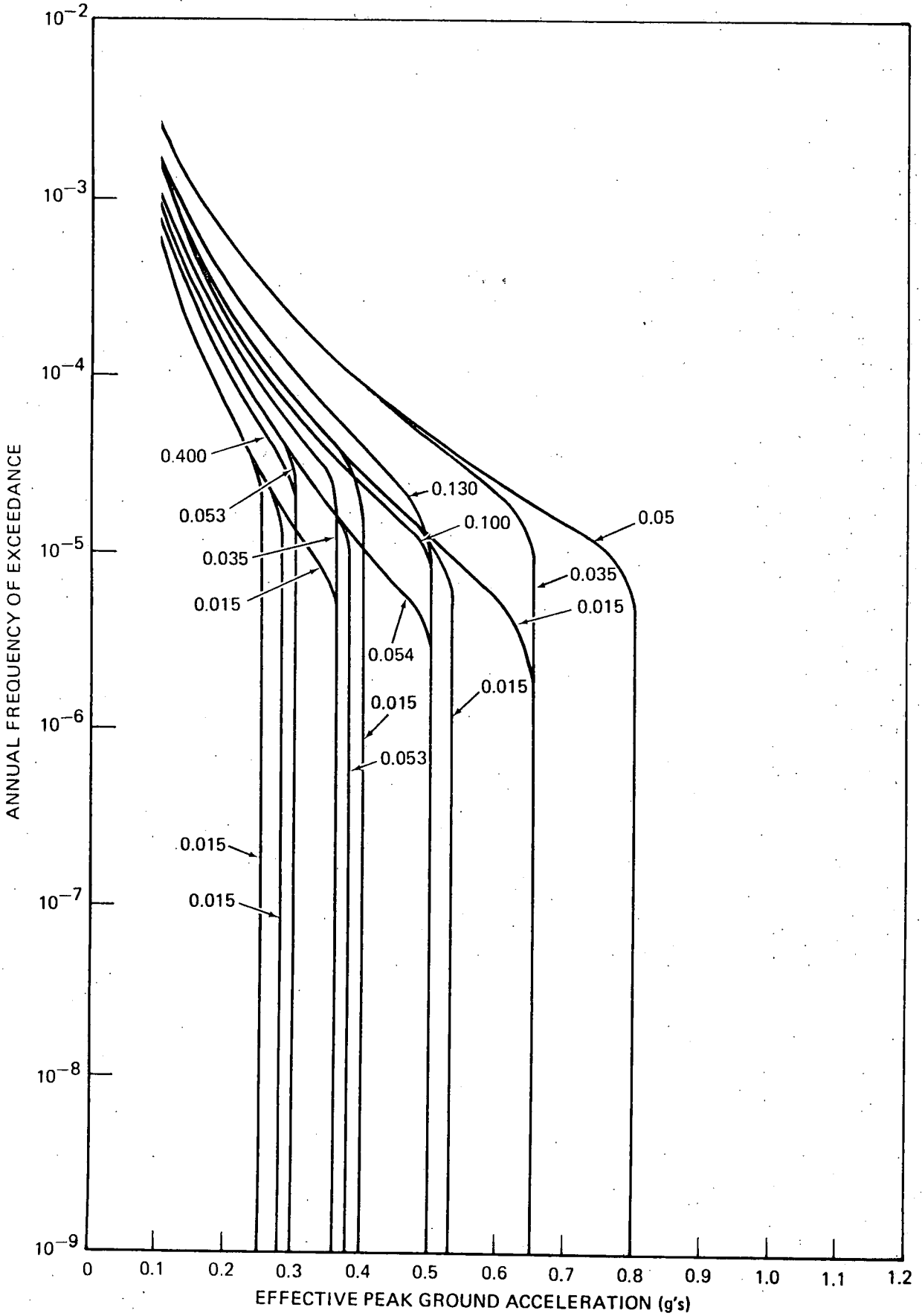


Figure 7.2-4. Seismicity Family Summary

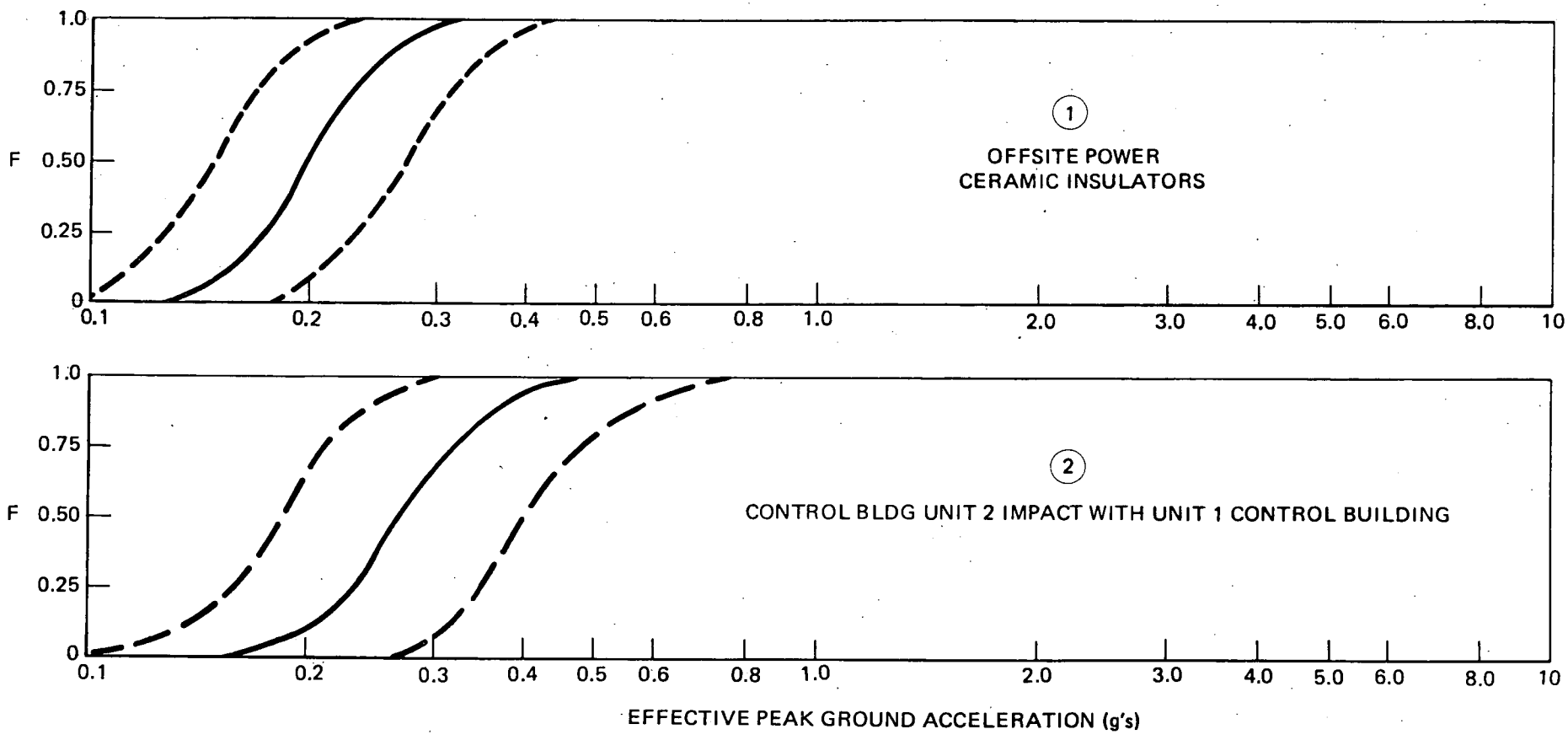


Figure 7.2-5. Fragility Families for Key Indian Point 2 Components (Sheet 1 of 5)

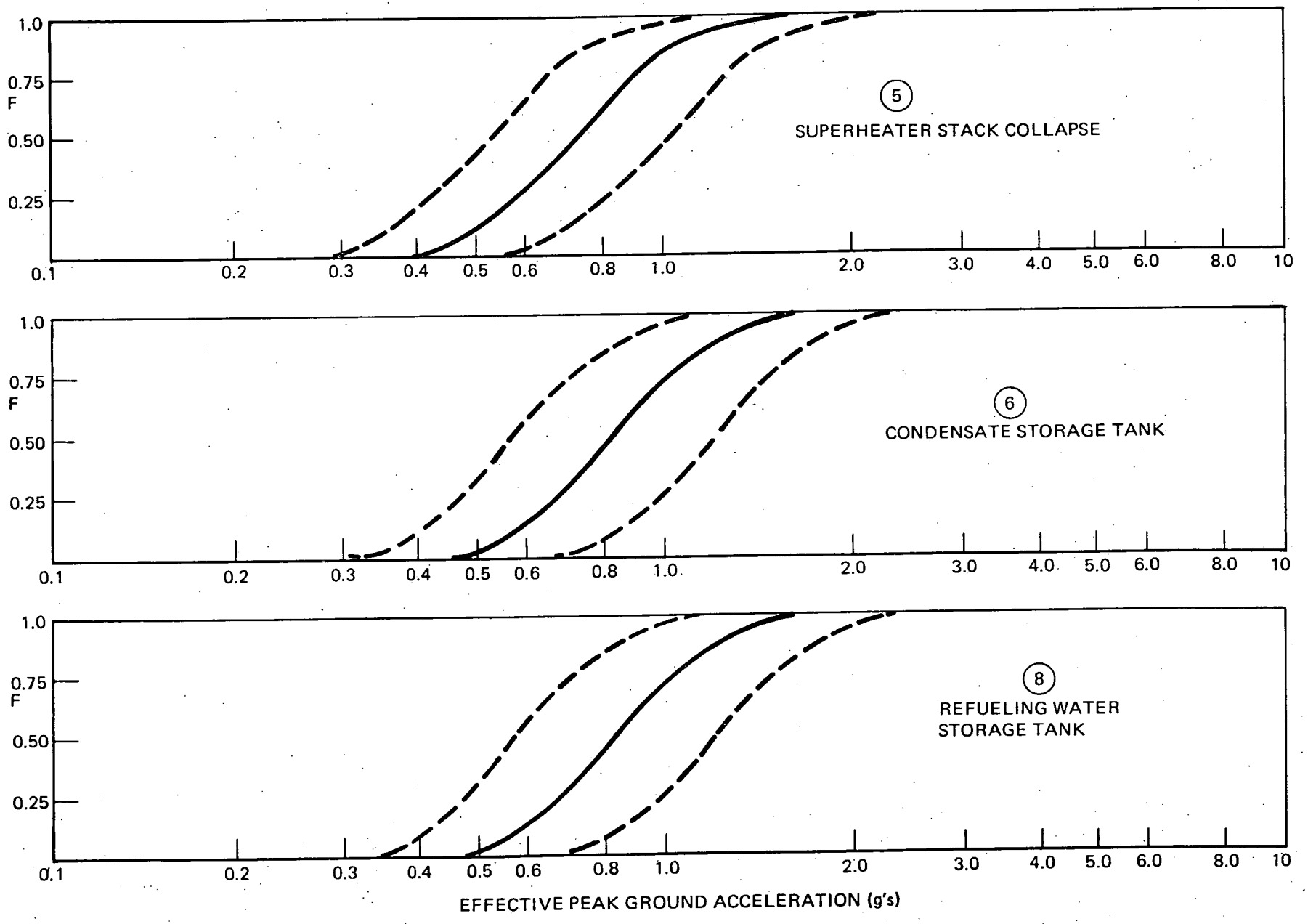


Figure 7.2-5. (Sheet 2 of 5)

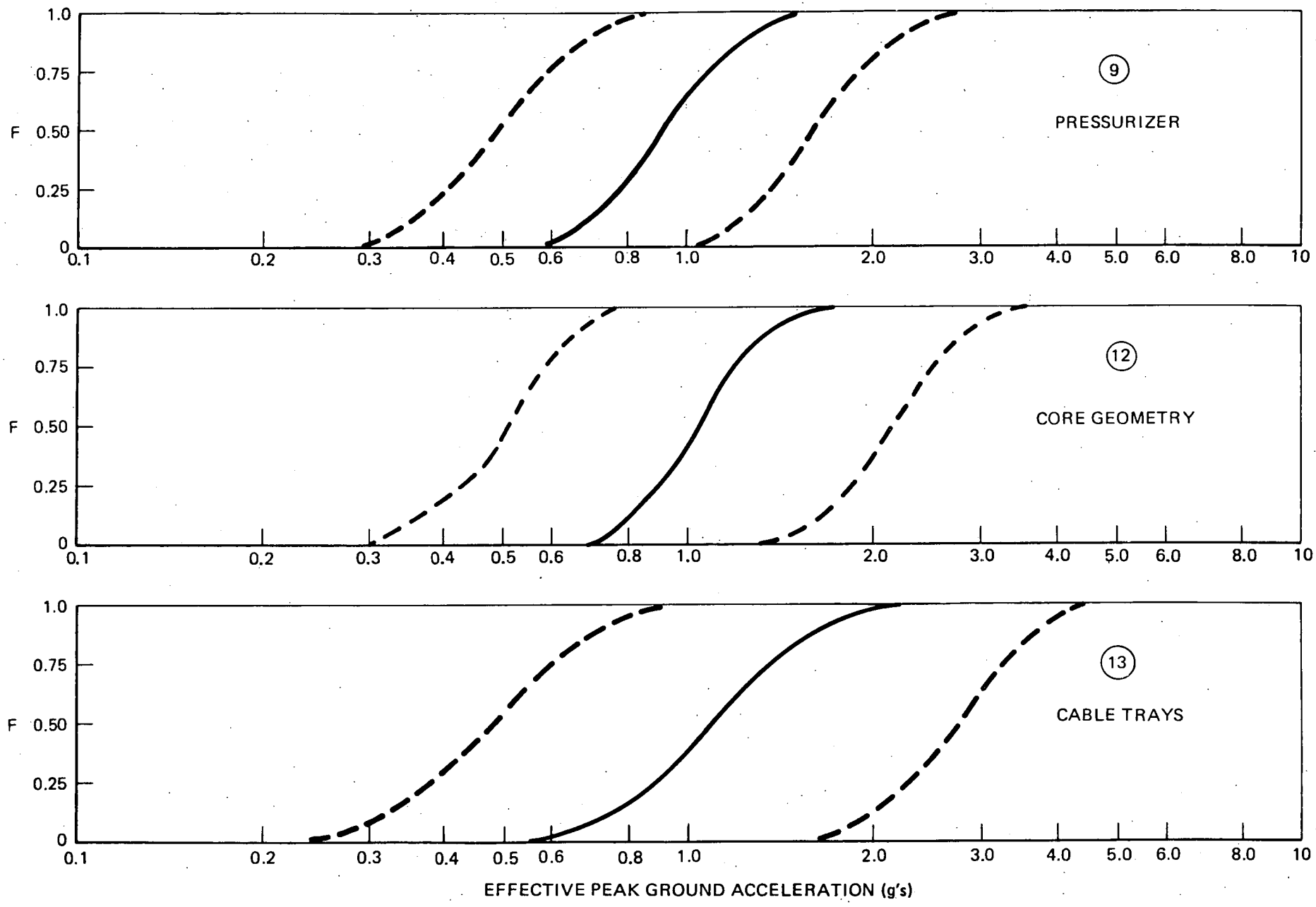


Figure 7.2-5. (Sheet 3 of 5)

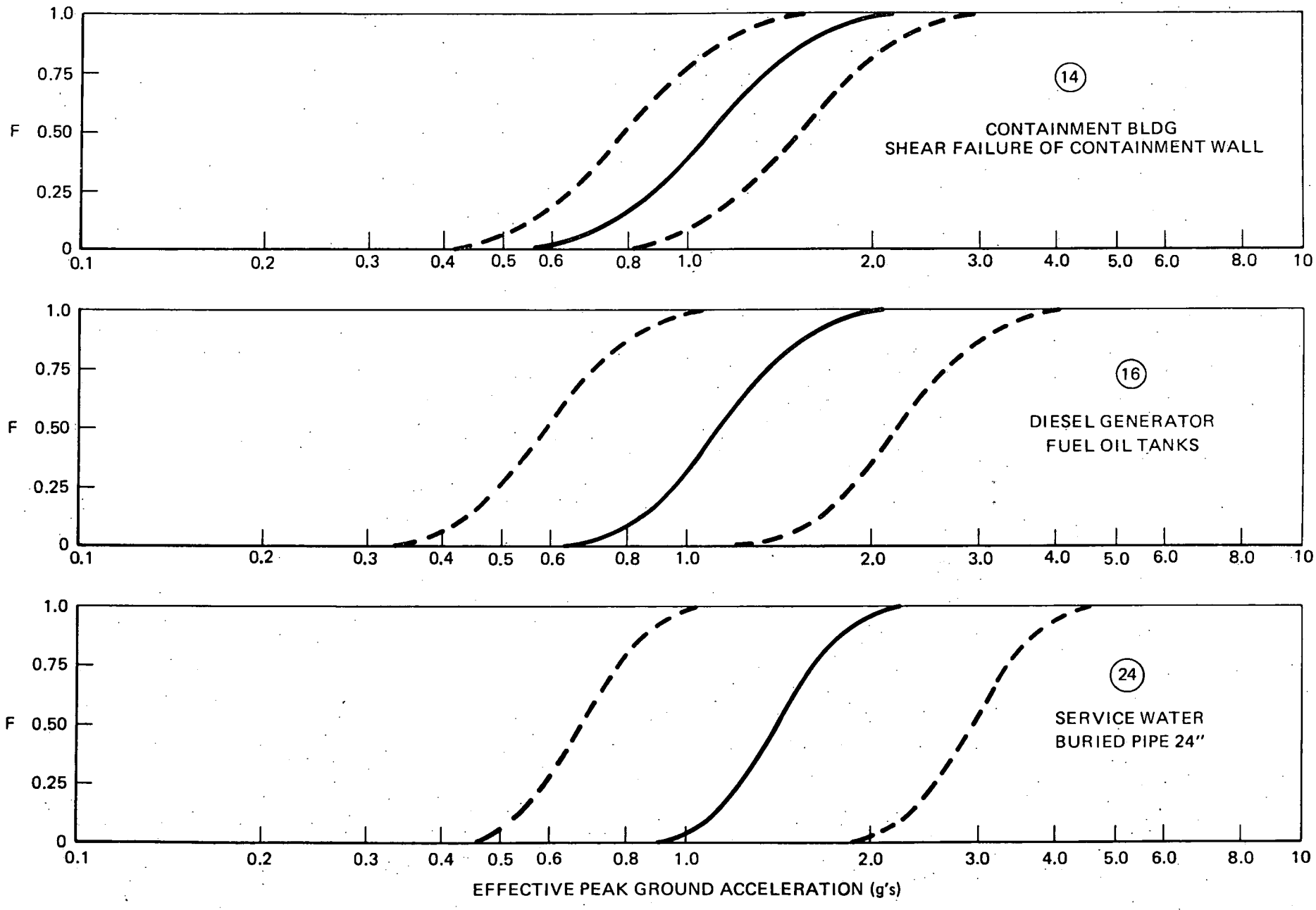


Figure 7.2-5. (Sheet 4 of 5)

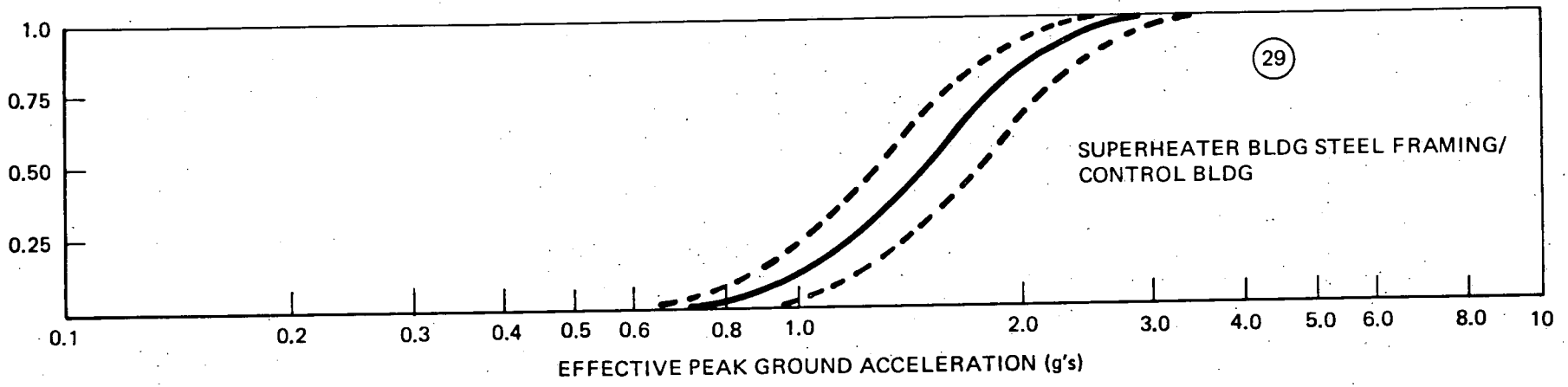
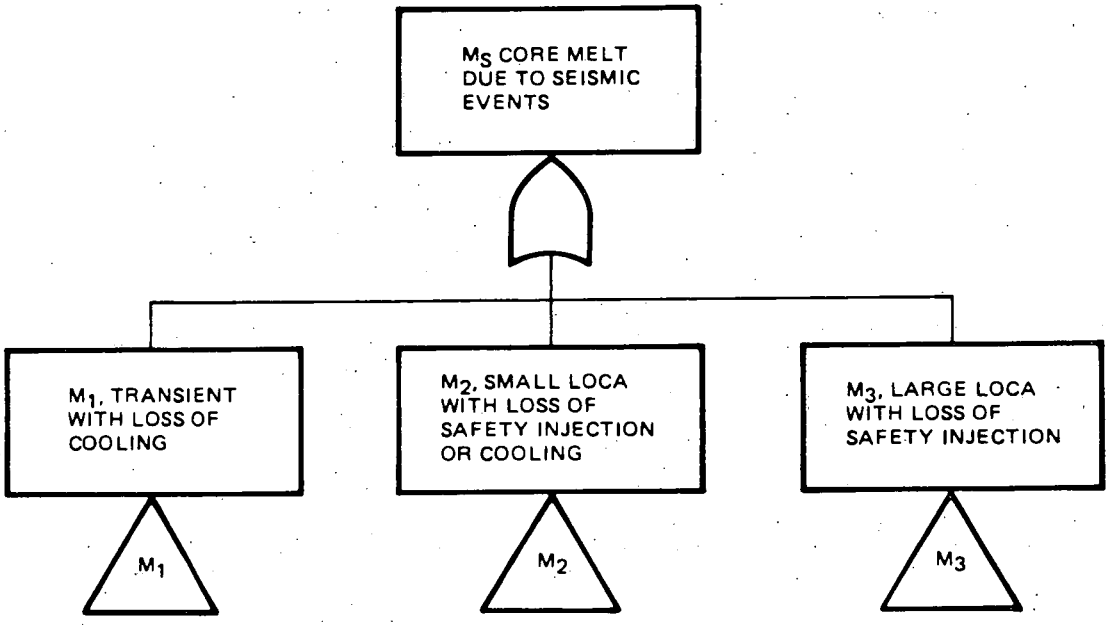


Figure 7.2-5. (Sheet 5 of 5)



NOTES:
1. SYMBOLS IN TRIANGLES Δ REFER TO OTHER FAULT TREE DEVELOPMENT.

Figure 7.2-6a. Indian Point Unit 2 Seismic Core Melt Fault Tree

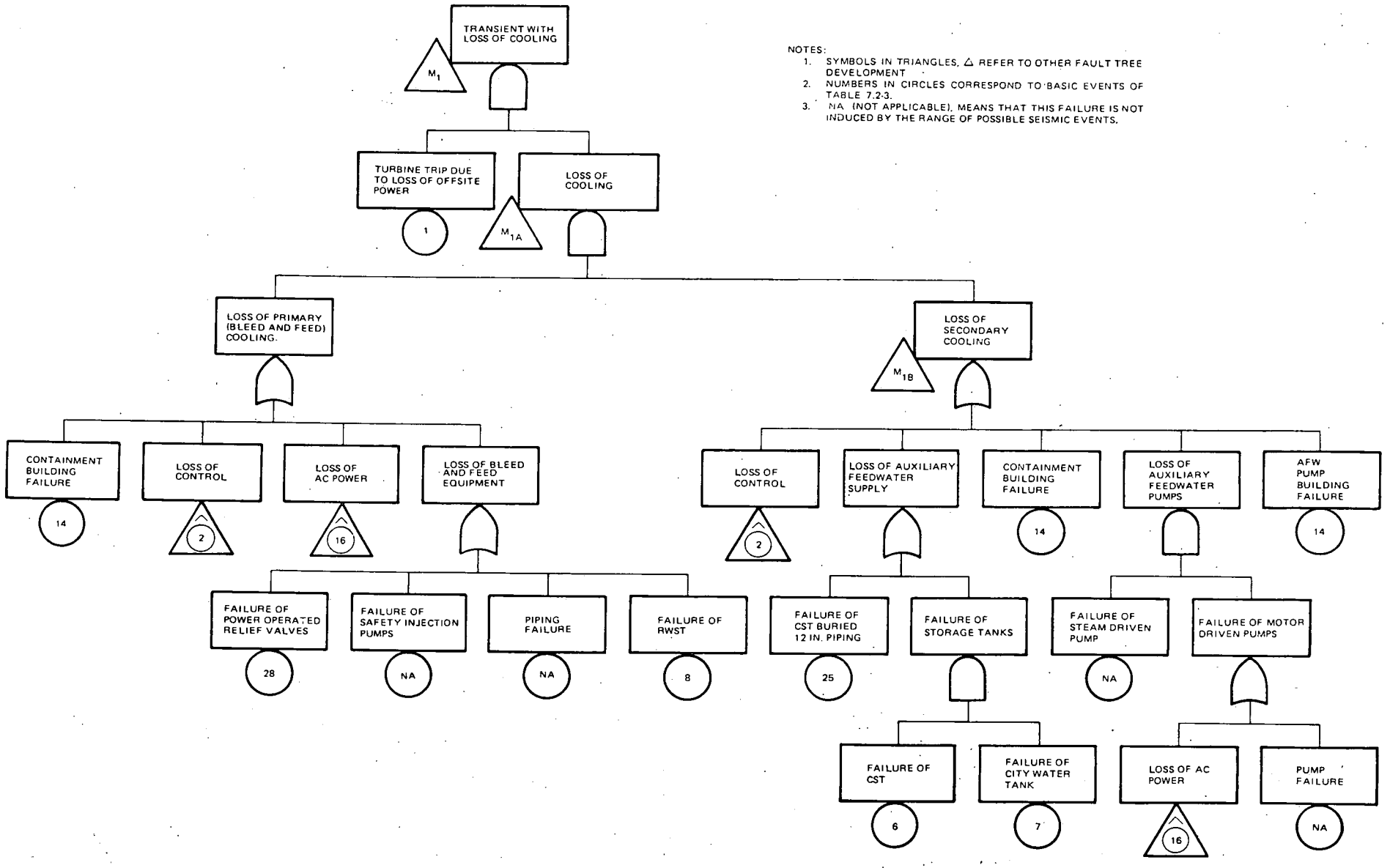
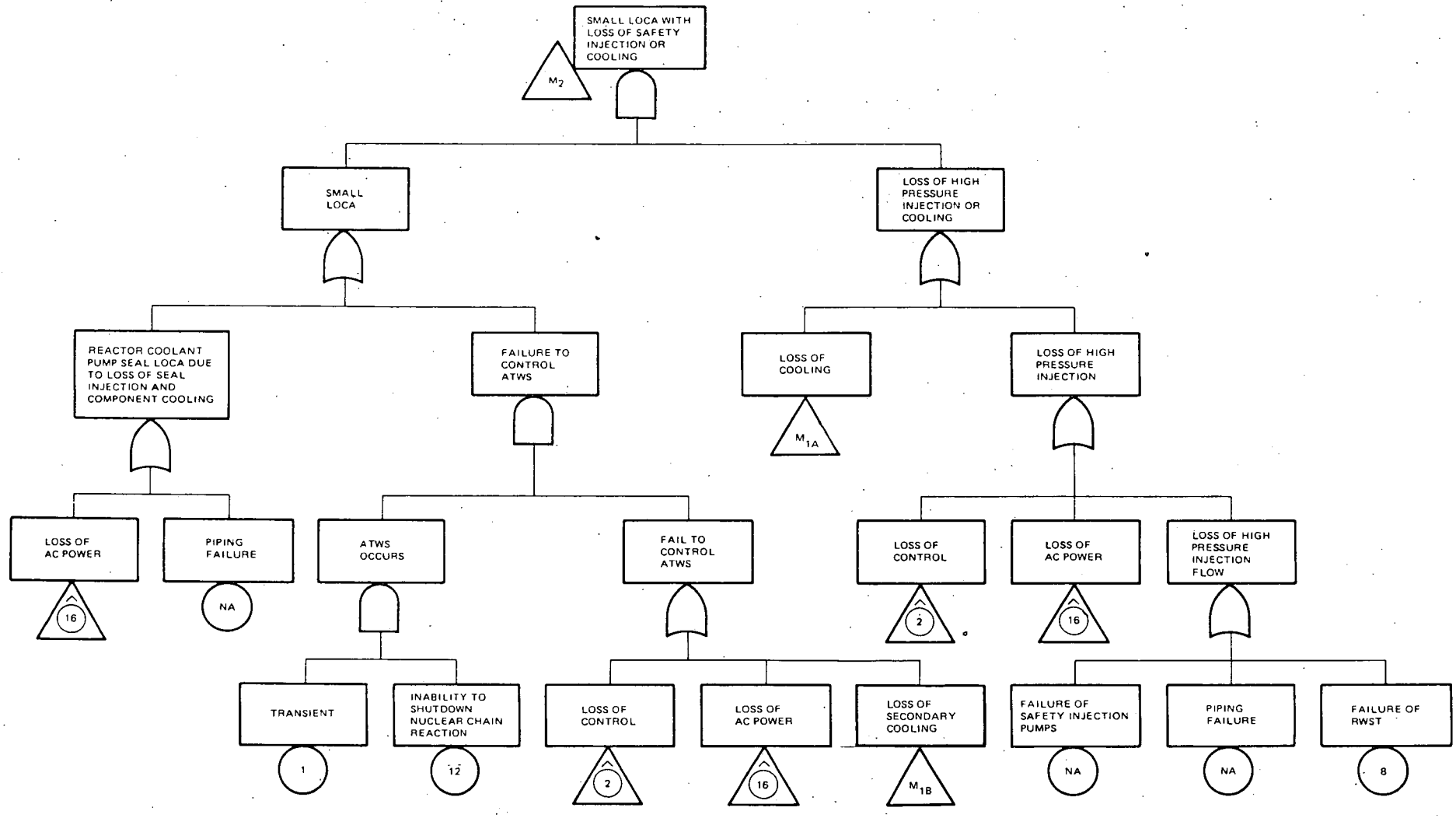
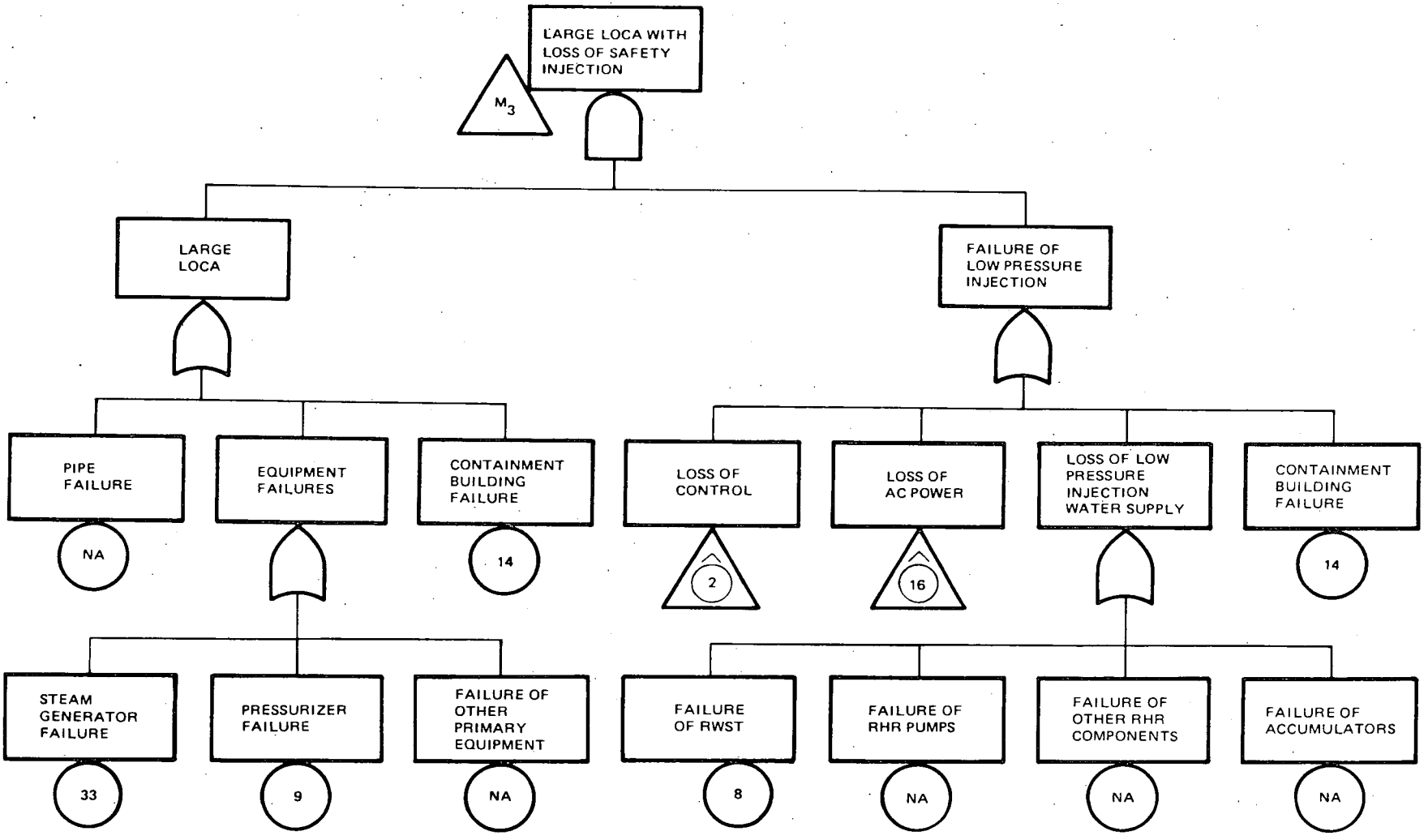


Figure 7.2-6b. Indian Point Unit 2 Seismic Core Melt Fault Tree (continued)



NOTES:
1. SYMBOLS IN TRIANGLES, Δ, REFER TO OTHER FAULT TREE DEVELOPMENT
2. NUMBERS IN CIRCLES CORRESPOND TO BASIC EVENTS OF TABLE 7.2-3
3. (NA) (NOT APPLICABLE), MEANS THAT THIS FAILURE IS NOT INDUCED BY THE RANGE OF POSSIBLE SEISMIC EVENTS.

Figure 7.2-6c. Indian Point Unit 2 Seismic Core Melt Fault Tree (continued)



NOTES:

1. SYMBOLS IN TRIANGLES, △ REFER TO OTHER FAULT TREE DEVELOPMENT.
2. NUMBERS IN CIRCLES CORRESPOND TO BASIC EVENTS OF TABLE 7.2-3.
3. (NA) (NOT APPLICABLE), MEANS THAT THIS FAILURE IS NOT INDUCED BY THE RANGE OF POSSIBLE SEISMIC EVENTS.

Figure 7.2-6d. Indian Point Unit 2 Seismic Core Melt Fault Tree (continued)

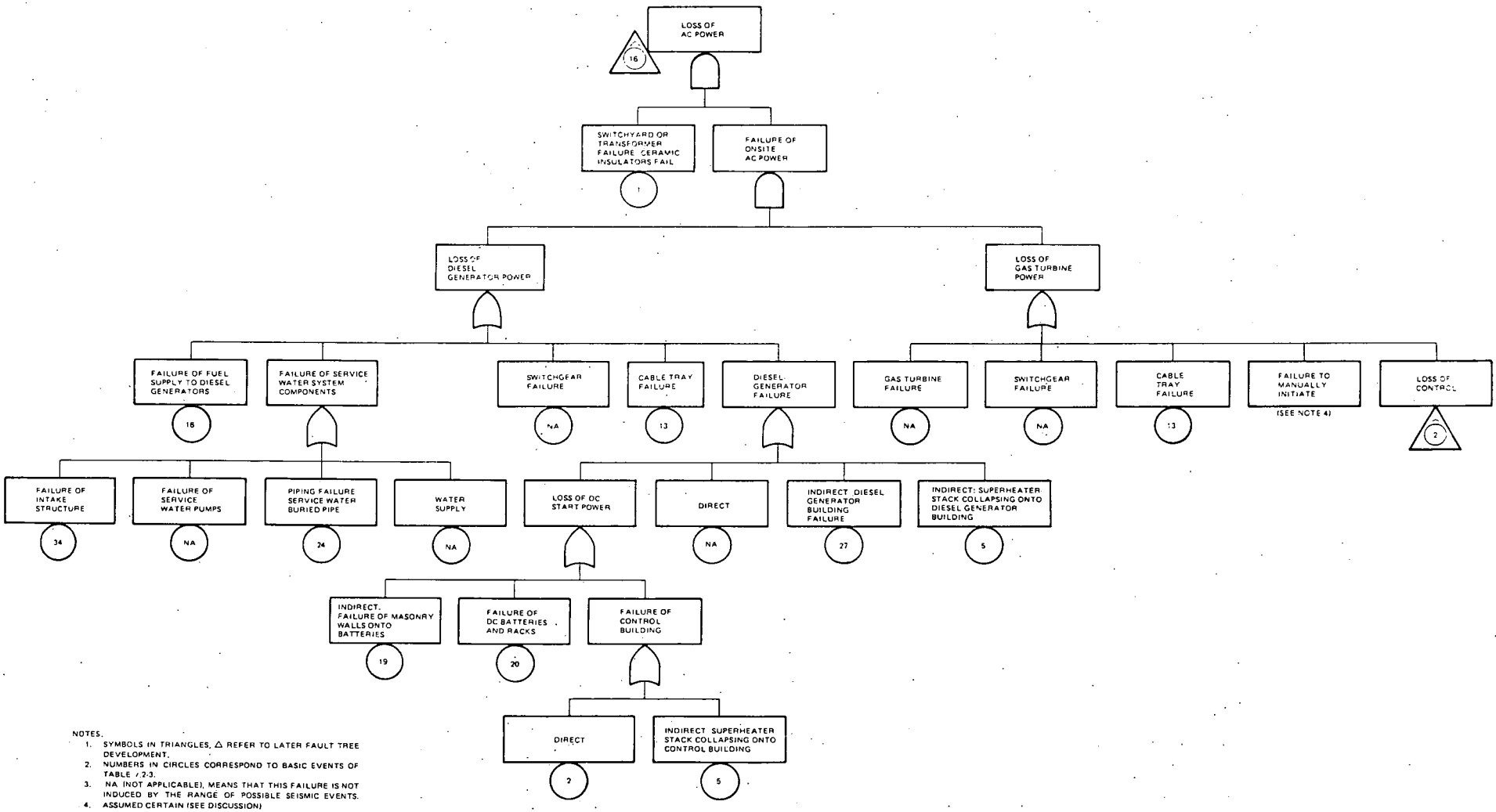
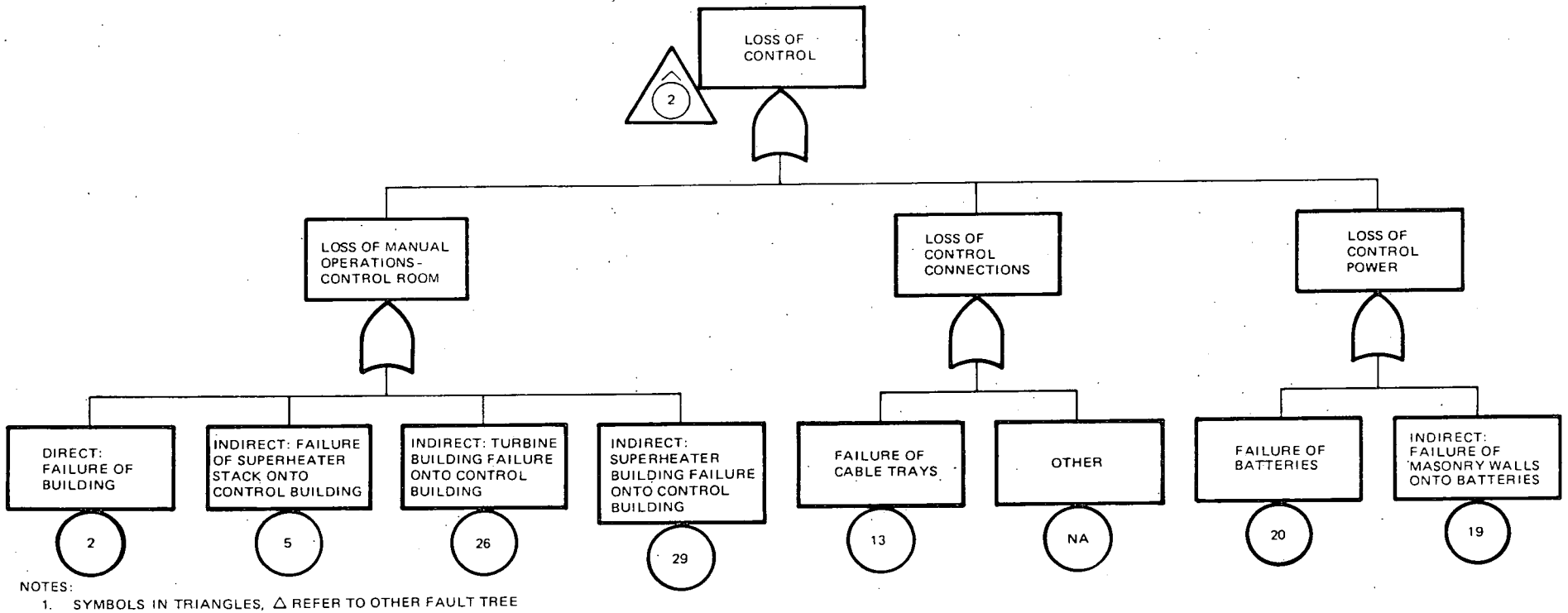


Figure 7.2-6e. Indian Point Unit 2 Seismic Core Melt Fault Tree (continued)



NOTES:

1. SYMBOLS IN TRIANGLES, △ REFER TO OTHER FAULT TREE DEVELOPMENT.
2. NUMBERS IN CIRCLES CORRESPOND TO BASIC EVENTS OF TABLE 7.2-3.
3. NA (NOT APPLICABLE), MEANS THAT THIS FAILURE IS NOT INDUCED BY THE RANGE OF POSSIBLE SEISMIC EVENTS.

Figure 7.2-6f. Indian Point Unit 2 Seismic Core Melt Fault Tree (continued)

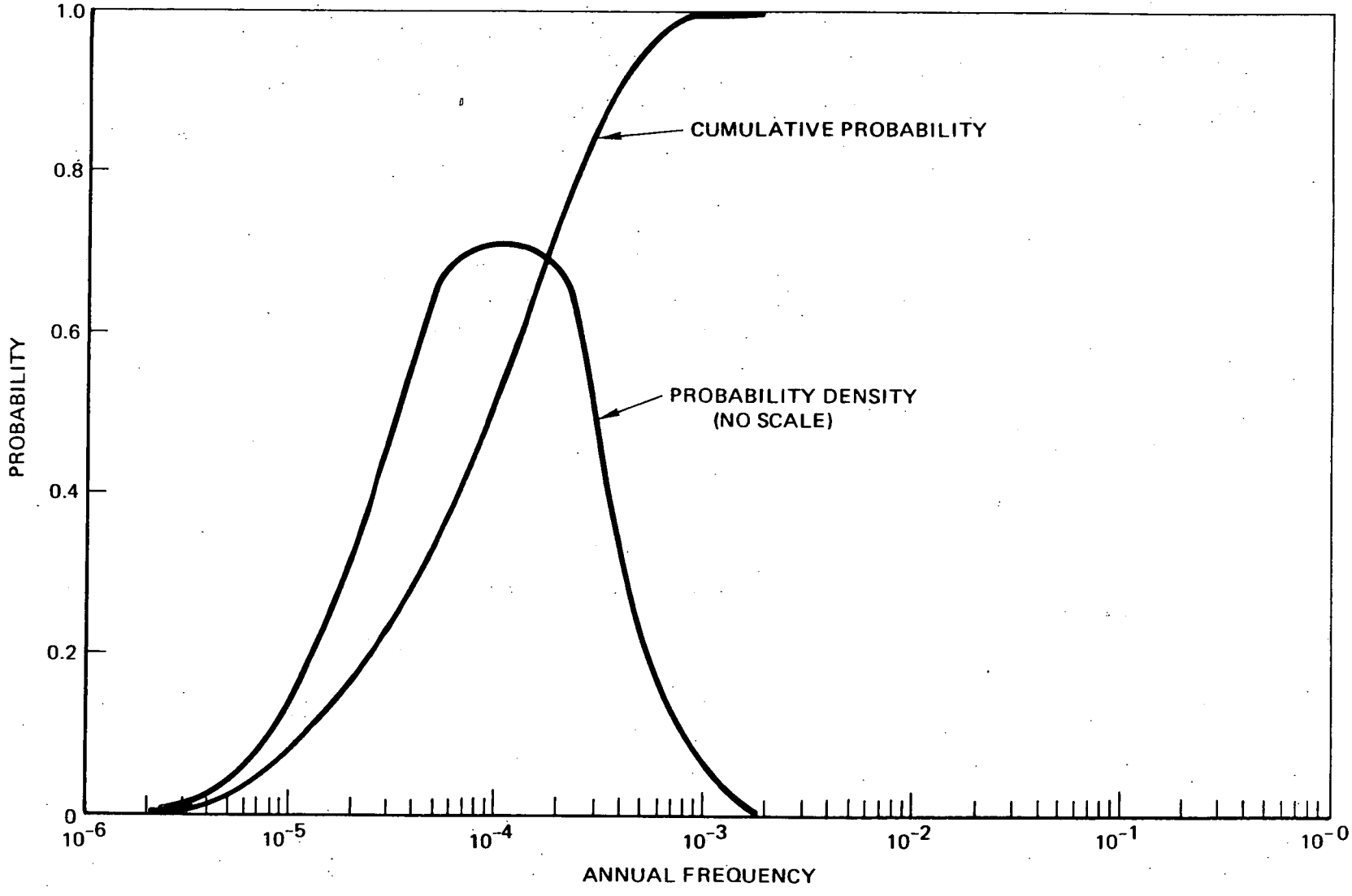
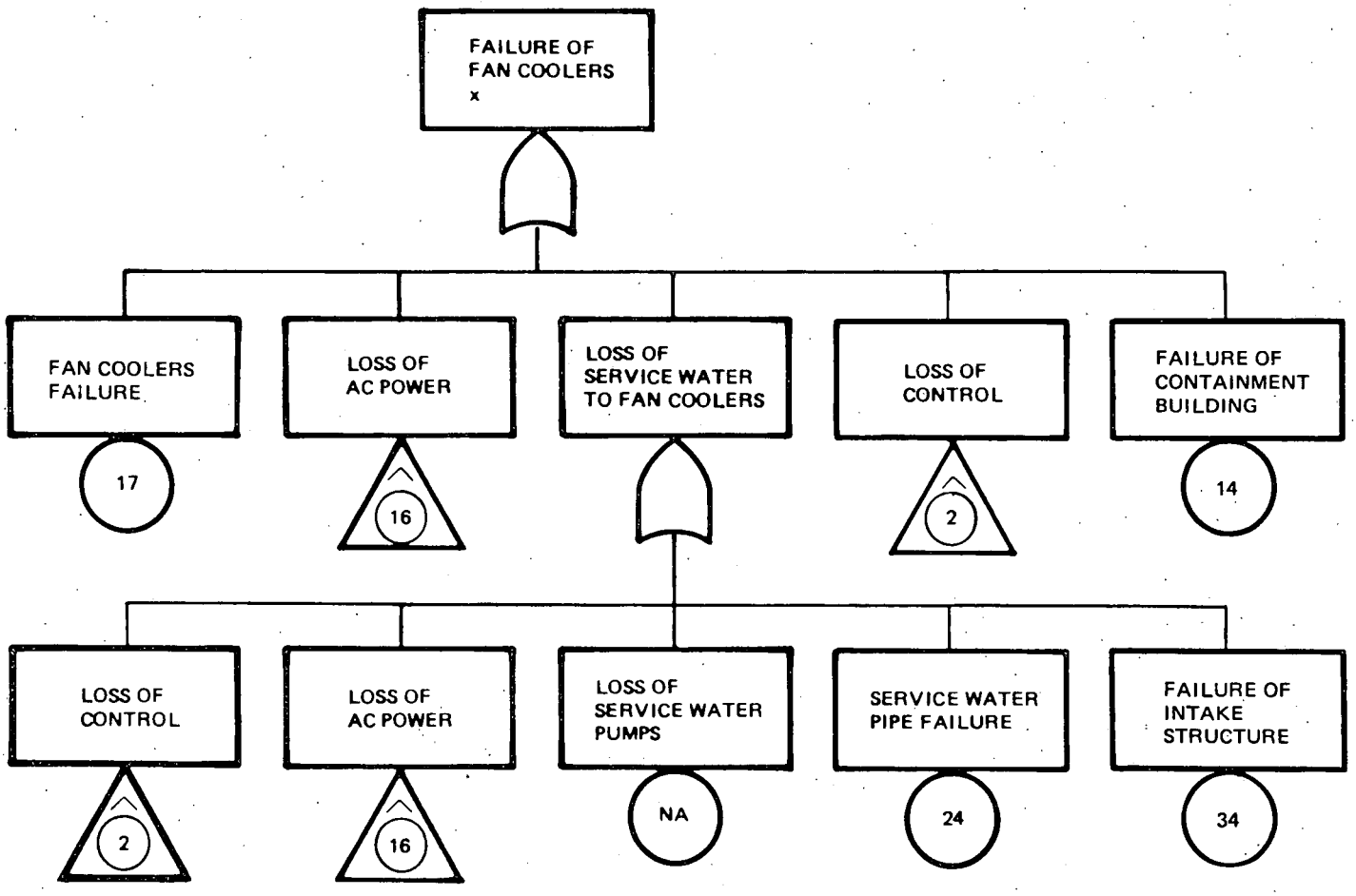


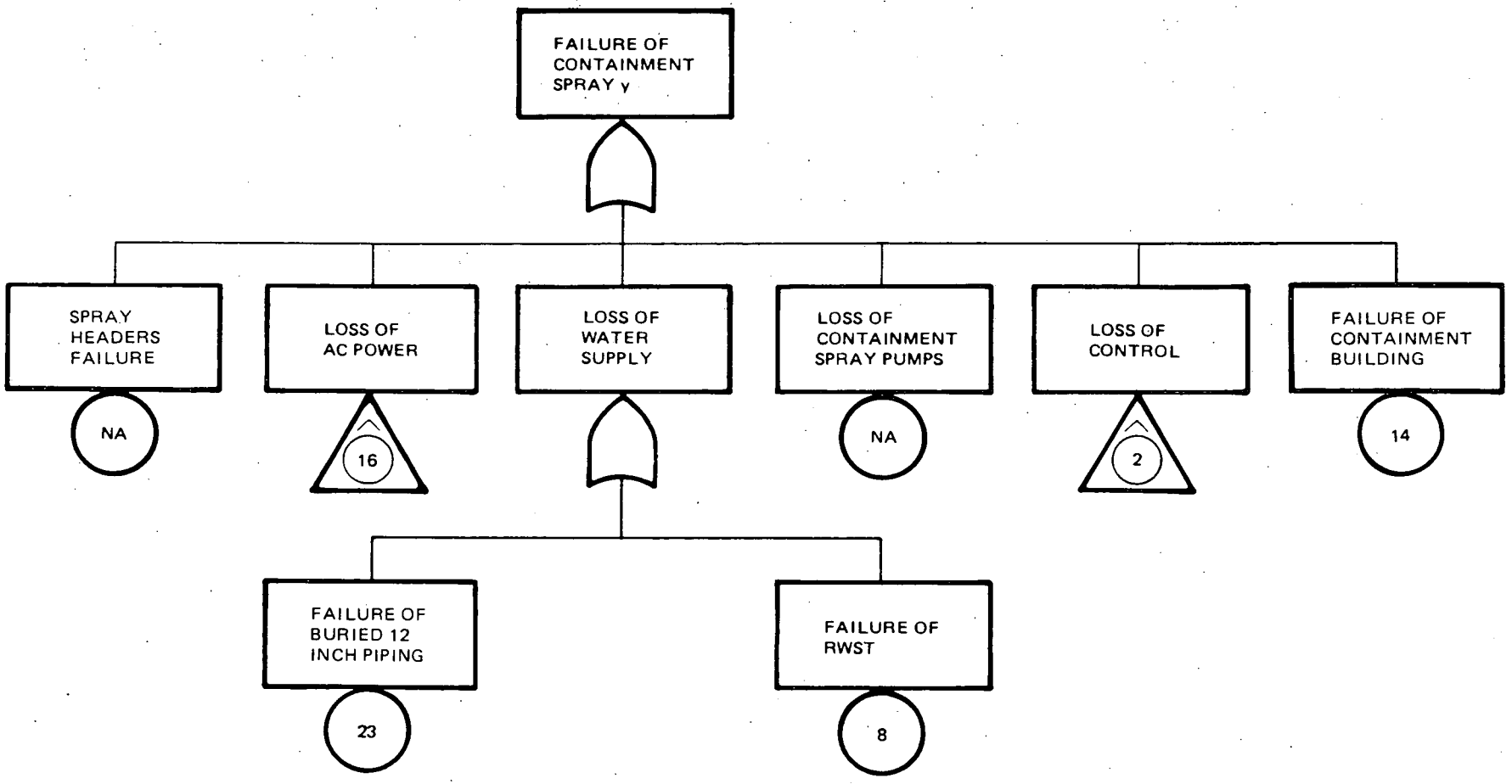
Figure 7.2-7. Indian Point Unit 2 Seismic Core Melt Frequency



NOTES:

1. SYMBOLS IN TRIANGLES, Δ, REFER TO OTHER FAULT TREE DEVELOPMENT.
2. NUMBERS IN CIRCLES CORRESPOND TO BASIC EVENTS OF TABLE 7.2-3.
3. (NA) (NOT APPLICABLE) MEANS THAT THIS FAILURE IS NOT INDUCED BY THE RANGE OF POSSIBLE SEISMIC EVENTS.

Figure 7.2-8. Indian Point Unit 2 Seismic Fan Coolers Fault Tree



NOTES:

1. SYMBOLS IN TRIANGLES, Δ, REFER TO OTHER FAULT TREE DEVELOPMENT.
2. NUMBERS IN CIRCLES CORRESPOND TO BASIC EVENTS OF TABLE 7.2-3.
3. (NA) (NOT APPLICABLE) MEANS THAT THIS FAILURE IS NOT INDUCED BY THE RANGE OF POSSIBLE SEISMIC EVENTS.

Figure 7.2-9. Indian Point Unit 2 Seismic Containment Spray Fault Tree

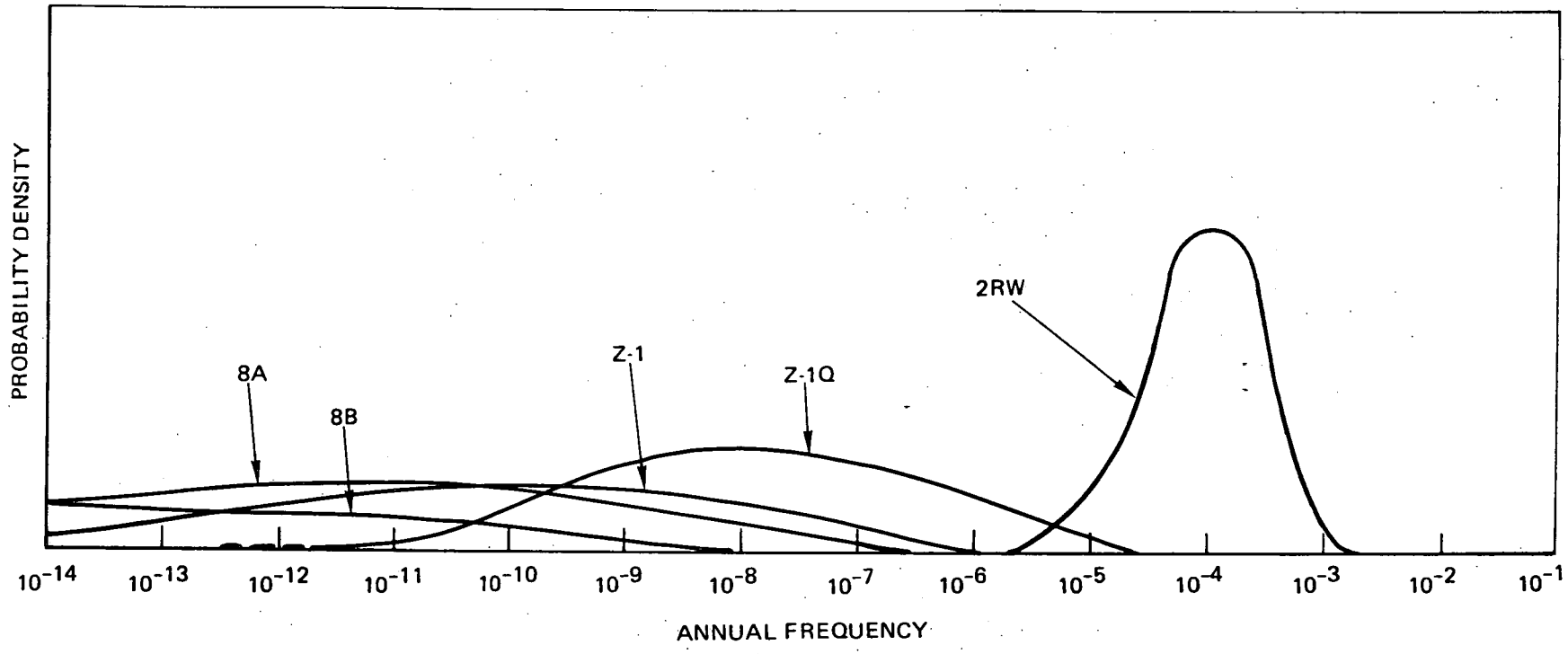


Figure 7.2-10. Release Frequency from Seismic Events - Indian Point Unit 2

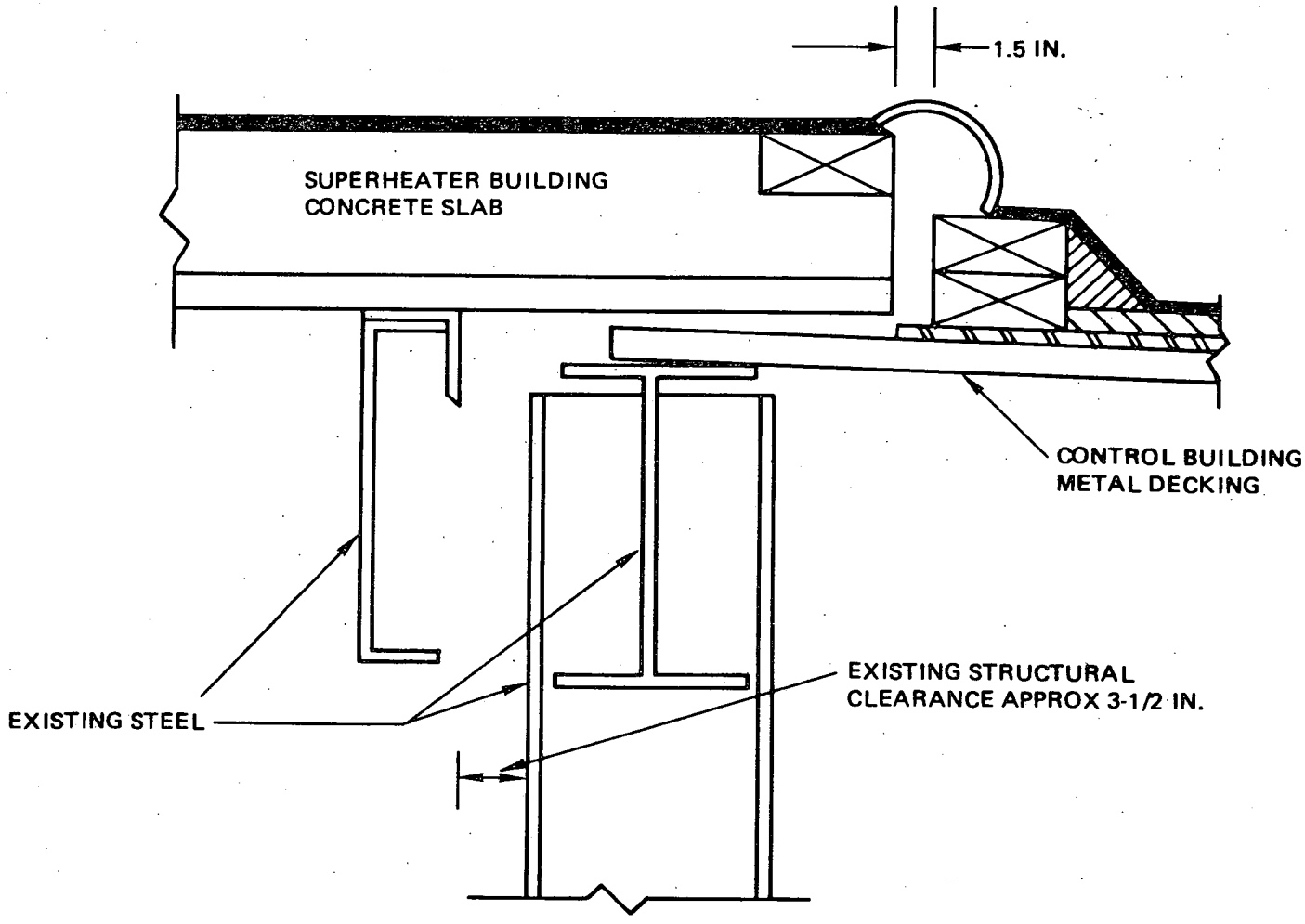


Figure 7.2.10A-1. Existing Configuration of Control Building and Superheater Building at Elevation 72'-0" (Indian Point 2)

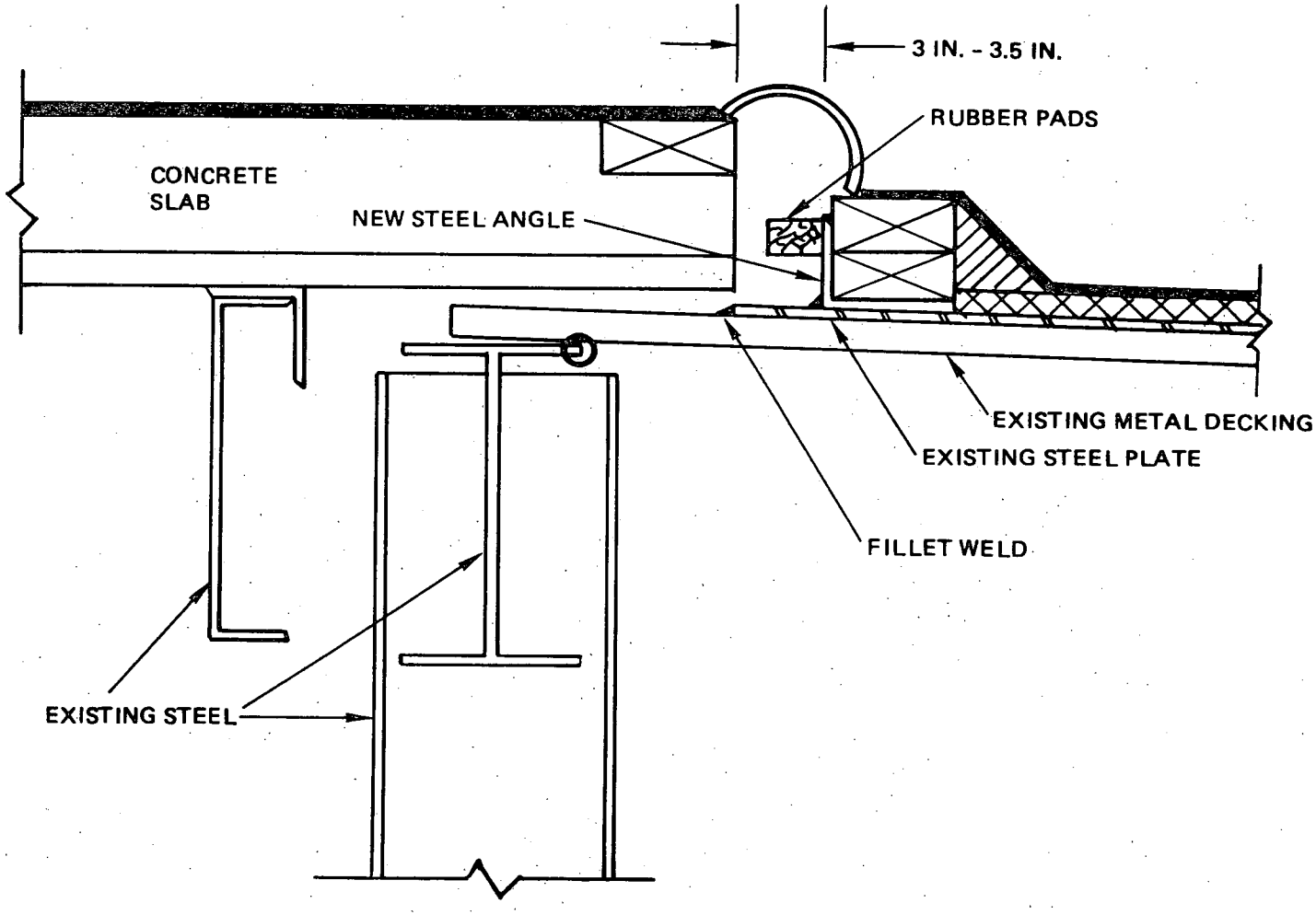


Figure 7.2.10A-2. Method for Adding Rubber Pads Between Control Building and Superheater Building (Indian Point 2)

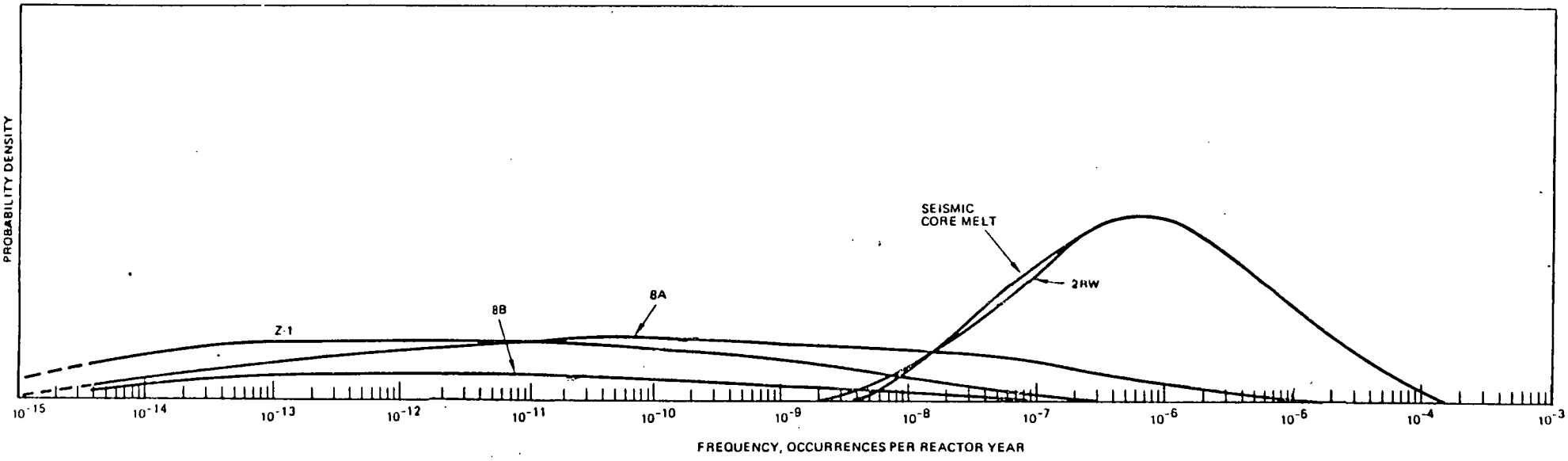


Figure 7.2 10A-3. Release Frequency from Seismic Events, Indian Point 2
(After Modification to the Control Building)

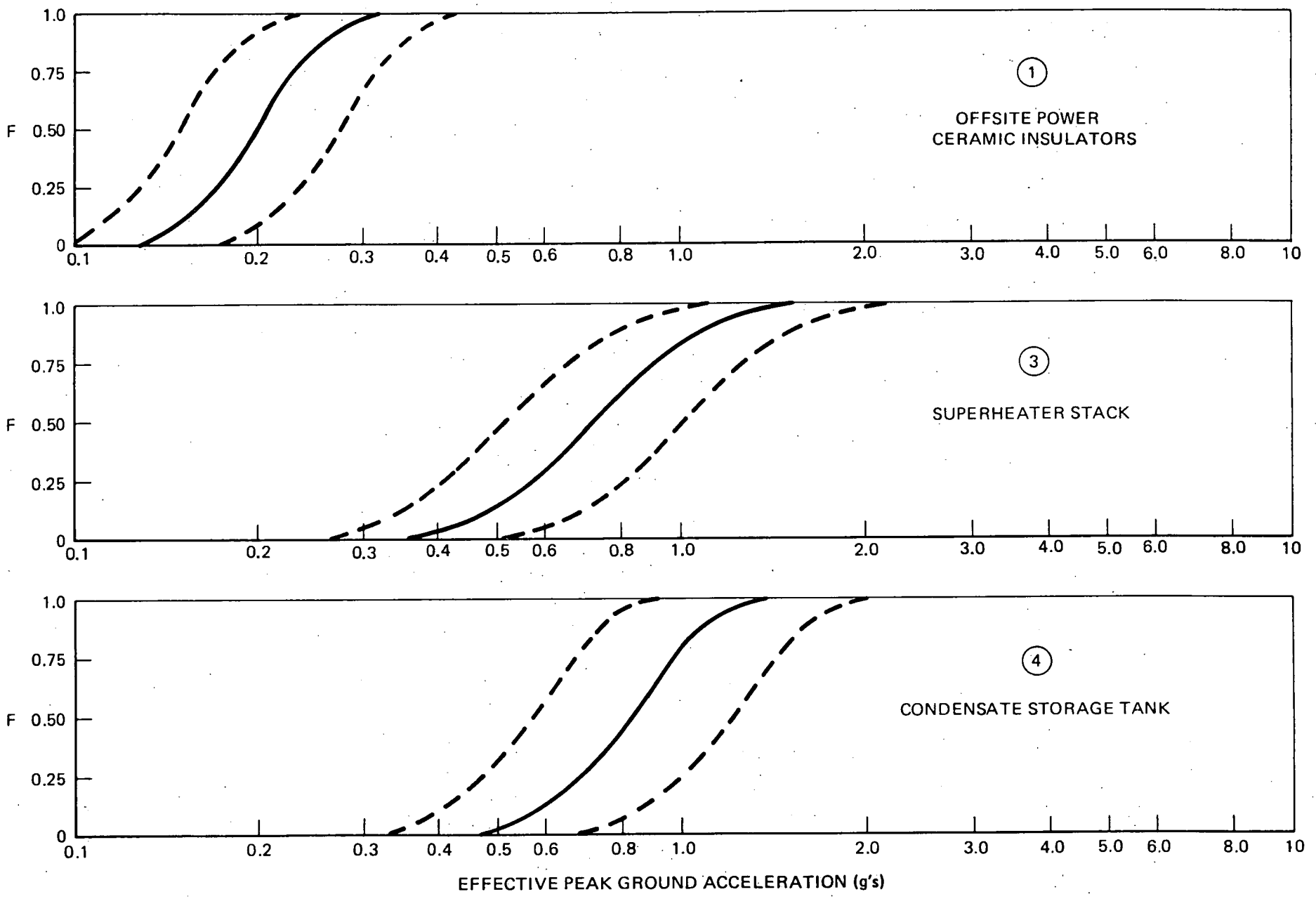


Figure 7.2-11. Fragility Families for Key Indian Point 3 Components (Sheet 1 of 5)

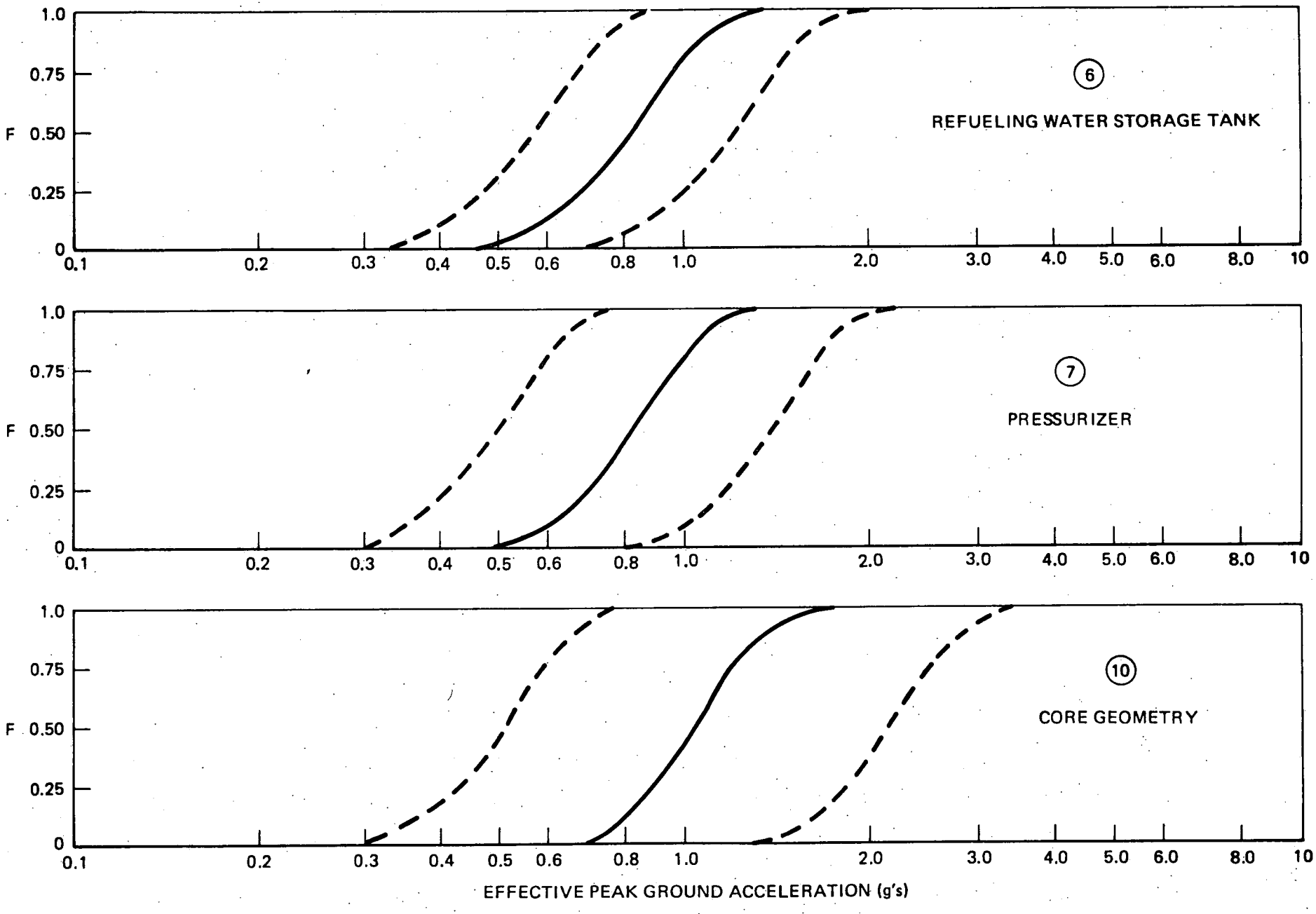


Figure 7.2-11. (Sheet 2 of 5)

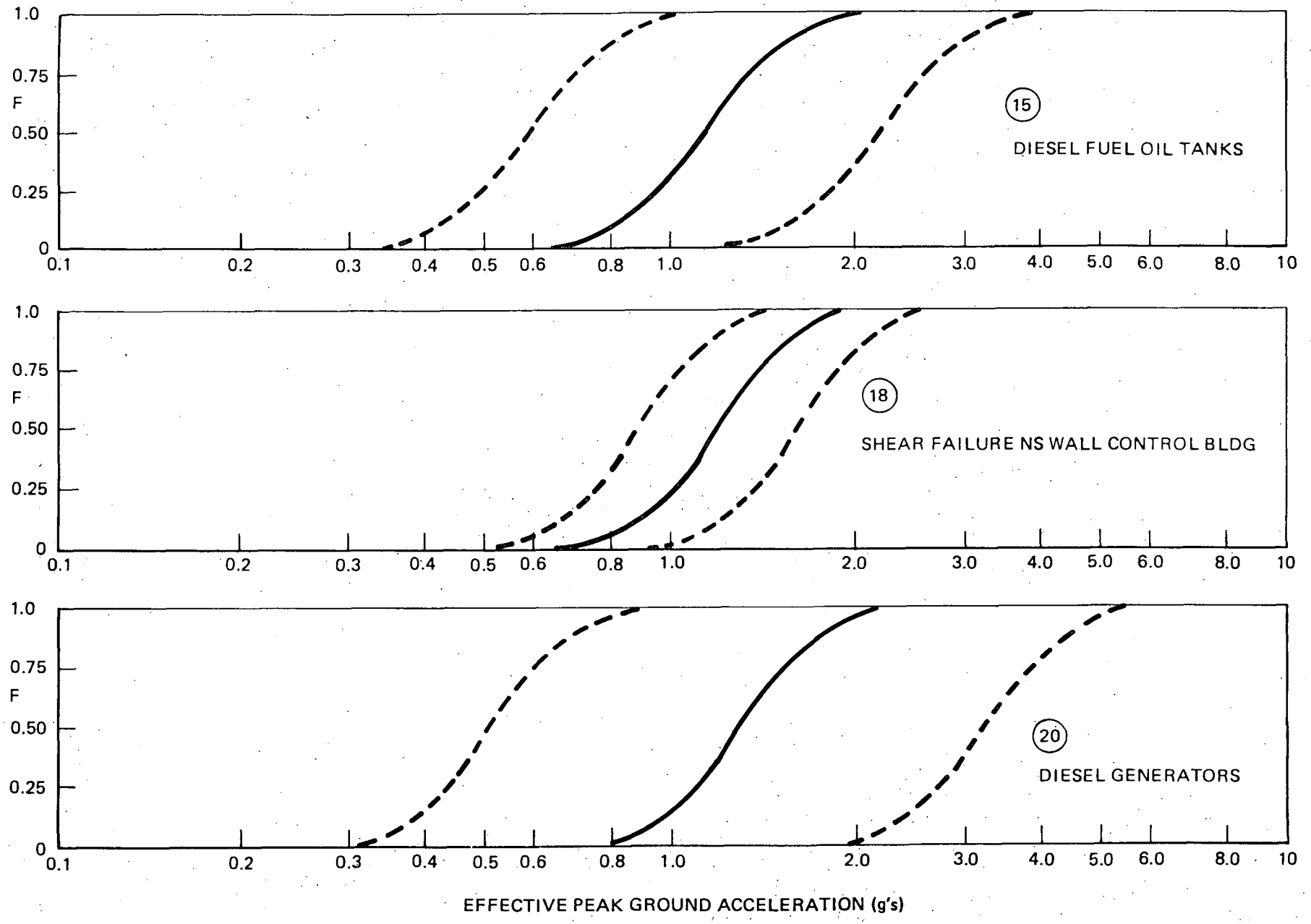


Figure 7.2-11. (Sheet 3 of 5)

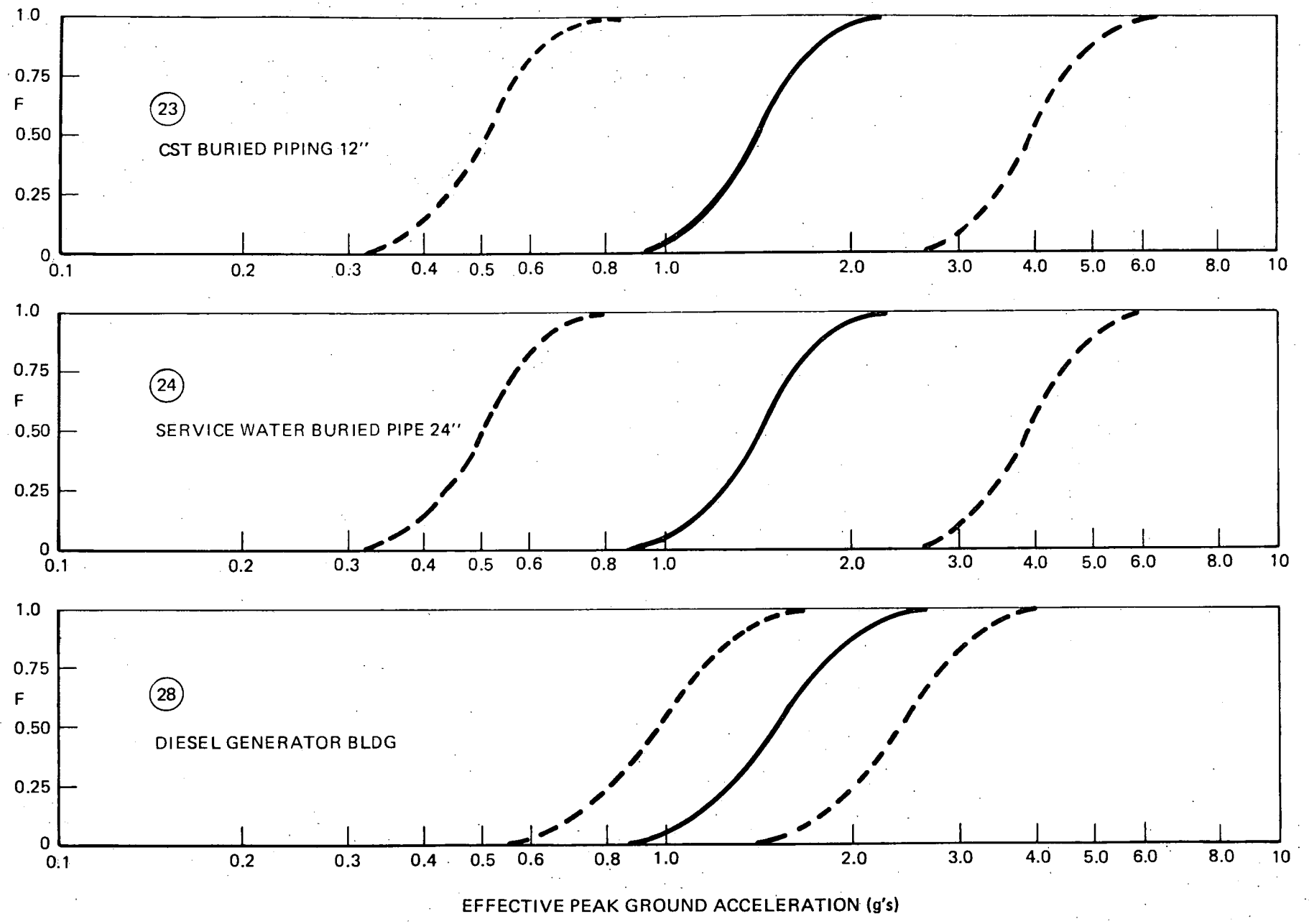


Figure 7.2-11. (Sheet 4 of 5)

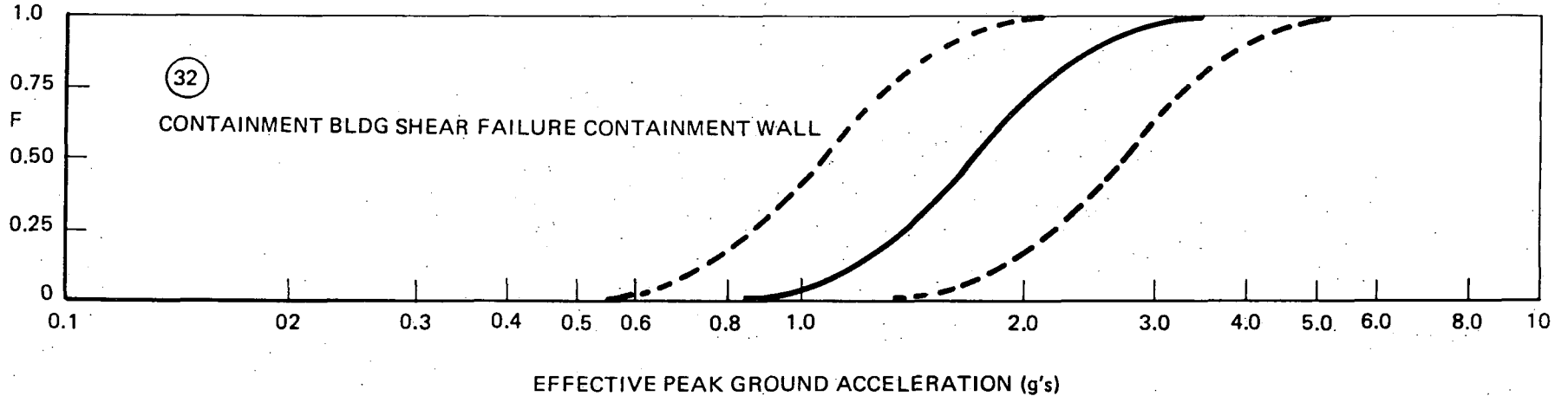
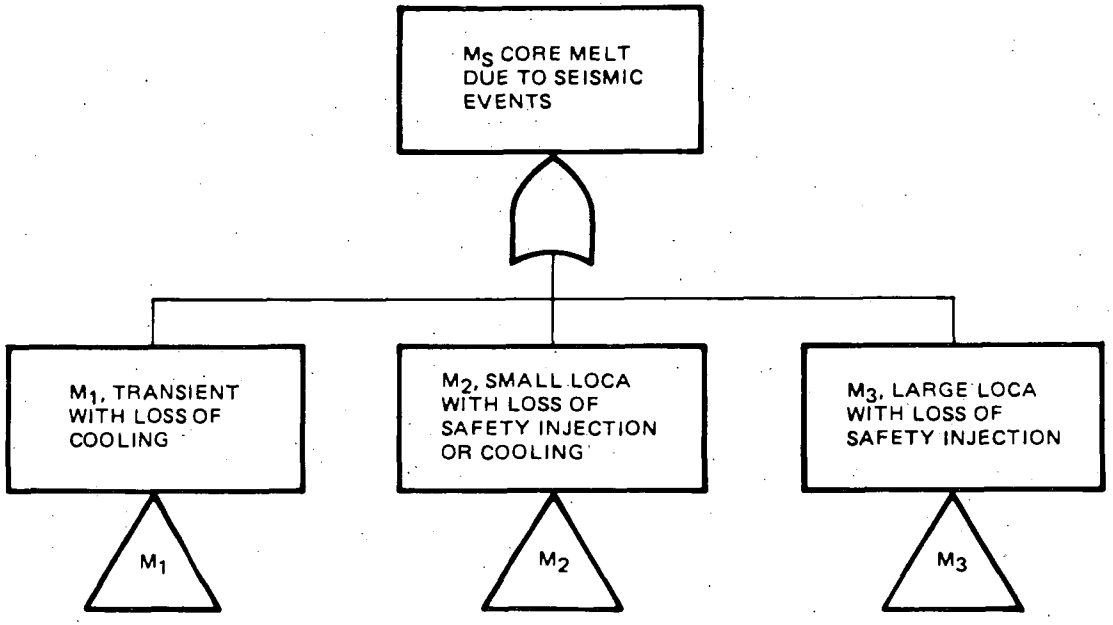


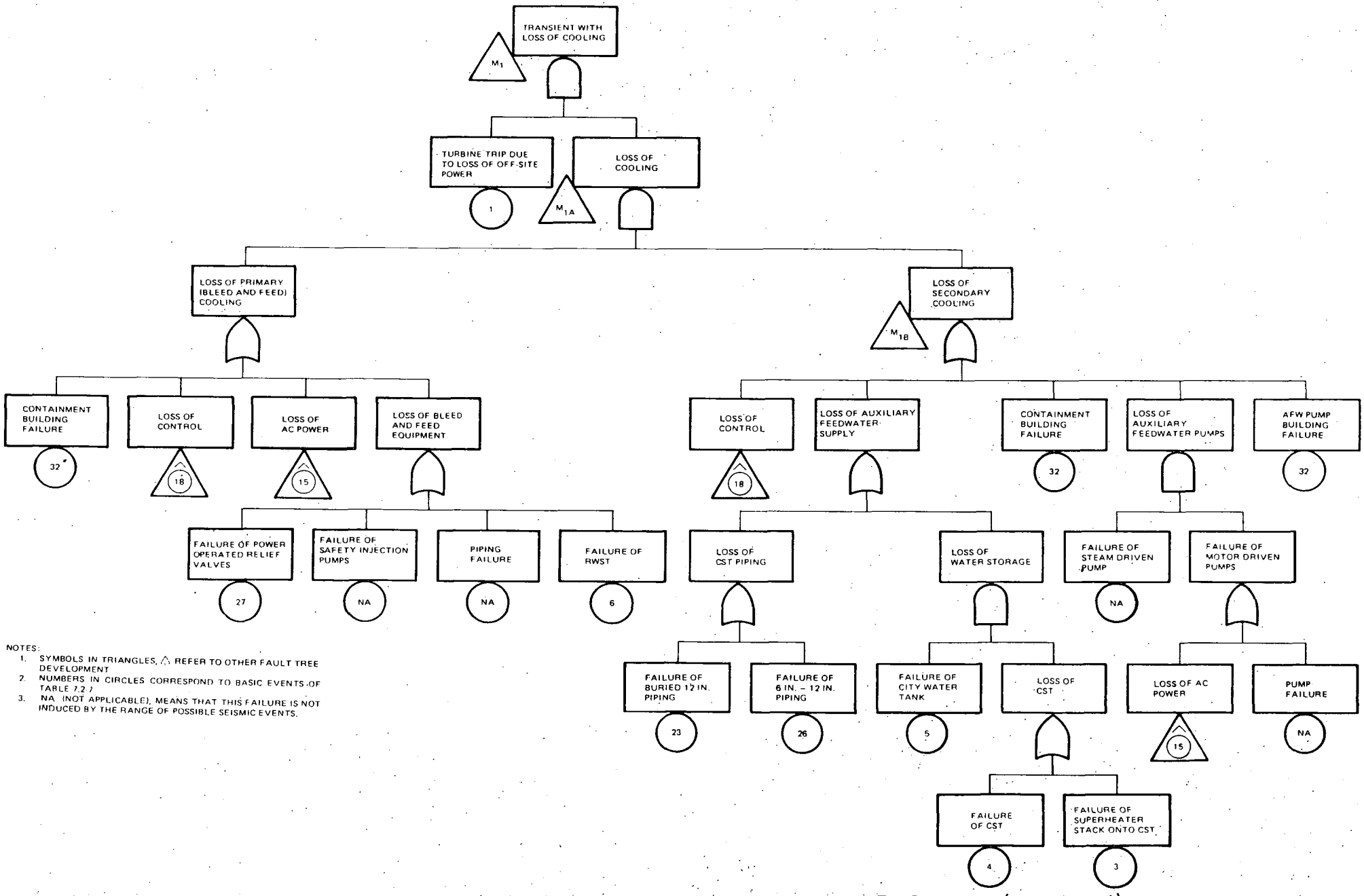
Figure 7.2-11. (Sheet 5 of 5)



NOTES:

1. SYMBOLS IN TRIANGLES Δ REFER TO OTHER FAULT TREE DEVELOPMENT.

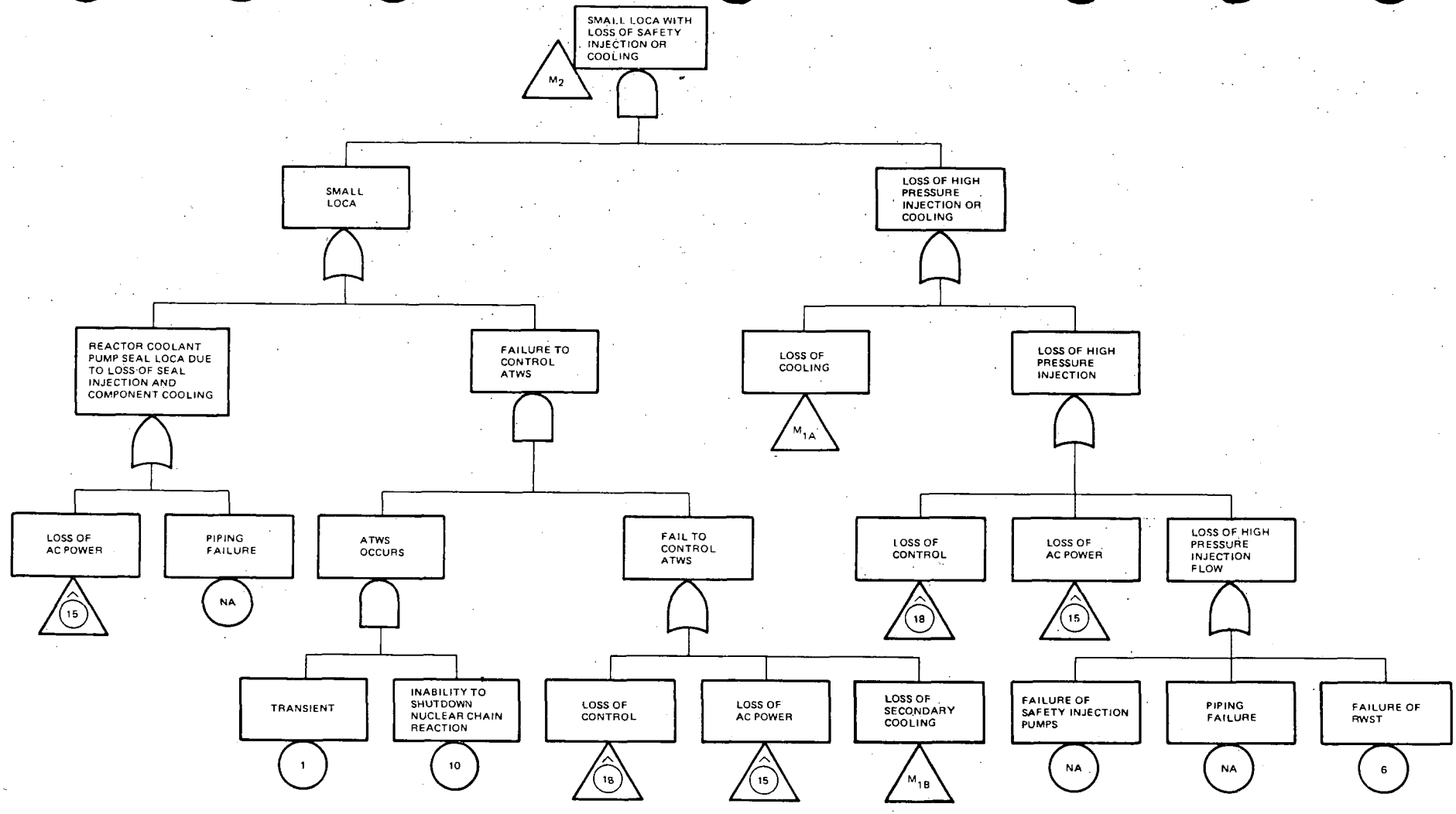
Figure 7.2-12a. Indian Point Unit 3 Seismic Core Melt Fault Tree



NOTES:

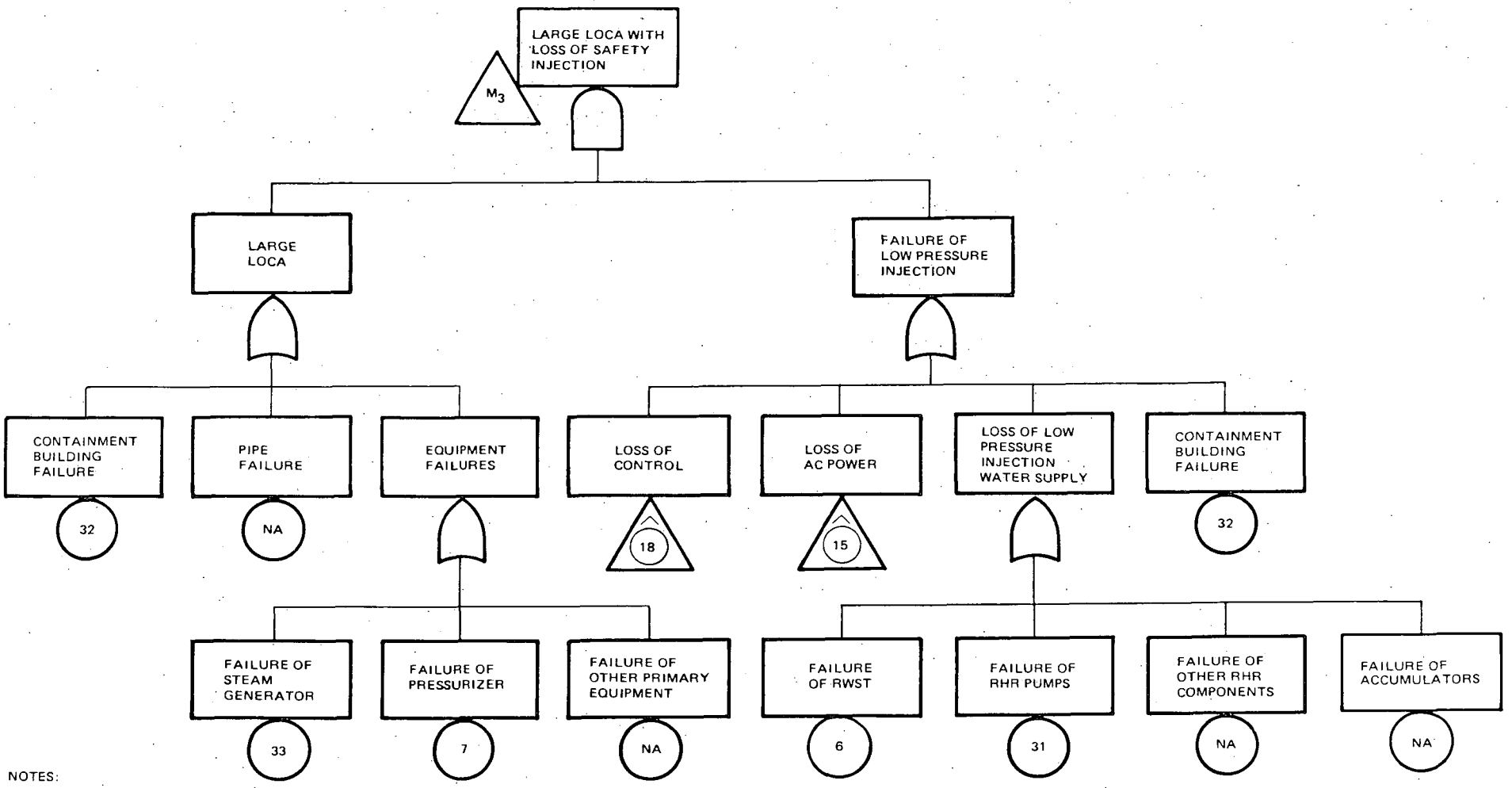
1. SYMBOLS IN TRIANGLES, △ REFER TO OTHER FAULT TREE DEVELOPMENT
2. NUMBERS IN CIRCLES CORRESPOND TO BASIC EVENTS OF TABLE 7.2-7
3. NA (NOT APPLICABLE), MEANS THAT THIS FAILURE IS NOT INDUCED BY THE RANGE OF POSSIBLE SEISMIC EVENTS.

Figure 7.2-12b. Indian Point Unit 3 Seismic Core Melt Fault Tree (continued)



NOTES:
1. SYMBOLS IN TRIANGLES, Δ, REFER TO OTHER FAULT TREE DEVELOPMENT
2. NUMBERS IN CIRCLES CORRESPOND TO BASIC EVENTS OF TABLE 7.2-7
3. (NA) (NOT APPLICABLE), MEANS THAT THIS FAILURE IS NOT INDUCED BY THE RANGE OF POSSIBLE SEISMIC EVENTS.

Figure 7.2-12c. Indian Point Unit 3 Seismic Core Melt Fault Tree (continued)



NOTES:

1. SYMBOLS IN TRIANGLES, △ REFER TO OTHER FAULT TREE DEVELOPMENT.
2. NUMBERS IN CIRCLES CORRESPOND TO BASIC EVENTS OF TABLE 7.2-7.
3. NA (NOT APPLICABLE), MEANS THAT THIS FAILURE IS NOT INDUCED BY THE RANGE OF POSSIBLE SEISMIC EVENTS.

Figure 7.2-12d. Indian Point Unit 3 Seismic Core Melt Fault Tree (continued)

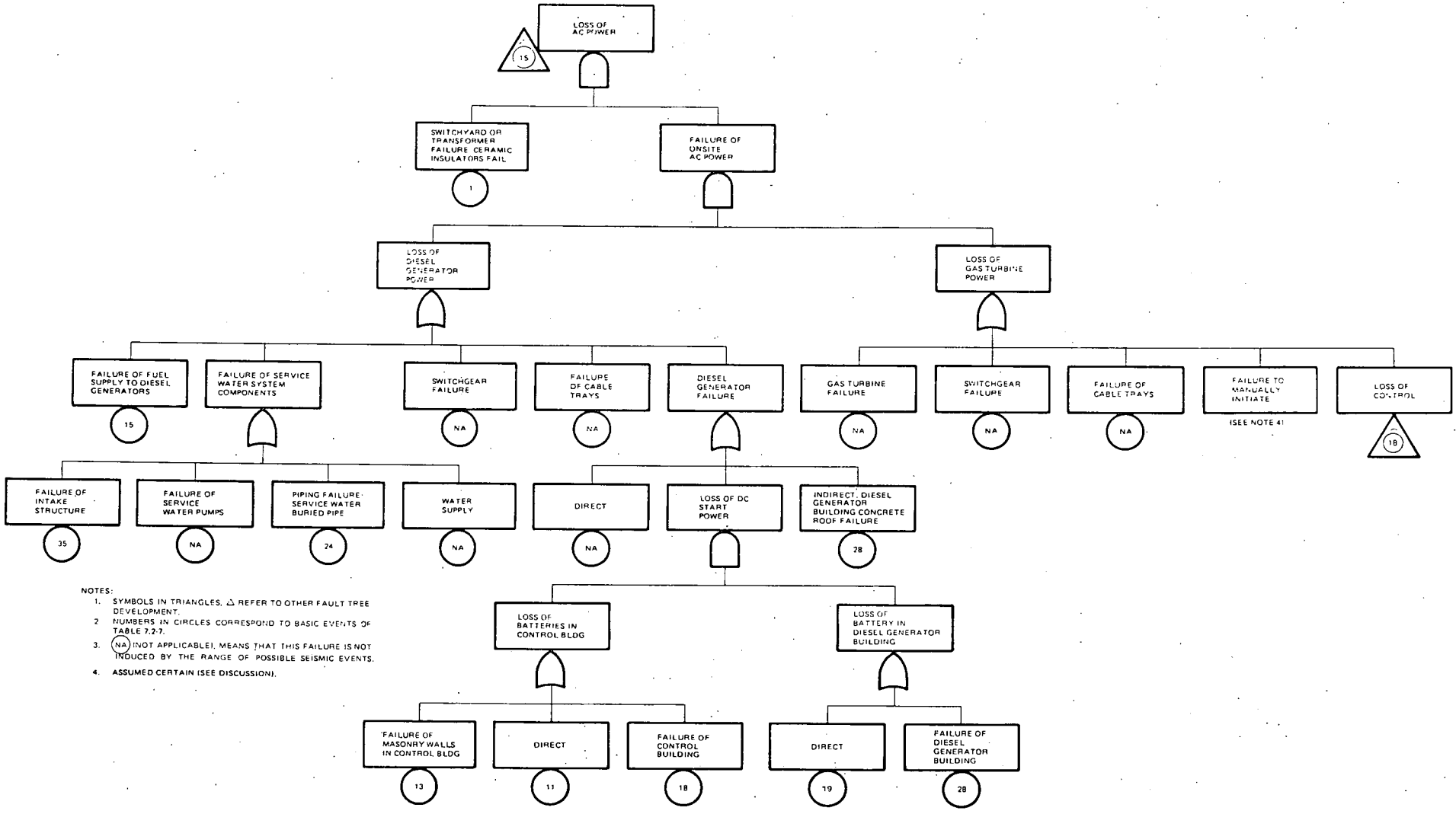
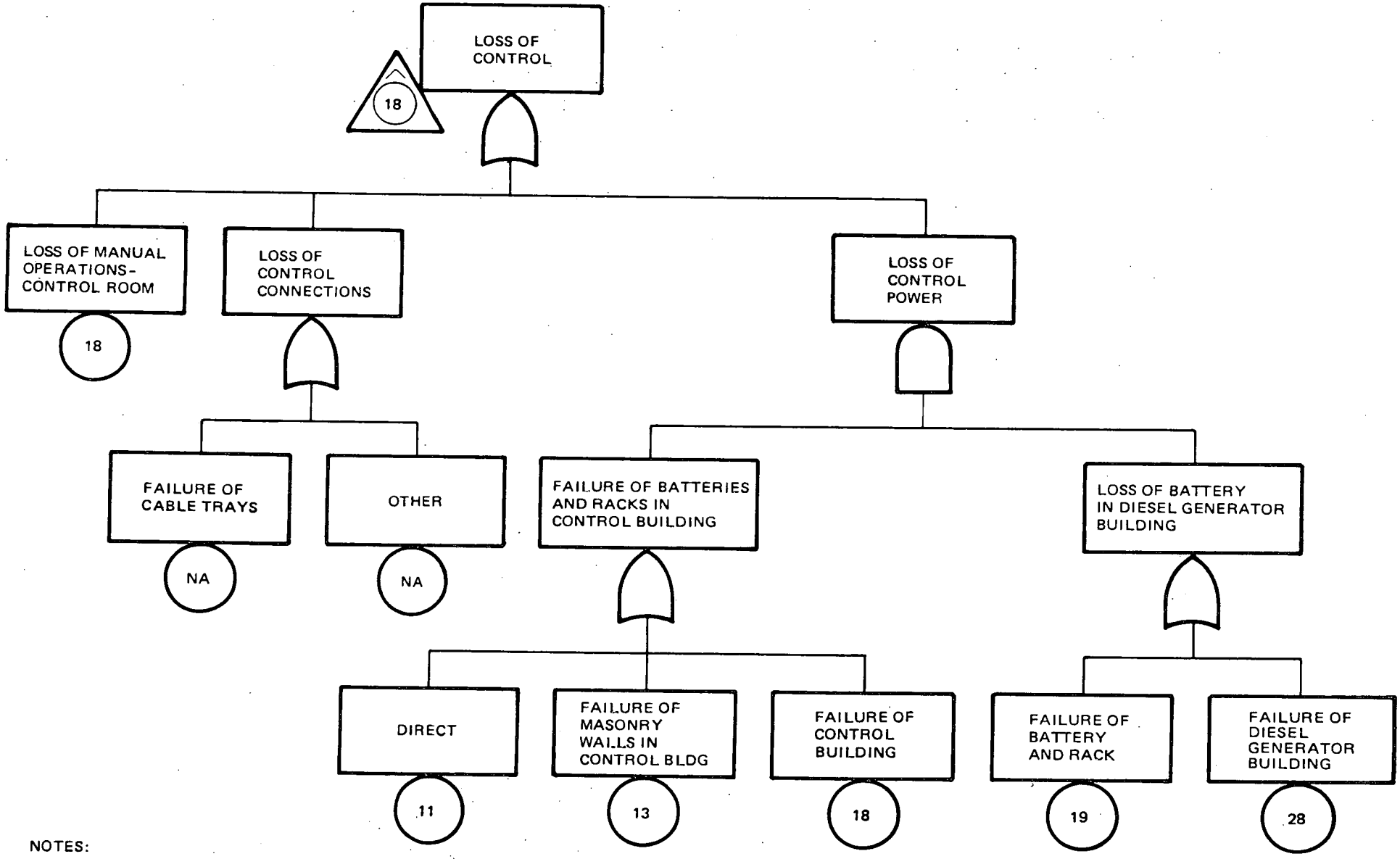


Figure 7.2-12e. Indian Point Unit 3 Seismic Core Melt Fault Tree (continued)



NOTES:

1. SYMBOLS IN TRIANGLES, Δ REFER TO OTHER FAULT TREE DEVELOPMENT.
2. NUMBERS IN CIRCLES CORRESPOND TO BASIC EVENTS OF TABLE 7.2-7.
3. (NA) (NOT APPLICABLE), MEANS THAT THIS FAILURE IS NOT INDUCED BY THE RANGE OF POSSIBLE SEISMIC EVENTS.

Figure 7.2-12f. Indian Point Unit 3 Seismic Core Melt Fault Tree (continued)

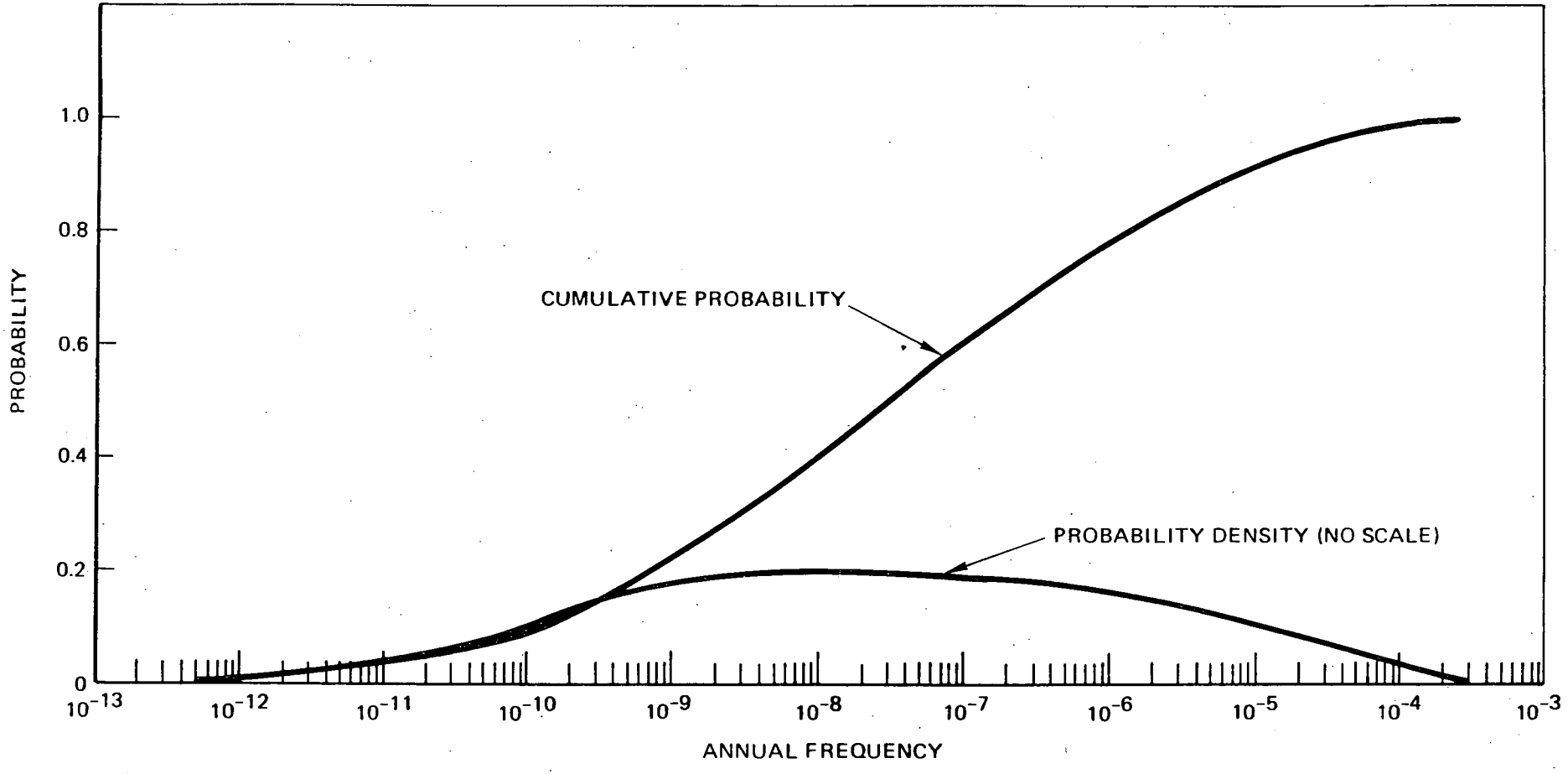
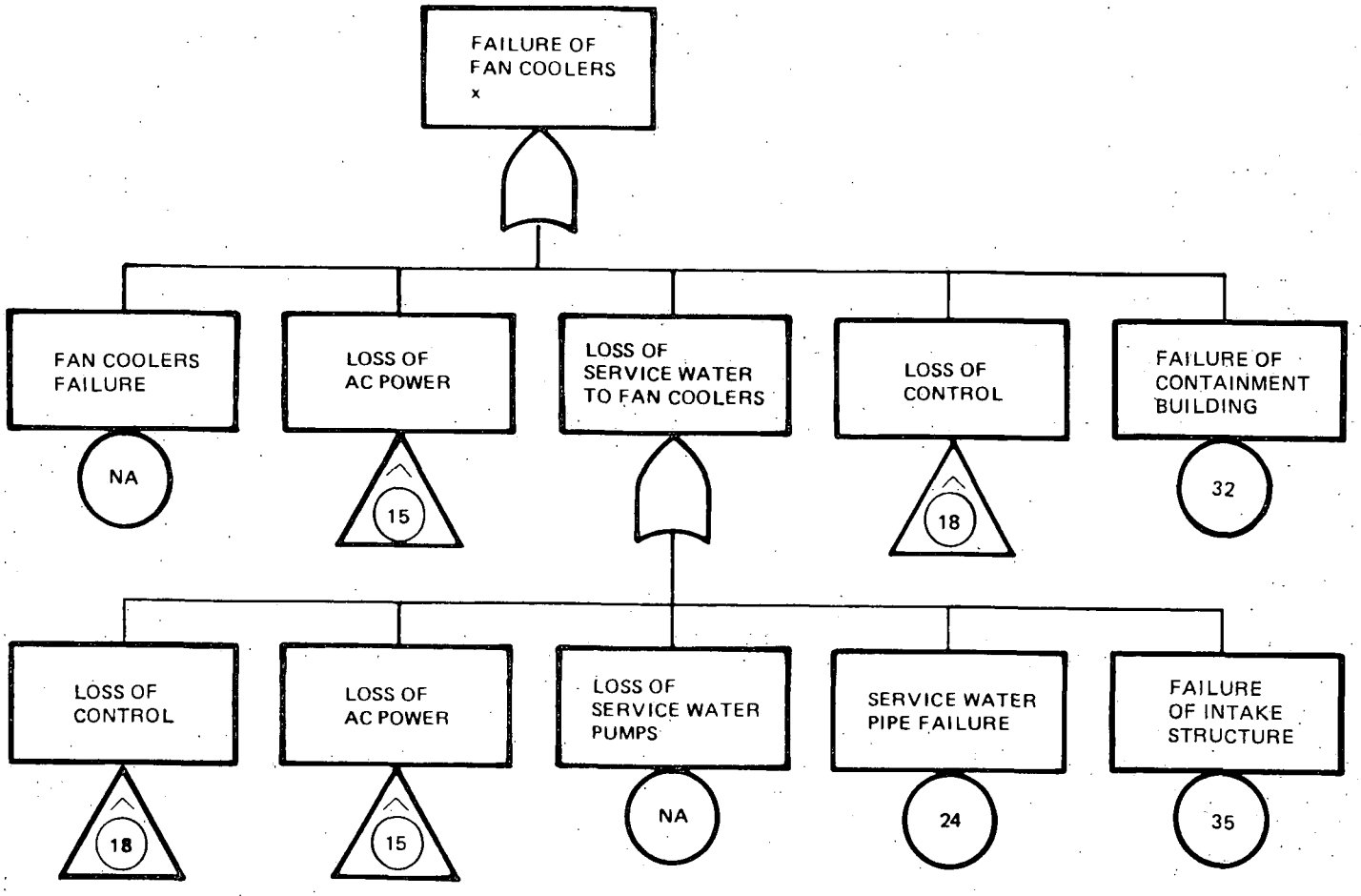


Figure 7.2-13. Indian Point Unit 3 Seismic Core Melt Frequency



NOTES:

1. SYMBOLS IN TRIANGLES, Δ, REFER TO OTHER FAULT TREE DEVELOPMENT.
2. NUMBERS IN CIRCLES CORRESPOND TO BASIC EVENTS OF TABLE 7.2-7.
3. (NA) (NOT APPLICABLE) MEANS THAT THIS FAILURE IS NOT INDUCED BY THE RANGE OF POSSIBLE SEISMIC EVENTS.

Figure 7.2-14. Indian Point Unit 3 Seismic Fan Coolers Fault Tree

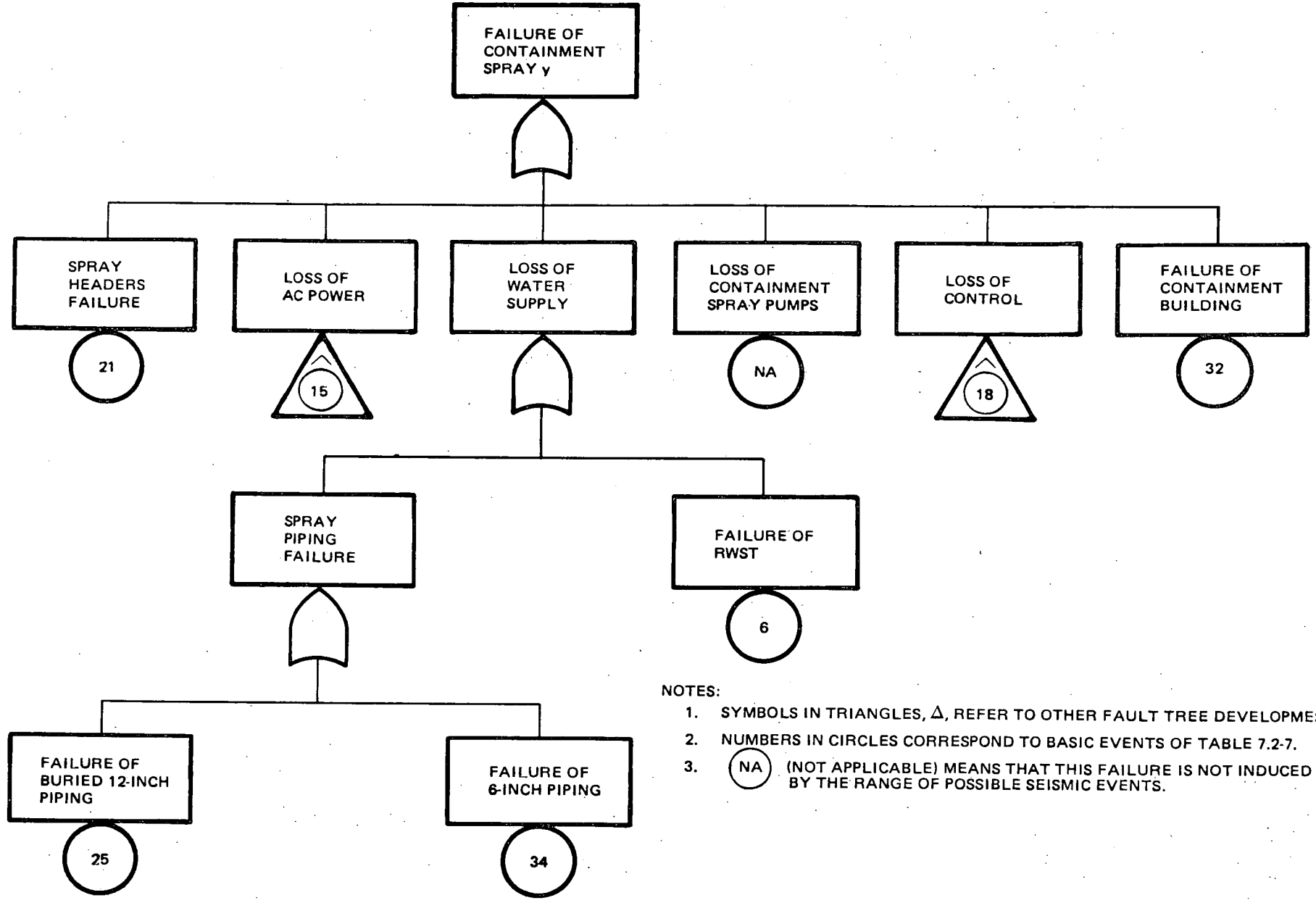


Figure 7.2-15. Indian Point Unit 3 Seismic Containment Spray Fault Tree

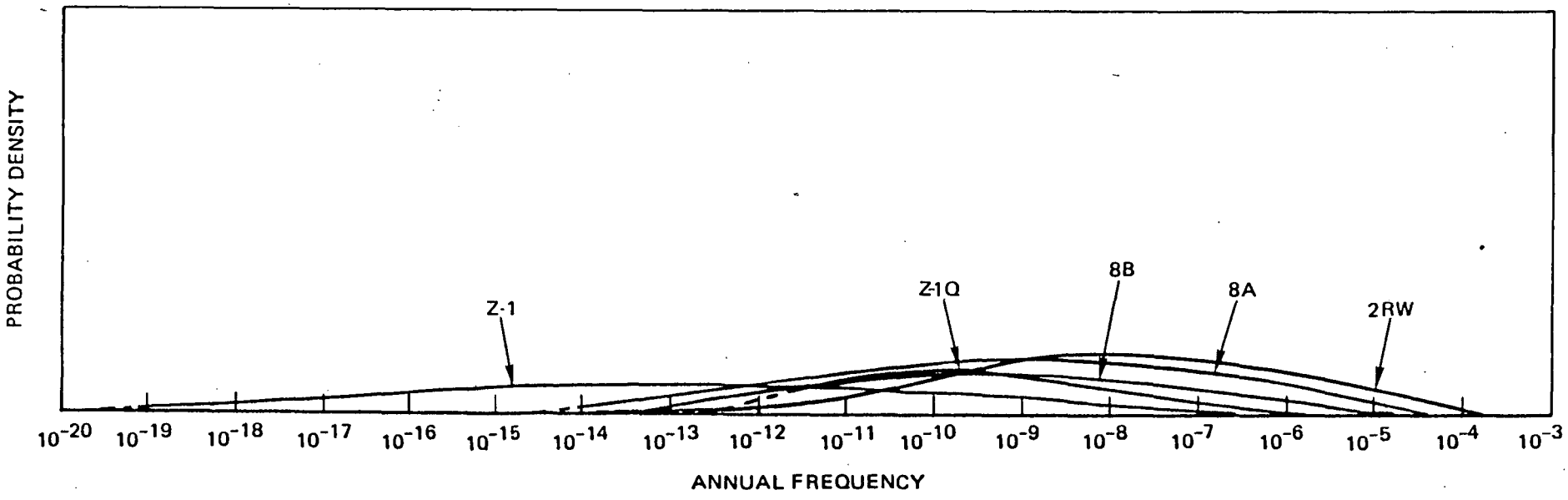


FIGURE 7.2-16. RELEASE FREQUENCY FROM SEISMIC EVENTS - INDIAN POINT UNIT 3

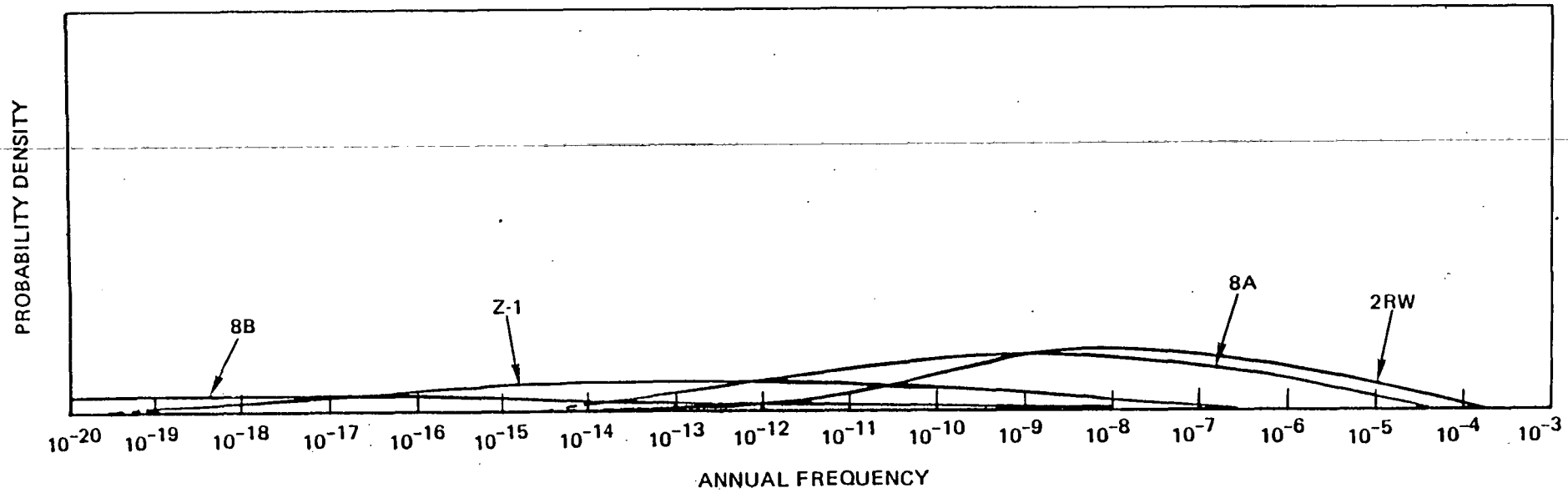


FIGURE 7.2-17. REVISED RELEASE FREQUENCY FROM SEISMIC EVENTS - INDIAN POINT UNIT 3

7.3 FIRE

7.3.1 INDIAN POINT 2 FIRE ANALYSIS

7.3.1.1 Summary

The evaluation of risk from fires is comprised of six major steps:

1. Identification of critical areas where fires can cause an initiating event and, simultaneously, the failure of redundant engineered safety functions.

2. Calculation of the probability distribution of the frequency of fires in these areas.

3. Calculation of fire propagation and of effects of fire extinguishing.

4. Assessment of the effects of fires on LOCAs and transients.

5. Assessment of the effects of fires on accident sequences originating from the initiating events identified in step 4.

6. Calculation of the frequencies of the various containment event tree states.

A preliminary analysis is carried out to identify the locations that require a more detailed investigation. The criterion for qualifying an area as critical is that a fire occurring in that location must be capable of causing an initiating event (a LOCA or a transient). Given that this postulated fire could cause an initiating event, the investigation proceeds to determine whether the same fire could induce failures that would prevent the following:

1. Reaching and maintaining a condition of negative reactivity.
2. Removing core decay heat.
3. Monitoring and controlling the primary system coolant inventory.

The cable spreading room, the switchgear room, the two portions of the electrical tunnel, the MCC area, and the electrical penetration area satisfy these criteria. The diesel generator building is also evaluated because of its importance in mitigating a loss of offsite power incident.

The core melt frequency has the following characteristic values:

5th Percentile:	6.0×10^{-6} ry^{-1}
Median:	6.5×10^{-5} ry^{-1}
95th Percentile:	7.3×10^{-4} ry^{-1}
Mean:	2.0×10^{-4} ry^{-1}

The main contributors to this frequency are fires in the switchgear room and the two portions of the electrical tunnel.

The following table summarizes the results for the frequencies of entering containment event tree entry states TEFC, TE, SLF, SEFC, SEF, and SE. The other entry states have insignificant frequencies.

State	Frequency (per reactor year)			
	Mean	5th Percentile	Median	95th Percentile
TEFC	1.6×10^{-6}	1.9×10^{-10}	6.0×10^{-8}	4.0×10^{-6}
TE	3.0×10^{-7}	$<10^{-10}$	7.3×10^{-9}	5.9×10^{-7}
SLF	4.9×10^{-5}	4.3×10^{-8}	7.4×10^{-6}	1.3×10^{-4}
SEFC	9×10^{-7}	6×10^{-8}	5×10^{-7}	3×10^{-6}
SEF	2.0×10^{-7}	4.9×10^{-10}	7.4×10^{-8}	6.4×10^{-7}
SE	1.4×10^{-4}	4.0×10^{-7}	2.8×10^{-5}	7.1×10^{-4}

Entry states TEFC and TE are primarily due to fires in the cable spreading room. Entry states SLF and SEF are due to fire in the two portions of the electrical tunnel, and fires in the switchgear room as well as the electrical tunnels are a major contributor to entry state SE. Entry state SEFC is due to loss of offsite power (due to causes other than the fire) and loss of all three diesel generators due to a fire.

The following table summarizes the results for the frequencies of release categories 2RW, 8A, and 8B as could be caused by a fire in Indian Point 2. The other release categories have insignificant frequencies.

Release Category	Frequency (per reactor year)			
	Mean	5th Percentile	Median	95th Percentile
8B	2.5×10^{-6}	1.2×10^{-7}	8.6×10^{-7}	2.2×10^{-5}
8A	5.0×10^{-5}	1.2×10^{-7}	9.0×10^{-6}	1.6×10^{-4}
2RW	1.4×10^{-4}	5.0×10^{-7}	2.8×10^{-5}	7.1×10^{-4}

The main contributors to the release category 8B are fires in the diesel generator building that could lead to containment event tree entry state SEFC, and fires in the cable spreading room that could lead to entry state TEFC. The main containment event tree entry state leading to release category 8A is SLF, which could be caused by fires in the electrical tunnels. Containment event tree entry state SE is the predominant factor in release category 2RW. The main contributors to entry state SE are certain fires in the switchgear room and the electrical tunnels.

The occurrence of fires and their effects on plant safety are very complex issues which have not received as detailed attention as have other parts of risk assessment in previous studies. Therefore, major assumptions had to be conservative in order to perform the analysis. The following remarks will place the results of this study into perspective:

1. The analysis was made for rooms where it was judged the most damage can occur. It is anticipated that the results of a more detailed study would not change the conclusions significantly because the predominant contributors to fire risk have been evaluated.

2. The frequencies of fires are derived from evidence collected from all U.S. nuclear power generating stations. They are average frequencies and do not necessarily reflect the conditions that exist at Indian Point 2. For example, it is debatable whether some actual fire occurrences, such as Browns Ferry, should be part of the data base because modifications have been implemented as a result of that fire. Nevertheless, all these fires have been included in the data base.

3. Simple models are used to assess the propagation of fires in cable trays and the temperature rise in compartments due to the heat released by the fire.

4. Detailed analysis of the accident sequences is not done. Such an analysis would explicitly include the timing of events, the possibility of restoration of lost functions, the possibility of errors of commission, etc.

5. Whenever a fire is postulated in an area where it can affect instrumentation, the question of completeness of the analysis becomes very important. It is very difficult to know what information reaches the operators and how they respond. However, the impact of such events on the fire risk is judged to be covered by the uncertainties of the dominant scenarios.

Additional assumptions pertaining to the analysis of individual rooms are given in the rest of this section. Equipment and systems failure frequencies not associated with fire are taken from Section 1 of this study.

7.3.1.2 Cable Spreading Room (Fire Zone 11, Control Building)

7.3.1.2.1 Characteristics of the Room and Critical Areas

Equipment in this area consists of the motor generator sets, reactor trip breakers, DC power panels, the DC inverters, and the battery chargers (Reference 7.3-1). Power, control, and instrumentation cables of all safety divisions are also present except for the power cables to the service water pumps and auxiliary feedwater pumps. In some cases, they share the same cable tray but 4-inch high dividers are installed to separate them (Reference 7.3-2). Also, wherever a power tray is located beneath an instrument or control tray or heavy power cables, a 1/4-inch thick transite barrier is installed between the trays.

In studying the fire effects in this area, the following information is useful:

1. The cable spreading room is a controlled access area.

2. The primary combustible materials permanently present in the room are cable insulation, motor lubricant, paint, and transient fuel. The total heat content of the room is estimated (Reference 7.3-1, page 9-54) to be 527,000 Btu. The transient fuels contribute more than 80% of this (439,000 Btu). This includes 15 lbs. of wood, 8 lbs. of paper, 8 lbs. of plastic, 5 lbs. of oil, and 10 lbs. of grease.

3. The room has ionization detectors, which annunciate in the control room, as well as portable extinguishers. A manual hose station outside the cable spreading room has access to this room. There is also a manual Halon system which is sized to cover the volume of the spreading room and the connected portion of the electric tunnel. The electrical tunnel ventilation fans are arranged such that smoke from a fire would be withdrawn from the cable spreading room in the opposite direction from which the fire brigade would be entering to fight the fire, thereby facilitating access for fire fighting activities. All the openings to this room, other than the passageway into the electrical tunnel, have shutters, louvers, or dampers that are automatically closed upon Halon system activation.

4. Control cables of all three auxiliary feedwater pumps and their regulator valves are located in this area. For the turbine-driven pump the speed indication is electronic, while the speed control mechanism is strictly pneumatic. If the air system is lost, this pneumatic control system does not depressurize instantaneously. The power cables of the two motor-driven pumps are independent of this area and therefore, these pumps could be operated locally. The turbine-driven pump starts automatically at minimum speed only and can be operated manually, independent of the cable spreading room.

5. For service water pumps, only the control cables, and not power cables, run through this area.

6. For charging pumps, safety injection pumps, component cooling pumps, containment spray pumps, containment fan coolers, pressurizer relief valves, secondary atmospheric relief valves, and residual heat removal pumps, both power and control cables run through the area. The power cables are located only in the eastern end of the room at the entrance to the electrical tunnel.

Figure 7.3.1-1 shows a top view of the cable spreading room. The control cables that enter the control room are laid on two stacks of cable trays that run in an east/west direction and are at elevations greater than 12 feet above the floor. These two stacks of trays contain cables of different divisions. The ones in the southern stack cross over to the northern side at 18 feet above the floor to enter the control room along with the cables of the other division that are run in the northern stack.

Two critical areas are identified. The first one is the center of the northern wall next to the ceiling where many redundant and diverse control cables come very close to each other before going through the control room floor. This area is immediately below the safeguards supervisory panels in the control room above. The second area is at the eastern end, at the entrance to the electrical tunnel. All power cables of the cable spreading room are located in this area. Figure 7.3.1-2 shows a cross-section of the trays and their contents. The same configuration is preserved throughout the electrical tunnel. Those power cables cover only a very small portion of the cable spreading room. Therefore, their contribution to the fire risk is calculated as part of the contribution of the electrical tunnel. Obviously, one can produce many fire propagation scenarios by postulating fires at various locations in the cable spreading room that would affect these critical areas. The total frequency of core damage would then be the appropriate sum of the frequencies of these scenarios. We choose representative cases to model these fire propagation scenarios.

7.3.1.2.2 The Frequency of Fires

Reference 7.3-3 presents distributions for the average frequency of fires per year in the following areas: control room, cable spreading room, diesel room, containment, turbine building, and auxiliary building. These distributions are derived using Bayes' theorem as follows.

The prior distributions are almost noninformative and therefore the evidence dominates the results. This evidence is derived from actual fire incidents as reported to the American Nuclear Insurers (ANI) (a survey of ANI records is reported in Reference 7.3-4). The room-years as of May 1, 1978, are calculated by surveying the FSARs of operating reactors.

In 301.3 room-years there were two reported fires in cable spreading rooms. The posterior distribution of the fire frequency is a gamma distribution* with parameters $\alpha = 2.182$, and $\beta = 302.26$ having the following characteristic values (per year):

$$\lambda_{CSR,05} = 1.4 \times 10^{-3}, \quad \lambda_{CSR,50} = 6.2 \times 10^{-3}, \quad \lambda_{CSR,95} = 1.7 \times 10^{-2},$$

$$\alpha_{\lambda_{CSR}} = 7.2 \times 10^{-3}$$

This distribution is generic, i.e., it is the distribution of the frequency of fires averaged over all existing cable spreading rooms. It is a conservative distribution because it includes the Browns Ferry fire and does not take into account the changes in procedures and/or design that resulted from that fire. It is felt that removal of the Browns Ferry fire from the data base would raise a controversy similar to that on the "rectifiability" notion proposed by EPRI in connection with the ATWS problem. In order to be conservative, the Browns Ferry fire was included, even though the frequency of fires in cable spreading rooms has probably been reduced. The derived distribution represents fires of any magnitude. The only criterion for their inclusion in the data base is that they have been reported to ANI, which has stricter reporting requirements than the NRC.

7.3.1.2.3 Fire Propagation and Extinguishing in Cable Spreading Room

As discussed in Section 7.3.1.2.1, fires which involve the control cable trays elevated 18 feet above the floor at the center of the northern wall are considered. These trays are not directly visible from the floor; additional horizontal trays with a vertical separation of 1 foot are located beneath this zone, with the lowest tray being 12 feet above the floor. We assume that the fire has reached a critical size when the trays 18 feet above the floor are ignited.

7.3.1.2.3.1 Propagation Analysis. Fire propagation is modeled in this area with a representative scenario involving a large exposure fire on the floor underneath the cable trays. Fires that start within the cable trays are not considered, because even the lowest trays are 12 feet above the floor, and because there are no power cables in this area.

In the representative scenario, the ground based exposure fire first ignites the lowest cable tray after τ_1 minutes. The fire then spreads through the higher cable trays, and reaches the critical trays at 18 feet τ_2 minutes after the lowest tray was ignited. Fire spread through the trays is considerably quicker than the fire spread

*The probability density function for the gamma distribution is

$$p(\lambda) = \frac{\beta^{\alpha}}{\Gamma(\alpha)} \lambda^{\alpha-1} \exp(-\beta\lambda), \quad \alpha, \beta, \lambda > 0.$$

described in Section 7.3.4 (Appendix I), because the external fire, which remains burning throughout the duration of the fire, augments the intensity of the fire on the lower trays. The characteristic fire propagation time for this scenario, τ_G, is the sum of τ_1 and τ_2.

The exposure fire is modeled as a 1-foot diameter oil fire located immediately under the stack of cable trays. Using COMPBRN (Reference 7.3-5), our reference model prediction for τ_1, called $\tau_{1,DRM}$, is about 8 minutes. Approximately 1 gallon of fuel is burned.

To quantify our uncertainty in COMPBRN's predictions, we define an error factor ψ such that

$$\tau_1 = \psi\tau_{1,DRM} \qquad (7.3.1\text{-}1)$$

ψ is judged to be lognormally distributed, with characteristic parameters

$$\psi_{05} = 0.8, \qquad \psi_{50} = 1.26, \qquad \psi_{95} = 2.0, \qquad \alpha_\psi = 1.31$$

We note that ψ plays the same role as the error factor ϕ defined in Section 7.3.4 (Appendix I) but has a tighter distribution. This reduced uncertainty stems from our relatively good state of knowledge concerning the characteristics of the fixed exposure fire.

The predicted time for fire spread to the uppermost level given ignition of the lowest tray, $\tau_{2,DRM}$, is computed to be approximately 6 minutes. This prediction is essentially constant for all allowable values of θ, the dimensionless parameter based on the cable insulation physical properties (see Section 7.3.4, Appendix I). The lack of variation in $\tau_{2,DRM}$ can be attributed to the strength of the large exposure fire as a driving force in fire propagation. Once more, we employ an error factor to quantify our uncertainties in COMPBRN's predictions,

$$\tau_2 = \phi\tau_{2,DRM} \qquad (7.3.1\text{-}2)$$

where we have employed ϕ because of the larger uncertainties inherent in propagating fire growth through a number of fuel elements.

Thus, the time required for fire propagation, τ_G, is given by

$$\tau_G = \psi\tau_{1,DRM} + \phi\tau_{2,DRM} \qquad (7.3.1\text{-}3)$$

The characteristic values of τ_G are (minutes)

$$\tau_{G,05} = 12.3, \qquad \tau_{G,50} = 21.2, \qquad \tau_{G,95} = 33.0 \qquad \alpha_{\tau_G} = 22.6$$

The amount of oil needed to sustain this fire ranges from 1.0 to 2.8 gallons.

It should be noted that the heat flux from the exposure fire to the lowest tray decreases if the fire is not located immediately under the cable trays. If the exposure fire is fueled by a less flammable material, the heat flux impinging on the lower trays will also decrease, and the fire growth time will therefore increase. For a 2-foot diameter polymethylmethacrylate (PMMA) fire, $\tau_{1,DRM}$ is equal to approximately 20 minutes (corresponding to 2.1 kg of this flammable plastic). If the exposure fire is much smaller, ignition of the lowest tray is unlikely before the fire is extinguished. For example, $\tau_{1,DRM}$ calculated for a 1-foot diameter PMMA fire is about 2.25 hours.

On the other hand, should the exposure fire be more severe than the one postulated, our results will not change dramatically, because τ_1 and τ_2 are small to begin with, and because the upper trays cannot be directly affected by the exposure fire.

The chosen exposure fire is representative of the large exposure fires which can initiate a fire in the elevated trays. Less severe exposure fires can also ignite the elevated trays, but they require much longer times to ignite the lowest trays. Furthermore, the effect of horizontal displacement of the smaller exposure fire, away from the position directly underneath the cable trays, is much more strongly pronounced.

7.3.1.2.3.2 Fire Detection and Extinguishment. The distribution for τ_G is derived without consideration of extinguishing efforts. To account for extinguishing, we define $Q(t)$ to be the conditional frequency that a fire is not extinguished by time t, given a fire. Thus, $Q(\tau_G)$ is the conditional frequency of fire growth in the critical zone studied.

The extinguishing process is modeled exponentially with a mean extinguishing time τ_s. $Q(t)$ is then given by

$$Q(t) = \exp(-t/\tau_s) \qquad (7.3.1\text{-}4)$$

The distribution for τ_s is based on two sources of information: (1) the fire detection and extinguishing capabilities available in the cable spreading room, and (2) fire suppression data given in Reference 7.3-6. Table 7.3.1-1 gives the histogram for τ_s.

There are many scenarios for fire extinguishing in the cable spreading room, of which a typical scenario would be: the control room is informed about a fire in a certain location, the control room operators dispatch a nuclear plant operator to check the fire, the latter enters the fire zone and assesses the severity of the fire, calls back the control room, and the control room operators or the watch supervisor dispatch the fire brigade to fight the fire. There are two important parts in these scenarios: (1) the mode of fire detection, and (2) the mode of fire fighting.

Fire detection can be either remote or local. For remote detection, there are smoke detectors in the cable spreading room that annunciate in the control room. The typical response time of smoke detectors, quoted

in the literature, is on the order of 5 minutes. It should be noted that detector response time is strongly dependent on the room and fire characteristics. In Reference 7.3-6, we find that the majority (75%) of fires in nuclear power plants in commercial operation have been detected locally by plant personnel. Of course, this may be lower for the cable spreading room because a considerable part of that data comes from dissimilar areas, the time before the Browns Ferry incident when the generic plant modifications as a result of that incident were not implemented.

There is also an indirect method for detection, via the control board indicators and readouts. If the fire affects instrumentation or control cables before it is detected, it may inform the control room operators of problems in the cable spreading room. In the preceding section, we have found that fire propagation to the cables is on the order of 8 minutes.

Local detection may be instantaneous (i.e., plant personnel would be present at the time of fire ignition) or it may be delayed. Thus, local detection time competes with the remote detection process provided by the smoke detectors. It should be noted that the fires considered in the preceding section are rather large. A representative detection time (including both remote and local combined) for the fires considered in the preceding section is on the order of a few minutes and the uncertainties may range from a few seconds to approximately 15 minutes. The latter bound is the sum of fire propagation time (8 minutes) and the time before the operators realize that the cause of the control board abnormalities is a fire in the cable spreading room. This assumes that the smoke detectors have not responded and none of the personnel are in the fire area. Very large response times are deemed to be very unlikely because of the large fires considered and because the control board is affected upon cable failure.

The extinguishing process can be divided into two parts: first, a decision is made on the strategy of combatting the fire, and second, the extinguishing agent (e.g., Halon, water, CO_2) is applied. This two part process is repeated until the fire is completely extinguished. If some plant personnel are present when the fire ignites, they may choose to use the available portable extinguishers. This may not be sufficient with the fire severities considered here (see Section 7.3.1.2.3.1). The control room operators may send a nuclear plant operator (NPO) to assess the situation or may send the fire brigade even before the NPO is dispatched. At the fire location, the NPO or the fire brigade could decide whether to flood the room with Halon or to enter the room and fight the fire directly using the other locally available extinguishing agents. The Halon would certainly reduce the severity of the fire significantly. However, because of the uncertainty about whether the fire will be completely extinguished, it was decided that the fire brigade has to enter the room and complete the extinguishing process manually.

Thus, the process of fire extinguishing may take from a few minutes (personnel present in the area using portable extinguishers or local hose stations) to about half an hour (NPO is dispatched to the area,

calls for fire brigade help and they put out the fire manually) to several hours (several fire extinguishing attempts fail to put the fire out completely and it reignites).

Reference 7.3-6 estimates the duration of actual fires. This duration is defined as the time from ignition to the time when maximum damage has occurred. The estimates of Reference 7.3-6, which are the results of expert evaluation, demonstrated that, of the 18 fires studied, approximately 80% were extinguished manually. The experts estimated that seven (40%) of them were extinguished within 5 minutes. Four of the 18 fires were estimated to have been extinguished between 5 and 25 minutes after initiation, and another group of four fires had extinguishment times of between 30 and 35 minutes. There were two fires that were extinguished after 60 minutes but before 85 minutes. Finally, the Browns Ferry fire was extinguished in approximately 7 hours. These are expert estimates, not statistical data. While these 18 fires were of all sizes, the analysis is limited to large fires (Section 7.3.1.2.3.1) in this case. Thus, the discrete model (Table 7.3.1-1) is consistent with the fire protection systems available for the cable spreading room and with the experts' estimates. To be conservative, the seven fires that were extinguished within 5 minutes were deleted because the time to extinguish fires of this severity was considered to be too short. Small probabilities are assigned to the longer mean extinguishment times (60 and 120 minutes) in light of the extinguishing capabilities in the cable spreading room. Another source of conservatism is that slowing down of the propagation of the fire is not explicitly modeled.

A second distribution for τ_s (Table 7.3.1-4) is derived, for smaller fires, based on the same set of information. In this case the largest probability is given to 5 minutes because the fires are small and adequate fire protection equipment is available. Based on the same arguments, the largest mean time for extinguishment is judged to be 60 minutes.

7.3.1.2.3.3 Conditional Frequency of Large Exposure Fires. As seen in Section 7.3.1.2.3.1, a number of different exposure fires can initiate fires in the critical zone in a reasonable amount of time. Less severe fires, e.g., less than 1-foot diameter oil fires or nonoil fueled fires of less than 2 feet in diameter, require much larger times to reach the uppermost cable tray. In view of the mean times for extinguishment listed in Table 7.3.1-4, it is concluded that these less severe fires are unlikely to spread to the upper trays. Note, furthermore, that the large exposure fire must be near the critical zone. The exposure fire severity factor, f_{es} represents the fraction of cable spreading room exposure fires which are large enough and close enough to cause damage. The distribution for f_{es} is assessed to be lognormal with the following characteristic values:

$$f_{es,05} = 2.5 \times 10^{-4} \qquad f_{es,50} = 5.0 \times 10^{-3}$$

$$f_{es,95} = 0.1, \qquad \alpha_{f_{es}} = 2.6 \times 10^{-2}$$

Some additional observations used in deriving this distribution are:

- Generally, no maintenance work is performed in this zone during power operation.
- The zone is not used as a passageway in general and especially not for large amounts of combustibles.
- Unauthorized personnel do not have access to this room.
- Administrative procedures prohibit the personnel to take actions that may increase the fire hazard in this room without a fire watch being present.
- The critical area constitutes only a small fraction (approximately 0.1) of the total cable spreading room floor area.
- One of the two fires in the data base, the Browns Ferry fire, was very large, initially fueled by large quantities of highly flammable material, and occurred at a critical area.
- A significant fraction (approximately 0.1) of the cable insulation fires reported in Reference 7.3-6 was estimated to be large.

7.3.1.2.3.4 Combined Propagation and Extinguishment. The conditional frequency of two divisions being within the fire can now be derived given that a fire has started. The conditional frequency of fire propagation among the critical control cables, given a large exposure fire under the cable trays, is given by $\exp(-\tau_G/\tau_S)$ [Equation (7.3.1-4)]. Thus, the conditional frequency of fire propagation $Q(\tau_G)$, given a large exposure fire, has the following characteristic values:

$$Q_{05}(\tau_G) = 0.09, \quad Q_{50}(\tau_G) = 0.43, \quad Q_{95}(\tau_G) = 0.81, \quad \alpha_{Q(\tau_G)} = 0.46$$

7.3.1.2.4 Effects of Cable Spreading Room Fires on Accident Sequences

7.3.1.2.4.1 Large LOCA. For a large LOCA to occur, loss of coolant through an opening larger than 6 inches in equivalent diameter must be induced by the fire. This can happen by the spurious opening of both RHR isolation valves (MOVs 731 and 730) if the valves are energized.

Figure 7.3.1-3 shows the control circuit for opening one of the valves. The control switch and the pressure interlock can be bypassed if the segments A and B of the wires in the cable spreading room touch each other, creating a "hot short," thus closing the circuit and energizing coil "O" which would generate an open signal to the valves.

During reactor operation, however, these valves are deenergized in the closed position by locking out their circuit breakers at their respective motor control centers (MCCs). In addition, even in the unlikely

event that the control circuits are energized and a simultaneous command to open the valves is generated by the fire, it is extremely unlikely that the valves would open. This is because the motors are undersized such that these valves cannot open against the large differential pressure which exists across the valve seat. Therefore, a large LOCA has a negligibly small frequency.

7.3.1.2.4.2 Medium LOCA. For a medium LOCA to occur, there would have to be an opening of 2 to 6 inches in equivalent diameter. There is no credible way in which a cable spreading room fire could initiate a medium LOCA.

7.3.1.2.4.3 Small LOCA. A small LOCA, which involves an opening of less than 2 inches in equivalent diameter, could occur by the simultaneous spurious opening of isolation valve MOV 536 or 535 (Figure 7.3.1-4) and of the associated power-operated relief valve (PORV) PCV-456 or PCV-455C, respectively. The small LOCA is very likely to be terminated by the fire because the hot shorts which caused the spurious openings will become open circuits due to further loss of insulation, in which case the wires contact the grounded trays. When this happens, the air-operated valves close, thus terminating the LOCA.

The inadvertent opening of a letdown line (Figure 7.3.1-5) may lead to a small LOCA as well. The normal letdown line (an orificed 3-inch pipe) is normally open and the coolant pressure drops from 2,235 psig to 225 to 275 psig when flowing through one of the orifices. The design pressure of the piping downstream of the orifices is 600 psig. If air-operated valve 201 or 202 (upstream of the nonregenerative heat exchanger) closes, the coolant pressure downstream of the orifices will increase. This will lead to the opening of relief valve 203 at 600 psig that would discharge the primary coolant into the pressurizer relief tank, thus a small LOCA. The operators can isolate this LOCA by closing AOV-459 or all three AOVs: 200A, 200B, and 200C. Furthermore, AOV-459 would close automatically at low pressurizer level or the 200 series AOVs would close upon receipt of a containment isolation phase A signal. The fire may even lead to the closure of these valves because they are of fail closed type and grounding of the wires to the solenoid will deenergize the control circuit of the valve.

The excess letdown line (Figure 7.3.1-5) is normally closed. For a small LOCA, the two series air-operated isolation valves (AOV-213 and HCV-123) would have to be opened simultaneously by hot shorts. Similar to the PORVs, they will be closed when the hot shorts become open circuits due to further loss of insulation in which case the wires contact the grounded trays.

Failure of the reactor coolant pump seals also leads to a small LOCA. This may occur due to simultaneous loss of the component cooling system and the charging pumps (see Section 1.3.3.8 for more details). A total maximum leak rate of 1,200 gpm from all four pumps might occur. This mode of small LOCA cannot be isolated. Figure 7.3.1-6 shows an event tree for this event. We assume that the availability of the refueling

water storage tank, reactor trip, and safety injection actuation are certainties. This type of small LOCA can occur due to a fire in the electrical tunnel or the electrical tunnel entrance area in the cable spreading room. As mentioned earlier, we analyze the contribution of this area as part of the electrical tunnel.

7.3.1.2.4.4 Transients. A transient can occur in many different ways (e.g., reactor trip, turbine trip, closure of main steam line isolation valves, etc.). Figure 7.3.1-7 shows a simple event tree for transients. It is assumed that, given a fire, a reactor trip, and therefore a transient, is a certainty.

7.3.1.2.4.4.1 Effects of Fires at the Center of the Northern Wall. The control cables of many safety related components come very close to each other near the ceiling at the center of the northern wall. The control room safeguards supervisory panels are immediately above the cable spreading room. The control cables of many redundant components run parallel to each other next to the northern and southern walls. At the center of the southern wall, the cables of this side go up into the cable trays next to the ceiling (18 feet above the floor) and cross the width of the cable spreading room to enter the control room at the center of the northern wall.

This area thus contains the control cables of the three auxiliary feedwater pump trains, the three safety injection pumps, the two containment spray pump trains, and all five containment fan cooler units. The control cables of the charging pumps, the PORVs, and the PORV block valves are located below the flight panel in the control room and are therefore independent of this area.

If a fire causes the failure of all these cables, the turbine-driven auxiliary feedwater pump would start at minimum speed. Local operator action can start this pump or one of the two motor-driven auxiliary feedwater pumps because the power cables would remain intact. Furthermore, the PORVs and the block valves are available in this case. Therefore, if the operators energize the safety injection pumps from the switchgears, the bleed and feed mode of operation is also possible.

7.3.1.2.4.4.2 Core Melt Frequency from Transients. The frequency of core melt can be expressed as

$$\phi_{CM,CSR} = \lambda_{CSR} f_{es} Q(\tau_G) Q_s \qquad (7.3.1\text{-}5)$$

where

λ_{CSR} = frequency of fires in the cable spreading room

f_{es} = fraction of cable spreading room fires that are large and near the center of the northern wall

$Q(\tau_G)$ = conditional frequency of fire growth

Q_s = frequency of failure to activate the auxiliary feedwater system

Human error is the main contributor to the frequency of failure to activate the auxiliary feedwater system. The following histogram gives the frequency of failure to bring the turbine-driven pump up to speed under accident conditions (from Section 1.5.3.9 of this report):

Q_S	Probability	Cumulative Probability
2.0×10^{-3}	0.05	0.05
6.8×10^{-3}	0.24	0.29
2.3×10^{-2}	0.42	0.71
8.0×10^{-2}	0.24	0.95
2.8×10^{-1}	0.05	1.00

The operators can also activate either one of the motor-driven pumps locally because the pump power cables are independent of this fire zone. These two actions (i.e., bringing the turbine-driven pump up to speed and activating either motor-driven pump) are dissimilar. Therefore, the related human errors have a low level of dependence. Reference 7.3-7 suggests that a conditional frequency of about 0.05 or greater be used for low levels of dependence (see Section 1.8.1.4.2 for a discussion on this conditional frequency). For moderate levels of dependence, this frequency is 0.14 or greater. In this case it is judged to be approximately 0.1. The operator controls the auxiliary feedwater pump output to maintain the proper steam generator levels. There are pneumatic indicators inside the containment at the airlock. There are also special procedures for safe shutdown from outside the control room. Furthermore, the primary bleed and feed mode of operation is possible because the safety injection (SI) pumps can be activated from the outside of the control room and the PORVs and their block valves can be opened from the control room. Based on this information, and given the effects of a large fire at the center of the northern wall, the conditional frequency of failure to achieve safe shutdown, Q_S, is judged to be lognormally distributed with median 5×10^{-3} and has an error factor of 20. The characteristic values are

$$Q_{S,05} = 2.5 \times 10^{-4}, \quad Q_{S,50} = 5 \times 10^{-3}, \quad Q_{S,95} = 0.1$$

$$\alpha_{Q_S} = 2.5 \times 10^{-2}$$

All the necessary data for $\phi_{CM,CSR}$, the frequency of core melt is now available. Using DPD arithmetic the following characteristic values are obtained:

5th Percentile: 3.0×10^{-10} ry^{-1}

Median: 7.3×10^{-8} ry^{-1}

95th Percentile: 3.3×10^{-6} ry^{-1}

Mean: 1.9×10^{-6} ry^{-1}

7.3.1.2.4.4.3 Containment Event Tree Entry States. In the event tree of Figure 7.3.1-7, we see that, after the postulated core melt, the status of containment cooling functions determines what containment event tree entry state would be obtained. The control cables of the two containment spray pumps and all of the five containment fan coolers would be affected by a fire in the center of the northern wall. Therefore, the fan coolers may fail and high containment pressure may not lead to the activation of the containment heat removal systems. The operators, however, can restore components by closing the corresponding breakers at the switchgear. The local start controls of the fan coolers are installed in the switchgear room. Although a significant containment pressure increase would occur only after core melt, it is very likely that the operators will restart some of the fan coolers before core melt. This is because the fans are normally operational. Furthermore, there are approximately 6 hours between melt and containment breach, thus local manual actuation of the containment spray system is also very likely. The conditional frequency of failure to activate containment heat removal systems, Q_{HE}, is derived based on these facts. It should be noted here that a major contributor to the frequency of failure to establish secondary cooling, Q_S, is human error. In view of the dependency among human actions, it is judged that Q_{HE} is lognormally distributed with a median of 0.1 and an error factor 5. The characteristic values are

$$Q_{HE,05} = 0.02, \quad Q_{HE,50} = 0.1, \quad Q_{HE,95} = 0.5, \quad \alpha_{Q_{HE}} = 0.16$$

Thus, either of the two entry states, TEFC or TE, may result. The frequency of the former is the product of $\phi_{CM,CSR}$ with the complement of Q_{HE}. The complement has the following characteristic values:

$$Q_{\overline{HE},05} = 0.5, \quad Q_{\overline{HE},50} = 0.9, \quad Q_{\overline{HE},95} = 0.98, \quad \alpha_{Q_{\overline{HE}}} = 0.84$$

The product of these two distributions is the frequency of entering state TEFC due to a fire at the center of the northern wall, $\phi_{TEFC,CSR}$ and is presented in Table 7.3.1-2. The characteristic values are

5th Percentile: 1.9×10^{-10} ry^{-1}

Median: 6.0×10^{-8} ry^{-1}

95th Percentile: 4.0×10^{-6} ry^{-1}

Mean: 1.6×10^{-6} ry^{-1}

The frequency of entering state TE due to a fire at the center of the northern wall, $\phi_{TE,CSR}$, is the product of Q_{HE} and the frequency of

core melt. The results are presented in Table 7.3.1-3. The characteristic values are

5th Percentile: less than 10^{-10} ry^{-1}

Median: 7.2×10^{-9} ry^{-1}

95th Percentile: 5.9×10^{-7} ry^{-1}

Mean: 3.0×10^{-7} ry^{-1}

7.3.1.2.5 Contributions from Other Areas in the Cable Spreading Room

We have already analyzed the effects of fires at the center of the northern wall. The eastern end of the cable spreading room is analyzed as part of the electrical tunnel. Fire in all other areas in the cable spreading room except for the northwestern quarter would not affect the auxiliary feedwater system. The overall unavailability of this system due to causes other than fire is very low, approximately 10^{-6}. Therefore, the overall impact on fire risk is very small.

The control cables of the two motor-driven auxiliary feedwater pumps, safety injection pumps 21 and 23, containment spray pump train 21, and containment fan coolers 23 and 24 are located in the northwestern quarter outside the center area of the northern wall. Many important components (for example, SI pump 22 and the PORVs) are independent of this area. Therefore, the contribution of fires in this quarter to the overall fire risk is also small.

7.3.1.3 Some Areas in the Primary Auxiliary Building, the Fan House, and the Control Building

Three buildings, the primary auxiliary building (PAB), the control building (CB), and the fan house (FH) are analyzed simultaneously because they are similar to auxiliary buildings typically found in other nuclear power plants. Several areas within these buildings (except for the cable spreading room) are analyzed and, given a fire, the conditional frequency of containment event tree entry states is computed. The weighted sums of these frequencies are the conditional frequencies of the entry states caused by fires postulated in these three buildings. For the unconditional frequencies, the latter is multiplied with the frequency of fires.

7.3.1.3.1 The Frequency of Fires

There are 10 reported fires in auxiliary buildings for the industry and the number of building years is 303.3. The state of knowledge distribution is a gamma with parameters $\alpha = 10.32$ and $\beta = 303.59$, and with the following characteristic values (per year):

$\lambda_{AUX,05} = 0.015$, $\lambda_{AUX,50} = 0.033$, $\lambda_{AUX,95} = 0.053$,

$\alpha_{\lambda_{AUX}} = 0.034$

Three areas of the primary auxiliary building, the fan house, and the control building were determined to require detailed analysis. They are fire zones 1A (electrical tunnel PAB side), 14 (switchgear room), and 32A (electrical tunnel CB side) (see Reference 7.3-1 for zone designations). Two other areas, fire zones 27A (safety related MCC-26A and MCC-26B) and 74A (containment electrical penetration area), have been considered also; however, they are not significant when compared to the two portions of the electrical tunnel and the switchgear room (see Sections 7.3.1.6 and 7.3.1.8).

The fraction of auxiliary building fires that would occur in each specific area is estimated based on the following observations:

- Both portions of the cable tunnel have the same characteristics except that, in one of them (zone 32A), an automatic sprinkler system is installed.
- In the switchgear room, equipment with moving parts (air compressors) and breakers for electric power are installed.
- There are more than 25 compartments in these three buildings that have characteristics similar to these three fire zones; they contain pumps, cable trays, etc.
- The majority of fires in auxiliary buildings in the data base involved electrical circuitry components (e.g., breakers, relays, coils, MCCs).
- The electrical tunnel is similar to the cable spreading room except that it is less frequented by personnel and that the cable spreading room contains reactor trip breakers, motor generator sets, and DC power panels in addition to the cables.

Fires are judged to be more likely in the switchgear room than in the cable spreading room, because of the fourth observation above. If all compartments of these three buildings were alike, then the conditional frequency of fire occurrence in one of them would be less than

$$\frac{1}{25} = 0.04$$

However, a review of the fire incident data, compiled in Reference 7.3-6, reveals that the majority of auxiliary building fires involved electrical components typically found in switchgear rooms (e.g., coils, relays, etc.). Therefore, the fraction of switchgear fires may be larger than the uniform fraction. Based on this, the fraction of PAB, CB, and FH fires that could occur in the switchgear room, f_{SWG}, is judged to be lognormally distributed with the following characteristic values:

$$f_{SWG,05} = 0.05, \quad f_{SWG,50} = 0.20, \quad f_{SWG,95} = 0.80, \quad \alpha_{f_{SWG}} = 0.285$$

Note that the unconditional frequency of fires in the switchgear (i.e., the product of λ_{AUX} and f_{SWG}) has the following characteristic values (per reactor year):

$$(\lambda_{AUX}f_{SWG})_{05} = 1.1 \times 10^{-3}, \quad (\lambda_{AUX}f_{SWG})_{50} = 6.5 \times 10^{-3},$$

$$(\lambda_{AUX}f_{SWG})_{95} = 2.2 \times 10^{-2}, \quad \alpha_{\lambda_{AUX}f_{SWG}} = 9.4 \times 10^{-3}$$

Based on the last observation above, the frequency of electrical tunnel fires is expected to be lower than that for cable spreading room fires. The fraction of PAB, CB, and FH fires that could occur in a given electrical tunnel, f_T, is judged to be lognormally distributed with the following characteristic values:

$$f_{T,05} = 8.0 \times 10^{-3}, \quad f_{T,50} = 4.0 \times 10^{-2}, \quad f_{T,95} = 2.0 \times 10^{-1}$$

$$\alpha_{f_T} = 6.5 \times 10^{-2}$$

The unconditional frequency of fires in an electrical tunnel has the following characteristic values (per reactor year):

$$(\lambda_{AUX}f_T)_{05} = 1.7 \times 10^{-4}, \quad (\lambda_{AUX}f_T)_{50} = 1.3 \times 10^{-3},$$

$$(\lambda_{AUX}f_T)_{95} = 5.6 \times 10^{-3}, \quad \alpha_{\lambda_{AUX}f_T} = 2.2 \times 10^{-3}$$

The two unconditional frequencies should be compared with the cable spreading room frequency (see Section 7.3.1.2.2). The relative magnitudes of these frequencies support the judgment for f_T. It should also be noted that if these two conditional frequencies (f_{SWG} and f_T) are treated as independent variables, there is a small probability that their sum will become greater than unity. Because this probability is small, the dependency between f_{SWG} and f_T is not included in the calculations.

7.3.1.4 Fire Zone 1A (Electrical Tunnel, PAB Side)

7.3.1.4.1 Characteristics of the Area

This zone is also known as the electrical and piping tunnel and piping penetration area. It is located in the primary auxiliary building at Elevation 51'.

The only safety related equipment in this area are the electrical cables. This includes power cables for the containment spray pumps, safety injection pumps, component cooling pumps, containment fan coolers, and residual heat removal pumps. It also includes power and control cables

for the charging pumps, pressurizer relief valves (PORVs), PORV block valves, secondary atmospheric relief valves, and control cable (only) for the auxiliary feedwater pump trains. The cable routing configuration in this compartment is identical to the cable tunnel entrance area in the cable spreading room. Figure 7.3.1-2 shows a cross-section of the tunnel, the cable trays, and their contents. The separation between the cables of different divisions follows the same rules as those for the cable spreading room (see Section 7.3.1.2.2).

This area is a controlled access area. The primary combustible is cable insulation. The heat released from burning transient fuels (5 lbs. of wood, 2 lbs. of paper, and 2 lbs. of plastic) is 76,000 Btus (Reference 7.3-1). The area contains smoke detectors and hand extinguishers. A manual hose station at the west end of the primary auxiliary building has access to this area.

7.3.1.4.2 Fire Propagation and Extinguishment in the Cable Tunnel

Three basic fire propagation patterns are of interest in this zone. The first two involve fire initiation in a tray on either the left or right side of the tunnel (Figure 7.3.1-2) and propagation among the cables on that fire-initiated side. The fire will probably not spread to the trays on the other side due to the low heat release rate of cable insulation fires and the approximately inverse relationship of the radiated thermal heat fluxes with the square of the distance to those trays. The third fire propagation pattern involves an exposure fire occurring in the aisle which passes between the two stacks of cable trays.

7.3.1.4.2.1. First Propagation Pattern. In the first fire propagation pattern, the fire is initiated in a control cable tray. The fire spreads upward and horizontally with a characteristic spread time τ_V. The distribution of τ_V as a function of Q_p, the mean heat content of the pilot fuel which initiates the fire, is developed in Section 7.3.4 (Appendix I).

The distribution of Q_p for this location is as follows:

$$Pr(Q_p = 400 \text{ Btu}) = 0.10$$

$$Pr(Q_p = 4000 \text{ Btu}) = 0.45$$

$$Pr(Q_p = 40000 \text{ Btu}) = 0.45$$

This distribution reflects the belief that a fire in the cable trays will probably involve additional fuels as well as cable insulation, because cable insulation is generally quite difficult to ignite. To provide some physical basis for the choice of Q_p, we note that 400 Btu from a 1-foot square fuel packet corresponds roughly to cable insulation burning for 1 minute (i.e., the initial fuel bed is essentially only cable insulation). Four thousand Btu can be associated with wood, paper, or plastic burning for 2 minutes, and 40,000 Btu can be equated with approximately 1 quart of oil burning in 1 minute. We note that a

quantity of wood burning for 2.5 minutes will release approximately the same amount of heat as a similarly sized oil fire burning for 1 minute; a strict equivalence between Q_p and the representative fuels mentioned is not intended.

The resulting distribution for τ_V for this location has the following characteristic values (minutes):

$$\tau_{V,05} = 2.0, \quad \tau_{V,50} = 9.5, \quad \tau_{V,95} = 37.0, \quad \alpha_{\tau_V} = 14.4$$

7.3.1.4.2.2 Second Propagation Pattern. The second propagation pattern involves fire initiation in a power cable tray. Because a 1/4-inch thick transite barrier is placed above power cable trays and the analysis of Section 7.3.4 (Appendix I) indicates that the barrier inhibits fire spread to trays above, only horizontal spread across the tray is considered. Two vertical metal barriers separated by a small air gap are located in the tray. Fire propagation across the tray is not prevented, however, because the flames on one side extend above the height of the barriers and can radiate heat to the opposite side.

The distribution for the spread time, τ_H, has the following characteristic values expressed in minutes:

$$\tau_{H,05} = 6.2, \quad \tau_{H,50} = 27.6, \quad \tau_{H,95} = 108.7, \quad \alpha_{\tau_H} = 44.0$$

This distribution is developed from the previous distribution for Q_p and the distributions for horizontal fire spread given in Section 7.3.4 (Appendix I).

7.3.1.4.2.3 Third Propagation Pattern. The third fire propagation pattern involves exposure fires in the center aisle, because a large fire in this location may ignite and/or seriously damage cables on both sides of the aisle.

Simple heat flux calculations, similar to those done in Section 7.3.6 (Appendix III), are performed to determine the damage potential of an exposure fire. The two exposure fires used to represent this case are fueled with oil and are located in the middle of the aisle. Their diameters are 2 feet and 1 foot, respectively.

The heat flux impinging on the cable trays is modeled by considering the heat flux falling on a small, horizontal area located 3 feet away from the fire's axis, or about 0.5 feet in from the tray edge. The elevation is that of the flame's base. To be conservative, the shielding effects of the tray sides and of the trays immediately above and below are neglected. The heat flux from the 2-foot diameter exposure fire is then computed to be 7,100 W/m^2, and for the 1-foot diameter fire, it is 2,900 W/m^2.

Using the above heat fluxes and a spontaneous ignition temperature of 825°K, the respective ignition times are computed to be 12 and 71 minutes [see Equation (7.3.4.1-9)]. The amounts of fuel required to sustain the 2-foot and 1-foot diameter fires for these durations are approximately 4.2 and 6.3 gallons, respectively.

Because the larger diameter exposure fire requires less fuel than the smaller one, it is judged to be a more reasonable and more conservative representative of the class of exposure fires which can lead to ignition of cables on both sides of the aisle.

It is noted that fires of similar size fueled by materials other than oil will take significantly longer to propagate; a 2-foot diameter polymethylmethacrylate (PMMA) fire located in the middle of the aisle requires approximately 3 hours to ignite the cable trays.

Note also that exposure fires located closer to one stack of cable trays will ignite that stack more quickly. The same PMMA fire discussed above requires only 50 minutes to ignite the trays, if it is located immediately next to the trays. However, the farther stack of trays will ignite more slowly. Therefore, it is judged that the central placement of the exposure fire is reasonable for our representative propagation pattern studied here.

The actual fire propagation time for the aisle fire, τ_A, is the product of the calculated spread time (12 minutes) and the error factor ψ, defined earlier in Section 7.3.1.2, which quantifies our uncertainty in the modeling. To be conservative, the time required for the flames to spread horizontally across the width of the tray is neglected. This spread is expected to be fairly rapid because the exposure fire heat flux increases the burning rate of the ignited fuel and preheats the unignited fuel. The distribution of τ_A has the following characteristic values (minutes):

$$\tau_{A,05} = 9.6, \quad \tau_{A,50} = 15.2, \quad \tau_{A,95} = 24.0, \quad \alpha_{\tau_A} = 15.8$$

7.3.1.4.2.4 Combined Propagation and Extinguishment. The distributions for τ_V, τ_H, and τ_A, given above are derived without consideration for efforts at extinguishing the fire. To account for extinguishment of the cable tray initiated fires (propagation patterns one and two), the extinguishment model described in Section 7.3.1.2.3.2 is used, i.e.,

$$Q(t) = \exp(-t/\tau_S) \qquad (7.3.1\text{-}6)$$

The distribution for the mean extinguishment time, τ_S, has been derived in Section 7.3.1.2.3.2 and is given in Table 7.3.1-4. This distribution applies to the first two propagation patterns. $Q(\tau_V)$

and $Q(\tau_H)$ are the respective conditional frequencies of fire propagation for the first two patterns. The probability distribution of $Q(\tau_V)$ has the following characterisic values:

$$Q_{05}(\tau_V) = 1.6 \times 10^{-3}, \quad Q_{50}(\tau_V) = 0.45, \quad Q_{95}(\tau_V) = 0.86,$$

$$\alpha_{Q(\tau_V)} = 0.44$$

The probability distribution of $Q(\tau_H)$ has the following characteristic values:

$$Q_{05}(\tau_H) = \text{smaller than } 10^{-8}, \quad Q_{50}(\tau_H) = 7.3 \times 10^{-2},$$

$$Q_{95}(\tau_H) = 0.68, \quad \alpha_{Q(\tau_H)} = 0.21$$

As for extinguishing a large aisle fire (i.e., the third growth pattern), we note that there are no automatic fire extinguishment systems in this portion of the electrical tunnel. However, smoke detectors will alert plant personnel within a short period of time after ignition and there are methods for fighting intense fires in small enclosures. Because of the geometry of the tunnel, the intensity of the exposure fire, and the relatively short time (i.e., approximately 15 minutes) for failure of vital components, the postulated aisle fire is judged to burn until propagation is complete. Thus, $Q(\tau_A) = 1.0$, and the frequency of fire propagation due to a large aisle fire is the frequency of that fire.

7.3.1.4.3 Conditional Frequencies of Fire Propagation Scenarios

The large aisle fires discussed in the preceding section form a subset of all possible fires in the electrical tunnel. The fraction of large electrical tunnel fires which burn highly combustible fuels (e.g., oil), and are in the aisle is defined as f_A. It should be noted that fires involving less flammable fuels must consume considerably larger amounts of fuel to have the same effect as those burning highly combustible fuels. Furthermore, in Section 7.3.1.4.2.3, it was found that only a certain set of fires may lead to cable failure within a reasonable fire duration. Therefore, it is judged that f_A is rather small with a median of 0.01. The data used in deriving λ_{AUX}, however, were mainly fires significant enough to be reportable. Thus, 0.10 was chosen for its 95th percentile. A lognormal distribution fitted to these two percentiles yields the following characteristic values:

$$f_{A,05} = 1.0 \times 10^{-3}, \quad f_{A,50} = 1.0 \times 10^{-2}, \quad f_{A,95} = 1.0 \times 10^{-1},$$

$$\alpha_{f_A} = 2.66 \times 10^{-2}$$

Some additional observations used in deriving this distribution are:

- Generally, no maintenance work is performed in this zone during power operation.

- The zone is not used for carrying large amounts of combustibles.
- Administrative procedures prohibit the personnel to take actions that may increase the fire hazard in this zone without a fire watch being present.
- The critical area constitutes a large fraction (approximately 0.4) of the total electrical tunnel floor area.
- A significant fraction (approximately 0.1) of the cable insulation fires reported in Reference 7.3-6 was estimated to be large.

To be conservative, the fraction of cable tray fires, f_C, is modeled as the complement of f_A. Because the latter is smaller than 0.1, its complement is almost unity. There are two similar stacks of cable trays. Therefore, the fraction of electrical tunnel fires in a given stack of trays, f_R, is half of f_C. Thus,

$$f_R \simeq 0.5$$

7.3.1.4.4 Effects of Fire in the Left Stack of Trays on Accident Sequences

The power cables to many redundant and diverse safety related components are located in the two bottom-most layers of trays. A 1/4-inch thick transite barrier is installed between these two sets of trays (Figure 7.3.1-2). The results of Section 7.3.4 (Appendix I) show that fire spread through the transite barrier is not likely. Because a serious fire must involve both trays, the effects of a fire initiated in the left stack of trays are deemed less significant than fires on the right stack of trays or in the aisle.

7.3.1.4.5 Effects of Fires in the Right Cable Trays on Accident Sequences

Figure 7.3.1-2 shows that the third layer of cable trays in the right stack of trays contains the power cables for all three component cooling pumps, all three charging pumps, both containment spray pumps, and both safety related MCCs, 26A and 26B. Two sets of initiating events may occur due to cable damage in this stack of trays. If all component cooling pumps and all charging pumps fail, a small LOCA would develop by causing the failure of the seals of all four reactor coolant pumps. If this initiating event does not occur, the fire would lead to a transient, e.g., a reactor trip.

Auxiliary feedwater and the high pressure injection systems would not be affected by a fire in the right stack of cable trays. In the case of a transient, the availability of the former (i.e., the auxiliary feedwater system) is sufficient for accident mitigation. Section 1.5.2.3.3, shows

that the unavailability of this system has the following characteristic values:

5th Percentile: 2.8×10^{-6} ry^{-1}

Median: 1.1×10^{-5} ry^{-1}

95th Percentile: 4.7×10^{-5} ry^{-1}

As seen later, other fire scenarios are the major contributors to the fire risk.

In the case of a small LOCA, both the auxiliary feedwater system (AFWS) and the high pressure injection system (HPIS) should be available. If both are available, failure of the low head recirculation system (Figure 7.3.1-6) could lead to containment event tree entry state SLF. The recirculation system is not required to operate until approximately 10 hours after the small LOCA. Because of such a long period, the effects of fire would be minimal by the time the recirculation mode of operation would become necessary. However, if the MCCs are not restored by the time it becomes necessary to operate the recirculation system, all MOVs would not be remotely operational. Therefore, MOVs 885A, 885B, and 888A or 888B (Figure 7.3.1-8) would have to be opened manually and the RHR pumps would have to be used. The recirculation pumps cannot be used because MOVs 1802A and 1802B inside containment would be inoperable. The RHR pumps would not be affected by the fire at the right stack of trays.

The block valves of the PORVs and the containment spray pumps would be unavailable. Therefore, the possible event sequences are 1, 3, 4, 6, 14, 16, 18, and 20 (Figure 7.3.1-6). The "nonsuccess" event sequences are quantified hereafter:

- Event Sequence 3. The HPIS, AFWS, and containment fan coolers are available in this sequence. About 10 hours or more after the small LOCA, the recirculation system should be activated. It can only be achieved by local manual actions. By this time, many people would be following the shutdown process. In Section 1.5.2.3.4, the frequency of failure of the recirculation system because of human error (about 10 hours after the accident) is estimated to have the following characteristic values:

  $Q_{05} = 3.7 \times 10^{-6}$, $Q_{50} = 7.5 \times 10^{-5}$, $Q_{95} = 1.5 \times 10^{-3}$

  $\alpha_Q = 3.9 \times 10^{-4}$

  In this sequence of events, the process is different because the actions have to be performed manually. The procedure for LOCA mitigation does not explicitly spell out this mode of external recirculation alignment. However, the control room operators are familiar with this mode of operation because of training, and because it is discussed in the emergency procedure for loss of component cooling.

Based on this information, the frequency of recirculation system failure is judged to be lognormally distributed with the following characteristic values:

$$Q_{LH,05} = 0.002, \quad Q_{LH,50} = 0.02, \quad Q_{LH,95} = 0.20,$$

$$\alpha_{Q_{LH}} = 0.05$$

This is the conditional frequency of Event Sequence 3, Q_3, given a fire that has failed the power cables of the right stack of trays.

- Event Sequence 6. The HPIS and AFWS are available. The containment fan coolers are independent from the fire and they are normally running. Therefore, the accident sequence does not have any impact on their availability. The unavailability of the fan coolers is discussed in Section 1.5.2.3.6 and has the following characteristic values:

$$Q_{CF,05} = 1.1 \times 10^{-7}, \quad Q_{CF,50} = 5.3 \times 10^{-7},$$

$$Q_{CF,95} = 3.6 \times 10^{-6}, \quad \alpha_{Q_{CF}} = 1.4 \times 10^{-6}$$

The remainder of this event sequence is identical to that of Sequence 3. Given that a fire has failed the power cables of the right stack of trays, the conditional frequency of Event Sequence 6, Q_6, is the product of Q_{CF} with Q_{LH}. Using DPD arithmetic, the following characteristic values are obtained:

$$Q_{6,05} = 2.0 \times 10^{-10}, \quad Q_{6,50} = 2.3 \times 10^{-8}, \quad Q_{6,95} = 2.7 \times 10^{-6}$$

$$\alpha_{Q_6} = 1.5 \times 10^{-6}$$

- Event Sequence 14. The HPIS and the containment fan coolers are available. The AFWS is independent from the fire. The operators, as top priority action, will ensure that at least one auxiliary feedwater pump is delivering water to the steam generators. In Section 1.5.2.3.9, the unavailability of the AFWS has been analyzed. It has the following characteristic values:

$$Q_{AFWS,05} = 2.8 \times 10^{-6}, \quad Q_{AFWS,50} = 1.1 \times 10^{-5},$$

$$Q_{AFWS,95} = 4.7 \times 10^{-5}, \quad \alpha_{Q_{AFWS}} = 1.9 \times 10^{-5}$$

This is the conditional frequency of Event Sequence 14, Q_{14}, given that a fire has failed the power cables of the right stack of trays.

- Event Sequence 16. The only available system is the HPIS. Both the AFWS and containment fan coolers are independent of the fire zone. Their unavailabilities, Q_{AFWS} and Q_{CF}, are given in the previous

two sequence descriptions. Given that a fire has failed the power cables of the right stack of trays, the conditional frequency of Event Sequence 16, Q_{16}, is the product of these two unavailabilities. The characteristic values are:

$$Q_{16,05} = 5.6 \times 10^{-13}, \quad Q_{16,50} = 6.1 \times 10^{-12},$$

$$Q_{16,95} = 6.6 \times 10^{-11}, \quad \alpha_{Q_{16}} = 1.7 \times 10^{-11}$$

- Event Sequence 18. Only the fan coolers are available in this sequence. The HPIS is independent of the fire zone. The operators would start the system if the automatic start signals were not generated. In Section 1.5.2.3.1, the unavailability of this system for a small LOCA is analyzed. Its characteristic values are:

$$Q_{HPIS,05} = 3.3 \times 10^{-5}, \quad Q_{HPIS,50} = 1.7 \times 10^{-4},$$

$$Q_{HPIS,95} = 4.4 \times 10^{-4}, \quad \alpha_{Q_{HPIS}} = 1.9 \times 10^{-4}$$

This is the conditional frequency of Event Sequence 18, Q_{18}, given a fire that has failed the power cables of the right stack of trays.

- Event Sequence 20. The HPIS and the fan coolers are unavailable in this sequence. Given that a fire has failed the power cables of the right stack of trays, the conditional frequency of this sequence, Q_{20}, is the product of Q_{HPIS} and Q_{CF}. The characteristic values are:

$$Q_{20,05} = 1.1 \times 10^{-11}, \quad Q_{20,50} = 8.9 \times 10^{-11},$$

$$Q_{20,95} = 7.5 \times 10^{-10}, \quad \alpha_{Q_{20}} = 2.1 \times 10^{-10}$$

The conditional frequencies of the containment event tree entry states can now be evaluated using Figure 7.3.1-6. For example, the conditional frequency of SEF is the sum of the conditional frequencies of Event Sequences 14 and 18. Table 7.3.1-5 summarizes the results.

7.3.1.4.6 Effects of Fires in the Aisle on Accident Sequences

In Section 7.3.1.4.2.3, it was found that a large fire in the aisle between the cable trays can affect the cables on both sides of the tunnel. In such a case, the power feeds to the charging pumps, the containment spray pumps, the component cooling pumps, and MCCs 26A and 26B would become unavailable as well as to the normal control of the auxiliary feedwater pumps and the power to the SI pumps, PORVs, and all five containment fan coolers.

The postulated small LOCA through failure of the reactor coolant pump seals is also a possibility in this case because all component cooling pumps and all charging pumps could be lost. This can be prevented by energizing one charging pump from the alternate shutdown system

(Reference 7.3-8), which requires attachment of a power cable from the alternate shutdown system to the desired charging pump. Plant personnel would have approximately 30 minutes to put a charging pump on line before the reactor coolant pump seals are damaged. If the small LOCA does not occur, transients are certain. The question is, given a large fire in the aisle which initiating event would occur?

The transients may lead to containment event tree entry state TE (Figure 7.3.1-7) which is slightly more severe than entry state SE (to which a small LOCA may lead). Either the AFWS or primary coolant bleed and feed are sufficient to mitigate a transient. For a small LOCA, however, the HPIS should be available in addition to the AFWS or primary coolant bleed and feed. This means that the latter is a more demanding case than the transients; therefore, it is conservatively assumed that, given a large fire in the aisle, a small LOCA is certain. No credit is given for the possibility of energizing a charging pump from the alternate shutdown system because of the short time window (approximately 30 minutes).

Figure 7.3.1-6 indicates that when the HPIS, fan coolers, and containment spray pumps are unavailable, containment event tree entry state SE would occur. In the case of a large fire in the aisle, it is conservatively assumed that this entry state is certain.

7.3.1.4.7 Frequencies of the Containment Event Tree Entry States

The frequencies of the significant containment event tree entry states as caused by a fire in the PAB side of the electrical tunnel are evaluated in this section. The entry states that are not mentioned here have a very small frequency of occurrence.

- Entry State SLF. The main contributor to the frequency of this entry state is a fire in the right stack of cable trays. The frequency of this entry state, $\phi_{SLF,1A}$ can be evaluated using the following formula:

$$\phi_{SLF,1A} = \lambda_{AUX} f_T f_R Q(\tau_V) Q_{LH} \qquad (7.3.1\text{-}7)$$

where

λ_{AUX} = frequency of fires in the PAB, the control building (CB) or the fan house (FH),

f_T = fraction of PAB, CB and FH fires that occur in the electrical tunnel in the PAB,

f_R = fraction of electrical tunnel fires that occur in the right stack of trays,

$Q(\tau_V)$ = conditional frequency of fire propagation, and

Q_{LH} = frequency of failure of the recirculation system given the loss of MCC buses 26A and 26B due to the fire.

Using DPD arithmetic in Equation (7.3.1-7), the distribution for $\phi_{SLF,1A}$ is evaluated and given in Table 7.3.1-6. The characteristic values are:

5th Percentile:	2.1×10^{-8} ry^{-1}
Median:	3.7×10^{-6} ry^{-1}
95th Percentile:	6.7×10^{-5} ry^{-1}
Mean:	2.4×10^{-5} ry^{-1}

- Entry State SEF. The main contributor to the frequency of this entry state is a fire in the right stack of cable trays. The frequency of this entry state can be evaluated using the following formula:

$$\phi_{SEF,1A} = \lambda_{AUX} f_T f_R Q(\tau_V)(Q_{AFWS} + Q_{HPIS}) \qquad (7.3.1\text{-}8)$$

where

Q_{HPIS} = frequency of failure of the HPIS independent from the fire

Q_{AFWS} = frequency of failure of the AFWS independent from the fire

The remaining terms have been defined earlier in this section. Using DPD arithmetic, $\phi_{SEF,1A}$ is obtained. Table 7.3.1-7 gives the histogram. The characteristic values are:

5th Percentile:	2.4×10^{-10} ry^{-1}
Median:	3.7×10^{-8} ry^{-1}
95th Percentile:	3.2×10^{-7} ry^{-1}
Mean:	1.0×10^{-7} ry^{-1}

- Entry State SE. The main contribution to the frequency of this entry state is a fire in the aisle between the two stacks of cable trays. The frequency of this entry state can be evaluated using the following formula:

$$\phi_{SE,1A} = \lambda_{AUX} f_T f_A \qquad (7.3.1\text{-}9)$$

where

f_A = fraction of electrical tunnel fires that are large and occur in the aisle portion.

Using DPD arithmetic, the probability distribution of $\phi_{SE,1A}$ is obtained. Table 7.3.1-8 gives the histogram. The characteristic values are:

5th Percentile:	1.9×10^{-8} ry^{-1}
Median:	6.1×10^{-6} ry^{-1}
95th Percentile:	1.2×10^{-4} ry^{-1}
Mean:	5.6×10^{-5} ry^{-1}

7.3.1.5 Switchgear Room (Fire Zone 14)

7.3.1.5.1 Characteristics of the Room

This room is located at Elevation 15' of the control building. Its safety related equipment consists of 480V switchgear numbers 2A, 3A, 5A, and 6A in two parallel rows facing each other (Figure 7.3.1-9). The cables feeding the switchgear cabinets enter the cabinets from above. They include power and control cables for charging, safety injection, component cooling, auxiliary feedwater and containment spray pumps, containment fan coolers, service water and residual heat removal pumps, and MCCs 26A and 26B. This equipment occupies half of the room; instrument air compressors are located in the other half. This room is a controlled access area.

The transient fuels in this area are assessed in Reference 7.3-1 as 15 lbs. of wood, 8 lbs. of paper, 8 lbs. of plastic, 5 lbs. of oil, and 10 lbs. of grease. The in situ combustibles are lightly loaded cable trays stacked 3 feet high at most. The lubricating fluid in the air compressors (7 gallons each) is "Anderol," which has a very high ignition temperature. There are 14 ionization-type detectors in the area. The fire fighting equipment consists of three 15-lb. carbon dioxide bottles inside the room and a master hose station in a stairwell outside the room. Also, there are hydrants and hose cabinets in the outside transformer yard which can be used for the switchgear room through a door in the north wall.

There are two areas in this room where a postulated fire would be of particular interest: the cable trays next to the ceiling in the eastern half of the room, and the switchgear cabinets. The typical separation between two cable trays of different divisions is approximately 1 foot and the fire propagation analysis is performed accordingly. Because fires caused by the switchgear would not have sufficient fuel to propagate to adjacent cabinets and because of the relatively low burning intensity of the cabinet fire, only external fires are considered.

Large outside fires propagating into the room are judged to be unlikely. A 3-hour fire barrier is installed on the north wall to protect the area from an exterior transformer fire. Similarly, a 3-hour fire barrier is installed between this room and the turbine building to protect against fires initiating in the turbine building.

7.3.1.5.2 Fire Propagation and Extinguishment in the Switchgear Room

Two fire scenarios are identified (see Section 7.3.1.5.2.3). The first involves two sets of cable trays elevated 12 feet above the floor and separated horizontally by a distance of 3 feet. The second involves a transient fuel exposure fire located in an aisle between the switchgear cabinets.

7.3.1.5.2.1 Cable Tray Fires. There are three horizontal cable trays in the zone of interest. Two are stacked vertically with a separation distance of 1 foot, with the lower tray being 12 feet above the floor. A 1/4-inch transite barrier is located a few inches below the upper tray. The remaining tray is parallel to the other two but is 3 feet to the south. This last tray is 13 feet above the floor. It is necessary to consider fire propagation to all three trays, and in particular, fire propagation to the upper northern tray.

The analysis of fire propagation in this zone is similar to that used for the cable spreading room (Section 7.3.1.2.3.1). However, the horizontal separation between the two tray stacks and the transite barrier in the northern stack must be taken into account.

In the cable spreading room analysis, the effect of a large exposure fire immediately underneath a critical stack of cable trays was investigated. To determine the location for the representative exposure fire in this analysis, the exposure fire was placed on the floor underneath the northern stack of trays, underneath the southern tray, and in between the two tray groups. The time to ignition of the lower trays in both groups was not significantly different for these three cases. In this analysis, therefore, the exposure fire is assumed to be underneath the northern trays.

The transite barrier inhibits rapid fire propagation to the upper northern tray from the lower one. The barrier model developed in Section 7.3.4 (Appendix I) was used, noting that the combination of heat fluxes from the barrier and from the burning southern tray may cause ignition of the upper northern tray.

Using COMPBRN (Reference 7.3-5) and an assumed 1-foot diameter oil fueled exposure fire, the time required for fire propagation to the upper northern tray is calculated to be about 12 minutes. The thermal barrier somewhat retards fire propagation in the case of this large fire.

The distribution for the characteristic propagation time, τ_G, is then constructed using the error factor, ϕ, defined in Section 7.3.4 (Appendix I).

$$\tau_G = \phi \tau_{G,DRM} \qquad (7.3.1\text{-}10)$$

where $\tau_{G,DRM}$ is 12 minutes in this case. τ_G is lognormally distributed with the following characteristic values (minutes):

$$\tau_{G,05} = 9.6, \quad \tau_{G,50} = 21.5, \quad \tau_{G,95} = 48, \quad \alpha_{\tau_G} = 24.2$$

To account for extinguishment, Equation (7.3.1-4) can be used where t is replaced with τ_G. The histogram of Table 7.3.1-1 should be used for τ_S because only large fires can reach the cable trays at 12 feet above the floor. Therefore, the conditional frequency of fire propagation to these cable trays, $Q(\tau_G)$ has the following characteristic values:

$$Q_{05}(\tau_G) = 0.04 \quad Q_{50}(\tau_G) = 0.44, \quad Q_{95}(\tau_G) = 0.82,$$

$$\alpha_{Q(\tau_G)} = 0.46$$

7.3.1.5.2.2 Aisle Exposure Fire. In this section, the effect of a large fire located in the aisle between the switchgear cabinets is considered. Because there is no permanent fuel bed in the aisle, the fire can only be fueled by transient combustibles.

The switchgear room electrical cabinets are modeled as metal boxes measuring 7.52m long by 1.46m deep by 2.44m high. A fire is considered to be serious if it causes a temperature rise to at least 120°C in two cabinets (which are separated by a 1.76m wide aisle). This is the maximum design temperature of typical electrical components (Reference 7.3-9).

Using the calculations described in Section 7.3.5 (Appendix II), the following regression for the asymptotic cabinet air temperature due to a steady heat flux $\dot{q}''_{in}$ (W/m^2) impinging on the front face of the cabinet is derived

$$T_A = 0.81 \, (\dot{q}''_{in})^{0.55} \, ^{o}C \qquad (7.3.1\text{-}11)$$

The critical heat flux required to cause a temperature rise to above 120°C, according to this model, is approximately 8,800 W/m^2. The heat flux attenuation model from Section 7.3.6 (Appendix III) shows that this corresponds to an oil pool fire 2 feet in diameter, located 3 feet away from the cabinet (i.e., in the middle of the aisle).

7.3.1.5.2.3 Conditional Frequency of Large Exposure Fires. The frequency of severe consequences from fires in the switchgear room can be written as the sum of the four frequencies derived for: (1) fires in the cable trays (Figure 7.3.1-9), (2) large fires on the floor affecting the cable trays, (3) fires in the aisle between the switchgear cabinets, and (4) fires inside a cabinet.

Because the cable trays are relatively inaccessible due to their elevation, the frequency of the large floor-level fires which affect the elevated trays is greater than the frequency of serious fires initiated within the cable trays. This greater frequency, in turn, is lower than the overall frequency of fires in the switchgear room. Not only must the exposure fire be very large (see Section 7.3.1.5.2.1), but it must also be located near the east/west cable trays running from the center of the room to the eastern wall. These trays, which contain all exposed

power cable (except those for the auxiliary feedwater pumps and the service water pumps), are widely separated until they reach this portion of the room. Of course, a much larger exposure fire may affect the widely separated section of trays also, but the frequency of such a fire is extremely low.

For the switchgear cabinets, the results of Section 7.3.1.5.2.2 indicate that a very large aisle fire is also required to raise the air temperatures of two cabinets of two different divisions above 120°C. Fires starting within a cabinet will not propagate to a different division because their intensity will be too low.

Note that in the case of an exposure fire involving the switchgear cabinets, some safety system trains would remain available for accident mitigation unless the fire involves nearly all cabinets lining the aisle. This is extremely unlikely because the size of the fire required to damage only two cabinets is already quite large. Because the fire in this location can only be fueled by transient combustibles, propagation over a permanent fuel bed is not possible; a larger exposure fire requires a larger amount of transient fuel in the aisle.

Based on the above discussions, the dominant scenario is a fire affecting the east/west running cable trays. The fraction of large fires, f_{SL}, in the switchgear room that could occur in the cable tray area is lognormally distributed with a median of 5×10^{-3} and an error factor of 4. The characteristic values are

$$f_{SL,05} = 5 \times 10^{-4}, \quad f_{SL,50} = 5 \times 10^{-3}, \quad f_{SL,95} = 5 \times 10^{-2},$$

$$\alpha_{f_{SL}} = 1.33 \times 10^{-2}$$

Note that most of the auxiliary building fires involved components typically found in a switchgear area. The magnitudes of all of them, however, were much smaller than the fires considered in Section 7.3.1.5.2.1. Furthermore, the main combustibles were not of the transient type.

7.3.1.5.3 Effects of Fires on Accident Sequences

The configuration of the power cables in the two sets of cable trays at the eastern part of the switchgear room (Figure 7.3.1-9) is identical to that of the electrical tunnel. Similar to the analysis for the tunnel, three different cases are identified: (1) fire affects the northern cable trays only, (2) fire affects the southern cable trays only, and (3) fire affects both sets of trays. The first case is equivalent to fire in the left stack of trays in the electrical tunnel. In this case, there are no transite barriers between the trays. The second case is equivalent to fires in the right stack of trays in the electrical tunnel. The third case is similar to the aisle fire discussed in Section 7.3.1.4.6.

7.3.1.5.3.1 Effects of Fires in the Northern Cable Trays on Accident Sequences. The power cables to all three safety injection pumps, all five containment fan coolers, and both recirculation pumps are run through the northern cable trays. Failure of the cables in these trays would not lead to a LOCA. Some types of transients may occur. The auxiliary feedwater system is independent from this area. Its unavailability is evaluated in Section 1.5.2.3.3. The 95th percentile is 6.2×10^{-6}. This is an upper bound for the conditional frequency of core melt resulting from a transient, given that a fire in the switchgear room has affected the northern set of cable trays only. Because of the low frequency of switchgear fires, the frequencies of containment event tree entry states TEFC, TEF, TEC, and TE from a fire that affects the northern trays are considered to be less than 10^{-7} per reactor year.

7.3.1.5.3.2 Effects of Fires in the Southern Cable Trays on Accident Sequences. The effect of fires in the southern cable trays on accident sequences is similar to the effect of fires in the right stack of trays in the electrical tunnel (Section 7.3.1.4.5). That is, a small LOCA may occur and MCCs 26A and 26B and the containment spray pumps may not be available. Therefore, the conditional frequencies given in Table 7.3.1-5 are applicable to this case also.

7.3.1.5.3.3 Effects of Fires on Both Sets of Cable Trays on Accident Sequences. The discussions in Section 7.3.1.4.6 apply to this case also; that is, a small LOCA would occur and the HPIS, the containment fan coolers, and the containment spray system would be affected. Therefore, the containment event tree entry state SE, given a fire affecting both sets of trays is certain.

7.3.1.5.4 Containment Event Tree Entry States Due to a Fire in the Switchgear Room

In Section 7.3.1.5.2, the fire propagation calculations show that, in the case of a large fire that affects one set of cable trays, there is a good chance that the other set of cable trays would also be affected. Therefore, containment event tree entry state SE dominates (Section 7.3.1.5.3.3). Its frequency can be written as

$$\Phi_{SE,14} = \lambda_{AUX} f_{SWG} f_{SL} Q(\tau_G) \qquad (7.3.1\text{-}12)$$

where

λ_{AUX} = the frequency of fires in PAB, CB, and FH

f_{SWG} = the fraction of PAB, CB, and FH fires that may occur in the switchgear room

f_{SL} = the conditional frequency of large exposure fire underneath the cable trays running east/west given a fire in the switchgear room

$Q(\tau_G)$ = the fraction of large switchgear room fires that would damage the cables in trays running east/west

The remaining terms have been defined earlier. Using DPD arithmetic, the histogram of Table 7.3.1-9 is obtained. $\phi_{SE,14}$ has the following characteristic values:

5th Percentile: 1.8×10^{-8} ry^{-1}

Median: 5.4×10^{-6} ry^{-1}

95th Percentile: 1.3×10^{-4} ry^{-1}

Mean: 5.6×10^{-5} ry^{-1}

7.3.1.6 Corridor (Fire Zone 27A)

This corridor at Elevation 98' of the primary auxiliary building contains the safety related motor control centers 26A and 26B. The controls of all safety related motor-operated valves pass through these motor control centers. It is a controlled access area. The auxiliary feedwater system, however, is totally independent from this area. The unavailability of the AFWS because of other causes is presented in Section 1.5.2.3.9 and the characteristic values are:

5th Percentile: 2.75×10^{-6}

50th Percentile: 1.06×10^{-5}

95th Percentile: 4.67×10^{-5}

Considering the frequency of fires in other areas and the fire propagation analysis performed for other areas, the frequency of failing both of the MCCs is judged to be less than 10^{-2} per reactor year. A LOCA cannot be caused by a fire in this area. Therefore, the frequency of core melt given a fire is the product of this frequency and the failure frequency of the auxiliary feedwater system. The fire risk from this area is thus much less than the risk from the two areas previously discussed.

7.3.1.7 Electrical Tunnel, CB Side (Fire Zone 32A)

This zone is the electrical tunnel portion that is located in the control building (CB). It is a controlled access area. It is the continuation of fire zone 1A and has identical characteristics except that a closed head preaction fire extinguishment sprinkler system is also installed. The heat detectors in the area have temperature settings lower than the sprinkler heads. These detectors open the deluge valves that isolate the fire water from the sprinkler heads. Therefore, the sprinkler system piping fills with water before the sprinkler heads are activated (at temperatures higher than that of the heat detectors). This portion of the cable tunnel is connected to the eastern end of the cable spreading room and has the same characteristics as the cable spreading room/electrical tunnel entrance area. The same fire scenarios and accident mitigation scenarios that apply to this zone also apply to zone 1A.

7.3.1.7.1 Fire Scenarios and Accident Sequences

The fire propagation scenario at the right stack of trays is identical to that discussed for zone 1A in Section 7.3.1.4.5. The same extinguishment model can be used because it has a large weight to manual extinguishment (40% probability to 5-minute extinguishment time). The effects of the cable tray fires on accident sequences are the same. Therefore, the significant containment event tree entry states are SLF, SL, SEF, and SE. See Table 7.3.1-5 for the conditional frequencies of these entry states given a cable tray fire at the right stack of trays.

The analysis of an aisle fire is similar to that of fire zone 1A except that the sprinkler systems should be taken into account also.

Replacing t with τ_A in Equation (7.3.1-4) and the histogram of Table 7.3.1-1 for τ_S, the conditional frequency of fire propagation in the aisle section, $Q(\tau_A)$, is evaluated. The characteristic values are

$$Q_{05}(\tau_A) = 0.19, \quad Q_{50}(\tau_A) = 0.56, \quad Q_{95}(\tau_A) = 0.86,$$

$$\alpha_{Q(\tau_A)} = 0.57$$

The effect of aisle fires on accident sequences is the same as that for fire zone 1A (Section 7.3.1.4.6). Given a large fire in the aisle, containment event tree entry state SE would occur.

7.3.1.7.2 Frequencies of Containment Event Tree Entry States

The frequencies of the significant containment event tree entry states caused by a fire in the electrical tunnel of the control building are evaluated in this section. The entry states that are not mentioned have a very small frequency of occurrence.

- Entry State SLF. For this entry state, the conditions are identical to those described in Section 7.3.1.4.7. Therefore, Equation (7.3.1-7) and its input quantities apply to this case also, and Table 7.3.1-6 gives the results. The characteristic values of $\Phi_{SLF,32A}$ are:

  5th Percentile: 2.1×10^{-8} ry^{-1}

  Median: 3.7×10^{-6} ry^{-1}

  95th Percentile: 6.7×10^{-5} ry^{-1}

  Mean: 2.4×10^{-5} ry^{-1}

- Entry State SEF. For this entry state, the conditions are identical to those described in Section 7.3.1.4.7. Therefore, Equation (7.3.1-8) and its input quantities apply to this case also,

and Table 7.3.1-7 gives the results. The characteristic values of $\phi_{SEF,32A}$ are

5th Percentile: 2.4×10^{-10} ry^{-1}

Median: 3.7×10^{-8} ry^{-1}

95th Percentile: 3.2×10^{-7} ry^{-1}

Mean: 1.0×10^{-7} ry^{-1}

- Entry State SE. The main contributor to the frequency of this entry state, similar to fire zone 1A, is a fire in the aisle between the two stacks of cable trays. The frequency of this entry state can be evaluated using the following formula:

$$\phi_{SE,32A} = \lambda_{AUX} f_T f_A Q(\tau_A) \qquad (7.3.1\text{-}13)$$

where

$Q(\tau_A)$ = the conditional frequency of fire growth given a fire in the aisle

The remaining entries of this equation have been defined in Section 7.3.1.4.7. Using DPD arithmetic, the probability distribution of $\phi_{SE,32A}$ is obtained. Table 7.3.1-10 gives the histogram. The characteristic values are

5th Percentile: 1.0×10^{-8} ry^{-1}

Median: 3.1×10^{-6} ry^{-1}

95th Percentile: 7.0×10^{-5} ry^{-1}

Mean: 3.2×10^{-5} ry^{-1}

7.3.1.8 Electrical Penetration Area (Fire Zone 74A)

This area is located in the fan house next to the containment and is a controlled access area. The control cables for the auxiliary feedwater pumps and their regulating valves, the power cables for the containment fan coolers, and the power and control cables for the PORVs and their associated block valves are located in this area. The conditions are similar to those of the left stack of trays in the electrical tunnel except that the power cables of the safety injection pumps are not run through this area. Similar to the left stack of trays there are 1/4-inch thick transite barriers above the power cables (the two bottommost cable trays). In Section 7.3.1.4.4, it was found that fire propagation through the barriers is very unlikely. At most, therefore, an exposure fire can only fail the containment fan coolers, the controls for the auxiliary feedwater pumps, and the control and power for the PORVs and their associated block valves. The containment spray system

would not be affected by such a fire. Since the unavailability of the containment spray system from causes other than fires is on the order of 10^{-5}, the contribution of zone 74A to the fire risk is dominated by other areas.

7.3.1.9 Diesel Generator Building

Loss of all AC power would result if all three diesel generators are disabled in a loss of offsite power condition. The disablement of the diesels as caused by fires is the subject of this section. The loss of offsite power is assumed to be due to all causes; that is, loss of offsite power simultaneously with all the initiating events (LOCAs and transients) and due to causes external to the plant.

7.3.1.9.1 Characteristics of the Area

All three diesel generators of this unit are housed inside one building. It is a controlled access area. Figures 7.3.1-10 and 7.3.1-11 show the layout of this area. Each day tank contains 175 gallons of fuel oil. The fuel line leaves the bottom of this tank and runs straight down to the area underneath the gratings on the floor. There, it travels horizontally and parallel to the engine and comes up at different locations to meet the fuel injection lines. Wet type sprinklers are installed to protect the day tanks and feed lines.

A pit underneath each engine catches leaking oil and water. Drainage of these pits is sufficient to ensure that oil does not collect under normal conditions. In addition, each diesel pit drain has a check valve to prevent backflow from one diesel pit from entering the others. Wet type sprinklers are installed underneath each engine and at the top of the pits.

All three diesels take suction from within the building. The air intake system includes filters and superchargers. The intake openings are on the southern end of the engine and are immediately below the exhaust pipe. There are several small lines and filters for fuel oil and lube oil below the air intake openings.

The portions of the engines above the floor grating are separated by a 1/8-inch aluminum splash shield that prevents accidentally ejected pressurized oil from reaching an adjacent engine.

The local control board for all three engines is installed on a 5-foot high platform against the west wall. The board is shielded from the westernmost diesel generator by a 14-foot concrete wall. Figure 7.3.1-10 gives the details on the relative position of these items.

The structural members of this building are coated with fire retardant materials so that their fire rating has been upgraded to a minimum of 2 hours. There are 21 heat detectors in the area with setpoints of 180^{0}F. They alarm in the control room.

This building has two doors, one at the eastern end and the other at the western end where the control panels are located. In case of a large fire, plant personnel can enter and fight the fire from either of the

two entrances. A fire hydrant and hose cabinet are located outside the diesel generator building, and fire extinguishers are also provided for this area.

7.3.1.9.2 The Frequency of Fires

The number of reported fires on diesel generators for the industry is 10 and the number of diesel years is 593.0. The average number of diesel generator start ups is estimated to be two per month or 14,232 trials. The state of knowledge distribution is beta distribution* with parameters p = 10 and q = 14,222 and with the following characteristic values (per demand):

$$Q_{DG,05} = 3.9 \times 10^{-4},\ Q_{DG,50} = 6.7 \times 10^{-4},\ Q_{DG,95} = 1.1 \times 10^{-3},$$

$$\alpha_{Q_{DG}} = 7.0 \times 10^{-4}$$

7.3.1.9.3 Diesel Engine Failures

There are several mechanisms by which a fire can fail one or more diesels. These include explosions, missiles and the release of excessive amounts of smoke, which could stall the engines due to lack of oxygen. To gain insight into these mechanisms, we analyzed 16 incidents reported in Nuclear Power Experience (NPE) (Reference 7.3-13).

Most of the 16 fires were small and were extinguished quickly by plant personnel. A typical cause is leaking fuel oil igniting upon contacting the exhaust manifold. There were no coupled failures (mainly because, in most plants, the diesels are in separate rooms) and in only eight cases even the engine on which the fire occurred was declared inoperable. In two cases, however, the fires were "large" in the sense that they released large amounts of heat and smoke, and they damaged other components in the vicinity of the engines. These were the Zion 2 (September, 1976) and San Onofre 1 (July, 1981) fires.

7.3.1.9.4 Accident Analysis

The diesel generators are essential only on loss of offsite power. In the following subsections we quantify the unavailability of one, two and three diesels due to fire.

7.3.1.9.4.1 One Diesel Failure. An inspection of the diesel generator fire occurrence reports reveals that not all fires have led to engine failure. For this study it is conservatively assumed that given a fire,

*The probability density functions for the beta distribution is

$$b(Q\ p,q) = \frac{\Gamma(p+q)}{\Gamma(p)\Gamma(q)} Q^{p-1}\ (1-Q)^{q-1}$$

$$0 \leq Q \leq 1$$

$$0 \leq p,q$$

the involved engine becomes unavailable. It is further assumed that only large fires have the potential of affecting more than one engine. Thus the frequency of only one diesel generator failure due to fire is equal to the frequency of small fires.

Of the 16 diesel fire incidents that have been studied, only 2 are judged to be large. The state of knowledge uncertainty about the fraction of large fires f_L is beta with parameters p = 2 and q = 16, and the following characteristic values:

$$f_{L,05} = 1.0 \times 10^{-2},\ f_{L,50} = 9.2 \times 10^{-2},\ f_{L,95} = 2.0 \times 10^{-1},$$

$$\alpha_{f_L} = 0.13$$

The unavailability of at least one of the three diesels due to fires can be written as

$$\phi_{1DG} = 3(1 - f_L)\, Q_{DG}$$

Using DPD arithmetic the following characteristic values of ϕ_{1DG} are obtained:

$$\phi_{1DG,05} = 7.7 \times 10^{-4},\ \phi_{1DG,50} = 1.8 \times 10^{-3},\ \phi_{1DG,95} = 2.8 \times 10^{-3}$$

$$\alpha_{\phi_{1DG}} = 1.8 \times 10^{-3}$$

This unavailability when compared with the results of Section 1.2.1.1, is an insignificant contributor to diesel generator unavailability due to other causes. Thus further investigation of the impact of one diesel failure due to fire is not warranted.

7.3.1.9.4.2 Two Diesels Failure. It is judged that only large fires have the potential of affecting more than one diesel. The dominant scenarios for the failure of only two out of three diesels is a large fire at the two end diesels, judging that the adjacent engine would shield the third from both blast waves and thermal exposure. The frequency of the simultaneous failure of two diesels becomes

$$\phi_{2DG} = 2 f_L Q_{DG}$$

Using DPD arithmetic the characteristic values of ϕ_{2DG} are evaluated as

$$\phi_{2DG,05} = 2.0 \times 10^{-5},\ \phi_{2DG,50} = 1.2 \times 10^{-4},\ \phi_{2DG,95} = 3.5 \times 10^{-4},$$

$$\alpha_{\phi_{2DG}} = 1.6 \times 10^{-4}$$

This unavailability as compared with the results of Section 1.2.1.1, is a small contributor to the unavailability of two diesels due to other causes. Thus, further investigations of the impact of two diesel failures due to fire is not warranted.

7.3.1.9.4.3 Three Diesel Failure. In Section 7.3.1.9.3, it is concluded that only large fires have the potential of affecting more than one diesel. The dominant scenario for the failure of all three diesels is a large fire involving the central engine. The frequency of this event can be written as

$$\phi_{3DG} = f_L Q_{DG}$$

Using DPD arithmetic, the following characteristic values of ϕ_{3DG} are evaluated:

$$\phi_{3DG,05} = 1.0 \times 10^{-5}, \ \phi_{3DG,50} = 6.0 \times 10^{-5}, \ \phi_{3DG,95} = 1.8 \times 10^{-4},$$

$$\alpha_{\phi_{DG}} = 8.0 \times 10^{-5}$$

7.3.1.9.5 Core Melt From Diesel Fires.

A core melt may occur if a loss of offsite power is followed by loss of all three diesels due to fire and power is not restored to at least one of the essential buses for more than 1 hour. From the information given in Section 1.3.2.2, the frequency of electric power nonrecovery within the first hour, ϕ_{NR1}, given permanent loss of all three diesels is calculated. Its characteristic values are:

$$\phi_{NR1,05} = 0.025, \ \phi_{NR1,50} = 0.05, \ \phi_{NR1,95} = 0.10, \ \alpha_{\phi_{NR1}} = 0.54$$

The core melt frequency can be written as

$$\phi_{CM,DG} = \lambda_{LOS} f_L Q_{DG} \phi_{NR1}$$

where λ_{LOS} is the frequency of loss of offsite power and the remaining parameters have been defined earlier in this section. From Section 1.1.1, the following characteristic values are found for λ_{LOS} (per reactor year):

$$\lambda_{LOS,05} = 3.0 \times 10^{-2}, \ \lambda_{LOS,50} = 1.6 \times 10^{-1}, \ \lambda_{LOS,95} = 4.6 \times 10^{-1},$$

$$\alpha_{\lambda_{LOS}} = 2.0 \times 10^{-1}$$

Using DPD arithmetic the state of knowledge distribution for $\phi_{CM,DG}$ is evaluated. It yields the following characteristic values (per reactor year):

$$\phi_{CM,DG,05} = 5.9 \times 10^{-8}, \ \phi_{CM,DG,50} = 5.0 \times 10^{-7}, \ \phi_{CM,DG,95} = 3.0 \times 10^{-6},$$

$$\alpha_{\phi_{CM,DG}} = 8.9 \times 10^{-7}$$

7.3.1.9.6 Containment Event Tree Entry State SEFC from Diesel Fires

The containment event tree entry state SEFC would result if power to an essential bus were recovered between 1 and 3 hours after failure of all three diesels. Since the frequency of nonrecovery within 3 hours is very small, frequency of SEFC from diesel generator fires $\phi_{SEFC,DG}$ is almost equal to the core melt frequency $\phi_{CM,DG}$.

7.3.1.9.7 Containment Event Tree Entry State SE from Diesel Fires

The containment event tree entry state SE would result if power to an essential bus were not recovered within the first 3 hours after station blackout. From information given in Section 1.3.2.2, the frequency of electric power nonrecovery within the first 3 hours, ϕ_{NR3}, given permanent loss of all three diesels is calculated. Its characteristic values are

$$\phi_{NR3,05} = 1.2 \times 10^{-4}, \quad \phi_{NR3,50} = 1.3 \times 10^{-3}, \quad \phi_{NR3,95} = 8.3 \times 10^{-3},$$

$$\alpha_{\phi_{NR3}} = 2.7 \times 10^{-3}$$

The frequency for SE can be written as

$$\phi_{SE,DG} = \lambda_{LOS} f_L Q_{DG} \phi_{NR3}$$

Using DPD arithmetic, the state of knowledge distribution for $\phi_{SE,DG}$ is evaluated. It yields the following characteristics values (per reactor year):

$$\phi_{SE,DG,05} = 1.0 \times 10^{-9}, \quad \phi_{SE,DG,50} = 1.8 \times 10^{-8}, \quad \phi_{SE,DG,95} = 1.3 \times 10^{-7},$$

$$\alpha_{\phi_{SE,DG}} = 4.4 \times 10^{-8}$$

7.3.1.10 Smoke Propagation

Smoke can have an impact on a fire-initiated accident scenario by corroding components and causing their failure or by reducing personnel effectiveness. Because the corrosion process is rather slow, component failures due to smoke would not have a significant impact on accident (e.g., LOCA) mitigation. Smoke may have a long term effect on component availability; however, the possibility of smoke causing an initiating event (i.e., LOCA, transients) is inconceivable.

The effects of smoke on the accident sequences due to its impact on plant personnel in certain critical plant areas are discussed hereafter. Areas of the plant not discussed either do not contain safety

related items or do not require operator action in those areas. The results of the preceding sections apply in the following plant areas:

- Control Room. The ventilation system of the control room is independent of the rest of the plant. It can be switched to several modes of operation. One such mode is the circulation of the control room air through filters. Smoke from fires in other parts of the plant can not propagate into this area. Therefore, in the case of fire in any of the critical areas that were discussed in the preceding section, the control room would remain inhabitable.

- Cable Spreading Room. The exhaust fans at the end of the electrical tunnel would draw the smoke toward the east end of the cable spreading room, through the electrical tunnel, and exhaust it to the tranformer yard. Smoke from this area would not propagate to other areas (e.g., switchgear room) where manual actions would be necessary.

- Electrical Tunnel (Fire Zones 32A and 1A). Similar to the cable spreading room, the exhaust fans would draw the smoke from the CB portion of the tunnel (fire zone 32A) toward the east end of the tunnel and out into the transformer yard. Smoke from this area would not propogate to other areas (e.g., switchgear room) where manual actions would be necessary. The entire PAB, including fire zone 1A (except the boric acid evaporator building), is ventilated through the PAB ventilation system.

- Switchgear Room. Three exhaust fans can draw the smoke out of this room. Each fan has about 20,000 cfm capacity and all are powered from MCC 29. The smoke from a turbine building fire may propagate into this area which would lead to automatic closure of the dampers at that interface. However, manual actions in this area would not be necessary in the case of such fires.

  A fire in the switchgear room may also cause the failure of the exhaust fans. In the preceding sections, a large fire in this area was found to lead to containment event tree entry state SE. The uncertainities in the frequencies of those accident sequences also cover the scenarios where exhaust fans are unavailable.

- Diesel Generator Building. This building stands free from the rest of the plant. Large capacity ventilating fans are provided for this area. Smoke propagation into this building is judged to have a very small impact on the frequencies of accident sequences because of the backup electrical power sources available for the plant (e.g., the offsite AC power and the gas turbine generators).

- Fire Zone 27A. This area contains MCCs 26A and 26B. If these MCCs are affected, the valve operations can be performed at the valve location by turning the handwheels. All the necessary MOVs are located outside the containment.

- Auxiliary Feedwater Pump Room (Fire Zone 23). All three auxiliary feedwater pumps are housed in this area. In the case of loss of control or power to the auxiliary feedwater pumps, the operators can start the turbine-driven pump from this area or they can switch the power of one of the motor-operated pumps to the alternate shutdown system. The building containing the auxiliary feedwater pumps is independent of the critical areas identified earlier in this section.

7.3.1.11 Flooding Due to Suppression Activities

The only areas that contain both a fixed fire water system and safety related shutdown equipment are the control building side of the electrical tunnel (fire zone 32A) and the diesel generator building. Drainage is provided by floor and hub drains. In the unlikely event of failure of the drainage system in the electrical tunnel, the water from the sprinklers will flow down the tunnel to the cable spreading room. Flooding of the cable spreading room may lead to the failure of the batteries. Although it is unlikely, the water may also penetrate the switchgear ceiling at the power cable seals. It may affect the air compressors. It will not, however, reach the switchgear cabinets because they are located at the far end of the cable trays. The impact of flooding from the sprinkler system in the cable tunnel on the frequencies of severe consequences is therefore judged to be minimal.

Flooding from the use of fire hose stations cannot have a significant impact on the frequencies of severe consequences because floor drains are provided. Because the process is manual, uncontrolled conditions would be avoided.

The impact of a flooding in the diesel generator building from an unlikely failure of the drainage system would be limited to the diesel generator sets only. Therefore, its impact on the overall fire risk is very small.

7.3.1.12 Core Melt Frequency Due to Fires at Indian Point 2

The total frequency of core melt caused by fires is the sum of the core melt frequencies from different fire zones. For the cable spreading room, it was explicitly calculated. For the electrical tunnels, two scenarios are the main contributors to core melt frequency. These two scenarios lead to entry states SLF and SE. For the switchgear room, the core melt frequency is dominated by the frequency of entry state SE. Therefore, the total core melt frequency can be written as

$$\phi_{CM} = \phi_{CM,CSR} + \phi_{SLF,1A} + \phi_{SE,1A} + \phi_{SE,14} + \phi_{SLF,32A} + \phi_{SE,32A} + \phi_{CM,DG} \qquad (7.3.1\text{-}16a)$$

or

$$\phi_{CM} = \phi_{CM,CSR} + \lambda_{AUX}[f_T(2f_R Q(\tau_V) Q_{LH} + f_A(1 + Q(\tau_A)) + f_{SWG} f_{SL} Q(\tau_{G,SWG})] + \phi_{CM,DG} \qquad (7.3.1\text{-}16b)$$

The probability distribution of the core melt frequency is given in Table 7.3.1-16 and has the following characteristic values:

5th Percentile:	6.0×10^{-6} ry^{-1}
Median:	6.5×10^{-5} ry^{-1}
95th Percentile:	7.6×10^{-4} ry^{-1}
Mean:	2.0×10^{-4} ry^{-1}

7.3.1.13 Frequencies of Containment Event Tree Entry States Due to Fires at Indian Point 2

The frequencies of containment event tree entry states caused by a fire in the power plant can now be evaluated. In the analyses of the preceding subsections, the frequencies of entry states caused by fires were calculated for specific areas. The frequencies of only six entry states are significant. Each state is discussed separately.

- Entry State TEFC. The main contributor to the frequency of this entry state is a fire in the cable spreading room. The probability distribution of ϕ_{TEFC} is given by Table 7.3.1-2. The characteristic values are

5th Percentile:	1.9×10^{-10} ry^{-1}
Median:	6.0×10^{-8} ry^{-1}
95th Percentile:	4.0×10^{-6} ry^{-1}
Mean:	1.6×10^{-6} ry^{-1}

- Entry State TE. The main contributor to the frequency of this entry state is a fire in the cable spreading room. The probability distribution of ϕ_{TE} is given by Table 7.3.1-3. The characteristic values are

5th Percentile:	less than 10^{-10} ry^{-1}
Median:	7.3×10^{-9} ry^{-1}
95th Percentile:	5.9×10^{-7} ry^{-1}
Mean:	3.0×10^{-7} ry^{-1}

- Entry State SEFC. The main contributors for this entry state are fires in the diesel generator building. Therefore,

$$\phi_{SEFC} = \phi_{SEFC,DG}$$

The characteristic values of ϕ_{SEFC} are:

5th Percentile: 4.2×10^{-8}

Median: 5.0×10^{-7}

95th Percentile: 3.0×10^{-6}

Mean: 8.9×10^{-7}

- Entry State SLF. The main contributors to the frequency of this entry state are fires in the two portions of the electrical tunnel (fire zones 1A and 32A). Therefore,

$$\phi_{SLF} = 2\phi_{SLF,1A} \qquad (7.3.1\text{-}17)$$

Table 7.3.1-11 gives the result of this multiplication. The characteristic values of ϕ_{SLF} are

5th Percentile: 4.3×10^{-8} ry^{-1}

Median: 7.4×10^{-6} ry^{-1}

95th Percentile: 1.3×10^{-4} ry^{-1}

Mean 4.9×10^{-5} ry^{-1}

- Entry State SEF. The main contributors to the frequency of this entry state are fires in the two portions of the electrical tunnel (fire zones 1A and 32A). Therefore,

$$\phi_{SEF} = 2\phi_{SEF,1A} \qquad (7.3.1\text{-}18)$$

Table 7.3.1-12 gives the result of this multiplication. The characteristic values of ϕ_{SEF} are

5th Percentile: 4.9×10^{-10} ry^{-1}

Median: 7.4×10^{-8} ry^{-1}

95th Percentile: 6.4×10^{-7} ry^{-1}

Mean: 2.0×10^{-7} ry^{-1}

- Entry State SE. The main contributors to the frequency of this entry state are fires in the two portions of the electrical tunnel (fire zones 1A and 32A) and the switchgear room. Therefore,

$$\phi_{SE} = \phi_{SE,1A} + \phi_{SE,32A} + \phi_{SE,14}$$

$$= \lambda_{AUX}\left[\left(1 + Q(\tau_A)\right) f_T f_A + f_{SWG} f_{SL} Q(\tau_G)\right] \qquad (7.3.1\text{-}19)$$

Table 7.3.1-13 gives the result. The characteristic values of ϕ_{SE} are

5th Percentile: 4.0×10^{-7} ry^{-1}

Median: 2.8×10^{-5} ry^{-1}

95th Percentile: 7.1×10^{-4} ry^{-1}

Mean: 1.4×10^{-4} ry^{-1}

7.3.1.14 Frequencies of Release Categories from Fires at Indian Point 2

The release categories that fires may lead to are 8A, 8B, and 2RW. The frequencies of other categories caused by fires are very small in comparison.

- Release Category 8A. The containment event tree entry states SLF and SEF lead to this release category. Its frequency can be written as

$$\phi_{8A} = \phi_{SLF} + \phi_{SEF} = 2\lambda_{AUX} f_T f_R Q(\tau_V) (Q_{LH} + Q_{AFWS} + Q_{HPIS}) \quad (7.3.1\text{-}20)$$

Table 7.3.1-14 gives the result. The characteristic values are

5th Percentile: 1.2×10^{-7} ry^{-1}

Median: 9.0×10^{-6} ry^{-1}

95th Percentile: 1.6×10^{-4} ry^{-1}

Mean: 5.0×10^{-5} ry^{-1}

The main contributor to this release category is containment event tree entry state SLF, which is caused by fires in the right stack of trays in either portion of the electrical tunnel.

- Release Category 8B. The containment event tree entry states TEFC and SEFC lead to this release category. Their frequencies can be written as:

$$\phi_{8B} = \phi_{TEFC} + \phi_{SEFC}$$

The characteristic values are

5th Percentile: 1.2×10^{-7} ry^{-1}

Median: 8.6×10^{-7} ry^{-1}

95th Percentile: 2.2×10^{-5} ry^{-1}

Mean: 2.5×10^{-6} ry^{-1}

- Release Category 2RW. The containment event tree entry states SE and TE lead to this release category. Its frequency can be written as

$$\Phi 2RW = \Phi TE + \Phi SE \qquad (7.3.1\text{-}21)$$

Table 7.3.1-15 gives the result of this summation. The characteristic values are

5th Percentile: 5.0×10^{-7} ry^{-1}

Median: 2.8×10^{-5} ry^{-1}

95th Percentile: 7.1×10^{-4} ry^{-1}

Mean: 1.4×10^{-4} ry^{-1}

The main contributor to this release category is containment event tree entry state SE, which is primarily caused by aisle fires in the switchgear room and the two portions of the electrical tunnel.

7.3.1A ADDITIONAL FEATURES, INDIAN POINT UNIT 2

7.3.1A.1 Introduction

In Section 7.3.1, the overall risk due to fires is found to be dominated by two fire zones: (1) the switchgear room, and (2) the electrical tunnel. In this section, the impact of a plant modification to reduce the frequency of fire initiated core melt events is evaluated.

The fire scenarios originating in those zones proceed through these stages: occurrence, propagation, and extinguishment of the fire itself, and the impact of the fire on the safety components. Modifications can be proposed to affect one or more aspects of fire occurrence and lead to reduction in the overall fire risk. The most effective modification is the installation of additional transfer switches in the already existing alternate shutdown system (ASDS) and relocating of the alternate pneumatic indicators for steam generator levels and pressurizer level and pressure to outside the containment. The additional transfer switches would facilitate a quicker connection to an alternate power source for one train of component cooling pumps, charging pumps, and service water pumps.

The dominant fire scenario in Section 7.3.1 is loss of the component cooling system (CCS) and the normal charging system (CVCS) (due to power cable failure) and loss of all mitigating systems. A small LOCA via reactor coolant pump (RCP) seal failure results from CCS and charging system failure.

To quantify the frequencies of core melt and release categories after the modification is completed, we need a more detailed list of contributors. This is because, when the dominant contributors are reduced, other formerly noncontributing areas may gain importance. The frequencies are reviewed in Section 7.3.1A.2.

The different aspects of a fire incident are analyzed in Section 7.3.1A.3. The details of the modification and all the necessary assumptions for evaluating the impact of this modification are given in Section 7.3.1A.4. The impact of the modification is evaluated in Section 7.3.1A.5. The results are summarized in Table 7.3.1A-17.

7.3.1A.2 Fire Risk Before the Modification

Fire risk results before the modification are needed for: (1) choosing the type of modification; and (2) measuring the reduction in the frequencies of core melt and release categories. In Section 7.3.1 these frequencies are calculated in terms of the dominant contributors. Most of the fire zones were not explicitly analyzed quantitatively, judging that their contribution would be insignificant. Typically, these fire zones contained only a few safety related components. The proposed modification would certainly change the pattern of contributors to the release categories and core melt. The fire risk from all fire zones not

explicitly quantified in Section 7.3.1 are now so quantified. Table 7.3.1A-18 summarizes the results and Section 7.3.1A.6 gives the details. The fire zone designating numbers are taken from Reference 7.3-1. All the areas that contain some safety components per Reference 7.3-1 are included here. The results of Section 7.3.1 are directly used in Table 7.3.1A-18. For areas not originally quantified in Section 7.3.1, point values (mean frequencies) are estimated per formulations given in Section 7.3.1A.6. The fire zones analyzed in Section 7.3.1 are found to be (as expected) the dominant contributors to core melt and damage states SE and TE. However, the mean frequency of other damage states are found to be dominated by fire zones not explicitly quantified in Section 7.3.1. Two comments are in order here. First, the increased frequency of these damage states has very little impact on the overall frequency of the damage states. The mean frequency of release category 8A increases from 4.8×10^{-5} per reactor year (from Table 8.3-2) to 4.9×10^{-5} per reactor year. Second, the main contributors to this increase are computed by conservative methods, and a more rigorous evaluation is expected to yield smaller frequencies and an overall 8A frequency very close to that presented in Section 7.3.1. The overall mean frequency of release category 8B is 9.1×10^{-5} per reactor year (from Table 8.3-2) and is significantly larger than 1.8×10^{-5}, the new frequency of 8B due to fires. The latter is now dominated by contributions from fire zones that were not explicitly quantified in Section 7.3.1. In Section 7.3.1A.6, we find that many conservative measures are incorporated in the quantification of these dominating fire zones.

7.3.1A.3 Basis for Modification

In this section, the basis for the proposed modification is examined. A typical quantification process for a critical fire area can be written as

$$\Phi_{Damage} = \lambda_{Fire} Q_{Plant}$$

where λ_{Fire} represents fire phenomenology and Q_{Plant} represents the impact of fire on accident sequences. By fire phenomenology we mean the occurrence of fire in critical areas, its propagation to vital components, and failure of extinguishment features to put out the fire in time to prevent the failure of vital components. The conditional frequency (given the fire) Q_{Plant} represents the frequency of failure of vital components, the frequency of failure in restoring a failed component, and the unavailability of components independent from fire. The frequency of fires is obtained from statistical data.

Plant response to a fire incident can be altered by introducing new equipment or new power sources to existing equipment. In Section 7.3.1, we find that there are two important areas (the switchgear room and the electrical tunnel) through which the power cables of almost all vital components are routed. Also, we find that the dominant accident sequence is a small LOCA via RCP seal failure and multiple loss of engineered safeguards. If seal failure can be prevented, core melt due to other initiating events (we have assumed a reactor trip as the enveloping

initiating event) would depend on the availability of the turbine-driven or a motor-driven auxiliary feedwater pump. The turbine-driven pump can be started and brought up to speed independent of the switchgear room or the electrical tunnel. A motor-driven auxiliary feedwater pump can be powered from the alternate shutdown system.

In Section 7.3.1, we find that the existing alternate shutdown system configuration does not provide adequate protection to prevent RCP seal failure. This is because to power a charging pump and/or a component cooling pump from the alternate shutdown source, a cable (or cables) must be run from disconnect switch(es) near the pump(s), replacing the original power cable(s). The process was judged to take longer than a half hour, thereby not preventing RCP seal failure. It should be noted that the half hour is the conservatively assumed time to RCP seal failure in the absence of seal water injection and thermal barrier cooling.

The process can be expedited by installing fixed alternate cabling and transfer switches and connecting both normal and alternate power cables to the switches. The operators can then switch to the alternate shutdown system by simply throwing the transfer switches. If the seal failure is prevented, the plant can be safely shut down using the secondary side cooling features. However, it is necessary to monitor the steam generator levels and pressurizer level and pressure. It is proposed that the existing alternate pneumatic indicators for these parameters be relocated outside the containment. More details about this modification are given in the following section.

7.3.1A.4 Description of the Modification

The most effective modification is the installation of transfer switches for one train of service water pumps, charging pumps, and component cooling pumps and relocating pneumatic level and pressure indicators outside the containment. The switches will allow an operator to transfer the power source for these pumps to the Indian Point Unit 1 switchgear within the first half hour of an accident that disables the component cooling and charging pumps. Figure 7.3.1A-12 shows the transfer switch that is already installed for a motor-driven auxiliary feedwater pump. It is assumed that the proposed ones will be very similar to this one.

This modification is judged to be the most effective because it complements another major modification, the alternate shutdown system installed previously. It does not require major rewiring of power or control circuits or installation of new major components.

The alternate shutdown system is described in Reference 7.3-14. It uses Indian Point Unit 1 switchgear and power cables are run to supply at least one service water pump, one motor-driven auxiliary feedwater pump, one component cooling pump, and one charging pump. With the proposed modification, the operators can transfer the power source of the dedicated pumps by manually throwing a switch near the pump location. Of course, they have to load the Unit 1 switchgear (which must be accomplished locally) prior to engaging the transfer switch(es). The

power cables of the alternate shutdown system are routed through areas independent from the switchgear room, the electrical tunnel, the cable speading room, the control room, containment spray pump room (fire zone 2), and the primary makeup pump area (fire zone 2B). It is assumed in this analysis that the procedures will be modified to address the addition of the new switches and the system will be functionally tested prior to service. Furthermore, as part of this modification, the pneumatic indicators installed near the airlock in the containment for steam generator level and pressurizer level and pressure will be relocated to outside the containment.

7.3.1A.5 Fire Risk After the Modification

The modification impacts mainly those fire scenarios such as fires in the electrical tunnel or switchgear room where many vital components may be affected. Table 7.3.1A-19 summarizes the results in terms of mean frequencies of the contributions from all fire zones. The modification has reduced the contributions from the electrical tunnel, the switchgear room, and the containment spray pump area. The other fire areas are either not affected by the modification or the impact is insignificant.

7.3.1A.5.1 Areas Not Affected

The cable spreading room and the control room fire scenarios are not significantly affected because in Section 7.3.1 provisions are included for the alternate shutdown system (before the proposed modification). In those scenarios, credit is given to the operators reactivating normally running components such as a charging pump and a component cooling pump provided that they are inadvertently stopped by a fire. Inadvertent stoppage of these pumps due to fire is deemed to be a comparatively lower frequency event. Thus, the possibility of an RCP seal failure (small LOCA) is not analyzed. It should be noted that in a cable spreading room or control room fire, only control and instrumentation circuits are affected. Even if it is assumed that all indications are lost, the operators can use the existing pneumatic indicators and activate the pumps from the switchgear room to safely shut down the plant.

The modification cannot have a significant impact on the contribution from pump rooms such as fire zone 1 for CCS pumps or zone 9 for the SI pumps. For these cases, the fire will disable all power feeds to the pumps or the pumps themselves, thus the fire would render the proposed transfer switch ineffective. For the remaining areas, the modification cannot help the restoration of the affected system because the components within those areas are not powered by the alternate shutdown system.

7.3.1A.5.2 Impact on Switchgear Room Contribution

The main impact of the proposed modification on a switchgear room fire is decreasing the likelihood of an RCP seal LOCA. In a switchgear room fire, if both switchgear cabinets or the power cables are affected, the power to all CCS pumps and charging pumps would be lost. With the proposed modification, the operators can activate switchgear of Unit 1 (which has to be done locally) and throw the transfer switches of the CCS pump and/or the charging pump and reactivate the RCP seal cooling

function. The relevant valves would be in their normal operating position and it is deemed very unlikely for the switchgear room fire to cause inadvertent closure of these valves. The transfer to the Unit 1 switchgear has to be completed within the first half hour of loss of all RCP seal cooling.

The conditional frequency, Q_{S1}, of seal LOCA given a large fire in the switchgear room can then be written as

$$Q_{S1} = Q_{HE,S1} + Q_{SW} + Q_{CCS}$$

where

$Q_{HE,S1}$ ≡ human error; failure of the operators to reactivate the CCS pump within one-half hour.

Q_{SW} ≡ failure of the transfer switch.

Q_{CCS} ≡ failure of the component cooling pump.

and

$$Q_{CCS} = Q_{CCS,D} + 24\lambda_{CCS} + Q_{CCS,M}$$

where

$Q_{CCS,D}$ ≡ failure of the CCS pump on demand.

λ_{CCS} ≡ failure of the CCS pump during operation (per hour).

$Q_{CCS,M}$ ≡ unavailability of the CCS pump due to maintenance.

The total time period that the component cooling pump is needed to operate is taken to be 24 hours.

The main contributor to $Q_{HE,S1}$ is judged to be failure of the control room operators to initiate the process for transferring to the alternate shutdown system. The large fire in the switchgear room is judged to pose a medium to high stress level on the operators. There will be at least three operators involved in making the decision. Reference 7.3-7 gives human error frequencies and has defined levels of dependency among the operators. It is judged that one of the operators will be strongly dependent on the other two and the level of dependence of the other two on one another will be low. Reference 7.3-7 suggests 0.1 for the frequency of human error for one operator under very high levels of stress. For the conditional frequency of a second operator making the same error, Reference 7.3-7 suggests a point value of 0.15. Based on these suggested frequencies, we have chosed $Q_{HE,S1}$ to be lognormally distributed with the following characteristic values:

$$Q_{HE,S1,05} = 9.0 \times 10^{-3}$$

$$Q_{HE,S1,50} = 3.0 \times 10^{-2}$$

$$Q_{HE,S1,95} = 1.0 \times 10^{-1}$$

$$\alpha_{Q_{HE,S1}} = 3.9 \times 10^{-2}$$

Table 7.3.1A-20 gives the frequencies of Q_{SW}, $Q_{CCW,D}$, λ_{CCS} and $Q_{CCS,M}$. Using those frequencies and the previously given human error frequency the conditional frequency of seal LOCA is evaluated. Its characteristic values are:

$$Q_{S1,05} = 1.7 \times 10^{-2}$$

$$Q_{S1,50} = 3.7 \times 10^{-2}$$

$$Q_{S1,95} = 9.8 \times 10^{-2}$$

$$\alpha_{Q_{S1}} = 4.6 \times 10^{-2}$$

In a large switchgear room fire, all the small LOCA mitigating functions will be lost. Thus, if a seal LOCA occurs, the operators have to turn on at least one auxiliary feedwater pump and at least one SI pump. The turbine-driven auxiliary feedwater pump is independent of the switchgear room. A motor-driven auxiliary feedwater pump can be activated using the alternate shutdown system. However, the SI pumps would be affected by the fire and would not be available within 1 hour of seal failure.

Thus, core melt is taken to be certainty in the case of seal failure. The conditional frequency of core melt $Q_{CM,14}$ can then be written as

$$Q_{CM,14} = Q_{S1}$$

The characteristic values of $Q_{CM,14}$ are:

$$Q_{CM,14,05} = 1.7 \times 10^{-2}$$

$$Q_{CM,14,50} = 3.7 \times 10^{-2}$$

$$Q_{CM,14,95} = 9.8 \times 10^{-2}$$

$$\alpha_{Q_{CM,14}} = 4.6 \times 10^{-2}$$

The containment spray pumps and containment fan cooler units will be lost in a switchgear room fire. The alternate shutdown system does not have any provisions for restoring the power to these components. Thus, a core melt due to seal failure would lead to plant damage state SE. The unconditional frequency of damage state SE is then

$$\phi'_{SE,14} = \phi_{SE,14} Q_{CM,14}$$

where $\phi_{SE,14}$ is the base case frequency of state SE due to switchgear fires given in Section 7.3.1.

If the seal failure is prevented, the initiating event becomes a transient (reactor trip is assumed here). Safe shutdown can be achieved

if the AFWS or bleed and feed mode of core cooling is employed. The latter is not possible because the PORV block valves would be lost due to loss of both safety MCCs 26A and 26B. Also, there is no immediate power to SI pumps. Of the auxiliary feedwater system, either the turbine-driven pump or one motor-driven pump (by connecting to the alternate shutdown system) can be used. The conditional frequency, $Q_{CM,T}$, of core melt (given a large switchgear room fire and successful RCP seal cooling or injection) is then equal to the unavailability of AFWS. It is deemed that human error contribution is very small because the successful alignment of CCS and charging pumps would have a reassuring effect on the operators. The unavailability of AFWS due to other causes as evaluated in Section 1.5.2.3.9 is used here. The distribution is approximated by a lognormal distribution with the following characteristic values:

$$Q_{CM,T,14,05} = 4.7 \times 10^{-5}$$

$$Q_{CM,T,14,50} = 1.3 \times 10^{-4}$$

$$Q_{CM,T,14,95} = 3.6 \times 10^{-4}$$

$$\alpha Q_{CM,T,14} = 1.6 \times 10^{-4}$$

Then the unconditional frequency of damage state TE becomes

$$\phi'_{TE,14} = \phi_{SE,14}\, Q_{CM,T,14}$$

The frequency of damage state SE prior to the modification is used because it is equal to the frequency of large fires in the switchgear room. The mean of the frequency of damage state TE after the proposed modification is given in Table 7.3.1A-19.

7.3.1A.5.3 Impact on Electrical Tunnel Contribution

7.3.1A.5.3.1 Fire at the Right Stack of Trays. The electrical tunnel contribution is also affected by the proposed modification. If the fire affects only the right stack of trays, damage states SEF and SLF would result (in this study we only use SEF and include all SLF contributions in SEF). The operators can prevent seal failure as described earlier. The conditional frequency of failure to prevent seal LOCA is Q_{S1} which was evaluated earlier.

In the base case evaluation of fire risk, the electrical tunnel is evaluated in two parts: (1) fire zone 1A on the PAB side, and (2) 32A on the control building side. The unconditional frequencies of SEF due to fire in these areas can be written as

$$\phi'_{SEF,1A} = \phi'_{SEF,32A} = (\phi_{SEF,1A} + \phi_{SLF,1A})\, Q_{S1}$$

This equation reflects the fact that base case SEF and SLF frequencies of the portions of the tunnel are equal. The mean values are given in Table 7.3.1A-19.

If the seal failure is prevented, the initiating event becomes a transient (reactor trip is assumed here). Safe shutdown can be achieved if the AFWS or bleed and feed mode of core cooling is employed. The two safety MCCs will be failed in a fire in the right stack of trays. Thus, the PORV block valves will not be able to be opened for bleed and feed, and similar to the switchgear room fire, if AFWS is not activated core melt could occur. The auxiliary feedwater system is independent from this fire. From Section 1.5.2.3.9 the unavailability of AFWS is obtained. It is approximated with a lognormal distribution with the following characteristic values:

$$Q_{CM,T,ET,05} = 1.7 \times 10^{-6}$$

$$Q_{CM,T,ET,50} = 1.1 \times 10^{-5}$$

$$Q_{CM,T,ET,95} = 6.5 \times 10^{-5}$$

$$\alpha Q_{CM,T,ET} = 1.9 \times 10^{-5}$$

The containment spray system would also fail from a fire in the right stack of trays. Thus, the unconditional frequency of TEF becomes

$$\phi'_{TEF,1A} = \phi'_{TEF,32A} = \lambda_{AUX} f_T f_R Q(\tau V)\, Q_{CM,T,ET}$$

where

λ_{AUX} = frequency of fires in the PAB, the control building (CB) or the fan house (FH).

f_T = fraction of PAB, CB, and FH fires that occur in the electrical tunnel in the PAB.

f_R = fraction of electrical tunnel fires that occur in the right stack of trays.

$Q(\tau_V)$ = conditional frequency of fire propagation.

These parameters are evaluated in Section 7.3.1.4 and they are summarized in Table 7.3.1A-20. The mean frequencies of damage state TEF after the proposed modifications are given in Table 7.3.1A-19.

7.3.1A.5.3.2 Fire Affecting Both Stacks of Trays. If the fire affects both stacks of trays, from the base case study, damage state SE would result. The seal failure may be prevented using the modified alternate shutdown system. The conditional frequency of seal failure is again Q_{S1}. Thus, the unconditional frequency of damage state SE becomes:

$$\phi'_{SE,1A} = \phi_{SE,1A} Q_{S1}$$

$$\phi'_{SE,32A} = \phi_{SE,32A} Q_{S1}$$

If seal failure is prevented, a transient (we assume reactor trip) would occur. The bleed and feed mode of core cooling would not be available because the two safety MCCs would be lost. Two trains of AFWS can be made available manually. Similar to switchgear room fire, it is deemed that human error contribution is very small because the successful alignment of CCS and charging pumps would have a reassuring effect on the operators. The unavailability of AFWS due to other causes as evaluated in Section 1.5.2.3.9 is used here. Using the results from the switchgear room fire study, we write

$$Q_{CM,T,1A} = Q_{CM,T,32A} = Q_{CM,T,14}$$

and for the unconditional frequencies

$$\phi'_{TE,1A} = \phi_{SE,1A} Q_{CM,T,1A}$$

$$\phi'_{TE,32A} = \phi_{SE,32A} Q_{CM,T,32A}$$

The mean frequencies of damage state TE after the proposed modifications are given in Table 7.3.1A-19.

7.3.1A.5.4 Impact on Containment Spray Pump Area Fire Zones 2 and 2A

The power cables of all CCS pumps are routed through these two fire zones, where the containment spray pumps, the primary water makeup pumps, and the spray additive tank are located. Since the transfer switch and the power cable for one CCS pump from the alternate shutdown system would not be located in these areas, there is a very small likelihood for a single fire or coincident fires simultaneously affecting the contents of these fire zones and failing the power source transfer capability.

One component pump can be made available manually by transferring the power source to the alternate shutdown system, thus preventing seal failure. The conditional frequency, Q_{S1}, which was evaluated earlier in this appendix is also applicable here. The frequencies of damage states SEF and SE are reduced by Q_{S1}. Table 7.3.1A-19 shows the mean values. For damage state SEF, the unavailability of CCS is reduced by Q_{S1}. For damage state SE, the unavailabilities of CCS and the service water system (SWS) are reduced by Q_{S1}.

7.3.1A.5.5 Impact on the Release Categories Due to Fire

Three release categories, 8B, 8A, and 2RW, may result from a fire incident. Their frequencies of occurrence are evaluated from the major contributors as determined by the mean values of Table 7.3.1A-19. The results are summarized in Table 7.3.1A-17.

The frequency of release category 8B is dominated by the frequency of damage state TEC from fire zone 74A (electrical penetration area), by the

frequency of damage state TEFC from fire zone 23 (auxiliary boiler feed pump room), and by damage state TEFC from fire zone 11 (the cable spreading room).

$$\phi'_{8B} = \phi_{TEC,74A} + \phi_{TEFC,23} + \phi_{TEFC,11} = \lambda_{AUX} f_T Q(\tau_H)\, Q_S$$

$$+ \lambda_{AUX} f_1 (Q_{S1} + Q_{REC} + Q_{PORV}) + \lambda_{CSR} f_{ES} Q(\tau_G)\, Q_S\, Q_{HE}$$

All the parameters of this equation (such as λ_{AUX}, f_T, etc.) are defined and evaluated either in Section 7.3.1A.5.6 or in Section 7.3.1 of this report. The characteristic values of release category 8B after the proposed modifications are given in Table 7.3.1A-17.

The frequency of release category 8A from fires is dominated by the frequency of damage state SEF from fire zones 1A and 32A (both portions of the electrical tunnel).

$$\phi'_{8A} = \phi'_{SEF,1A} + \phi'_{SEF,32A} = 2\phi'_{SEF,1A}$$

$$= 2(\phi_{SEF,1A} + \phi_{SLF,1A})\, Q_{S1}$$

The base case frequencies, $\phi_{SEF,1A}$ and $\phi_{SLF,1A}$ are taken from Section 7.3.1. The parameter Q_{S1} is evaluated earlier in this section. The characteristic values of release category 8A after the proposed modifications are given in Table 7.3.1A-17.

The frequency of release category 2RW from fires is dominated by the frequency of damage state SE from fire zones 1A and 32A (both portions of the electrical tunnel), fire zone 14 (the switchgear room), and by the frequency of damage state TE from fire zone 11 (the cable spreading room).

$$\phi'_{2RW} = \phi'_{SE,1A} + \phi'_{SE,32A} + \phi'_{SE,14} + \phi'_{TE,11}$$

$$= \lambda_{AUX} f_T f_A [1 + Q(\tau_A)] Q_{S1} + \lambda_{AUX} f_{SWG} f_{SL} Q(\tau_G) Q_{CM,14}$$

$$+ \lambda_{CSR} f_{ES} Q(\tau_G) Q_S Q_{HE}$$

All the parameters of this equation (such as λ_{AUX}, f_T, etc.) are defined aand evaluated either in this section or in Section 7.3.1. The characteristic values of release category 2RW are given in Table 7.3.1A-17.

The frequency of core melt from fires is now dominated by the frequency of damage state TEC from fire zone 74A (the electrical penetration area), the frequency of state TEC from fire zone 23 (the auxiliary boiler feed pump room), the frequencies of damage states SEF and SE from fire

zones 1A and 32A (both portions of the electrical tunnel), and by the frequency of damage state TEFC from fire zone 11 (the cable spreading room).

$$\phi'_{CM} = \phi'_{TEC,74A} + \phi''_{TEFC,23} + \phi'_{SEF,1A} + \phi'_{SEF,32A} + \phi'_{SE,1A} + \phi'_{SE,32A} + \phi'_{SE,14A} + \phi_{TEFC,11}$$

All the parameters of this equation have been defined earlier in this section. Thus, the characteristic values of the core melt frequency after the fixes are given in Table 7.3.1A-17.

7.3.1A.6 Highlights of Base Case Quantification

In this section, the methods used for calculating the risk from the fire zones not explicitly quantified in Section 7.3.1 are described. The details of quantification for some areas are also highlighted.

7.3.1A.6.1 The General Formulations

In Section 7.3.1, it is found that fires cannot cause a large or medium LOCA. The simultaneous occurrence of these initiating events and a fire disabling part or most of the mitigating systems can be shown to be dominated by the frequencies of these sequences due to causes other than fire.

For a small LOCA, it is found that fire can only lead to a reactor coolant pump seal failure (thereby leading to a small LOCA) and cannot cause any other type of breach in the primary system (Section 7.3.1). To simplify the calculations, the delayed melts (e.g., due to failure of the recirculation system) are combined with early melts. Core melt is computed in two parts: (1) core melt due to a small LOCA, and (2) core melt due to a transient. The transients are grouped together and reactor trip is chosen to be the representing transient initiating event.

$$\phi_{\text{core melt}} = \phi_{CM,\text{small LOCA}} + \phi_{CM,\text{transient}}$$

$$\phi_{CM,\text{small LOCA}} = \lambda_{Fire}\left[Q_{EP} + Q_{SW} + Q_{CCS}(Q_{S1} + Q_{REC} + Q_{CF} + Q_{PORV} + Q_{AFWS})\right]$$

$$\phi_{CM,\text{transient}} = \lambda_{Fire}\left[(Q_{S1} + Q_{REC} + Q_{PORV})Q_{AFWS}\right]$$

where

λ_{Fire} = frequency of fire failing a specified group of vital components.

Q_i = unavailability of system i.

EP = electric power system.

SW = service water system.

CCS = component cooling water system.

SI = safety injection system.

REC = recirculation system.

CF = containment fan cooling system.

PORV = power-operated relief valves (block valves are used for bleed and feed operation).

AFWS = auxiliary feedwater system.

The equation for core melt due to a small LOCA is based on the event tree of Figure 7.3.1-6. The systems referenced previously are analyzed in Section 1.5.2, except for the PORV which is analyzed in Section 1.3.3.9. The unavailability of these systems is given in Section 1.5.2 for different boundary conditions. In that core melt equation, it is assumed that total loss of electric power or service water will lead to RCP seal failure and loss of all mitigating features. It is also assumed that total loss of component cooling leads to loss of the charging pumps and, consequently, a small LOCA via the RCP seals. The availability of the containment fan coolers determines the availability of the recirculation system when the component cooling system is not available.

The equation for core melt due to a transient is based on the event tree of Figure 7.3.1-7. The plant damage states are computed from the following equations:

$$\phi_{SEFC} = \lambda_{Fire}[Q_{CCS}(Q_{SI} + Q_{REC} + Q_{PORV}Q_{AFWS})]$$

$$\phi_{SEF} = \phi_{SEFC}Q_{CS}$$

$$\phi_{SEC} = \lambda_{Fire}[Q_{CCS}Q_{CF} + Q_{SW}]$$

$$\phi_{SE} = \lambda_{Fire}[Q_{EP} + Q_{SW}Q_{CS} + Q_{CCS}Q_{CF}Q_{CS}]$$

$$\phi_{TEFC} = \phi_{CM,transient}$$

$$\phi_{TEF} = \phi_{TEFC}Q_{CS}$$

$$\phi_{TEC} = \phi_{TEFC}Q_{CF}$$

$$\phi_{TE} = \phi_{TEFC}Q_{CF}Q_{CS}$$

where the different parameters are defined earlier and

Q_{CS} = unavailability of the containment spray system (this system is analyzed in Section 1.5.2.

The frequencies of the release categories are computed using:

$$\phi_{8B} = \lambda_{Fire}[Q_{SW} + Q_{CCS}(Q_{SI} + Q_{REC} + Q_{CF}) + (Q_{SI} + Q_{REC} + Q_{PORV})Q_{AFWS}]$$

$$\phi_{8A} = \lambda_{Fire}[Q_{CCS}(Q_{SI} + Q_{REC}) + (Q_{SI} + Q_{REC} + Q_{PORV})Q_{AFWS}]Q_{CS}$$

$$\phi_{2RW} = \lambda_{Fire}[Q_{EP} + Q_{SW}Q_{CS} + Q_{CCS}Q_{CF}Q_{CS} + (Q_{SI} + Q_{REC} + Q_{PORV})Q_{AFWS}Q_{CF}Q_{CS}]$$

The mean of the frequency of λ_{Fire} is conservatively taken as 10^{-3} for each fire zone in the primary auxiliary building (PAB), the fan house (FH), the control building (CB), and the containment. For those areas in which the core melt and damage state frequencies are evaluated, this mean frequency is reevaluated using distributions of the frequency of fires in the overall building and the fraction of those fires occurring in the specific area.

Table 7.3.1A-21 gives the results and input information for core melt and damage state calculations. All five zones are addressed. The details of some of the calculations are highlighted hereafter.

7.3.1A.6.2 Fire Zone 1, CCS Pump Room

Fire zone 1 is located at Elevation 68' of the PAB. The three component cooling pumps are installed in this area. The frequency of failure of all three pumps due to a fire incident, λ_{Fire}, is shown as a fraction of auxiliary building fires

$$\lambda_{Fire} = \lambda_{AUX} f_1$$

In Section 7.3.1, we find:

$$\lambda_{AUX,05} = 0.015 \text{ ry}^{-1}$$

$$\lambda_{AUX,50} = 0.033 \text{ ry}^{-1}$$

$$\lambda_{AUX,95} = 0.053 \text{ ry}^{-1}$$

$$\alpha_{\lambda_{AUX}} = 0.034 \text{ ry}^{-1}$$

The fraction f_1 is the fraction of fires that may occur in fire zone 1 and be of sufficient severity to fail all three CCS pumps. It is evaluated judgmentally based on the experience gained in doing the analysis of Section 7.3.1, and is chosen to be lognormally distributed with the following characteristic values:

$$f_{1,05} = 5.0 \times 10^{-4}$$

$$f_{1,50} = 5.0 \times 10^{-3}$$

$$f_{1,95} = 5.0 \times 10^{-2}$$

$$\alpha_{f_1} = 1.3 \times 10^{-2}$$

The product of these two distributions, λ_{Fire}, which is the frequency of fires in fires in fire zone 1 that would fail all three CCS pumps, yields the following characteristic values (per reactor year):

$$\lambda_{Fire,05} = 1.6 \times 10^{-5}$$

$$\lambda_{Fire,50} = 0.9 \times 10^{-4}$$

$$\lambda_{Fire,95} = 1.7 \times 10^{-3}$$

$$\alpha_{f_{Fire}} = 4.4 \times 10^{-4}$$

The mean unavailabilities of the mitigating systems are taken from Section 1.5.2. The formulations given in Section 7.3.1A.6.1 are used to evaluate the core melt and other plant damage states.

7.3.1A.6.3 Fire Zone 15, Control Room

The control room is directly above the cable spreading room and contains the control and instrumentation cables, controls, and readouts of virtually all the systems of the plant. There are no motive power cables in the area. The area is manned continuously. There are fire detectors inside the control cabinets. The fire extinguishment capability for the area consists of two hose stations and a Class A fire extinguisher adjacent to the zone and several 15-pound carbon dioxide extinguishers inside the control room. The operators also have access to breathing apparatus that can be used in case of smoke in the area.

The most critical area within the control room is the control cabinet of safety components (cabinet numbers SB1 and SB2) which are directly above the critical area in the cable spreading room that was analyzed in Section 7.3.1. A fire in these cabinets would have the same impact on plant safety as cable spreading room fire at the center of the northern wall. However, in this case, the operators would detect the fire almost immediately and attempt to extinguish it in a short period of time. Also, the transient fuels in the control room are judged to be significantly less than the cable spreading room. Not all control room fires would lead to the evacuation of the area because operators can wear breathing apparatus and the control room HVAC can purge the contaminated control room air.

Fires affecting cabinets other than those controlling the safety components (e.e., SB1 and SB2) will not have severe impact on the plant's safety margin. A fire affecting SB1 and SB2 will result in accident sequences similar to those analyzed for cable spreading room fires in

Section 7.3.1.2.4. It is judged that the frequency of core melt or other damage states from control room fires is just a fraction of the frequency of the same state from cable spreading room fires. This fraction, F_{CR}, is judged to have the following histogram:

f_{CR}	Probability	Cumulative Probability
0.01	0.05	0.05
0.03	0.20	0.25
0.10	0.25	0.50
0.30	0.25	0.75
0.75	0.20	0.95
1.00	0.05	1.00

The mean of this distribution is 0.31. For example, the core melt frequency from control room fires is obtained from

$$\phi_{CM,CR} = f_{CR}\phi_{CM,CSR}$$

where

$\phi_{CM,CSR}$ = core melt frequency from cable spreading room fires.

The mean frequencies are given in Table 7.3.1A-21.

7.3.1A.6.4 Fire Zone 27A, Corridor

This corridor at Elevation 98' of the primary auxiliary building contains the safety related motor control centers 26A and 26B. The controls of all safety related motor-operated valves pass through these motor control centers. It is a controlled access area. Considering the frequency of fires in other areas and the fire propagation analysis performed for other areas, the frequency of failing both the motor control centers is written as

$$\lambda_{Fire} = \lambda_{AUX} f_{27A} f_{PF}$$

where

λ_{AUX} = frequency of auxiliary building fires.

f_{27A} = the fraction of auxiliary building fires that may occur at the motor control center area.

f_{PF} = the fraction of motor control center area fires that may occur between the two safety cabinets and be large enough to fail both of them.

The fraction, f_{27A}, of auxiliary building fires in the motor control center area is assessed by comparing two similar parameters for the switchgear area, f_{SWG}, and electrical tunnel area, f_T, of Section 7.3.1. The probability distribution of f_{27A} is lognormal and has the following characteristic values:

$$f_{27A,05} = 0.03$$

$$f_{27A,50} = 0.1$$

$$f_{27A,95} = 0.3$$

$$\alpha_{f_{27A}} = 0.12$$

The fraction, f_{PF}, of motor control center fires that may occur between the two cabinets and be large enough to cause damage to both of them is assessed by comparing similar frequencies for cable spreading room fires, f_{es}; for the electrical tunnel fires, f_R; and switchgear room fires, f_{SL} of Section 7.3.1. The probability distribution of f_{PF} is lognormal and has the following characteristic values:

$$f_{PF,05} = 2.0 \times 10^{-3}$$

$$f_{PF,50} = 2.0 \times 10^{-2}$$

$$f_{PF,95} = 2.0 \times 10^{-7}$$

$$\alpha_{f_{PF}} = 5.3 \times 10^{-2}$$

The frequency of fires in fire zone 27A is computed by using probabilistic arithmetic. The resulting distribution has the following characteristic values (per reactor year):

$$\lambda_{Fire,05} = 4.9 \times 10\text{-}6$$

$$\lambda_{Fire,50} = 6.9 \times 10\text{-}5$$

$$\lambda_{Fire,95} = 8.2 \times 10\text{-}4$$

$$\alpha_{\lambda_{Fire}} = 2.2 \times 10^{-4}$$

Since the PORV block valves are normally closed and are powered from these motor control centers, it is assumed that their control and motive power will be lost and, therefore, they will fail closed. It is also assumed that the CCS, AFW, EP, and SW systems will not be adversely affected by the fire. This is because CCS and SW are normally in operation; their valves would fail as they are and the pumps would not be affected by the fire. The AFW valves fail open upon loss of power and the pump controls would not be affected by the MCC failure. The electric power is very likely to continue to provide power to the switchgears. It

is assumed that SI and recirculation unavailability would increase significantly. Even if they become unity, their impact on the frequency of core melt from fires in zone 27A woulld be insignificant because they will be dominated either by PORV unavailability (in the case of transient) or SW unavailability (in the case of a small LOCA).

7.3.1A.6.5 Fire Zone 74A, the Electrical Penetration Area

Fire zone 74A is the electrical penetration area at Elevation 51' of the fan house. It is the far end of the electrical tunnel. The cable trays of this area are stacked in a fashion similar to the electrical tunnel. The control cables for the auxiliary feedwater pumps and their regulating valves, the power cables for the containment fan coolers, and the power and control cables for the PORVs and their associated block valves are located in this area. The conditions are similar to those of the left stack of trays in the electrical tunnel except that the power cables of the safety injection pumps are not run through this area. Therefore, the frequency of fire, λ_{Fire}, that may fail a vital set of cables is derived using results from the electrical tunnel analysis part of the IPPSS. We write

$$\lambda_{Fire} = \lambda_{AUX} f_T Q(\tau_H)$$

where

f_T = the fraction of auxiliary building fires that may occur in fire zone 74A (this is defined in Section 7.3.3.1 for the electrical tunnel).

$Q(\tau_H)$ = the fraction of fires in fire zone 74A that are not extinguished in time to prevent vital component failures (derived in Section 7.3.1.4.2).

In Section 7.3.1.3.1, we find:

$$f_{T,05} = 8.0 \times 10^{-3}$$

$$f_{T,50} = 4.0 \times 10^{-2}$$

$$f_{T,95} = 2.0 \times 10^{-7}$$

$$\alpha_{f_T} = 6.5 \times 10^{-2}$$

In Section 7.3.1.4.2, we find:

$$Q_{05}(\tau_H) = \text{smaller than } 10^{-8}$$

$$Q_{50}(\tau_H) = 7.3 \times 10^{-2}$$

$$Q_{95}(\tau_H) = 0.68$$

$$\alpha_{Q(\tau_H)} = 0.21$$

The product of these distributions yields the following characteristic values for λ_{Fire} (per reactor year):

$\lambda_{Fire,05} = 5.9 \times 10^{-10}$

$\lambda_{Fire,50} = 1.0 \times 10^{-4}$

$\lambda_{Fire,95} = 2.1 \times 10^{-3}$

$\alpha_{\lambda_{Fire}} = 4.6 \times 10^{-4}$

7.3.1A.6.6 Fire Zone 75A, Outer Annulus of Containment

Fire zone 75A is the outer annulus of the containment at Elevation 46'. It contains the power and control cables for the PORVs and their block valves and the power cables of all fan cooling units. The frequency of fire, λ_{Fire}, that may occur in this area and fail the power cables to all the fan coolers and PORVs is written as

$$\lambda_{Fire} = \lambda_{CON} f_{75A}$$

where

λ_{CON} = the frequency of fires in the containment.

λ_{75A} = the fraction of containment fires that may occur in area 75A and fail the previously listed components.

The frequency of containment fires is taken from Reference 7.3-3. A lognormal distribution is fitted to the upper and lower bounds reported in that reference to simplify the quantification process. The characteristic values of λ_{CON} are (per reactor year):

$\lambda_{CON,05} = 6.2 \times 10^{-3}$

$\lambda_{CON,50} = 1.3 \times 10^{-2}$

$\lambda_{CON,95} = 2.8 \times 10^{-2}$

$\alpha_{\lambda_{CON}} = 1.5 \times 10^{-2}$

The fraction, f_{75A}, of containment fires occurring in fire zone 75A and failing the previously listed components is assessed by comparing two similar parameters for the switchgear area, f_{SWG}, and the electrical tunnel area, f_T, of Section 7.3.1. The probability distribution of f_{75A} is lognormal and has the following characteristic values:

$f_{75A,05} = 4.0 \times 10^{-3}$

$f_{75A,50} = 2.0 \times 10^{-2}$

$f_{75A,95} = 1.0 \times 10^{-7}$

$\alpha_{f_{75A}} = 3.2 \times 10^{-2}$

The product of these two distributions yields the following characteristic values for λ_{Fire} (per reactor year):

$\lambda_{Fire,05} = 4.3 \times 10^{-5}$

$\lambda_{Fire,50} = 2.9 \times 10^{-4}$

$\lambda_{Fire,95} = 1.5 \times 10^{-3}$

$\alpha_{\lambda_{Fire}} = 4.7 \times 10^{-4}$

7.3.1B CHANGES TO FIRE ANALYSIS, INDIAN POINT 2

7.3.1B.1 Introduction

In the unamended version of the Indian Point Probabilistic Safety Study (IPPSS) in Section 7.3.1, the risk from fires was evaluated explicitly. Some of the resulting sequences turned out to be dominant contributors to certain release categories. A modification was proposed and implemented to reduce the main fire contributors (see Section 7.3.1A, Amendment 1). As a result, fire zones of lesser importance had to be reevaluated more explicitly (see Table 7.3.1A-19) because the modification changed the relative order of contributors to the release categories and to core melt. A conservative approximate method was employed for these new areas because they were numerous and did not have a significant impact on risk prior to the modification. However, after the modification, two of these new fire zones, the electrical penetration area and the auxiliary feedwater pump room, became important contributors to the frequencies of core melt and release category 8B. In this amendment to the IPPSS, we requantify the fire risk from these two areas employing more refined methods.

For the electrical penetration area, the requantification leads to a significant reduction, mainly due to a better evaluation of accident mitigation efforts. For the case of the auxiliary feedwater pump room, a more realistic assumption is used for initiating event occurrence. The impact of these reductions on the overall fire risk is summarized in Tables 7.3.1B-22 and 7.3.1B-23. The latter is adapted from Table 7.3.1A-19 (Section 7.3.1A) of Amendment 1.

7.3.1B.2 Electrical Penetration Area (Fire Zone 74A)

The frequency of a fire that may fail a vital set of cables in the electrical penetration area (fire zone 74A), $\lambda_{Fire,74A}$, is evaluated in Section 7.3.1A.6.5. Its characteristic values (per reactor year) are:

$$\lambda_{Fire,74A,05} = 5.9 \times 10^{-10}$$

$$\lambda_{Fire,74A,50} = 1.0 \times 10^{-4}$$

$$\lambda_{Fire,74A,95} = 2.1 \times 10^{-3}$$

$$\alpha_{\lambda_{Fire,74A}} = 4.6 \times 10^{-4}$$

This frequency is then multiplied in Section 7.3.1A.6.5 with the conditional frequency of loss of the auxiliary feedwater system (AFWS) (see Section 7.3.1A.6.1) to obtain the frequency of damage state TEC. From Table 7.3.1A-21, we find that a conservative mean conditional frequency of 0.025 was used in Section 7.3.1A (Amendment 1) for AFWS unavailability without detailed modeling of feasible options. The

conditions for AFWS actuation in the case of a cable penetration fire are the same as those for the electrical tunnel, as discussed in Section 7.3.1A.5.3.2 (Amendment 1). The unavailability of the AFWS for the electrical tunnel fire scenarios can thus be used here. It has the following characteristic values:

$$Q_{CM,T,74A,05} = 4.7 \times 10^{-5}$$

$$Q_{CM,T,74A,50} = 1.3 \times 10^{-4}$$

$$Q_{CM,T,74A,95} = 3.6 \times 10^{-4}$$

$$\alpha_{Q_{CM,T,74A}} = 1.6 \times 10^{-4}$$

The unconditional frequency of damage state TEC becomes

$$\phi'_{TEC,74A} = \lambda_{Fire,74A}\, Q_{CM,T,74A}$$

Similarly, the unconditional frequency of damage state TE becomes

$$\phi'_{TE,74A} = \lambda_{Fire,74A}\, Q_{CM,T,74A}\, Q_{CS}$$

where

Q_{CS} = unavailability of the containment spray system.

The unavailability of the containment spray system, Q_{CS}, is taken from Section 1.5.2.3.5. It has the following characteristic values:

$$Q_{CS,05} = 2.0 \times 10^{-5}$$

$$Q_{CS,50} = 5.0 \times 10^{-5}$$

$$Q_{CS,95} = 1.5 \times 10^{-4}$$

$$\alpha_{Q_{CS}} = 7.5 \times 10^{-5}$$

The mean frequencies of these damage states are given in Table 7.3.1B-23.

7.3.1B.3. Auxiliary Feedwater Pump Room

The plant damage states from fires in the auxiliary feedwater pump room were calculated in Section 7.3.1A.6 (Amendment 1) using a generic fire occurrence frequency. In this requantification, more realistic frequencies of fire are established.

Two critical areas are identified in the AFWS pump room where a fire may simultaneously fail all three auxiliary feedwater pumps. The first critical area is near the door where the pneumatic controls of the turbine-driven pump and the control cables of the motor-driven pumps are in close proximity to each other. The other critical area is near the turbine-driven pump where the power cables of the two motor-driven pumps are located. The frequency of sufficiently severe fires in one of these critical areas that may fail all three pumps can be written as

$$\lambda_{Fire,23} = \lambda_{AUX} \, f_{23} \, f_{GS,23}$$

where

λ_{AUX} ≡ the frequency of fires in the primary auxiliary building, fan house, control building, and the AFWS pump house.

f_{23} ≡ fraction of λ_{AUX} associated with the AFWS pump house.

$f_{GS,23}$ ≡ fraction of AFWS pump house fires that are sufficiently severe and occur at one of the critical areas.

The frequency λ_{AUX} is given in Section 7.3.1.3.1. It has the following characteristic values (per reactor year):

$$\lambda_{AUX,05} = 0.015$$

$$\lambda_{AUX,50} = 0.033$$

$$\lambda_{AUX,95} = 0.053$$

$$\alpha_{\lambda_{AUX}} = 0.034$$

The fraction, f_{23}, of fires whose frequency of occurrence is represented by λ_{AUX} that may occur in the AFWS pump room is derived judgmentally based on the observations that there are more than 25 compartments covered by λ_{AUX} and that several pump fires are part of the data base for the λ_{AUX} derivation. The probability distribution of f_{23} is chosen to be lognormal with the following characteristic values:

$$f_{23,05} = 0.02$$

$$f_{23,50} = 0.09$$

$$f_{23,95} = 0.4$$

$$\alpha_{f_{23}} = 0.14$$

The fraction, $f_{GS,23}$, of AFWS pump room fires that may lead to the failure of all three AFWS pumps is also derived judgmentally based on the following observations:

- The critical areas constitute about 20% of the main floor area.
- Severe fires are needed at both critical locations to inflict damage to all three pumps. Near the door, the control cables are far from the pneumatic controls; and, at the turbine-driven pump area, the power cables are at a high elevation.

A lognormal distribution is chosen for $f_{GS,23}$ with the following characteristic values:

$$f_{GS,23,05} = 4.0 \times 10^{-3}$$

$$f_{GS,23,50} = 2.0 \times 10^{-2}$$

$$f_{GS,23,95} = 1.0 \times 10^{-1}$$

$$\alpha_{f_{GS,23}} = 3.2 \times 10^{-2}$$

Using these distributions we can calculate the probability distribution for $\lambda_{Fire,23}$. It has the following characteristic values (per reactor year):

$$\lambda_{Fire,23,05} = 7.2 \times 10^{-6}$$

$$\lambda_{Fire,23,50} = 6.4 \times 10^{-5}$$

$$\lambda_{Fire,23,95} = 5.8 \times 10^{-4}$$

$$\alpha_{\lambda_{Fire,23}} = 1.5 \times 10^{-4}$$

Plant damage state TEFC would be realized if an initiating event (such as reactor trip) occurs simultaneously with the damaging fire in the AFWS pumproom and the bleed and feed mode of core cooling is unavailable. It is assumed that initiating event occurrence is certain.

The conditional frequency of loss of bleed and feed is evaluated in Section 1.3.3.9 as Top Event OP-2 for the event trees. The probability distribution for Q_{OP-2} has the following characteristic values:

$$Q_{OP-2,05} = 3.1 \times 10^{-3}$$

$$Q_{OP-2,50} = 5.8 \times 10^{-3}$$

$$Q_{OP-2,95} = 1.1 \times 10^{-2}$$

$$\alpha_{Q_{OP-2}} = 6.3 \times 10^{-3}$$

The unconditional frequency of damage state TEFC can thus be written as

$$\Phi TEFC,23 = \lambda AUX \; f_{23} \; F_{GS,23} \; Q_{OP-2}$$

The mean frequency of this damage state is given in Table 7.3.1B-23.

7.3.1B.4 Overall Impact of Requantification

Table 7.3.1B-22 gives the probability distributions for the frequencies of core melt and the release categories after the requantification. The mean core melt frequency from all fires is reduced by about a factor of 2 and the mean frequency of release category 8B from all fires is reduced by a factor of 4. The significant fire scenarios for core melt are now the switchgear room, the elecrical tunnel, and the cable spreading room with almost equal contribution levels. For release category 8B, the significant contributors are the cable spreading room and the AFWS pump room. The contributors to release category 2RW remain unchanged and are dominated by the switchgear room and the electrical tunnel.

The frequency of release category 8A changes slightly from the result presented in Amendment 1 due to minor numerical corrections.

TABLE 7.3.1-1

HISTOGRAM OF THE MEAN EXTINGUISHING TIME FOR LARGE FIRES

τ_s (min)	Probability	Cumulative Probability
15	0.40	0.40
30	0.30	0.70
60	0.20	0.90
120	0.10	1.00

TABLE 7.3.1-2

HISTOGRAM OF THE FREQUENCY OF CONTAINMENT EVENT TREE ENTRY STATE TEFC FROM A FIRE IN THE CABLE SPREADING ROOM

ϕTEFC,CSR,ϕ8B (ry^{-1})	Probability	Cumulative Probability
1.9×10^{-10}	.047	.047
1.1×10^{-9}	.053	.100
2.4×10^{-9}	.046	.146
4.7×10^{-9}	.050	.197
7.9×10^{-9}	.047	.244
1.2×10^{-8}	.052	.296
1.9×10^{-8}	.051	.347
2.8×10^{-8}	.048	.394
4.1×10^{-8}	.053	.447
6.0×10^{-8}	.045	.492
8.2×10^{-8}	.052	.544
1.2×10^{-7}	.048	.593
1.7×10^{-7}	.053	.646
2.5×10^{-7}	.050	.696
3.5×10^{-7}	.054	.750
5.3×10^{-7}	.049	.799
8.4×10^{-7}	.048	.847
1.4×10^{-6}	.053	.899
4.0×10^{-6}	.046	.945
2.2×10^{-5}	.055	1.000

TABLE 7.3.1-3

HISTOGRAM OF THE FREQUENCY OF CONTAINMENT EVENT TREE ENTRY STATE TE FROM A FIRE IN THE CABLE SPREADING ROOM

$\phi_{TE,CSR}$ (ry^{-1})	Probability	Cumulative Probability
2.9×10^{-11}	.044	.044
1.2×10^{-10}	.054	.098
2.9×10^{-10}	.050	.147
5.4×10^{-10}	.047	.194
9.0×10^{-10}	.050	.244
1.5×10^{-9}	.050	.294
2.3×10^{-9}	.050	.343
3.4×10^{-9}	.052	.395
5.0×10^{-9}	.050	.445
7.2×10^{-9}	.051	.495
1.1×10^{-8}	.054	.550
1.5×10^{-8}	.044	.593
2.2×10^{-8}	.050	.643
3.2×10^{-8}	.052	.695
4.7×10^{-8}	.045	.740
7.3×10^{-8}	.057	.797
1.2×10^{-7}	.050	.847
2.3×10^{-7}	.053	.900
5.9×10^{-7}	.044	.943
4.3×10^{-6}	.057	1.000

TABLE 7.3.1-4

HISTOGRAM OF THE MEAN EXTINGUISHING TIME FOR CABLE TRAY FIRES

τ_s (min)	Probability	Cumulative Probability
5	0.4	0.4
15	0.3	0.7
30	0.2	0.9
60	0.1	1.0

TABLE 7.3.1-5

CONDITIONAL FREQUENCIES OF CONTAINMENT EVENT TREE ENTRY STATES GIVEN A FIRE THAT HAS CAUSED FAILURE OF THE POWER CABLES OF THE RIGHT STACK OF TRAYS

Entry State	Mean	5th Percentile	50th Percentile	95th Percentile
SLF	0.05	0.002	0.02	0.20
SL	1.5×10^{-6}	2.0×10^{-10}	2.3×10^{-8}	2.7×10^{-6}
SEF	2.2×10^{-4}	6.4×10^{-5}	1.8×10^{-4}	4.1×10^{-4}
SE	2.2×10^{-10}	2.0×10^{-11}	9.0×10^{-11}	7.5×10^{-10}

TABLE 7.3.1-6

HISTOGRAM OF THE FREQUENCY OF CONTAINMENT EVENT TREE ENTRY STATE SLF FROM A FIRE IN FIRE ZONE 1A

$\phi_{SLF,1A}$ (ry^{-1})	Probability	Cumulative Probability
2.1×10^{-8}	.050	.050
8.8×10^{-8}	.044	.093
2.1×10^{-7}	.055	.149
4.3×10^{-7}	.051	.199
6.7×10^{-7}	.049	.248
1.1×10^{-6}	.051	.299
1.4×10^{-6}	.046	.345
2.0×10^{-6}	.053	.398
2.7×10^{-6}	.045	.442
3.7×10^{-6}	.057	.499
4.8×10^{-6}	.046	.546
6.3×10^{-6}	.049	.595
8.3×10^{-6}	.053	.648
1.1×10^{-5}	.046	.693
1.4×10^{-5}	.049	.743
1.9×10^{-5}	.054	.796
2.7×10^{-5}	.053	.849
4.0×10^{-5}	.042	.891
6.7×10^{-5}	.054	.945
2.5×10^{-4}	.055	1.000

TABLE 7.3.1-7

HISTOGRAM OF THE FREQUENCY OF CONTAINMENT EVENT TREE ENTRY STATE SEF FROM A FIRE IN FIRE ZONE 1A

$\phi_{SLF,1A}$ (ry^{-1})	Probability	Cumulative Probability
2.4×10^{-10}	.049	.049
1.2×10^{-9}	.051	.099
3.0×10^{-9}	.048	.147
5.8×10^{-9}	.052	.199
9.4×10^{-9}	.050	.250
1.3×10^{-8}	.047	.297
1.8×10^{-8}	.052	.349
2.3×10^{-8}	.049	.398
3.0×10^{-8}	.051	.450
3.7×10^{-8}	.050	.499
4.5×10^{-8}	.050	.549
5.5×10^{-8}	.051	.600
6.7×10^{-8}	.047	.647
8.1×10^{-8}	.052	.700
1.0×10^{-7}	.050	.750
1.3×10^{-7}	.048	.798
1.6×10^{-7}	.051	.849
2.2×10^{-7}	.049	.898
3.2×10^{-7}	.049	.950
7.0×10^{-7}	.052	1.000

TABLE 7.3.1-8

HISTOGRAM OF THE FREQUENCY OF CONTAINMENT EVENT TREE ENTRY STATE SE FROM A FIRE IN FIRE ZONE 1A

$\phi_{SE,1A}$ (ry^{-1})	Probability	Cumulative Probability
1.9×10^{-8}	.049	.049
6.7×10^{-8}	.048	.097
1.4×10^{-7}	.045	.142
2.5×10^{-7}	.056	.198
4.5×10^{-7}	.044	.242
7.8×10^{-7}	.055	.296
1.5×10^{-6}	.046	.343
2.8×10^{-6}	.056	.399
4.4×10^{-6}	.051	.450
6.1×10^{-6}	.048	.498
8.1×10^{-6}	.044	.542
1.0×10^{-5}	.049	.591
1.3×10^{-5}	.054	.645
1.7×10^{-5}	.048	.698
2.1×10^{-5}	.056	.749
3.0×10^{-5}	.048	.798
4.1×10^{-5}	.052	.850
6.2×10^{-5}	.049	.899
1.2×10^{-4}	.050	.949
7.7×10^{-4}	.051	1.000

TABLE 7.3.1-9

HISTOGRAM OF THE FREQUENCY OF CONTAINMENT EVENT TREE ENTRY STATE SE FROM A FIRE IN THE SWITCHGEAR ROOM

$\phi_{SE,14}$ (ry^{-1})	Probability	Cumulative Probability
1.8×10^{-8}	.048	.048
5.5×10^{-8}	.050	.098
1.3×10^{-7}	.050	.147
2.4×10^{-7}	.050	.197
4.3×10^{-7}	.052	.249
7.5×10^{-7}	.044	.298
1.3×10^{-6}	.049	.347
2.3×10^{-6}	.053	.400
3.7×10^{-6}	.050	.450
5.4×10^{-6}	.048	.497
7.5×10^{-6}	.051	.548
9.9×10^{-6}	.050	.598
1.3×10^{-5}	.049	.647
1.7×10^{-5}	.051	.698
2.3×10^{-5}	.050	.748
3.0×10^{-5}	.049	.798
4.1×10^{-5}	.044	.846
6.3×10^{-5}	.053	.899
1.3×10^{-4}	.050	.949
7.5×10^{-4}	.051	1.000

TABLE 7.3.1-10

HISTOGRAM OF THE FREQUENCY OF CONTAINMENT EVENT TREE ENTRY STATE SE FROM A FIRE IN THE ELECTRICAL TUNNEL, CB SIDE

$\phi_{SE,32A}$ (ry^{-1})	Probability	Cumulative Probability
1.0×10^{-8}	.044	.049
3.4×10^{-8}	.049	.098
7.4×10^{-8}	.052	.150
1.4×10^{-7}	.048	.198
2.5×10^{-7}	.051	.249
4.5×10^{-7}	.050	.300
8.1×10^{-7}	.048	.348
1.4×10^{-6}	.049	.397
2.2×10^{-6}	.051	.448
3.1×10^{-6}	.051	.498
4.2×10^{-6}	.050	.548
5.5×10^{-6}	.050	.598
7.2×10^{-6}	.052	.650
9.3×10^{-6}	.050	.700
1.2×10^{-5}	.048	.748
1.6×10^{-5}	.051	.799
2.3×10^{-5}	.049	.848
3.5×10^{-5}	.047	.896
7.0×10^{-5}	.054	.949
4.4×10^{-4}	.051	1.000

TABLE 7.3.1-11

HISTOGRAM OF THE FREQUENCY OF CONTAINMENT EVENT TREE ENTRY STATE SLF

ϕ_{SLF} (ry^{-1})	Probability	Cumulative Probability
4.3×10^{-8}	.050	.050
1.8×10^{-7}	.044	.093
4.2×10^{-7}	.055	.149
8.6×10^{-7}	.051	.199
1.3×10^{-6}	.049	.248
2.2×10^{-6}	.051	.299
2.9×10^{-6}	.046	.345
4.1×10^{-6}	.053	.398
5.4×10^{-6}	.045	.442
7.4×10^{-6}	.057	.499
9.6×10^{-6}	.047	.546
1.3×10^{-5}	.049	.595
1.7×10^{-5}	.053	.648
2.1×10^{-5}	.046	.693
2.8×10^{-5}	.049	.743
3.9×10^{-5}	.054	.797
5.3×10^{-5}	.053	.849
8.0×10^{-5}	.042	.891
1.3×10^{-4}	.054	.945
5.1×10^{-4}	.055	1.000

TABLE 7.3.1-12

HISTOGRAM OF THE FREQUENCY OF CONTAINMENT EVENT TREE ENTRY STATE SEF

ϕ_{SEF} (ry^{-1})	Probability	Cumulative Probability
4.9×10^{-10}	.044	.049
2.3×10^{-9}	.051	.099
6.1×10^{-9}	.048	.147
1.2×10^{-8}	.052	.199
1.9×10^{-8}	.050	.250
2.7×10^{-8}	.047	.297
3.6×10^{-8}	.052	.349
4.6×10^{-8}	.049	.398
5.9×10^{-8}	.051	.450
7.4×10^{-8}	.050	.499
9.0×10^{-8}	.050	.549
1.1×10^{-7}	.051	.600
1.3×10^{-7}	.047	.647
1.6×10^{-7}	.052	.700
2.0×10^{-7}	.050	.750
2.5×10^{-7}	.048	.798
3.2×10^{-7}	.051	.849
4.3×10^{-7}	.049	.898
6.4×10^{-7}	.049	.948
1.4×10^{-6}	.052	1.000

TABLE 7.3.1-13

HISTOGRAM OF THE FREQUENCY OF CONTAINMENT
EVENT TREE ENTRY STATE SE

ϕSE (ry^{-1})	Probability	Cumulative Probability
4.0×10^{-7}	.049	.049
1.4×10^{-6}	.050	.099
3.2×10^{-6}	.047	.145
5.5×10^{-6}	.051	.196
8.3×10^{-6}	.050	.247
1.1×10^{-5}	.049	.296
1.5×10^{-5}	.052	.348
1.9×10^{-5}	.047	.395
2.3×10^{-5}	.050	.445
2.8×10^{-5}	.050	.495
3.4×10^{-5}	.050	.546
4.1×10^{-5}	.053	.599
5.0×10^{-5}	.049	.649
6.2×10^{-5}	.050	.698
7.8×10^{-5}	.048	.746
1.0×10^{-4}	.051	.796
1.5×10^{-4}	.052	.849
2.7×10^{-4}	.051	.899
7.1×10^{-4}	.049	.949
1.2×10^{-3}	.051	1.000

TABLE 7.3.1-14

HISTOGRAM OF THE FREQUENCY OF
RELEASE CATEGORY 8A

ϕ_{8A} (ry^{-1})	Probability	Cumulative Probability
1.2×10^{-7}	.049	.049
3.9×10^{-7}	.048	.098
7.9×10^{-7}	.051	.149
1.3×10^{-6}	.050	.198
2.0×10^{-6}	.051	.249
2.8×10^{-6}	.050	.298
4.0×10^{-6}	.050	.349
5.2×10^{-6}	.049	.398
7.0×10^{-6}	.050	.447
9.0×10^{-6}	.052	.500
1.2×10^{-5}	.049	.548
1.6×10^{-5}	.051	.599
2.0×10^{-5}	.050	.649
2.5×10^{-5}	.050	.699
3.2×10^{-5}	.049	.748
4.2×10^{-5}	.051	.799
5.5×10^{-5}	.050	.849
8.9×10^{-5}	.050	.899
1.6×10^{-4}	.048	.948
5.1×10^{-4}	.052	1.000

TABLE 7.3.1-15

HISTOGRAM OF THE FREQUENCY OF
RELEASE CATEGORY 2RW

ϕ_{2RW} (ry^{-1})	Probability	Cumulative Probability
5.0×10^{-7}	.049	.049
1.7×10^{-6}	.051	.100
3.8×10^{-6}	.050	.150
6.0×10^{-6}	.048	.198
8.8×10^{-6}	.050	.249
1.2×10^{-5}	.050	.298
1.5×10^{-5}	.051	.350
1.9×10^{-5}	.050	.400
2.3×10^{-5}	.048	.448
2.8×10^{-5}	.050	.498
3.4×10^{-5}	.050	.548
4.1×10^{-5}	.051	.599
5.0×10^{-5}	.049	.649
6.2×10^{-5}	.050	.698
7.9×10^{-5}	.050	.748
1.0×10^{-4}	.051	.799
1.5×10^{-4}	.050	.849
2.7×10^{-4}	.051	.899
7.0×10^{-4}	.049	.949
1.2×10^{-3}	.051	1.000

TABLE 7.3.1-16

HISTOGRAM OF THE TOTAL FREQUENCY OF CORE MELT

ϕ_{CM} (ry^{-1})	Probability	Cumulative Probability
2.9×10^{-6}	.008	.008
4.5×10^{-6}	.040	.049
7.6×10^{-6}	.003	.051
9.8×10^{-6}	.057	.108
1.6×10^{-5}	.064	.172
2.2×10^{-5}	.061	.232
2.9×10^{-5}	.059	.291
3.6×10^{-5}	.061	.352
5.0×10^{-5}	.144	.495
6.5×10^{-5}	.009	.504
8.3×10^{-5}	.145	.649
1.2×10^{-4}	.059	.708
1.6×10^{-4}	.060	.768
2.3×10^{-4}	.058	.826
4.4×10^{-4}	.063	.888
7.3×10^{-4}	.062	.850
1.3×10^{-3}	.050	1.000

TABLE 7.3.1A-17

CHARACTERISTIC VALUES OF THE FREQUENCIES OF RELEASE CATEGORIES AND CORE MELT DUE TO FIRE AFTER THE MODIFICATION OF INDIAN POINT 2

Release Category/ Core Melt	Probability Level	Frequency After Modification (per reactor year)
Release Category 8B	5th Percentile	1.2×10^{-6}
	Median	5.5×10^{-6}
	95th Percentile	1.6×10^{-4}
	Mean	1.8×10^{-5}
Release Category 8A	5th Percentile	8.2×10^{-8}
	Median	6.6×10^{-7}
	95th Percentile	2.1×10^{-5}
	Mean	2.6×10^{-6}
Release Category 2RW	5th Percentile	1.6×10^{-7}
	Median	1.6×10^{-6}
	95th Percentile	4.1×10^{-5}
	Mean	6.7×10^{-6}
Core Melt	5th Percentile	3.2×10^{-6}
	Median	1.3×10^{-5}
	95th Percentile	1.6×10^{-4}
	Mean	2.7×10^{-5}

TABLE 7.3.1A-18

MEAN FREQUENCIES OF FIRE CONTRIBUTORS BEFORE THE MODIFICATION

Fire Zone	CM	SEFC	SEC	SEF	SE	TEFC	TEC	TEF	TE	8B	8A	2RW
Electrical Tunnel 1A	8.0-5	-	-	2.4-5	5.6-5	-	-	-	-	-	2.4-5	5.6-5
SWG Room 14	5.6-5	-	-	-	5.6-5	-	-	-	-	-	-	5.6-5
Electrical Tunnel 32A	5.6-5	-	-	2.4-5	3.2-5	-	-	-	-	-	2.4-5	3.2-5
Electrical Penet. 74A	1.1-5	-	2.8-8	-	9.2-11	-	1.1-5	-	8.6-10	1.1-5	-	9.5-10
CSR 11	1.9-6	-	-	-	-	1.6-6	-	-	2.9-7	1.6-6	-	2.9-7
DG Room 10	9.0-7	8.5-7	-	-	4.4-8	-	-	-	-	8.5-7	-	4.4-8
AFWS Pump Room 23	3.0-6	-	-	-	-	3.0-6	3.0-12	2.3-10	2.3-16	3.0-6	2.3-10	2.3-16
CCS Pump Room 1	3.3-7	3.1-7	2.3-8	2.3-11	1.5-10	6.1-11	6.1-17	4.6-15	4.6-21	3.3-7	2.3-11	1.5-10
CS Pump Room 2	3.3-7	-	-	3.1-7	2.3-8	-	-	6.1-11	6.1-17	-	3.1-7	2.3-8
Makeup Pump Room 2A	3.3-7	-	-	3.1-7	2.3-8	-	-	6.1-11	6.1-17	-	3.1-7	2.3-8
Control Room 15	5.7-7	-	-	-	-	4.8-7	-	-	8.9-8	4.8-7	-	8.9-8
Containment 77A	3.3-8	3.4-12	2.3-8	2.6-16	9.4-11	9.4-9	5.6-13	7.1-13	4.2-17	3.3-8	7.1-13	9.4-11
REC Pump 78A	2.4-8	4.7-10	2.4-8	3.6-14	9.4-11	9.4-10	9.4-16	7.1-14	7.1-20	2.4-8	1.1-13	9.4-11
SI Pump Room 9	8.1-8	1.0-8	5.1-8	1.0-11	3.8-10	2.0-8	2.0-14	2.0-11	2.0-17	7.0-8	3.0-11	3.8-10
Valve Room 13A	8.1-8	1.0-8	5.1-8	1.0-11	3.8-10	2.0-8	2.0-14	2.0-11	2.0-17	7.0-8	3.0-11	3.8-10
Outer Annul 75A	3.7-8	-	2.8-8	-	9.4-11	-	9.4-9	-	7.1-13	3.7-8	-	9.5-11
RCP Area 70A	3.3-8	3.4-12	2.4-8	2.6-16	1.4-10	9.4-9	9.4-15	7.1-13	7.1-19	3.3-8	7.1-13	1.4-10
MCC Area 27A	2.6-8	-	-	1.4-9	1.1-8	-	-	1.5-8	1.5-14	-	1.6-8	1.1-8
RCP Area 71A	3.3-8	3.4-12	2.4-8	2.6-16	1.4-10	9.4-9	9.4-15	7.1-13	7.1-19	3.3-8	7.1-13	1.4-10
Total	2.1-4	1.4-6	2.8-7	4.9-5	1.4-4	5.1-6	1.1-5	1.5-8	3.8-7	1.8-5	4.9-5	1.4-4

Note: Exponential notation is indicated in abbreviated form; i.e., 8.0-5 = 8×10^{-5}.

TABLE 7.3.1A-19

MEAN FREQUENCIES OF FIRE CONTRIBUTORS AFTER THE MODIFICATION

Fire Zone	CM	SEFC	SEC	SEF	SE	TEFC	TEC	TEF	TE	8B	8A	2RW	Impact of Modification
Electrical Tunnel 1A	3.7-6	--	--	1.1-6	2.5-6	--	--	9.2-9	9.0-9	--	1.1-6	2.5-6	Affected
SWG Room 14	2.6-6	--	--	--	2.5-7	--	--	--	9.0-9	--	--	2.5-6	Affected
Electrical Tunnel 32A	2.6-6	--	--	1.1-6	1.4-6	--	--	9.2-9	5.1-9	--	1.1-6	1.4-6	Affected
Electrical Penet. 74A	1.1-5	--	2.8-8	--	9.2-11	--	1.1-5	--	8.6-10	1.1-5	--	9.5-10	No Effect
CSR 11	1.9-6	--	--	--	--	1.6-6	--	--	2.9-7	1.6-6	--	2.9-7	No Effect
DG Room 10	9.0-7	8.5-7	--	--	4.4-8	--	--	--	--	8.5-7	--	4.4-8	No Effect
AFWS Pump Room 23	3.0-6	--	--	--	--	3.0-6	3.0-12	2.3-10	2.3-16	3.0-6	2.3-10	2.3-16	No Effect
CCS Pump Room 1	3.3-7	3.1-7	2.3-8	2.3-11	1.5-10	6.1-11	6.1-17	4.6-15	4.6-21	3.3-7	2.3-11	1.5-10	No Effect
CS Pump Room 2	1.5-8	--	--	1.4-8	1.1-9	--	--	6.1-11	6.1-17	--	1.4-8	1.1-9	Affected
Makeup Pump Room 2A	1.5-8	--	--	1.4-8	1.1-9	--	--	6.1-11	6.1-17	--	1.4-8	1.1-9	Affected
Control Room 15	5.7-7	--	--	--	--	4.8-7	--	--	8.9-8	4.8-7	--	8.9-8	No Effect
Containment 77A	3.3-8	3.4-12	2.3-8	2.6-16	9.4-11	9.4-9	5.6-13	7.1-13	4.2-17	3.3-8	7.1-13	9.4-11	No Effect
REC Pump 78A	2.4-8	4.7-10	2.4-8	3.6-14	9.4-11	9.4-10	9.4-16	7.1-14	7.1-20	2.4-8	1.1-13	9.4-11	No Effect
SI Pump Room 9	8.1-8	1.0-8	5.1-8	1.0-11	3.8-10	2.0-8	2.0-14	2.0-11	2.0-17	7.0-8	3.0-11	3.8-10	No Effect
Valve Room 13A	8.1-8	1.0-8	5.1-8	1.0-11	3.8-10	2.0-8	2.0-14	2.0-11	2.0-17	7.0-8	3.0-11	3.8-10	No Effect

Note: Exponential notation is indicated in abbreviated form; i.e., 8.0-5 = 8×10^{-5}.

TABLE 7.3.1A-19 (continued)

MEAN FREQUENCIES OF FIRE CONTRIBUTORS AFTER THE MODIFICATION

Fire Zone	CM	SEFC	SEC	SEF	SE	TEFC	TEC	TEF	TE	8B	8A	2RW	Impact of Modification
Outer Annul 75A	3.7-8	--	2.8-8	--	9.4-11	--	9.4-9	--	7.1-13	3.7-8	--	9.5-11	No Effect
RCP Area 70A	3.3-8	3.4-12	2.4-8	2.6-16	1.4-10	9.4-9	9.4-15	7.1-13	7.1-19	3.3-8	7.1-13	1.4-10	No Effect
MCC Area 27A	2.6-8	--	--	1.4-9	1.1-8	--	--	1.5-8	1.5-14	--	1.6-8	1.1-8	No Effect
RCP Area 71A	3.3-8	3.4-12	2.4-8	2.6-16	1.4-10	9.4-9	9.4-15	7.1-13	7.1-19	3.3-8	7.1-13	1.4-10	No Effect
Total	2.7-5	1.4-6	2.8-7	2.2-6	6.7-6	5.1-6	1.1-5	3.4-8	4.0-7	1.8-5	2.2-6	6.7-6	

Note: Exponential notation is indicated in abbreviated form; i.e., 8.0-5 = 8×10^{-5}.

TABLE 7.3.1A-20

FREQUENCIES OF SEVERAL PARAMETERS USED IN SECTION 7.3.1A-5

Parameter	Distribution	Mean	Variance	Source
Q_{SW}	Lognormal	2.46×10^{-5}	1.84×10^{-8}	Table 1.5.1-4, item 29.
$Q_{CCS,D}$	Lognormal	6.41×10^{-3}	7.78×10^{-6}	Table 1.5.1-4, item 11.
λ_{CCS}	Lognormal	1.68×10^{-5} per hour	2.76×10^{-8} per hour	Table 1.5.1-4, item 16.
$Q_{CCS,M}$	Lognormal	5.6×10^{-5}	3.14×10^{-9}	Table 1.5.1-13 approximating techniques $T_m = 1.0$, $T_{Comp} = 17832.0$.
λ_{AUX}	Gamma	0.034 per year		Section 7.3.1.3.
f_T	Lognormal	6.51×10^{-2}	6.71×10^{-3}	Section 7.3.1.3.
f_R	Almost Certain	0.5	--	Section 7.3.1.4.3.
$Q(\tau_V)$	See the Source	0.44		Section 7.3.1.4.2.

TABLE 7.3.1A-21

FIRE CONTRIBUTIONS BEFORE THE MODIFICATION

Fire Area	Core Melt Related Components		Containment Related Components		Mean Frequency										Remarks
	Within Fire Area	Outside Fire Area	Within Fire Area	Outside Fire Area	Fire Frequency	Core Melt	SEFC	SEC	SEF	SE	TEFC	TEC	TEF	TE	
1: CCS Pump Room	CCS P (all)	CCS 1.0 (all) SIS 2.-4 AFWS 2.-5 EP 3.3-7 SWS 5.1-5 REC 5.-4 PORV 6.2-3 (from page 1.3-128 for OP1)	--	CS 7.5-5 (all) CF 1.-6	4.4-4	3.3-7	3.1-7	2.3-8	2.3-11	1.5-10	6.1-11	6.1-17	4.6-15	4.6-21	Part of CCS system. 8B = 3.3-7 8A = 2.3-11 2RW = 1.5-10 λ_{AUX} = 3.4-2 f_2 = 0.013 EP is 10 times higher than that of Table 1.5.2.2.1-2D
1A: Electrical Tunnel	SIS (all) P CCS P (all) RHR (all) P CHG P & C PORV P & C AFW Pumps C	CHG 1.0 CCS 1.0 SIS 1.0 AFWS 0.05 EP 3.3-7 SWS 5.1-4 REC 1.0 PORV 1.0	CS P (all) CF P (all)	CS 1.0 CF 1.0	See 7.3.1	8.-5	--	--	2.4-5	5.6-5	--	--	--	--	From Section 7.3.1 of the IPPSS, page 7.3-27.
2: Containment Spray Pump Room	CCS P (all)	See Fire Zone 1	CS (all)	CF 1.-6 (all) CS 1.0	4.4-4	3.3-7	--	--	3.1-7	2.3-8	--	--	6.1-11	6.1-17	8B = -- 8A = 3.1-7 2RW = 2.3-8 $\lambda_{AUX} f_2$

P = power cables; C = control cables; CHG = charging pumps; CCS = component cooling system; SIS = safety injection system; AFWS = auxiliary feedwater system; EP = electric power; SWS = service water system; REC = recirculation system; PORV = PORVs and block valves; RHR = residual heat removal; MCC = motor control center.

TABLE 7.3.1A-21 (continued)

FIRE CONTRIBUTIONS BEFORE THE MODIFICATION

Fire Area	Core Melt Related Components		Containment Related Components		Mean Frequency										Remarks
	Within Fire Area	Outside Fire Area	Within Fire Area	Outside Fire Area	Fire Frequency	Core Melt	SEFC	SEC	SEF	SE	TEFC	TEC	TEF	TE	
2A: Primary Water Makeup Pump Room	CCS (all) P CHG (all) C	CCS 1.0 SIS 2.-4 AFWS 2.-5 EP 3.-7 SW 5.-5 REC 5.-4 PORV 6.2-3	CS (all) P	CS 1.0 (all) CF 1.-6 (all)	4.4-4	3.3-7	--	--	3.1-7	2.3-8	--	--	6.1-11	6.1-17	8B = 3.1-7 8A = 3.1-7 2RW = 2.3-8 $\lambda_{AUX} f_2$
3: RHR Pump Room	RHR 22 P		--												Part of RHR system. Large LOCA not possible by fire.
3A: Corridor	RHR 21 and 22 P		--												Part of RHR system. Large LOCA not possible by fire.
4: RHR Pump Room	RHR 21 P														Part of RHR system. Large LOCA not possible by fire.
4A	--		--												
5: CHG Pump Room	CHG (all)		--												Part of CHG system analysis. CCS will prevent RCP seal LOCA.
5A	--		--												

P = power cables; C = control cables; CHG = charging pumps; CCS = component cooling system; SIS = safety injection system; AFWS = auxiliary feedwater system; EP = electric power; SWS = service water system; REC = recirculation system; PORV = PORVs and block valves; RHR = residual heat removal; MCC = motor control center.

TABLE 7.3.1A-21 (continued)

FIRE CONTRIBUTIONS BEFORE THE MODIFICATION

Fire Area	Core Melt Related Components		Containment Related Components		Mean Frequency										Remarks
	Within Fire Area	Outside Fire Area	Within Fire Area	Outside Fire Area	Fire Frequency	Core Melt	SEFC	SEC	SEF	SE	TEFC	TEC	TEF	TE	
6	CHG 22,23		--												Part of CHG system.
6A	CHG (all)		--												Part of CHG system analysis.
7	CHG 23		--												
7A	Remote S/D Panel CHG C CCSHX														Very small impact on components needed for safe S/D.
8	BAT 21 and 22		--												Part of CHG system.
8A	--		--												
9: SI Pump room	SIS (all)	CCS 1.-5 SIS 1.0 AFWS 2.-5 EP 3.3-7 SWS 5.1-5 REC 5.-4 PORV 6.2-3	--	CS 1.-3 CF 1.-6	10^{-3}	8.1-8	1.-8	5.1-8	1.-11	3.8-10	2.-8	2.-14	2.-11	2.-17	Part of SI system. 8B = 8.1-8 8A = 3.0-11 2RW = 3.8-10
9A	--		--												
10: DG Building	All three diesels		--		See 7.3.1	9.-7	8.5-7	--	--	4.4-8	--	--	--	--	See Section 7.3.1 for detail.
10A	--		--												

P = power cables; C = control cables; CHG = charging pumps; CCS = component cooling system; SIS = safety injection system; AFWS = auxiliary feedwater system; EP = electric power; SWS = service water system; REC = recirculation system; PORV = PORVs and block valves; RHR = residual heat removal; MCC = motor control center.

TABLE 7.3.1A-21 (continued)

FIRE CONTRIBUTIONS BEFORE THE MODIFICATION

Fire Area	Core Melt Related Components		Containment Related Components		Mean Frequency									Remarks
	Within Fire Area	Outside Fire Area	Within Fire Area	Outside Fire Area	Fire Frequency	Core Melt	SEFC	SEC	SEF	SE	TEFC	TEC	TEF	TE	
11: CSR						1.9-6	--	--	--	--	1.6-6	--	--	2.9.-7	See Section 7.3.1 for detail
11A	--		--												
12	Batteries														
12A	--		--												
13	Batteries														
13A: Valve Room	RHR 21 and 22 P SIS(all) C	CCS 1.-5 SIS 1.0 AFWS 2.-5 EP 3.-7 SW 5.-5 REC 5.-4 PORV 6.2-3	--	CS 1.-3 CF 1.-6	10^{-3}	8.1-8	1.-8	5.1-8	1.-11	3.8-10	2.-8	2.-14	2.-11	2.-17	8B = 8.-8 8A = 3.-11 2RW = 3.8-10
14: SWG Room						5.6-5	--	--	--	5.6-5	--	--	--	--	See Section 7.3.1
14A	--		--												
15: Control Room	Controls of all Components	Power of all Components	Controls of all Components	Power of all Components	See cable spreading room (CSR) study	5.7-7	--	--	--	--	4.8-7	--	--	8.9-8	Same as CSR except for factor f_{CR} ($\alpha f_{CR} = 0.3$) reduction due to human presence.

P = power cables; C = control cables; CHG = charging pumps; CCS = component cooling system; SIS = safety injection system; AFWS = auxiliary feedwater system; EP = electric power; SWS = service water system; REC = recirculation system; PORV = PORVs and block valves; RHR = residual heat removal; MCC = motor control center.

TABLE 7.3.1A-21 (continued)

FIRE CONTRIBUTIONS BEFORE THE MODIFICATION

Fire Area	Core Melt Related Components		Containment Related Components		Mean Frequency										Remarks
	Within Fire Area	Outside Fire Area	Within Fire Area	Outside Fire Area	Fire Frequency	Core Melt	SEFC	SEC	SEF	SE	TEFC	TEC	TEF	TE	
15A: Valve Room	--		--												
16	--		--												
16A	--		--												
17	--		--												
17A	--		--												
18	--		--												
18A	--		--												
19	--		--												
19A	--		--												
20	--		--												
20A	--		--												
21	--		--												
21A	--		--												
22: Intake Structure	SW (all)														Part of SWS analysis. Pumps in open area.

P = power cables; C = control cables; CHG = charging pumps; CCS = component cooling system; SIS = safety injection system; AFWS = auxiliary feedwater system; EP = electric power; SWS = service water system; REC = recirculation system; PORV = PORVs and block valves; RHR = residual heat removal; MCC = motor control center.

TABLE 7.3.1A-21 (continued)

FIRE CONTRIBUTIONS BEFORE THE MODIFICATION

Fire Area	Core Melt Related Components		Containment Related Components		Mean Frequency										Remarks
	Within Fire Area	Outside Fire Area	Within Fire Area	Outside Fire Area	Fire Frequency	Core Melt	SEFC	SEC	SEF	SE	TEFC	TEC	TEF	TE	
22A	--		--												
23: AFWS Pump Room	AFWS (all)	AFWS 1.0 SIS 2.-4 REC 5.-4 PORV 6.2-3 SW 5.-5 EP 3.-7 CCS 1.-5	--	CS 7.5-5 (all) CF 1.-6	4.4-4	3.0-6	--	--	--	--	3.0-6	3.0-12	2.3-10	2.3-16	Part of AFWS analysis. 8B = 3.1-6 8A = 2.3-10 2RW = 2.3-16
23A	--		--												
24A	--		--												
25A	--		--												
26A	--		--												
27A MCC Area	MCC 26A and 26B	PORV 1.0 AFWS 7.-5 EP 3.-7 SW 5.-5 REC 0.6 SIS 0.03	CS (MOVs)	CS 1.0 CF 10^{-6} (all)	2.2-4	2.6-8	--	--	1.4-9	1.1-8	--	--	1.5-8	1.5-14	f_{27A} = .121 ≡ fraction of auxiliary building fire in MCC area. f_{PF} = .053 ≡ fraction of MCC fire disabling both MCCs. λ_{AUX} = 0.034 8B = -- 8A = 1.6-8 2RW = 1.1-8
28A	--		--												

P = power cables; C = control cables; CHG = charging pumps; CCS = component cooling system; SIS = safety injection system; AFWS = auxiliary feedwater system; EP = electric power; SWS = service water system; REC = recirculation system; PORV = PORVs and block valves; RHR = residual heat removal; MCC = motor control center.

TABLE 7.3.1A-21 (continued)

FIRE CONTRIBUTIONS BEFORE THE MODIFICATION

Fire Area	Core Melt Related Components		Containment Related Components		Mean Frequency										Remarks
	Within Fire Area	Outside Fire Area	Within Fire Area	Outside Fire Area	Fire Frequency	Core Melt	SEFC	SEC	SEF	SE	TEFC	TEC	TEF	TE	
29A	--		--												
30A	SW Pipes														Part of SW system analysis. Not susceptible to fire.
31A	--		--												
32A: Tunnel						5.6-5	--	--	2.4-5	3.2-5	--	--	--	--	See Section 7.3.1.7 of the IPPSS, p. 7.3-34
33A	--		--												
39A	--		--												
40A	--		--												
41A	--		--												
42A	--		--												
43A	--		--												
44A	--		--												
45A	--		--												
46A	--		--												
47A	--		--												

P = power cables; C = control cables; CHG = charging pumps; CCS = component cooling system; SIS = safety injection system; AFWS = auxiliary feedwater system; EP = electric power; SWS = service water system; REC = recirculation system; PORV = PORVs and block valves; RHR = residual heat removal; MCC = motor control center.

TABLE 7.3.1A-21 (continued)

FIRE CONTRIBUTIONS BEFORE THE MODIFICATION

Fire Area	Core Melt Related Components		Containment Related Components		Mean Frequency										Remarks
	Within Fire Area	Outside Fire Area	Within Fire Area	Outside Fire Area	Fire Frequency	Core Melt	SEFC	SEC	SEF	SE	TEFC	TEC	TEF	TE	
48A	--		--												
49A	--		--												
50A	--		--												
51A	--		--												
52A	--		--												
53A	--		--												
55A	--		--												
56A	--		--												
57A	--		--												
58A	--		--												
59A	Charcoal Filters														Does not pose immediate safety concern.
60A	Secondary RV P & C Penetration Cooling System														The plant can be safety shut-down without these components.
61A	--		--												

P = power cables; C = control cables; CHG = charging pumps; CCS = component cooling system; SIS = safety injection system; AFWS = auxiliary feedwater system; EP = electric power; SWS = service water system; REC = recirculation system; PORV = PORVs and block valves; RHR = residual heat removal; MCC = motor control center.

TABLE 7.3.1A-21 (continued)

FIRE CONTRIBUTIONS BEFORE THE MODIFICATION

Fire Area	Core Melt Related Components		Containment Related Components		Mean Frequency										Remarks
	Within Fire Area	Outside Fire Area	Within Fire Area	Outside Fire Area	Fire Frequency	Core Melt	SEFC	SEC	SEF	SE	TEFC	TEC	TEF	TE	
62A	Boiler Feedwater Components														Part of AFWS study.
63A	--		--												
64A	--		--												
65A	Main Feed-water Related Atmos-pheric Relief Valves														The plant can be safely shut-down without these components.
70A RCP Area	PORV P & C	PORV 1. CCS 1.-5 SIS 2.-4 AFWS 2.-5 EP 2.-7 SW 5.-5 REC 5.-4	--	CS 7.5-5 CF 1.-6	4.7-4 see 75A	3.3-8	3.4-12	2.4-8	2.6-16	1.4-10	9.4-9	9.4-15	7.1-13	7.1-19	Part of PORV failure frequency. 8B = 3.3-8 8A = 7.1-13 2RW = 1.4-10
71A	PORV P & C SIS Valves RHR Valves CHG Valves	Same as 70A		Same as 70A	4.7-4 see 75A	3.3-8	3.4-12	2.4-8	2.6-16	1.4-10	9.4-9	9.4-15	7.1-13	7.1-19	Only PORV failure affects plant safety; others are in safe position /should be quantified as part of PORV failure frequency. See 70A.

P = power cables; C = control cables; CHG = charging pumps; CCS = component cooling system; SIS = safety injection system; AFWS = auxiliary feedwater system; EP = electric power; SWS = service water system; REC = recirculation system; PORV = PORVs and block valves; RHR = residual heat removal; MCC = motor control center.

TABLE 7.3.1A-21 (continued)

FIRE CONTRIBUTIONS BEFORE THE MODIFICATION

Fire Area	Core Melt Related Components		Containment Related Components		Mean Frequency										Remarks
	Within Fire Area	Outside Fire Area	Within Fire Area	Outside Fire Area	Fire Frequency	Core Melt	SEFC	SEC	SEF	SE	TEFC	TEC	TEF	TE	
72A	RHR Valves		CF 22 P												Failure of RHR valves has little effect on plant safety; this fire zone can be regarded as part of CF system failure analysis.
74A: Electrical Penetrations Fan House	AFWS C PORV P & C Atmosphere P & C	PORV 1.0 CCS 1.-5 SIS 2.-4 AFWS 0.025 (see page 7.3-14) SWS 5.-5 EP 2.-7	CF P	CF 1.0 CS 7.5-5	4.6-4	1.1-5	--	2.8-8	--	9.2-11	--	1.1-5	--	8.6-10	8B = 1.1-5 8A = -- 2RW = 8.6-10 λ_{AUX} = 2.4-2 f_T = 6.5-2 $Q(T)$ = 0.21
75A: Outer Annulus Containment	PORV P & C Przr Heaters	PORV 1.0 CCS 1.-5 SIS 2.-4 AFWS 2.-5 EP 2.-7 SWS 5.-5 REC 5.-4	CF P (all)	CF 1.0 CS 7.5-5	4.7-4	3.7-8	--	2.8-8	--	9.4-11	--	9.4-9	--	7.1-13	8B = 3.7-8 8A = -- 2RW = 9.5-11 $\lambda_{containment}$ = 1.5-2 f_{75A} = 3.2-2
76A: Containment	--		CF 23, 24, 25 P	CF 1.0 CS 1.-3											Part of CF failure study; plant can be safely shut down.

P = power cables; C = control cables; CHG = charging pumps; CCS = component cooling system; SIS = safety injection system; AFWS = auxiliary feedwater system; EP = electric power; SWS = service water system; REC = recirculation system; PORV = PORVs and block valves; RHR = residual heat removal; MCC = motor control center.

TABLE 7.3.1A-21 (continued)

FIRE CONTRIBUTIONS BEFORE THE MODIFICATION

Fire Area	Core Melt Related Components		Containment Related Components		Mean Frequency										Remarks
	Within Fire Area	Outside Fire Area	Within Fire Area	Outside Fire Area	Fire Frequency	Core Melt	SEFC	SEC	SEF	SE	TEFC	TEC	TEF	TE	
77A - Containment	PORV P	PORV 1.0 CCS 1.-5 SIS 2.-4 AFWS 2.-5 EP 2.-7 SW 5.-5 REC 5.-4	CF 25 P	CF 6.-5 CS 7.5-5	4.7-4 see 75A	3.3-8	3.4-12	2.3-8	2.6-16	9.4-11	9.4-9	5.6-13	7.1-13	4.2-17	8B = 3.3-8 8A = 7.1-13 2RW = 9.4-11
78A - Recirculation Pump Area	RHRHX REC Pumps CCS Valves for RHRHX cooling	PORV 6.2-3 SIS 2.-4 REC 0.1 AFWS 2.-5 EP 2.-7 SW 5.-5 CCS 1.-5	--	CF 1.-6 CS 7.5-5	4.7-4 See 75A	2.4-8	4.7-10	2.4-8	3.6-14	9.4-11	9.4-10	9.4-16	7.1-14	7.1-20	Recirculation failure if CF is failed. 8B = 2.4-8 8A = 1.1-13 2RW = 9.4-11
80A	--		CF 21												Part of CF system analysis.
81A	--		CF 23												Part of CF system analysis.
82A	--		CF 24												Part of CF system analysis.
83A	--		CF 25												Part of CF system analysis.

P = power cables; C = control cables; CHG = charging pumps; CCS = component cooling system; SIS = safety injection system; AFWS = auxiliary feedwater system; EP = electric power; SWS = service water system; REC = recirculation system; PORV = PORVs and block valves; RHR = residual heat removal; MCC = motor control center.

TABLE 7.3.1A-21 (continued)

FIRE CONTRIBUTIONS BEFORE THE MODIFICATION

Fire Area	Core Melt Related Components		Containment Related Components		Mean Frequency										Remarks
	Within Fire Area	Outside Fire Area	Within Fire Area	Outside Fire Area	Fire Frequency	Core Melt	SEFC	SEC	SEF	SE	TEFC	TEC	TEF	TE	
84A	--		CF 22												Part of CF system analysis.
85A	Incore Detector		--												Failure would not lead to severely adverse situations.
86A	Przr, SGS, CR Drives, Hydrogen Recom-biners														Fire cannot lead to mechanical component failure; therefore, this area is not critical.
87A	--		--												
90A	--		--												
91A	--		--												
94A	--		--												
95A	--		--												
96A	--		--												
97A	--		--												
98A	--		--												

P = power cables; C = control cables; CHG = charging pumps; CCS = component cooling system; SI: safety injection system; AFWS = auxiliary feedwater system; EP = electric power; SWS = service water system; REC = recirculation system; PORV = PORVs and block valves; RHR = residual heat removal; MCC = motor control center.

TABLE 7.3.1A-21 (continued)

FIRE CONTRIBUTIONS BEFORE THE MODIFICATION

Fire Area	Core Melt Related Components		Containment Related Components		Mean Frequency										Remarks
	Within Fire Area	Outside Fire Area	Within Fire Area	Outside Fire Area	Fire Frequency	Core Melt	SEFC	SEC	SEF	SE	TEF	TEC	TEF	TE	
99A	--		Charcoal Filters												No effect on risk.
100A	--		--												
101A	--		--												
105A	--		--												
106A	RWST		--												Part of RWST failure frequency.

P = power cables; C = control cables; CHG = charging pumps; CCS = component cooling system; SIS = safety injection system; AFWS = auxiliary feedwater system; EP = electric power; SWS = service water system; REC = recirculation system; PORV = PORVs and block valves; RHR = residual heat removal; MCC = motor control center.

TABLE 7.3.1B-22

INDIAN POINT 2 - CHARACTERISTIC VALUES OF THE FREQUENCIES OF RELEASE CATEGORIES AND CORE MELT DUE TO FIRE AFTER THE ALTERNATE SHUTDOWN SYSTEM MODIFICATIONS AND THE REQUANTIFICATION OF FIRE ZONES 74A AND 23

Release Category/ Core Melt	Probability Level	Frequency After Modification (per reactor year)
Release Category 8B (reduced)	5th Percentile	6.6×10^{-7}
	Median	2.4×10^{-6}
	95th Percentile	2.6×10^{-5}
	Mean	4.6×10^{-6}
Release Category 8A (revised)	5th Percentile	7.3×10^{-9}
	Median	3.5×10^{-7}
	95th Percentile	2.5×10^{-5}
	Mean	2.2×10^{-6}
Release Category 2RW (unchanged)	5th Percentile	1.6×10^{-7}
	Median	1.6×10^{-6}
	95th Percentile	4.1×10^{-5}
	Mean	6.7×10^{-6}
Core Melt (reduced)	5th Percentile	1.9×10^{-6}
	Median	7.4×10^{-6}
	95th Percentile	4.6×10^{-5}
	Mean	1.4×10^{-5}

TABLE 7.3.1B-23

MEAN FREQUENCIES OF FIRE CONTRIBUTORS AFTER THE ALTERNATE SHUTDOWN SYSTEM MODIFICATIONS AND THE REQUANTIFICATION OF FIRE ZONES 74A AND 23

Fire Zone	CM	SEFC	SEC	SEF	SE	TEFC	TEC	TEF	TE	8B	8A	2RW	Impact of Modification
Electrical Tunnel 1A	3.7-6	--	--	1.1-6	2.5-6	--	--	9.2-9	9.0-9	--	1.1-6	2.5-6	Affected
Switchgear Room 14	2.4-6	--	--	--	2.4-6	--	--	--	9.0-9	--	--	2.4-6	Affected
Electrical Tunnel 32A	2.6-6	--	--	1.1-6	1.4-6	--	--	9.2-9	5.1-9	--	1.1-6	1.4-6	Affected
Electrical Penetration 74A	1.0-7	--	2.8-8	--	9.2-11	--	7.4-8	--	5.6-12	1.0-7	--	9.8-11	No Effect
CSR 11	1.9-6	--	--	--	--	1.6-6	--	--	2.9-7	1.6-6	--	2.9-7	No Effect
Diesel Generator Room 10	9.0-7	8.5-7	--	--	4.4-8	--	--	--	--	8.5-7	--	4.4-8	No Effect
AFWS Pump Room 23	9.4-7	--	--	--	--	9.4-7	9.4-13	7.1-11	7.1-17	9.4-7	7.1-11	7.1-17	No Effect
CCS Pump Room 1	3.3-7	3.1-7	2.3-8	2.3-11	1.5-10	6.1-11	6.1-17	4.6-15	4.6-21	3.3-7	2.3-11	1.5-10	No Effect
CS Pump Room 2	1.5-8	--	--	1.4-8	1.1-9	--	--	6.1-11	6.1-17	--	1.4-8	1.1-9	Affected
Makeup Pump Room 2A	1.5-8	--	--	1.4-8	1.1-9	--	--	6.1-11	6.1-17	--	1.4-8	1.1-9	Affected
Control Room 15	5.7-7	--	--	--	--	4.8-7	--	--	8.9-8	4.8-7	--	8.9-8	No Effect
Containment 77A	3.3-8	3.4-12	2.3-8	2.6-16	9.4-11	9.4-9	5.6-13	7.1-13	4.2-17	3.3-8	7.1-13	9.4-11	No Effect

Note: Exponential notation is indicated in abbreviated form; i.e., 3.7-6 = 3.7 x 10^{-6}.

TABLE 7.3.1B-23 (continued)

Fire Zone	CM	SEFC	SEC	SEF	SE	TEFC	TEC	TEF	TE	8B	8A	2RW	Impact of Modification
Recirculating Pump 78A	2.4-8	4.7-10	2.4-8	3.6-14	9.4-11	9.4-10	9.4-16	7.1-14	7.1-20	2.4-8	1.1-13	9.4-11	No Effect
SI Pump Room 9	8.1-8	1.0-8	5.1-8	1.0-11	3.8-10	2.0-8	2.0-14	2.0-11	2.0-17	7.0-8	3.0-11	3.8-10	No Effect
Valve Room 13A	8.1-8	1.0-8	5.1-8	1.0-11	3.8-10	2.0-8	2.0-14	2.0-11	2.0-17	7.0-8	3.0-11	3.8-10	No Effect
Outer Annulus 75A	3.7-8	--	2.8-8	--	9.4-11	--	9.4-9	--	7.1-13	3.7-8	--	9.5-11	No Effect
RCP Area 70A	3.3-8	3.4-12	2.4-8	2.6-16	1.4-10	9.4-9	9.4-15	7.1-13	7.1-19	3.3-8	7.1-13	1.4-10	No Effect
Motor Control Center Area 27A	2.6-8	--	--	1.4-9	1.1-8	--	--	1.5-8	1.5-14	--	1.6-8	1.1-8	No Effect
RCP Area 71A	3.3-8	3.4-12	2.4-8	2.6-16	1.4-10	9.4-9	9.4-15	7.1-13	7.1-19	3.3-8	7.1-13	1.4-10	No Effect
Total	1.4-5	1.2-6	2.8-7	2.2-6	6.3-6	3.1-6	8.3-8	3.4-8	4.0-7	4.6-6	2.2-6	6.7-6	

Note: Exponential notation is indicated in abbreviated form; i.e., 2.4-8 = 2.4×10^{-8}.

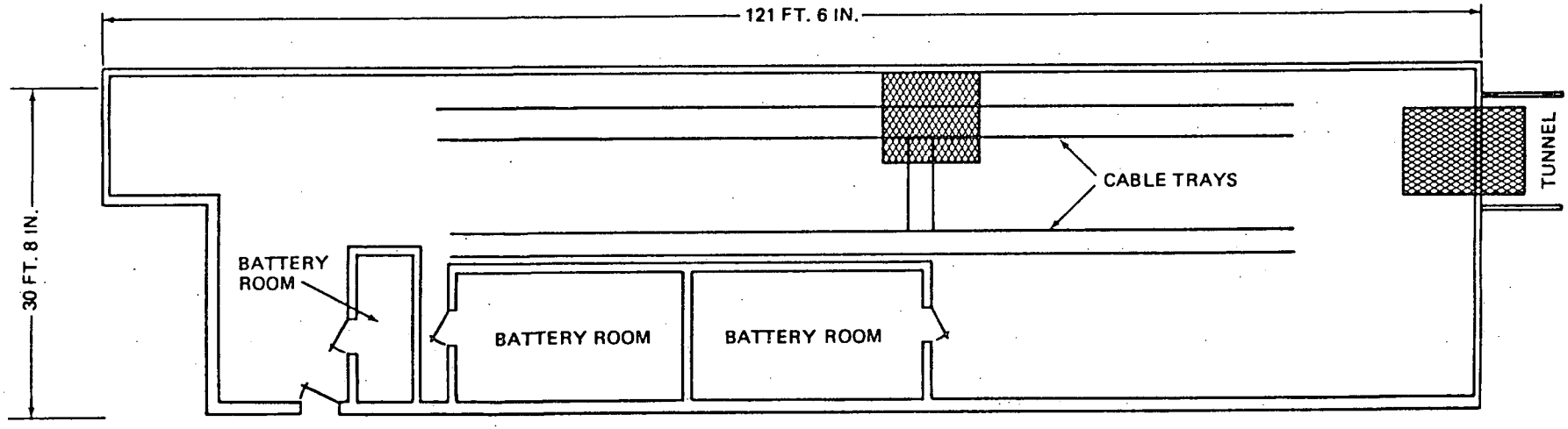
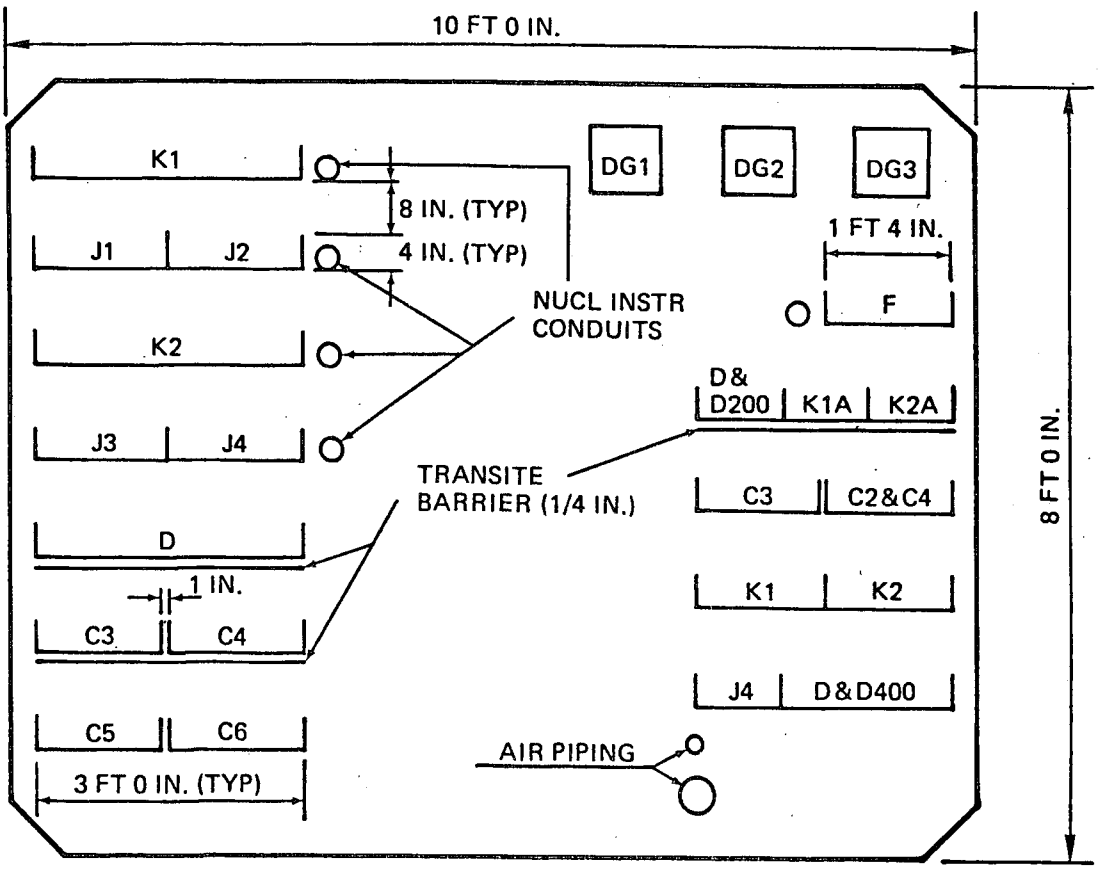


Figure 7.3.1-1. The Cable Spreading Room of Indian Point 2, as Viewed from the Top



TYPICAL SECTION CABLE TUNNEL

LEFT HAND SIDE TRAYS	K1	CONTROL TRAY ONE CHANNEL (FOR VALVE CONTROL) ETC
	J1-J2	2 INSTR TRAYS WITH BARRIERS – 2 CHANNELS
	K2	CONTROL TRAY ONE CHANNEL (FOR VALVE CONTROL) ETC
	J3 & J4	2 INSTR TRAYS WITH BARRIERS – 2 CHANNELS
	D	MAX NO. 12 WIRE FOR SMALL POWER & ONE CONTROL CHANNEL
	C4	(480V HEAVY POWER) CONT RECIRC FAN 21 SAF INJ PUMP 21 RECIRC PUMP 21
	C3	(480V HEAVY POWER) CONT RECIRC FAN 25 RES HT REM PUMP 22 SAF INJ PUMP 23 CONT RECIRC FAN 23
	C6	(480V HEAVY POWER) CONT RECIRC FAN 22 SAF INJ PUMP 22
	C5	(480V HEAVY POWER) RECIRC PUMP 22 RES HT REM PUMP 21 CONT RECIRC FAN 24
RIGHT HAND SIDE TRAYS	F	2ND CHANNELS FOR "F" CABLES DC SUPPLY (NORMAL) DIESEL GEN CONT PNL 22
	F	(1ST CHANNEL) DC SUPPLY (EMERG) DIESEL GEN CONT PNL 23 LTG & MOTOR FEEDERS
	D & D200-K1A-K2A	DIESEL GEN CONTROL – 3 CHANNELS
	C3	(480V HEAVY POWER) COMP CLG PUMP 23 MCC27 FEEDER MCC 26B FEEDER LTG SWGR TRANSF 22 CHARGING PUMP 22 CHARGING PUMP 23 CONT SPRAY PUMP 22
	C2	(480V HEAVY POWER) DC EMERG LTG FEEDER
	C4	CONT SPRAY PUMP 21 COMP COOLING PUMP 21 COMP COOLING PUMP 22 MCC 26A FEEDER LTG SWGR TRANSF 23 CHARGING PUMP 21
	K1-K2	CONTROL, – 2 CHANNELS
	J4	INSTR – 1 CHANNEL
	D & D400	MISC SMALL POWER & CONTROL – 1 CHANNEL

Figure 7.3.1-2. Cable Routing in Cable Tunnel

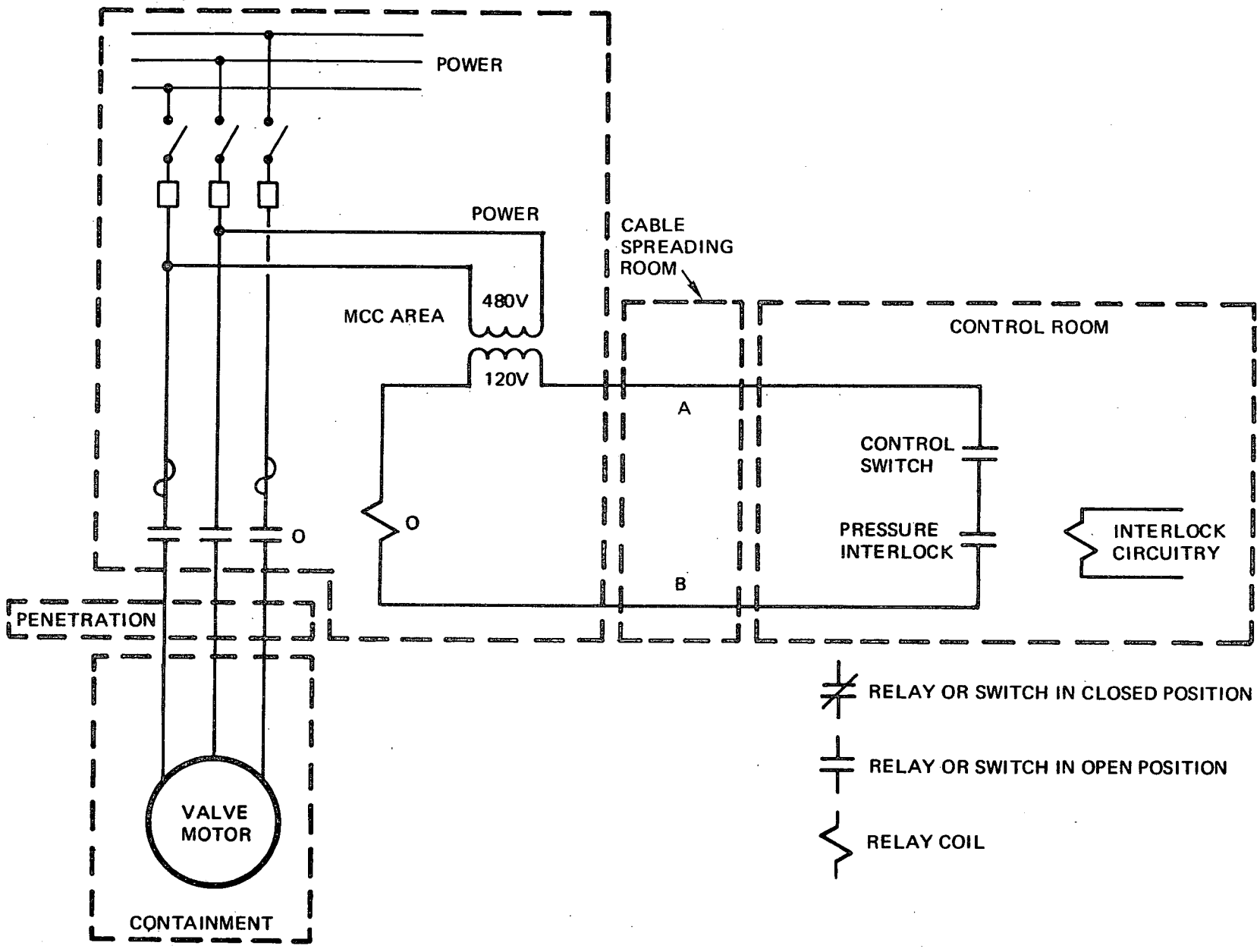


Figure 7.3.1-3. Simplified Diagram of the Control Circuitry for Opening an RHR Isolation MOV (730 or 731)

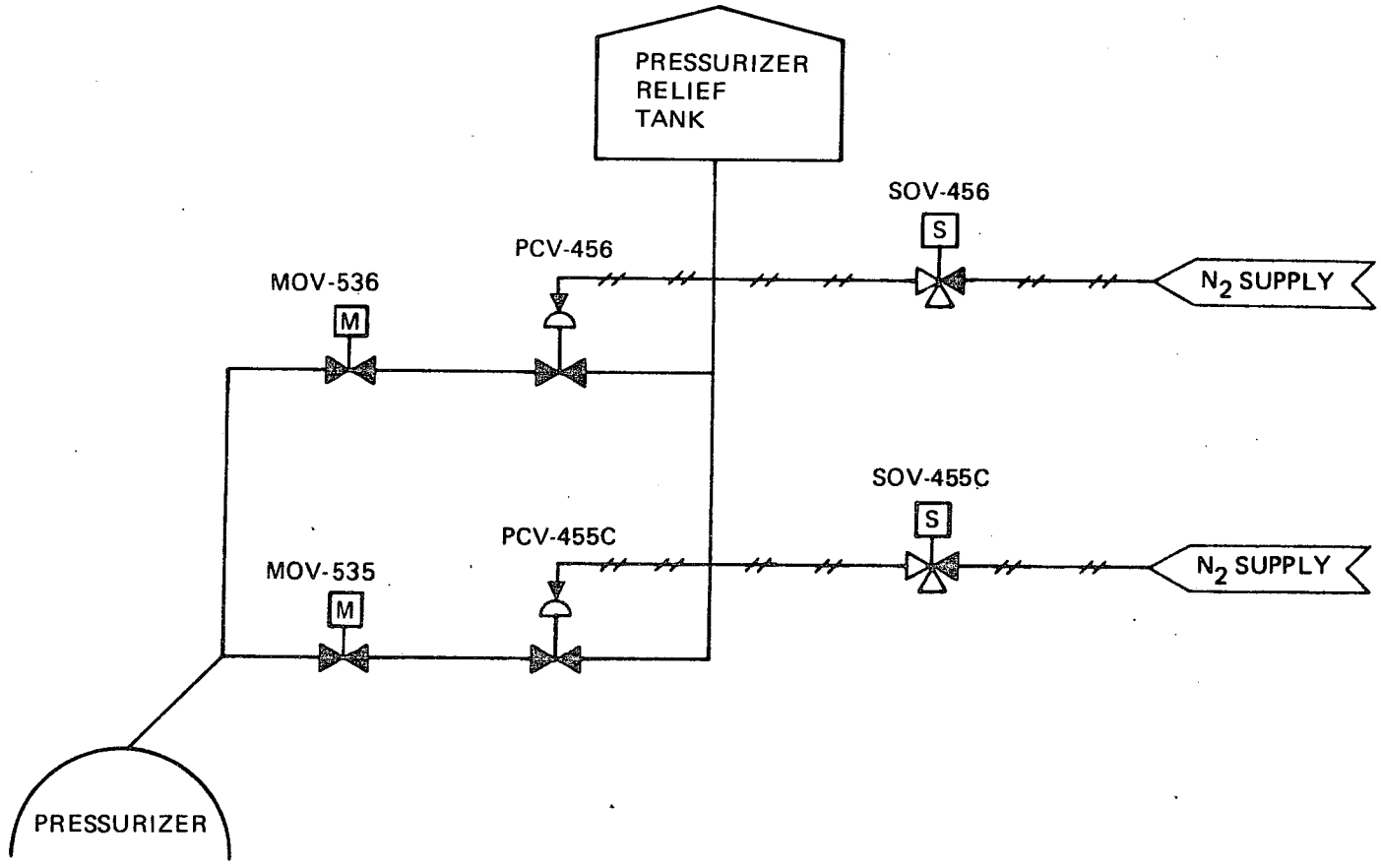


Figure 7.3.1-4. Valves with the Potential of Causing a Small LOCA

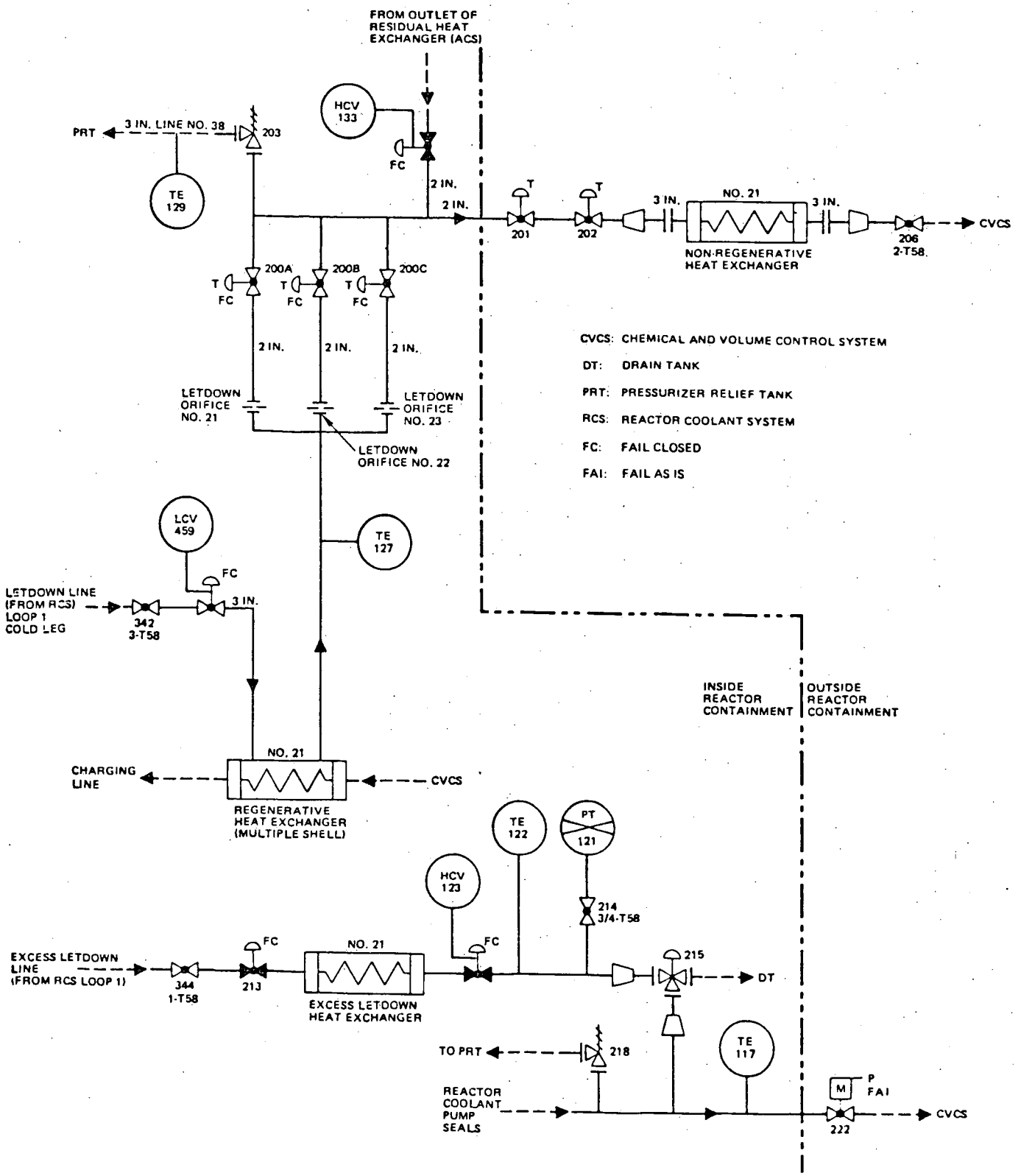


Figure 7.3.1-5. Normal and Excess Letdown Lines in Indian Point 2

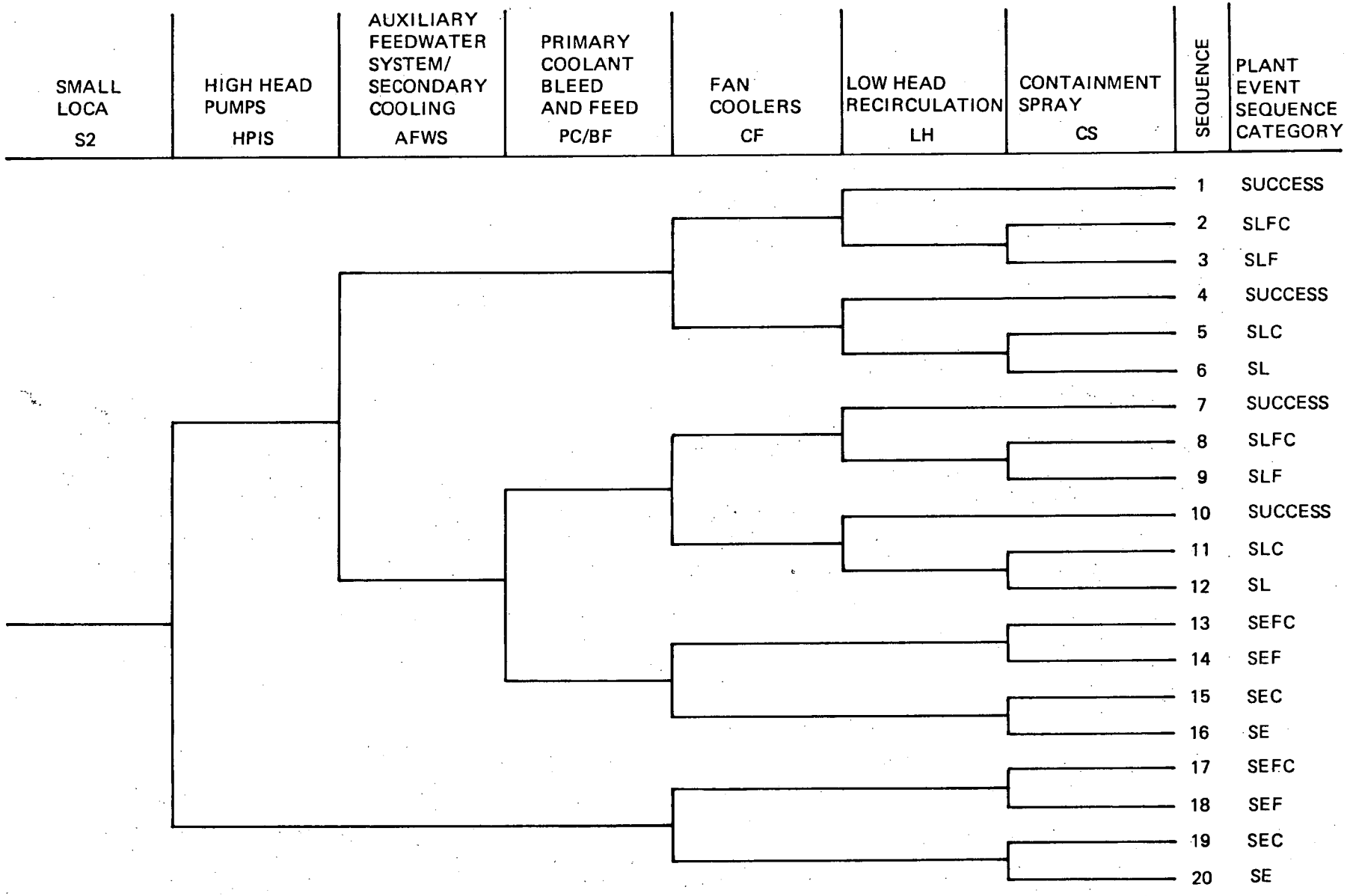


Figure 7.3.1-6. Simplified Event Tree for a Small LOCA

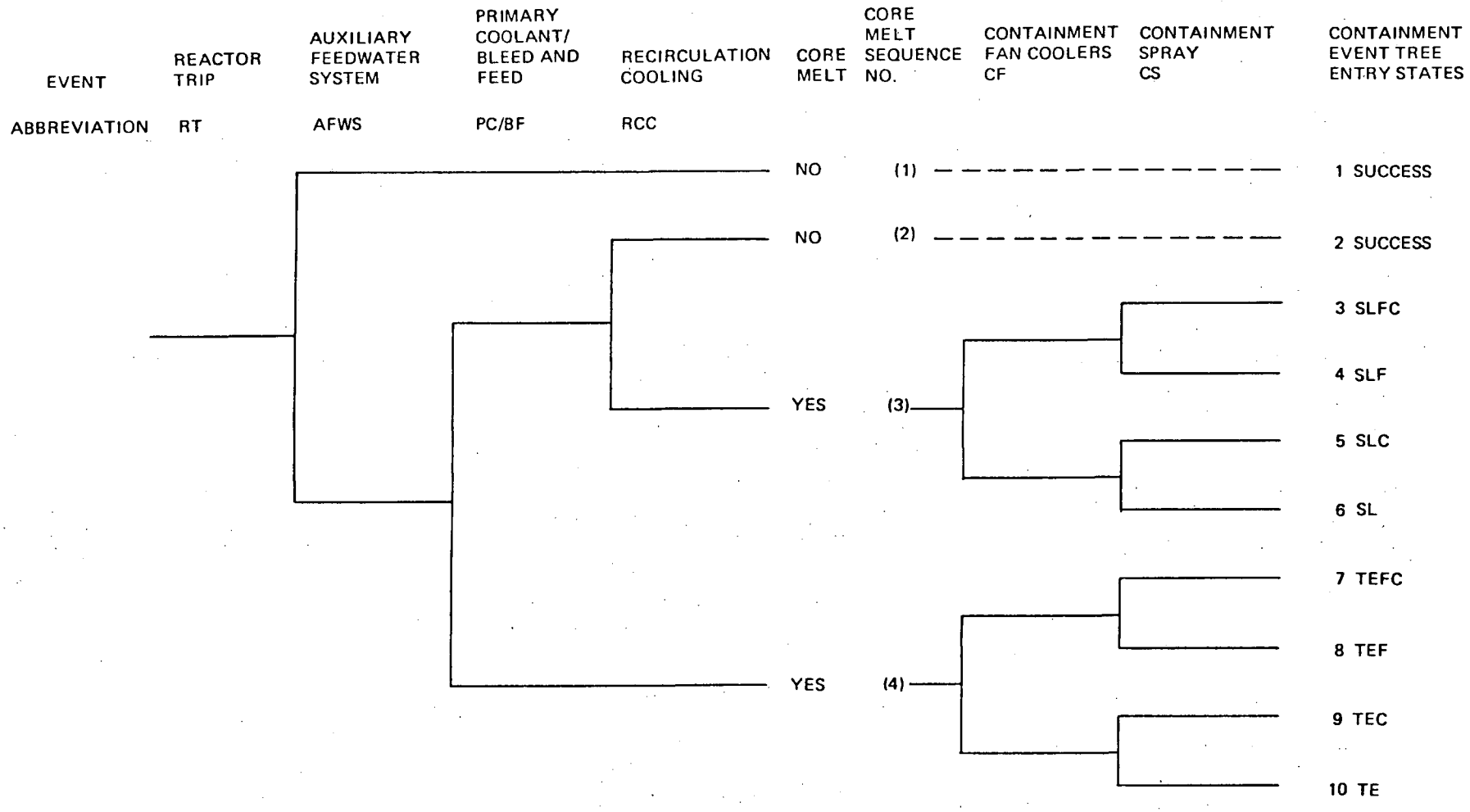


Figure 7.3.1-7. Simplified Event Tree for Transient Events

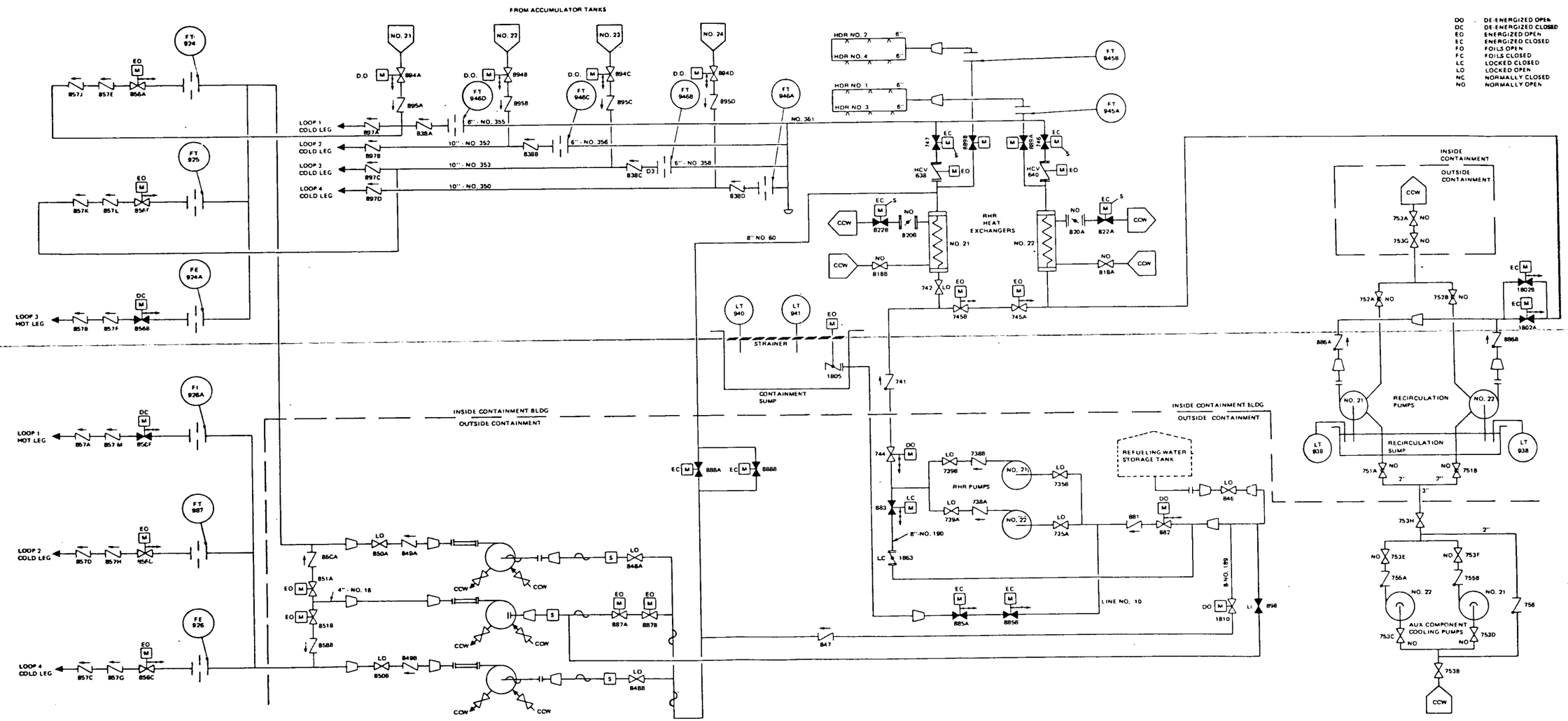


Figure 7.3.1-8. Recirculation System Simplified P&ID

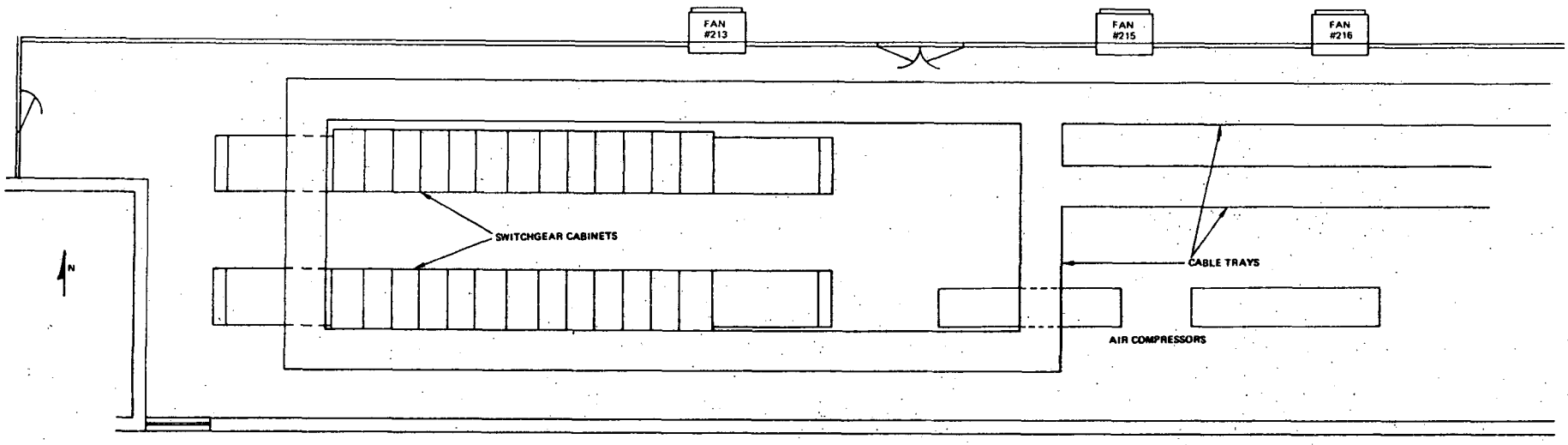


Figure 7.3.1-9. Top View of the Switchgear Room in Indian Point 2

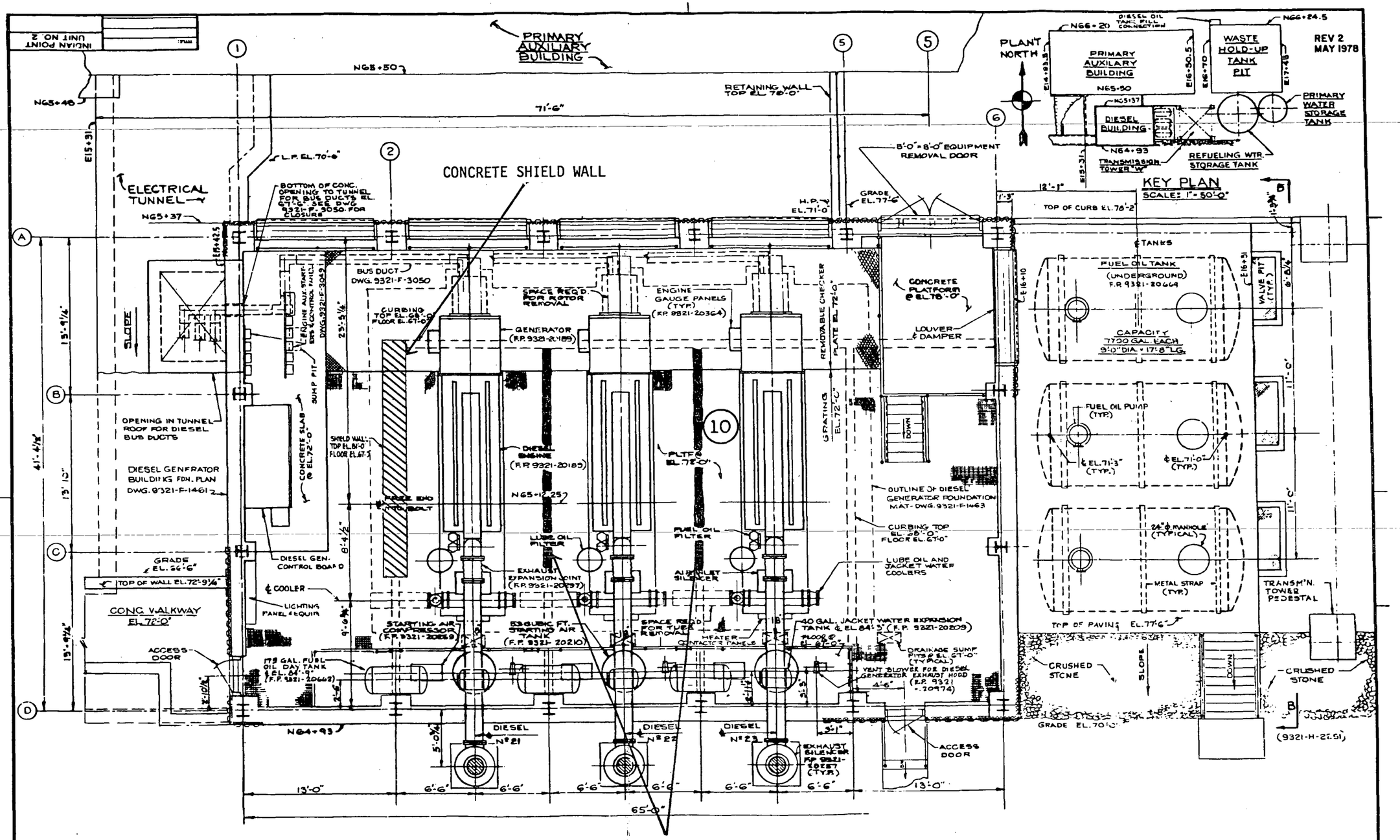
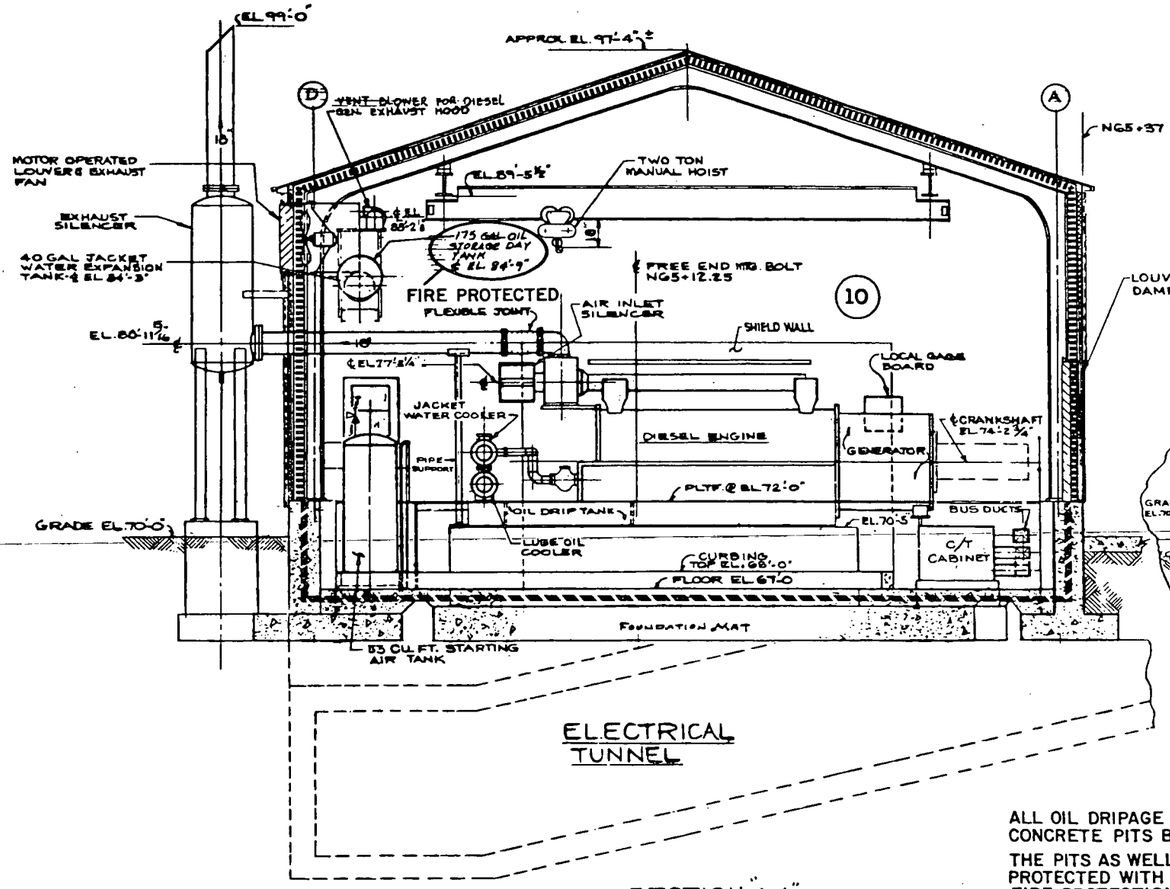


Figure 7.3.1-10. Layout of the Diesel Generator Building

INDIAN POINT
UNIT NO. 2

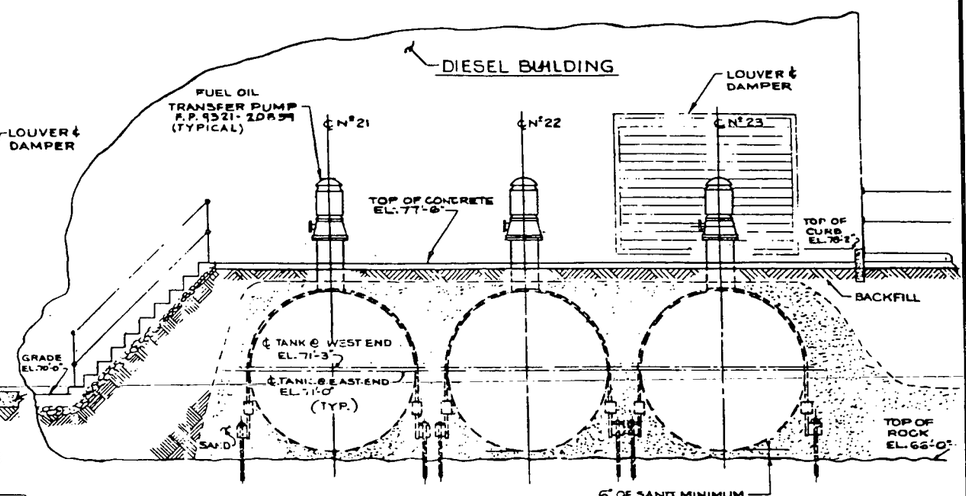
REV 2
MAY 1978



SECTION "A-A"
SCALE 1/4" = 1'-0"
(9321-H-2250)

ALL OIL DRIPAGE IS COLLECTED IN CONCRETE PITS BELOW DIESELS.

THE PITS AS WELL AS DAY TANKS ARE PROTECTED WITH WATER SPRAY FIRE PROTECTION.



SECTION "B-B"
SCALE: 1/4" = 1'-0"
(9321-H-2250)

LEGEND

- 3 HOUR RATED
- NO WALL OR FLOOR
- NON RATED WALL OR FLOOR

Figure 7.3.1-11. Side View of the Diesel Generator Building

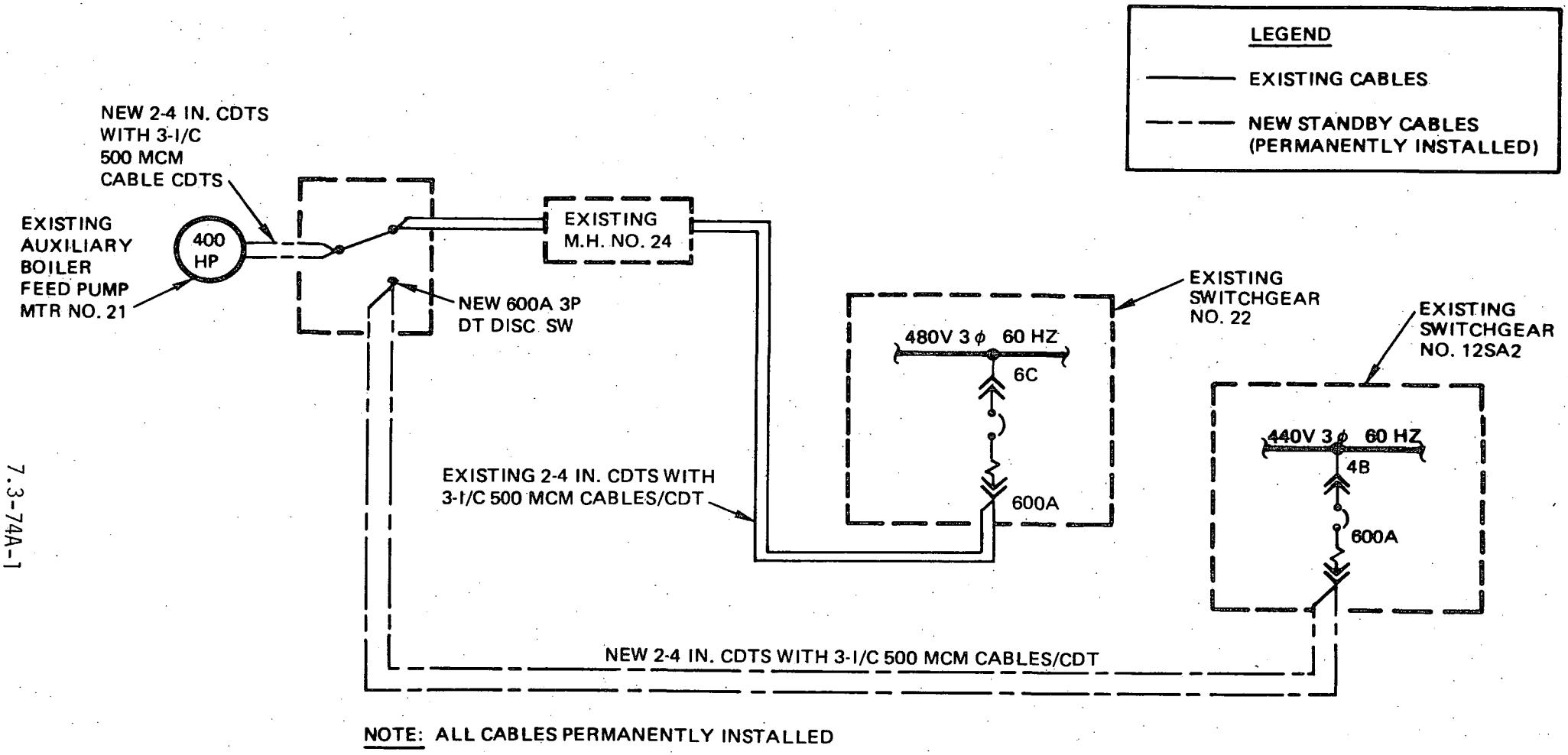


Figure 7.3.1A-12. Schematics of the Transfer Switch Installed for AFWS Pump 21

7.3.2 INDIAN POINT 3 FIRE ANALYSIS

7.3.2.1 Summary

The evaluation of risk due to fires comprises six major steps:

1. Identification of critical areas where fires could cause an initiating event and, simultaneously, cause failure of redundant engineered safety functions.

2. Calculation of the probability distribution of the frequency of fires in these areas.

3. Calculation of fire propagation and of effects of fire extinguishing.

4. Assessment of the effects of fires on LOCAs and transients.

5. Assessment of the effects of fires on accident sequences originating from the initiating events identified in step 4.

6. Calculation of the frequencies of the various containment event tree states.

A preliminary analysis is carried out to identify the locations that require a more detailed investigation. The criterion for qualifying an area as critical is that a fire occurring in that location must be capable of causing an inititating event (a LOCA or a transient). Given that this postulated fire could cause an initiating event, the investigation proceeds to determine whether the same fire could induce failures that will prevent:

1. Reaching and maintaining a condition of negative reactivity.
2. Removing core decay heat.
3. Monitoring and controlling the primary system coolant inventory.

The cable spreading room, the switchgear room, the upper electrical tunnel, the MCC area, and the electrical penetration area, satisfy these criteria.

The core melt frequency has the following characteristic values:

5th Percentile:	2.1×10^{-6} ry^{-1}
Median:	2.8×10^{-5} ry^{-1}
95th Percentile:	1.0×10^{-3} ry^{-1}
Mean:	9.8×10^{-5} ry^{-1}

The main contributors to this frequency are fires in the switchgear room and at the entrance to the electrical tunnel.

The following table summarizes the results for the frequencies of containment event tree entry states TEFC, TE, and SE. The other entry states have smaller frequencies.

State	Frequency (per reactor year)			
	Mean	5th Percentile	Median	95th Percentile
TEFC	1.6×10^{-6}	1.9×10^{-10}	6.0×10^{-8}	4.0×10^{-6}
TE	1.0×10^{-6}	1.2×10^{-9}	6.7×10^{-8}	9.2×10^{-6}
SE	9.5×10^{-5}	8.5×10^{-7}	2.5×10^{-5}	9.6×10^{-4}

Entry state TEFC is primarily due to fires in the control cables in the cable spreading room. Entry state TE is due to fires in the same area, as well as fires in the upper electrical tunnel. Entry state SE is primarily due to fires in the switchgear room and in the power cables in the cable spreading room.

The following table summarizes the results for the frequencies of release categories 2RW and 8B as caused by a fire in Indian Point 3. The other release categories have smaller frequencies.

Release Category	Frequency (per reactor year)			
	Mean	5th Percentile	Median	95th Percentile
8B	1.6×10^{-6}	1.9×10^{-10}	6.0×10^{-8}	4.0×10^{-6}
2RW	9.6×10^{-5}	1.5×10^{-6}	2.6×10^{-5}	9.7×10^{-4}

The main containment event tree entry state leading to release category 8B is TEFC, which could be caused by fires in the control cable spreading room. Containment event tree entry state SE is the predominant factor in release category 2RW. The main contributors to entry state SE are certain fires in the switchgear room and the entrance to the electrical tunnels.

The occurrence of fires and their effects on plant safety are very complex issues which have not received as detailed attention as have other parts of risk assessment in previous studies. Therefore, major

assumptions had to be conservative in order to perform the analysis. The following remarks will place the results of this study into perspective:

1. The analysis was made for rooms where it was judged the most damage can occur. It is anticipated that the results of a more detailed study would not change the conclusions significantly because the predominant contributors to fire risk have been evaluated.

2. The frequencies of fires are derived from evidence collected from all U.S. nuclear power generating stations. They are average frequencies and do not necessarily reflect the conditions that exist at Indian Point 3. For example, it is debatable whether some actual fire occurrences, such as Browns Ferry, should be part of the data base because modifications have been implemented as a result of that fire. Nevertheless, all these fires have been included in the data base.

3. Simple models are used to assess the propagation of fires in cable trays and the temperature rise in compartments due to the heat released by the fire.

4. Detailed analysis of the accident sequences is not done. Such an analysis would explicitly include the timing of events, the possibility of restoration of lost functions, the possibility of errors of commission, etc.

5. Whenever a fire is postulated in an area where it can affect instrumentation, the question of completeness of the analysis becomes very important. It is very difficult to know what information reaches the operators and how they respond.

Additional assumptions pertaining to the analysis of individual rooms are given in the rest of this section. Equipment and systems failure frequencies not associated with fire are taken from Section 1 of this study.

7.3.2.2 Cable Spreading Room (Fire Zone 11, Control Building)

7.3.2.2.1 Characteristics of the Room and Critical Areas

Equipment in this area consists of the motor generator sets, reactor trip breakers, DC power panels, the DC inverters, and the battery chargers (Reference 7.3-1). Power, control, and instrumentation cables of all safety divisions are also present except for the power cables to the service water pumps and auxiliary feedwater pumps. The power cable trays of two different divisions are separated vertically by 3 feet of free air (Reference 7.3-11). The instrumentation and control cables are separated by 1 foot. At areas where the 3-foot separation is not possible, metal or transite barriers are installed to separate the trays.

In studying the fire effects in this area, the following information is useful:

1. The cable spreading room is a controlled access area.

2. The primary combustible materials permanently present in the room are cable insulation, motor lubricant, paint, and transient fuel. The total heat content of the room is estimated (Reference 7.3-1, page 9 - 3,124) to be 791,000 Btu. The transient fuels contribute more than 55% of this (439,000 Btu). This includes 15 lbs. of wood, 8 lbs. of paper, 8 lbs. of plastic, 5 lbs. of oil, and 10 lbs. of grease.

3. The room has ionization detectors which annunciate in the control room as well as portable extinguishers. A manual hose station southeast of the cable spreading room (outside the door) has access to this room. There is also an automatic CO_2 system, activated by heat detectors, designed to cover the volume of the spreading room. Some of the power cable trays at the entrance to the electrical tunnel of this room have sprinkler heads (Reference 7.3-12). An electrically safe, 20-foot extension ladder is also located here. All the openings to this room have doors, shutters, louvers, or dampers that are automatically closed by carbon dioxide system activation.

4. Control cables of all three auxiliary feedwater pumps and their regulator valves are located in this area. For the turbine-driven pump the speed indication is electronic, while the speed control mechanism is strictly pneumatic. If the air system is lost this pneumatic control system does not depressurize instantaneously. The power cables of the two motor-driven pumps are independent of this area and, therefore, these pumps could be operated locally. The turbine-driven pump starts automatically at minimum speed only and can be operated manually independently of the cable spreading room.

5. For service water pumps, only the control cables, and no power cables run through this area.

6. For the charging pumps, safety injection pumps, component cooling pumps, containment spray pumps, containment fan coolers, pressurizer relief valves, secondary atmospheric relief valves, and residual heat removal pumps, both power and control cables run through the area. The power cables are located only in the eastern end of the room at the entrance to the electrical tunnel.

The electrical tunnel entrance area at the end of the cable spreading room is separated into two parts by a wall. A door in this wall, which is normally open, connects the cable spreading room to the electrical tunnels. In our analysis, we treat the area on the two sides and close to this wall (before the tunnel branches into upper and lower parts) as part of the cable spreading room. This is the tunnel entrance area.

Figure 7.3.2-1 shows a top view of the cable spreading room. The control cables that enter the control room are laid on two stacks of cable trays that run east-west and are at elevations greater than 9 feet above the floor. These two stacks of trays contain cables of different divisions. The ones in the southern stack cross over to the northern side at 16 feet above the floor to enter the control room along with the cables of the northern stack.

We choose representative cases to model these scenarios. Two critical areas are identified. The first one is the center of the northern wall next to the ceiling where many redundant and diverse control cables come very close to each other before going through the ceiling (i.e., the control room floor). This area is immediately below the safeguards supervisory panels in the control room. The second area is at the eastern end, at the entrance to the electrical tunnels. All power cables of the cable spreading room are located here. Figure 7.3.2-2 shows a cross-section of the trays and their contents. The same configuration is preserved throughout the two electrical tunnels (Figure 7.3.2-3). Obviously, postulating fires at various locations in the cable spreading room that would affect these critical areas can produce many fire propagation scenarios. The total frequency of core damage would then be the sum of the frequencies of these fire propagation scenarios.

7.3.2.2.2 The Frequency of Fires

Reference 7.3-3 presents distributions for the average frequency of fires per year in the following areas: control room, cable spreading room, diesel room, containment, turbine building, and auxiliary building. These distributions are derived using Bayes' theorem as follows.

The prior distributions are almost noninformative and, therefore, the evidence dominates the results. The evidence is derived from actual fire incidents as reported to the American Nuclear Insurers (ANI) (a survey of ANI records is reported in Reference 7.3-4). The room-years as of May 1, 1978, are calculated by surveying the FSARs of operating reactors.

In 301.3 room-years, there were two reported fires in cable spreading rooms. The posterior distribution of the fire frequency is a gamma distribution* with parameters $\alpha = 2.182$, and $\beta = 302.26$ having the following characteristic values (per year):

$$\lambda_{CSR,05} = 1.4 \times 10^{-3}, \quad \lambda_{CSR,50} = 6.2 \times 10^{-3}, \quad \lambda_{CSR,95} = 1.7 \times 10^{-2},$$

$$\alpha_{\lambda_{CSR}} = 7.2 \times 10^{-3}$$

*The probability density function for the gamma distribution is:

$$p(\lambda) = \frac{\beta^{\alpha}}{\Gamma(\lambda)} \lambda^{\alpha-1} \exp(-\beta\lambda), \quad \alpha, \beta, \lambda > 0$$

This distribution is generic, i.e., it is the distribution of the frequency of fires averaged over all existing cable spreading rooms. It is a conservative distribution because it includes the Browns Ferry fire and does not take into account the changes in procedures and/or design that resulted from that fire. It is felt that removal of the Browns Ferry fire from the data base would raise a controversy similar to that on the "rectifiability" notion proposed by EPRI in connection with the ATWS problem. In order to be conservative, the Browns Ferry fire was included even though the frequency of fires in cable spreading rooms has probably been reduced. The derived distribution represents fires of any magnitude. The only criterion for their inclusion in the data base is that they have been reported to ANI, which has stricter reporting requirements than the NRC.

7.3.2.2.3 Fire Propagation and Extinguishing in Cable Spreading Room

As discussed in Section 7.3.2.2.1, fires which involve the following are considered: (1) control cable trays 16 feet above the floor at the center of the northern wall, and (2) power cables at the eastern end of the room. The propagation and extinguishment of fires are discussed separately hereafter for these two critical areas in the cable spreading room.

7.3.2.2.3.1 Fire Propagation and Extinguishment at the Center of the Northern Wall. The control cable trays of interest at the center of the northern wall are 16 feet above the floor, and are not directly visible from the floor; additional horizontal trays with a vertical separation of 1 foot are located beneath this zone, with the lowest tray being 9 feet above the floor.

7.3.2.2.3.1.1 Propagation Analysis. Fire propagation is modeled in this area with a representative scenario involving a large exposure fire on the floor underneath the cable trays. Fires that start within the cable trays are not considered, because even the lowest trays are 9 feet above the floor, and because there are no power cables in this area.

In the representative scenario, the ground based exposure fire first ignites the lowest cable tray after τ_1 minutes. The fire then spreads through the higher cable trays, and reaches the critical trays at 16 feet τ_2 minutes after the lowest tray was ignited. Fire spread through the trays is considerably quicker than the fire spread described in Section 7.3.4 (Appendix I), because the external fire, which remains burning throughout the duration of the fire, augments the intensity of the fire on the lower trays. The characteristic fire propagation for this scenario, τ_G, is the sum of τ_1 and τ_2.

The exposure fire is modeled as a 1-foot diameter oil fire located immediately under the stack of cable trays. Using COMPBRN (Reference 7.3-5), our reference model prediction for τ_1, called $\tau_{1,DRM}$ about 8 minutes. Approximately 1 gallon of fuel is burned. To quantify our uncertainty in COMPBRN's predictions, we define an error factor ψ such that:

$$\tau_1 = \psi\tau_{1,DRM} \qquad (7.3.2\text{-}1)$$

ψ is judged to be lognormally distributed, with characteristic parameters:

$$\psi_{05} = 0.8, \qquad \psi_{50} = 1.3, \qquad \psi_{95} = 2.0, \qquad \alpha_{\psi} = 1.3$$

We note that ψ plays the same role as the error factor ϕ defined in Section 7.3.4 (Appendix I) but has a tighter distribution. This reduced uncertainty stems from the relatively good state of knowledge concerning the characteristics of the fixed exposure fire.

The predicted time for fire spread to the uppermost level given ignition of the lowest tray, $\tau_{2,DRM}$, is computed to be approximately 6 minutes. This prediction is essentially constant for all allowable values of θ, the dimensionless parameter based on the cable insulation physical properties (see Section 7.3.4, Appendix I). The lack of variation in $\tau_{2,DRM}$ can be attributed to the strength of the large exposure fire as a driving force in fire propagation. Once more, we employ an error factor to quantify our uncertainties in COMPBRN's predictions:

$$\tau_2 = \phi\tau_{2,DRM} \tag{7.3.2-2}$$

where we have employed ϕ because of the larger uncertainties inherent in fire propagation through a number of fuel elements.

Thus, the time required for fire propagation, τ_G, is given by:

$$\tau_G = \psi\tau_{1,DRM} + \phi\tau_{2,DRM} \tag{7.3.2-3}$$

The characteristic values of τ_G are (minutes):

$$\tau_{G,05} = 12.2, \qquad \tau_{G,50} = 19.8, \qquad \tau_{G,95} = 29.2, \qquad \alpha_{\tau_G} = 21.2$$

The amount of oil needed to sustain this fire ranges from 0.3 to 1.4 gallons.

It should be noted that the heat flux from the exposure fire to the lowest tray decreases if the fire is not located immediately under the cable trays. If the exposure fire is fueled by a less flammable material, the heat flux impinging on the lower trays will also decrease, and the fire propagation time will therefore increase. For a 2-foot diameter polymethylmethacrylate (PMMA) fire, $\tau_{1,DRM}$ is equal to approximately 20 minutes (corresponding to 2.1 kg of this flammable plastic). If the exposure fire is much smaller, ignition of the lowest tray is unlikely before the fire is extinguished. For example, $\tau_{1,DRM}$ calculated for a 1-foot diameter PMMA fire is about 2.25 hours.

On the other hand, should the exposure fire be more severe than the one postulated, our results will not change dramatically, because τ_1 and τ_2 are small to begin with, and because the upper trays cannot be directly affected by the exposure fire.

The chosen exposure fire is a representative of the large exposure fires which can initiate a fire in the elevated trays. Less severe exposure fires can also ignite the elevated trays, but they require much longer times to ignite the lowest trays. Furthermore, the effect of the horizontal displacement of the smaller exposure fire away from the position directly underneath the cable trays is much more strongly pronounced.

7.3.2.2.3.1.2 Fire Detection and Extinguishing. The distribution for τ_G is derived without consideration of extinguishing efforts. To account for extinguishing, we define Q(t) to be the conditional frequency that a fire is not extinguished by time t, given a fire. Thus, $Q(\tau_G)$ is the conditional frequency of fire propagation in the critical zone studied.

The extinguishing process is modeled exponentially with a mean extinguishing time, τ_S. Q(t) is then given by:

$$Q(t) = \exp(-t/\tau_S) \qquad (7.3.2\text{-}4)$$

The distribution for τ_S is based on two sources of information: (1) the fire detection and extinguishing capabilities available in the cable spreading room, and (2) fire extinguishing data given in Reference 7.3-6. Table 7.3.2-1 gives the histogram for τ_S.

There are many scenarios for fire extinguishing in the cable spreading room, of which a typical scenario would be: the control room is informed about a fire in a certain location, the control room operators dispatch a nuclear plant operator to check the fire, the latter enters the fire zone and accesses the severity of the fire, calls back the control room, and the control room operators or the watch supervisor dispatch the fire brigade to fight the fire. There are two important parts in these scenarios: 1) the mode of fire detection, and 2) the mode of fire fighting.

Fire detection can be either remote or local. For remote detection, there are smoke detectors in the cable spreading room that annunciate in the control room. The typical response time of the smoke detectors, quoted in the literature, is on the order of a few minutes. It should be noted that detector response time is strongly dependent on the room and fire characteristics. In Reference 7.3-6, we find that 75% of fires in the nuclear power plants (NPPs) under commercial operation have been detected locally by plant personnel. Of course, this fraction may be lower for the cable spreading room, because a considerable part of that data comes from other plants and the period before the Browns Ferry fire and before the resulting generic plant modifications were installed.

There is also an indirect method for detection via the control board indicators and readouts. If the fire affects instrumentation or control cables before it is detected, it may inform the control room operators of problems in the cable spreading room. In the preceding section, we have found that fire propagation to the cables is approximately 10 minutes.

Local detection may be instantaneous (i.e., plant personnel would be present at the time of fire ignition) or it may be delayed. Thus, local detection time competes with the remote detection process provided by the smoke detectors. It should be noted that the fires considered in the preceding section are rather large. A representative detection time (including both remote and local combined) for the fires considered in the preceding section is on the order of a few minutes and the uncertainties may range from a few seconds to approximately 15 minutes. The latter bound is the sum of fire propagation time (8 minutes) and the time before the operators realize that the cause of the control board abnormalities is a fire in the cable spreading room. (This assumes that the smoke detectors have not responded and none of the personnel are in the fire area.) Very large response times are deemed to be unlikely because of the large fires considered and because the control board is affected upon cable failure.

The extinguishing process can be divided into two parts: first, a decision is made on the strategy of combatting the fire, and second, the extinguishing agent (e.g., water, CO_2) is applied. This two part process is repeated until the fire is completely extinguished. If some plant personnel are present when the fire ignites, they may choose to use the available portable extinguishers. This may not be sufficient for the fire severities considered here (see the preceding section). The control room operators may send a nuclear plant operator (NPO) to assess the situation or may send the fire brigade even before the NPO is dispatched. At the fire location, the NPO or the fire brigade could decide whether to flood the room with carbon dioxide or to enter the room and fight the fire directly using the other locally available extinguishing agents. The carbon dioxide would certainly reduce the severity of the fire significantly. However, because of the uncertainty about whether the fire will be completely extinguished, it was decided that the fire brigade has to enter the room and complete the extinguishing process manually.

Thus, the process of fire extinguishing may take from a few minutes (personnel present in the area using portable extinguishers or local hose stations) to about half an hour (NPO is dispatched to the area, calls for fire brigade help and they put out the fire manually), to several hours (several fire extinguishing attempts fail to put the fire out completely and it reignites).

Reference 7.3-6 estimates the actual fire duration. This duration is defined as the time from ignition to the time when maximum damage has occurred. The estimates of Reference 7.3-6, which are the results of expert evaluation, demonstrated that of the 18 fires studied, approximately 80% were extinguished manually. The experts estimated that seven (40%) of them were extinguished within 5 minutes. Four of the 18 fires were estimated to have been extinguished between 5 and 25 minutes after initiation, and another group of 4 had extinguishment times of between 30 and 35 minutes. There were two fires that were extinguished after 60 minutes but before 85 minutes. Finally, the Browns Ferry fire was extinguished in approximately 7 hours. These are

expert estimates, not statistical data. While these 18 fires were of all sizes, the analysis is limited to large fires (Section 7.3.2.2.3.1.1) in this case. Thus, the discrete model (Table 7.3.2-1) is consistent with the fire protection systems available for the cable spreading room and with the experts' estimates. To be conservative, the seven fires that were extinguished within 5 minutes were deleted because the time to extinguish fires of this severity was considered to be too short. Small probabilities are assigned to the longer mean extinguishment times (60 and 120 minutes) in light of the extinguishing capabilities in the cable spreading room. Another source of conservatism is that slowing down of the propagation of the fire is not explicitly modeled.

A second distribution for τ_S (Table 7.3.2-2) is derived for smaller fires, based on the same set of information. In this case the largest probability is given to 5 minutes, because the fires are small and adequate fire protection equipment is available. Based on the same arguments the largest mean time for extinguishment is judged to be 60 minutes.

The conditional frequency of fire propagation among the critical control cables, given a large fire under the cable trays is $Q(\tau_G)$ (where t of Equation 7.3.2-4 is replaced with τ_G). The characteristic values of this conditional distribution are:

$$Q_{05}(\tau_G) = 0.12, \quad Q_{50}(\tau_G) = 0.45, \quad Q_{95}(\tau_G) = 0.8, \quad \alpha_{Q(\tau_G)} = 0.48$$

7.3.2.2.3.2 Fire Propagation and Extinguishment at Electrical Tunnel Entrance. Three basic fire propagation patterns are of interest in this area. The first two involve fire initiation in a tray on either the left or right side of the tunnel entrance (Figure 7.3.2-2) and propagation among the cables on the fire-initiated side. The fire will probably not spread to the trays on the other side due to the low heat release rate of cable insulation fires and the approximately inverse relationship of the radiated thermal heat fluxes with the square of the distance to those trays. The third fire propagation pattern involves an exposure fire occurring in the aisle which passes between the two stacks of cable trays.

7.3.2.2.3.2.1 First Propagation Pattern. In the first fire propagation pattern, the fire is initiated in a cable tray. The fire spreads upward and horizontally with a characteristic spread time τ_V. The distribution of τ_V as a function of Q_p, the heat content of the pilot fuel which initiates the fire, is developed in Section 7.3.4 (Appendix I).

The distribution of Q_p for this location is as follows:

$$\Pr(Q_p = 400 \text{ Btu}) = 0.10$$
$$\Pr(Q_p = 4000 \text{ Btu}) = 0.45$$
$$\Pr(Q_p = 40000 \text{ Btu}) = 0.45$$

This distribution reflects the belief that a fire in the cable trays will probably involve additional fuels as well as cable insulation, because cable insulation is generally quite difficult to ignite. To provide some physical basis for the choice of Q_p, we note that 400 Btu from a 1-foot square fuel packet corresponds roughly to cable insulation burning for 1 minute (i.e., the initial fuel bed is essentially only cable insulation). Four thousand Btu can be associated with wood, paper, or plastic burning for 2 minutes, and 40,000 Btu can be equated with approximately 1 quart of oil burning in 1 minute. We note that a quantity of wood burning for 2.5 minutes will release approximately the same amount of heat as a similarly sized oil fire burning for 1 minute; a strict equivalence between Q_p and the representative fuels mentioned is not intended.

The resulting distribution for τ_V for this location has the following characteristic values (minutes):

$$\tau_{V,05} = 2.0, \quad \tau_{V,50} = 9.5, \quad \tau_{V,95} = 37.0, \quad \alpha_{\tau_V} = 14.4$$

7.3.2.2.3.2.2 Second Propagation Pattern. The second propagation pattern involves fire initiation in a power cable tray. Because a 1/4-inch thick transite barrier is placed above power cable trays and the analysis of Section 7.3.4 (Appendix I) indicates that the barrier prevents fire spread to trays above, only horizontal spread across the tray is considered. Two vertical metal barriers separated by a small air gap are located in the tray. Fire propagation across the tray is not prevented, however, because the flames on one side extend above the height of the barriers and can radiate heat to the opposite side.

The distribution for the spread time, τ_H, has the following characteristic values expressed in minutes:

$$\tau_{H,05} = 6.2, \quad \tau_{H,50} = 27.6, \quad \tau_{H,95} = 108.7, \quad \alpha_{\tau_H} = 44.0$$

This distribution is developed from the previous distribution for Q_p and the distributions for horizontal fire spread given in Section 7.3.4 (Appendix I).

7.3.2.2.3.2.3 Third Propagation Pattern. The third fire propagation pattern involves exposure fires in the center aisle, because a large fire in this location may ignite and/or seriously damage cables on both sides of the aisle.

Simple heat flux calculations, similar to those done in Section 7.3.6 (Appendix III), are performed to determine the damage potential of an exposure fire. The two exposure fires used to represent this case are fueled with oil and are located in the middle of the aisle. Their diameters are 2 feet and 1 foot, respectively.

The heat flux impinging on the cable trays is modeled by considering the heat flux falling on a small, horizontal area located 3 feet away from the fire's axis, or about 0.5 feet in from the tray edge. The elevation of this area is that of the flame's base. To be conservative, the shielding effects of the tray sides and of the trays immediately above and below are neglected. The heat flux on this area from the 2-foot diameter exposure fire is then computed to be 7,100 W/m^2, and for the 1-foot diameter fire, it is 2,900 W/m^2.

Using the above heat fluxes and a spontaneous ignition temperature of 825^0K, the respective ignition times are computed to be 12 and 71 minutes (see Equation 7.3.4.1-9). The amounts of fuel required to sustain the 2-foot and 1-foot diameter fires for these durations are about 4.2 and 6.3 gallons, respectively.

Because the larger diameter exposure fire requires less fuel than the smaller one, it is judged to be more reasonably and more conservatively representative of the class of exposure fire which can lead to ignition of cables on both sides of the aisle.

It is noted that fires of similar size fueled by materials other than oil will take significantly longer to propagate; a 2-foot diameter polymethylmethacrylate (PMMA) fire located in the middle of the aisle requires approximately 3 hours to ignite the cable trays.

Note also that exposure fires located closer to one stack of cable trays will ignite that stack more quickly. The same PMMA fire discussed above requires only 50 minutes to ignite the trays, if it is located immediately next to the trays. However, the farther stack of trays will ignite more slowly. Therefore, the central placement of the exposure fire is judged to be reasonable for the representative propagation pattern studied here.

The actual fire propagation time for the aisle fire, τ_A, is the product of the calculated spread time (12 minutes) and the error factor ψ, defined earlier in Section 7.3.2.2.3.1.1, which quantifies our uncertainty in the modeling. To be conservative, the time required for the flames to spread horizontally across the width of the tray is neglected. This spread is expected to be fairly rapid because the exposure fire heat flux increases the burning rate of the ignited fuel and preheats the unignited fuel. The distribution of τ_A has the following characteristic values:

$$\tau_{A,05} = 9.6, \quad \tau_{A,50} = 15.2, \quad \tau_{A,95} = 24.0, \quad \alpha_{\tau_H} = 15.8$$

7.3.2.2.3.2.4 Combined Propagation and Extinguishment. The distributions for τ_V, τ_H, and τ_A, given above are derived without consideration for efforts at extinguishing the fire. To account for extinguishment of cable tray initiated fires (propagation patterns one and two), the extinguishment model described in Section 7.3.2.2.3.1.2 is used, i.e.,

$$Q(t) = \exp(-t/\tau_S) \qquad (7.3.2\text{-}5)$$

The distribution for the mean extinguishment time, τ_s, has been derived in Section 7.3.2.2.3.1.2 and is given in Table 7.3.2-2. This distribution applies to the first two propagation patterns. $Q(\tau_V)$ and $Q(\tau_H)$ are the respective conditional frequencies of fire propagation for the first two propagation patterns. The probability distribution of $Q(\tau_V)$ has the following characteristic values:

$$Q_{05}(\tau_V) = 1.6 \times 10^{-3}, \quad Q_{50}(\tau_V) = 0.45, \quad Q_{95}(\tau_V) = 0.86,$$

$$\alpha_{Q(\tau_V)} = 0.44$$

The probability distribution of $Q(\tau_H)$ has the following characteristic values:

$$Q_{05}(\tau_H) = \text{smaller than } 10^{-8}, \quad Q_{50}(\tau_H) = 7.3 \times 10^{-2}$$

$$Q_{95}(\tau_H) = 0.68, \quad \alpha_{Q(\tau_V)} = 0.21$$

To extinguish a large aisle fire, the histogram of Table 7.3.2-1 is used, because of the severity of such a fire. The conditional frequency of fire propagation in the aisle section, $Q(\tau_A)$ is evaluated by replacing τ with τ_A in Equation (7.3.2-6). The characteristic values are:

$$Q_{05}(t_A) = 0.19, \quad Q_{50}(t_A) = 0.45, \quad Q_{95}(\tau_A) = 0.86,$$

$$\alpha_{Q(\tau_A)} = 0.44$$

7.3.2.2.3.3 Conditional Frequency of Large Exposure Fires. As seen in Section 7.3.2.2.3.1, a number of different exposure fires can initiate fires in the critical zone in a reasonable amount of time. Less severe fires, e.g., less than 1 foot diameter oil fires or nonoil fueled fires of less than 2 feet in diameter, require much larger times to reach the uppermost cable tray. In view of the mean times for extinguishment listed in Table 7.3.2-2, it is concluded that these less severe fires have a small likelihood of spreading to the upper trays. Furthermore, note that the large exposure fire must be near the critical zone. The exposure fire severity factor f_{es}, represents that fraction of cable spreading room fires which are large enough and close enough to cause damage.

There are two critical areas in the cable spreading room and a separate exposure fire severity factor is assigned for each: $f_{es,cc}$ is the fraction of large exposure fires at the center of the northern wall, and $f_{es,te}$ is the fraction of large aisle fires at the electrical tunnel entrance.

The following values are the characteristics of f_{es}, which has been assessed as lognormally distributed:

$$f_{es,05} = 2.5 \times 10^{-4}, \quad f_{es,50} = 5.0 \times 10^{-3},$$

$$f_{es,95} = 0.1, \quad \alpha_{f_{es}} = 2.6 \times 10^{-2}$$

Similarly, $f_{es,te}$ is assessed as lognormally distributed with the following characteristic values:

$$f_{es,te,05} = 2.0 \times 10^{-5}, \quad f_{es,te,50} = 1.0 \times 10^{-3},$$

$$f_{es,te,95} = 5.0 \times 10^{2}, \quad \alpha_{f_{es}} = 1.69 \times 10^{-2}$$

Some additional observations used in deriving this distribution are:

- The zone is not used as a passageway in general and especially for carrying large amounts of combustibles.
- A guard patrols the area several times in a day.
- The operators walk through this area a few times during every work shift.
- Administrative procedures prohibit the personnel to take actions that may increase the fire hazard in this room without fire watch on hand.
- The critical area constitutes only a small fraction (approximately 0.1) of the total cable spreading room floor area.
- One of the two fires in the data base, the Browns Ferry fire, was very large, was initially fueled by large quantities of very flammable material, and occurred at a critical area.
- A significant fraction (approximately 0.1) of the cable insulation fires reported in Reference 7.3-6 was estimated to be large.

It is judged that $f_{es,te}$ is smaller than $f_{es,cc}$ because only a fire as severe as a large oil fire in the aisle could cause damage in both stacks of trays in the tunnel entrance. At the center of the northern wall, however, other combustibles may cause failure within a reasonable amount of time.

7.3.2.2.4 Effects of Cable Spreading Room Fires on the Initiating Events

7.3.2.2.4.1 Large LOCA. For a large LOCA to occur, loss of coolant through an opening larger than 6 inches in equivalent diameter must be induced by the fire. This can happen by the spurious opening of both RHR isolation valves (MOVs 731 and 730) if the valves are energized.

Figure 7.3.2-3 shows the control circuit for opening one of the valves. The control switch and the pressure interlock can be bypassed if the segments A and B of the wires in the cable spreading room touch each other, creating a "hot short," thus closing the circuit and energizing coil "O" which would generate an open signal to the valves.

During reactor operation, however, these valves are deenergized in the closed position by locking out their circuit breakers at their respective motor control centers (MCCs). In addition, even in the unlikely event that the control circuits are energized and a simultaneous command to open the valves is generated by the fire, it is extremely unlikely that the valves would open. This is because the motors are undersized such that these valves cannot open against the large differential pressure which exists across the valve seat. Therefore, a large LOCA has a negligibly small frequency from fires in the cable spreading room.

7.3.2.2.4.2 Medium LOCA. For a medium LOCA to occur, there would have to be an opening of 2 to 6 inches in equivalent diameter. There is no credible way in which a cable spreading room fire could initiate a medium LOCA.

7.3.2.2.4.3 Small LOCA. A small LOCA, which involves an opening less than 2 inches in equivalent diameter, could occur by the simultaneous spurious opening of isolation valve MOV 536 or 535 (Figure 7.3.2-4) and of the associated power-operated relief valve (PORVs) PCV-456 or PCV-455C, respectively. The small LOCA is very likely to be terminated by the fire because the hot shorts which cause the spurious openings will become open circuits due to further loss of insulation, in which case the wires contact the grounded trays. When this happens, the air-operated valves close thus terminating the LOCA.

The inadvertent opening of a letdown line (Figure 7.3.2-6) may lead to a small LOCA as well. The normal letdown line (an orificed 3-inch pipe) is normally open and the coolant pressure drops from 2,235 psig to approximately 275 psig when flowing through one of the orifices. The design pressure of the piping downstream of the orifices is 600 psig. If air-operated valve 201 or 202 (upstream of the nonregenerative heat exchanger) closes, the coolant pressure downstream of the orifices will increase. This will lead to the opening of relief valve 203 at 600 psig that would discharge the primary coolant into the pressurizer relief tank, thus a small LOCA. The operators can isolate this LOCA by closing LCV-459, LCV-460, or all three AOVs: 200A, 200B, and 200C. The fire may even lead to the closure of these valves because they are of the fail closed type and grounding of the wires to the solenoid will deenergize the control circuit of the valve.

The excess letdown line (Figure 7.3.2-6) is normally closed. For a small LOCA to occur, the two series air-operated isolation valves (AOV-213 and HCV-123) would have to be opened simultaneously by hot shorts. Similar to the PORVs, they will be closed when the hot shorts become open circuits due to further loss of insulation, in which case the wires contact the grounded trays.

Failure of the reactor coolant pump seals also leads to a small LOCA. This may occur due to simultaneous loss of the component cooling system and the charging pumps (see Section 1.3.3.8 for more detail). A total maximum leak rate of 1,200 gpm from all four pumps might occur. This mode of small LOCA cannot be isolated. Figure 7.3.2-7 shows an event tree for this event. We assume that the availability of the refueling water storage tank, reactor trip, and safeguards actuation are certainties. This type of small LOCA can occur due to a fire in the electrical tunnel entrance area in the cable spreading rooms.

7.3.2.2.4.4 Transients. A transient can occur in many different ways (e.g., reactor trip, turbine trip, closure of main steam line isolation valves, etc.). Figure 7.3.2-8 shows a simple event tree for transients. It is assumed that given a fire, a reactor trip, and therefore a transient, is a certainty.

7.3.2.2.4.5 Effects of Fires at the Center of the Northern Wall on Accident Sequences. The control cables of many safety related components come very close to each other near the ceiling at the center of the northern wall. The control room safeguards supervisory panels are immediately above the cable spreading room. The control cables of many redundant components run parallel to each other next to the northern and southern walls. At the center of the southern wall, the cables of this side go up into the cable trays next to the ceiling (16 feet above the floor) and cross the width of the cable spreading room to enter the control room at the center of the northern wall.

This area thus contains the control cables of the three auxiliary feedwater pump trains, the three safety injection pumps, the two containment spray pump trains, and all five containment fan cooler units. The control cables of the charging pumps, the PORVs, and the PORV block valves are located below the flight panel in the control room and are therefore independent of this area.

If a fire causes failure of all these cables, a transient would occur and the turbine-driven auxiliary feedwater pump would start at minimum speed. Local operator action can start this pump or one of the motor-driven auxiliary feedwater pumps because the power cables would remain intact. Furthermore, the PORVs and the block valves are available in this case; therefore, if the operators energize the safety injection pumps from the switchgears, the bleed and feed mode of operation is also possible.

7.3.2.2.4.5.1 Core Melt Frequency from Transients. The frequency of core melt can be expressed as:

$$\phi_{CM,CSR} = \lambda_{CSR} f_{es,cc} Q(\tau_G) Q_s \qquad (7.3.2\text{-}6)$$

where

λ_{CSR} = frequency of fires in the cable spreading room

f_{es} = fraction of cable spreading room fires that are large and near the center of the northern wall

$Q(\tau_G)$ = conditional frequency of fire propagation

Q_S = frequency of failure to activate the auxiliary feedwater system.

The main contributor to the frequency of failure to activate the auxiliary feedwater system is human error. The following histogram gives the frequency of failure to bring the turbine-driven pump up to speed under accident conditions (from Section 1.6.3.9 of this report):

Q_S	Probability	Cumulative Probability
2.0×10^{-3}	0.05	0.05
6.8×10^{-3}	0.24	0.29
2.3×10^{-2}	0.42	0.71
8.0×10^{-2}	0.24	0.95
2.8×10^{-1}	0.05	1.00

The operators can also activate either one of the motor-driven pumps locally because the pump power cables are independent of this fire zone. These two actions (i.e., bringing the turbine-driven pump up to speed and activating either motor-driven pump) are dissimilar. Therefore, the related human errors have a low level of dependence. Reference 7.3-7 suggests that a conditional frequency of about 0.05 or greater be used for low levels of dependence (see Section 1.8.1.4.2 for a discussion on this conditional frequency). For moderate levels of dependence, this frequency is 0.14 or greater. In this case, it is judged to be approximately 0.1. The operator controls the auxiliary feedwater pump output to maintain the proper steam generator levels. There are pneumatic indicators inside containment at the airlock. There are also special procedures for safe shutdown from outside the control room. Furthermore, the primary bleed and feed mode of operation is possible because the safety injection (SI) pumps can be activated from the outside of the control room and the PORVs and their block valves can be opened from the control room. Based on this information and given the effects of a large fire at the center of the northern wall, the conditional frequency of failure to achieve safe shutdown, Q_S, is judged to be lognormally distributed with median 5×10^{-3} and has an error factor of 20. The characteristic values are:

$$Q_{S,05} = 2.5 \times 10^{-4}, \quad Q_{S,50} = 5 \times 10^{-3}, \quad Q_{S,95} = 0.1$$

$$\alpha_{Q_S} = 2.62 \times 10^{-2}$$

All the necessary data for $\phi_{CM,CSR}$, the frequency of core melt is now available. Using DPD arithmetic the following characteristic values are obtained:

5th Percentile: 3.0×10^{-10} ry^{-1}

Median: 7.3×10^{-8} ry^{-1}

95th Percentile: 3.3×10^{-6} ry^{-1}

Mean: 1.9×10^{-6} ry^{-1}

7.3.2.2.4.5.2 Containment Event Tree Entry States. In the event tree of Figure 7.3.2-8, we see that, after the postulated core melt, the status of containment cooling functions determines what containment event tree entry state would be obtained. The control cables of the two containment spray pumps and all of the five containment fan coolers would be affected by a fire in the center of the northern wall. Therefore, the fan coolers may fail and high containment pressure may not lead to the activation of the containment heat removal systems. The operators, however, can restore components by closing the corresponding breakers at the switchgear. The local start controls of the fan coolers are installed in the switchgear room. Although a significant containment pressure increase would occur only after core melt, it is very likely that the operators will restart some of the fan coolers before core melt. This is because the fans are normally operational. Furthermore, there are approximately 6 hours between melt and containment breach, thus, local manual actuation of the containment spray system is also very likely. The conditional frequency of failure to activate containment heat removal systems, Q_{HE}, is derived based on these facts. It should be noted here that a major contributor to the frequency of failure to establish secondary cooling, Q_S, is human error. In view of the dependency among human actions, it is judged that Q_{HE} is lognormally distributed with a median of 0.1 and an error factor 5. The characteristic values are:

$$Q_{HE,05} = 0.02, \quad Q_{HE,50} = 0.1, \quad Q_{HE,95} = 0.5, \quad \alpha_{Q_{HE}} = 0.16$$

Thus, either of the two entry states, TEFC or TE, may result. The frequency of the former is the product of $\phi_{CM,CC}$ with the complement of Q_{HE}. The complement has the following characteristic values:

$$Q_{\overline{HE},05} = 0.5, \quad Q_{\overline{HE},50} = 0.9, \quad Q_{\overline{HE},95} = 0.98, \quad \alpha_{Q_{\overline{HE}}} = 0.84$$

The product of these two distributions is the frequency of entering state TEFC due to a fire at the center of the northern wall, $\phi_{TEFC,CC}$, and is presented in Table 7.3.2-3. The characteristic values are:

5th Percentile: 1.9×10^{-10} ry^{-1}

Median: 6.0×10^{-8} ry^{-1}

95th Percentile: 4.0×10^{-6} ry^{-1}

Mean: 1.6×10^{-6} ry^{-1}

The frequency of entering state TE due to a fire at the center of the northern wall, $\phi_{TE,CC}$, is the product of Q_{HE} and the frequency of core melt. The results are presented in Table 7.3.2-3. The characteristic values are:

5th Percentile: less than 10^{-10} ry^{-1}

Median: 7.3×10^{-9} ry^{-1}

95th Percentile: 5.9×10^{-7} ry^{-1}

Mean: 3.0×10^{-7} ry^{-1}

7.3.2.2.4.6 Fires at the Electrical Tunnel Entrance. Figure 7.3.2-2 shows the location of the power cables of several safety related components at the entrance of the electrical tunnel inside the cable spreading room. Based on the fire propagation analysis of Section 7.3.2.2.3.2, three scenarios can be visualized here: (1) fire only at the left stack of trays, (2) fire only at the right stack of trays, or (3) large fire in the aisle.

7.3.2.2.4.6.1 Effects of Fires at the Left Stack of Cables on Accident Sequences. A fire at the left stack of trays has the potential to cause the failure of (Figure 7.3.2-2) auxiliary feedwater pump 33, SI pump 33, charging pumps 32 and 33, recirculation pump 32, both RHR pumps, power to MCCs 36A and 37, containment spray (CS) pump 32, and component cooling pump 33. Because charging pump 31 and component cooling pumps 31 and 32 would not be affected, the occurrence of a small LOCA is very unlikely; however, transients would almost certainly occur. Two AFWS trains, three fan cooler units, and one containment spray would be available in such a fire. Because the failure frequencies of these components are small, the frequencies of containment event tree entry states due to the fire at the left stack of trays should be very small.

7.3.2.2.4.6.2 Effects of Fires at the Right Stack of Cables on Accident Sequences. A fire at the right stack of trays has the potential to cause the failure of (Figure 7.3.2-2) auxiliary feedwater pump 32, SI pumps 31 and 32, charging pump 31, containment fan coolers 31, 33, and 32, recirculation pump 31, MCC 36A, containment spray pump 31, and component cooling pump 33. The outcome of a fire here is very similar to that of the left stack of trays. Thus, as described in Section 7.3.2.4.6.1, the frequencies of containment event tree entry states should be very small.

7.3.2.2.4.6.3 Effects of Fires in the Aisle on Accident Sequences. In Section 7.3.2.2.3.2.3, it was found that a large fire in the aisle between the cable trays can affect the cables on both sides of the tunnel. In such a case, the power feeds to the charging pumps, the

containment spray pumps, the component cooling pumps, and MCCs 36A and 36B would become unavailable. In addition to the normal control of the auxiliary feedwater pumps and the power to the SI pumps, PORVs and all five containment fan coolers would become unavailable.

The small LOCA via the failure of the reactor coolant pump seals is possible in this case because all component cooling pumps and all charging pumps could be lost.

The transients may lead to containment event tree entry state TE (Figure 7.3.2-8) which is slightly more severe than entry state SE (to which a small LOCA may lead). Either the AFWS or primary coolant bleed and feed will mitigate the transient. However, for a small LOCA, the HPIS should be available in addition to the AFWS or primary coolant bleed and feed. This means that the latter is more demanding than the transients; therefore, given a large fire in the aisle, a conservative assessment concludes that a small LOCA is a certainty.

Figure 7.3.2-7 shows that when the HPIS, fan coolers, and containment spray pumps are unavailable, containment event tree entry state SE is realized. In the case of a large fire in the aisle, it is conservatively assumed that this entry state is a certainty.

The frequency of entry state SE can then be written as:

$$\phi_{SE,PC} = \lambda_{CSR} f_{es,TE} Q(\tau_A) \qquad (7.3.2\text{-}7)$$

where

$Q(\tau_A)$ = conditional frequency of fire propagation given a large fire in the aisle section

The remaining two terms have been defined earlier in this section. Using DPD arithmetic, $\phi_{SE,PC}$ is evaluated. The resulting histogram is given in Table 7.3.2-5 and the characteristic values are:

5th percentile:	3.6×10^{-8} ry^{-1}
Median:	4.1×10^{-6} ry^{-1}
95th percentile:	7.5×10^{-5} ry^{-1}
Mean:	2.4×10^{-5} ry^{-1}

7.3.2.2.5 Contributions from Other Areas in the Cable Spreading Room

The effects of fires at the center of the northern wall and the eastern end of the cable spreading room, the entrance of the electrical tunnel, have already been analyzed. Fire in all other areas in the cable spreading room except for the northwestern quarter would not affect the auxiliary feedwater system. The overall unavailability of this system due to causes other than fire is very low, approximately 10^{-6}. Therefore, the overall impact on fire risk is very small.

The control cables of the two motor-driven auxiliary feedwater pumps, PORV 455C and block valve 536, and containment spray pump trains 31 and 32 are located in the northeastern quarter outside the center area of the northern wall. Many important components (e.g., the SI pumps and the fan coolers) are independent of this area. Therefore, the contribution of fires in this quarter to the overall fire risk is small.

7.3.2.3 Some Areas in the Primary Auxiliary Building, the Fan House, and the Control Building

Three buildings, the primary auxiliary building (PAB), the control building (CB), and the fan house (FH) are analyzed simultaneously because they are similar to auxiliary buildings typically found in other nuclear power plants. Several areas within these buildings (except for the cable spreading room) are analyzed and, given a fire, the conditional frequency of containment event tree entry states is computed. The weighted sums of these frequencies are the conditional frequencies of the entry states caused by fires postulated in these three buildings. For the unconditional frequencies, the latter is multiplied with the frequency of fires.

7.3.2.3.1 The Frequency of Fires

There are 10 reported fires in auxiliary buildings for the industry and the number of building-years is 303.3. The state of knowledge distribution is a gamma with parameters $\alpha = 10.32$ and $\beta = 303.59$, and with the following characteristic values (per year):

$$\lambda_{AUX,05} = 0.015, \quad \lambda_{AUX,50} = 0.033, \quad \lambda_{AUX,95} = 0.053,$$

$$\alpha_{\lambda_{AUX}} = 0.034$$

Three areas of the primary auxiliary building, the fan house, and the control building were determined to require detailed analysis. They are fire zones 60A (upper electrical tunnel), 14 (switchgear room), and 73A (upper electrical penetration areas) (see Reference 7.3-1 for zone designations). Another area, fire zone 17A, has been considered also; however, it is a less important area than the upper tunnel and the switchgear room (see Section 7.3.2.6).

The fraction of auxiliary building fires that would occur in each specific area is estimated based on the following observations:

- In the switchgear room, equipment with moving parts (air compressors) and breakers for electric power are installed.
- There are more than 25 compartments in these three buildings that have characteristics similar to these three fire zones; they contain pumps, cable trays, etc.

- The majority of fires in auxiliary buildings in the data base involved electrical circuitry components (e.g., breakers, relays, coils, MCCs).

- The electrical tunnels are similar to the cable spreading room except that they are less frequented by personnel and that the cable spreading room contains reactor trip breakers, motor generator sets, and DC power panels in addition to the cables.

Fires are judged to be more likely in the switchgear room than in the cable spreading room, because of the fourth observation above. If all compartments of these three buildings were alike, then the conditional frequency of fire occurrence in one of them would be less than:

$$\frac{1}{25} = 0.04$$

However, a review of the fire incident data, compiled in Reference 7.3-6, reveals that the majority of auxiliary building fires involved electrical components typically found in switchgear rooms (e.g., coils, relays, etc.). Therefore, the fraction of switchgear fires may be larger than the uniform fraction. Based on this, the fraction of PAB, CB, and FH fires that could occur in the switchgear room, f_{SWG}, is judged to be lognormally distributed with the following characteristic values:

$$f_{SWG,05} = 0.05, \quad f_{SWG,50} = 0.20, \quad f_{SWG,95} = 0.80, \quad \alpha_{f_{SWG}} = 0.285$$

Note that the unconditional frequency of fires in the switchgear (i.e., the product of λ_{AUX} and f_{SWG}) has the following characteristic values (per reactor year):

$$\left(\lambda_{AUX} f_{SWG}\right)_{05} = 1.0 \times 10^{-3}, \quad \left(\lambda_{AUX} f_{SWG}\right)_{50} = 8.0 \times 10^{-3},$$

$$\left(\lambda_{AUX} f_{SWG}\right)_{95} = 2.1 \times 10^{-3}, \quad \alpha_{\lambda_{AUX} f_{SWG}} = 9.8 \times 10^{-3}$$

Based on the last observation above, the frequency of electrical tunnel fires is expected to be lower than that for cable spreading room fires. The fraction of PAB, CB, and FH fires that could occur in a given electrical tunnel, f_T, is judged to be lognormally distributed with the following characteristic values:

$$f_{T,05} = 8.0 \times 10^{-3}, \quad f_{T,50} = 4.0 \times 10^{-2}, \quad f_{T,95} = 2.0 \times 10^{-1}$$

$$\alpha_{f_T} = 6.5 \times 10^{-2}$$

The unconditional frequency of fires in an electrical tunnel has the following characteristic values (per reactor year):

$$\left(\lambda_{AUX} f_T\right)_{05} = 1.7 \times 10^{-4}, \quad \left(\lambda_{AUX} f_T\right)_{50} = 1.5 \times 10^{-3},$$

$$\left(\lambda_{AUX} f_T\right)_{95} = 5.4 \times 10^{-3}, \quad \alpha_{\lambda_{AUX} f_T} = 2.2 \times 10^{-3}$$

The two unconditional frequencies should be compared with the cable spreading room frequency (see Section 7.3.2.2.2). The relative magnitudes of these frequencies support the judgment for f_T. It should also be noted that if these two conditional frequencies (f_{SWG} and f_T) are treated as independent variables, there is a small probability that their sum will become greater than unity. Because this probability is rather small, the dependency between f_{SWG} and f_T is not included in the calculations.

7.3.2.4 Fire Zone 60A (Upper Electrical Tunnel

7.3.2.4.1 Characteristics of the Area

This zone is also known as the upper electrical tunnel. It is located in the primary auxiliary building and control building at elevation 43 feet.

The only safety related equipment in this area are the electrical cables. This includes power cables for both of the containment spray pumps, safety injection pumps 31 and 33, component cooling pumps 31 and 33, containment fan coolers 31, 33, and 35, and residual heat removal pump 32. It also includes power and control cables for charging pumps 31 and 32, pressurizer relief valves (PORVs), PORV block valves, secondary atmospheric relief valves, the auxiliary feedwater pump 33 trains, and the power feeds to both safety related MCCs 36A and 36B. Figure 7.3.2-2 shows a cross-section of the tunnel, the cable trays, and their contents.

This area is a controlled access area. The primary combustible is cable insulation. The heat released from burning transient fuels (5 lbs. of wood, 2 lbs. of paper, and 2 lbs. of plastic) is 76,000 Btus (Reference 7.3-1). The area contains smoke detectors, temperature sensors, and a closed head, preaction sprinkler system.

7.3.2.4.2 Fire Propagation and Extinguishment

The situation here is similar to that in Section 7.3.2.2.3.2 where fire propagation and extinguishment at the electrical tunnel entrance area is analyzed. The same three propagation patterns, and consequently $Q(\tau_V)$, $Q(\tau_H)$, and $Q(\tau_A)$, are applicable here.

7.3.2.4.3 Conditional Frequencies of Fire Propagation Scenarios

The large aisle fires discussed in the preceding section form a subset of all possible fires in the electrical tunnel. The fraction of large electrical tunnel fires which burn highly combustible fuels (e.g., oil) and are in the aisle is defined as f_A. Fires involving less flammable fuels must consume a considerably larger amount of fuel to have the same effect as those burning highly combustible fuels. Furthermore, in Section 7.3.2.4.2.3, it was found that only a certain set of fires may lead to cable failure within a reasonable fire duration. Therefore, f_A is judged to be rather small with a median of 0.01. The data used in deriving λ_{AUX}, however, were mainly fires that were significant enough to be reportable. Thus, 0.10 was chosen as its 95th percentile. A lognormal distribution fitted to these two percentiles yields the following characteristic values:

$$f_{A,05} = 1.0 \times 10^{-3}, \quad f_{A,50} = 1.0 \times 10^{-2}, \quad f_{A,95} = 1.0 \times 10^{-1},$$

$$\alpha_{f_A} = 2.66 \times 10^{-2}$$

Some additional observations used in deriving this distribution are:

- Generally, no maintenance work is performed in this zone during power operation.
- The zone is not used as a passageway in general and especially for carrying large amounts of combustibles.
- Administrative procedures prohibit the personnel to take actions that may increase the fire hazard in this zone without a fire watch being present.
- The critical area constitutes a large fraction (approximately 0.4) of the total electrical tunnel.
- A significant fraction (approximately 0.1) of the cable insulation fires reported in Reference 7.3-6 were estimated to be large.

7.3.2.4.4 Effects of Fires in the Left Stack of Trays on Accident Sequences

A fire at the left stack of trays can potentially cause failure of the power cables to auxiliary feedwater pump 33, fan cooler 35, recirculation pump 32, safety injection pump 33, charging pump 33, RHR pump 32, MCCs 36A and 37, containment spray pump 33, and component cooling pump 33. The failure of those components would not lead to a small LOCA. Although it is very likely that a transient would occur, many redundant safety related components would not be affected by such a fire. Therefore, the frequencies of the containment event tree entry states because of a fire at the left stack of cables are very small.

7.3.2.4.5 Effects of Fires in the Right Cable Trays on Accident Sequences

A fire at the right stack of trays can potentially cause failure of the power cables to the fan coolers 31 and 33, recirculation pump 31, SI pump 31, charging pump 31, component cooling pump 31, MCCs 36A, and containment spray pump 31. As with the left stack of trays, only transients can occur, and several redundant components would not be affected. Therefore, the frequencies of the containment event tree entry states because of a fire at the right stack of cables are very small.

7.3.2.4.6 Effects of Aisle Fire on Accident Sequences

Section 7.3.2.4.1 lists the power cables that an aisle fire may damage. Both of the sets of power cables discussed in Sections 7.3.2.4.4 and 7.3.2.4.5, respectively, are affected. As in the previous two cases, the frequency of a small LOCA is small because the power cables of the charging pump 32 and component cooling pump 32 are routed through the lower tunnel. It is assumed that a transient is a certainty. Figure 7.3.2-8 gives a simplified event tree. Either of two sequences, number 1 or number 10, are possibilities in this fire scenario because the primary bleed and feed would be unavailable due to the loss of both safety related MCCs, 36A and 36B. Thus, core melt sequences 2 and 3 cannot occur. Furthermore, both containment spray pumps and three out of five fan coolers would become unavailable. Thus, if core melt sequence 4 occurs, it would lead to sequence number 10 which then leads to containment event tree entry state TE.

The frequency of entry state TE because of a fire at the upper electrical tunnel, can be written as:

$$\Phi_{TE,60A} = \lambda_{AUX} f_T f_A \, Q(\tau_A) \, Q_S \qquad (7.3.2\text{-}8)$$

where

λ_{AUX} = frequency of fires in the PAB, the control building (CB), or the fan house (FH)

f_T = fraction of PAB, CB, and FH fires that occur in the electrical tunnel

f_A = fraction of electrical tunnel fires that are large and occur in the aisle portion

$Q(\tau_A)$ = conditional frequency of propagation of large aisle fires

Q_S = frequency of failure to activate the auxiliary feedwater system

Auxiliary feedwater pumps 31 and 32 are independent of fires at the upper electrical tunnel. The turbine driven pump requires operator actions to come up to speed. The other pump, which is motor-driven, would either start automatically or would be started by the operators in the control room. Although the situation here is different from that described in Section 7.3.2.2.4.5.1 (where failure of the auxiliary feedwater system because of human error and fire in the cable spreading room is discussed), the probability distribution for Q_S, which is given in that section, also applies to this case. The main difference between the cases is the availability of the controls of the motor-driven pump 31. A fire in the aisle of the upper tunnel would cause the failure of many other control and instrumentation cables, in addition to the aforementioned power cables, and may lead to wrong or conflicting information on the control board. Because the effects of these control board malfunctions on the control room operators is not known, the failure frequency of these two pump trains because of human error is judged to be much higher than their combined failure frequency from other causes (see Table 1B of Section 1.5.2.3.9).

Using DPD arithmetic in Equation (7.3.2-8), the distribution for $\Phi_{TE,60A}$ is evaluated and given in Table 7.3.2-6. The characteristic values are:

5th Percentile:	less than 10^{-10} ry^{-1}
Median:	1.3×10^{-8} ry^{-1}
95th Percentile:	1.2×10^{-6} ry^{-1}
Mean:	7.8×10^{-7} ry^{-1}

7.3.2.5 Switchgear Room (Fire Zone 14)

7.3.2.5.1 Characteristics of the Room

This room is located at elevation 15 feet of the control building. Its safety related equipment consists of 480V switchgear numbers 2A, 3A, 5A, and 6A in two parallel rows facing each other (Figure 7.3.2-9). The cables feeding the switchgear cabinets enter the cabinets from above. They include power and control cables for charging pumps, safety injection pumps, component cooling pumps, auxiliary feedwater pumps, containment spray pumps, containment fan coolers, service water pumps, residual heat removal pumps, and MCCs 36A and 36B. This equipment occupies half of the room; instrument air compressors are located in the other half. This room is a controlled access area.

The transient fuels in this area are assessed in Reference 7.3-1 as 15 lbs. of wood, 8 lbs. of paper, 8 lbs. of plastic, 5 lbs. of oil, and 10 lbs. of grease. The in situ combustibles are lightly loaded cable trays stacked three high at most. The lubricating fluid in the air compressors (7 gallons each) is "Anderol," which has a very high ignition temperature. There are 14 ionization-type detectors in the

area. The fire fighting equipment consists of an automatic total flooding carbon dioxide system, two 15-pound carbon dioxide bottles inside the room, and a hose station in the turbine building.

There are two areas in this room where a fire may lead to severe consequences: the cable trays next to the ceiling in the eastern end of the room and the switchgear cabinets. The typical separation between two cable trays of different divisions is approximately 1 foot and the fire propagation analysis is performed accordingly. Because fires caused by the switchgear would not have sufficient fuel to propagate to adjacent cabinets and because of the relatively low burning intensity of the cabinet fire, only external fires are considered. Large outside fires propagating into the room are not considered.

7.3.2.5.2 Fire Propagation and Extinguishing In the Switchgear Room

Two fire scenarios are identified (see Section 7.3.2.5.1). The first involves cable trays elevated above the switchgear cabinets, and the second involves the cabinets themselves.

7.3.2.5.2.1 Cable Tray Fire. Four groups of trays, as shown in Figure 7.3.2-9, are considered. Each group is composed of a stack of three trays, with a vertical separation of 1 foot. The horizontal separation between the groups ranges from 4 to 5 feet, and the lowest tray in each group is elevated 10 feet above the floor. The trays are 2-1/4 feet wide.

The analysis of a fire in these trays is similar to that used for the cable spreading room (Section 7.3.2.2.3.1), except that multiple stacks of trays must be considered.

The large exposure fire analyzed is 2 feet in diameter, and is fueled with oil. The fire is located in the aisle which separates the switchgear cabinets, and is immediately underneath tray stack D. Two large station transformers prevent the occurrence of an exposure fire under tray groups A and B, and a fire located near tray stack C would require a much longer propagation time than the case considered. The exposure fire analyzed is thus conservative and represents all severe exposure fires in this area.

The analysis in Section 7.3.2.5.3 indicates that a fire involving tray groups A, D, and B would initiate the same accident sequence as a fire involving all four tray groups. The time from fire initiation to full involvement of groups A, D, and B is defined as τ_3.

The predicted fire propagation times, $\tau_{3,DRM}$, is obtained using COMPBRN (Reference 7.3-5); its respective value is about 10 minutes, and is fairly independent of the numerical values for the cable insulation physical properties used in the calculations.

Using the error factor ψ to quantify our uncertainties in the calculated fire propagation times when a well defined, fixed exposure fire is involved, the distribution for τ_3 was developed as follows:

$$\tau_3 = \psi\tau_{3,DRM} \qquad (7.3.2\text{-}9)$$

τ_3 is lognormally distributed with the following characteristic values expressed in minutes

$$\tau_{3,05} = 8, \quad \tau_{3,50} = 13, \quad \tau_{3,95} = 20, \quad \alpha_{\tau_3} = 13$$

To account for fire extinguishing activities, the basic model presented in Equation (7.3.2-4) was used, i.e., Q(t), the conditional frequency of fire propagation by time t, given a fire and an extinguishing time τ_S, is exponential with mean τ_S.

For fire propagation among tray groups B, C, and D

$$Q_3 = \exp(-\tau_3/\tau_S) \qquad (7.3.2\text{-}10/11)$$

In evaluating Equation (7.3.2-10), the histogram for τ_S presented in Table 7.3.2-1 is used. This stems from the restriction of fire scenarios to only those which involve very large exposure fires; smaller fires at floor level are not likely to propagate to the elevated trays. The resulting conditional frequencies of fire propagation have the following characteristic values:

$$Q_{3,05} = 0.2 \qquad Q_{3,50} = 0.4, \qquad Q_{3,95} = 0.47,$$

$$\alpha_{Q_3} = 0.39$$

7.3.2.5.2.2 Aisle Exposure Fire. In this section, the effect of a large fire located in the aisle between the switchgear cabinets is considered. Because there is no permanent fuel bed in the aisle, the fire can only be fueled by transient combustibles.

The switchgear room electrical cabinets are modeled as metal boxes measuring 7.52m long by 1.46m deep by 2.44m high. A fire is considered to be serious if it causes a temperature rise of at least 120°C in two cabinets (which are separated by a 1.76m wide aisle). This is the maximum design temperature of typical electrical components (Reference 7.3-9).

Using the calculations described in Section 7.3.5 (Appendix II), the following regression for the asymptotic cabinet air temperature due to a steady heat flux $\dot{q}''_{in}$ (W/m^2) impinging on the front face of the cabinet is derived:

$$T_A = 0.81 \, (\dot{q}''_{in})^{0.55} \quad {}^{\circ}C \qquad (7.3.2\text{-}12)$$

The critical heat flux required to cause a 120°C rise, according to this model, is approximately 8,800 W/m^2. Using the heat flux attenuation model from Section 7.3.6, (Appendix III), this corresponds to an oil pool fire 2 feet in diameter, located 3 feet away from the cabinet (i.e., in the middle of the aisle).

7.3.2.5.2.3 Conditional Frequency of Large Exposure Fires. The frequency of severe consequences from fires in the switchgear room can be written as the sum of four frequencies derived for: (1) fires in the cable trays (Figure 7.3.2-9), (2) large fires on the floor affecting the cable trays, (3) fires in the aisle between the switchgear cabinets, and (4) fires inside a cabinet.

Because the cable trays are relatively inaccessible due to their elevation, the frequency of the large floor-level fires which affect the elevated trays is greater than the frequency of serious fires initiated within the cable trays. This frequency, in turn, is lower than the overall frequency of fires in the switchgear room; not only must the exposure fire be very large (see Section 7.3.2.5.2.1), but it must also be located near the cable trays running from the cabinets toward the eastern wall. These trays contain all exposed power cables except those for the service water pumps.

For the switchgear cabinets, the results of Section 7.3.2.5.2.2 indicate that a very large aisle fire is also required to raise the air temperatures of two cabinets of two different divisions above 120°C. Fires starting within a cabinet will not propagate to a different division because their intensity will be too low.

Note that in the case of an exposure fire involving the switchgear cabinets, some safety system trains would remain available for accident mitigation unless the fire involves nearly all cabinets lining the aisle. This is extremely unlikely because the size of the fire required to damage only two cabinets is already quite large. Because a severe fire in this location can only be fueled by transient combustibles, propagation over a permanent fuel bed is not possible; a larger exposure fire requires a larger amount of transient fuel in the aisle.

The air compressors and related lubricating fluids are located at the western half of the room. Therefore, a fire there would not have significant impact on the switchgear and associated power cables.

Based on the above discussions, it is judged that the dominant scenario is a fire affecting the east/west running cable trays. The fraction of large fires, f_{SL}, in the switchgear room that could occur in the cable tray area is lognormally distributed with a median of 5×10^{-2} and an error of factor 4. The characteristic values are:

$$f_{SL,05} = 5 \times 10^{-4}, \quad f_{SL,50} = 5 \times 10^{-3}, \quad f_{SL,95} = 5 \times 10^{-2},$$

$$\alpha f_{SL} = 1.33 \times 10^{-2}$$

It should be noted that most of the auxiliary building fires involved components typically found in a switchgear area. However, their magnitudes were much smaller than those of the fires considered in Section 7.3.2.5.2.1. Furthermore, the main combustibles were not of a transient type.

7.3.2.5.3 Effects of Fires on Accident Sequences

Several fire scenarios are identified for this area. They affect one stack of trays, or two or more adjacent stack of trays. From Figure 7.3.2-9, we can see that in the case of the failure of one or two adjacent stacks of trays, several safety related components remain available. Thus, the frequencies of severe consequences for these smaller fires must be very low. Three fire scenarios are considered: two for the failure of three adjacent trays (C, A, D or A, D, B) and one for all of the trays. In Section 7.3.2.5.2.1, the likelihood of only failing C, A, and D, and not B, however, was found to be very small. The remaining two scenarios are therefore analyzed.

7.3.2.5.3.1 Cable Tray Stacks A, D, and B Affected by a Fire. An RCP seal failure would occur if all the cables of trays A, D, and B (Figure 7.3.2-9) are damaged by a fire because all component cooling pumps would be lost and the charging pumps are dependent on these pumps. The situation is very similar to that of an aisle fire at the electrical tunnel entrance area inside the cable spreading room. Because the power leads to both SI pumps (see Figure 7.3.2-7), both containment spray pumps and all four fan coolers would be affected, this fire scenario would lead to containment event tree entry state SE. The frequency of entry state SE can be written as:

$$\Phi_{SE,14} = \lambda_{AUX} f_{SWG} f_{SL} Q_3 \qquad (7.3.2\text{-}13/14)$$

where

λ_{AUX} = frequency of fires in PAB, CB, or FH.

f_{SWG} = the fraction of PAB, CB, or FH fires that would occur in the switchgear room.

f_{SL} = fraction of switchgear room fires that are large and under the cable trays.

Q_3 = conditional frequency of fire propagation to the three stacks of trays.

Using DPD arithmetic, the histogram of Table 7.3.2-7/8 for $\phi_{SE,4}$ is obtained. The characteristic values are:

5th Percentile: 4.6×10^{-8} ry^{-1}

Median: 7.5×10^{-6} ry^{-1}

95th Percentile: 4.2×10^{-4} ry^{-1}

Mean: 7.1×10^{-5} ry^{-1}

7.3.2.5.3.2 All Four Cable Tray Stacks Affected By a Fire. The impact of this fire scenario is the same as the fire affecting A, D, and B trays. This is because the additional failures (i.e., one charging pump and one fan cooler unit) do not have any further impact on the accident sequence; that is, RCP seal failure and loss of makeup and containment cooling. The fire propagation time to the fourth tray is longer than $\tau_{3,DRM}$, thus the conditional frequency of cable failures before suppression is smaller than Q_3. However, Equation (7.3.2-13/14) does cover fire scenarios leading to the failure of all four stacks of trays because we have not subtracted the former conditional frequency from Q_3 to exclude the fires propagating to the last stack of trays. Thus, any further analysis of this scenario is not necessary.

7.3.2.6 Corridor (Fire Zone 27A)

This corridor at Elevation 98' of the primary auxiliary building contains the safety related motor control centers 36A and 36B. The controls of all safety related motor-operated valves pass through these motor control centers. The auxiliary feedwater system is totally independent from this area, however. The unavailability of the AFWS due to other causes is presented in Section 1.5.2.3.9 and the characteristic values are:

5th Percentile: 1.1×10^{-6}

50th Percentile: 7.6×10^{-6}

95th Percentile: 8.2×10^{-5}

In view of the frequency of fires in other areas and the fire propagation analysis performed for other areas, the frequency of failing both of the MCCs is judged to be less than 10^{-2} per reactor year. The frequency of core melt given a fire is the product of this frequency and that of the auxiliary feedwater system. The fire risk from this area is thus much less than the two areas previously discussed.

7.3.2.7 Upper Electrical Penetration Area (Fire Zone 73A)

This area is located in the fan house next to the containment. The control cables for the auxiliary feedwater pumps and their regulating valves, the power cables for the containment fan coolers, and the power

and control cables for the PORVs and their associated block valves are located in this area. These conditions are similar to those of the upper electrical tunnel, except that the power cables of the safety injection pumps, and of several other pumps, do not run through this area. The remaining two auxiliary feedwater pump trains can provide adequate cooling. Thus, the frequencies of containment event tree entry states are very low.

7.3.2.8 Smoke Propagation

Smoke can have an impact on a fire initiated accident scenario by corroding components and causing their failure or by reducing personnel effectiveness. Because the corrosion process is rather slow, component failures due to smoke would not have a significant impact on accident (e.g., LOCA) mitigation. Smoke may have a long term effect on component availability; however, the possibility of smoke causing an initiating event (i.e., LOCA, transients) is inconceivable.

The effects of smoke on the accident sequences due to its impact on plant personnel in certain critical plant areas are discussed. Areas of the plant not discussed either do not contain safety related items or do not require operator action. The results of the preceding sections apply in the following plant areas:

- Control Room. The ventilation system of the control room is independent of the rest of the plant. Smoke from fires in other parts of the plant cannot propagate to this area. Thus, in the case of fire in any of the critical areas discussed in the preceding sections, the control room operators would be able to use the control board. Furthermore, breathing apparatus are provided in this area, in case of smoke, to allow the operators to stay in the control room. Special emergency procedures for plant shutdown from outside the control room also exist. The effects of a fire in the control room (the most likely source of smoke in the area) are very similar to a fire in the control cables in the cable spreading room except that habitability of the control room is an important factor. The frequency of fires in the control room (Reference 7.3.3) is less than the frequency of fires in the cable spreading room. Extinguishment would be initiated almost immediately after ignition because of the continuous presence of the operators. Fires in the safety related supervisory panels may only lead to the failure of several redundant safety systems. Because breathing apparatus are provided, not all fires would require evacuation of the control room. Therefore, the frequencies of severe consequences from a fire in the control room are covered within the uncertainties of those frequencies evaluated for the cable spreading room.

- Cable Spreading Room. Two exhaust fans would remove the smoke from the cable spreading room into the electrical tunnels. Smoke from this area would not propagate to other areas (e.g., switchgear room) where manual actions would be necessary.

- Switchgear Room. Two exhaust fans can draw the smoke out of this room. Manual actions in the switchgear room are not necessary even though smoke from a turbine building fire may enter this area. A fire in the switchgear room may also cause the failure of the exhaust fans. In the preceding sections, a large fire in this area was found to lead to severe consequences with a small likelihood of mitigation. The uncertainties in the frequencies of those accident sequences also cover the scenarios where exhaust fans are unavailable.

- The Corridor Containing MCCs 36A and 36B (Fire Zone 27A). The manual actions in this area would only involve the control of motor-operated valves which can also be performed at the valve location itself by turning the handwheels. In the preceding sections, all the necessary MOVs were found to be located outside the containment.

- Auxiliary Feedwater Pump Room (Fire Zone 23). All three auxiliary feedwater pumps are housed in this area. In the case of loss of control or power to the feedwater pumps, the operators can start the turbine-driven pump from this area or they can switch the power of one of the motor-operated pumps to the alternate shutdown system. The building containing the auxiliary feedwater pumps is independent of the critical areas identified earlier in this section. Two wall exhaust fans are also provided for this area. Therefore, smoke from other areas cannot propagate to this room.

7.3.2.9 Flooding Due to Extinguishing Activities

Four general areas contain fixed fire water systems and safety related shutdown equipment: the diesel generator rooms, the upper and lower electrical tunnel and penetration, and elevation 55 feet of primary auxiliary building.

A dry pipe preaction sprinkler system that upon activation, alarms in the control room is installed at elevation 55 feet of the primary auxiliary building. The two safety related MCCs, 36A and 36B, are the most critical items of this area. In Section 7.3.2.6, we have found that simultaneous failure of these MCCs does not contribute significantly to the fire risk.

Fire zones 7A and 60A (lower and upper electrical tunnels) are protected by a preaction dry pipe sprinkler system that alarms in the control room. Drainage is provided by floor drains and hub drains. In the case of failure of this drainage system, the water from the sprinklers will flow to the cable spreading room. Flooding of the cable spreading room may lead to the failure of the batteries. The water may also penetrate the switchgear ceiling at the power cable seals. It may reach the switchgear cabinets because they are located very close to the ceiling

penetrations, thus leading to failures inside the cabinets. Several unlikely events would have to occur to have severe consequences: failure of water through the seal in the floor, and water reaching the switchgear cabinets after traveling horizontally on the cable trays. The effects of these events would be similar to a large fire in the switchgear room or at the tunnel entrance in the cable spreading room. The impact of flooding from the sprinkler system in the cable tunnel on the frequencies of severe consequences is thus judged to be minimal.

Flooding due to use of fire hose stations cannot have a significant impact on the frequencies of severe consequences because floor drains are provided and since the process is manual, uncontrolled conditions would be avoided.

7.3.2.10 Core Melt Frequency Due to Fires at Indian Point 3

The total frequency of core melt caused by fires is the sum of the core melt frequencies from different fire zones. In most cases, only one containment event tree entry state resulted. For example, entry state TE results from an aisle fire in the upper electrical tunnel. Therefore, the freqencies of these entry states are equal to the core melt frequencies. Thus, we can write:

$$\begin{aligned}\Phi CM &= \Phi CM,CC + \Phi SE,PC + \Phi TE,60A + \Phi SE,14 \\ &= \lambda_{CSR}\left[f_{es,cc}Q(\tau_G)Q_S + f_{cs,TE}Q(\tau_A)\right] \\ &+ \lambda_{AUX}\left[f_T f_A Q(\tau_A)Q_S + f_{SWG}f_{SL}Q_3\right]\end{aligned} \qquad (7.3.2\text{-}15)$$

The probability distribution of the core melt frequency is given in Table 7.3.2-12 and has the following characteristic values:

5th Percentile:	2.2×10^{-6} ry^{-1}
Median:	2.8×10^{-5} ry^{-1}
95th Percentile:	1.0×10^{-3} ry^{-1}
Mean:	9.8×10^{-5} ry^{-1}

7.3.2.11 Frequencies of Containment Event Tree Entry States Due to Fires at Indian Point 3

The frequencies of containment event tree entry states as caused by a fire in the power plant can now be evaluated. In the analyses of the preceding subsections, the frequencies of entry states as caused by fires was calculated for specific areas. The frequencies of only three entry states are significant. Each state is discussed separately.

- Entry State TEFC. The main contributor to the frequency of this entry state is a fire in the cable spreading room. Thus, the

probability distribution of ϕ_{TEFC} is given by Table 7.3.2-3. The characteristic values are:

5th Percentile: 1.9×10^{-10} ry^{-1}

Median: 6.0×10^{-8} ry^{-1}

95th Percentile: 4.0×10^{-6} ry^{-1}

Mean: 1.6×10^{-6} ry^{-1}

- Entry State TE. The main contributors to the frequency of this entry state are fires in the cable spreading room, the upper electrical tunnel, and the switchgear room. Thus,

$$\phi_{TE} = \phi_{TE,CC} + \phi_{TE,60A}$$

$$= \lambda_{CSR} f_{es} \exp\left(-\frac{\tau_G}{\tau_s}\right) Q_s Q_{HE} + \lambda_{AUX}\left[f_T f_A \exp\left(-\frac{\tau_A}{\tau_s}\right) Q_s + f_{SWG} f_{SL} \exp\left(-\frac{\tau_3}{\tau_s}\right)\right] \quad (7.3.2\text{-}16)$$

Table 7.3.2-9 gives the result. The characteristic values of ϕ_{TE} are:

5th Percentile: 1.2×10^{-9} ry^{-1}

Median: 6.7×10^{-8} ry^{-1}

95th Percentile: 9.2×10^{-6} ry^{-1}

Mean: 1.0×10^{-6} ry^{-1}

- Entry State SE. The main contributors to the frequency of this entry state are fires in the cable spreading room and the switchgear room. Thus,

$$\phi_{SE} = \phi_{SE,PC} + \phi_{SE,14}$$

$$= \lambda_{CSR} f_{es} \exp\left(-\frac{\tau_A}{\tau_s}\right) + \lambda_{AUX} f_{SWG} f_{SL} \exp\left(-\frac{\tau_3}{\tau_s}\right) \quad (7.3.2\text{-}17)$$

Table 7.3.2-10 gives the result. The characteristic values of ϕ_{SE} are:

5th Percentile: 8.5×10^{-7} ry^{-1}

Median: 2.5×10^{-5} ry^{-1}

95th Percentile: 9.6×10^{-4} ry^{-1}

Mean: 9.5×10^{-5} ry^{-1}

7.3.2.12 Frequencies of Release Categories Due to Fires at Indian Point 3

Fires may lead to release categories 8B and 2RW. The frequencies of other categories caused by fires are very small.

- Release Category 8B. The containment event tree entry state TEFC leads to this release category. Its frequency can be written as:

$$\Phi 8B = \Phi TEFC \qquad (7.3.2\text{-}18)$$

Table 7.3.2-3 gives the result. The characteristic values are:

5th Percentile: 1.9×10^{-10} ry^{-1}

Median: 6.0×10^{-8} ry^{-1}

95th Percentile: 4.0×10^{-6} ry^{-1}

Mean: 1.6×10^{-6} ry^{-1}

Fires at the center of the northern wall in the cable spreading room are the main contributors.

- Release Category 2RW. The containment event tree entry states SE and TE lead to this release category. Its frequency can be written as:

$$\Phi 2RW = \Phi TE + \Phi SE \qquad (7.3.2\text{-}19)$$

Since the core melt frequency $\Phi CM,CC$ is small, this equation gives the same result as Equation (7.3.2-15). Table 7.3.2-11 gives the result. The characteristic values are:

5th Percentile: 1.5×10^{-6} ry^{-1}

Median: 2.6×10^{-5} ry^{-1}

95th Percentile: 9.7×10^{-4} ry^{-1}

Mean: 9.6×10^{-5} ry^{-1}

The main contributor is containment event tree entry state SE, which is primarily caused by fires in the switchgear room and the entrance to the electrical tunnels.

7.3.2A ADDITIONAL FEATURES, INDIAN POINT UNIT 3

7.3.2A.1 Introduction

A modification was proposed in Reference 7.3-15 to enable Indian Point Unit 3 to comply with Appendix R to 10CFR50. In this section, the effects of the proposed modification on the frequencies of core melt accidents and radionuclide releases caused by fires in Indian Point Unit 3 are evaluated. These frequencies as evaluated in Section 7.3.2 present estimates of the fire risk from the plant prior to implementation of the proposed modification. Thus, the frequencies and the methodology of Section 7.3.2 are used in this section.

In Section 7.3.2, it is found that the overall fire risk is dominated by two fire zones: the switchgear room and the electrical tunnel entrance area. In both cases, the power cables of many vital components are in close proximity. A large fire in either of these two areas can lead to reactor coolant pump (RCP) seal failure with loss of many components necessary to mitigate core melt and to prevent containment failure. The modification is tailored so that it reduces the likelihood of fire as the cause of an accident initiating event (RCP seal failure in this case). Table 7.3.2A-13 gives the frequencies of core melt and release categories 8A, 8B, and 2RW as influenced by this modification.

7.3.2A.2 Fire Risk Before Modification

The fire risk results in Section 7.3.2 are needed for measuring the reduction in the frequencies of core melt and release categories. In Section 7.3.2, these frequencies are calculated in terms of the dominant contributors. Most of the fire zones were not explicitly analyzed quantitatively, based on judgment that their contribution would be insignificant. Typically, these fire zones contained only a few safety related components. The proposed modifications would probably change the relative order of contributors to the release categories and core melt. Therefore, the fire risk from other fire zones not explicitly quantified in Section 7.3.2 is now so quantified. All the areas that contain some safety components per Reference 7.3-1 are included here. Table 7.3.2A-14 summarizes the results and Section 7.3.2A.5 gives the details.

The fire zone designating numbers used in Table 7.3.2A-14 are taken from Reference 7.3-1. For areas not originally quantified in Section 7.3.2, point values (mean frequencies) are estimated per formulas given in Section 7.3.2A.5. The fire zones analyzed in Section 7.3.2 are found (as expected) to be the dominant contributors to core melt and damage states SE and TE. However, the mean frequency of other damage states is found to be dominated by fire zones not explicitly quantified in Section 7.3.2. Two comments are in order here. First, the increased frequency of these damage states has very little impact on the overall frequency of the damage states given in Table 8.3-3. The overall mean frequency of release category 8B is 1.3×10^{-4} per reactor year (from Table 8.3-3) and is significantly larger than 6.7×10^{-6}, the new

frequency of 8B (before the modification) due to fires. The latter is now dominated by contributions from fire zones that were not explicitly quantified in Section 7.3.2. In Section 7.3.2A.3, we find that many conservative assumptions are incorporated in the quantification of these dominating fire zones; therefore, a more rigorous evaluation is expected to yield smaller frequencies and less significant contribution to the overall 8B frequency.

7.3.2A.3 Description of the Modification

The modification is the same as Avenue 2 of Reference 7.3-15. It utilizes the nonsafety switchgears 313 and 312 which are located in the turbine building as an alternate power source for one CCS pump, one charging pump, one service water pump, and the instrumentation cabinet located in the penetration area. The source of the electrical power to the switchgears is the 138 kV or 13.8 kV feed from the Buchanan substation. Figure 7.3.2A-10 gives the one-line diagram of the power supply. Figure 7.3.2A-11 gives the routing of the power cables from switchgears 313 and 312 to the pumps and the instrumentation cabinet. Note that the alternate power cables do not pass through any of the critical fire locations. Transfer switches (see Figure 7.3.2A-10) will be installed for the CCS pump and charging pump. For the service water system, the backup pumps will be connected directly (without any transfer switches) to switchgear 312. An alternate power cable will feed the instrumentation isolation cabinet.

The alternate power cable for the instrumentation power supply at the electrical penetration area will be routed in a fashion similar to the preceding two alternate feed cables. Manual switches in the power supply cabinet can isolate the instrumentation circuitry from the cable spreading room and control room. The application of these switches reactivates the wide range steam generator level indicators in the auxiliary feedwater pump room and one channel of pressurizer pressure and level indicators outside the charging pump room.

In addition to these three alternate feed cables, Reference 7.3-15 proposes to install fire barriers in the electrical penetration area and inside the containment. These barriers will provide further separation between channels A, C, and B, D of instrumentation cable trays.

In the case of a fire in the switchgear room or electrical tunnel entrance area, the operators would have to reactivate at least one component cooling pump within one-half hour of loss of all CCS pumps to prevent seal failure. One operator would have to be stationed at switchgear 313 and another at the pump location. The transfer switch would have to be applied first. The operator at switchgear 313 could then close the associated breaker and restart a CCS pump. The same process can then be followed to reactivate a charging pump.

If vital instrumentation were also lost, the operators could reactivate the instrumentation power supply cabinet following the same procedure as for the CCS pumps. However, they would have to isolate the cabinet from the control room by applying switches at the cabinet (in the penetrations area). They could then follow the vital parameters at two locations: the auxiliary feedwater pump room and the charging pump room.

Core cooling would be achieved by running an auxiliary feedwater pump. In the case of a switchgear room fire, the turbine-driven pump can be controlled from the control room. The Appendix R study had identified that the power cable for the steam supply valve is coupled to cables in the switchgear room. However, the resultant effect of postulated interactions was determined not to impair the turbine-driven pump operability. In the case of an electrical tunnel entrance fire, the turbine-driven pump can be controlled at the pump location. Also, in the latter case, the power cable for one motor-driven auxiliary pump would remain available.

The following summarizes our assumptions about this modification:

- The power source (i.e., power at switchgears 312 and 313) is offsite power and provisions to connect to other sources are not available for several hours.
- Switchgears 312 and 313 are in the turbine building and their power source can be isolated from the switchgear room (fire zone 14), the electrical tunnels (fire zones 7A and 60A), and the cable spreading room (fire zone 11).
- The switchgear would provide an alternate power source to the charging pump, component cooling pump, backup service water pump, and the power supply for the instrumentation cabinet in the penetration area.
- Cable routing from the new switchgear to all affected components would not pass through the control room, cable spreading room, or switchgear room.
- Some of the alternate feed cables will be routed partly through the upper electrical tunnel.
- The transfer switches would be installed in areas readily accessible to the operators and would be close to the related component to minimize the length of single portion of the power cable feeding the pump.
- The availability of the new switchgear should not be dependent on support systems that could be affected by a fire in the existing switchgear room, electrical tunnels, control room, or cable spreading room.
- The existing alternate indicators of steam generator level and pressurizer pressure and level will be provided with alternate feed cables for their power supply, and are independent from the control room, cable speading room, the electrical tunnels, and the switchgear room.
- Procedures for using the alternate feeds and instrumentation would be written and practiced by all control room operators.
- Access to the transfer switches would not be hindered by smoke from the above-mentioned fire zones.

7.3.2A.4 Fire Risk After the Modification

The modification impacts mainly those fire scenarios that originate in the electrical tunnel or switchgear room where many vital components may be affected. Table 7.3.2A-15 summarizes the results in terms of mean frequencies of the contributions from all fire zones. The modification reduces the contribution from the electrical tunnel entrance area, and switchgear room. The other fire areas are either not affected by the modification or the impact is insignificant.

7.3.2A.4.1 Areas Not Affected

The control cable part of the cable spreading room and the control room fire scenarios are not significantly affected by this modification because the study in Section 7.3.2 includes provisions for manually activating vital pumps and achieving hot shutdown conditions from outside the control room. Power cables are not affected by a fire in these areas. Control cables of almost all safety components can be affected by these fires. Hot shorts in these cables may stop already running pumps. However, credit is given to the operators reactivating normally running components such as a charging pump and a component cooling pump if they are stopped by a fire which fails only control cables. Prolonged stoppage of these pumps due to control cable fires is deemed to be a comparatively low frequency event. Thus, the possibility of an RCP seal failure (a small loss of coolant accident) is not analyzed. Many vital instrumentation channels would also be affected. The existing isolation switches in the penetrations area would have to be applied to transfer the vital instrumentation to the alternate points (i.e., auxiliary feedwater pump room and the charging pump room).

The modification cannot have a significant impact on the contribution from pump rooms such as fire zone 1 for the CCS pumps. For these cases, the fire will disable all power feeds to the pumps or the pumps themselves, and thus render the proposed transfer switch ineffective. Finally, for the remaining areas, this modification has an insignificant effect because the components connected to the alternate switchgear are not affected by a fire in those areas.

7.3.2A.4.2 Impact on the Switchgear Room

The main impact of this modification on a switchgear room fire is that of decreasing the likelihood of an RCP seal LOCA. In a switchgear room fire, if all four switchgear cabinets are affected or the power cables at the eastern end of the room are affected (three of the four stacks of trays), the power to all CCS pumps would be lost. With the proposed modification, the operators can activate the alternate switchgear and throw the transfer switches of one CCS pump and/or one charging pump, and reactivate the RCP seal cooling function. The relevant valves would be in their normal operating positions because it is impossible for a switchgear room fire to cause inadvertent closure of these valves as the valve cables are not routed through the switchgear room. Transfer to the alternate switchgear must be completed within the first half hour of loss of all RCP seal cooling.

The conditional frequency, Q_{S1}, of a small LOCA (via RCP seal failure) given a large fire in the switchgear room can then be written as

$$Q_{S1} = Q_{HE,S1} + Q_{SW} + Q_{CCS}$$

where

$Q_{HE,S1}$ ≡ human error; failure of the operators to reactivate the CCS pump within one-half hour of a large fire.

Q_{SW} ≡ failure of the transfer switch.

Q_{CCS} ≡ failure of the component cooling pump.

and

$$Q_{CCS} = Q_{CCS,D} + 24\lambda_{CCS} + Q_{CCS,M}$$

where

$Q_{CCS,D}$ ≡ failure of the CCS pump on demand.

λ_{CCS} ≡ failure of the CCS pump during operation.

$Q_{CCS,M}$ ≡ unavailability of CCS pump due to maintenance.

The total time period that the component cooling pump is needed to operate is taken to be 24 hours.

The main contributor to $Q_{HE,S1}$ is judged to be failure of the control room operators to initiate the process of transferring to the alternate switchgear. The large fire in the switchgear room is judged to pose a medium to high stress level on the operators. There will be at least three operators involved in making the decision. Reference 7.3-7 is used for human error frequencies and the definitions of levels of dependencies among the operators. It is judged that one of the operators will be strongly dependent on the other two and the level of dependence of the other two to one another will be low. Reference 7.3-7 suggests 0.1 for the frequency of human error for one operator under very high levels of stress. For the conditional frequency of a second operator making the same error, it suggests a point value of 0.15. Based on these suggested frequencies, we have chosen $Q_{HE,S1}$ to be lognormally distributed with the following characteristic values:

$$Q_{HE,S1,05} = 9.0 \times 10^{-3}$$

$$Q_{HE,S1,50} = 3.0 \times 10^{-2}$$

$$Q_{HE,S1,95} = 1.0 \times 10^{-1}$$

$$\alpha_{Q_{HE,S1}} = 3.9 \times 10^{-2}$$

Table 7.3.2A-16 gives the frequencies of Q_{SW}, $Q_{CCS,D}$, λ_{CCS}, and $Q_{CCS,M}$. Using those frequencies and the previously given human error frequency, the conditional frequency of a seal LOCA is evaluated. Its characteristic values are:

$$Q_{S1,05} = 1.8 \times 10^{-2}$$

$$Q_{S1,50} = 3.7 \times 10^{-2}$$

$$Q_{S1,95} = 9.9 \times 10^{-2}$$

$$\alpha_{Q_{S1}} = 4.7 \times 10^{-2}$$

It should be noted that the unavailability of the electric power is not an important contributor to Q_{S1}. This unavailability, Q_{EP}, can be written as

$$Q_{EP} = \lambda_{LOP} t + Q_{LOP/TT}$$

where

λ_{EP} ≡ frequency of loss of offsite power due to causes other than an Indian Point 3 turbine trip.

t ≡ exposure time.

$Q_{LOP/TT}$ ≡ loss of offsite power given an Indian Point 3 turbine trip.

Table 7.3.2A-16 gives the frequencies λ_{LOP} and $Q_{LOP/TT}$. The exposure time is taken to be 24 hours. The mean of the distribution for Q_{EP} is

$$\alpha_{Q_{EP}} = 1.1 \times 10^{-3}$$

Thus, loss of electric power has an insignificant contribution to the unavailability of the alternate feed system for preventing RCP seal failure.

The simple event tree of Section 7.3.2 (Figure 7.3.2-7) for the mitigation of a small LOCA is used here. In a large switchgear room fire, all the small LOCA mitigating functions would be lost. For example, the SI pumps would be affected by the fire and would not be available.

Thus, core melt is taken to be a certainty in case of seal failure for this scenario. The conditional frequency of core melt $Q_{CM,14}$ can then be written as

$$Q_{CM,14} = Q_{S1}$$

The containment spray pumps and containment fan cooler units would also be lost in a switchgear room fire. Thus, a core melt due to seal failure would lead to plant damage state SE (event sequence 20 of Figure 7.3.2-7). The unconditional frequency of damage state SE is then

$$\phi'_{SE,14,F} = \phi_{SE,14}\, Q_{CM,14} = \phi_{SE,14}\, Q_{S1}$$

where $\phi_{SE,14}$ is the frequency of state SE due to switchgear room fires prior to the implementation of the modification. The mean frequency of this damage state becomes

$$\alpha_{\phi'_{SE,14,F}} = 3.3 \times 10^{-6} \text{ (per reactor year)}$$

If seal failure were prevented, the initiating event would become a transient (reactor trip is assumed here). Safe shutdown could be achieved if the auxiliary feedwater system (AFWS) or bleed and feed mode of core cooling were employed (see Figure 7.3.2-8 for the event tree). Moreover, bleed and feed would not be possible because the block valves of the power-operated relief valves would be lost due to loss of both safety related motor control centers. Also, the power cables of the SI pumps would be affected by the fire. Of the auxiliary feedwater systems, only the turbine-driven pump could be used in its normal mode. It is deemed that human error in locally activating the turbine-driven AFW pump would not be exceptionally high because the successful alignment of the CCS and charging pumps would have a reassuring effect on the operators. The unavailability of AFWS with loss of power to all electrical buses as evaluated in Section 1.6.2.3.9 is used here. Human error contributes to about half of this frequency. The distribution is approximated by a lognormal distribution with the following characteristic values:

$$Q_{TD1,05} = 3.5 \times 10^{-3}$$

$$Q_{TD1,50} = 1.2 \times 10^{-2}$$

$$Q_{TD1,95} = 4.1 \times 10^{-2}$$

$$\alpha_{Q_{TD1}} = 1.6 \times 10^{-2}$$

The unconditional frequency of damage state TE can be written as

$$\phi'_{TE,14,F} = \phi_{SE,14}(1-Q_{S1})\, Q_{TD1}$$

The mean frequency of this damage state becomes

$$\alpha_{\phi'_{TE,14,F}} = 1.1 \times 10^{-6} \text{ (per reactor year)}$$

7.3.2A.4.3 Impact on Electrical Tunnel Entrance Area Contribution

The contribution of the electrical tunnel entrance area to plant risk is also affected by the proposed modification. From Section 7.3.2, we find that damage state SE would result when a fire affects both stacks of trays. The seal failure may be prevented using the alternate feeds. The conditions here are very similar to those of the switchgear room fire except that in this case, many control cables and instrumentation cables may also be affected. It is deemed that the human error rate $Q_{HE,S1}$ of the switchgear room is evaluated conservatively so that in spite of the additional failures, it is also applicable to this case. Thus, the conditional frequency of seal failure is again Q_{S1}, and the unconditional frequency of damage state SE becomes:

$$\phi'_{SE,11PC,F} = \phi_{SE,PC} Q_{S1}$$

where $\phi_{SE,PC}$ is the frequency of damage state SE as calculated in Section 7.3.2. The mean frequency of this damage state becomes

$$\alpha_{\phi'_{SE,11PC,F}} = 1.1 \times 10^{-6} \text{ (per reactor year)}$$

If seal failure were prevented, a transient (we assume reactor trip) would occur. The event tree for transients is shown in Figure 7.3.2-8. The bleed and feed mode of core cooling would not be available because both the PORVs and the SI pumps would be failed. Two trains of the AFWS could be made available manually: the turbine-driven pump and one motor-driven pump. The latter would have to be activated at the switchgears because its control cables would be affected by the fire. However, the overall unavailability of motor-driven pumps is dominated by human error in restoring them. The unavailabliity of AFWS, $Q_{AF3,11PC}$, can be written as

$$Q_{AF3,11PC} = Q_{TD2}\, Q_{MD1}$$

where Q_{TD2} is the unavailability of the turbine-driven pump and Q_{MD} is the unavailability of the motor-driven pump. The turbine-driven auxiliary feedwater pump has to be activated locally. The human error frequency is higher in this case because control and instrumentation cables are affected. The results of Section 1.6.2.3.9 are still applicable here. For Q_{TD2} we can write

$$Q_{TD2} = Q_{TD,D} + Q_{TD,M} + Q_{TD2,HE}$$

where

$Q_{TD,D}$ ≡ failure of the turbine-driven AFW pump to start due to mechanical failures.

TD2,HE ≡ unavailability of the turbine-driven AFW pump due to human error.

$Q_{TD,M}$ ≡ unavailability of the turbine-driven AFW pump due to maintenance.

Table 7.3.2A-16 gives the characteristic values of these frequencies. The human error contribution $Q_{TD2,HE}$ is also taken from Section 1.6.2.3.9 for pump activation from outside the control room. It is judged that the stress levels and dependencies modeled in that section are applicable to the situation here. Thus, the unavailability of the turbine-driven pump has a mean of

$$\alpha_{Q_{TD2}} = 5.3 \times 10^{-2}$$

The conditional frequency of failure of the motor-driven pump given the failure of the turbine-driven pump, Q_{MD1}, is deemed to be dominated by the human error of manually closing the associated breaker at the switchgear cabinets. The stress levels would be high because of the fire and the failure of the turbine-driven pump. The available time before severe core damage would be about 3 hours. At least three control room operators and one shift technical advisor (STA) would be available for the operation within this time period. The basic human error rate is about 0.1. Because of the earlier failures (of the turbine-driven pump), the dependency between two of the operators is taken to be complete. The dependency of the first two with the third operator is taken to be high. Some (high) level of dependency is taken for the STA and the rest of the team. The unavailability of both motor driven-pumps, Q_{MD1}, is judged to be lognormally distributed with the following characteristic values:

$$Q_{MD1,05} = 1.5 \times 10^{-3}$$

$$Q_{MD1,50} = 3.0 \times 10^{-2}$$

$$Q_{MD1,95} = 6.0 \times 10^{-1}$$

$$\alpha_{Q_{MD1}} = 1.6 \times 10^{-1}$$

The mean frequency of $Q_{AF3,11PC}$ becomes

$$\alpha_{Q_{AF3,11PC}} = 8.5 \times 10^{-3}$$

For the unconditional frequency of damage state TE we get

$$\phi'_{TE,11PC,F} = \phi_{SE,PC}\, Q_{AF3,11PC}\, (1 - Q_{S1})$$

The mean frequency of this damage state is

$$\alpha_{\phi'_{TE,11PC,F}} = 1.8 \times 10^{-7} \text{ (per reactor year)}$$

7.3.2A.4.4 Impact on the Upper Electrical Tunnel, Fire Zone 60A

The power cables of many vital components are routed through this electrical tunnel, the details of which are given in Section 7.3.2.4.1. At least one train of all vital systems remains unaffected by a large fire in this area except for the containment spray system. The additional power source has an insignificant impact on the availability of the components needed to prevent core damage. Thus, the results of Section 7.3.2 are used here.

7.3.2A.4.5 Total Core Melt and Release Category Frequencies

In Table 7.3.2A-15, the total mean frequencies of core melt, plant damage states, and release categories are given. The probability distribution of these total frequencies of core melt and the release categories are calculated in two stages. First, the distributions for the dominant fire zones for plant damage states are calculated. These frequencies are indicated in Table 7.3.2A-15 by an asterisk. In the second stage, an appropriate set of these probability distributions are summed (using probabilisitc arithmetic) to obtain the distribution for core melt and the release categories. Tables 7.3.2A-17 through 7.3.2A-20 give the probability distributions for core melt and release categories 8B, 8A, and 2RW, respectively.

Table 7.3.2A-15 shows that approximately 40% of the total core melt frequency is from areas that were not originally analyzed in the IPPSS fire study. This confirms our earlier expectation that by reducing the frequencies of the dominant contributors, other fire areas may gain in relative importance. These new areas are addressed in Section 7.3.2A.5 to this study. By comparing Tables 7.3.2A-14 and 7.3.2A-15, we can see that the mean core melt frequency has decreased by about a factor of 7 due to the modification.

The frequencies of release categories 8B and 8A are not affected by the modification. The frequencies of both are dominated by fire areas that were not included in Section 7.3.2. The contribution from these areas is calculated in Section 7.3.2A.5. It should be noted that fire initiated release categories 8A and 8B do not have significant impact on the overall frequency of these categories for the plant.

The probability distribution of release category 2RW is given in Table 7.3.2A-20. Table 7.3.2A-15 shows that this frequency (similar to the frequency of 2RW prior to the modification) is dominated by fires in the switchgear room and the electrical tunnel entrance area. However, other areas (such as the cable spreading room and the upper electrical tunnel) have some impact on this total frequency. The switchgear room and the tunnel entrance area contributes to about 84% of the total frequency as opposed to the 99% contribution that they had prior to the modification. The modification has lead to a reduction in the total frequency by a factor of about 14.

7.3.2A.5 Highlights of Base Case Quantifications

In this section, the methods used for calculating the risk from the fire zones not explicitly quantified in Section 7.3.2 are described. The details of quantification for some areas are also highlighted.

7.3.2A.5.1 The General Formulas

In Section 7.3.2, it is found that fires cannot cause a large or medium loss of coolant accident. The simultaneous occurrence of these initiating events and a fire disabling part or most of the mitigating systems can be shown to be dominated by the frequencies of these sequences due to causes other than fire.

For a small LOCA, it is found that fire can only lead to a reactor coolant pump seal failure (thereby leading to a small LOCA) and cannot cause any other type of breach in the primary system (Section 7.3.2). To simplify the calculations, the delayed melts (e.g., due to failure of the recirculation system) are combined with early melts. For dominant scenarios, in the main text these two types of melts are clearly differentiated. Core melt is computed in two parts: (1) core melt due to a small LOCA, and (2) core melt due to a transient. The transients are grouped together and reactor trip is chosen to be the representing transient initiating event. The following formulas are used for quantifying fire risk.

$$\phi_{\text{core melt}} = \phi_{CM,\text{small LOCA}} + \phi_{CM,\text{transient}}$$

$$\phi_{CM,\text{small LOCA}} = \lambda_{Fire}[Q_{EP} + Q_{SW} + Q_{CCS}(Q_{SI} + Q_{REC} + Q_{CF} + Q_{PORV} + Q_{AFWS})]$$

$$\phi_{CM,\text{transient}} = \lambda_{Fire}[(Q_{SI} + Q_{REC} + Q_{PORV})Q_{AFWS}]$$

where

λ_{Fire} = frequency of fire failing a specified group of vital components.

Q_i = unavailability of system i.

EP = electric power system (both trains).

SWS = service water system.

CCS = component cooling system.

SIS = safety injection system.

REC = recirculation system.

CF = containment fan cooling system.

PORV = power-operated relief valves and block valves (used for bleed and feed operation).

AFWS = auxiliary feedwater system.

The equation for core melt due to a small LOCA is based on the event tree of Figure 7.3.2-7. The systems referenced previously are analyzed in Section 1.6.2, except for the poweroperated relief valve which is analyzed in Section 1.3.3.9. The unavailability of these systems is given in Section 1.6.2 for different boundary conditions. In the core melt equation above, it is assumed that total loss of electric power or service water will lead to reactor coolant pump seal failure and loss of all mitigating features. It is also assumed that total loss of component cooling leads to loss of the charging pumps and, consequently, a small LOCA via the RCP seals. The availability of the containment fan coolers determines the availability of the recirculation system when the component cooling system is not available. The partial failures of support systems such as the electric power system were found to have insignificant contributions to core melt.

The equation for core melt due to a transient is based on the event tree of Figure 7.3.2-8. The plant damage states are computed from the following equations:

$$\phi_{SEFC} = \lambda_{Fire}[Q_{CCS}(Q_{SI} + Q_{REC} + Q_{PORV}Q_{AFWS})]$$

$$\phi_{SEF} = \phi_{SEFC}Q_{CS}$$

$$\phi_{SEC} = \lambda_{Fire}[Q_{CCS}Q_{CF} + Q_{SW}]$$

$$\phi_{SE} = \lambda_{Fire}[Q_{EP} + Q_{SW}Q_{CS} + Q_{CCS}Q_{CF}Q_{CS}]$$

$$\phi_{TEFC} = \phi_{CM,transient}$$

$$\phi_{TEF} = \phi_{TEFC}Q_{CS}$$

$$\phi_{TEC} = \phi_{TEFC}Q_{CF}$$

$$\phi_{TE} = \phi_{TEFC}Q_{CF}Q_{CS}$$

where the different parameters are defined earlier and

Q_{CS} = unavailability of the containment spray system (this system is analyzed in Section 1.6.2).

The frequencies of the release categories are computed using:

$$\phi_{8B} = \lambda_{Fire}\,[Q_{SW} + Q_{CCS}(Q_{SI} + Q_{REC} + Q_{CF}) + (Q_{SI} + Q_{REC} + Q_{PORV})Q_{AFWS}]$$

$$\phi_{8A} = \lambda_{Fire}\,[Q_{CCS}(Q_{SI} + Q_{REC}) + (Q_{SI} + Q_{REC} + Q_{PORV})Q_{AFWS}]Q_{CS}$$

$$\phi_{2RW} = \lambda_{Fire}\,[Q_{EP} + Q_{SW}Q_{CS} + Q_{CCS}Q_{CF}Q_{CS} + (Q_{SI} + Q_{REC} + Q_{PORV})Q_{AFWS}Q_{CF}Q_{CS}]$$

The contribution from each fire zone to the frequencies of core melt and release categories are calculated using the above formulations. The fire zones and the safety components contained within them are taken from Reference 7.3-1. The mean of the frequency of λ_{Fire} is conservatively taken as 10^{-3} for each fire zone in the primary auxiliary building (PAB), the fan house (FH), the control building, and the containment. For those areas in which the core melt and damage state frequencies are found to be significant, this mean frequency is reevaluated using distributions of the frequency of fires in the overall building and the fraction of those fires occurring in the specific area.

Table 7.3.2A-21 gives the results and input information for core melt and damage state calculations. All fire zones containing safety related components are addressed. The details of some of the calculations are highlighted hereafter.

7.3.2A.5.2 Fire Zone 1, CCS Pump Room

Fire zone 1 is located at Elevation 41' of the PAB. The three component cooling pumps are installed in this area. The frequency of failure of all three pumps due to a fire incident, λ_{Fire}, is shown as a fraction of auxiliary building fires

$$\lambda_{Fire} = \lambda_{AUX} f_1$$

In Section 7.3.2, we find:

$$\lambda_{AUX,05} = 0.015\ ry^{-1}$$

$$\lambda_{AUX,50} = 0.033\ ry^{-1}$$

$$\lambda_{AUX,95} = 0.053\ ry^{-1}$$

$$\alpha_{\lambda_{AUX}} = 0.034\ ry^{-1}$$

The fraction f_1 is the fraction of auxiliary building fires that may occur in fire zone 1 and be of sufficient severity to fail all three component cooling system pumps. This fraction is evaluated judgmentally

based on the experience gained in doing the analysis for Section 7.3. The three pumps are separated from each other by at least 10 feet. The conduits containing their power cables penetrate through the wall that is shared with fire zone 58A at elevations close to the ceiling. Only an extremely large fire can fail all three power cables inside the conduits. For this reason, f_1 is chosen to be rather small. It is chosen to be lognormally distributed with the following characteristic values:

$$f_{1,05} = 1.0 \times 10^{-4}$$

$$f_{1,50} = 1.0 \times 10^{-3}$$

$$f_{1,95} = 1.0 \times 10^{-2}$$

$$\alpha_{f_1} = 2.7 \times 10^{-3}$$

The product of these two distributions, λ_{Fire}, which is the frequency of fires in fire zone 1 that would fail all three CCS pumps, yields the following characteristic values (per reactor year):

$$\lambda_{Fire,05} = 3.2 \times 10^{-6}$$

$$\lambda_{Fire,50} = 3.8 \times 10^{-5}$$

$$\lambda_{Fire,95} = 3.4 \times 10^{-4}$$

$$\alpha_{\lambda_{Fire}} = 9.1 \times 10^{-5}$$

This frequency can be compared with the frequency of large fires at the critical locations in the upper tunnel and the switchgear room. The mean frequencies per Section 7.3.2 of the first area (i.e., the upper tunnel) is 3.2×10^{-5} and the mean frequency of the second area is 1.3×10^{-4} per reactor year.

The mean unavailabilities of the mitigating systems are taken from Section 1.6.2. The formulas given in Section 7.3.2A.5.1 are used to evaluate the core melt and other plant damage states.

7.3.2A.5.3 Fire Zone 7A, Lower Tunnel

The conditions in this fire zone are very similar to those of fire zone 60A, the upper tunnel. The latter was analyzed in Section 7.3.2. It is deemed that the same frequency of fires and conditional frequency of fire propagation applies here. From that section, we can write

$$\lambda_{Fire} = \lambda_{AUX} f_T f_A Q(\tau_A)$$

where

f_T ≡ fraction of auxiliary building fires that may occur in the lower electrical tunnel.

f_A ≡ fraction of lower tunnel fires that may occur in the aisle and are sufficiently large to affect both tray stacks.

$Q(\tau_A)$ ≡ fraction of large aisle fires that will not be extinguished before vital cables are damaged.

These parameters are quantified in Section 7.3.2 and a summary of their characteristic values are given in Table 7.3.2A-21. The product of these distributions yield the following characteristic values for λ_{Fire} (per reactor year).

$$\lambda_{Fire,05} = 1.0 \times 10^{-8}/ry^{-1}$$

$$\lambda_{Fire,50} = 3.1 \times 10^{-6}/ry^{-1}$$

$$\lambda_{Fire,95} = 7.0 \times 10^{-5}/ry^{-1}$$

$$\alpha_{\lambda_{Fire}} = 3.2 \times 10^{-5}/ry^{-1}$$

7.3.2A.5.4 Fire Zone 15, Control Room

The control room is directly above the cable spreading room and contains the control and instrumentation cables, controls, and readouts of virtually all the systems of the plant. There are no power cables in the area. The area is manned continuously. The fire suppression system for the area consists of hose stations adjacent to the zone. The operators also have access to breathing apparatus that can be used in case of smoke in the area.

The most critical area within the control room is the control cabinet of safety components (cabinet numbers SB1 and SB2) which are directly above the critical area in the cable spreading room that was analyzed in Section 7.3.2. A fire in these cabinets would have the same impact on plant safety as a cable spreading room fire at the center of the northern wall. However, in this case, the operators would detect the fire almost immediately and attempt to extinguish it in a short period of time. Also, the transient fuels in the control room are judged to be significantly less than the cable spreading room. Not all control room fires would lead to the evacuation of the area because operators can wear breathing apparatus and the control room air can be purged, to some extent, by shutting down the air conditioning system and using the toilet and locker area exhaust system.

Fires affecting cabinets other than those controlling the safety components (i.e., SB1 and SB2) will not have severe impact on the plant's safety margin. A fire affecting SB1 and SB2 will result in accident sequences similar to those analyzed for cable spreading room fires in Section 7.3.2.2.4. It is judged that the frequency of core melt or other damage states from control room fires is just a fraction of the frequency of the same state from cable spreading room fires. This fraction, f_{CR}, is judged to have the following histogram:

f_{CR}	Probability	Cumulative Probability
0.01	0.05	0.05
0.03	0.20	0.25
0.10	0.25	0.50
0.30	0.25	0.75
0.75	0.20	0.95
1.00	0.05	1.00

The mean of this distribution is 0.31. For example, the core melt frequency from control room fires is obtained from

$$\phi_{CM,CR} = f_{CR}\phi_{CM,CSR}$$

where

$\phi_{CM,CSR}$ = core melt frequency from cable spreading room fires.

The mean frequencies are given in Table 7.3.2A-21.

7.3.2A.5.5 Fire Zone 17A, Corridor

This corridor at Elevation 55' of the primary auxiliary building contains the safety related motor control centers 36A and 36B. The controls of all safety related motor-operated valves pass through these motor control centers. It is a controlled access area. Considering the frequency of fires in other areas and the fire propagation analysis performed for other areas, the frequency of failing both of the motor control centers is written as

$$\lambda_{Fire} = \lambda_{AUX} f_{17A} f_{PF}$$

where

λ_{AUX} = frequency of auxiliary building fires.

f_{17A} = the fraction of auxiliary building fires that may occur at the motor control center area.

f_{PF} = the fraction of motor control center area fires that may occur between the two safety cabinets and be large enough to fail both of them.

The fraction, f_{17A}, of auxiliary building fires in the motor control center area is assessed by comparing two similar parameters for the switchgear area, f_{SWG}, and electrical tunnel area, f_T, of Section 7.3.2. The probability distribution of f_{17A} is lognormal and has the following characteristic values:

$$f_{17A,05} = 0.03$$

$$f_{17A,50} = 0.1$$

$$f_{17A,95} = 0.3$$

$$\alpha_{f_{17A}} = 0.12$$

The fraction, f_{PF}, of motor control center fires that may occur between the two cabinets and be large enough to cause damage to both of them is assessed by comparing similar frequencies for cable spreading room fires, f_{es}; for the electrical tunnel fires, f_R; and switchgear room fires, f_{SL} of Section 7.3.1. The probability distribution of f_{PF} is lognormal and has the following characteristic values:

$$f_{PF,05} = 2.0 \times 10^{-3}$$

$$f_{PF,50} = 2.0 \times 10^{-2}$$

$$f_{PF,95} = 2.0 \times 10^{-7}$$

$$\alpha_{f_{PF}} = 5.3 \times 10^{-2}$$

The frequency of fires in fire zone 17A is computed by using probabilistic arithmetic. The resulting distribution has the following characteristic values (per reactor year):

$$\lambda_{Fire,05} = 4.9 \times 10^{-6}$$

$$\lambda_{Fire,50} = 6.9 \times 10^{-5}$$

$\lambda_{Fire,95} = 8.2 \times 10^{-4}$

$\alpha_{\lambda_{Fire}} = 2.2 \times 10^{-4}$

Since the PORV block valves are normally closed and are powered from these motor control centers, it is assumed that their control and motive power will be lost and, therefore, they will fail closed. It is also assumed that the CCS, AFW, electric power, and service water systems will not be adversely affected by the fire. This is because CCS and service water are normally in operation, their valves would fail as they are, and the pumps would not be affected by the fire. The AFW valves fail open upon loss of power and the pump controls would not be affected by the motor control center failure. The electric power is very likely to continue to provide power to the switchgears. It is assumed that SI and recirculation unavailability would increase significantly. Even if they become unity, their impact on the frequency of core melt from fires in zone 17A would be insignificant because they will be dominated either by PORV unavailability (in the case of transients) or SW unavailability (in the case of a small LOCA).

7.3.2A.5.6 Fire Zone 23, Auxiliary Feedwater Pump Room

The power and control cables of all three AFWS trains are located in fire zone 23. A sufficiently severe fire in this zone can disable the AFWS for at least several hours. This fire would not lead to any initiating event unless the operators chose to shut down the plant. They can initiate an orderly shutdown or turbine-generator runback using the condensate pumps and the main feedwater pumps, and remove the decay heat through the main condenser. This mode of operation can continue for a very long time.

The unreliability of the condensate and main feedwater system, Q_{MF}, has not been analyzed in Section 7.3.2. In none of the accident sequences was credit given to its availabilty. It is deemed conservatively that its unreliability is equal to the unreliability of the turbine-driven pump train of the AFWS. Its characteristic values are:

$Q_{MF,05} = 5.35 \times 10^{-3}$

$Q_{MF,50} = 1.15 \times 10^{-2}$

$Q_{MF,95} = 3.07 \times 10^{-2}$

$\alpha_{Q_{MF}} = 1.57 \times 10^{-2}$

The frequency of a large fire failing all three pumps in this fire zone is a fraction of the auxiliary building fires.

$\lambda_{Fire} = \lambda_{AUX} f_{23}$

The fraction f_{23} is the fraction of auxiliary building fires that may occur in fire zone 23 and be of sufficient severity to fail all three AFWS pumps. This fraction is evaluated judgmentally based on the experience gained in doing the analysis for Section 7.3.2. It is chosen to be lognormally distributed with the following characteristic values:

$$f_{23,05} = 5.0 \times 10^{-4}$$

$$f_{23,50} = 5.0 \times 10^{-3}$$

$$f_{23,95} = 5.0 \times 10^{-2}$$

$$\alpha_{f_{23}} = 1.3 \times 10^{-2}$$

The product of these two distributions, λ_{Fire}, which is the frequency of fires in fire zone 23 that would fail all three AFWS pumps, yields the following characteristic values (per reactor year):

$$\lambda_{Fire,05} = 1.6 \times 10^{-5}$$

$$\lambda_{Fire,50} = 1.9 \times 10^{-4}$$

$$\lambda_{Fire,95} = 1.7 \times 10^{-3}$$

$$\alpha_{\lambda_{Fire}} = 4.4 \times 10^{-4}$$

7.3.2A.5.7 Fire Zone 58A, Piping Tunnel

Reference 7.3-1 indicates that the power cables of all component cooling pumps and all charging pumps are run through fire zone 58A. These cables are actually inside conduits that are imbedded inside the concrete slab of the ceiling. A fire within zone 58A cannot affect these cables unless it is severe enough to raise the temperature within the ceiling well above 500°F. It is deemed that this type of fire is very unlikely and its effect is dominated by fires in zone 1. Fire zone 1 contains cables identical to fire zone 58A.

7.3.2A.5.8 Fire Zone 73A, The Electrical Penetration Area

Fire zone 73A is the electrical penetration area at Elevation 46' of the fan house. It is the far end of the electrical tunnels. The cable trays of this area are stacked in a fashion similar to the electrical tunnels. The control cables for the auxiliary feedwater pumps and their regulating valves, the power cables for the containment fan coolers, and

the power and control cables for the PORVs and their associated block valves are located in this area. These conditions are similar to those of the upper electrical tunnel, except that the power cables of the safety injection pumps, and of several other pumps, do not run through this area. Therefore, the frequency of fires, λ_{Fire}, that may fail a vital set of cables is derived using results from the electrical tunnel analysis part of the IPPSS. We write

$$\lambda_{Fire} = \lambda_{AUX} f_T Q(\tau_V)$$

where

f_T = the fraction of auxiliary building fires that may occur in fire zone 73A (this is defined in Section 7.3.2.3.1 for the upper electrical tunnel).

$Q(\tau_V)$ = the fraction of fires in fire zone 73A that are not extinguished in time to prevent vital component failures (derived in Section 7.2.2.3.2.4).

In Section 7.3.2.3.1, we find:

$$f_{T,05} = 8.0 \times 10^{-3}$$

$$f_{T,50} = 4.0 \times 10^{-2}$$

$$f_{T,95} = 2.0 \times 10^{-7}$$

$$\alpha_{f_T} = 6.5 \times 10^{-2}$$

In Section 7.2.2.3.2.4, we find:

$$Q_{05}(\tau_V) = 1.0 \times 10^{-2}$$

$$Q_{50}(\tau_V) = 0.45$$

$$Q_{95}(\tau_V) = 0.90$$

$$\alpha_{Q(\tau_V)} = 0.44$$

The product of these distributions yields the following characteristic values for λ_{Fire} (per reactor year):

$$\lambda_{Fire,05} = 6.7 \times 10^{-6}$$

$$\lambda_{Fire,50} = 4.6 \times 10^{-4}$$

$$\lambda_{Fire,95} = 3.6 \times 10^{-3}$$

$$\alpha_{\lambda_{Fire}} = 9.7 \times 10^{-4}$$

7.3.2A.5.9 Fire Zone 75A, Outer Annulus of Containment

Fire zone 75A is the outer annulus of the containment at Elevation 46'. It contains the power and control cables for the PORVs and their block valves and the power cables of all fan cooling units. The frequency of fire, λ_{Fire}, that may occur in this area and fail the power cables to all the fan coolers and PORVs is written as

$$\lambda_{Fire} = \lambda_{CON} f_{75A}$$

where

λ_{CON} = the frequency of fires in the containment.

f_{75A} = the fraction of containment fires that may occur in area 75A and fail the previously listed components.

The frequency of containment fires is taken from Reference 7.3-3. A lognormal distribution is fitted to the upper and lower bounds reported in that reference to simplify the quantification process. The characteristic values of λ_{CON} are (per reactor year):

$$\lambda_{CON,05} = 6.2 \times 10^{-3}$$

$$\lambda_{CON,50} = 1.3 \times 10^{-2}$$

$$\lambda_{CON,95} = 2.8 \times 10^{-2}$$

$$\alpha_{\lambda_{CON}} = 1.5 \times 10^{-2}$$

The fraction, f_{75A}, of containment fires occurring in fire zone 75A and failing the previously listed components is assessed by comparing two similar parameters for the switchgear area, f_{SWG}, and the electrical tunnel area, f_T, of Section 7.3.2. It should be added that all the containment fires involved reactor coolant pumps. The probability distribution of f_{75A} is chosen to be lognormal with the following characteristic values:

$$f_{75A,05} = 4.0 \times 10^{-3}$$

$$f_{75A,50} = 2.0 \times 10^{-2}$$

$f_{75A,95} = 1.0 \times 10^{-1}$

$\alpha_{f_{75A}} = 3.2 \times 10^{-2}$

TABLE 7.3.2-1

HISTOGRAM OF THE MEAN EXTINGUISHING TIME FOR LARGE FIRES

τ_s (min)	Probability	Cumulative Probability
15	0.40	0.40
30	0.30	0.70
60	0.20	0.90
120	0.10	1.00

TABLE 7.3.2-2

HISTOGRAM OF THE MEAN EXTINGUISHING TIME FOR CABLE TRAY FIRES

τ_s (min)	Probability	Cumulative Probability
5	0.4	0.4
15	0.3	0.7
30	0.2	0.9
60	0.1	1.0

TABLE 7.3.2-3

HISTOGRAM OF THE FREQUENCY OF CONTAINMENT EVENT TREE ENTRY STATE TEFC OR CONTAINMENT EVENT TREE ENTRY STATE 8B FROM A FIRE AT THE CENTER OF THE NORTHERN WALL

ϕTEFC,CC,ϕ8B (ry^{-1})	Probability	Cumulative Probability
1.9×10^{-10}	.047	.047
1.1×10^{-9}	.053	.100
2.4×10^{-9}	.046	.146
4.7×10^{-9}	.050	.197
7.8×10^{-9}	.047	.244
1.2×10^{-8}	.052	.296
1.9×10^{-8}	.051	.347
2.8×10^{-8}	.048	.394
4.1×10^{-8}	.053	.447
6.0×10^{-8}	.045	.492
8.2×10^{-8}	.052	.544
1.2×10^{-7}	.048	.593
1.7×10^{-7}	.053	.646
2.5×10^{-7}	.050	.696
3.5×10^{-7}	.054	.750
5.3×10^{-7}	.049	.799
8.4×10^{-7}	.048	.847
1.4×10^{-6}	.053	.899
4.0×10^{-6}	.046	.945
2.2×10^{-5}	.055	1.000

TABLE 7.3.2-4

HISTOGRAM OF THE FREQUENCY OF CONTAINMENT EVENT TREE ENTRY STATE TE FROM A FIRE AT THE CENTER OF THE NORTHERN WALL

$\phi_{TE,CC}$ (ry^{-1})	Probability	Cumulative Probability
2.9×10^{-11}	.044	.044
1.2×10^{-10}	.054	.098
2.9×10^{-10}	.050	.147
5.4×10^{-10}	.047	.194
9.0×10^{-10}	.050	.244
1.5×10^{-9}	.050	.294
2.3×10^{-9}	.050	.343
3.4×10^{-9}	.052	.395
5.0×10^{-9}	.050	.445
7.2×10^{-9}	.051	.495
1.1×10^{-8}	.054	.550
1.5×10^{-8}	.044	.593
2.2×10^{-8}	.050	.643
3.2×10^{-8}	.052	.695
4.7×10^{-8}	.045	.740
7.3×10^{-8}	.057	.797
1.2×10^{-7}	.050	.847
2.3×10^{-7}	.053	.900
5.9×10^{-7}	.044	.943
4.3×10^{-6}	.057	1.000

TABLE 7.3.2-5

HISTOGRAM OF THE FREQUENCY OF CONTAINMENT EVENT TREE ENTRY STATE SE FROM A FIRE AT THE POWER CABLES IN THE CABLE SPREADING ROOM

$\phi_{SE,PC}$ (ry^{-1})	Probability	Cumulative Probability
3.6×10^{-8}	.049	.049
9.2×10^{-8}	.048	.098
2.0×10^{-7}	.052	.149
4.1×10^{-7}	.050	.200
7.1×10^{-7}	.048	.247
1.1×10^{-6}	.050	.298
1.6×10^{-6}	.050	.348
2.3×10^{-6}	.048	.394
3.1×10^{-6}	.052	.448
4.1×10^{-6}	.050	.498
5.5×10^{-6}	.051	.549
7.6×10^{-6}	.049	.599
1.0×10^{-5}	.049	.648
1.4×10^{-5}	.049	.694
1.9×10^{-5}	.051	.748
2.5×10^{-5}	.051	.799
3.4×10^{-5}	.048	.844
4.6×10^{-5}	.051	.898
7.5×10^{-5}	.051	.949
2.1×10^{-4}	.051	1.000

TABLE 7.3.2-6

HISTOGRAM OF THE FREQUENCY OF CONTAINMENT EVENT TREE ENTRY STATE TE FROM A FIRE IN FIRE ZONE 60A

$\phi_{TE,60A}$ (ry^{-1})	Probability	Cumulative Probability
2.3×10^{-11}	.048	.048
9.9×10^{-11}	.046	.093
2.9×10^{-10}	.055	.148
6.3×10^{-10}	.051	.200
1.2×10^{-9}	.048	.247
2.0×10^{-9}	.045	.292
3.2×10^{-9}	.052	.344
5.3×10^{-9}	.055	.399
8.4×10^{-9}	.045	.444
1.3×10^{-8}	.054	.498
2.0×10^{-8}	.046	.544
3.1×10^{-8}	.053	.596
4.8×10^{-8}	.053	.650
7.3×10^{-8}	.049	.693
1.0×10^{-7}	.042	.740
1.6×10^{-7}	.055	.796
2.7×10^{-7}	.054	.850
5.1×10^{-7}	.049	.899
1.2×10^{-6}	.050	.949
1.3×10^{-5}	.051	1.000

TABLE 7.3.2-7/8

HISTOGRAM OF THE FREQUENCY OF CONTAINMENT EVENT TREE ENTRY STATE SE FROM A FIRE IN THE SWITCHGEAR ROOM

$\Phi_{SE,4}$ (ry^{-1})	Probability	Cumulative Probability
3.1×10^{-8}	.049	.049
1.0×10^{-7}	.050	.099
2.2×10^{-7}	.051	.150
3.8×10^{-7}	.048	.198
6.5×10^{-7}	.050	.248
1.2×10^{-6}	.052	.300
2.0×10^{-6}	.048	.348
3.4×10^{-6}	.050	.398
5.1×10^{-6}	.051	.449
7.0×10^{-6}	.051	.500
9.0×10^{-6}	.048	.548
1.2×10^{-5}	.052	.600
1.5×10^{-5}	.050	.650
1.9×10^{-5}	.050	.700
2.5×10^{-5}	.051	.751
3.3×10^{-5}	.050	.801
4.6×10^{-5}	.045	.846
7.3×10^{-5}	.052	.898
1.6×10^{-4}	.052	.950
9.9×10^{-4}	.050	1.000

TABLE 7.3.2-9

HISTOGRAM OF THE FREQUENCY OF CONTAINMENT EVENT TREE ENTRY STATE TE FROM A FIRE IN INDIAN POINT 3

Φ_{TE} (ry^{-1})	Probability	Cumulative Probability
5.9×10^{-10}	.050	.050
2.0×10^{-9}	.049	.099
4.0×10^{-9}	.051	.150
6.6×10^{-9}	.049	.199
1.0×10^{-8}	.051	.250
1.5×10^{-8}	.048	.298
2.1×10^{-8}	.051	.349
2.4×10^{-8}	.050	.399
4.0×10^{-8}	.050	.449
5.3×10^{-8}	.050	.499
7.2×10^{-8}	.049	.548
8.6×10^{-8}	.051	.599
1.2×10^{-7}	.051	.650
1.8×10^{-7}	.049	.699
2.3×10^{-7}	.050	.749
4.0×10^{-7}	.051	.800
5.7×10^{-7}	.048	.848
1.2×10^{-6}	.051	.899
4.4×10^{-6}	.051	.950
1.3×10^{-5}	.050	1.000

TABLE 7.3.2-10

HISTOGRAM OF THE FREQUENCY OF CONTAINMENT EVENT TREE ENTRY STATE SE FROM A FIRE IN INDIAN POINT 3

Φ_{SE} (ry^{-1})	Probability	Cumulative Probability
4.4×10^{-7}	.049	.049
1.4×10^{-6}	.050	.099
2.8×10^{-6}	.050	.149
4.5×10^{-6}	.050	.199
6.5×10^{-6}	.050	.249
8.8×10^{-6}	.050	.299
1.1×10^{-5}	.050	.349
1.4×10^{-5}	.049	.398
1.8×10^{-5}	.052	.450
2.2×10^{-5}	.049	.499
2.6×10^{-5}	.051	.550
3.2×10^{-5}	.050	.600
3.8×10^{-5}	.049	.649
4.7×10^{-5}	.048	.697
5.7×10^{-5}	.052	.749
7.5×10^{-5}	.049	.798
9.2×10^{-5}	.050	.848
2.7×10^{-4}	.051	.899
2.3×10^{-6}	.050	.949
1.0×10^{-3}	.051	1.000

TABLE 7.3.2-11

HISTOGRAM OF THE FREQUENCY OF
RELEASE CATEGORY 2RW

Φ2RW (ry^{-1})	Probability	Cumulative Probability
6.9×10^{-7}	.049	.049
1.9×10^{-6}	.050	.099
3.5×10^{-6}	.049	.148
5.4×10^{-6}	.050	.198
7.5×10^{-6}	.050	.248
1.0×10^{-5}	.050	.298
1.3×10^{-5}	.050	.348
1.6×10^{-5}	.050	.398
1.9×10^{-5}	.051	.449
2.3×10^{-5}	.050	.499
2.7×10^{-5}	.051	.550
3.3×10^{-5}	.050	.600
3.9×10^{-5}	.050	.650
4.8×10^{-5}	.049	.699
5.8×10^{-5}	.051	.750
7.6×10^{-5}	.051	.801
7.3×10^{-5}	.051	.849
1.7×10^{-4}	.051	.900
2.2×10^{-4}	.050	.950
1.0×10^{-3}	.050	1.000

TABLE 7.3.2-12

HISTOGRAM OF THE FREQUENCY OF CORE MELT

Φ_{CM} (ry^{-1})	Probability	Cumulative Probability
1.2×10^{-6}	.048	.048
2.7×10^{-6}	.049	.097
4.5×10^{-6}	.050	.147
6.6×10^{-6}	.050	.197
9.2×10^{-6}	.050	.247
1.2×10^{-5}	.052	.299
1.5×10^{-5}	.050	.349
1.9×10^{-5}	.048	.397
2.2×10^{-5}	.050	.447
2.7×10^{-5}	.050	.497
3.1×10^{-5}	.050	.547
3.7×10^{-5}	.050	.597
4.3×10^{-5}	.050	.647
5.2×10^{-5}	.052	.699
6.2×10^{-5}	.049	.748
7.9×10^{-5}	.050	.798
9.6×10^{-5}	.049	.847
1.7×10^{-4}	.052	.899
2.4×10^{-4}	.050	.949
1.0×10^{-3}	.051	1.000

TABLE 7.3.2A-13

CHARACTERISTIC VALUES OF THE FREQUENCIES OF RELEASE CATEGORIES AND CORE MELT DUE TO FIRE AFTER THE APPENDIX R MODIFICATON TO INDIAN POINT 3

Description	Percentile	Annual Frequency			
		Core Melt	8B	8A	2RW
Avenue 2 of Appendix R - Alternate Feeds and Transfer Switches for One Backup SWS Pump, One CCS Pump, and One Charging Pump and Power Supply of Vital Instrumentation	5th Median 95th Mean	1.7-5 7.1-6 4.8-5 1.4-5	2.7-7 2.6-6 2.5-5 6.7-6	5.3-11 7.7-10 9.4-9 3.4-9	5.7-7 3.0-6 2.6-6 6.8-6

Note: Exponential notation is indicated in abbreviated form; i.e., 5.5-6 = 5.5×10^{-6}.

TABLE 7.3.2A-14

MEAN FREQUENCIES OF FIRE CONTRIBUTORS FOR INDIAN POINT 3 BEFORE THE MODIFICATION

Fire Zone	CM	SEFC	SEC	SEF	SE	TEFC	TEC	TEF	TE	8B	8A	2RW
SWG 14	7.1-5	--	--	--	7.1-5	--	--	--	--	--	--	7.1-5
CSR 11cc	1.9-6	--	--	--	--	1.6-6	--	--	2.9-7	1.6-6	--	2.0-7
CSR 11pc	2.4-5	--	--	--	2.4-5	--	--	--	--	--	--	2.4-5
AFW 23	3.7-6	--	--	--	--	3.7-6	2.3-12	1.2-10	7.3-17	3.7-6	1.2-10	7.3-17
CCS 1	3.8-7	3.8-7	7.6-9	1.1-11	1.9-12	1.1-11	7.0-18	3.4-16	2.2-22	3.8-7	1.1-11	1.9-12
Upper Tunnel 60A	7.4-7	--	--	--	--	--	--	--	7.4-7	--	--	7.4-7
Control Room 15	5.7-7	--	--	--	--	4.8-7	--	--	8.9-8	4.8-7	--	8.9-8
Electric Penet. 73A	1.8-7	--	8.3-8	--	2.3-11	--	9.7-8	--	4.6-13	9.8-8	--	2.3-11
RCP Area 70A	4.7-8	5.2-12	4.0-8	1.6-16	1.1-11	7.1-9	4.4-15	2.2-13	1.4-19	4.7-8	2.2-13	1.1-11
RCP Area 71A	4.7-8	5.2-12	4.0-8	1.6-16	1.1-11	7.1-9	4.4-15	2.2-13	1.4-19	4.7-8	2.2-13	1.1-11
RCP Area 78A	4.7-8	5.2-11	4.0-8	1.6-15	1.1-11	7.1-9	4.4-15	2.2-13	1.4-19	4.7-8	2.2-13	1.1-11
Outer Annulus 75A	4.7-8	--	4.0-8	--	1.1-11	--	7.1-9	--	2.2-13	4.7-8	--	1.1-11
Outer Annulus 77A	4.0-8	5.2-12	4.0-8	1.6-16	1.1-11	7.1-10	2.0-14	2.2-14	6.1-19	4.0-8	2.2-14	1.1-11
SI Pump 9	4.5-8	4.8-11	3.8-8	1.5-15	1.0-11	6.6-9	4.2-15	2.1-13	1.3-19	4.5-8	2.1-13	1.0-11
Piping Penet. 59A	4.5-8	4.8-11	3.8-8	1.5-15	1.0-11	6.6-9	4.2-15	2.1-13	1.3-19	4.5-8	2.1-13	1.0-11
Makeup Pump Room 2A	3.8-8	--	--	1.8-13	3.8-8	--	--	5.5-11	3.5-17	--	5.5-11	3.8-8
Corridor 4A	3.8-8	3.4-12	3.8-8	1.1-16	8.8-12	5.6-11	3.5-17	1.7-15	1.1-21	3.8-8	1.8-15	8.8-12
Corridor 12A	3.8-8	1.4-10	3.8-8	4.3-15	9.6-12	5.6-11	3.5-17	1.7-15	1.1-21	3.8-8	6.-15	9.6-12
MCC Area 17A	2.1-8	--	--	1.5-11	1.9-8	--	--	3.3-9	2.1-15	--	3.3-9	1.9-8
Lower Tunnel 7A	6.3-9	2.4-13	2.8-9	7.5-18	7.3-13	3.5-9	3.9-11	1.1-13	1.2-15	6.3-9	1.1-13	7.3-13
Total	1.0-4	3.8-7	4.4-7	2.6-11	9.5-5	5.8-6	1.0-7	3.5-9	1.1-6	6.7-6	3.4-9	9.6-5

Note: Exponential notation is indicated in abbreviated form; i.e., 7.1-5 = 7.1×10^{-5}.

TABLE 7.3.2A-15

MEAN FREQUENCIES OF FIRE CONTRIBUTORS AFTER APPENDIX R MODIFICATION IS IMPLEMENTED

Fire Zone	CM	SEFC	SEC	SEF	SE	TEFC	TEC	TEF	TE	8B	8A	2RW	Impact of Modification
SWG 14	4.4-6	--	--	--	3.3-6*	--	--	--	1.1-6*	--	--	4.4-6	Affected
CSR 11cc	1.9-6	--	--	--	--	1.6-6*	--	--	2.9-7*	1.6-6	--	2.0-7	Minor Impact
CSR 11pc	1.3-6	--	--	--	1.1-6*	--	--	--	1.8-7*	--	--	1.3-6	Affected
AFW 23	3.7-6	--	--	--	--	3.7-6	2.3-12	1.2-10*	7.3-17	3.7-6	1.2-10	7.3-17	No Effect
CCS 1	3.8-7	3.8-7*	7.6-9	1.1-11	1.9-12	1.1-11	7.0-18	3.4-16	2.2-22	3.8-7	1.1-11	1.9-12	No Effect
Upper Tunnel 60A	7.4-7	--	--	--	--	--	--	--	7.4-7*	--	--	7.4-7	Minor Impact
Control Room 15	5.7-7	--	--	--	--	4.8-7*	--	--	8.9-8*	4.8-7	--	8.9-8	Minor Impact
Electric Penetration 73A	1.8-7	--	8.3-8*	--	2.3-11	--	9.7-8*	--	4.6-13	9.8-8	--	2.3-11	Minor Impact
RCP Area 70A	4.7-8	5.2-12	4.0-8*	1.6-16	1.1-11	7.1-9	4.4-15	2.2-13	1.4-19	4.7-8	2.2-13	1.1-11	No Effect
RCP Area 71A	4.7-8	5.2-12	4.0-8	1.6-16	1.1-11	7.1-9	4.4-15	2.2-13	1.4-19	4.7-8	2.2-13	1.1-11	No Effect
RCP Area 78A	4.7-8	5.2-11	4.0-8	1.6-15	1.1-11	7.1-9	4.4-15	2.2-13	1.4-19	4.7-8	2.2-13	1.1-11	No Effect
Outer Annulus 75A	4.7-8	--	4.0-8*	--	1.1-11	--	7.1-9*	--	2.2-13	4.7-8	--	1.1-11	No Effect
Outer Annulus 77A	4.0-8	5.2-12	4.0-8*	1.6-16	1.1-11	7.1-10	2.0-14	2.2-14	6.1-19	4.0-8	2.2-14	1.1-11	No Effect
SI Pump 9	4.5-8	4.8-11	3.8-8	1.5-15	1.0-11	6.6-9	4.2-15	2.1-13	1.3-19	4.5-8	2.1-13	1.0-11	No Effect
Piping Penetration 59A	4.5-8	4.8-11	3.8-8	1.5-15	1.0-11	6.6-9	4.2-15	2.1-13	1.3-19	4.5-8	2.1-13	1.0-11	No Effect
Makeup Pump Room 2A	3.8-8	--	--	1.8-13	3.8-8	--	--	5.5-11	3.5-17	--	5.5-11	3.8-8	No Effect
Corridor 4A	3.8-8	3.4-12	3.8-8	1.1-16	8.8-12	5.6-11	3.5-17	1.7-15	1.1-21	3.8-8	1.8-15	8.8-12	Assumed No Effect
Corridor 12A	3.8-8	1.4-10	3.8-8	4.3-15	9.6-12	5.6-11	3.5-17	1.7-15	1.1-21	3.8-8	6.-15	9.6-12	Minor Impact
MCC Area 17A	2.1-8	--	--	1.5-11	1.9-8*	--	--	3.3-9*	2.1-15	--	3.3-9	1.9-8	No Effect
Lower Tunnel 7A	6.3-9	2.4-13	2.8-9	7.5-18	7.3-13	3.5-9	3.9-11	1.1-13	1.2-15	6.3-9	1.1-13	7.3-13	Assumed No Effect
Total	1.4-5	3.8-7	4.4-7	2.6-11	4.5-6	5.8-6	1.0-7	3.5-9	2.4-6	6.7-6	3.4-9	6.8-6	

*The probability distribution of this frequency has been quantified.

Note: Exponential notation is indicated in abbreviated form; i.e., 7.1-5 = 7.1×10^{-5}.

TABLE 7.3.2A-16

FREQUENCIES OF SEVERAL PARAMETERS USED IN THE STUDY

Parameter	Distribution	Mean	Variance	Source
Q_{SW}	Lognormal	1.33-3	5.57-6	Table 1.6.1-4, Item 29
$Q_{CCS,D}$	Lognormal	1.36-3	1.22-6	Table 1.6.1-4, Item 11
λ_{CCS}	Lognormal	3.26-6 per hour	2.47-11 per hour	Table 1.6.1-4, Item 15
$Q_{CCS,M}$	Lognormal	4.92-3	8.23-8	Table 1.6.1-13 Approximation Techniques, T_M = 394.0, T_{comp} = 59760.0
λ_{LOP}	Lognormal	3.0-5 per hour	6.0-10 per hour	Table 1.61-31, Item 116
$Q_{LOP/TT}$	Lognormal	3.4-4	3.3-5	Section 1.6.2.2
$Q_{TD,D}$	Lognormal	4.5-3	3.7-5	Table 1.6.2.3.9.7F
$Q_{TD,M}$	Lognormal	4.2-3	4.3-7	Table 1.6.2.3.9-13
$Q_{TD2,HE}$	Discretized	4.4-2	———	Page 1.6-883

Note: Exponential notation is indicated in abbreviated form; i.e., 1.33-3 = 1.33×10^{-3}.

TABLE 7.3.2A-17

HISTOGRAM OF THE FREQUENCY OF CORE MELT IN INDIAN POINT 3 DUE TO FIRE AFTER THE MODIFICATION

Φ_{CM} (ry^{-1})	Probability	Cumulative Probability
7.6×10^{-7}	.009	.009
1.4×10^{-6}	.038	.047
1.7×10^{-6}	.004	.051
2.1×10^{-6}	.055	.106
2.7×10^{-6}	.060	.166
3.3×10^{-6}	.054	.220
4.0×10^{-6}	.067	.287
4.6×10^{-6}	.054	.341
5.9×10^{-6}	.149	.490
7.0×10^{-6}	.008	.498
7.1×10^{-6}	.003	.501
8.8×10^{-6}	.140	.641
1.2×10^{-5}	.064	.705
1.4×10^{-5}	.066	.771
1.9×10^{-5}	.060	.831
2.3×10^{-5}	.059	.880
3.7×10^{-5}	.060	.950
4.8×10^{-5}	.003	.953
6.8×10^{-5}	.037	.990
1.3×10^{-4}	.010	1.000

TABLE 7.3.2A-18

HISTOGRAM OF RELEASE CATEGORY 8B
IN INDIAN POINT 3 DUE TO FIRE

Φ_{8B} (ry^{-1})	Probability	Cumulative Probability
9.2×10^{-8}	.009	.009
1.9×10^{-7}	.037	.046
2.7×10^{-7}	.003	.049
3.5×10^{-7}	.058	.107
5.3×10^{-7}	.055	.162
7.5×10^{-7}	.061	.223
9.6×10^{-7}	.059	.282
1.3×10^{-6}	.064	.346
1.7×10^{-6}	.146	.492
2.6×10^{-6}	.005	.497
2.6×10^{-6}	.001	.498
2.8×10^{-6}	.147	.645
4.1×10^{-6}	.062	.707
4.9×10^{-6}	.058	.765
6.7×10^{-6}	.062	.827
1.1×10^{-5}	.060	.887
1.9×10^{-5}	.060	.947
2.4×10^{-5}	.001	.948
4.6×10^{-5}	.039	.987
1.2×10^{-4}	.013	1.000

TABLE 7.3.2A-19

HISTOGRAM OF THE FREQUENCY OF RELEASE CATEGORY 8A
IN INDIAN POINT 3 DUE TO FIRE

Φ_{8A} (ry^{-1})	Probability	Cumulative Probability
1.6×10^{-11}	.009	.009
4.0×10^{-11}	.038	.047
5.5×10^{-11}	.004	.051
8.2×10^{-11}	.058	.109
1.4×10^{-10}	.061	.170
2.0×10^{-10}	.058	.228
2.6×10^{-10}	.058	.286
3.9×10^{-10}	.063	.349
5.4×10^{-10}	.141	.490
7.6×10^{-10}	.006	.496
7.8×10^{-10}	.007	.503
1.1×10^{-9}	.144	.647
1.5×10^{-9}	.059	.706
2.2×10^{-9}	.059	.765
3.1×10^{-9}	.061	.826
4.8×10^{-9}	.060	.886
8.8×10^{-9}	.058	.944
9.3×10^{-9}	.003	.947
2.4×10^{-8}	.038	.985
8.7×10^{-8}	.015	1.000

TABLE 7.3.2A-20

HISTOGRAM OF THE FREQUENCY OF RELEASE CATEGORY 2RW IN INDIAN POINT 3 DUE TO FIRE AFTER THE MODIFICATION

ϕ2RW (ry^{-1})	Probability	Cumulative Probability
2.2×10^{-7}	.009	.009
4.4×10^{-7}	.038	.047
5.7×10^{-7}	.004	.051
7.3×10^{-7}	.061	.112
1.0×10^{-6}	.059	.171
1.3×10^{-6}	.055	.226
1.5×10^{-6}	.047	.273
1.9×10^{-6}	.077	.350
2.5×10^{-6}	.140	.490
3.0×10^{-6}	.008	.498
3.1×10^{-6}	.004	.502
3.9×10^{-6}	.146	.648
5.3×10^{-6}	.056	.704
7.3×10^{-6}	.064	.768
8.9×10^{-6}	.058	.826
1.2×10^{-5}	.061	.887
1.9×10^{-5}	.061	.948
2.6×10^{-5}	.002	.950
3.3×10^{-5}	.038	.988
1.0×10^{-4}	.012	1.000

TABLE 7.3.2A-21

FIRE AREA ANALYSIS

Fire Area	Core Melt Related Components		Containment Related Components		Mean Frequency										Remarks
	Within Fire Area	Outside Fire Area	Within Fire Area	Outside Fire Area	Fire Frequency	Core Melt	SEFC	SEC	SEF	SE	TEFC	TEC	TEF	TE	
1: CCS Pump Room	CCS pumps (all) P CHG 32/33 P	SI 1.4-4 AFWS 1.5-5 EP 2.-8 SWS 8.6-5 REC 4.-3 PORV 4.3-3 CCS 1.0	--	CF (all) 6.3-7 CS (all) 3.1-5	9.1-5	3.8-7	3.8-7	7.6-9	1.1-11	1.9-12	1.1-11	7.0-18	3.4-16	2.2-22	8B = 3.8-7 8A = 1.1-11 2RW = 1.9-12 λ_{AUX} = 3.4-2 f_1 = 2.7-3
1A	--		--												
2	--	all	CS (all)	CF (all)											Part of CS system analysis (impact very small on plant risk).
2A: Primary Makeup Water Pump Room	CHG 33 P	SI 1.4-4 AFWS 1.5-5 EP 2.-8 SWS 8.6-5 REC 4.-3 PORV 4.3-3 CCS 1.1-7	CS (all) P	CF (all) 6.3-7 CS (all) 1.0	4.4-4	3.8-8	--	--	1.8-13	3.8-8	--	--	5.5-11	3.5-17	Part of CS system analysis. Impact on CS total failure very small and charging pump impact on overall risk is very small. 8B = -- 8A = 5.5-11 2RW = 3.8-8
3	RHR 31 Pump + P, 32 P		--												Part of LPIS system analysis (fire cannot lead to large LOCA).

P = power cables; C = control cables; CHG = charging pumps; CCS = component cooling system; SIS = safety injection system; AFWS = auxiliary feedwater system; EP = electric power; SWS = service water system; REC = recirculation system; PORV = PORVs and block valves; RHR = residual heat removal; MCC = motor control center.

Note: Exponential notation is indicated in abbreviated form; i.e., 8.0-5 = 8×10^{-5}.

TABLE 7.3.2A-21 (continued)

FIRE AREA ANALYSIS

Fire Area	Core Melt Related Components		Containment Related Components		Mean Frequency										Remarks
	Within Fire Area	Outside Fire Area	Within Fire Area	Outside Fire Area	Fire Frequency	Core Melt	SEFC	SEC	SEF	SE	TEFC	TEC	TEF	TE	
3A	CHR 33 P		--												Very small impact on plant risk due to CHG pump failure.
4	RHR 32 PMP + P		--												Part of LPIS system/fire cannot lead to large LOCA.
4A Corridor	CCS 31 P CHG 31 P SI 31 P RHR 31/32 P	SI 32/33 1.4-4 AFWS 1.5-5 EP 2.-8 SWS 8.6-5 REC 4.-3 PORV 4.3-3 CCS 32/33 1.8-6	--	CS (all) 3.1-5 CF (all) 6.3-7	4.4-4	3.8-8	3.4-12	3.8-8	1.1-16	8.8-12	5.6-11	3.5-17	1.7-15	1.1-21	Recirculation system unavailability does not increase significantly from RHR pump failure. 8B = 3.8-8 8A = 1.8-15 2RW = 8.8-12
5	CHG 31 PMP + P														See Area 3A.
5A	--		--												
6	CHG 32 PMP		--												See Area 3A.
6A															

P = power cables; C = control cables; CHG: charging pumps; CCS: component cooling system; SIS: safety injection system; AFWS: auxiliary feedwater system; EP: electric power; SWS: service water system; REC: recirculation system; PORV: PORVs and block valves; RHR: residual heat removal; MCC: motor control center.

Note: Exponential notation is indicated in abbreviated form; i.e., 8.0-5 = 8×10^{-5}.

TABLE 7.3.2A-21 (continued)

FIRE AREA ANALYSIS

Fire Area	Core Melt Related Components		Containment Related Components		Mean Frequency										Remarks
	Within Fire Area	Outside Fire Area	Within Fire Area	Outside Fire Area	Fire Frequency	Core Melt	SEFC	SEC	SEF	SE	TEFC	TEC	TEF	TE	
7	CHG 33 PMP + P		--												See Area 3A.
7A: Lower Tunnel	CCS 32 P RHR 31/32 P PORV P + C CHG 32 P+C AFWS C 31	SI 1.4-4 AFWS (32/33) 1.1-4 EP 2.-8 SWS 8.6-5 REC 4.-3 PORV 1.0 CCS 1.8-6	CF 34/32	CF (31,33,35) 1.1-2 CS 3.1-5	3.2-5	6.3-9	2.4-13	2.8-9	7.5-18	7.3-13	3.5-9	3.9-11	1.1-13	1.2-13	See Section 7.3.2.4.6 for frequency f_{AUX_T} = 2.2-3, f_A = 2.7-2, Q(T) = 0.6 8B = 6.3-9 8A = 1.1-13 2RW = 7.3-13
8	Boric Acid Tanks 31/32		--												Part of HPIS system; not readily susceptible to fire.
8A	--		--												
9: SI Pump Room	SI (all) P and PMP	SI 1.0 AFWS 1.5-5 EP 2.-8 SWS 8.6-5 REC 4.-3 PORV 4.3-3 CCS 1.1-7	--	CS 3.1-5 CF 6.3-7	4.4-4	4.5-8	4.8-11	3.8-8	1.5-15	1.0-11	6.6-9	4.2-15	2.1-13	1.3-19	8B = 4.5-8 8A = 2.1-13 2RW = 1.0-11
9A	RHR 31/32		--												Part of LPIS system.
10	DG 31		--												Part of EP system.

P = power cables; C = control cables; CHG = charging pumps; CCS = component cooling system; SIS = safety injection system; AFWS = auxiliary feedwater system; EP = electric power; SWS = service water system; REC = recirculation system; PORV = PORVs and block valves; RHR = residual heat removal; MCC = motor control center.

Note: Exponential notation is indicated in abbreviated form; i.e., 8.0-5 = 8×10^{-5}.

0682P110432

TABLE 7.3.2A-21 (continued)

FIRE AREA ANALYSIS

Fire Area	Core Melt Related Components		Containment Related Components		Mean Frequency										Remarks
	Within Fire Area	Outside Fire Area	Within Fire Area	Outside Fire Area	Fire Frequency	Core Melt	SEFC	SEC	SEF	SE	TEFC	TEC	TEF	TE	
10A	SI 32 P		--												Part of HPIS system.
11: CSR Center of North Wall	Control Cables					1.9-6	--	--	--	--	1.6-6	--	--	3.-7	See Section 7.3.2 of IPPSS,
Tunnel Entrance Room	Power Cables					2.4-5	--	--	--	2.4-5	--	--	--	--	p. 7.3-3.
12	Emergency Batteries		--												Part of EP System
12A: Corridor	RHR 31/32 P CHG 32 P SI 33 P CCS 31/33 P	SI 31/32 1.4-4 AFWS 1.5-5 EP 2.2-8 SWS 8.6-5 REC 4-3 PORV 4.3-3 CCS 32 8.3-5	--	CS (all) 3.1-5 CF (all) 6.3-7	4.4-4	3.8-8	1.4-10	3.8-8	4.3-15	9.6-12	5.6-11	3.5-17	1.7-15	1.1-21	8B = 3.8-8 8A = 6.0-15 2RW = 9.6-12
13	Batteries		--												Part of EP system analysis.
13A	--		--												
14: Switchgear Room						3.7-5	--	--	--	3.6-5	--	--	--	7.-7	See Section 7.3.2, of the IPPSS page 7.3-105

P = power cables; C = control cables; CHG = charging pumps; CCS = component cooling system; SIS = safety injection system; AFWS = auxiliary feedwater system; EP = electric power; SWS = service water system; REC = recirculation system; PORV = PORVs and block valves; RHR = residual heat removal; MCC = motor control center.

Note: Exponential notation is indicated in abbreviated form; i.e., 8.0-5 = 8×10^{-5}.

0623D110182

TABLE 7.3.2A-21 (continued)

FIRE AREA ANALYSIS

Fire Area	Core Melt Related Components		Containment Related Components		Mean Frequency										Remarks
	Within Fire Area	Outside Fire Area	Within Fire Area	Outside Fire Area	Fire Frequency	Core Melt	SEFC	SEC	SEF	SE	TEFC	TEC	TEF	TE	
14A	--		--												
15: Control Room	Controls of all components instrumentation	Power of all components	Controls of all components	Power of all components	See CSR study	5.7-7	--	--	--	--	4.8-7	--	--	8.9-8	Same as CSR except for power cables factor of f_{CR}, αf_{CR} = .31 f_{CR} = 0.31 introduced for human presence
15A	--		--												
16	--		--												
16A	--		--												
17	--		--												
17A MCC Area	MCCs 36A and 36B Power to All MOVs	PORV 1.0 CCS 1.1-7 AFWS 1.5-5 EP (pump power only) 2.-8 SWS 8.6-5 REC 0.6 SI 0.03	CS (MOVs)	CS 1.0 CF 6.3-7	2.2-4	2.1-8	--	--	1.5-11	1.9-8	--	--	3.3-9	2.1-15	Assumed CS not available f_{17A} factor of auxiliary building fires in 17A f_{PF}: fire large enough to fail both MCCs λ_{AUX} = 3.4-2 f_{17A} = 0.121 f_{PF} = 0.053 8B = -- 8A = 3.3-8 2RW = 1.9-8

P = power cables; C = control cables; CHG = charging pumps; CCS = component cooling system; SIS = safety injection system; AFWS = auxiliary feedwater system; EP = electric power; SWS = service water system; REC = recirculation system; PORV = PORVs and block valves; RHR = residual heat removal; MCC = motor control center.

Note: Exponential notation is indicated in abbreviated form; i.e., 8.0-5 = 8 x 10^{-5}.

TABLE 7.3.2A-21 (continued)

FIRE AREA ANALYSIS

Fire Area	Core Melt Related Components		Containment Related Components		Mean Frequency										Remarks
	Within Fire Area	Outside Fire Area	Within Fire Area	Outside Fire Area	Fire Frequency	Core Melt	SEFC	SEC	SEF	SE	TEFC	TEC	TEF	TE	
18	--		--												
18A	CHG 32 C	See area 3A	--												See area 3A
19	--		--												
19A	CHG 32 C	See area 3A	--												See area 3A
20	--		--												
20A	--		--												
21	--		--												
21A	--		--												
22	SWS (all)		--												Very large fire necessary to fail all six safety SWS C pumps/pumps in open area backup pumps away from these six.
22A	--		--												

P = power cables; C = control cables; CHG = charging pumps; CCS = component cooling system; SIS = safety injection system; AFWS = auxiliary feedwater system; EP = electric power; SWS = service water system; REC = recirculation system; PORV = PORVs and block valves; RHR = residual heat removal; MCC = motor control center.

Note: Exponential notation is indicated in abbreviated form; i.e., 8.0-5 = 8×10^{-5}.

TABLE 7.3.2A-21 (continued)

FIRE AREA ANALYSIS

Fire Area	Core Melt Related Components		Containment Related Components		Mean Frequency										Remarks
	Within Fire Area	Outside Fire Area	Within Fire Area	Outside Fire Area	Fire Frequency	Core Melt	SEFC	SEC	SEF	SE	TEFC	TEC	TEF	TE	
23: AFW Pump Room	AFW 31, 32 and 33 PMP P C	CCW (all) 1.1-7 SI (all) 1.4-4 EP (all) 2.-8 SW 8.6-5 REC 4.-3 PORV 4.3-3 AFWS 1.0	--	CS (all) 3.1-5 CF (all) 6.3-7	4.4-4 See Fire Area 2A	3.7-6	--	--	--	--	3.7-6	2.3-12	1.2-10	7.3-17	Part of AFWS 8B = 3.7-6 8A = 1.2-10 2RW = 7.3-17
23A	--		--												
24	--		--												
25A	--		--												
26A	--		--												
27A	--		--												
28A	--		--												
29A	--		--												
30A	--		--												
31A	--		--												
32A	--		--												

P = power cables; C = control cables; CHG = charging pumps; CCS = component cooling system; SIS = safety injection system; AFWS = auxiliary feedwater system; EP = electric power; SWS = service water system; REC = recirculation system; PORV = PORVs and block valves; RHR = residual heat removal; MCC = motor control center.

Note: Exponential notation is indicated in abbreviated form; i.e., 8.0-5 = 8×10^{-5}.

TABLE 7.3.2A-21 (continued)

FIRE AREA ANALYSIS

Fire Area	Core Melt Related Components		Containment Related Components		Mean Frequency										Remarks
	Within Fire Area	Outside Fire Area	Within Fire Area	Outside Fire Area	Fire Frequency	Core Melt	SEFC	SEC	SEF	SE	TEFC	TEC	TEF	TE	
33A	--		--												
34A	--		--												
35A	Control Room Ventilation		--												Minor impact on plant safety.
36A	--		--												
37A	--		--												
38A	--		--												
39A	--		--												
40A	--		--												
41A	--		--												
42A	--		--												
43A	--		--												
44A	--		--												
45A	--		--												
46A	--		--												
47A	--		--												
48A	--		--												

P = power cables; C = control cables; CHG = charging pumps; CCS = component cooling system; SIS = safety injection system; AFWS = auxiliary feedwater system; EP = electric power; SWS = service water system; REC = recirculation system; PORV = PORVs and block valves; RHR = residual heat removal; MCC = motor control center.

Note: Exponential notation is indicated in abbreviated form; i.e., 8.0-5 = 8×10^{-5}.

TABLE 7.3.2A-21 (continued)

FIRE AREA ANALYSIS

Fire Area	Core Melt Related Components		Containment Related Components		Mean Frequency										Remarks
	Within Fire Area	Outside Fire Area	Within Fire Area	Outside Fire Area	Fire Frequency	Core Melt	SEFC	SEC	SEF	SE	TEFC	TEC	TEF	TE	
49A	--		--												
50A	--		--												
51A	--		--												
52A	Secondary RV Containment Heat and Cooling		--												Part of AFWS minor impact on plant safety.
53A	--		--												
54A	--		--												
55A	--		--												
56A	--		--												
57A	P and C for Secondary Side Valves		--												AFW not affected. Therefore, a fire in this area only contributes to main feedwater reliability.
58A	CHG 31/32 P CCS all P Imbedded		--												

P = power cables; C = control cables; CHG = charging pumps; CCS = component cooling system; SIS = safety injection system; AFWS = auxiliary feedwater system; EP = electric power; SWS = service water system; REC = recirculation system; PORV = PORVs and block valves; RHR = residual heat removal; MCC = motor control center.

Note: Exponential notation is indicated in abbreviated form; i.e., 8.0-5 = 8×10^{-5}.

TABLE 7.3.2A-21 (continued)

FIRE AREA ANALYSIS

Fire Area	Core Melt Related Components		Containment Related Components		Mean Frequency									Remarks
	Within Fire Area	Outside Fire Area	Within Fire Area	Outside Fire Area	Fire Frequency	Core Melt	SEFC	SEC	SEF	SE	TEFC	TEC	TEF	TE	
59A: Piping Penetration Area	MOVs of CHG RHR CCS SI	CCS 1.1-7 AFWS 1.5-5 EP 2.-8 SWS 8.6-5 REC 1.0 PORV 4.3-3 SI 1.4-4	--	CS 3.1-5 CF 6.3-7	4.4-4	4.5-8	4.8-11	3.8-8	1.5-15	1.0-11	6.6-9	4.2-15	2.1-13	1.3-19	Power cable or MOV motors may be affected by the fire. All valves are in SI position except for REC related ones (CCW valves of RHR HX). 822A and 822B valves are far apart. 8B = 4.5-8 8A = 2.1-13 2RW = 8.8-11
60A: Upper Tunnel	SI 31/33 P CCW 31/33 P RHR 32 P AFWS 33 C P CHG 31/32 C P PORV	See text	CS (all) CF (31,33, 35)	See text		8.-7	--	--	--	--	--	--	--	8.-7	See Section 7.3.2.4 page 7.3-97.
61A	MOV for RWST to RHR Pumps		--												Part of LPIS minor impact on risk.
62A	MOV of SWS to CF		--												Part of CF system minor impact on risk.

P = power cables; C = control cables; CHG = charging pumps; CCS = component cooling system; SIS = safety injection system; AFWS = auxiliary feedwater system; EP = electric power; SWS = service water system; REC = recirculation system; PORV = PORVs and block valves; RHR = residual heat removal; MCC = motor control center.

Note: Exponential notation is indicated in abbreviated form; i.e., 8.0-5 = 8×10^{-5}.

TABLE 7.3.2A-21 (continued)

FIRE AREA ANALYSIS

Fire Area	Core Melt Related Components		Containment Related Components		Mean Frequency										Remarks
	Within Fire Area	Outside Fire Area	Within Fire Area	Outside Fire Area	Fire Frequency	Core Melt	SEFC	SEC	SEF	SE	TEFC	TEC	TEF	TE	
63A	--		--												
64A	--		--												
65A	--		--												
66A	--		--												
67A	--		--												
68A	CHG 33 P		CS (all) P												All three power cables are encased in concrete. Therefore, we do not further analyze.
69A	RHR 32 P		--												Part of LPIS.
70A: Containment RCP Area	MOVs for SIS pumps (recirculation affected) PORV P, C	AFWS 1.5-5 EP 2.-8 CCW 1.1-7 PORV 1.0 REC 0.1 SWS 8.6-5 SI 1.4-4	--	CS (all) 3.1-5 CF (all) 6.3-7	4.7-4	4.7-8	5.2-12	4.0-8	1.6-16	1.1-11	7.1-9	4.4-15	2.2-13	1.4-12	Power cables to REC pumps are not known where routed. Therefore, assumed that affected by a RCP fire because of proximity. 8B = 4.7-8 8A = 2.2-13 2RW = 1.1-11 λ_{Cont} = 1.5-2 f_{70A} = 0.032

P = power cables; C = control cables; CHG = charging pumps; CCS = component cooling system; SIS = safety injection system; AFWS = auxiliary feedwater system; EP = electric power; SWS = service water system; REC = recirculation system; PORV = PORVs and block valves; RHR = residual heat removal; MCC = motor control center.

Note: Exponential notation is indicated in abbreviated form; i.e., 8.0-5 = 8×10^{-5}.

TABLE 7.3.2A-21 (continued)

FIRE AREA ANALYSIS

Fire Area	Core Melt Related Components		Containment Related Components		Mean Frequency										Remarks
	Within Fire Area	Outside Fire Area	Within Fire Area	Outside Fire Area	Fire Frequency	Core Melt	SEFC	SEC	SEF	SE	TEFC	TEC	TEF	TE	
71A RCP Area	PORV P, C SI, CHG, and RHR MOVs (recirculation affected)	See area 70A	--	See area 70A	4.7-4	9.8-8	1.1-11	8.3-8	3.4-16	1.9-11	1.5-8	9.1-15	4.5-13	2.9-19	See 70A.
72A Outer Annulus	RHR MOVs		CF 32 P												Part of CF system analysis.
73A: Electric Penetration	AFWS 33 P and C PORV P 32 C RCS Prsr level	CCW (all) 1.1-7 SI (all) 1.4-4 AFWS 1.1-4 EP 2.-8 SWS 8.6-5 REC 4.-3 PORV 1.0 Narrow range SG levels	CF (all) P	CS (all) 3.1-5 CF 1.0	9.7-4	1.8-7	--	8.3-8	--	2.3-11	--	9.7-8	--	4.6-13	8B = 9.8-8 8A = -- 2RW = 2.3-11
74A	AFWS 31 C														Part of AFWS.
75A: Outer Annulus Containment	PORV P, C	CCW 1.1-7 SI 1.4-4 AFWS 1.5-5 EP 2.0-8 SWS 8.6-5 REC 4.-3 PORV 1.0	CF (all) P	CS (all) 3.1-5 CF 1.0	4.7-4	4.7-8	--	4.0-8	--	1.1-11	--	7.1-9	--	2.2-13	8B = 4.7-8 8A = -- 2RW = 1.1-11 λ_{CNT} = 1.6-2 f_{75A} = .032

P = power cables; C = control cables; CHG = charging pumps; CCS = component cooling system; SIS = safety injection system; AFWS = auxiliary feedwater system; EP = electric power; SWS = service water system; REC = recirculation system; PORV = PORVs and block valves; RHR = residual heat removal; MCC = motor control center.

Note: Exponential notation is indicated in abbreviated form; i.e., 8.0-5 = 8×10^{-5}.

TABLE 7.3.2A-21 (continued)

FIRE AREA ANALYSIS

Fire Area	Core Melt Related Components		Containment Related Components		Mean Frequency										Remarks
	Within Fire Area	Outside Fire Area	Within Fire Area	Outside Fire Area	Fire Frequency	Core Melt	SEFC	SEC	SEF	SE	TEFC	TEC	TEF	TE	
76A	--		CF 33,34, 35 P	CS (all) -3											Part of CF system.
77A: Outer Annulus Containment	SI MOVs P (recirculation affected)	CCW 1.1-7 SI 1.4-4 AFWS 1.5-5 EP 2.-8 SWS 8.6-5 REC 0.1 PORV 4.3-3	CF 35 P	CF (31-34) 2.8-5 CS (all) 3.1-5	4.7-4 See 75A	4.0-8	5.2-12	4.0-8	1.6-16	1.1-11	7.1-10	2.0-14	2.2-14	6.1-19	Assume recirculation system affected. 8B = 4.0-8 8A = 2.2-14 2RW = 1.1-11
78A: Containment Recirculation Pump Area	RHR Hx REC Pump PORV	CCW 1.1-7 SI 1.6-4 AFWS 1.5-5 EP 2.-8 SWS 8.6-5 REC 1.0 PORV 1.0	--	CS 3.1-5 CF 6.3-7	4.7-4	4.7-8	5.2-11	4.0-8	1.6-15	1.1-11	7.1-9	4.4-15	2.2-13	1.4-19	See 70A 8B = 4.7-8 8A = 2.2-13 2RW = 1.1-11
79A															
80A	--		CF 31,33, 34, 35 P	CS 3.1-5 CF 1.0											Part of CF system; minor impact on risk.
81A	--		CF 33,34, 35 P	CF 1.0											Part of CF system; minor impact on risk.
82A	--		CF 34/35 P												Part of CF system; minor impact on risk.

P = power cables; C = control cables; CHG = charging pumps; CCS = component cooling system; SIS = safety injection system; AFWS = auxiliary feedwater system; EP = electric power; SWS = service water system; REC = recirculation system; PORV = PORVs and block valves; RHR = residual heat removal; MCC = motor control center.

Note: Exponential notation is indicated in abbreviated form; i.e., 8.0-5 = 8×10^{-5}.

TABLE 7.3.2A-21 (continued)

FIRE AREA ANALYSIS

Fire Area	Core Melt Related Components		Containment Related Components		Mean Frequency										Remarks
	Within Fire Area	Outside Fire Area	Within Fire Area	Outside Fire Area	Fire Frequency	Core Melt	SEFC	SEC	SEF	SE	TEFC	TEC	TEF	TE	
83A	--		CF 35 P												Part of CF system; minor impact on risk.
84A	--		CS (NIOH) CF (32) P	CF - 5											
85A	Incore Detector Drive Mechanism		--												
86A	Control Rod Drive P and SG		Hydrogen Recombiner												Minor impact on internal risk.
87A	--		--												
88A	--		Charcoal Filters												No effect on risk.
89A	--		--												
90A	--		--												
91A	--		--												
94A	--		--												
95A	--		--												
96A	--		--												
97A	--		--												

P = power cables; C = control cables; CHG = charging pumps; CCS = component cooling system; SIS = safety injection system; AFWS = auxiliary feedwater system; EP = electric power; SWS = service water system; REC = recirculation system; PORV = PORVs and block valves; RHR = residual heat removal; MCC = motor control center.

Note: Exponential notation is indicated in abbreviated form; i.e., 8.0-5 = 8×10^{-5}.

TABLE 7.3.2A-21 (continued)

FIRE AREA ANALYSIS

Fire Area	Core Melt Related Components		Containment Related Components		Mean Frequency										Remarks
	Within Fire Area	Outside Fire Area	Within Fire Area	Outside Fire Area	Fire Frequency	Core Melt	SEFC	SEC	SEF	SE	TEFC	TEC	TEF	TE	
98A	--		--												
101A	DG 31		--												Part of EP system.
102A	DG 32		--												Part of EP system.
105A	Primary Water Storage Tank		--												Part of internal risk study.
106A	RWST		--												Part of SI study.

P = power cables; C = control cables; CHG = charging pumps; CCS = component cooling system; SIS = safety injection system; AFWS = auxiliary feedwater system; EP = electric power; SWS = service water system; REC = recirculation system; PORV = PORVs and block valves; RHR = residual heat removal; MCC = motor control center.

Note: Exponential notation is indicated in abbreviated form; i.e., 8.0-5 = 8×10^{-5}.

TABLE 7.3.2A-22

CHARACTERISTIC VALUES OF SEVERAL PARAMETERS USED IN THE QUANTIFICATION OF BASE CASE FIRE RISK

Probability Level	Parameter		
	f_T	f_A	$Q(\tau_A)$
Distribution	Lognormal	Lognormal	Histogram
5th Percentile	8.0-3	1.0-3	0.2
Median	4.0-2	1.0-2	0.55
95th Percentile	2.0-1	1.0-1	0.87
Mean	6.5-2	2.7-2	0.57

Note: Exponential notation is indicated in abbreviated form; i.e., 8.0-5 = 8×10^{-5}.

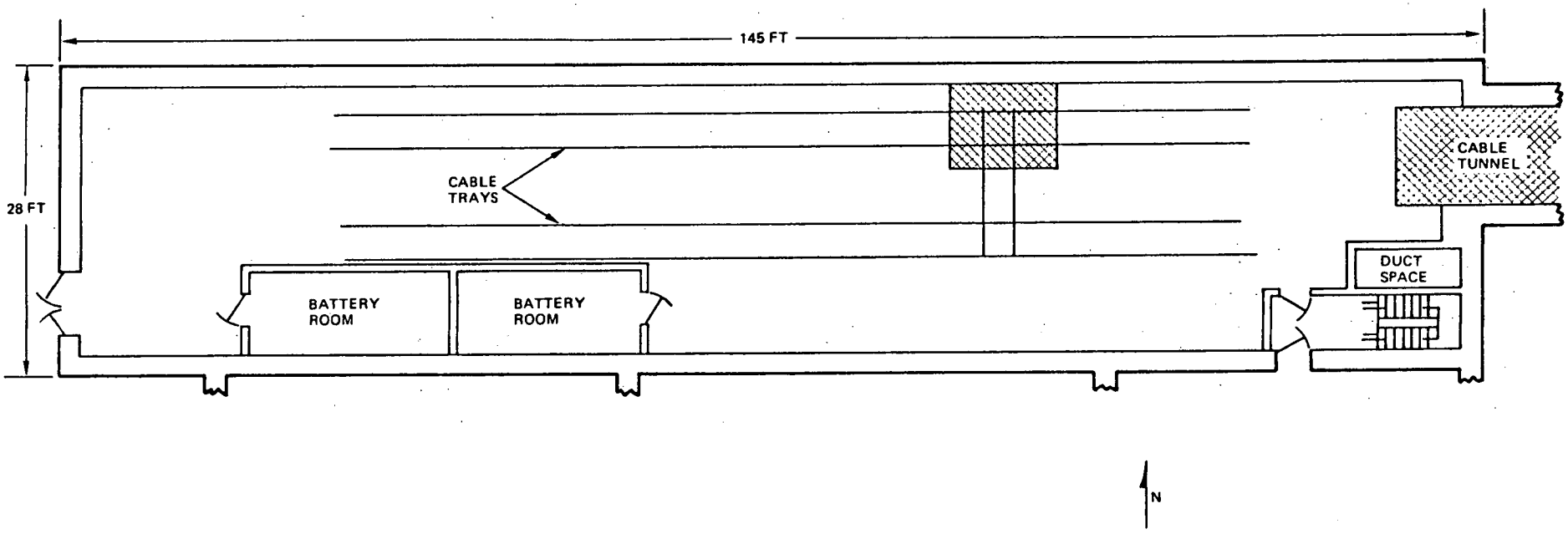


Figure 7.3.2-1. The Cable Spreading Room of Indian Point 3, as Viewed from the Top

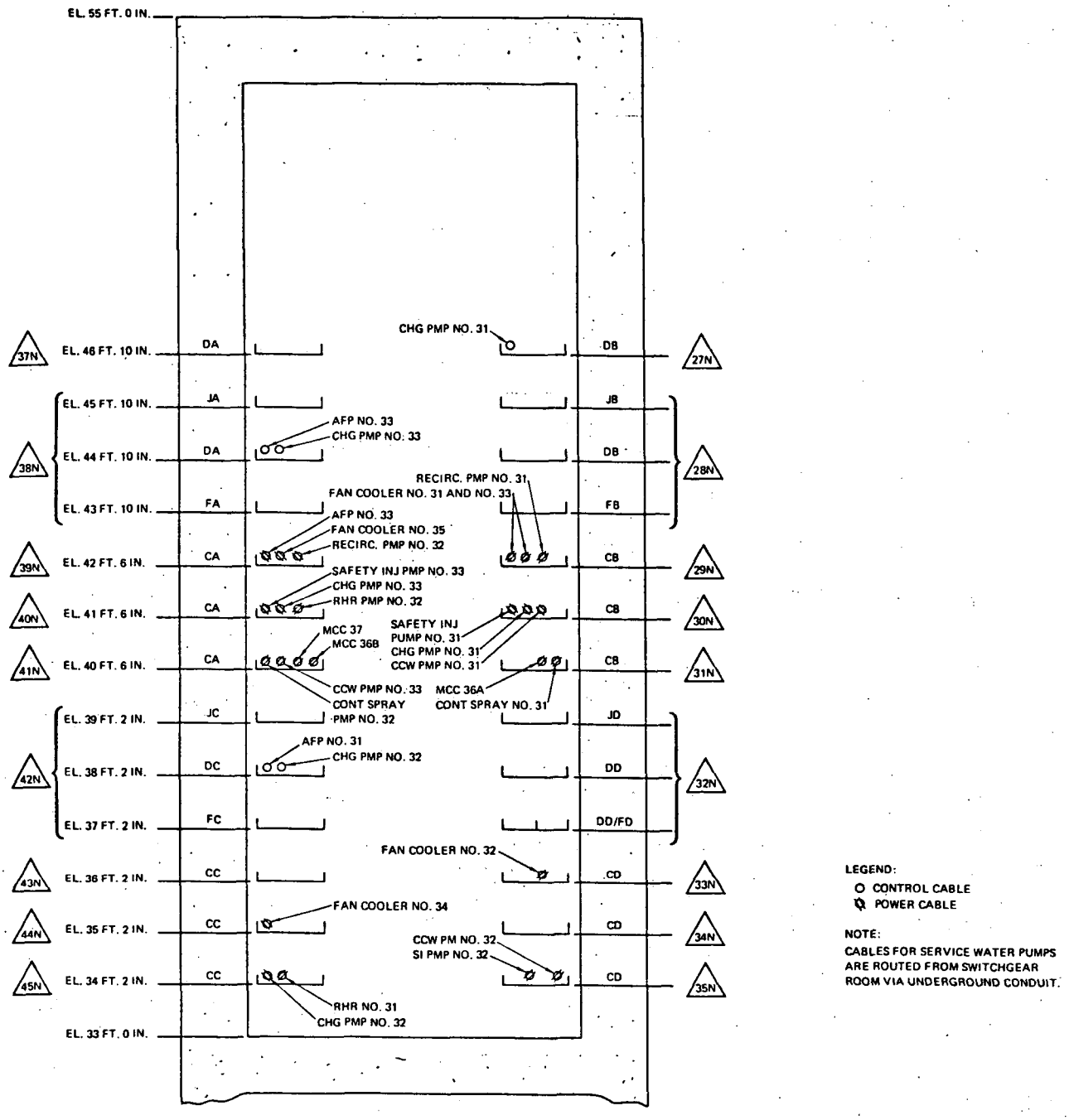


Figure 7.3.2-2. View Looking East into Cable Tunnel

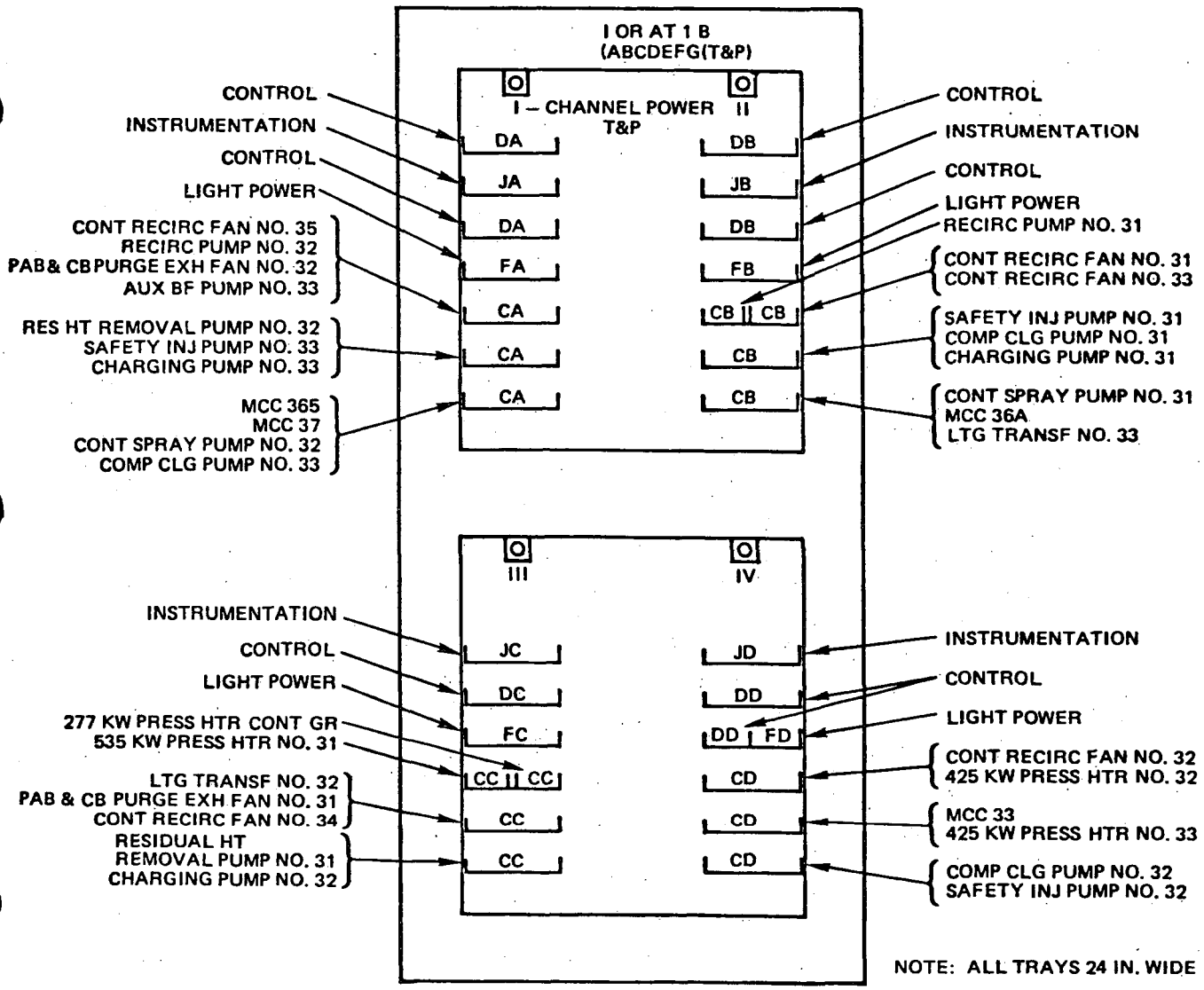


Figure 7.3.2-3. Typical Section in Tunnel
Looking from Control Building, Indian Point 3

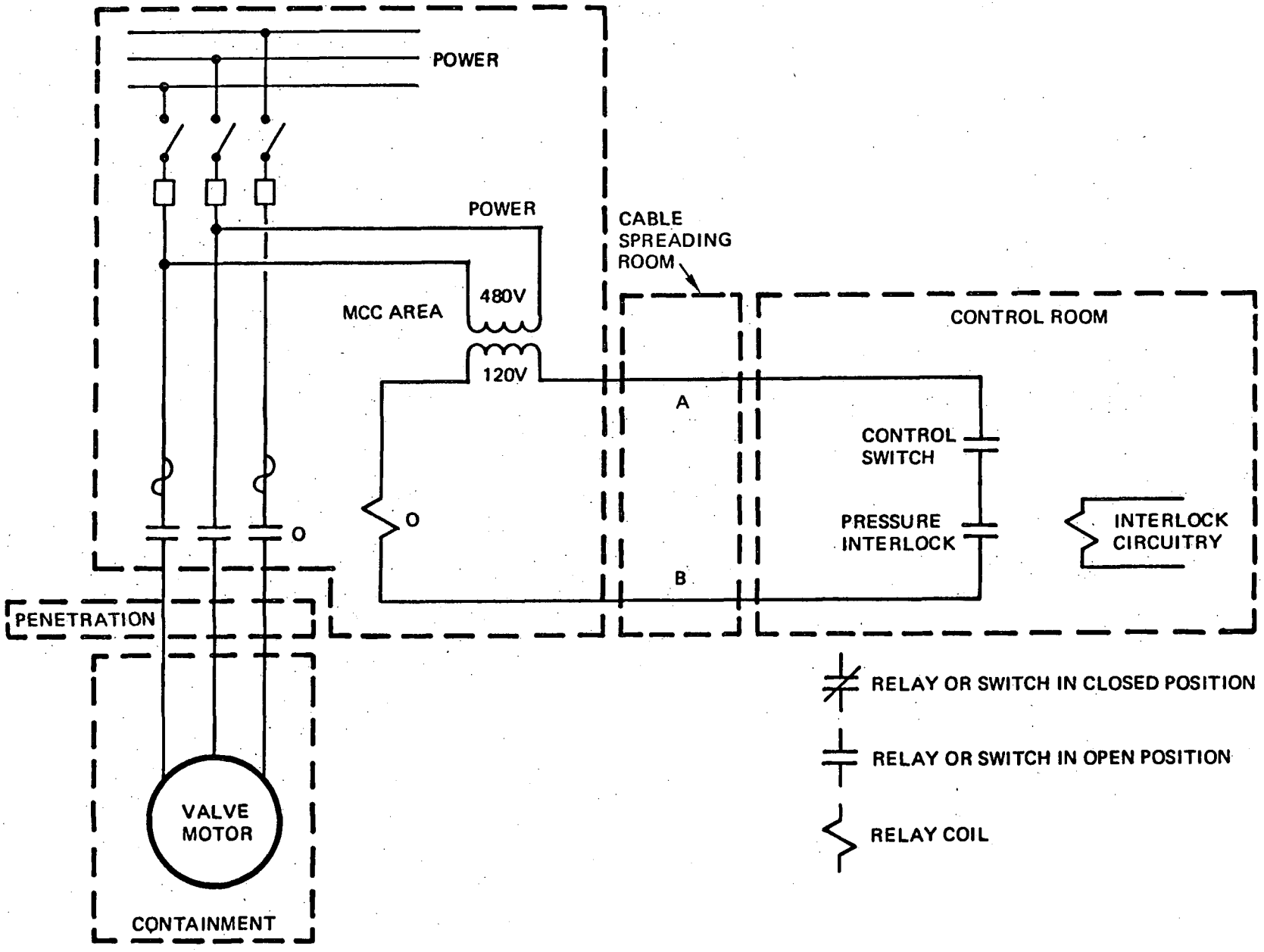


Figure 7.3.2-4. Simplified Diagram of the Control Circuitry for Opening an RHR Isolation MOV (731 or 730)

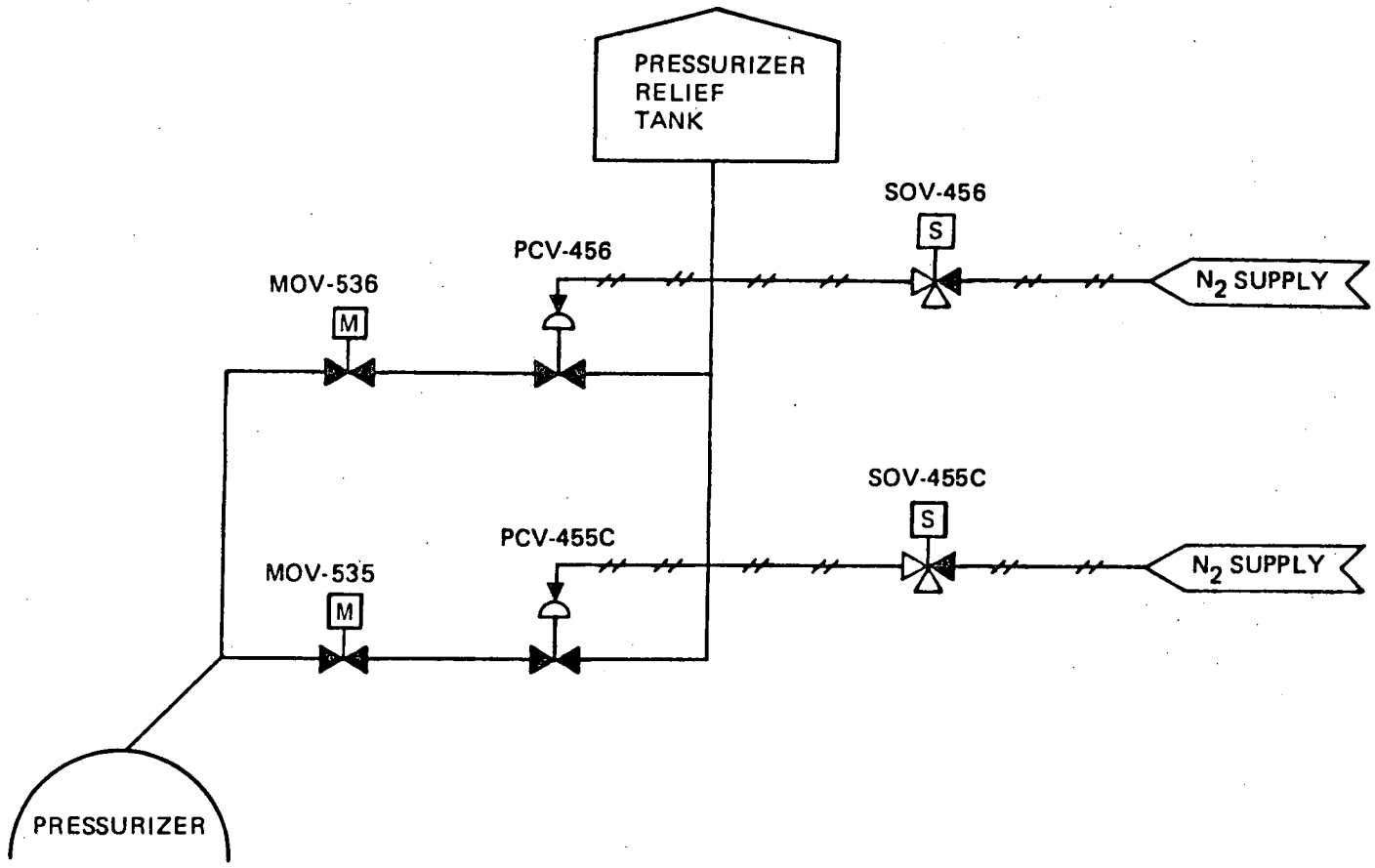


Figure 7.3.2-5. Valves with the Potential of Causing a Small LOCA

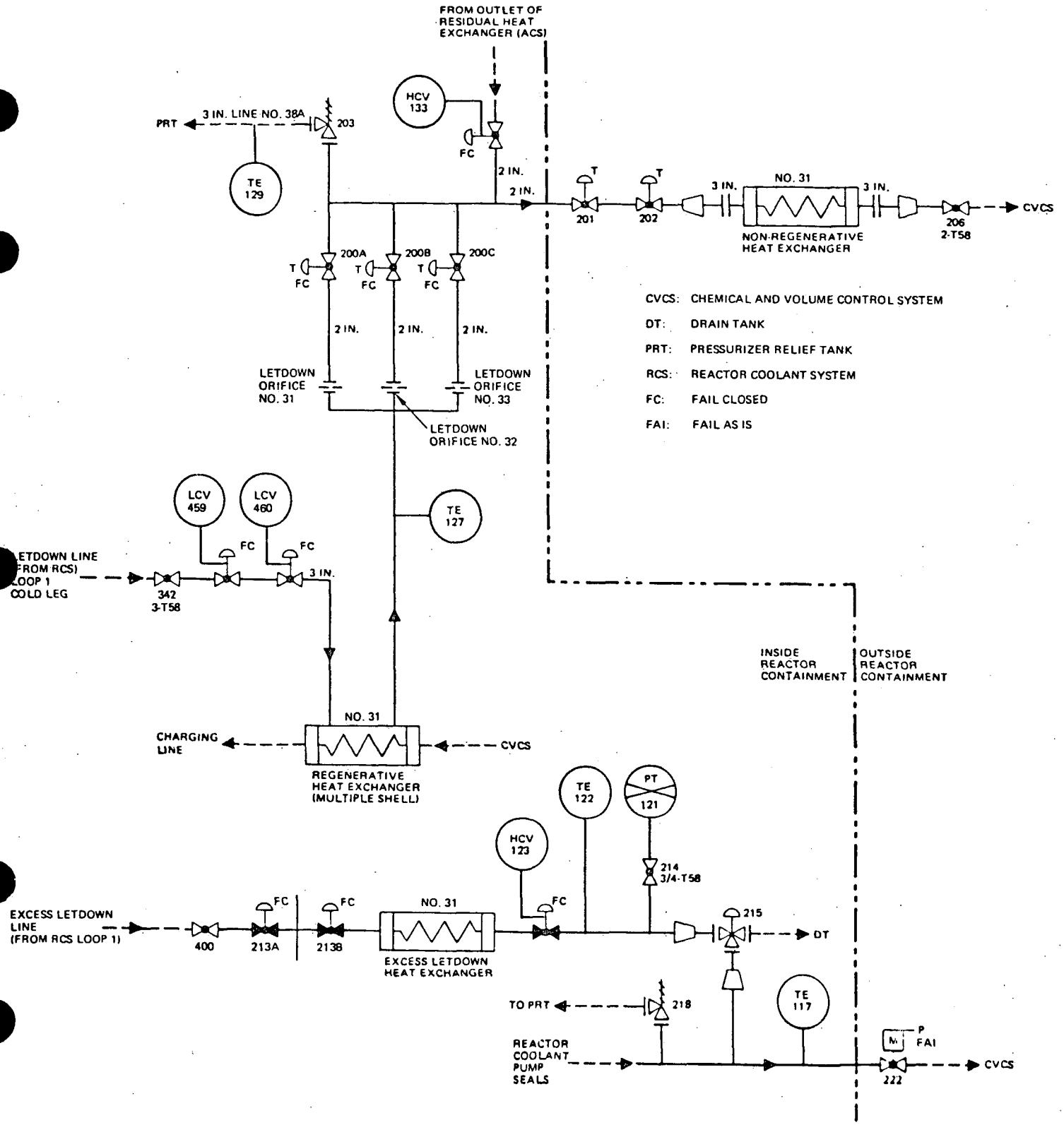


Figure 7.3.2-6. Normal and Excess Letdown Lines in Indian Point 3

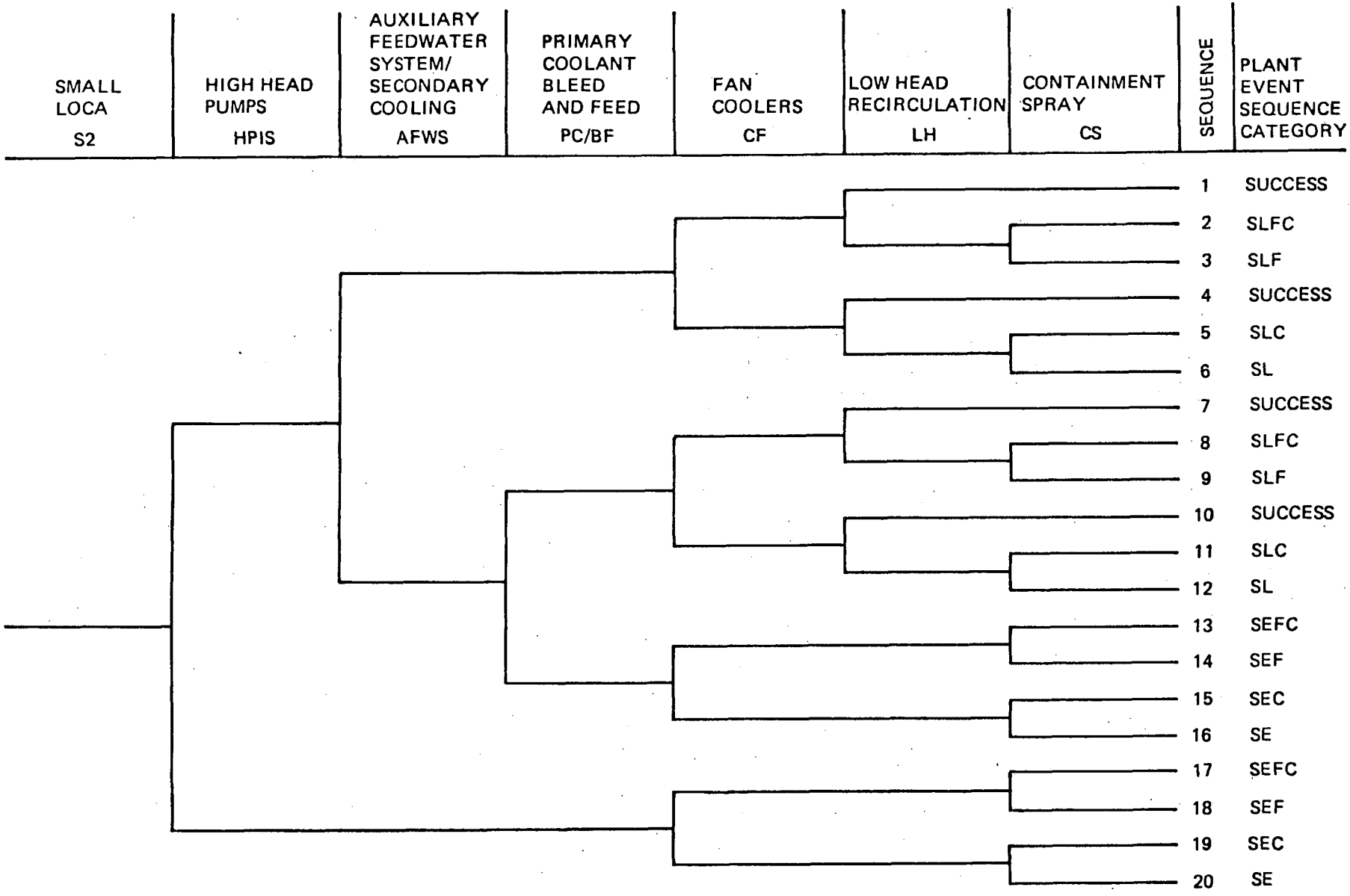


Figure 7.3.2-7. Simplified Event Tree for a Small LOCA

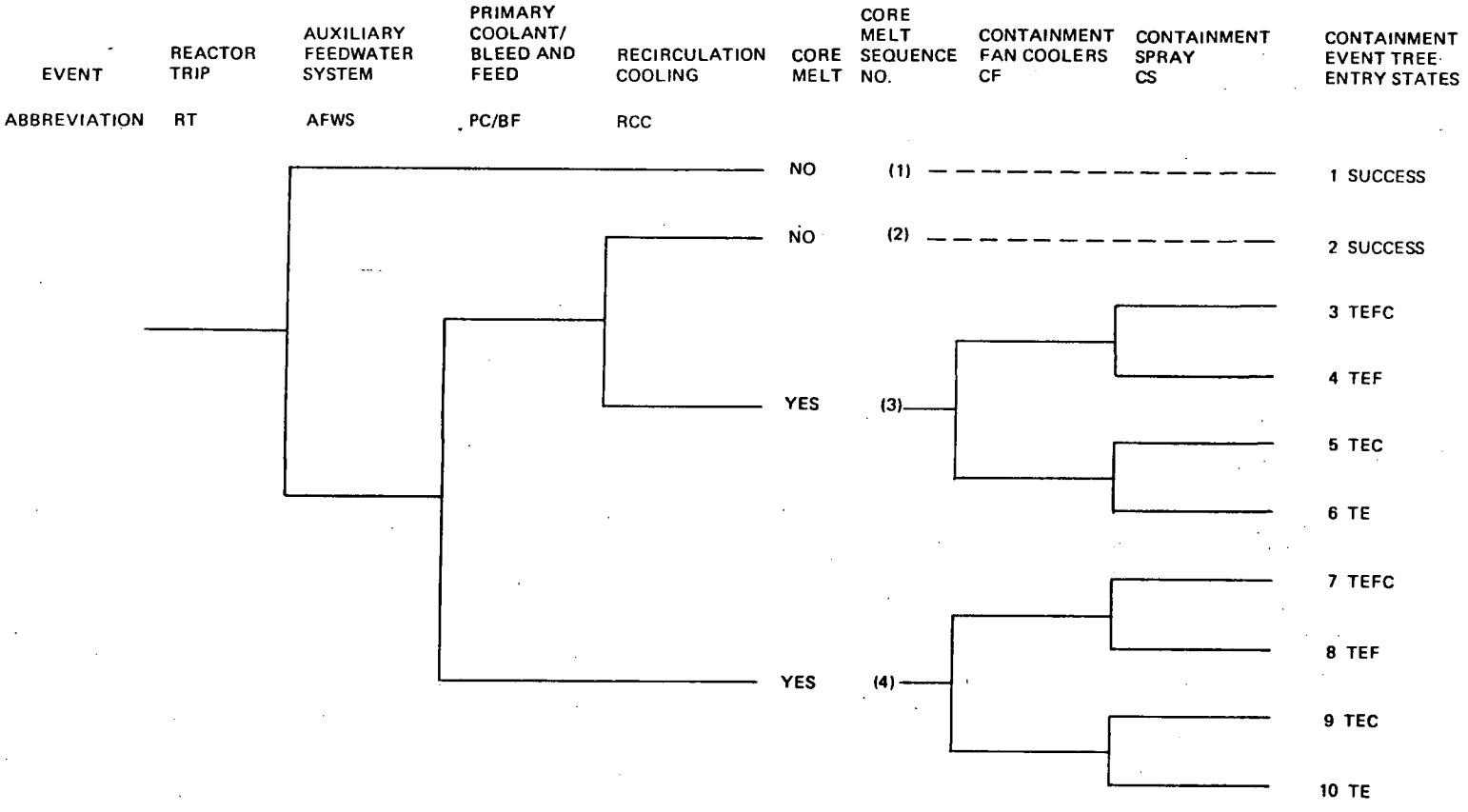
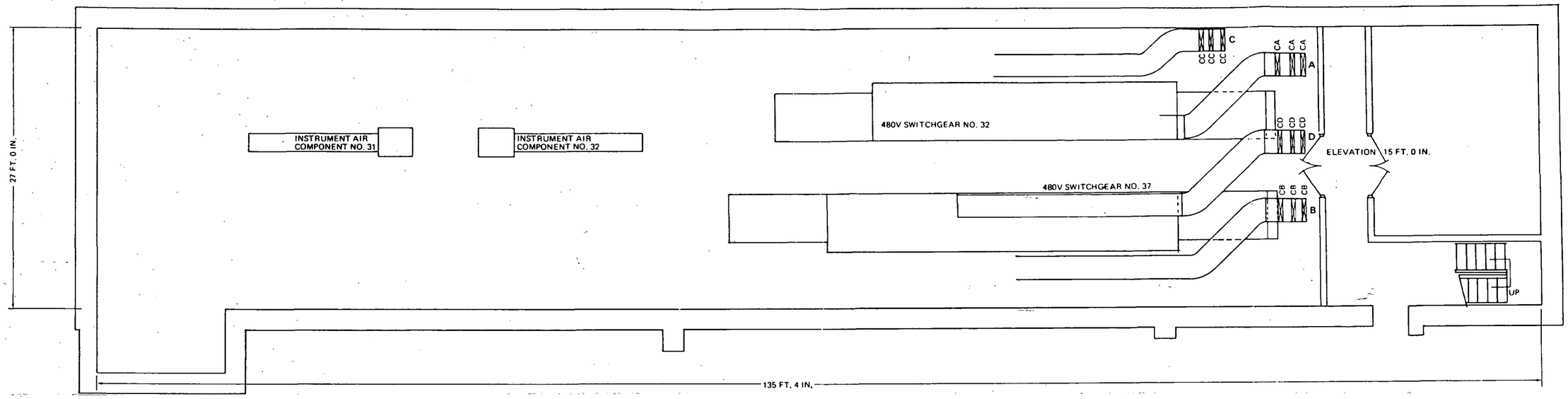


Figure 7.3.2-8. Simplified Event Tree for Transient Events



CABLE TRAY STACK	CONTENTS (POWER CABLES)	
C	CHARGING PMP	32
	CONTAINMENT FAN COOLER	34
	RHR PMP	31
A	AUX. FEED PMP	33
	CHARGING PMP	33
	CONTAINMENT FAN COOLER	35
	CONTAINMENT SPRAY	32
	COMPONENT COOLING PMP	33
	MCC	36B
	RECIRCULATION PMP	32
	RHR PMP	32
	SAFETY INJ.	33
D	AUX. FEED PMP	32
	COMPONENT COOLING PMP	32
	CONTAINMENT FAN COOLER	32
	SAFETY INJ.	32
B	CHARGING PMP	31
	COMPONENT COOLING PMP	31
	CONTAINMENT FAN COOLER	31, 33
	CONTAINMENT SPRAY	31
	MCC	36A
	RECIRCULATION PMP	31
	SAFETY INJECTION	31

Figure 7.3.2-9. Simplified Top View of the Switchgear Room in Indian Point 3

AMENDMENT 1
IPPSS DEC 1982

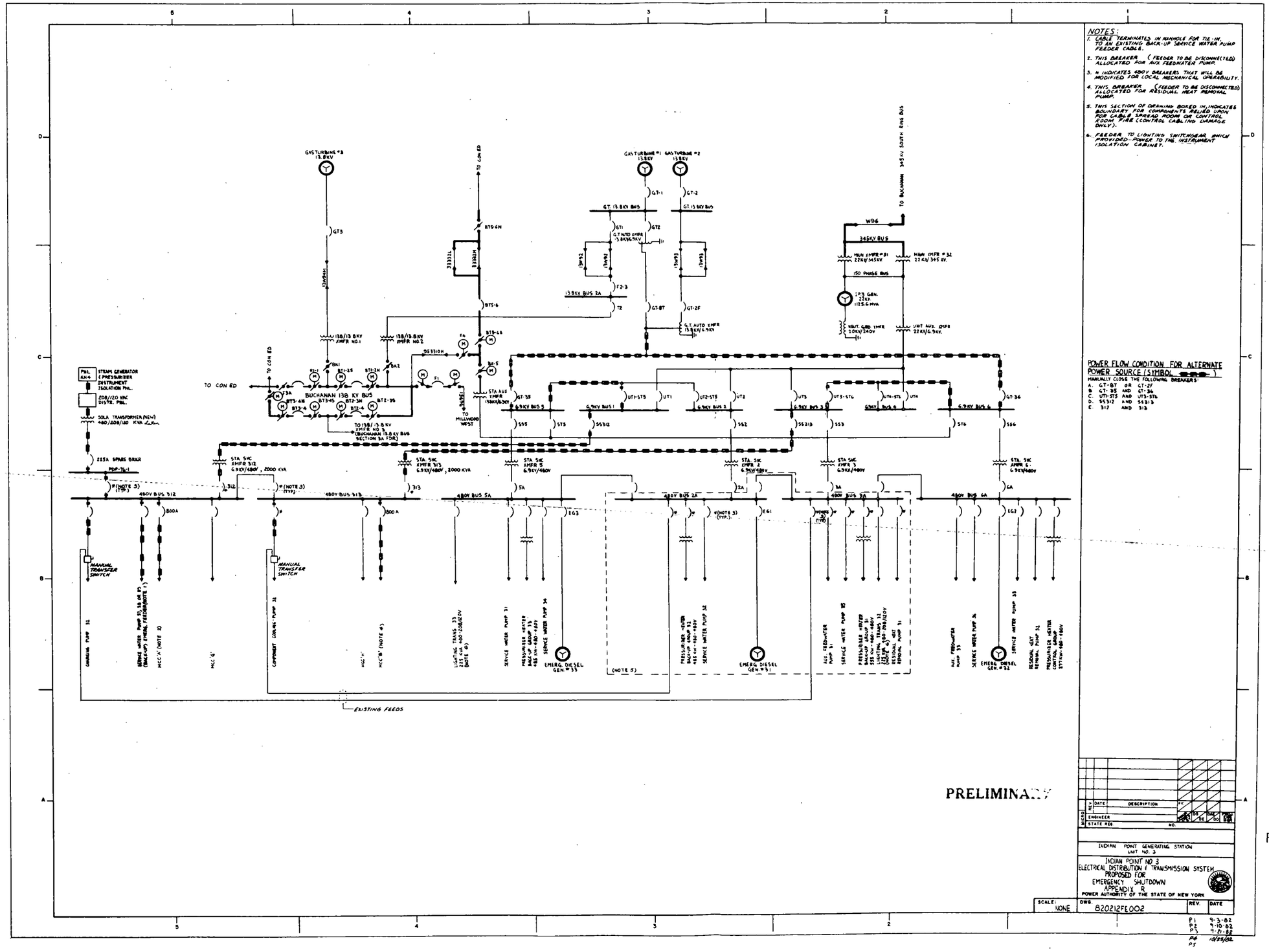


Figure 7.3.2A-10. Schematic of Appendix R Modification

AMENDMENT 1
IPPSS DEC 1982

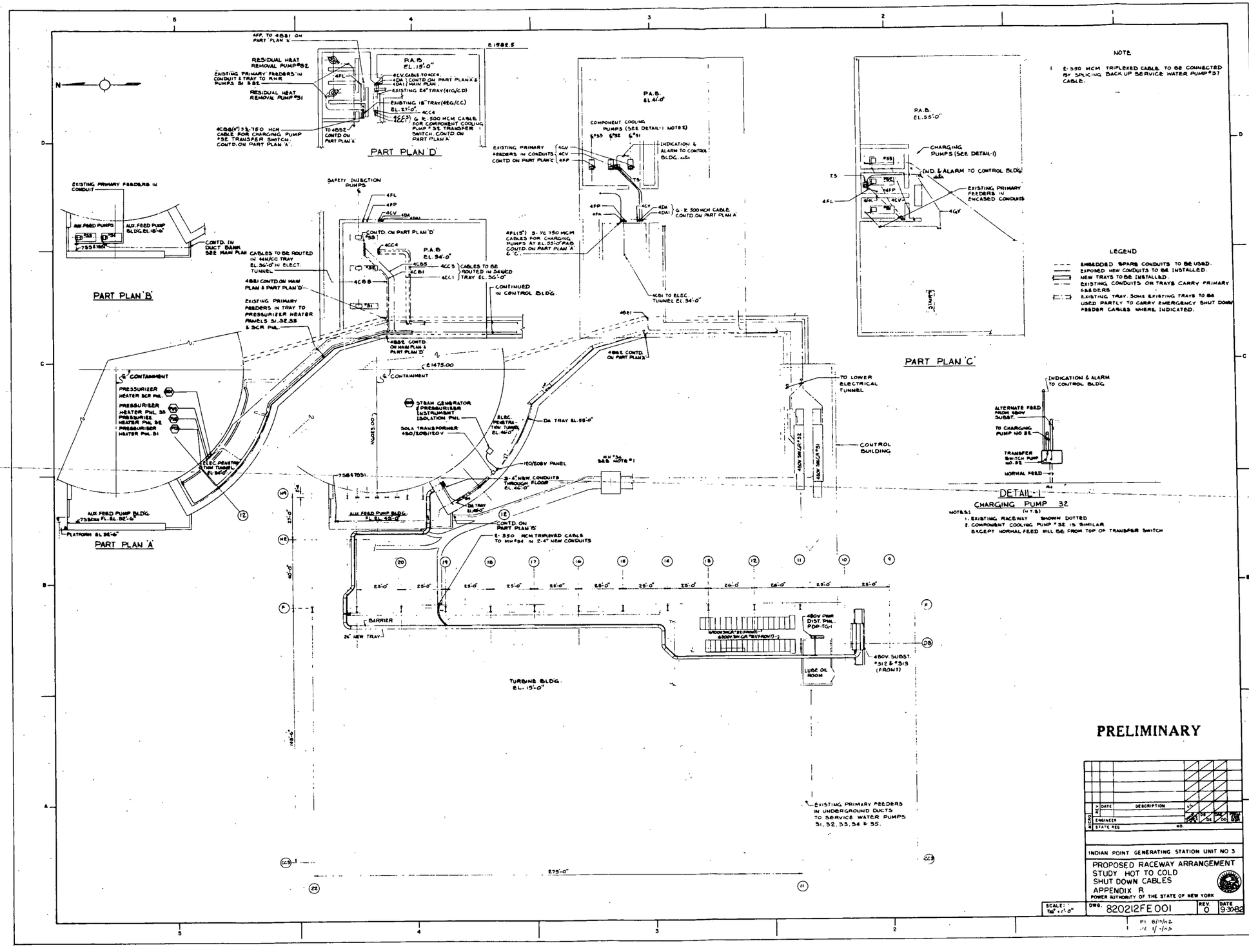


Figure 7.3.2A-11. Cable Routing of the Alternate Feed System

7.3.3 REFERENCES

7.3-1 "Review of the Indian Point Station Fire Protection Program," Consolidated Edison Company of New York and Power Authority of the State of New York, April 1977.

7.3-2 "Supplement 3 to the Indian Point Unit 2 Final Safety Analysis Report," Answer to Question 7.6, November 1969.

7.3-3 Apostolakis, G., and M. Kazarians, "The Frequency of Fires in Light Water Reactor Compartments," paper presented at the ANS/ENS Topical Meeting on Thermal Reactor Safety, Knoxville, Tennessee, April 6-9, 1980.

7.3-4 Sideris, A. G., R. W. Hockenbury, M. L. Yeater, and W. E. Vesely, "Nuclear Plant Fire Incident Data File," Nuclear Safety, 20, 308-317, 1979.

7.3-5 Siu, N. O., "Probabilistic Models for the Behavior of Compartment Fires," UCLA-ENG-8090, University of California, Los Angeles, 1980.

7.3-6 Fleming, K. N., W. J. Houghton, and F. P. Scaletta, "A Methodology for Risk Assessment of Major Fires and its Application to an HTGR Plant," GA-A15402, General Atomic Co., July 1979.

7.3-7 Swain, A. D., and H. E. Guttman, "Handbook of Human Reliability," NUREG/CR-1278, Sandia Laboratories, Albuquerque, New Mexico, October 1980.

7.3-8 "Indian Point 2 Alternate Shutdown System," Consolidated Edison Company of New York, Inc., Letters to the NRC dated September 18, 1978 and December 12, 1978.

7.3-9 Dummer, G. W. A., and N. B. Griffin, Electronics Reliability Calculation and Design, Pergamon Press, 1966.

7.3-10 Thomas, P. H., "The Size of Flames from Natural Fires," Tenth Symposium (Int'l.) on Combustion, 844-859 (1963).

7.3-11 United Engineers and Constructors, Inc., "Electrical Separation Implementation Design Guide - Indian Point Generating Station, Unit 3," Revision 6, June 18, 1975.

7.3-12 U. S. Nuclear Regulatory Commission, "Supplement to the Fire Protection Safety Evaluation Report, Indian Point Unit 3," Letter to PASNY dated May 2, 1980.

7.3-13 Nuclear Power Experience, a Division of Petroleum Information Corporation, "Nuclear Power Experience," August 1981.

7.3.3A.1 References for Section 7.3.1A

7.3-14 Response to Staff Position P9 on Indian Point 2 Fire Protection Program, attached to letter from William J. Cahill, Jr., of Consolidated Edison Company of New York to Victor Stello, Jr., of NRC, September 1978.

7.3.3A.2 References for Section 7.3.2A

7.3-15 Enclosure 2 to letter from J. P. Bayne, Power Authority of the State of New York, to S. A. Varga, U.S. Nuclear Regulatory Commission, July 1, 1982.

7.3.4 APPENDIX I -- FIRE PROPAGATION MODEL

This appendix presents a general model for constructing fire propagation time probability distributions. This model incorporates the predictions of a simple physical model, whose features are outlined below, judgment concerning the accuracy of the physical model, and subjective distributions for the parameters used in the physical model. The model is used to derive histograms for three cases: (1) vertical fire propagation within a stack of horizontal cable trays, (2) horizontal propagation across the width of a horizontal tray, and (3) fire propagation among a group of separated trays when an external exposure fire is present.

7.3.4.1 The Physical Model

The physical model used is in the form of the computer program COMPBRN. The general outline of the model follows; a more complete description of the model and the code can be found in Reference 7.3.4-1.

The basic model is as follows:

1. A burning fuel element releases a certain amount of heat at a rate $\dot{Q}(W)$.

2. This heat is transmitted by convection and/or radiation. If a barrier intervenes between the flame and an element, a special model must be introduced.

3. After absorbing a critical amount of heat, an element will ignite and add its heat to the fire.

7.3.4.1.1 Heat Release

The heat release rate is given by

$$\dot{Q} = \dot{m}'' A_f H_f \ (W) \qquad (7.3.4.1\text{-}1)$$

where

$\dot{m}''$ = specific burning rate of fuel (kg/m^2s)

A_f = area of fuel (m^2)

H_f = heating value of fuel (J/kg)

In COMPBRN, the fuel bed is divided into discrete elements (typically square) and so A_f is fixed. H_f is usually quite well known for most fuels. For fuel surface controlled fires; that is, fires not restricted by the available ventilation,

$$\dot{m}'' = \dot{m}''_o + C_s \dot{q}''_{ext} \ (kg/m^2s) \qquad (7.3.4.1\text{-}2)$$

where

$\dot{m}''_o$, C_s = characteristic constants for a given material

$\dot{q}''_{ext}$ = external heat flux on burning element

C_s is usually fairly well known. However, $\dot{m}''_o$ is not well known for cable insulation. Note that $\dot{m}''_o$ may be negative for "nonflammable" materials, which will not burn unless a threshold external heat flux is provided.

7.3.4.1.2 Heat Transmission

The heat transferred to other fuel elements from the flame is modeled as follows:

$$\dot{q}''_o = \text{heat flux received by an element} = \dot{q}''_{rad} + \dot{q}''_{convection} \quad (7.3.4.1\text{-}3)$$

where

$\dot{q}''_{convection} = h\left(T(z)-T_o\right)$ where $T(z)$ is given by correlation

$\dot{q}''_{rad} = F_{o \to s}\dot{q}''_s$

$F_{o \to s}$ = shape factor from the element to the heat source (purely geometry dependent, the source being a cylinder whose height equals the flame height and is given by correlation, and whose radius equals the equivalent radius of the fuel base)

$$\dot{q}''_s = \gamma\dot{Q}/A_{fl} \quad (7.3.4.1\text{-}4)$$

where

γ = fraction of total heat production which is radiated (~.20 to .40)

A_{fl} = surface area of flame

If a thermal barrier is interposed between the flame and the element of interest (e.g., between the upper and lower cable trays in Figure 7.3.4-1), the radiative heat flux on this element is still the product of a source heat flux and an appropriate shape factor. The source heat flux, however, emanates from the side of the barrier opposite the flame. This heat flux, $\dot{q}''_{s,B}$, is computed as follows.

The thermal barrier is modeled as a slab of thickness L. The face exposed to the flame is called the "hot" face; the opposite face is called the "cold" face.

Let $\dot{q}''_B$ represent the heat flux from the flame to the barrier, computed as previously described. Heat balances at the hot and cold faces yield

1. Hot Face (X=0)

$$\varepsilon \dot{q}''_B = h_B[T(0) - T_e] + \sigma\varepsilon_B[T^4(0) - T_e^4] - k_B \left(\frac{dT}{dx}\right)_{X=0} \quad (7.3.4.1\text{-}5)$$

2. Cold Face (X=L)

$$-k_B \left(\frac{dT}{dx}\right)_{X=L} = h_B[T(L) - T_e] + \sigma\varepsilon_B[T^4(L) - T_e^4] \quad (7.3.4.1\text{-}6)$$

where

σ = Stefan-Boltzmann constant

ε_B = barrier emissivity

k_B = barrier thermal conductivity

h_B = heat transfer coefficient

T_e = environment temperature

If steady state conditions are assumed, the temperature profile within the slab is linear, i.e.,

$$T(X) = T(0) + [T(L) - T(0)] \frac{X}{L} \quad (7.3.4.1\text{-}7)$$

The above three equations can be solved iteratively to find T(0) and T(L). If the heat flux leaving the barrier cold face is assumed to be primarily radiative, a valid assumption when T(L) is large, then

$$\dot{q}''_{s,B} = \varepsilon_B[T^4(L) - T_e^4] \quad (7.3.4.1\text{-}8)$$

Note that the steady state assumption is a conservative one, because it ignores the time required for a thermal wave to penetrate the barrier. This time is of the order

$$t_B \sim \frac{L^2}{\alpha_B}$$

where

α_B = barrier thermal diffusivity

or about 1.5 minutes for a 1/4-inch thick slab of concrete. While this value seems to be rather small, it must be remembered that steady state conditions will be reached only after a number of time constants, that

other materials have longer time constants (for asbestos, $\tau_B \sim 2.6$ min.), and that the time scale for extinguishing the fire is approximately 5 minutes.

7.3.4.1.3 Ignition

The time to ignition of a combustible fuel element is given by

$$t^* = \frac{\pi}{4\alpha}\left[\frac{k(T^* - T_o)^2}{\dot{q}''_o}\right] \qquad (7.3.4.1\text{-}9)$$

where

k, α = material properties of element (thermal conductivity, thermal diffusivity)

T^* = ignition temperature of element (either piloted or spontaneous)

T_o = element temperature (assumed constant)

$\dot{q}''_o$ = heat flux on element

The above equation results from the solution of the transient heat conduction equation for a semi-infinite medium.

7.3.4.2 Uncertainties in Modeling

The uncertainties in the modeling can be thought of as uncertainties in the value of the fuel parameters used, uncertainties in the basic structure, formulas, etc., of the physical model, and uncertainties arising from the practical application of the model to actual problems.

7.3.4.2.1 Fuel Parameter Values

A substantial number of the fuel bed's physical properties must be used as input to the COMPBRN code. Most of these properties are fixed by the problem formulation (e.g., the problem geometry), are known to a high degree of accuracy, or have relatively little effect on the computations when varied over a realistic range of values. The three parameters chosen, whose variations characterize the uncertainty in the physical properties of the cable insulation considered, are the specific burning rate $\dot{m}''_o$, the fuel heating value H_f, and the spontaneous ignition temperature, T^*_s.

The following distributions express the probability of the parameter values for cable insulation-fueled fires, and are derived from information given in Reference 7.3.4-2.

$\dot{m}''_o$ = lognormally distributed with $\mu = -6.91$ and $\sigma = 0.865$ (median = 10^{-3} kg/m^{2}s, error factor = 4)

H_f = uniformly distributed between 1.85×10^7 J/kg and 2.7×10^7 J/kg

T^*_s = uniformly distributed between 800^0 and 850^0K

7.3.4.2.2 Basic Modeling

This section presents the uncertainties in the physical models used by COMPBRN. The models are discussed in the order presented in Section 7.3.4.1.

The burning rate equation, Equation (7.3.4.1-1), is empirical; the actual physical processes occurring at the fuel surface are extremely complex. As a result, $\dot{m}''_0$ is not really a purely fuel dependent constant but varies somewhat from fire to fire.

Uncertainties also arise in the calculation of $\dot{q}''_{ext}$, because radiation attenuation due to smoke and gases is not accounted for. Thus, to be conservative, the feedback heat flux is larger in the model than it should be. This conservatism becomes more important for fuels which release large amounts of smoke when burning.

The combustion efficiency has been assumed to be 1.0 in the heat release equation, a reasonable, if conservative, assumption for fires not limited by available ventilation.

The modeling uncertainties in the heat transmittal calculation are due to the assumption of a uniform heat source (actually, the flame temperature decreases continuously with height), the use of simplified shapes to represent the source and the object (the latter being represented by a differential surface element), and the neglect of radiation attenuation by smoke and gases between source and object. This last source of uncertainty is probably the largest.

The use in the ignition model of the semi-infinite slab solution for surface temperature as a function of time is a fair approximation, especially for poor thermal conductors such as cable insulation. The concept of a critical ignition temperature, however, is fairly controversial, because this quantity is partially dependent on the problem setup as well as the material involved.

An important factor in the ignition model is the disregarding of both convective and radiative heat losses at the fuel surface. This is especially conservative as the fuel element approaches ignition, because the losses increase rapidly with rising surface temperature.

Finally, Equation (7.3.4.1-9) also assumes that the incoming heat flux is constant. In the actual computation, a time-averaged value is used.

7.3.4.2.3 Practical Implementation

The two most crucial sources of uncertainty in the COMPBRN program are also sources of conservatism. These are the disregarding of heat flux attenuation through gases and smoke, and the disregarding of heat losses from an element, as discussed previously.

Another conservatism arises from the way the code models a fuel bed. Essentially, any three dimensional object is modeled as either a horizontal or vertical flat slab. The heat fluxes on the slab's bottom and top are added to determine the heat flux on the object's "surface." In particular, cables in a horizontal cable tray are assumed to be exposed to both heat fluxes on the top layer of cables and on the metal tray underlying the cables.

7.3.4.3 Code Benchmarking

COMPBRN has been used to simulate a number of wood, plastic, and oil fires. Results have been good for flammable materials. As discussed below, however, simulations of cable tray fires indicate wide uncertainties, partly because of uncertainties in the parameter values to be used, and partly because cable insulation is generally difficult to burn. The heat losses from melting as well as from radiation and convection are nearly comparable to the heat gains. Such a situation requires a more accurate accounting of the physics in the region of the fuel surface.

The vertical cable tray burning tests conducted by Przybyla and Christian (Reference 7.3.4-3) involve a single vertical tray loaded with PVC-insulated cable, ignited by a propane ribbon burner. The burner was left on for the duration of the test. The average velocity (defined as the maximum vertical propagation distance divided by the time to reach that distance) is estimated to be between 0.10 cm/s and 0.31 cm/s.

A COMPBRN simulation of these experiments yields an average velocity of approximately 0.6 cm/s. If we assume that the ratio of simulation to experimental velocity equals the inverse ratio of the propagation times, we get

$$2 \lesssim \frac{\tau^*}{\tau^*_{sim}} \lesssim 6 \qquad (7.3.4.3\text{-}1)$$

where τ^* is the characteristic propagation time.

Note that in some cases the experimental fire never reached the top of the burning tray, whereas the fire predicted by COMPBRN invariably does so.

The above result indicates that the COMPBRN prediction is rather conservative for the particular vertical tray configuration. To check COMPBRN's accuracy for horizontal trays, note that Pinkel (Reference 7.3.4-4) quotes an "average propagation velocity" of 1 inch per minute or 0.037 cm/s. Calculation of the flame front velocity along a 1-foot wide horizontal tray indicates that

$$0.02 \lesssim \overline{V} \lesssim 0.14 \text{ cm/s}$$

where the variability is due to input parameter variations. Again, letting the ratio of simulation velocity to the referenced value approximate the ratio of the actual propagation time to the predicted time, the result is

$$0.5 \lesssim \frac{\tau^*}{\tau^*_{sim}} \lesssim 3.8$$

As in the case of the vertical tray, the COMPBURN prediction is adequate, and generally conservative.

7.3.4.4 Development of Fire Propagation Histograms

In this section, the previous material is used to derive fire propagation time histograms for three cases: (1) vertical propagation from tray 1 to tray 2 (see Figure 7.3.4-1), (2) horizontal propagation across tray 1, and (3) propagation to tray C (see Figure 7.3.4-2). The first two cases involve fires that are initiated within the cable tray stack, while the third is driven by an external exposure fire.

7.3.4.4.1 Vertical Propagation Among Cable Trays

The distribution for τ_V^*, the time required for the fire to propagate from tray 1 to tray 2, depends on a variety of physical parameters. These include $\dot{m}_o''$, H_f and T_s^*, as discussed in Section 7.3.4.2.1, and also Q_p, a parameter used to model the pilot fuels which initiate the fire.

7.3.4.4.1.1 Pilot Fuels. Cable insulation, in general, is a fuel which is difficult to ignite and to burn. It is expected, therefore, that the fire in the lower tray is often initiated with a quantity of a more flammable fuel such as oil. Because these pilot fuels may burn more intensely than the cable insulation, the type and quantity of pilot fuel plays an important role in the ensuing fire propagation phase.

To model the effect of the pilot fuels, a quantity Q_p representing the amount of heat which can be released by burning the entire quantity of pilot fuel is defined.

The spectrum of possible values for Q_p is divided into three discrete classes: Q_p = 400 Btu (4×10^5 J), Q_p = 4,000 Btu (4×10^6 J), and Q_p = 40,000 Btu (4×10^7 J). To provide some physical reference points for the choices of Q_p, note that 400 Btu from a 1-foot square fuel packet whose surface is covered with cables corresponds roughly to cable insulation burning for 1 minute (i.e., the pilot fuel is a negligible contributor to growth), 4,000 Btu corresponds roughly to wood chips and paper burning for 2 minutes, and 40,000 Btu can be associated with oil burning for 1 minute.

7.3.4.4.1.2 Response Surface

An approximate functional relationship between $\tau_{V,DRM}$, the calculated propagation time, and the four input variables $\dot{m}_o''$, H_f, T_s^*, and Q_p, was developed using COMPBRN.

This relationship, or response surface, enables uncertainties in the input variables to be efficiently carried through the physical model.

The Latin Hypercube Sampling technique (Reference 7.3.4-5) was used to select the input vectors. The ranges of parameters used were

$$10^{-5} < \dot{m}''_o < 3 \times 10^{-3} \text{ kg/m}^2\text{s}$$

$$1.85 \times 10^7 < H_f < 2.7 \times 10^7 \text{ J/kg}$$

$$800 < T_s^* < 850^0\text{K}$$

Q_p = 400 Btu, 4,000 Btu, and 40,000 Btu

Important fixed parameters were

$$C_s = 1.8 \times 10^{-7} \text{ kg/J}$$

T_p^* (piloted ignition temperature) = $T_s^* - 40^0$K

$$k = 0.092 \text{ W/m}^0\text{K}$$

$$\alpha = 5.13 \times 10^{-8} \text{ m}^2\text{/s}$$

$$\gamma = 0.40$$

When the results are grouped by pilot fuel, $\tau_{V,DRM}$ is found to be well correlated by the dimensionless parameter θ, where

$$\theta = \left(\frac{\dot{m}''_o A_f}{M_f}\right)\left(\frac{\pi}{4\alpha}\right)\left(\frac{7k(T_s^* - T_o)}{\gamma \dot{m}''_o H_f}\right)^2 \qquad (7.3.4.4\text{-}1)$$

(M_f/A_f) is the amount of fuel per unit area. The other parameters have been previously defined. Substituting for the constant values, the following is obtained:

$$\theta = \frac{3.96 \times 10^6}{\dot{m}''_o}\left(\frac{T_s^* - 298}{H_f}\right)^2 \qquad (7.3.4.4\text{-}2)$$

θ represents the ratio of a characteristic ignition time (see Equation (7.3.4.1-9)) and a characteristic self-extinguishment time. This latter quantity, whose inverse is the first term of Equation (7.3.4.4-1), is simply the ratio of the available fuel mass to the mass burning rate. Note that using the ranges for $\dot{m}''_o$, H_f, and T_s^* given earlier, the following is obtained:

$$0.23 < \theta < 175$$

The correlation is of the form

$$\tau_{V,DRM} = C_1 + C_2\,\theta \qquad (7.3.4.4\text{-}3)$$

When there is no thermal barrier separating the two trays, C_1 and C_2 are as follows:

Vertical Propagation Time (τ_V)		
Q_p (Btu)	C_1 (min)	C_2 (min)
400	1.7	4.5
4,000	3.4	1.1
40,000	2.8	1.0

The distribution for τ_V changes dramatically when a thermal barrier is interposed between the lower and upper trays. If a 0.25-inch thick horizontal thermal barrier is located 2 inches below the top tray, COMPBRN calculations indicate that the heat flux received by the top tray is insufficient to cause ignition before the fuel in the lower tray is exhausted.

A case with oil as the pilot fuel is presented to illustrate this point. In these circumstances, the peak heat flux on the upper tray is approximately 1 W/cm^2; using Equation (7.3.4.1-9) and an ignition temperature of 800^0K, this translates to an ignition time of 5.5 minutes. Because the burning rate required to achieve this heat flux level is approximately 0.018 kg/ft^2s, approximately 6 kg of oil per square foot of tray are required to sustain this fire. Because the trays are 3 inches deep, however, they will hold approximately 6 kg of oil per square foot at most; and this, only when they do not hold anything else (including cables).

Thus for the problem geometry considered, vertical fire propagation through a thermal barrier is an unlikely event. Propagation to tray 2 in this case is not impossible, because noncombusted flammable gases released by the fire on tray 1 may slip around the barrier and ignite underneath tray 2 (Reference 7.3.4-6).

7.3.4.4.1.3 Fire Propagation Histograms. As discussed in Section 7.3.4.2, our uncertainties in our model's predictions, given a pilot fuel, stem from uncertainties in the values of $\dot{m}''_0$, H_f, and T^*_s, and from uncertainties in the various submodels used to construct the overall model. The fuel parameter uncertainties are characterized by the distributions given in Section 7.3.4.2.1, and are carried through Equation (7.3.4.4-3) to form a histogram for $\tau_{V,DRM}$ for each of the pilot fuels. These histograms are presented in Tables 7.3.4-1 through 7.3.4-3.

To incorporate the uncertainty in the basic model's predictions, the actual spread time τ_V^* is modeled as the product of COMPBRN's propagation time prediction and an error factor ϕ

$$\tau_V^*(Q_p) = \phi\tau_{V,DRM}(Q_p) \qquad (7.3.4.4\text{-}4)$$

Because our data base has little information for τ_V^*, a subjective distribution for ϕ is made using the evidence presented in Section 7.3.4.4.3, as well as our knowledge of COMPBRN's conservatisms and limitations. The distribution is made intentionally wide to reflect a rather diffuse state of knowledge, and is lognormal with a 95% upper bound of 4.0 and a 5% lower bound of 0.8. Some important parameters are

$\mu\phi$: 0.582

$\sigma\phi$: 0.489

Mean: 2.0

Median: 1.8

Mode: 1.4

The distribution for $\tau_{V,DRM}$ can now be combined with the distribution for ϕ using DPD arithmetic to obtain the histograms in Tables 7.3.4-4 through 7.3.4-6 for τ_V^*, the actual time for propagation between trays 1 and 2 and across tray 1.

7.3.4.4.2 Horizontal Propagation Across Cable Tray

The distribution for τ_H^*, the characteristic time for fire propagation across tray 1 in Figure 7.3.4-1, is derived in a manner identical to that used to derive τ_V^*. The response surface for the COMPBRN predictions is

$$\tau_{H,DRM} = C_1 + C_2 \qquad (7.3.4.4\text{-}5)$$

where C_1 and C_2 are as follows:

Horizontal Propagation Time (τ_H)		
Q_p (Btu)	C_1 (min)	C_2 (min)
400	2.6	9.6
4,000	4.7	6.2
40,000	3.0	4.3

These coefficients do allow for a vertical thermal barrier inserted in the tray. This barrier retards propagation, but does not prevent it, because the cable tray flames can radiate heat over the barrier to the other side.

Three distributions for $\tau_{H,DRM}$ which reflect parameter uncertainties are given in Tables 7.3.4-7 through 7.3.4-9. Each distribution applies to a particular value of Q_p. The distributions for τ_H^*, which also incorporate modeling uncertainties via the error factor ϕ defined in Equation (7.3.4.4-4), are presented in Tables 7.3.4-10 through 7.3.4-12.

7.3.4.4.3 Propagation Among Separate Tray Groups

Consider the cable trays shown in Figure 7.3.4-2. Direct fire propagation between trays A and C is unlikely for the reasons discussed in Section 7.3.4.4.1.2. Furthermore, tray B is sufficiently far away that a fire on that tray would probably not initiate a fire on tray C by itself. If a large external fire is burning beneath the two tray groups, however, the combined heat fluxes from both trays A and B may be sufficient to ignite tray C. A 2-foot diameter oil fire is assumed to be burning at location X in Figure 7.3.4-2, and the distribution of the time to propagate to tray C is derived in the following sections.

7.3.4.4.3.1 Response Surface. The response surface for the fire propagation time, τ_C^*, is derived in Section 7.3.4.4.1.2. Thirty-two triplets of values for $\dot{m}_o''$, H_f, and T_s^* were created from the given ranges for these parameters, using the Latin Hypercube Sampling technique. These triplets, or input vectors, were then processed by COMPBRN to determine the "response" of the model to the input.

In 17 of the 32 calculations, the fire did not propagate to tray C. In these cases, the fires on trays A and B exhausted their available fuel before tray C absorbed enough heat to ignite. We define a new dimensionless parameter χ to help us model this phenomenon as follows.

Let H_i represent a characteristic amount of heat needed to raise the cable insulation temperature to ignition levels

$$H_i = {}_fC_p(T_s^*-T_A) \quad (J) \qquad (7.3.4.4-6)$$

Furthermore, let H_A represent a characteristic amount of heat available to be radiated from a given fuel packet

$$H_A = {}_f\gamma H_f \quad (J) \qquad (7.3.4.4-7)$$

We define the ratio of H_i to H_A as χ, or

$$\chi = \frac{C_p(T_s^* - T_A)}{\gamma H_f} \qquad (7.3.4.4-8)$$

Substituting in appropriate values for C_p and γ (see Section 7.3.4.4.1.2), we obtain

$$\chi = 2610 \left(\frac{T_s^* - 298}{H_f} \right) \qquad (7.3.4.4\text{-}9)$$

Using χ and the previously defined parameter θ (Equation 7.3.4.4-2), our correlation for $\tau_{C,DRM}$ (min) is

$$\tau_{C,DRM} = \begin{cases} \frac{610}{\infty} \chi - 18, & \chi < .0544 + .00407\,\theta \\ \text{otherwise} \end{cases} \qquad (7.3.4.4\text{-}10)$$

7.3.4.4.3.2 Fire Propagation Histogram. Monte Carlo sampling calculations off of Equation (7.3.4.4-10) using the distributions for $\dot{m}_o''$, H_f and T_s^* given in Section 7.3.4.2.1 indicate that the probability of nonpropagation is about 0.31. The uncertainty quantified by this probability stems from uncertainties in the actual values of $\dot{m}_o''$, H_f, and T_s^*. All fires are conservatively assumed to propagate to tray C, and large values of $\tau_{C,DRM}$ are assigned to the ones that did not actually propagate.

The distribution for $\tau_{C,DRM}$ is given in Table 7.3.4-13. Note that the exposure fire considered ignited tray A in approximately 1 minute, and tray B in approximately 8 minutes.

The distribution for τ_C^*, the actual time for fire propagation to tray C, is the product of the above histogram for $\tau_{C,DRM}$ and the error factor ϕ defined in Section 7.3.4.4.1.3. The resulting histogram is given in Table 7.3.4-14. The treatment of the nonpropagation cases is not especially critical; most of the fires with long propagation times will be extinguished before they can actually propagate to tray C.

7.3.4.5 References

7.3.4-1 Siu, N. O., "Probabilistic Models for the Behavior of Compartment Fires," UCLA-ENG-8090, University of California, Los Angeles, 1980.

7.3.4-2 "Review of the Indian Point Station Fire Protection Program," Consolidated Edison Company of New York and Power Authority of the State of New York, April 1977.

7.3.4-3 Przybyla, L. and W. J. Christian, "Development and Verification of Fire Tests for Cable Systems and System Components," Quarterly Reports 2 and 3, September 1, 1977 to February 28, 1978, NUREG/CR-0152, Underwriters Laboratories, Inc., June 1978.

7.3.4-4 Pinkel, I. I., "Estimating Fire Hazards Within Enclosed Structures as Related to Nuclear Power Stations," BNL-23892, Brookhaven National Laboratory, January 1978.

7.3.4-5 Iman, R. L., J. C. Helton, and J. E. Campbell, "Risk Methodology for Geologic Disposal of Radioactive Waste: Sensitivity Analysis Techniques," NUREG/CR-0394, 1978.

7.3.4-6 Hunter, L. W., "Models of Horizontal Electric Cables and Cable Trays Exposed to a Fire Plume," Combustion and Flame, v.35, 311-322 (1979).

TABLE 7.3.4-1

HISTOGRAM OF THE PREDICTED VERTICAL SPREAD FIRE PROPAGATION TIME ($\tau_{V,DRM}$), NO BARRIER, Q_p = 400 BTU, INCLUDING PARAMETER UNCERTAINTIES ONLY

$\tau_{V,DRM}$ (min)	Probability	Cumulative Probability
2.5	0.111	0.111
7.5	0.322	0.433
12.5	0 211	0.644
17.5	0.117	0.761
22.5	0.075	0.836
27.5	0.046	0.882
32.5	0.032	0.914
37.5	0.022	0.936
42.5	0.064	1.000

TABLE 7.3.4-2

HISTOGRAM OF THE PREDICTED VERTICAL SPREAD FIRE PROPAGATION TIME ($\tau_{V,DRM}$), NO BARRIER, Q_p = 4,000 BTU, INCLUDING PARAMETER UNCERTAINTIES ONLY

$\tau_{V,DRM}$ (min)	Probability	Cumulative Probability
2.5	0.335	0.335
7.5	0.542	0.877
12.5	0 088	0.965
17.5	0.022	0.987
22.5	0.013	1.000

TABLE 7.3.4-3

HISTOGRAM OF THE PREDICTED VERTICAL SPREAD FIRE PROPAGATION TIME ($\tau_{V,DRM}$), NO BARRIER, Q_p = 40,000 BTU, INCLUDING PARAMETER UNCERTAINTIES ONLY

$\tau_{V,DRM}$ (min)	Probability	Cumulative Probability
2.5	0.470	0.470
7.5	0.428	0.898
12.5	0 071	0.969
17.5	0.020	0.989
22.5	0.013	1.000

TABLE 7.3.4-4

HISTOGRAM OF THE
VERTICAL SPREAD FIRE PROPAGATION
TIME (τ_V^*), NO BARRIER, Q_p = 400 BTU,
INCLUDING MODELING UNCERTAINTIES

τ_V^* (min)	Probability	Cumulative Probability
2.8	0.011	0.041
6.3	0.125	0.167
11.5	0 163	0.330
17.8	0.170	0.500
24.4	0.139	0.638
35.0	0.154	0.792
60.0	0.157	0.948
120.0	0.051	1.000

TABLE 7.3.4-5

HISTOGRAM OF THE
VERTICAL SPREAD FIRE PROPAGATION
TIME (τ_V^*), NO BARRIER, Q_p = 4,000 BTU,
INCLUDING MODELING UNCERTAINTIES

τ_V^* (min)	Probability	Cumulative Probability
1.7	0.018	0.018
3.5	0.176	0.194
6.1	0.146	0.341
7.8	0.065	0.406
11.4	0.244	0.649
16.4	0.133	0.782
24.3	0.164	0.946
46.6	0.054	1.000

TABLE 7.3.4-6

HISTOGRAM OF THE
VERTICAL SPREAD FIRE PROPAGATION
TIME (τ_V^*), NO BARRIER, Q_p = 40,000 BTU,
INCLUDING MODELING UNCERTAINTIES

τ_V^* (min)	Probability	Cumulative Probability
1.7	0.026	0.026
2.9	0.136	0.161
4.4	0.123	0.285
6.4	0.207	0.492
9.8	0.126	0.617
13.1	0.114	0.731
20.5	0.214	0.944
43.6	0.056	1.000

TABLE 7.3.4-7

HISTOGRAM OF THE PREDICTED HORIZONTAL SPREAD FIRE PROPAGATION TIME ($\tau_{H,DRM}$), NO BARRIER, Q_p = 400 BTU, INCLUDING MODELING UNCERTAINTIES

$\tau_{H,DRM}$ (min)	Probability	Cumulative Probability
2.5	0.008	0.008
7.5	0.120	0.128
12.5	0 154	0.282
17.5	0.139	0.421
22.5	0.113	0.534
27.5	0.086	0.620
32.5	0.071	0.691
37.5	0.055	0.746
45.0	0.076	0.822
55.0	0.052	0.874
67.5	0.046	0.920
92.5	0.048	0.968
115.0	0.032	1.000

TABLE 7.3.4-8

HISTOGRAM OF THE PREDICTED HORIZONTAL SPREAD FIRE PROPAGATION TIME ($\tau_{H,DRM}$), NO BARRIER, Q_p = 4,000 BTU, INCLUDING MODELING UNCERTAINTIES

$\tau_{H,DRM}$ (min)	Probability	Cumulative Probability
2.5	0.001	0.0001
7.5	0.152	0.153
12.5	0 231	0.384
17.5	0.177	0.561
22.5	0.121	0.682
27.5	0.086	0.768
32.5	0.058	0.826
40.0	0.069	0.895
52.5	0.052	0.947
87.5	0.046	0.993
117.5	0.007	1.000

TABLE 7.3.4-9

HISTOGRAM OF THE PREDICTED HORIZONTAL SPREAD FIRE PROPAGATION TIME ($\tau_{H,DRM}$), NO BARRIER, Q_p = 40,000 BTU, INCLUDING MODELING UNCERTAINTIES

$\tau_{H,DRM}$ (min)	Probability	Cumulative Probability
2.5	0.045	0.045
7.5	0.338	0.383
12.5	0 240	0.623
17.5	0.134	0.757
22.5	0.080	0.837
27.5	0.048	0.885
35.0	0.056	0.941
55.0	0.046	0.987
95.0	0.013	1.000

TABLE 7.3.4-10

HISTOGRAM OF THE
HORIZONTAL SPREAD FIRE PROPAGATION
TIME (τ_H^*), NO BARRIER, Q_p = 400 BTU,
INCLUDING MODELING UNCERTAINTIES

τ_H^* (min)	Probability	Cumulative Probability
4.9	0.049	0.049
9.2	0.083	0.132
15.9	0.104	0.236
21.4	0.107	0.343
33.3	0.138	0.481
46.8	0.107	0.588
60.8	0.104	0.692
87.4	0.145	0.837
149.0	0.112	0.949
280.0	0.051	1.000

TABLE 7.3.4-11

HISTOGRAM OF THE
HORIZONTAL SPREAD FIRE PROPAGATION
TIME (τ_H^*), NO BARRIER, Q_p = 4,000 BTU,
INCLUDING MODELING UNCERTAINTIES

τ_H^* (min)	Probability	Cumulative Probability
5.6	0.081	0.081
10.9	0.140	0.221
19.6	0.157	0.378
32.6	0.192	0.570
47.1	0.128	0.698
67.0	0.150	0.848
100.0	0.084	0.932
200.0	0.068	1.000

TABLE 7.3.4-12

HISTOGRAM OF THE
HORIZONTAL SPREAD FIRE PROPAGATION
TIME (τ_H^*), NO BARRIER, Q_p = 40,000 BTU,
INCLUDING MODELING UNCERTAINTIES

τ_H^* (min)	Probability	Cumulative Probability
3.2	0.049	0.049
5.4	0.092	0.141
8.1	0.112	0.253
14.5	0.096	0.349
20.7	0.218	0.567
33.6	0.174	0.741
47.5	0.098	0.839
67.1	0.087	0.926
137.0	0.074	1.000

TABLE 7.3.4-13

HISTOGRAM OF THE PREDICTED SPREAD TIME TO TRAY C ($\tau_{C,DRM}$), INCLUDING PARAMETER UNCERTAINTIES ONLY

$\tau_{C,DRM}$ (min)	Probability	Cumulative Probability
12.5	0.190	0.190
17.5	0.320	0.510
22.5	0.135	0.645
27.5	0.050	0.695
32.5	0.050	0.745
37.5	0.050	0.795
42.5	0.050	0.845
47.5	0.050	0.895
52.5	0.050	0.945
57.5	0.055	1.000

TABLE 7.3.4-14

HISTOGRAM OF THE SPREAD TIME TO TRAY C (τ_C*), INCLUDING MODELING UNCERTAINTIES

τ_C* (min)	Probability	Cumulative Probability
8.3	0.074	0.074
12.2	0.127	0.201
22.4	0.114	0.315
35.4	0.163	0.478
48.3	0.206	0.684
70.9	0.151	0.835
117.2	0.097	0.932
152.0	0.068	1.000

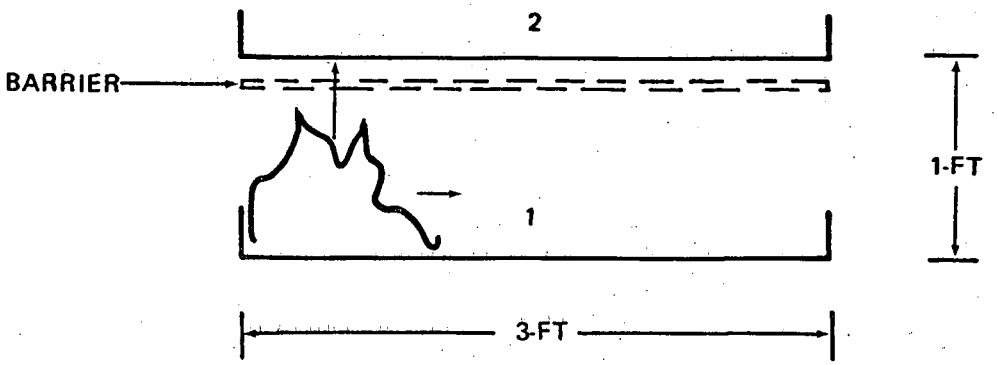


Figure 7.3.4-1. Cable Tray Configuration in the Indian Point 2 Cable Spreading Room

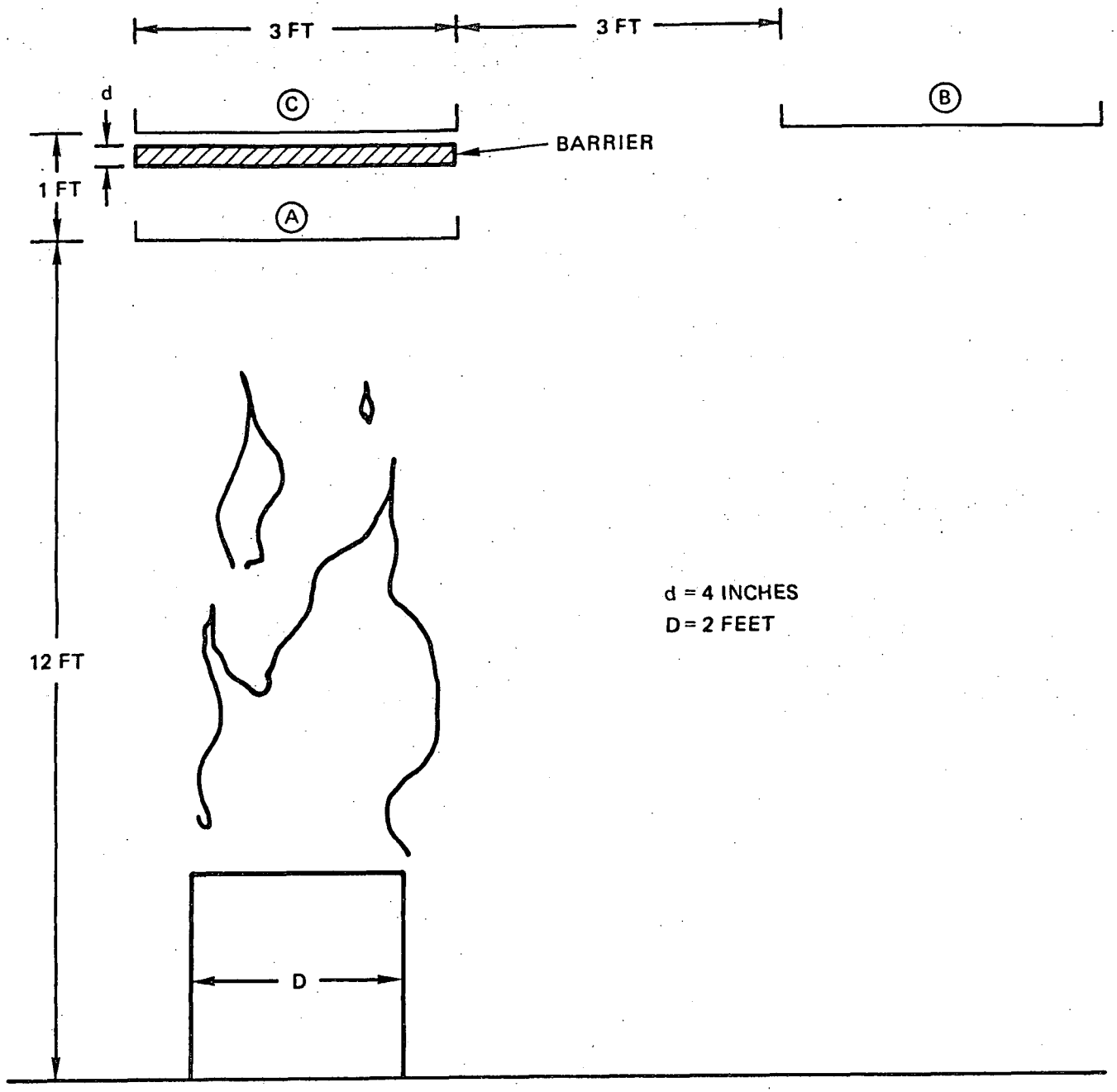


Figure 7.3.4-2. Fire Spread Through Elevated Trays

7.3.5 APPENDIX II -- A SIMPLE CABINET AIR TEMPERATURE MODEL

Consider the situation pictured in Figure 7.3.5-1. The following illustrates the computation of the temperature rise in the cabinet due to the impinging external heat flux $\dot{q}''_{cab}$. Heat balances at three nodes are performed. The first node represents the exposed cabinet wall (the "hot wall" or HW), the second represents the cold wall (CW), and the third represents the air inside the cabinet (A).

The heat fluxes entering and leaving the hot wall are pictured in Figure 7.3.5-2. Equating the gains to the losses leads to

$$\dot{q}''_{cab} = \rho\dot{q}''_{cab} + h_{H,o}(T_{HW} - T_\infty) + \varepsilon\sigma(T_{HW}^4 - T_\infty^4) + h_{H,i}(T_{HW} - T_A) + \varepsilon\sigma(T_{HW}^4 - T_A^4) \qquad (7.3.5\text{-}1)$$

ρ = reflectivity of cabinet wall

ε = $1-\rho$
= emissivity of cabinet wall

σ = Stefan-Boltzmann constant
= 5.6697×10^{-8} ($W/m^2\ {}^0K^4$)

T_∞ = ambient air temperature (298^0K)

$h_{H,o}$ = convective heat transfer coefficient for outside of cabinet hot wall ($W/m^2\ {}^0K$)

$h_{H,i}$ = convective heat transfer coefficient for inside of cabinet hot wall ($W/m^2\ {}^0K$)

Because the wall is thin and has a high thermal conductivity, the wall temperature is assumed to equilibrate instantaneously (i.e., no transient terms are included in the heat balance) and conduction losses across the wall are also neglected.

In a similar manner, the heat balance for the cold wall (all cabinet surfaces not directly exposed to the fire) yields (see Figure 7.3.5-2):

$$h_{C,i}(T_A - T_{CW}) + \varepsilon\sigma(T_A^4 - T_{CW}^4) = h_{C,o}(T_{CW} - T_\infty) + \varepsilon\sigma(T_{CW}^4 - T_\infty^4) \qquad (7.3.5\text{-}2)$$

Using Figures 7.3.5-2 and 7.3.5-3, the heat balance for the cabinet air node may also be written

$$A_H[h_{H,i}(T_{HW} - T_A) + \varepsilon\sigma(T_{HW}^4 - T_A^4)] = A_C[h_{C,i}(T_A - T_{CW}) + \varepsilon\sigma(T_A^4 - T_{CW}^4)] \qquad (7.3.5\text{-}3)$$

A_H = area of hot wall (m^2)

A_C = area of cold wall (m^2)

Equations (7.3.5-1) through (7.3.5-3) represent a set of coupled, nonlinear algebraic equations. The solution of these equations is relatively easy; a Newton-Raphson-type iteration scheme was used.

The heat sink effect of the components in the cabinet or of the floor was not modeled. The asymptotic temperature is calculated because time dependent calculations indicate that steady state conditions are achieved extremely rapidly.

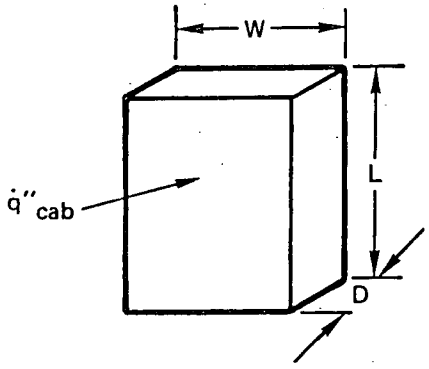


Figure 7.3.5-1. Problem Setup

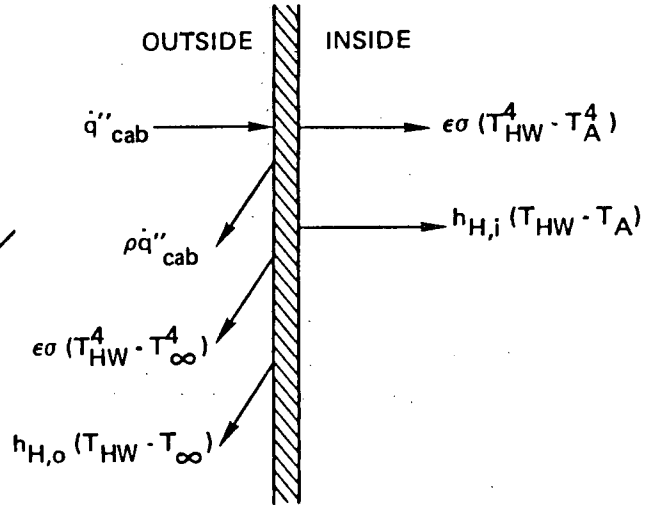


Figure 7.3.5-2. Hot Wall Heat Balance

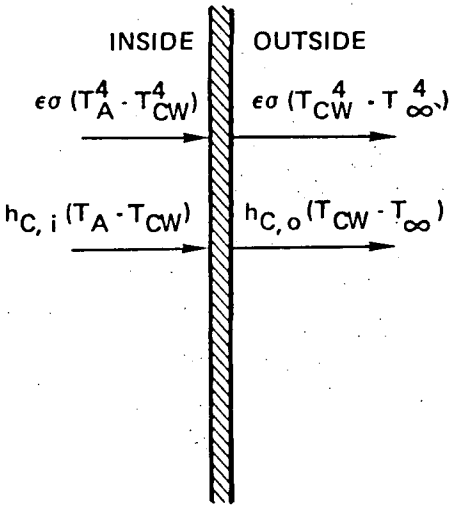


Figure 7.3.5-3. Cold Wall Heat Balance

7.3.6 APPENDIX III -- HEAT FLUXES FROM AN OIL POOL FIRE

This appendix uses the heat flux equations presented in Section 7.3.4 (Appendix I), Equations (7.3.4.1-3) and (7.3.4.1-4), to calculate the heat flux from an oil pool fire.

Consider the fire shown in Figure 7.3.6-1. Because the target does not lie within the hot buoyant plume above the flames, the heat flux to the target is primarily radiative. The source heat flux at the flame boundary is then given by

$$\dot{q}''_R = \gamma \dot{Q}/A_{f\ell} (W/m^2) \qquad (7.3.6\text{-}1)$$

Modeling the flame as a cylinder of radius R and height $Z_{f\ell}$,

$$\dot{q}''_R = \gamma \dot{m}'' H_f \left(\frac{R}{R + 2Z_{f\ell}} \right) \qquad (7.3.6\text{-}2)$$

The specific burning rate, $\dot{m}''$, is constant when there are no heat sources external to the fire. The fraction of heat released which is radiated away from the fire, γ, ranges between 0.20 and 0.40 for most fires (Reference 7.3.6-1); the latter value is conservatively used. For an oil pool fire, representative values for $\dot{m}''$ and H_f are

$$\dot{m}'' = 0.061 \text{ kg/m}^2\text{s}$$

$$H_f = 4.20 \times 10^7 \text{ J/kg}$$

The flame height, $Z_{f\ell}$, can be calculated from Thomas' correlation (Reference 7.3.6-2) for pool fires as

$$Z_{f\ell} = 84R \left(\frac{\dot{m}''}{\rho_A \sqrt{2gR}} \right)^{0.61} = 30.6(\dot{m}'')^{0.61}(R)^{0.695}(M) \qquad (7.3.6\text{-}3)$$

To determine the heat flux impinging on the target, the following is used:

$$\dot{q}''_t = F_{t\text{-}f\ell} \dot{q}''_R$$

$F_{t\text{-}f\ell}$ = shape factor from target to flame

If the target face is parallel to the flame axis as shown in Figure 7.3.6-1, and is represented by a differential surface located at the height of the flame (or at the base), a distance X_c away, the shape factor is given by

$$F_{t\text{-}f\ell} = \frac{1}{\pi Y} \tan^{-1}\left(\frac{X}{\sqrt{Y^2 - 1}} \right) + \frac{X}{\pi} \left[\frac{A-2Y}{Y\sqrt{AB}} \tan^{-1} \sqrt{\frac{A(Y-1)}{B(Y+1)}} \right.$$

$$\left. - \frac{1}{Y} \tan^{-1} \sqrt{\frac{Y-1}{Y+1}} \right] \qquad (7.3.6\text{-}4)$$

where

$$X = H/R$$

$$Y = X_c/R$$

$$A = (1+Y)^2 + X^2$$

$$B = (1-Y)^2 + X^2$$

For a similarly located target whose face is perpendicular to the flame axis, the shape factor is given by:

$$F_{t\text{-}f\ell} = \frac{1}{\pi}\left[\tan^{-1}\sqrt{\frac{X+R'}{X-R'}} - \frac{A}{B}\tan^{-1}\sqrt{\frac{X-R'}{X+R'}}\right] \qquad (7.3.6\text{-}5)$$

where

$$X = X_c/H$$

$$R' = R/H$$

$$A = 1 + X^2 - R'^2$$

$$B = 1 + X^2 + R'^2$$

Of course, the pool fire considered cannot act as a heat source indefinitely. The burning rate is given by

$$\dot{m} = \dot{m}'' \pi R^2 \qquad (7.3.6\text{-}6)$$

For an oil fire,

$$\dot{m} = 11.5R^2 (\text{kg/min}) \qquad (7.3.6\text{-}7)$$

Thus, the fire acts as a source of strength $\dot{q}_R''$, until the self-extinguishment time τ_{se} is reached, whereupon its source strength is reduced to zero

$$\tau_{se} = \frac{M_f}{\dot{m}} \qquad (7.3.6\text{-}8)$$

where M_f is the mass of the fuel available for burning.

References

7.3.6-1 Siu, N. O. "Probabilistic Models for the Behavior of Compartment Fires," UCLA-ENG-8090, University of California, Los Angeles, 1980.

7.3.6-2 Thomas, P. H., "The Size of Flames from Natural Fires," Tenth Symposium (Int'l) on Combustion, 844-859 (1963).

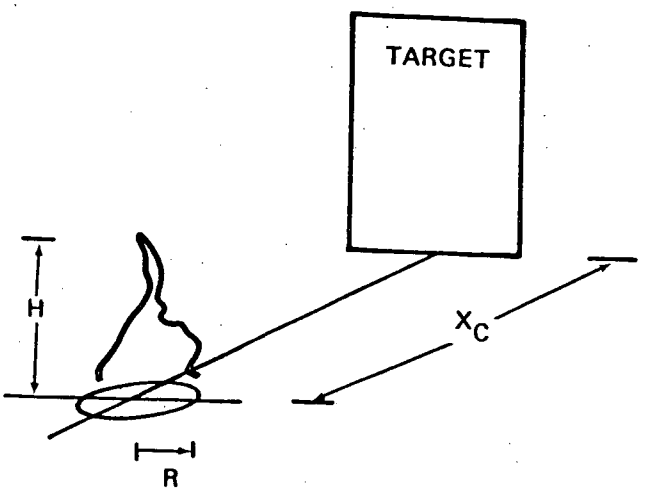


Figure 7.3.6-1. Model for Computing Heat Fluxes from a Pool Fire

7.4 FLOODING

This section examines flooding as an initiator of an accident sequence leading to core melt. External and internal flood sources are considered.

7.4.1 EXTERNAL FLOODING

The grade elevation at the plant embankment adjoining the river is 14.0 feet. The elevation increases to above 14.0 feet at all buildings and exterior vessels and equipment at the site. An evaluation was previously made of the probable maximum flood at Indian Point as a result of high tidal surge conditions during a severe hurricane (Reference 7.4-1). Based on predictions by the U.S. Corps of Engineers of the maximum tidal surge in New York Harbor resulting from the maximum probable hurricane (Reference 7.4-2), the high water mark at Indian Point was estimated to be 10.4 feet, with a maximum high water mark of 13.1 feet at maximum spring high tide of 2.7 feet. The study was based on records since 1635 with only one recorded occurrence of a maximum surge of 11 feet in New York Harbor (7.5 feet at Indian Point). This maximum elevation corresponds to an annual frequency of occurrence of 3×10^{-3}.

A 1971 study (Reference 7.4-3) concluded that the maximum sustained water surface elevation at the Indian Point site is 14.0 feet, based on the extraordinary combination of a Hudson River maximum flood, probable maximum precipitation over the Esopus Creek Basin resulting in failure of the Ashokan Dam, and a hurricane at New York Bay. The maximum flood and hurricane used in the study were defined by the U.S. Corps of Engineers. The frequency of occurrence of each of these was estimated in the study as being between 1.0×10^{-3} and 1.0×10^{-4}. Collectively, these events and the dam failure have an estimated annual frequency of 10^{-8} to 10^{-12}.

The response (Reference 7.4-4) to NRC Question 2.11, regarding maximum hurricane surges during spring tides, reevaluated earlier work using considerations of estuary effects in the Hudson River from a surge at the mouth, the Battery. The study considered variations along the Hudson River in channel geometry, friction coefficient, and hurricane stages at the Battery as a function of time. The river is about 5,000 feet wide at Indian Point and the maximum water surface elevation at this location from hurricanes, wind surges, and high tides was determined to be 12.4 feet above mean sea level.

In view of the foregoing flood levels and the grade elevations which exceed Elevation 14.0' at the critical facilities of the plant, external flooding contribution to core melt frequency is extremely small.

7.4.2 INTERNAL FLOODING

7.4.2.1 NonCategory I Systems

The nonCategory I systems and components at Indian Point 2 have been extensively reviewed by Consolidated Edison and by the Nuclear Regulatory Commission. References 7.4-5 through 7.4-8 present the reviews that Consolidated Edison has made of these systems. Reference 7.4-9 presents the NRC's Safety Evaluation Report on the Susceptibility of Safety Related Systems to Flooding From Failure of NonCategory I Systems for Indian Point Nuclear Power Station Unit 2. The results of these reviews and reports demonstrate that failure of these nonCategory I systems at Indian Point 2 will not impair the operation of safety systems necessary for plant protection. Because of the similarities in design of Indian Point Units 2 and 3, these results generally apply to Indian Point Unit 3 also.

7.4.2.1.1 Quantification of Internal Flooding From NonCategory I Sources

7.4.2.1.1.1 Circulating Water Failure. Flooding from this source has the potential for flooding the lowest level (Elevation 15') of the control building. This elevation in the control building contains the Class 1E 480V distribution switchgear. Loss of this switchgear initiates a station blackout.

Given a circulating water pipe failure, Reference 7.4-5 estimates the flooding must continue for 10 minutes to potentially affect the Class 1E switchgear. Indication of the flooding is available in the control room of Unit 2 from two independent level detectors in the Unit 1 condenser pit area. The flooding is mitigated by: (1) securing the affected condenser section circulating water pump, or (2) opening the rollup doors on Elevation 15' of the turbine building.

This event is self-limiting in that flooding from this source will flood the condensate pump motors and the 6.9 kV switchgear which provides power to the circulating water pumps. Flooding of the condensate pumps results in a reactor trip due to loss of main feed flow. Flooding of the 6.9 kV switchgear, results in a loss of offsite power supply to the unit and a unit trip.

The access to the control building from the turbine building is controlled, normally closed, and locked. The effect of the closed door, in conjunction with failure of the 6.9 kV switchgear, serves to prevent damage to or loss of the vital 480V switchgear with flooding occurring in the turbine building.

With no credit taken for operator corrective actions, flooding from the circulating water system will initiate a reactor trip and loss of offsite power with a frequency equal to the frequency of occurrence of the flooding. If the frequency of occurrence is as high as 1.0×10^{-3} per plant year (which corresponds to a failure rate of approximately 1.0×10^{-7} per hour), this event does not contribute significantly to

plant risk when compared to the frequency of occurrence of reactor trip and the frequency of occurrence of a loss of offsite power due to other causes.

7.4.2.1.1.2 Fire Protection System Failure. The fire protection system is the other nonCategory I system which contains or has available enough water to cause flooding in localized areas if rupture were to occur. Reference 7.4-8 discusses flooding from the fire protection system for the following safety related areas of the plant:

- Electrical Tunnel Flooding. Flooding of the electrical tunnel from the fire protection system requires coincident occurrence of the following events: (1) deluge valve tripping open to supply water to the headers, (2) rupture of piping tripping open spray nozzles, and (3) plugging of a 10-inch floor drain at Elevation 33'. Even with all of these events occurring, cable failure due to flooding should not occur due to the design of the cable. If the frequency of failure of the deluge valve is 1.0×10^{-3} per plant year (approximately 1.0×10^{-7} per hour) for failing open, and the frequency of pipe rupture is 1.0×10^{-3} per plant year, the frequency of occurrence of rupture of the fire protection system in the electrical tunnel is 1.0×10^{-6} per plant year. This frequency is less than the frequency of occurrence of fire in the electrical tunnel and is, therefore, not a significant contributor to plant risk.

- Diesel Generator Building Flooding. Flooding of the diesel generator building from the fire protection system requires coincident rupture or inadvertent actuation of the fire protection system and plugging of a 12-inch drain line in the pit area. Flooding of the diesel generators does not initiate a plant transient; however, the plant would be shut down due to technical specification requirements. Rupture or excessive flow from the fire protection system to the diesel generator building is alarmed in the control room on panel "SO." If no credit is taken for operator action to isolate the source of the flooding in response to the indicated alarm, and no credit is taken for the drain line, and the expected outage time per event is assumed to be 10 hours, then the expected unavailability of all three diesel generators due to flooding from the fire protection system is approximately 1.0×10^{-6} (1.0×10^{-7} failures per hour times 10 hours). To cause plant damage, this flooding must exist concurrently with a transient which requires diesel generator operation. The contribution to frequency of diesel generator failure on demand from this event is approximately 1.0×10^{-6} and is negligible in relation to other causes of diesel generator failure.

- Charcoal Filter Flooding. Because of the location of the charcoal filter units, the design of the filter housing and associated drainage system, and the small amount of water involved, flooding from this source is not quantified.

7.4.2.2 Category I Systems

Failures of Category I systems and components also have a potential for affecting safety related systems in various areas of the plant. A discussion of the involved areas, systems, and components, is presented in the following sections.

7.4.2.2.1 Primary Auxiliary Building (PAB)

For both units, the PAB houses most of the Category I engineered safety features systems in addition to housing nonCategory I reactor support systems. The building contains several floors, all of which drain to Elevation 15'. The residual heat removal (RHR) pumps are the only Category I pumps located at the 15' level of the PAB. Any flooding source which is capable of flooding the Elevation 15' level could cause loss of the RHR pumps due to loss of the motors. It is estimated that 31,500 gallons are necessary to cause loss of the RHR pump motors by flooding. Some protection is afforded by a door flap to the transformer yard at Elevation 18'-8". This flap will drain an estimated 800 gpm with water level at Elevation 19'-0". Potential sources of flooding of this magnitude and the results of such flooding are:

1. Refueling Water Storage Tank (RWST) Supply to the Containment Spray Pumps, Safety Injection Pumps and the RHR Pumps. The RWST contains 350,000 gallons of water for use by the safeguards systems in the event of a LOCA. Rupture of the supply lines from the RWST inside the PAB would result in flooding of the Elevation 15' level of the PAB, but this event would not initiate a plant transient. Indication of this event is available from RWST level indicators and alarms and from plant operators stationed in the PAB. Loss of the RWST supply would result in a plant shutdown due to technical specification limits on water level. The effect of loss of the RWST during accidents is quantified in the event trees for Indian Point 2 and Indian Point 3. Loss of the RWST due to pipe rupture is included with the frequency of failure of the RWST and, for this reason, is not quantified in this section.

2. Service Water System. Among other services, the service water system supplies the component cooling heat exchangers located in the PAB between Elevations 68' and 98' (41' to 73' for IP3). (The PAB also contains service water supply and return lines for services contained in other buildings.) Failure of the service water supply or return line(s) (18-inch diameter) for the component cooling heat exchanger(s) would cause flooding of Elevation 15' in the PAB and loss of the RHR pumps. In addition, such line failures could cause loss of the component cooling pumps which are located below the heat exchangers. Loss of component cooling would result in a plant shutdown. Reactor coolant pump (RCP) seal cooling in Unit 2 would be maintained by the charging system, with the charging pumps provided with cooling water from the city water system. Therefore, no plant transient is expected for Unit 2. Indications of flooding from this source include: component cooling temperature and pressure alarms,

service water header pressure indications and alarms, and plant operators stationed in the PAB. Quantification of the failure of the service water piping to the component cooling water system is included in the quantification of the service water system frequency of failure. For this reason, the quantification of this failure is not included in this section.

3. Component Cooling System. Rupture or a large leak from this system would lead to a plant shutdown due to the loss of component cooling to the RCPs. This would result in a plant shutdown with RCP seal cooling being provided by the charging system as described in 2, above. Indications of this event are provided by component cooling surge tank level alarms, component cooling temperature and header pressure alarms, and plant operators stationed in the PAB. Failure of this piping is included in the frequency of failure of the component cooling quantified in the systems analysis and is, therefore, not included in this section.

7.4.2.2.2 Diesel Generator Building (DGB)

Service water is supplied to the jacket water coolers and the lube oil coolers for all three emergency diesel generators. Failure in a service water supply or return line should not cause loss of the emergency diesel generators as the DGB is drained by several 12-inch drain lines. Flooding of the emergency diesel generators would not cause a plant transient; however, the plant would be shut down due to technical specification requirements. The effect of concurrent failure of this piping and the occurrence of a plant transient requiring the emergency diesel generators is included in the quantification of the frequency of failure of the service water system and is, therefore, not quantified in this section.

7.4.2.2.3 Auxiliary Feed Pump Building (AFPB)

The drainage capabilities of this building (i.e., door flap to the transformer yard similar to the PAB) have been designed to handle the water discharged from a feedwater line break. Failure of the Category I piping from the condensate storage tank will not result in flooding of the AFPB because of the size of the lines involved, and the capacity of the drainage provisions. Indication of flooding from this source is available from CST level indicators and alarms. Loss of water from this tank would result in a plant shutdown due to technical specification limits. The effect of concurrent CST failure and auxiliary feedwater system initiation is included in the quantification performed to determine the frequency of failure of the auxiliary feedwater system. For this reason, it is not included in this section.

7.4.2.2.4 Control Building (CB)

The service water system supplies the instrument air compressor closed loop cooling system heat exchangers located at Elevation 15' of this building. Also located at this elevation, are the vital 480V switchgear buses. Flooding of this elevation could result in loss of power to the unit and a reactor scram.

The two 3-inch service water supply and return lines penetrate the CB in the vicinity of the closed loop cooling heat exchangers which are located away from the 480V switchgear buses. This results in relatively short piping runs, and no immediate loss of the buses in the event of a large leak or rupture of the service water pipes.

Drainage of the CB consists of two 4-inch floor drains and seven 4-inch hub drains. These drains are sized to remove the runoff of water used to combat fires in this area and are, therefore, adequate to remove the water from a possible service water line break.

Using a frequency of failure of piping due to rupture of 8.48×10^{-10} per hour (reference data section, item 44) and four sections of pipe, the frequency of service water pipe rupture in this area is 3.4×10^{-5} per plant year. If the probability of operator error, failure to isolate the source, is as high as 1 in 10, the frequency of occurrence of loss of power due to this cause is 3.0×10^{-6} per plant year. Including the frequency of drain failure (plugging) would further reduce this frequency. However, the estimated frequency of occurrence of loss of loss of power due to this flooding is less than the calculated frequency of loss of power due to other causes and is, therefore, not quantified for its effect on plant risk.

7.4.2.2.5 Containment Building

Recent experience has shown that the Category I service water piping to the containment fan coolers is susceptible to leakage which can lead to flooding in the containment building. The detailed investigation into the causes and consequences of the Unit 2, October 17, 1980, flooding event has lead to numerous hardware and administrative changes for both units (detailed in References 7.4-10 and 7.4-11 for Unit 2), including for both units:

- Improved level control and indication devices for the containment sump pumps.
- Upgrading of the reactor cavity pumps control and CCR cavity level indication.
- Revised technical specifications regarding limiting conditions for operation of the various leakage detection systems and operating leakage limits.
- Continuous containment sump level indication in the control room.

In addition, for Unit 2 there are new design fan cooler heat exchangers with rolled rather than brazed tubes and improved access to the tubes via water boxes, television camera monitoring of the containment water levels, and improved fan cooler and weir system and dew point recorder.

As a result of these and many other improvements, substantial leakage or flooding in the containment building will be detected and controlled, which reduces the probability of damage to safety related equipment and decreases the frequency of occurrence of flooding inside the containment building.

The impact on plant risk due to concurrent service water system rupture and LOCA was investigated for possible increases in plant risk (due primarily to increased water in the containment sump and possible flooding of equipment necessary for the recirculation phase).

This event is an insignificant contributor to plant risk and is not quantified for the following reasons:

1. The service water pipe rupture must either occur as a result of the LOCA or occur randomly after the start of the LOCA.

2. If the service water pipe were to rupture, the individual service water lines to the containment fan cooler units can be readily isolated from outside the containment building (two MOVs in series in each of the inlet lines and two MOVs in series in each of the fan cooler outlet and fan cooler motor outlet service water lines for Unit 2, and similar manual valves for Unit 3).

3. Flow and temperature indication is available to allow rapid detection of a failed service water line.

7.4.3 CONCLUSIONS

Extensive review of the nonCategory I systems and components at Indian Point Units 2 and 3 has demonstrated that flooding from these sources will not initiate a plant transient. Failures in Category I systems and components could lead to local flooding; however, no plant transient would result, and in most cases damage would be limited to those safety related components in the vicinity of the failure.

7.4.4 REFERENCES

7.4-1 Indian Point Unit 3, PSAR, Supplement 1, Item 18.

7.4-2 Corps of Engineers, Proceedings of the American Society of Civil Engineers, Journal of Waterways and Harbors Division, Hurricane Study of New York Harbor, February 1962, Issue No. 1.

7.4-3 Quirk, Lawler, and Matusky, "Supplemental Study of Flooding Conditions at Indian Point Nuclear Generating Unit No. 3," June 1971.

7.4-4 Indian Point Unit 3, FSAR, Supplement 10, January 1973.

7.4-5 Letter from William J. Cahill, Jr., Vice President, Consolidated Edison Company of New York, Inc., to Mr. Richard C. DeYoung, Assistant Director for Pressurized Water Reactors, Directorate of Licensing, U.S. Atomic Energy Commission, dated December 18, 1972.

7.4-6 Letter from Carl L. Newman, Vice President, Consolidated Edison Company of New York, Inc., to Mr. George Lear, Chief, Operating Reactor Branch #3, Directorate of Licensing, U.S. Nuclear Regulatory Commission, dated January 20, 1975.

7.4-7 Letter from William J. Cahill, Jr., Vice President, Consolidated Edison Company of New York, Inc., to Mr. George Lear, Chief, Operating Reactor Branch #3, Directorate of Licensing, U.S. Nuclear Regulatory Commission, dated February 18, 1975.

7.4-8 Letter from Peter Zarakas, Vice President, Consolidated Edison Company of New York, Inc. to Mr. Steven A. Varga, Chief, Operating Reactor Branch #1, Directorate of Licensing, U.S. Nuclear Regulatory Commission, dated July 14, 1980.

7.4-9 Letter from Steven A. Varga, Chief, Operating Reactor Branch #1, Directorate of Licensing, U.S. Nuclear Regulatory Commission to Mr. John D. O'Toole, Assistant Vice President, Nuclear Affairs and Quality Assurance, Consolidated Edison Company of New York, Inc., dated December 18, 1980.

7.4-10 Consolidated Edison Company of New York, Inc., letter to the U.S. Nuclear Regulatory Commission, dated December 22, 1980.

7.4-11 Consolidated Edison Company of New York, Inc., letter to the U.S. Nuclear Regulatory Commission, dated January 5, 1981.

7.5 WINDS AND WIND INDUCED MISSILES

Strong winds can affect safety related (or critical) structures at the plant site in at least two ways. If the wind forces exceed the load capacity of a building or other external facility, the incident walls or framing might collapse or the structure might overturn. If the winds are strong enough, such as in a hurricane or tornado, the wind might be capable of lifting materials and thrusting them against some of these facilities. If a wind induced missile broke through a facility's wall, critical components or other equipment inside the structure might be damaged or lost.

7.5.1 WIND EVENTS

A study was performed by Research Triangle Institute to predict the wind speed exceedance frequencies for specific structures at the Indian Point site (see Appendix 7.9.5). Models were developed for determining tornado and extreme wind exceedance frequencies using historical data for tornadoes, hurricanes, cyclones, and other extreme winds. Computer simulation of tornado strikes at the plant site was included.

Wind speed exceedance frequency curves were developed for extreme winds, extra tropical cyclones, hurricanes, and tornadoes. Factors such as site and building exposure, wind velocity variability with elevation, and gust effects differ between tornadoes and other wind types. Therefore, separate exceedance frequency curves were provided for tornadoes and for the other winds. Their use will be discussed shortly. The velocities indicated for extreme winds and hurricanes are for the fastest mile (highest wind velocity in a 1-mile distance) traditionally presented for nontornado winds. The curves for tornadoes indicate the faster quarter mile wind speeds. These are seen in Figures 7.5-1 and 7.5-2, respectively.

The wind speed exceedance frequency curves were developed for an elevation of 10 meters, or 33 feet, above the ground surface. However, wind velocities vary with building elevation and exposure. In order to use the curves in Figures 7.5-1 and 7.5-2 for structures of heights other than 33 feet, correction factors for actual structure elevations were incorporated in the structure wind fragility analysis.

7.5.2 TORNADO MISSILES AND WINDS ON CONCRETE STRUCTURES

Reinforced concrete and reinforced masonry structures are typically comprised of relatively rigid and massive members as compared with steel or wood structures. The wall thicknesses of the vital concrete structures are over 12 to 14 inches and have weights of over 150 pounds per square foot. These structures, designed for seismic loading of 0.15g and greater depending on structure response characteristics, are, therefore, effectively analyzed for horizontal loading of over 25 psf. Because of the rigidity of these materials, little deflection results under this loading. More significantly, however, exterior walls are designed to carry the roof or floor loads above as well as the weight of the wall. These vertical loads induce compressive stresses in the walls

that essentially reduce the tendency toward the development of tensile stresses in the concrete that might otherwise lead to wall failure. Typically, therefore, and as evidenced by the resistance of reinforced concrete and concrete block structures to wind loading, failure from wind loading is not expected for these types of structures except at extraordinarily high velocities.

Tornado missile hazard analysis involves information about the likelihood of a spectrum of available missiles in the plant vicinity, representation of the wind field in the tornado, and aerodynamic calculations relative to lift-off and flight of the potential missile. The analysis leads to a spectrum of missiles and missile impact velocities with their respective frequencies. A detailed analysis which integrated all these effects for typical plant layouts has previously been accomplished (Reference 7.5-1). The results of that work were used to examine the potential hazard of tornado missiles at Indian Point.

In this study, calculations were made using tornado histories of each tornado region defined by the NRC. It used a typical plant layout to establish the target envelope, and the spectrum of missiles defined in the NRC Standard Review Plan, Section 3.5.1.4 (wood plank, steel pipe, steel rod, utility pole, automobile). Calculations were made for a small and a large (6,000) number of missiles at a plant site. Considering the key concrete structures, the study indicated the following annual frequencies for both cases for NRC tornado region 1 which includes the Indian Point site (Reference 7.5-1, Table 2):

	Quantity of Various Missiles	
	Small Number	Large Number
Annual frequency of missile hitting a structure	$< 10^{-7}$	$< 10^{-4}$
Annual frequency of hitting a structure at high velocities	$< 10^{-9}$	$< 10^{-6}$
Annual frequency of inside scabbing of 6-inch thick wall	$< 10^{-8}$	$< 10^{-4}$
Annual frequency of inside scabbing of 12 to 18-inch thick wall	$< 10^{-9}$	$< 10^{-6}$

Tornado frequencies at Indian Point are lower than the worst cases contained elsewhere in region 1. Therefore, the annual frequency of a tornado missile hitting a key plant structure can be inferred to be less than about 10^{-5}.

Because the concrete structures of interest at the site have wall thicknesses of more than 14 inches (several feet in some cases) we can infer from the referenced study that the annual frequency of inside wall scabbing is less than about 10^{-7}. If equipment in the structure were hit by the scabs, the equipment can conservatively be assumed to fail, thereby also having an annual frequency of failure of less than about 10^{-7}. The frequency of this failure resulting in a core melt would be much less.

It is recognized that these results are for an assumed plant configuration and without using site specific tornado data; the Indian Point case could lead to somewhat different results. The approach and results of the referenced study, however, are considered to be reasonable estimates.

A 1968 study (Reference 7.5-2) evaluated the penetration of hypothesized 300 mph tornado missiles in concrete and steel structures at Indian Point. It concluded that for 300 mph winds, corrugated sheet siding, bolted wood decking, a passenger car, or a cedar fence post acting as a missile might penetrate mass concrete up to 0.4 inches at impact velocity, with the result that the missile would not cause the concrete wall to fail. It is possible for thin, reinforced concrete walls hit by a heavy, bulky missile such as a car to extensively fracture the wall. Reinforcing steel could, however, keep the wall from totally collapsing. Even if scabbing of the inner surface were to take place, there is a question of whether the spalling would have sufficient impact to cause damage to a vital component. The evaluation results compare with the findings of the other study.

In summary, it is not likely that a tornado missile would be capable of penetrating the critical reinforced concrete structures at Indian Point. Therefore, the frequency of core melt from such potential tornado missiles is considered to be included in the other computations of wind and tornado initiated core melt frequency.

7.5.3 TORNADO MISSILES AND WINDS ON METAL STRUCTURES

There are some steel framed structures with metal siding and roofing that contain critical equipment. The Unit 2 control building and diesel generator building are steel framed structures with insulated steel wall and roof panels. A portion of the upper story of the Unit 2 PAB containing the safeguards MCCs, and component cooling system heat exchangers and surge tank is also metal covered. The auxiliary feed pump buildings at Units 2 and 3 are constructed partly of steel. In addition, critical exterior vessels at both units are the 3/16-inch thick carbon steel condensate storage tanks (CST), the 1/4-inch minimum thick stainless steel refueling water storage tanks (RWST), and the city water tank which backs up the CSTs. If the steel superheater stack collapsed, it could impact on critical structures. Also, exterior to both units of the plant are the service water pumps that cool component cooling water and the diesel generators, the offsite power supply including the station auxiliary transformers, and the gas turbines that could supply backup power under emergency conditions. These metal facilities may all be subject to failure from negative or positive pressures generated by winds through tornado levels or from penetration by tornado missiles.

In Reference 7.5-2, it was concluded that tornado missiles of the type previously described could penetrate steel plate 5/8-inch thick. Formed steel siding could, therefore, more easily be penetrated. Under such missile loading, we can expect the critical exterior vessels to be penetrated or deformed sufficiently to fail and thus lose their contents. We can also expect under tornado winds that service water pumps, the gas turbines and their control panels, metal buildings containing critical equipment, and transformers are all subject to loss of function from tornado missile impact. Therefore, for these facilities, we estimate that the frequency of a metal facility or of equipment being damage by a tornado missile is equal to the hit frequency. Tornadoes of velocities less than 200 mph are capable of lifting heavy objects. This is reflected in the fragility family in Figure 7.5-3.

Considering wind loading, the Unit 2 control building, diesel generator building, auxiliary feed pump building, and PAB are all protected to some extent by other plant structures in close proximity. For example, the Unit 1 containment building is almost 200 feet in diameter with its top at Elevation 164'. The top of the Unit 1 turbine building is at Elevation 135'. The top of the Unit 2 containment building is at Elevation 262'. These large structures will certainly influence the wind loading patterns on smaller nearby structures at the site. In addition, there is a significant variance in topography at the site. The wind flow through the site will have to accommodate the wind resistant structures in its path and the topography, and will thereby cause a wide range of pressures to occur on surfaces in the wind stream. Some of these pressures will be negative and may cause roofing or siding to pull away from their fastenings, or cause vessels to deform. Some assumptions are made about the influence of the ground contours and ground roughness on structure loading. However, the influence of nearby structures is best judged from wind tunnel tests of a site model. Median value fragility curves presented in this section have not allowed for an increase or decrease in local wind pressure due to specific adjacent structures. These effects are considered to be contained within the uncertainty bounds of the wind speed exceedance curves and structure capacity curves.

The wind speed exceedance curves being used in the analysis are based on winds at a standard height of 33 feet above grade. Actual elevations of the structures being evaluated differ from the standard so it is necessary to adjust the wind loads to actual elevations of the structures. Elevations greater than 33 feet will be subject to higher wind loads than reflected by the wind speed exceedance curves, and lower structure elevations will be subjected to lower wind loads. Also, the wind speed exceedance curves do not reflect the possible variations that result from different exposures of the buildings and site. For example, a large area containing tall buildings, hilly surfaces, or forests will interrupt the wind stream and cause incident pressures to be lower than at the shoreline where the exposure is greater. As will be discussed, a wind load correction, or safety factor, SF_L, is used to estimate the

variability in effective wind that might be experienced by each structure as a function of structure elevation and exposure, and the structure response to gusts, when using the wind speed exceedance curves.

Another factor which is considered in evaluating the margin of safety in wind resistant metal structures is the allowable stress level that governs the structure design. Structural members will begin to fail at yield stresses or, in the case of slender structural members in compression, may fail earlier if buckling stresses are reached before yield. The safety factor for these stress levels is identified as SF_Y.

The third factor that has been considered in judging the margin of safety against failure relates to the increase in working stresses that may have been taken in the design for combined loading conditions such as dead load and wind load. The increased allowable stress, when taken, has the effect of reducing the margin of safety, and is represented by SF_I.

The overall safety factor, SF, is then given by

$$SF = SF_L \cdot SF_Y \cdot SF_I$$

The structure capacity to wind loading is determined by multiplying SF by the design wind load.

Let us first examine the wind loading design basis of key structures. The metal siding and roofing of buildings at the site were specified to resist 30 psf wind loading with the result that deflections would not exceed 1/180 of the span. Most metal buildings and structures were designed for 30 psf wind loading without any increase in allowable stress above the American Institute of Steel Construction recommended working stress level of 20,000 psi in tension. The Unit 2 control and diesel generator buildings, the gas turbine enclosures, and auxiliary feed pump buildings were all designed on this basis. Because the gas turbine enclosures were obtained as commercially packaged units, however, it is assumed that a one-third increase in allowable working stress for the combined loading was used in their design.

The response to FSAR Supplement 2, Question 1.11, October 1969, cites information from the siding manufacturer who supplied the siding for the Unit 2 PAB and control building (auxiliary feed pump and diesel generator buildings were constructed using the same siding). The siding panels will blow out at 170 psf (equivalent to 1.18 psi) negative pressure and will fail at 60 psf external pressure, which is equivalent to 162 mph external wind load. The response also indicated that the girts which support the siding will fail at 90 psf; therefore the siding failure would govern the external loading condition.

The transmission lines and towers from Buchanan substation to the plant were designed to resist 30 psf wind loading on flat surfaces and 20 psf on round surfaces. These were also designed for a 1/2 inch radial ice coating on wires and tower surfaces, combined with 13 psf wind on flat

surfaces, and 8 psf on curved surfaces. In both cases, no increase in allowable working stress was used. The offsite power lines were designed for 30 psf (50 psf on flats) wind on rounds, but for failure stresses instead of allowable working stresses. This would appear to make their resistance to wind loads about the same as the onsite lines. The Buchanan poles are stronger, however, because they were also designed for an ice condition on the lines, thereby providing them with additional strength to resist high winds with no ice. At many locations, the critical load for the offsite towers was the 30 psf (wind on rounds) loading. Thus the Buchanan poles can resist greater wind velocity than the offsite system.

The Unit 1 superheater stack was initially designed for a 40 psf wind loading with a 0.6 reduction for its curved surface. Subsequently, the stack was reevaluated for tornado wind loading (Reference 7.5-3). The analysis indicated that the stack would have a factor of safety of 1.02 against buckling failure from 300 mph winds. It also indicated that the stack, shortened by 80 feet in height, would have a similar factor of safety against buckling from 360 mph winds. The stack was subsequently shortened by 80 feet.

The refueling water storage is normally maintained full, and the condensate water storage and city water storage tanks are normally about 2/3 to 3/4 full. Their resultant uniform internal pressures range to over 2,000 psf at the bottom walls. So long as the tanks have such a capacity, large external wind pressures cannot develop sufficiently to cause asymmetrical loads that would threaten buckling of the tanks, although the tank top might be blown out from negative pressures. This, however, would not cause failure of the tank walls.

The design wind pressure for the key metal structures is tabulated in Table 7.5-1.

To assess the first safety factor, SF_L, as it pertains to structure capacity for resisting extra-tropical cyclones and hurricanes, the American National Standards Institute standard (Reference 7.5-4) is used to determine the effective wind loading as a function of differences in actual structure elevation and site exposure. As previously stated, the wind speed exceedance curves used in this study were established for an elevation above grade of 33 feet and an average exposure. By using the reference document, the difference between the wind loading at 33-foot elevation and average exposure conditions, and the actual building heights and extremes in exposure conditions, including consideration of structure response and gusting, the range in SF_L for the design loads used can be estimated.

Basic wind speeds of 75 mph and 90 mph are designated in Reference 7.5-4 for the Indian Point region to reflect 50-year and 100-year recurrence periods, respectively. These are based on observed air flow in open country. In addition, three categories of exposure are defined to account for terrain effects. Exposure A is for centers of large cities and very rough hilly terrain. Exposure B is for suburban areas, towns,

wooded areas, and rolling terrain. Exposure C is for flat, open country or coastal areas and grassland. Exposure B is most applicable to the Indian Point site. Upper and lower bounds in SF_L can be estimated by varying the basic wind speed recurrence period, exposure, and structure elevation.

Using the values recommended by Reference 7.5-4, Table 5, the standard design wind pressures for the Indian Point location are tabulated in Table 7.5-1 based first on variations in elevation, then on variations in exposure and recurrence period for basic wind. Lower, median, and upper bound values for the products of the loading factors are based on the following assignments:

Upper Bound -- 50-year recurrence of basic wind speed, wind pressure at minimum structure height, Exposure A

Median -- An average of the 50-year and 100-year recurrence of basic wind speed, wind pressure at structure average height, Exposure B

Lower Bound -- 100-year recurrence basic wind speed, wind pressure at maximum structure height, Exposure C

Upper and lower bounds on the safety factor SF_L, were determined by the ratio of average standard pressure load as obtained from the reference tables to minimum and maximum loads, respectively.

SF_L for tornado wind loading is now assessed. Appendix 7.9.5 discusses the variability in wind speed probability with elevation. Gusting and site exposure considerations are not particularly applicable to tornado phenomena. Also, structural dynamic response characteristics may differ for tornado phenomena; however, this is not sufficiently understood to warrant its inclusion in the analysis. The variability of tornado wind speed probability with elevation was determined by the expression

$$f(z) = 2.0[1 - e^{-0.013(z + 20)}]$$ (reference Appendix 7.9.5)

where f(z) is the ratio of wind speed frequency at elevation z above grade to wind speed frequency at 33-foot elevation. This ratio was applied to the tornado wind speed curves for various elevations from which the change in effective wind speed was determined. Ratios of wind speed changes with elevation were inverted to reflect the variability of the safety factor in structure design loading, SF_L, from tornadoes. The results are seen in Table 7.5-2.

The second safety factor, SF_Y, is the ratio of the maximum design stress to the material's yield stress or buckling stress, whichever is closer to its critical stress. The yield stress is a function of the tensile strength of the material, typically for structural steel in most of these buildings about 33,000 psi for 60,000 to 72,000 psi tensile

strength material (American Institute Steel Construction). Thus, while steel production sampling assures 33,000 psi minimum yield stress, the actual value might be somewhat higher. Therefore, with design tensile stresses limited to 20,000 psi, for steel members stressed to that level, the safety factor against yield might be between 1.65 and 1.95, with a median safety factor $SF_\gamma = 1.8$. In the case of the superheater building stack, however, the earlier analysis determined that failure would be from excessive buckling stresses. The analysis based on 360 mph winds determined that the safety factor against buckling for the assumed wind loading was about 1.0. Therefore, for the stack, SF_γ is 1.0. Similarly, in the design of the offsite transmission lines, the stresses were taken to yield under the maximum wind design condition (30 psf). Therefore, SF_γ for these is also 1.0. Tables 7.5-2 and 7.5-3 summarize the assigned SF_γ values.

SF_I, the safety factor (reduction) for having used allowable increases in working stresses is now evaluated. In typical design practices, structures designed under combined loading conditions would be permitted stress increases of up to one-third the allowable working stresses for materials under combined dead, live, and wind loading conditions. Because not all the stress results from wind loads (the wind proportion could be large or small depending on the structure configuration and the magnitude of other loads), we judge that the allowable working stress directly related to wind loading alone is effectively between 1.0 and 1.3 times normal working stresses. This represents a reduction in the safety factor. A median safety factor $SF_I = 0.8$, is therefore assigned for these cases. Such an increase in allowable working stress was not taken in the design of the control building, diesel generator building, auxiliary feed pump building, the PAB, and the transmission lines. The SF_I values are seen in Tables 7.5-2 and 7.5-3.

If the overall wind safety factor is now examined on the basis of the products of the three contributing safety factors, the combined SF and capacities indicated in Table 7.5-3 for extra-tropical cyclones and hurricane winds, and Table 7.5-2 for tornado loading, are obtained in terms of psf and then in terms of mph (converted from $q = 0.00256V^2$). The capacity of the stack is based on the failure analysis performed previously (Reference 7.5-3) for a tornado loading of 360 mph distributed uniformly with stack height.

Figure 7.5-4 indicates the plotted extra-tropical cyclone and hurricane wind fragilities for each of the key facilities, including the uncertainty limits on these values. The curves are developed from Table 7.5-3 for extreme wind velocities. Similarly, Figure 7.5-5 provides structure fragilities for tornado winds, using Table 7.5-2. The solid curves represent the variability of the wind loading and material strength while the dashed curves reflect the uncertainty. A 25% uncertainty in median value was the basis for establishing the upper bound dashed curves. This considers that structural components designed for wind loading traditionally are: (1) not designed up to allowable stresses, (2) designed assuming the maximum wind pressures are uniform when, in fact, they may be substantially nonuniformly lower, and (3) conservatively designed to include assumed live loading at the same time as wind loading; if the resultant is higher component stresses, the

lower bound dashed curve was established to reflect the high unlikelihood that structures designed for horizontal wind loading would fail at loads less than design due to the conservatism incorporated in the application of design loads and stress limits. The upper and lower bound curves are weighted 0.1 each, while the median curves are weighted 0.8.

Before discussing the plant logic, it is important to examine the consequence of some of the structure failures noted. The portion of the upper story of the Unit 2 PAB that is enclosed by metal siding and roofing contains the component cooling system heat exchangers and surge tank as well as the motor control centers for the safeguards valves. Failure of the motor control centers would leave the motor-operated valves in their required position for plant hot shutdown. As discussed in Section 1, hot shutdown can be maintained without the entire component cooling system by using the charging pumps (cooled by city water) for RCP seal injection and the auxiliary feedwater system for removing decay heat. Either the turbine-driven auxiliary feedwater pump or, if power is available, one of the two motor-driven auxiliary feedwater pumps, can supply secondary cooling until the primary water supply (CST) is depleted. This will occur in about 24 hours under the condition of meeting minimum required decay heat removal at hot shutdown conditions. In that period, manual operation of the MOVs would enable cold shutdown to be accomplished, should that be desirable. If not, hot shutdown conditions can continue to be maintained using the secondary city water supply to the auxiliary feedwater pumps.

It is important to consider the consequences of a postulated collapse of the auxiliary feed pump building of either unit. The lower story containing the auxiliary feedwater pumps is constructed of reinforced concrete and provides wind and tornado protection of these pumps and the auxiliary feedwater discharge lines from the pump. Above the second story, the structure is steel framed with metal siding and roof decking, except for the turbine missile shield wall on the west side that extends to about the 80-foot elevation. Failure of the steel structure (and of the steam and feedwater lines in the bridge crossing to the turbine building) will probably cause the failure of the main steam, feedwater, and auxiliary feedwater lines because they are supported by the structure.

Failure of the main 4-inch diameter auxiliary feedwater lines, which join the main feedwater lines just outside containment, would result in a loss of the auxiliary feedwater in that line. The supply to each line can be isolated from the control room. Failure of the main feedwater lines does not necessarily cause loss of auxiliary feedwater because check valves in the main feedwater lines near containment prevent backflow. Failure of the main steam or feedwater lines at the containment penetration, however, could theoretically cause the penetration pipe sleeve or the closure plate between the pipe and pipe sleeve on the containment side to fail. Such failures suggest a loss of containment. An analysis was made of the load capacity of each of these pipes and their penetrations on the auxiliary feed pump building side of the pipe restraint just outside of containment (Reference 7.5-5). This restraint represents the point where building failure from the horizontal loading would transfer the load to all the pipes. Although early hairline

cracking of the end closure plate weld to the pipe could occur, the piping and penetration would not fail and cause an opening in containment as a result of wind load failure. Their total capacity is such that it equates to a uniform wind loading on the exposed north or south building walls of over 500 psf, far exceeding the maximum wind loading corresponding to the wind velocities seen in Figures 7.5-1 and 7.5-2.

There are two gas turbines located near the Buchanan substation approximately a half mile from the plant and one located adjacent to the Unit 1 turbine building. Under normal procedures, one turbine is started after tornado watch notification by the Energy Control Center. Also, should offsite power be lost, starting of a gas turbine is generally initiated. Should the offsite gas turbines fail because of wind loading, the onsite unit adjacent to the Unit 1 turbine building can be started. If the enclosure for this gas turbine fails, but the control breaker panels inside the structure do not fail (if breakers trip they can be reset), then an operable gas turbine can supply safeguards power.

If the onsite gas turbine fails but the Unit 2 breakers within the structure (GT, GT1, GT2, GTA), the Unit 3 outdoor breakers (52GT/BT, 52GT/2F), and the outdoor gas turbine auto transformers (2) are intact, power from one of the Unit 3 diesel generators, which are protected from the wind and tornadoes, can be transferred to Unit 2. Although the breakers and auto transformers are not qualified for this loading condition and the Unit 3 diesel power transfer has not yet been tested, it is estimated that the transfer could be made within 1/2 to 1-1/2 hours. In any of these cases, however, the power supply is to the Unit 2 480 VAC switchgear which is located in the Unit 2 control building.

The city water tank supplies water to both units. Its lines are underground, and air-operated valves controlled from each unit's control room enable this supply to be tied into the lines from the condensate storage tanks, providing a backup water supply for the auxiliary feedwater system. The city water tank also provides a backup supply of cooling water for the Unit 2 charging pumps.

7.5.4 INDIAN POINT UNIT 2

7.5.4.1 Plant Logic

As in the case of seismically initiated events, wind initiated events and the resulting failures that could lead to core melt can be expressed by three basic fault trees. The first, M_1, consists of a transient, such as loss of offsite power, followed by turbine trip and loss of cooling. A wind initiated event may induce a reactor coolant system rupture and failure of safeguards systems that could also lead to core melt. We designate the failures starting with a small LOCA followed by a loss of safety injection and cooling, M_2, and those starting with a large LOCA followed by a loss of safety injection, M_3. Thus, we can expect core melt if either M_1, M_2, or M_3 occurs.

The fault trees for Unit 2 are given in Figure 7.5-6, starting with the master logic tree. Each component is denoted by a circle symbol, (1), (2), etc., with a subscript $\bigcirc_W$ for wind induced failures and/or a

subscript $\bigcirc_T$ for tornado induced failures. When both exist they are an "or" relationship for the loading function.

The results of these trees are summarized below using the Boolean algebra symbols

$\wedge$ = "and"
$\vee$ = "or"

From the fault tree in Figure 7.5-6a, core melt occurs for

$$M_W = M_1 \vee M_2 \vee M_3$$

In terms of the basic component failures and beginning with the fault tree in Figure 7.5-6b, we have

$$M_1 = (②_W \vee ②_T) \wedge (\hat{④} \vee \hat{②} \vee ⑨_T) \wedge [\hat{④} \vee (⑧_T \wedge ⑩_T) \vee ③_W \vee ③_T]$$

where from Figure 7.5-6f

$$\hat{②} = (②_W \vee ②_T) \wedge (④_W \vee ④_T \vee 0.13 \times ⑦_W \vee 0.13 \times ⑦_T \vee ⑪_T \vee ④_W \vee ④_T \vee 0.13 \times ⑦_W \vee 0.13 \times ⑦_T \vee ⑥_W \vee ⑥_T \vee 0.05 \times ⑦_W \vee 0.05 \times ⑦_T)$$

where $0.05 \times ⑦$ is the probability of the Unit 1 superheater stack falling on the diesel generator building and $0.13 \times ⑦$ is the probability of the superheater stack falling on the control building.

Note that, in this instance, the unavailability of gas turbine power is conservatively assumed for several reasons. While two gas turbines which are located up the hill and to the east of the plant can be started from the control room, the operator must access the Buchanan substation to perform local switching operations before either of these gas turbines can be placed online. Under severely adverse weather conditions, it may not be possible to gain access to the substation. GT-1, which is located adjacent to the Unit 1 turbine building, however, can be started and placed online from the control room. Even in this case, both nuclear plant units may place a demand on the gas turbine at the same time, causing its unavailability to one or the other unit. Further, even under normal operations, each gas turbine has a probability of failing to start on demand of approximately 0.15, not considering operator actions under this external event and turbine unavailability due to maintenance. Even under the most optimistic conditions, a gas turbine would not normally supply power for at least 30 minutes following a loss of offsite and plant power. Therefore, gas turbine unavailability has been assumed to be 1.0.

Then,

$$\hat{②} = (②_W \vee ②_T) \wedge (④_W \vee ④_T \vee ⑥_W \vee ⑥_T \vee ⑪_T \vee 0.18 \times ⑦_W \vee 0.18 \times ⑦_T)$$

From Figure 7.5-6e

$$\hat{④} = ④_W \vee ④_T \vee 0.13 \times ⑦_W \vee 0.13 \times ⑦_T \vee ④_W \vee ④_T \vee 0.13 \times ⑦_W \vee 0.13 \times ⑦_T$$

which reduces to

$$\hat{④} = ④_W \vee ④_T \vee 0.13 \times ⑦_W \vee 0.13 \times ⑦_T$$

Then, M_1 reduces to

$$M_1 = (②_W \vee ②_T) \wedge \{\hat{④} \vee [(\hat{②} \vee ⑨_T) \wedge \{③_W \vee ③_T \vee (⑧_T \wedge ⑩_T)\}]\}$$

From Figure 7.5-6c

$$M_2 = \{\hat{②} \vee [(⑤_W \vee ⑤_T \vee ⑪_T) \wedge (⑩_T \vee ⑨_T)]\} \wedge \{\hat{④} \vee [(\hat{②} \vee ⑨_T) \wedge \{③_W \vee ③_T \vee (⑧_T \wedge ⑩_T)\}] \vee \hat{④} \vee \hat{②} \vee ⑨_T\}$$

which reduces to

$$M_2 = \hat{②} \vee [(⑤_W \vee ⑤_T \vee ⑪_T) \wedge (⑨_T \vee \{⑩_T \wedge \hat{④}\})]$$

From Figure 7.5-6d, we see that M_3, large LOCA, does not occur since the components which might cause the LOCA are located in the containment building and are protected from wind effects. Therefore, the expression for core melt becomes

$$M_W = M_1 \vee M_2$$

$$M_W = \{((②_W \vee ②_T) \wedge [(\hat{④} \vee ⑥_W \vee ⑥_T \vee ⑪_T) \vee \{⑨_T \wedge [③_W \vee ③_T \vee (⑧_T \wedge ⑩_T)]\}]\} \vee \{[⑨_T \vee (\hat{④} \wedge ⑩_T)] \wedge (⑤_W \vee ⑤_T \vee ⑪_T)\}$$

This Boolean equation expresses the logical relationship between the occurrence of melt and the failure of various components. The probability of failure of each individual component, as a function of wind velocity, is described by its family of fragility curves as seen in Figures 7.5-3 and 7.5-5 for tornado loading and Figure 7.5-4 for other winds. These individual families of fragility curves can now be combined for each respective loading type through the logic of the Boolean equation, to obtain a plant level family of fragility curves for the occurrence of core melt.

7.5.4.2 Wind Core Melt Frequencies

The fragility families are now combined with the appropriate wind speed family (tornado or other wind curves). When core melt frequencies are combined for both wind types, a probability curve showing our state of knowledge about the frequency of core melt due to wind or tornado loading is obtained. The result is seen in Figure 7.5-7. From the cumulative probability curve it is seen that the median annual frequency

of core melt due to wind events is about 2.5×10^{-5} with a 90% confidence that it is between 1.2×10^{-4} and 2.9×10^{-6}. The mean annual frequency of core melt is 4.3×10^{-5}.

7.5.4.3 Initial Assembly Leading To Release Category Frequencies

In the previous section we developed a Boolean expression for the state "core melt" in terms of plant components. Now, in order to develop risk curves and integrate the wind analysis with the rest of the study, we need to know which type of core melt, plant state, and release category occurs. That is, we need to develop Boolean expressions for each of the plant states defined in Section 1 and then aggregate them according to the containment state and release category to which they contribute. For this purpose, we introduce two new expressions:

x = failure of fan coolers
y = failure of containment spray

The fault trees of Figures 7.5-8 and 7.5-9 give the logic for x and y. Summarizing,

$$x = \hat{(2)} \vee \hat{(4)} \vee (11)_T$$

$$y = \hat{(2)} \vee \hat{(4)} \vee (9)_T$$

Now, from the definitions of the plant states in Section 1, only the following plant states might occur from a wind initiating event:

Plant State	Boolean Expression
AEFC	$M_3 \wedge \bar{x} \wedge \bar{y}$
AEF	$M_3 \wedge \bar{x} \wedge y$
AEC	$M_3 \wedge x \wedge \bar{y}$
AE	$M_3 \wedge x \wedge y$
SEFC	$M_2 \wedge \overline{M_3} \wedge \bar{x} \wedge \bar{y}$
SEF	$M_2 \wedge \overline{M_3} \wedge \bar{x} \wedge y$
SEC	$M_2 \wedge \overline{M_3} \wedge x \wedge \bar{y}$
SE	$M_2 \wedge \overline{M_3} \wedge x \wedge y$
TEFC	$M_1 \wedge \overline{M_2} \wedge \overline{M_3} \wedge \bar{x} \wedge \bar{y}$
TEF	$M_1 \wedge \overline{M_2} \wedge \overline{M_3} \wedge \bar{x} \wedge y$
TEC	$M_1 \wedge \overline{M_2} \wedge \overline{M_3} \wedge x \wedge \bar{y}$
TE	$M_1 \wedge \overline{M_2} \wedge \overline{M_3} \wedge x \wedge y$

Bars over the symbols denote negation. Thus, $\bar{x}$ means that fan coolers do not fail, and so on.

Next, these plant states are aggregated in terms of the containment state (failure or no failure of containment) and the release category to which they contribute.

Because M_3 cannot occur, AEFC, AEF, AEC, and AE all equal zero and, since Release Category Z-1 = AE, Z-1 = 0. Now, since containment does not fail from wind loading,

$$2RW = SE \vee TE$$

$$= (M_1 \vee M_2) \wedge x \wedge y$$

Substituting the components for M_1, M_2, x, and y, and reducing,

$$2RW = [(\textcircled{2}_W \vee \textcircled{2}_T) \wedge (\hat{\textcircled{4}} \vee \textcircled{6}_W \vee \textcircled{6}_T \vee \textcircled{11}_T)] \vee \{[\textcircled{9}_T \vee (\hat{\textcircled{4}} \wedge \textcircled{10}_T)] \wedge (\textcircled{5}_W \vee \textcircled{5}_T \vee \textcircled{11}_T) \wedge [\hat{\textcircled{4}} \vee (\textcircled{11}_T \wedge \textcircled{9}_T)]\}$$

Also,

$$8B = SEFC \vee SEC \vee TEFC \vee TEC$$

$$= (M_1 \vee M_2) \wedge \bar{y}$$

This cannot occur since the components in $\bar{y}$ must fail in order to have core melt $M_1 \vee M_2$.

Also,

$$8A = SEF \vee TEF$$

$$= (M_1 \vee M_2) \wedge \bar{x} \wedge y$$

$$= \hat{\textcircled{4}} \wedge \overline{\textcircled{11}}_T \wedge \textcircled{9}_T \wedge \{[\overline{\textcircled{2}}_W \wedge \overline{\textcircled{2}}_T \wedge (\textcircled{5}_W \vee \textcircled{5}_T)] \vee [(\textcircled{2}_W \vee \textcircled{2}_T) \wedge \overline{\textcircled{6}}_W \wedge \overline{\textcircled{6}}_T \wedge (\textcircled{3}_W \vee \textcircled{3}_T \vee \textcircled{5}_W \vee \textcircled{5}_T \vee \{\textcircled{8}_T \wedge \textcircled{10}_T\})]\}$$

These Boolean equations express the logical relationships between component failures and occurrence of the various release categories. Using these expressions and the fragility families for the components, the plant level fragility family for each release category is obtained. This family, in numerical form, consititutes the wind MC^W matrix. The uncertainties in the component fragility curves translate through this process into uncertainty in the MC^W matrix. This uncertainty is represented in Tables 7.5-4 and 7.5-5 for extra-tropical cyclones and hurricanes, and tornadoes, respectively, by showing five different values of the MC^W matrix with 20% probability assigned to each. This table, thus, is an example of the DPD process applied at the matrix

level as discussed in Section 0.8.4.2. The numbers entered in the tables are elements of the MC^W matrix and give the conditional frequencies of occurrence of the various release categories, given wind velocities specified in the left column. The MC^W matrix, when combined with the windspeed hazard curves, gives us the frequency of wind initiated release categories. Figure 7.5-10 presents the resultant probability of frequency curves.

The dominant contributors to release category 2RW are loss of offsite power lines and failure of the control building housing the switchgear and batteries for starting the diesel generator.

The dominant contributors to release category 8A are failure of offsite power lines, a portion of the PAB top story, the auxiliary feed pump building, and the refueling water storage tank.

7.5.4A ADDITIONAL ANALYSES, UNIT 2

The initial wind effects analysis in Section 7.9.5 considered that any potential increases in windspeeds at the Indian Point site due to wind channelization effects along the Hudson River Valley would be more than offset by the conservatisms in the study. For example, the methods used in the analysis to account for terrain roughness and for attenuation of basic offshore windspeeds to windspeeds at the site gave conservative results. Also, peak winds were assumed in the initial study to occur from any direction.

The effects of adjacent buildings increasing or decreasing wind pressures on Unit 2 buildings of interest were treated in the initial study by analyzing buildings for variations in fastest mile wind pressures as a function of extremes in building exposures and building elevations, using the ANSI wind pressure tables. Further, the likelihood of the turbine buildings or the Unit 1 superheater building failing and damaging other buildings of interest was judged to be small and was not explicitly modeled.

An additional analysis has been accomplished for Unit 2 to give greater attention to these points. One of the unique features of this analysis to gain greater realism is that it is based on wind hazards and structure fragilities for each of four principal directions. The following discussion considers the additional analyses conducted for wind hazard and structure fragilities for wind and tornado missiles and presents revised plant logic and revised core melt and release frequencies.

7.5.4A.1 Wind Hazard

An additional study was performed by Research Triangle Insititute (RTI) and York Research Corporation to maximize the use of site specific wind data in the study and to account for wind channelization, wind attenuation with distance inland, terrain roughness in the vicinity of the site, and directional effects (see Section 7.9.5.1).

The wind simulation model was expanded to obtain hazard curves for each of the four principal wind directions. The model was compared to empirical wind field models and additional data on velocity attenuation of hurricanes that cross the coastline and reach the plant site. It also was refined to recognize the sheltered location of the site in comparison to velocity measurements available from weather stations. These were determined using site wind velocity data of specific storms and comparing it with data from weather stations for the same storms. Site data included information for heights up to 400 feet above grade. These data and topographic maps and photographs of the area surrounding the plant site were analyzed to provide directionally dependent friction and wind channelization factors. These considerations were incorporated into the HURRISK computer model.

The terrain in the vicinity of the Indian Point station is complex and hilly with 1,100-foot peaks on the west shoreline and 500 to 600-foot hills east of the site. South of the plant on the opposite shore of the Hudson River are 600 to 1,200-foot peaks and north of the plant across Peekskill Bay are 700 to 900-foot hills. Mean grade at the plant is about 18 feet MSL. These features tend to significantly influence the direction, speed, and turbulence characteristics of surface windspeeds that the structures at the plant will experience in storm-driven severe wind conditions. The data presented in Reference 24 of Section 7.9.5.1 tend to confirm the conservatism of the previous assumptions of open wind exposure conditions. The mean hourly 33-foot (10-m) windspeeds are from one-fourth to one-third of those at 400 feet, as measured by the instruments at the site. The available data also do not support the hypothesis (Reference 7.5-6) that low level (10-m) topographic speedups occur from the south-southeast or southeast directions. The extreme annual windspeeds measured at the site are significantly less than those recorded at stations that have much more open exposure conditions, such as LaGuardia, Bridgeport, or Westchester County airports. Thus, the position of the plant at 18 feet MSL on a razorback in the river valley with virtually solid valley walls to 200 feet MSL results in significantly reduced surface windspeeds as measured by onsite instruments.

The hurricane wind hazard curves are significantly lower than those presented in Appendix 7.9.5, which were based on conservative open terrain conditions. Site data were obtained and analyzed to provide a more realistic assessment of the boundary layer winds at Indian Point. These data indicated that the 33-foot winds at Indian Point were about one-third of the 400-foot winds for storm-driven conditions. When these adjustments were made to the simulation model with other updated data and a formal uncertainty analysis procedure, the resulting wind hazard curves are less than those given in Appendix 7.9.5. These results compare favorably to the NOAA Technical Report NWS 23 probable maximum hurricane calculations and to the observed windspeeds measured at the site, which were much lower than those measured offshore during Hurricane Doria.

For extratropical cyclone winds, 13 years of site data were collected, reviewed, and analyzed to assess the conservatism of the use of the LaGuardia data in Appendix 7.9.5. The data indicated that the site annual wind extremes are consistently less than the LaGuardia data.

A site specific extreme value analysis of the 13 years of data has been made using the WINDRISK computer code. The uncertainty analysis included contributing factors such as data interpretation, height adjustment, fastest mile windspeed conversion, sample size, and statistical modeling. These uncertainties were propagated through the modeling and analysis in a Monte Carlo calculation to yield a family of windspeed curves for each plant direction sector. The resulting windspeed exceedance frequencies are more than a factor of 10 less than the previous estimates in Appendix 7.9.5.

In this updated analysis, the hurricane winds dominate the combined wind hazard curves for winds from the north and west directions, up to about 100 to 125 mph windspeeds. Such high wind velocities are rare events with extremely low frequencies. The maximum wind velocity recorded near the Indian Point site is about 80 mph at 400 feet in height; wind velocities nearer the surface would be from 1/4 to 1/3 of that velocity. Extratropical cyclone and hurricane winds dominate the wind hazard curves for the plant east and south directions up to about 90 mph. At windspeeds greater than 125 mph, the tornado hazard dominates the plant wind risk for all the directions. Therefore, in this analysis, we were able to produce a single set of windspeed hazard curves for each of the four principal directions. These are seen in Figures 7.5-16 through 7.5-19.

7.5.4A.2 Structure Wind Fragilities

The capacity of key structures to resist extremes in wind loading has been analyzed by Structural Mechanics Associates, Inc. (SMA). Their report is presented in Section 7.9.6.

Building design calculations and drawings were reviewed, information was obtained from the siding manufacturer for the analysis, and a site inspection was made. Various modes of failure were assessed for extreme wind loadings in each of the four principal wind directions. The analysis considered building shape factors, roofing and siding failures from impinging winds and negative pressures, and building frame and anchorage failures. Cermak/Peterka & Associates, Inc., specialists in wind tunnel tests and influences of adjacent structures on building wind pressures, assisted SMA in the estimation of funneling and shielding effects on buildings of interest at the site. Their work is incorporated in the appendix of Section 7.9.6.

Three major factors of safety were estimated for each building: strength of materials; modeling of the wind pressures on the buildings' exteriors and loading of the building frame; and funneling and shielding effects of nearby structures (given fastest mile wind velocities). Wind gusts and building heights were considered in the evaluation. The overall factor of safety for each structure was multiplied by the wind pressure used in the structure's design to determine the best estimate of wind velocity at failure.

the uncertainty in wind capacity was determined to be well represented by a lognormal standard distribution, using the best estimate as the median value, $\tilde{v}$. For each factor of safety, a coefficient, β_U, on the standardized Gaussian random variable, f, was selected so that the velocity capacity, v, could be expressed by

$$v = \tilde{v} \cdot \exp(f \cdot \beta_U)$$

The results of the wind fragility analysis are summarized in Table 7.5-7 for each of the key structures on each principal building axis. The table indicates the median wind velocity capacity, $\tilde{v}$, and β_U for frame failure, $\tilde{v}_F$, siding or roofing failing from impinging loads, $\tilde{v}_S$, or siding or roofing failing from suction loads, $\tilde{v}_{S-}$ or $\tilde{v}_{R-}$.

Note that in addition to impinging or suction loads on siding or roofing, the capacity was determined by SMA for center and edge locations due to the wide variability of wind pressures over a building face. In the table, however, the impinging or suction pressure capacities presented for the roof or all walls of a building conservatively are those which are the lower of all the face locations.

The capacity of the control building roof, $\tilde{v}_R$, due to negative pressures is based on a loss of the additional steel roof plate without affecting the roof decking which has a higher capacity due to its greater weld attachment to the building frame. The impinging wind capacity, $\tilde{v}_{Sa}$, of the upper level control building siding is based on the capacity of the steel plate that is fastened to the frame along with the siding. The wind suction capacity of the upper level control building siding, $\tilde{v}_{S-}$, however, is not affected by the presence of the added steel plate in that story because the wall capacity under suction loading is governed by failure of the girt connections. $\tilde{v}_{Sb}$ denotes the impingement load capacity of siding elsewhere on the building.

The capacities of the turbine building frames are based on the operating deck floor slab transmitting lateral column loads to the turbine pedestal for all but the interior columns opposite the heat exchanger cutouts in the floor slab. These columns opposite the floor openings will fail earlier than the others and, in failure, will tend to be restrained from collapsing into the yard because of purlins, girts, and struts that tie them back to the other frames. However, as will be seen later, some chance is assigned to the possibility of their collapsing into the yard, twisting, and somehow impacting on the control building. The capacity of these interior frames is denoted by $\tilde{v}_{FI}$, and for the other frames is denoted by $\tilde{v}_{FE}$.

The superheater stack was designed to withstand a 360-mph wind velocity without exceeding allowable design stresses. Considering also that the design loading was based on a conservative distribution of wind pressure with height, it is judged that a capacity of 360 mph conservatively can represent the 5th percentile and that a capacity of about 1.5 times the equivalent wind pressure for this velocity is a reasonable representation

of the 95th percentile in wind pressure capacity. This corresponds to a 440-mph windspeed capacity since wind pressures are proportional to the squares of their respective wind velocities. The analysis is based on a lognormal standard distribution through these bounds to obtain the value, $\tilde{v}_F$, for the stack. Because of the high capacity of the stack, greater accuracy in this value is unwarranted.

SMA indicates that, based on failure evidence, there is a lower bound below which engineered building frames and siding definitely will not fail. This lower limit in fragility is at three standard deviations below the median velocity capacity.

7.5.4A.3 Structure Tornado Missile Fragilities

As referenced in Section 7.5.2, a study was performed to evaluate the probability of tornado missiles impinging on nuclear power plant facilities in various tornado regions (Reference 7.5-1, later published in full as Tornado Missile Risk Analysis, EPRI NP-768). In the study, the probability of hitting specific building targets for a two-unit plant configuration was analyzed where one unit was still in construction and the site contained a large number of potential missiles. The results of that study are used here to represent the probability of damaging the contents of buildings of interest from tornado missiles. This approach is conservative for the following reasons:

1. The Indian Point site is not in construction and does not have as many potential missiles as might typically be found at a plant in construction.

2. The Indian Point stuctures are considered to have greater protection from missiles because of the closer proximity of its many stuctures, as compared with the referenced study model.

3. In this additional Indian Point study, the frequency of damaging all of a building's contents is taken to be the frequency of a missile hitting the building.

In using the results of the referenced study in this analysis, it is desirable to determine the probability of impinging structures conditional on the tornado frequency. In this way, the wind and tornado hazard curves in the current analysis can be used to quantify the damage frequency using site specific tornado frequencies. The hit probabilities, P_N, for each of the key stuctures in the referenced study that most nearly apply to the Indian Point facilities of interest are seen in Table 7.5-8. These mean values were based on an estimated tornado strike frequency in Tornado Region I of 2.3×10^{-3} per year. As a result, the column for mean value of P_M represents the conditional hit frequency and was determined by dividing P_N in the reference study by 2.3×10^{-3}. The referenced study indicated that analysis showed the 95% confidence bound to be generally less than three times the reported mean values. Consequently, the last column of Table 7.5-8 indicates the 95th percentile value of P_M for use in the current analysis. A

lognormal standard distribution for the conditional building damage frequency was determined from these values and was used in the computations.

7.5.4A.4 Plant Logic

The potential building failures from excessive wind loading can result in the building frame collapse or in the loss of building siding or roofing from impinging wind pressure or from negative pressures on the leeward and side faces of the building. Building frame failures are considered to cause a loss of all building contents.

Failure of building siding from impinging loads is considered to generally take the form of bowing of the siding with gross leakage of wind into the building, thereby relieving girt loads. It would not necessarily result in the siding tearing away from its girt supports, particularly since the siding often is continuous over its supports. However, as will be seen, some chance is assigned to the failed siding being released into the building and causing damage to the building contents. In the case of the control room, failure of the siding or roof panels was considered to disrupt the activities of the operators sufficiently so that the operators could no longer control the plant.

Negative wind pressures on the leeward, top, and side faces of buildings are considered to cause panels comprised of siding and girts or roof panels and purlins to fail by their detachment from the building, thereby exposing the building contents. This condition would not particularly be hazardous to building contents because the wind flows inside the building would be significantly lower than those on roofing and siding outside the building, resulting in greatly reduced negative wind pressures, if any, on equipment surfaces. However, it is considered that loss of the siding or roofing around the control room from negative pressures will interfere with the operators performing necessary control functions. It is conservatively assumed that loss of control room siding or roofing will result in a loss of control.

Consideration is given to the effect of failure of the Unit 1 superheater building and the superheater stack on adjacent buildings of interest. In general, it was judged that superheater building frame failures from winds in any direction would fail the adjacent Unit 2 control building. The impact of the superheater building and stack failure on other structures is considered only when structure dimensions and distances justify such an assumption for winds in any of the four directions. For example, the gas turbine shelter is considered to be impacted by failure of the superheater building from winds in any direction except the south. Also, the superheater building dimensions are such that the building's failure occurring along its major axis would not affect the diesel generator building, except for the case where winds from the west fail the superheater building, causing stack collapse onto the Unit 1 reactor building roof and its subsequent impact on the diesel generator building. Stack failure to the west and onto the Unit 1 turbine building could result in the stack's impact, then, on the control building or gas turbine shelter.

The Unit 1 turbine building was determined in the fragility analysis to be dependent on the strength of the superheater building since the two are structurally tied together. The southernmost bay of the Unit 2 turbine building overlaps the control building so that failure of that bay and perhaps the next bay as well would likely cause a failure of the control building, including a loss of control and AC and DC power. The third bay from the south end of the Unit 2 turbine building contains cross bracing which forms a box structure that would resist failed adjacent frames from falling into the yard under westerly wind loading and possibly impacting the control building. This is a consideration for failure of the turbine building since the fragility analysis assigns a higher east-west wind velocity capacity to the building bays not opposite the operating floor slab cutouts. That analysis indicates the operating floor slab is capable of transmitting east-west lateral loads from these outer bays to the turbine-generator pedestal while the heat exchanger slab cutouts in the other bays preclude such load transfers. Consequently, these interior bays have a lower capacity and are treated as an independent source of failure.

Table 7.5-9 summarizes these potential failure sources and the conditional probability, k, of each source's failure from wind in each of the directions impacting on the target structure of interest. The left subscript on k represents the source structure number and the right subscript represents the target structure number. These subscripts are presented after the item numbers used in Figure 7.5-3. The items are presented as follows and additionally include the superheater and turbine buildings:

(1) Gas Turbine Shelter

(2) Offsite Power Service

(3) Auxiliary Feed Pump Building

(4) Unit 2 - Control Building

(5) Unit 2 - Portion of PAB

(6) Unit 2 - Diesel Generator Building

(7) Unit 1 - Superheater Stack

(8) Condensate Storage Tank

(9) Refueling Water Storage Tank

(10) City Water Tank

(11) Service Water Pumps

(12) Superheater Building

(13) Unit 1 or Unit 2 Turbine Building

The k values in Table 7.5-9 are used as applicable in the Booleans to be discussed next. Seen earlier in Section 7.5.4, the wind initiated events and the resulting failures that could lead to core melt can be expressed by a fault tree. Figure 7.5-6a and the discussion indicated that core melt can occur from either of two scenarios: M_1, a transient such as loss of offsite power followed by turbine trip and loss of cooling; or M_2, a small rupture in the reactor coolant system and failure of safety injection and cooling. The potential sources of failure and impacts of these events as determined in the current analysis are modeled in Figure 7.5-20a for M_1 and Figure 7.5-20b for M_2. As before, the circled numbers refer to the item as defined earlier in this section and the symbols in triangles refer to fault trees seen in Figure 7.5-20c for loss of power and in Figure 7.5-20d for loss of control.

Each of the failure events noted on the fault trees can result variously from building frame failures, siding or roofing failures, or from the impact of tornado-driven missiles. Using the fault trees of Figures 7.5-20a through 7.5-20d, Booleans are developed for M_1 and M_2 and, therefore, for core melt, M_W, which is

$$M_W = M_1 \vee M_2$$

In terms of the structure failures, and considering the probability of failure from impacts by nearby buildings,

$$M_1 = \hat{4} \vee \{(\hat{2} \vee 9) \wedge [(8 \wedge 10) \vee 3]\}$$

$$M_2 = \hat{2} \vee \{(5 \vee 11) \wedge [9 \vee (\hat{4} \wedge 10)]\}$$

and

$$M_W = \hat{2} \vee \hat{4} \vee \{9 \wedge [3 \vee 5 \vee 11 \vee (8 \wedge 10)]\}$$

where, conceding (2),

$$(\hat{2} \vee \hat{4}) = \hat{4a} \vee 12 \vee ({}_{13}k_1 + {}_{13}k_4)\ 13 \vee ({}_{7}k_1 + {}_{7}k_4 + {}_{7}k_6)\ 7$$
$$\vee [(4b \vee 6 \vee 11) \wedge (1 \vee \text{GTFS})]$$

and

$$\hat{4a} = 4 \vee 4a$$

The failure probability of the gas turbine to start on demand, GTFS, is obtained from Section 1.5. Impact failure probability values of k are obtained for each direction of wind loading from Table 7.5-9. The items in the Boolean may fail from building frame failures, siding or roofing failures from impinging or negative pressure loads, or from tornado missile impacts. It is therefore necessary to express the logic of these possible failure modes where applicable for each structure. This logic is presented in the form of Booleans in Table 7.5-10. Each of the items

in the M_W expression above for core melt is replaced by the appropriate Boolean in Table 7.5-10 in determining M_W. In these Booleans, values for failure fractions F_F, F_S, F_{S-}, and F_{R-} correspond with the failure fraction for median wind velocity capacities, $\tilde{v}_F$, $\tilde{v}_S$, $\tilde{v}_{S-}$, and $\tilde{v}_{R-}$, respectively, obtained from Table 7.5-7; and values for P_M are obtained from Table 7.5-8; all for each of the four wind directions.

The expression for M_W gives the logical relationship between the occurrence of melt and the failure of various components. The individual components can now be combined through the Boolean equation by means of the SEIS code to obtain a plant level family of fragility curves for the occurrence of core melt.

7.5.4A.5 Wind Core Melt Frequencies

The plant level fragility family for each wind direction can then be combined with the appropriate wind and tornado hazard curves using the SEIS code. When these are combined for all four wind directions through the DPD process, we obtain the probability curve shown in Figure 7.5-21 indicating our state of knowledge about the frequency of core melt due to wind and tornadoes. The median annual frequency is about 1.8×10^{-5} and the mean is 3.6×10^{-5}.

7.5.4A.6 Wind Release Category Frequencies

The fault trees indicating failures which lead to a loss of the fan coolers, x, and to a loss of containment spray, y, are seen in Figures 7.5-22 and 7.5-23, respectively. These allow us to develop logic expressions for each release category where, as described in Section 7.5.4.3,

$$2RW = (M1 \vee M2) \wedge x \wedge y$$

$$8B = (M1 \vee M2) \wedge \bar{y}$$

$$8A = (M1 \vee M2) \wedge \bar{x} \wedge y$$

A bar over a symbol indicates failure negation. From the figures,

$$x = \hat{2} \vee \hat{4} \vee 11$$

$$y = \hat{2} \vee \hat{4} \vee 9$$

Substituting in the above expressions for release categories and reducing,

$$2RW = \hat{2} \vee \hat{4} \vee (11 \wedge 9)$$

$$8B = \text{cannot occur}$$

$$8A = \hat{2} \wedge \hat{4} \wedge \overline{11} \wedge 9 \wedge [3 \vee 5 \vee (8 \wedge 10)]$$

Using these expressions of failures and the occurrence of release categories, the plant level fragility is determined from the component Booleans in Table 7.5-10, and the values of $\tilde{v}_F$, $\tilde{v}_S$, $\tilde{v}_{S-}$, and $\tilde{v}_{R-}$ in Table 7.5-7, P_M in Table 7.5-8, and k in Table 7.5-9 for each of the four wind directions. These are combined with the wind hazard curves for each of the wind directions using the SEIS code. These results are then combined for all four directions using the DPD process. Figure 7.5-24 presents the resultant probability of frequency curves for release categories 2RW and 8A.

The major contributors to the frequency of core melt and release category 2RW are failure of the control room causing a loss of control, and failure of the gas turbine and diesel generator buildings causing a loss of emergency power.

7.5.5 INDIAN POINT UNIT 3

7.5.5.1 Plant Logic

As in the case of wind initiated events for Indian Point 2, the failures leading to core melt can be expressed by three basic fault trees. The first, M_1, consists of a transient, such as loss of offsite power, followed by turbine trip and loss of cooling. A wind initiated event may induce a reactor coolant system rupture and failure of safeguards systems that could also lead to core melt. We designate the failures starting with a small LOCA followed by a loss of safety injection and cooling, M_2, and those starting with a large LOCA followed by a loss of safety injection, M_3. Thus, we can expect core melt if either M_1, M_2, or M_3 occurs.

The fault trees for wind initiated Unit 3 failures leading to core melt are seen in Figure 7.5-11. From the fault tree in Figure 7.5-11a, core melt occurs for

$$M_W = M_1 \vee M_2 \vee M_3$$

From Figure 7.5-11b

$$M_1 = (\textcircled{2}_W \vee \textcircled{2}_T) \wedge \{(\hat{\textcircled{2}} \vee \textcircled{9}_T) \wedge [(\textcircled{8}_T \vee 0.05 \times \textcircled{7}_W \vee 0.05 \times \textcircled{7}_T) \wedge \textcircled{10}_T] \vee \textcircled{3}_W \vee \textcircled{3}_T\}$$

where 0.05 = probability of the superheat stack falling on the CST.

From Figure 7.5-11e

$$\hat{\textcircled{2}} = (\textcircled{2}_W \vee \textcircled{2}_T) \wedge \textcircled{11}_T$$

Note that, in this instance, the unavailability of gas turbine power is conservatively assumed for several reasons. While two gas turbines which are located up the hill and to the east of the plant can be

level as discussed in Section 0.8.4.2. The numbers entered in the tables are elements of the MC^W matrix and give the conditional frequencies of occurrence of the various release categories, given wind velocities specified in the left column. The MC^W matrix, when combined with the wind speed hazard curves, gives us the frequency of wind initiated release categories. Figure 7.5-10 presents the resultant probability of frequency curves.

The dominant contributors to Release Category 2RW are loss of offsite power lines and failure of the control building housing the switchgear and batteries for starting the diesel generator.

The dominant contributors to Release Category 8A are failure of offsite power lines, a portion of the PAB top story, the auxiliary feed pump building, and the refueling water storage tank.

7.5.5 INDIAN POINT UNIT 3

7.5.5.1 Plant Logic

As in the case of wind initiated events for Indian Point 2, the failures leading to core melt can be expressed by three basic fault trees. The first, M_1, consists of a transient, such as loss of offsite power, followed by turbine trip and loss of cooling. A wind initiated event may induce a reactor coolant system rupture and failure of safeguards systems that could also lead to core melt. We designate the failures starting with a small LOCA followed by a loss of safety injection and cooling, M_2, and those starting with a large LOCA followed by a loss of safety injection, M_3. Thus, we can expect core melt if either M_1, M_2, or M_3 occurs.

The fault trees for wind initiated Unit 3 failures leading to core melt are seen in Figure 7.5-11. From the fault tree in Figure 7.5-11a, core melt occurs for

$$M_W = M_1 \vee M_2 \vee M_3$$

From Figure 7.5-11b

$$M_1 = (②_W \vee ②_T) \wedge \{(\hat{②} \vee ⑨_T) \wedge [(⑧_T \vee 0.05 \times ⑦_W \vee 0.05 \times ⑦_T) \wedge ⑩_T] \vee ③_W \vee ③_T\}$$

where 0.05 = probability of the superheater stack falling on the CST.

From Figure 7.5-11e

$$\hat{②} = (②_W \vee ②_T) \wedge ⑪_T$$

Note that, in this instance, the unavailability of gas turbine power is conservatively assumed for several reasons. While two gas turbines which are located up the hill and to the east of the plant can be

started from the control room, the operator must access the Buchanan substation to perform local switching operations before either of these gas turbines can be placed online. Under severely adverse weather conditions, it may not be possible to gain access to the substation. GT-1, which is located adjacent to the Unit 1 turbine building, however, can be started and placed online from the control room. Even in this case, both nuclear plant units may place a demand on the gas turbine at the same time, causing its unavailability to one or the other unit. Further, even under normal operations, each gas turbine has a probability of failing to start on demand of approximately 0.15, not considering operator actions under this external event and turbine unavailability due to maintenance. Even under the most optimistic conditions, a gas turbine would not normally supply power for at least 30 minutes following a loss of offsite and plant power. Therefore, gas turbine unavailability has been assumed to be 1.0.

Then M_1 reduces to

$$M_1 = (②_W \vee ②_T) \wedge (⑨_T \vee ⑪_T) \wedge [③_W \vee ③_T \vee (⑩_T \wedge \{⑧_T \vee 0.05 \times ⑦_W \vee 0.05 \times ⑦_T\})]$$

From Figure 7.5-11c,

$$M_2 = \{\hat{②} \vee [⑪_T \wedge (⑨_T \vee ⑪_T)]\} \wedge \{\hat{②} \vee ⑨_T \vee M_{1A}\}$$

which reduces to

$$M_2 = ⑪_T \wedge (②_W \vee ②_T \vee ⑨_T)$$

From Figure 7.5-11d, we see that M_3, large LOCA, does not occur. Therefore, our expression for core melt becomes

$$M_W = M_1 \vee M_2$$

$$= \{[③_W \vee ③_T \vee (⑩_T \wedge \{⑧_T \vee 0.05 \times ⑦_W \vee 0.05 \times ⑦_T\})] \wedge ⑨_T \wedge (②_W \vee ②_T)\} \vee \{⑪_T \wedge [(②_W \vee ②_T) \vee ⑨_T]\}$$

This Boolean equation expresses the logical relationship between the occurrence of melt and the failure of various components. The probability of failure of each individual component, as a function of wind velocity, is described by its family of fragility curves. These individual families of fragility curves can now be combined through the logic of the Boolean equation, to obtain a plant level family of fragility curves for the occurrence of core melt for each type of wind loading.

7.5.5.2 Wind Core Melt Frequencies

The fragility family is now combined with the wind speed families of Figures 7.5-1 and 7.5-2 to obtain a probability curve showing our state of knowledge about the frequency of core melt due to wind or tornado

loading. The result is seen in Figure 7.5-12. From the cumulative probability curve it is seen that the median annual frequency of core melt due to wind events is about 4.9×10^{-8} with a 90% confidence that it is between zero and 6.5×10^{-6}. The mean annual frequency of core melt is 1.3×10^{-6}.

7.5.5.3 Initial Assembly Leading To Release Category Frequencies

In the previous section we developed a Boolean expression for the state "core melt" in terms of plant components. Now, to develop risk curves and to integrate wind analysis with the rest of the study, we need to know which type of core melt, plant state, and release category occurs. That is, we need to develop Boolean expressions for each of the plant states defined in Section 1 and then aggregate them according to the containment state and release category to which they contribute. For this purpose, we introduce two new expressions:

x = failure of fan coolers
y = failure of containment spray

The fault trees of Figures 7.5-13 and 7.5-14 give the logics for x and y. Summarizing,

$$x = \hat{(2)} \vee (11)_T$$

which reduces to

$$x = (11)_T$$

and

$$y = \hat{(2)} \vee (9)_T$$

Now, from the definitions of the plant states in Section 1, only the following plant states might occur from a wind initiating event:

Plant State	Boolean Expression
AEFC	$M_3 \wedge \bar{x} \wedge \bar{y}$
AEF	$M_3 \wedge \bar{x} \wedge y$
AEC	$M_3 \wedge x \wedge \bar{y}$
AE	$M_3 \wedge x \wedge y$
SEFC	$M_2 \wedge \overline{M_3} \wedge \bar{x} \wedge \bar{y}$
SEF	$M_2 \wedge \overline{M_3} \wedge \bar{x} \wedge y$

Plant State	Boolean Expression
SEC	$M_2 \wedge \overline{M_3} \wedge x \wedge \overline{y}$
SE	$M_2 \wedge \overline{M_3} \wedge x \wedge y$
TEFC	$M_1 \wedge \overline{M_2} \wedge \overline{M_3} \wedge \overline{x} \wedge \overline{y}$
TEF	$M_1 \wedge \overline{M_2} \wedge \overline{M_3} \wedge \overline{x} \wedge y$
TEC	$M_1 \wedge \overline{M_2} \wedge \overline{M_3} \wedge x \wedge \overline{y}$
TE	$M_1 \wedge \overline{M_2} \wedge \overline{M_3} \wedge x \wedge y$

Bars over the symbols denote negation. Thus, $\overline{x}$ means that fan coolers do not fail, and so on.

Next, these plant states are aggregated in terms of the containment state (failure or no failure of containment) and the release category to which they contribute.

Because M_3 cannot occur, AEFC, AEF, AEC, and AE all equal zero and, because Release Category Z-1 = AE, Z-1 = 0. Now, since containment does not fail,

$$2RW = SE \vee TE$$

$$= (M_1 \vee M_2) \wedge x \wedge y$$

Substituting the components for M_1, M_2, x, and y, and reducing,

$$2RW = \textcircled{11}_T \wedge (\textcircled{2}_W \vee \textcircled{2}_T \vee \textcircled{9}_T)$$

Also,

$$8B = SEFC \vee SEC \vee TEFC \vee TEC$$

$$= (M_1 \vee M_2) \wedge \overline{y}$$

This cannot occur since the components of y must fail in order to have core melt $M_1 \vee M_2$.

Also,

$$8A = SEF \vee TEF$$

$$= (M_1 \vee M_2) \wedge \overline{x} \wedge y$$

$$= \overline{\textcircled{11}}_T \wedge \textcircled{9}_T \wedge [\textcircled{3}_W \vee \textcircled{3}_T \vee (\textcircled{10}_T \wedge \{\textcircled{8}_T \vee 0.05 \times \textcircled{7}_W \vee 0.05 \times \textcircled{7}_T\})] \wedge (\textcircled{2}_W \vee \textcircled{2}_T)$$

These Boolean equations for each release category express the logical relationships between component failures and occurrence of the various release categories. Using these expressions and the fragility families for the components, the plant level fragility family for each release category is obtained. This family, in numerical form, consititutes the wind MC^W matrix. The uncertainties in the component fragility curves translate through this process into uncertainty in the MC^W matrix. This uncertainty is represented in Table 7.5-6 for tornadoes by showing five different values of the MC^W matrix with 20% probability assigned to each. The values in the MC^W matrix for extra-tropical cyclones and hurricanes are essentially zero for all release categories. This table, thus, is an example of the DPD process applied at the matrix level as discussed in Section 0.8.4.2. The numbers entered in the table (and zero for extra-tropical cyclones and hurricanes) are elements of the MC^W matrix and give the conditional frequencies of occurrence of the various release categories, given wind velocities specified in the left column. The MC^W matrix, when combined with the wind speed hazard curves, gives us the frequency of wind initiated release categories. Figure 7.5-15 presents the resultant probability of frequency curves.

The dominant contributors to Release Category 2RW are the loss of offsite power, failure of the auxiliary feed pump building, and failure of the service water pumps.

The dominant contributors to Release Category 8A are the loss of offsite power, failure of the auxiliary feed pump building, and failure of the refueling water storage tank.

7.5.6 SUMMARY

The preceding sections have provided, in effect, the matrix ϕ^W, i.e., the frequencies of wind initiating events; the matrix M^W, i.e., the conditional plant damage state frequencies; and the matrix ϕMC^W, the release frequencies. In Section 8, the latter matrix is combined with the matrix S to produce the total wind risk in terms of the five damage indices.

7.5.7 REFERENCES

7.5-1 Twisdale, L. A., W. L. Dunn, and J. Cho, "Tornado Missile Simulation and Risk Analysis," Meeting on Probabilistic Analysis of Nuclear Safety, ANS, Newport Beach, May 1978.

7.5-2 United Engineers and Constructors, Inc., "Indian Point Generating Station - Unit No. 2, Report - Plant Capability to Withstand Tornadoes," January 26, 1968.

7.5-3 Consolidated Edison Company, Indian Point, Unit 2, FSAR response to Question 1.3, August 1970.

7.5-4 American National Standards Institute, Inc., "Building Code Requirements For Minimum Design Loads in Buildings and Other Structures," ANSI A58.1-1972.

7.5-5 Structural Mechanics Associates letter to Pickard, Lowe and Garrick, Inc., dated August 5, 1981.

7.5-6 Sandia National Laboratories, "Review and Evaluation of the Indian Point Probabilistic Safety Study," NUREG/CR-2934, December 1982.

TABLE 7.5-1

VARIABILITY FOR EXTRA-TROPICAL CYCLONES AND HURRICANE WIND LOADING - INDIAN POINT UNITS 2 AND 3

Structure	Design Wind Pressure (psf)	Factor, Elevation Variability (Exposure B, 50-Year Recurrence)					Factor, Exposure Variability and Recurrence Period (Elevation 33')					Load Variability, SF_L		
		@ 33' (psf)	@ Max Height (psf)	Height Factor	@ Base (psf)	Height Factor	Exposure B 50-Year (psf)	Exposure C 100-Year (psf)	Exposure Factor	Exposure A 50-Year (psf)	Exposure Factor	Lower Bound	Median	Upper Bound
Unit 2 Control Building	30	11.5	13.5	0.85	9.0	1.27	11.5	18.5	0.62	6.0	1.92	0.53	1.0	2.44
Unit 2 Diesel Generator Building	30	11.5	9.0	1.27	9.0	1.27	11.5	18.5	0.62	6.0	1.92	0.79	1.0	1.61
Unit 2 PAB-Portion of Top Story	30	11.5	12.5	0.92	9.0	1.27	11.5	18.5	0.62	6.0	1.92	0.57	1.0	2.44
Units 2 and 3 AFW Pump Building	30	11.5	15.5	0.74	9.0	1.27	11.5	18.5	0.62	6.0	1.92	0.46	1.0	2.44
Gas Turbine Enclosure	30	11.5	9.0	1.27	9.0	1.27	11.5	18.5	0.62	6.0	1.92	0.79	1.0	2.44
Superheater Stack	331*	11.5	26.7	0.43	19.5	0.59	11.5	18.5	0.62	6.0	1.92	0.27	1.0	1.13
Transmission Lines	50 (30 on rounded surfaces)	11.5	15.5	0.74	9.0	1.27	11.5	18.5	0.62	6.0	1.92	0.46	1.0	2.44

*Calculated from 360 mph tornado wind by $q = 0.00256V^2$, where q = wind load in psf and V = wind velocity in mph.

TABLE 7.5-2

STRUCTURE CAPACITIES FOR TORNADO WINDS - INDIAN POINT UNITS 2 AND 3

Structure	Tornado Load Variability, SF_L			SF_Y			S_I	$SF_L SF_Y SF_I$			Capacity (psf)			Capacity (mph)*		
	Lower Bound	Median	Upper Bound	Lower Bound	Median	Upper Bound		Lower Bound	Median	Upper Bound	Lower Bound	Median	Upper Bound	Lower Bound	Median	Upper Bound
Unit 2 Control Building	0.9	1.0	1.4	1.7	1.8	2.0	1.0	1.5	1.8	2.8	45	54	84	132	145	181
Unit 2 Diesel Generator Building	0.9	1.0	1.4	1.7	1.8	2.0	1.0	1.5	1.8	2.8	45	54	84	132	145	181
Unit 2 PAB-Portion of Top Story	0.9	1.0	1.4	1.7	1.8	2.0	1.0	1.5	1.8	2.8	45	54	84	132	145	181
Units 2 and 3 AFW Pump Building	0.8	1.0	1.4	1.7	1.8	2.0	1.0	1.4	1.8	2.8	42	54	84	128	145	181
Gas Turbine Enclosure	1.0	1.2	1.4	1.7	1.8	2.0	0.8	1.4	1.7	2.2	42	51	66	128	141	160
Superheater Stack	0.5	1.0	1.4	1.0	1.0	1.0	1.0	0.5	0.5	1.4	165	331	463	254	360	425
Transmission Lines	0.8	1.0	1.4	1.0	1.0	1.0	1.0	0.8	1.0	1.4	40	50	70	125	140	165

*Equivalent wind velocity, V, from $q = 0.00256V^2$, where q = psf capacity.

TABLE 7.5-3

STRUCTURE CAPACITIES FOR EXTRA-TROPICAL CYCLONE AND HURRICANE WINDS - INDIAN POINT UNITS 2 AND 3

Structure	Load Variability, SF_L			SF_Y			SF_I	$SF_L SF_Y SF_I$			Capacity (psf)			Capacity (mph)*		
	Lower Bound	Median	Upper Bound	Lower Bound	Median	Upper Bound		Lower Bound	Median	Upper Bound	Lower Bound	Median	Upper Bound	Lower Bound	Median	Upper Bound
Unit 2 Control Building	0.53	1.0	2.44	1.7	1.8	2.0	1.0	0.90	1.80	4.88	27	54	146	103	145	238
Unit 2 Diesel Generator Building	0.79	1.0	1.61	1.7	1.8	2.0	1.0	1.34	1.80	3.22	40	54	07	125	145	195
Unit 2 PAB-Portion of Top Story	0.57	1.0	2.44	1.7	1.8	2.0	1.0	0.97	1.80	4.88	29	54	146	106	145	238
Units 2 and 3 AFW Pump Building	0.46	1.0	2.44	1.7	1.8	2.0	1.0	0.78	1.80	4.88	23	54	146	94	145	238
Gas Turbine Enclosure	0.79	1.0	2.44	1.7	1.8	2.0	0.8	1.07	1.44	3.90	32	43	117	112	130	214
Superheater Stack	0.27	1.0	1.13	1.0	1.0	1.0	1.0	0.27	1.0	1.13	90	331	374	187	360	382
Transmission Lines	0.46	1.0	2.44	1.0	1.0	1.0	1.0	0.46	1.0	2.44	23	50	122	95	140	218

*Equivalent wind velocity, V, from $q = 0.00256V^2$, where q = psf capacity.

TABLE 7.5-4

INDIAN POINT 2 CONDITIONAL RELEASE FREQUENCIES -
EXTRA-TROPICAL CYCLONE AND HURRICANE WIND MATRIX MC^W

20% Probability Each Table

Wind Velocity (mph)	Release Category	
	2RW	8A
70	0	0
90	5.60E-05	0
110	1.83E-03	0
130	3.29E-02	0
150	2.34E-01	0
170	5.15E-01	0
190	7.13E-01	0
210	8.41E-01	0
230	9.20E-01	0
250	9.55E-01	0
270	9.90E-01	0
290	1.00E+00	0
310	1.00E+00	0
330	1.00E+00	0

Wind Velocity (mph)	Release Category	
	2RW	8A
70	0	0
90	7.92E-04	0
110	1.30E-02	0
130	1.22E-01	0
150	4.57E-01	0
170	7.38E-01	0
190	8.64E-01	0
210	9.40E-01	0
230	1.00E+00	0
250	1.00E+00	0
270	1.00E+00	0
290	1.00E+00	0
310	1.00E+00	0
330	1.00E+00	0

Wind Velocity (mph)	Release Category	
	2RW	8A
70	0	0
90	8.00E-04	0
110	1.34E-02	0
130	1.29E-01	0
150	4.87E-01	0
170	7.54E-01	0
190	8.66E-01	0
210	9.40E-01	0
230	1.00E+00	0
250	1.00E+00	0
270	1.00E+00	0
290	1.00E+00	0
310	1.00E+00	0
330	1.00E+00	0

Wind Velocity (mph)	Release Category	
	2RW	8A
70	0	0
90	8.00E-04	0
110	1.50E-02	0
130	1.38E-01	0
150	4.93E-01	0
170	7.55E-01	0
190	8.67E-01	0
210	9.40E-01	0
230	1.00E+00	0
250	1.00E+00	0
270	1.00E+00	0
290	1.00E+00	0
310	1.00E+00	0
330	1.00E+00	0

Wind Velocity (mph)	Release Category	
	2RW	8A
70	0	0
90	1.35E-02	0
110	2.77E-01	0
130	2.01E-01	0
150	5.63E-01	0
170	7.87E-01	0
190	8.95E-01	0
210	9.70E-01	0
230	1.00E+00	0
250	1.00E+00	0
270	1.00E+00	0
290	1.00E+00	0
310	1.00E+00	0
330	1.00E+00	0

TABLE 7.5-5

INDIAN POINT 2 CONDITIONAL RELEASE FREQUENCIES - TORNADO WIND MATRIX MC^W

20% Probability Each Table

Wind Velocity (mph)	Release Category	
	2RW	8A
70	0	0
90	0	0
110	0	0
130	6.53E-04	0
150	3.26E-01	0
170	5.24E-01	0
190	9.88E-01	0
210	1.00E+00	0
230	1.00E+00	0
250	1.00E+00	0
270	1.00E+00	0
290	1.00E+00	0
310	1.00E+00	0
330	1.00E+00	0

Wind Velocity (mph)	Release Category	
	2RW	8A
70	0	0
90	0	0
110	0	0
130	2.12E-03	0
150	7.96E-01	0
170	9.87E-01	0
190	1.00E+00	0
210	1.00E+00	0
230	1.00E+00	0
250	1.00E+00	0
270	1.00E+00	0
290	1.00E+00	0
310	1.00E+00	0
330	1.00E+00	0

Wind Velocity (mph)	Release Category	
	2RW	8A
70	0	0
90	0	0
110	0	0
130	2.36E-03	0
150	8.58E-01	0
170	9.98E-01	0
190	1.00E+00	0
210	1.00E+00	0
230	1.00E+00	0
250	1.00E+00	0
270	1.00E+00	0
290	1.00E+00	0
310	1.00E+00	0
330	1.00E+00	0

Wind Velocity (mph)	Release Category	
	2RW	8A
70	0	0
90	0	0
110	0	0
130	2.83E-03	0
150	8.62E-01	0
170	9.99E-01	0
190	1.00E+00	0
210	1.00E+00	0
230	1.00E+00	0
250	1.00E+00	0
270	1.00E+00	0
290	1.00E+00	0
310	1.00E+00	0
330	1.00E+00	0

Wind Velocity (mph)	Release Category	
	2RW	8A
70	0	0
90	0	0
110	0	0
130	6.52E-03	0
150	8.99E-01	0
170	1.00E+00	5.45E-04
190	1.00E+00	2.12E-05
210	1.00E+00	2.06E-06
230	1.00E+00	0
250	1.00E+00	0
270	1.00E+00	0
290	1.00E+00	0
310	1.00E+00	0
330	1.00E+00	0

TABLE 7.5-6

INDIAN POINT 3 CONDITIONAL RELEASE FREQUENCIES - TORNADO WIND MATRIX MC^W

20% Probability Each Table

Wind Velocity (mph)	Release Category	
	2RW	8A
70	0	0
90	0	0
110	0	0
130	0	0
150	0	0
170	0	0
190	0	0
210	0	0
230	5.00E-02	1.06E-02
250	2.50E-01	1.75E-02
270	4.80E-01	3.92E-03
290	6.40E-01	0
310	9.00E-01	0
330	1.00E+00	0

Wind Velocity (mph)	Release Category	
	2RW	8A
70	0	0
90	0	0
110	0	0
130	0	0
150	0	0
170	0	0
190	0	0
210	0	0
230	1.00E-01	8.84E-02
250	5.00E-01	2.48E-01
270	9.50E-01	4.70E-02
290	1.00E+00	0
310	1.00E+00	0
330	1.00E+00	0

Wind Velocity (mph)	Release Category	
	2RW	8A
70	0	0
90	0	0
110	0	0
130	0	0
150	0	0
170	0	0
190	0	0
210	0	0
230	1.00E-01	9.00E-02
250	5.00E-01	2.50E-01
270	9.50E-01	4.75E-02
290	1.00E+00	0
310	1.00E+00	0
330	1.00E+00	0

Wind Velocity (mph)	Release Category	
	2RW	8A
70	0	0
90	0	0
110	0	0
130	0	0
150	0	0
170	0	0
190	0	0
210	0	0
230	1.00E-01	9.00E-02
250	5.00E-01	2.50E-01
270	9.50E-01	4.75E-02
290	1.00E+00	0
310	1.00E+00	0
330	1.00E+00	0

Wind Velocity (mph)	Release Category	
	2RW	8A
70	0	0
90	0	0
110	0	0
130	0	0
150	0	0
170	2.29E-02	2.00E-02
190	4.99E-02	4.84E-02
210	2.75E-01	2.59E-01
230	5.25E-01	4.43E-01
250	7.50E-01	4.85E-01
270	9.75E-01	4.52E-01
290	1.00E+00	3.34E-01
310	1.00E+00	9.80E-02
330	1.00E+00	0

TABLE 7.5-7

UNIT 2 BUILDING WIND FRAGILITY SUMMARY

Building[a]	Wind Direction							
	North		South		East		West	
	$\tilde{v}$(mph)	β_U	$\tilde{v}$(mph)	β_U	$\tilde{v}$(mph)	β_U	$\tilde{v}$(mph)	β_U
Unit 2 Turbine Building								
$\tilde{v}_{F_E}$	161[b]	0.11	278[b]	0.23	153[c]	0.14	132[c]	0.12
$\tilde{v}_{F_I}$	161[b]	0.11	278[b]	0.23	137[c]	0.14	119[c]	0.12
$\tilde{v}_S$	128	0.12	(Unit 1)		123	0.11	107	0.10
$\tilde{v}_{S-}$	128	0.12	108	0.12	108	0.16	94	0.12
$\tilde{v}_{R-}$	219	0.13	219	0.13	219	0.13	219	0.13
PAB (Metal Portion)								
$\tilde{v}_F$	426	0.19	381	0.23	>>[d]		>>[d]	
$\tilde{v}_S$	178	0.14	178	0.11	178	0.12	>>[d]	
$\tilde{v}_{S-}$	132	0.11	145	0.11	153	0.11	174	0.11
$\tilde{v}_{R-}$	242	0.16	242	0.16	242	0.16	242	0.16

a. $\tilde{v}_F$ = structure; $\tilde{v}_S$ = siding, impinging wind; $\tilde{v}_{S-}$ = siding, wind suction; $\tilde{v}_{R-}$ = roofing, wind suction.
b. Dependent.
c. Independent.
d. Fully shielded; extremely high capacity.

TABLE 7.5-7 (continued)

UNIT 2 BUILDING WIND FRAGILITY SUMMARY

Building[a]	Wind Direction							
	North		South		East		West	
	$\tilde{v}$(mph)	β_U	$\tilde{v}$(mph)	β_U	$\tilde{v}$(mph)	β_U	$\tilde{v}$(mph)	β_U
Diesel Generator Building								
$\tilde{v}_F$	304	0.22	219	0.17	208	0.17	292	0.22
$\tilde{v}_S$	194	0.27	141	0.12	123	0.11	157	0.16
$\tilde{v}_{S-}$	235	0.17	164	0.12	157	0.12	174	0.13
$\tilde{v}_{R-}$	132	0.15	132	0.15	132	0.15	132	0.15
Auxiliary Feed Pump Building								
$\tilde{v}_F$	440	0.14	547	0.19	404	0.23	314	0.20
$\tilde{v}_S$	197	0.13	240	0.23	298	0.18	>>[b]	
$\tilde{v}_{S-}$	222	0.19	222	0.19	222	0.19	222	0.19
Unit 1 Superheater Building								
$\tilde{v}_F$	319	0.16	294	0.11	232	0.14	200	0.10

a. $\tilde{v}_F$ = structure; $\tilde{v}_S$ = siding, impinging wind; $\tilde{v}_{S-}$ = siding, wind suction; $\tilde{v}_{R-}$ = roofing, wind suction.
b. Fully shielded; extremely high capacity.

TABLE 7.5-7 (continued)

UNIT 2 BUILDING WIND FRAGILITY SUMMARY

Building[a]	Wind Direction							
	North		South		East		West	
	$\tilde{v}$(mph)	β_U	$\tilde{v}$(mph)	β_U	$\tilde{v}$(mph)	β_U	$\tilde{v}$(mph)	β_U
Unit 1 Turbine Building								
$\tilde{v}_F$	319	0.16	294	0.11	232	0.14	200	0.10
Control Building								
$\tilde{v}_F$	319	0.16	294	0.11	282	0.13	469	0.23
$\tilde{v}_{Sa}$ (control room)	194	0.12	N/A		202	0.13	N/A	
$\tilde{v}_{Sb}$ (elsewhere)	171	0.12	N/A		178	0.13	N/A	
$\tilde{v}_{S-}$	149	0.12	168	0.12	157	0.11	167	0.12
$\tilde{v}_{R-}$	400	0.28	400	0.28	400	0.28	400	0.28
Gas Turbine Shelter								
$\tilde{v}_F$	181	0.26	181	0.26	181	0.26	104	0.21
$\tilde{v}_S$	94	0.26	94	0.26	94	0.26	83	0.22

a. $\tilde{v}_F$ = structure; $\tilde{v}_S$ = siding, impinging wind; $\tilde{v}_{S-}$ = siding, wind suction; $\tilde{v}_{R-}$ = roofing, wind suction.

TABLE 7.5-8

UNIT 2 BUILDING TORNADO MISSILE FRAGILITIES

Component Number	Structure	Similar Target Number (referenced study)	P_N	P_M	
				Mean	95th Percentile
(1)	Gas Turbine Shelter	7	3.3-6	1.4-3	4,2-3
(3)	Auxiliary Feed Pump Building	3	3.1-5	1.3-2	3.9-2
(4)	Control Building	4	2.6-5	1.1-2	3.3-2
(5)	PAB	3	3.1-5	1.3-2	3.9-2
(6)	Diesel Generator	7	3.3-6	1.4-3	4.2-3
(7)	Superheater Stack		(Nil - too high)		
(8)	Condensate Storage Tank	7	3.3-6	1.4-3	4.2-3
(9)	Refueling Water Storage Tank	7	3.3-6	1.4-3	4.2-3
(10)	City Water Tank	7	3.3-6	1.4-3	4.2-3
(11)	Service Water Pumps	6	1.4-6	6.1-4	2.4-3

NOTES:

1. Exponential notation is indicated in abbreviated form; i.e., 2.6-5 = 2.6×10^{-5}.
2. Data do not permit a discretization of tornadoes as a function of direction at the site. Therefore, these values of P_M are used for each of the directions considered.

TABLE 7.5-9

CONDITIONAL PROBABILITY OF IMPACT

Source Failure	Target Impacted	k Designator	Probability of Impact for Wind Direction			
			North	South	East	West
Superheater Building and Unit 1 Turbine Building	Control Building	$12^{k}4$	1.0	1.0	1.0	1.0
	Gas Turbine	$12^{k}1$	1.0	0	1.0	1.0
	Diesel Generator Building	$12^{k}6$	0	0	0	0
	Stack onto Diesel Generator Building	$12^{k}6$	0	0	0	0.5*
Unit 2 Turbine Building	Service Water System	$13^{k}11$	1.0	1.0	1.0	1.0
	Gas Turbine	$13^{k}1$	1.0	0	0	0
	Exterior Bays onto Control Building	$13E^{k}4$	1.0	1.0	1.0	1.0
	Interior Bays onto Control Building**	$13I^{k}4$	1.0	1.0	0.5	0.5
Superheater Building Stack	Control Building	$7^{k}4$	0	1.0	0.5*	0
	Gas Turbine	$7^{k}1$	1.0	0	0.5*	0
	Diesel Generator Building	$7^{k}6$	0	0.16*	0	0.5*

*Calculated from potential subtended angle of failure.
**Only applies given no failure of the exterior bays.

TABLE 7.5-10

UNIT 2 COMPONENT BOOLEANS

Component		Boolean Expression
(1)	Gas Turbine Shelter	$F_S \vee F_F \vee P_{M_1}$
(2)	Transmission Lines	Concede at Probability = 1.0
(3)	Auxiliary Feed Pump Building Top Portion	$0.2\ F_S \vee (F_F \wedge \overline{F}_S) \vee P_{M_3}$
(4)	Control Building	$(F_F \wedge \overline{F}_{Sb}) \vee P_{M_4}$
(4a)	Control Room	$F_{Sa} \vee F_{S-} \vee P_{M_4}$
(4b)	Control Building Siding (except for control room)	$0.5F_{Sb} \vee P_{M_4}$
$\hat{(4a)}$	= (4) ∨ (4a)	$F_{S_a} \vee F_{S-} \vee (F_F \wedge \overline{F}_{Sb}) \vee P_{M_4}$
(5)	PAB Top Portion	$0.7\ F_S \vee (F_F \wedge \overline{F}_S) \vee P_{M_5}$
(6)	Diesel Generator Building	$0.7\ F_S \vee (F_F \wedge \overline{F}_S) \vee P_{M_6}$
(7)	Unit 1 Superheater Stack	F_F
(8)	Condensate Storage Tank	P_{M_8}
(9)	Refueling Water Storage Tank	P_{M_9}
(10)	City Water Tank	$P_{M_{10}}$
(11)	Service Water Pumps	$P_{M_{11}}$
(12)	Unit 1 Superheater Building and Turbine Building	F_F
(13)	Unit 2 Turbine Building	$(F_{FE} \vee 0.5F_{FI}) \wedge \overline{F}_S$

NOTES:

1. F_F = frame failure fraction for specific structure.
2. F_S = wall failure fraction from wind pressure impingement.
3. F_{S-} = wall or roof failure fraction from negative wind pressure.
4. P_M = building penetration from tornado missile.
5. $\overline{F}^M$ = denotes no failure.

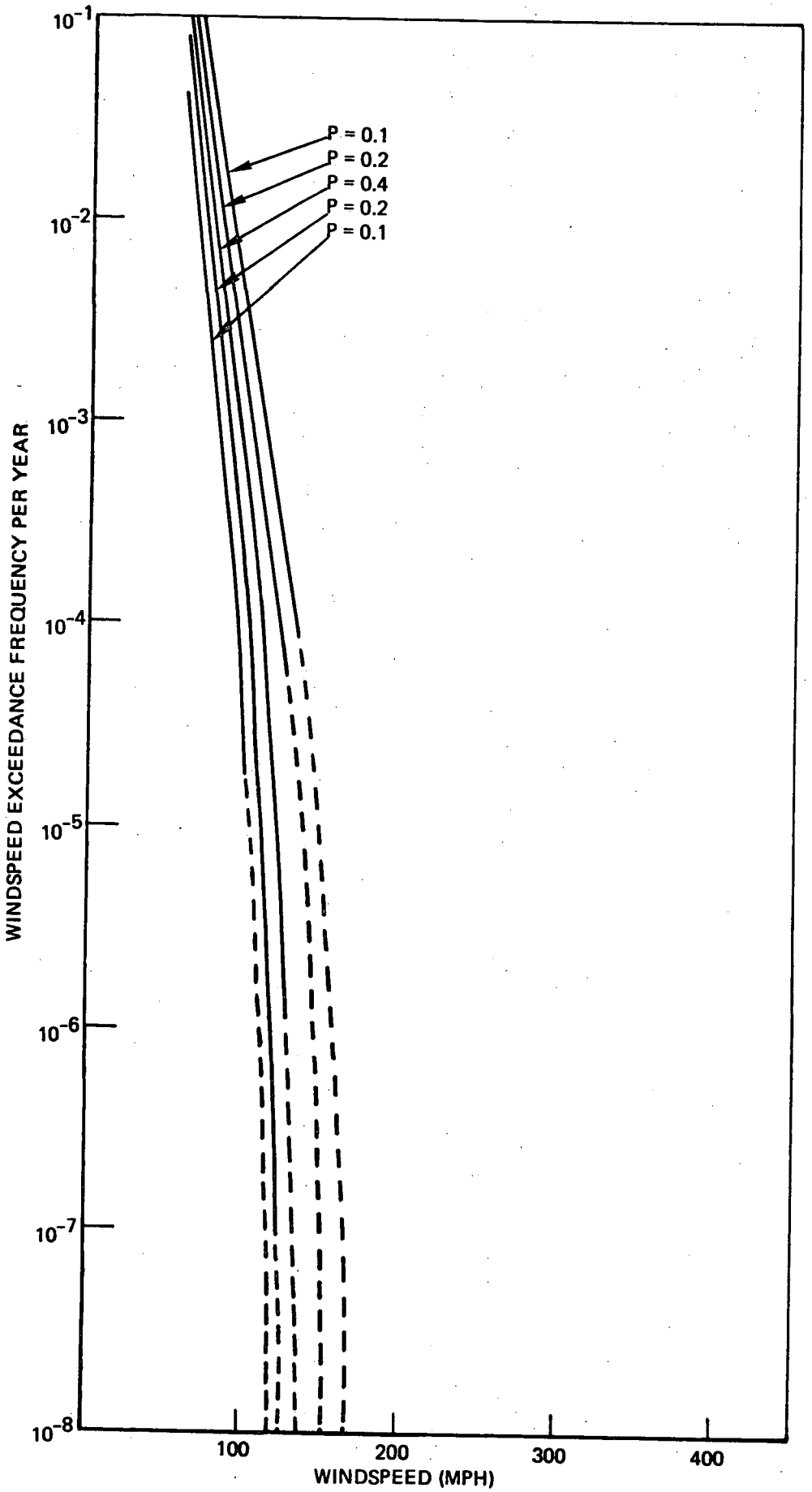


Figure 7.5-1. Hurricane and Extra-Tropical Cyclone Windspeed Exceedance Probabilities at Elevation 33' (Fastest Mile)

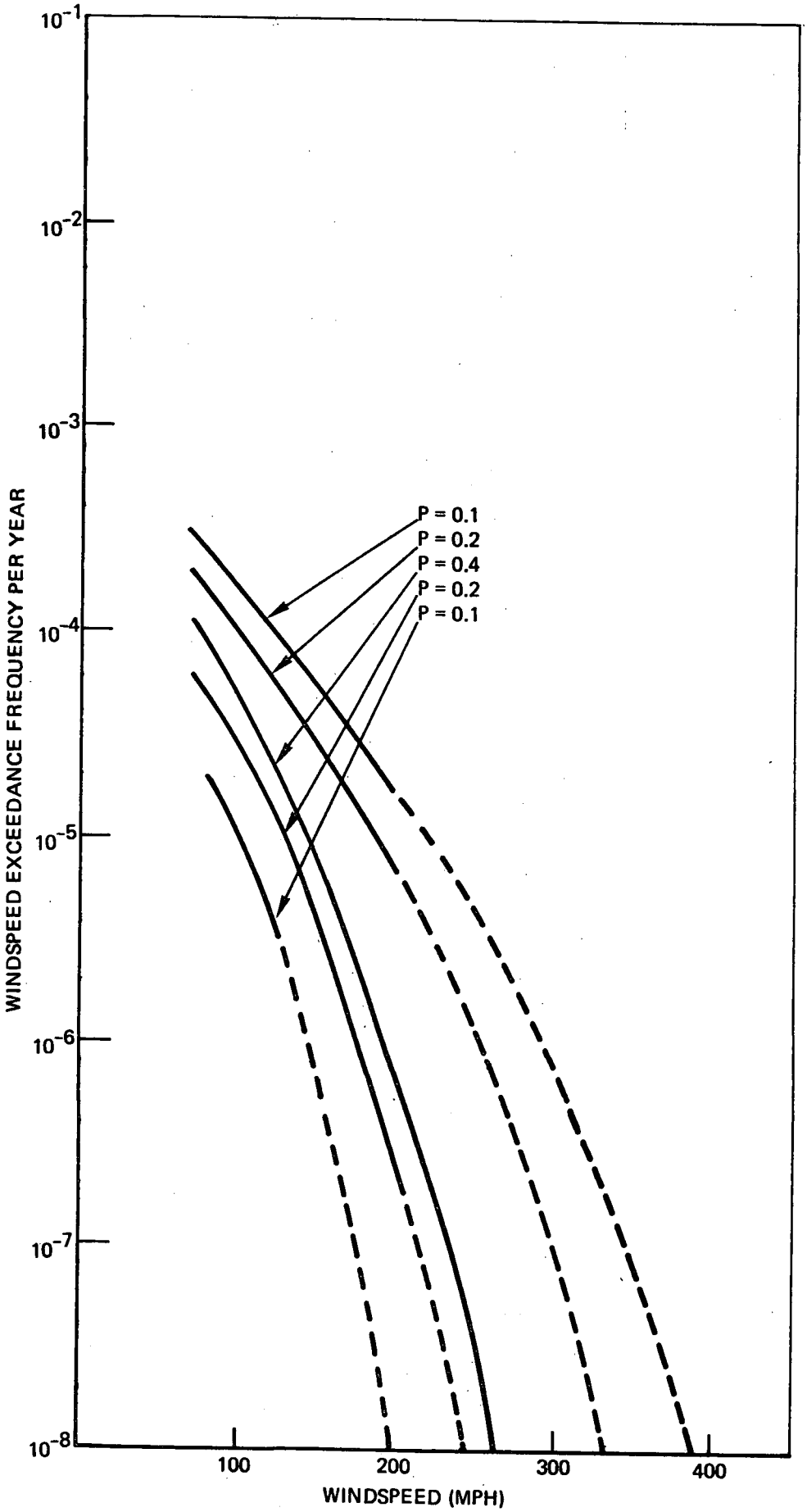


Figure 7.5-2. Tornado Windspeed Exceedance Probabilities at Elevation 33' (Fastest Quarter Mile)

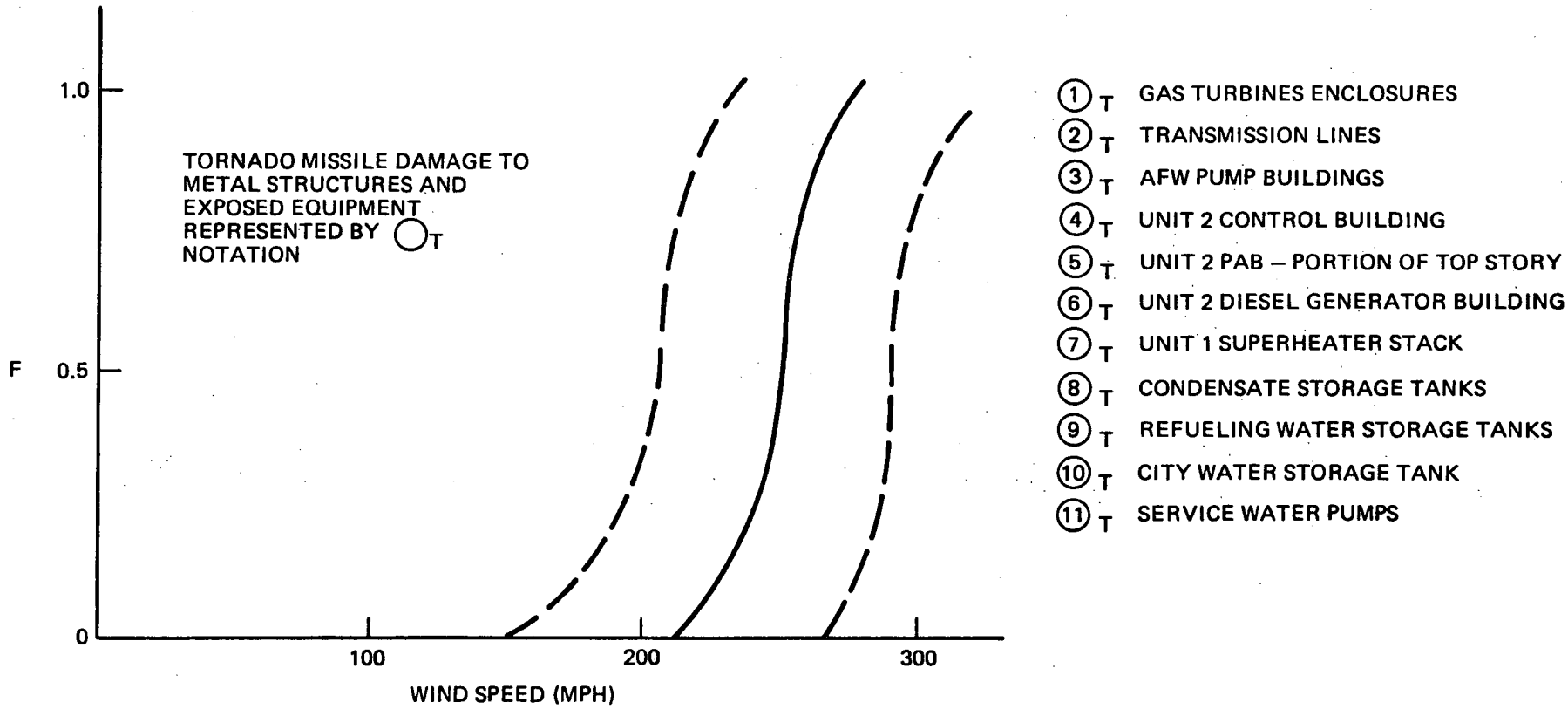


Figure 7.5-3. Structure Tornado Missile Capacities

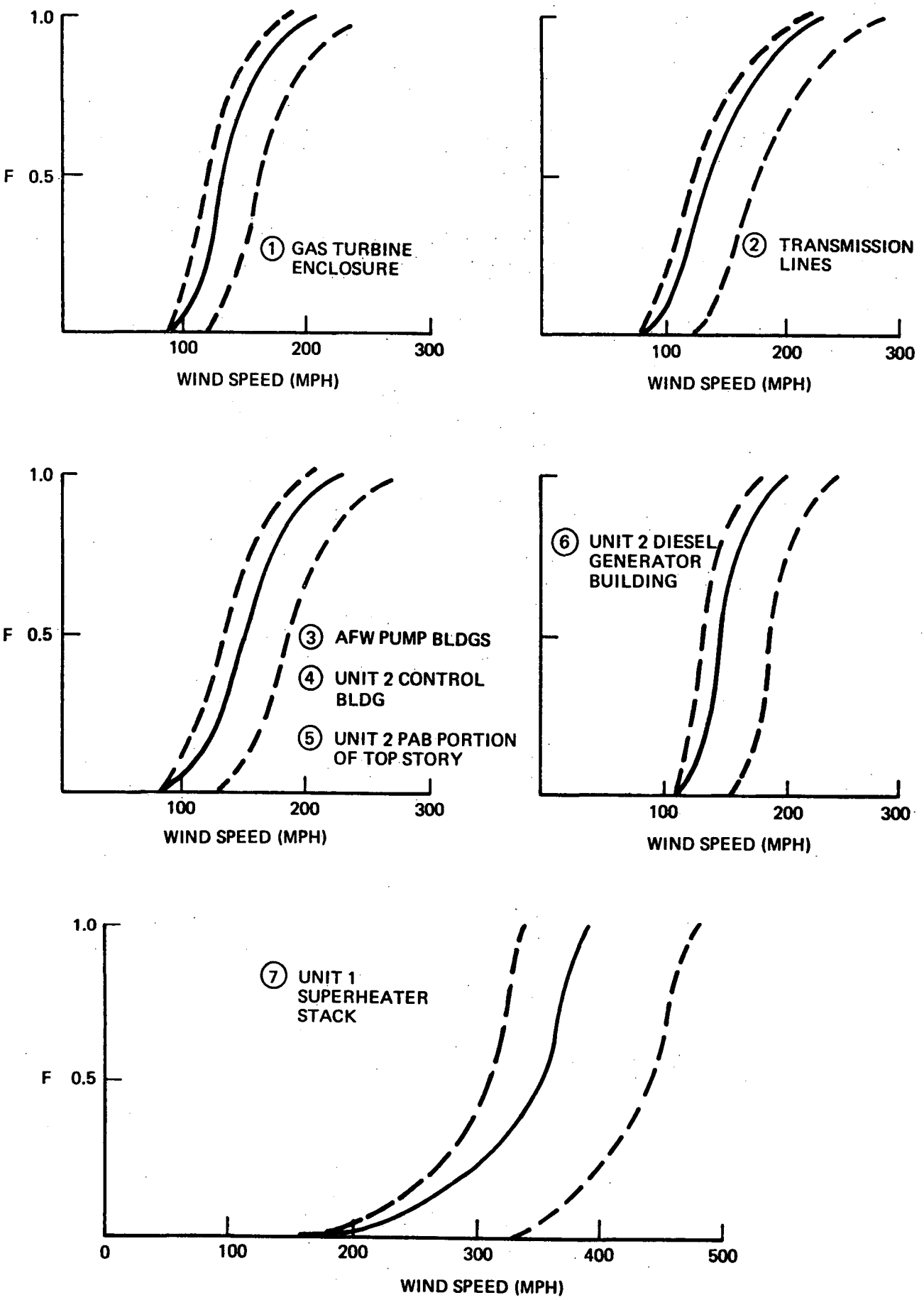


Figure 7.5-4. Structure Hurricane and Extra-Tropical Cyclone Wind Capacities

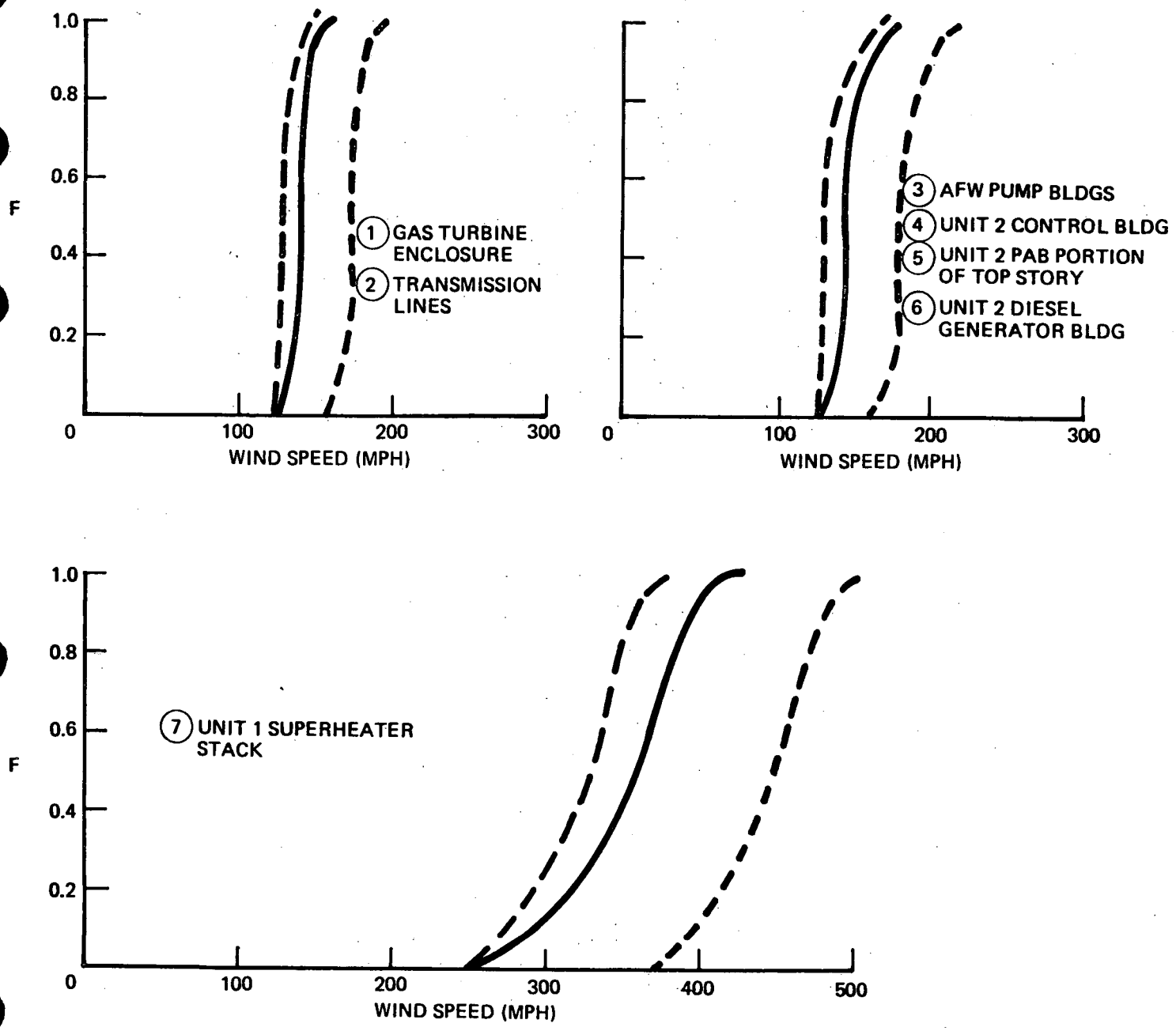
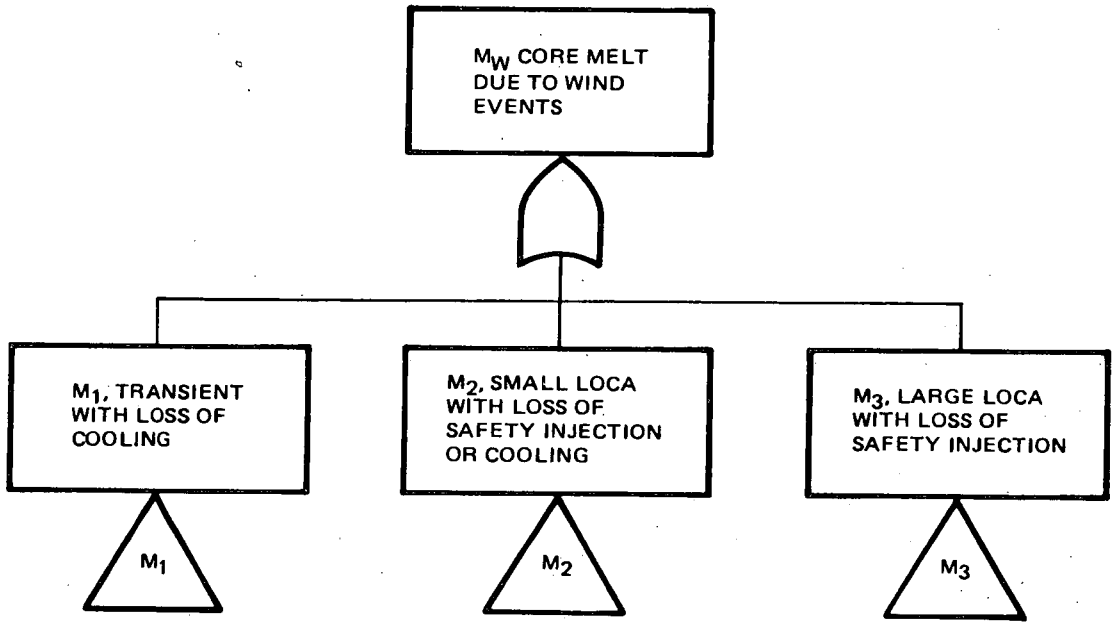


Figure 7.5-5. Structure Tornado Wind Capacities



NOTES:

1. SYMBOLS IN TRIANGLES △ REFER TO LATER FAULT TREE DEVELOPMENT.

Figure 7.5-6a. Indian Point Unit 2 Wind and Tornado Missile Core Melt Fault Tree

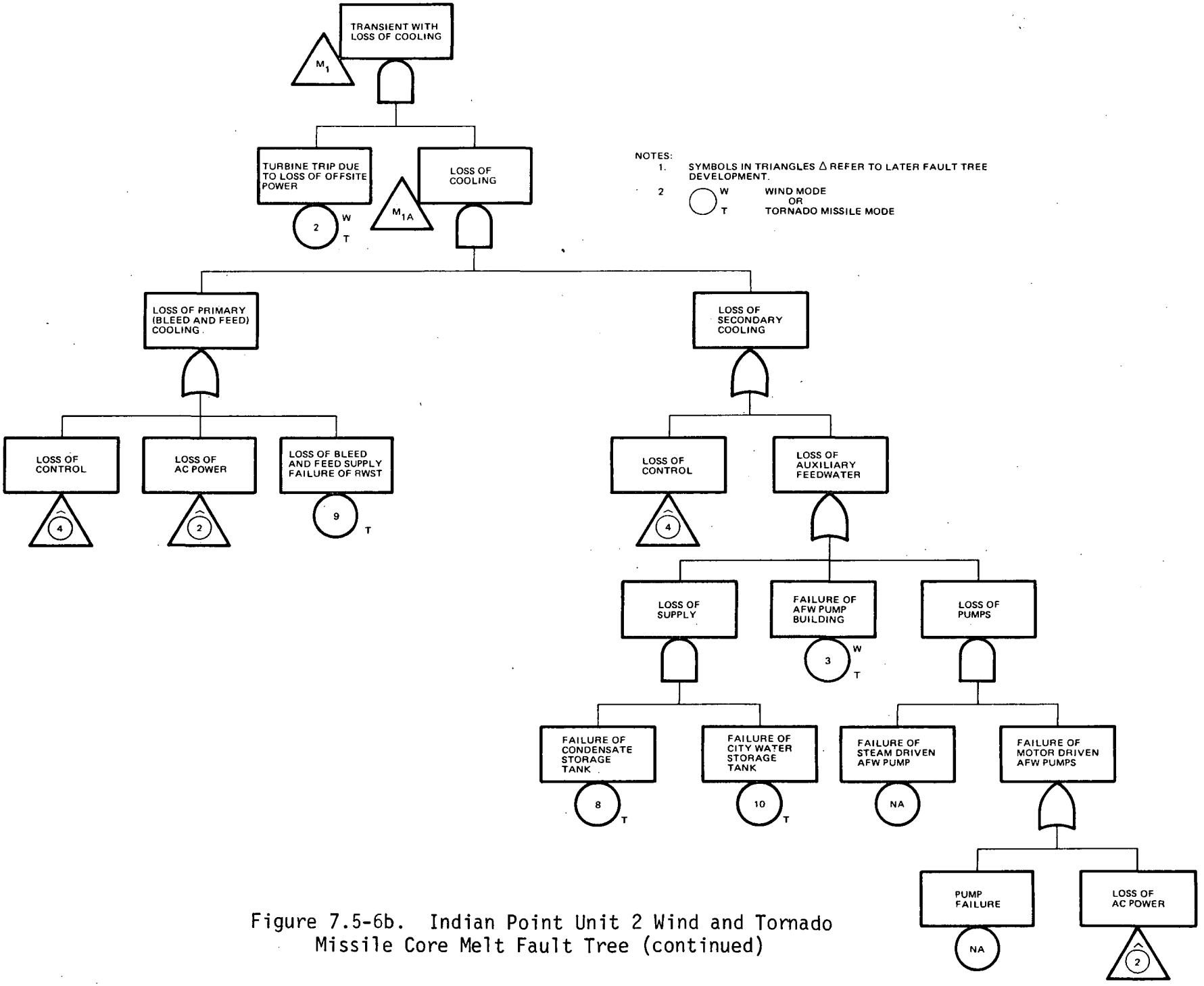


Figure 7.5-6b. Indian Point Unit 2 Wind and Tornado Missile Core Melt Fault Tree (continued)

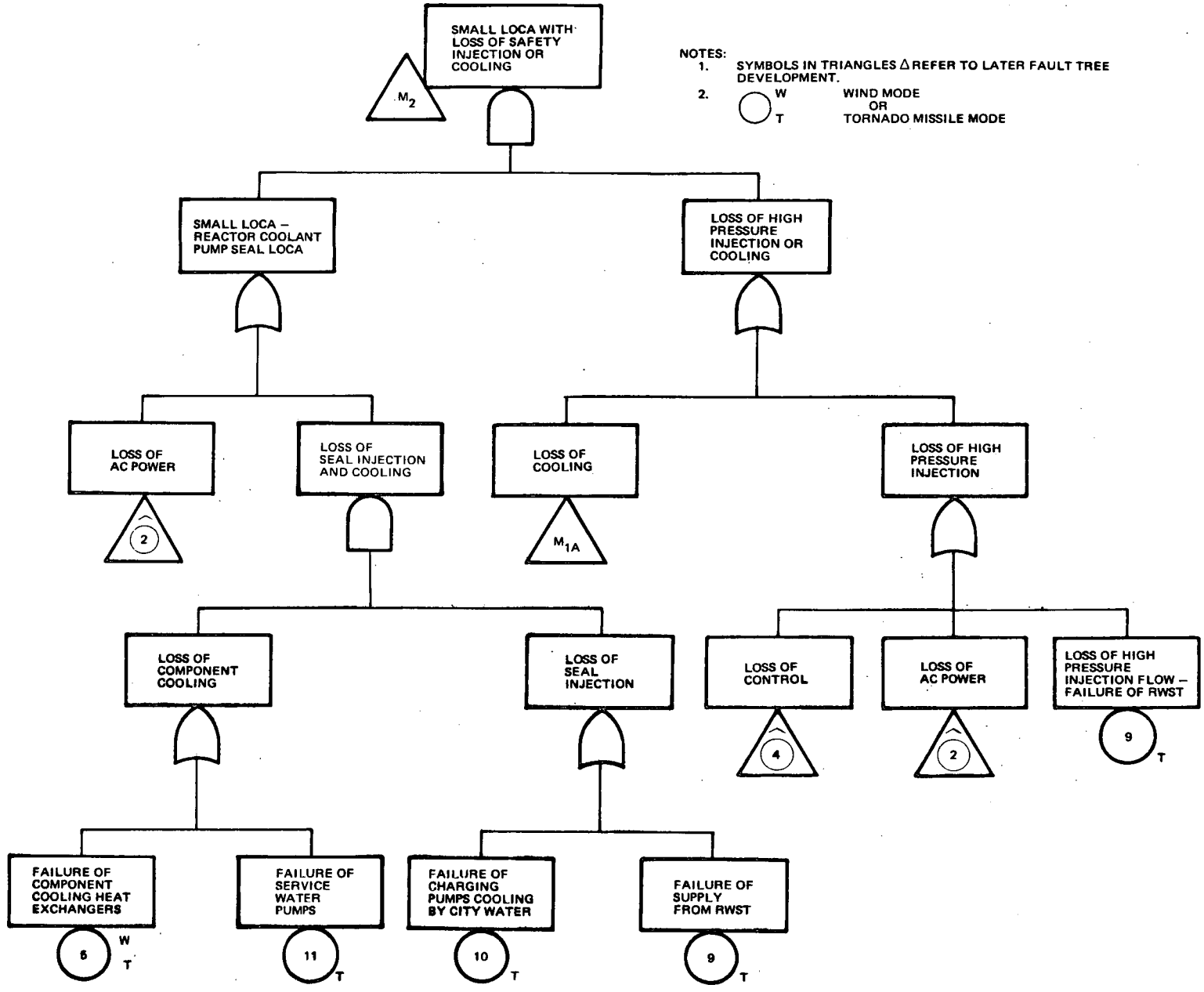
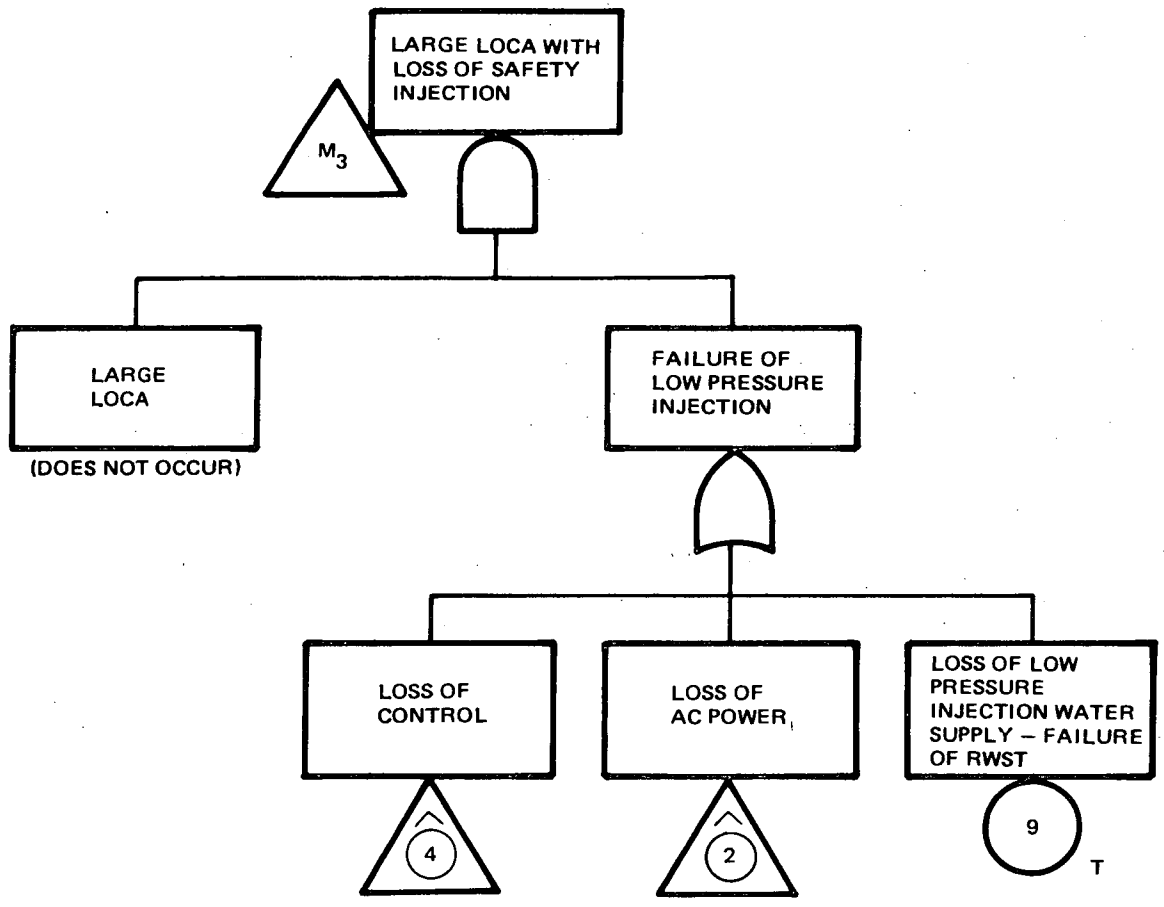


Figure 7.5-6c. Indian Point Unit 2 Wind and Tornado Missile Core Melt Fault Tree (continued)



NOTES:

1. SYMBOLS IN TRIANGLES △ REFER TO LATER FAULT TREE DEVELOPMENT.
2. W / T — WIND MODE OR TORNADO MISSILE MODE

Figure 7.5-6d. Indian Point Unit 2 Wind and Tornado Missile Core Melt Fault Tree (continued)

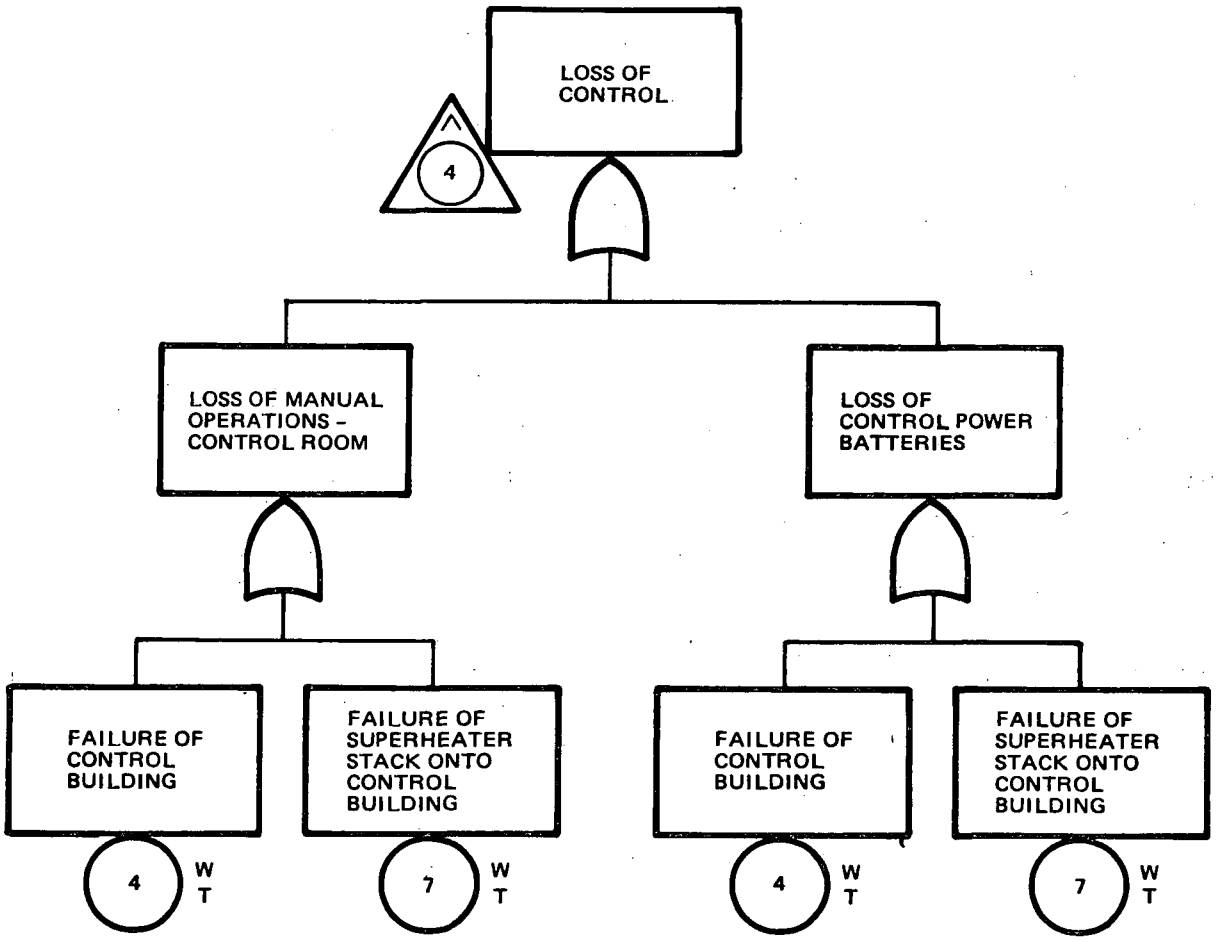


Figure 7.5-6e. Indian Point Unit 2 Wind and Tornado Missile Core Melt Fault Tree (continued)

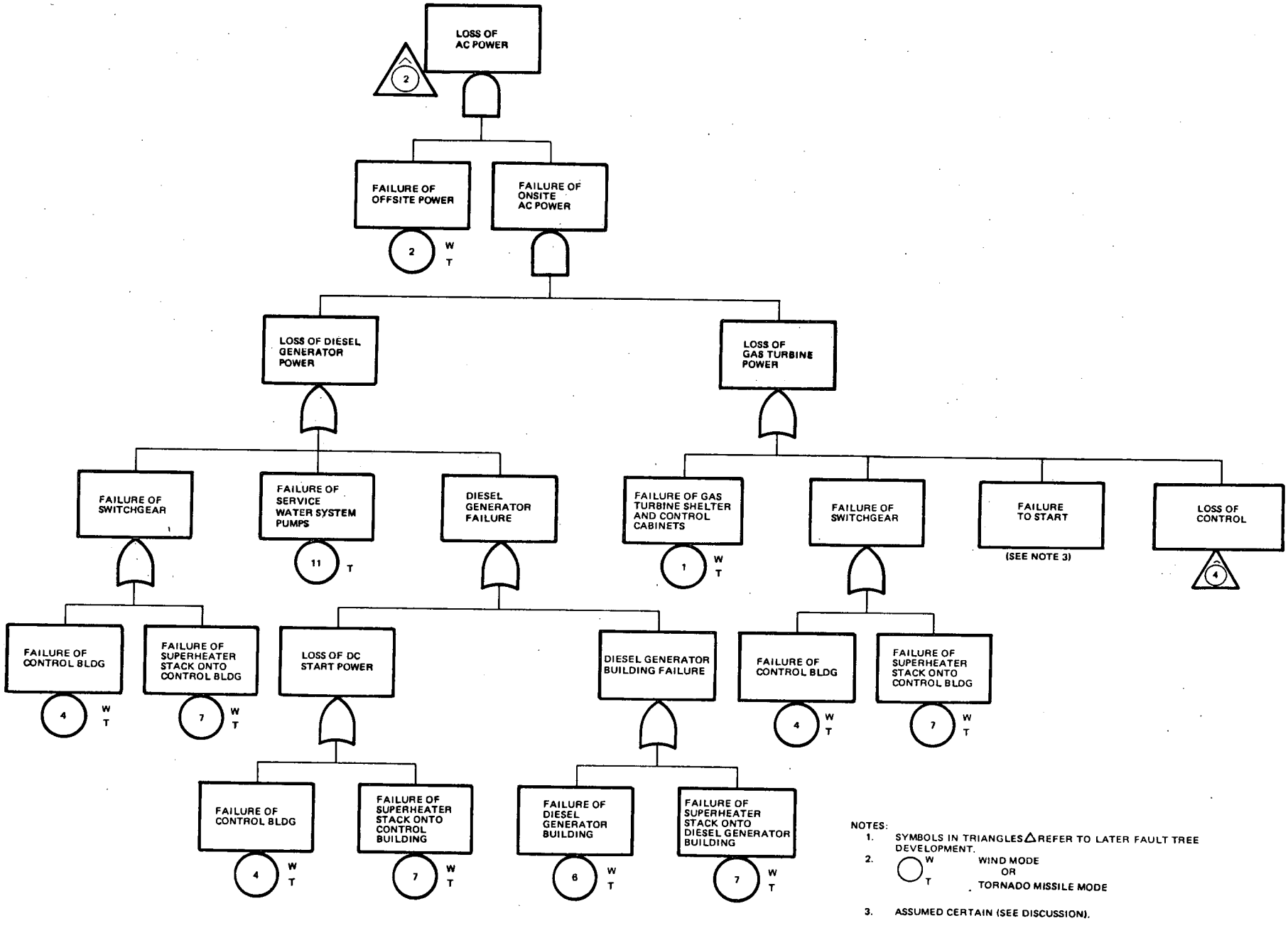


Figure 7.5-6f. Indian Point Unit 2 Wind and Tornado Missile Core Melt Fault Tree (continued)

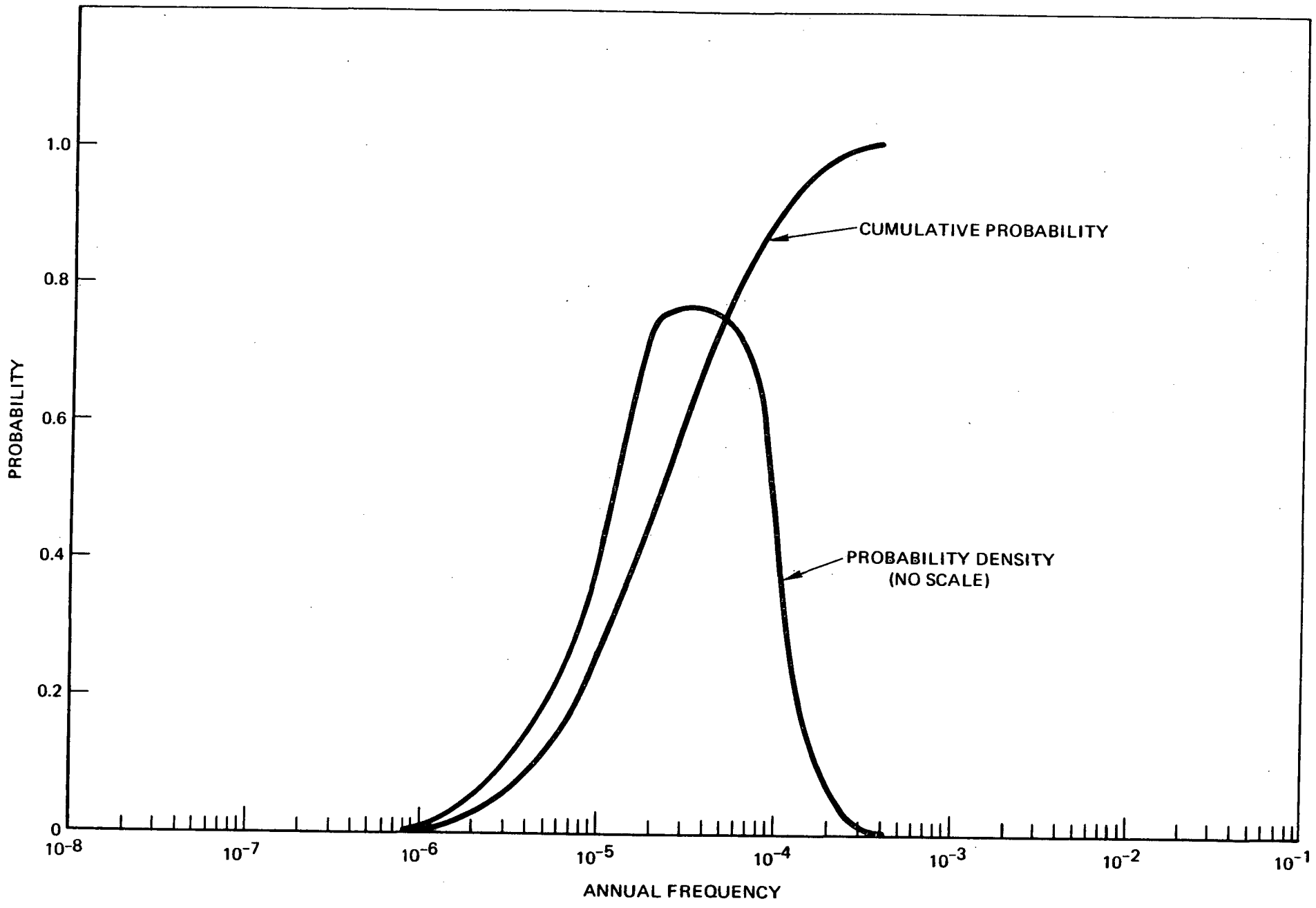
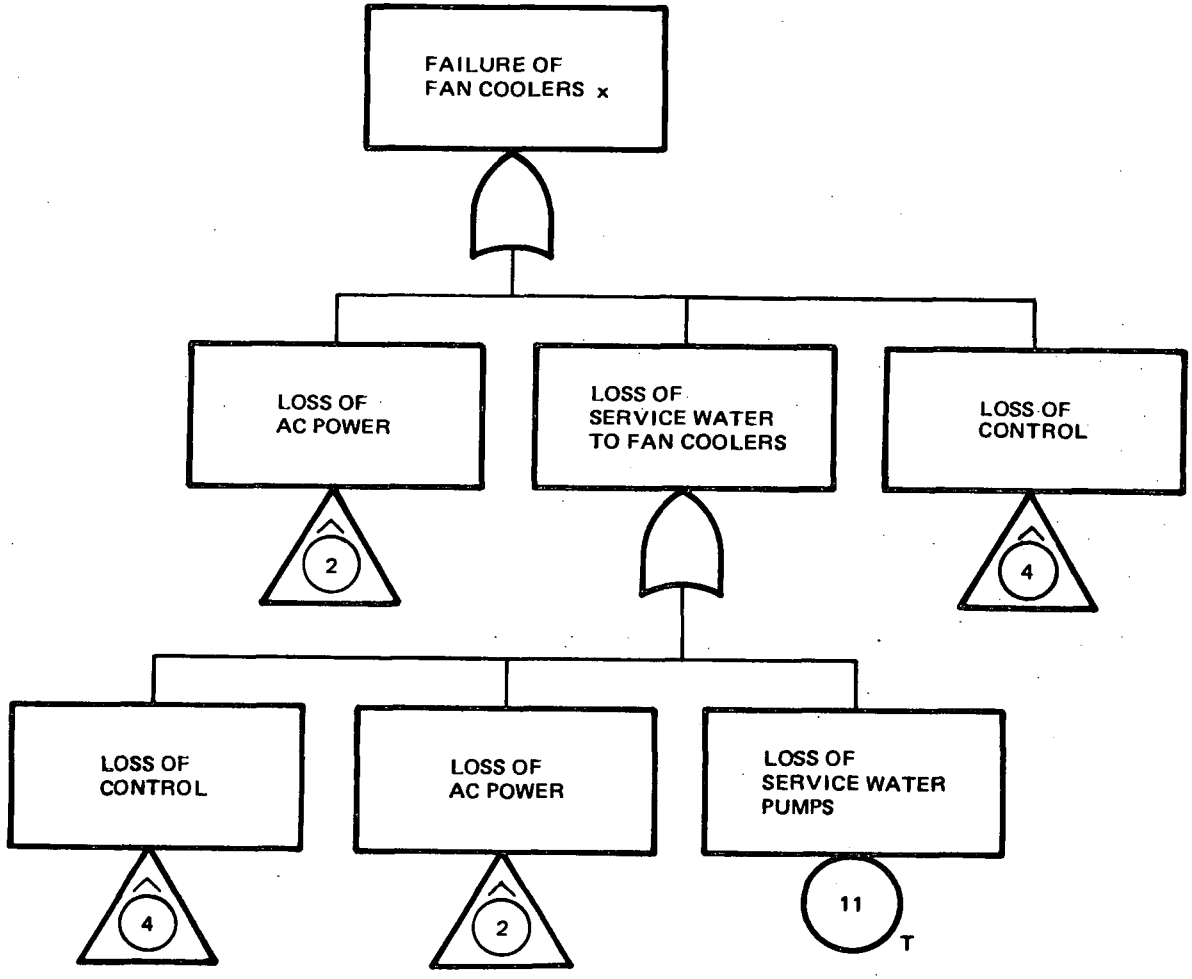


Figure 7.5-7. Core Melt Frequency from Wind Events - Indian Point 2



NOTES:

1. SYMBOLS IN TRIANGLES △ REFER TO LATER FAULT TREE DEVELOPMENT.
2. ○ W / T — WIND MODE OR TORNADO MISSILE MODE

Figure 7.5-8. Indian Point Unit 2 Wind and Tornado Missile Fault Tree for Failure of Fan Coolers

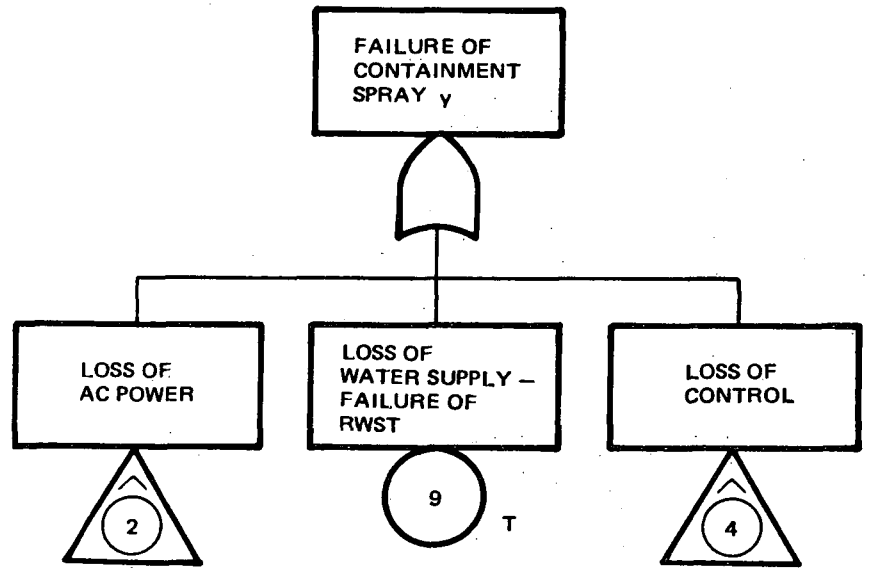


Figure 7.5-9. Indian Point Unit 2 Fault Tree for Wind and Tornado Missile Failure of Containment Spray

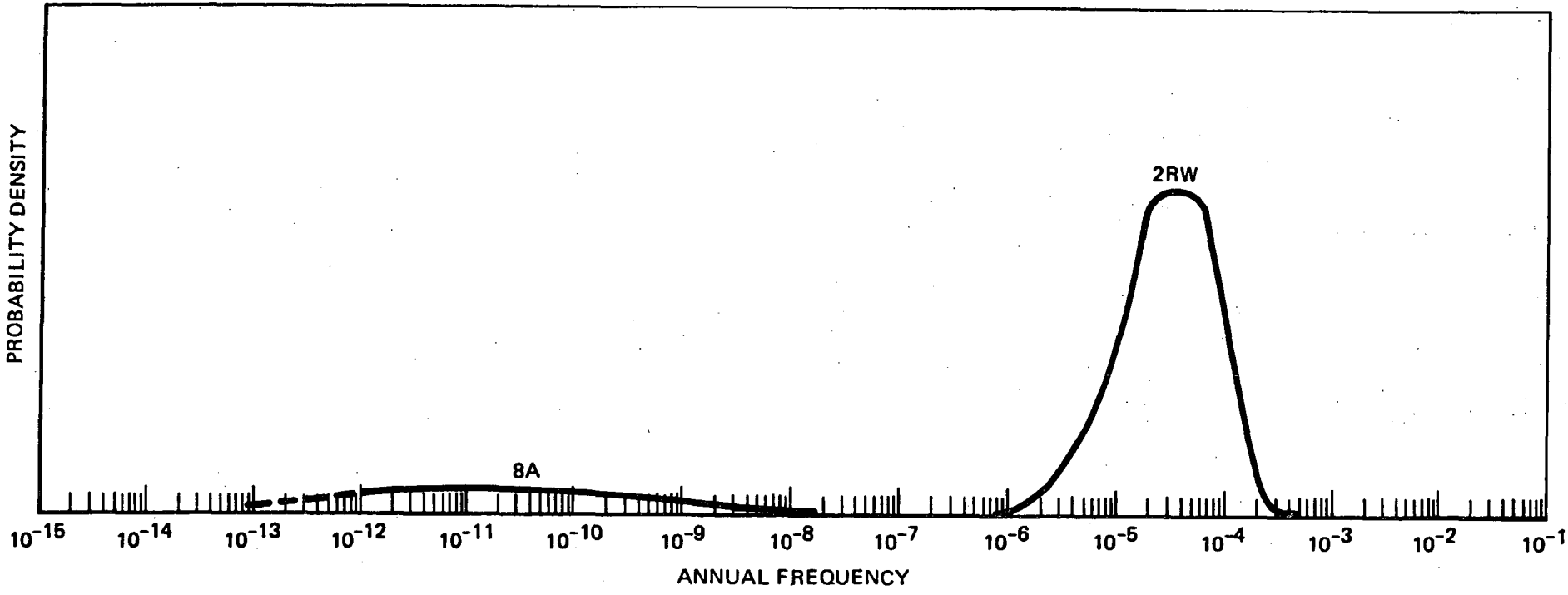
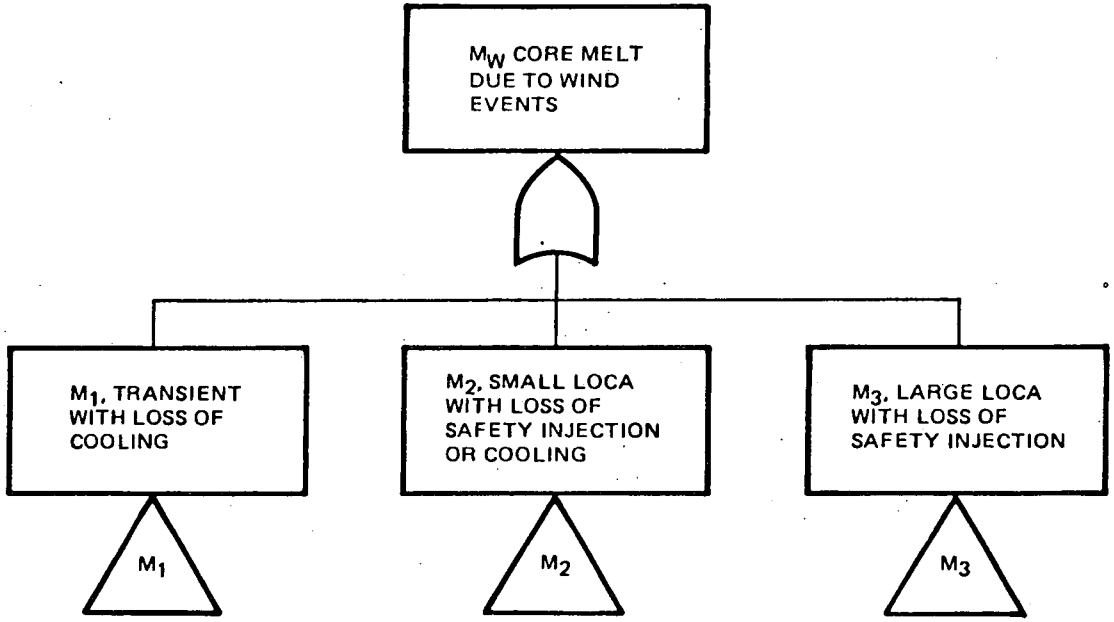


Figure 7.5-10. Release Frequency from Wind Events - Indian Point Unit 2



NOTES:
1. SYMBOLS IN TRIANGLES △ REFER TO LATER FAULT TREE DEVELOPMENT.

Figure 7.5-11a. Indian Point Unit 3 Wind and Tornado Missile Core Melt Fault Tree

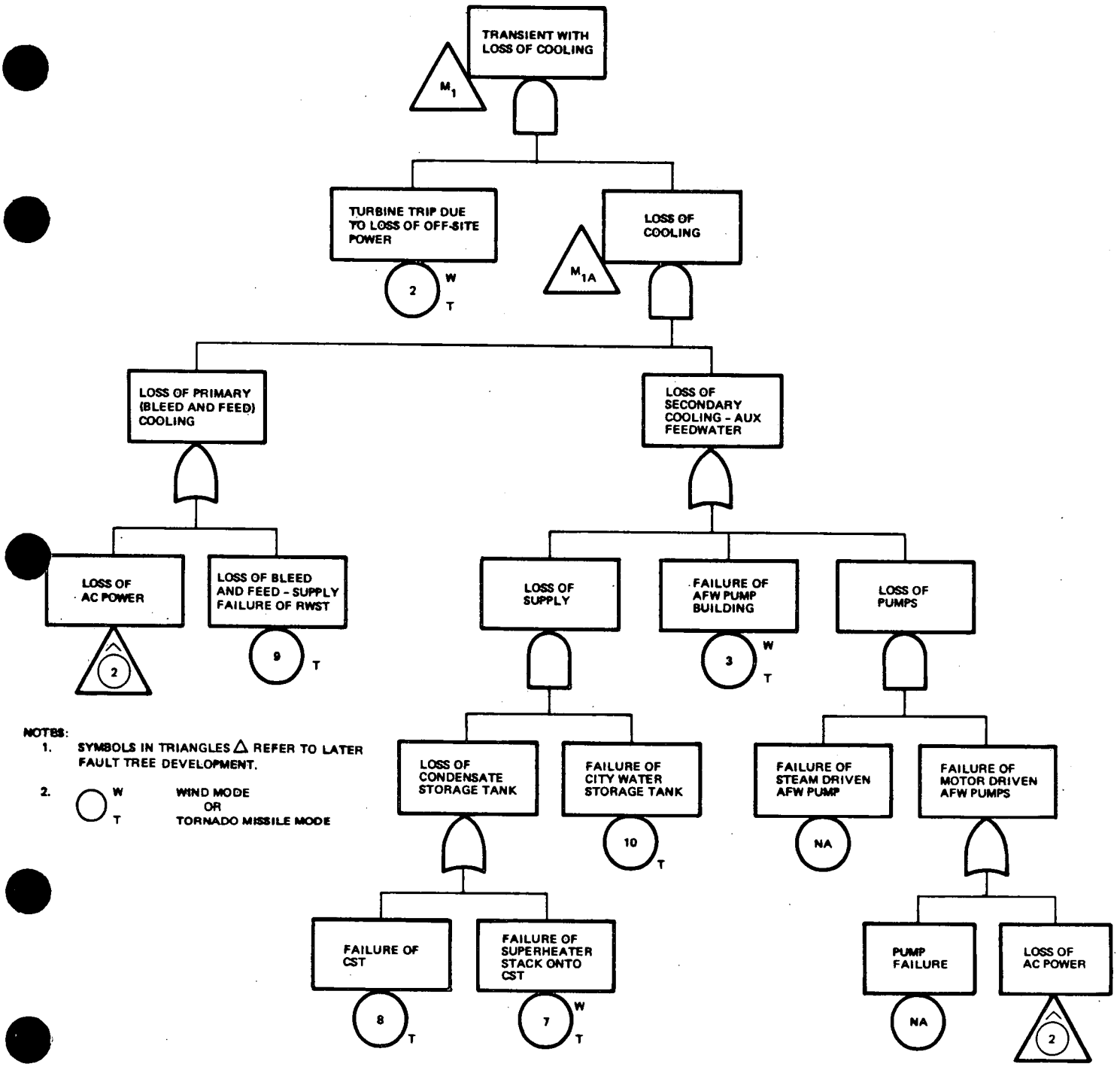


Figure 7.5-11b. Indian Point Unit 3 Wind and Tornado Missile Core Melt Fault Tree (continued)

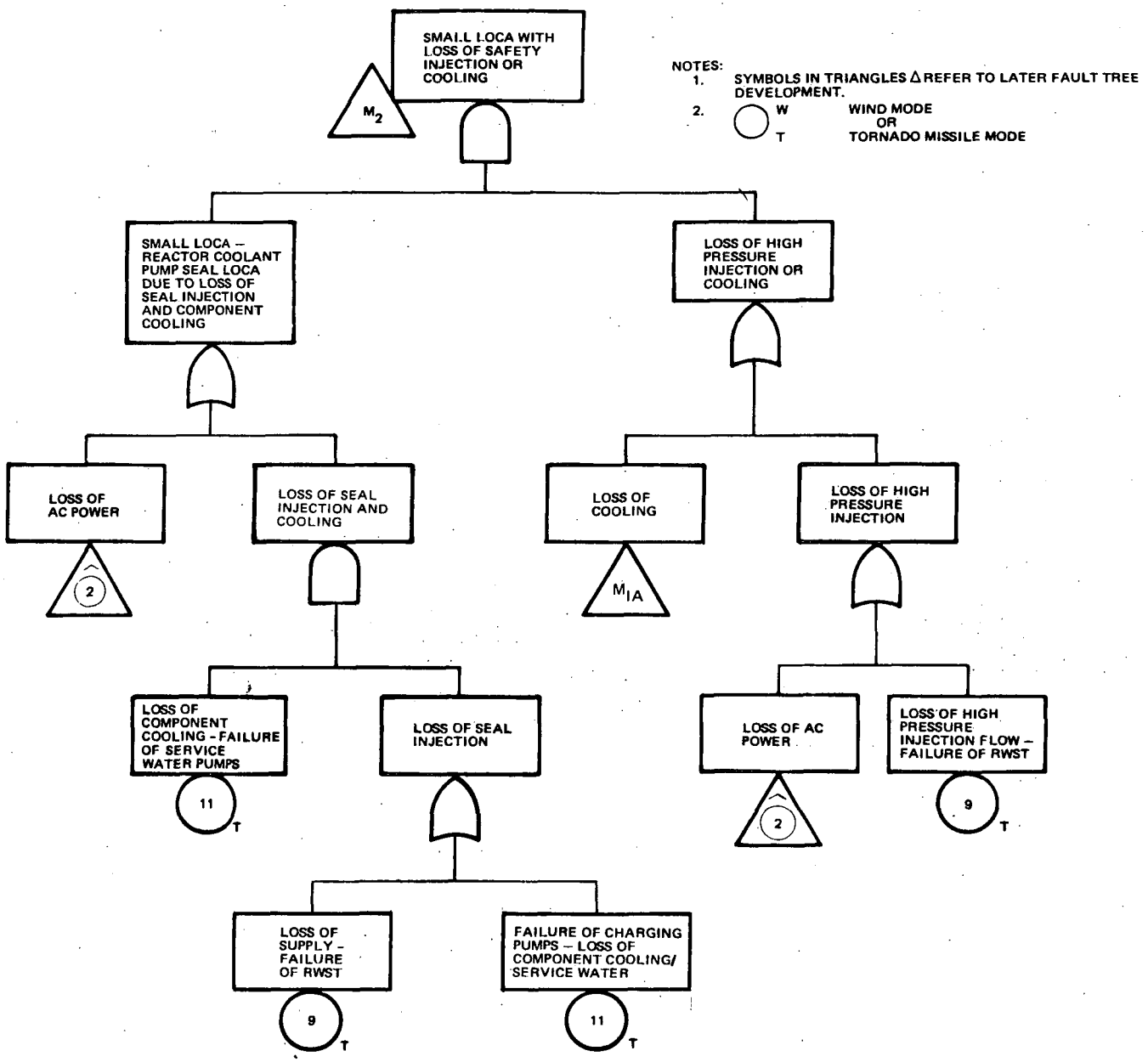
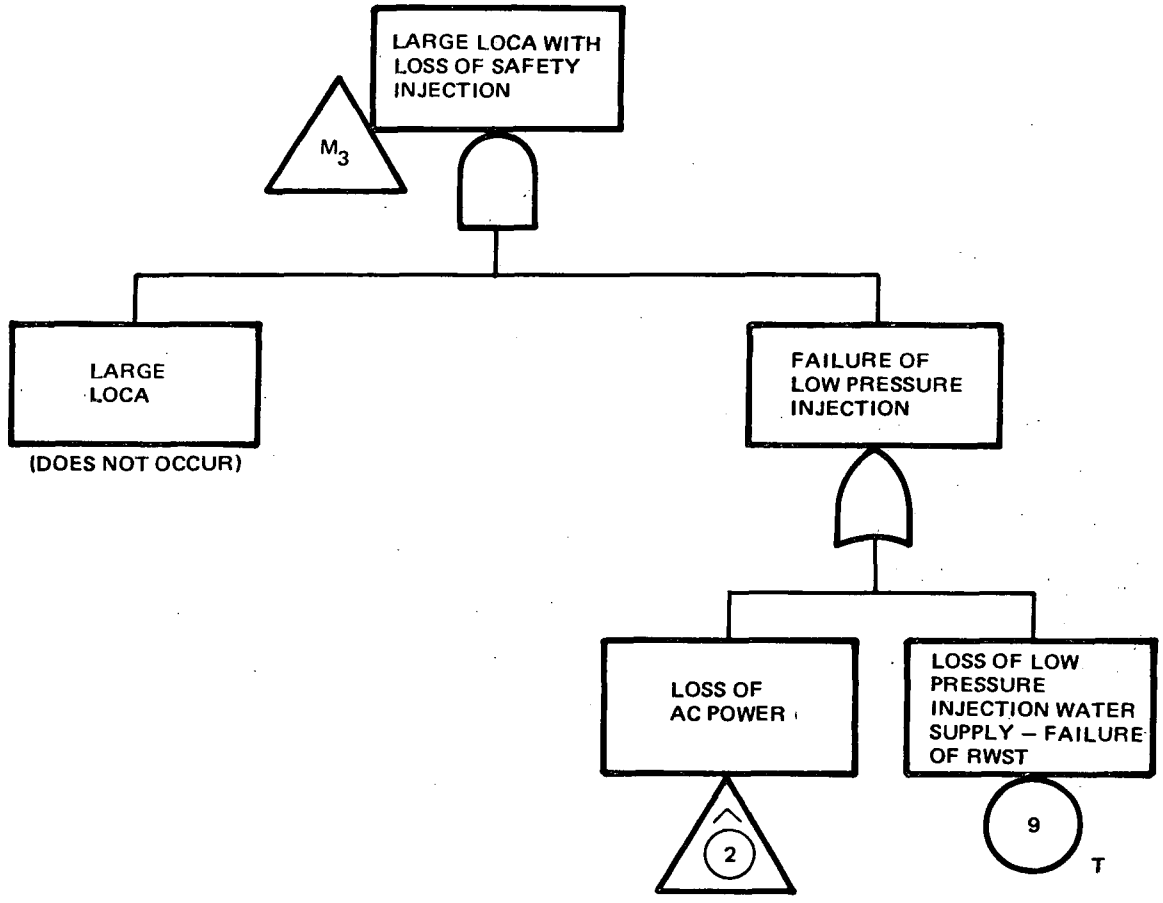


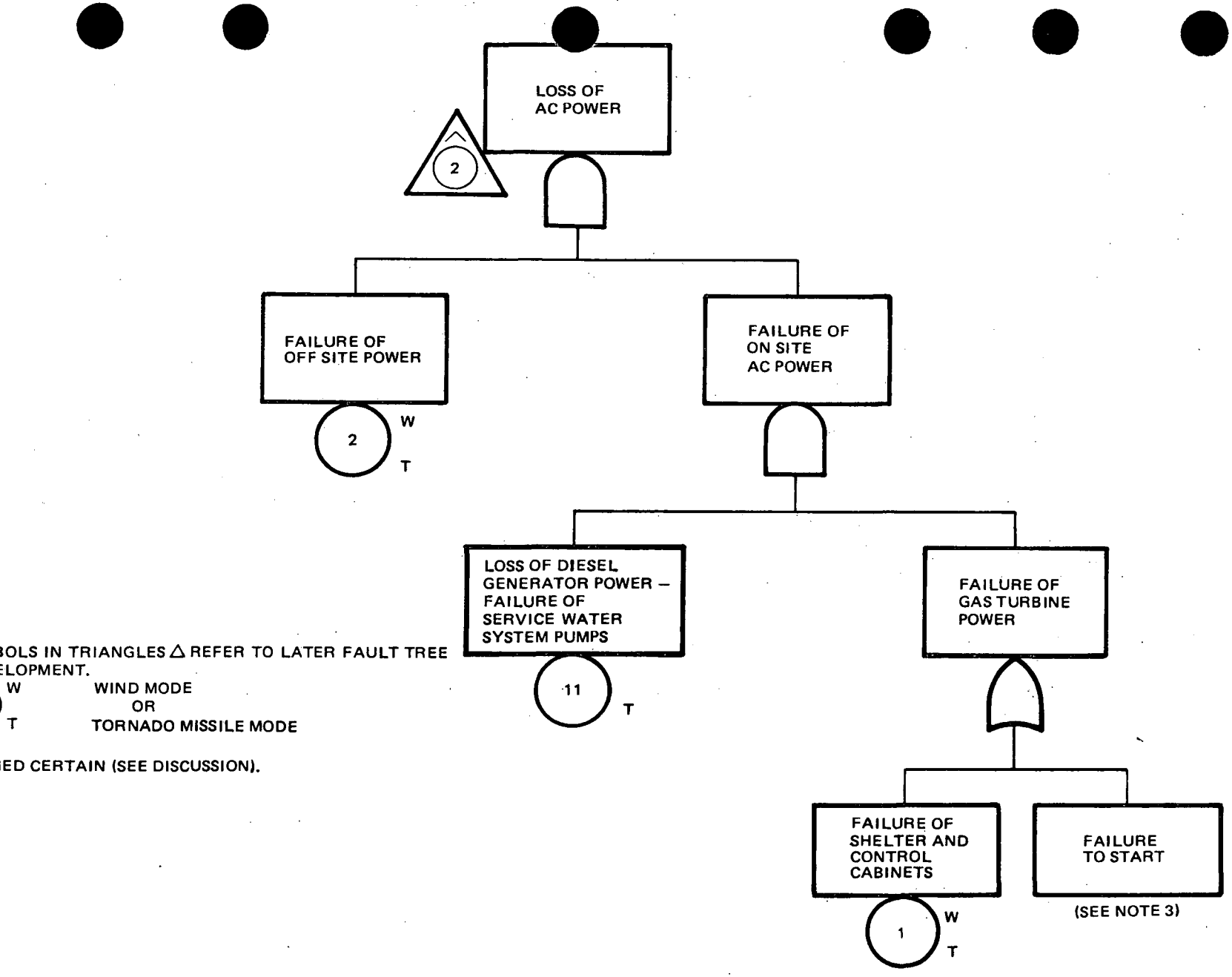
Figure 7.5-11c. Indian Point Unit 3 Wind and Tornado Missile Core Melt Fault Tree (continued)



NOTES:

1. SYMBOLS IN TRIANGLES △ REFER TO LATER FAULT TREE DEVELOPMENT.
2. W, T — WIND MODE OR TORNADO MISSILE MODE

Figure 7.5-11d. Indian Point Unit 3 Wind and Tornado Missile Core Melt Fault Tree (continued)



NOTES:

1. SYMBOLS IN TRIANGLES △ REFER TO LATER FAULT TREE DEVELOPMENT.
2. W / T — WIND MODE OR TORNADO MISSILE MODE
3. ASSUMED CERTAIN (SEE DISCUSSION).

Figure 7.5-11e. Indian Point Unit 3 Wind and Tornado Missile Core Melt Fault Tree (continued)

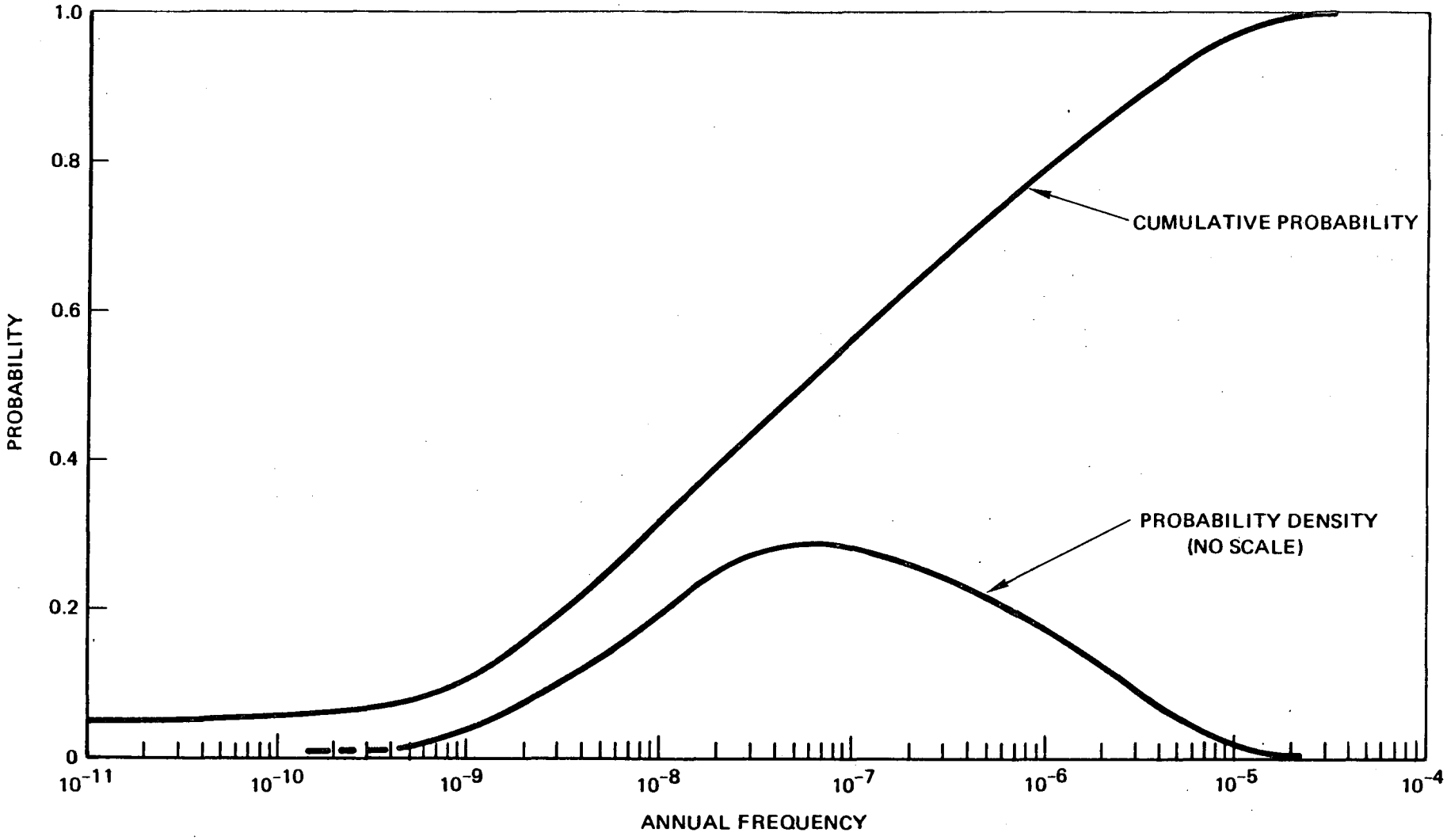
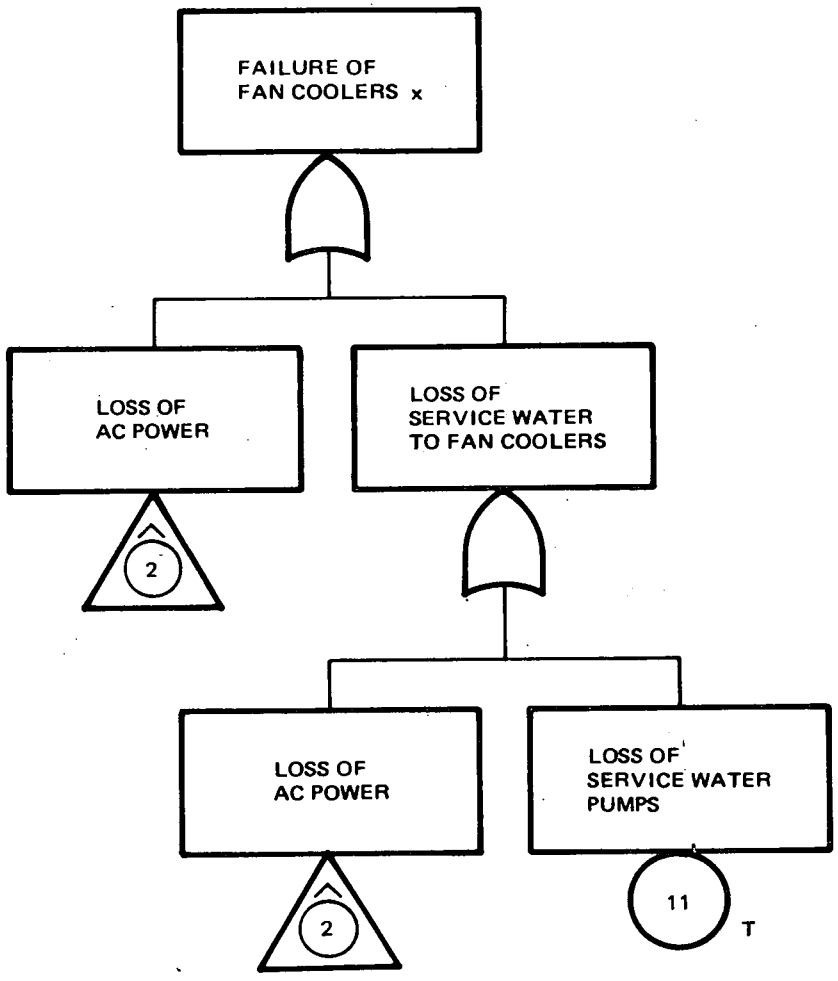


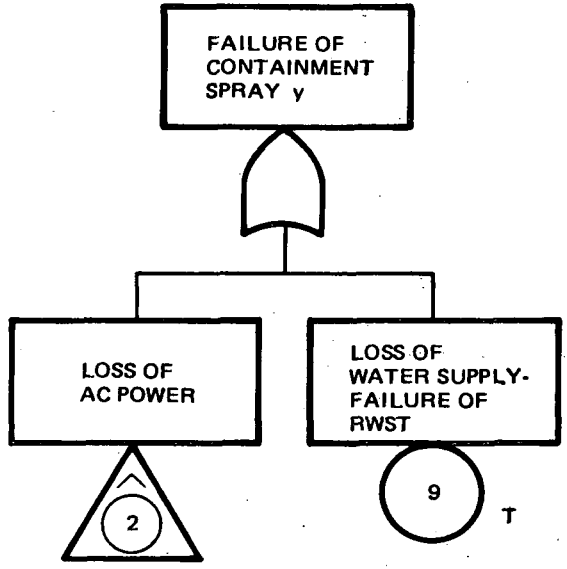
Figure 7.5-12. Core Melt Frequency from Wind Events - Indian Point Unit 3



NOTES:

1. SYMBOLS IN TRIANGLES △ REFER TO LATER FAULT TREE DEVELOPMENT.
2. W / T — WIND MODE OR TORNADO MISSILE MODE

Figure 7.5-13. Indian Point Unit 3 Wind and Tornado Missile Fault Tree for Failure of Fan Coolers



NOTES:

1. SYMBOLS IN TRIANGLES △ REFER TO LATER FAULT TREE DEVELOPMENT.
2. ◯ W — WIND MODE
   OR
   T — TORNADO MISSILE MODE

Figure 7.5-14. Indian Point Unit 3 Fault Tree for Wind and Tornado Missiles Failure of Containment Spray

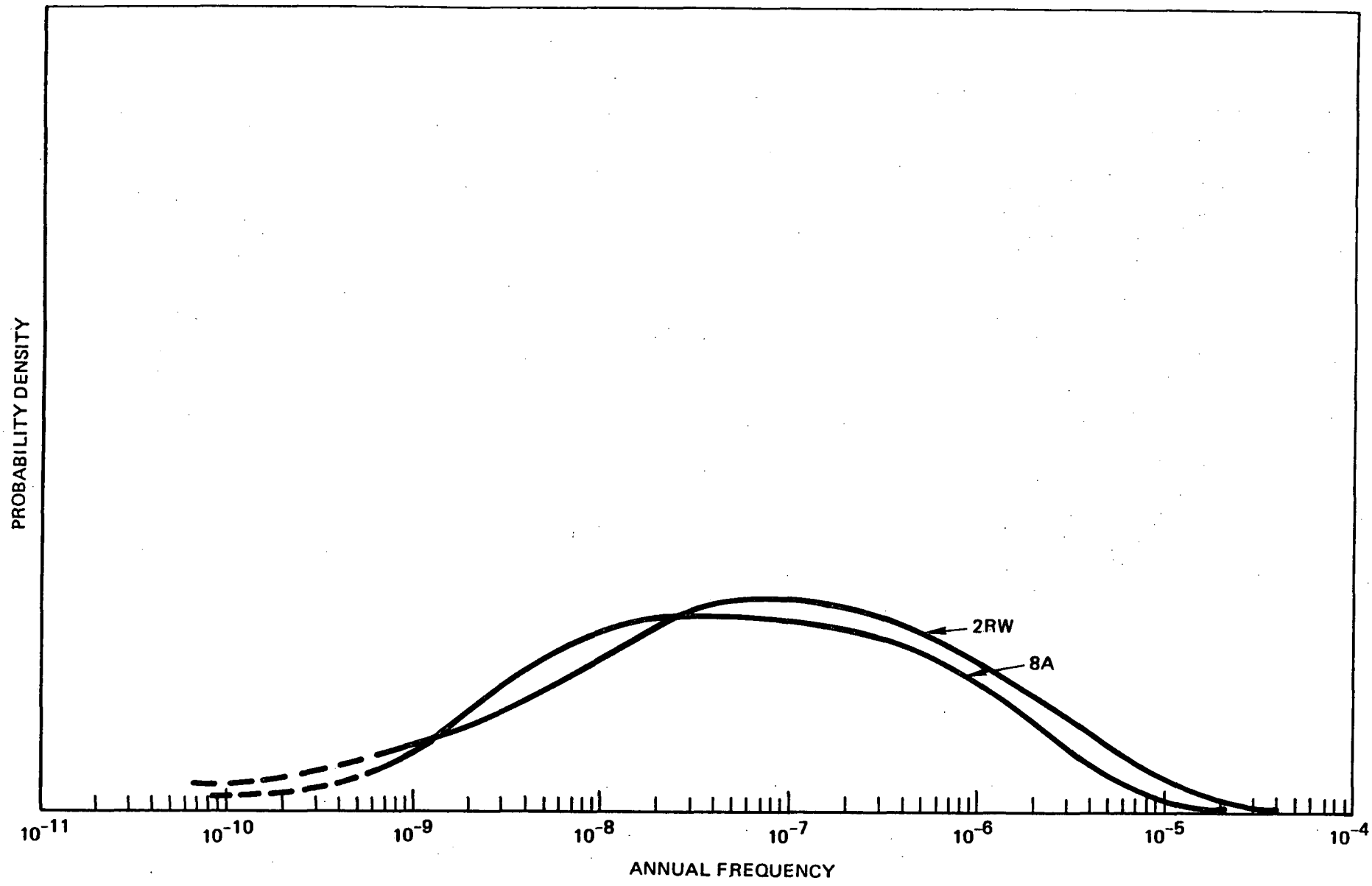


Figure 7.5-15. Release Frequency from Wind Events - Indian Point Unit 3

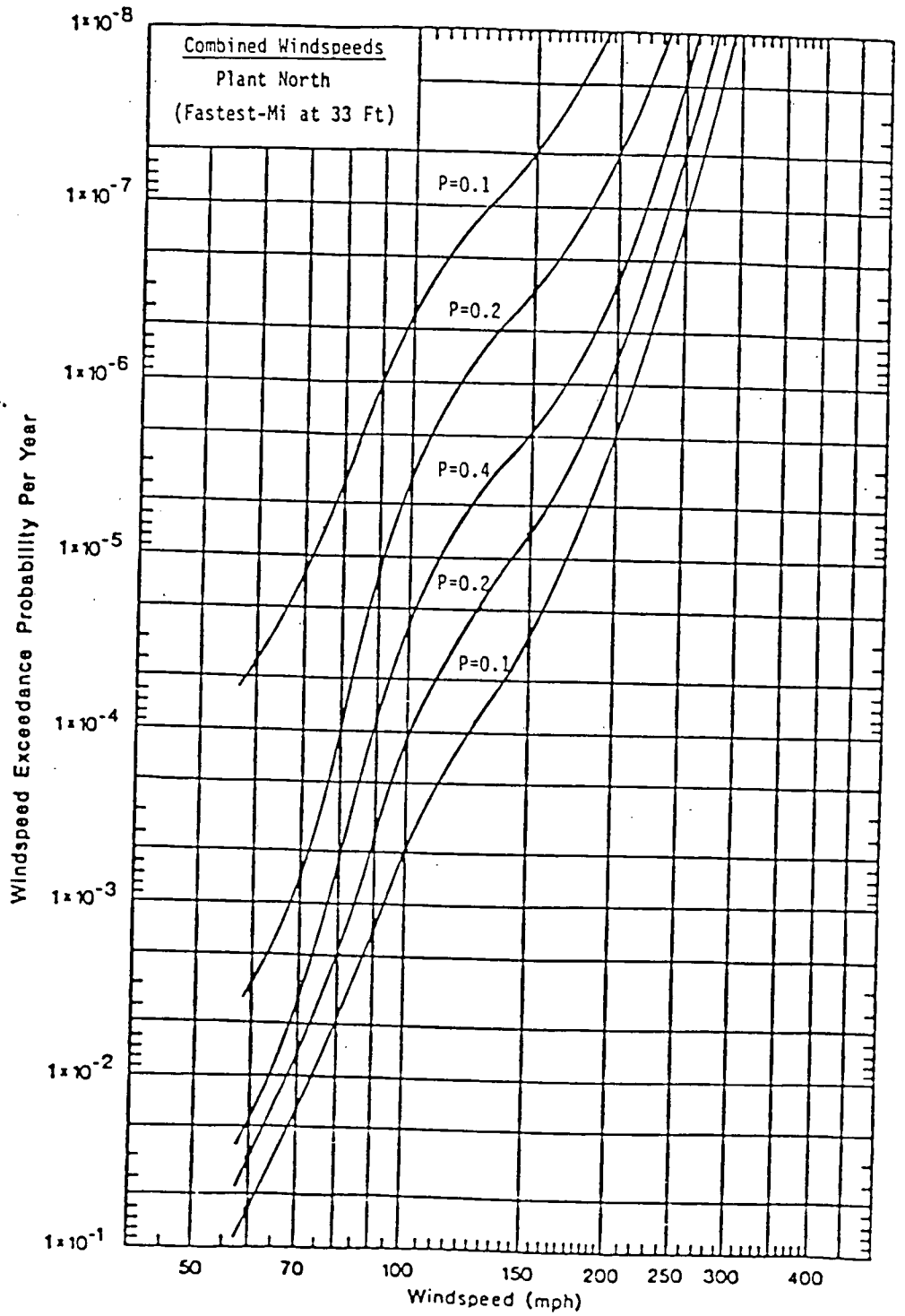


Figure 7.5-16. Plant North Combined Windspeed Exceedance Probabilities

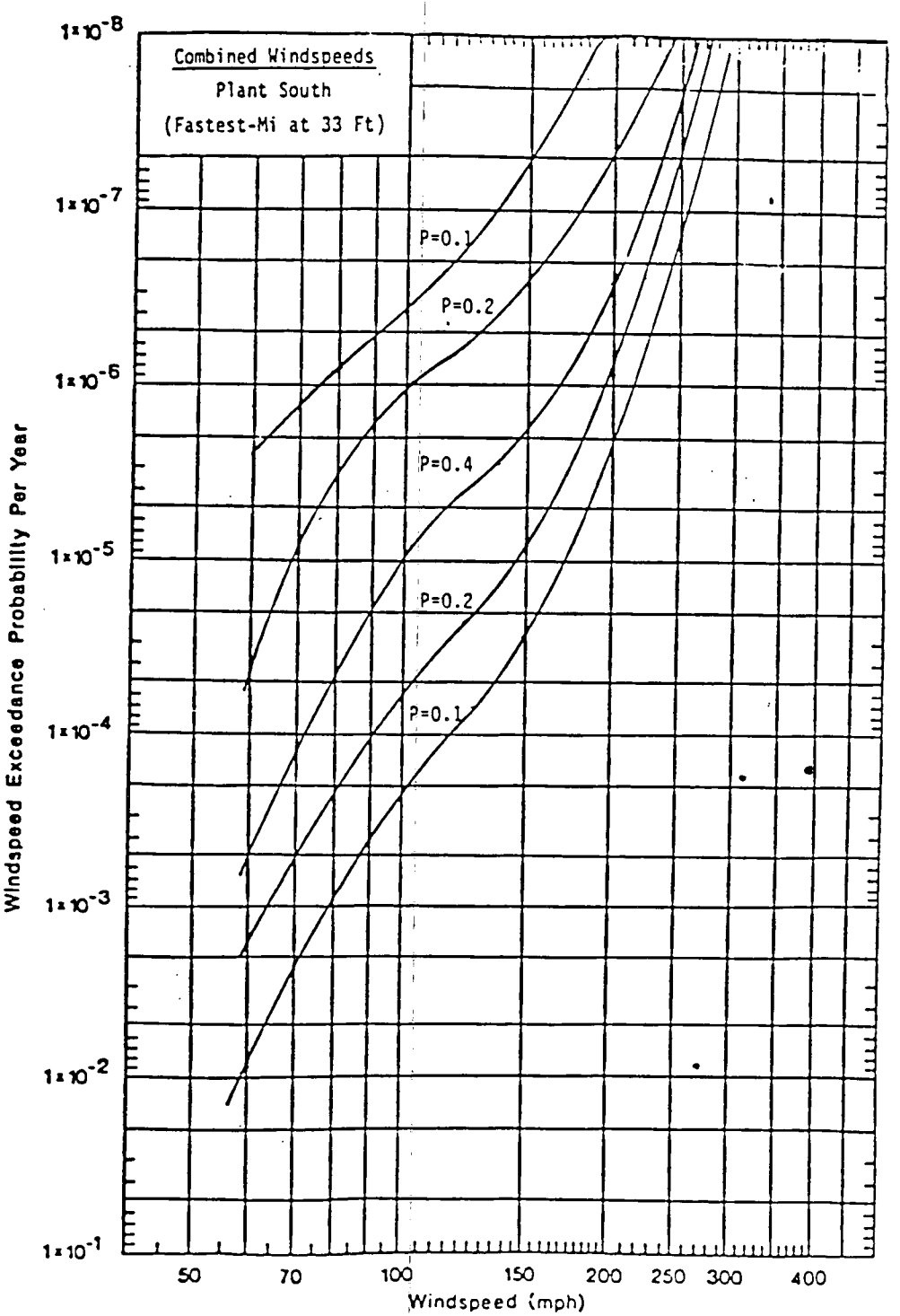


Figure 7.5-17. Plant South Combined Windspeed Exceedance Probabilities

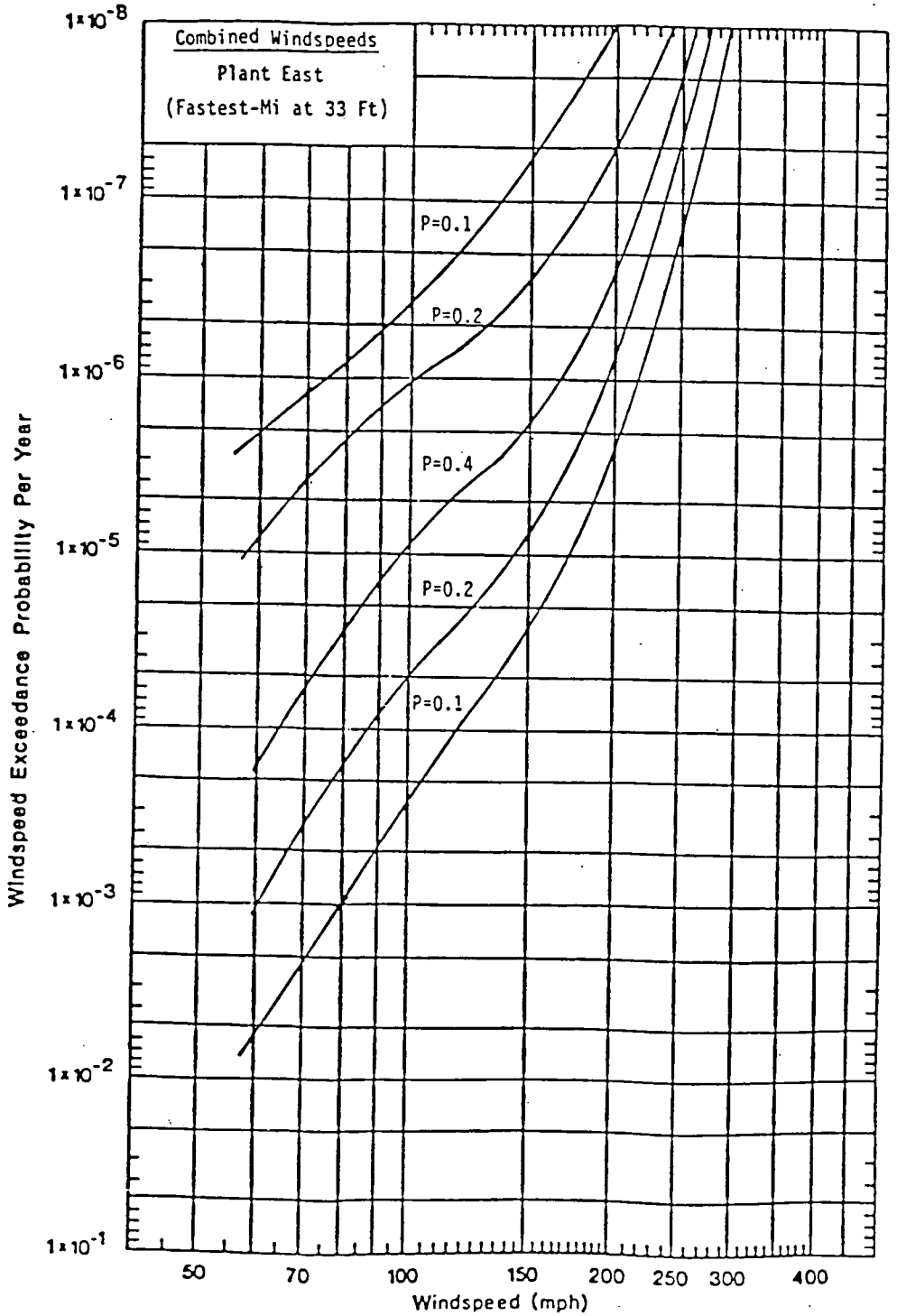


Figure 7.5-18. Plant East Combined Windspeed Exceedance Probabilities

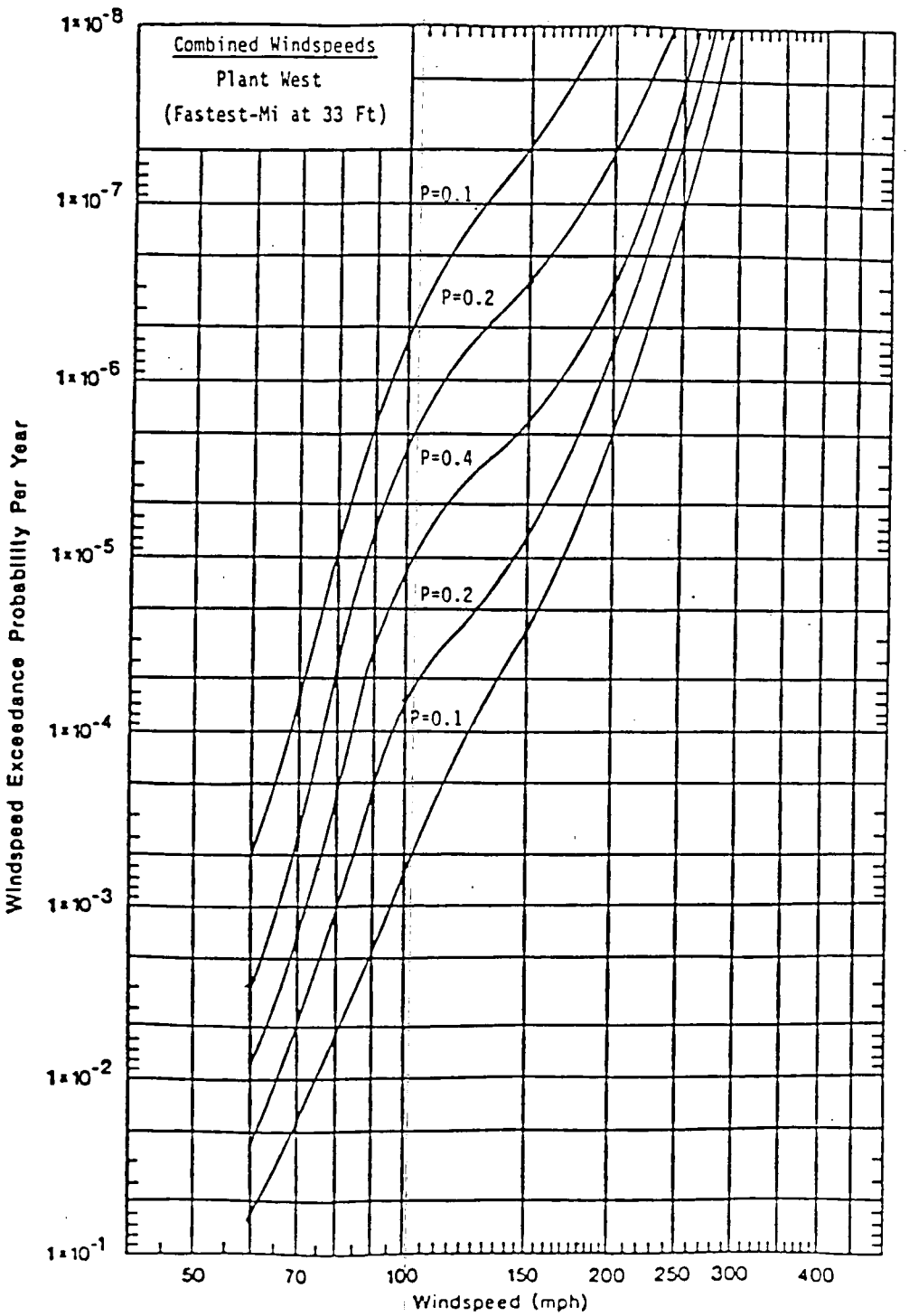


Figure 7.5-19. Plant West Combined Windspeed Exceedance Probabilities

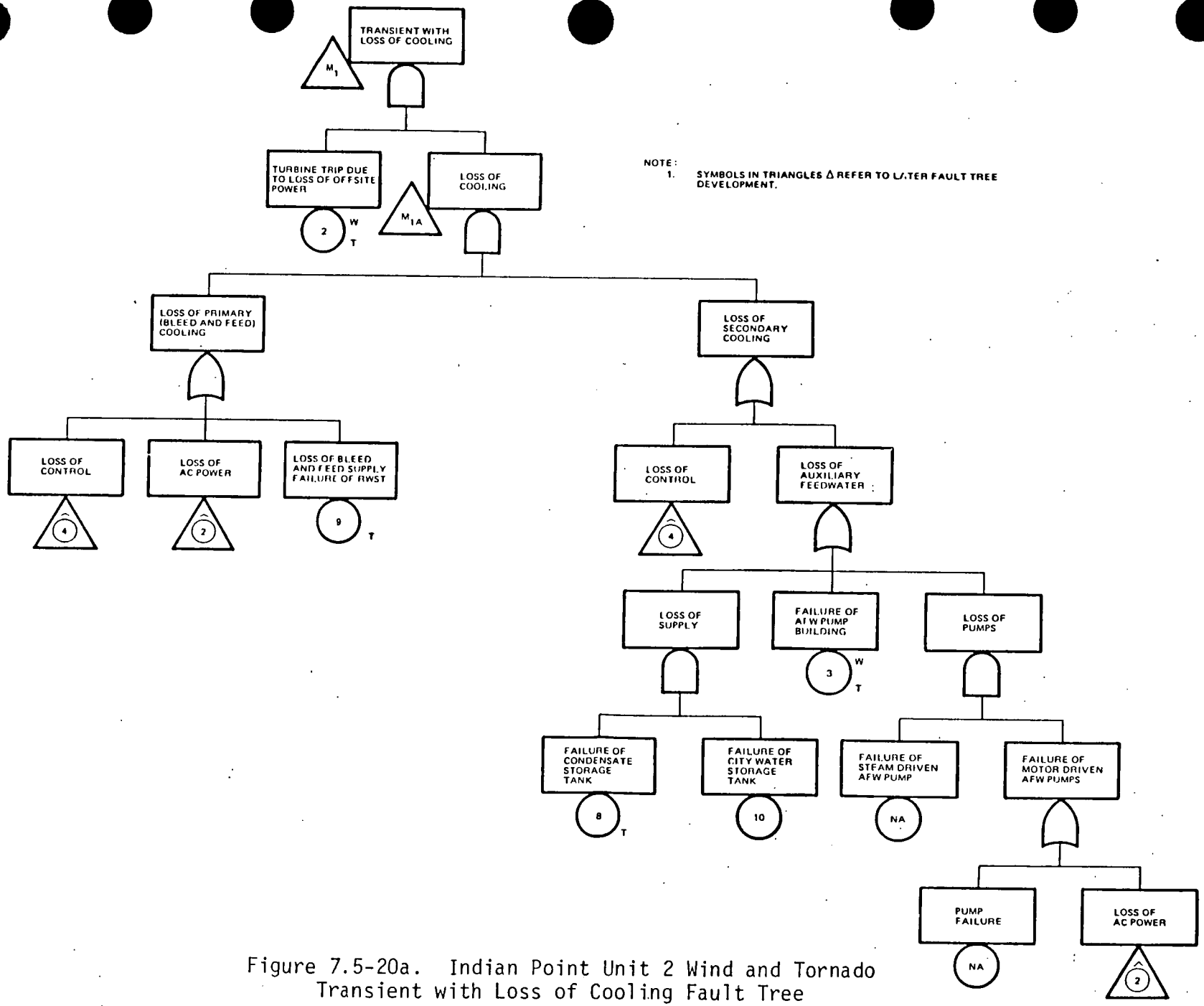


Figure 7.5-20a. Indian Point Unit 2 Wind and Tornado Transient with Loss of Cooling Fault Tree

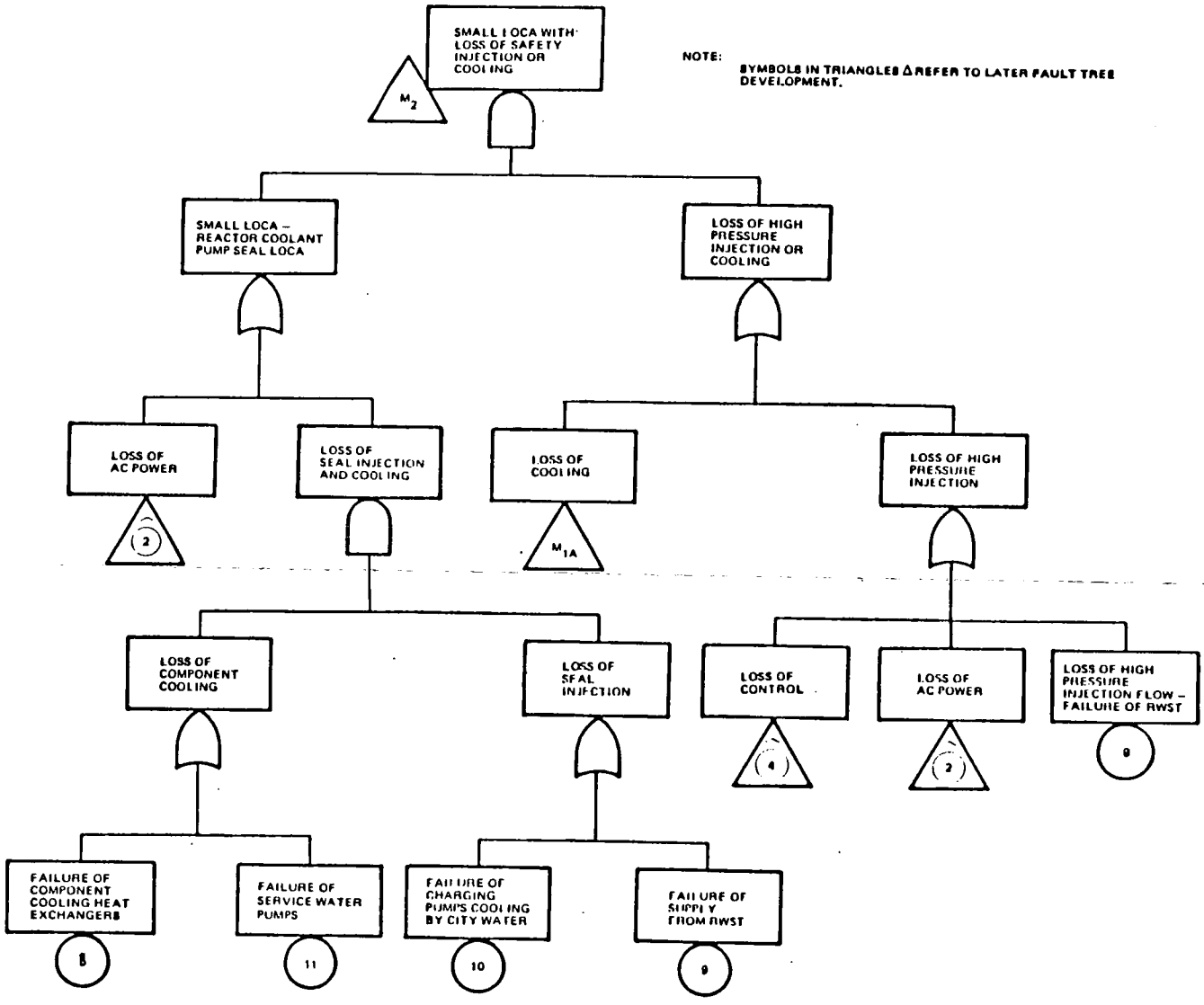


Figure 7.5-20b. Indian Point Unit 2 Wind and Tornado
Small LOCA with Loss of Injection or Cooling

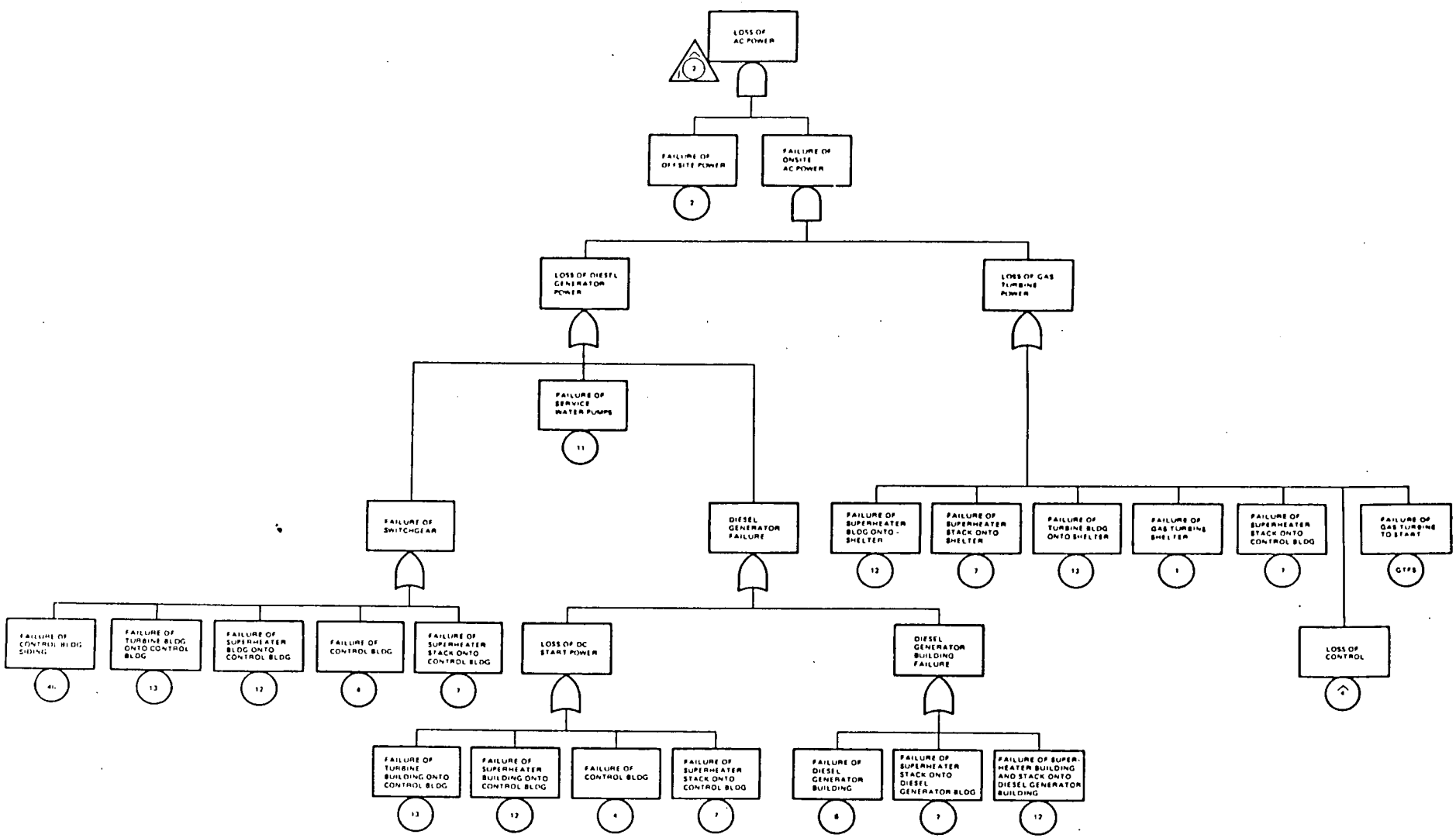


Figure 7.5-20c. Indian Point Unit 2 Wind and Tornado Loss of AC Power

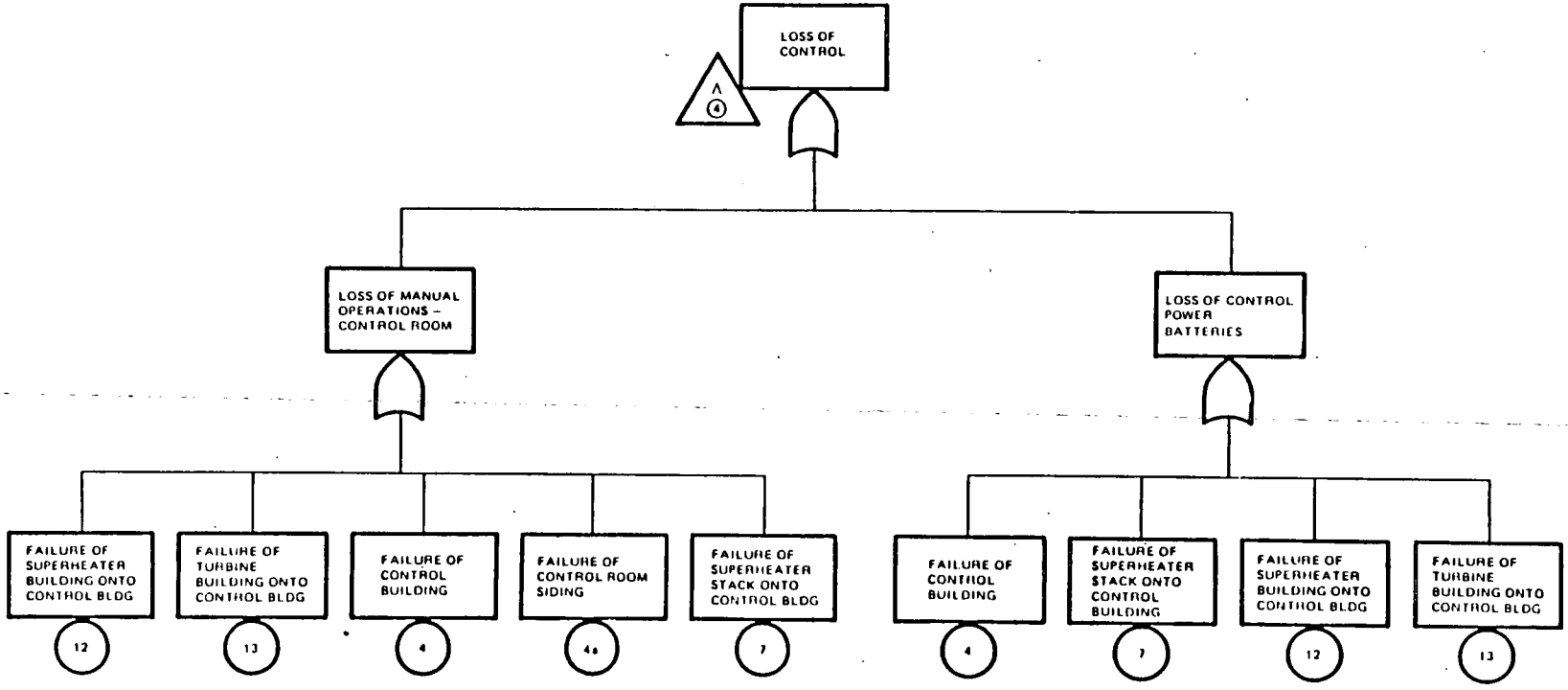


Figure 7.5-20d. Indian Point Unit 2 Wlind and Torando Loss of Control

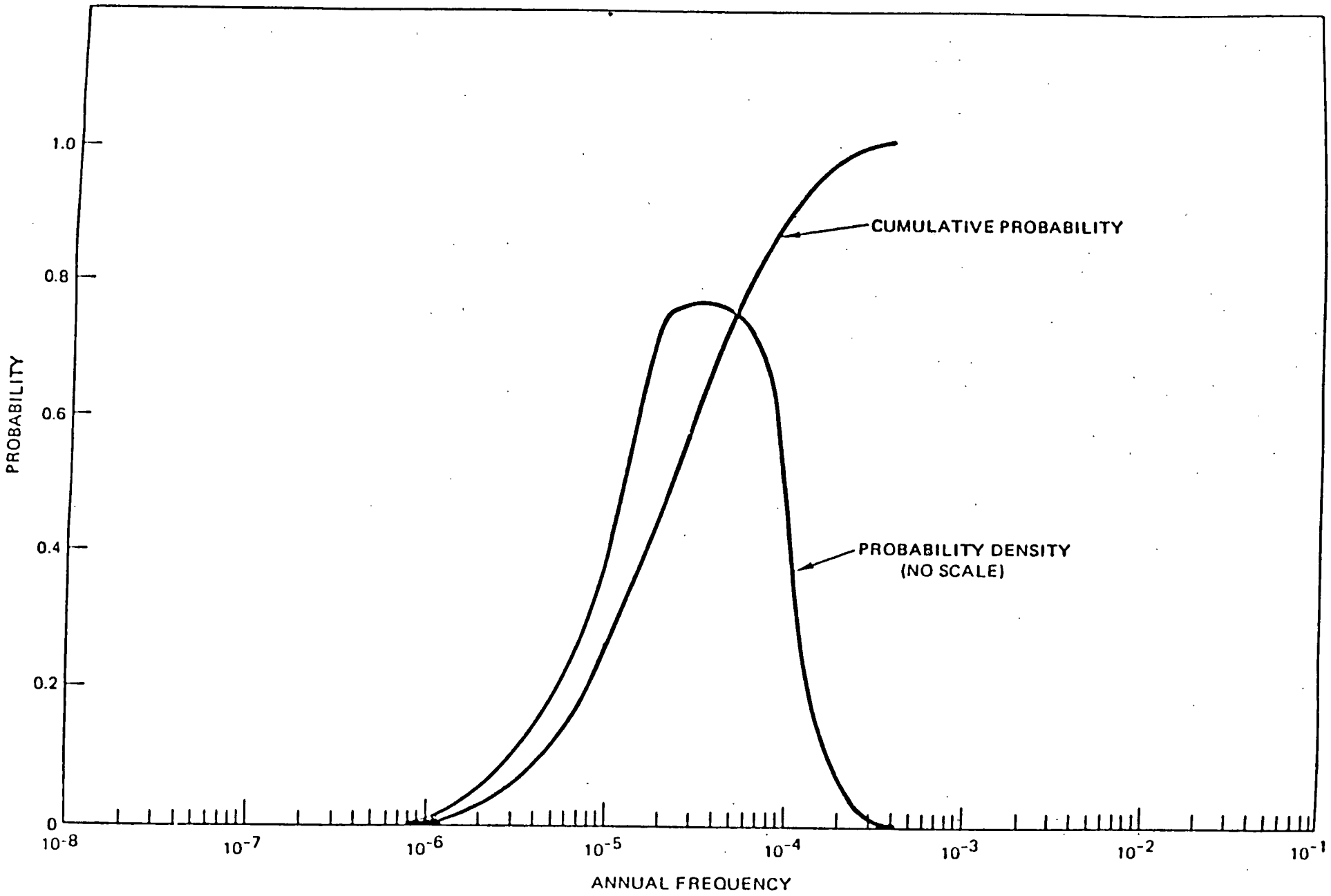
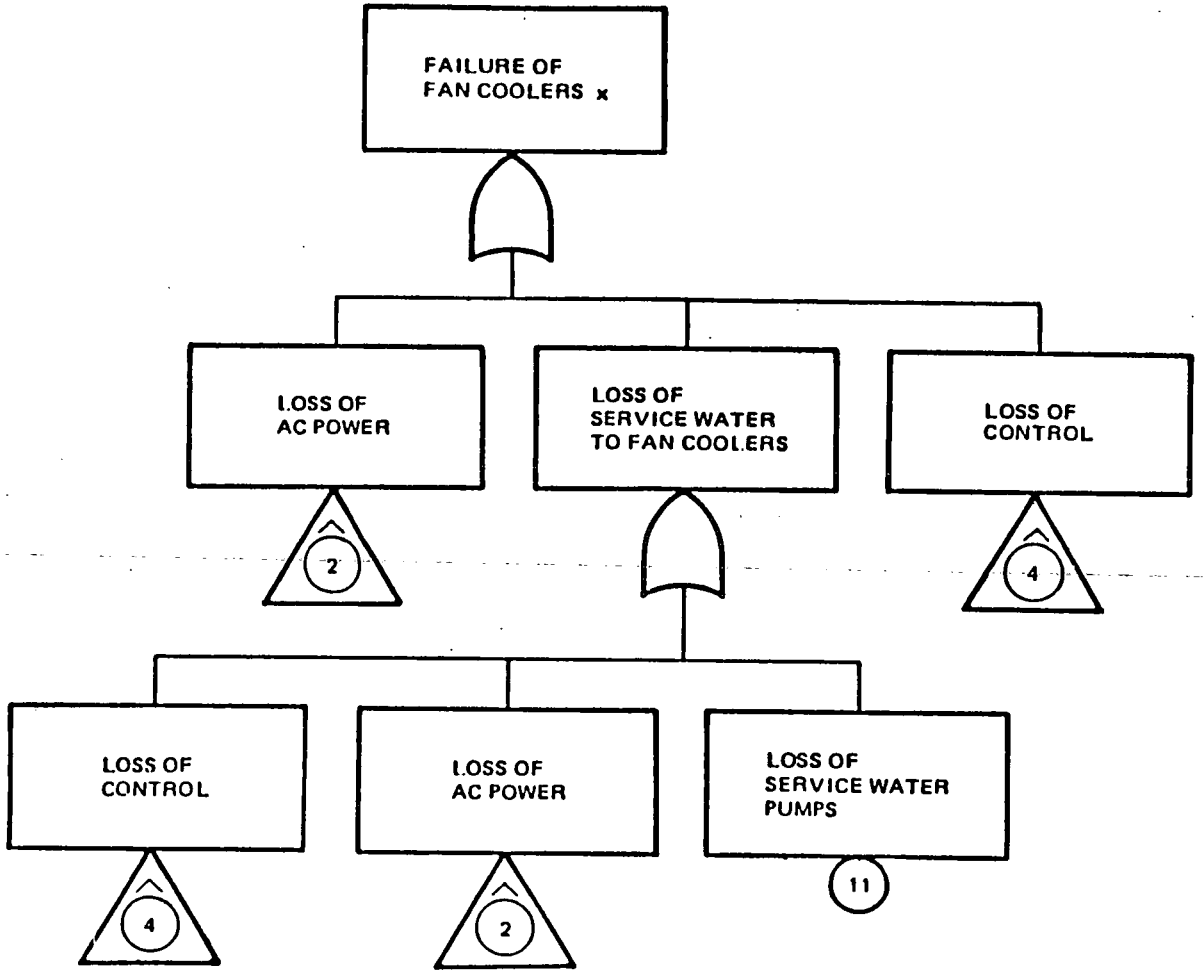


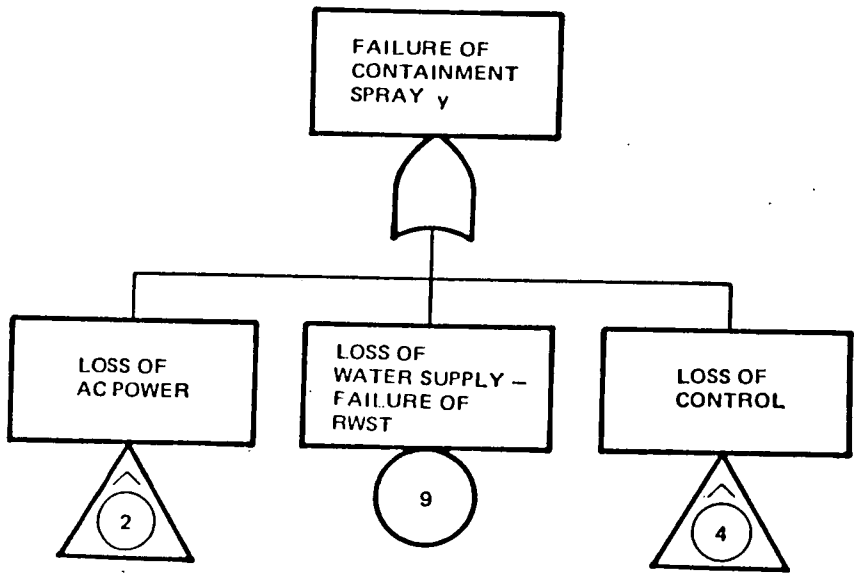
Figure 7.5-21. Core Melt Frequency from Wind Events - Indian Point 2



NOTE:

SYMBOLS IN TRIANGLES Δ REFER TO LATER FAULT TREE DEVELOPMENT

Figure 7.5-22. Indian Point Unit 2 Wind and Tornado Missile Fault Tree for Failure of Fan Coolers



NOTE:

1. SYMBOLS IN TRIANGLES △ REFER TO LATER FAULT TREE DEVELOPMENT.

Figure 7.5-23. Indian Point Unit 2 for Wind and Tornado Missile Failure of Containment Spray

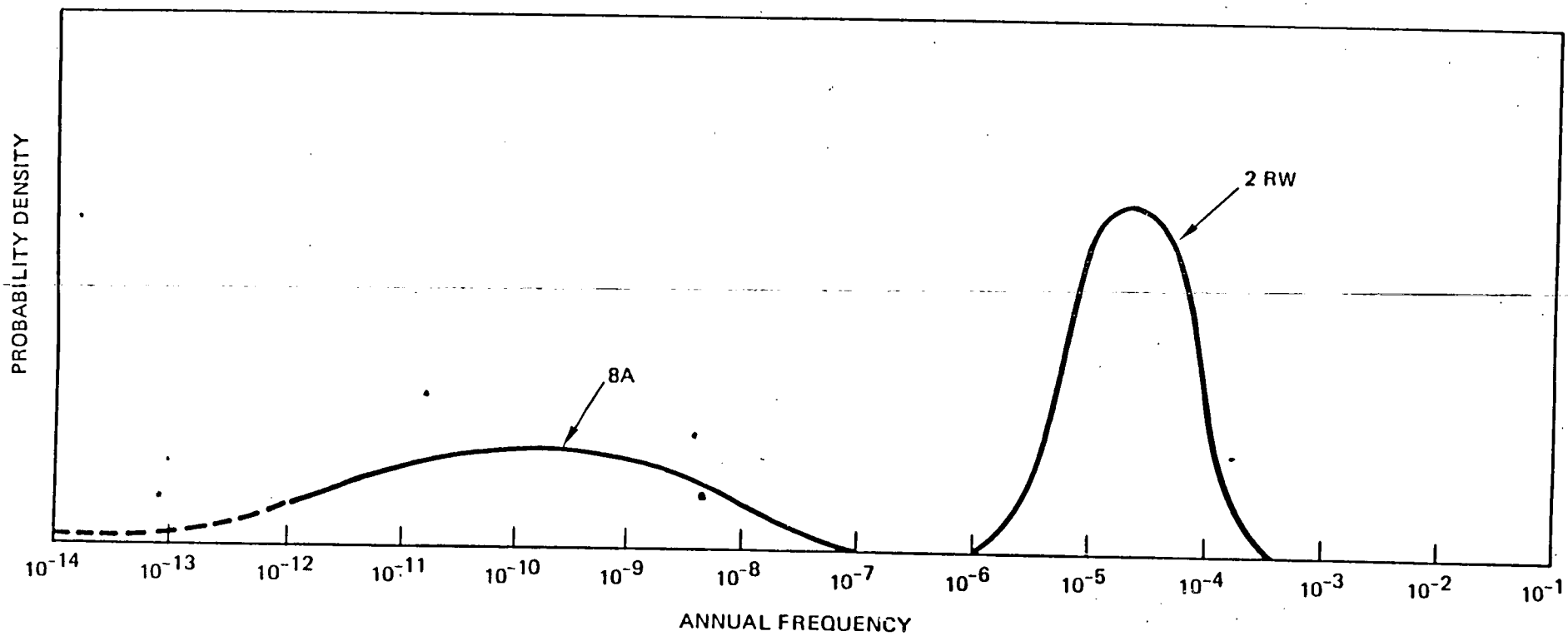


Figure 7.5-24. Release Frequency from Wind Events - Indian Point Unit 2